FUNCTIONALISATION OF SP3 C-O BONDS AND OLEFINS ENABLED BY NICKEL CATALYSIS

Laura Talavera Codina

UNIVERSITAT
ROVIRA i VIRGILI

Functionalisation of *sp*^{3} C–O bonds and olefins enabled by nickel catalysis

Laura Talavera Codina

DOCTORAL THESIS
2023

UNIVERSITAT ROVIRA I VIRGILI
FUNCTIONALISATION OF SP3 C-O BONDS AND OLEFINS ENABLED BY NICKEL CATALYSIS
Laura Talavera Codina

UNIVERSITAT ROVIRA I VIRGILI
FUNCTIONALISATION OF SP3 C-O BONDS AND OLEFINS ENABLED BY NICKEL CATALYSIS
Laura Talavera Codina

Functionalisation of sp^3 C–O bonds and olefins enabled by nickel catalysis

Laura Talavera Codina

DOCTORAL THESIS
Supervised by Prof. Rubén Martín Romo
Institut Català d'Investigació Química (ICIQ)
Universitat Rovira i Virgili (URV)
Department of Analytical Chemistry and Organic Chemistry

UNIVERSITAT ROVIRA i VIRGILI

ICIQ

Tarragona 2023

UNIVERSITAT ROVIRA I VIRGILI
FUNCTIONALISATION OF SP3 C-O BONDS AND OLEFINS ENABLED BY NICKEL CATALYSIS
Laura Talavera Codina

Prof. Rubén Martín Romo, Group Leader at the Institute of Chemical Research of Catalonia (ICIQ) and Research Professor at the Catalan Institution for Research and Advanced Studies (ICREA),

I STATE that the present study, entitled "Functionalisation of sp^3 C-O bonds and olefins enabled by nickel catalysis", presented by Laura Talavera Codina for the award of the degree of Doctor, has been carried out under my supervision at the Institute of Chemical Research of Catalonia (ICIQ).

Tarragona, June 2023

Doctoral Thesis Supervisor

Prof. Rubén Martín Romo

UNIVERSITAT ROVIRA I VIRGILI
FUNCTIONALISATION OF SP3 C-O BONDS AND OLEFINS ENABLED BY NICKEL CATALYSIS
Laura Talavera Codina

“It is not the mountain we conquer, but ourselves”
Edmund Hillary

UNIVERSITAT ROVIRA I VIRGILI
FUNCTIONALISATION OF SP3 C-O BONDS AND OLEFINS ENABLED BY NICKEL CATALYSIS
Laura Talavera Codina

Acknowledgements

First of all, I would like to express my deepest gratitude to my PhD supervisor, **Prof. Rubén Martín**, for providing me with the opportunity to pursue my doctoral studies under his guidance and mentorship. Thanks for believing in my potential and for helping me transition from an industrial mindset to an academic one. During these past four years I have expanded my horizons in ways I never thought possible, and I have not only grown as a scientist but also as a person.

Secondly, I would like to thank the members of my committee, **Prof. Igor Larrosa**, **Prof. Mariola Tortosa**, and **Dr. Alexandr Shafir** for accepting our invitation to read and assess my work.

Additionally, I would also like to acknowledge the collaborators that I have worked with during the projects summarised in this work: **Dr. Shang-Zheng**, **Philipp Spieß** and **Dr. Craig Day**, then **Dr. Ciro Romano** and **Prof. Enrique Gomez-Bengoa**, and most recently **Dr. Robert R. A. Freund**, **Huihui Zhang**, **Dr. Matthew Wakeling** and **Mara Jensen**. I am truly thankful for your support, expertise, and contributions; this work would not have been possible without you.

A special thank you is dedicated to **Dr. Eloisa Serrano** for providing me with the opportunity to undertake a 5-month industrial placement at Boehringer Ingelheim. Your guidance, mentorship, and passion for research have been truly inspiring.

I am very grateful to **David Sadaba** for taking care of the group. Thanks for making our lives easier, and for being there whenever there is a problem, you are gem! I would also like to acknowledge the **ICIQ research support units** for their assistance and support throughout these past four years. **Xisco Caldentey** and **Maria Hueso**, thank you for your constant support and willingness to provide guidance and advice whenever needed.

I would like to express my heartfelt gratitude to the **past and present members of the Martin group**, you have made my time in the lab an unforgettable experience. Those Martinis who were there when I first started. **Andreu**, **Rosie**, **Yaya**, **Jessica**, **Jacob**, **Hongfei**, and **Fei** thanks for all the help and advice. **Raul**, thanks for making my life easier in Tarragona. Your energy and enthusiasm were infectious, and I genuinely miss you. **Shang-Zheng**, I am immensely grateful for your kindness when I first joined the 2.12 lab. Your willingness to transfer knowledge and guide me through the 1,1-difunctionalisation project was invaluable, thanks for such a good mentorship. **Bradley**, what a chaos you are, but honey I adore you for it. I'm grateful for the moments we shared and for the genuine connection we formed. The lads, **Roman**, **Robert**, **Matt**, **Franz**, you all brought an incredible energy to the group, and I miss the times when we were all together. From the lab to our outings to Twins and the beach volleyball in l'Arrabassada, those were some of the best moments our group has witnessed!! **Carlota**, we have been together in this journey since day 1, and we have shared everything I could think of: the lab, the house, and even a lock down. Despite our differences, I would

like to thank you for being there. **Julien**, thanks for the fresh air you have brought to the lab, and for the climbing sessions in Monobloc, CET and outdoors! **Adrian**, your energy for partying is truly impressive, thanks for making me feel a little older! **Jesus**, our Rosalia sessions will forever remain me of the good times in 2.7, thanks for all the help and for being there when I needed. **Alvaro**, thanks for always being happy to lend a helping hand, and for your positive energy, keep it high. **Shuai**, the latest addition to our group, thanks for taking care of the project, I wish you good luck in your PhD studies. **Huihui**, tía, I will miss you tremendously, but I hope we can see each other again! You are an amazing person! **Cris**, although you are not from the group, you have been one of the most important persons during this journey. Thank you for being there for me, always. **Julieta**, you have become an incredible friend, thanks for being there for me through thick and thin, I can't imagine this PhD without you, te quiero beba! **Ciro**, our journey has had its ups and downs ;), but I am deeply grateful for your patience and support. From the great times in the lab to the joyful moments outside of it!! I will never be able to thank you enough for the countless discussions, and guidance you have provided. I truly miss having you here. I also want to thank the rest of the current members of the group, **Tomás**, **Liangliang**, **Zhong**, **Xinyang**, **Dimitry**, **Wen-Jun**, **Jinhong**, **Hao**, **Filip**, **Joan**, **Clarence**, **Yubiao**, **Wei** and **Paula** for creating the wonderful atmosphere we have today.

I want to thank the **people in BI** for welcoming me to the beautiful village of Biberach. Thanks for making my internship a very special time. I want to specially thank **Dr. Marco Santagostino**, **Philipp Kollmu** and **Paolo Piacentini** for kindly accepting me in the TEC lab, and for all the help. A gigantic thanks goes to **Kilian Frank** and the people from PR1, **Andrea Ardemani**, **Arne Guta**, and **Vanessa Koot**, for such as smooth introduction to the lab, and for accepting me without having second thoughts. And also, the climbing and non-climbing people for the great time I had with them outside the lab: **Paolo**, **Lucia**, **Julian**, **Dora**, **Camilla**, **James**, **Jörg**, **Raphy**, and **Bart**. **Christoph**, I will never forget the "famous" Spanish song, thanks for the introduction to the good German music, now I wake up happier every day!

També m'agradaria donar les gracies a les meves amigues, a les de **Lleida**, les de tota la vida, i la família d'**Esteve**! Gràcies per estar sempre al meu costat quan us he necessitat, i per fer que tot segueixi igual malgrat hi haver-me vist desaparèixer en més ocasions del que m'agradaria.

També vull donar les gràcies a la meva família, especialment als meus pares i germans. **mama**, **papa**, **Gerard** i **Sergi**, gràcies per haver cregut sempre en mi, per acompanyar-me en tots els meus camins, però sobretot, per haver fet possible que hagi arribat aquí. I finalment, m'agradaria donar les gràcies a l'**Adrià**. Gràcies per ser la meva escapatòria per tenir tanta paciència i per estimar-me durant els bons i els mals moments d'aquest viatge.

List of publications

At the time of printing, the results reported herein have been published as:

1. **Talavera, L.***; Freund, R. A. R.*; Zhang, H.; Wakeling, M.; Jensen, M.; Martin, R. Nickel-catalyzed 1,1-Aminoborylation of Unactivated Terminal Alkenes. *ACS Catal.* **2023**, *13*, 5538-5543.
2. Romano, C.*; **Talavera, L.***; Gómez-Bengoa, E.; Martin, R. Site-selective Functionalization of Unactivated sp^3 C–O Bonds in Cyclic Acetals. *J. Am. Chem. Soc*. **2022**, *144*, 11558-11563
3. Sun, S-Z.*; **Talavera, L**.*; *Spieß*, P.; Day, C.; Martin, R. sp^3 Bis-organometallic Reagents via Catalytic 1,1-Difunctionalization of Unactivated Olefins. *Angew. Chem. Int. Ed.* **2021**, *60*, 11740-11744.

*indicates equal contribution

UNIVERSITAT ROVIRA I VIRGILI
FUNCTIONALISATION OF SP3 C-O BONDS AND OLEFINS ENABLED BY NICKEL CATALYSIS
Laura Talavera Codina

Table of contents

Preface

The work presented in this dissertation has been performed at the Catalan Institute of Chemical Research (ICIQ) during the period of September 2019 to June 2023 under the supervision of Professor Rubén Martín Romo. The present manuscript is divided into five main parts: a general introduction, three research chapters, and a final chapter in which general conclusions of the work are presented. Each of the research chapters consists of an introduction and a summary of the aims of the project, followed by a discussion of the experimental results, conclusions, and finally an experimental section. References are independently organed in each chapter.

The first chapter provides an introduction to the background of Ni-catalysed cross-coupling reactions. It highlights the significance of nickel catalysis in the functionalisation of strong σ-bonds and recognises the potential of nickel/photoredox dual catalysis as a manifold to build up molecular complexity.

The second chapter, "*Site-selective functionalisation of unactivated sp^3 C–O bonds in cyclic acetals*", presents our efforts towards the development of a nickel/photoredox dual catalysis for the functionalisation of unbiased sp^3 C–O bonds in cyclic acetals. This methodology demonstrates the significance of conformational flexibility in achieving both reactivity and site-selectivity. The work described has been performed in collaboration with Dr. Ciro Romano and Prof. Enrique Gómez-Bengoa. This technique was published in *J. Am. Chem. Soc*. **2022**, *144*, 11558-11563.

The third chapter, "*sp^3 bis-organometallic reagents via catalytic 1,1-difunctionalisation of unactivated olefins*", discloses a catalytic 1,1-difunctionalisation of unactivated olefins to generate sp^3 bis-organometallic B,B(Si)-reagents. This protocol is characterised by exceptional reaction rates, mild conditions, wide scope, and exquisite pattern, providing a new platform to access sp^3 organometallics. This work was conducted in collaboration with Dr. Shang-Zheng Sun, Philipp Spieß, and Dr. Craig Day. This methodology was published in *Angew. Chem. Int. Ed.* **2021**, *60*, 11740-11744.

The fourth chapter, "*Nickel-catalysed 1,1-aminoborylation of unactivated terminal olefins*", discusses the development of a 1,1-difunctionalisation of unactivated olefins via nickel catalysis. This approach allows the incorporation of two different heteroatom motifs across an olefin backbone, enabling the synthesis α-aminoboronic acid derivatives from readily available precursors. This work has been performed in collaboration with Dr. Robert R. A. Freund, Huihui Zhang, Dr. Matthew Wakeling, and Mara Jensen. This protocol was published in *ACS Catal.* **2023**, *13*, 5538-5543.

Abbreviations

acac	acetylacetonate
AIBN	Azobisisobutyronitrile
NaBARF	sodium tetrakis 3,5-bis(trifluoromethyl)phenyl borate
Bdan	2,3-dihydro-1*H*-naphtho[1,8-*de*][1,3,2]diazaborinine
BDE	bond dissociation energy
Bpiy/bpy	2,2'-bipyridine
Bneop	5,5-dimethyl-1,3,2-dioxaborinane
BPin	4,4,5,5-tetramethyl-1,2,3 dioxaboronic ester
BTMG	2-*tert*-Butyl-1,1,3,3-tetramethylguanidine
CCDC	Cambridge crystallographic data centre
CFL	compact fluorescent light bulb
COD	1,5-cyclooctadiene
CPhos	2-Dicyclohexylphosphino-2′,6′-bis(*N*,*N*-dimethylamino)biphenyl
DCC	*N*,*N*′-Dicyclohexylcarbodiimide
DCM	dichloromethane
dcype	1,2-bis(dicyclohexylphosphino)ethane
DEMS	Dimethoxydimethylsilane
DFT	density functional theory
DG	directing group
DIPEA	*N*,*N*-diisopropylethylamine
DMA	dimethylacetamide
DMAP	4-(dimethylamino)pyridine
DME	1,2-dimethoxyethane
DMF	*N*,*N*-dimethylformamide
DMPU	1,3-dimethyltetrahydropyrimidin-2(1*H*)-one, *N,N*′-Dimethylpropylene urea
DMSO	dimethylsulfoxide
dppf	1,1′-Ferrocenediyl-bis(diphenylphosphine)
dr	diastereomeric ratio
dtbbpy	4,4'-di-*tert*-butylbipyridine
DTBP	di-*tert*-butyl peroxide
dtbpe	1,2-bis(di-*tert*-butylphosphino)ethane
ee	enantiomeric excess
equiv	equivalent(s)
EDA	electron donor-acceptor
EnT	energy transfer
E_T	triplet energy

HAT	hydrogen atom transfer
HMDSO	hexamethyldisiloxane
LiHMDS	Lithium bis(trimethylsilyl)amide
IPr·HCl	1,3-Bis-(2,4,6-Tribenzhydrylphenyl)-1*H*-imidazol-3-ium chloride
KTC	Kumada-Tamao-Corriu
LDA	Lithium diisopropylamide
LED	light-emitting diode
LMCT	ligand-to-metal charge transfer
LUMO	lowest unoccupied molecular orbital
mesitylene/Ms	1,3,5-trimethylbenzene
MTBE	Methyl *tert*-butyl ether
NBS	N-Bromosuccinimide
NHC	*N*-heterocyclic carbene
NHP	*N*-hydroxyphtalamide
NMP	*N*-methyl-2-pyrrolidone
PBI	Polybenzimidazole
PC	photocatalyst
PMHS	polymethylhydrosiloxane
PyrOx	pyroxamide
(R)-SEGPHOS	(*R*)-(+)-5,5′-Bis(diphenylphosphino)-4,4′-bi-1,3-benzodioxole
RuPhos	dicyclohexyl(2',6'-diisopropoxy-[1,1'-biphenyl]-2-yl)phosphane
rr	regiomeric ratio
RT	room temperature
SET	single electron-transfer
SIMes	1,3-bis(2,4,6-trimethylphenyl)-2-imidazolidinylidene
*t*AmOH	*tert*-Amyl alcohol, 2-methylbutan-2-ol
TBA	tetrabutyl ammonium
TBAB	tetrabutyl ammonium bromide
TEMPO	2,2,6,6-tetramethylpiperidin-1-yl)oxyl
TES	Triethoxysilane
THF	tetrahydrofuran
THP	Tetrahydropyran
TIPS	triisopropyl silane
TLC	thin layer chromatography
TMHD	2,2,6,6-tetramethyl-3,5-heptanedionate
TMS	Tetramethylsilane

Abstract

In recent years, nickel catalysis has gained considerable momentum as a vehicle to enable bond-forming reactions with exceptional efficiency. This is probably due to the ease at which nickel catalysts trigger single-electron transfer events, activation of strong C–X bonds and functionalisation of π-components, offering new vistas to promote reactions that would otherwise be difficult to accomplish by other means.[1–5]

In line with our ongoing interest in developing strategies to functionalise strong σ-bonds and the functionalisation of readily available starting materials,[6–8] this Doctoral Thesis has been focused on two main areas: *i*) the functionalisation of unactivated C–O bonds (Chapter 2), and *ii*) the 1,1-difunctionalisation of unactivated olefins (Chapters 3 and 4).

Despite the significant progress on the functionalisation of sp^3 C–O derivatives – requiring in most instances the utilisation of electron-withdrawing groups adjacent to the oxygen atom –, the sp^3 C–O functionalisation of unactivated alkyl ethers still remains challenging.[9] The first study explores the functionalisation of unactivated C–O bonds in cyclic acetals through metallaphotoredox catalysis. The reaction is triggered by an appropriate σ*−p orbital overlap prior to sp^3 C–O cleavage, highlighting the significance of conformational flexibility in achieving both reactivity and site selectivity. The protocol is characterised by its excellent chemoselectivity profile, thus offering new possibilities for activating strong σ sp^3 C–O linkages (Chapter 2).

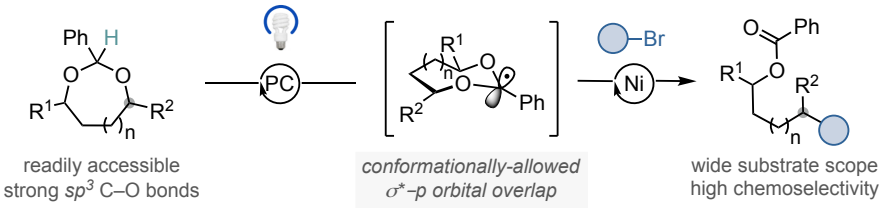

Scheme 1. Site-Selective sp^3 C–O Arylation and Alkylation of Cyclic Acetals

In a distinct effort, we directed our attention towards the 1,1-difunctionalisation of olefins to enhance molecular complexity using readily available starting materials.[10–12] Unlike the extensively studied 1,2-difunctionalisation of alkenes,[13–17] we recognised that the development of a platform that might enable 1,1-difunctionalisation of olefins would expand the repertoire of bond disconnections available in modern organic synthesis. Initially we demonstrated the synthesis of *bis*-organometallic reagents bearing both B and Si motifs (Chapter 3). Building upon the success of this transformation, we envisioned the development of a generic platform for synthesising α-aminoboronic acids. Unlike the remarkable achievements using alkynes[18] and well-defined vinyl boronates[19,20] as

precursors, we recognised that the use of readily accessible olefins and commercially available B_2Pin_2 as starting materials would offer enhanced synthetic flexibility and reduced costs.

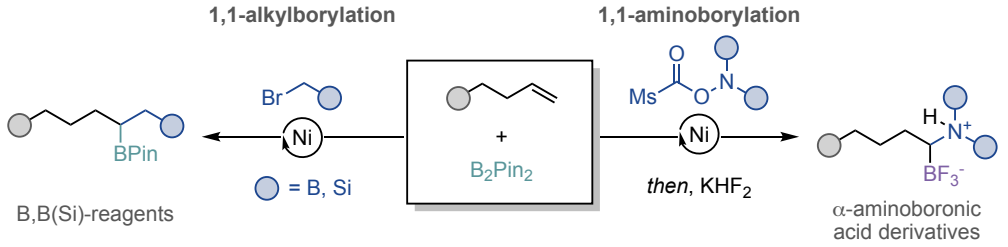

Scheme 2. Nickel-catalysed 1,1-difunctionalisation of olefins

In conclusion, we have developed new methods that highlight the versatility and distinct reactivity modes of nickel catalysis, providing valuable tools for the functionalisation of unactivated C–O bonds via metallaphotoredox strategies and the synthesis of diverse sp^3 functionalised linkages using olefins as readily available starting materials.

References

(1) Chernyshev, V. M.; Ananikov, V. P. Nickel and Palladium Catalysis: Stronger Demand than Ever. *ACS Catal.* **2022**, *12* (2), 1180–1200. https://doi.org/10.1021/acscatal.1c04705.
(2) Diccianni, J. B.; Diao, T. Mechanisms of Nickel-Catalyzed Cross-Coupling Reactions. *Trends Chem.* **2019**, *1* (9), 830–844. https://doi.org/10.1016/j.trechm.2019.08.004.
(3) Chan, A. Y.; Perry, I. B.; Bissonnette, N. B.; Buksh, B. F.; Edwards, G. A.; Frye, L. I.; Garry, O. L.; Lavagnino, M. N.; Li, B. X.; Liang, Y.; Mao, E.; Millet, A.; Oakley, J. V.; Reed, N. L.; Sakai, H. A.; Seath, C. P.; MacMillan, D. W. C. Metallaphotoredox: The Merger of Photoredox and Transition Metal Catalysis. *Chem. Rev.* **2022**, *122* (2), 1485–1542. https://doi.org/10.1021/acs.chemrev.1c00383.
(4) Li, Y.; Wu, D.; Cheng, H.; Yin, G. Difunctionalization of Alkenes Involving Metal Migration. *Angew. Chem. Int. Ed.* **2020**, *59* (21), 7990–8003. https://doi.org/10.1002/anie.201913382.
(5) Ye, Y.; Lin, Y.; Mao, N.-D.; Yang, H.; Ye, X.-Y.; Xie, T. Recent Progress in Nickel-Catalyzed Carboboration of Alkenes. *Org. Biomol. Chem.* **2022**, *20* (47), 9255–9271. https://doi.org/10.1039/D2OB01855A.
(6) Cornella, J.; Zarate, C.; Martin, R. Metal-Catalyzed Activation of Ethers via C–O Bond Cleavage: A New Strategy for Molecular Diversity. *Chem. Soc. Rev.* **2014**, *43* (23), 8081–8097. https://doi.org/10.1039/C4CS00206G.
(7) Zarate, C.; van Gemmeren, M.; Somerville, R. J.; Martin, R. Chapter Four - Phenol Derivatives: Modern Electrophiles in Cross-Coupling Reactions. In *Advances in Organometallic Chemistry*; Pérez, P. J., Ed.; Academic Press, 2016; Vol. 66, pp 143–222. https://doi.org/10.1016/bs.adomc.2016.07.001.
(8) Juliá-Hernández, F.; Moragas, T.; Cornella, J.; Martin, R. Remote Carboxylation of Halogenated Aliphatic Hydrocarbons with Carbon Dioxide. *Nature* **2017**, *545* (7652), 84–88. https://doi.org/10.1038/nature22316.
(9) Anwar, K.; Merkens, K.; Aguilar Troyano, F. J.; Gómez-Suárez, A. Radical Deoxyfunctionalisation Strategies**. *Eur. J. Org. Chem.* **2022**, *2022* (26), e202200330. https://doi.org/10.1002/ejoc.202200330.
(10) Dong, Z.; Ren, Z.; Thompson, S. J.; Xu, Y.; Dong, G. Transition-Metal-Catalyzed C–H Alkylation Using Alkenes. *Chem. Rev.* **2017**, *117* (13), 9333–9403. https://doi.org/10.1021/acs.chemrev.6b00574.
(11) Dhungana, R. K.; Kc, S.; Basnet, P.; Giri, R. Transition Metal-Catalyzed Dicarbofunctionalization of Unactivated Olefins. *Chem. Rec.* **2018**, *18* (9), 1314–1340. https://doi.org/10.1002/tcr.201700098.
(12) Patel, M.; Desai, B.; Sheth, A.; Dholakiya, B. Z.; Naveen, T. Recent Advances in Mono- and Difunctionalization of Unactivated Olefins. *Asian J. Org. Chem.* **2021**, *10* (12), 3201–3232. https://doi.org/10.1002/ajoc.202100666.
(13) Giri, R.; KC, S. Strategies toward Dicarbofunctionalization of Unactivated Olefins by Combined Heck Carbometalation and Cross-Coupling. *J. Org. Chem.* **2018**, *83* (6), 3013–3022. https://doi.org/10.1021/acs.joc.7b03128.
(14) Tu, H.-Y.; Zhu, S.; Qing, F.-L.; Chu, L. Recent Advances in Nickel-Catalyzed Three-Component Difunctionalization of Unactivated Alkenes. *Synthesis* **2020**, *52* (09), 1346–1356. https://doi.org/10.1055/s-0039-1690842.
(15) Badir, S. O.; Molander, G. A. Developments in Photoredox/Nickel Dual-Catalyzed 1,2-Difunctionalizations.

Chem **2020**, *6* (6), 1327–1339. https://doi.org/10.1016/j.chempr.2020.05.013.

(16) Derosa, J.; Apolinar, O.; Kang, T.; Tran, V. T.; Engle, K. M. Recent Developments in Nickel-Catalyzed Intermolecular Dicarbofunctionalization of Alkenes. *Chem. Sci.* **2020**, *11* (17), 4287–4296. https://doi.org/10.1039/C9SC06006E.

(17) Qi, X.; Diao, T. Nickel-Catalyzed Dicarbofunctionalization of Alkenes. *ACS Catal.* **2020**, *10* (15), 8542–8556. https://doi.org/10.1021/acscatal.0c02115.

(18) Gao, D.-W.; Gao, Y.; Shao, H.; Qiao, T.-Z.; Wang, X.; Sanchez, B. B.; Chen, J. S.; Liu, P.; Engle, K. M. Cascade CuH-Catalysed Conversion of Alkynes into Enantioenriched 1,1-Disubstituted Products. *Nat. Catal.* **2020**, *3* (1), 23–29. https://doi.org/10.1038/s41929-019-0384-6.

(19) Nishikawa, D.; Hirano, K.; Miura, M. Asymmetric Synthesis of α-Aminoboronic Acid Derivatives by Copper-Catalyzed Enantioselective Hydroamination. *J. Am. Chem. Soc.* **2015**, *137* (50), 15620–15623. https://doi.org/10.1021/jacs.5b09773.

(20) Zhang, Y.; Qiao, D.; Duan, M.; Wang, Y.; Zhu, S. Enantioselective Synthesis of α-Aminoboronates by NiH-Catalysed Asymmetric Hydroamidation of Alkenyl Boronates. *Nat. Commun.* **2022**, *13* (1), 5630. https://doi.org/10.1038/s41467-022-33411-9.

Chapter 1.

General introduction

UNIVERSITAT ROVIRA I VIRGILI
FUNCTIONALISATION OF SP3 C-O BONDS AND OLEFINS ENABLED BY NICKEL CATALYSIS
Laura Talavera Codina

1.1. Transition metal-catalysed reactions

Metal-catalysed cross-coupling reactions represent a reliable and modular approach to build C–C and C–heteroatom bonds and have undoubtedly revolutionised the landscape of modern synthetic chemistry.[1] Indeed, the recognition of their importance is evident from the three Nobel Prizes awarded in Chemistry for the development of stereoselective catalysis, olefin metathesis, and palladium-catalysed cross-couplings. These highly efficient, mild, and functional group tolerant transformations have found widespread use in diverse fields, ranging from complex natural product synthesis and drug discovery to manufacturing. In fact, the use of palladium-catalysed cross-coupling reactions alone accounts for more than 40% of C–C bond forming reactions in pharmaceutical synthesis,[2] which can be attributed to its predictable and controllable catalytic properties.[3] However, the high cost of palladium has encouraged chemist to find more sustainable and less toxic alternatives using earth-abundant first-raw transition metals. In this context, nickel, which is located above palladium in the periodic table, not only represents a cheaper alternative but also offers complementary reactivity/selectivity due to its unique properties.[4–7]

Despite the widespread use of palladium catalysis, the use of nickel predates that of Pd. The origins of nickel can be traced back to the 1890s with the seminal works from Mond and Sabatier.[8,9] Sabatier, in particular, was awarded the 1912 Nobel Prize in Chemistry for his pioneering work on the nickel-catalysed hydrogenation of ethylene. Since then, numerous outstanding catalytic systems and powerful practical applications have been discovered. These include the industrial applications of the Shell Higher Olefin Process (SHOP) for the production of α-olefins and the DuPont's hydrocyanation of butadiene for the synthesis of adiponitrile.[10,11]

1.1.1. General properties of nickel catalysis

Despite both nickel and palladium belonging to the group 10 metals in the periodic table, they display several differences in their catalytic properties (Scheme 1). For instance, as a first-raw metal, nickel exhibits a higher pairing energy of the d orbitals. This characteristic enables the formation of more stable open-shell electronic configurations compared to its second and third row counterparts. Consequently, activation of electrophiles by Ni can occur via one-electron pathways alongside the classical two-electron oxidative addition. Due to its smaller radius and higher nucleophilicity, nickel can promote oxidative addition of particularly strong σ-bonds, such as C–O or C–N bonds. Additionally, the coupling of sp^3 carbon fragments is favoured with Ni catalyst, as slow β-hydride elimination from Ni-alkyl complexes is observed. The slower β-hydride elimination observed in Ni-alkyl compounds can be attributed to the lower electronegativity of Ni, resulting in a weaker agnostic interaction relative to Pd, as well as its smaller radius, which leads to a more strained geometry in the

transition state.[12–14] Finally, nickel exhibits strong π-back donation, resulting in tight binding to unsaturated systems, thus facilitating the activation of alkenes and alkynes.[15–18]

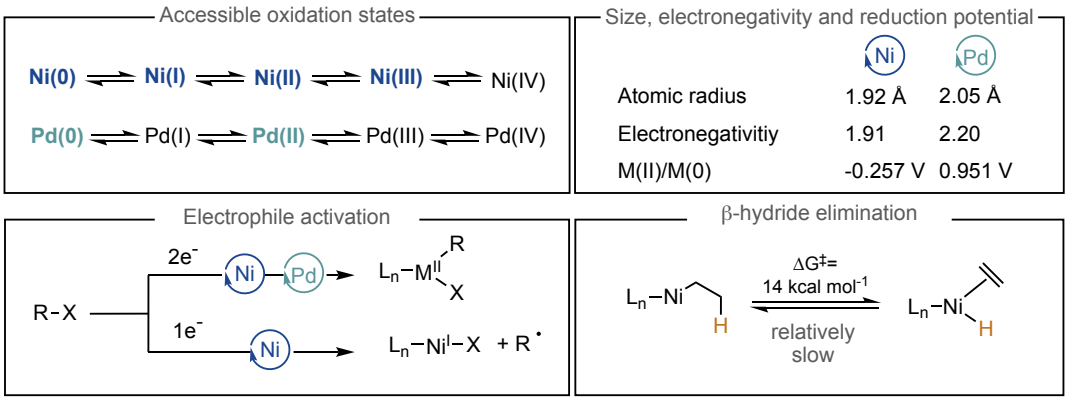

Scheme 1. Characteristics of nickel and palladium

As a result of its distinct properties when compared to palladium, nickel has been recognised to participate in a number of processes, such as *i*) single-electron transfer events, *ii*) activation of strong C–X bonds historically considered inert in cross-coupling reactions, and *iii*) difunctionalisation of olefins, thus, providing opportunities for reaching new reactivity modes.

1.2. Functionalisation of strong σ-bonds via nickel catalysis

Although the use of organic halides as coupling partners in metal-catalysed reactions has become routine, their toxicity, associated to the formation of halogenated waste, along with their limited accessibility, have prompted chemists to seek for alternatives that offer improved flexibility, practicality, and modularity.

In recent years, carbon-oxygen electrophiles have emerged as viable substitutes to organic halides in the cross-coupling arena.[6,19–23] This can be attributed to *i*) the lack of halogenated waste generation, *ii*) their greater availability compared to aryl/alkyl halides, and *iii*) the opportunity to develop orthogonal reactions to “traditional” Pd-catalysed reactions. Besides (pseudo)halide electrophiles, the direct functionalisation of carbon-hydrogen bonds represents and ideal scenario to build up molecular complexity, considering the ubiquitous nature of C–H bonds in organic molecules. Indeed, C–H functionalisation is particularly attractive in the context of late-stage functionalisation wherein molecules featuring high structural complexity can be diversified without the need for lengthy synthetic route redesign.[24–28]

Despite the great advantages offered by their direct manipulation, simple alcohols or C–H bonds still represent challenging targets in metal-catalysed cross-coupling reactions, due to the high activation barrier required for effecting the cleavage of such strong bonds. Initial efforts in the context of C–O activation were directed towards the utilisation of activated C–O bonds,[29] while typical methods for C–H bond activation were observed through the direct oxidative addition of highly reactive, low valent, noble metals to alkanes, forming a carbon-metal bond.[30–34]

In this section, nickel-catalysed functionalisation of strong C–O and C–H bonds will be discussed. However, the utilisation of especially activated allyl, propargyl, and allenyl and/or biased phenol derivatives with particularly weak C–O bonds such as phosphates, sulfonates, phenyl esters, carbamates, carbonates, and carboxylic acids is beyond the scope of this thesis.[22] Likewise, more recent photoredox approaches based on single-electron pathways will not be covered in this section.[35]

1.2.1. Functionalisation of C–O bonds

1.2.1.1. C(sp^2)–O functionalisation

The harder and more electropositive character of nickel when compared to palladium has led to the development of metal-catalysed cross-coupling reactions using unactivated phenol derivatives. While aryl sulfonates are commonly employed in palladium catalysis, stronger C–O bonds such as aryl ethers or esters are not viable substrates for Pd catalysts. Conversely, Ni(0) complexes have demonstrated the ability to insert into these bonds (Scheme 2).[36–38]

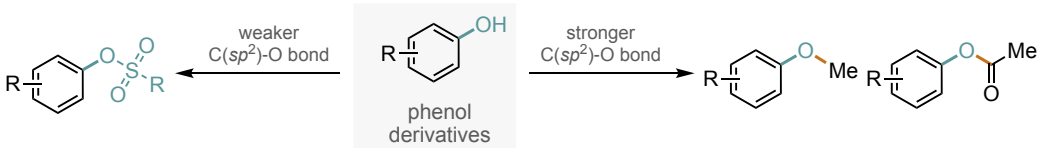

Scheme 2. Phenol derivatives

Aryl methyl ethers

Aryl methyl ethers, the simplest phenols derivatives, have emerged as highly attractive carbon electrophiles from both step- and atom-economical points of views. Their commercially availability, ease of synthesis and great stability under commonly employed conditions make them ideal precursors for C(sp^2)-synthons in cross-coupling reactions. Nevertheless, their traditional utilisation has been limited to serving as directing groups in electrophilic aromatic substitutions or metalation reactions.[19,20,23,39]

Although the inherent challenge for promoting C(sp^2)–OMe cleavage led to the general perception that aryl methyl ethers could not be applied as electrophiles in cross-coupling reactions, pioneering work by Wenkert in 1979, already demonstrated the ability of nickel to engage in C(sp^2)–OMe manipulation.[40–42] This study described a Kumada-Tamao-Corriu-type cross-coupling reaction of aryl and vinyl methyl ethers with Grignard reagents, resulting in the formation of alkylated and arylated products using $Ni(PPh_3)_2Cl_2$ as the precatalyst (Scheme 3, *top*). However, it was not until two decades later that the potential of this transformation was fully recognised by Dankwardt.[43] In this seminal work, the use of bulky and electron-rich phosphines in combination with a nickel catalyst provided improved reactivity, extending the methodology to regular arenes lacking π-extended backbones, even at room temperature (Scheme 3, *bottom*).

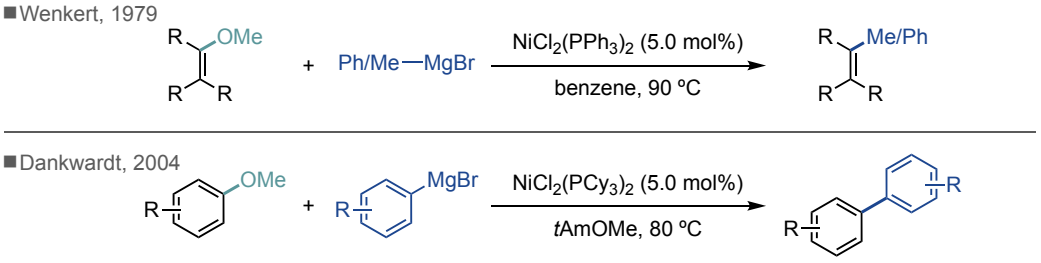

Scheme 3. Wenkert's seminal work and Dankwardt's reinvestigation of KTC-type cross-coupling reactions

Based on the abovementioned reports, one might think that C(sp^2)–O scission is preferred over C(sp^3)–O, however it is important to note that the latter is energetically favoured in anisole derivatives. In fact, Milstein and co-workers reported that site-selectivity of the C–O bond cleavage can be controlled by the judicious choice of transition metal.[44] Nucleophilic Rh(I) complexes promote C(sp^2)–O bond scission, whereas the more electrophilic Ni(II) species underwent activation of the weaker C(sp^3)–O bond. These findings imply that electron-rich transition metal catalyst promote C(sp^2)–OMe cleavage, in agreement with the early discoveries by Wenkert and Dankwardt, showing that electron-donating phosphines – PCy_3 or PCy_2Ph – were the most active ligands.[40,43]

In 2012, the group of Agapie conducted a series of mechanistic investigations to shed light on the chemoselectivity of Ni(0) catalysed C(sp^2)–OMe bond cleavage. These studies focused on the stoichiometric oxidative addition of **I** into $Ni(COD)_2$.[45] By utilising NMR spectroscopy, they were able to detect intermediate **III** and isolate and characterise the complex resulting from the subsequent β-hydride elimination (**IV**), confirming that oxidative addition occurred at the C(sp^2)–O bond. Furthermore, complex **II** was also characterised by NMR and X-ray, constituting the first evidence of a η^2-complex and elucidating the mechanism by which site-selectivity operates in anisole derivatives.

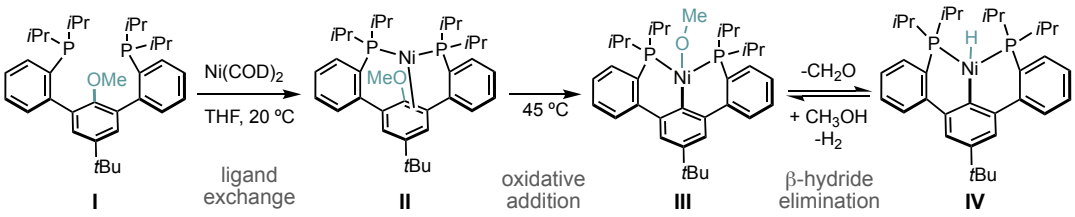

Scheme 4. Agapie's mechanistic studies on Ni insertion into the C(sp^2)–O bond

Recent studies have focused on the investigation of the mechanistic intricacies during the C(sp^2)–OMe bond cleavage and have proposed the existence of alternative pathways other than "classical" oxidative addition to Ni(0) species. For example, Lewis acid-assisted oxidative addition of alkyl-nickelate complexes have been proposed by our group and others, which have been supported by both computational and experimental evidence.[38,46–49]

These findings served as inspiration for several research groups to expand the substrate scope of viable electrophiles by fine-tuning the Ni(0) source, the ligand backbone, and/or the substrate properties. In addition to the methods described earlier, aryl ethers can be coupled with other nucleophiles rather than Grignard reagents under nickel catalysis.[1–3,48,50–56] Representative examples include coupling with organoboron reagents[57–59], amines[60,61], hydrosilanes[36,62] and silylboranes,[63] showcasing the opportunity to access a range of C–X bond-forming reactions and reductive cleavage (Scheme 5).

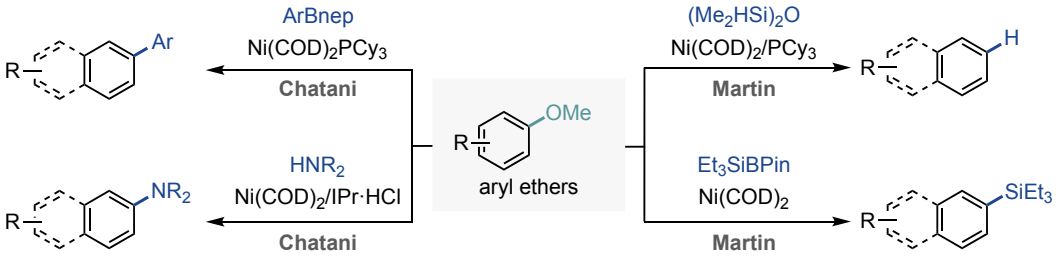

Scheme 5. Selected examples of Ni-catalysed cross-coupling of aryl methyl ethers

Aryl esters

When discussing the functionalisation of aryl esters, site-selectivity issues arise, similar to those observed with aryl methyl ethers. Seminal work by Yamamoto and co-workers described the factors that influence the functionalisation of aryl C(sp^2)–O *vs* acyl C(sp^2)–O bonds in aryl and vinyl carboxyesters.[64,65] The authors observed that selectivity is primarily determined by the nature of the ester. Specifically, vinyl esters exhibit a preference for reacting at the aryl C(sp^2)–O site, whereas phenyl esters are more prone to undergo functionalisation at the acyl C(sp^2)–O group (Scheme 6).

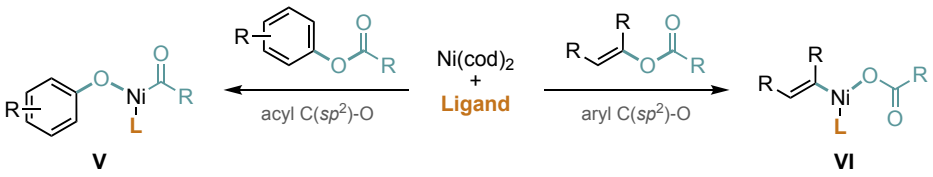

Scheme 6. Differences in site-selectivity of nickel oxidative addition with aryl and vinyl ester derivatives

While this report demonstrated the feasibility of aryl esters as electrophiles using nickel, it was not until 2008 that Shi and Garg groups independently reported the first catalytic C(sp^2)–OPiv functionalisation.[51,66,67] Shi utilised aryl boroxines and stoichiometric amounts of water or organozinc as nucleophilic partners, while Garg employed boronic acids. It is worth noting that in both cases, aryl pivalates were used to prevent undesired reactions arising from the acyl C(sp^2)–O bond cleavage. Later on, Liu and co-workers conducted a theoretical study that supported the experimental findings, demonstrating that the mechanism is consistent with the functionalisation of the stronger C(sp^2)–O bond. The group proposed that a monophosphate pathway is energetically favoured over the diphosphine pathway proposed by Shi (Scheme 7).[68]

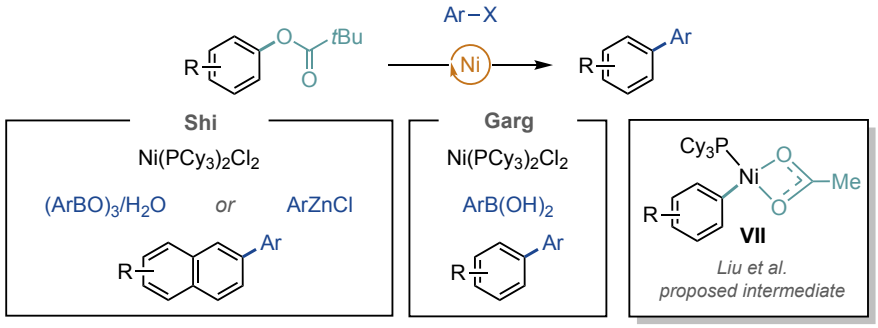

Scheme 7. Pioneering works on aryl ester C(sp^2)–O bond functionalisation

The reactivity differences between aryl pivalates and aryl benzoate esters were exemplified by Yamaguchi and Itami groups in the context of Ni-catalysed C–O/C–H coupling.[69] This report revealed that the use of aryl pivalates esters led to exclusive aryl C(sp^2)–O functionalisation, whereas activation at the weaker acyl C(sp^2)–O bond occurred with aryl benzoate esters, followed by decarbonylative C–H arylation (Scheme 8).[70] This study highlighted the ability to selectively target different C–O bonds based on the structure of the ester substrate employed.

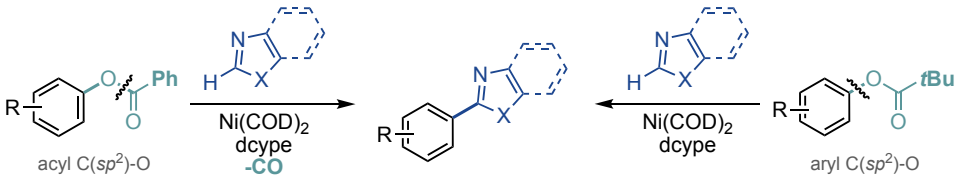

Scheme 8. Differences in reactivity between aryl pivalates and aryl benzoate esters

Following these seminal works, several theoretical and experimental mechanistic studies were conducted by Houk, Itami, Yamaguchi and Lei. [68,71,72] Houk, studied the Ni(0)/dcype system for C–O selectivity with aryl pivalates and aryl benzoate esters substrates and found that the reaction at the weaker acyl C(sp^2)–O bond is favoured in both cases.[72] However, after oxidative addition, aryl pivalates undergo decarbonylation with the formation of a highly unstable Ni(dcype)(*t*Bu)(OAr) intermediate (**IX**), such intermediate is destabilised by unfavourable steric interactions between the *t*Bu group and the bulky dcype ligand. The increased energy barrier for acyl C(sp^2)–O bond activation, due to this steric clash, accounts for the selective functionalisation of aryl C(sp^2)–O bond in aryl pivalates using the Ni(0)/dcype system. On the contrary, the complex resulting from the decarbonylation of aryl esters (**X**) is relatively more stable, due to reduced steric demand and favourable d-π* interaction between the nickel centre and the phenyl group, making the coupling via acyl C(sp^2)–O bond cleavage feasible (Scheme 9).

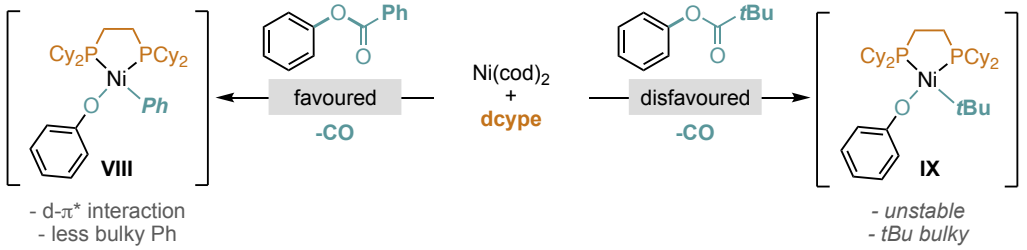

Scheme 9. Mechanistic insights into the acyl C(sp^2)–O bond cleavage/decarbonylation pathways

Notably, Itami, Yamaguchi, and Lei reported for the first time the isolation of an oxidative addition complex between nickel and an aryl pivalate (**X**), providing experimental evidence to support their mechanistic studies (Scheme 10, *left*).[73] To further highlight the ability of nickel to insert into the C(sp^2)–O bond, Love described the activation of non π-extended aryl esters with dtbpe at room temperature (Scheme 10, *middle*).[74] Subsequent studies conducted by our group showed that the oxidative addition can occur using monodentate phosphines – PCy_3 – with both π-extended and non π-extended systems. Initial investigations indicated that the more flexible coordination sphere and the complex unsaturated nature of these complexes posed difficulties in their isolation: only off-cycle dimeric species **XIII**, deriving from comproportionation with Ni(0), could be isolated and characterised.

Nonetheless, a later study demonstrated that on-cycle species **XIV** could be isolated and characterised when synthesised by anion metathesis of the sterically congested mesitylene derivative, representing a milestone step forward in the fundamental understanding of C–O functionalisation reactions (Scheme 10, *right*).[75,76]

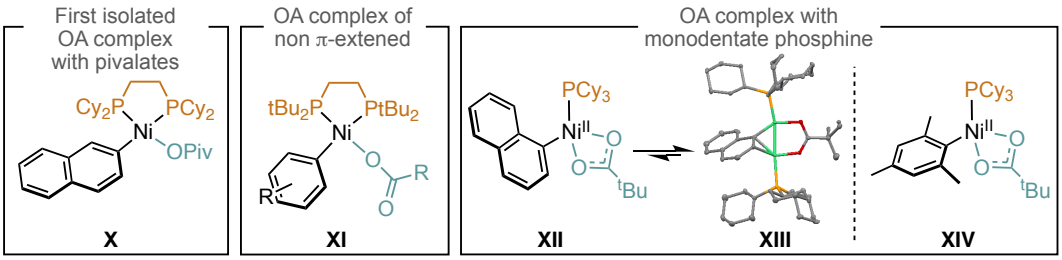

Scheme 10. Isolated nickel complexes for the functionalisation of aryl esters

While these pioneering studies founded the origins of C(sp^2)–O bond cleavage, over the last decades numerous research groups have demonstrated the remarkable versatility of nickel-catalysed cross-coupling reactions using aryl pivalates. These methods have shown that aryl esters functionalisation expands far beyond C–C bond formation,[77–81] encompassing a wide range of transformations, such as amidations,[82] carboxylations,[83] aminations,[84] borylations, stannylations,[85] phosphorylations[86,87] and silylations reactions[88] (Scheme 11).

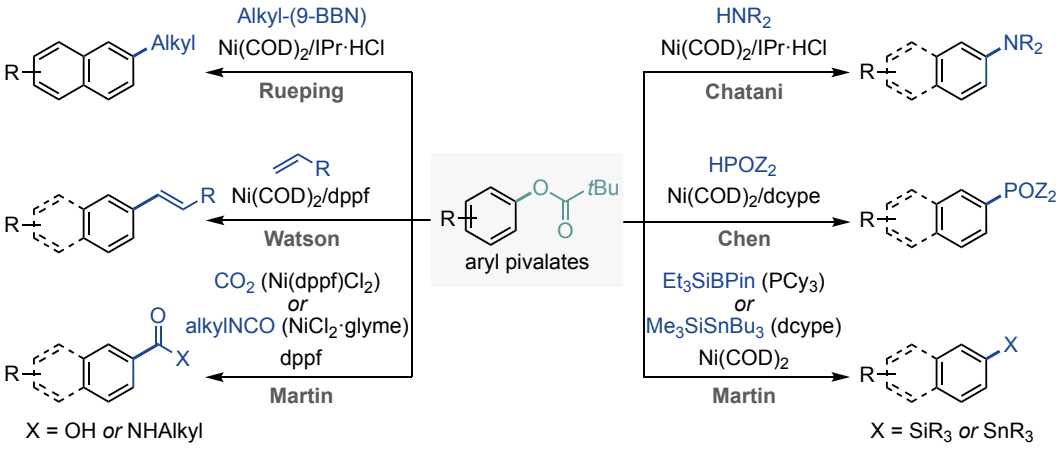

Scheme 11. Selected examples of Ni-catalysed cross-coupling of aryl pivalates

1.2.1.2. C(sp^3)–O functionalisation

Benzylic and allylic derivatives

Although the use of sp^2 C–O electrophiles has become routine, limitations remain with respect to the activation and coupling of sp^3 C–O counterparts. In this context, the use of benzylic and allylic alcohol derivatives has offered ways to overcome the high activation

barrier of unactivated sp^3 C–O. Moreover, the change in participating orbitals when compared to sp^2 C–O bond activation has led to the development of new activation methods, enabling stereospecific Ni-catalysed C–O functionalisations.

Although stereoconvergent coupling reactions of benzylic C–O bonds employing enantioselective nickel catalysis were pioneered by the Fu group in 2009 (Scheme 12, *top*),[89] Jarvo and co-workers developed a complementary approach via a stereospecific cross-coupling reaction (Scheme 12, *bottom*). [90]

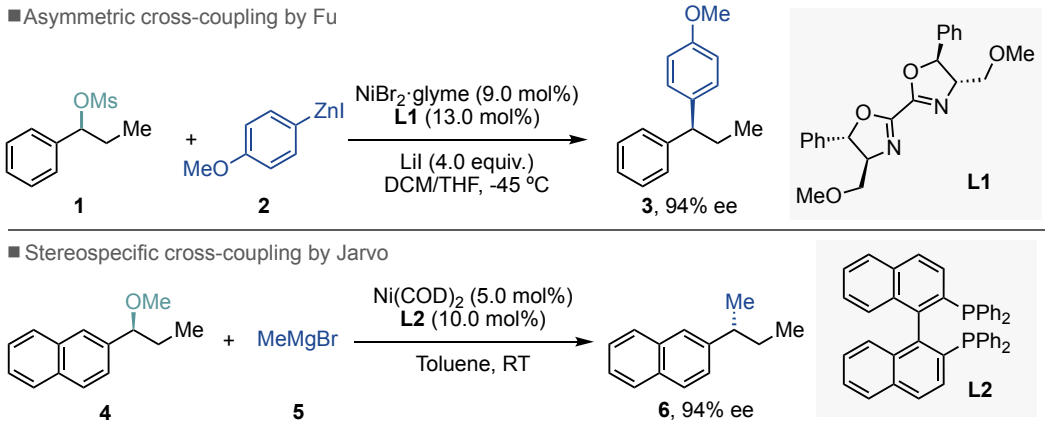

Scheme 12. Initial reports on enantioselective and stereospecific cross-coupling with benzylic C–O electrophiles

Later, the same group reported a stereospecific nickel-catalysed cross-coupling of benzylic carbamates and pivalates with aryl boronic esters, in which the stereospecificity of the transformation was controlled by the nature of the ligand. PCy_3 exhibited high selectivity towards stereoretentive C–C bond formation, while SIMes led to a stereoinvertive process (Scheme 13, *top*).[91] Theoretical studies conducted by Jarvo and Hong provided insights into the reaction mechanism, revealing that nickel can cleave the benzylic and allylic C(sp^3)–O bonds through either a stereoretentive chelation-assisted model or a streoinvertive S_N2-type back-side attack. In both cases, Ni(0) undergoes cleavage of the benzylic C–O bond, leading to the formation of benzyl nickel(II) species and, according to the oxidative addition mechanism, enantoisomeric benzyl nickel(II) species are formed (**XV** *vs* **XVI**). The nature of the ligand plays a crucial role. PCy_3 interacts with nickel primarily through σ-donation, thus favouring a stereoretentive benzylic C–O activation. On the other hand, SIMes features additional d(metal)-p(ligand) back-donation with nickel, resulting in a more rigid environment, thereby promoting a stereoinvertive oxidative addition step. These findings are consistent with the experimental results (Scheme 13, *bottom*).[92,93]

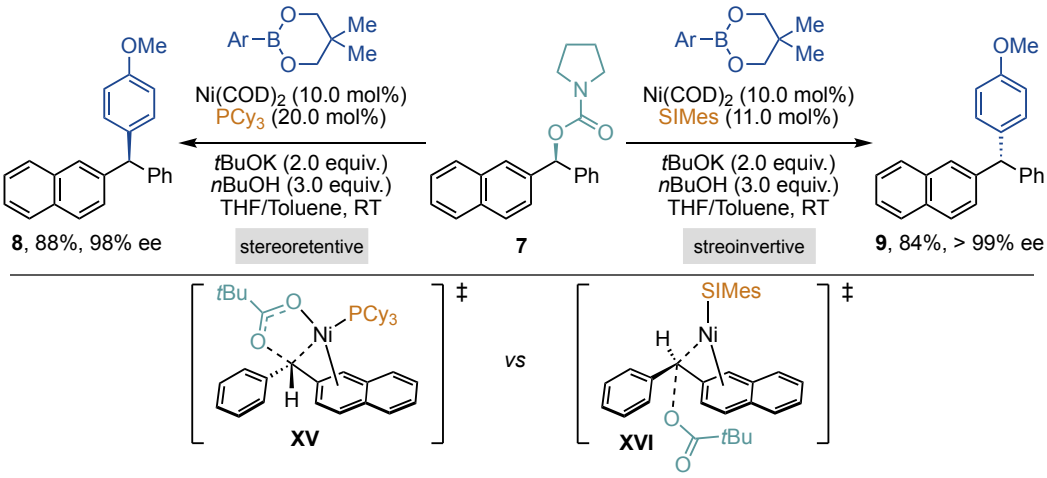

Scheme 13. Stereospecificity controlled by the nature of the ligand

The stereospecificity of these reactions is not only influenced by the choice of the ligand but also by the reaction solvent and substrate structure. The group of Watson reported a nickel-catalysed Miyaura borylation of allylic pivalates, in which the stereospecificity of C–B bond formation depended on the solvent used.[94] Mechanistic investigations revealed that solvents with low polarity deliver stereoretentive borylation products, while highly polar solvents led to stereoinverted products. The latter observation can be attributed to a zwitterionic S_N2-type transition state that causes inversion of the allylic stereogenic centre.[93,95] Interestingly, Jarvo and co-workers found that KTC-type coupling of benzylic ethers proceeds exclusively with stereoinvertion, whereas a cross-electrophile coupling solely produces the stereoretented product.[96,97] This finding is attributed to the ability of Lewis acidic MgI_2, formed in the KTC-type cross-coupling, to coordinate the oxygen leaving group and stabilise the S_N2-type back-side attack transition state.[93,98]

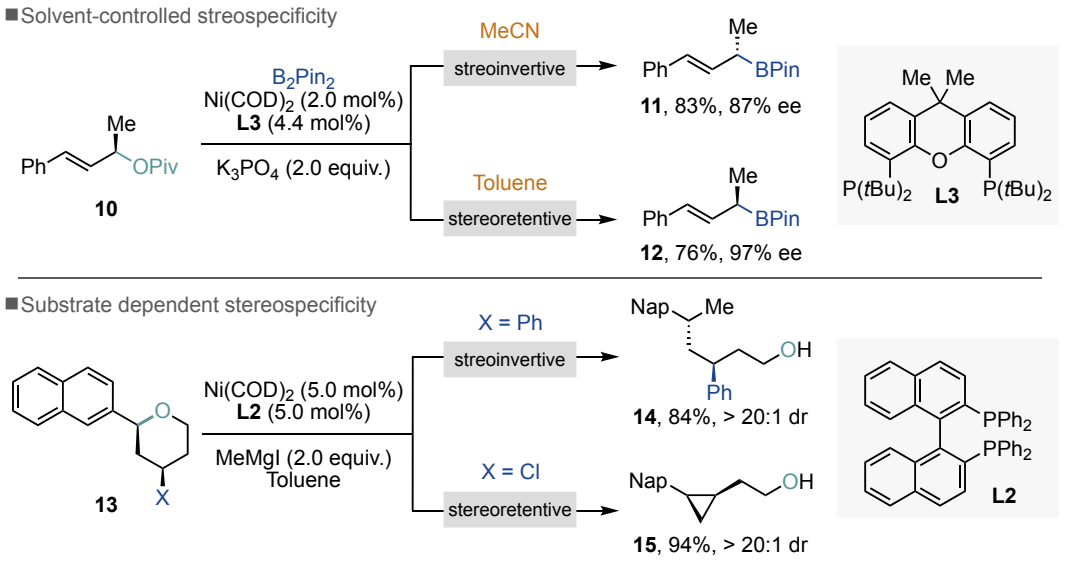

Scheme 14. Solvent and substrate dependent stereospecificity

These reports highlight representative examples of the distinct mechanisms described for the coupling of allylic and benzylic sp^3 C–O bonds and spurred the development of novel stereospecific cross-coupling reactions via nickel-catalysed C–N and C–O bond activation.[83,99–108]

Aliphatic derivatives

While benzylic and allylic alcohols represent activated electrophiles bearing a sp^2-hydridised carbon adjacent to the electrophilic centre, the use of purely aliphatic counterparts has proved particularly challenging under standard conditions. The difficulty in using alkyl electrophiles arises from the high activation barrier to cleave the C(sp^3)–O linkage, as well as the need to avoid competitive homocoupling side reactions and β-hydride elimination.

In 2016, Morken disclosed an elegant enantioselective cross-coupling between symmetric cyclic sulfates and aryl Grignard reagents using a chiral nickel catalyst (Scheme 15).[109]

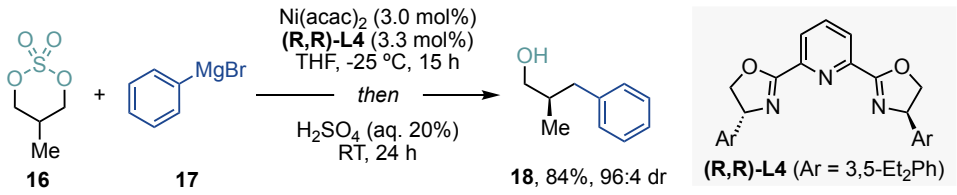

Scheme 15. Asymmetric Kumada-Tamao-Corriu type cross-coupling of cyclic sulfates

Nonetheless, direct activation of aliphatic alcohols has remained scarce and current efforts have focused on the use of pre-activation of the hydroxy functionality, using either *in*

situ or *ex situ* techniques. Recent methods include the coupling of alcohol-derived alkyl sulfonates via halide intermediates[108,110–113], *in situ* bromination of alcohols[114], Zn-mediated single-electron transfer of alkyl oxalates[115,116], photoinduced generation of carbon-centred radical from alcohol derived redox-active esters, among others.[117–121] These strategies will be discussed more in details in Chapter 2.

1.2.2. Functionalisation of C–H bonds

The direct functionalisation of C–H bonds is one of the most powerful techniques in organic synthesis. However, the development of catalytic systems to achieve regio-, chemo-, and stereo-stereoselectivity is tremendously challenging, due to the presence of multiple C–H bonds with comparable bond dissociation energies within organic molecules.

The first Ni-catalysed C(sp^2)–H bond functionalisation was reported by Kleiman and Dubeck in 1963, for the activation of azobenzene.[122] However, when compared to precious metals (e.g., Ir, Rh, Pd, Pt), nickel-catalysed C–H bond functionalisation protocols have remained relatively underdeveloped and are limited to the use of directing-group strategies or the functionalisation of particularly acidic C–H bonds.[123–125]

1.2.2.1. Non-directing group strategies

In non-directing group strategies, acidic C–H bonds are typically targeted. Therefore, advances have been achieved especially with substrates containing highly electron-negative heteroatoms or electron-withdrawing groups. However, these requirements limit the methods' generality to polyfuloroarenes, imidazoles, pyridines and thereof.

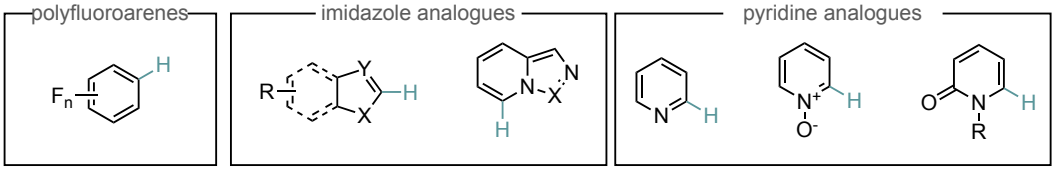

Scheme 16. Electron-deficient arenes traditionally employed in non-directed C–H functionalisations

The use of perfluoroarenes in nickel-catalysed C–H functionalisation was popularised by the Hiyama group in 2008, which described the alkylation of fluoroarenes.[126]

In the case of imidazole analogues, a pioneering example was demonstrated by Cavell in 2004, who reported the coupling of imidazolium salts with alkenes using a $Ni(COD)_2/PPh_3$ system.[127] Since then, the functionalisation of imidazole analogues has seen remarkable levels of sophistication due to the prevalence of heteroarenes in drug molecules, agrochemical compounds, and organic materials.[124,125]

Similarly to imidazole analogues, C–H bonds at the C2 and C4 position of pyridine and pyridine *N*-oxides are also acidic, thus spurring the development of functionalisation strategies at these positions. In 2008, Nakao and co-workers used a monophosphine ligand in combination with a Ni-Zn bimetallic catalyst system to achieve C2 alkenylation of pyridines (Scheme 17, *top*),[128] whereas in 2010 the activation at the C4 position was attained by replacing the phosphine ligand with a bulky *N*-heterocyclic carbene (Scheme 17, *middle*).[129,130] However, a recent notable advance in the field was disclosed by Yu and co-workers, who reported the C3-alkylation of pyridines by cooperative Ni/Al catalysis. The authors were able to override the intrinsic C2/C4 selectivity by the use of a reversible template-substrate anchoring strategy. In fact, the catalyst was able to block the C2 position through a steric clash between the ligand and the Lewis acid, and disfavour the reaction at the C4 position via ring-strain imparted by the ligand length (Scheme 17, *bottom*).[131]

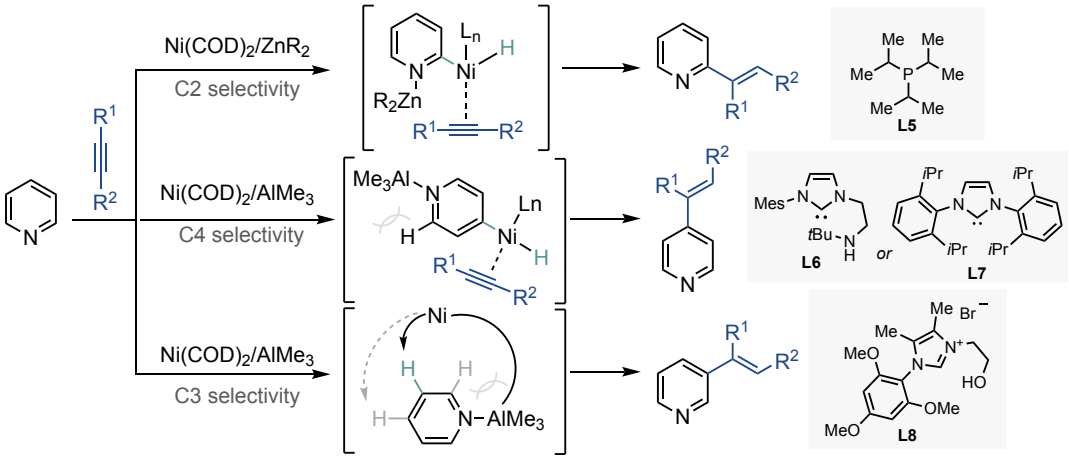

Scheme 17. Alkenylation of pyridines at the C2, C4 and C3 position

Despite C–H activation typically occurring at acidic C–H sites, in 2019, Nakao and Hartwig described the first undirected hydroarylation of unactivated alkenes enabled by the use of a nickel catalyst in combination with a highly sterically hindered NHC ligand, demonstrating the ability to activate unbiased C–H bonds.[132]

Initially, nickel-catalysed C–H functionalisation was proposed to proceed via a direct oxidative addition. However, theoretical and experimental mechanistic studies by Peruts, Sakaki, Hartwig, and others have revealed that these reactions occur through a ligand-to-ligand hydrogen transfer (LLHT) mechanism. In LLHT, oxidative addition of C–H bonds and migratory insertion of an unsaturated co-reactant occur simultaneously without the formation of a Ni(II)-hydride intermediate (Scheme 18).[132–135]

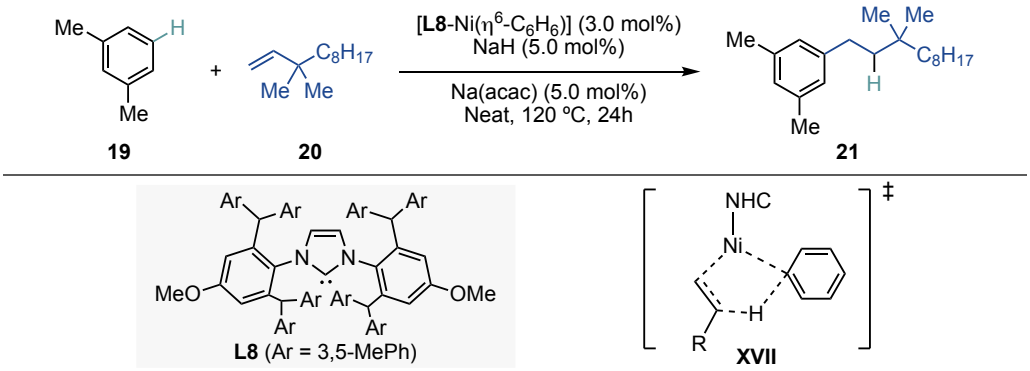

Scheme 18. Ligand-to-ligand hydrogen transfer (LLHT) mechanism in C–H bond activation

1.2.2.2. Directing group strategies

Directing group strategies have emerged as a powerful tool to activate C–H bonds that are not inherently acidic. This approach is based on the coordination of a metal centre to a pending functional group, which brings the catalyst into close proximity of a specific C–H bond.

Among the most commonly employed directing groups, *N,N*-bidentate systems such as 8-aminoquinoline, 2-(pyridine-2-yl)isopropylamine, and 2-pyrimidyl have proven to be effective in achieving C–H bond activation. The groups of Chatani, Akerman, Shi, Ge, and Zhang, among others, have made significant contributions to the development of chelation-assisted systems utilising these directing groups, enabling the formation of C–C, C–X and C–S bonds.[123]

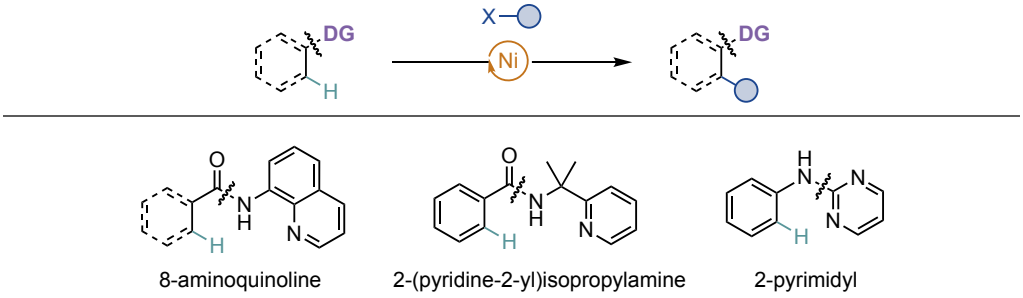

Scheme 19. Selected directing groups used in nickel-catalysed C–H functionalisation strategies

The use of 8-aminoquinoline, initially discovered by Daugulis,[136] has been extensively exploited for the formation of a number of C–X bonds, and has been successfully applied to activate both C(sp^2)–H and C(sp^3)–H sites.[123] As a result, several theoretical and experimental studies have been conducted by Liu and Love to elucidate the mechanism by which nickel activates the C–H bond. It has been concluded that the C–H cleavage step is

the rate-determining step and occurs through a concerted metalation-deprotonation (CMD) mechanism.[137,138]

1.3. Nickel/photoredox dual catalysis

The reactivity and selectivity of transition metal-catalysed reactions can be controlled through ligand design or modulation of the oxidation state of the catalyst.[139–142] The ligand can exert steric and electronic control over the metal environment, thereby affecting the reactivity of the metal complex, whereas the modulation of the metal oxidation state can accelerat sluggish elementary steps. Nevertheless, ligand design requires extensive theoretical and experimental efforts and often offers low degree of control over intrinsic reactivity, while modulation of the metal oxidation state frequently involves the use of stoichiometric oxidants/reductants, ultimately affecting the overall reaction mixture.

To address these challenges, the integration of photoredox catalysis within the context of transition metal chemistry has emerged as a powerful alternative. This approach utilises light-mediated radical generation to activate non-traditional cross-coupling electrophiles or to access high-energy oxidation levels and electronically excited states on the transition metal complex.[143,144]

In 2007, pioneering studies by Osawa and co-workers demonstrated the potential use of $Ru(bpy)_3^{2+}$ as a "light-harvesting" photocatalyst for a copper-free Sonogashira coupling reaction.[145] While this report established the genesis of metallaphotocatalysis, it was Sanford and co-workers who recognised the potential of merging photoredox with transition metal catalysis, disclosing the directed C–H arylation of 2-arylpyridines with aryl diazonium salts (Scheme 20).[146] This work, together with the ability of nickel catalysts to access a range of oxidation states via one-electron pathways and facilitate the coupling of sp^3-hybridised fragments, inspired the early works by MacMillan, Doyle and Molander on the nickel/photoredox dual catalytic manifold.

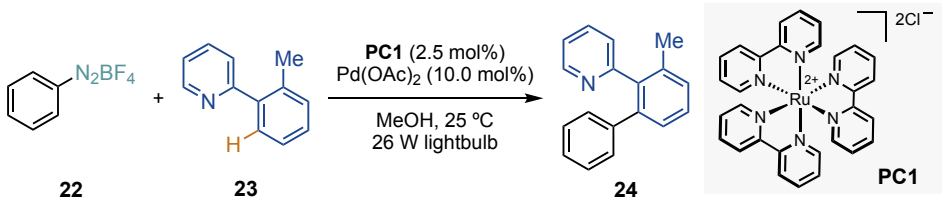

Scheme 20. Seminal work on the potential of merging photoredox and transition metal catalysis

Although beyond the scope of this thesis, it is worth noting that metallaphotoredox catalysis has also been described using other metals than nickel, with major focus on the use of palladium, copper, gold and cobalt among others.[143,144,147,148]

1.3.1. Redox-active substrates

In 2014, MacMillan and Doyle reported a decarboxylative cross-coupling of carboxylic acids with aryl halide electrophiles, to forge new C(sp^2)–C(sp^3) bonds (Scheme 21).[149] The proposed mechanism, involves two consecutive single electron-transfer (SET) events from the excited state of the photocatalyst to the Ni(II) precatalyst, accessing the active Ni(0) species. The electron-transfer event is triggered by the generation of a highly oxidising *Ir(III) complex generated upon photo-excitation and singlet-to-triplet intersystem crossing of the photocatalyst (**PC2**). Subsequently, Ni(0) undergoes oxidative addition with the aryl iodide to deliver the nickel-aryl species (**I**). Concurrently, the *Ir(III) intermediate interacts with the carboxylate by a SET event, releasing an Ir(II) photocatalyst and a carboxy-radical. The *O*-centred radical rapidly decarboxylates to release a nucleophilic *C*-centred alkyl radical, **XVIII**. The latter is captured by **XX** to afford a high valent Ni(III) intermediate (**XXI**) that rapidly undergoes reductive elimination to yield the desired product and a Ni(I) specie. Finally, a SET between the highly reductant Ir(II) and nickel(I) closes both catalytic cycles, regenerating the active species.

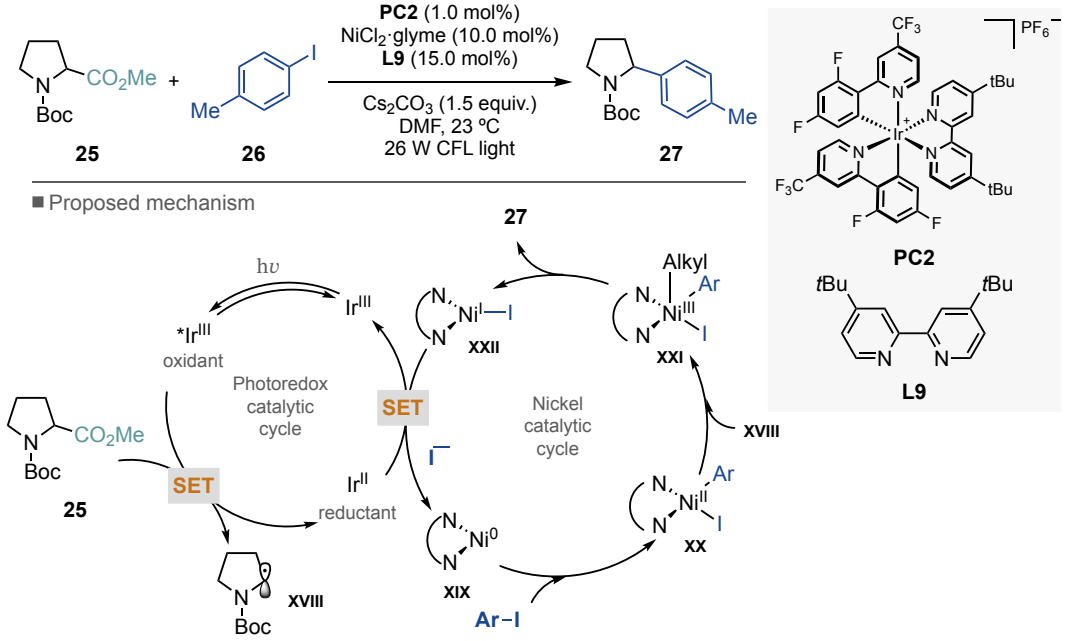

Scheme 21. Metallaphotoredox decarboxylative arylation

Analogously, Molander and co-workers described the merger of Ni catalysis within the photoredox arena using benzyltrifluoroborates as benzylic radical precursors, which were generated upon SET with the excited photocatalyst.[150] In this case, however, a revised mechanism proposes an initial capture of the carbon-centred radical by the Ni(0) species, to

afford a Ni(I)-alkyl intermediate (**XXV**). Oxidative addition of the aryl iodide, then, affords the key high valent Ni(III) species (**XXVI**) (Scheme 22).[151]

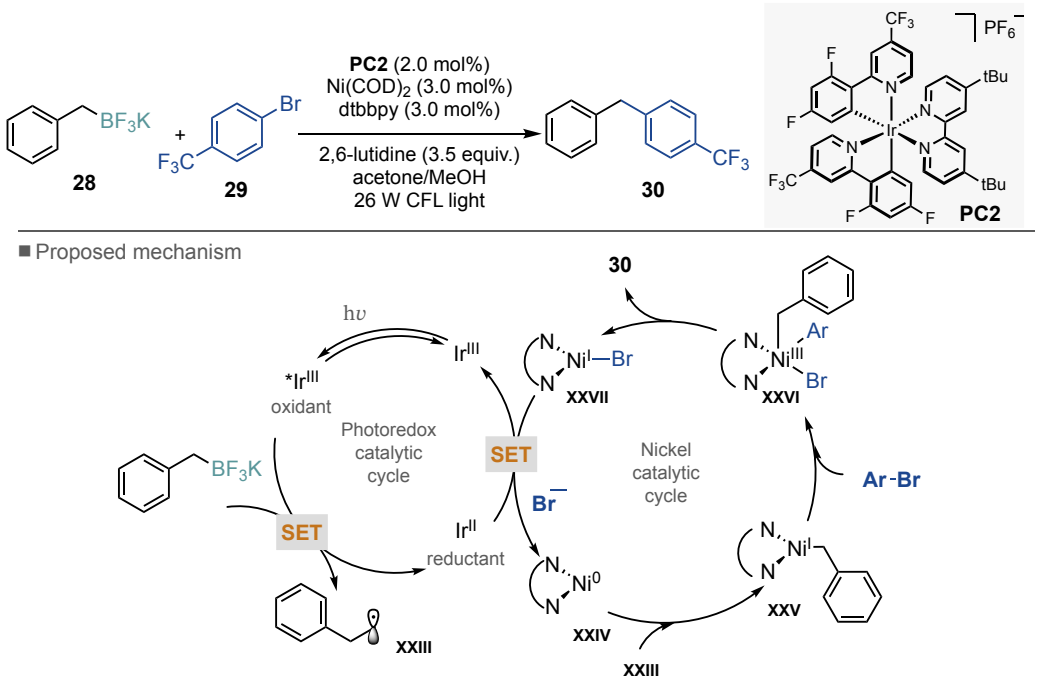

Scheme 22. Benzyl trifluoroborate cross-coupling with aryl bromides using nickel/photoredox dual catalysis

Subsequently, this concept has been expanded to an array of other functionalities, enabling structural manipulation at unconventional sites by novel activation modes based on the generation of alkyl radicals from redox-active substrates, hence complementary to traditional metal-catalysed cross-coupling platforms (Scheme 23).[143,144,147] However, in some cases, the high oxidation potentials to overcome for the generation of the key radical intermediates limit the functional group compatibility.

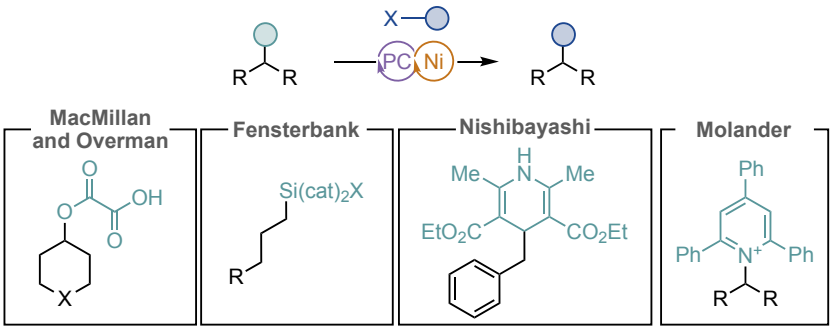

Scheme 23. Selected examples of redox-active substrates

1.3.2. Hydrogen atom transfer

To decouple the redox properties of the substrate from the mode of action, hydrogen atom transfer (HAT) can be utilised. In this context, the development of new photocatalysts has contributed significantly to the direct activation of R–H bonds in a highly selective manner, eliminating the need for preliminary installation of activated functional groups. Upon excitation, according to the photoredox catalyst employed, various types of HAT process can be initiated, which can be classified into *direct* and *indirect* methods. [152–154]

1.3.2.1. Direct HAT approaches

Direct HAT strategies rely on the inherent reactivity of the photocatalyst in its excited state to directly abstract a hydrogen atom from the substrate. In this context, aromatic ketones and polyoxomelates, such as decatungstate anion, are the most relevant in this field. These species possess a highly electrophilic oxygen site, which enables the desired HAT step.

Aromatic ketones

In 2018, our group reported the use of aromatic ketones as HAT catalyst in a light-mediated nickel-catalysed cross-coupling reaction. The authors developed a C(sp^3)–H bond arylation and alkylation platform employing a benzophenone catalyst under CFL irradiation.[155] Mechanistic investigations supported the hypothesis of the $Ni(acac)_2$ reduction by the photoexcited diarylketone, resulting in the formation of the active Ni(0) species. The latter, undergoes oxidative addition with the aryl halide, releasing an electrophilic Ni(II) intermediate (**XXX**). Concurrently, HAT transfer occurs from the long-lived triplet excited state of the aromatic ketone, furnishing a nucleophilic carbon-centred radical **XXVIII**, which then recombines with **XXX** to generate a high-valent Ni(III). The desired product is ultimately obtained through reductive elimination. The propagating species are generated upon SET from the highly reducing ketyl radical and a Ni(I) species. Interestingly, the diaryl ketone employed possesses a “push-pull” structure, featuring a higher molar absorption coefficient in the visible region and a higher stability of the corresponding ketyl radical, providing optimal results (Scheme 24).

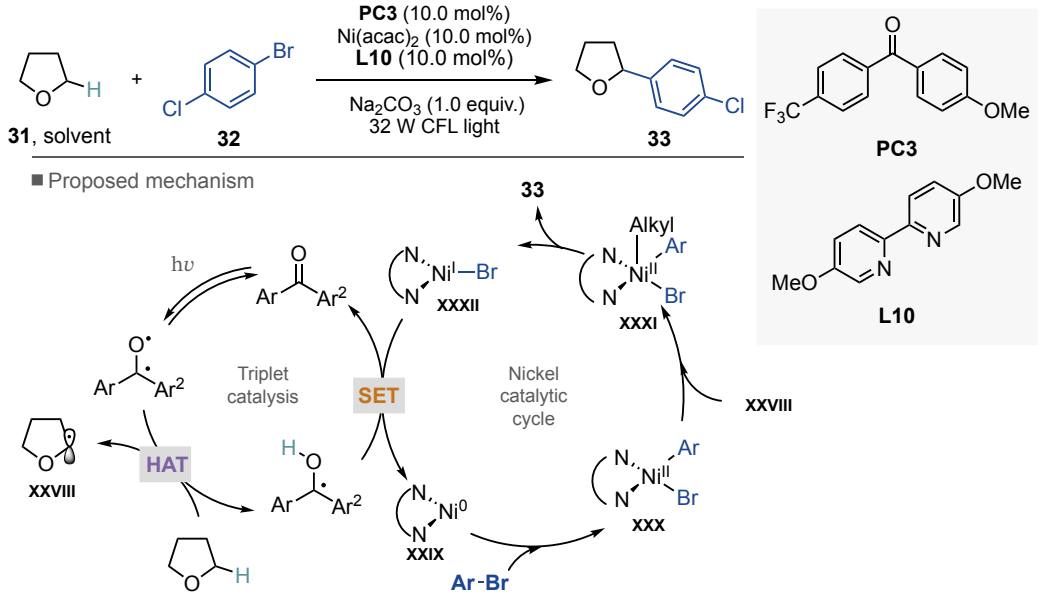

Scheme 24. Diaryl ketones photocatalyst in metallaphotoredox cross-coupling

Decatungstate anion

Although several polyoxometalates are known for their photochemical activity, the decatungstate anion $[W_{10}O_{32}]^{4-}$ has been recently recognised by MacMillan and co-workers to productively engage in a nickel dual-catalytic C–H cross-coupling reaction.[156] The success of this reaction is probably attributed to the decatungstate anion properties, which includes its highly oxidising excited state, well-studied selectivity in HAT step, and suitable potentials for the electron-transfer events. Specifically, HAT from a neutral C(sp^3)–H by the excited state of decatungstate ($^*[W_{10}O_{32}]^{4-}$) affords $[W_{10}O_{32}]^{5-}$H and a nucleophilic carbon-centred radical (**XXXIII**), which is subsequently captured by a nickel(II)-aryl species. After reductive elimination, a final single-electron transfer between the Ni(I) species and the doubly reduced decatungstate regenerates the active catalysts. It is worth noting that this approach is highly versatile and applicable to the functionalisation of natural products and chemical feedstocks, enabling the functionalisation at previously inert sites.

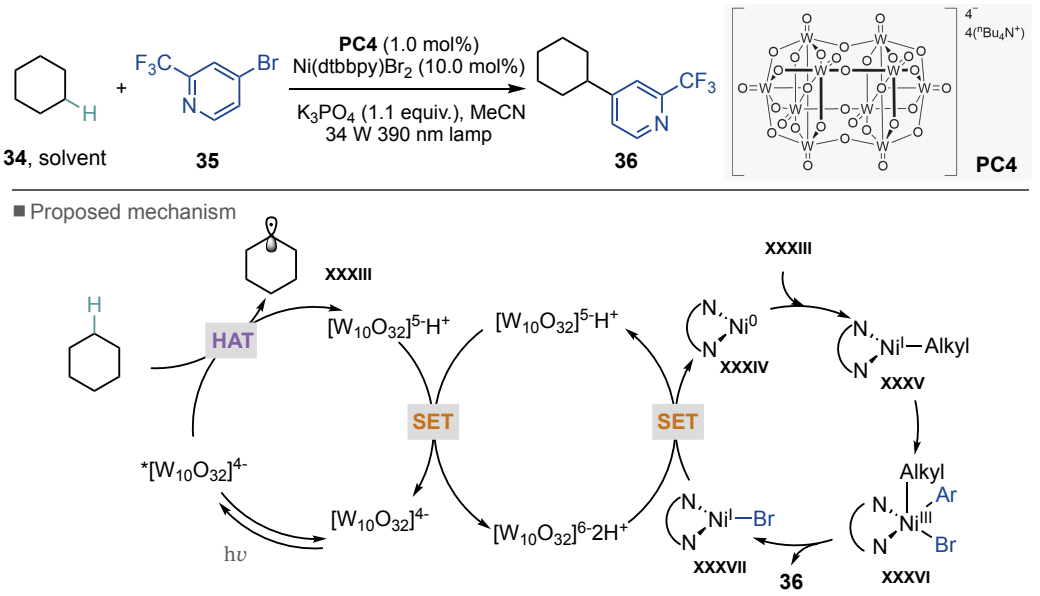

Scheme 25. Decatungstate photocatalyst in metallaphotoredox cross-coupling

1.3.2.2. Indirect HAT approaches

Due to the limited availability of photocatalyst capable of directly performing HAT upon excitation, indirect strategies have emerged as an alternative. In these cases, the excited state of the photocatalyst generates a radical species, through SET or energy transfer (EnT) events, in which the latter is responsible for the HAT step, facilitating the desired transformation.

Electrophilic nitrogen-centred radicals

MacMillan and co-workers disclosed a HAT-based approach to activate electron-rich α-amino C–H bonds in protected amines, employing 3-acetoxyquinuclidine as the HAT reagent (Scheme 26). Tertiary amines can serve as reductive quenchers,[157] which means that SET from the excited photocatalyst to the amine furnishes the corresponding amine radical cation. The latter abstracts the hydridic C–H hydrogen atom at the alpha position with respect to the protected amine via a polarity-matched HAT, affording a *C*-centred radical. The utility of this method was further demonstrated by expanding the scope from the C(sp^2)-C(sp^3) coupling to the more challenging C(sp^3)-C(sp^3) bond-forming reaction using alkyl bromides as electrophiles.[158]

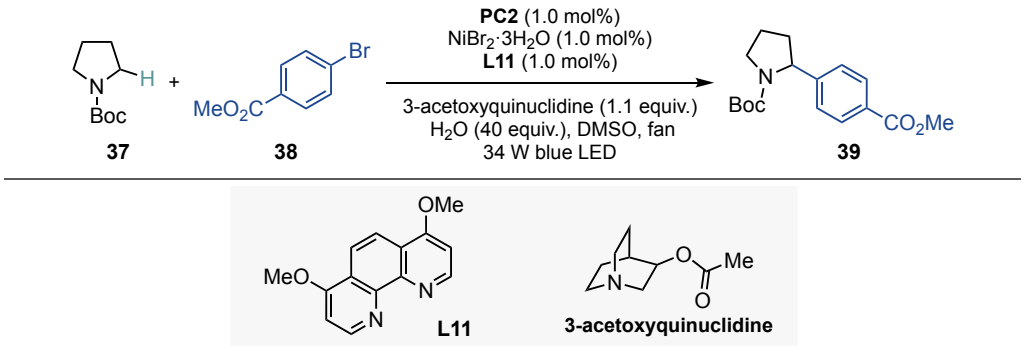

Scheme 26. Ni-catalysed cross-coupling of aryl bromides with C(sp^3)–H bonds using 3-acetoxyquinuclidine as the HAT reagent

A detailed computation analysis was carried out to elucidate the critical aspects of the reaction mechanism. DFT studies revealed that the nickel(II) precatalyst initially undergoes SET with the excited photocatalyst, delivering a Ni(I) complex (**XXXIX**). A second single electron reduction to form Ni(0) was found to be thermodynamically unfavourable. The generated Ni(I) complex captures the carbon-centred radical to form **XXXVIII**, which is subsequently reduced by Ir(II) intermediate. The oxidative addition of the alkyl bromide occurs at **XLI**, leading to a nickel(III) complex (**XLII**), followed by reductive elimination to yield the desired product (Scheme 27).[159]

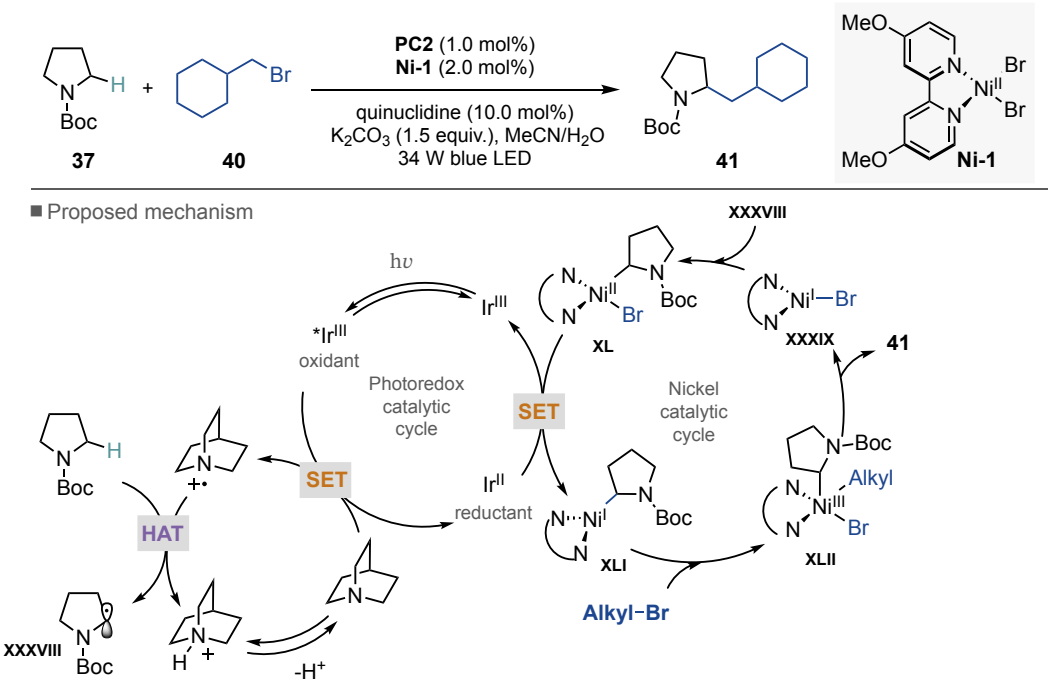

Scheme 27. Mechanistic proposal for the C(sp^3)–C(sp^3) cross-coupling using alkyl bromides as electrophiles

Halogen radicals

Besides electrophilic nitrogen-centred radicals, halogen radicals have also been demonstrated to effectively participate in HAT events. In this context, the Doyle group disclosed the cross-coupling of ethereal solvents with aryl chlorides, whose key intermediates are depicted in Scheme 28.[160] The initial step involves the oxidative addition of the aryl chloride to Ni(0), producing Ni(II) aryl chloride intermediate (**XLIII**). Subsequent oxidation by the excited state iridium photocatalyst via a SET yields Ni(III) complex (**XLIV**). Under the reaction conditions, homolysis of Ni(III)-Cl bond occurs via *ligand-to-metal charge transfer* (LMCT) to produce a chloride radical and a Ni(II)-Ar species (**XLV**).[161] The resulting Cl• abstracts the α-oxy C–H bond of the ethereal solvent ($BDE_{H\text{-}Cl}$ = 102 kcal mol^{-1}, BDE_{THF} = 92 kcal mol^{-1}) via HAT to generate **XXXVII**, which recombines with **XLV** prior to reductive elimination. Mechanistic experiments using stochiometric Ni(II) oxidative adduct **XLIII** and emission quenching experiments provided evidence for the oxidation-photoexcitation mechanism. Indeed, the ability of related Ni(III)-Cl complexes to undergo photoinduced homolysis to produce chlorine radicals was initially described by Nocera and co-workers in 2015.[162]

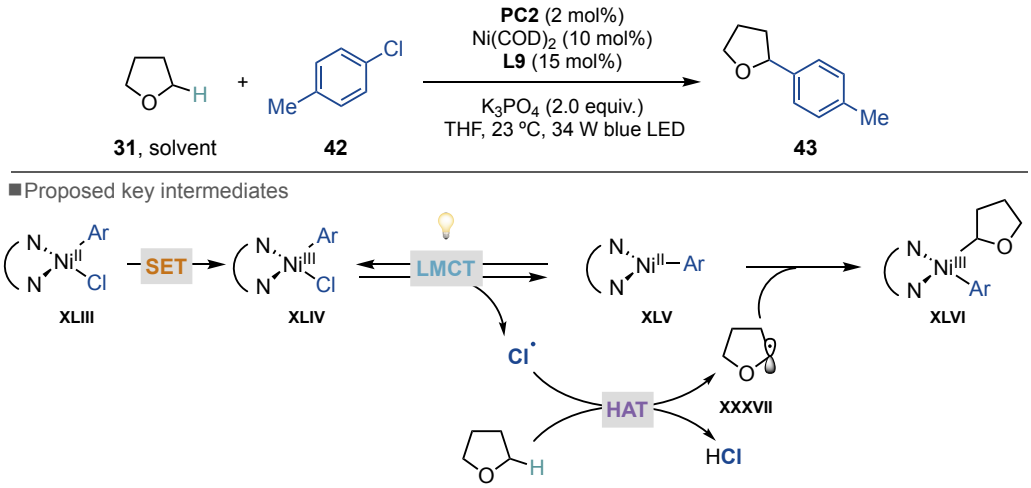

Scheme 28. Chlorine radicals generated via LMCT

Simultaneously, Molander and co-workers reported a similar transformation for the coupling of ethereal solvents using aryl bromides and dimethoxybenzophenone as co-catalyst.[163] Although, mechanistic studies using different photocatalyst indicated that bromine radicals were generated upon triplet-triplet energy transfer from an excited iridium or benzophenone photocatalyst to the Ni(II) aryl chloride intermediate (**XLIII**), the photoinduced homolysis of Ni(III)-Br bond described by Nocera and Doyle could not be fully ruled out.[160,162]

1.3.3. Modulation of the oxidation state of the metal catalyst

In addition to the well documented ability of nickel complexes to participate in a wide variety of C–C bond forming reactions in the context of metallaphotoredox catalysis, the ability to forge new C–O linkages using nickel catalysis has received much less attention. Pioneering studies by Hillhouse and others have demonstrated that the challenging reductive elimination step from aryl-nickel(II)alkoxide intermediates can be overcome by simple exposure of this species to molecular oxygen, which results in the formation of the desired product by accessing high-valent Ni(III) intermediates.[140,164,141,165–167]

Common approaches relay on the use of stoichiometric oxidants or electrochemical oxidation to induce reductive elimination. However, in some cases, these reagents may be incompatible with other catalytic elementary steps.[168,169] Alternatively, the MacMillan group has pioneered the use of photocatalysis to modulate the oxidation state of the transition metal complexes, enabling the use of nickel catalysis in ether synthesis (Scheme 29).[170] Initially, the authors proposed that an excited Ir-photocatalyst promotes the oxidation of a Ar-Ni(II)-OR intermediate to a nickel(III) complex, facilitating the critical C–O bond-forming event. However, recent mechanistic studies have provided evidence supporting oxidative addition of aryl halides at Ni(I) (**XLVIII**) and the existence of a “dark” Ni(I)/Ni(III) cycle.[171–176]

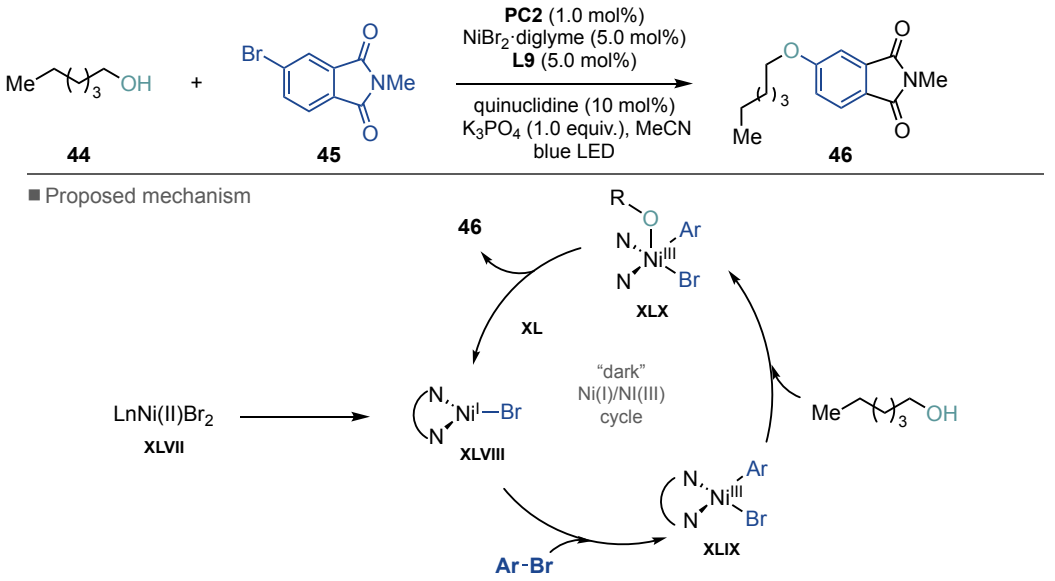

Scheme 29. C–O formation via nickel photoredox catalysis

It should be noted that there is ongoing debate regarding the exact mechanism, as multiple mechanisms have been proposed for the generation of the active Ni(I) species (Scheme 30). While Nocera suggested that the active Ni(I) species (**XLXII**) are obtained

through reduction of a Ni(II) chloride precatalyst by the iridium photocatalyst, with quinuclidine hypothesised to act as a sacrificial reductant of the excited-state iridium (III) to generate the active iridium (II) species, thereby turning over the photocatalyst,[144,171,173] Mirica and Miyake groups have described the generation of the key Ni(I) intermediate (**XLXIV**) through oxidative quenching of the iridium photoexcited state, where in this case halide anions were found to reduce the oxidised form of the PC.[175,176] Additionally, in 2020, Doyle and co-workers reported the photoinduced homolysis of the nickel-aryl bond as a method for generating nickel(I) species (**XLXVI**).[174]

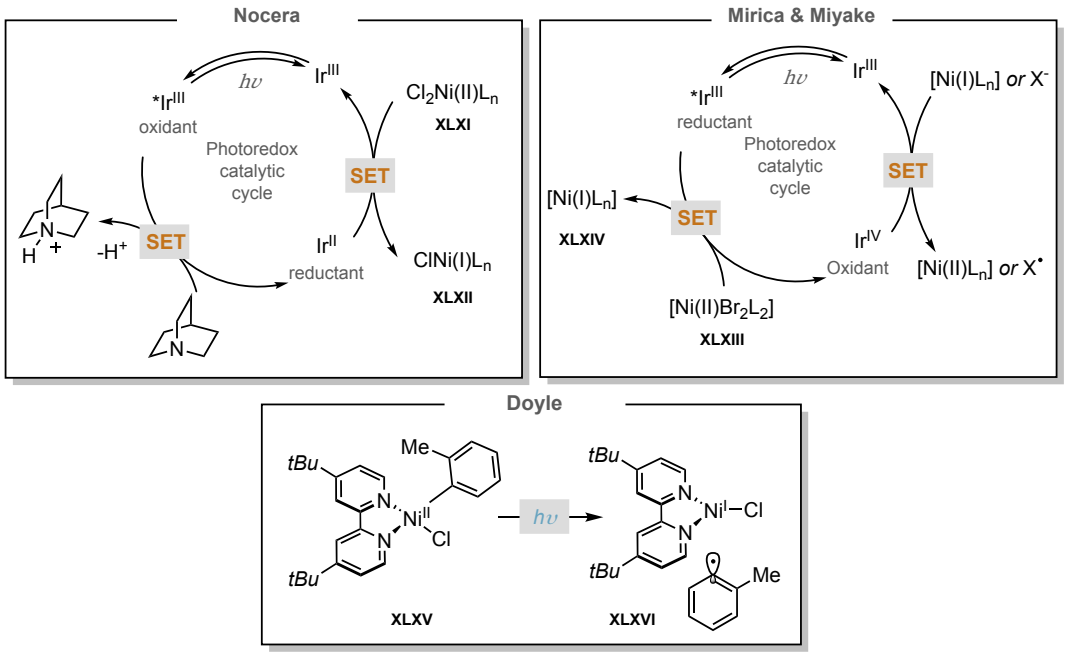

Scheme 30. Proposed mechanisms for the generation of Ni(I) species

Unprecedented reactivity paradigms can potentially be mapped out by accessing excited states metal centres via triple-triplet energy transfer to organometallic species.[177–180] MacMillan and McClusker questioned whether the documented energy-transfer mechanism could target the challenging C–O bond formation reactions to deliver aryl esters from the coupling of carboxylic acids and aryl halides, by inducing reductive elimination from the aryl-nickel(II)-carboxylate complex (**XI**).[181] In accordance to Molander's report,[163] stoichiometric experiments proved that the reactivity of **XI** is highly dependent on the photocatalyst triplet energy (E_T), and anticorrelated to the oxidising power of the photocatalyst, thus suggesting that the critical reductive elimination step occurs from nickel(II) excited state (Scheme 31). Subsequent studies in collaboration with the Scholes group confirmed the energy-transfer pathway.[182]

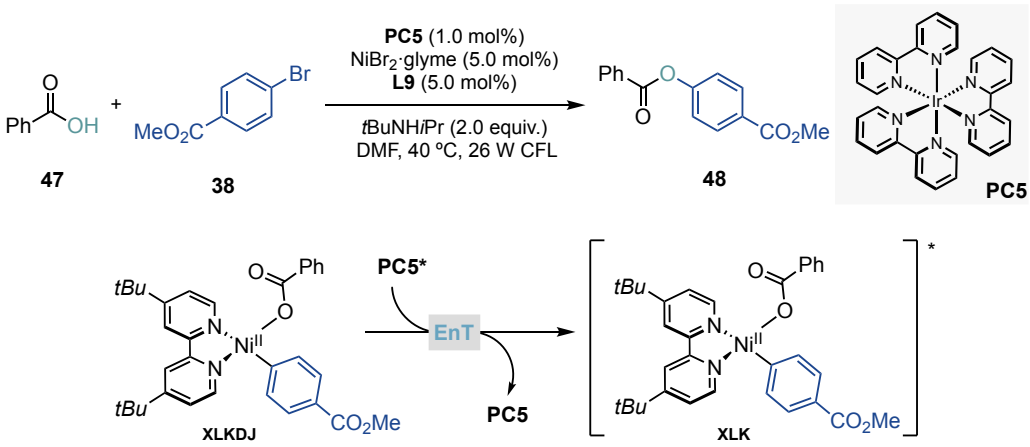

Scheme 31. Nickel-catalysed C–O coupling of carboxylic acids with aryl halides

The opportunity to modulate the metal oxidation state by photochemistry was also recognised in the context of C–N bond formation, in which Jamison, MacMillan and Buchwald played a pivotal role for their pioneering reports.[183,184]

Overall, the merger of transition metal and photoredox catalysis has *i*) enabled the activation of previously unreactive starting materials, by generating alkyl radicals which can be trapped by transition metals, and *ii*) has allowed the modulation of the metal oxidation state without the need for strongly oxidising conditions. However, despite the recent success, detailed mechanistic understanding remains elusive, and multiple possible redox process can occur between Ni at various oxidation states and the photocatalyst. The knowledge attainable by dissecting each elementary step at a molecular level will be pivotal for further advancements in the field and will surely incentive the disclosure of novel activation modes and overcome current limitations.

1.4. General objectives of this doctoral thesis

During the last two decades, significant progress has been made in the research area of Ni-catalysed metallaphotoredox reactions, along with the difunctionalisation of olefins. Although remarkable levels of sophistication have been achieved, several challenges still persist in these endeavours. Motivated by our group's interest in the functionalisation of strong σ-bonds, and the development of new C(sp^2)–C(sp^3) and C(sp^3)–C(sp^3) bond forming reactions, we have established the following three main objectives for this PhD thesis:

1. To develop a site-selective functionalisation of unactivated sp^3 C–O bonds enabled by a nickel/photoredox dual catalysis.

2. To broaden the scope of Ni-catalysed 1,1-difunctionalisation strategies by utilising α-haloboranes and α-halosilanes, thereby enabling access to bis-organometallic reagents.

3. To expand the scope of Ni-catalysed 1,1-difunctionalisation strategies to incorporate two different heteroatom motifs across the olefin backbone, leading to the generation α-aminoboronic acid derivatives.

1.5. References

(1) *Metal-Catalyzed Cross-Coupling Reactions and More: DeMeijere/Metal-Catalyzed Cross-Coupling Reactions and More*; De Meijere, A., Bräse, S., Oestreich, M., Eds.; Wiley-VCH Verlag GmbH & Co. KGaA: Weinheim, Germany, 2014. https://doi.org/10.1002/9783527655588.

(2) Magano, J.; Dunetz, J. R. Large-Scale Applications of Transition Metal-Catalyzed Couplings for the Synthesis of Pharmaceuticals. *Chem. Rev.* **2011**, *111* (3), 2177–2250. https://doi.org/10.1021/cr100346g.

(3) Johansson Seechurn, C. C. C.; Kitching, M. O.; Colacot, T. J.; Snieckus, V. Palladium-Catalyzed Cross-Coupling: A Historical Contextual Perspective to the 2010 Nobel Prize. *Angew. Chem. Int. Ed.* **2012**, *51* (21), 5062–5085. https://doi.org/10.1002/anie.201107017.

(4) Tasker, S. Z.; Standley, E. A.; Jamison, T. F. Recent Advances in Homogeneous Nickel Catalysis. *Nature* **2014**, *509* (7500), 299–309. https://doi.org/10.1038/nature13274.

(5) Standley, E. A.; Tasker, S. Z.; Jensen, K. L.; Jamison, T. F. Nickel Catalysis: Synergy between Method Development and Total Synthesis. *Acc. Chem. Res.* **2015**, *48* (5), 1503–1514. https://doi.org/10.1021/acs.accounts.5b00064.

(6) Su, B.; Cao, Z.-C.; Shi, Z.-J. Exploration of Earth-Abundant Transition Metals (Fe, Co, and Ni) as Catalysts in Unreactive Chemical Bond Activations. *Acc. Chem. Res.* **2015**, *48* (3), 886–896. https://doi.org/10.1021/ar500345f.

(7) Chernyshev, V. M.; Ananikov, V. P. Nickel and Palladium Catalysis: Stronger Demand than Ever. *ACS Catal.* **2022**, *12* (2), 1180–1200. https://doi.org/10.1021/acscatal.1c04705.

(8) Wilke, G. Contributions to Organo-Nickel Chemistry. *Angew. Chem. Int. Ed. Engl.* **1988**, *27* (1), 185–206. https://doi.org/10.1002/anie.198801851.

(9) Keim, W. Nickel: An Element with Wide Application in Industrial Homogeneous Catalysis. *Angew. Chem. Int. Ed. Engl.* **1990**, *29* (3), 235–244. https://doi.org/10.1002/anie.199002351.

(10) Schneider, C.; Leischner, T.; Ryabchuk, P.; Jackstell, R.; Junge, K.; Beller, M. Development of Bulk Organic Chemical Processes—History, Status, and Opportunities for Academic Research. *CCS Chem.* **2021**, *3* (3), 512–530. https://doi.org/10.31635/ccschem.021.202000680.

(11) Clevenger, A. L.; Stolley, R. M.; Aderibigbe, J.; Louie, J. Trends in the Usage of Bidentate Phosphines as Ligands in Nickel Catalysis. *Chem. Rev.* **2020**, *120* (13), 6124–6196. https://doi.org/10.1021/acs.chemrev.9b00682.

(12) Leatherman, M. D.; Svejda, S. A.; Johnson, L. K.; Brookhart, M. Mechanistic Studies of Nickel(II) Alkyl Agostic Cations and Alkyl Ethylene Complexes: Investigations of Chain Propagation and Isomerization in (α-Diimine)Ni(II)-Catalyzed Ethylene Polymerization. *J. Am. Chem. Soc.* **2003**, *125* (10), 3068–3081. https://doi.org/10.1021/ja021071w.

(13) Xu, H.; White, P. B.; Hu, C.; Diao, T. Structure and Isotope Effects of the β-H Agostic (α-Diimine)Nickel Cation as a Polymerization Intermediate. *Angew. Chem. Int. Ed.* **2017**, *56* (6), 1535–1538. https://doi.org/10.1002/anie.201611282.

(14) Structural Characterization of B-Agostic Bonds in Pd-Catalyzed Polymerization. *Organometallics* **2017**, *36* (21), 4099–4102. https://doi.org/10.1021/acs.organomet.7b00666.

(15) Macgregor, S. A.; Neave, G. W.; Smith, C. Theoretical Studies on C–Heteroatom Bond Formation via Reductive Elimination from Group 10 M(PH3)2(CH3)(X) Species (X = CH3, NH2, OH, SH) and the Determination of Metal–X Bond Strengths Using Density Functional Theory. *Faraday Discuss.* **2003**, *124* (0), 111–127. https://doi.org/10.1039/B212309F.

(16) Ananikov, V. P. Nickel: The “Spirited Horse” of Transition Metal Catalysis. *ACS Catal.* **2015**, *5* (3), 1964–1971. https://doi.org/10.1021/acscatal.5b00072.

(17) Diccianni, J. B.; Diao, T. Mechanisms of Nickel-Catalyzed Cross-Coupling Reactions. *Trends Chem.* **2019**, *1* (9), 830–844. https://doi.org/10.1016/j.trechm.2019.08.004.

(18) Diccianni, J.; Lin, Q.; Diao, T. Mechanisms of Nickel-Catalyzed Coupling Reactions and Applications in Alkene

Functionalization. *Acc. Chem. Res.* **2020**, *53* (4), 906–919. https://doi.org/10.1021/acs.accounts.0c00032.

(19) Cornella, J.; Zarate, C.; Martin, R. Metal-Catalyzed Activation of Ethers via C–O Bond Cleavage: A New Strategy for Molecular Diversity. *Chem. Soc. Rev.* **2014**, *43* (23), 8081–8097. https://doi.org/10.1039/C4CS00206G.

(20) Tobisu, M.; Chatani, N. Cross-Couplings Using Aryl Ethers via C–O Bond Activation Enabled by Nickel Catalysts. *Acc. Chem. Res.* **2015**, *48* (6), 1717–1726. https://doi.org/10.1021/acs.accounts.5b00051.

(21) Zeng, H.; Qiu, Z.; Domínguez-Huerta, A.; Hearne, Z.; Chen, Z.; Li, C.-J. An Adventure in Sustainable Cross-Coupling of Phenols and Derivatives via Carbon–Oxygen Bond Cleavage. *ACS Catal.* **2017**, *7* (1), 510–519. https://doi.org/10.1021/acscatal.6b02964.

(22) Tobisu, M. C□O Bond Transformations. In *Nickel Catalysis in Organic Synthesis*; John Wiley & Sons, Ltd, 2020; pp 123–149. https://doi.org/10.1002/9783527813827.ch7.

(23) Boit, T. B.; Bulger, A. S.; Dander, J. E.; Garg, N. K. Activation of C–O and C–N Bonds Using Non-Precious-Metal Catalysis. *ACS Catal.* **2020**, *10* (20), 12109–12126. https://doi.org/10.1021/acscatal.0c03334.

(24) Cernak, T.; Dykstra, K. D.; Tyagarajan, S.; Vachal, P.; Krska, S. W. The Medicinal Chemist's Toolbox for Late Stage Functionalization of Drug-like Molecules. *Chem. Soc. Rev.* **2016**, *45* (3), 546–576. https://doi.org/10.1039/C5CS00628G.

(25) Moir, M.; Danon, J. J.; Reekie, T. A.; Kassiou, M. An Overview of Late-Stage Functionalization in Today's Drug Discovery. *Expert Opin. Drug Discov.* **2019**, *14* (11), 1137–1149. https://doi.org/10.1080/17460441.2019.1653850.

(26) Guillemard, L.; Kaplaneris, N.; Ackermann, L.; Johansson, M. J. Late-Stage C–H Functionalization Offers New Opportunities in Drug Discovery. *Nat. Rev. Chem.* **2021**, *5* (8), 522–545. https://doi.org/10.1038/s41570-021-00300-6.

(27) Jana, R.; Begam, H. M.; Dinda, E. The Emergence of the C–H Functionalization Strategy in Medicinal Chemistry and Drug Discovery. *Chem. Commun.* **2021**, *57* (83), 10842–10866. https://doi.org/10.1039/D1CC04083A.

(28) Bellotti, P.; Huang, H.-M.; Faber, T.; Glorius, F. Photocatalytic Late-Stage C–H Functionalization. *Chem. Rev.* **2023**. https://doi.org/10.1021/acs.chemrev.2c00478.

(29) Rosen, B. M.; Quasdorf, K. W.; Wilson, D. A.; Zhang, N.; Resmerita, A.-M.; Garg, N. K.; Percec, V. Nickel-Catalyzed Cross-Couplings Involving Carbon−Oxygen Bonds. *Chem. Rev.* **2011**, *111* (3), 1346–1416. https://doi.org/10.1021/cr100259t.

(30) Arndtsen, B. A.; Bergman, R. G.; Mobley, T. A.; Peterson, T. H. Selective Intermolecular Carbon-Hydrogen Bond Activation by Synthetic Metal Complexes in Homogeneous Solution. *Acc. Chem. Res.* **1995**, *28* (3), 154–162. https://doi.org/10.1021/ar00051a009.

(31) Shilov, A. E.; Shul'pin, G. B. Activation of C−H Bonds by Metal Complexes. *Chem. Rev.* **1997**, *97* (8), 2879–2932. https://doi.org/10.1021/cr9411886.

(32) Introduction: CH Activation. *Chem. Rev.* **2017**, *117* (13), 8481–8482. https://doi.org/10.1021/acs.chemrev.7b00307.

(33) Rogge, T.; Kaplaneris, N.; Chatani, N.; Kim, J.; Chang, S.; Punji, B.; Schafer, L. L.; Musaev, D. G.; Wencel-Delord, J.; Roberts, C. A.; Sarpong, R.; Wilson, Z. E.; Brimble, M. A.; Johansson, M. J.; Ackermann, L. C–H Activation. *Nat. Rev. Methods Primer* **2021**, *1* (1), 1–31. https://doi.org/10.1038/s43586-021-00041-2.

(34) Gensch, T.; Hopkinson, M. N.; Glorius, F.; Wencel-Delord, J. Mild Metal-Catalyzed C–H Activation: Examples and Concepts. *Chem. Soc. Rev.* **2016**, *45* (10), 2900–2936. https://doi.org/10.1039/C6CS00075D.

(35) Anwar, K.; Merkens, K.; Aguilar Troyano, F. J.; Gómez-Suárez, A. Radical Deoxyfunctionalisation Strategies**. *Eur. J. Org. Chem.* **2022**, *2022* (26), e202200330. https://doi.org/10.1002/ejoc.202200330.

(36) Álvarez-Bercedo, P.; Martin, R. Ni-Catalyzed Reduction of Inert C−O Bonds: A New Strategy for Using Aryl Ethers as Easily Removable Directing Groups. *J. Am. Chem. Soc.* **2010**, *132* (49), 17352–17353. https://doi.org/10.1021/ja106943q.

(37) Luo, Y.-R. *Handbook of Bond Dissociation Energies in Organic Compounds*; CRC Press: Boca Raton, 2002.

https://doi.org/10.1201/9781420039863.

(38) Cornella, J.; Gómez-Bengoa, E.; Martin, R. Combined Experimental and Theoretical Study on the Reductive Cleavage of Inert C–O Bonds with Silanes: Ruling out a Classical Ni(0)/Ni(II) Catalytic Couple and Evidence for Ni(I) Intermediates. *J. Am. Chem. Soc.* **2013**, *135* (5), 1997–2009. https://doi.org/10.1021/ja311940s.

(39) Zarate, C.; van Gemmeren, M.; Somerville, R. J.; Martin, R. Chapter Four - Phenol Derivatives: Modern Electrophiles in Cross-Coupling Reactions. In *Advances in Organometallic Chemistry*; Pérez, P. J., Ed.; Academic Press, 2016; Vol. 66, pp 143–222. https://doi.org/10.1016/bs.adomc.2016.07.001.

(40) Wenkert, E.; Michelotti, E. L.; Swindell, C. S. Nickel-Induced Conversion of Carbon-Oxygen into Carbon-Carbon Bonds. One-Step Transformations of Enol Ethers into Olefins and Aryl Ethers into Biaryls. *J. Am. Chem. Soc.* **1979**, *101* (8), 2246–2247. https://doi.org/10.1021/ja00502a074.

(41) Wenkert, E.; Michelotti, E. L.; Swindell, C. S.; Tingoli, M. Transformation of Carbon-Oxygen into Carbon-Carbon Bonds Mediated by Low-Valent Nickel Species. *J. Org. Chem.* **1984**, *49* (25), 4894–4899. https://doi.org/10.1021/jo00199a030.

(42) Wenkert, E.; Leftin, M. H.; Michelotti, E. L. A Synthesis of Conjugated Dienes from Aromatic, Five-Membered Heterocycles. *J. Chem. Soc. Chem. Commun.* **1984**, No. 9, 617–618. https://doi.org/10.1039/C39840000617.

(43) Dankwardt, J. W. Nickel-Catalyzed Cross-Coupling of Aryl Grignard Reagents with Aromatic Alkyl Ethers: An Efficient Synthesis of Unsymmetrical Biaryls. *Angew. Chem. Int. Ed.* **2004**, *43* (18), 2428–2432. https://doi.org/10.1002/anie.200453765.

(44) van der Boom, M. E.; Liou, S.-Y.; Ben-David, Y.; Shimon, L. J. W.; Milstein, D. Alkyl− and Aryl−Oxygen Bond Activation in Solution by Rhodium(I), Palladium(II), and Nickel(II). Transition-Metal-Based Selectivity. *J. Am. Chem. Soc.* **1998**, *120* (26), 6531–6541. https://doi.org/10.1021/ja9738889.

(45) Kelley, P.; Lin, S.; Edouard, G.; Day, M. W.; Agapie, T. Nickel-Mediated Hydrogenolysis of C–O Bonds of Aryl Ethers: What Is the Source of the Hydrogen? *J. Am. Chem. Soc.* **2012**, *134* (12), 5480–5483. https://doi.org/10.1021/ja300326t.

(46) Cornella, J.; Martin, R. Ni-Catalyzed Stereoselective Arylation of Inert C–O Bonds at Low Temperatures. *Org. Lett.* **2013**, *15* (24), 6298–6301. https://doi.org/10.1021/ol4031815.

(47) Ogawa, H.; Minami, H.; Ozaki, T.; Komagawa, S.; Wang, C.; Uchiyama, M. How and Why Does Ni0 Promote Smooth Etheric C□O Bond Cleavage and C□C Bond Formation? A Theoretical Study. *Chem. – Eur. J.* **2015**, *21* (40), 13904–13908. https://doi.org/10.1002/chem.201502114.

(48) Tobisu, M.; Takahira, T.; Morioka, T.; Chatani, N. Nickel-Catalyzed Alkylative Cross-Coupling of Anisoles with Grignard Reagents via C–O Bond Activation. *J. Am. Chem. Soc.* **2016**, *138* (21), 6711–6714. https://doi.org/10.1021/jacs.6b03253.

(49) Liu, X.; Hsiao, C.-C.; Kalvet, I.; Leiendecker, M.; Guo, L.; Schoenebeck, F.; Rueping, M. Lewis Acid Assisted Nickel-Catalyzed Cross-Coupling of Aryl Methyl Ethers by C−O Bond-Cleaving Alkylation: Prevention of Undesired β-Hydride Elimination. *Angew. Chem. Int. Ed.* **2016**, *55* (20), 6093–6098. https://doi.org/10.1002/anie.201510497.

(50) Guan, B.-T.; Xiang, S.-K.; Wu, T.; Sun, Z.-P.; Wang, B.-Q.; Zhao, K.-Q.; Shi, Z.-J. Methylation of ArenesviaNi-Catalyzed Aryl C–O/F Activation. *Chem. Commun.* **2008**, No. 12, 1437–1439. https://doi.org/10.1039/B718998B.

(51) Li, B.-J.; Li, Y.-Z.; Lu, X.-Y.; Liu, J.; Guan, B.-T.; Shi, Z.-J. Cross-Coupling of Aryl/Alkenyl Pivalates with Organozinc Reagents through Nickel-Catalyzed C□O Bond Activation under Mild Reaction Conditions. *Angew. Chem. Int. Ed.* **2008**, *47* (52), 10124–10127. https://doi.org/10.1002/anie.200803814.

(52) Iglesias, M. J.; Prieto, A.; Nicasio, M. C. Kumada–Tamao–Corriu Coupling of Heteroaromatic Chlorides and Aryl Ethers Catalyzed by (IPr)Ni(Allyl)Cl. *Org. Lett.* **2012**, *14* (17), 4318–4321. https://doi.org/10.1021/ol302112q.

(53) Zhang, J.; Xu, J.; Xu, Y.; Sun, H.; Shen, Q.; Zhang, Y. Mixed NHC/Phosphine Ni(II) Complexes: Synthesis and Their Applications as Versatile Catalysts for Selective Cross-Couplings of ArMgX with Aryl Chlorides, Fluorides, and Methyl Ethers. *Organometallics* **2015**, *34* (24), 5792–5800.

https://doi.org/10.1021/acs.organomet.5b00874.

(54) Márquez, I. R.; Fuentes, N.; Cruz, C. M.; Puente-Muñoz, V.; Sotorrios, L.; Marcos, M. L.; Choquesillo-Lazarte, D.; Biel, B.; Crovetto, L.; Gómez-Bengoa, E.; González, M. T.; Martin, R.; Cuerva, J. M.; Campaña, A. G. Versatile Synthesis and Enlargement of Functionalized Distorted Heptagon-Containing Nanographenes. *Chem. Sci.* **2017**, *8* (2), 1068–1074. https://doi.org/10.1039/C6SC02895K.

(55) Tobisu, M.; Takahira, T.; Chatani, N. Nickel-Catalyzed Cross-Coupling of Anisoles with Alkyl Grignard Reagents via C–O Bond Cleavage. *Org. Lett.* **2015**, *17* (17), 4352–4355. https://doi.org/10.1021/acs.orglett.5b02200.

(56) Tobisu, M.; Takahira, T.; Ohtsuki, A.; Chatani, N. Nickel-Catalyzed Alkynylation of Anisoles via C–O Bond Cleavage. *Org. Lett.* **2015**, *17* (3), 680–683. https://doi.org/10.1021/ol503707m.

(57) Tobisu, M.; Yasutome, A.; Kinuta, H.; Nakamura, K.; Chatani, N. 1,3-Dicyclohexylimidazol-2-Ylidene as a Superior Ligand for the Nickel-Catalyzed Cross-Couplings of Aryl and Benzyl Methyl Ethers with Organoboron Reagents. *Org. Lett.* **2014**, *16* (21), 5572–5575. https://doi.org/10.1021/ol502583h.

(58) Nakamura, K.; Tobisu, M.; Chatani, N. Nickel-Catalyzed Formal Homocoupling of Methoxyarenes for the Synthesis of Symmetrical Biaryls via C–O Bond Cleavage. *Org. Lett.* **2015**, *17* (24), 6142–6145. https://doi.org/10.1021/acs.orglett.5b03151.

(59) Guo, L.; Liu, X.; Baumann, C.; Rueping, M. Nickel-Catalyzed Alkoxy–Alkyl Interconversion with Alkylborane Reagents through C−O Bond Activation of Aryl and Enol Ethers. *Angew. Chem. Int. Ed.* **2016**, *55* (49), 15415–15419. https://doi.org/10.1002/anie.201607646.

(60) Tobisu, M.; Shimasaki, T.; Chatani, N. Ni0-Catalyzed Direct Amination of Anisoles Involving the Cleavage of Carbon–Oxygen Bonds. *Chem. Lett.* **2009**, *38* (7), 710–711. https://doi.org/10.1246/cl.2009.710.

(61) Tobisu, M.; Yasutome, A.; Yamakawa, K.; Shimasaki, T.; Chatani, N. Ni(0)/NHC-Catalyzed Amination of N-Heteroaryl Methyl Ethers through the Cleavage of Carbon–oxygen Bonds. *Tetrahedron* **2012**, *68* (26), 5157–5161. https://doi.org/10.1016/j.tet.2012.04.005.

(62) Tobisu, M.; Yamakawa, K.; Shimasaki, T.; Chatani, N. Nickel-Catalyzed Reductive Cleavage of Aryl–Oxygen Bonds in Alkoxy- and Pivaloxyarenes Using Hydrosilanes as a Mild Reducing Agent. *Chem. Commun.* **2011**, *47* (10), 2946–2948. https://doi.org/10.1039/C0CC05169A.

(63) Zarate, C.; Nakajima, M.; Martin, R. A Mild and Ligand-Free Ni-Catalyzed Silylation via C–OMe Cleavage. *J. Am. Chem. Soc.* **2017**, *139* (3), 1191–1197. https://doi.org/10.1021/jacs.6b10998.

(64) Ishizu, J.; Yamamoto, T.; Yamamoto, A. Selective Cleavage of c–o Bonds in Esters through Oxidative Addition to Nickel(0) Complexes. *Chem. Lett.* **1976**, *5* (10), 1091–1094. https://doi.org/10.1246/cl.1976.1091.

(65) Yamamoto, T.; Ishizu, J.; Kohara, T.; Komiya, S.; Yamamoto, A. Oxidative Addition of Aryl Carboxylates to Nickel(0) Complexes Involving Cleavage of the Acyl-Oxygen Bond. *J. Am. Chem. Soc.* **1980**, *102* (11), 3758–3764. https://doi.org/10.1021/ja00531a016.

(66) Guan, B.-T.; Wang, Y.; Li, B.-J.; Yu, D.-G.; Shi, Z.-J. Biaryl Construction via Ni-Catalyzed C−O Activation of Phenolic Carboxylates. *J. Am. Chem. Soc.* **2008**, *130* (44), 14468–14470. https://doi.org/10.1021/ja8056503.

(67) Quasdorf, K. W.; Tian, X.; Garg, N. K. Cross-Coupling Reactions of Aryl Pivalates with Boronic Acids. *J. Am. Chem. Soc.* **2008**, *130* (44), 14422–14423. https://doi.org/10.1021/ja806244b.

(68) Li, Z.; Zhang, S.-L.; Fu, Y.; Guo, Q.-X.; Liu, L. Mechanism of Ni-Catalyzed Selective C−O Bond Activation in Cross-Coupling of Aryl Esters. *J. Am. Chem. Soc.* **2009**, *131* (25), 8815–8823. https://doi.org/10.1021/ja810157e.

(69) Muto, K.; Yamaguchi, J.; Itami, K. Nickel-Catalyzed C–H/C–O Coupling of Azoles with Phenol Derivatives. *J. Am. Chem. Soc.* **2012**, *134* (1), 169–172. https://doi.org/10.1021/ja210249h.

(70) Dzik, W. I.; Lange, P. P.; Gooßen, L. J. Carboxylates as Sources of Carbon Nucleophiles and Electrophiles: Comparison of Decarboxylative and Decarbonylative Pathways. *Chem. Sci.* **2012**, *3* (9), 2671–2678. https://doi.org/10.1039/C2SC20312J.

(71) Xu, H.; Muto, K.; Yamaguchi, J.; Zhao, C.; Itami, K.; Musaev, D. G. Key Mechanistic Features of Ni-Catalyzed C–H/C–O Biaryl Coupling of Azoles and Naphthalen-2-Yl Pivalates. *J. Am. Chem. Soc.* **2014**, *136* (42),

14834–14844. https://doi.org/10.1021/ja5071174.

(72) Hong, X.; Liang, Y.; Houk, K. N. Mechanisms and Origins of Switchable Chemoselectivity of Ni-Catalyzed C(Aryl)–O and C(Acyl)–O Activation of Aryl Esters with Phosphine Ligands. *J. Am. Chem. Soc.* **2014**, *136* (5), 2017–2025. https://doi.org/10.1021/ja4118413.

(73) Muto, K.; Yamaguchi, J.; Lei, A.; Itami, K. Isolation, Structure, and Reactivity of an Arylnickel(II) Pivalate Complex in Catalytic C–H/C–O Biaryl Coupling. *J. Am. Chem. Soc.* **2013**, *135* (44), 16384–16387. https://doi.org/10.1021/ja409803x.

(74) Desnoyer, A. N.; Friese, F. W.; Chiu, W.; Drover, M. W.; Patrick, B. O.; Love, J. A. Exploring Regioselective Bond Cleavage and Cross-Coupling Reactions Using a Low-Valent Nickel Complex. *Chem. – Eur. J.* **2016**, *22* (12), 4070–4077. https://doi.org/10.1002/chem.201504959.

(75) Somerville, R. J.; Hale, L. V. A.; Gómez-Bengoa, E.; Burés, J.; Martin, R. Intermediacy of Ni–Ni Species in Sp2 C–O Bond Cleavage of Aryl Esters: Relevance in Catalytic C–Si Bond Formation. *J. Am. Chem. Soc.* **2018**, *140* (28), 8771–8780. https://doi.org/10.1021/jacs.8b04479.

(76) *Deciphering the dichotomy exerted by Zn(ii) in the catalytic sp2 C–O bond functionalization of aryl esters at the molecular level | Nature Catalysis*. https://www.nature.com/articles/s41929-020-00560-3 (accessed 2023-05-03).

(77) Ehle, A. R.; Zhou, Q.; Watson, M. P. Nickel(0)-Catalyzed Heck Cross-Coupling via Activation of Aryl C–OPiv Bonds. *Org. Lett.* **2012**, *14* (5), 1202–1205. https://doi.org/10.1021/ol203322v.

(78) Guo, L.; Hsiao, C.-C.; Yue, H.; Liu, X.; Rueping, M. Nickel-Catalyzed Csp2–Csp3 Cross-Coupling via C–O Bond Activation. *ACS Catal.* **2016**, *6* (7), 4438–4442. https://doi.org/10.1021/acscatal.6b00801.

(79) Takise, R.; Muto, K.; Yamaguchi, J.; Itami, K. Nickel-Catalyzed α-Arylation of Ketones with Phenol Derivatives. *Angew. Chem. Int. Ed.* **2014**, *53* (26), 6791–6794. https://doi.org/10.1002/anie.201403823.

(80) Koch, E.; Takise, R.; Studer, A.; Yamaguchi, J.; Itami, K. Ni-Catalyzed α-Arylation of Esters and Amides with Phenol Derivatives. *Chem. Commun.* **2014**, *51* (5), 855–857. https://doi.org/10.1039/C4CC08426H.

(81) Cornella, J.; Jackson, E. P.; Martin, R. Nickel-Catalyzed Enantioselective C□C Bond Formation through C□O Cleavage in Aryl Esters. *Angew. Chem. Int. Ed.* **2015**, *54* (13), 4075–4078. https://doi.org/10.1002/anie.201412051.

(82) Correa, A.; Martin, R. Ni-Catalyzed Direct Reductive Amidation via C–O Bond Cleavage. *J. Am. Chem. Soc.* **2014**, *136* (20), 7253–7256. https://doi.org/10.1021/ja5029793.

(83) Correa, A.; León, T.; Martin, R. Ni-Catalyzed Carboxylation of C(Sp2)– and C(Sp3)–O Bonds with CO2. *J. Am. Chem. Soc.* **2014**, *136* (3), 1062–1069. https://doi.org/10.1021/ja410883p.

(84) Shimasaki, T.; Tobisu, M.; Chatani, N. Nickel-Catalyzed Amination of Aryl Pivalates by the Cleavage of Aryl C□O Bonds. *Angew. Chem. Int. Ed.* **2010**, *49* (16), 2929–2932. https://doi.org/10.1002/anie.200907287.

(85) Gu, Y.; Martín, R. Ni-Catalyzed Stannylation of Aryl Esters via C−O Bond Cleavage. *Angew. Chem. Int. Ed.* **2017**, *56* (12), 3187–3190. https://doi.org/10.1002/anie.201611720.

(86) Yang, J.; Chen, T.; Han, L.-B. C–P Bond-Forming Reactions via C–O/P–H Cross-Coupling Catalyzed by Nickel. *J. Am. Chem. Soc.* **2015**, *137* (5), 1782–1785. https://doi.org/10.1021/ja512498u.

(87) Yang, J.; Xiao, J.; Chen, T.; Han, L.-B. Nickel-Catalyzed Phosphorylation of Phenol Derivatives via C–O/P–H Cross-Coupling. *J. Org. Chem.* **2016**, *81* (9), 3911–3916. https://doi.org/10.1021/acs.joc.6b00289.

(88) Zarate, C.; Martin, R. A Mild Ni/Cu-Catalyzed Silylation via C–O Cleavage. *J. Am. Chem. Soc.* **2014**, *136* (6), 2236–2239. https://doi.org/10.1021/ja412107b.

(89) Do, H.-Q.; Chandrashekar, E. R. R.; Fu, G. C. Nickel/Bis(Oxazoline)-Catalyzed Asymmetric Negishi Arylations of Racemic Secondary Benzylic Electrophiles to Generate Enantioenriched 1,1-Diarylalkanes. *J. Am. Chem. Soc.* **2013**, *135* (44), 16288–16291. https://doi.org/10.1021/ja408561b.

(90) Taylor, B. L. H.; Swift, E. C.; Waetzig, J. D.; Jarvo, E. R. Stereospecific Nickel-Catalyzed Cross-Coupling Reactions of Alkyl Ethers: Enantioselective Synthesis of Diarylethanes. *J. Am. Chem. Soc.* **2011**, *133* (3), 389–391. https://doi.org/10.1021/ja108547u.

(91) Harris, M. R.; Hanna, L. E.; Greene, M. A.; Moore, C. E.; Jarvo, E. R. Retention or Inversion in Stereospecific

Nickel-Catalyzed Cross-Coupling of Benzylic Carbamates with Arylboronic Esters: Control of Absolute Stereochemistry with an Achiral Catalyst. *J. Am. Chem. Soc.* **2013**, *135* (9), 3303–3306. https://doi.org/10.1021/ja311783k.

(92) Zhang, S.-Q.; Taylor, B. L. H.; Ji, C.-L.; Gao, Y.; Harris, M. R.; Hanna, L. E.; Jarvo, E. R.; Houk, K. N.; Hong, X. Mechanism and Origins of Ligand-Controlled Stereoselectivity of Ni-Catalyzed Suzuki–Miyaura Coupling with Benzylic Esters: A Computational Study. *J. Am. Chem. Soc.* **2017**, *139* (37), 12994–13005. https://doi.org/10.1021/jacs.7b04973.

(93) Zhang, S.-Q.; Hong, X. Mechanism and Selectivity Control in Ni- and Pd-Catalyzed Cross-Couplings Involving Carbon–Oxygen Bond Activation. *Acc. Chem. Res.* **2021**, *54* (9), 2158–2171. https://doi.org/10.1021/acs.accounts.1c00050.

(94) Zhou, Q.; Srinivas, H. D.; Zhang, S.; Watson, M. P. Accessing Both Retention and Inversion Pathways in Stereospecific, Nickel-Catalyzed Miyaura Borylations of Allylic Pivalates. *J. Am. Chem. Soc.* **2016**, *138* (36), 11989–11995. https://doi.org/10.1021/jacs.6b07396.

(95) Chen, P.-P.; Zhang, H.; Cheng, B.; Chen, X.; Cheng, F.; Zhang, S.-Q.; Lu, Z.; Meng, F.; Hong, X. How Solvents Control the Stereospecificity of Ni-Catalyzed Miyaura Borylation of Allylic Pivalates. *ACS Catal.* **2019**, *9* (10), 9589–9598. https://doi.org/10.1021/acscatal.9b02636.

(96) Tollefson, E. J.; Dawson, D. D.; Osborne, C. A.; Jarvo, E. R. Stereospecific Cross-Coupling Reactions of Aryl-Substituted Tetrahydrofurans, Tetrahydropyrans, and Lactones. *J. Am. Chem. Soc.* **2014**, *136* (42), 14951–14958. https://doi.org/10.1021/ja5076426.

(97) Tollefson, E. J.; Erickson, L. W.; Jarvo, E. R. Stereospecific Intramolecular Reductive Cross-Electrophile Coupling Reactions for Cyclopropane Synthesis. *J. Am. Chem. Soc.* **2015**, *137* (31), 9760–9763. https://doi.org/10.1021/jacs.5b03870.

(98) Chen, P.-P.; Lucas, E. L.; Greene, M. A.; Zhang, S.-Q.; Tollefson, E. J.; Erickson, L. W.; Taylor, B. L. H.; Jarvo, E. R.; Hong, X. A Unified Explanation for Chemoselectivity and Stereospecificity of Ni-Catalyzed Kumada and Cross-Electrophile Coupling Reactions of Benzylic Ethers: A Combined Computational and Experimental Study. *J. Am. Chem. Soc.* **2019**, *141* (14), 5835–5855. https://doi.org/10.1021/jacs.9b00097.

(99) Greene, M. A.; Yonova, I. M.; Williams, F. J.; Jarvo, E. R. Traceless Directing Group for Stereospecific Nickel-Catalyzed Alkyl−Alkyl Cross-Coupling Reactions. *Org. Lett.* **2012**, *14* (16), 4293–4296. https://doi.org/10.1021/ol300891k.

(100) Wisniewska, H. M.; Swift, E. C.; Jarvo, E. R. Functional-Group-Tolerant, Nickel-Catalyzed Cross-Coupling Reaction for Enantioselective Construction of Tertiary Methyl-Bearing Stereocenters. *J. Am. Chem. Soc.* **2013**, *135* (24), 9083–9090. https://doi.org/10.1021/ja4034999.

(101) Zhou, Q.; Srinivas, H. D.; Dasgupta, S.; Watson, M. P. Nickel-Catalyzed Cross-Couplings of Benzylic Pivalates with Arylboroxines: Stereospecific Formation of Diarylalkanes and Triarylmethanes. *J. Am. Chem. Soc.* **2013**, *135* (9), 3307–3310. https://doi.org/10.1021/ja312087x.

(102) Yonova, I. M.; Johnson, A. G.; Osborne, C. A.; Moore, C. E.; Morrissette, N. S.; Jarvo, E. R. Stereospecific Nickel-Catalyzed Cross-Coupling Reactions of Alkyl Grignard Reagents and Identification of Selective Anti-Breast-Cancer Agents. *Angew. Chem. Int. Ed.* **2014**, *53* (9), 2422–2427. https://doi.org/10.1002/anie.201308666.

(103) Tollefson, E. J.; Hanna, L. E.; Jarvo, E. R. Stereospecific Nickel-Catalyzed Cross-Coupling Reactions of Benzylic Ethers and Esters. *Acc. Chem. Res.* **2015**, *48* (8), 2344–2353. https://doi.org/10.1021/acs.accounts.5b00223.

(104) Lucas, E. L.; Jarvo, E. R. Stereospecific and Stereoconvergent Cross-Couplings between Alkyl Electrophiles. *Nat. Rev. Chem.* **2017**, *1* (9), 1–7. https://doi.org/10.1038/s41570-017-0065.

(105) Pound, S. M.; Watson, M. P. Asymmetric Synthesis via Stereospecific C–N and C–O Bond Activation of Alkyl Amine and Alcohol Derivatives. *Chem. Commun.* **2018**, *54* (87), 12286–12301. https://doi.org/10.1039/C8CC07093H.

(106) Sanford, A. B.; Thane, T. A.; McGinnis, T. M.; Chen, P.-P.; Hong, X.; Jarvo, E. R. Nickel-Catalyzed Alkyl–

Alkyl Cross-Electrophile Coupling Reaction of 1,3-Dimesylates for the Synthesis of Alkylcyclopropanes. *J. Am. Chem. Soc.* **2020**, *142* (11), 5017–5023. https://doi.org/10.1021/jacs.0c01330.

(107) Xu, J.; Bercher, O. P.; Talley, M. R.; Watson, M. P. Nickel-Catalyzed, Stereospecific C–C and C–B Cross-Couplings via C–N and C–O Bond Activation. *ACS Catal.* **2021**, *11* (3), 1604–1612. https://doi.org/10.1021/acscatal.0c05484.

(108) Chen, P.-P.; McGinnis, T. M.; Lin, P. C.; Hong, X.; Jarvo, E. R. A Nickel-Catalyzed Cross-Electrophile Coupling Reaction of 1,3-Dimesylates for Alkylcyclopropane Synthesis: Investigation of Stereochemical Outcomes and Radical Lifetimes. *ACS Catal.* **2023**, *13* (8), 5472–5481. https://doi.org/10.1021/acscatal.3c00905.

(109) Eno, M. S.; Lu, A.; Morken, J. P. Nickel-Catalyzed Asymmetric Kumada Cross-Coupling of Symmetric Cyclic Sulfates. *J. Am. Chem. Soc.* **2016**, *138* (25), 7824–7827. https://doi.org/10.1021/jacs.6b03384.

(110) Prinsell, M. R.; Everson, D. A.; Weix, D. J. Nickel-Catalyzed, Sodium Iodide-Promoted Reductive Dimerization of Alkyl Halides, Alkyl Pseudohalides, and Allylic Acetates. *Chem. Commun.* **2010**, *46* (31), 5743–5745. https://doi.org/10.1039/C0CC01716G.

(111) Liang, Z.; Xue, W.; Lin, K.; Gong, H. Nickel-Catalyzed Reductive Methylation of Alkyl Halides and Acid Chlorides with Methyl p-Tosylate. *Org. Lett.* **2014**, *16* (21), 5620–5623. https://doi.org/10.1021/ol502682q.

(112) Molander, G. A.; Traister, K. M.; O'Neill, B. T. Engaging Nonaromatic, Heterocyclic Tosylates in Reductive Cross-Coupling with Aryl and Heteroaryl Bromides. *J. Org. Chem.* **2015**, *80* (5), 2907–2911. https://doi.org/10.1021/acs.joc.5b00135.

(113) Kranthikumar, R. Recent Advances in C(Sp3)–C(Sp3) Cross-Coupling Chemistry: A Dominant Performance of Nickel Catalysts. *Organometallics* **2022**, *41* (6), 667–679. https://doi.org/10.1021/acs.organomet.2c00032.

(114) Chi, B. K.; Widness, J. K.; Gilbert, M. M.; Salgueiro, D. C.; Garcia, K. J.; Weix, D. J. In-Situ Bromination Enables Formal Cross-Electrophile Coupling of Alcohols with Aryl and Alkenyl Halides. *ACS Catal.* **2022**, *12* (1), 580–586. https://doi.org/10.1021/acscatal.1c05208.

(115) Liu, J.; Ye, Y.; Sessler, J. L.; Gong, H. Cross-Electrophile Couplings of Activated and Sterically Hindered Halides and Alcohol Derivatives. *Acc. Chem. Res.* **2020**, *53* (9), 1833–1845. https://doi.org/10.1021/acs.accounts.0c00291.

(116) Ye, Y.; Chen, H.; Sessler, J. L.; Gong, H. Zn-Mediated Fragmentation of Tertiary Alkyl Oxalates Enabling Formation of Alkylated and Arylated Quaternary Carbon Centers. *J. Am. Chem. Soc.* **2019**, *141* (2), 820–824. https://doi.org/10.1021/jacs.8b12801.

(117) Zhang, X.; MacMillan, D. W. C. Alcohols as Latent Coupling Fragments for Metallaphotoredox Catalysis: Sp3–Sp2 Cross-Coupling of Oxalates with Aryl Halides. *J. Am. Chem. Soc.* **2016**, *138* (42), 13862–13865. https://doi.org/10.1021/jacs.6b09533.

(118) Li, H.; Guo, L.; Feng, X.; Huo, L.; Zhu, S.; Chu, L. Sequential C–O Decarboxylative Vinylation/C–H Arylation of Cyclic Oxalates via a Nickel-Catalyzed Multicomponent Radical Cascade. *Chem. Sci.* **2020**, *11* (19), 4904–4910. https://doi.org/10.1039/D0SC01471K.

(119) Kariofillis, S. K.; Shields, B. J.; Tekle-Smith, M. A.; Zacuto, M. J.; Doyle, A. G. Nickel/Photoredox-Catalyzed Methylation of (Hetero)Aryl Chlorides Using Trimethyl Orthoformate as a Methyl Radical Source. *J. Am. Chem. Soc.* **2020**, *142* (16), 7683–7689. https://doi.org/10.1021/jacs.0c02805.

(120) Kariofillis, S. K.; Jiang, S.; Żurański, A. M.; Gandhi, S. S.; Martinez Alvarado, J. I.; Doyle, A. G. Using Data Science To Guide Aryl Bromide Substrate Scope Analysis in a Ni/Photoredox-Catalyzed Cross-Coupling with Acetals as Alcohol-Derived Radical Sources. *J. Am. Chem. Soc.* **2022**, *144* (2), 1045–1055. https://doi.org/10.1021/jacs.1c12203.

(121) Sakai, H. A.; MacMillan, D. W. C. Nontraditional Fragment Couplings of Alcohols and Carboxylic Acids: C(Sp3)–C(Sp3) Cross-Coupling via Radical Sorting. *J. Am. Chem. Soc.* **2022**, *144* (14), 6185–6192. https://doi.org/10.1021/jacs.2c02062.

(122) Kleiman, J. P.; Dubeck, Michael. The Preparation of Cyclopentadienyl [o-(Phenylazo)Phenyl]Nickel. *J. Am. Chem. Soc.* **1963**, *85* (10), 1544–1545. https://doi.org/10.1021/ja00893a040.

(123) Khake, S. M.; Chatani, N. Chelation-Assisted Nickel-Catalyzed C−H Functionalizations. *Trends Chem.* **2019**, *1* (5), 524–539. https://doi.org/10.1016/j.trechm.2019.06.002.

(124) Gandeepan, P.; Müller, T.; Zell, D.; Cera, G.; Warratz, S.; Ackermann, L. 3d Transition Metals for C–H Activation. *Chem. Rev.* **2019**, *119* (4), 2192–2452. https://doi.org/10.1021/acs.chemrev.8b00507.

(125) Khake, S. M.; Chatani, N. Nickel-Catalyzed C−H Functionalization Using A Non-Directed Strategy. *Chem* **2020**, *6* (5), 1056–1081. https://doi.org/10.1016/j.chempr.2020.04.005.

(126) Nakao, Y.; Kashihara, N.; Kanyiva, K. S.; Hiyama, T. Nickel-Catalyzed Alkenylation and Alkylation of Fluoroarenes via Activation of C−H Bond over C−F Bond. *J. Am. Chem. Soc.* **2008**, *130* (48), 16170–16171. https://doi.org/10.1021/ja807258m.

(127) Clement, N. D.; Cavell, K. J. Transition-Metal-Catalyzed Reactions Involving Imidazolium Salt/N-Heterocyclic Carbene Couples as Substrates. *Angew. Chem. Int. Ed.* **2004**, *43* (29), 3845–3847. https://doi.org/10.1002/anie.200454166.

(128) Nakao, Y.; Kanyiva, K. S.; Hiyama, T. A Strategy for C−H Activation of Pyridines: Direct C-2 Selective Alkenylation of Pyridines by Nickel/Lewis Acid Catalysis. *J. Am. Chem. Soc.* **2008**, *130* (8), 2448–2449. https://doi.org/10.1021/ja710766j.

(129) Nakao, Y.; Yamada, Y.; Kashihara, N.; Hiyama, T. Selective C-4 Alkylation of Pyridine by Nickel/Lewis Acid Catalysis. *J. Am. Chem. Soc.* **2010**, *132* (39), 13666–13668. https://doi.org/10.1021/ja106514b.

(130) Tsai, C.-C.; Shih, W.-C.; Fang, C.-H.; Li, C.-Y.; Ong, T.-G.; Yap, G. P. A. Bimetallic Nickel Aluminun Mediated Para-Selective Alkenylation of Pyridine: Direct Observation of H2,H1-Pyridine Ni(0)−Al(III) Intermediates Prior to C−H Bond Activation. *J. Am. Chem. Soc.* **2010**, *132* (34), 11887–11889. https://doi.org/10.1021/ja1061246.

(131) Zhang, T.; Luan, Y.-X.; Lam, N. Y. S.; Li, J.-F.; Li, Y.; Ye, M.; Yu, J.-Q. A Directive Ni Catalyst Overrides Conventional Site Selectivity in Pyridine C–H Alkenylation. *Nat. Chem.* **2021**, *13* (12), 1207–1213. https://doi.org/10.1038/s41557-021-00792-1.

(132) Saper, N. I.; Ohgi, A.; Small, D. W.; Semba, K.; Nakao, Y.; Hartwig, J. F. Nickel-Catalysed Anti-Markovnikov Hydroarylation of Unactivated Alkenes with Unactivated Arenes Facilitated by Non-Covalent Interactions. *Nat. Chem.* **2020**, *12* (3), 276–283. https://doi.org/10.1038/s41557-019-0409-4.

(133) Guihaumé, J.; Halbert, S.; Eisenstein, O.; Perutz, R. N. Hydrofluoroarylation of Alkynes with Ni Catalysts. C–H Activation via Ligand-to-Ligand Hydrogen Transfer, an Alternative to Oxidative Addition. *Organometallics* **2012**, *31* (4), 1300–1314. https://doi.org/10.1021/om2005673.

(134) Tang, S.; Eisenstein, O.; Nakao, Y.; Sakaki, S. Aromatic C–H σ-Bond Activation by Ni0, Pd0, and Pt0 Alkene Complexes: Concerted Oxidative Addition to Metal vs Ligand-to-Ligand H Transfer Mechanism. *Organometallics* **2017**, *36* (15), 2761–2771. https://doi.org/10.1021/acs.organomet.7b00256.

(135) Nett, A. J.; Montgomery, J.; Zimmerman, P. M. Entrances, Traps, and Rate-Controlling Factors for Nickel-Catalyzed C–H Functionalization. *ACS Catal.* **2017**, *7* (10), 7352–7362. https://doi.org/10.1021/acscatal.7b02919.

(136) Zaitsev, V. G.; Shabashov, D.; Daugulis, O. Highly Regioselective Arylation of Sp3 C−H Bonds Catalyzed by Palladium Acetate. *J. Am. Chem. Soc.* **2005**, *127* (38), 13154–13155. https://doi.org/10.1021/ja054549f.

(137) Omer, H. M.; Liu, P. Computational Study of Ni-Catalyzed C–H Functionalization: Factors That Control the Competition of Oxidative Addition and Radical Pathways. *J. Am. Chem. Soc.* **2017**, *139* (29), 9909–9920. https://doi.org/10.1021/jacs.7b03548.

(138) Beattie, D. D.; Grunwald, A. C.; Perse, T.; Schafer, L. L.; Love, J. A. Understanding Ni(II)-Mediated C(Sp3)–H Activation: Tertiary Ureas as Model Substrates. *J. Am. Chem. Soc.* **2018**, *140* (39), 12602–12610. https://doi.org/10.1021/jacs.8b07708.

(139) Tsou, T. T.; Kochi, J. K. Reductive Coupling of Organometals Induced by Oxidation. Detection of Metastable Paramagnetic Intermediates. *J. Am. Chem. Soc.* **1978**, *100* (5), 1634–1635. https://doi.org/10.1021/ja00473a067.

(140) Matsunaga, P. T.; Hillhouse, G. L.; Rheingold, A. L. Oxygen-Atom Transfer from Nitrous Oxide to a Nickel Metallacycle. Synthesis, Structure, and Reactions of [Cyclic] (2,2'-Bipyridine)Ni(OCH2CH2CH2CH2). *J. Am.*

Chem. Soc. **1993**, *115* (5), 2075–2077. https://doi.org/10.1021/ja00058a085.

(141) Han, R.; Hillhouse, G. L. Carbon−Oxygen Reductive-Elimination from Nickel(II) Oxametallacycles and Factors That Control Formation of Ether, Aldehyde, Alcohol, or Ester Products. *J. Am. Chem. Soc.* **1997**, *119* (34), 8135–8136. https://doi.org/10.1021/ja9714999.

(142) Ruiz-Castillo, P.; Buchwald, S. L. Applications of Palladium-Catalyzed C–N Cross-Coupling Reactions. *Chem. Rev.* **2016**, *116* (19), 12564–12649. https://doi.org/10.1021/acs.chemrev.6b00512.

(143) Twilton, J.; Le, C. (Chip); Zhang, P.; Shaw, M. H.; Evans, R. W.; MacMillan, D. W. C. The Merger of Transition Metal and Photocatalysis. *Nat. Rev. Chem.* **2017**, *1* (7), 1–19. https://doi.org/10.1038/s41570-017-0052.

(144) Chan, A. Y.; Perry, I. B.; Bissonnette, N. B.; Buksh, B. F.; Edwards, G. A.; Frye, L. I.; Garry, O. L.; Lavagnino, M. N.; Li, B. X.; Liang, Y.; Mao, E.; Millet, A.; Oakley, J. V.; Reed, N. L.; Sakai, H. A.; Seath, C. P.; MacMillan, D. W. C. Metallaphotoredox: The Merger of Photoredox and Transition Metal Catalysis. *Chem. Rev.* **2022**, *122* (2), 1485–1542. https://doi.org/10.1021/acs.chemrev.1c00383.

(145) Osawa, M.; Nagai, H.; Akita, M. Photo-Activation of Pd-Catalyzed Sonogashira Coupling Using a Ru/Bipyridine Complex as Energy Transfer Agent. *Dalton Trans.* **2007**, No. 8, 827–829. https://doi.org/10.1039/B618007H.

(146) Kalyani, D.; McMurtrey, K. B.; Neufeldt, S. R.; Sanford, M. S. Room-Temperature C–H Arylation: Merger of Pd-Catalyzed C–H Functionalization and Visible-Light Photocatalysis. *J. Am. Chem. Soc.* **2011**, *133* (46), 18566–18569. https://doi.org/10.1021/ja208068w.

(147) Tellis, J. C.; Kelly, C. B.; Primer, D. N.; Jouffroy, M.; Patel, N. R.; Molander, G. A. Single-Electron Transmetalation via Photoredox/Nickel Dual Catalysis: Unlocking a New Paradigm for Sp3–Sp2 Cross-Coupling. *Acc. Chem. Res.* **2016**, *49* (7), 1429–1439. https://doi.org/10.1021/acs.accounts.6b00214.

(148) Ackerman-Biegasiewicz, L. K. G.; Kariofillis, S. K.; Weix, D. J. Multimetallic-Catalyzed C–C Bond-Forming Reactions: From Serendipity to Strategy. *J. Am. Chem. Soc.* **2023**, *145* (12), 6596–6614. https://doi.org/10.1021/jacs.2c08615.

(149) Zuo, Z.; Ahneman, D. T.; Chu, L.; Terrett, J. A.; Doyle, A. G.; MacMillan, D. W. C. Merging Photoredox with Nickel Catalysis: Coupling of α-Carboxyl Sp3-Carbons with Aryl Halides. *Science* **2014**, *345* (6195), 437–440. https://doi.org/10.1126/science.1255525.

(150) Tellis, J. C.; Primer, D. N.; Molander, G. A. Single-Electron Transmetalation in Organoboron Cross-Coupling by Photoredox/Nickel Dual Catalysis. *Science* **2014**, *345* (6195), 433–436. https://doi.org/10.1126/science.1253647.

(151) Gutierrez, O.; Tellis, J. C.; Primer, D. N.; Molander, G. A.; Kozlowski, M. C. Nickel-Catalyzed Cross-Coupling of Photoredox-Generated Radicals: Uncovering a General Manifold for Stereoconvergence in Nickel-Catalyzed Cross-Couplings. *J. Am. Chem. Soc.* **2015**, *137* (15), 4896–4899. https://doi.org/10.1021/ja513079r.

(152) Capaldo, L.; Ravelli, D. Hydrogen Atom Transfer (HAT): A Versatile Strategy for Substrate Activation in Photocatalyzed Organic Synthesis. *Eur. J. Org. Chem.* **2017**, *2017* (15), 2056–2071. https://doi.org/10.1002/ejoc.201601485.

(153) Sarkar, S.; Cheung, K. P. S.; Gevorgyan, V. C–H Functionalization Reactions Enabled by Hydrogen Atom Transfer to Carbon-Centered Radicals. *Chem. Sci.* **2020**, *11* (48), 12974–12993. https://doi.org/10.1039/D0SC04881J.

(154) Holmberg-Douglas, N.; Nicewicz, D. A. Photoredox-Catalyzed C–H Functionalization Reactions. *Chem. Rev.* **2022**, *122* (2), 1925–2016. https://doi.org/10.1021/acs.chemrev.1c00311.

(155) Shen, Y.; Gu, Y.; Martin, R. Sp3 C–H Arylation and Alkylation Enabled by the Synergy of Triplet Excited Ketones and Nickel Catalysts. *J. Am. Chem. Soc.* **2018**, *140* (38), 12200–12209. https://doi.org/10.1021/jacs.8b07405.

(156) Perry, I. B.; Brewer, T. F.; Sarver, P. J.; Schultz, D. M.; DiRocco, D. A.; MacMillan, D. W. C. Direct Arylation of Strong Aliphatic C–H Bonds. *Nature* **2018**, *560* (7716), 70–75. https://doi.org/10.1038/s41586-018-0366-x.

(157) Prier, C. K.; Rankic, D. A.; MacMillan, D. W. C. Visible Light Photoredox Catalysis with Transition Metal

Complexes: Applications in Organic Synthesis. *Chem. Rev.* **2013**, *113* (7), 5322–5363. https://doi.org/10.1021/cr300503r.

(158) Le, C.; Liang, Y.; Evans, R. W.; Li, X.; MacMillan, D. W. C. Selective Sp3 C–H Alkylation via Polarity-Match-Based Cross-Coupling. *Nature* **2017**, *547* (7661), 79–83. https://doi.org/10.1038/nature22813.

(159) Maity, B.; Zhu, C.; Yue, H.; Huang, L.; Harb, M.; Minenkov, Y.; Rueping, M.; Cavallo, L. Mechanistic Insight into the Photoredox-Nickel-HAT Triple Catalyzed Arylation and Alkylation of α-Amino Csp3–H Bonds. *J. Am. Chem. Soc.* **2020**, *142* (40), 16942–16952. https://doi.org/10.1021/jacs.0c05010.

(160) Shields, B. J.; Doyle, A. G. Direct C(Sp3)–H Cross Coupling Enabled by Catalytic Generation of Chlorine Radicals. *J. Am. Chem. Soc.* **2016**, *138* (39), 12719–12722. https://doi.org/10.1021/jacs.6b08397.

(161) Juliá, F. Ligand-to-Metal Charge Transfer (LMCT) Photochemistry at 3d-Metal Complexes: An Emerging Tool for Sustainable Organic Synthesis. *ChemCatChem* **2022**, *14* (19), e202200916. https://doi.org/10.1002/cctc.202200916.

(162) Hwang, S. J.; Anderson, B. L.; Powers, D. C.; Maher, A. G.; Hadt, R. G.; Nocera, D. G. Halogen Photoelimination from Monomeric Nickel(III) Complexes Enabled by the Secondary Coordination Sphere. *Organometallics* **2015**, *34* (19), 4766–4774. https://doi.org/10.1021/acs.organomet.5b00568.

(163) Heitz, D. R.; Tellis, J. C.; Molande, G. A. Photochemical Nickel-Catalyzed C–H Arylation: Synthetic Scope and Mechanistic Investigations. *J. Am. Chem. Soc.* **2016**, *138* (39), 12715–12718. https://doi.org/10.1021/jacs.6b04789.

(164) Matsunaga, P. T.; Mavropoulos, J. C.; Hillhouse, G. L. Oxygen-Atom Transfer from Nitrous Oxide (N□N□O) to Nickel Alkyls. Syntheses and Reactions of Nickel(II) Alkoxides. *Polyhedron* **1995**, *14* (1), 175–185. https://doi.org/10.1016/0277-5387(94)00330-H.

(165) Macgregor, S. A.; Neave, G. W.; Smith, C. Theoretical Studies on C–Heteroatom Bond Formation via Reductive Elimination from Group 10 M(PH3)2(CH3)(X) Species (X = CH3, NH2, OH, SH) and the Determination of Metal–X Bond Strengths Using Density Functional Theory. *Faraday Discuss.* **2003**, *124* (0), 111–127. https://doi.org/10.1039/B212309F.

(166) Camasso, N. M.; Sanford, M. S. Design, Synthesis, and Carbon-Heteroatom Coupling Reactions of Organometallic Nickel(IV) Complexes. *Science* **2015**, *347* (6227), 1218–1220. https://doi.org/10.1126/science.aaa4526.

(167) Zhou, W.; Schultz, J. W.; Rath, N. P.; Mirica, L. M. Aromatic Methoxylation and Hydroxylation by Organometallic High-Valent Nickel Complexes. *J. Am. Chem. Soc.* **2015**, *137* (24), 7604–7607. https://doi.org/10.1021/jacs.5b04082.

(168) Lau, W.; Huffman, J. C.; Kochi, J. K. Electrochemical Oxidation-Reduction of Organometallic Complexes. Effect of the Oxidation State on the Pathways for Reductive Elimination of Dialkyliron Complexes. *Organometallics* **1982**, *1* (1), 155–169. https://doi.org/10.1021/om00061a027.

(169) Lanci, M. P.; Remy, M. S.; Kaminsky, W.; Mayer, J. M.; Sanford, M. S. Oxidatively Induced Reductive Elimination from (TBu2bpy)Pd(Me)2: Palladium(IV) Intermediates in a One-Electron Oxidation Reaction. *J. Am. Chem. Soc.* **2009**, *131* (43), 15618–15620. https://doi.org/10.1021/ja905816q.

(170) Terrett, J. A.; Cuthbertson, J. D.; Shurtleff, V. W.; MacMillan, D. W. C. Switching on Elusive Organometallic Mechanisms with Photoredox Catalysis. *Nature* **2015**, *524* (7565), 330–334. https://doi.org/10.1038/nature14875.

(171) Sun, R.; Qin, Y.; Ruccolo, S.; Schnedermann, C.; Costentin, C.; Nocera, D. G. Elucidation of a Redox-Mediated Reaction Cycle for Nickel-Catalyzed Cross Coupling. *J. Am. Chem. Soc.* **2019**, *141* (1), 89–93. https://doi.org/10.1021/jacs.8b11262.

(172) Shields, B. J.; Kudisch, B.; Scholes, G. D.; Doyle, A. G. Long-Lived Charge-Transfer States of Nickel(II) Aryl Halide Complexes Facilitate Bimolecular Photoinduced Electron Transfer. *J. Am. Chem. Soc.* **2018**, *140* (8), 3035–3039. https://doi.org/10.1021/jacs.7b13281.

(173) Sun, R.; Qin, Y.; Nocera, D. G. General Paradigm in Photoredox Nickel-Catalyzed Cross-Coupling Allows for Light-Free Access to Reactivity. *Angew. Chem. Int. Ed.* **2020**, *59* (24), 9527–9533.

https://doi.org/10.1002/anie.201916398.

(174) Ting, S. I.; Garakyaraghi, S.; Taliaferro, C. M.; Shields, B. J.; Scholes, G. D.; Castellano, F. N.; Doyle, A. G. 3d-d Excited States of Ni(II) Complexes Relevant to Photoredox Catalysis: Spectroscopic Identification and Mechanistic Implications. *J. Am. Chem. Soc.* **2020**, *142* (12), 5800–5810. https://doi.org/10.1021/jacs.0c00781.

(175) Na, H.; Mirica, L. M. Deciphering the Mechanism of the Ni-Photocatalyzed C–O Cross-Coupling Reaction Using a Tridentate Pyridinophane Ligand. *Nat. Commun.* **2022**, *13* (1), 1313. https://doi.org/10.1038/s41467-022-28948-8.

(176) Chrisman, C. H.; Kudisch, M.; Puffer, K. O.; Stewart, T. K.; Lamb, Y. M. L.; Lim, C.-H.; Escobar, R.; Thordarson, P.; Johannes, J. W.; Miyake, G. M. Halide Noninnocence and Direct Photoreduction of Ni(II) Enables Coupling of Aryl Chlorides in Dual Catalytic, Carbon–Heteroatom Bond-Forming Reactions. *J. Am. Chem. Soc.* **2023**, *145* (22), 12293–12304. https://doi.org/10.1021/jacs.3c02784.

(177) Creutz, S. E.; Lotito, K. J.; Fu, G. C.; Peters, J. C. Photoinduced Ullmann C–N Coupling: Demonstrating the Viability of a Radical Pathway. *Science* **2012**, *338* (6107), 647–651. https://doi.org/10.1126/science.1226458.

(178) Hwang, S. J.; Powers, D. C.; Maher, A. G.; Anderson, B. L.; Hadt, R. G.; Zheng, S.-L.; Chen, Y.-S.; Nocera, D. G. Trap-Free Halogen Photoelimination from Mononuclear Ni(III) Complexes. *J. Am. Chem. Soc.* **2015**, *137* (20), 6472–6475. https://doi.org/10.1021/jacs.5b03192.

(179) Kainz, Q. M.; Matier, C. D.; Bartoszewicz, A.; Zultanski, S. L.; Peters, J. C.; Fu, G. C. Asymmetric Copper-Catalyzed C-N Cross-Couplings Induced by Visible Light. *Science* **2016**, *351* (6274), 681–684. https://doi.org/10.1126/science.aad8313.

(180) Strieth-Kalthoff, F.; James, M. J.; Teders, M.; Pitzer, L.; Glorius, F. Energy Transfer Catalysis Mediated by Visible Light: Principles, Applications, Directions. *Chem. Soc. Rev.* **2018**, *47* (19), 7190–7202. https://doi.org/10.1039/C8CS00054A.

(181) Welin, E. R.; Le, C.; Arias-Rotondo, D. M.; McCusker, J. K.; MacMillan, D. W. C. Photosensitized, Energy Transfer-Mediated Organometallic Catalysis through Electronically Excited Nickel(II). *Science* **2017**, *355* (6323), 380–385. https://doi.org/10.1126/science.aal2490.

(182) Tian, L.; Till, N. A.; Kudisch, B.; MacMillan, D. W. C.; Scholes, G. D. Transient Absorption Spectroscopy Offers Mechanistic Insights for an Iridium/Nickel-Catalyzed C–O Coupling. *J. Am. Chem. Soc.* **2020**, *142* (10), 4555–4559. https://doi.org/10.1021/jacs.9b12835.

(183) Tasker, S. Z.; Jamison, T. F. Highly Regioselective Indoline Synthesis under Nickel/Photoredox Dual Catalysis. *J. Am. Chem. Soc.* **2015**, *137* (30), 9531–9534. https://doi.org/10.1021/jacs.5b05597.

(184) Corcoran, E. B.; Pirnot, M. T.; Lin, S.; Dreher, S. D.; DiRocco, D. A.; Davies, I. W.; Buchwald, S. L.; MacMillan, D. W. C. Aryl Amination Using Ligand-Free Ni(II) Salts and Photoredox Catalysis. *Science* **2016**, *353* (6296), 279–283. https://doi.org/10.1126/science.aag0209.

Chapter 1.

Chapter 2.

Site-selective functionalisation of unactivated sp^3 C–O bonds in cyclic acetals

Research carried out in collaboration with

Ciro Romano and Enrique Gómez-Bengoa

Published in: *J. Am. Chem. Soc.* **2022**, *144*, 11558-11563.

UNIVERSITAT ROVIRA I VIRGILI
FUNCTIONALISATION OF SP3 C-O BONDS AND OLEFINS ENABLED BY NICKEL CATALYSIS
Laura Talavera Codina

2.1. Introduction

Due to their natural abundance, low toxicity and widespread availability, alcohols could serve as ideal reagents in organic chemistry, providing a powerful alternative to the commonly employed organohalides counterparts. Although the use of sp^2 C–O derivatives has become routine, deoxygenative transformations of *unactivated* sp^3 C–O bonds, possessing β-hydrogens, remains highly underexplored.

Achieving deoxyfunctionalisation reactions on primary or secondary alcohols can be readily accomplished using classical nucleophilic substitution chemistry. However, the challenge arises when attempting such transformations with tertiary or sterically hindered secondary and primary alcohols. Additionally, the exploitation of S_N1 or S_N2 mechanisms imposes the use of nucleophilic coupling partners and restricts the variety of achievable architectures. To overcome this inherent reactivity boundaries, one promising strategy is the use of radical deoxyfunctionalisation paradigms, which can be achieved through a variety of mechanisms.[1–10] Nonetheless, in most cases, pre-activation of the alcohol substrate is required either via either *ex situ* or *in situ* manifolds.[11–18] In these processes, the activated alcohol undergoes single-electron transfer, followed by homolytic cleavage, generating a primary, secondary, or tertiary radical that can participate in subsequent transformations.

2.1.1. Photoredox radical-based deoxygenation strategies

Barton-McCombie-type xanthate-based approaches

Since the pioneering work of Barton and McCombie in 1975, the radical deoxygenation of alcohols has emerged as one of the most widely utilised approaches for the reduction of sp^3 C–O to sp^3 C–H bonds.[19] The described reaction proceeds via the formation of a thiocarbonyl precursor (**2**), which subsequently reacts with stannyl radicals, leading to intermediate **I**. The latter, undergoes preferential β-scission of the carbon-oxygen bond, resulting in the formation of a *C*-centred radical (**III**). The desired reduced product (**3**) is then obtained through hydrogen abstraction from tributyltin hydride. It is worth noting that the unstable by-product **II** decomposes delivering carbon oxygensulfide (Scheme 1).

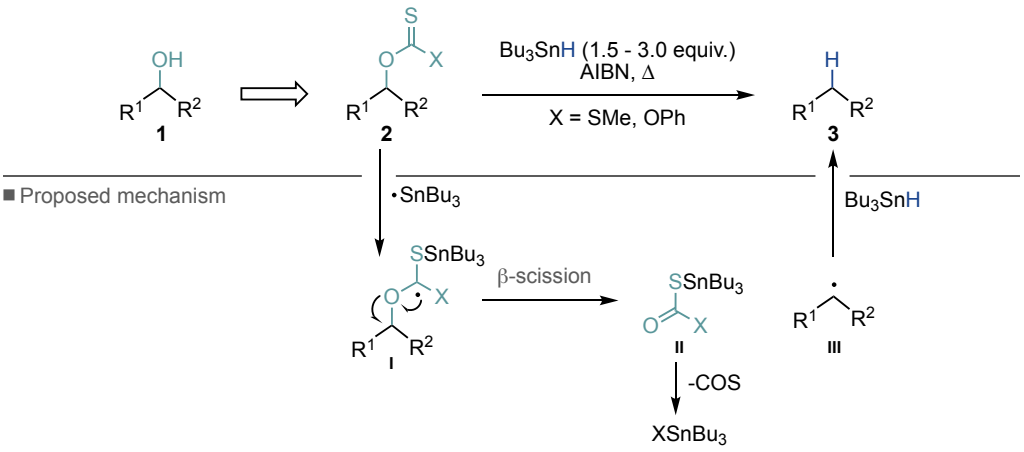

Scheme 1. Barton-McCombie deoxygenation of secondary alcohols

Despite the initial use of highly toxic tin hydride sources, significant progress has been made in the deoxygenation of alcohols towards the utilisation of less hazardous alternatives. Preliminary success was demonstrated by Fu in 1997, who introduced a variation of the method that employed catalytic amounts of Bu_3SnH and phenylsilane as the hydride source, thus reducing the reliance on toxic reagents.[20] Subsequently, in 2000, Tongo and co-workers developed a tin-free deoxygenation method using xanthates and tetraphenyldisilane.[21] Further improvements were achieved in 2005 by Wood, who introduced the use of water as the hydrogen source in combination with trialkylboranes, offering an even more benign and environmentally friendly option.[22] Together, these developments have expanded the possibilities for safer and more sustainable approaches to alcohol deoxygenation reactions.

In 2014, inspired by the resurgence of photoredox catalysis, the groups of Fensterbank, Goddard and Ollivier reported a photocatalysed tin-free Barton-McCombie-type deoxygenation reaction of secondary and tertiary thiocarbamates.[23] The proposed mechanism involves the reduction of *O*-thiocarbamate by the photoexcited iridium catalyst, to afford a carbon-centred radical via C–O cleavage. Subsequently, hydrogen atom transfer occurs from the base (DIPEA), resulting in the formation of the desired product. The base serves not only as the hydrogen source but also as the reductant to regenerate Ir(III). The applicability of the method was demonstrated by the successful application to protected sugars and steroids (Scheme 2).

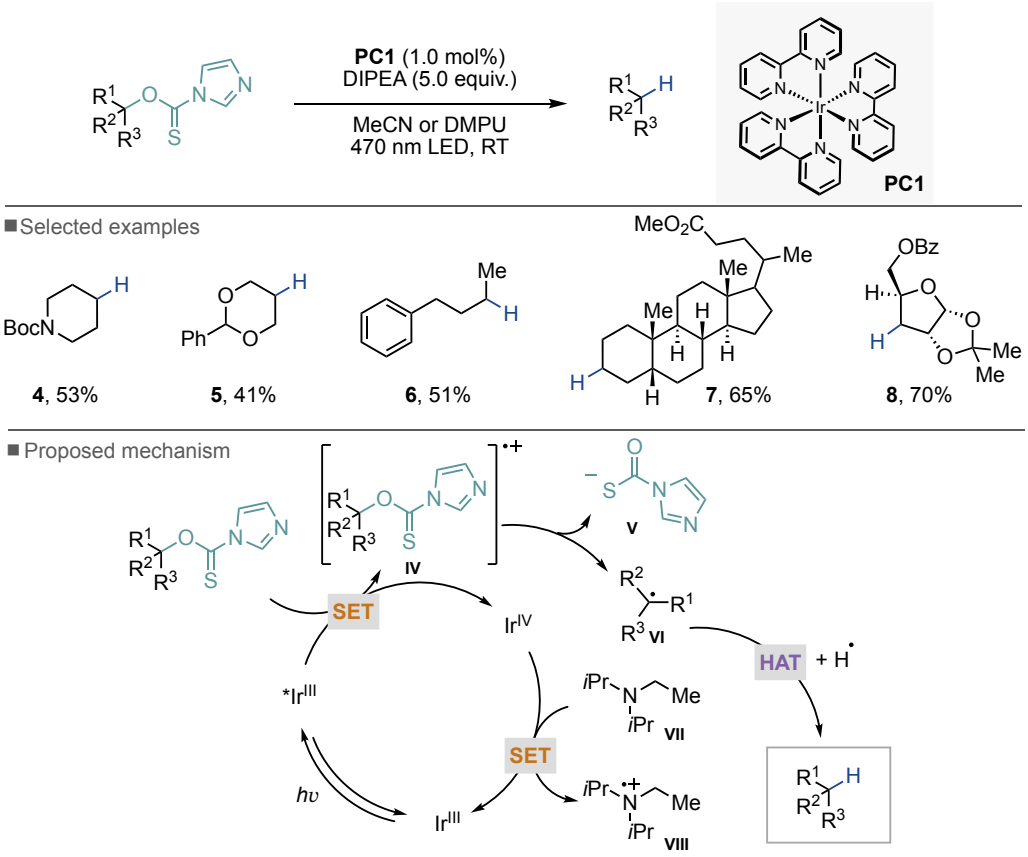

Scheme 2. Photocatalytic deoxygenation of *O*-thiocarbamates

Phosphine-mediated approaches

In 2008, Rovis, Doyle and co-workers reported a novel deoxygenative strategy for the generation of primary benzylic radicals from the corresponding alcohols under visible-light photoredox conditions without the need for pre-activation.[17] This strategy, inspired by the studies of Bentrude and others on C–O bond activation with phosphoranyl radicals,[24] exploits the unique reactivity of these radicals. In this system, the photoexcited *Ir(III) catalyst undergoes SET with triphenylphosphine to afford a phosphine radical cation (**IX**). This species reacts with the corresponding alcohol to form a phosphoranyl radical intermediate (**X**), which upon β-scission generates an alkyl radical (**XI**) and triphenylphosphine oxide. A subsequent HAT event from an aryl thiol affords the desired product. A final reduction of the thiyl radical and proton transfer to the thiolate regenerates the active catalyst. It is worth noting that although it represents a significant advancement in the field, this approach is limited to the deoxygenation of primary benzylic alcohols.

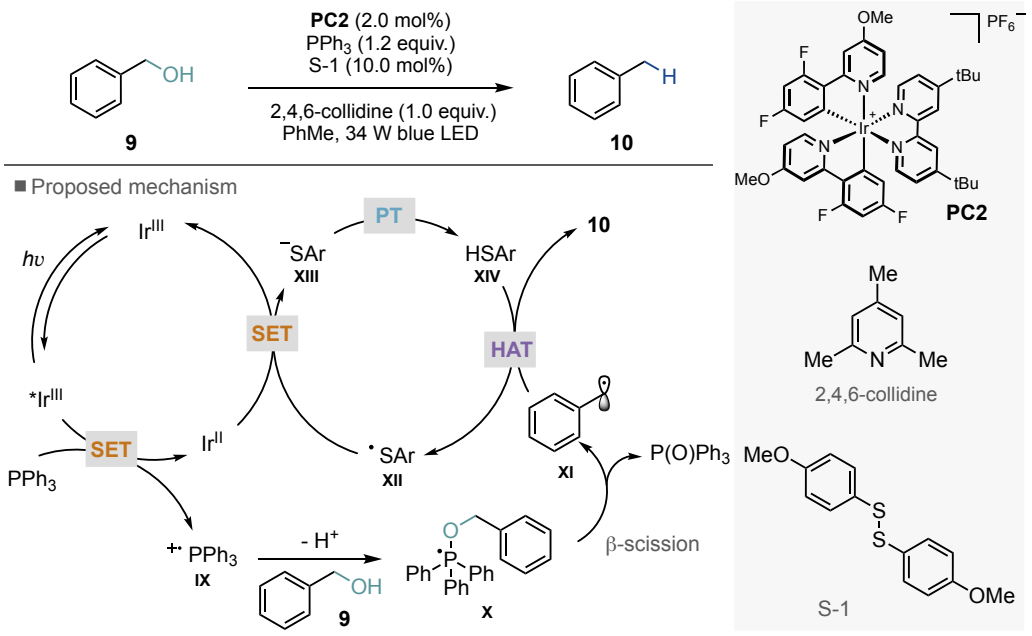

Scheme 3. Deoxygenation of benzylic alcohols using phosphoranyl radicals

2.1.2. Photoredox deoxyfunctionalisation strategies

With the development of efficient and controllable methodologies for the generation of radicals via photoredox catalysis, there has been a growing interest in the design of novel strategies for bond formation, specially through radical sp^3 C–O bond cleavage.

2.1.2.1. sp^3 C–O bond cleavage strategies using redox-active esters

Oxalates and xanthates

In 2013, Overman introduced *N*-phthalimidoyl oxalates as radical precursors and successfully employed them in a light-mediated Giese-type approach to construct quaternary carbon centres from tertiary alcohols.[25] As suggested by Okada in a similar methodology,[26] the reaction proceeds through a single-electron reduction of *N*-phthalimidoyl oxalate, which delivers an alcoxycarbonyl radical (**XVI**) and phthalimide by-product, upon N–O bond homolytic cleavage and subsequent decarboxylation. A slower, second decarboxylation event generates the tertiary radical (**XVII**), which adds to an electron-deficient alkene, ultimately yielding the desired product (Scheme 4). The rate of the second decarboxylation is determined by the stability of the resulting radical, thus elucidating the requirement for elevated temperatures in the case of secondary alcohols, while primary alcohols are not amendable for this strategy.

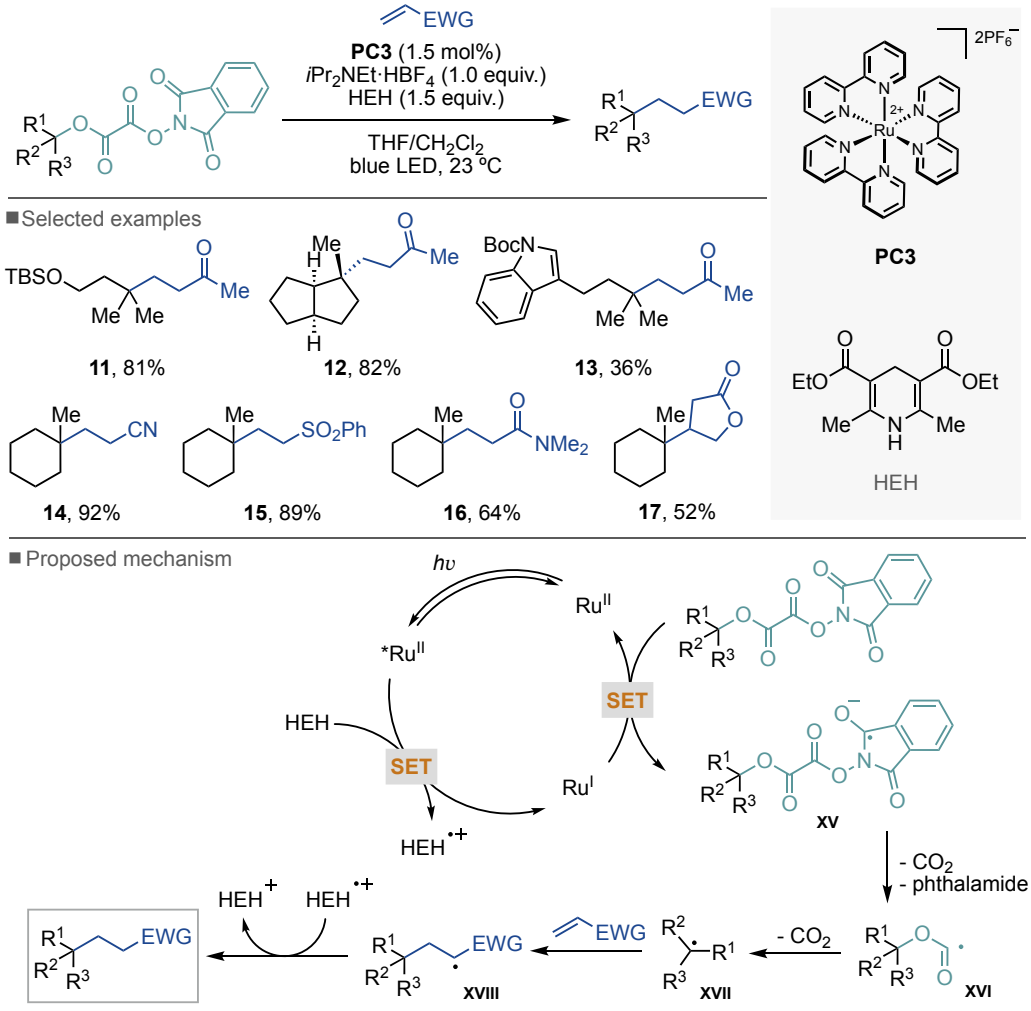

Scheme 4. Light-mediated Giese-type approach using *N*-phtalimidoyl oxalates

Building on these discoveries, in 2015, a collaboration between the Overman's and the MacMillan's groups unveiled a novel redox-neutral protocol that utilised alkyl oxalates as alcohol precursors.[27] This activating group exhibits opposite redox properties to those of *N*-phthalimidoyl oxalate and can be activated through a redox-neutral manifold. Unlike the previously described reductive coupling, a photoexcited iridium photocatalyst is reductively quenched by the tertiary alcohol-derived caesium oxalate, which delivers the corresponding tertiary radical, upon two consecutive decarboxylation steps. The resulting radical adds to the activated olefin and yields the desired product, via single-electron transfer from Ir(II) and subsequent protonation (Scheme 5).

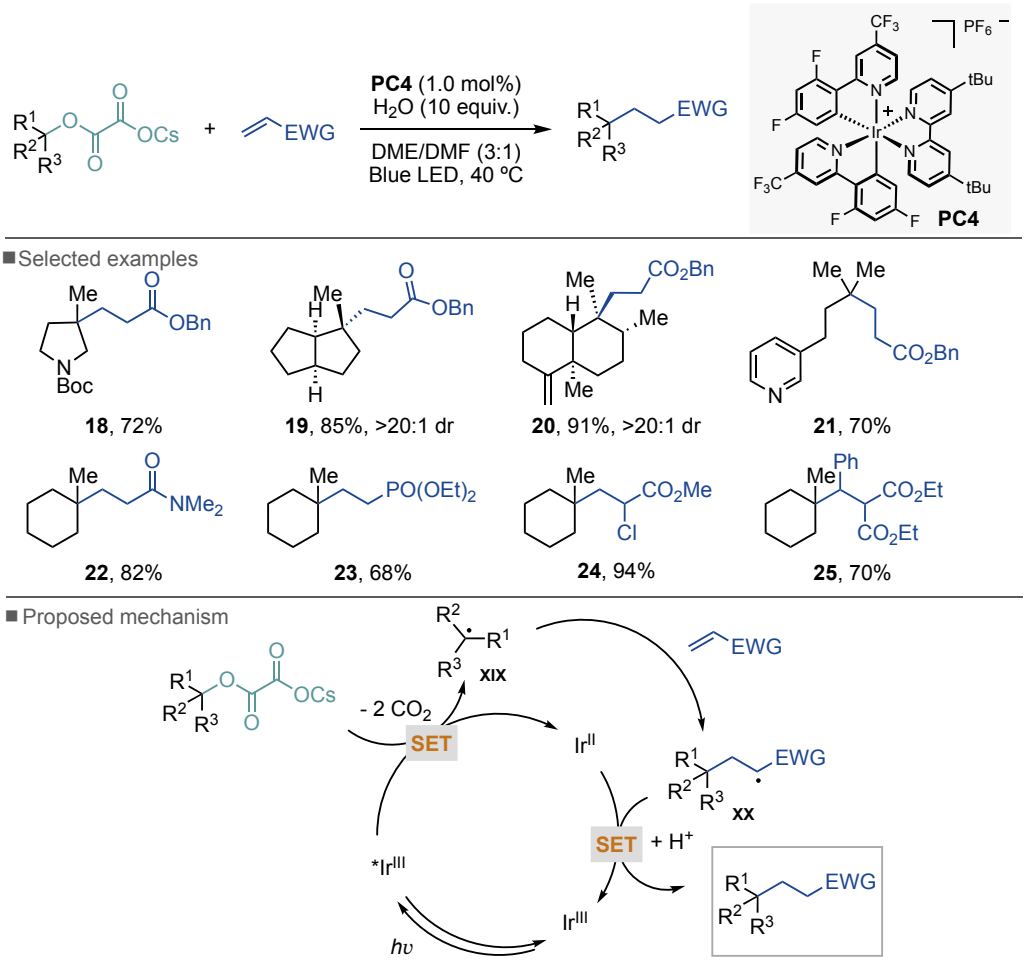

Scheme 5. Light-mediated Giese-type approach using caesium oxalates

While the implementation of a redox-neutral approach eliminated the need for stoichiometric reductants, the scope of the reaction remained largely limited to tertiary alcohols. Nevertheless, this innovative approach undoubtedly paved the way for diverse radical transformations, thereby significantly expanding the chemical space within reach. A representative selection of some of these methodologies is depicted in Scheme 6.[28–32]

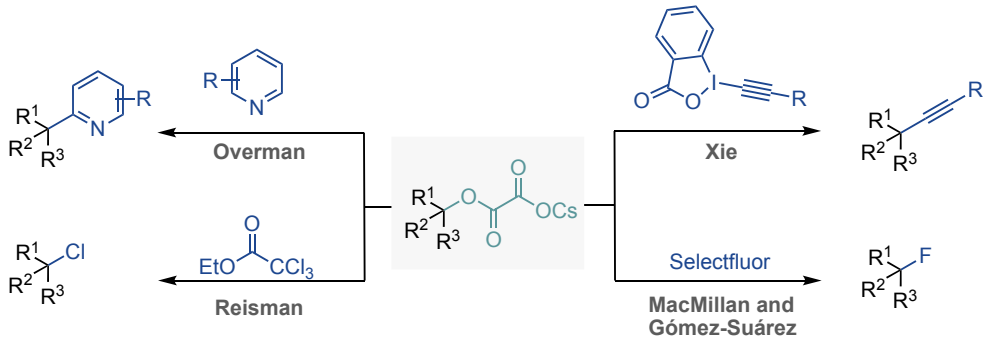

Scheme 6. Selected examples using caesium oxalates

In 2016, MacMillan and co-workers demonstrated the utilisation of oxalates as radical precursors in a metallaphotoredox reaction to construct challenging C*sp*³–C*sp*² bonds.[33] Particularly noteworthy was the ability to provide the desired products using secondary (both cyclic and acyclic) and primary alcohol-derived oxalates, albeit in moderate yields (Scheme 7).

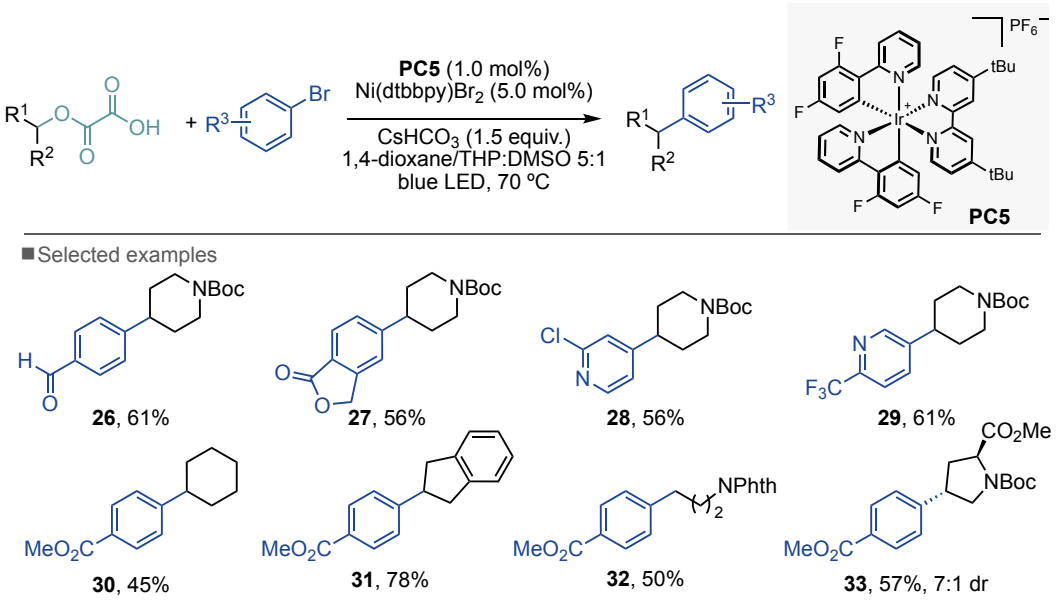

Scheme 7. Metallaphotoredox cross-coupling between oxalates and (hetero)arylbromides

This strategy employed a similar mechanism to the one described in Scheme 5, wherein the generation of the carbon-centred radical occurred through SET from the photoexcited state of **PC5**, followed by two consecutive decarboxylation events. Concurrently, oxidative addition of the aryl bromide to Ni(0) generates a Ni(II)-aryl species, which oxidatively captures the radical to afford a high valent Ni(II) intermediate. Reductive elimination yields

the desired product and a Ni(I) species. A final SET between the photocatalyst and Ni(I) regenerates the active species, closing both catalytic cycles (Scheme 8).

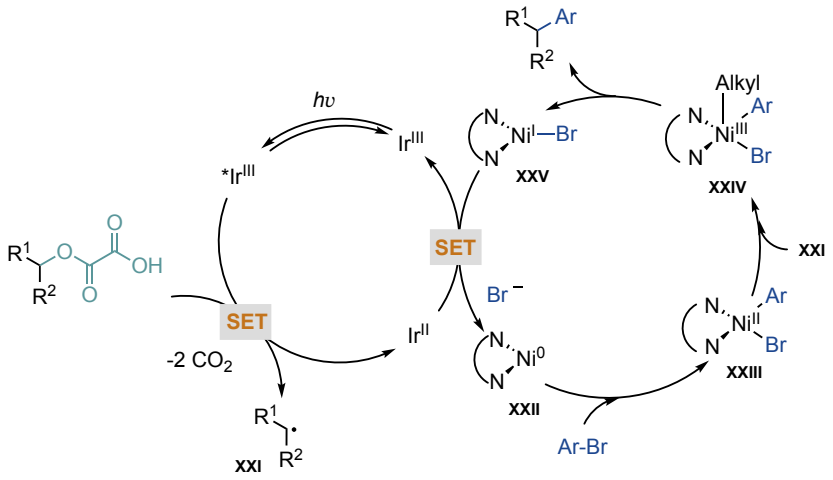

Scheme 8. Proposed mechanism for the metallaphotoredox cross-coupling between oxalates and (hetero)arylbromides

Later on, Overman's and Chu's research groups independently expanded on this discovery. The former showcased the synthesis of siprolactones through a photoredox-mediated alkoxycarbonyl radical 5-exo cyclisation triggered by the loss of a single equivalent of CO_2 (Scheme 9, *top*).[34] On the other hand, Chu and co-workers reported a multicomponent radical cascade of saturated cyclic hydrocarbons via a decarboxylative vinylation. The vinyl radical intermediate undergoes 1,5-HAT followed by a Csp^3–Csp^2 cross-coupling to deliver the targeted product (Scheme 9, *bottom*).[35]

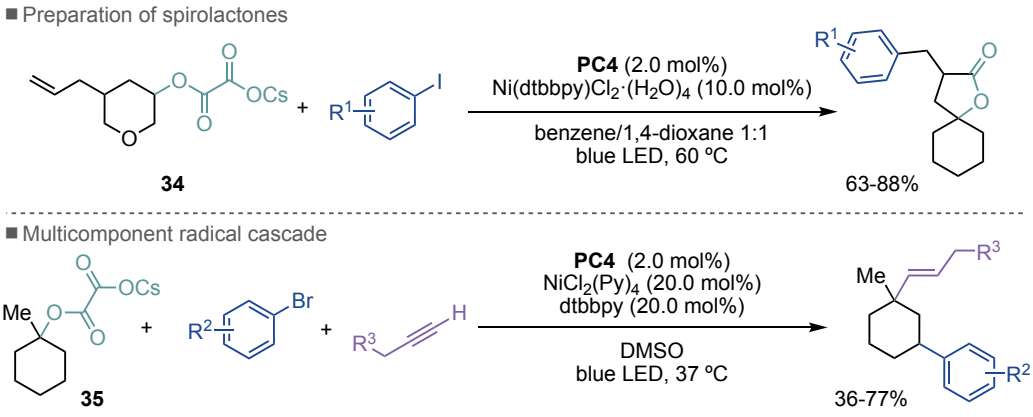

Scheme 9. Metallaphotoredox strategies reported by Overman and Chu

Over the past years, significant attention has been directed towards the development of methods to access alkylboronic esters through photoredox deoxygenative strategies. This is primarily due to the remarkable versatility of the C–B bond in downstream transformations.

In 2019, Studer and co-workers successfully demonstrated a Barton-McCombie-inspired deoxygenative radical borylation of tertiary alcohols activated with neutral dialkyl oxalates using Ir photoredox catalysis (Scheme 10, *path a*).[36] Concurrently, the Aggarwal group reported a similar transformation using 2-iodophenyl-thianocarbonate-derived secondary alcohols, which proceeded under visible-light irradiation without the need for a photocatalyst (Scheme 10, *path b*).[37] Mechanistic investigations revealed the importance of the iodide on thionocarbonates, ruling out a mechanism involving the direct single-electron reduction of the thiocarbonyl moiety. UV-vis spectroscopy, ^{11}B and ^{13}C NMR, and cyclic voltammetry experiments provided evidence for the formation of an electron donor-acceptor (EDA) complex between triethylamine, B_2cat_2 and the aryl iodide moiety. The proposed mechanism is shown in Scheme 10, *bottom*. Upon irradiation of the EDA complex, a photoinduced electron transfer generates an aryl iodide radical anion **XXVI** and a radical cation complex **XXVII**. Subsequent elimination of iodide from **XXVI** forms the aryl radical **XXVIII**, which undergoes 5-endo-trig cyclisation and fragmentation, yielding the key alkyl radical and cyclic thionocarbonate (**XXX**). The resulting alkyl radical is then trapped by B_2cat_2, affording the targeted alkyl boronic ester. Inspired by these findings, Liu and Gong developed a photo-induced metal-free borylation of tertiary alcohols – activated as methyl oxalates – and secondary alcohols – activated as *O*-thiocarbamate – (Scheme 10, *path c*).[38] This transformation followed a mechanistic pathway similar to that described by Aggarwal, further expanding the scope of photoredox deoxygenative strategies for the synthesis of alkylboronic esters.

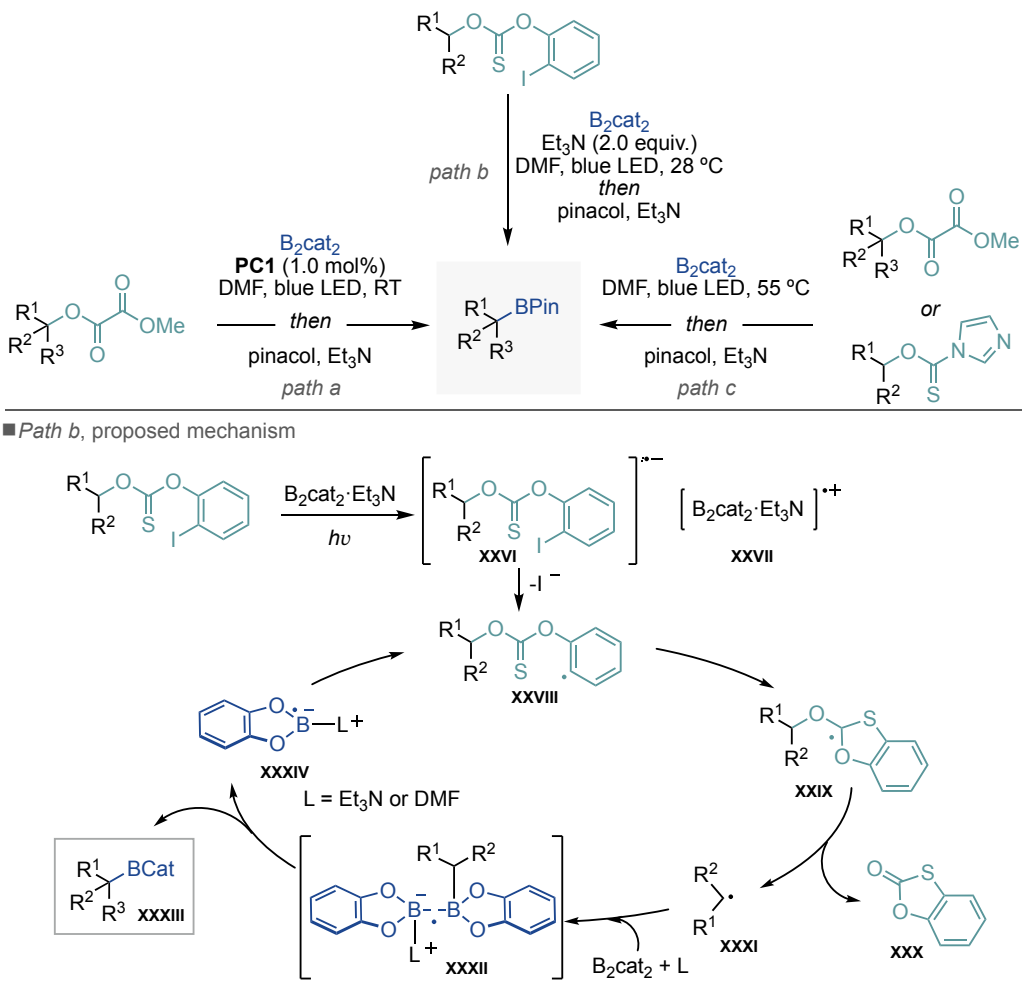

Scheme 10. Photoinduced deoxygenative borylation reactions

Dihydropyridine

Spurred by the interest in the synthesis of novel *C*-aryl glycosides, Diao and co-workers described a new cross-coupling approach for their preparation (Scheme 11).[39] The anomeric alcohol moiety was linked to a 4-carboxy dihydropyridine derivative, attaining the two-fold effect of imparting stability to the resulting glycosyl linkage and allowing the exploitation of a similar mechanistic scenario than the one described above. It is worth noting that the anomeric stereochemistry of the cross-coupled products is dictated by the electronic and steric properties of the sugar starting material. The presence of bulky substituents or electron-donating/withdrawing groups influences the orientation and reactivity of the glycosyl ester during the cross-coupling reaction, leading to the preferential formation of the α- or β-anomer.

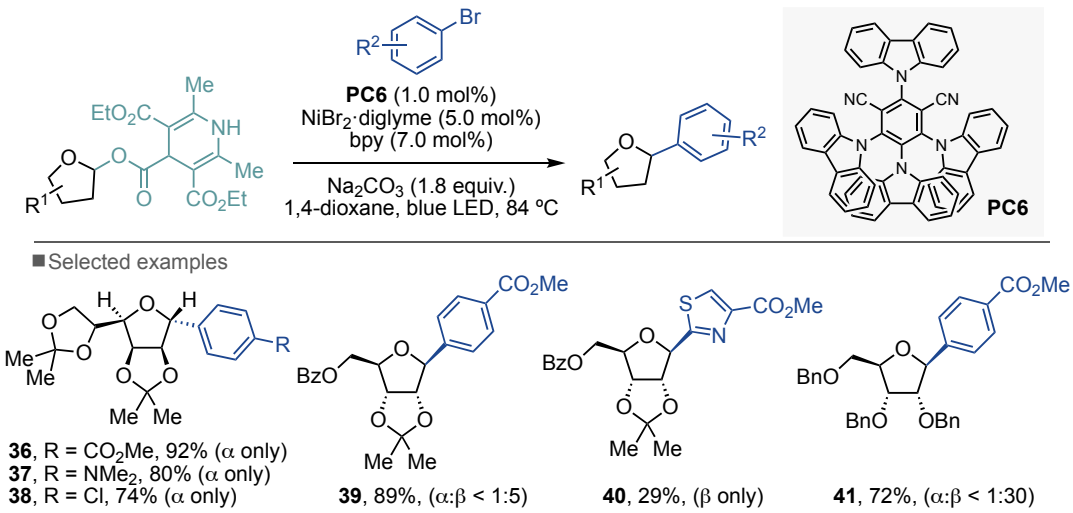

Scheme 11. Diastereoselective synthesis of *C*-aryl glycosides

Benzoxazole

In 2021, MacMillan reported an elegant method to selectively couple primary, secondary and tertiary alcohols with (hetero)aryl bromides and chlorides (Scheme 12, *left*).[40] The key feature of this approach is the *in situ* pre-activation of the alcohol moiety through condensation with a benzoxazolium salt, resulting on the formation of an activated NHC-alcohol adduct (**XXXV**). In this case, the excited-state *Ir(III) oxidises the anilinic nitrogen of **XXXV** via a single-electron transfer mechanism, as supported by Stern-Volmer experiments. Subsequently, deprotonation of the C–H bond adjacent to the resulting nitrogen radical yields an α-amino radical (**XXXVII**). Rapid β-scission from **XXXVII** gives alkyl radical **XXXIX**, and carbamate **XXXVIII**. Importantly, the formation of the carbamate moiety provides the necessary thermodynamic driving force for the homolysis of the C–O bond to take place. (Scheme 12, *middle*). The synthetic value of this transformation was demonstrated by the functionalisation of a wide number of primary, secondary, and tertiary alcohols, as well as the modification of saccharides. Notably, C2-symmetric 1,2- and 1,4-diols were diversified into complex arylated products with excellent diastereoselectivites (Scheme 12, *bottom left*). An extension of this method was released by the same group in 2022.[41] In this case, the challenging C(sp^3)–C(sp^3) cross-coupling of alcohols with carboxylic acids was accomplished, using a nickel catalyst that effectively differentiates between two alkyl radical species (Scheme 12, *right*). The distinct relative stabilities of the generated alkyl radicals and the differences in nickel-carbon bond strengths play a crucial role in this transformation. Interestingly, this methodology has been successfully applied to the construction of highly congested quaternary carbon centres. Additionally, alkylation with deuterated acetic acid has

also been demonstrated, furnishing a straightforward approach to the synthesis of labelled molecules (Scheme 12, bottom right).

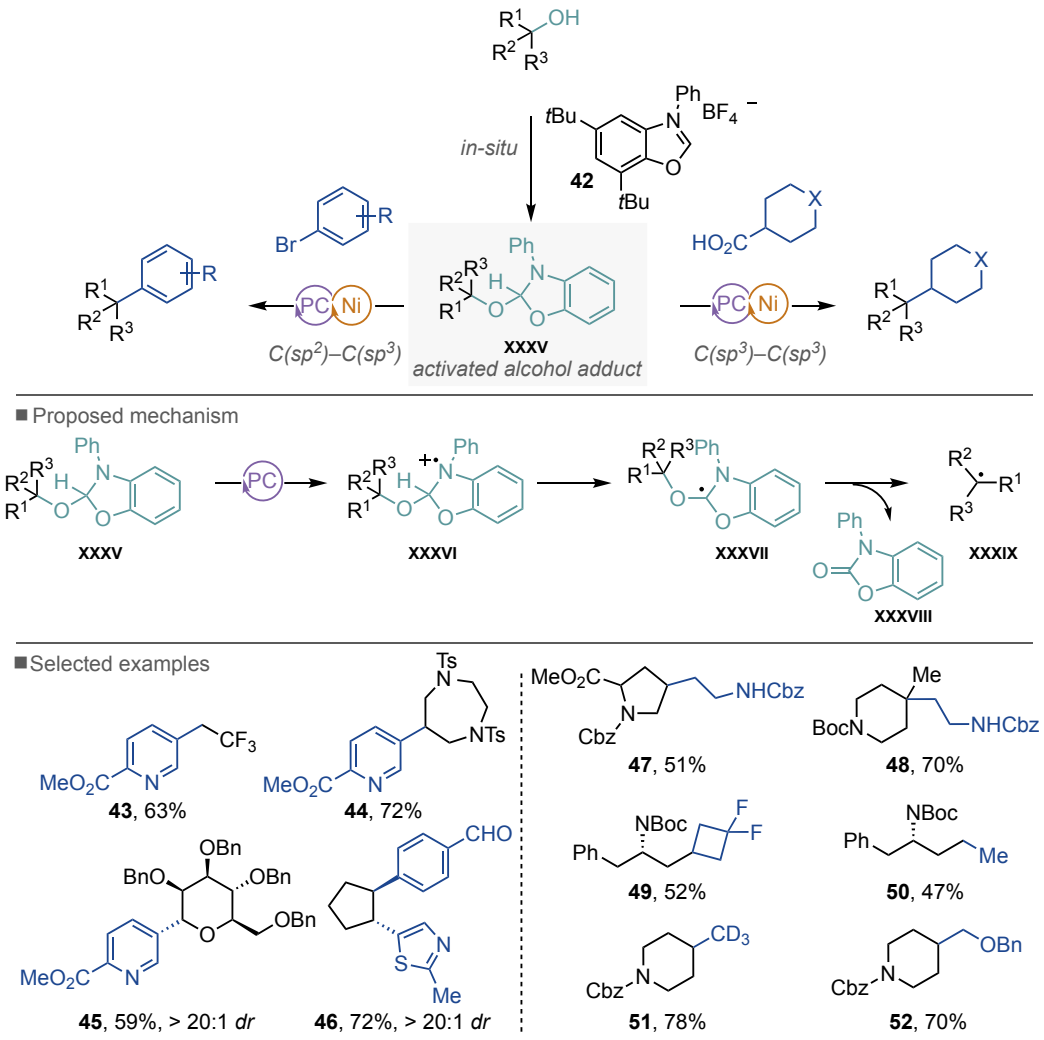

Scheme 12. Ni-metallaphotoredox C(sp^2)–C(sp^3) and C(sp^3)–C(sp^3) cross-coupling of benzoxazole-activated alcohols with (hetero)aryl halides or carboxylic acids

2.1.2.2. sp^3 C–O bond cleavage strategies via HAT

As described in Chapter 1, C–H activation by hydrogen atom transfer has been recognised as a powerful alternative to the use of redox-active substrates. In this context, Xie et al. developed a trifluoromethylthiolation method that employs dialkyl acetals as masked alcohols under a dual photocatalytic manifold (Scheme 38).[42] Initially, the excited 4CzIPN undergoes SET with the thiophosphate co-catalyst, which is oxidised to form a thiyl radical. The resulting electrophilic thiyl radical performs a highly regioselective HAT at the

most hydridic α-C–H group of the ether to generate a dialkoxyl radical. The latter evolves through β-C–O cleavage delivering a tertiary carbon-centred radical, which is finally intercepted by the *N*-(trifuoromethylthio)phthalimide and provides the targeted product.

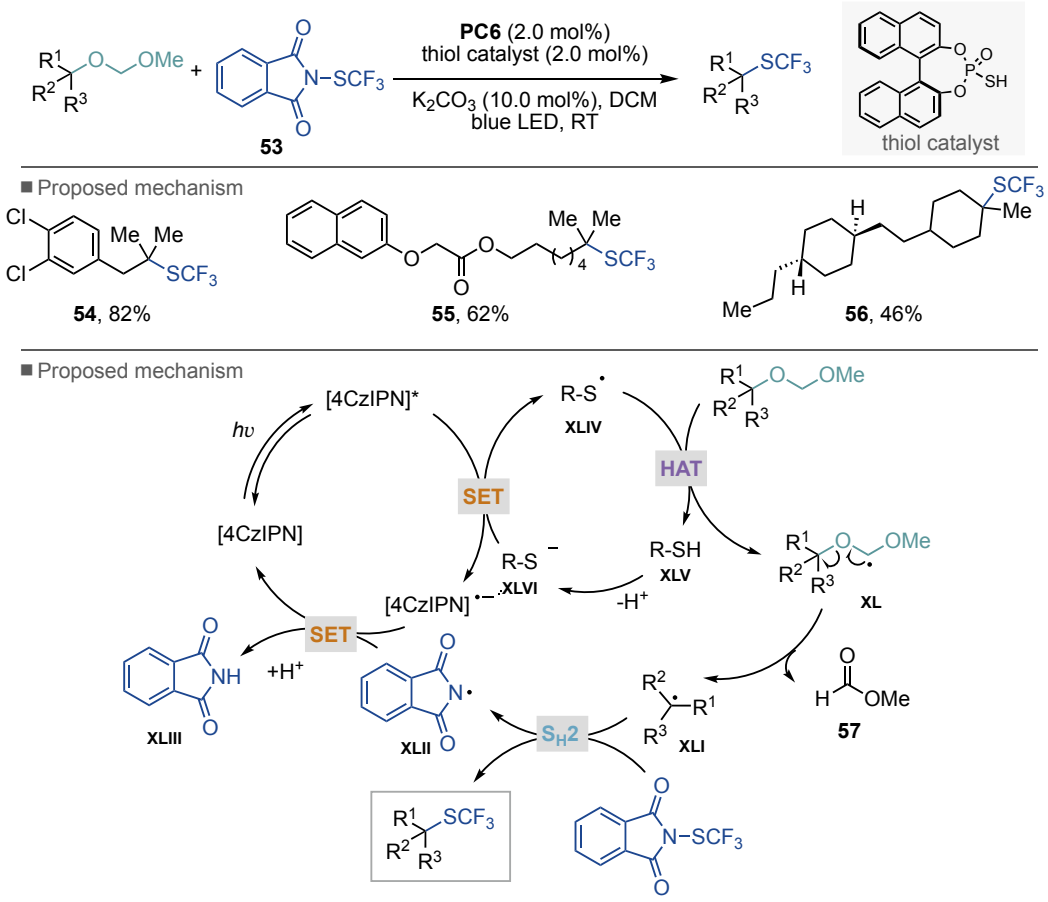

Scheme 13. Dialkyl acetals as masked alcohols

In 2022, Doyle and co-workers reported the use of benzaldehyde di(alkyl)acetals as alkyl radical precursors and engaged them in the methylation and alkylation of aryl halides.[43] In this case, the key HAT event is mediated by the bromine radical, which selectively abstracts the weak acetal *sp*³ C–H bond, triggering the following β-scission and delivering the desired alkyl radical. Stern-Volmer quenching studies provided evidence for bromide oxidation over bromine photoelimination pathway from the nickel complex.[44,45]

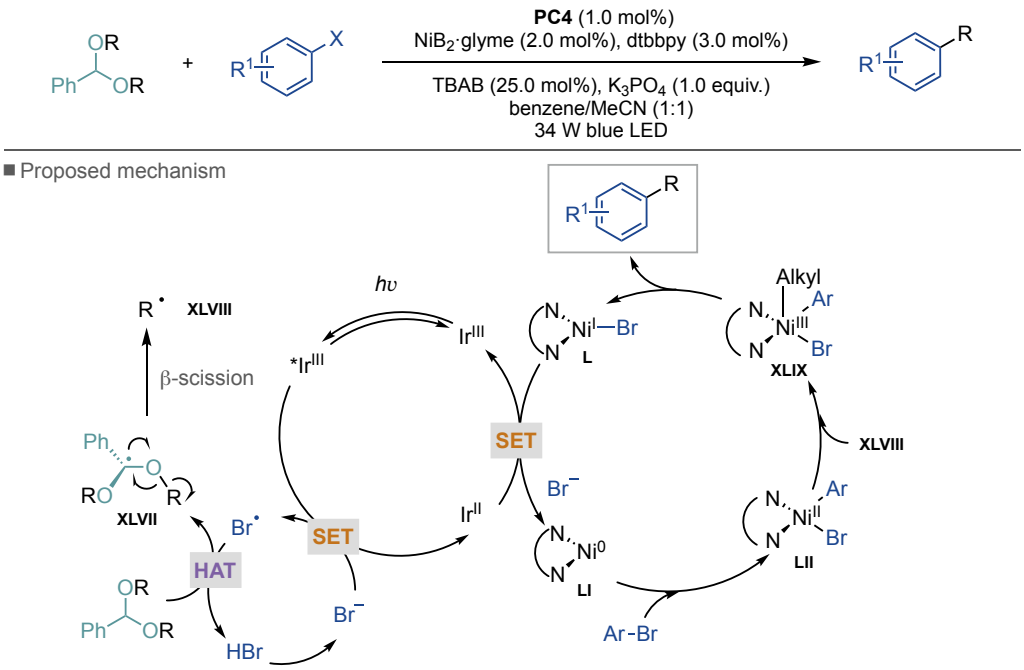

Scheme 14. Benzaldehyde di(alkyl)acetals in sp^3 C–O bond cleavage

2.1.3. Zn-mediated single-electron transfer of alkyl oxalates

Although the use of oxalate derivatives in photocatalysis was previously recognised, it was not until 2018 – when Shu firstly described it – that they started to be employed as radical precursors in the realm of nickel catalysed reductive cross-couplings.[46] The group disclosed the coupling of benzyl oxalates with primary and secondary alkyl bromides, using zinc as stoichiometric reductant. Subsequently, Gong and co-workers broadened the methodology to encompass the utilisation of methyl and *tert*-butyl oxalate derivatives for the generation of tertiary alkyl radicals.[13] This methodology permitted the synthesis of sterically hindered quaternary C–C bonds using a diverse range of electrophilic Michael-acceptors (Scheme 15, *method a*). Interestingly, in the absence of Ni catalyst, lower yields were observed for the Giese-type addition, indicating that nickel may play a non-negligible role in promoting the reaction. This protocol has been expanded to a wide array of transformations,[2,47] including arylation with aryl chlorides (Scheme 15, *method b*),[13] arylation of α-hydroxyl ester-derived oxalates,[48] arylation of cyclopropanol rings,[15] and even in the context of Fe-catalysed reactions.[49,50]

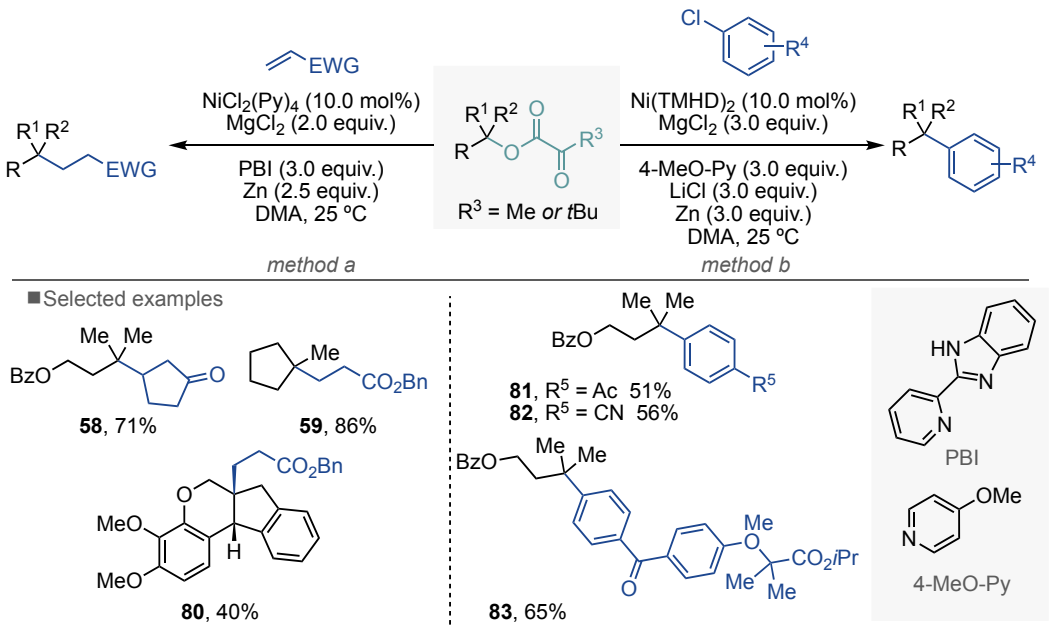

Scheme 15. Giese-type addition and arylation of tertiary alkyl radicals

From a mechanistic perspective, the reduction of dialkyl oxalates by Zn is thermodynamically unfavourable based on the reduction potentials ($E°_{red}$ = −1.26 V vs SCE in CH_3CN for *t*Butyl-methyl oxalate and $E°(Zn^{2+}/Zn)$ = −0.76 V in water and −1.0 V in DMA vs SCE, Figure 1).[51] However, in the presence of $MgCl_2$, the Mg^{2+} chelates the oxalate, lowering the energy of the carbonyl-centred LUMO, thereby facilitating the single-electron reduction from Zn. After SET, the generated radical anion can potentially undergo competitive HAT, followed by decomposition to yield an alcohol. This pathway is unproductive and dominates when secondary and primary dialkyl oxalates are employed, explaining why these methodologies are limited to the use of tertiary alcohols (Scheme 16).

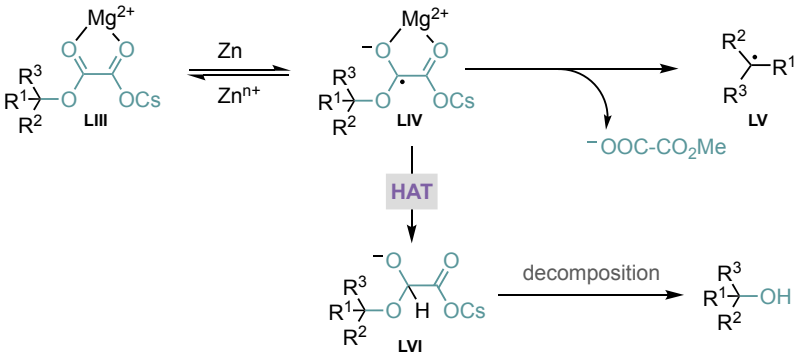

Scheme 16. Cooperative effect of Zn and $MgCl_2$ on the oxalate reduction

It is worth mentioning that several other methodologies for radical deoxygenation and deoxyfuncionalisation of sp^3 C–O bonds have been disclosed, however in most of the cases *in situ* halogenation of the corresponding alcohol moiety or activated/benzylic alcohols have been used.[2] Nonetheless, these important contributions are beyond the scope of this chapter, which deals exclusively with the strategies aimed at the functionalisation of *unactivated* sp^3 C–O bonds.

2.2. General aim of the project

At the outset of our investigation, significant progress via photoredox strategies had been made towards the functionalisation of sp^3 C–O derivatives bearing electron-withdrawing groups adjacent to the oxygen atom. However, the sp^3 C–O functionalisation of unactivated alkyl ethers still remained challenging. This is largely due to the lower tendency of alkoxides to act as leaving groups, the high activation barrier required to cleave alkyl sp^3 C–O bonds, and the site-selectivity issues arising from the possibility to cleave both alkyl sp^3 C–O sites.

Nevertheless, we recognised that a platform for the functionalisation of alkyl sp^3 C–O bonds would unravel the potential of unactivated sp^3 C–O in metallaphotoredox strategies, providing a powerful alternative to the use of pre-functionalisation methods via *in situ* or *ex situ* generation of the "active" intermediates.

Unlike the elegant reports from Doyle and co-workers, who exploited symmetrical acyclic acetals as alkyl radical precursors, we hypothesised that benzylidene cyclic acetals could be used as vehicles to enable site-selective functionalisation of unbiased sp^3 C–O bonds, culminating in a high atom economical transformation – by preserving the integrity of the whole molecule – and offering the opportunity to discriminate between three similar sp^3 C–O sites.

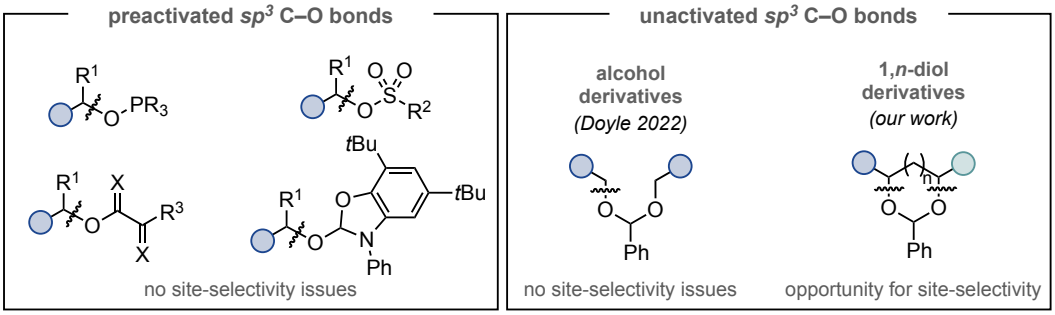

Scheme 17. Overview of sp^3 C–O electrophiles employed in cross-coupling reactions

We anticipated that a favourable SET between the excited photocatalyst and an electron-donor (quinuclidine), would generate an electrophilic radical (quinuclidinium radical cation), able to perform selective, polarity-matched, hydrogen-abstraction from the weak acetal sp^3 C–H bond. Subsequently, β-fragmentation would occur from **LVII** via an appropriate σ*–p orbital overlap enabling sp^3 C–O cleavage, generating an alkyl radical (**LVIII**). The latter could be captured by a nickel(II) complex (**LVXI**), furnishing the key aryl-Ni(III)-alkyl intermediate (**LVIX**). Reductive elimination and SET between the oxidised PC and Ni(I) species would afford the desired product and regenerate the active catalysts.

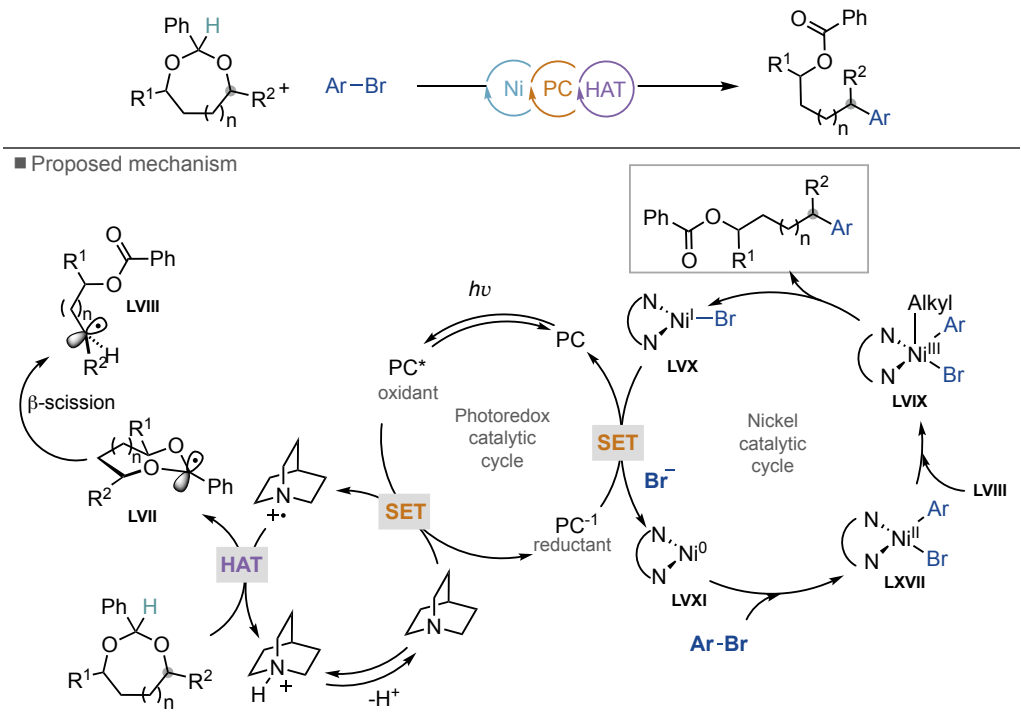

Scheme 18. Proposed catalytic cycle for site-selective functionalisation of unactivated sp^3 C–O bonds in cyclic acetals

2.3. Site-selective functionalisation of unactivated *sp*³ C–O bonds in cyclic acetals

2.3.1. Optimisation of the reaction conditions

According to the rationale design depicted in Scheme 18, we anticipated that the β-fragmentation event would only occur if a certain degree of conformational flexibility was granted upon generation of the radical at the weak acetal *sp*³ C–H bond.

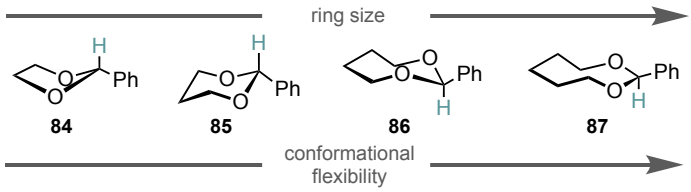

Scheme 19. Flexibility according to the ring size

To assess this hypothesis, considerable screening of the reaction conditions – *e.g.* ligands, nickel sources, temperature, photocatalysts, and HAT reagents – was performed using 5- and 6-memebered benzylidene acetals. However, we were not able to detect even traces of products arising from *sp*³ C–O bond cleavage using either five-membered 2-phenyl-1,3-dioxolane or six-membered 2-phenyl-1,3-dioxane as substrates. Therefore, our study continued by investigating the reaction of more flexible seven-membered analogue (**86**) – easily accessed by the reaction of 1,4-butanediol with benzaldehyde dimethyl acetal – with commercially available methyl 4-bromobenzoate, **88**.

The initial fine-tuning of the reaction conditions was based on the preliminary screening using 5- and 6-memebered benzylidene acetals. Our first efforts focused on the identification of an optimal solvent system that afforded the desired product in high selectivity (Table 1). The best results were achieved when using pivalonitrile, benzene or hindered alcohols (*t*BuOH and *t*AmOH). In contrast, solvents prone to undergo parasitic HAT, such as MeCN, acetone or MeOH, resulted in lower yields. It is important to note that under optimal reaction conditions different batches of *t*BuOH gave inconsistent results, probably due to variations in the water content. Interestingly, increasing the concentration to 0.2 M led to an overall yield improvement from 70 to 78%.

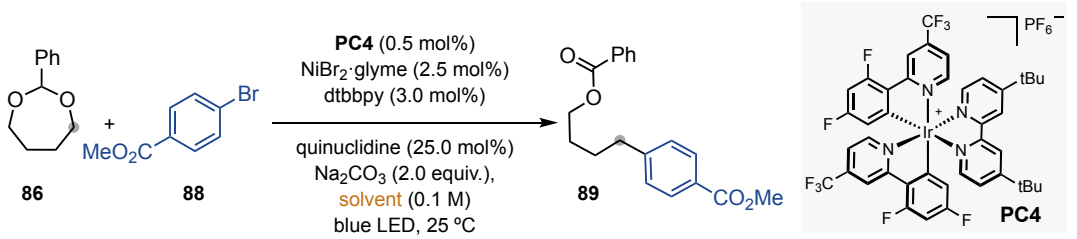

Entry	Solvent	**3a** (%)
1	MeCN	33
2	pivalonitirle	64
3	benzene	63
4	acetone	34
5	MeOH	traces
6	*t*BuOH	63
7	*t*AmOH	70
8	*t*AmOH (0.2 M)	78

Reaction conditions: **1a** (0.40 mmol, 2.0 equiv.), **2a** (0.20 mmol, 1.0 equiv.), **PC4** (0.5 mol%), $NiBr_2$·glyme (2.5 mol%), dtbbpy (3.0 mol%), quinuclidine (25.0 mol%), Na_2CO_3 (0.40 mmol), solvent (0.10 M) under blue LED irradiation, 25 ºC for 16 h. GC yields using decane as internal standard.

Table 1. Solvent screening

Next, we investigated the impact of the inorganic base on the reaction system (Table 2). Starting with carbonate bases, we rapidly realised that the choice of the counterion had a non-negligible effect. Lithium carbonate dramatically decreased the yield, while the more soluble caesium carbonate provided the product with reduced yields compared to sodium carbonate (56% vs 78%). Phosphate bases were also effective in promoting the reaction, although the weak base $(n\text{BuO})_2PO_2K$ lead to diminished yields. Likewise, weaker bases like NaOAc proved also successful.

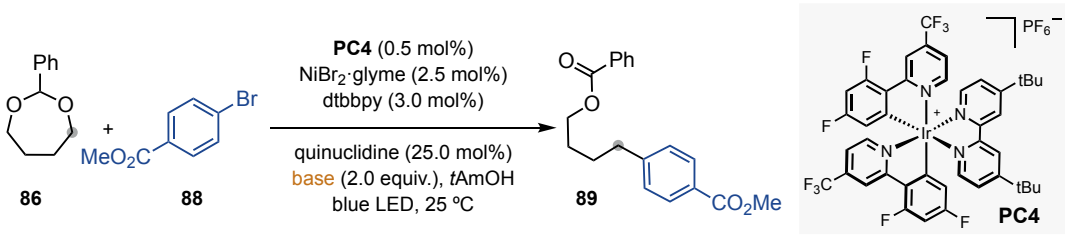

Entry	Base	**3a** (%)
1	Na_2CO_3	78
2	Li_2CO_3	traces
3	Cs_2CO_3	56
4	K_3PO4	72
5	$(n\text{BuO})_2PO_2K$	34
6	NaOAc	63

Reaction conditions: **1a** (0.40 mmol, 2.0 equiv.), **2a** (0.20 mmol, 1.0 equiv.), **PC4** (0.5 mol%), $NiBr_2$·glyme (2.5 mol%), dtbbpy (3.0 mol%), quinuclidine (25.0 mol%), base (0.40 mmol), *t*AmOH (0.20 M) under blue LED irradiation, 25 ºC for 16 h. GC yields using decane as internal standard.

Table 2. Screening of inorganic bases

As expected, the nature of the ligand employed had a profound influence on the reaction outcome (Scheme 20). Bipyridine ligands bearing electron-rich substituents on the fourth position exhibited good reactivity (**L1**, **L2** and **L3**), with the sterically demanding *tert*-butyl group providing the best results (78%). Despite the high efficiency of phenanthroline or terpyridine-type ligands in other related nickel metallaphotoredox strategies,[52–54] negligible amounts of product were obtained when using them (**L6**, and **L8**). Interestingly, while PyrOx ligands displayed comparable yields, no enantioselectivity could not be induced, despite several attempts.

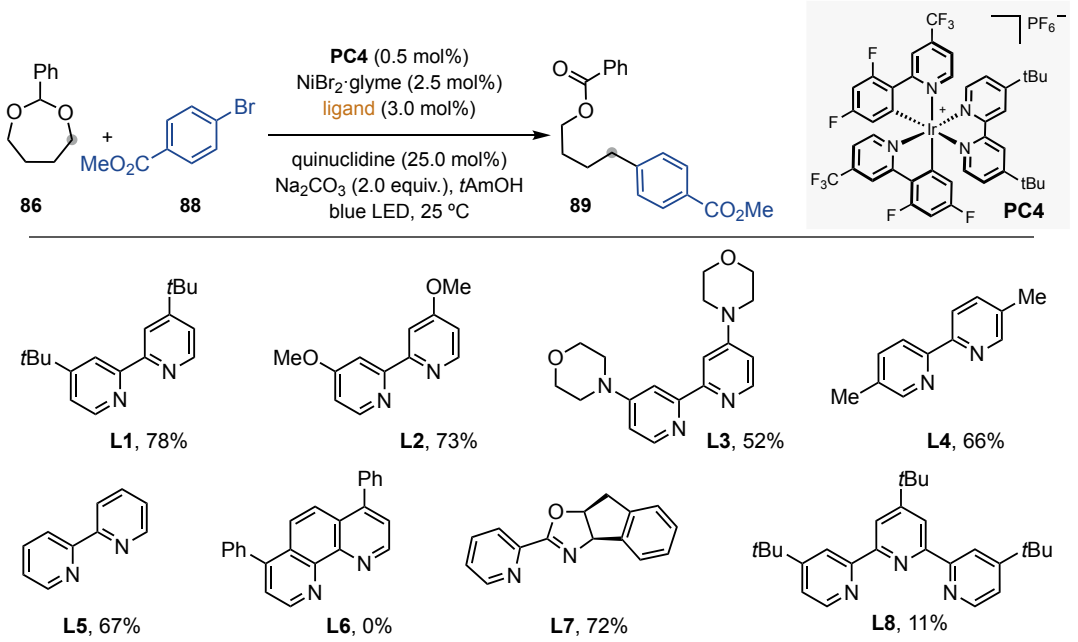

Reaction conditions: **1a** (0.40 mmol, 2.0 equiv.), **2a** (0.20 mmol, 1.0 equiv.), **PC4** (0.5 mol%), $NiBr_2$·glyme (2.5 mol%), ligand (3.0 mol%), quinuclidine (25.0 mol%), Na_2CO_3 (0.40 mmol), *t*AmOH (0.20 M) under blue LED irradiation, 25 ºC for 16 h. GC yields using decane as internal standard.

Scheme 20. Ligand screening

With these results in hand, we shifted our focus to investigating the effect of the nickel precatalyst (Table 3). Interestingly, both Ni(II) and Ni(0) sources rendered similar yields (entries 1, 5-6). However, the use of nickel halide salts other than $NiBr_2$·glyme resulted in diminished yields. The superior results obtained with bromine counterions can be tentatively attributed to the generation of bromine radicals, which could potentially act as HAT catalysts, as already reported by Molander and Doyle in related halogen atom-mediated C–H arylations.[43,44,55]

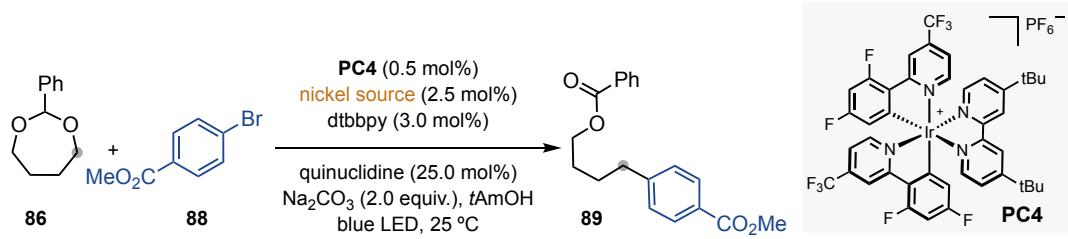

Entry	Nickel precatalyst	**3a** (%)
1	$NiBr_2$·glyme	78
2	$NiCl_2$·glyme	38
3	$Ni(OAc)_2$	0
4	NiI_2	0
5	$Ni(acac)_2$	68
6	$Ni(COD)_2$	70

Reaction conditions: **1a** (0.40 mmol, 2.0 equiv.), **2a** (0.20 mmol, 1.0 equiv.), **PC4** (0.5 mol%), nickel precatalyst (2.5 mol%), dtbbpy (3.0 mol%), quinuclidine (25.0 mol%), Na_2CO_3 (0.40 mmol), *t*AmOH (0.20 M) under blue LED irradiation, 25 ºC for 16 h. GC yields using decane as internal standard.

Table 3. Screening of nickel precatalysts

Table 4 shows the influence of different photocatalysts in the reaction outcome. The use of Ir- and Ru- photocatalyst with lower and/or higher oxidising powers resulted in lower yields or no product formation, indicating a poorer rate match between the catalytic cycles. Similarly, the use of organic photocatalyst such as 4CzIPN, or the use of photo-responsive diaryl ketones, only afforded traces of the desired cross-coupling product. Moreover, any attempt to correlate the reaction yields to the photocatalysts' triplet energy was unsuccessful, ruling out the involvement of substrate activation by energy transfer events. The results obtained during this part of the screening suggest that the choice of the photocatalyst is crucial for reaction success.

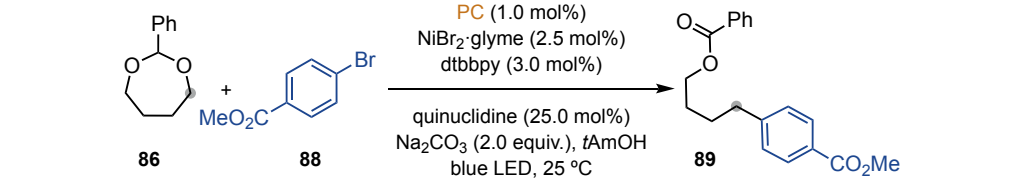

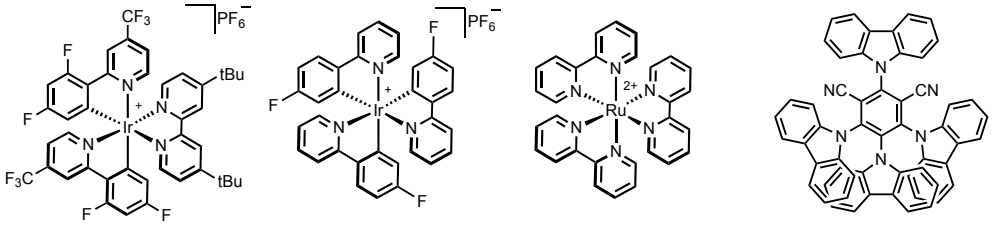

Entry	Photocatalyst	E_T (kcal·mol^{-1})	$^*E_{red}$ ($^*PC^n/PC^{n-1}$)	E_{red} ($^*PC^n/PC^{n-1}$)	**3a** (%)
1	PC4	60.0	+1.21 V	-1.37 V	78
2	PC5	49.0	+0.77 V	-1.33 V	0
3	PC3	60.1	+0.77 V	-2.00 V	0
4	PC6	55.3	+1.35 V	-1.21 V	traces
5	Ph_2CO (30 mol%)	69.1	-	-2.20 V	traces

Reaction conditions: **1a** (0.40 mmol, 2.0 equiv.), **2a** (0.20 mmol, 1.0 equiv.), **PC** (1.0 mol%), $NiBr_2$·glyme (2.5 mol%), dtbbpy (3.0 mol%), quinuclidine (25.0 mol%), Na_2CO_3 (0.40 mmol), *t*AmOH (0.20 M) under blue LED irradiation, 25 ºC for 16 h. GC yields using decane as internal standard.

Table 4. Screening of photocatalysts

Prompted by the optimal results observed when using bromine counterions, we embarked in the evaluation of a series of HAT reagents and bromide additives (Table 5). While the use of other electrophilic amines or exogenous bromide sources did not increase the efficiency of the reaction, control experiments revealed that product was obtained in the absence of quinuclidine, albeit in lower yields (entry 1 vs 8). This finding suggests that bromide, expelled by a photoexcited Ni-complex or accumulated in the reaction media at each catalytic cycle, might act as the main HAT catalyst. On the other hand, quinuclidine may operate through multiple pathways, acting as the HAT catalyst (as suggested by the ability to obtain the desired product when using aryl chlorides, entry 9), or as an organic, more soluble base (phase-transfer reagent).

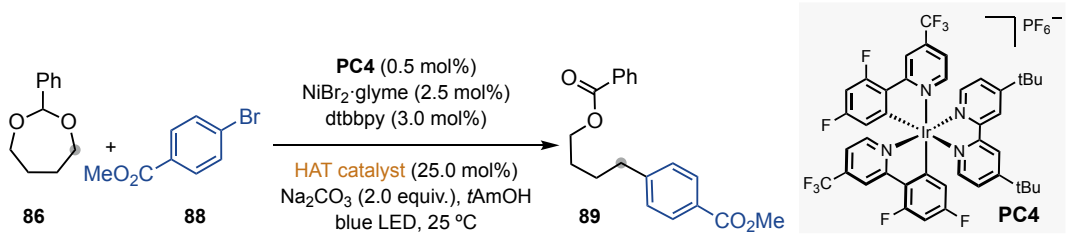

Entry	HAT catalyst	**3a** (%)
1	quinuclidine (25.0 mol%)	78
2	3-acetoxyquinuclidine (25.0 mol%)	70
3	DABCO (25.0 mol%)	47
4	TBAB (25.0 mol%)	58
5	quinuclidine and TBAB (25.0 mol% each)	62
6	quinuclidine (10.0 mol%)	76
7	quinuclidine (100.0 mol%)	29
8	-	65
9	Aryl chloride (**88-Cl**)	49

Reaction conditions: **86** (0.40 mmol, 2.0 equiv.), **88** (0.20 mmol, 1.0 equiv.), **PC4** (0.5 mol%), $NiBr_2$·glyme (2.5 mol%), dtbbpy (3.0 mol%), HAT catalyst (X mol%), Na_2CO_3 (0.40 mmol), *t*AmOH (0.20 M) under blue LED irradiation, 25 ºC for 16 h. GC yields using decane as internal standard.

Table 5. Screening of HAT catalysts

Subsequently, the stoichiometry of the reaction components was evaluated (Table 6). Interestingly, the reaction still proceeds when using a lower stoichiometry of **86**, albeit with reduced efficiencies (entries 4-5). Conversely, increasing the photocatalyst, nickel precatalyst or ligand loadings has a negative impact on the reaction outcome (entries 2,3,6).

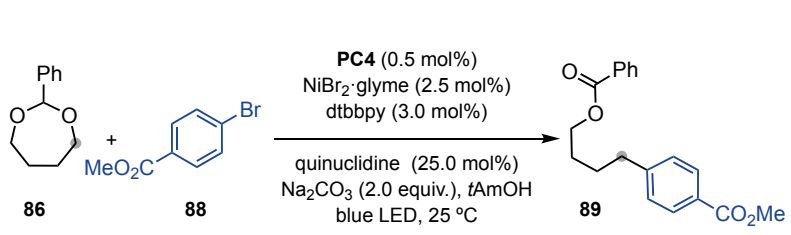

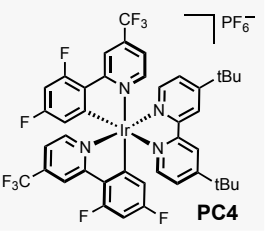

Entry	Deviation from standard conditions	**3a** (%)
1	none	78
2	5.0 mol% $NiBr_2$·glyme and 6.0 mol% dtbbpy	70
3	3.75 mol% dtbbpy	47
4	1.2 equiv. of **86**	58
5	1.5 equiv. of **86**	62
6	1.0 mol% **PC4**	76

Reaction conditions: **86** (0.40 mmol, 2.0 equiv.), **88** (0.20 mmol, 1.0 equiv.), **PC4** (1.0 mol%), $NiBr_2$·glyme (2.5 mol%), dtbbpy (3.0 mol%), quinuclidine (25.0 mol%), Na_2CO_3 (0.40 mmol), *t*AmOH (0.20 M) under blue LED irradiation, 25 ºC for 16 h. GC yields using decane as internal standard.

Table 6. Screening of the reaction components' stoichiometry

Finally, control experiments confirmed the metallaphotoredox nature of the process by the lack of reactivity in absence of light, photocatalyst or nickel precatalyst (Table 7). It is worth mentioning that critical to the success of this reaction was the use of photoreactors with low light intensity (<1 W, vs 34 W for Kessil lamps), which minimised the formation of by-products arising from protodehalogenation (entry 6).

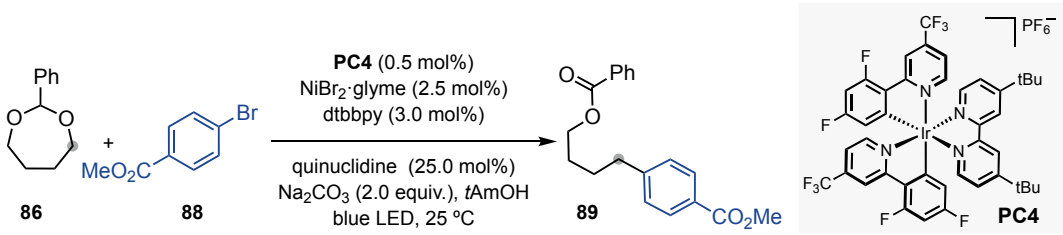

Entry	Deviation from standard conditions	**3a** (%)
1	none	78
2	No ligand	70
3	No nickel precatalyst	47
4	No PC	58
5	No light	62
6	Kessil lamps (34 W)	28

Reaction conditions: **86** (0.40 mmol, 2.0 equiv.), **88** (0.20 mmol, 1.0 equiv.), **PC4** (1.0 mol%), $NiBr_2$·glyme (2.5 mol%), dtbbpy (3.0 mol%), quinuclidine (25.0 mol%), Na_2CO_3 (0.40 mmol), *t*AmOH (0.20 M) under blue LED irradiation, 25 ºC for 16 h. GC yields using decane as internal standard.

Table 7. Control experiments

2.3.2. Substrate scope

With the optimised conditions in hand, we explored the preparative scope of our sp^3 C–O functionalisation. First, we examined the generality of our transformation with respect to the cyclic acetals (Scheme 21 and Scheme 22). As shown, when using 4-substituted 1,3-dioxepanes arylation occurred exclusively at the secondary carbon site, delivering products **92** and **94** in 83% and 69% yield, respectively. As anticipated, 5-substituted 1,3-dioxepanes (**98**) gave lower regioselectivity (2:1), however, it is worth noting that the major isomer resulted from the activation at C4, suggesting a certain stabilisation of the corresponding alkyl radical intermediate by hyperconjugation.[56]

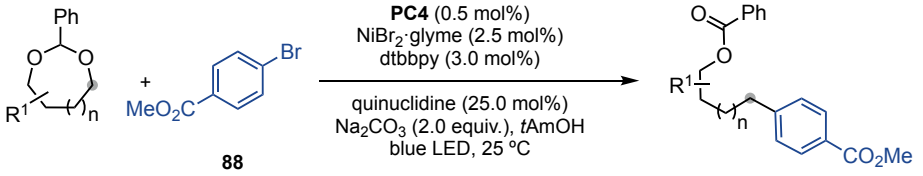

Cyclic acetal	arylated product	Cyclic acetal	arylated product
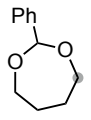 **86**	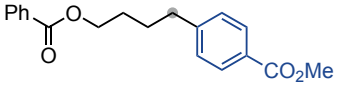 **89**, 86%	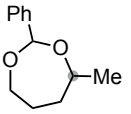 **91**	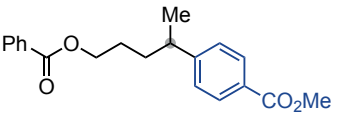 **92**, 83%
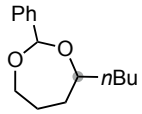 **93**	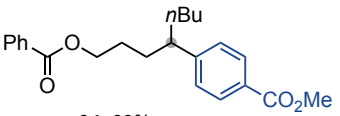 **94**, 69%	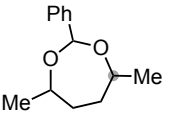 **95**	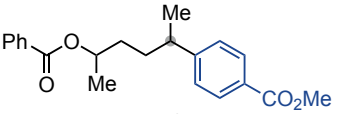 **96**, 80%[a]
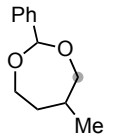 **97**	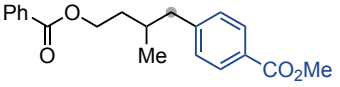 **98**, 74%[b]		

Reaction conditions: **86** (0.40 mmol, 2.0 equiv.), **88** (0.20 mmol, 1.0 equiv.), **PC4** (0.5 mol%), $NiBr_2$·glyme (2.5 mol%), dtbbpy (3.0 mol%), quinuclidine (25.0 mol%), Na_2CO_3 (0.40 mmol), *t*AmOH (0.20 M) under blue LED irradiation, 25 °C for 16 h. [a]*dr* 1:1. [b]*rr* 2:1. Isolated yields, average of two different independent runs.

Scheme 21. Scope of cyclic acetals (**I**)

Intriguingly, ring-fused 1,3-dioxepanes were well accommodated, requiring slightly higher reaction temperatures (35 ºC), probably to overcome the higher rigidity posed by the fused bicyclic structure, affecting the key σ*–p orbital overlap required for the β-fragmentation (Scheme 22). Equally interesting was the ability to prepare **104** despite the presence of five different *sp*³ C–H bonds amendable for HAT. Moreover, the product from **105,** which contains seven nucleophilic carbinolic *sp*³ C–H bonds adjacent to oxygen atoms, could also be obtained in a low 34% yield as a single product. A simple esterification of the pending hydroxyl moieties led to the corresponding product (**108**) in greatly enhanced yields. Markedly, our *sp*³ C–O functionalisation methodology was not limited to 7-membered cyclic acetals but could also be extended to larger 8-membered dioxocanes with equal ease under otherwise identical reaction conditions (**111**, **113**).

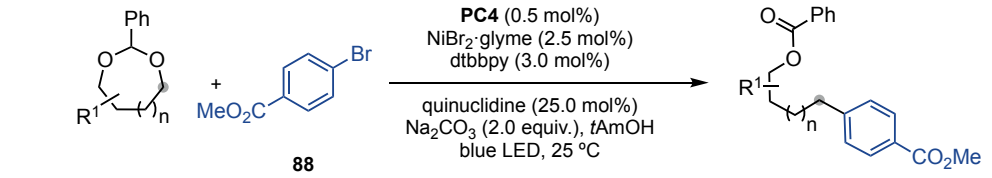

Cyclic acetal	arylated product	Cyclic acetal	arylated product
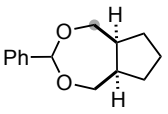 **99**	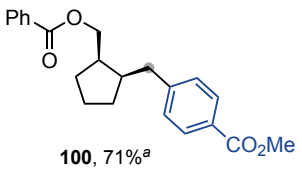 **100**, 71%[a]	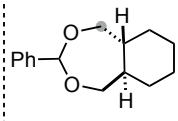 **101**	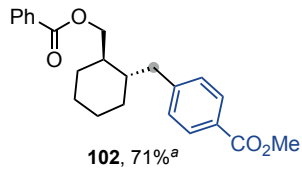 **102**, 71%[a]
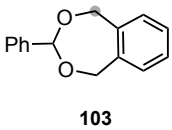 **103**	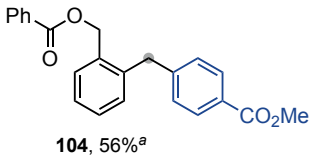 **104**, 56%[a]	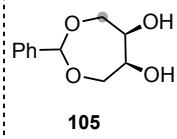 **105**	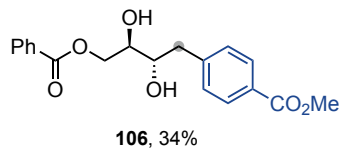 **106**, 34%
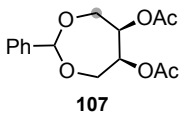 **107**	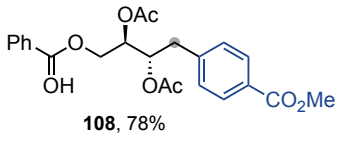 **108**, 78%	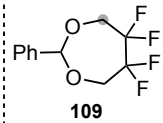 **109**	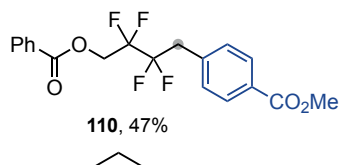 **110**, 47%
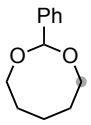 **111**	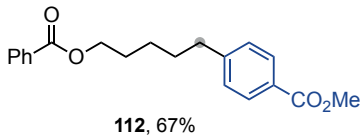 **112**, 67%	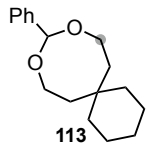 **113**	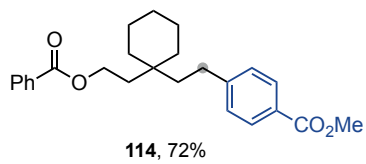 **114**, 72%

Reaction conditions: **99-113** (0.40 mmol, 2.0 equiv.), **88** (0.20 mmol, 1.0 equiv.), **PC4** (0.5 mol%), $NiBr_2$·glyme (2.5 mol%), dtbbpy (3.0 mol%), quinuclidine (25.0 mol%), Na_2CO_3 (0.40 mmol), *t*AmOH (0.20 M) under blue LED irradiation, 25 ºC for 16 h. [a]35 ºC. Isolated yields, average of two different independent runs.

Scheme 22. Scope of cyclic acetals (**II**)

Next, we moved our attention to test different aryl bromides (Scheme 23). The present method accommodates both electron-rich and electron-poor aryl bromides, the latter typically providing higher yields. The presence of sulfonamides (**123**), alcohols (**127**), nitriles (**126**) or ketones (**128**, **134**, **136**) showed the good chemoselectivity profile of the procedure. Moreover, product **124** was obtained in good yield (60%) despite the presence of allylic and ethereal hydrogens, which can potentially lead to unproductive HAT pathways. Boronic esters (**120**) or chlorides (**115**) were tolerated as well, leaving an additional handle for further derivatisations. Even heteroaryl bromides, containing benzofuran, thiophen, pyridine or quinoline cores did not interfere with productive cross-coupling. Interestingly, no racemisation was found for compounds bearing enantioenriched stereocenters (**135**).

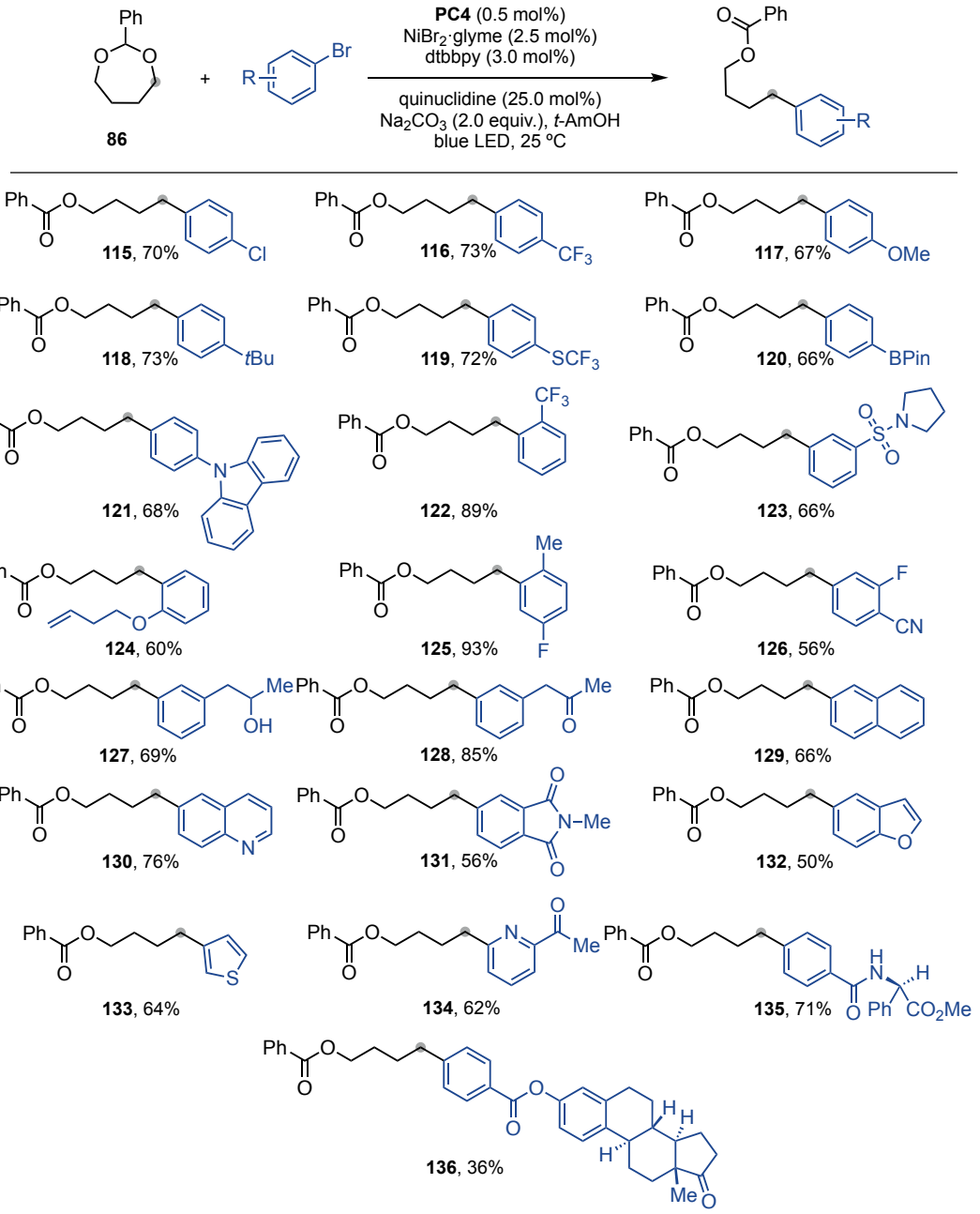

Reaction conditions: **86** (0.40 mmol, 2.0 equiv.), **2b-m** (0.20 mmol, 1.0 equiv.), **PC4** (0.5 mol%), $NiBr_2$·glyme (2.5 mol%), dtbbpy (3.0 mol%), quinuclidine (25.0 mol%), Na_2CO_3 (0.40 mmol), *t*AmOH (0.20 M) under blue LED irradiation, 25 ºC for 16 h. Isolated yields, average of two independent runs.

Scheme 23. Scope of aryl bromides

The opportunity to extend this approach beyond the construction of C(sp^3)–aryl linkages would arguably increase its synthetic applicability, due to the increasing demand of *C*(sp^3)-enriched molecules in medicinal chemistry programmes. However, the coupling of two C(sp^3) fragments and the formation of C(sp^3)–vinyl bonds still represent a challenging endeavour in the realm of unactivated sp^3 C–O manipulation strategies. Nonetheless, after fine-tuning of the reaction conditions, we found that our protocol could be extended to vinyl bromides and unactivated alkyl halides, albeit with slightly diminished yields (Scheme 24).

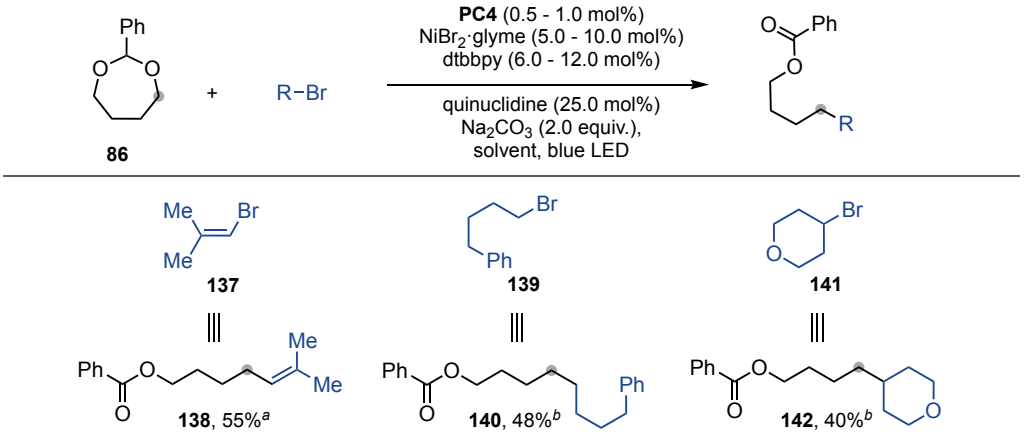

Reaction conditions: [a] **86** (0.40 mmol, 2.0 equiv.), **137** (0.20 mmol, 1.0 equiv.), **PC4** (1.0 mol%), $NiBr_2$·glyme (5.0 mol%), dtbbpy (6.0 mol%), quinuclidine (25.0 mol%), Na_2CO_3 (0.40 mmol), *t*AmOH (0.20 M) under blue LED irradiation, 25 ºC for 16 h. [b] **86** (0.40 mmol, 2.0 equiv.), **139-141** (0.20 mmol, 1.0 equiv.), **PC4** (0.5 mol%), $NiBr_2$·glyme (10 mol%), dtbbpy (12 mol%), quinuclidine (25.0 mol%), Na_2CO_3 (0.40 mmol), 5Å MS (30 mg), benzene (0.20 M) under blue LED irradiation, 25 ºC for 48 h. Isolated yields, average of two different independent runs.

Scheme 24. Scope of vinyl halides and unactivated alkyl bromides

2.3.3. Preliminary mechanistic studies

To gain further information about the mechanistic subtilities of the reaction, we decide to conduct a series of control experiments. We initiated our studies by performing a kinetic isotope effect experiment (KIE) by comparing the initial rates of **86** and **143** at different reaction times. The results showed a k_H/k_D = 1, suggesting that the sp^3 C–H cleavage might not be involved in the rate-determining-step (Scheme 25).

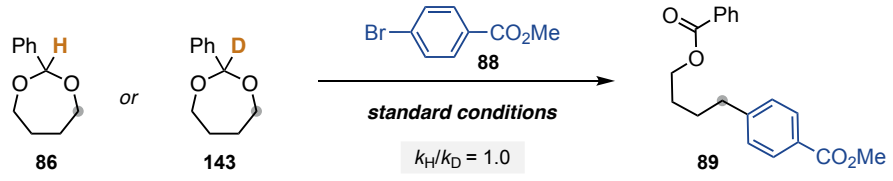

Scheme 25. Kinetic isotope effect

As described in Scheme 18, we anticipated a selective HAT at the weak benzylidene position of **I**, from either the bromine radical or the electrophilic quinuclidinium radical cation. To determine if the HAT event is highly selective or a reversible process which evolves further only when the acetalic radical is formed, we prepared **144** and analysed any erosion in deuterium content. The formation of only one product (**154**), demonstrates the lack of D/H scrambling, supporting that HAT occurs exclusively at the benzylidene position (Scheme 26).

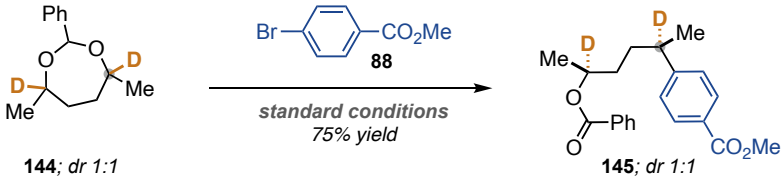

Scheme 26. Competitive HAT at different *sp*³ C–H sites

To confirm the radical nature of the C–O cleavage, we conducted the standard reaction in presence of TEMPO (2,2,6,6-tetramethylpiperidin-1-yl)oxyl) as radical scavenger (Scheme 27). Under these reaction conditions no product was formed, while **89-TEMPO** adduct could be detected by GC-MS analysis, and its identity supported by the corresponding fragmentation pattern.

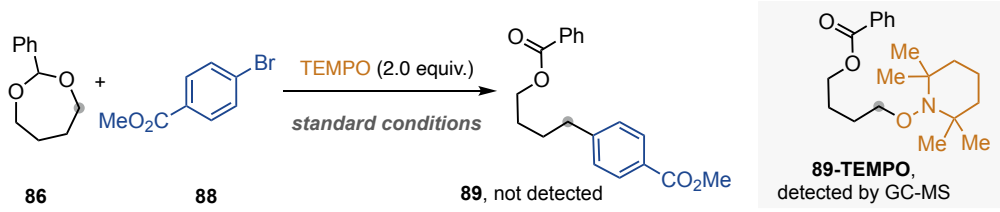

Scheme 27. Radical-trapping experiments

Finally, we found the oxidative addition complex (**Ni-X**) to be catalytically competent, although somehow less active than the one formed *in situ* (Scheme 28). However, the current result does not allow us to determine the exact role of the nickel complex (**Ni-X**) in the catalytic cycle.

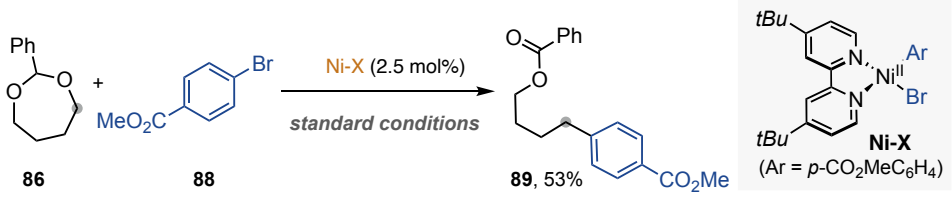

Scheme 28. Reaction performance using the oxidative addition complex **Ni-X**

With all this information in hand, we proposed two mechanistic scenarios, differing by the nature of the HAT catalyst (quinuclidine or bromine radical).

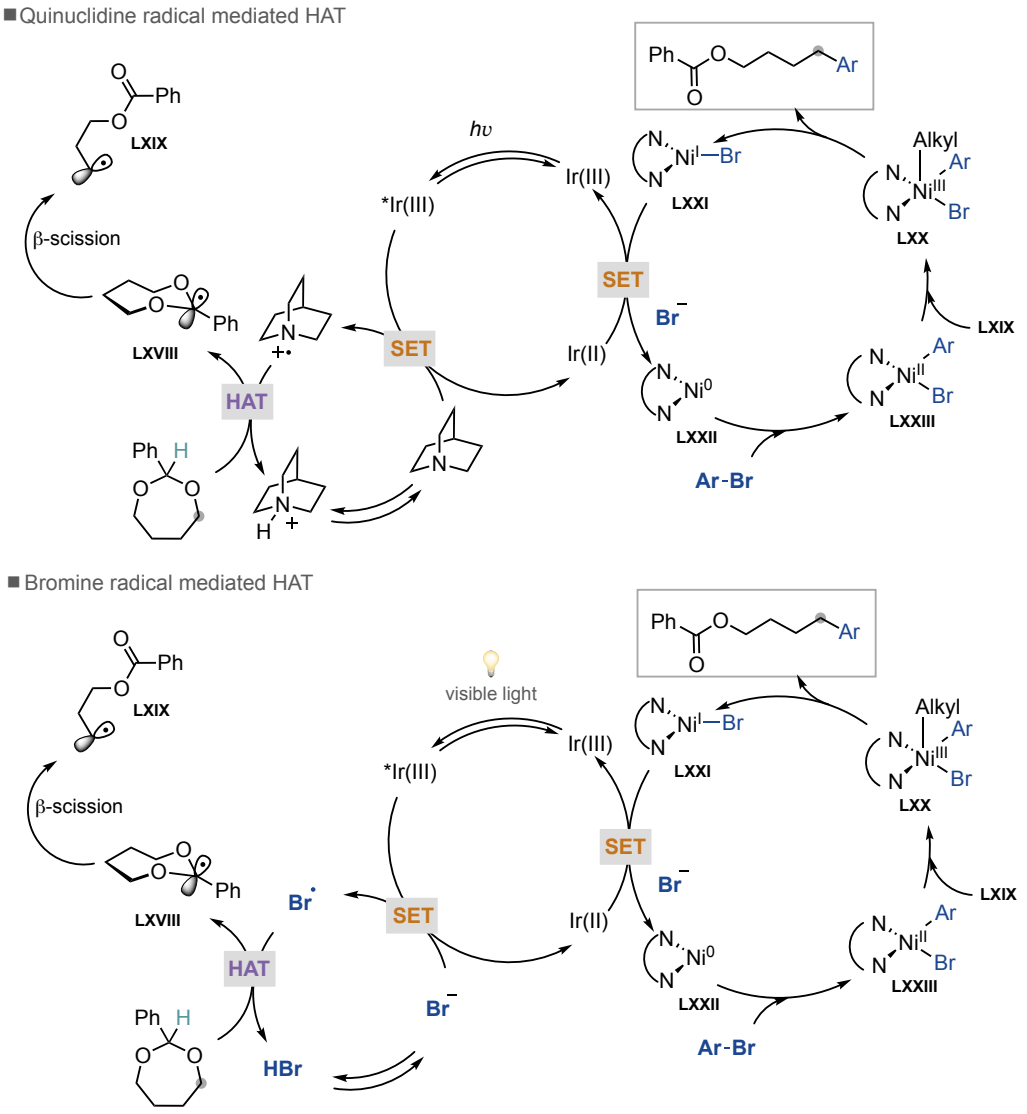

Scheme 29. Proposed mechanistic scenarios

2.3.4. DFT studies

As anticipated by the unsuccessful attempts to promote the sp^3 C–O functionalisation of five- and six-membered benzylidene acetals, it is evident that the fragmentation step only occurs when a certain degree of conformational flexibility is allowed upon radical generation. The higher degree of freedom in larger rings facilitates the necessary σ*-p orbital overlap.

To validate this hypothesis and assess the energy profiles in different ring sizes, DFT calculations were conducted out by Prof. Enrique Gomez-Bengoa at UPV/EHU (San Sebastian). In the case of six-membered rings, a noticeable accumulation of ring strain is

observed as the reaction proceeds. Notably, when comparing the stability of the resulting radical from six-membered and seven-membered acetals, a significant destabilisation of 2.9 kcal·mol^{-1} is observed for the former. This destabilisation is likely attributed to the higher distortion of the chair conformation in the case of six-membered rings when accommodating the planar *sp*^{2}-hybridised carbon in the radical intermediate.

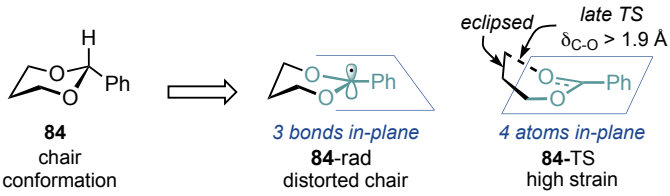

84
chair
conformation

84-rad
distorted chair

84-TS
high strain

Cyclic acetal	ΔG_{eq} (kcal·mol^{-1})	$\Delta\Delta G^{‡}$ (kcal·mol^{-1})
6-membered	2.9	21.0
7-membered	0	18.0
8-membered	1.2	18.3

Scheme 30. Relative stabilities of the generated radical

A detailed examination of the fragmentation transition state of the 6-membered acetal is particularly illustrative, as it reveals the difficult planarisation of four atoms together, along with a non-favourable eclipsed conformation of the CH_2–CH_2 fragment.

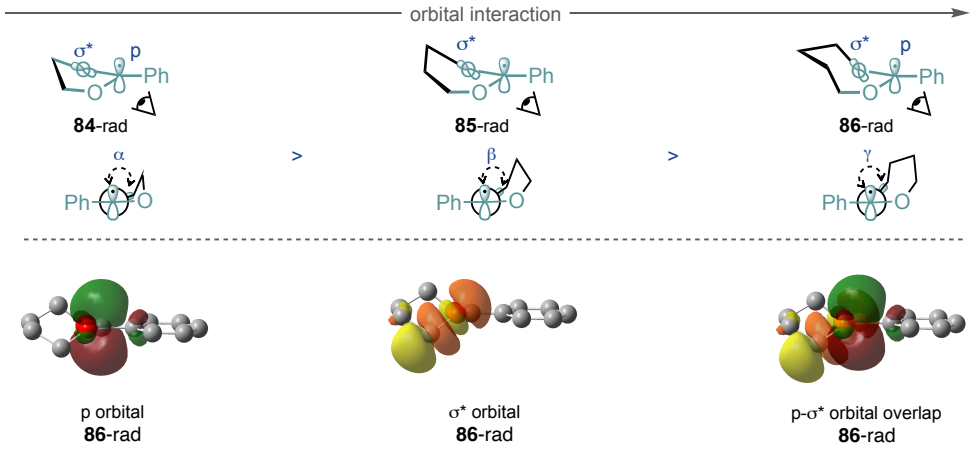

Scheme 31. Schematic representations of the interacting σ*-p orbitals within different ring sizes (*top*) and 3D-visualisation of the isolated and overlapping p and σ* orbitals (*bottom*)

Taken together, DFT calculations confirmed conformational flexibility as a key contributing factor for success in our *sp*^{3} C–O cleavage event, further explaining why all our efforts to promote the *sp*^{3} C–O arylation of either 5- and 6-memebered acetals were met with failure.

2.3.5. Preliminary ring opening and functionalisation of bicyclic benzylidene acetals

A comprehensive review of the literature reveals that in 2002, Roberts and co-workers described the regioselective ring opening via β-scission of 2-phenyl-1,3- dioxan-2-yl radicals derived from bicyclic benzylidene acetals.[57] The reported method employs a thiol-catalysed radical-chain redox rearrangement to generate benzoate esters from cyclic benzylidene acetals derived from 1,2- and 1,3-diols. This transformation occurs at 130 ºC under refluxing conditions in octane, utilising di-*tert*-butyl peroxide as the initiator in combination with triisopropylsilanethiol as the catalyst, thus greatly limiting the functional group tolerance of this method. The formation of benzoate esters is achieved through β-scission of intermediate benzylidene radicals when fused cyclohexane or cyclopentane rings are employed. The transformation illustrates two distinct modes of cleavage for each bicyclic structure, resulting in the formation of either a primary or a secondary radical. The regioselectivity of β-scission is dictated by whether the ring junction is *cis* or *trans*. In the case of the *trans*-isomer, the primary alkyl radical is preferentially obtained, whereas the *cis*-isomer affords primarily the secondary radical (with fused five membered rigs giving higher regioselectivity on the cleavage) (Scheme 32). Furthermore, DFT calculations suggest that the β-scission process occurs through a product-like transition state, where the geometry at the emerging radical centre is nearly planar. The observed regioselectivity in the β-scission of these bicyclic 1,3-dioxan-2-yl radicals can be rationalised by considering the interplay between the thermodynamic driving force, charge-transfer stabilisation of the transition state, and the degree of umbrella angle strain at the emerging radical centre.

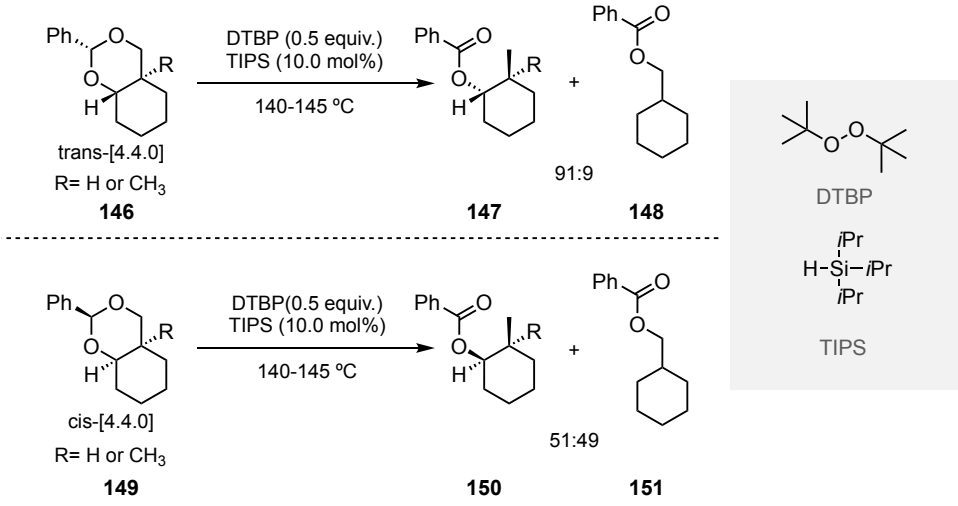

Scheme 32. Regioselective ring opening via β-scission of 2-phenyl-1,3- dioxan-2-yl radicals

Thus, we explored the applicability of our developed strategy to induce such cleavage. As depicted in Scheme 33, the desired cross-coupled product could be preliminary obtained in low yield, setting the basis for expanding the current methodology. Although preliminary, these results are rather interesting giving the paucity of this method for the direct functionalisation of carbohydrates at positions other than the anomeric carbon, unless orthogonal functional group protection/deprotection strategies are employed.

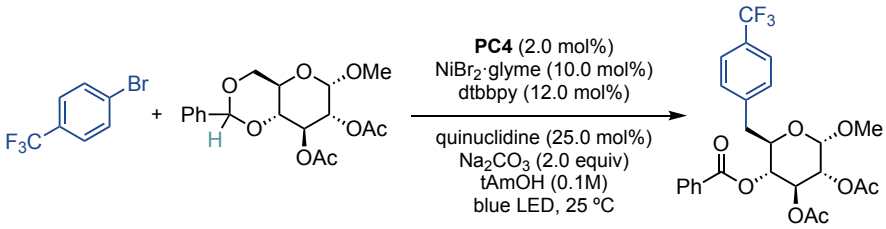

152 (1.0 equiv.) **153** (1.1 equiv.) **154**, 25%

Scheme 33. Preliminary results for the ring opening of bicyclic benzylidene acetals in carbohydrates

2.4. Conclusions

In summary, we have successfully developed a dual catalytic strategy for the functionalisation of unactivated sp^3 C−O bonds in cyclic acetals with aryl and alkyl halides. Both experimental and computational investigations have empathised the importance of conformational flexibility in both reactivity and site-selectivity. The method exhibits a broad scope, encompassing a wide number of cyclic acetals and aryl/alkyl halides, thus offering a promising avenue to improve upon existing sp^3 C−O functionalisation scenarios.

The information gathered through the optimisation of reaction conditions together with the mechanistic experiments suggests a Ni(0)/Ni(II)/Ni(III) catalytic cycle, wherein bromine radicals or quinuclidine serve as HAT reagents to selectively abstract the benzylidene C–H bond. Additional experiments, however, are required to confirm these observations and to provide further information on each elementary step.

Presently, the methodology is restricted to the use of 7- and 8-memebered cyclic acetals. However, preliminary results indicate that bicyclic 4,6-*O*-benzylidene glucoside derivatives can yield the desired product. In this case, selective β-scission of the intermediate dioxanyl radical delivers preferentially the primary C(6)-centred radical, which is subsequently trapped by nickel through and oxidative process. Ongoing investigations in our group aim to further explore and expand upon these findings.

2.5. Experimental section

2.5.1. General information

Analytical methods

^{1}H and ^{13}C NMR spectra were recorded on Bruker 400 MHz and Bruker 500 MHz at 20 °C. All ^{1}H NMR spectra are reported in parts per million (ppm) downfield of TMS and were calibrated using the residual solvent peak of $CHCl_3$ (7.26 ppm), unless otherwise indicated. All ^{13}C NMR spectra are reported in ppm relative to TMS, were calibrated using the signal of residual $CHCl_3$ (77.16 ppm) and ^{19}F NMR were obtained with ^{1}H decoupling unless otherwise indicated. Coupling constants, *J*, are reported in Hertz. Gas chromatographic analyses were performed on Hewlett-Packard 6890 gas chromatography instrument with FID detector. Flash chromatography was performed with Sigma-Aldrich silica gel, pore size 60 Å (230-400 mesh). Thin layer chromatography was used to monitor reaction progress and analyse fractions from column chromatography. To this purpose TLC Silica gel 60 F_{254} aluminium sheets from Sigma-Aldrich were used and visualisation was achieved using UV irradiation and/or staining with potassium permanganate solution. The yields reported in Table XX refer to isolated yields and represent an average of at least two independent runs. In the cases the High-Resolution Mass Spectra of the molecular ion could not be obtained using ESI and APCI ionisation modes the GC-MS of the compound was given. SFC analysis were carried out on an Agilent 1260 Infinity II SFC system.

Light Source

All reactions were performed with 451 nm LEDs (OSRAM Oslon® SSL 80 royal-blue LEDs), which were installed at the bottom of a custom-made 8 flat-bottom Schlenk tubes holder, equipped with a cooling system (the temperature was set at 20 °C) and a magnetic stirrer (~ 500 rpm).

Reagents

Commercially available materials were used as received without further purification. Nickel (II) bromide ethylene glycol dimethyl ether complex ($NiBr_2$·dme) and quinuclidine were purchased from Sigma-Aldrich and stored in a nitrogen-filled glovebox. Sodium carbonate was purchased from Sigma-Aldrich, dried at 100 ºC under vacuum overnight using P_2O_5, and stored in a nitrogen-filled glovebox. 4,4′-Di-*tert*-butyl-2,2′-dipyridyl (dtbbpy, 98% purity), Anhydrous 2-methyl-2-butanol (*tert*-Amyl alcohol, 99% purity) and Anhydrous Benzene (99.8% purity), were purchased from Sigma-Aldrich. ($Ir[dF(CF_3)ppy]_2(dtbbpy)PF_6$) was prepared according to literature.[58] 1,3-dioxepanes and 1,3-dioxecane were prepared according to **general procedure A** (see below). Commercially available aryl bromides were

purchased and used without further purification. Oxidative addition complex **Ni-I** was prepared according to a known literature procedure.[59]

2.5.2. Optimisation of the reaction conditions

General procedure used for reaction optimisation (Tables XX – XX):

To a 5 mL Crimp Top vial equipped with magnetic stirring was charged methyl 4-bromobenzoate (43.0 mg, 0.20 mmol, 1.0 equiv.), the corresponding ligand (0.03 mmol, 3.0 mol%) and photocatalyst (0.005 mmol, 0.5 mol%). Subsequently the vial was brought inside a nitrogen-filled glovebox, and the corresponding base (0.40 mmol, 2.0 equiv.), HAT reagent (0.25 mmol, 25.0 mol%) and nickel precatalyst (0.025 mmol, 2.5 mol%) were added. Then, the vial was sealed with a crimp cap and taken outside the glovebox, solvent (1.0 mL, 0.2 M) and 2-phenyl-1,3-dioxepane (71.3 mg, 0.4 mmol, 2.0 equiv.) were added sequentially via syringe. The reaction was stirred at 500 rpm under blue LED irradiation with a cooling system set at 20ºC for 16 hours. After the reaction was completed, the mixture was diluted with EtOAc, washed with water and the organic layer filtered through silica plug. The yields were determined by GC FID analysis using decane (39 μl, 0.2 mmol, 1.0 equiv.) as internal standard.

2.5.3. Starting materials synthesis

Commercially available compounds were used as received without further purification. Non-commercially available aryl bromides: 1-bromo-2-(but-3-en-1-yloxy)benzene (**2k**)[60] 1-(3-bromophenyl)propan-2-ol (**2n**)[61], methyl (*R*)-2-(4-bromobenzamido)-2-phenylacetate (**2v**)[62] and 8*R*,9*S*,13*S*,14*S*)-13-methyl-17-oxo-7,8,9,11,12,13,14,15,16,17-decahydro-6*H*-cyclopenta[*a*]phenanthren-3-yl 4-bromobenzoate (**2w**)[63] were prepared by known literature procedures. Non-commercially available diols: **1c'**, **1e'**, **1g'**, **1h'**, and **1m'** were prepared according to literature. The NMR data for all these compounds is in agreement with reported literature values.

Synthesis of 1,4- and 1,5-diols

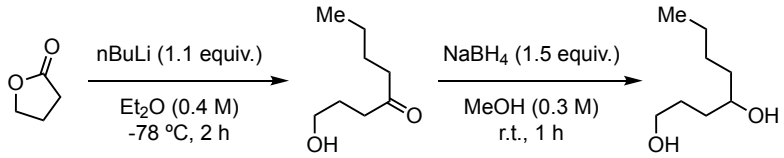

Octane-1,4-diol (**1c'**): γ-butyrolactone (6.0 mmol, 517 mg) was used for the synthesis of 1-hydroxyoctan-4-one, following a reported procedure.[64] After workup, the crude product was used in the next step without further purification. Reduction of the intermediate keto alcohol was conducted with $NaBH_4$ (9 mmol, 1.5 equiv., 340 mg) in methanol (30 mL) at room

temperature for 1 h. The reaction was quenched with sat. aq. NH_4Cl, extracted with EtOAc (x 3), dried over Na_2SO_4 and evaporated under vacuum. After hydrolytic workup, the crude product was subjected to a subsequent acetalisation without any purification.

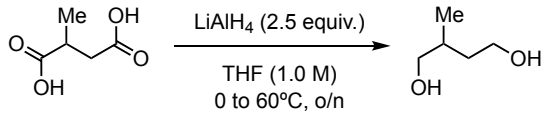

2-methylbutane-1,4-diol (**1e'**): 2-methyl succinic acid (10.0 mmol, 1.30 g) was used for the synthesis of 2-methylbutane-1,4-diol, following a reported procedure.[65] After hydrolytic workup, the crude product was subjected to a subsequent acetalisation without any purification.

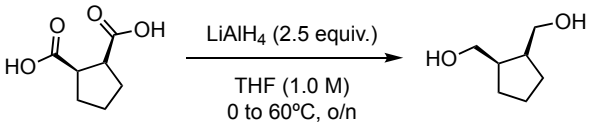

***cis*-cyclopentane-1,2-diyl)dimethanol** (**1g'**): (±)-cis-Cyclopentane-1,2-dicarboxylic acid (5 mmol, 791 mg) was used for the synthesis of *cis*-cyclopentane-1,2-diyl)dimethanol, following a reported procedure.[65] After hydrolytic workup, the crude product was subjected to a subsequent acetalisation without any purification.

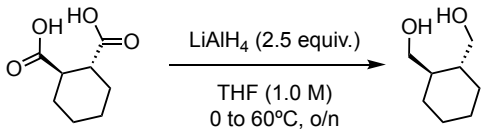

***trans*-cyclohexane-1,2-diyl)dimethanol** (**1h'**): *trans*-1,2-Cyclohexanedicarboxylic acid (5 mmol, 861 mg) was used for the synthesis of *trans*-cyclohexane-1,2-diyl)dimethanol, following a reported procedure.[65] After hydrolytic workup, the crude product was subjected to a subsequent acetalisation without any purification.

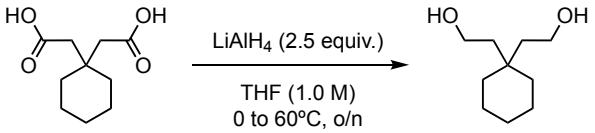

2,2'-(cyclohexane-1,1-diyl)bis(ethan-1-ol) (**1m'**): 2,2'-(cyclohexane-1,1-diyl)diacetic acid (10.0 mmol, 1.20 g) was used for the synthesis of 2-methylbutane-1,4-diol, following a reported procedure.[65] After hydrolytic workup, the crude product was subjected to a subsequent acetalisation without any purification.

Synthesis of 1,3-dioxepane and 1,3-dioxecane

General procedure A: 1,3-dioxepanes **1a-g** were prepared in analogy to a literature procedure.[66] A flame-dried 2-neck round bottom flask equipped with magnetic stirring was charged with 4 Å molecular sieves (500 mg/mmol) and then evacuated and backfilled with Ar three times. Thereafter, dry DCM (0.1M), the corresponding 1,n-diol (1.0 equiv. 8.0 mmol), benzaldehyde dimethyl acetal (1.2 equiv.) and Amberlyst® 15 hydrogen form (10 mol%) were added sequentially. The reaction mixture was stirred at room temperature for 24 hours. After that, the reaction mixture was filtered through Celite® 545, washed with DCM and concentrated under reduced pressure. The crude was then filtered through a short silica plug eluting with Toluene and concentrated under reduced pressure. Purification by Kugelrohr distillation under high vacuum afforded the title compound. Purified compounds were stored at 2–8 ºC under nitrogen atmosphere.

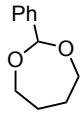

2-phenyl-1,3-dioxepane (**1a**): Following the **general procedure A**, using (8.0 mmol), the product was purified by distilling off the remaining reagents by Kugelrohr distillation (90 ºC, 3 mbar). The product **1a** was obtained in 61% yield (864 mg) as a colourless oil. **^{1}H NMR** (400 MHz, d_8-Toluene) δ 7.61 – 7.59 (m, 2H), 7.23 – 7.18 (m, 2H), 7.14 – 7.11 (m, 1H), 5.66 (s, 1H), 3.73 – 3.67 (m, 2H), 3.54 – 3.48 (m, 2H), 1.45 – 1.40(m, 4H) ppm. **^{13}C NMR** (101 MHz, d_8-Toluene) δ 141.0, 128.2, 128.1, 126.9, 100.6, 64.8, 29.7 ppm. **IR** (neat, 3089, 3062, 3032, 2940, 2874, 1495, 1451, 1438, 1377, 1359, 1336, 1311, 1286, 1274, 1231, 1221, 1204, 1174, 1131, 1108, 1081, 1053, 1028, 1007, 936, 922, 866, 832, 738, 697, 671, 530 cm^{-1}). **HRMS**: m/z calcd. for ($C_{11}H_{14}O_2$) $[M]^+$: 178.0994 found 178.2950, ($C_{11}H_{15}O_2$) $[M+H]^+$: 179.1067 found 179.1045.

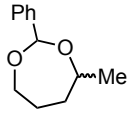

4-methyl-2-phenyl-1,3-dioxepane (**1b**): Following the **general procedure A**, using pentane-1,4-diol (10.0 mmol), the product was purified by flash column chromatography on silica gel deactivated with 1% v/v Et_3N (*n*-hexane/EtOAc 98:2). The product **1b** was obtained in 29% yield (550 mg, *d.r.* 1.4:1), as a colourless oil. **^{1}H NMR** (400 MHz, d_8-Toluene) δ 7.66 – 7.58 (m, 2H), 7.23 – 7.17 (m, 2H), 7.16 – 7.11 (m, 1H), 5.66 (s, 1H), 3.89 – 3.45 (m, 3H), 1.59 – 1.28 (m, 4H), 1.17 and 1.03 (d, 6.3 Hz, 3H) ppm.**^{13}C NMR** (101 MHz, d_8-Toluene): δ 141.2, 128.4, 128.2, 128.11, 128.09, 128.0, 127.2, 127.0, 126.9, 102.7, 100.1, 99.4, 74.0, 67.9, 66.6, 62.7, 51.8, 36.7, 36.6, 29.8, 29.1, 22.73, 22.70 ppm. **IR** (neat, 3089, 3062, 3032, 2969, 2933, 2873, 1494, 1450, 1378, 1360, 1337, 1279, 1234, 1205, 1174, 1132, 1104,

1083, 1040, 988, 962, 934, 882, 828, 743, 700, 629, 532 cm^{-1}). **HRMS**: m/z calcd. for ($C_{12}H_{16}NaO_2$) $[M+Na]^+$: 215.1053 found 215.1046.

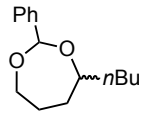

4-butyl-2-phenyl-1,3-dioxepane (**1c**): Following the **general procedure A**, using octane-1,4-diol (**1c'**) from previous step without any further purification, the product was obtained by distilling off the remaining reagents by Kugelrohr distillation (90 ºC, 3 mbar). The product **1c** was obtained in 35% yield (484 mg, *d.r.* 2:1) over three steps, as a colourless oil. **^{1}H NMR** (400 MHz, d_8-Toluene) δ 7.64 – 7.58 (m, 2H), 7.23 – 7.17 (m, 3H), 5.70 (s, 1H), 3.92 – 3.49 (m, 3H), 1.65 – 0.96 (m, 10H), 0.91 and 0.73 (t, *J* = 7.2 Hz, 3H) ppm. **^{13}C NMR** (101 MHz, d_8-Toluene) δ 141.3, 140.9, 128.1, 127.3, 126.9, 100.5, 99.7, 78.0, 71.0, 67.0, 62.7, 36.9, 36.7, 35.1, 35.0, 29.8, 29.2, 28.6, 28.1, 23.2, 22.8, 14.3, 14.2 ppm. **IR** (neat, 3089, 3063, 3032, 2933, 2872, 2860, 1494, 1451, 1378, 1358, 1345, 1279, 1234, 1205, 1175, 1109, 1077, 1041, 968, 928, 888, 743, 700, 631 cm^{-1}). **HRMS**: m/z calcd. for ($C_{15}H_{22}NaO_2$) $[M+Na]^+$: 257.1512 found 257.1507.

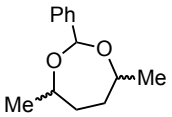

4,7-dimethyl-2-phenyl-1,3-dioxepane (**1d**): Following the **general procedure A**, using hexane-2,5-diol (10.0 mmol, mixture of diastereoisomers), the product was purified by flash column chromatography on silica gel deactivated with 1% v/v Et_3N (*n*-hexane/EtOAc 98:2). The product **1d** was obtained in 36% yield (739 mg, *d.r.* 3.9:1), as a colourless oil. **^{1}H NMR** (400 MHz, d_8-Toluene) δ 7.66 – 7.63 (m, 2H), 7.23 – 7.19 (m, 2H), 7.14 – 7.11 (m, 1H), 5.72 (s, 1H), 3.91 – 3.76 (m, 2H), 1.44 – 1.30 (m, 4H), 1.18 (d, *J* = 6.4 Hz, 3H), 1.04 (d, *J* = 6.3 Hz, 3H) ppm. **^{13}C NMR** (101 MHz, d_8-Toluene) δ 141.4, 128.1, 128.0, 127.0, 98.7, 73.1, 67.5, 36.7, 36.3, 22.8, 22.7 ppm. **IR** (neat, 3090, 3063, 3032, 2970, 2929, 2869, 1494, 1449, 1377, 1358, 1323, 1300, 1205, 1175, 1156, 1133, 1097, 1075, 1043, 1028, 1007, 937, 924, 890, 870, 847, 749, 709, 696, 628 cm^{-1}). **HRMS** m/z calcd. for ($C_{13}H_{18}NaO_2$) $[M+Na]^+$: 229.1199 found 229.1200.

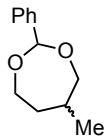

5-methyl-2-phenyl-1,3-dioxepane (**1e**): Following the **general procedure A**, using 2-methylbutane-1,4-diol (**1e'**, 6.3 mmol) prepared from the previous step without any further

purification, the product was obtained by distilling off the remaining reagents by Kugelrohr distillation (90 ºC, 3 mbar). The product **1e** was obtained in 49% yield (602 mg, *d.r.* 1:1), as a colourless oil. **^{1}H NMR** (400 MHz, d_8-Toluene) δ 7.63 – 7.60 (m, 2H), 7.24 – 7.19 (m, 2H), 7.15 – 7.10 (m, 1H), 5.71 and 5.69 (s, 1H), 3.80 – 3.68 (m, 1H), 3.65 – 3.55 (m, 1H), 3.51 – 3.31 (m, 2H), 1.73 – 1.59 (m, 1H), 1.50 – 1.38 (m, 1H), 1.26 – 1.16 (m, 1H), 0.71 and 0.65 (d, *J* = 6.9 Hz, and 6.9 Hz, 3H) ppm. **^{13}C NMR** (101 MHz, d_8-Toluene): δ 141.0, 128.1, 126.9, 100.6, 100.5, 71.7, 68.6, 64.5, 61.5, 38.2, 38.0, 34.6, 34.5, 17.1, 16.9 ppm. **IR** (neat, 3090, 3063, 3032, 2951, 2932, 2872, 1495, 1451, 1432, 1338, 1310, 1277, 1259, 1228, 1206, 1176, 1142, 1108, 1084, 1046, 1029, 974, 931, 896, 828, 738, 698, 671, 557 cm^{-1}). **HRMS**: m/z calcd. for ($C_{12}H_{16}NaO_2$) $[M+Na]^+$: 215.1043 found 215.1048.

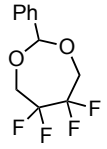

5,5,6,6-tetrafluoro-2-phenyl-1,3-dioxepane (**1f**): Following the **general procedure A**, using 2,2,3,3-tetrafluorobutane-1,4-diol (2.0 mmol), the product was purified by distilling off the remaining reagents by Kugelrohr distillation (90 ºC, 3 mbar). The product **1f** was obtained in 79% yield (395 mg) as a white solid. m.p.: 49-51 ºC. **^{1}H NMR** (400 MHz, d_8-Toluene): δ 7.29 – 7.27 (m, 2H), 7.13 – 7.07 (m, 3H), 5.26 (s, 1H), 3.61 – 3.51 (m, 2H), 3.39 – 3.30 (m, 2H) ppm. **^{13}C NMR** (101 MHz, d_8-Toluene) δ 136.9, 129.3, 128.6, 126.6, 117.3 (t, $^{2}J_{CF}$ = 30.3 Hz), 114.8 (t, $^{2}J_{CF}$ = 30.3 Hz), 100.4, 61.5 – 60.9 (m) ppm. **^{19}F NMR** (376 MHz, Tol) δ -127.5 □ -127.7 (m) ppm. **IR** (neat, 3068, 3031, 3021, 2988, 2944, 2916, 1690, 1494, 1454, 1445, 1389, 1366, 1340, 1311, 1270, 1234, 1200, 1130, 1107, 1053, 1027, 1008, 943, 925, 908, 861, 748, 710, 698, 674, 663, 633, 570, 550, 523, 511, 412cm^{-1}). **HRMS**: m/z calcd. for ($C_{11}H_{11}F_4O_2$) $[M+H]^+$: 251.0690 found 251.0686.

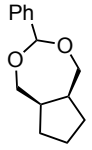

(+/-) 3-phenylhexahydro-1*H*-cyclopenta[*e*][1,3]dioxepine (**1g**): Following the **general procedure A**, using *cis*-cyclopentane-1,2-diyl)dimethanol (**1g'**, 4.1 mmol) prepared from previous step without any further purification, the product was obtained by distilling off the remaining reagents by Kugelrohr distillation (120 ºC, 3 mbar). The product **1g** was obtained in 54% yield (587 mg) over two steps, as a white solid. m.p.: 40-43 ºC. **^{1}H NMR** (400 MHz, d_8-Toluene) δ 7.66 – 7.59 (m, 2H), 7.23 – 7.18 (m, 3H), 5.50 and 5.49 (s, 1H), 3.78 (dd, *J* = 12.2, 4.2 Hz, 1H), 3.70 (dd, *J* = 12.3, 4.9 Hz, 1H), 3.56 – 3.52 (m, 1H), 3.39 (dd, *J* = 12.2, 8.8 Hz, 1H), 2.19 – 2.11 (m, 1H), 1.94 – 1.88 (m, 1H), 1.58 – 1.45 (m, 4H), 1.38 – 1.26 (m,

1H), 1.20 – 1.11 (m, 1H) ppm. **^{13}C NMR** (101 MHz, d_8-Toluene) δ 140.8, 140.7, 128.1, 126.93, 126.89, 104.0, 103.1, 68.4, 67.5, 43.6, 43.5, 28.5, 28.2, 25.3, 24.5 ppm. **IR** (neat, 3088, 3062, 3032, 2945, 2858, 1495, 1473, 1448, 1388, 1369, 1349, 1314, 1279, 1255, 1212, 1175, 1158, 1111, 1028, 1005, 975, 945, 923, 914, 740, 698, 666, 594, 546 cm^{-1}). **HRMS**: m/z calcd. for ($C_{14}H_{18}NaO_2$) $[M+Na]^+$: 241.1199 found 241.1196.

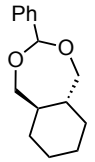

(+/-) 3-phenyloctahydrobenzo[*e*][1,3]dioxepine (**1h**): Following the **general procedure A**, using *trans*-cyclohexane-1,2-diyl)dimethanol (**1h'**, 4.15 mmol) prepared from previous step without any further purification, the product was obtained by distilling off the remaining reagents by Kugelrohr distillation (90 ºC, 3 mbar). The product **1h** was obtained in 76% yield (883 mg) over two steps, as a white solid. m.p.: 53-60 ºC. **^{1}H NMR** (400 MHz, d_8-Toluene) δ 7.66 - 7-64 (m, 2H), 7.26 – 7.22 (m, 2H), 7.17 – 7.12 (m, 1H), 5.76 (s, 1H), 3.67 (dd, *J* = 11.4, 2.9 Hz, 1H), 3.52 – 3.39 (m, 2H), 3.24 (dd, *J* = 11.7, 2.7 Hz, 1H), 1.61 – 1.53 (m, 2H), 1.35 – 1.01 (m, 6H), 0.73 – 0.63 (m, 1H), 0.61 – 0.50 (m, 1H) ppm. **^{13}C NMR** (101 MHz, d_8-Toluene) δ 141.2, 128.2, 128.1, 127.0, 100.0, 72.1, 67.0, 46.5, 46.3, 28.82, 28.75, 26.60, 26.56 ppm. **IR** (neat, 3061, 3032, 2928, 2870, 1720, 1483, 1448, 1348, 1310, 1280, 1323, 1202, 1145, 1104, 1027,993, 976, 940, 919, 901, 855, 744, 698, 671, 583 cm^{-1}). **HRMS**: m/z calcd. for ($C_{15}H_{20}NaO_2$) $[M+Na]^+$: 255.1356 found 255.1349.

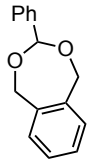

3-phenyl-1,5-dihydrobenzo[*e*][1,3]dioxepine (**1i**): Following the **general procedure A**, using 1,2-phenylenedimethanol (3.6 mmol), the product was purified by distilling off the remaining reagents by Kugelrohr distillation (90 ºC, 3 mbar). The product **1i** was obtained as in 85% yield (691 mg) as a white solid. m.p.: 76-78 ºC. **^{1}H NMR** (400 MHz, d_8-Toluene) δ 7.63 – 7.60 (m, 2H), 7.23 – 7.19 (m, 2H), 7.16 – 7.13 (m, 1H), 6.97 – 6.95 (m, 2H), 6.79 – 6.76 (m, 2H), 5.75 (s, 1H), 4.73 (d, *J* = 13.9 Hz, 2H), 4.59 (d, *J* = 13.9 Hz, 2H) ppm. **^{13}C NMR** (101 MHz, d_8-Toluene) δ 139.4, 128.5, 128.3, 127.1, 127.0, 126.9, 104.0, 69.2 ppm. **IR** (neat, 3051, 3028, 3016, 2960, 2918, 2869, 2715, 2663, 1967, 1720, 1603, 1494, 1447, 1372, 1349, 1338, 1312, 1290, 1279, 1254, 1208, 1173, 1108, 1077, 1043, 1026, 966, 942, 926, 870, 855, 742, 697, 645, 620, 424 cm^{-1}). **HRMS**: m/z calcd. for ($C_{15}H_{15}O_2$) $[M+H]^+$: 227.1067 found 227.1056.

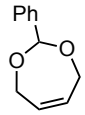

2-phenyl-4,7-dihydro-1,3-dioxepine (**1j'**): Following the **general procedure A**, using (*Z*)-but-2-ene-1,4-diol (8.0 mmol), the product was purified by distilling off the remaining reagents by Kugelrohr distillation (90 ºC, 3 mbar). The product **1j'** was obtained in 83% yield (1.2 g) as a colourless oil. **^{1}H NMR** (400 MHz, d_8-Toluene) δ 7.60 – 7.58 (m, 2H), 7.21 – 7.16 (m, 2H), 7.14 – 7.11 (m, 1H), 5.73 (s, 1H), 5.41 (t, *J* = 1.8 Hz, 2H), 4.18 – 4.11 (m, 2H), 4.00 – 3.93 (m, 2H) ppm. **^{13}C NMR** (101 MHz, d_8-Toluene) δ 139.8, 130.2, 128.4, 128.2, 127.0, 102.0, 64.2 ppm. **IR** (neat, 3088, 3063, 3031, 2974, 2941, 2897, 2856, 1723, 1703, 1493, 1451, 1387, 1371, 1341, 1312, 1258, 1207, 1108, 1072, 1030, 999, 862, 785, 739, 698, 635 cm^{-1}). **HRMS**: m/z calcd. for ($C_{11}H_{12}NaO_2$) $[M+Na]^+$: 199.0730 found 199.0722.

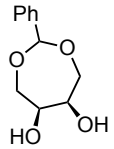

(5,6-*cis*)-2-phenyl-1,3-dioxepane-5,6-diol (**1j**): 2-phenyl-4,7-dihydro-1,3-dioxepine (**1j'**, 4.2 mmol), obtained from previous step, was dissolved in an acetone/tBuOH/water 18:1:1mixture (28 mL), then N-Methylmorpholine-oxide (NMO, 1.5 equiv., 738 mg) and OsO4 (2 mol%, 21 mg) were added. The reaction was stirred overnight at room temperature, then quenched with an aq. sat. solution of Na_2SO_3. After stirring for 2h, the mixture was extracted with EtOAc (3 x 50 mL), dried over Na_2SO_4 and the solvent was removed in vacuo. Recrystallisation from EtOAc/*n*-hexane mixture afforded **1j** in 80% yield (710 mg, *d.r.* 2:1), as a white solid. m.p.: 67-74 ºC. **^{1}H NMR** (400 MHz, d_8-Toluene) δ 7.43 – 7.39 (m, 2H), 7.19 – 7.09 (m, 3H), 5.43 (s, 1H), 3.50 – 3.18 (m, 6H), 2.21 (bd, 1H), 2.07 (bd, 1H) ppm. **^{13}C NMR** (101 MHz, d_8-Toluene) δ 139.4, 128.4, 128.3, 126.7, 126.6, 100.8, 100.5, 71.0, 70.7, 63.9, 63.1 ppm. **IR** (neat, 3439, 3372, 3063, 3035, 2969, 2938, 2891, 1453, 1401, 1374, 1348, 1334, 1268, 1243, 1212, 1159, 1122, 1097, 1072, 1049, 1030, 990, 924, 903, 818, 744, 737, 695, 636, 605, 513 cm^{-1}). **HRMS**: m/z calcd. for ($C_{11}H_{14}NaO_4$) $[M+Na]^+$: 233.0784 found 233.0781.

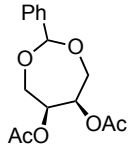

(5,6-cis)-2-phenyl-1,3-dioxepane-diyl diacetate (**1k**): In a flamed-dried 2-necked flask, 5,6-*cis*)-2-phenyl-1,3-dioxepane-5,6-diol (**1j**, 1.0 mmol, 210 mg), obtained from the previous step, was dissolved in dry pyridine (10 mL). To this solution, DMAP (0.1 mmol, 10 mol%, 12 mg) and acetic anhydride (6 mmol, 6 equiv., 0.57 mL) were added and stirred at room

temperature overnight. The reaction was quenched with brine, extracted with Et_2O (x 3) and washed multiple times with brine to remove the excess of pyridine. The organic phases were collected, dried over Na_2SO_4 and evaporated in vacuo to obtain product **1k** in 80% yield (235 mg, *d.r.* 1.6:1), as a white solid. m.p.: 52-61 ºC. **^{1}H NMR** (400 MHz, d_8-Toluene) δ 7.53 – 7.41 (m, 2H), 7.20 – 7.08 (m, 3H), 5.60 (s, 1H), 5.15 – 5.06 (m, 2H), 3.92 – 3.70 (m, 2H), 3.52 – 3.31 (m, 2H), 1.74 and 1.68 (s, 6H) ppm. **^{13}C NMR** (101 MHz, d_8-Toluene) δ 169.23, 169.17, 139.5, 139.2, 128.3, 126.8, 100.4, 100.3, 70.71, 70.66, 61.94, 61.92 ppm. **IR** (neat, 3033, 2953, 2889, 1737, 1495, 1451, 1369, 1337,1299, 1219, 1174, 1124, 1096, 1045, 1019, 948, 902, 877, 854, 742, 700, 671, 606 cm^{-1}). **HRMS**: m/z calcd. for ($C_{15}H_{18}NaO_6$) $[M+Na]^+$: 317.0996 found 317.0996.

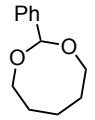

2-phenyl-1,3-dioxocane (**1l**): Following the **general procedure A**, using pentane-1,5-diol (5 mmol), the product was purified by distilling off the remaining reagents by Kugelrohr distillation (95 ºC, 3 mbar). The product **1l** was obtained in 5% yield (37 mg) as a colourless oil. **^{1}H NMR** (400 MHz, d_8-Toluene) δ 7.58 – 7.55 (m, 2H), 7.21 – 7.17 (m, 2H), 7.13-7.11 (m, 1H), 5.55 (s, 1H), 3.71 – 3.64 (m, 2H), 3.50 – 3.44 (m, 2H), 1.66 – 1.44 (m, 6H) ppm. **^{13}C NMR** (101 MHz, d_8-Toluene): δ 140.3, 1.30.4, 128.5, 128.1,101.1, 65.7, 30.4, 24.2 ppm. **IR** (neat, 3089, 3062, 3032, 2926, 2861, 1722, 1494, 1449, 1384, 1344, 1294, 1273, 1212, 1174, 1140, 1109, 1076, 1043, 988, 962, 934, 900, 737, 698 cm^{-1}). **HRMS**: m/z calcd. for ($C_{12}H_{16}O_2$) $[M]^+$: 192.1145 found 192.1136.

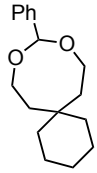

10-phenyl-9,11-dioxaspiro[5.7]tridecane (**1m**): Following the **general procedure A**, using 2,2'-(cyclohexane-1,1-diyl)bis(ethan-1-ol) (**1m'**, 6 mmol) prepared from the previous step without any further purification, the product was obtained by distilling off the remaining reagents by rotavapor distillation (40 ºC, 15 mbar). The product **1m** was obtained in 13% yield (205 mg) over two steps, as a colourless oil. **^{1}H NMR** (400 MHz, d_8-Toluene) δ 7.58 – 7.56 (m, 2H), 7.22 – 7.18 (m, 2H), 7.14 - 7.11 (m, 1H), 5.62 (s, 1H), 3.79 (ddd, *J* = 12.3, 9.4, 3.9 Hz, 2H), 3.55 (ddd, *J* = 12.4, 5.8, 4.5 Hz, 2H), 1.64 (ddd, *J* = 14.2, 9.4, 4.5 Hz, 2H), 1.48 – 1.26 (m, 12H) ppm. **^{13}C NMR** (101 MHz, d_8-Toluene): δ 140.4, 128.3, 128.2, 128.1, 127.1, 100.7, 62.5, 38.7, 35.7, 34.8, 26.8, 22.4, 22.2 ppm. **IR** (neat, 3088, 3062, 3031, 2922, 2855, 1994, 1451, 1346, 1310, 1283, 1265, 1235, 1204, 1175, 1123, 1108, 1082, 1058, 1028,

1016, 929, 888, 739, 699 cm^{-1}). **HRMS**: m/z calcd. for ($C_{17}H_{24}O_2$) $[M]^+$: 260.1771 found 260.1761.

2.5.4. General procedures for arylated and alkylated products

General procedure B (Schemes XX-XX): To a 5 mL Crimp Top vial equipped with magnetic stirring was charged methyl 4-bromobenzoate (**2a**, 43.0 mg, 0.20 mmol, 1.0 equiv.), cyclic acetal (*if solid*, 0.4 mmol, 2.0 equiv.), dtbbpy (1.6 mg, 0.03 mmol, 3 mol%) and ($Ir[dF(CF_3)ppy]_2(dtbbpy)PF_6$) (1.1 mg, 0.005 mmol, 0.5 mol%). Subsequently the vial was brought inside a nitrogen-filled glovebox, and Na_2CO_3 (42.4 mg, 0.40 mmol, 2.0 equiv.), quinuclidine (5.6 mg, 0.25 mmol, 25 mol%) and $NiBr_2$·dme (1.5 mg, 0.025 mmol, 2.5 mol%) were added. Then the vial was sealed with a crimp cap and taken outside the glovebox, were *tert*-Amyl alcohol (1.0 mL, 0.2 M) and cyclic acetal (*if liquid*, 0.4 mmol, 2.0 equiv.) were added sequentially via syringe. The reaction was stirred at 500 rpm under blue LED irradiation with a cooling system set at 20ºC for 16 hours. After the reaction was completed, the mixture was diluted with EtOAc and washed with water. The aqueous phase was washed with EtOAc (2 times), dried over anhydrous Na_2SO_4 and concentrated under reduced pressure. The crude was purified by column chromatography (see details below).

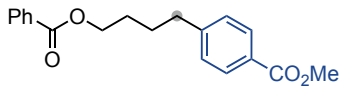

methyl 4-(4-(benzoyloxy)butyl)benzoate (**3a**): Following the **general procedure B**, using 2-phenyl-1,3-dioxepane (**1a**), the crude was purified by flash column chromatography (*n*-hexane/EtOAc, gradient: 95 :5 to 9:1), to afford **3a** (54 mg, 86% yield) as a white solid. m.p.: 57-59 ºC. **^{1}H NMR** (400 MHz, $CDCl_3$): δ 8.05 – 8.02 (m, 2H), 7.98 – 7.95 (m, 2H), 7.58 – 7.53 (m, 1H), 7.46 – 7.41 (m, 2H), 7.28 – 7.25 (m, 2H), 4.36 – 4.33 (m, 2H), 3.90 (s, 3H), 2.76 – 2.73 (m, 2H), 1.84 – 1.78 (m, 4H) ppm. **^{13}C NMR** (101 MHz, $CDCl_3$): δ 167.2, 166.7, 147.7, 133.0, 130.5, 129.9, 129.7, 128.6, 128.5, 128.1, 64.8, 52.1, 35.6, 28.4, 27.6 ppm. **IR** (neat, 3062, 3034, 2955, 2873, 1714, 1609, 1584, 1451, 1435, 1418, 1379, 1313, 1269, 1178, 1108, 1069, 1019, 967, 855, 829, 775, 707, 688, 675 cm^{-1}). **HRMS**: m/z calcd. for ($C_{19}H_{20}NaO_4$) $[M+Na]^+$: 335.1254 found 335.1255.

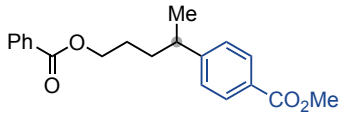

methyl 4-(5-(benzoyloxy)pentan-2-yl)benzoate (**3b**): Following the **general procedure B**, using 4-methyl-2-phenyl-1,3-dioxepane (**1b**), the crude was purified by flash column chromatography (*n*-hexane/EtOAc, 97:3), to afford **3b** (54 mg, 83% yield) as a colourless oil. **^{1}H NMR** (400 MHz, $CDCl_3$): δ 8.03 – 8.00 (m, 2H), 7.99 – 7.96 (m, 2H), 7.57 – 7.52 (m, 1H),

7.45 – 7.41 (m, 2H), 7.28 – 7.26 (m, 2H), 4.27 (t, *J* = 6.3 Hz, 2H), 3.90 (s, 3H), 2.82 (h, *J* = 6.9 Hz, 1H), 1.76 – 1.59 (m, 4H), 1.29 (d, *J* = 6.9 Hz, 3H) ppm. **^{13}C NMR** (101 MHz, $CDCl_3$) δ 167.2, 166.7, 152.6, 133.0, 130.5, 130.0, 129.6, 128.4, 128.2, 127.1, 64.9, 52.1, 39.9, 34.4, 27.0, 22.2 ppm. **IR** (neat, 3061, 3034, 2955, 2873, 1714, 1609, 1584, 1574, 1451, 1435, 1418, 1379, 1313, 1269, 1178, 1108, 1069, 1025, 1019, 967, 855, 829, 775, 707, 688, 675 cm^{-1}). **HRMS**: m/z calcd. for ($C_{20}H_{22}NaO_4$) $[M+Na]^+$: 349.1410 found 349.1415.

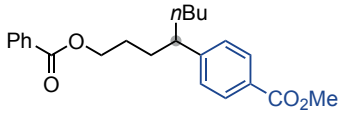

methyl 4-(1-(benzoyloxy)octan-4-yl)benzoate (**3c**): Following the **general procedure B**, using 4-butyl-2-phenyl-1,3-dioxepane (**1c**), the crude was purified by flash column chromatography (*n*-hexane/EtOAc, 97:3), to afford **3b** (51 mg, 69% yield) as a colourless oil. **^{1}H NMR** (400 MHz, $CDCl_3$): δ 8.05 – 7.92 (m, 4H), 7.57 – 7.53 (m, 1H), 7.46 – 7.41 (m, 2H), 7.24 -7.21 (m, 2H), 4.24 (t, *J* = 6.3 Hz, 2H), 3.90 (s, 3H), 2.66 – 2.58 (m, 1H), 1.87 – 1.77 (m, 1H), 1.74 – 1.51 (m, 5H), 1.32 – 1.02 (m, 4H), 0.81 (t, *J* = 7.2 Hz, 3H) ppm. **^{13}C NMR** (101 MHz, $CDCl_3$) δ 167.2, 166.7, 151.3, 133.0, 130.5, 129.9, 129.6, 128.5, 128.3, 127.8, 65.0, 52.1, 46.0, 36.6, 33.1, 29.8, 26.9, 22.8, 14.1 ppm. **IR** (neat, 3033, 2953, 2928, 2871, 2857, 1716, 1609, 1584, 1451, 1435, 1417, 1380, 1313, 1269, 1178, 1109, 1070, 1026, 1020, 966, 938, 855, 774, 708, 688, 675 cm^{-1}). **HRMS:** m/z calcd. for ($C_{23}H_{28}NaO_4$) $[M+Na]^+$: 391.1880 found 391.1883.

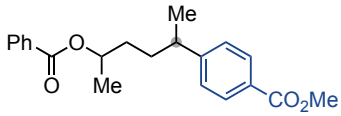

methyl 4-(5-(benzoyloxy)hexan-2-yl)benzoate (**3d**): Following the **general procedure B**, using 4,7-dimethyl-2-phenyl-1,3-dioxepane (**1d**), the crude was purified by flash column chromatography (*n*-hexane/EtOAc, 97:3), to afford **3d** (55 mg, 80% yield) as a colourless oil. dr = 1:1, determined by ^{1}H NMR. **^{1}H NMR** (400 MHz, $CDCl_3$): δ 8.03 – 7.94 (m, 4H), 7.57 – 7.52 (m, 1H), 7.45 – 4.41 (m, 2H), 7.26 – 7.23 (m, 2H), 5.18 – 5.07 (m, 1H), 3.90 and 3.90 (s, 3H), 2.77 (dp, *J* = 13.6, 6.8 Hz, 1H), 1.78 – 1.53 (m, 4H), 1.29 – 1.25 (m, 6H) ppm. **^{13}C NMR** (101 MHz, $CDCl_3$) δ 167.22, 167.21, 166.3, 166.2, 152.73, 152.69, 132.89, 132.87, 130.85, 130.85, 130.0, 129.9, 129.6, 128.42, 128.41, 128.2, 127.2, 127.1, 71.7, 71.4, 52.1, 40.1, 40.0, 34.3, 34.1, 34.0, 33.7, 22.4, 22.2, 20.2, 20.1 ppm. **IR** (neat, 3062, 3033, 2953, 2872, 1712, 1610, 1584, 1574, 1451, 1435, 1418, 1379, 1353, 1313, 1271, 1179, 1108, 1069, 1025, 1019, 1002, 968, 916, 855, 829, 773, 707, 688, 674 cm^{-1}). **HRMS:** m/z calcd. for ($C_{21}H_{24}NaO_4$) $[M+Na]^+$: 363.1567 found 363.1570.

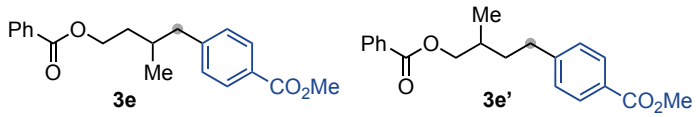

methyl 4-(4-(benzoyloxy)-2-methylbutyl)benzoate and methyl 4-(4-(benzoyloxy)-3-methylbutyl)benzoate (**3e**): Following the **general procedure B**, using 5-methyl-2-phenyl-1,3-dioxepane (**1e**), the crude was purified by flash column chromatography (*n*-hexane/EtOAc, gradient 97:3 to 96:4), to afford **3e** (48 mg, 74% yield, **3e**:**3e'=** 2:1) as a colourless oil. **^{1}H NMR** (400 MHz, $CDCl_3$): δ 8.05 – 8.00 (m, 2H), 7.97 – 7.94 (m, 2H), 7.58 – 7.54 (m, 1H), 7.46 – 7.42 (m, 2H), 7.27 – 7.22 (m, 2H), 4.44 – 4.17 (m, 2H), 3.90 (s, 3H), 2.83 – 2.51 (m, 2H), 2.04 – 1.94 (m, 1H), 1.89. – 1.80 (m, 1H), 1.65 – 1.55 (m, 1H), 1.10 and 0.96 (d, *J* = 6.7 Hz, 3H) ppm. **^{13}C NMR** (101 MHz, $CDCl_3$) δ 167.2, 167.2, 166.7, 147.9, 146.5, 133.0, 133.0, 130.49, 130.47, 129.9, 129.7, 129.6, 129.3, 128.50, 128.48, 128.1, 128.0, 69.5, 63.3, 52.1, 43.6, 35.3, 35.0, 33.4, 32.5, 32.2, 19.5, 17.1 ppm. **IR** (neat, 3062, 3033, 2952, 1714, 1610, 1584, 1451, 1435, 1416, 1389, 1313, 1269, 1177, 1105, 1070, 1021, 967, 838, 755, 709, 675 cm^{-1}). **HRMS:** m/z calcd. for ($C_{20}H_{22}NaO_4$) $[M+Na]^+$: 349.1410 found 349.1408.

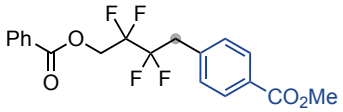

methyl 4-(4-(benzoyloxy)-2,2,3,3-tetrafluorobutyl)benzoate benzoate (**3f**): Following the **general procedure B**, using 5,5,6,6-tetrafluoro-2-phenyl-1,3-dioxepane (**1f**), the crude was purified by flash column chromatography (*n*-hexane/EtOAc, 97:3), to afford **3f** (36 mg, 47% yield) as a white solid. m.p.: 92-100 ºC. **^{1}H NMR** (400 MHz, $CDCl_3$): δ 8.09 – 8.01 (m, 4H), 7.62 – 7.58 (m, 1H), 7.49 – 7.44 (m, 2H), 7.40 – 7.38 (m, 2H), 4.80 (t, *J* = 13.9 Hz, 2H), 3.92 (s, 3H), 3.48 – 3.39 (m, 2H) ppm. **^{13}C NMR** (101 MHz, $CDCl_3$) δ 166.9, 165.4, 135.4, 133.8, 131.0, 130.1, 129.8, 128.92, 128.90 (d, $^{2}J_{CF}$ = 222,2 Hz), 128.7, 116.6 (d, $^{1}J_{CF}$ = 191.9 Hz), 60.0 (t, $^{1}J_{CF}$ = 27.0), 52.3, 36.5 (t, $^{1}J_{CF}$ = 22.5), 29.8 ppm. **^{19}F NMR** (376 MHz, $CDCl_3$) δ -113.1, 119.7 ppm. **IR** (neat, 2957, 2923, 2851, 1725, 1707, 1614, 1602, 1578, 1436, 1420, 1399, 1369, 1315, 1262, 1225, 1189, 1177, 1141, 1109, 1064, 1013, 968, 951, 903, 868, 810, 790, 759, 730, 701, 684, 673, 638, 571, 489 cm^{-1}). **HRMS:** m/z calcd. for ($C_{19}H_{16}F_4NaO_4$) $[M+Na]^+$: 407.0877 found 407.0882.

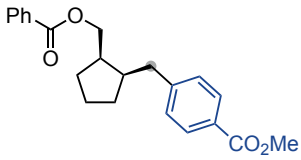

***(cis)* methyl 4-((2-((benzoyloxy)methyl)cyclopentyl)methyl)benzoate** (**3g**): Following the **general procedure B**, using (+/-) 3-phenylhexahydro-1*H*-cyclopenta[*e*][1,3]dioxepine (**1g**), at 35ºC for 48 hours, the crude was purified by flash column chromatography (*n*-hexane/EtOAc, 97:3), to afford **3g** (50 mg, 71% yield) as a colourless oil. **^{1}H NMR** (400 MHz, $CDCl_3$): δ 8.05 – 8.02 (m, 2H), 7.96 – 7.93 (m, 2H), 7.59 – 7.54 (m, 1H), 7.47 – 7.43 (m, 2H), 7.26 – 7.24 (m, 2H), 4.41 – 4.29 (m, 2H), 3.90 (s, 3H), 2.94 (dd, *J* = 13.4, 5.1 Hz, 1H), 2.55 – 2.46 (m, 2H), 2.44 – 2.34 (m, 1H), 1.93 – 1.73 (m, 2H), 1.67 – 1.58 (m, 3H), 1.44 – 1.37 (m, 1H) ppm. **^{13}C NMR** (101 MHz, $CDCl_3$) δ 167.3, 166.8, 147.5, 133.1, 130.5, 129.8, 129.7, 128.9, 128.5, 128.0, 65.8, 52.1, 43.3, 41.4, 36.3, 30.6, 28.3, 22.8 ppm. **IR** (neat, 3063, 3033, 2950, 2872, 1714, 1609, 1584, 1450, 1434, 1416, 1392, 1313, 1268, 1177, 1107, 1069, 1021, 966, 864, 805, 756, 708 cm^{-1}). **HRMS:** m/z calcd. for ($C_{22}H_{24}NaO_4$) $[M+Na]^+$: 375.1567 found 375.1568.

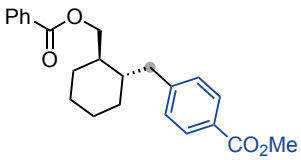

***(trans)* methyl 4-((2-((benzoyloxy)methyl)cyclohexyl)methyl)benzoate** (**3h**): Following the **general procedure B**, using (+/-) 3-phenyloctahydrobenzo[*e*][1,3]dioxepine (**1h**), at 35ºC for 48 hours, the crude was purified by flash column chromatography (*n*-hexane/EtOAc, gradient 98:2 to 97:3), to afford **3h** (52 mg, 71% yield) as a white solid. m.p.: 61-65 ºC. **^{1}H NMR** (400 MHz, $CDCl_3$): δ 8.08 -8.05 (m, 2H), 7.94 – 7.91 (m, 2H), 7.60 – 7.56 (m, 1H), 7.48 -7.45 (m, 2H), 7.22 -7.18 (m, 2H), 4.44 (qd, *J* = 11.2, 4.3 Hz, 2H), 3.89 (s, 3H), 3.16 (dd, *J* = 13.3, 3.2 Hz, 1H), 2.35 (dd, *J* = 13.3, 9.2 Hz, 1H), 1.93 – 1.90 (m, 1H), 1.75 – 1.57 (m, 5H), 1.37 – 1.25 (m, 2H), 1.23 -1.09 (m, 1H), 1.00 – 0.90 (m, 1H) ppm. **^{13}C NMR** (101 MHz, $CDCl_3$) δ 167.3, 166.8, 146., 133.1, 130.5, 129.68, 129.66, 129.4, 128.6, 128.0, 67.8, 52.1, 42.1, 40.8, 40.3, 31.4, 30.2, 25.9 ppm. **IR** (neat, 2993, 2924, 2854, 1714, 1609, 1585, 1449, 1435, 1415, 1383, 1313, 1268, 1206, 1176, 1159, 1107, 1069, 1022, 964, 948, 857, 756, 708, 688, 677 cm^{-1}). **HRMS:** m/z calcd. for ($C_{23}H_{26}NaO_4$) $[M+Na]^+$: 389.1723 found 389.1715.

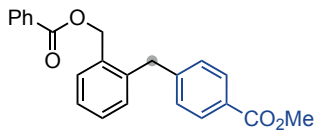

methyl 4-(2-((benzoyloxy)methyl)benzyl)benzoate (**3i**): Following the **general procedure B**, using 3-phenyl-1,5-dihydrobenzo[*e*][1,3]dioxepine (**1i**), at 35ºC for 48 hours, the crude was purified by flash column chromatography (*n*-hexane/EtOAc, 96:4), to afford **3i** (40 mg, 56% yield) as a white solid. m.p.: 77-81 ºC. **^{1}H NMR** (400 MHz, $CDCl_3$): δ 7.91 – 7.88 (m, 4H), 7.54 – 7.49 (m, 2H), 7.39 – 7.30 (m, 4H), 7.22 – 7.18 (m, 3H), 7.22 -7.18 (m, 2H), 5.32 (s, 2 H), 4.20 (s, 2H), 3.88 (s, 3H) ppm. **^{13}C NMR** (101 MHz, $CDCl_3$) δ 167.1, 166.4, 145.9, 138.8, 134.3, 133.1, 131.0, 130.5, 130.0, 129.97, 129.7, 129.1, 128.8, 128.4, 128.3, 127.2, 65.0, 52.1, 38.8 ppm. **IR** (neat, 3075, 3023, 2975, 2955, 2913, 2848, 1703, 1608, 1583, 1572, 1493, 1464, 1443, 1414, 1379, 1316, 1264, 1196, 1177, 1158, 1111, 1094, 1070, 1017, 968, 934, 883, 839, 783, 739, 710, 686, 643, 615, 593, 499, 481 cm^{-1}). **HRMS:** m/z calcd. for ($C_{23}H_{20}NaO_4$) $[M+Na]^+$: 383.1254 found 383.1262.

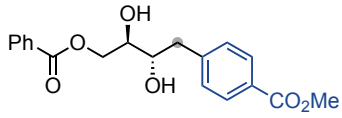

methyl 4-(4-(benzoyloxy)-2,3-dihydroxybutyl)benzoate (**3j**): Following the **general procedure B**, using 2-phenyl-1,3-dioxepane-5,6-diol (**1j**), the crude was purified by flash column chromatography (*n*-hexane/EtOAc, gradient 7:3 to 6:4), to afford **3j** (23mg, 34% yield) as a white solid. m.p.: 124-130 ºC. **^{1}H NMR** (400 MHz, $CDCl_3$): δ 8.06 – 8.03 (m, 2H), 7.99 – 7.96 (m, 2H), 7.61 – 7.56 (m, 1H), 7.47 – 7.43 (m, 2H), 7.36 – 7-33 (m, 2H), 4.61 – 4.57 (m, 2H), 4.04 – 3.92 (m, 2H), 3.90 (s, 3H), 3.12 – 3.08 (m, 1H), 2.89 – 2.84 (m, 1H) 2.36 (bs, 1H), 1.72 (bs, 1H) ppm. **^{13}C NMR** (101 MHz, $CDCl_3$) δ 167.5, 167.2, 143.7, 133.6, 130.01, 120.98, 129.9, 129.71, 129.65, 128.7, 128.6, 73.0, 72.9, 66.4, 52.2, 39.2 ppm. **IR** (neat, 3398, 3322, 3071, 2953, 2922, 2851, 1710, 1692, 1612, 1601, 1585, 1578, 1451, 1435, 1417, 1402, 1383, 1319, 1304, 1270, 1186, 1177, 1135, 110, 1057, 1021, 963, 927, 838, 765, 705, 684, 650, 551, 480 cm^{-1}). **HRMS:** m/z calcd. for ($C_{19}H_{20}NaO_6$) $[M+Na]^+$: 367.1152 found 367.1159.

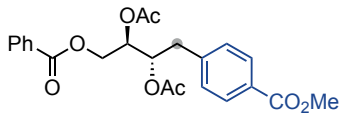

1-(benzoyloxy)-4-(4-(methoxycarbonyl)phenyl)butane-2,3-diyl diacetate (**3k**): Following the **general procedure B**, using 2-phenyl-1,3-dioxepane-5,6-diyl diacetate (**1k**), the crude was purified by flash column chromatography (*n*-hexane/EtOAc, gradient 9:1 to 8:2), to afford **3k** (67 mg, 78% yield) as a white solid. m.p.: 121-124 ºC. **^{1}H NMR** (400 MHz, $CDCl_3$): δ 8.03

– 7.94 (m, 4H), 7.59 – 7.54 (m, 1H), 7.46 – 7.42 (m, 2H), 7.29 – 7.26 (m, 2H), 5.45 (dt, *J* = 8.6, 4.9 Hz, 1H), 5.34 (ddd, *J* = 6.6, 5.0, 3.4 Hz, 1H), 4.62 (dd, *J* = 12.1, 3.4 Hz, 1H), 4.39 (dd, *J* = 12.1, 6.5 Hz, 1H), 3.89 (s, 3H), 3.09 – 2.96 (m, 2H), 2.06 (s, 3H), 1.95 (s, 3H) ppm. **^{13}C NMR** (101 MHz, $CDCl_3$) δ 170.1, 169.8, 166.9, 166.2, 141.8, 133.4, 129.9, 129.8, 129.6, 129.4, 129.0, 128.6, 71.9, 71.8, 62.5, 52.1, 36.9, 21.0, 20.8 ppm. **IR** (neat, 2928, 2858, 1733, 1716, 1606, 1491, 1452, 1414, 1372, 1315, 1261, 1221, 1173, 1148, 1119, 1067, 1009, 953, 914, 890, 847, 819, 756, 711, cm^{-1}. **HRMS:** m/z calcd. for ($C_{23}H_{24}NaO_8$) $[M+Na]^+$: 451.1363 found 451.1379.

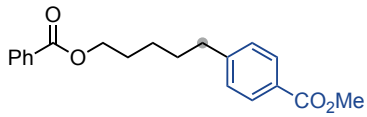

methyl 4-(5-(benzoyloxy)pentyl)benzoate benzoate (**3l**): Following the **general procedure B**, using 2-phenyl-1,3-dioxocane (**1l**), the crude was purified by flash column chromatography (*n*-hexane/EtOAc, gradient 97:3 to 96:4), to afford **3l** (44 mg, 67% yield) as a colourless oil. **^{1}H NMR** (400 MHz, $CDCl_3$): δ 8.03 – 8.01 (m, 2H), 7.96 – 7.93 (m, 2H), 7.58 – 7.53 (m, 1H), 7.46 – 7.41 (m, 2H), 7.25 – 7.23 (m, 2H), 4.32 (t, *J* = 6.6 Hz, 2H), 3.90 (s, 3H), 2.70 (t, *J* = 7.7 Hz, 2H), 1.84 – 1.68 (m, 4H), 1.53 – 1.45 (m, 2H) ppm. **^{13}C NMR** (101 MHz, $CDCl_3$) δ 167.3, 166.8, 148.0, 133.0, 130.6, 129.8, 129.7, 128.6, 128.5, 127.9, 64.9, 52.1, 35.9, 30.8, 28.7, 25.7 ppm. **IR** (neat, 3062, 3033, 2938, 2859, 1714, 1609, 1584, 1451, 1435, 1415, 1386, 1313, 1269, 1777, 1106, 1070, 1021, 965, 856, 762, 709, 675 cm^{-1}). **HRMS:** m/z calcd. for ($C_{20}H_{22}NaO_4$) $[M+Na]^+$: 349.1410 found 349.1413.

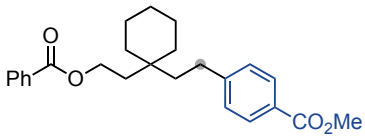

methyl 4-(2-(1-(2-(benzoyloxy)ethyl)cyclohexyl)ethyl)benzoate (**3m**): Following the **general procedure B**, using 10-phenyl-9,11-dioxaspiro[5.7]tridecane (**1m**), the crude was purified by flash column chromatography (*n*-hexane/EtOAc, gradient 97:3 to 96:4), to afford **3m** (57 mg, 72% yield) as a colourless oil. **^{1}H NMR** (400 MHz, $CDCl_3$): δ 8.05 – 8.02 (m, 2H), 7.95 – 7.92 (m, 2H), 7.58 – 7.53 (m, 1H), 7.45 – 7.40 (m, 2H), 7.26 – 7.24 (m, 2H), 4.44 – 4.40 (m, 2H), 3.90 (s, 3H), 2.67 – 2.62 (m, 2H), 1.89 – 1.85 (m, 2H), 1.68 – 1.62 (m, 2H), 1.53 – 1.40 (m, 10H) ppm. **^{13}C NMR** (101 MHz, $CDCl_3$) δ 167.3, 166.9, 148.9, 133.0, 130.5, 129.9, 129.7, 128.51, 128.47, 127.8, 61.8, 52.1, 39.7, 36.1, 35.1, 35.0, 29.9, 26.4, 21.7 ppm. **IR** (neat, 3032, 2925, 2852, 1715, 1609, 1584, 1451, 1435, 1415, 1392, 1313, 1269, 1176, 1107, 1070, 1021, 964, 863, 838, 767, 709, 688, 676 cm^{-1}). **HRMS:** m/z calcd. for ($C_{25}H_{30}NaO_4$) $[M+Na]^+$: 417.2036 found 417.2034.

General procedure C (Schemes XX-XX): To a 5 mL Crimp Top vial equipped with magnetic stirring was charged the corresponding aryl bromide (*if solid*, 0.20 mmol, 1.0 equiv.), dtbbpy (1.6 mg, 0.03 mmol, 3 mol%) and ($Ir[dF(CF_3)ppy]_2(dtbbpy)PF_6$) (1.1 mg, 0.005 mmol, 0.5 mol%). Subsequently the vial was brought inside a nitrogen-filled glovebox, and Na_2CO_3 (42.4 mg, 0.40 mmol, 2.0 equiv.), quinuclidine (5.6 mg, 0.25 mmol, 25 mol%) and $NiBr_2$·dme (1.5 mg, 0.025 mmol, 2.5 mol%) were added. Then the vial was sealed with a crimp cap and taken outside the glovebox, were *tert*-Amyl alcohol (1.0 mL, 0.2 M), 2-phenyl-1,3-dioxepane (**1a**, 71.3 mg, 0.4 mmol, 2.0 equiv.) and aryl bromide (*if liquid*, 0.2 mmol, 1.0 equiv.) were added sequentially via syringe. The reaction was stirred at 500 rpm under blue LED irradiation with a cooling system set at 20ºC for 16 hours. After the reaction was completed, the mixture was diluted with EtOAc and washed with water. The aqueous phase was washed with EtOAc (2 times), dried over anhydrous Na_2SO_4 and concentrated under reduced pressure. The crude was purified by column chromatography (see details below).

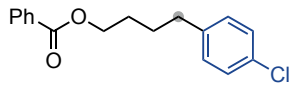

4-(4-chlorophenyl)butyl benzoate (**4a**): Following the **general procedure C**, using 1-bromo-4-chlorobenzene (**2b**), the crude was purified by flash column chromatography (*n*-hexane/EtOAc, 99:1), followed by further drying under high vacuum at 120ºC for 2 hours, to afford **4a** (40 mg, 70% yield) as a colourless oil. **^{1}H NMR** (400 MHz, $CDCl_3$): δ 8.08 – 8.05 (m, 2H), 7.60 – 7.55 (m, 1H), 7.48 – 7.44 (m, 2H), 7.29 – 7.25 (m, 2H), 7.16 – 7.12 (m, 2H), 4.36 (t, *J* = 6.3 Hz, 2H), 2.68 (t, *J* = 7.3 Hz, 2H), 1.86 – 1.74 (m, 4H) ppm. **^{13}C NMR** (101 MHz, $CDCl_3$) δ 166.7, 140.5, 133.0, 131.7, 130.5, 129.9, 129.7, 128.6, 128.58, 128.53, 128.47, 128.45, 64.8, 34.9, 28.3, 27.8 ppm. **IR** (neat, 3062, 3031, 2941, 2861, 1715, 1602, 1585, 1491, 1451, 1407, 1386, 1314, 1269, 1175, 1113, 1069, 1026, 1015, 958, 831, 804, 708, 687, 675, 659 cm^{-1}). **HRMS:** m/z calcd. for ($C_{17}H_{17}ClNaO_2$) $[M+Na]^+$: 311.0809 found 311.0818.

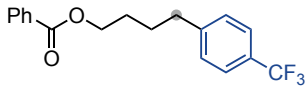

4-(4-(trifluoromethyl)phenyl)butyl benzoate (**4b**): Following the **general procedure C**, using 1-bromo-4-(trifluoromethyl)benzene (**2c**), the crude was purified by flash column chromatography (*n*-hexane/EtOAc, 100:1), followed by further drying under high vacuum at 120ºC for 2 hours, to afford **4b** (47 mg, 73% yield) as a white solid. m.p.: 42-44 ºC. **^{1}H NMR** (400 MHz, $CDCl_3$): δ 8.06 – 8.03 (m, 2H), 7.58 – 7.53 (m, 3H), 7.47 – 7.42 (m, 2H), 7.32 – 7.30 (m, 2H), 4.37 – 4.34 (m, 2H), 2.77 – 2.74 (m, 2H), 1.86 – 1.77 (m, 4H) ppm. **^{13}C NMR** (101 MHz, $CDCl_3$) δ 166.8, 146.2 (q, $^5J_{CF}$ = 1.4 Hz), 133.1, 130.5, 129.7, 128.8, 128.5, 128.4 (q, $^3J_{CF}$ = 32.2 Hz), 125.4 (q, $^3J_{CF}$ = 3.8 Hz), 124.5 (q, $^1J_{CF}$ = 271.7 Hz), 64.7, 35.4, 28.4, 27.7

ppm. **^{19}F NMR** (376 MHz, $CDCl_3$) δ -62.40 ppm. **IR** (neat, 3067, 3036, 2942, 2866, 1716, 1617, 1600, 1584, 1451, 1418, 1324, 1271, 1161, 1110, 1066, 1017, 959, 840, 821, 740, 710, 687, 675, 633, 595cm^{-1}). **HRMS:** m/z calcd. for ($C_{18}H_{17}F_3NaO_2$) $[M+Na]^+$: 345.1073 found 345.1071.

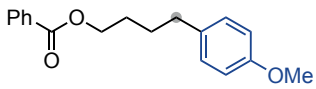

4-(4-methoxyphenyl)butyl benzoate (**4c**): Following the **general procedure C**, using 1-bromo-4-methoxybenzene (**2d**), the crude was purified by flash column chromatography (*n*-hexane/EtOAc, 97:3), to afford **4c** (38 mg, 67% yield) as a colourless oil. **^{1}H NMR** (400 MHz, $CDCl_3$): δ 8.06 – 8.03 (m, 2H), 7.58 – 7.54 (m, 1H), 7.46 – 7.42 (m, 2H), 7.14 – 7.10 (m, 2H), 6.86 – 6.83 (m, 2H), 4.35 (t, *J* = 6.3 Hz, 2H), 3.79 (s, 3H), 2.64 (t, *J* = 7.2 Hz, 2H), 1.85 – 1.72 (m, 4H) ppm. **^{13}C NMR** (101 MHz, $CDCl_3$) δ 166.8, 157.9, 134.2, 133.0, 130.6, 129.7, 129.4, 128.5, 113.9, 65.0, 55.4, 34.7, 28.4, 28.2 ppm. **IR** (neat, 3062, 3032, 2995, 2937, 2859, 2835, 1714, 1611, 1584, 1511, 1451, 1386, 1314, 1270, 1243, 1175, 1110, 1069, 1027, 951, 830, 709, 674, 562, 516 cm^{-1}). **HRMS:** m/z calcd. for ($C_{18}H_{20}NaO_3$) $[M+Na]^+$: 307.1305 found 307.1305.

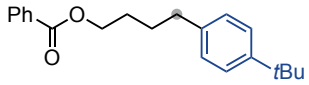

4-(4-(*tert*-butyl)phenyl)butyl benzoate (**4d**): Following the **general procedure C**, using 1-bromo-4-(*tert*-butyl)benzene (**2e**), the crude was purified by flash column chromatography (*n*-hexane/EtOAc, 100:1), followed by further drying under high vacuum at 120ºC for 2 hours, to afford **4d** (45 mg, 73% yield) as a colourless oil. **^{1}H NMR** (400 MHz, $CDCl_3$): δ 8.08 – 8.06 (m, 2H), 7.59 – 7.55 (m, 1H), 7.48 – 7.43 (m, 2H), 7.35 – 7.32 (m, 2H), 7.18 – 7.14 (m, 2H), 4.37 (t, *J* = 6.3 Hz, 2H), 2.69 (t, *J* = 7.1 Hz, 2H), 1.89 – 1.77 (m, 4H), 1.34 (s, 9H) ppm. **^{13}C NMR** (101 MHz, $CDCl_3$) δ 166.8, 148.8, 139.1, 132.9, 130.6, 129.7, 128.4, 128.2, 125.4, 65.0, 35.1, 34.5, 31.5, 28.5, 27.9 ppm. **IR** (neat, 3089, 3060, 3024, 2956, 2865, 1717, 1602, 1585, 1510, 1491, 1451, 1392, 1363, 1314, 1269, 1204, 1175, 1110, 1069, 1026, 936, 909, 831, 709, 570 cm^{-1}). **HRMS:** m/z calcd. for ($C_{21}H_{26}NaO_2$) $[M+Na]^+$: 333.1825 found 333.1823.

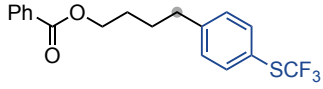

4-(4-((trifluoromethyl)thio)phenyl)butyl benzoate (**4e**): Following the **general procedure C**, using (4-bromophenyl)(trifluoromethyl)sulfane (**2f**), the crude was purified by flash column chromatography (*n*-hexane/EtOAc, 100:1), followed by further drying under high vacuum at 120ºC for 2 hours, to afford **4e** (43 mg, 71% yield) as a colourless oil. **^{1}H NMR** (400 MHz, $CDCl_3$): δ 8.06 – 8.03 (m, 2H), 7.58 – 7.54 (m, 3H), 7.46 – 7.42 (m, 2H), 7.26 – 7.24 (m, 2H),

4.37 – 4.34 (m, 2H), 2.75 – 2.71 (m, 2H), 1.87 – 1.76 (m, 4H) ppm. **^{13}C NMR** (101 MHz, $CDCl_3$) δ 166.7, 145.5, 136.6, 133.0, 130.5, 129.8 (q, $^1J_{CF}$ = 309.0 Hz), 129.71, 129.67, 128.5, 121.6 (q, $^3J_{CF}$ = 3.0 Hz), 64.7, 35.3, 28.5, 27.7 ppm. **^{19}F NMR** (376 MHz, $CDCl_3$) δ -43.12 ppm. **IR** (neat, 3064, 3032, 2944, 2863, 1716, 1601, 1585, 1492, 1452, 1406, 1386, 1315, 1271, 1151, 1108, 1084, 1069, 1026, 1016, 935, 834, 806, 755, 709, 573, 513 cm^{-1}). **HRMS:** m/z calcd. for ($C_{18}H_{17}F_3NaO_2S$) $[M+Na]^+$: 377.0794 found 377.0795.

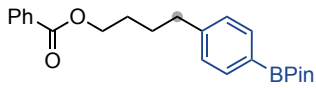

4-(4-(4,4,5,5-tetramethyl-1,3,2-dioxaborolan-2-yl)phenyl)butyl (**4f**) Following the **general procedure C**, using 2-(4-bromophenyl)-4,4,5,5-tetramethyl-1,3,2-dioxaborolane (**2g**), the crude was purified by flash column chromatography (*n*-hexane/EtOAc, gradient: 95:5 to 9:1), to afford **3s** (50 mg, 66% yield) as a colourless oil. **^{1}H NMR** (400 MHz, $CDCl_3$): δ 8.06 – 8.03 (m, 2H), 7.77 – 7.75 (m, 2H), 7.58 – 7.53 (m, 1H), 7.46 – 7.42 (m, 2H), 7.22 – 7.21 (m, 2H), 4.36 – 4.33 (m, 2H), 2.73 – 2.70 (m, 2H), 1.84 – 1.75 (m, 4H), 1.35 (s, 12H) ppm. **^{13}C NMR** (101 MHz, $CDCl_3$) δ 166.8, 145.6, 135.1, 132.95, 132.92, 130.5, 129.7, 128.4, 128.0, 83.8, 64.9, 35.8, 28.4, 27.8, 25.0 ppm. **IR** (neat, 3046, 2977, 2937, 2860, 1717, 1611, 1585, 1518, 1451, 1398, 1358, 1316, 1269, 1214, 1143, 1110, 1088, 1070, 1022, 962, 859, 827, 710, 657 cm^{-1}). **HRMS:** m/z calcd. for ($C_{23}H_{29}NaO_4{}^{11}B$) $[M+Na]^+$: 403.2051 found 403.2041.

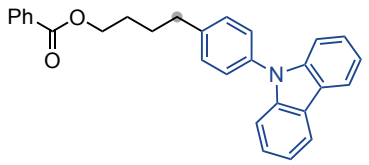

4-(4-(9*H*-carbazol-9-yl)phenyl)butyl benzoate (**4g**): Following the **general procedure C**, using 9-(4-bromophenyl)-9*H*-carbazole (**2h**), the crude was purified by flash column chromatography (*n*-hexane/EtOAc, 50:1), to afford **4g** (56 mg, 68% yield) as a white solid. m.p.: 111-116 ºC. **^{1}H NMR** (400 MHz, $CDCl_3$): δ 8.19 – 8.16 (m, 2H), 8.13 – 8.09 (m, 2H), 7.61 – 7.57 (m, 1H), 7.51 – 7.47 (m, 4H), 7.46 – 7.42 (m, 6H), 7.34 – 7.29 (m, 2H), 4.46 – 4.43 (m, 2H), 2.86 – 2.83 (m, 2H), 1.98 – 1.88 (m, 4H) ppm. **^{13}C NMR** (101 MHz, $CDCl_3$) δ 166.8, 141.5, 141.1, 135.6, 133.0, 130.5, 129.9, 129.7, 128.5, 128.4, 127.2, 126.0, 123.4, 120.4, 119.9, 109.9, 64.9, 35.3, 28.6, 27.9 ppm. **IR** (neat, 3061, 3035, 2938, 2857, 1715, 1596, 1512, 1476, 1450, 1395, 1361, 1336, 1313, 1273, 1229, 1173, 1119, 1071, 1046, 1022, 955, 910, 838, 807, 752, 741, 725, 705, 687, 675, 627 cm^{-1}). **HRMS:** m/z calcd. for ($C_{29}H_{25}NNaO_2$) $[M+Na]^+$: 442.1777 found 442.1780.

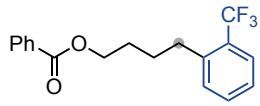

4-(2-(trifluoromethyl)phenyl)butyl benzoate (**4h**): Following the **general procedure C**, using 1-bromo-2-(trifluoromethyl)benzene (**2i**), the crude was purified by flash column chromatography (*n*-hexane/EtOAc, 95:5), followed by further drying under high vacuum at 120ºC for 2 hours, to afford **4h** (57 mg, 89% yield) as a colourless oil. **^{1}H NMR** (400 MHz, $CDCl_3$): δ 8.07 – 8.04 (m, 2H), 7.64 – 7.61 (m, 1H), 7.58 – 7.54 (m, 1H), 7.49 – 7.44 (m, 3H), 7.36 – 7.34 (m, 1H), 7.31 – 7.27 (m, 1H), 4.37 (t, J = 6.3 Hz, 2H), 2.89 – 2.85 (m, 2H), 1.92 – 1.77 (m, 4H) ppm. **^{13}C NMR** (101 MHz, $CDCl_3$) δ 166.8, 141.0 (q, J_{CF} = 1.9 Hz), 133.0, 131.9 (d, J_{CF} = 1.0 Hz) 131.0, 130.5, 129.7, 128.6 (q, $^2J_{CF}$ = 29.7 Hz), 128.5, 126.4, 126.1 (q, $^3J_{CF}$ = 5.5 Hz), 124.8 (q, $^1J_{CF}$ = 273.9 Hz), 64.8, 32.4 (m), 28.8, 28.3 ppm. **^{19}F NMR** (376 MHz, $CDCl_3$) δ -59.29 ppm. **IR** (neat, 3065, 3036, 2952, 2877, 1716, 1604, 1584, 1493, 1452, 1387, 1311, 1270, 1158, 1109, 1069, 1059, 1027, 955, 767, 743, 709, 687, 675, 653, 600 cm^{-1}). **HRMS:** m/z calcd. for ($C_{18}H_{17}F_3NaO_2$) $[M+Na]^+$: 345.1073 found 345.1074.

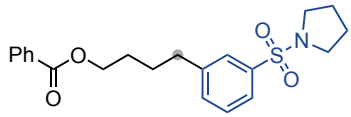

4-(3-(pyrrolidin-1-ylsulfonyl)phenyl)butyl benzoate (**4i**): Following the **general procedure C**, using 1-((3-bromophenyl)sulfonyl)pyrrolidine (**2j**), the crude was purified by flash column chromatography (*n*-hexane/EtOAc, 8:2), to afford **4i** (51 mg, 66% yield) as a colourless oil. **^{1}H NMR** (400 MHz, $CDCl_3$): δ 8.05 – 8.02 (m, 2H), 7.67 – 7.64 (m, 2H), 7.58 – 7.54 (m, 1H), 7.46 – 7.40 (m, 4H), 4.36 – 4.33 (m, 2H), 3.26 – 3.21 (m, 4H), 2.80 – 2.75 (m, 2H), 1.85 – 1.80 (m, 4H), 1.77 – 1.70 (m, 4H) ppm. **^{13}C NMR** (101 MHz, $CDCl_3$) δ 166.8, 143.4, 137.1, 133.1, 132.8, 130.4, 129.7, 129.2, 128.5, 127.4, 125.2, 64.7, 48.1, 35.4, 28.4, 27.8, 25.4 ppm. **IR** (neat, 3063, 2948, 2868, 1714, 1601, 1584, 1475, 1451, 1386, 1343, 1314, 1271, 1200, 1153, 1113, 1089, 1069, 1026, 1009, 996, 910, 796, 753, 711, 690, 626, 589, 566 cm^{-1}). **HRMS:** m/z calcd. for ($C_{21}H_{25}NNaO_4S$) $[M+Na]^+$: 410.1396 found 410.1391.

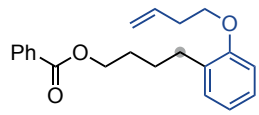

4-(2-(but-3-en-1-yloxy)phenyl)butyl benzoate (**4j**): Following the **general procedure C**, using 1-bromo-2-(but-3-en-1-yloxy)benzene (**2k**), the crude was purified by flash column chromatography (*n*-hexane/EtOAc, 99:1), followed by further drying under high vacuum at 120 ºC for 2 hours, to afford **4j** (39 mg, 60% yield) as a colourless oil. **^{1}H NMR** (400 MHz, $CDCl_3$): δ 8.07 – 8.04 (m, 2H), 7.58 – 7.53 (m, 1H), 7.46 – 7.41 (m, 2H), 7.19 – 7.13 (m, 2H),

6.88 (td, *J* = 7.4, 1.1 Hz, 2H), 6.85 – 6.82 (m, 1H), 5.91 (ddt, *J* = 17.0, 10.2, 6.7 Hz, 1H), 5.16 (dq, *J* = 17.2, 1.6 Hz, 1H), 5.09 (ddt, *J* = 10.2, 2.1, 1.2 Hz, 1H), 4.35 (t, *J* = 6.3 Hz, 2H), 4.02 (t, *J* = 6.5 Hz, 2H), 2.70 (t, *J* = 7.2 Hz, 2H), 2.55 (qt, *J* = 6.6, 1.4 Hz, 2H), 1.86 – 1.72 (m, 4H) ppm. **^{13}C NMR** (101 MHz, $CDCl_3$) δ 166.8, 156.9, 134.9, 132.9, 130.8, 130.7, 130.1, 129.7, 128.4, 127.2, 120.5, 117.0, 111.3, 67.2, 65.2, 34.0, 30.1, 28.7, 26.5 ppm. **IR** (neat, 3069, 3033, 2929, 2866, 1716, 1642, 1601, 1586, 1493, 1471, 1452, 1385, 1314, 1271, 1240, 1191, 1176, 1112, 1069, 1048, 1026, 989, 916, 750, 709, 687, 674 cm^{-1}). **HRMS:** m/z calcd. for ($C_{21}H_{24}NaO_3$) $[M+Na]^+$: 347.1618 found 347.1618.

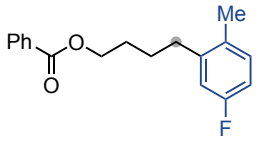

4-(5-fluoro-2-methylphenyl)butyl benzoate (**4k**): Following the **general procedure C**, using 2-bromo-4-fluoro-1-methylbenzene (**2l**), the crude was purified by flash column chromatography (*n*-hexane/EtOAc, 99:1), followed by further drying under high vacuum at 120 ºC for 2 hours, to afford **4k** (53 mg, 93% yield) as a colourless oil. **^{1}H NMR** (400 MHz, $CDCl_3$): δ 8.07 – 8.04 (m, 2H), 7.59 – 7.54 (m, 1H), 7.47 – 7.42 (m, 2H), 7.08 (dd, *J* = 8.4, 6.0 Hz, 1H), 6.87 (dd, *J* = 9.9, 2.8 Hz, 1H), 6.80 (td, *J* = 8.4, 2.8 Hz, 1H), 4.37 (t, *J* = 6.4 Hz, 2H), 2.67 – 2.64 (m, 2H), 2.26 (s, 3H), 1.90 – 1.83 (m, 2H), 1.79 – 1.71 (m, 2H) ppm. **^{13}C NMR** (101 MHz, $CDCl_3$) δ 166.8, 161.4 (d, $^{1}J_{CF}$ = 242.4 Hz), 142.4 (d, $^{3}J_{CF}$ = 6.9 Hz), 133.0, 131.36 (d, $^{3}J_{CF}$ = 7.9 Hz), 131.41 (d, $^{3}J_{CF}$ = 3.0 Hz), 130.5, 129.7, 128.5, 115.4 (d, $^{2}J_{CF}$ = 20.9 Hz), 112.6 (d, $^{2}J_{CF}$ = 20.6 Hz), 64.8, 32.9 (d, $^{4}J_{CF}$ = 1.8 Hz), 28.7, 26.4, 18.7 ppm. **^{19}F NMR** (376 MHz, $CDCl_3$) δ -118.16 ppm. **IR** (neat, 3064, 3033, 2946, 2870, 1715, 1612, 1602, 1589, 1496, 1451, 1415, 1384, 1314, 1270, 1247, 1202, 1175, 1149, 1111, 1069, 1026, 1000, 951, 938, 867, 807, 739, 709, 687, 675, 461 cm^{-1}). **HRMS:** m/z calcd. for ($C_{18}H_{19}FNaO_2$) $[M+Na]^+$: 309.1261 found 309.1259.

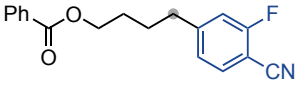

4-(4-cyano-3-fluorophenyl)butyl benzoate (**4l**): Following the **general procedure C**, using 4-bromo-2-fluorobenzonitrile (**2m**), the crude was purified by flash column chromatography (*n*-hexane/EtOAc, 9:1), to afford **4l** (33 mg, 56% yield) as a white solid. m.p.: 49-53 ºC. **^{1}H NMR** (500 MHz, $CDCl_3$): δ 8.04 – 8.01 (m, 2H), 7.59 – 7.51 (m, 2H), 7.47 – 7.42 (m, 2H), 7.10 – 7.04 (m, 2H), 4.37 – 4.34 (m, 2H), 2.77 – 2.74 (m, 2H), 1.86 – 1.75 (m, 4H) ppm. **^{13}C NMR** (101 MHz, $CDCl_3$) δ 166.7, 163.4 (d, $^{1}J_{CF}$ = 258.8 Hz), 151.1 (d, $^{3}J_{CF}$ = 7.7 Hz), 133.4, 133.1, 130.3, 129.6, 128.5, 125.1 (d, $^{4}J_{CF}$ = 3.2 Hz), 116.4 (d, $^{2}J_{CF}$ = 19.1 Hz), 114.3, 99.0 (d, $^{2}J_{CF}$ = 15.6 Hz), 64.4, 35.6 (d, $^{4}J_{CF}$ = 1.5 Hz), 28.3, 27.2 ppm. **^{19}F NMR** (376 MHz, $CDCl_3$) δ -107.00 ppm. **IR** (neat, 3067, 2961, 2937, 2898, 2870, 2235, 1705, 1621, 1601, 1585,

1568, 1501, 1476, 1450, 1432, 1393, 1379, 1331, 1314, 1274, 1218, 1179, 1157, 1120, 1069, 1028, 964, 956, 939, 874, 851, 822, 807, 822, 807, 774, 741, 709, 685, 676, 613, 584, 502 cm^{-1}). **HRMS:** m/z calcd. for ($C_{18}H_{16}FNNaO_2$) $[M+Na]^+$: 320.1057 found 320.1060.

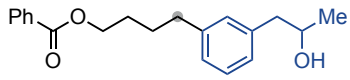

4-(3-(2-hydroxypropyl)phenyl)butyl benzoate (**4m**): Following the **general procedure C**, using 1-(3-bromophenyl)propan-2-ol (**2n**), the crude was purified by flash column chromatography (*n*-hexane/EtOAc, gradient 9:1 to 8:2) to afford **4m** (43 mg, 69% yield) as a colourless oil. **^{1}H NMR** (400 MHz, $CDCl_3$): δ 8.06 – 8.03 (m, 2H), 7.58 – 7.53 (m, 1H), 7.46 – 7.42 (m, 2H), 7.26 – 7.22 (m, 1H), 7.09 – 7.04 (m, 3H), 4.34 (t, *J* = 6.1 Hz, 2H), 4.06 – 3.98 (m, 1H), 2.77 (dd, *J* = 13.4, 4.8 Hz, 1H), 2.70 – 2.63 (m, 3H), 1.84 – 1.78 (m, 4H), 1.68 (brs, 1H), 1.25 (d, *J* = 6.2 Hz, 3H) ppm. **^{13}C NMR** (101 MHz, $CDCl_3$) δ ^{13}C NMR (101 MHz, $CDCl_3$) δ 166.8, 142. 5, 138.7, 133.0, 130.5, 129.7, 128.7, 128.5, 127.0, 126.7, 69.0, 64.9, 45.9, 35.5, 28.5, 27.9, 22.9 ppm. **IR** (neat, 3412, 3060, 3022, 2962, 2929, 2859, 1715, 1603, 1585, 1488, 1451, 1387, 1374, 1315, 1271, 1204, 1176, 1113, 1070, 1026, 939, 785, 709, 687, 675 cm^{-1}). **HRMS:** m/z calcd. for ($C_{20}H_{24}NaO_3$) $[M+Na]^+$: 335.1618 found 335.1613.

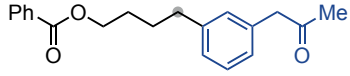

4-(3-(2-oxopropyl)phenyl)butyl benzoate (**4n**): Following the **general procedure C**, using 1-(3-bromophenyl)propan-2-one (**2o**), the crude was purified by flash column chromatography (*n*-hexane/EtOAc, gradient 9:1 to 8:2), to afford **4n** (53 mg, 85% yield) as a colourless oil. **^{1}H NMR** (400 MHz, $CDCl_3$): δ 8.05 – 8.03 (m, 2H), 7.58 – 7.53 (m, 1H), 7.46 – 7.41 (m, 2H), 7.2 – 7.24 (m, 1H), 7.12 – 7.10 (m, 1H) 7.05 – 7.03 (m, 2H), 4.36 – 4.33 (m, 2H), 3.67 (s, 2H), 2.68 (t, *J* = 7.1 Hz, 2H), 2.14 (s, 3H), 1.84 – 1.74 (m, 4H) ppm. **^{13}C NMR** (101 MHz, $CDCl_3$) δ 206.6, 166.8, 142.7, 134.4, 133.0, 130.6, 129.7, 129.6, 128.9, 128.5, 127.3, 127.1, 64.9, 51.2, 35.5, 29.4, 28.5, 27.9 ppm. **IR** (neat, 3246, 2958, 1719, 1687, 1601, 1583, 1449, 1435, 1361, 1325, 1275, 1191, 1116, 1070, 1025, 777, 708, 679, 658 cm^{-1}). **HRMS:** m/z calcd. for ($C_{20}H_{22}NaO_3$) $[M+Na]^+$: 333.1461 found 333.1472.

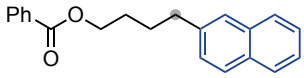

4-(naphthalen-2-yl)butyl benzoate (**4o**): Following the **general procedure C**, using 2-bromonaphthalene (**2p**), the crude was purified by flash column chromatography (*n*-hexane/EtOAc, 100:1), followed by further drying under high vacuum at 120 ºC for 2 hours, to afford **4o** (40 mg, 66% yield) as a colourless oil. **^{1}H NMR** (400 MHz, $CDCl_3$): δ 8.09 – 8.06 (m, 2H), 7.84 – 7.79 (m, 3H), 7.65 – 7.65 (m, 1H), 7.59 – 7.55 (m, 1H), 7.49 – 7.42 (m, 4H), 7.37 (dd, *J* = 8.4, 1.7 Hz, 1H), 4.39 (t, *J* = 6.2 Hz, 2H), 2.88 (t, *J* = 7.1 Hz, 2H), 1.96 – 1.80

(m, 4H) ppm. **^{13}C NMR** (101 MHz, $CDCl_3$) δ 166.8, 139.6, 133.7, 133.0, 132.2, 130.6, 129.7, 128.5, 128.1, 127.7, 127.5, 127.4, 126.6, 126.0, 125.3, 64.9, 35.7, 28.5, 27.8 ppm. **IR** (neat, 3054, 2939, 2858, 1713, 1633, 1601, 1584, 1508, 1492, 1451, 1385, 1314, 1269, 1175, 1111, 1069, 1026, 958, 889, 854, 817, 746, 708, 619, 475 cm^{-1}). **HRMS:** m/z calcd. for ($C_{21}H_{20}NaO_2$) $[M+Na]^+$: 327.1356 found 327.1356.

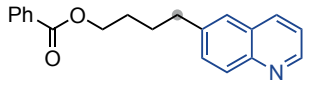

4-(quinolin-6-yl)butyl benzoate (**4p**): Following the **general procedure C**, using 6-bromoquinoline (**2q**), the crude was purified by flash column chromatography (*n*-hexane/EtOAc, gradient: 9:1 to 7:1), to afford **4p** (46 mg, 76% yield) as a yellowish oil. **^{1}H NMR** (400 MHz, $CDCl_3$): 8.86 (dd, *J* = 4.2, 1.7 Hz, 1H), 8.11 – 8.08 (m, 1H), 8.05 – 8.02 (m, 3H), 7.60 – 7.5 (m, 3H), 7.45 – 7.42 (m, 2H), 7.37 (dd, *J* = 8.3, 4.2 Hz, 1H), 4.37 (t, *J* = 6.2 Hz, 2H), 2.89 (t, *J* = 7.1 Hz, 2H), 1.94 – 1.82 (m, 4H) ppm. **^{13}C NMR** (101 MHz, $CDCl_3$) δ 166.8, 149.8, 147.3, 140.6, 135.8, 133.0, 131.1, 130.5, 129.7, 129.5, 128.53, 128.50, 126.3, 121.3, 64.9, 35.6, 28.5, 27.7 ppm. **IR** (neat, 3063, 3032, 3012, 2939, 2859, 1712, 1595, 1570, 1585, 1500, 1451, 1382, 1314, 1270, 1175, 1112, 1069, 1026, 883, 835, 798, 709, 687, 674, 615 cm^{-1}). **HRMS:** m/z calcd. for ($C_{20}H_{20}NO_2$) $[M+H]^+$: 306.1489 found 306.1487.

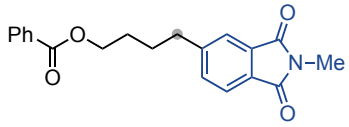

4-(2-methyl-1,3-dioxoisoindolin-5-yl)butyl benzoate (**4q**): Following the **general procedure C**, using 5-bromo-2-methylisoindoline-1,3-dione (**2r**), the crude was purified by flash column chromatography (*n*-hexane/EtOAc, gradient 95:5 to 85:5), to afford **4q** (38 mg, 56% yield) as a white solid. m.p.: 75-81 ºC. **^{1}H NMR** (400 MHz, $CDCl_3$): δ 8.03 – 8.00 (m, 2H), 7.73 (d, *J* = 7.6 Hz, 1H), 7.67 – 7.66 (m, 1H), 7.57 – 7.52 (m, 1H), 7.51 – 7.49 (m, 1H), 7.45 – 7.40 (m, 2H), 4.36 – 4.33 (m, 2H), 3.15 (s, 3H), 2.84 – 2.81 (m, 2H), 1.86 – 1.78 (m, 4H) ppm. **^{13}C NMR** (101 MHz, $CDCl_3$) δ 168.7, 168.6, 166.7, 149.3, 134.0, 133.0, 132.8, 130.3, 130.2, 129.6, 128.5, 123.4, 123.2, 64.5, 35.9, 28.3, 27.6, 24.0 ppm. **IR** (neat, 3454, 2983, 2953, 2934, 2865, 2853, 1767, 1705, 1618, 1598, 1584, 1545, 1484, 1463, 1451, 1441, 1422, 1371, 1315, 1292, 1266, 1246, 1185, 1173, 1106, 1097, 1069, 1024, 1003, 979, 951, 900, 853, 829, 801, 787, 744, 709, 695, 607, 566, 538, 475 cm^{-1}). **HRMS:** m/z calcd. for ($C_{20}H_{19}NNaO_4$) $[M+Na]^+$: 360.1206 found 360.1204.

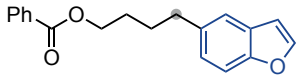

4-(benzofuran-5-yl)butyl benzoate (**4t**): Following the **general procedure C**, using 5-bromobenzofuran (**2s**), the crude was purified by flash column chromatography (*n*-hexane/EtOAc, 99:1), followed by further drying under high vacuum at 120 ºC for 2 hours, to afford **4r** (29 mg, 50% yield) as a yellowish oil. **^{1}H NMR** (400 MHz, $CDCl_3$): δ 8.07 – 8.04 (m, 2H), 7.60 (d, *J* = 2.2 Hz, 1H), 7.60 – 7.58 (m, 1H), 7.46 – 7.42 (m, 4H), 7.14 (dd, *J* = 8.3, 1.9 Hz, 1H), 6.72 (dd, *J* = 2.2, 0.9 Hz, 1H), 4.38 – 4.35 (m, 2H), 2.81 – 2.78 (m, 2H), 1.88 – 1.80 (m, 4H) ppm. **^{13}C NMR** (101 MHz, $CDCl_3$) δ 166.8, 153.7, 145.2, 136.6, 133.0, 130.6, 129.7, 128.5, 127.7, 125.0, 120.6, 111.2, 106.5, 65.0, 35.5, 28.5, 28.4 ppm. **IR** (neat, 3064, 2938, 2858, 1713, 1602, 1584, 1537, 1468, 1451, 1386, 1314, 1270, 1196, 1176, 1110, 1069, 1027, 939, 882, 808, 766, 735, 708, 687, 675, 640, 422 cm^{-1}). **HRMS:** m/z calcd. for ($C_{19}H_{18}NaO_3$) $[M+Na]^+$: 317.1148 found 317.1153.

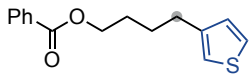

4-(thiophen-3-yl)butyl benzoate (**4s**): Following the **general procedure C**, using 3-bromothiophene (**2t**), the crude was purified by flash column chromatography (*n*-hexane/EtOAc, 100:1), followed by further drying under high vacuum at 120 ºC for 2 hours, to afford **4s** (33 mg, 64% yield) as a colourless oil. **^{1}H NMR** (400 MHz, $CDCl_3$): δ 8.06 – 8.04 (m, 2H), 7.58 – 7.54 (m, 1H), 7.47 – 7.42 (m, 2H), 7.27 – 7.25 (m, 1H), 6.96 – 6.95 (m, 2H), 4.37 – 4.34 (m, 2H), 2.73 (t, *J* = 7.0 Hz, 2H), 1.87 – 1.76 (m, 4H) ppm. **^{13}C NMR** (101 MHz, $CDCl_3$) δ 166.8, 142.5, 133.0, 130.6, 129.7, 128.5, 128.3, 125.5, 120.3, 64.9, 30.0, 28.5, 27.1 ppm. **IR** (neat, 3102, 3063, 3033, 2939, 2860, 1714, 1601, 1584, 1491, 1451, 1410, 1386, 1359, 1314, 1269, 1210, 1175, 1112, 1069, 1026, 1002, 952, 938, 855, 833, 805, 772, 708, 686, 674, 633 cm^{-1}). **HRMS:** m/z calcd. for ($C_{15}H_{16}NaO_2S$) $[M+Na]^+$: 283.0763 found 283.0757.

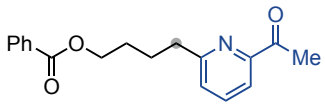

4-(6-acetylpyridin-2-yl)butyl benzoate (**4t**): Following the **general procedure C**, using 1-(6-bromopyridin-2-yl)ethan-1-one (**2u**), the crude was purified by flash column chromatography (*n*-hexane/EtOAc, 9:1), to afford **4t** (37 mg, 62% yield) as a colourless oil. **^{1}H NMR** (500 MHz, $CDCl_3$): δ 8.05 – 8.02 (m, 2H), 7.84 (dd, *J* = 7.7, 0.9 Hz, 1H), 7.71 (t, *J* = 7.7 Hz, 1H), 7.57 – 7.53 (m, 1H), 7.45 – 7.41 (m, 2H), 7.31 (dd, *J* = 7.7, 0.9 Hz, 1H), 4.38 (t, *J* = 6.4 Hz, 2H), 2.92 (t, *J* = 7.5 Hz, 2H), 2.70 (s, 3H), 2.01 – 1.93 (m, 2H), 1.91 – 1.83 (m, 2H) ppm. **^{13}C NMR** (101 MHz, $CDCl_3$) δ 200.8, 166.7, 161.2, 153.4, 137.1, 133.0, 130.5,

129.6, 128.5, 126.3, 119.1, 64.8, 37.5, 28.4, 25.84, 25.82 ppm. **IR** (neat, 3062, 3008, 2984, 2942, 2896, 1715, 1697, 1586, 1452, 1419, 1385, 1356, 1314, 1270, 1176, 1154, 1110, 1070, 1026, 994, 955, 807, 753, 710, 688, 675, 599 cm^{-1}). **HRMS:** m/z calcd. for ($C_{18}H_{19}NNaO_3$) $[M+Na]^+$: 320.1257 found 320.1254.

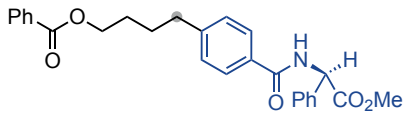

(*R*)-4-(4-((2-methoxy-2-oxo-1-phenylethyl)carbamoyl)phenyl)butyl benzoate (**4u**): Following the **general procedure C**, using methyl (*R*)-2-(4-bromobenzamido)-2-phenylacetate (**2v**), the crude was purified by flash column chromatography (*n*-hexane/EtOAc, 8:2), to afford **4u** (63 mg, 71% yield) as a white solid. m.p.: 76-79 ºC. **^{1}H NMR** (400 MHz, $CDCl_3$): δ 8.04 – 8.02 (m, 2H), 7.77 – 7.74 (m, 2H), 7.57 – 7.53 (m, 1H), 7.45 – 7.41 (m, 4H), 7.39 – 7.33 (m, 3H), 7.27 – 7.25 (m, 2H), 7.15 (d, *J* = 7.0 Hz, 1H), 5.78 (d, *J* = 7.0 Hz, 1H), 4.35 – 4.32 (m, 2H), 3.76 (s, 3H), 2.75 – 2.71 (m, 2H), 1.83 – 1.76 (m, 4H) ppm. **^{13}C NMR** (101 MHz, $CDCl_3$) δ 171.7, 166.7, 166.6, 146.5, 136.7, 133.0, 131.4, 130.4, 129.6, 129.1, 128.75, 128.68, 128.5, 127.4, 64.7, 56.9, 53.0, 35.4, 28.3, 27.6 ppm. **IR** (neat, 3339, 3061, 3033, 2949, 2863, 1744, 1710, 1637, 1611, 1585, 1570, 1522, 1494, 1451, 1436, 1396, 1355, 1315, 1283, 1568, 1205, 1192, 1175, 1148, 1121, 1112, 1098, 1070, 1027, 1003, 966, 945, 847, 766, 755, 736, 708, 698, 638, 618, 597, 541 cm^{-1}). **HRMS:** m/z calcd. for ($C_{27}H_{27}NNaO_5$) $[M+Na]^+$: 468.1781 found 468.1774.

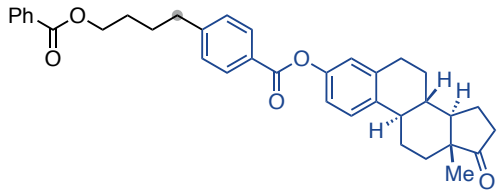

(8*R*,9*S*,13*S*,14*S*)-8,13-dimethyl-17-oxo-7,8,9,11,12,13,14,15,16,17-decahydro-6*H*-cyclopenta[*a*]phenanthren-3-yl 4-(4-(benzoyloxy)butyl)benzoate (**4v**): Following the **general procedure C**, using (8*R*,9*S*,13*S*,14*S*)-8,13-dimethyl-17-oxo-7,8,9,11,12,13,14,15,16,17-decahydro-6*H*-cyclopenta[*a*]phenanthren-3-yl 4-bromobenzoate (**2w**), the crude was purified by flash column chromatography (*n*-hexane/EtOAc, gradient 85:5 to 70:3) to afford **4v** (40 mg, 36% yield) as a white solid. m.p.: 156-159 ºC. **^{1}H NMR** (400 MHz, $CDCl_3$): δ 8.13 – 8.10 (m, 2H), 8.05 – 8.03 (m, 2H), 7.58 – 7.54 (m, 1H), 7.47 – 7.42 (m, 2H), 7.34 – 7.32 (m, 3H), 6.99 – 6.94 (m, 2H), 4.38 – 4.35 (m, 2H), 2.90 – 2.92 (m, 2H), 2.81 – 2.77 (m, 2H), 2.55 – 2.46 (m, 1H), 2.46 – 1.96 (m, 6H), 1.85 – 1.82 (m, 4H), 1.69 – 1.39 (m, 6H), 0.92 (s, 3H) ppm. **^{13}C NMR** (101 MHz, $CDCl_3$) δ 166.7, 165.5, 149.0, 148.4, 138.1, 137.5, 133.0, 130.5, 129.6, 128.7, 128.5, 127.5, 126.5, 121.8, 119.0, 64.7, 50.5, 48.1, 44.3, 38.2, 36.0, 35.7, 31.7, 29.5, 28.4, 27.6, 26.5, 25.9, 21.7, 14.0 ppm. **IR** (neat, 2928,

2858, 1733, 1716, 1606, 1491, 1452, 1414, 1372, 1315, 1261, 1221, 1173, 1148, 1119, 1067, 1009, 953, 914, 890, 847, 819, 756, 711cm^{-1}). **HRMS:** m/z calcd. for ($C_{36}H_{38}NaO_5$) [M+Na]$^+$: 573.2611 found 573.2609.

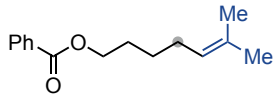

6-methylhept-5-en-1-yl benzoate (**5**): Following the **general procedure C**, using 1-bromo-2-methylprop-1-ene (**4**), 5 mol% $NiBr_2$·dme, 6 mol% dtbbpy, the crude was purified by flash column chromatography (*n*-hexane/EtOAc, 200:1) to afford **5** (26 mg, 55% yield) as a colourless oil. **^{1}H NMR** (400 MHz, $CDCl_3$): δ 8.06 – 8.04 (m, 2H), 7.57 – 7.53 (m, 1H), 7.46 – 7.41 (m, 2H), 5.15 – 5.11 (m, 1H), 4.32 (t, *J* = 6.6 Hz, 2H), 2.06 (q, *J* = 7.3 Hz, 2H), 1.81 – 1.74 (m, 2H), 1.70 (s, 3H), 1.61 (s, 3H), 1.53 – 1.45 (m, 2H) ppm. **^{13}C NMR** (101 MHz, $CDCl_3$) δ 166.8, 132.9, 132.1, 130.7, 129.7, 128.5, 124.3, 65.2, 28.5, 27.8, 26.4, 25.9, 17.8 ppm. **IR** (neat, 3063, 2927, 2857, 1719, 1602, 1451, 1378, 1314, 1271, 1176, 1112, 1069, 1027, 710 cm^{-1}). **HRMS:** m/z calcd. for ($C_{15}H_{20}NaO_2$) [M+Na]$^+$: 255.1356 found 255.1362.

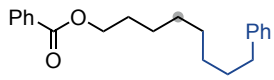

8-phenyloctyl benzoate (**7**): Following the **general procedure C**, using (4-bromobutyl)benzene (**6**) the crude was purified by flash column chromatography (*n*-hexane/EtOAc, 100:1), followed by further drying under high vacuum at 120 ºC for 2 hours, to afford **7** (30 mg, 48% yield) as a colourless oil. **^{1}H NMR** (400 MHz, $CDCl_3$): δ 8.07 – 8.04 (m, 2H), 7.58 – 7.54 (m, 1H), 7.46 – 7.42 (m, 2H), 7.30 – 7.26 (m, 2H), 7.19 – 7.16 (m, 3H), 4.32 (t, *J* = 6.7 Hz, 1H), 2.63 – 2.59 (m, 1H), 4.32 (t, *J* = 6.6 Hz, 2H), 2.06 (q, *J* = 7.3 Hz, 2H), 1.83 – 1.73 (m, 2H), 1.70 (d, *J* = 0.9 Hz, 2H), 1.80 – 1.73 (m, 2H), 1.66 – 1.58 (m, 2H), 1.49 – 1.41 (m, 2H), 1.38 – 1.33 (m, 6H) ppm. **^{13}C NMR** (101 MHz, $CDCl_3$) δ 166.8, 143.0, 132.9, 130.7, 129.7, 128.53, 128.48, 128.4, 125.7, 65.3, 36.1, 31.6, 29.5, 29.37, 29.35, 28.9, 26.2 ppm. **IR** (neat, 3061, 3026, 2927, 2854, 1717, 1602, 1495, 1451, 1386, 1314, 1270, 1210, 1176, 1155, 1101, 1069, 1026, 1002, 959, 747, 709, 698 cm^{-1}). **HRMS:** m/z calcd. for ($C_{21}H_{26}NaO_2$) [M+Na]$^+$: 333.1825 found 333.1825.

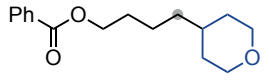

4-(tetrahydro-2*H*-pyran-4-yl)butyl benzoate (**9**): Following the **general procedure C**, using 4-bromotetrahydro-2*H*-pyran (**8**), 10 mol% $NiBr_2$·dme, 12 mol% dtbbpy and stirring for 72h, the crude was purified by flash column chromatography (*n*-hexane/EtOAc, 95:5) to afford **9** (21 mg, 40% yield) as a colourless oil. **^{1}H NMR** (400 MHz, $CDCl_3$): δ 8.06 – 7.03 (m, 2H), 7.58 – 7.53 (m, 1H), 7.46 – 7.42 (m, 2H), 4.32 (t, *J* = 6.6 Hz, 2H), 3.97 – 3.93 (m, 2H),

3.36 (td, *J* = 11.8, 2.1 Hz, 2H), 1.80 – 1.73 (m, 2H), 1.62 – 1.58 (m, 2H), 1.53 – 1.43 (m, 3H), 1.34 – 1.25 (m, 4H) ppm. **^{13}C NMR** (101 MHz, $CDCl_3$) δ 166.8, 133.0, 130.6, 129.7, 128.5, 68.3, 65.1, 36.7, 35.0, 33.3, 29.0, 23.0 ppm. **IR** (neat, 2958, 2927, 2863, 2841, 2759, 1715, 1600, 1584, 1476, 1464, 1450, 1387, 1356, 1333, 1313, 1273, 1228, 1177, 1147, 1114, 1097, 1069, 1027, 1013, 981, 955, 901, 859, 814, 712, 687, 675, 610 cm^{-1}). **HRMS:** m/z calcd. for ($C_{16}H_{22}NaO_3$) $[M+Na]^+$: 285.1461 found 285.1459.

2.5.5. Mechanistic investigations

Kinetic isotope effect (KIE)

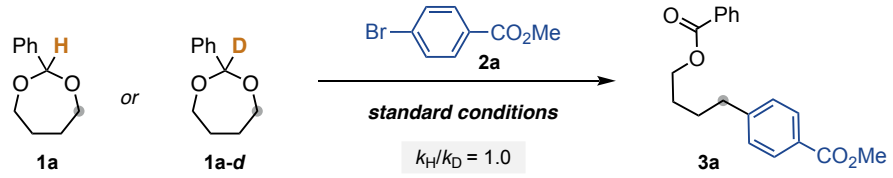

To a 5 mL Crimp Top vial equipped with magnetic stirring was charged methyl 4-bromobenzoate (**2a**, 43.0 mg, 0.20 mmol, 1.0 equiv.), dtbbpy (1.6 mg, 0.03 mmol, 3 mol%) and ($Ir[dF(CF_3)ppy]_2(dtbbpy)PF_6$) (1.1 mg, 0.005 mmol, 0.5 mol%). Subsequently the vial was brought inside a nitrogen-filled glovebox, and Na_2CO_3 (42.4 mg, 0.40 mmol, 2.0 equiv.), quinuclidine (5.6 mg, 0.25 mmol, 25 mol%) and $NiBr_2$·dme (1.5 mg, 0.025 mmol, 2.5 mol%) were added. Then the vial was sealed with a crimp cap and taken outside the glovebox, were *tert*-Amyl alcohol (1.0 mL, 0.2 M) and 2-phenyl-1,3-dioxepane (**1a**, 71.3 mg, 0.4 mmol, 2.0 equiv.) or 2-phenyl-1,3-dioxepane-2-*d* (**1a-*d***, 72.0 mg, 0.4 mmol, 2.0 equiv.) were added sequentially via syringe. The reaction was stirred at 500 rpm under blue LED irradiation with a cooling system set at 20 ºC. decane (39 μl, 0.2 mmol, 1.0 equiv.), as internal standard, was added to the reaction mixture and aliquots were taken at 4, 8, 12, 14, and 16 hours. The reaction mixture was diluted with EtOAc, washed with water and the organic layer filtered through silica gel. The organic phase was analysed by GC FID analysis. The k_H/k_D was calculated to be 1.0 by plotting the data points and comparing the slopes of the two curves.

Deuterium scrambling

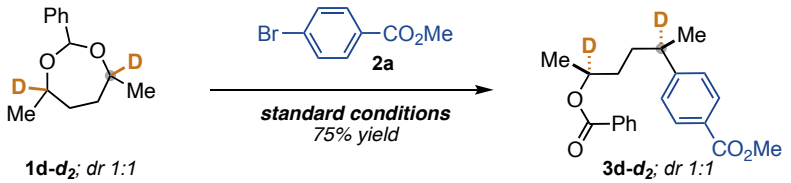

To a 5 mL Crimp Top vial equipped with magnetic stirring was charged methyl 4-bromobenzoate (**2a**, 43.0 mg, 0.20 mmol, 1.0 equiv.) dtbbpy (1.6 mg, 0.03 mmol, 3 mol%)

and (Ir[dF(CF_3)ppy]$_2$(dtbbpy)PF_6) (1.1 mg, 0.005 mmol, 0.5 mol%). Subsequently the vial was brought inside a nitrogen-filled glovebox, and Na_2CO_3 (42.4 mg, 0.40 mmol, 2.0 equiv.), quinuclidine (5.6 mg, 0.25 mmol, 25 mol%) and $NiBr_2$·dme (1.5 mg, 0.025 mmol, 2.5 mol%) were added. Then the vial was sealed with a crimp cap and taken outside the glovebox, were *tert*-Amyl alcohol (1.0 mL, 0.2 M) and 4,7-dimethyl-2-phenyl-1,3-dioxepane-4,7-d_2 (**1d-d^2,** 83.3 mg, 0.4 mmol, 2.0 equiv.) were added sequentially via syringe. The reaction was stirred at 500 rpm under blue LED irradiation with a cooling system set at 20 ºC for 16 hours at 20ºC. After the reaction was completed, the mixture was diluted with EtOAc and washed with water. The aqueous phase was washed with EtOAc (2 times), dried over anhydrous Na_2SO_4 and concentrated under reduced pressure. The crude was purified by flash column chromatography (*n*-hexane/EtOAc, gradient 95:5 to 9:1) to afford **3d-d_2** (51 mg, 75% yield) as a colourless oil. No deuterium scrambling was observed which argues against a 1,3-HAT process.

methyl 4-(5-(benzoyloxy)hexan-2-yl-2,5-d_2)benzoate (**3d-d_2**): **^{1}H NMR** (400 MHz, $CDCl_3$): δ 8.06 – 7.97 (m, 4H), 7.59 – 7.54 (m, 1H), 7.47 – 4.43 (m, 2H), 7.29 – 7.25 (m, 2H), 3.93 and 3.92 (s, 3H), 1.79 – 1.45 (m, 4H), 1.30 – 1.27 (m, 6H) ppm. **^{13}C NMR** (101 MHz, $CDCl_3$) δ 167.2, 166.3, 166.2, 152.7, 152.6, 132.89, 132.87, 130.9, 130.8, 130.0, 129.9, 129.6, 128.42, 128.41, 128.2, 127.14, 127.12, 71.4, 71.3, 71.1, 70.8, 52.1, 39.9, 39.7, 39.5, 39.3, 34.1, 34.0, 33.8, 33.5, 22.3, 22.1, 20.1, 20.0 ppm.

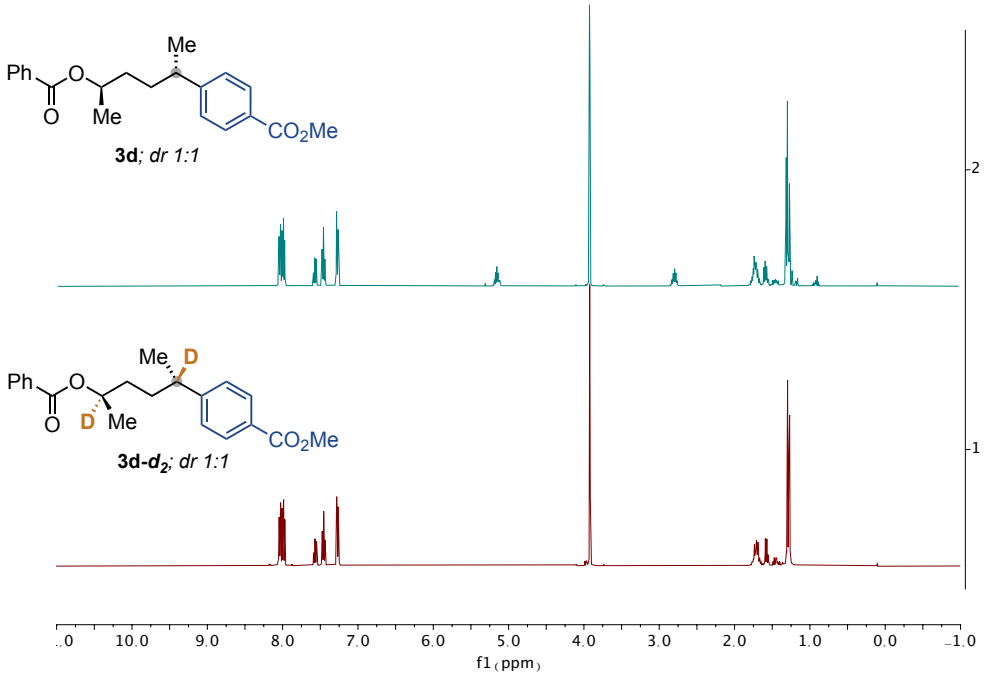

Radical-trapping experiments

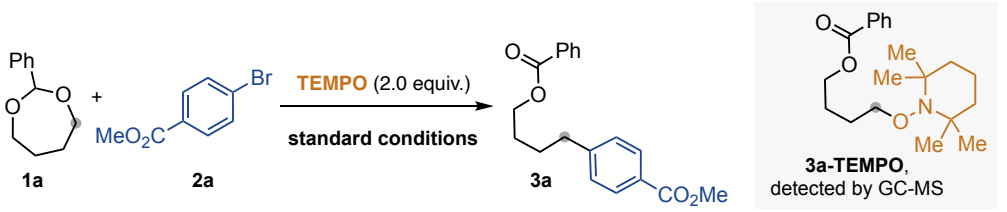

To a 5 mL Crimp Top vial equipped with magnetic stirring was charged methyl 4-bromobenzoate (**2a**, 43.0 mg, 0.20 mmol, 1.0 equiv.), dtbbpy (1.6 mg, 0.03 mmol, 3 mol%), (Ir[dF(CF_3)ppy]$_2$(dtbbpy)PF_6) (1.1 mg, 0.005 mmol, 0.5 mol%) and TEMPO (2.0 equiv.). Subsequently the vial was brought inside a nitrogen-filled glovebox, and Na_2CO_3 (42.4 mg, 0.40 mmol, 2.0 equiv.), quinuclidine (5.6 mg, 0.25 mmol, 25 mol%) and $NiBr_2$·dme (1.5 mg, 0.025 mmol, 2.5 mol%) were added. Then the vial was sealed with a crimp cap and taken outside the glovebox, were *tert*-Amyl alcohol (1.0 mL, 0.2 M) and 2-phenyl-1,3-dioxepane (**1a**, 71.3 mg, 0.4 mmol, 2.0 equiv.) were added sequentially via syringe. The reaction was stirred at 500 rpm for 16 hours at 20ºC under blue LED irradiation. After the reaction was completed, the mixture was diluted with EtOAc, washed with water and the organic layer filtered through silica gel. The crude was analysed by GC-MS and ^{1}H NMR analysis and **3a-TEMPO** adduct was detected (69% yield based on relative integration with remaining **1a**). **GC-MS** ($C_{20}H_{31}NO_3$) [M]: found t = 9.122 min, m/z 333.3.

Pre-formed oxidative addition complex

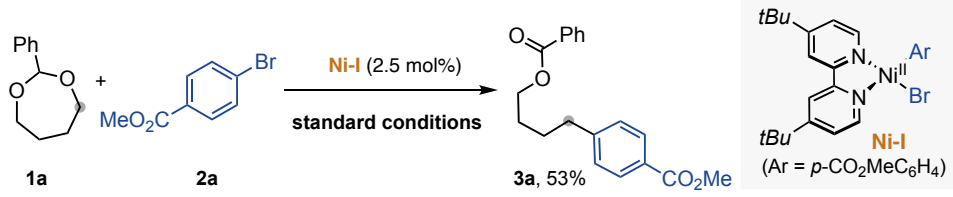

To a 5 mL Crimp Top vial equipped with magnetic stirring was charged methyl 4-bromobenzoate (**2a**, 43.0 mg, 0.20 mmol, 1.0 equiv.) and (Ir[dF(CF_3)ppy]$_2$(dtbbpy)PF_6) (1.1 mg, 0.005 mmol, 0.5 mol%). Subsequently the vial was brought inside a nitrogen-filled glovebox, and Na_2CO_3 (42.4 mg, 0.40 mmol, 2.0 equiv.), quinuclidine (5.6 mg, 0.25 mmol, 25 mol%) and **Ni-I** precomplex (2.7 mg, 0.025 mmol, 2.5 mol%) were added.[2] Then the vial was sealed with a crimp cap and taken outside the glovebox, were *tert*-Amyl alcohol (1.0 mL, 0.2 M) and 2-phenyl-1,3-dioxepane (**1a**, 71.3 mg, 0.4 mmol, 2.0 equiv.) were added sequentially via syringe. The reaction was stirred at 500 rpm for 16 hours at 20ºC under blue LED irradiation. After the reaction was completed, the mixture was diluted with EtOAc and washed with water. The aqueous phase was washed with EtOAc (2 times), dried over

anhydrous Na_2SO_4 and concentrated under reduced pressure. The crude was purified by flash column chromatography (*n*-hexane/EtOAc, gradient 95:5 to 9:1) to afford **3a** (33 mg, 53% yield) as a white solid.

Computational studies

All structures were optimised using density functional theory (DFT) as implemented in Gaussian 16,[10] with M06-2X[11] as functional and 6-311++G(d,p) as basis set, introducing solvation factors with the IEF-PCM[12] method (2-methyl-2-propanol as solvent). The stationary points were characterised by frequency calculations in order to verify that they have the right number of imaginary frequencies.

In the main text, the most stable conformation of the six-membered radical species has been shown **85**-rad, which shows a distorted chair structure. The distorted boat radical was also computed and found to be 1.5 kcal/mol higher in energy. The opposite preference was found during the transition states. The lowest in energy is **85**-TS, a boat like transition state, as shown in the manuscript. Meanwhile, the chair like TS, **85**-TS-chair is even higher in energy ($\Delta\Delta G^{\ddagger}$ = 23.4 kcal/mol), due to its enhanced distortion and larger breaking C–O bond, *ca*. 2.0 Å

85-rad G = 0 distorted chair | **85**-rad-boat G = 1.5 distorted boat | **85**-TS $\Delta\Delta G^{\ddagger}$ = 21.0 | **85**-TS-chair $\Delta\Delta G^{\ddagger}$ = 23.4

For the relative stabilities of the different radical species **85**-rad, **86**-rad and **87**-rad, the corresponding equilibria between radical and C–H species were computed. For example, in the comparison between the six and seven membered cycles, the equilibrium (shown below) is shifted to the left by 2.9 kcal/mol, corroborating the preferential formation (>100:1) of **86**-rad over **85**-rad.

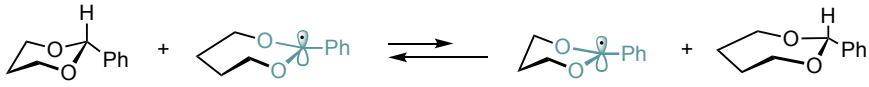

85-H **86**-rad **85**-rad **86**-H

Compound	E (M06-2X)	Correction to G	G (M06-2X)	ΔG	Negative Frequency
85-H	-538.650538	0.167918	-538.482621	--	
85-rad	-538.005909	0.154734	-537.851175	0.0	
85-TS	-537.967969	0.150213	-537.817757	21.0	-1200.1
85-rad-boat	-538.002924	0.154179	-537.848745	1.5	
85-TS-chair	-537.964020	0.150088	-537.813932	23.4	-1022.8
86-H	-577.953082	0.196423	-577.756659	--	
86-rad	-577.311761	0.181963	-577.129799	0.0	
87-TS	-577.279236	0.178166	-577.101070	18.0	-909.6
87-H	-617.255225	0.224363	-617.030863	--	
87-rad	-616.611824	0.209614	-616.402210	0.0	
87-TS	-616.579769	0.206768	-616.373000	18.3	-828.8

Table 8. Energies of the structures studied in the main text and figure above. Energies are given in Hartress. ΔG in kcal·mol^{-1}

2.5.6. NMR spectra

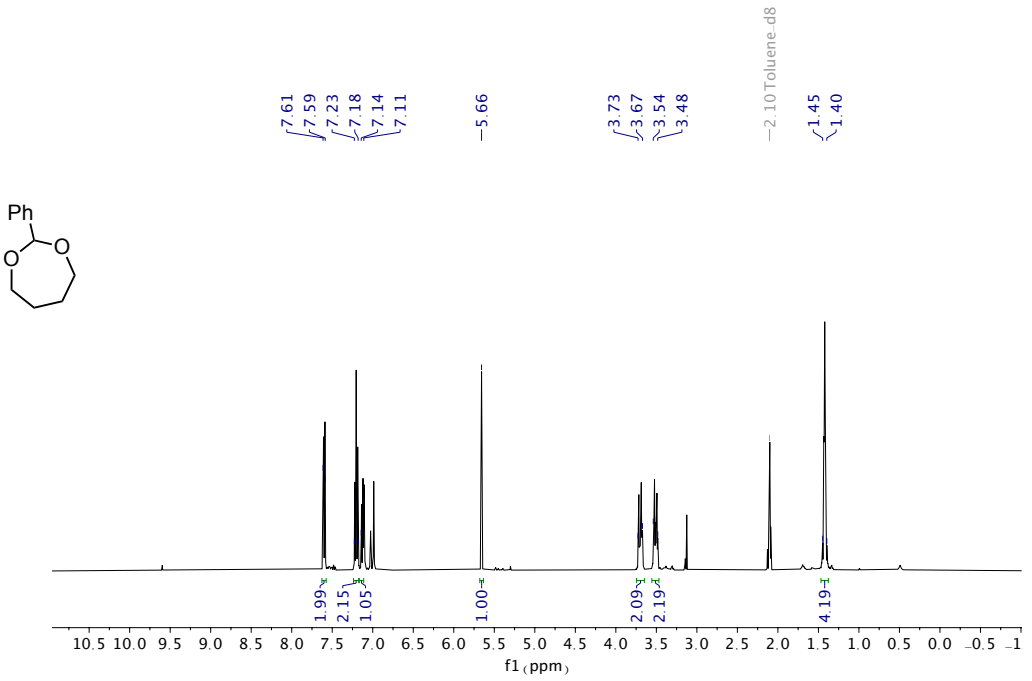

*[1]H NMR spectra (400 MHz) of **1a***

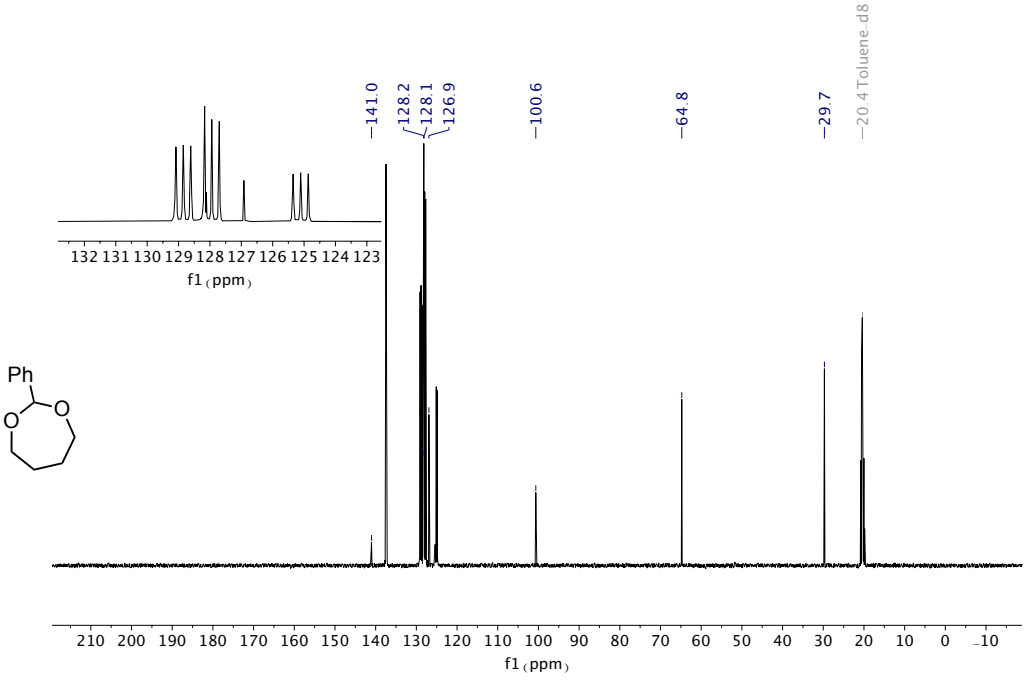

*[13]C NMR spectra (101 MHz) of **1a***

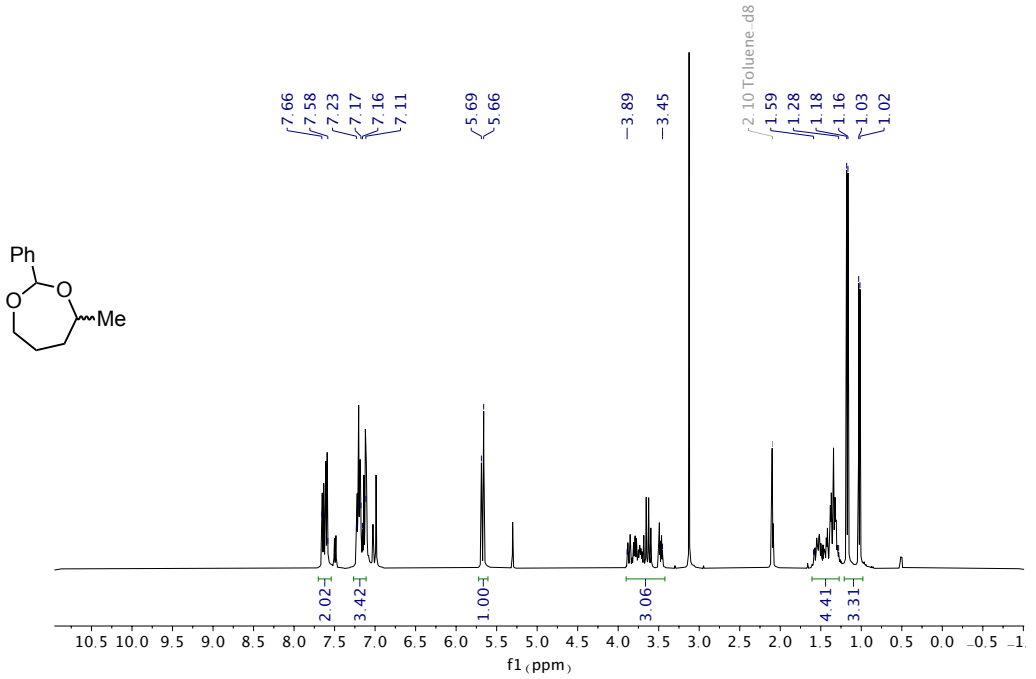

*[1]H NMR spectra (400 MHz) of **1b***

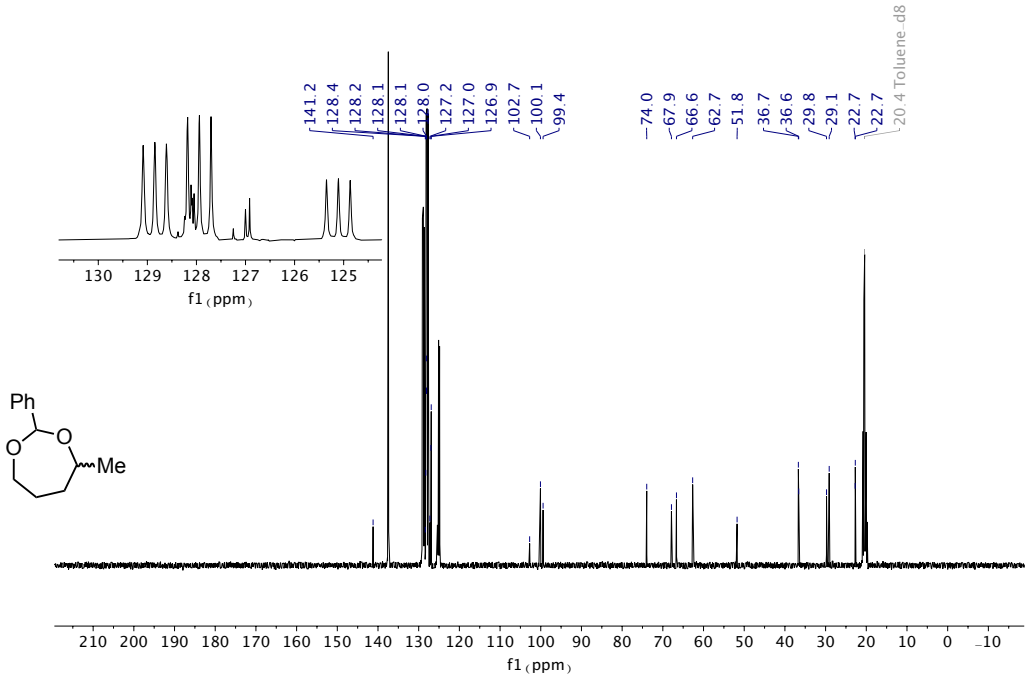

*[13]C NMR spectra (101 MHz) of **1b***

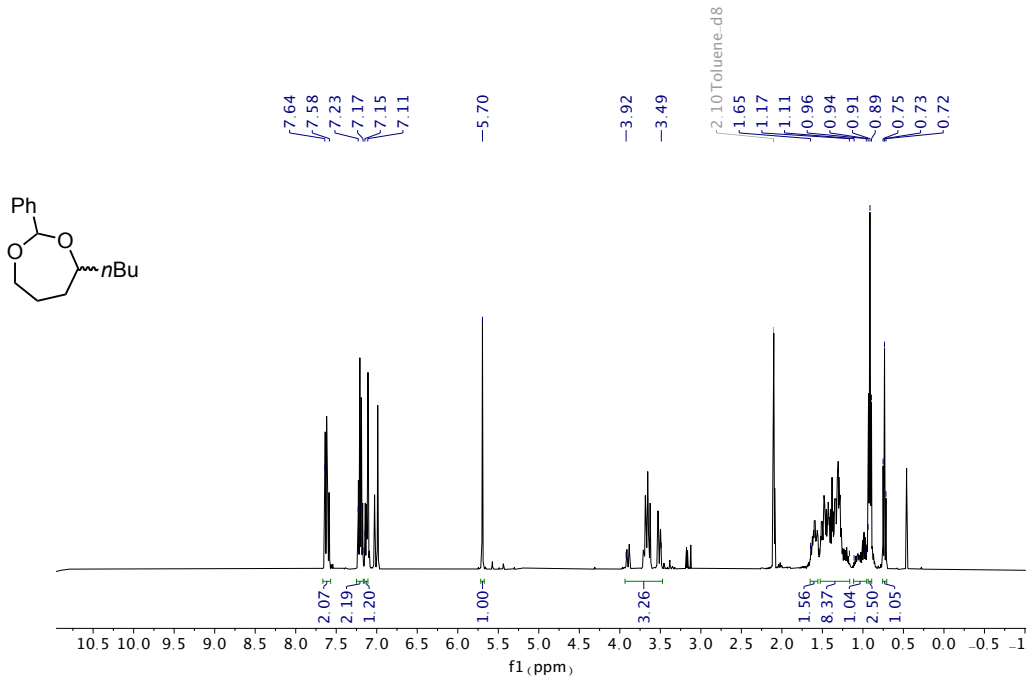

[1]H NMR spectra (400 MHz) of ***1c***

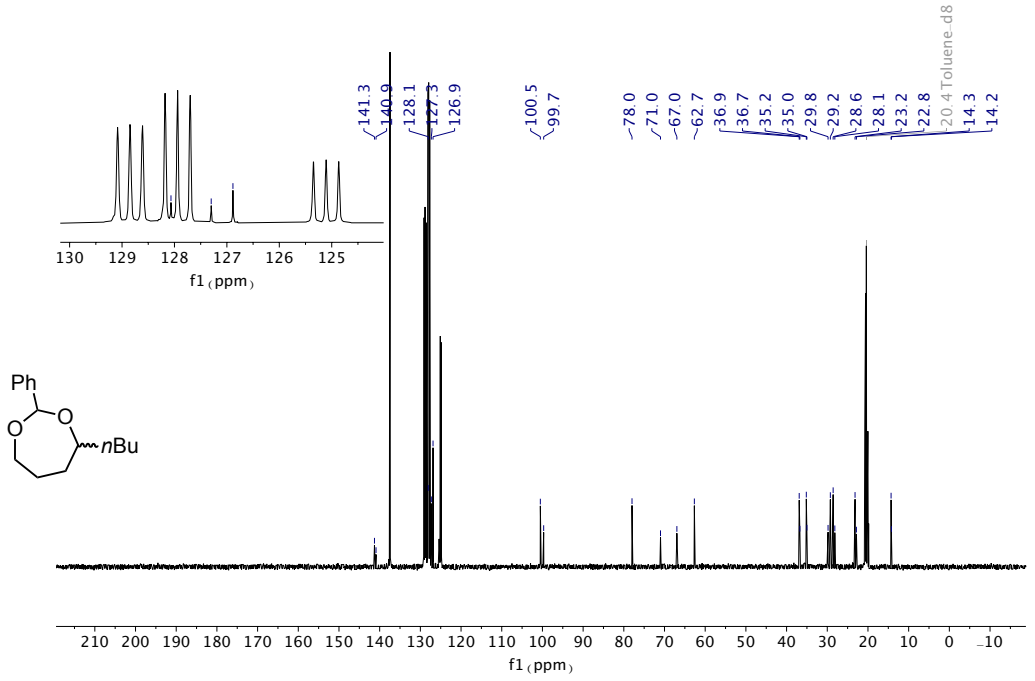

[13]C NMR spectra (101 MHz) of ***1c***

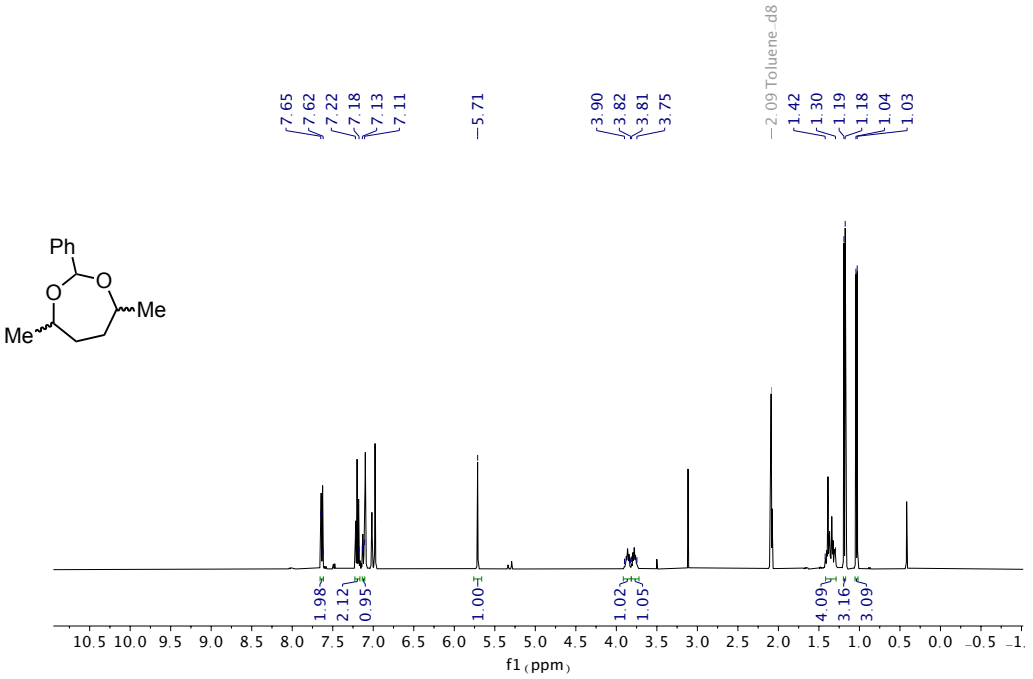

*^{1}H NMR spectra (400 MHz) of **1d***

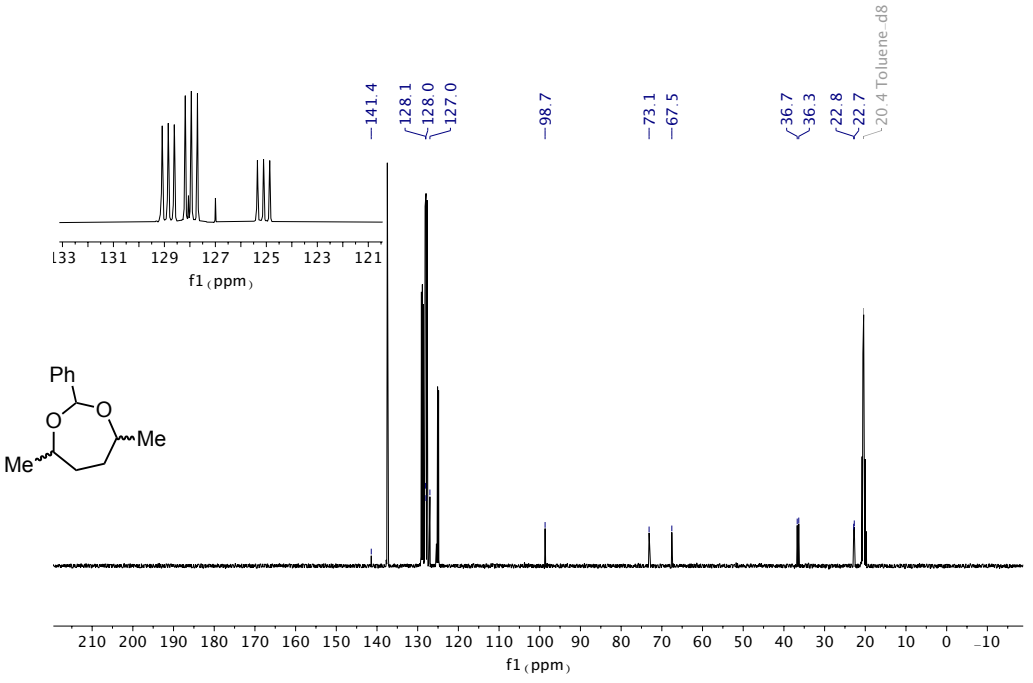

*^{13}C NMR spectra (101 MHz) of **1d***

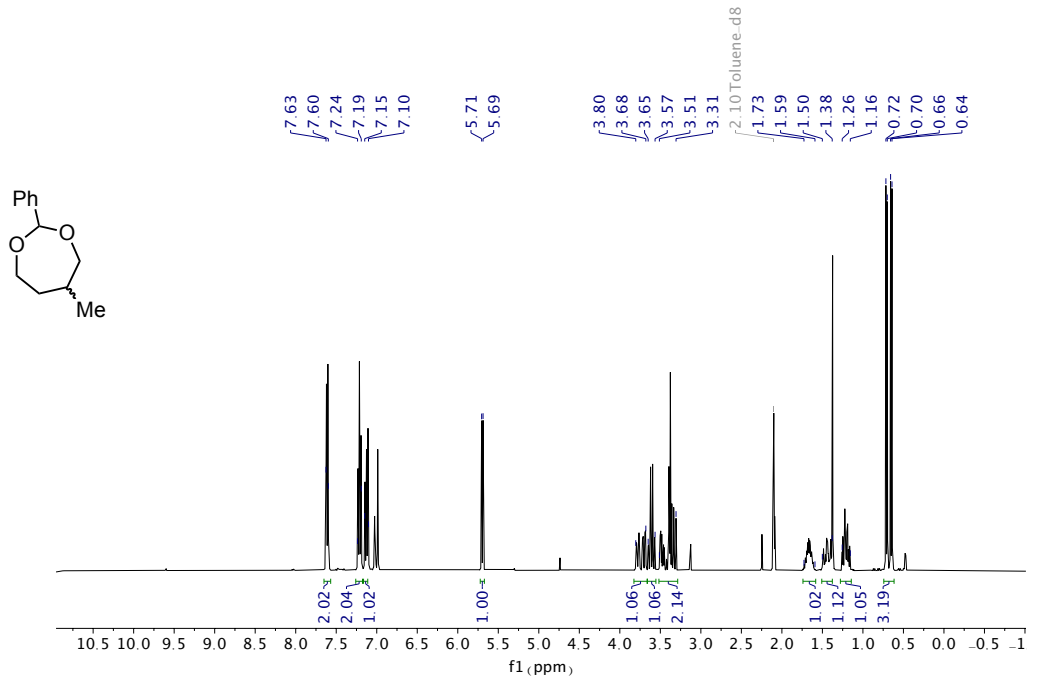

*[1]H NMR spectra (400 MHz) of **1e***

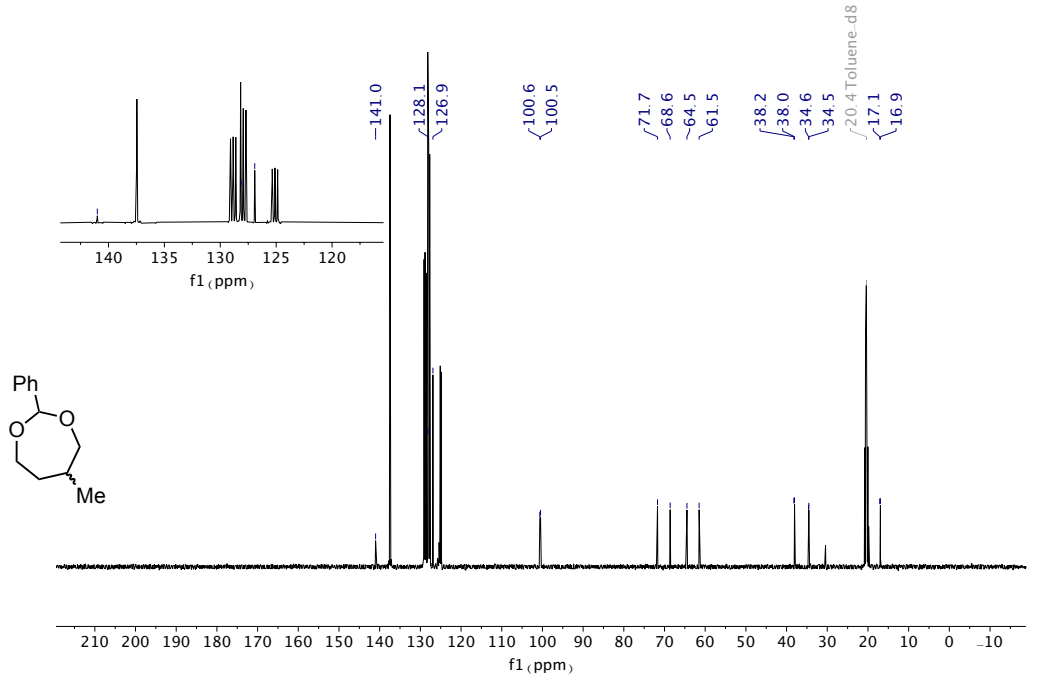

*[13]C NMR spectra (101 MHz) of **1e***

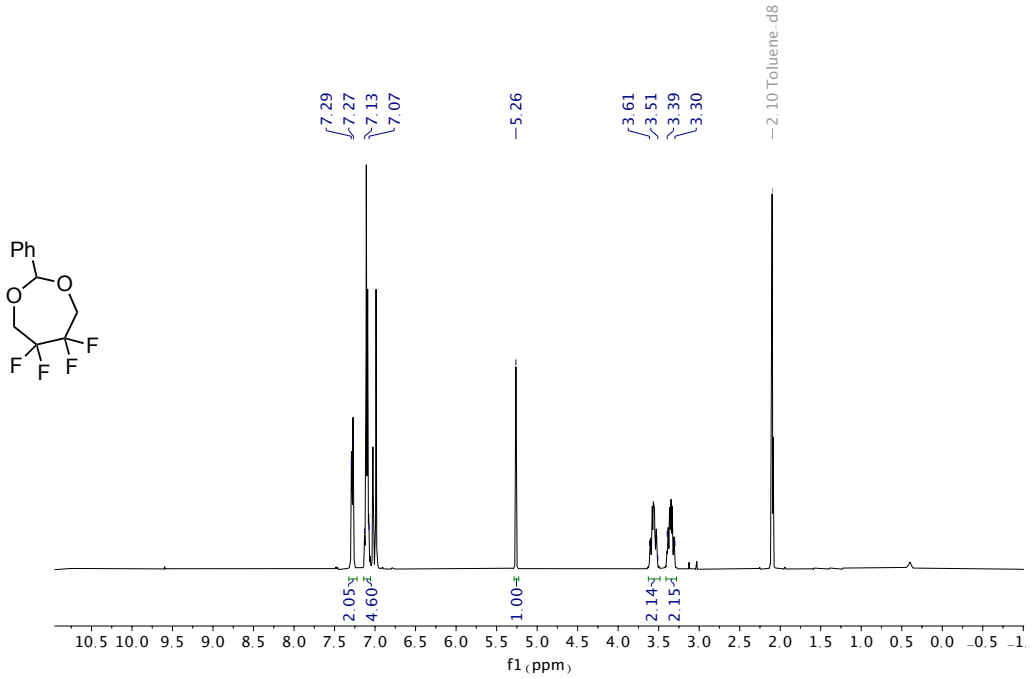

*[1]H NMR spectra (400 MHz) of **1f***

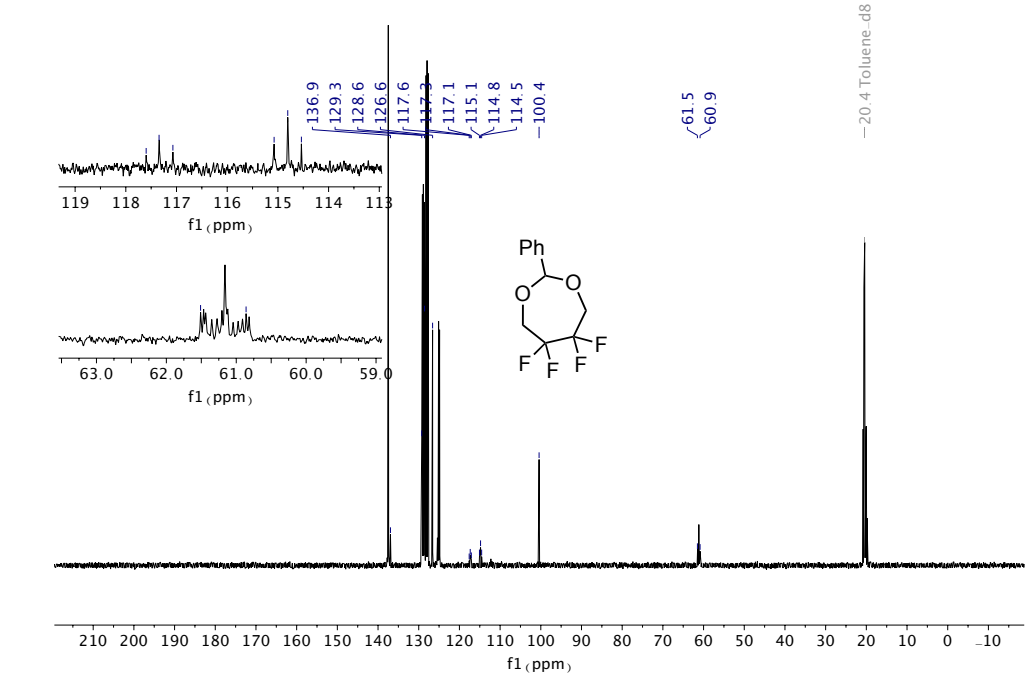

*[13]C NMR spectra (101 MHz) of **1f***

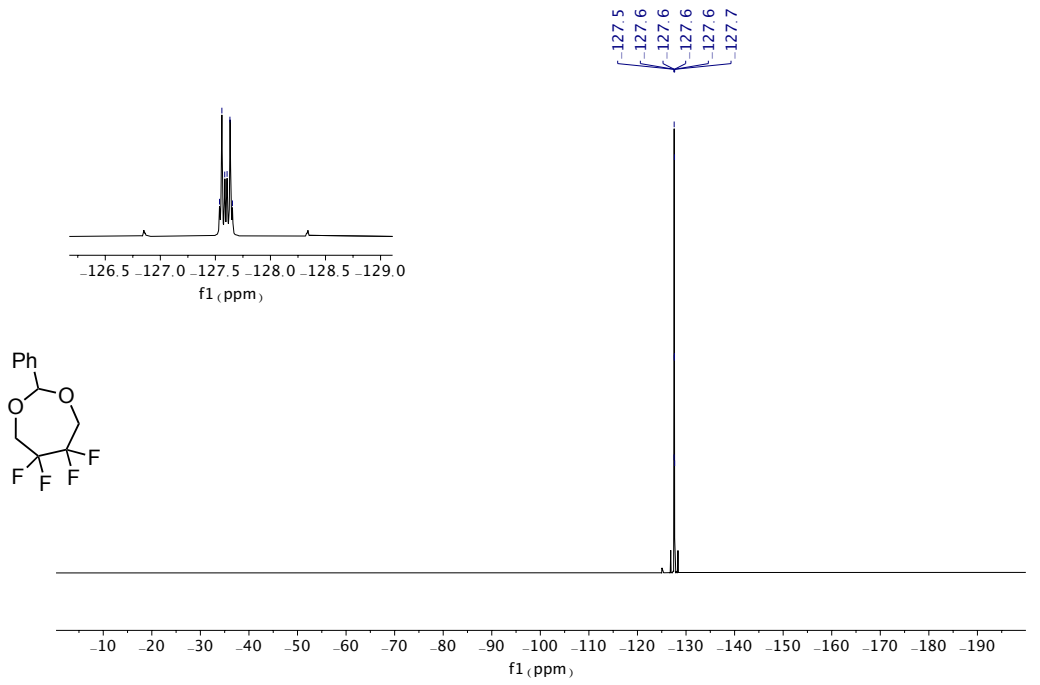

*[19]F NMR spectra (376 MHz) of **1g***

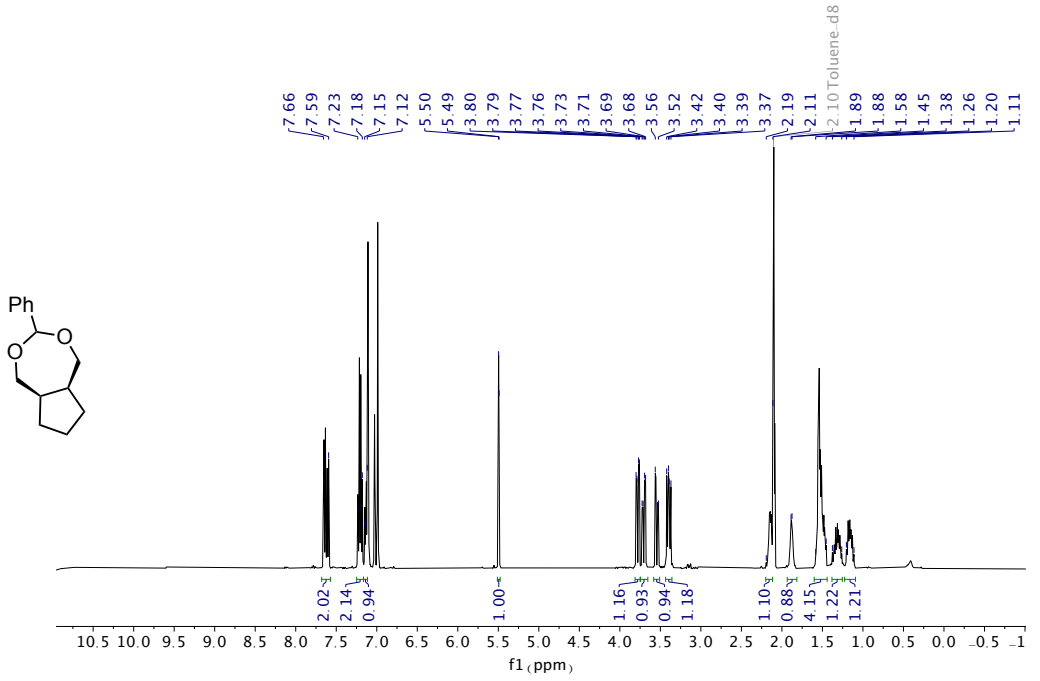

*[1]H NMR spectra (400 MHz) of **1g***

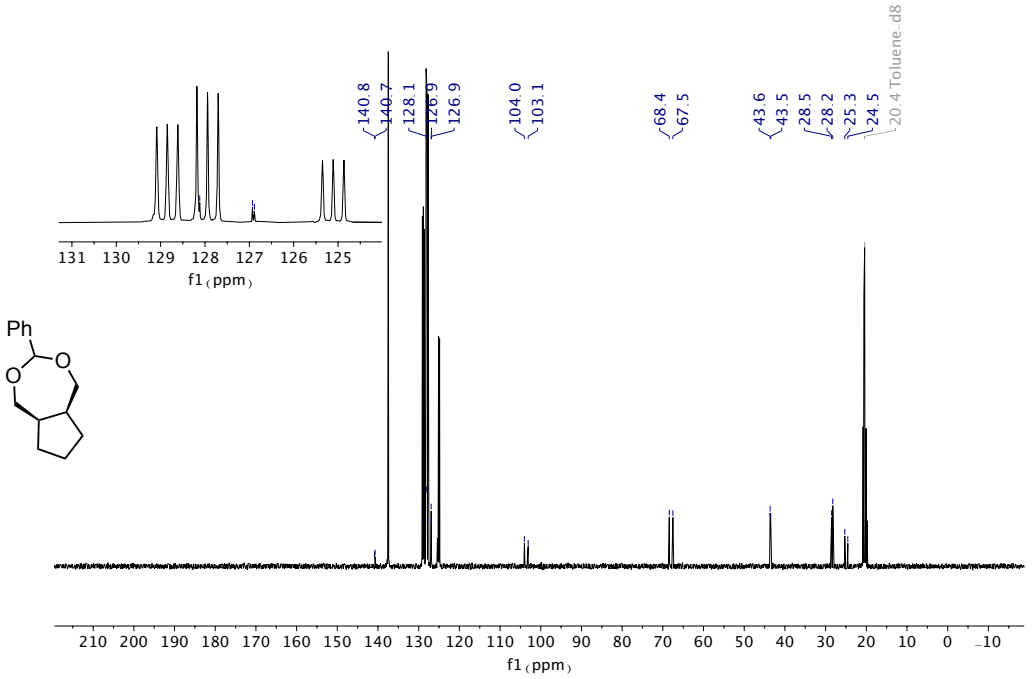

*^{13}C NMR spectra (101 MHz) of **1g***

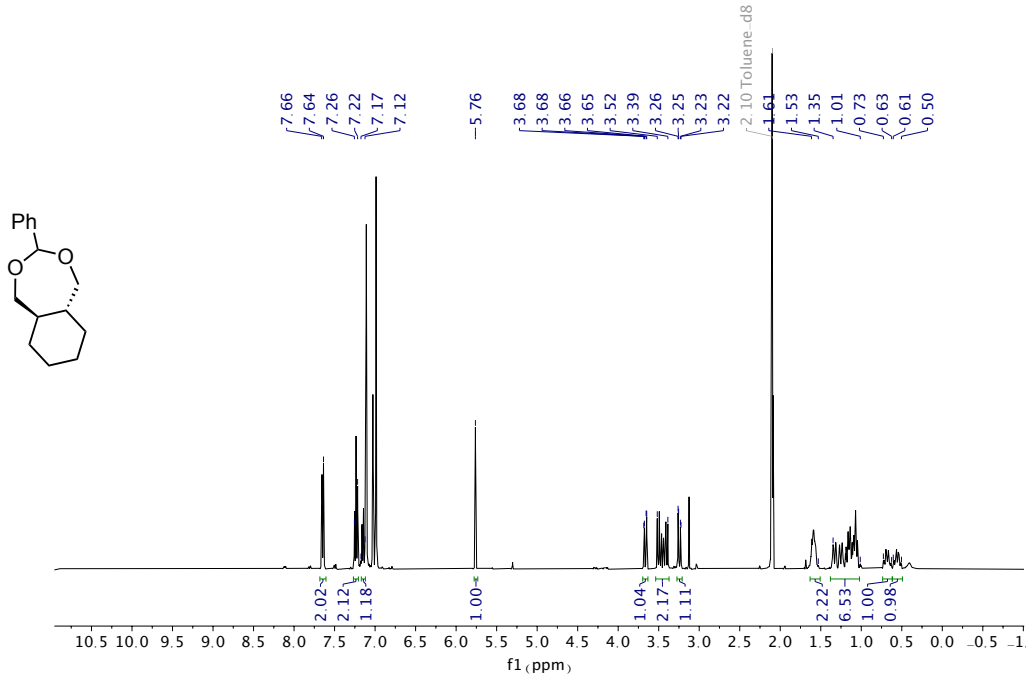

*^{1}H NMR spectra (400 MHz) of **1h***

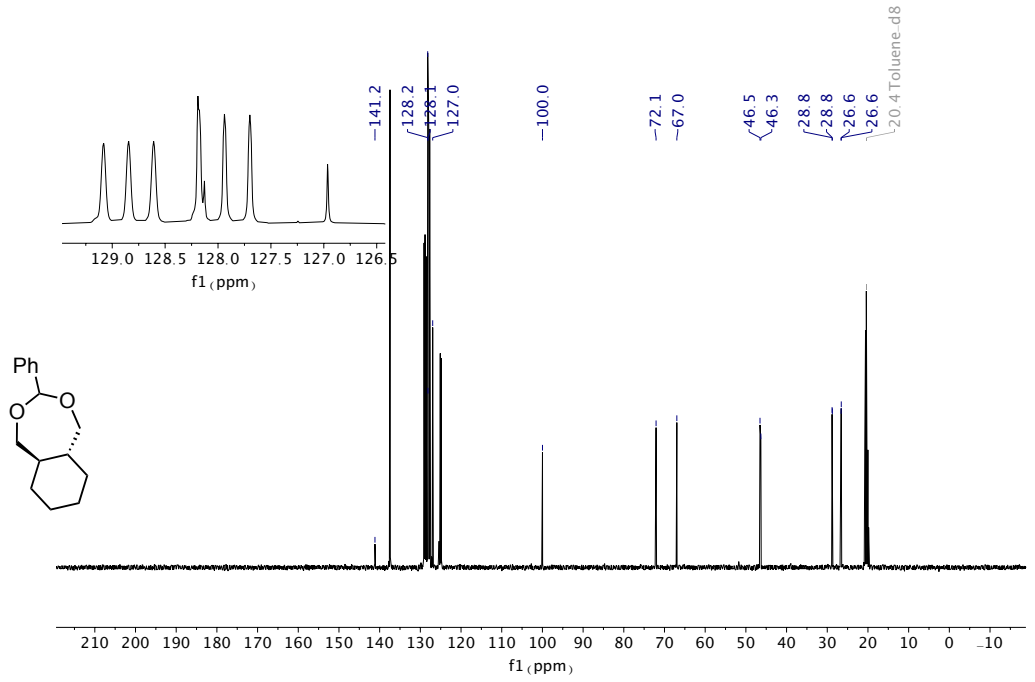

*[13]C NMR spectra (101 MHz) of **1h***

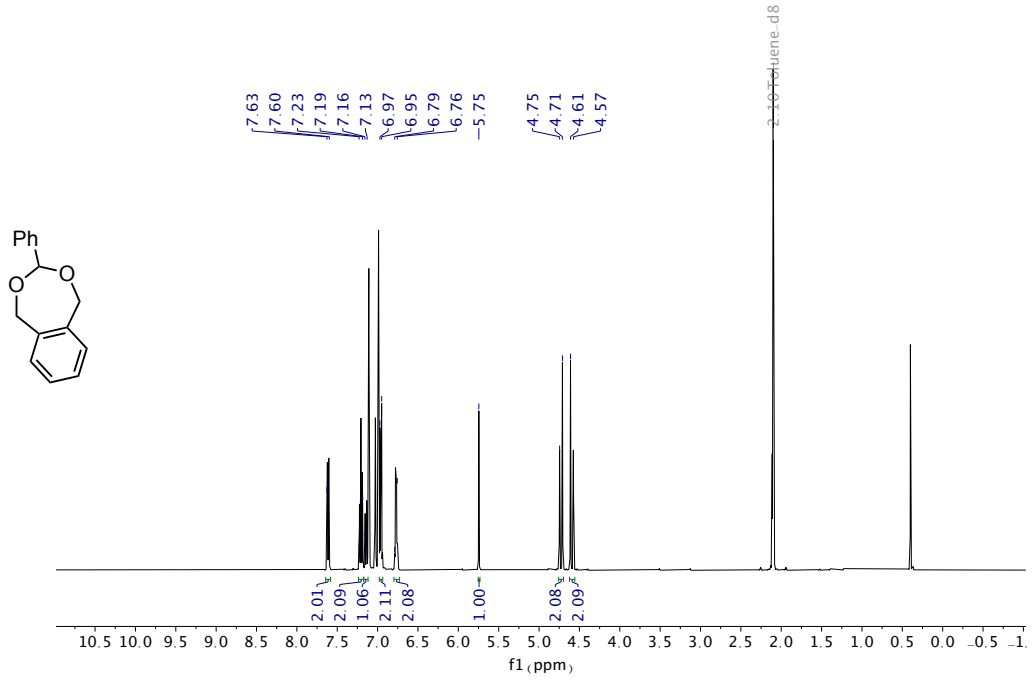

*[1]H NMR spectra (400 MHz) of **1i***

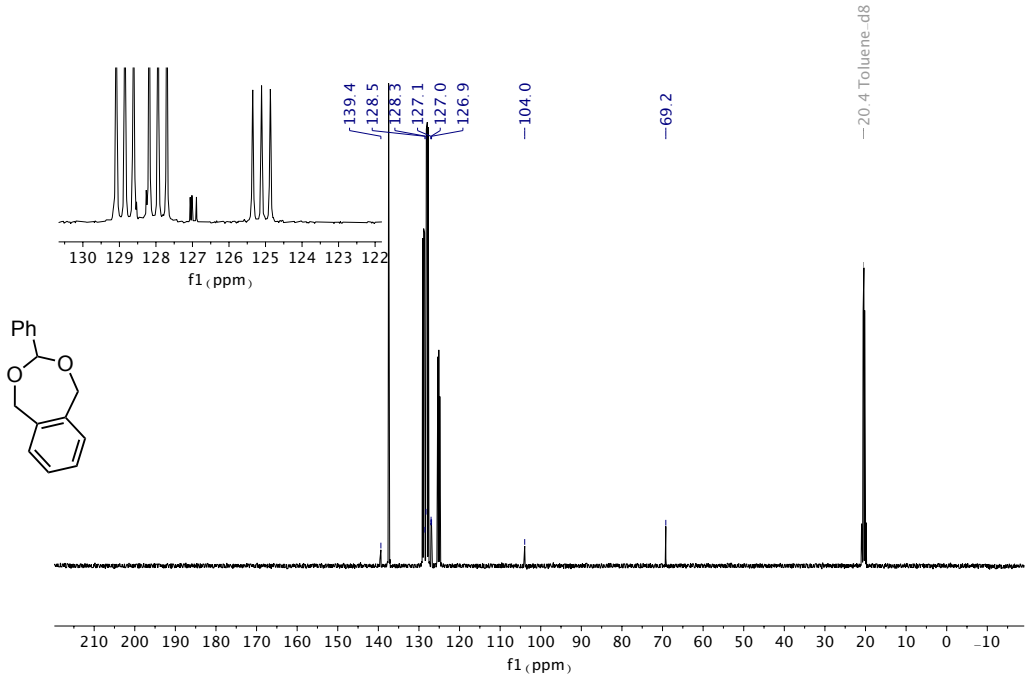

*^{13}C NMR spectra (101 MHz) of **1i***

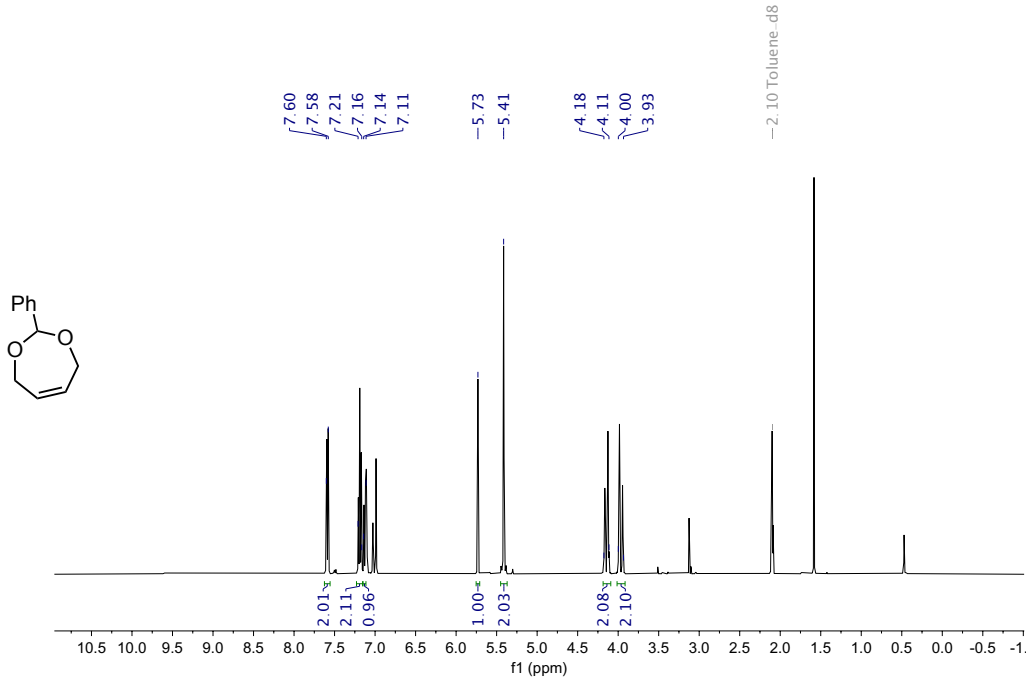

*^{1}H NMR spectra (400 MHz) of **1j'***

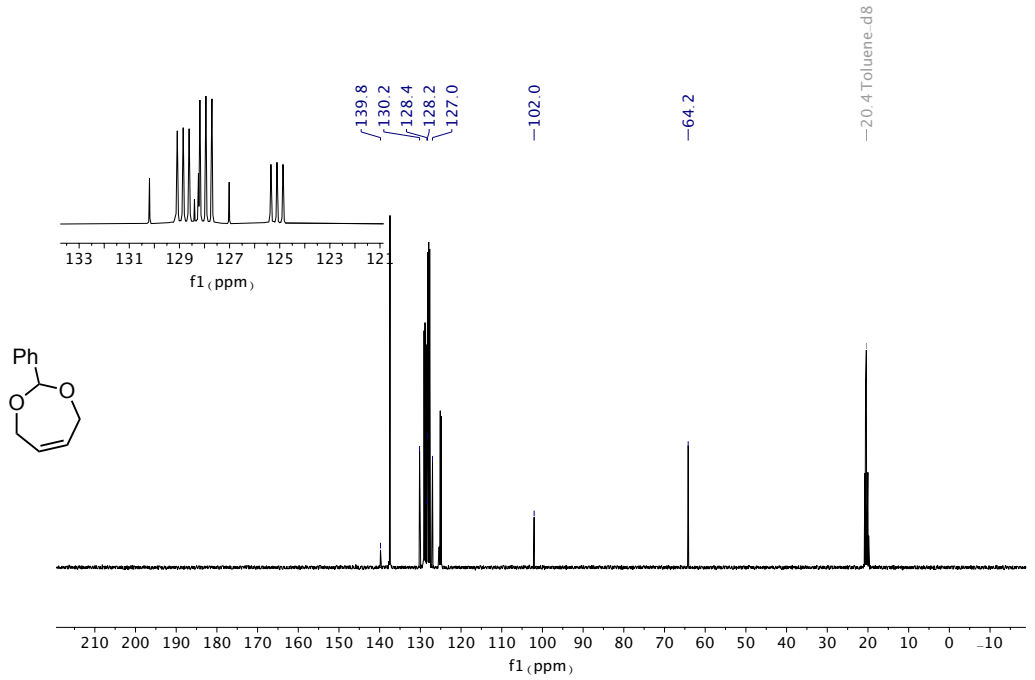

*^{13}C NMR spectra (101 MHz) of **1j'***

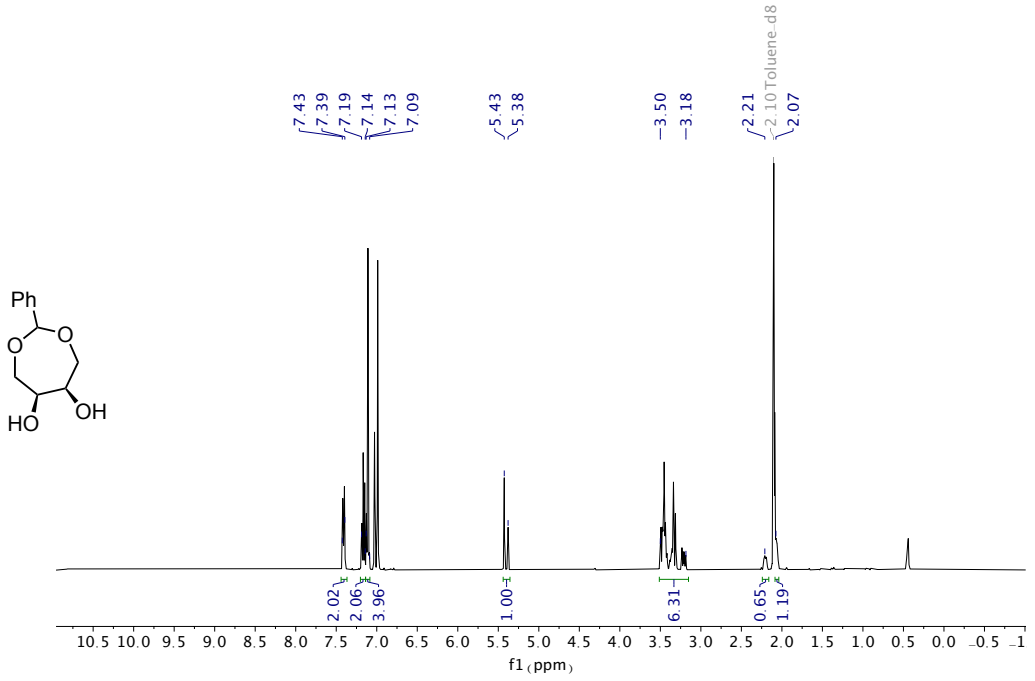

*^{1}H NMR spectra (400 MHz) of **1j***

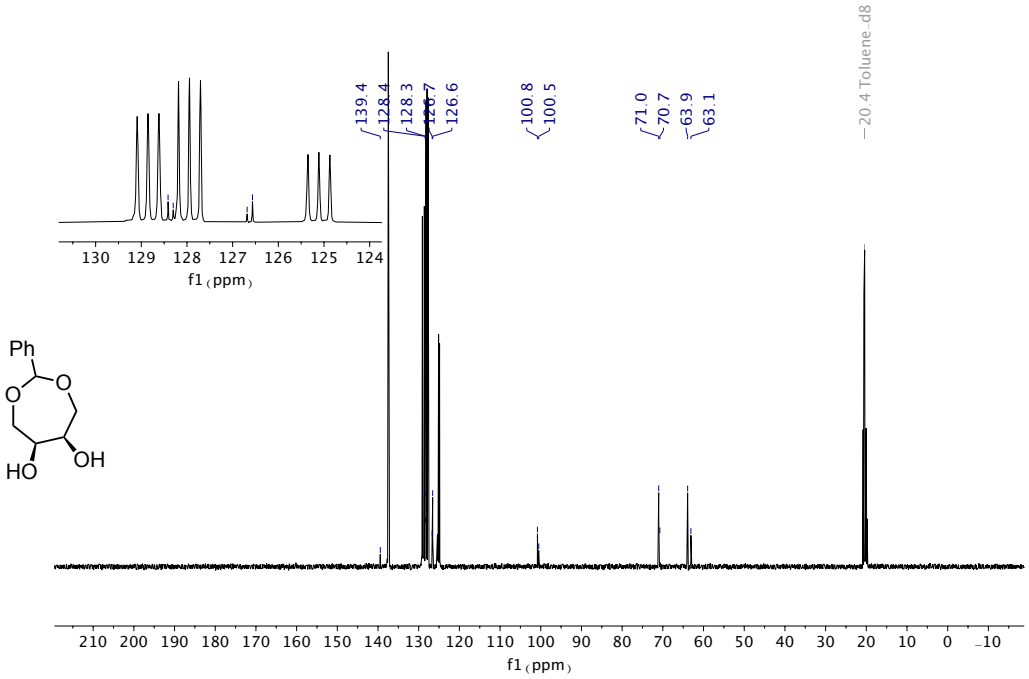

*^{13}C NMR spectra (101 MHz) of **1j***

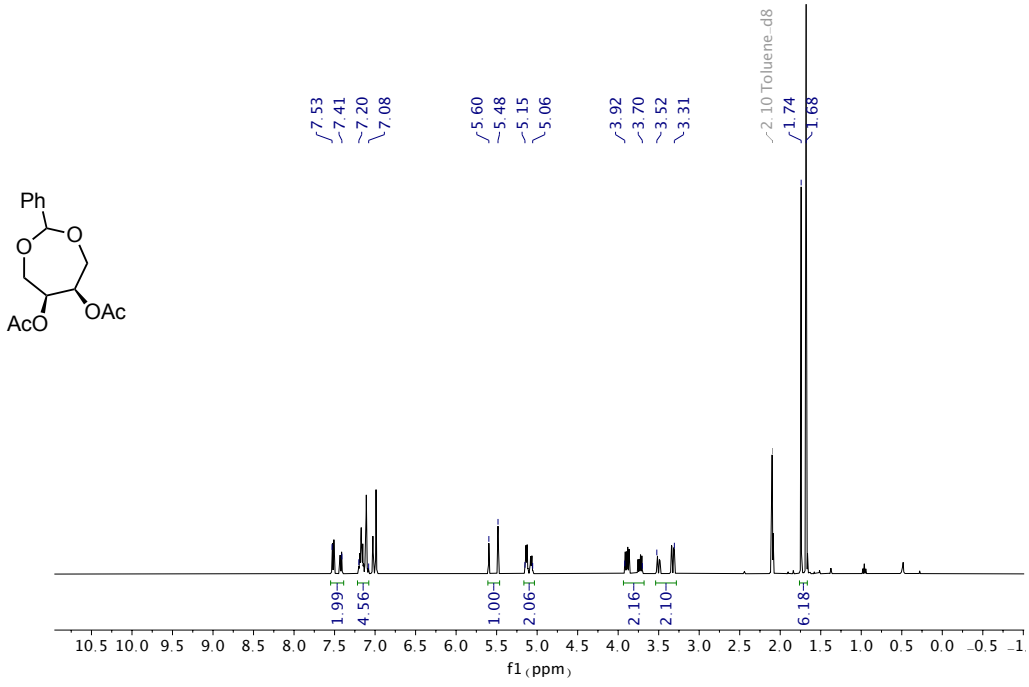

*^{1}H NMR spectra (400 MHz) of **1k***

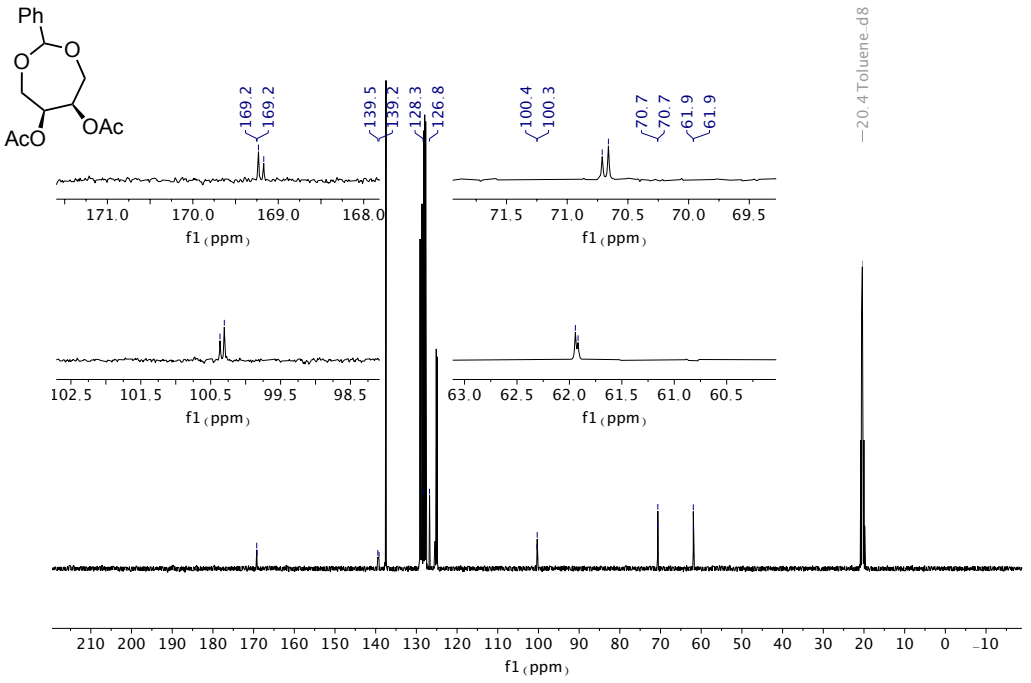

*[13]C NMR spectra (101 MHz) of **1k***

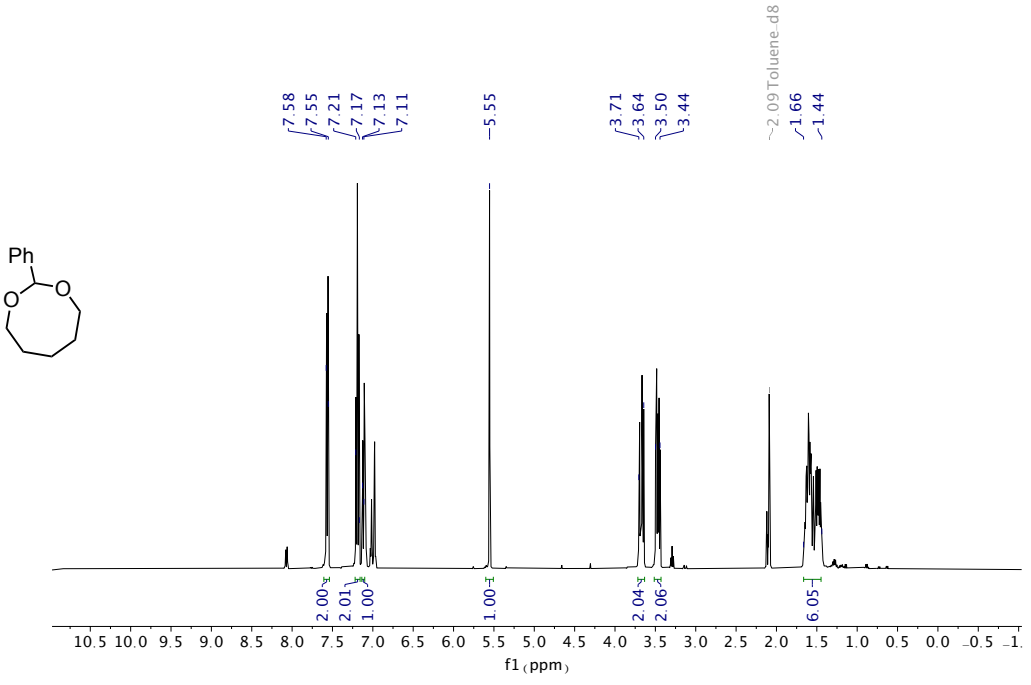

*[1]H NMR spectra (400 MHz) of **1l***

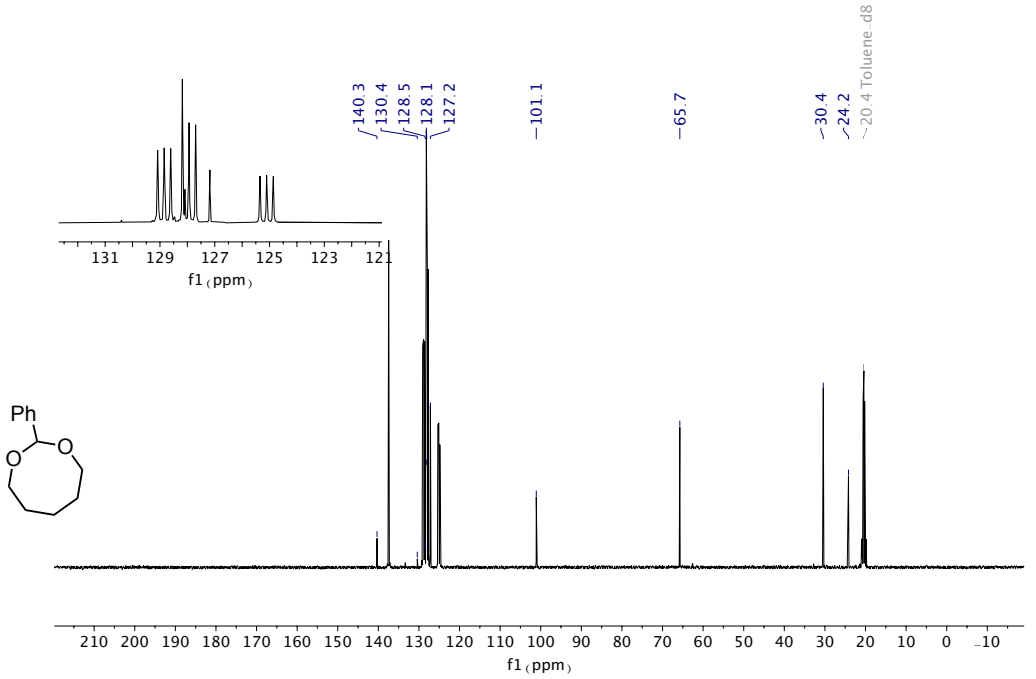

*^{13}C NMR spectra (101 MHz) of **1l***

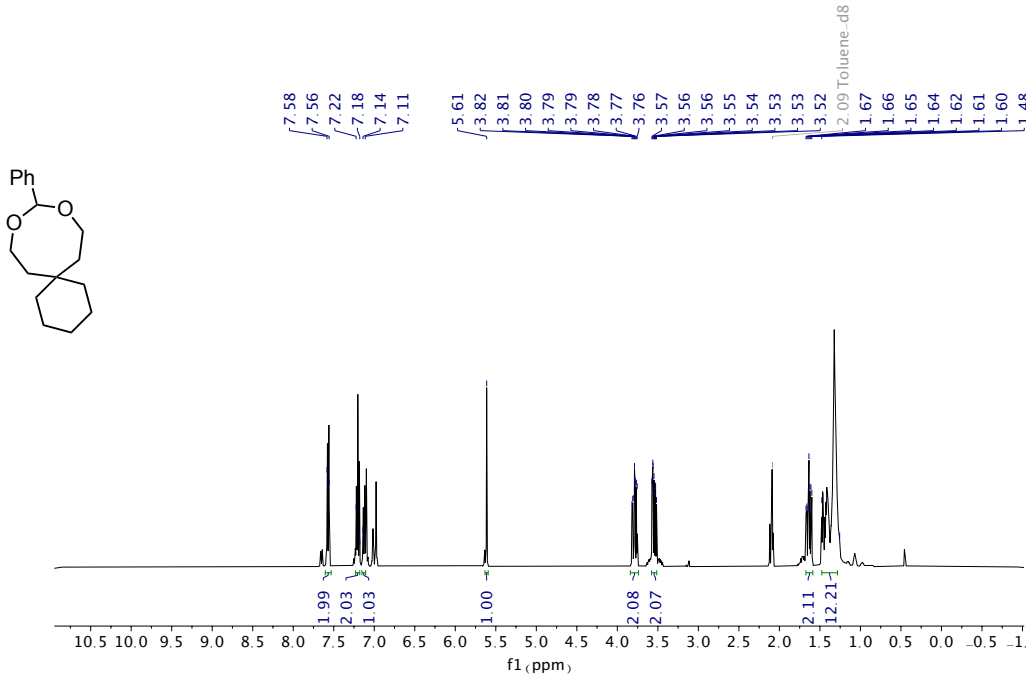

*^{1}H NMR spectra (400 MHz) of **1m***

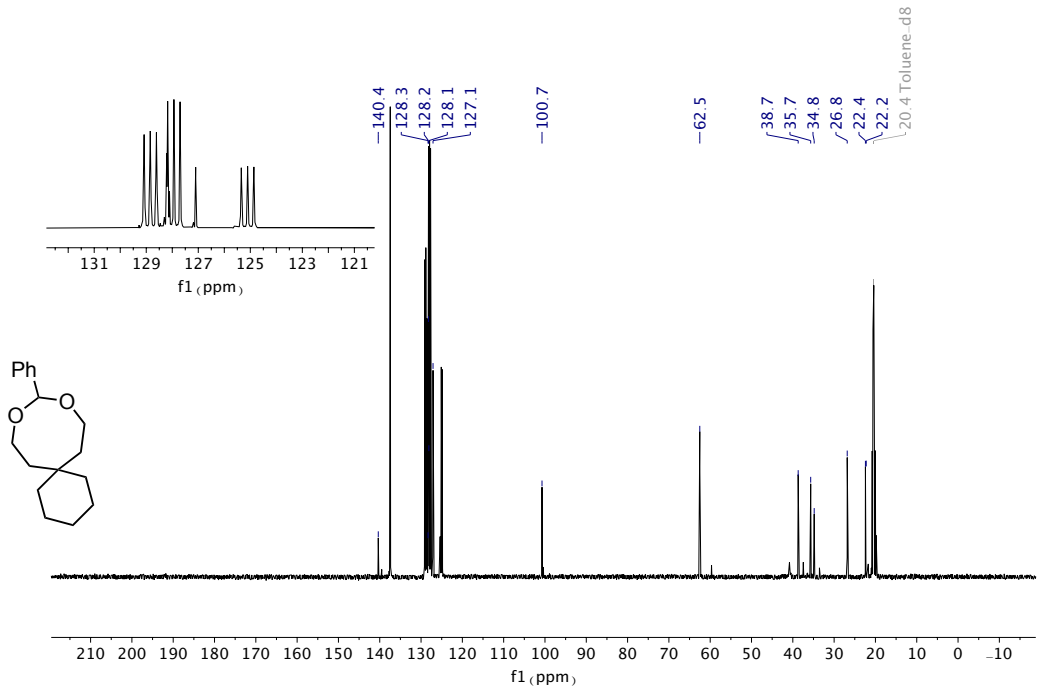

*^{13}C NMR spectra (101 MHz) of **1m***

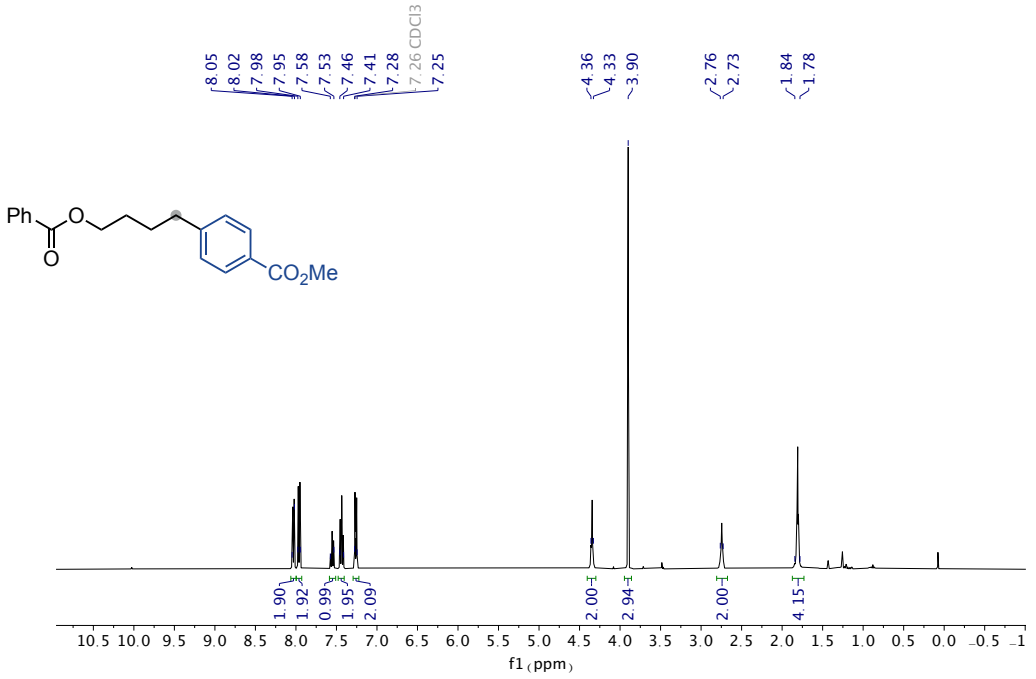

*^{1}H NMR spectra (400 MHz) of **3a***

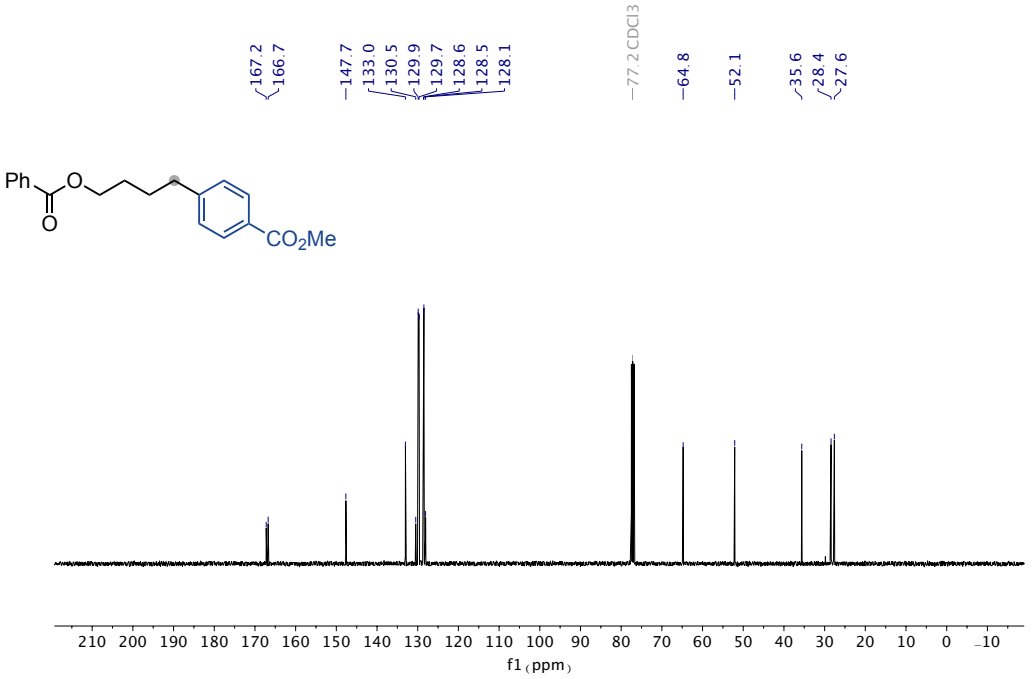

*^{13}C NMR spectra (101 MHz) of **3a***

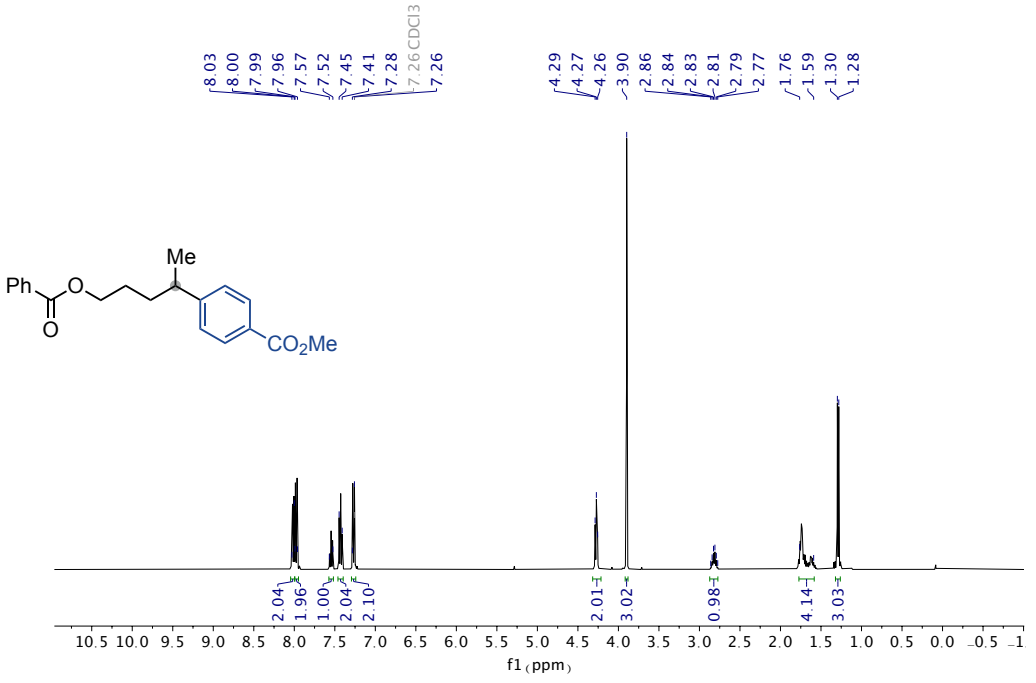

*^{1}H NMR spectra (400 MHz) of **3b***

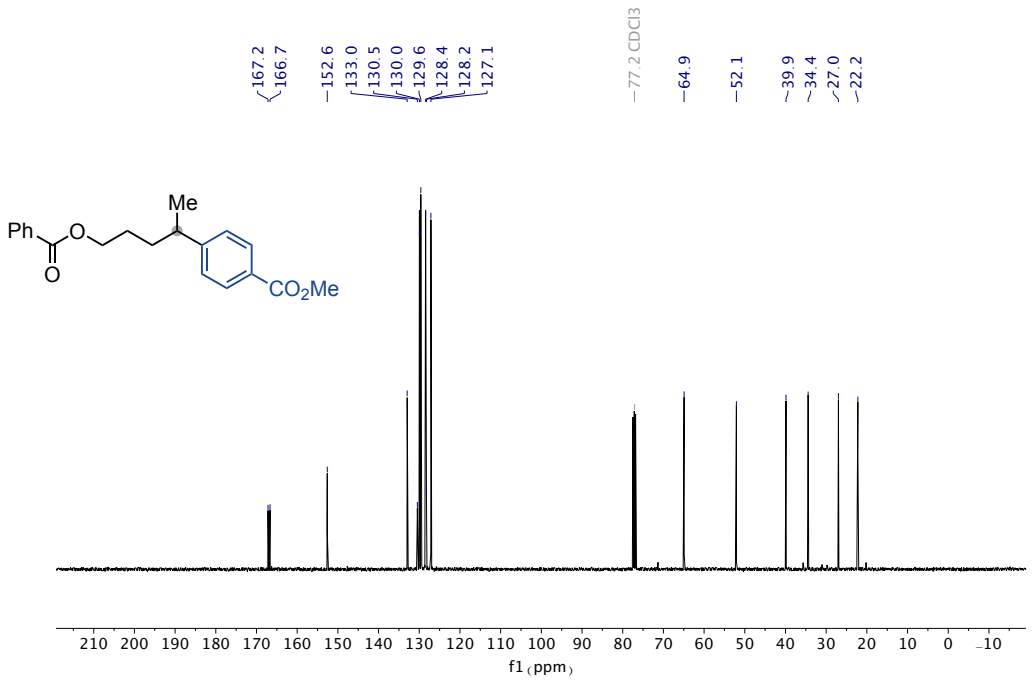

*[13]C NMR spectra (101 MHz) of **3b***

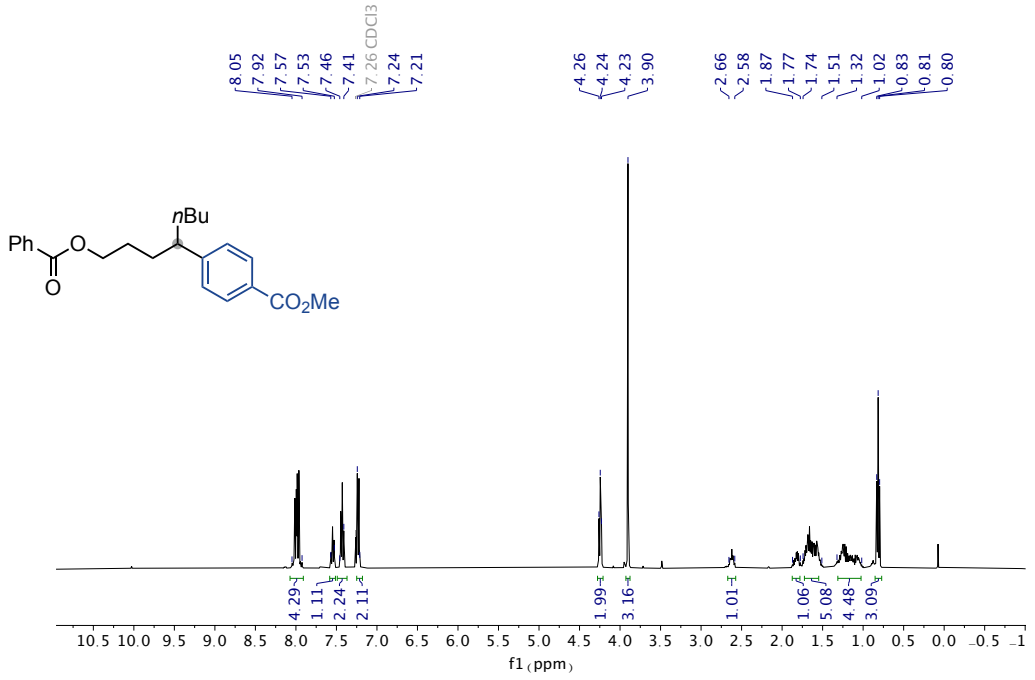

*[1]H NMR spectra (400 MHz) of **3c***

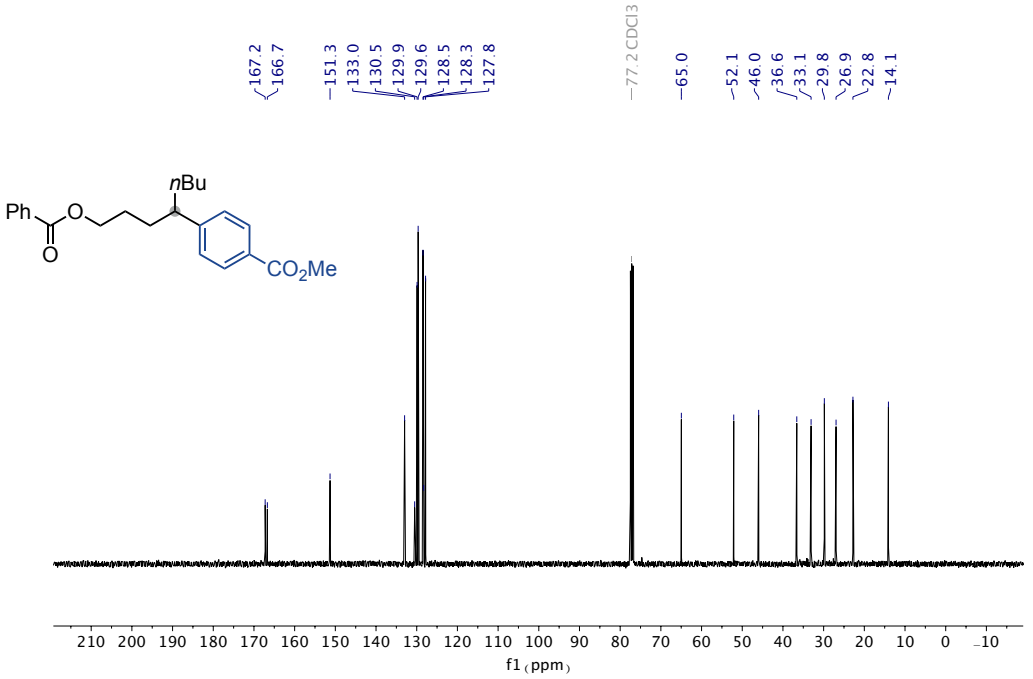

*^{13}C NMR spectra (101 MHz) of **3c***

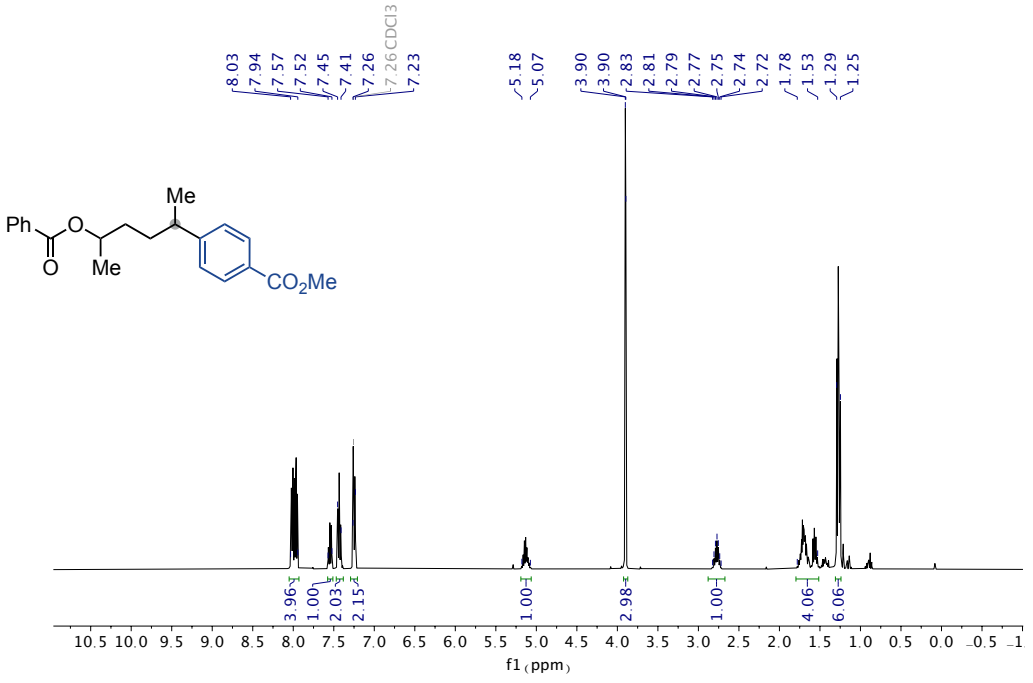

*^{1}H NMR spectra (400 MHz) of **3d***

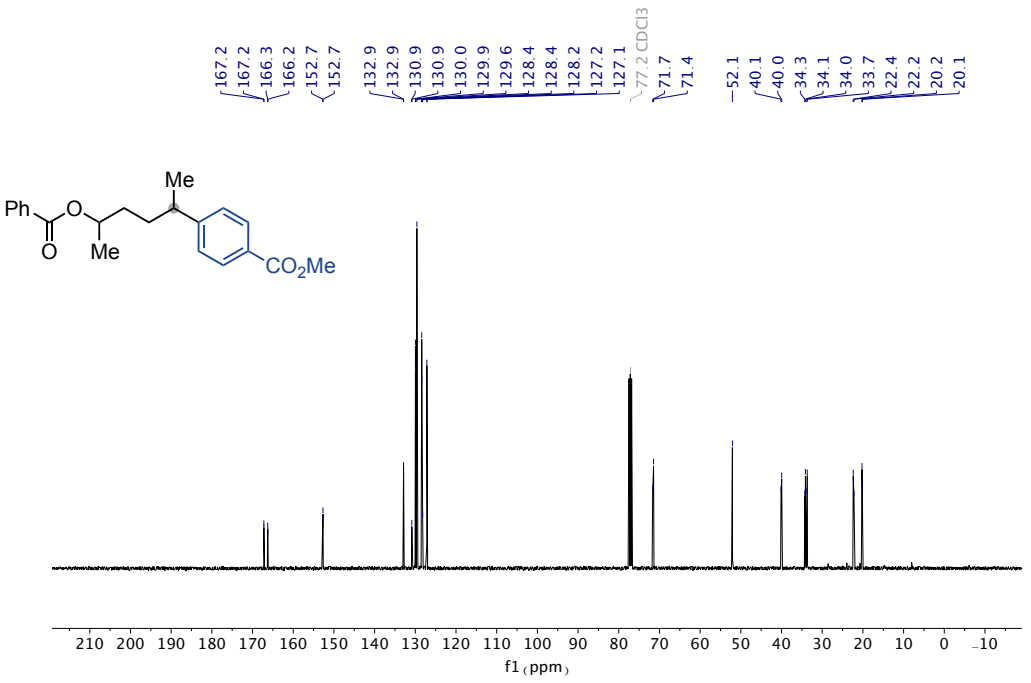

*[13]C NMR spectra (101 MHz) of **3d***

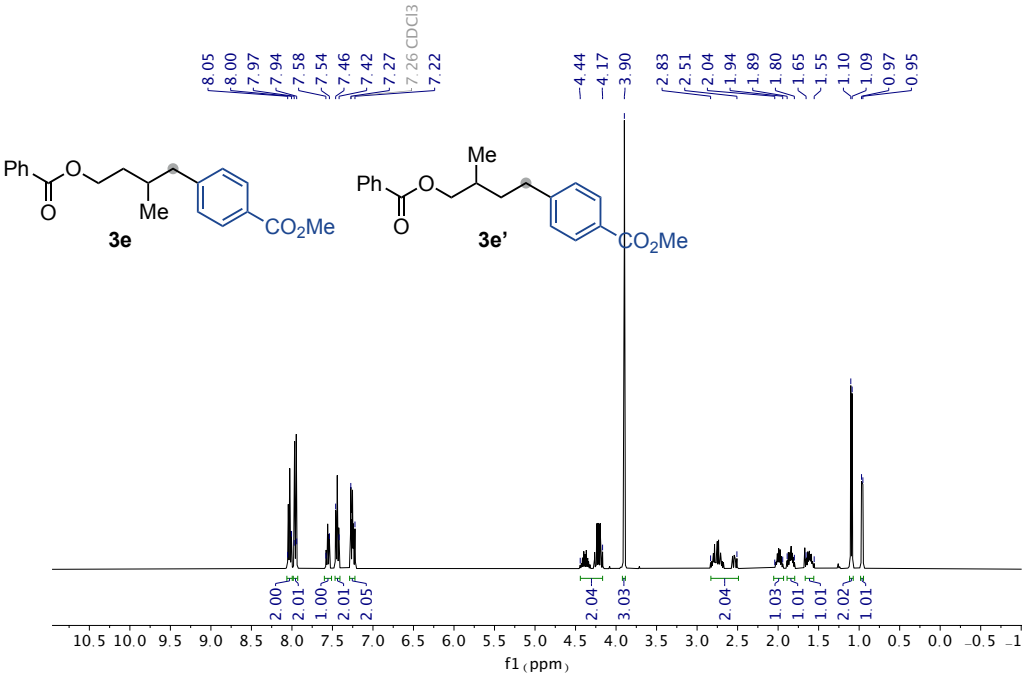

*[1]H NMR spectra (400 MHz) of **3e/3e'***

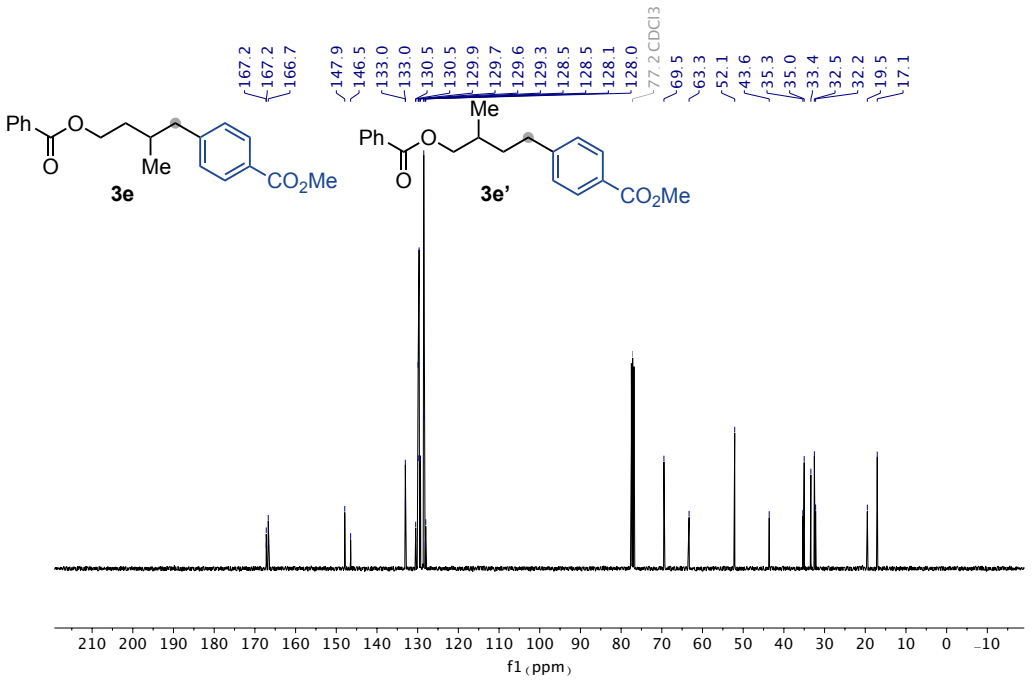

*[13]C NMR spectra (101 MHz) of **3e/3e'***

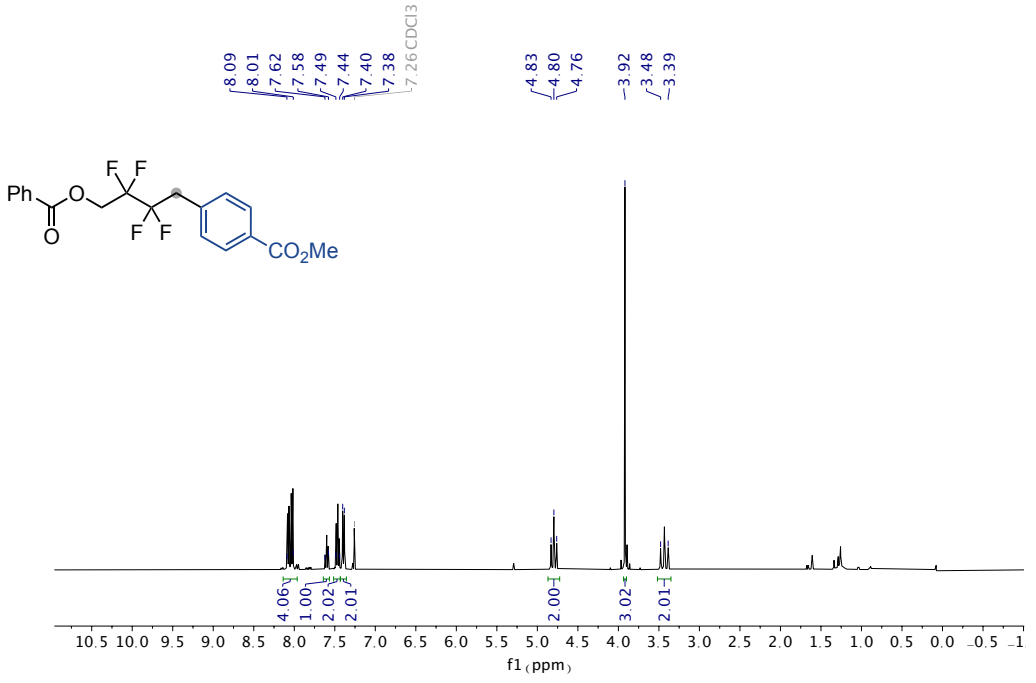

*[1]H NMR spectra (400 MHz) of **3f***

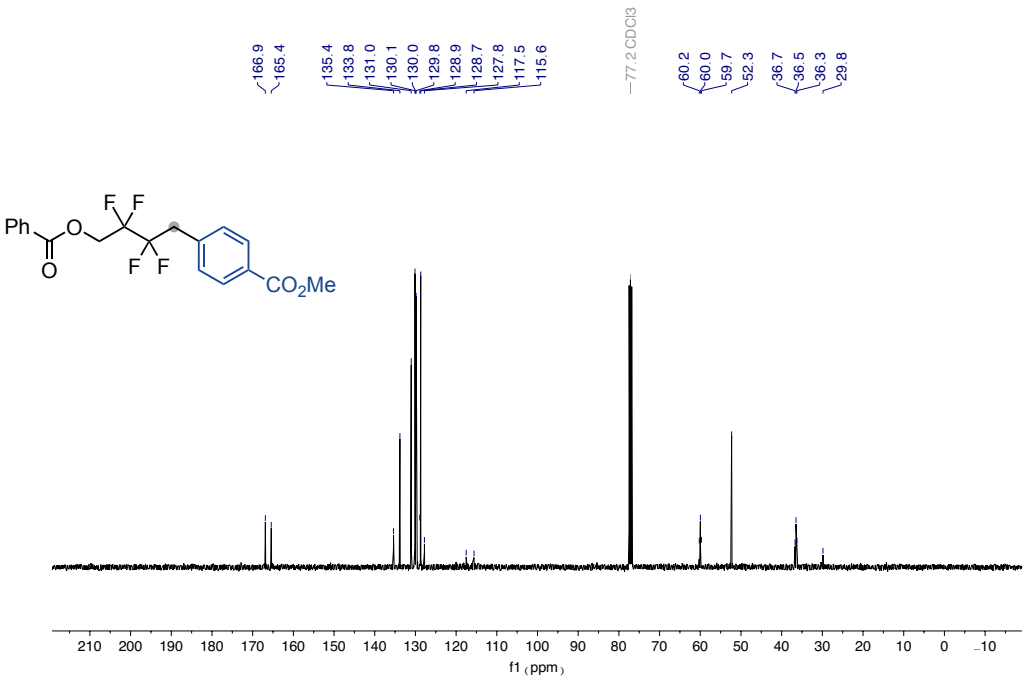

*[13]C NMR spectra (101 MHz) of **3f***

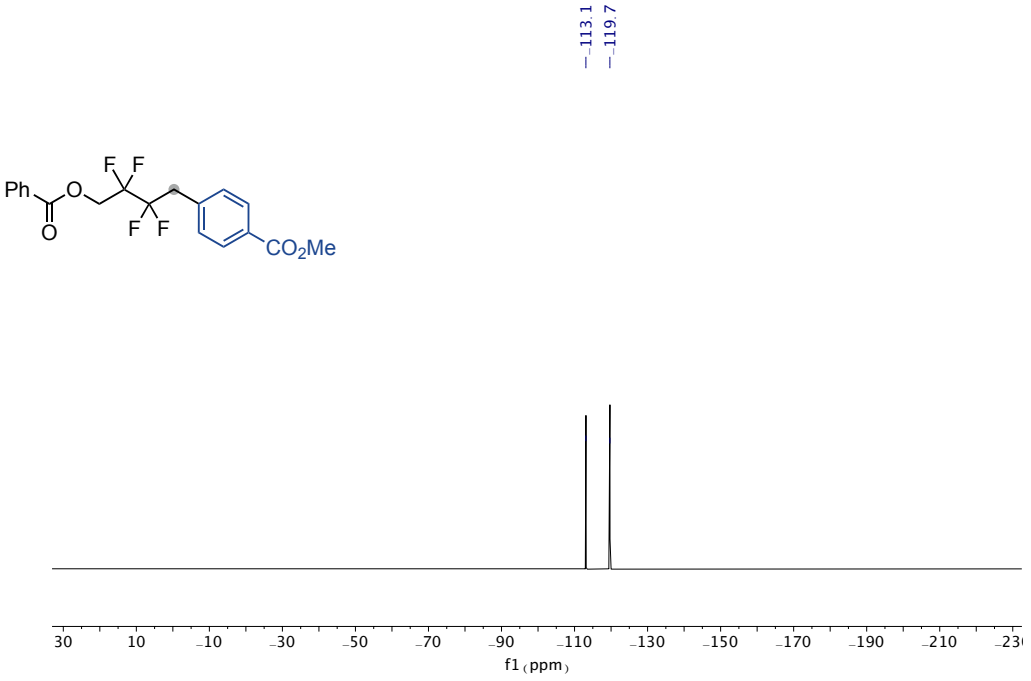

*[19]F NMR spectra (376 MHz) of **3f***

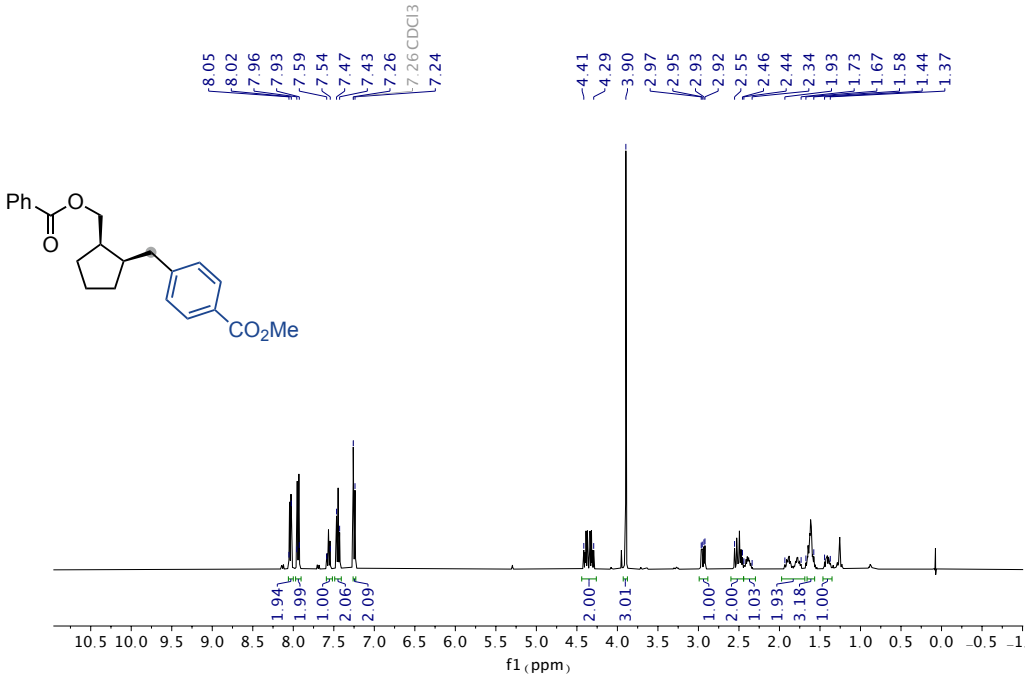

*^{1}H NMR spectra (400 MHz) of **3g***

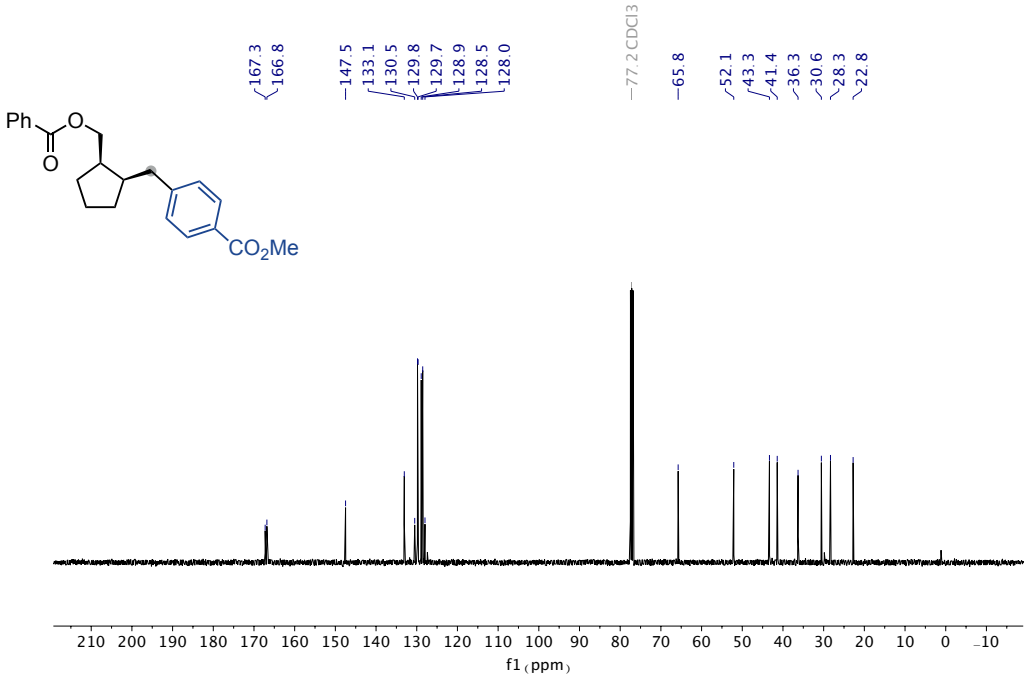

*^{13}C NMR spectra (101 MHz) of **3g***

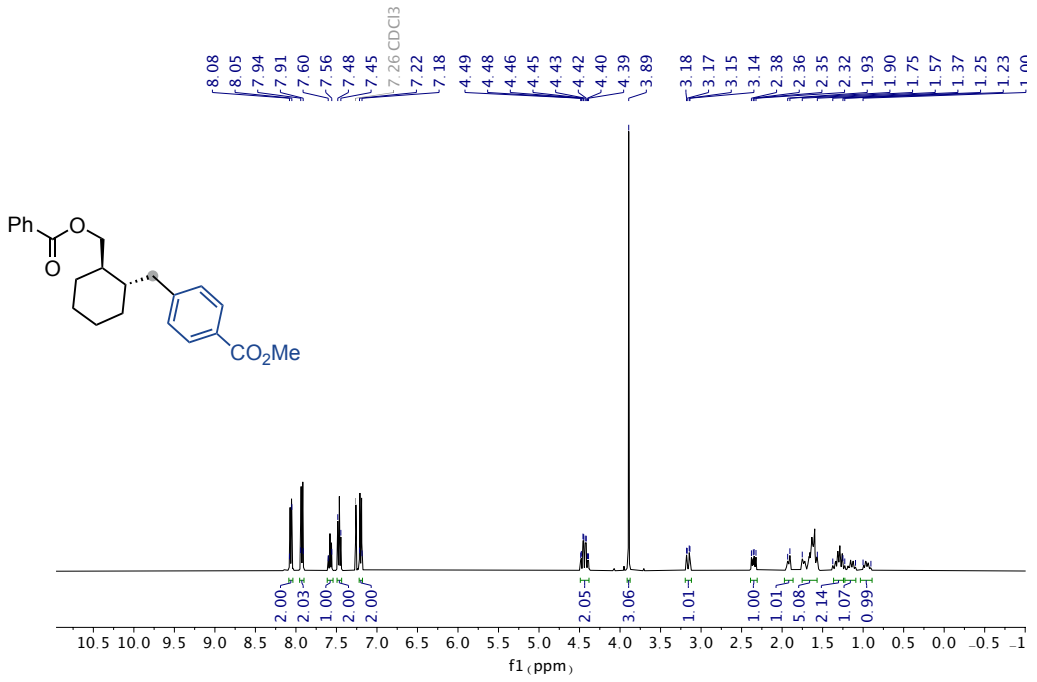

*[1]H NMR spectra (400 MHz) of **3h***

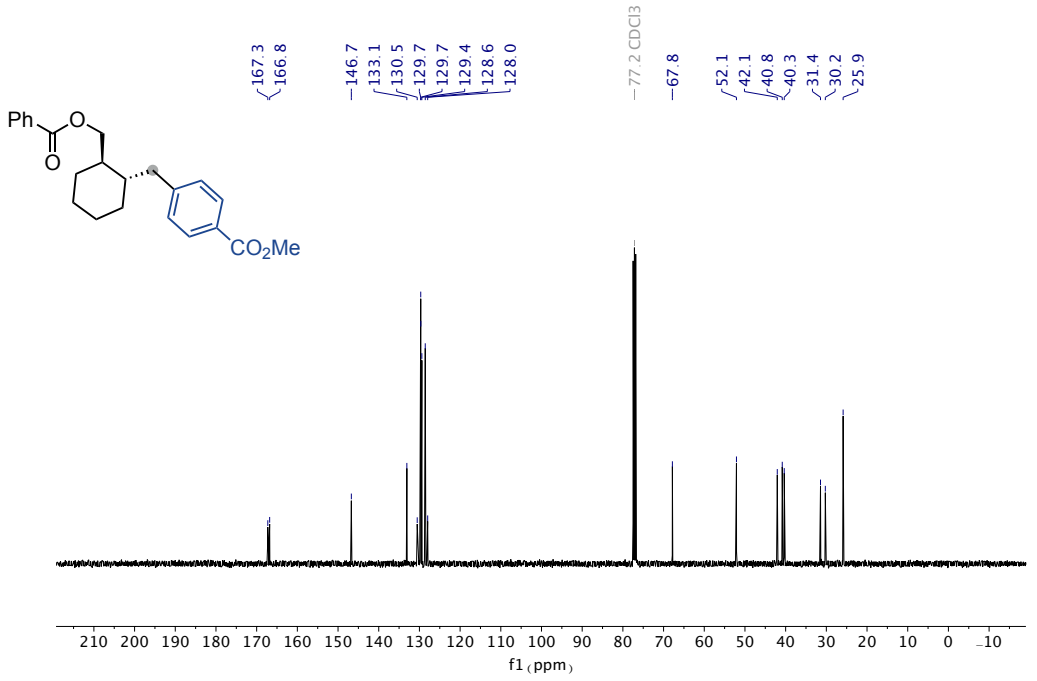

*[13]C NMR spectra (101 MHz) of **3h***

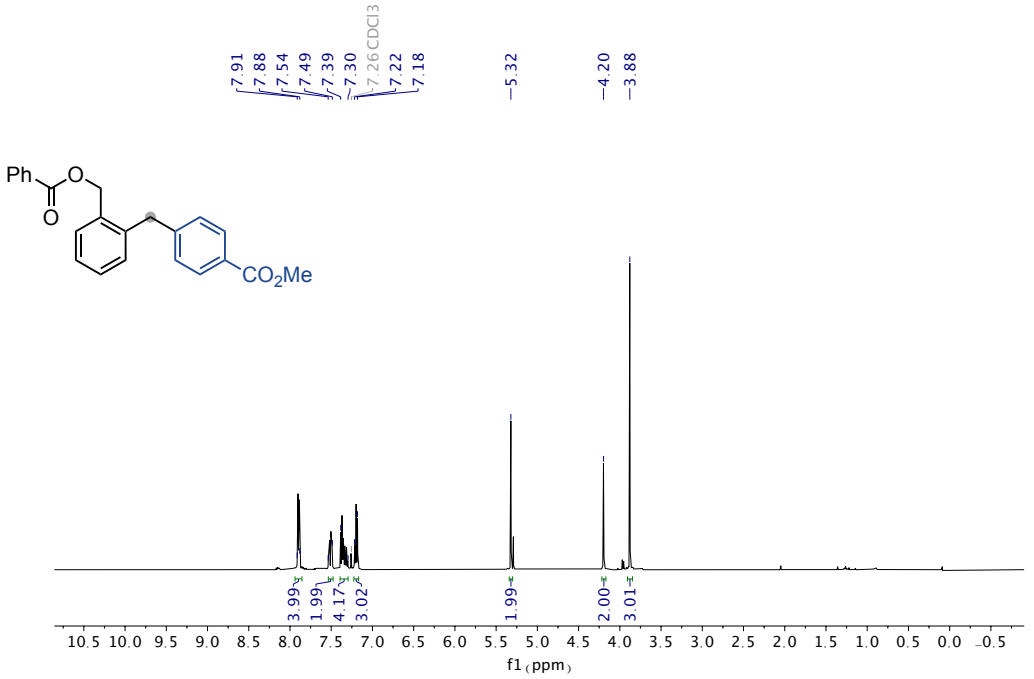

*[1]H NMR spectra (400 MHz) of **3i***

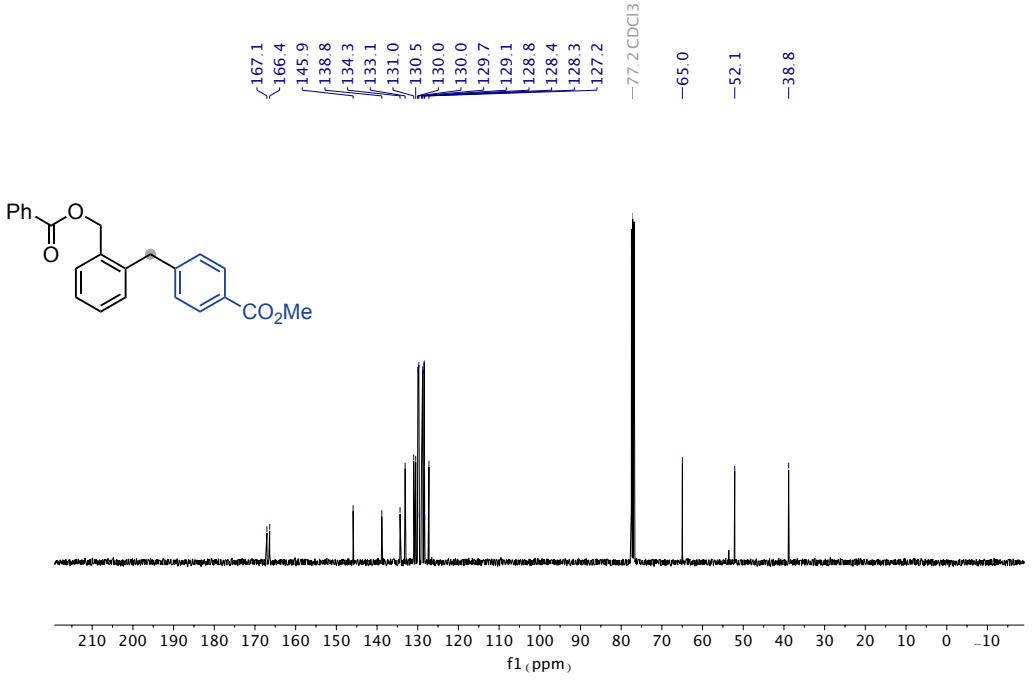

*[13]C NMR spectra (101 MHz) of **3i***

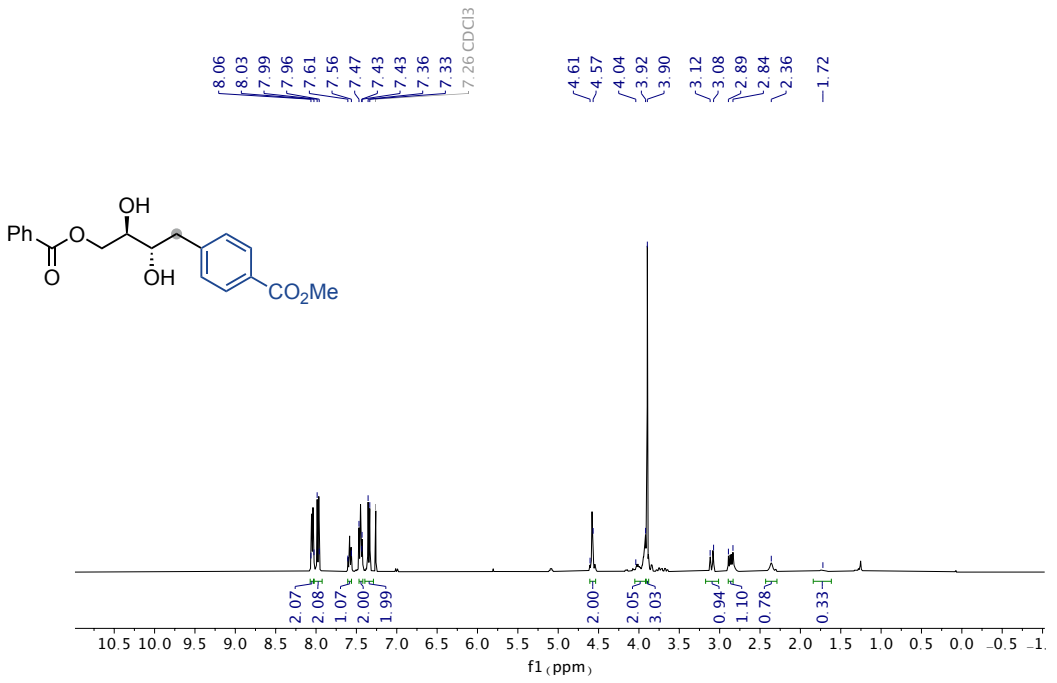

*[1]H NMR spectra (400 MHz) of **3j***

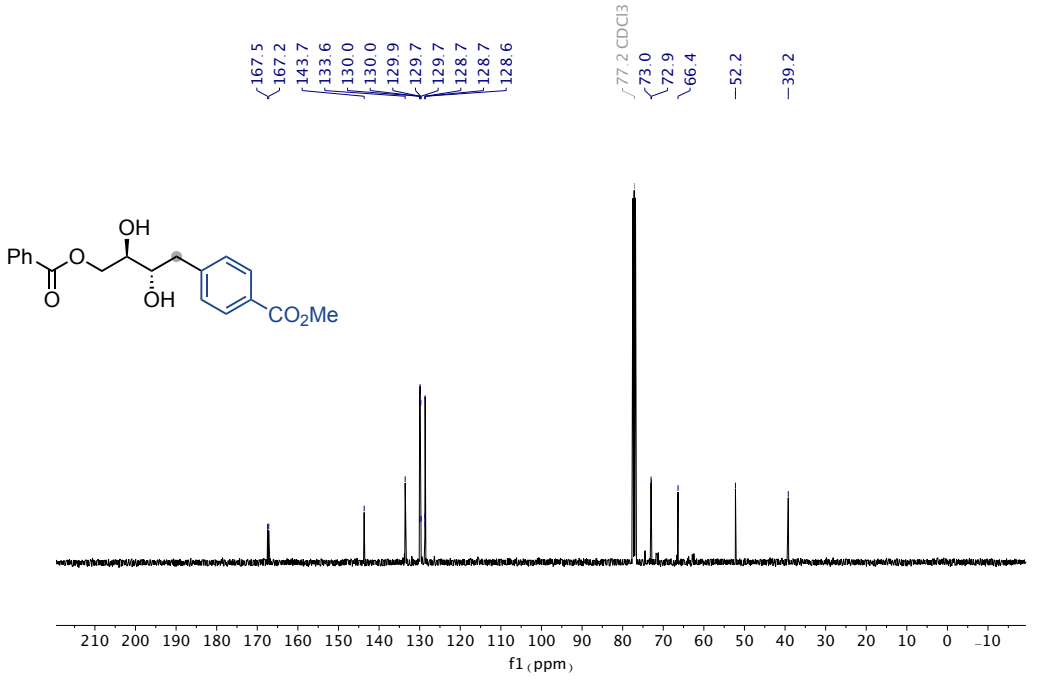

*[13]C NMR spectra (101 MHz) of **3j***

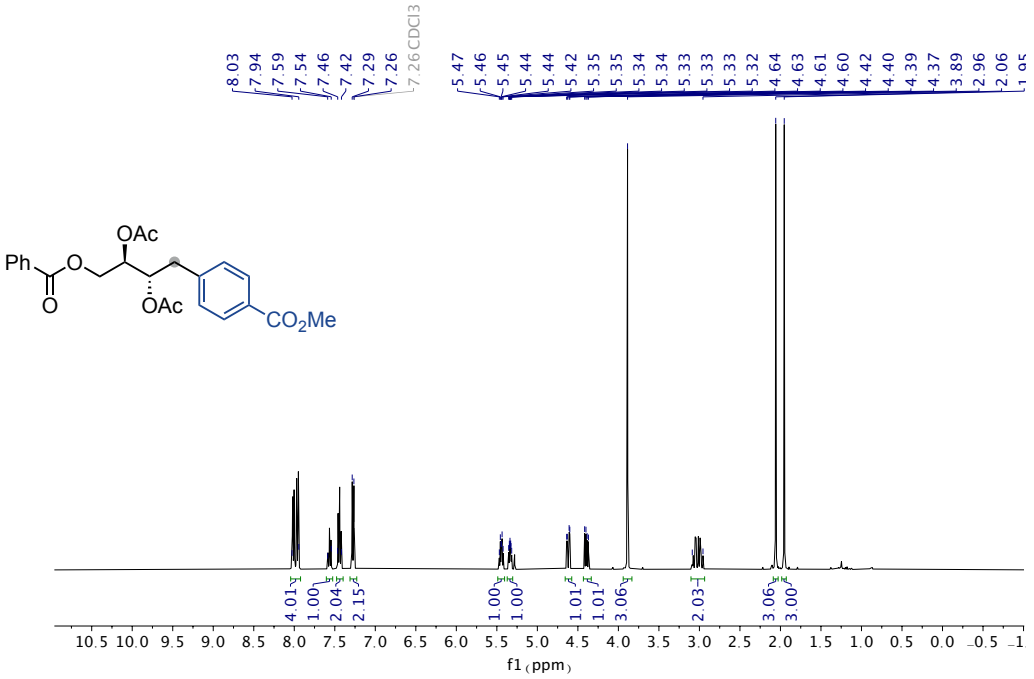

*^{1}H NMR spectra (400 MHz) of **3k***

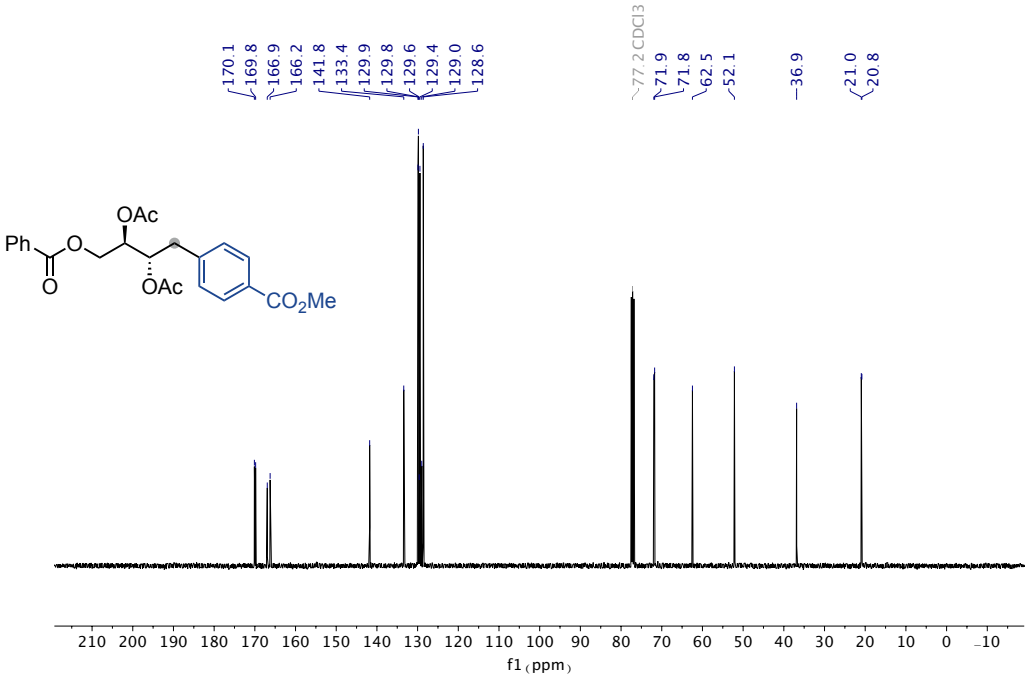

*^{13}C NMR spectra (101 MHz) of **3k***

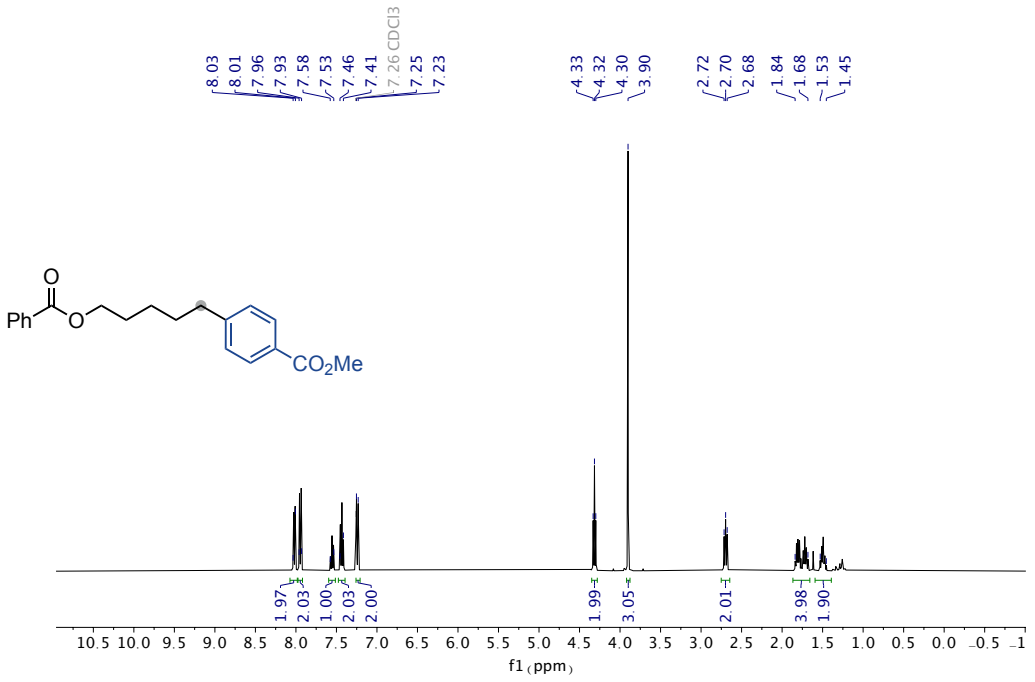

*[1]H NMR spectra (400 MHz) of **3l***

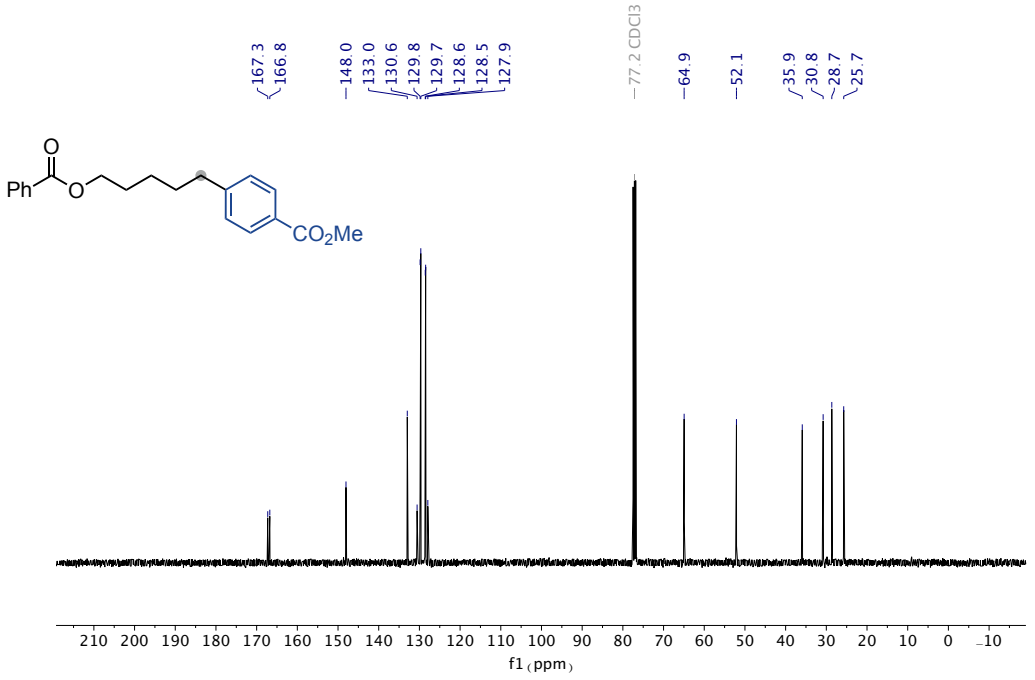

*[13]C NMR spectra (101 MHz) of **3l***

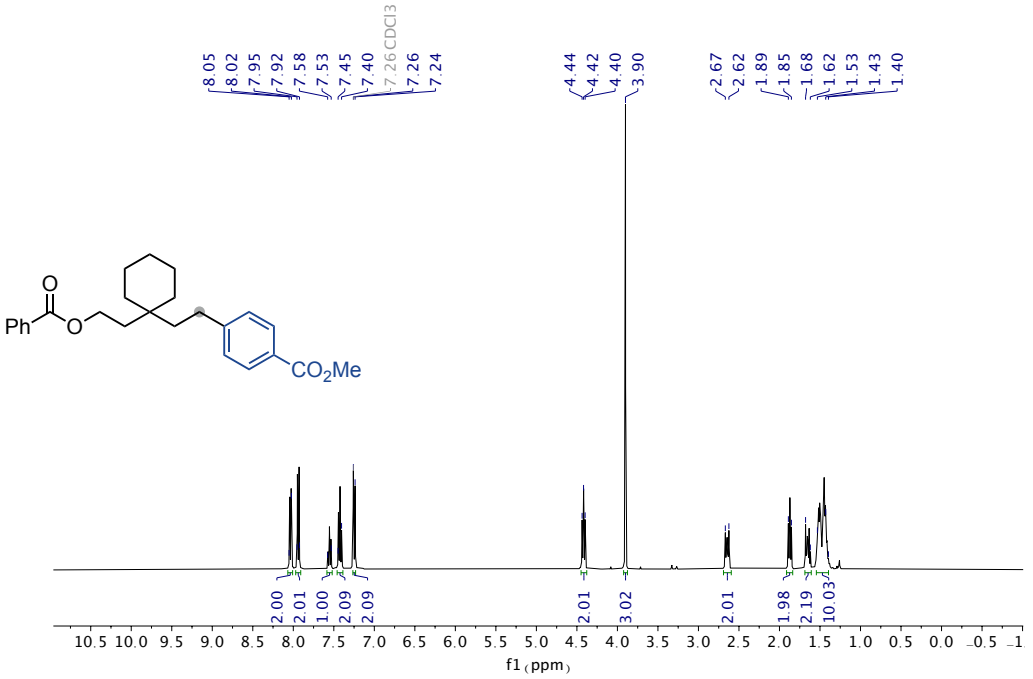

*[1]H NMR spectra (400 MHz) of **3m***

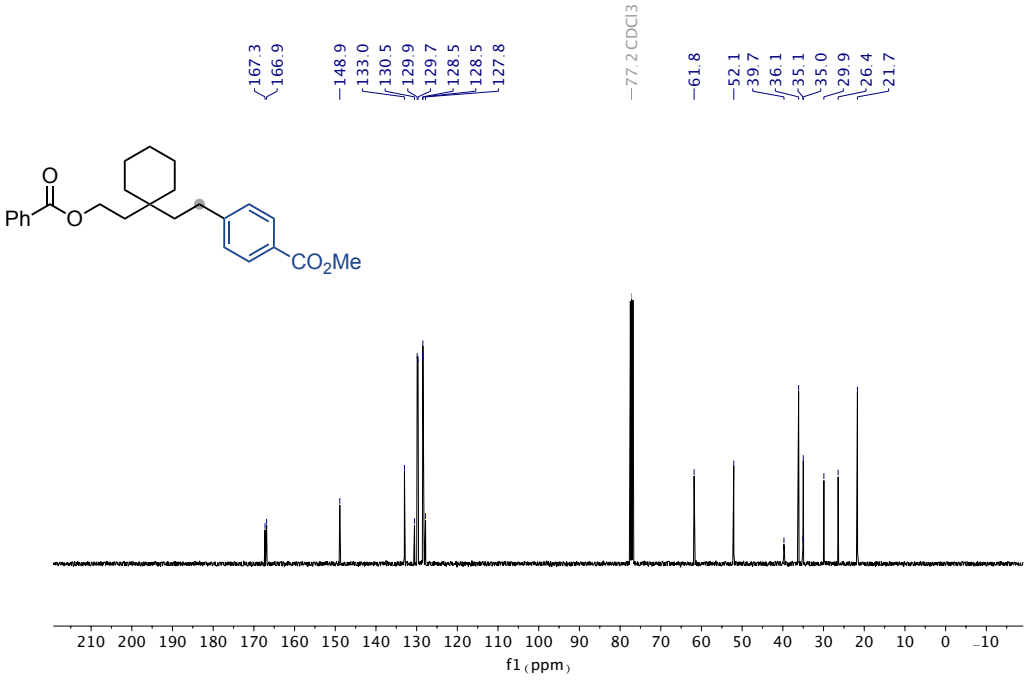

*[13]C NMR spectra (101 MHz) of **3m***

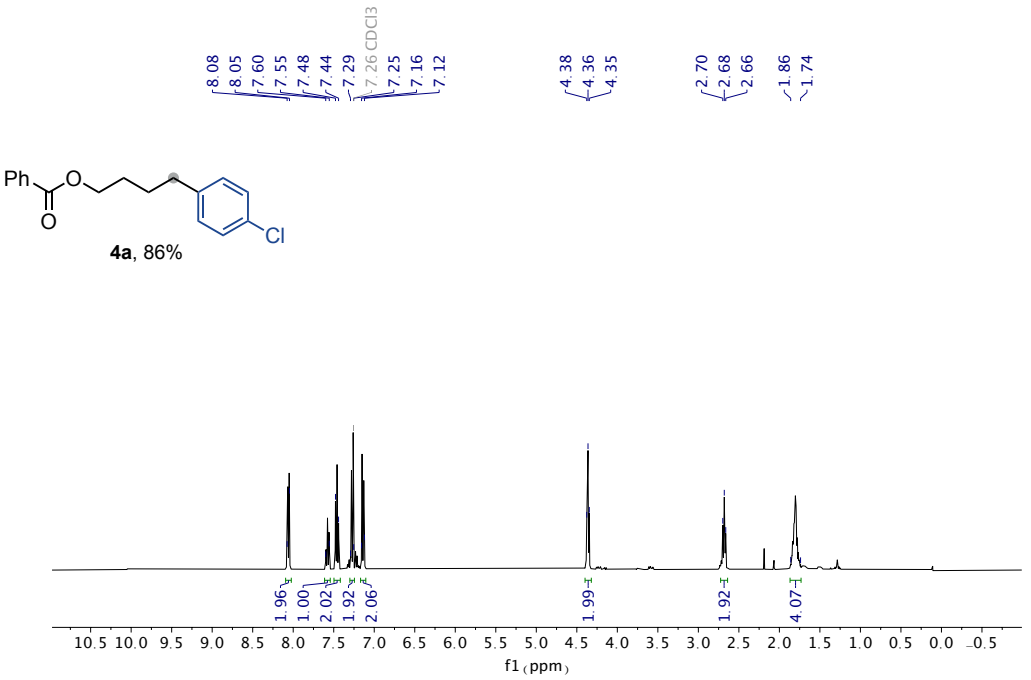

*[1]H NMR spectra (400 MHz) of **4a***

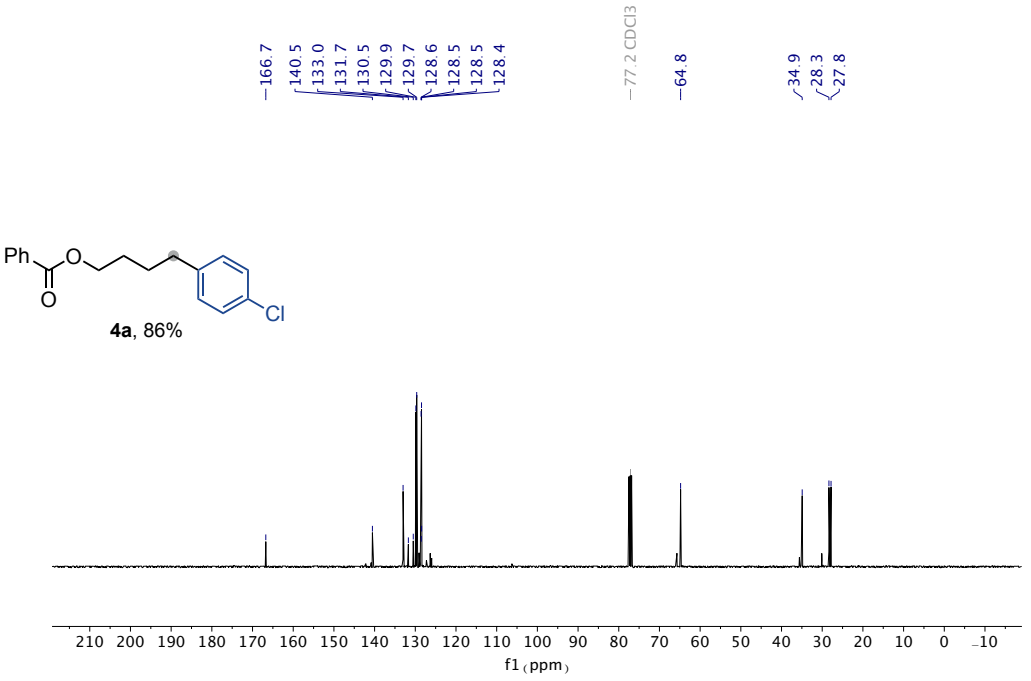

*[13]C NMR spectra (101 MHz) of **4a***

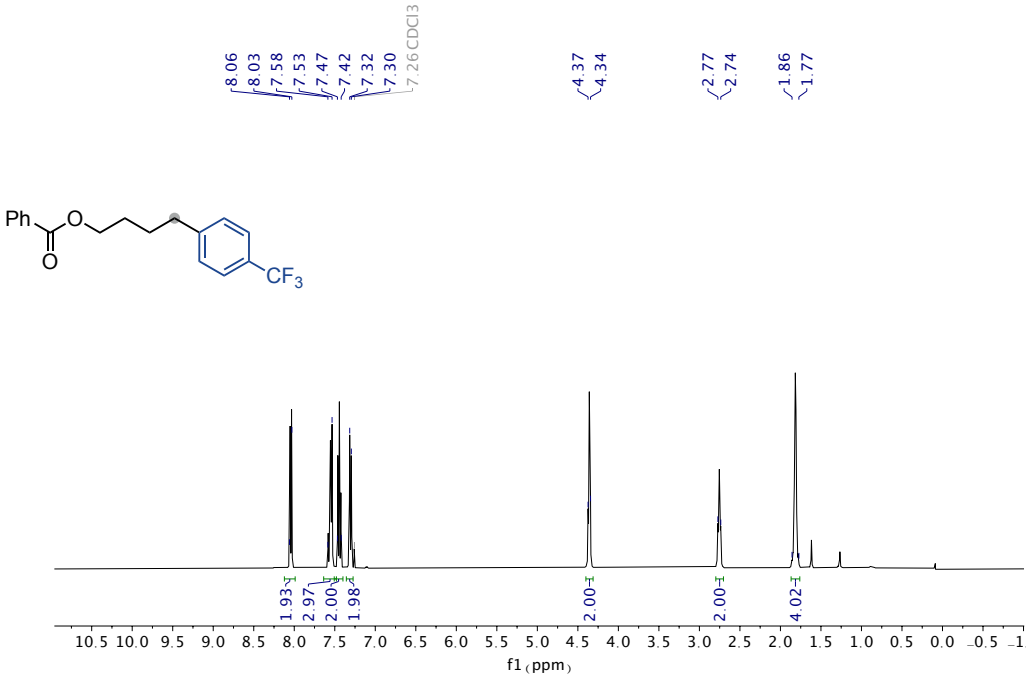

*^{1}H NMR spectra (400 MHz) of **4b***

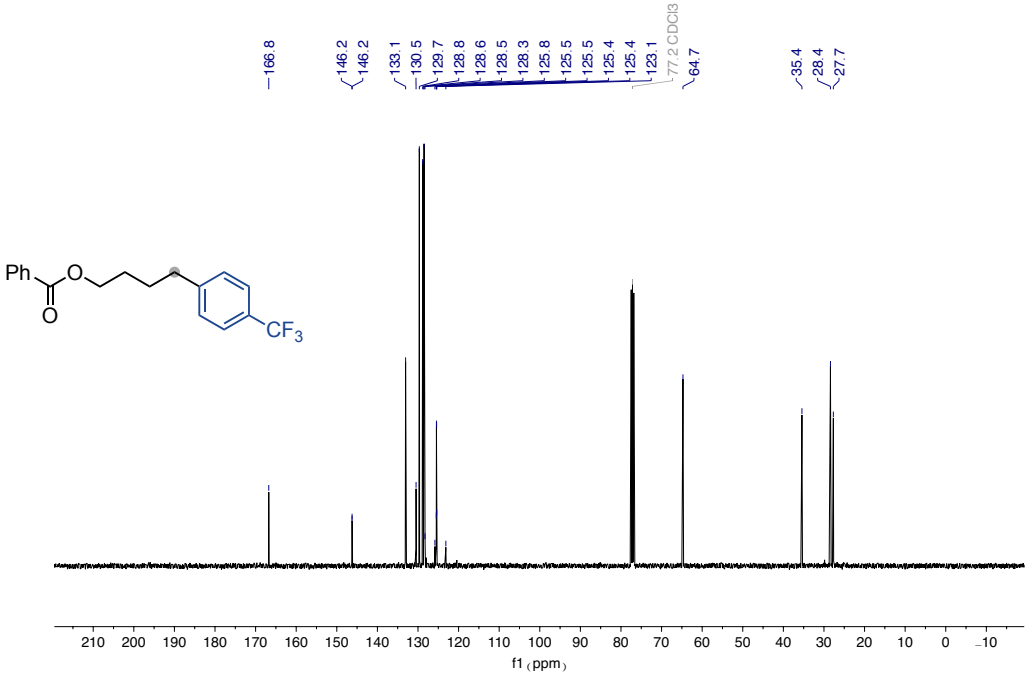

*^{13}C NMR spectra (101 MHz) of **4b***

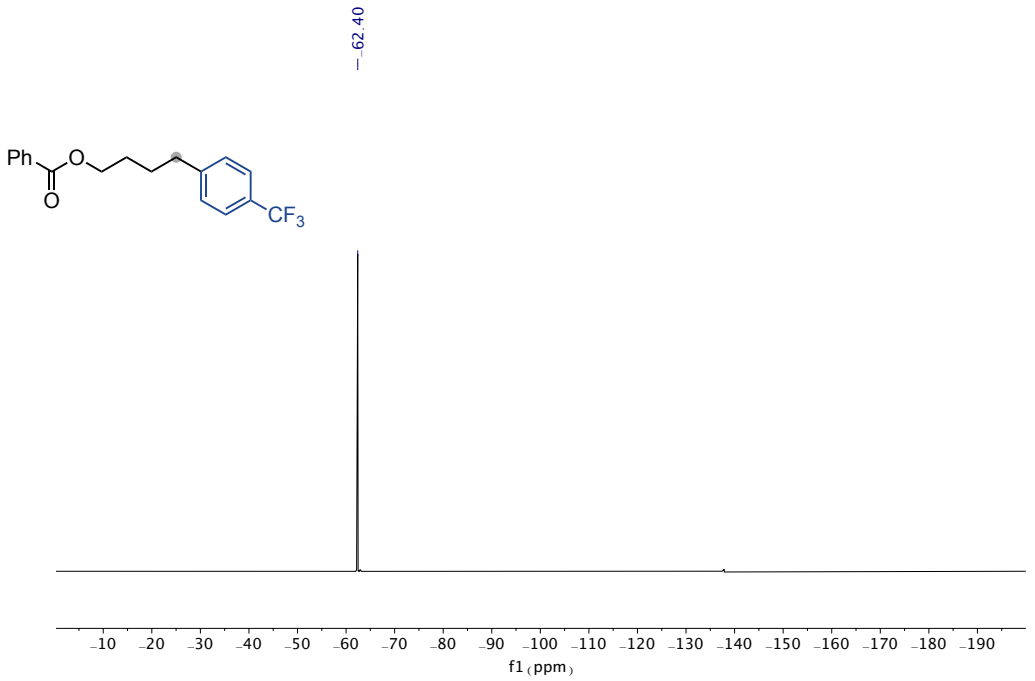

*[19]F NMR spectra (376 MHz) of **4c***

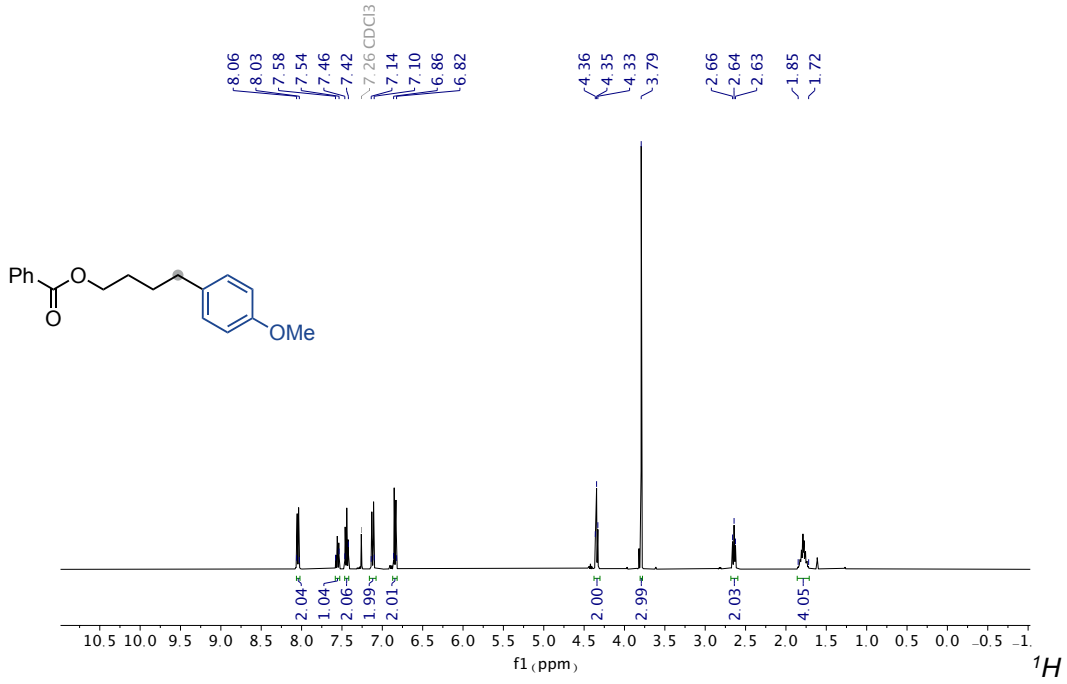

*[1]NMR spectra (400 MHz) of **4c***

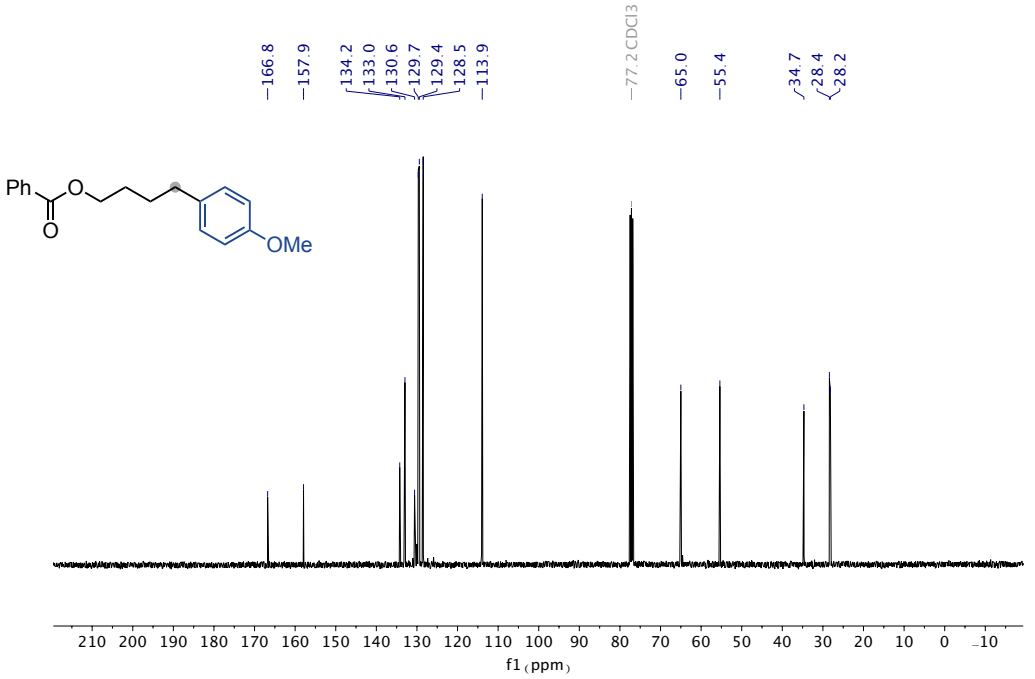

*^{13}C NMR spectra (101 MHz) of **4d***

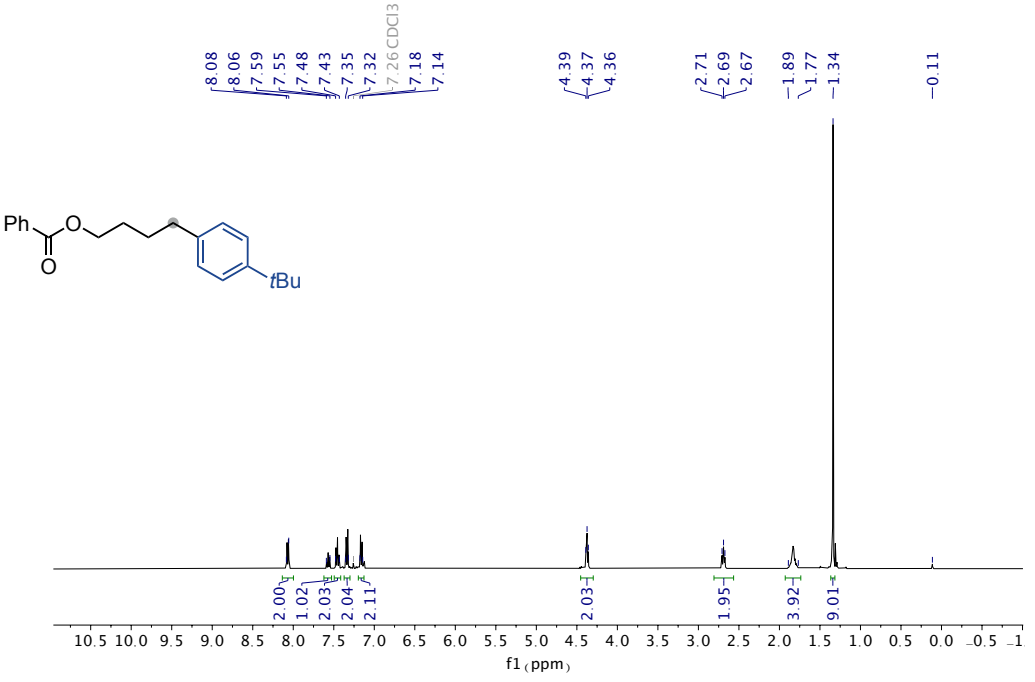

*^{1}H NMR spectra (400 MHz) of **4d***

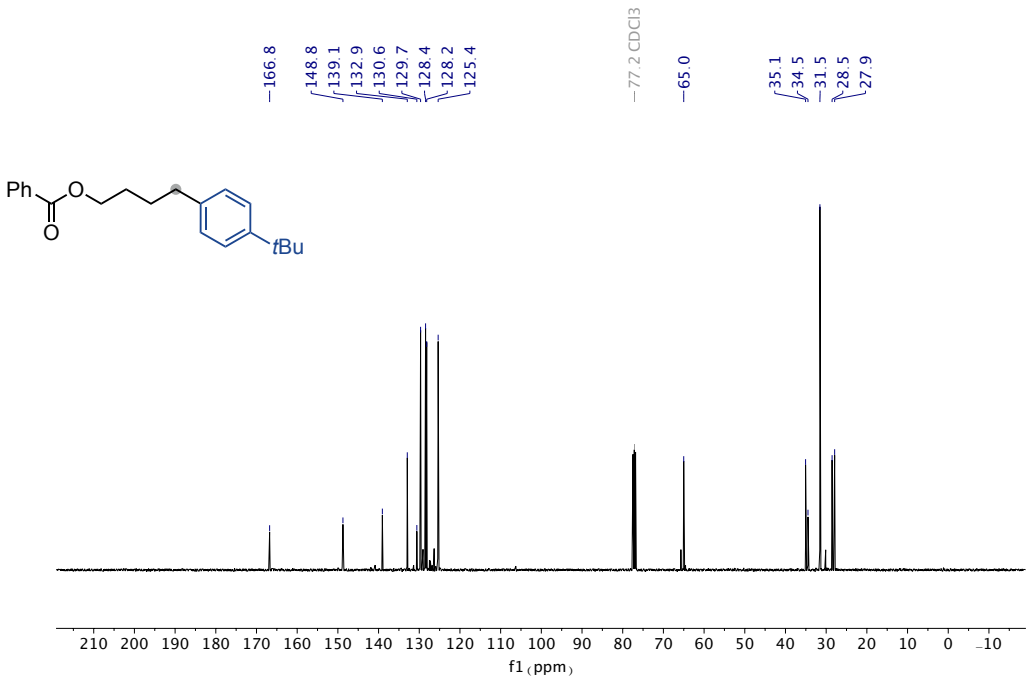

*[13]C NMR spectra (101 MHz) of **4d***

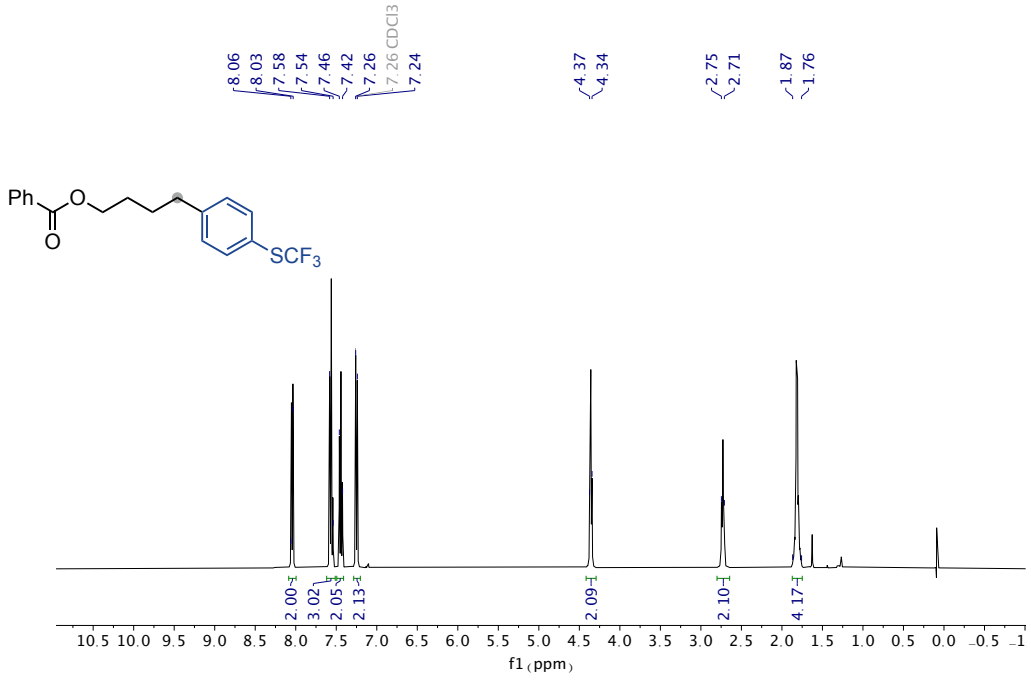

*[1]H NMR spectra (400 MHz) of **4e***

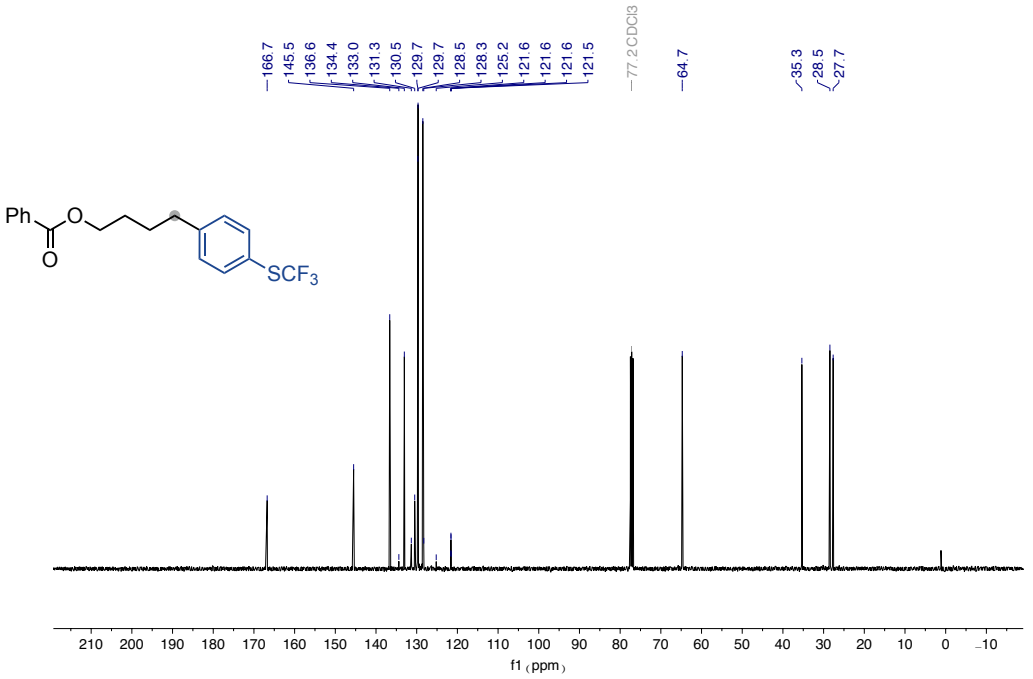

*^{13}C NMR spectra (101 MHz) of **4e***

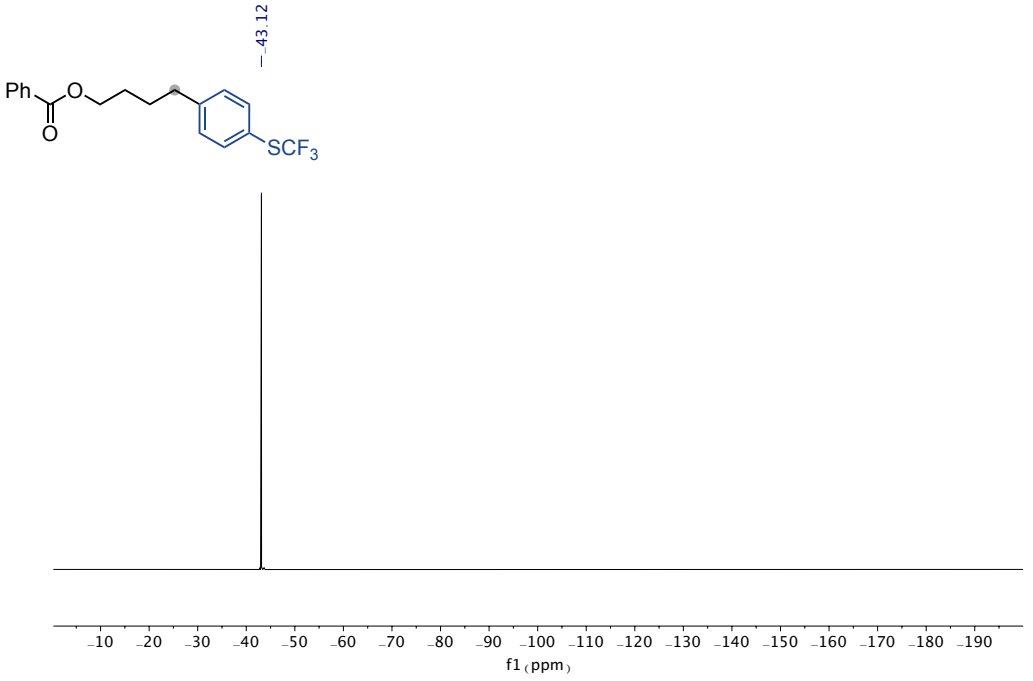

*^{19}F NMR spectra (376 MHz) of **4e***

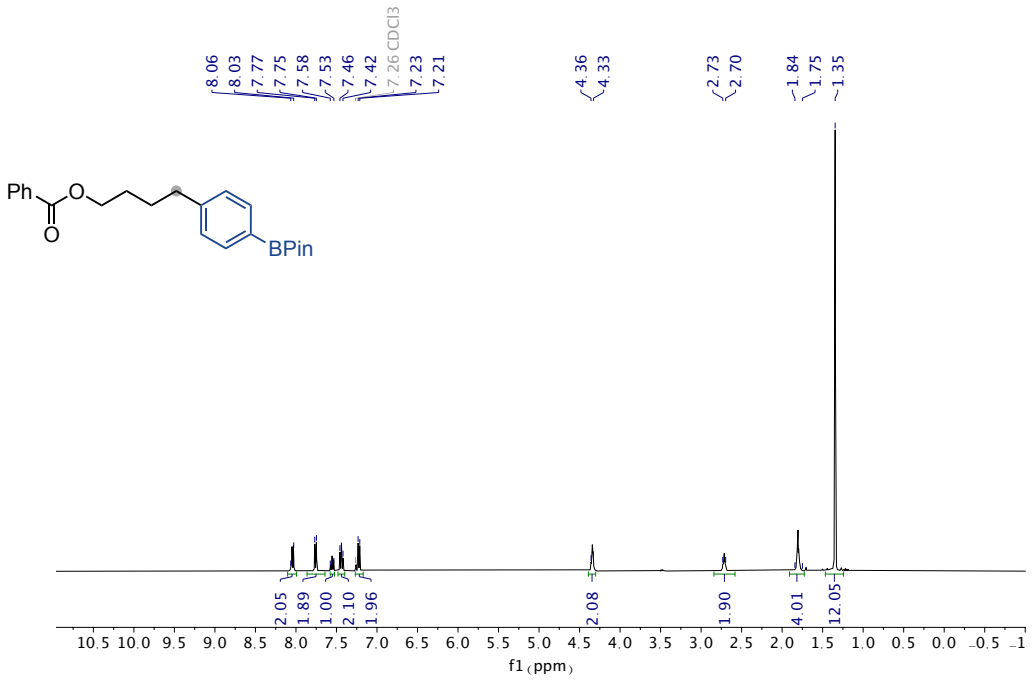

*[1]H NMR spectra (400 MHz) of **4f***

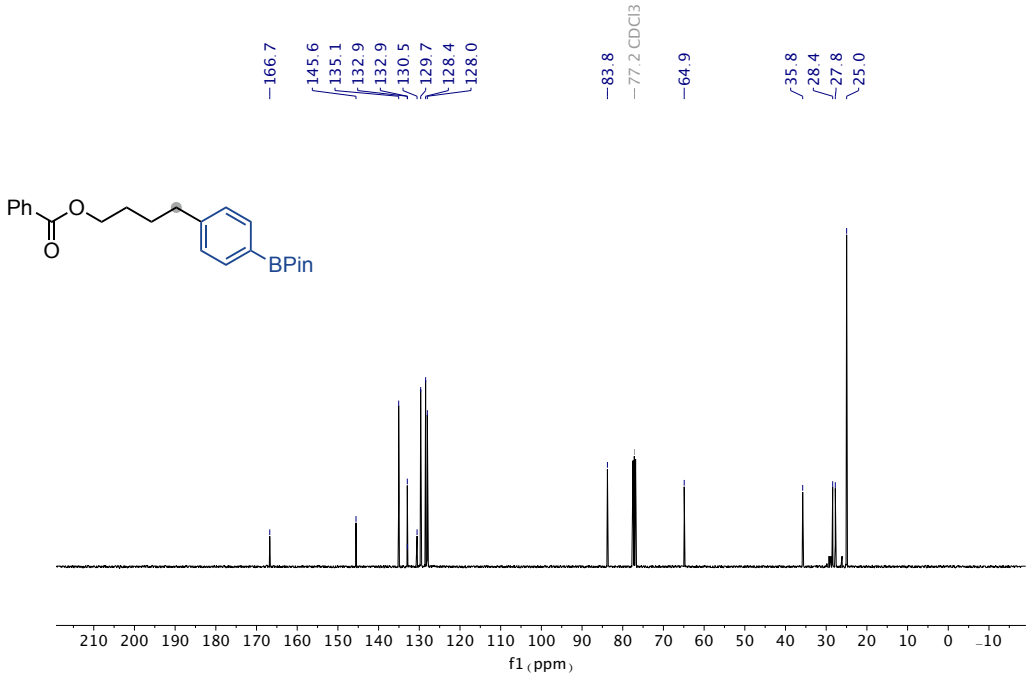

*[13]C NMR spectra (101 MHz) of **4f***

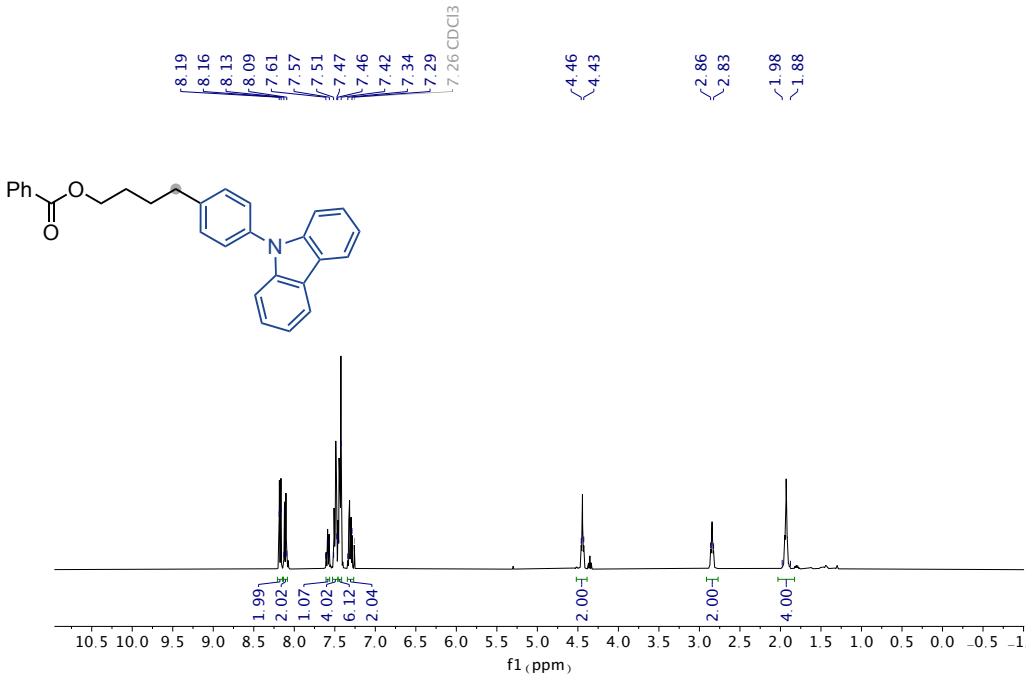

*^{1}H NMR spectra (400 MHz) of **4g***

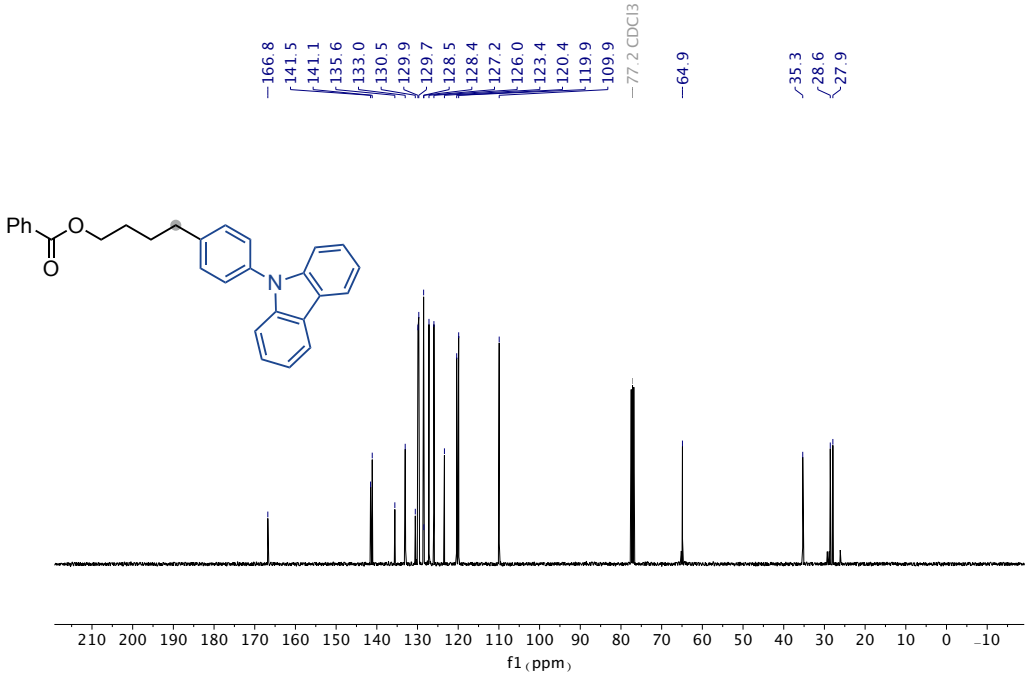

*^{13}C NMR spectra (101 MHz) of **4g***

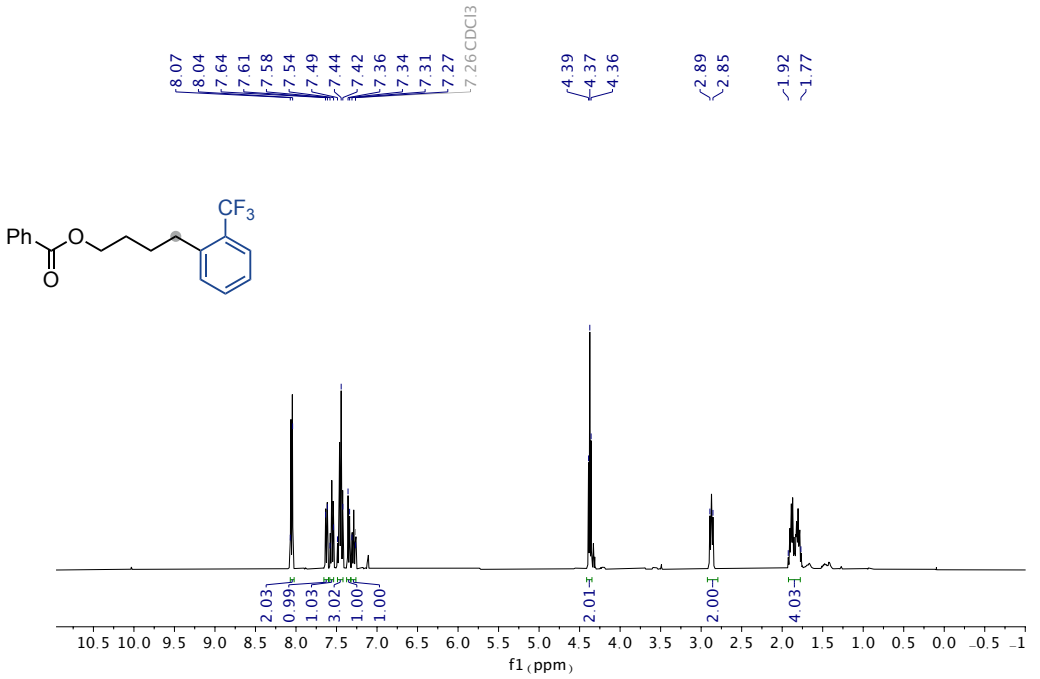

*[1]H NMR spectra (400 MHz) of **4h***

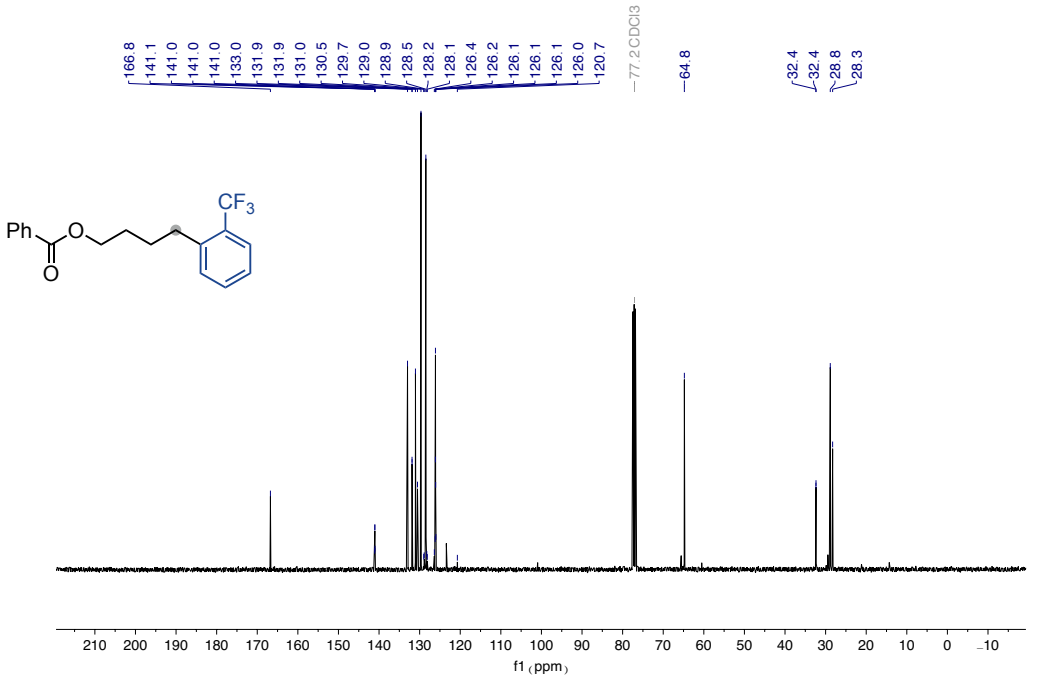

*[13]C NMR spectra (101 MHz) of **4h***

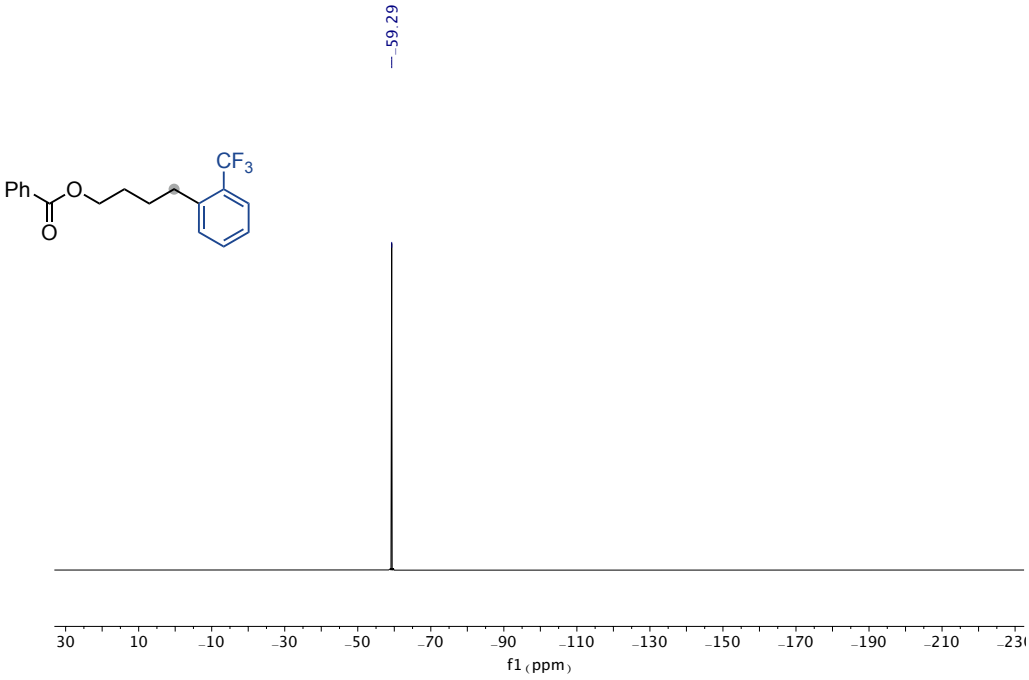

*^{19}F NMR spectra (376 MHz) of **4h***

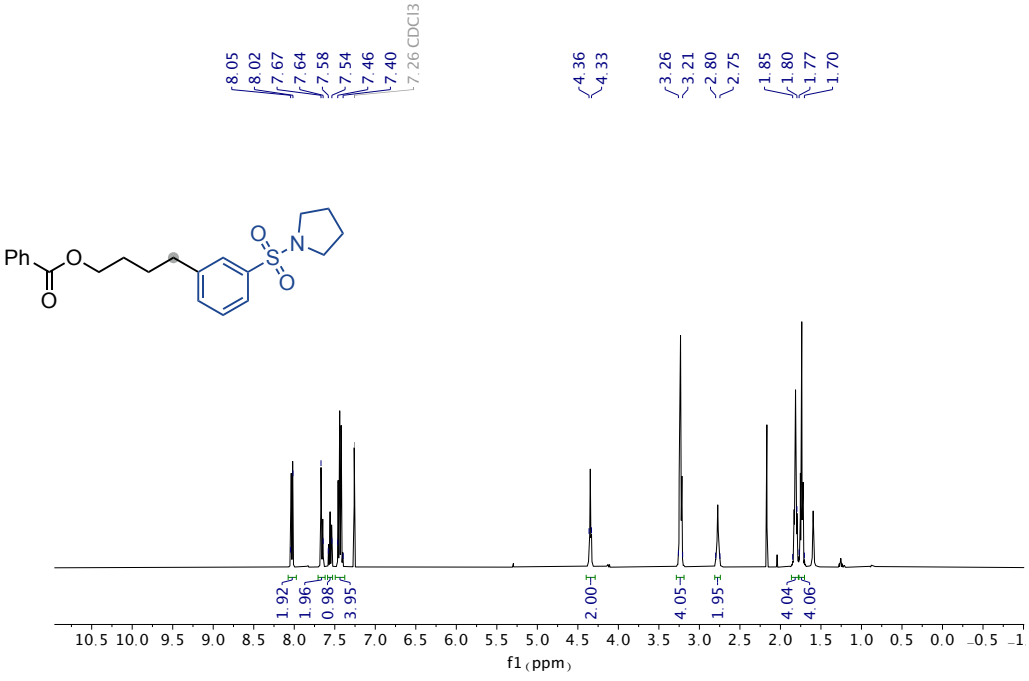

*^{1}H NMR spectra (400 MHz) of **4i***

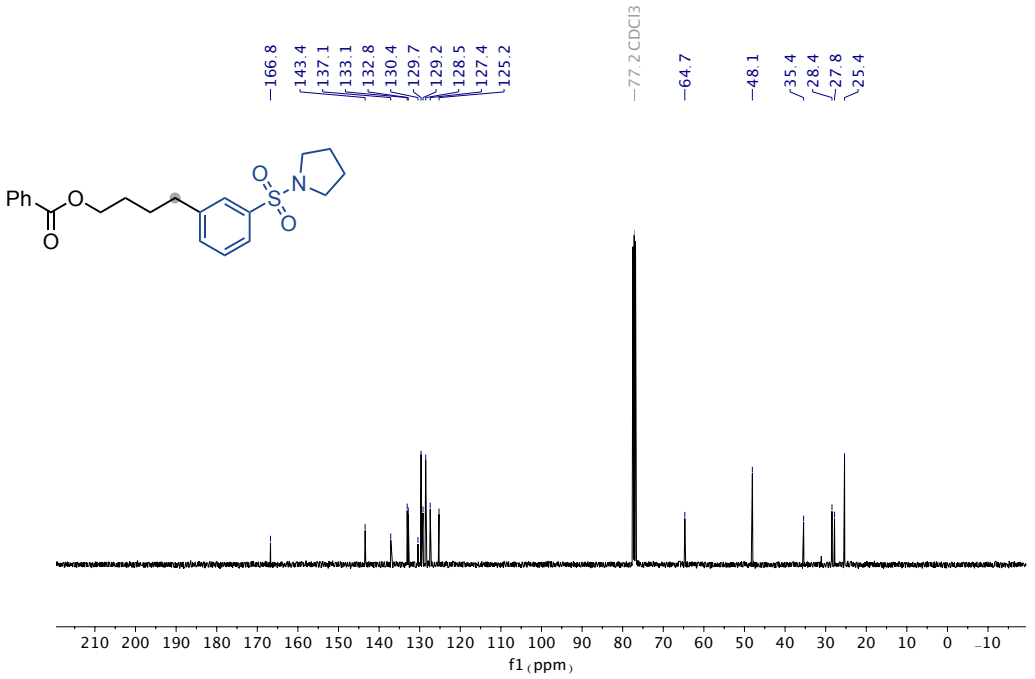

*[13]C NMR spectra (101 MHz) of **4i***

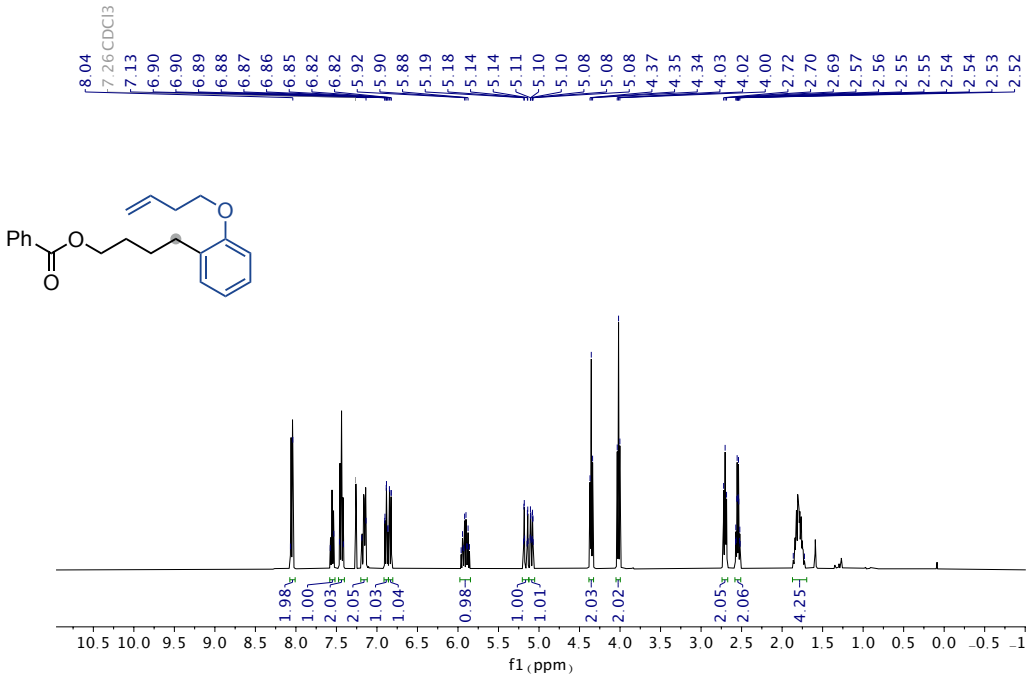

*[1]H NMR spectra (400 MHz) of **4j***

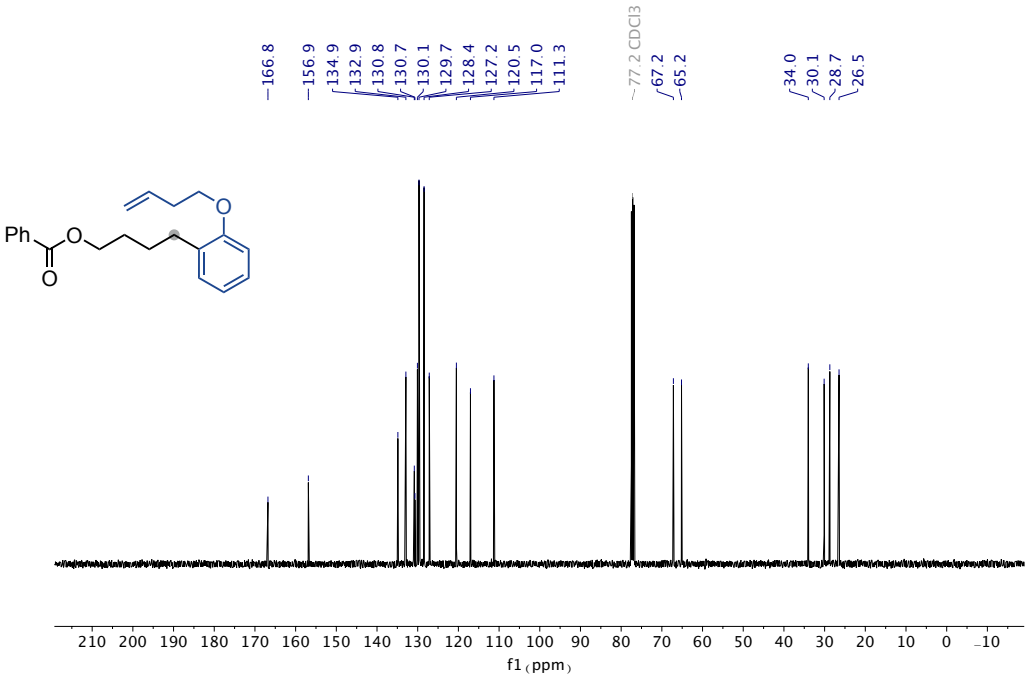

*^{13}C NMR spectra (101 MHz) of **4j***

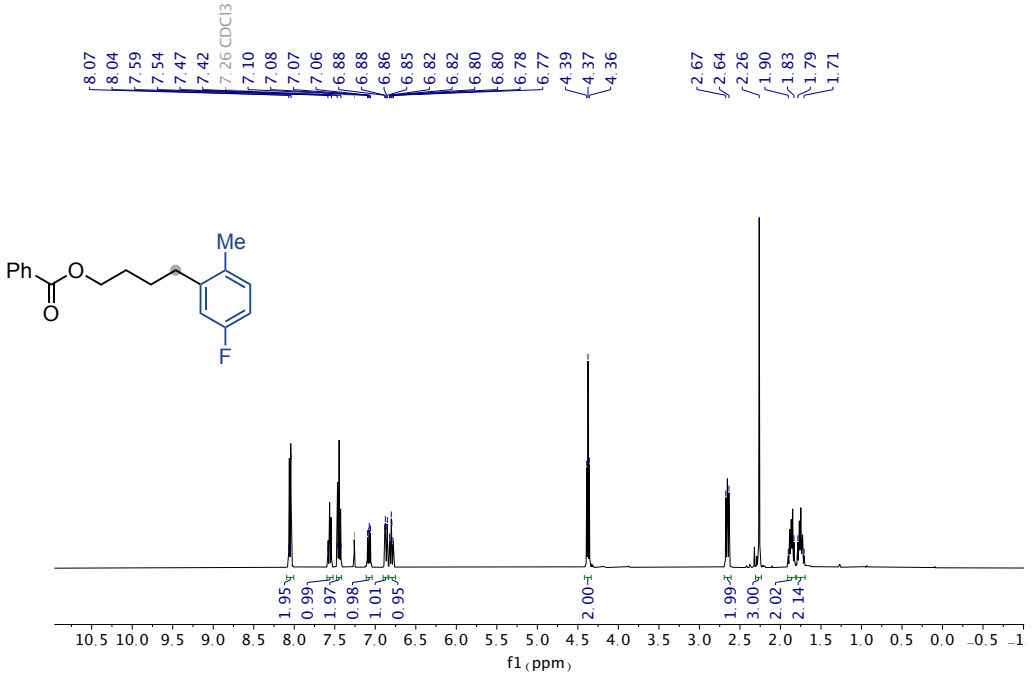

*^{1}H NMR spectra (400 MHz) of **4k***

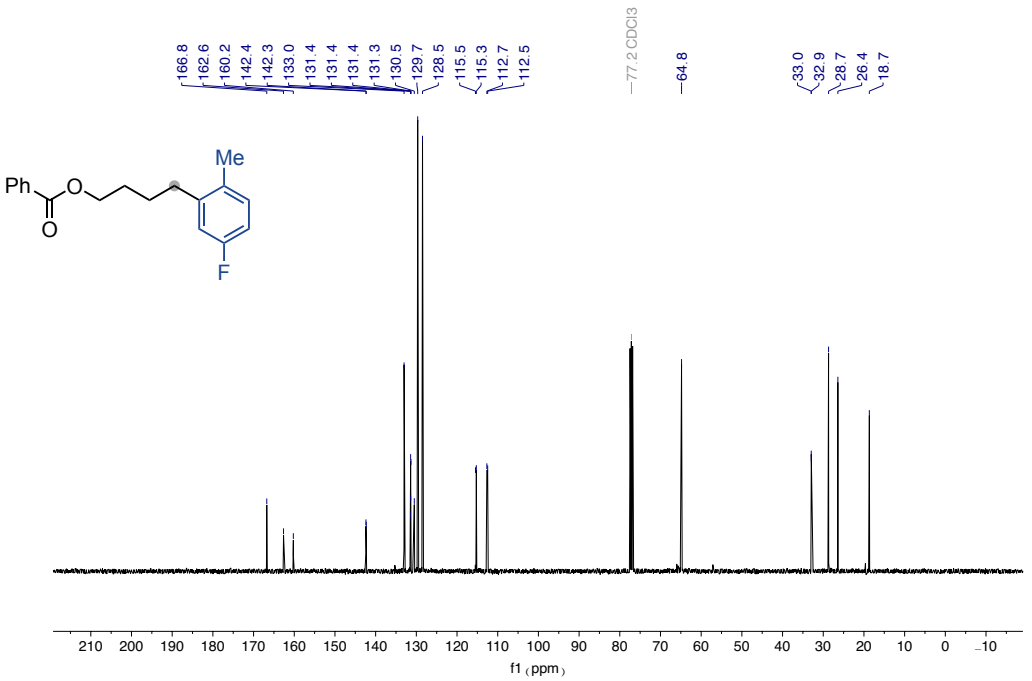

*[13]C NMR spectra (101 MHz) of **4k***

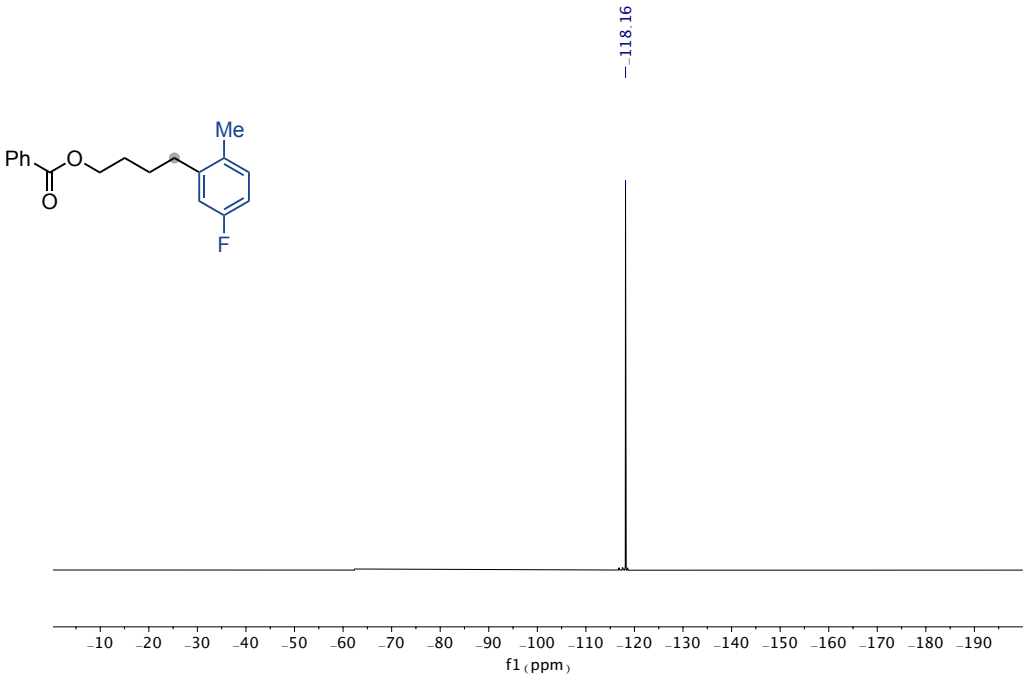

*[19]F NMR spectra (376 MHz) of **4k***

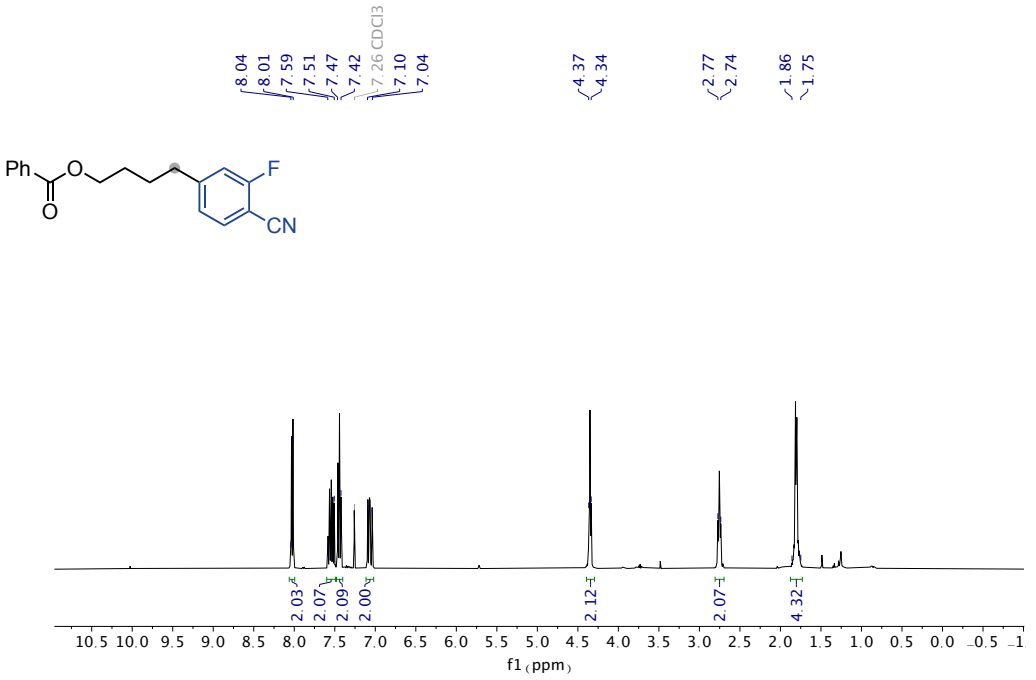

*^{1}H NMR spectra (500 MHz) of **4l***

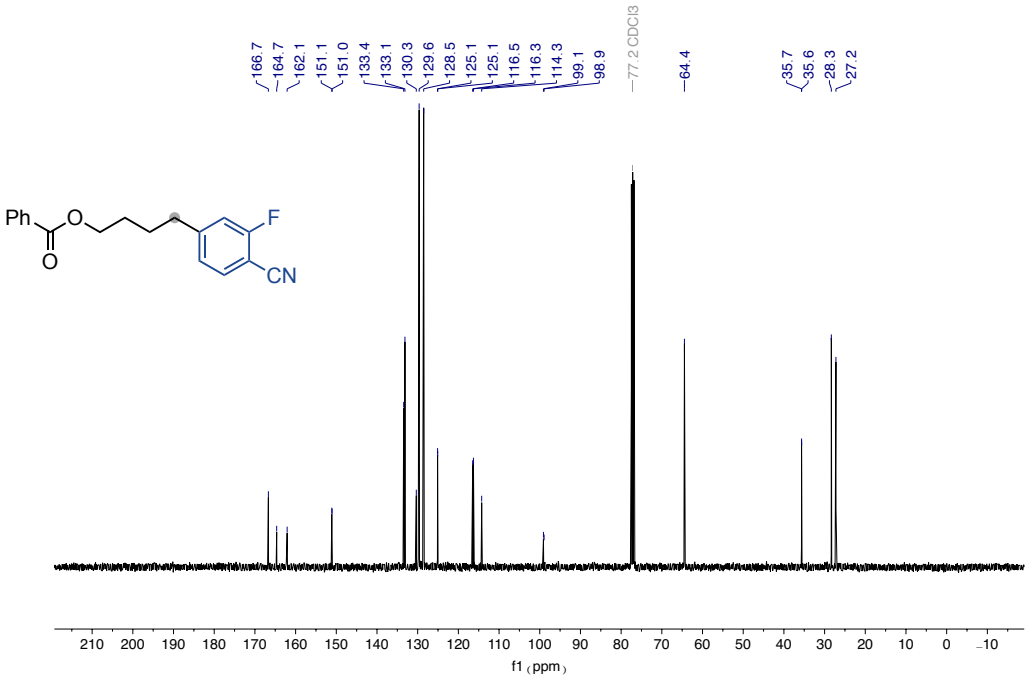

*^{13}C NMR spectra (101 MHz) of **4l***

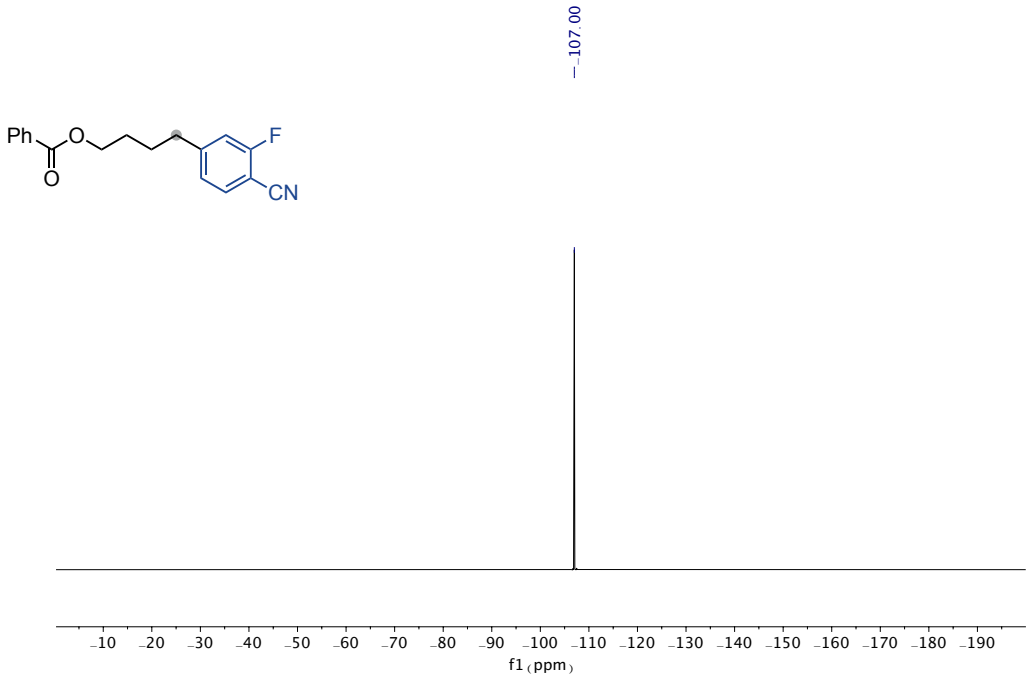

*[19]F NMR spectra (376 MHz) of **4l***

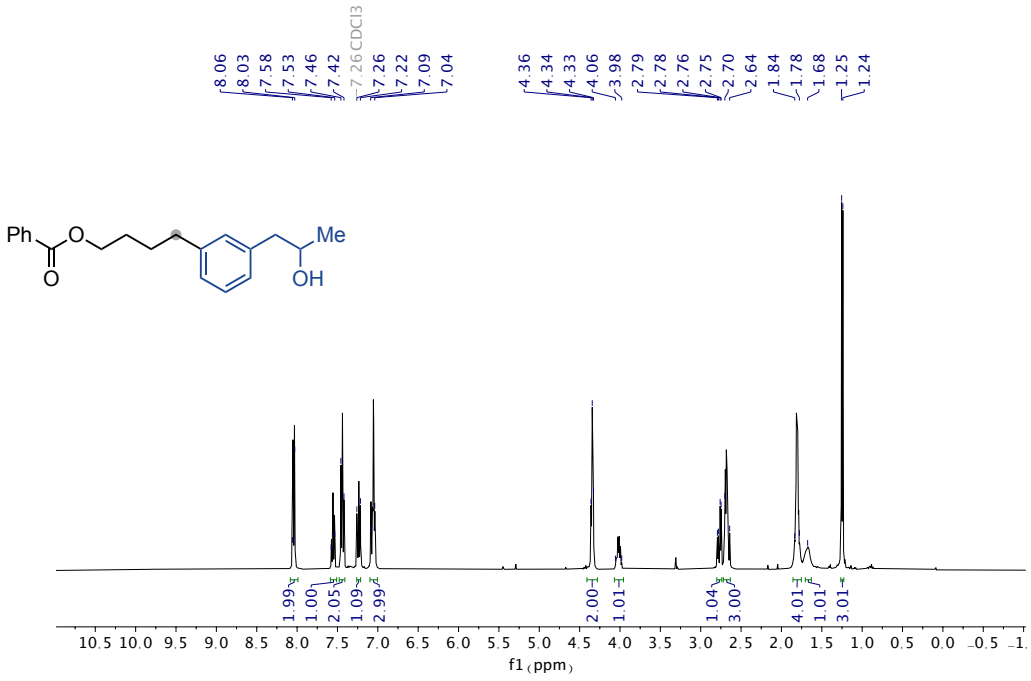

*[1]H NMR spectra (400 MHz) of **4m***

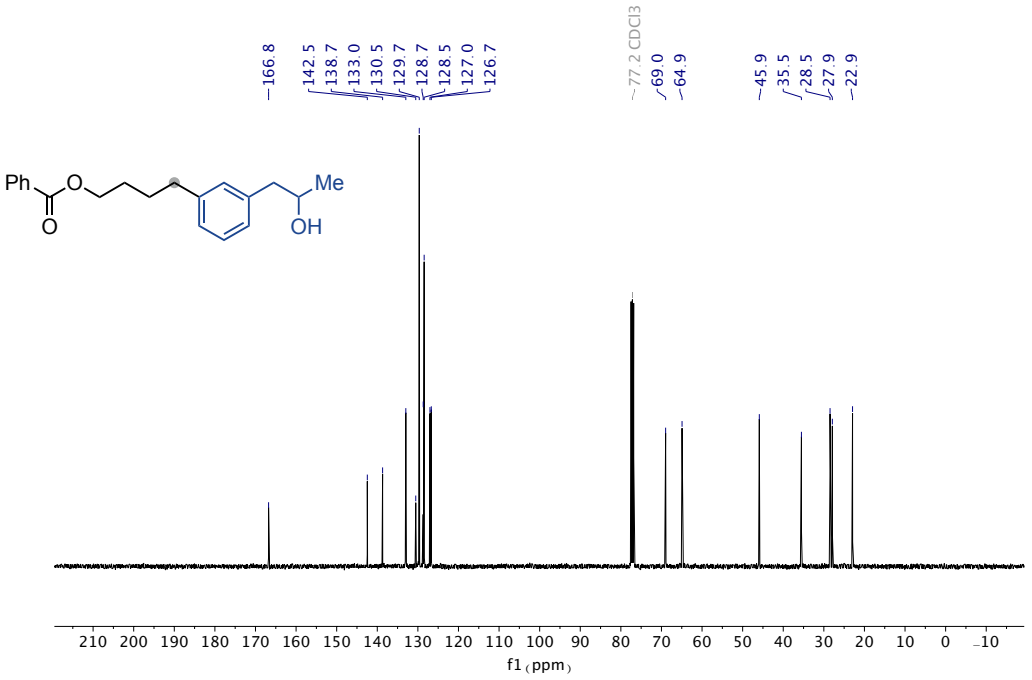

*^{13}C NMR spectra (101 MHz) of **4m***

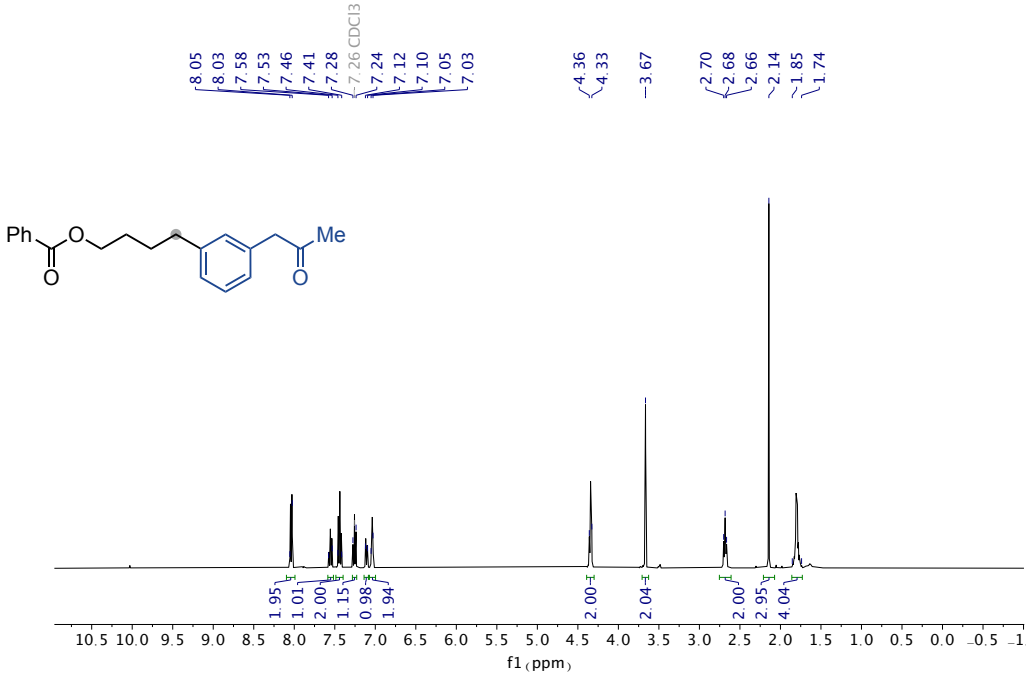

*^{1}H NMR spectra (400 MHz) of **4n***

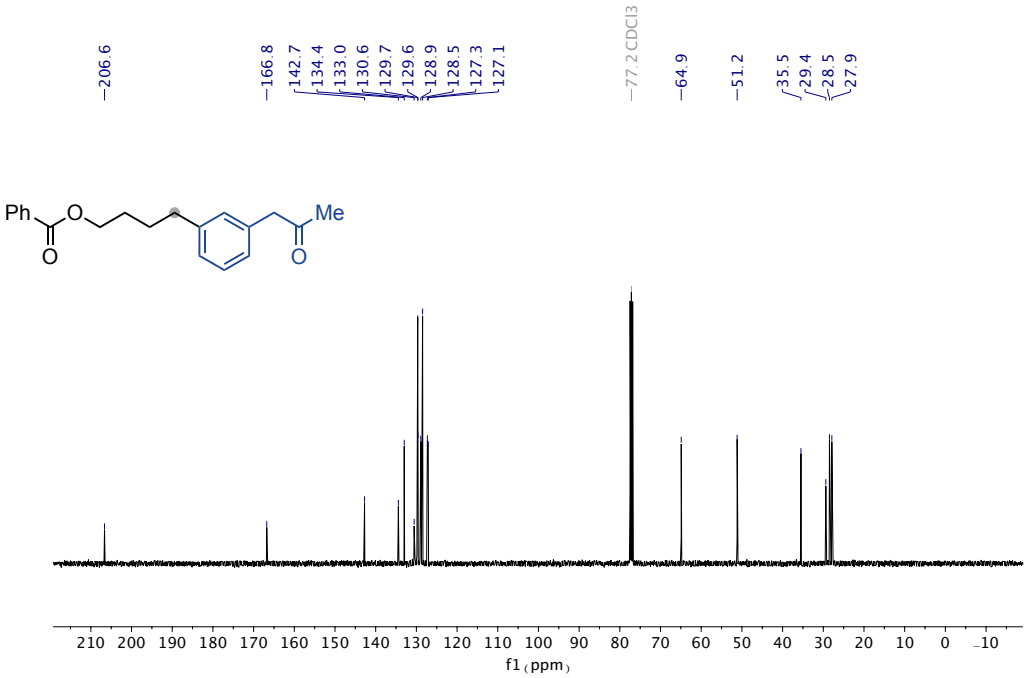

*[13]C NMR spectra (101 MHz) of **4n***

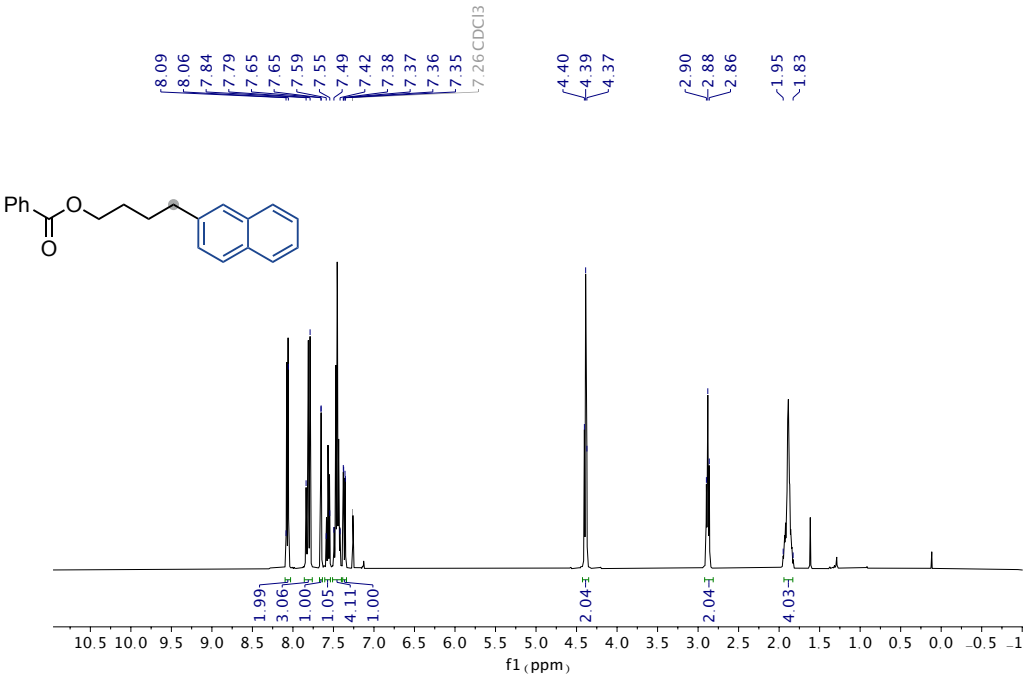

*[1]H NMR spectra (400 MHz) of **4o***

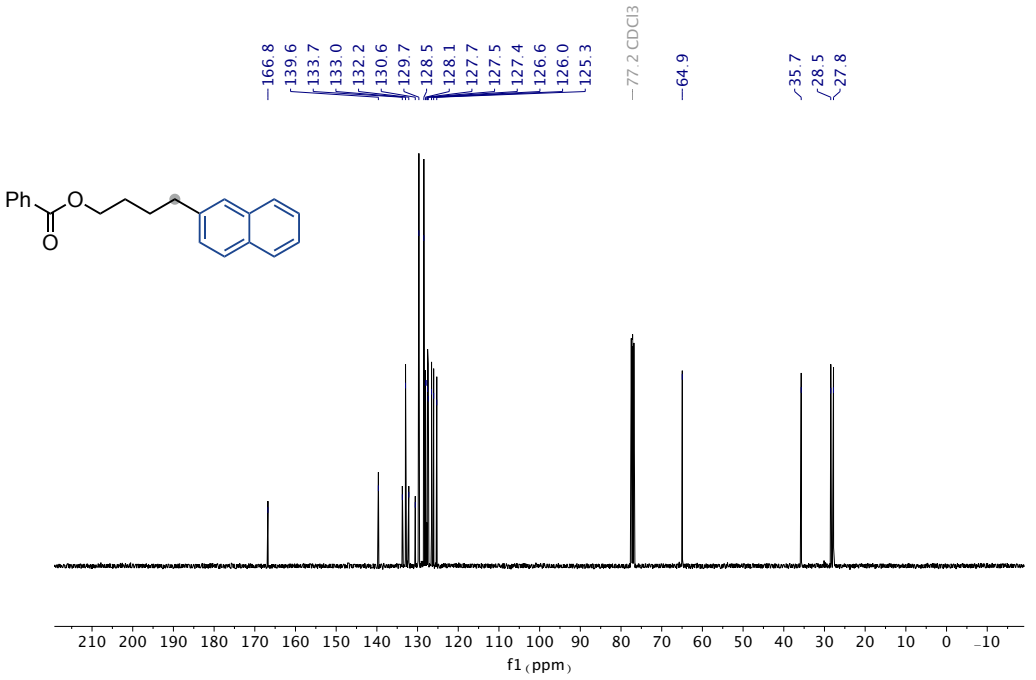

*^{13}C NMR spectra (101 MHz) of **4o***

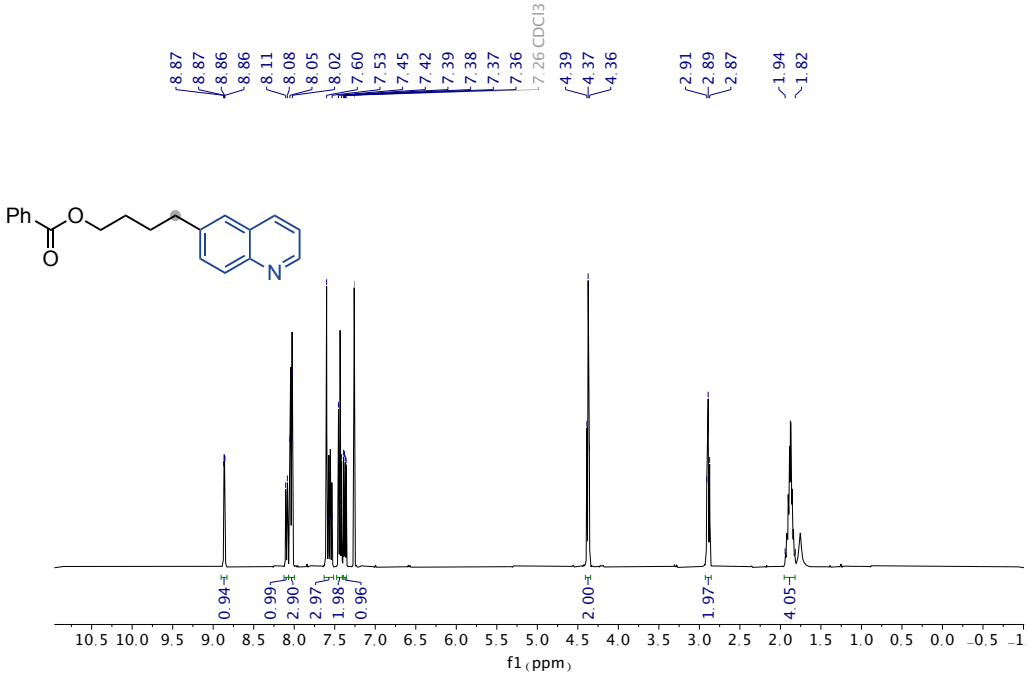

*^{1}H NMR spectra (400 MHz) of **4p***

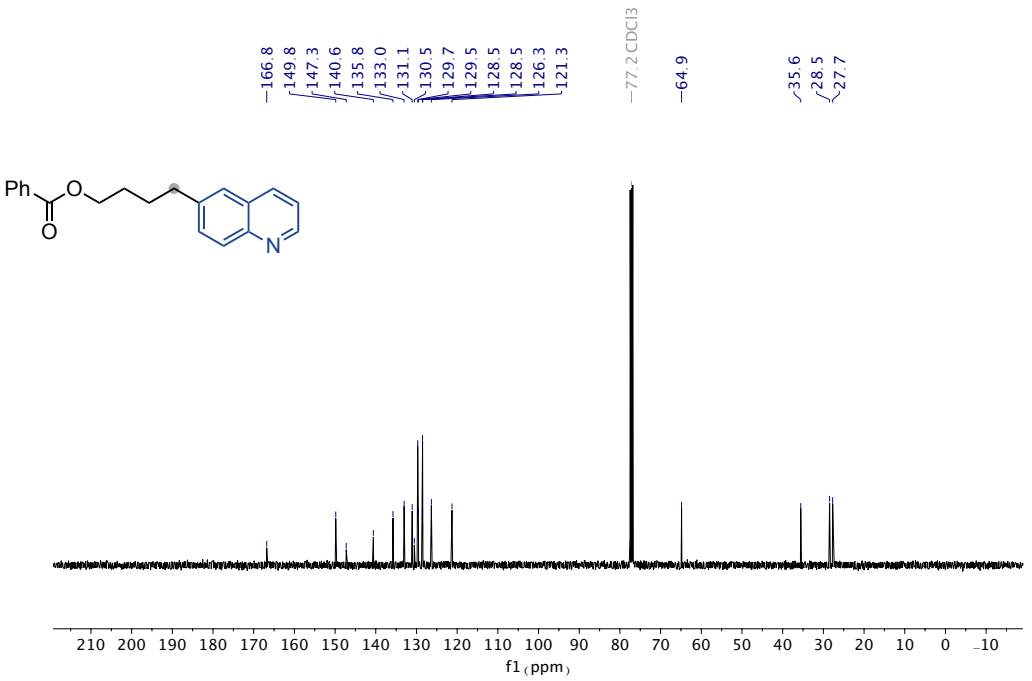

*[13]C NMR spectra (101 MHz) of **4p***

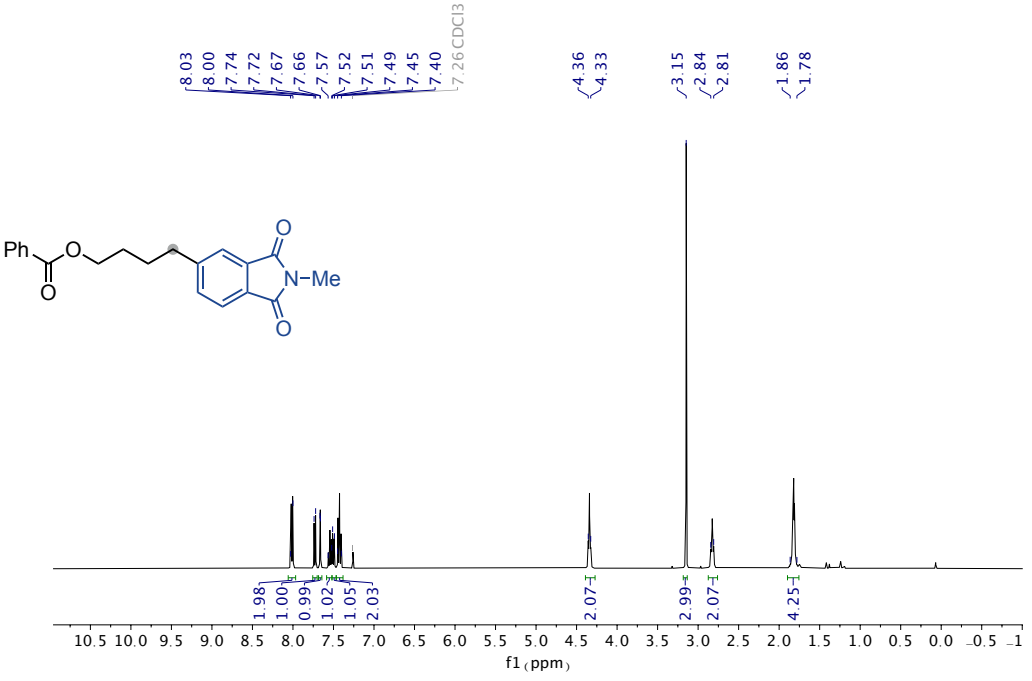

*[1]H NMR spectra (400 MHz) of **4q***

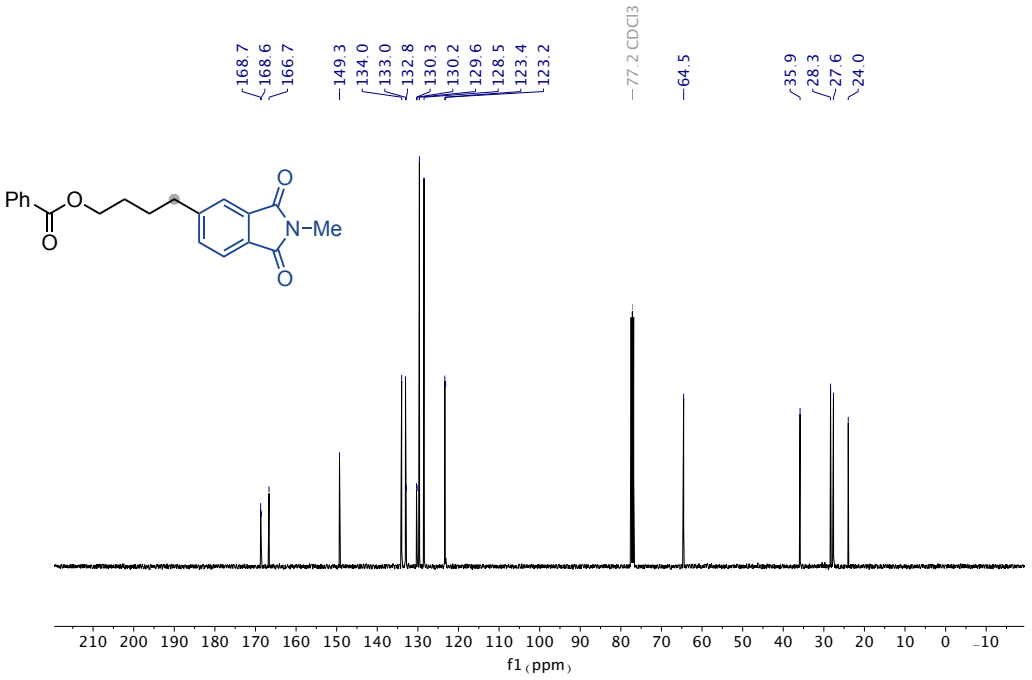

*^{13}C NMR spectra (101 MHz) of **4q***

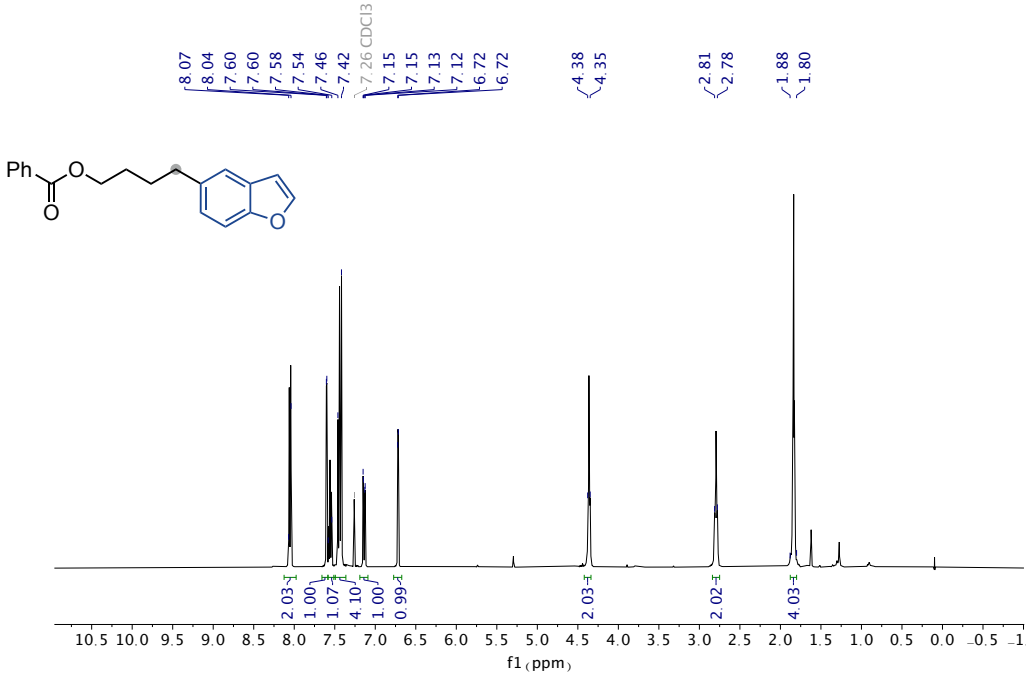

*^{1}H NMR spectra (400 MHz) of **4r***

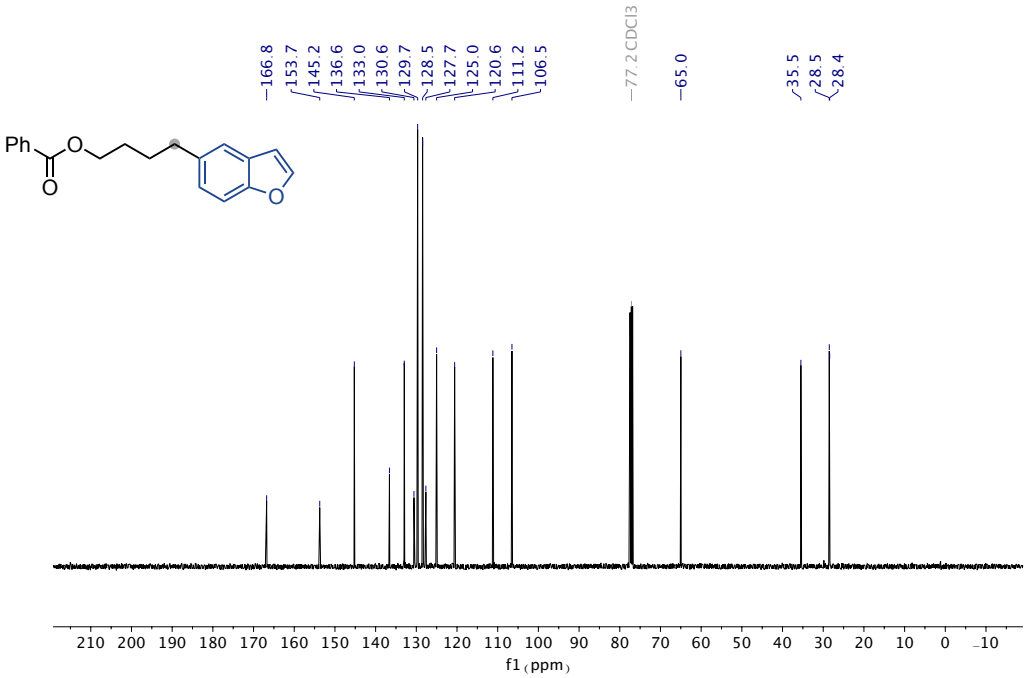

*[13]C NMR spectra (101 MHz) of **4r***

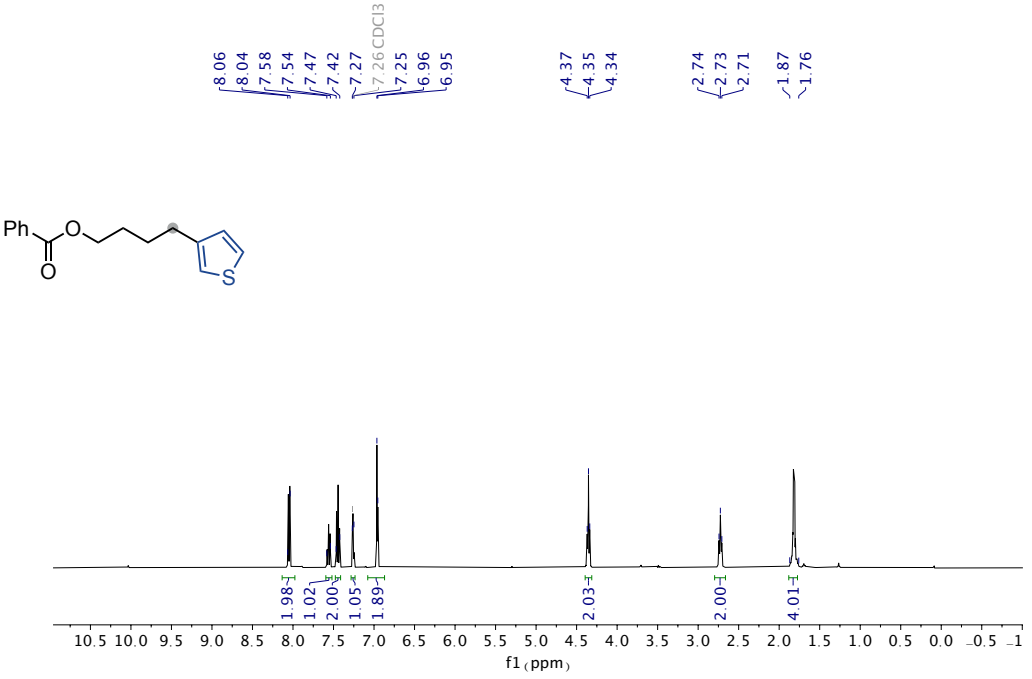

*[1]H NMR spectra (400 MHz) of **4s***

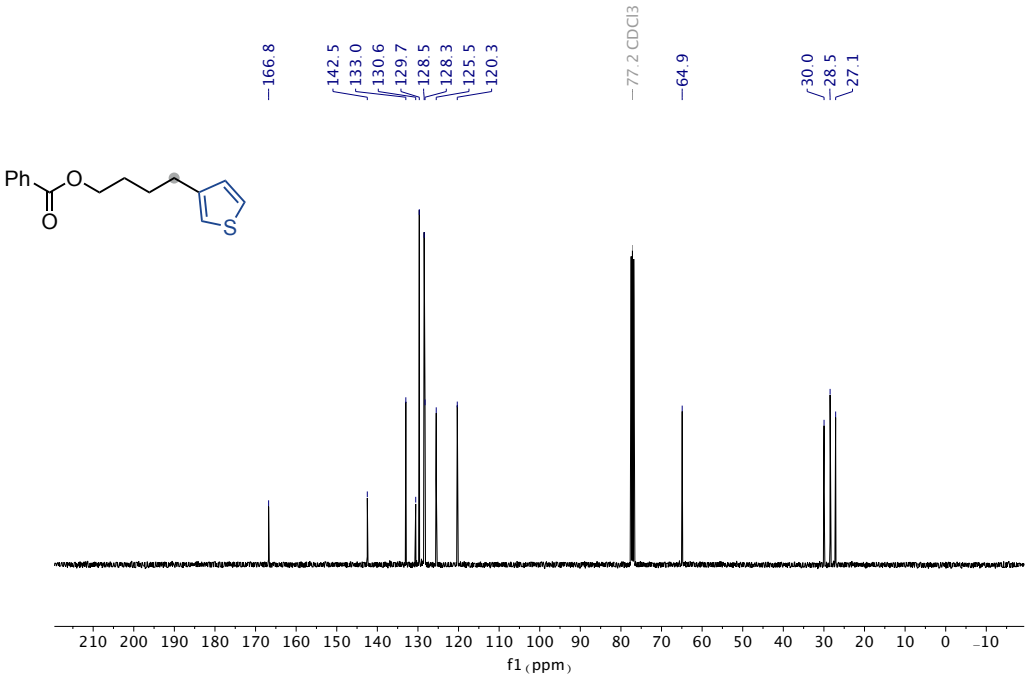

*^{13}C NMR spectra (101 MHz) of **4s***

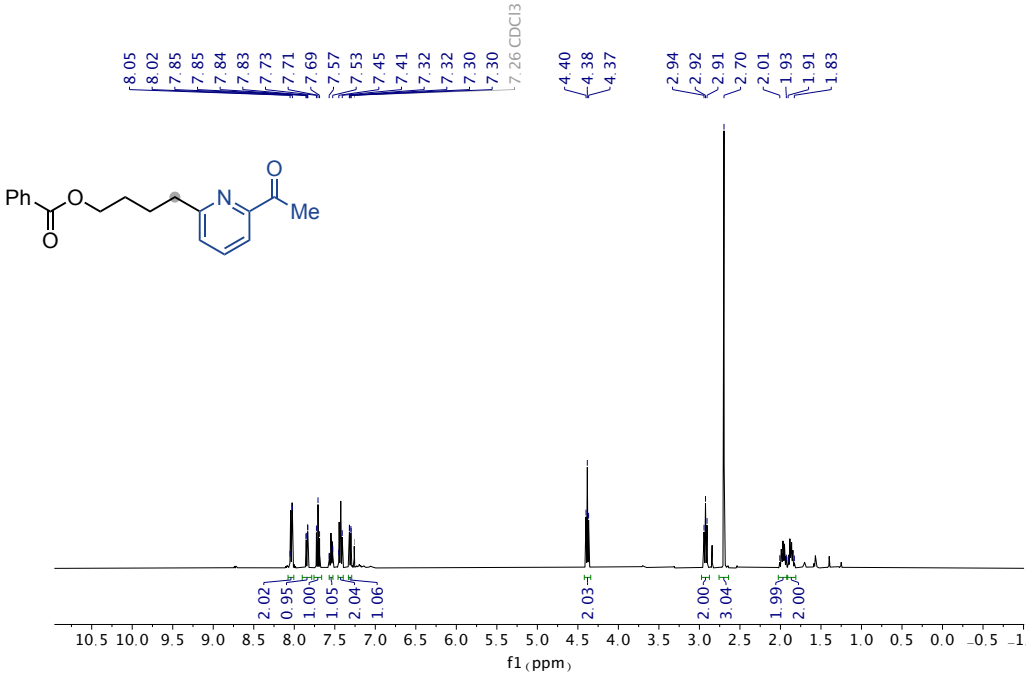

*^{1}H NMR spectra (500 MHz) of **4t***

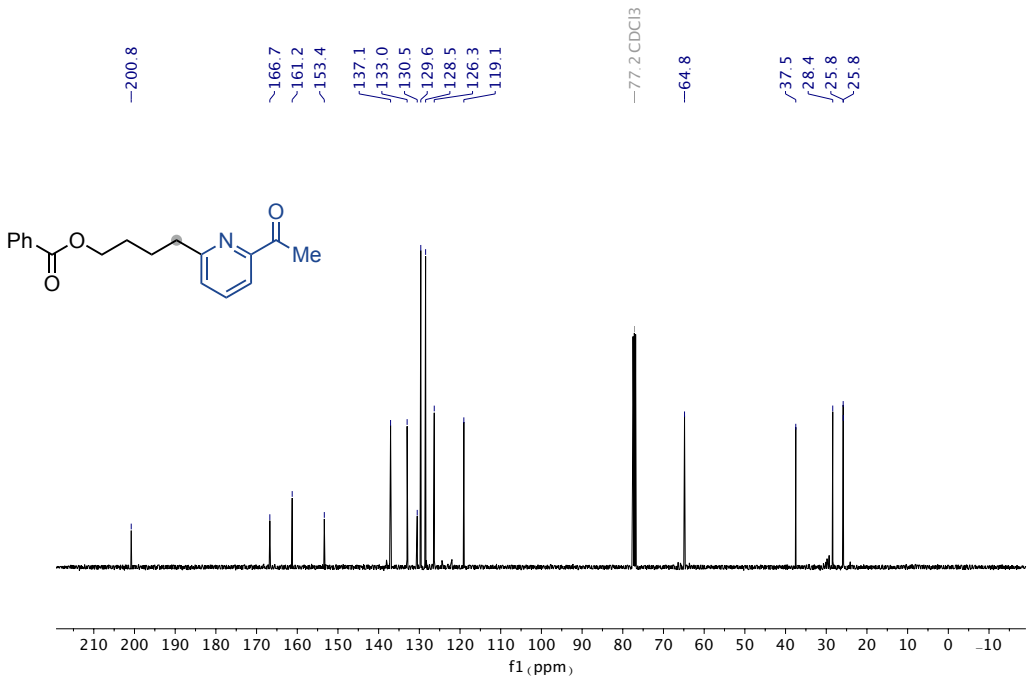

*[13]C NMR spectra (101 MHz) of **4t***

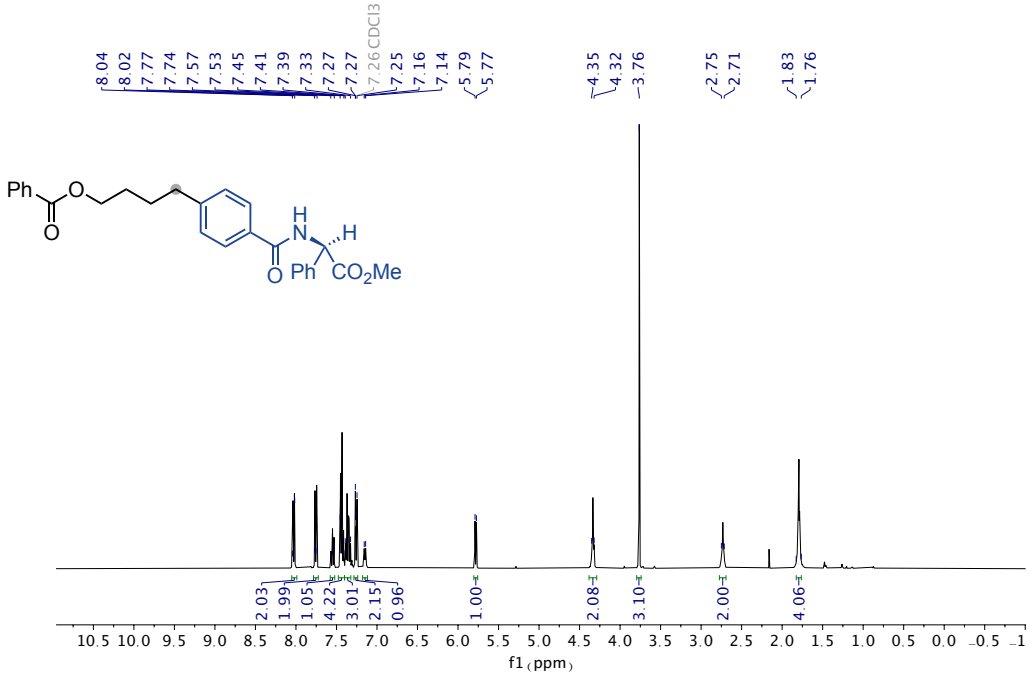

*[1]H NMR spectra (400 MHz) of **4u***

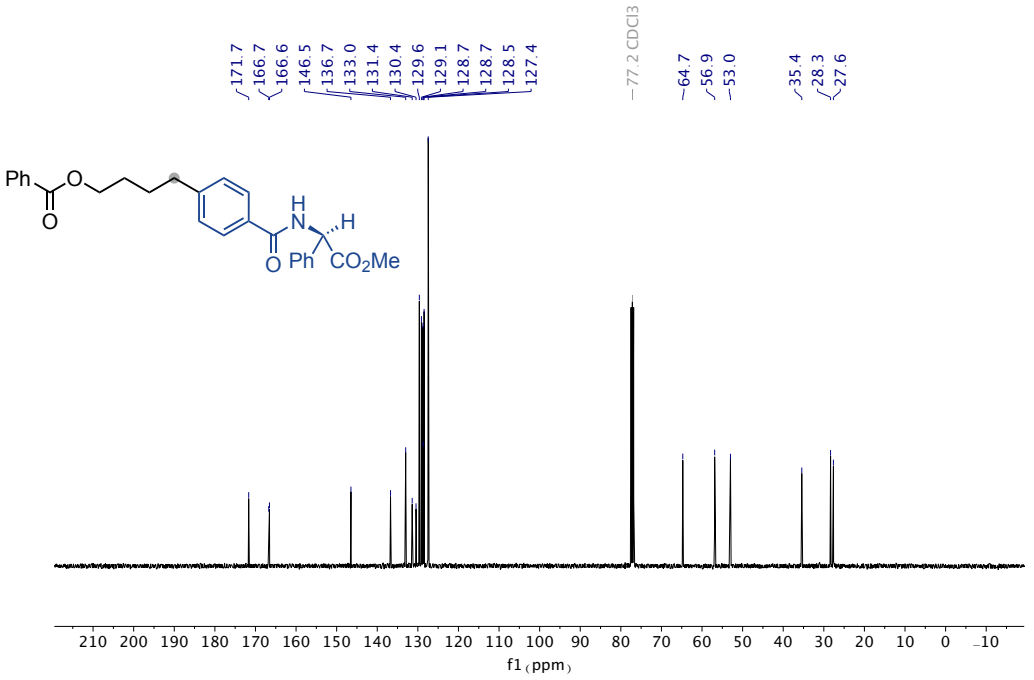

*^{13}C NMR spectra (101 MHz) of **4u***

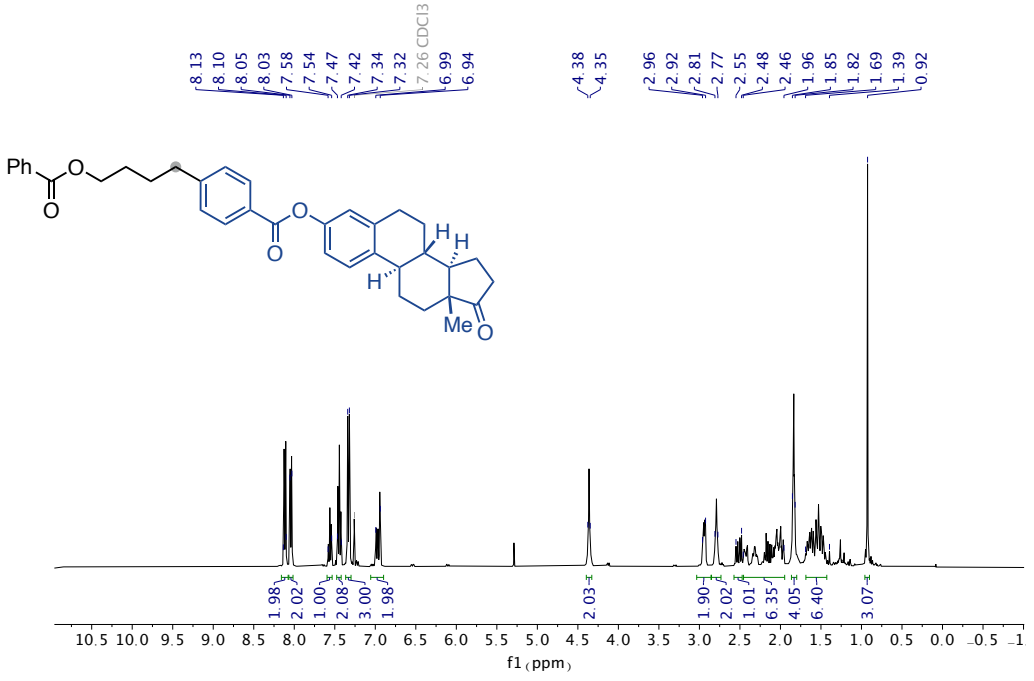

*^{1}H NMR spectra (400 MHz) of **4v***

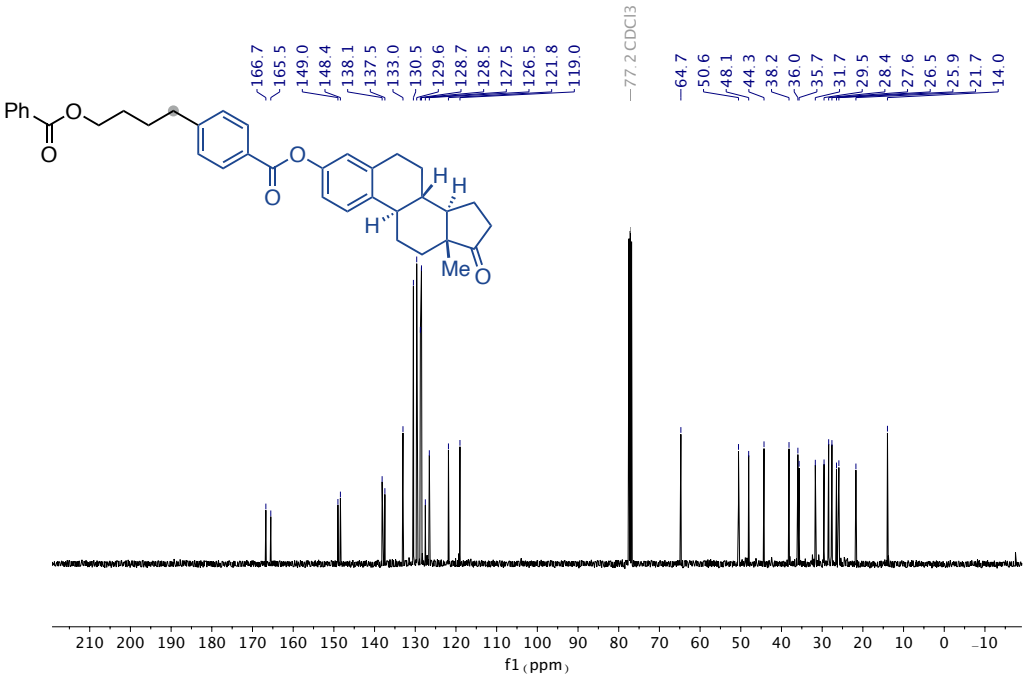

*[13]C NMR spectra (101 MHz) of **4v***

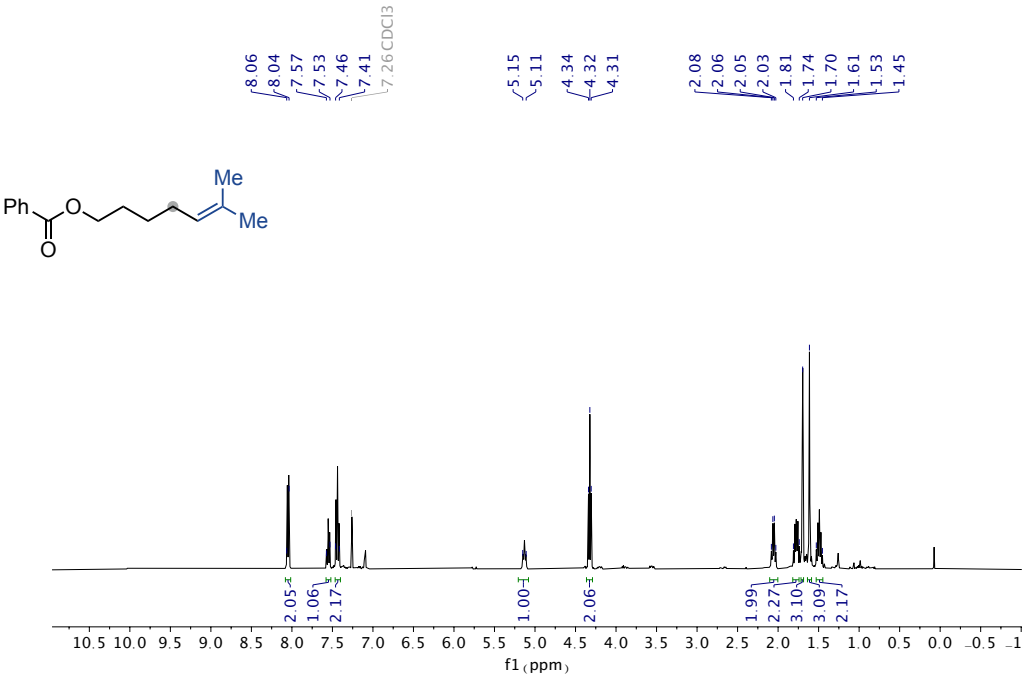

*[1]H NMR spectra (400 MHz) of **5***

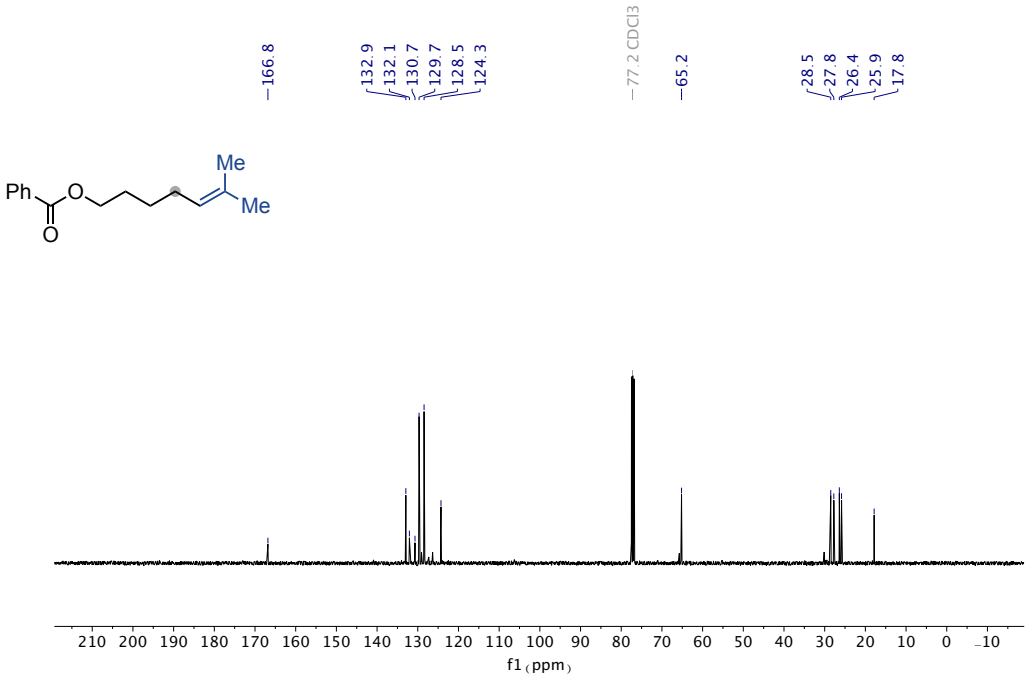

*^{13}C NMR spectra (101 MHz) of **5***

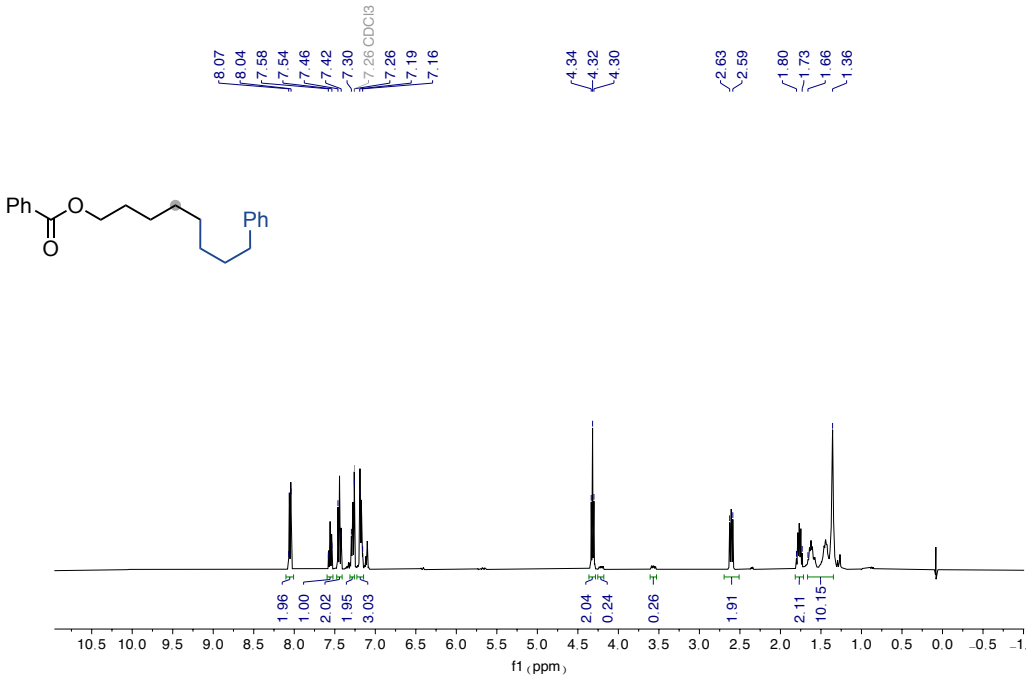

*^{1}H NMR spectra (400 MHz) of **7***

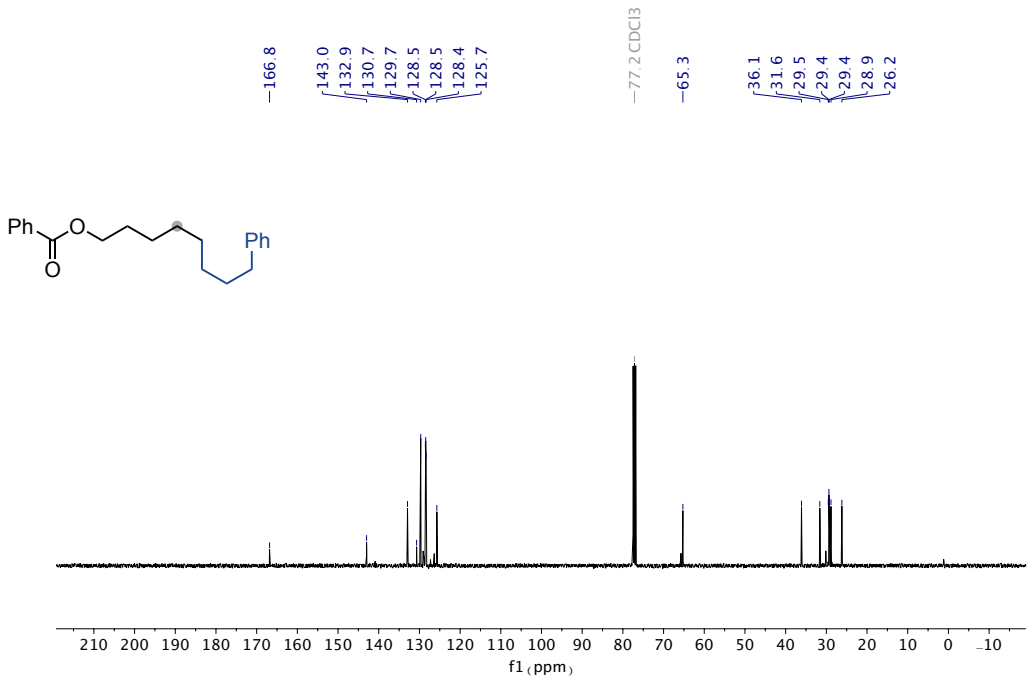

*[13]C NMR spectra (101 MHz) of **7***

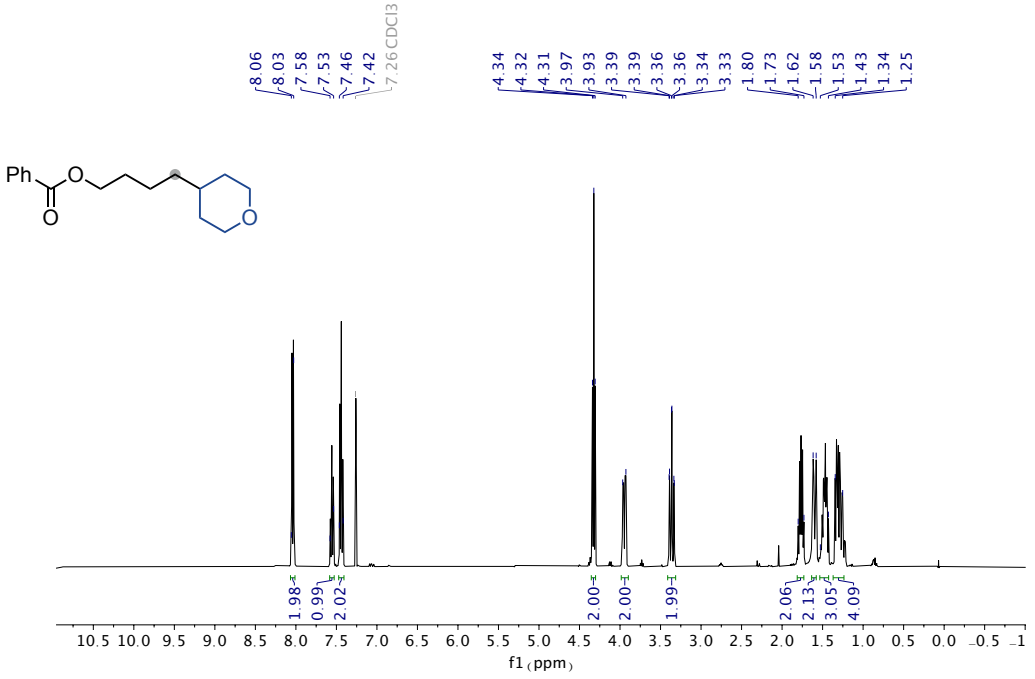

*[1]H NMR spectra (400 MHz) of **9***

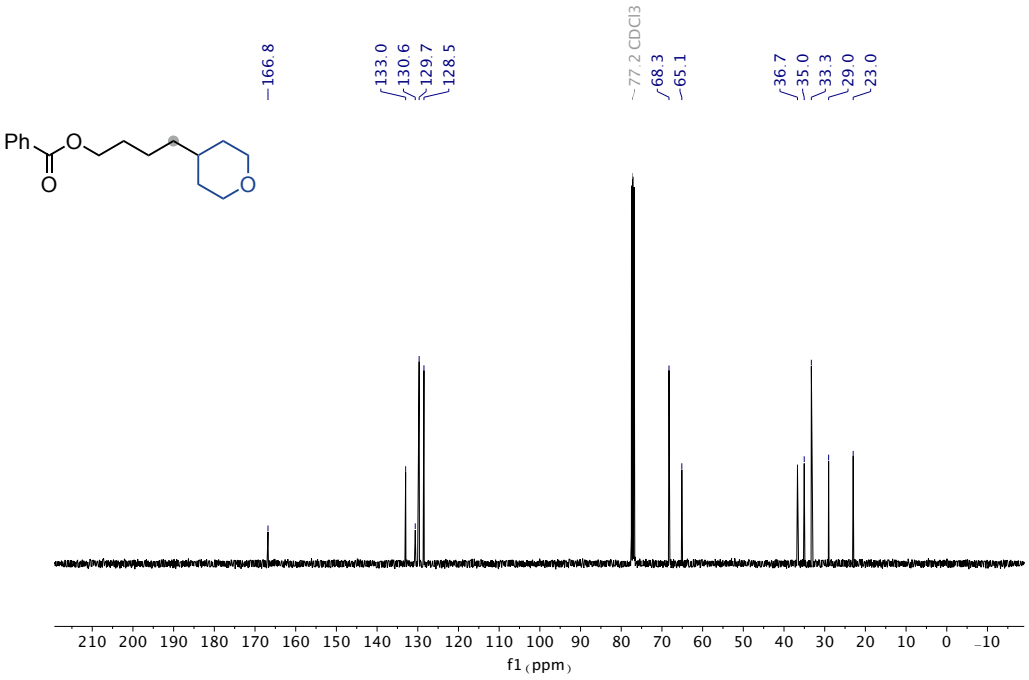

*^{13}C NMR spectra (101 MHz) of **9***

2.6. References

(1) Huang, C.-Y.; Li, J.; Li, C.-J. Photocatalytic C(Sp3) Radical Generation via C–H, C–C, and C–X Bond Cleavage. *Chem. Sci.* **2022**, *13* (19), 5465–5504. https://doi.org/10.1039/D2SC00202G.

(2) Anwar, K.; Merkens, K.; Aguilar Troyano, F. J.; Gómez-Suárez, A. Radical Deoxyfunctionalisation Strategies**. *Eur. J. Org. Chem.* **2022**, *2022* (26), e202200330. https://doi.org/10.1002/ejoc.202200330.

(3) Sanford, A. B.; Thane, T. A.; McGinnis, T. M.; Chen, P.-P.; Hong, X.; Jarvo, E. R. Nickel-Catalyzed Alkyl–Alkyl Cross-Electrophile Coupling Reaction of 1,3-Dimesylates for the Synthesis of Alkylcyclopropanes. *J. Am. Chem. Soc.* **2020**, *142* (11), 5017–5023. https://doi.org/10.1021/jacs.0c01330.

(4) Chen, P.-P.; McGinnis, T. M.; Lin, P. C.; Hong, X.; Jarvo, E. R. A Nickel-Catalyzed Cross-Electrophile Coupling Reaction of 1,3-Dimesylates for Alkylcyclopropane Synthesis: Investigation of Stereochemical Outcomes and Radical Lifetimes. *ACS Catal.* **2023**, *13* (8), 5472–5481. https://doi.org/10.1021/acscatal.3c00905.

(5) Li, Z.; Sun, W.; Wang, X.; Li, L.; Zhang, Y.; Li, C. Electrochemically Enabled, Nickel-Catalyzed Dehydroxylative Cross-Coupling of Alcohols with Aryl Halides. *J. Am. Chem. Soc.* **2021**, *143* (9), 3536–3543. https://doi.org/10.1021/jacs.0c13093.

(6) Xie, H.; Guo, J.; Wang, Y.-Q.; Wang, K.; Guo, P.; Su, P.-F.; Wang, X.; Shu, X.-Z. Radical Dehydroxylative Alkylation of Tertiary Alcohols by Ti Catalysis. *J. Am. Chem. Soc.* **2020**, *142* (39), 16787–16794. https://doi.org/10.1021/jacs.0c07492.

(7) Xie, H.; Wang, S.; Wang, Y.; Guo, P.; Shu, X.-Z. Ti-Catalyzed Reductive Dehydroxylative Vinylation of Tertiary Alcohols. *ACS Catal.* **2022**, *12* (2), 1018–1023. https://doi.org/10.1021/acscatal.1c05530.

(8) Suga, T.; Takahashi, Y.; Miki, C.; Ukaji, Y. Direct and Unified Access to Carbon Radicals from Aliphatic Alcohols by Cost-Efficient Titanium-Mediated Homolytic C−OH Bond Cleavage. *Angew. Chem. Int. Ed.* **2022**, *61* (10), e202112533. https://doi.org/10.1002/anie.202112533.

(9) Zhang, K.; Chang, L.; An, Q.; Wang, X.; Zuo, Z. Dehydroxymethylation of Alcohols Enabled by Cerium Photocatalysis. *J. Am. Chem. Soc.* **2019**, *141* (26), 10556–10564. https://doi.org/10.1021/jacs.9b05932.

(10) Chen, Y.; Wang, X.; He, X.; An, Q.; Zuo, Z. Photocatalytic Dehydroxymethylative Arylation by Synergistic Cerium and Nickel Catalysis. *J. Am. Chem. Soc.* **2021**, *143* (13), 4896–4902. https://doi.org/10.1021/jacs.1c00618.

(11) Lin, Q.; Ma, G.; Gong, H. Ni-Catalyzed Formal Cross-Electrophile Coupling of Alcohols with Aryl Halides. *ACS Catal.* **2021**, *11* (22), 14102–14109. https://doi.org/10.1021/acscatal.1c04239.

(12) Chi, B. K.; Widness, J. K.; Gilbert, M. M.; Salgueiro, D. C.; Garcia, K. J.; Weix, D. J. In-Situ Bromination Enables Formal Cross-Electrophile Coupling of Alcohols with Aryl and Alkenyl Halides. *ACS Catal.* **2022**, *12* (1), 580–586. https://doi.org/10.1021/acscatal.1c05208.

(13) Ye, Y.; Chen, H.; Sessler, J. L.; Gong, H. Zn-Mediated Fragmentation of Tertiary Alkyl Oxalates Enabling Formation of Alkylated and Arylated Quaternary Carbon Centers. *J. Am. Chem. Soc.* **2019**, *141* (2), 820–824. https://doi.org/10.1021/jacs.8b12801.

(14) Gao, M.; Sun, D.; Gong, H. Ni-Catalyzed Reductive C–O Bond Arylation of Oxalates Derived from α-Hydroxy Esters with Aryl Halides. *Org. Lett.* **2019**, *21* (6), 1645–1648. https://doi.org/10.1021/acs.orglett.9b00174.

(15) Mills, L. R.; Monteith, J. J.; dos Passos Gomes, G.; Aspuru-Guzik, A.; Rousseaux, S. A. L. The Cyclopropane Ring as a Reporter of Radical Leaving-Group Reactivity for Ni-Catalyzed C(Sp3)–O Arylation. *J. Am. Chem. Soc.* **2020**, *142* (30), 13246–13254. https://doi.org/10.1021/jacs.0c06904.

(16) Zhang, L.; Koreeda, M. Radical Deoxygenation of Hydroxyl Groups via Phosphites. *J. Am. Chem. Soc.* **2004**, *126* (41), 13190–13191. https://doi.org/10.1021/ja0462777.

(17) Stache, E. E.; Ertel, A. B.; Rovis, T.; Doyle, A. G. Generation of Phosphoranyl Radicals via Photoredox Catalysis Enables Voltage–Independent Activation of Strong C–O Bonds. *ACS Catal.* **2018**, *8* (12), 11134–11139. https://doi.org/10.1021/acscatal.8b03592.

(18) Guo, H.-M.; Wu, X. Selective Deoxygenative Alkylation of Alcohols via Photocatalytic Domino Radical

Fragmentations. *Nat. Commun.* **2021**, *12* (1), 5365. https://doi.org/10.1038/s41467-021-25702-4.

(19) Barton, D. H. R.; McCombie, S. W. A New Method for the Deoxygenation of Secondary Alcohols. *J. Chem. Soc. Perkin 1* **1975**, No. 16, 1574–1585. https://doi.org/10.1039/P19750001574.

(20) Lopez, R. M.; Hays, D. S.; Fu, G. C. Bu3SnH-Catalyzed Barton−McCombie Deoxygenation of Alcohols. *J. Am. Chem. Soc.* **1997**, *119* (29), 6949–6950. https://doi.org/10.1021/ja971400y.

(21) Togo, H.; Matsubayashi, S.; Yamazaki, O.; Yokoyama, M. Deoxygenative Functionalization of Hydroxy Groups via Xanthates with Tetraphenyldisilane. *J. Org. Chem.* **2000**, *65* (9), 2816–2819. https://doi.org/10.1021/jo991715r.

(22) Spiegel, D. A.; Wiberg, K. B.; Schacherer, L. N.; Medeiros, M. R.; Wood, J. L. Deoxygenation of Alcohols Employing Water as the Hydrogen Atom Source. *J. Am. Chem. Soc.* **2005**, *127* (36), 12513–12515. https://doi.org/10.1021/ja052185l.

(23) Chenneberg, L.; Baralle, A.; Daniel, M.; Fensterbank, L.; Goddard, J.-P.; Ollivier, C. Visible Light Photocatalytic Reduction of O-Thiocarbamates: Development of a Tin-Free Barton–McCombie Deoxygenation Reaction. *Adv. Synth. Catal.* **2014**, *356* (13), 2756–2762. https://doi.org/10.1002/adsc.201400729.

(24) Bentrude, W. G. Phosphoranyl Radicals - Their Structure, Formation, and Reactions. *Acc. Chem. Res.* **1982**, *15* (4), 117–125. https://doi.org/10.1021/ar00076a004.

(25) Lackner, G. L.; Quasdorf, K. W.; Overman, L. E. Direct Construction of Quaternary Carbons from Tertiary Alcohols via Photoredox-Catalyzed Fragmentation of Tert-Alkyl N-Phthalimidoyl Oxalates. *J. Am. Chem. Soc.* **2013**, *135* (41), 15342–15345. https://doi.org/10.1021/ja408971t.

(26) Okada, K.; Okamoto, K.; Morita, N.; Okubo, K.; Oda, M. Photosensitized Decarboxylative Michael Addition through N-(Acyloxy)Phthalimides via an Electron-Transfer Mechanism. *J. Am. Chem. Soc.* **1991**, *113* (24), 9401–9402. https://doi.org/10.1021/ja00024a074.

(27) Nawrat, C. C.; Jamison, C. R.; Slutskyy, Y.; MacMillan, D. W. C.; Overman, L. E. Oxalates as Activating Groups for Alcohols in Visible Light Photoredox Catalysis: Formation of Quaternary Centers by Redox-Neutral Fragment Coupling. *J. Am. Chem. Soc.* **2015**, *137* (35), 11270–11273. https://doi.org/10.1021/jacs.5b07678.

(28) Pitre, S. P.; Muuronen, M.; Fishman, D. A.; Overman, L. E. Tertiary Alcohols as Radical Precursors for the Introduction of Tertiary Substituents into Heteroarenes. *ACS Catal.* **2019**, *9* (4), 3413–3418. https://doi.org/10.1021/acscatal.9b00405.

(29) Su, J. Y.; Grünenfelder, D. C.; Takeuchi, K.; Reisman, S. E. Radical Deoxychlorination of Cesium Oxalates for the Synthesis of Alkyl Chlorides. *Org. Lett.* **2018**, *20* (16), 4912–4916. https://doi.org/10.1021/acs.orglett.8b02045.

(30) Li, M.; Liu, T.; Li, J.; He, H.; Dai, H.; Xie, J. Visible-Light-Mediated Deoxyalkynylation of Activated Tertiary Alcohols. *J. Org. Chem.* **2021**. https://doi.org/10.1021/acs.joc.1c01356.

(31) González-Esguevillas, M.; Miró, J.; Jeffrey, J. L.; MacMillan, D. W. C. Photoredox-Catalyzed Deoxyfluorination of Activated Alcohols with Selectfluor®. *Tetrahedron* **2019**, *75* (32), 4222–4227. https://doi.org/10.1016/j.tet.2019.05.043.

(32) Aguilar Troyano, F. J.; Ballaschk, F.; Jaschinski, M.; Özkaya, Y.; Gómez-Suárez, A. Light-Mediated Formal Radical Deoxyfluorination of Tertiary Alcohols through Selective Single-Electron Oxidation with TEDA2+. *Chem. – Eur. J.* **2019**, *25* (62), 14054–14058. https://doi.org/10.1002/chem.201903702.

(33) Zhang, X.; MacMillan, D. W. C. Alcohols as Latent Coupling Fragments for Metallaphotoredox Catalysis: Sp3–Sp2 Cross-Coupling of Oxalates with Aryl Halides. *J. Am. Chem. Soc.* **2016**, *138* (42), 13862–13865. https://doi.org/10.1021/jacs.6b09533.

(34) Weires, N. A.; Slutskyy, Y.; Overman, L. E. Facile Preparation of Spirolactones by an Alkoxycarbonyl Radical Cyclization–Cross-Coupling Cascade. *Angew. Chem. Int. Ed.* **2019**, *58* (25), 8561–8565. https://doi.org/10.1002/anie.201903353.

(35) Li, H.; Guo, L.; Feng, X.; Huo, L.; Zhu, S.; Chu, L. Sequential C–O Decarboxylative Vinylation/C–H Arylation of Cyclic Oxalates via a Nickel-Catalyzed Multicomponent Radical Cascade. *Chem. Sci.* **2020**, *11* (19), 4904–

4910. https://doi.org/10.1039/D0SC01471K.

(36) Friese, F. W.; Studer, A. Deoxygenative Borylation of Secondary and Tertiary Alcohols. *Angew. Chem. Int. Ed.* **2019**, *58* (28), 9561–9564. https://doi.org/10.1002/anie.201904028.

(37) Wu, J.; Bär, R. M.; Guo, L.; Noble, A.; Aggarwal, V. K. Photoinduced Deoxygenative Borylations of Aliphatic Alcohols. *Angew. Chem. Int. Ed.* **2019**, *58* (52), 18830–18834. https://doi.org/10.1002/anie.201910051.

(38) Ma, G.; Chen, C.; Talukdar, S.; Zhao, X.; Lei, C.; Gong, H. Metal Catalyst-Free Photo-Induced Alkyl C–O Bond Borylation. *Chem. Commun.* **2020**, *56* (70), 10219–10222. https://doi.org/10.1039/D0CC04776G.

(39) Wei, Y.; Ben-zvi, B.; Diao, T. Diastereoselective Synthesis of Aryl C-Glycosides from Glycosyl Esters via C−O Bond Homolysis. *Angew. Chem. Int. Ed.* **2021**, *60* (17), 9433–9438. https://doi.org/10.1002/anie.202014991.

(40) Dong, Z.; MacMillan, D. W. C. Metallaphotoredox-Enabled Deoxygenative Arylation of Alcohols. *Nature* **2021**, *598* (7881), 451–456. https://doi.org/10.1038/s41586-021-03920-6.

(41) Sakai, H. A.; MacMillan, D. W. C. Nontraditional Fragment Couplings of Alcohols and Carboxylic Acids: C(Sp3)–C(Sp3) Cross-Coupling via Radical Sorting. *J. Am. Chem. Soc.* **2022**, *144* (14), 6185–6192. https://doi.org/10.1021/jacs.2c02062.

(42) Xu, W.; Ma, J.; Yuan, X.-A.; Dai, J.; Xie, J.; Zhu, C. Synergistic Catalysis for the Umpolung Trifluoromethylthiolation of Tertiary Ethers. *Angew. Chem. Int. Ed.* **2018**, *57* (32), 10357–10361. https://doi.org/10.1002/anie.201805927.

(43) Kariofillis, S. K.; Jiang, S.; Żurański, A. M.; Gandhi, S. S.; Martinez Alvarado, J. I.; Doyle, A. G. Using Data Science To Guide Aryl Bromide Substrate Scope Analysis in a Ni/Photoredox-Catalyzed Cross-Coupling with Acetals as Alcohol-Derived Radical Sources. *J. Am. Chem. Soc.* **2022**, *144* (2), 1045–1055. https://doi.org/10.1021/jacs.1c12203.

(44) Shields, B. J.; Doyle, A. G. Direct C(Sp3)–H Cross Coupling Enabled by Catalytic Generation of Chlorine Radicals. *J. Am. Chem. Soc.* **2016**, *138* (39), 12719–12722. https://doi.org/10.1021/jacs.6b08397.

(45) Hwang, S. J.; Anderson, B. L.; Powers, D. C.; Maher, A. G.; Hadt, R. G.; Nocera, D. G. Halogen Photoelimination from Monomeric Nickel(III) Complexes Enabled by the Secondary Coordination Sphere. *Organometallics* **2015**, *34* (19), 4766–4774. https://doi.org/10.1021/acs.organomet.5b00568.

(46) Yan, X.-B.; Li, C.-L.; Jin, W.-J.; Guo, P.; Shu, X.-Z. Reductive Coupling of Benzyl Oxalates with Highly Functionalized Alkyl Bromides by Nickel Catalysis. *Chem. Sci.* **2018**, *9* (19), 4529–4534. https://doi.org/10.1039/C8SC00609A.

(47) Liu, J.; Ye, Y.; Sessler, J. L.; Gong, H. Cross-Electrophile Couplings of Activated and Sterically Hindered Halides and Alcohol Derivatives. *Acc. Chem. Res.* **2020**, *53* (9), 1833–1845. https://doi.org/10.1021/acs.accounts.0c00291.

(48) Liu, J.; Ren, Q.; Zhang, X.; Gong, H. Preparation of Vinyl Arenes by Nickel-Catalyzed Reductive Coupling of Aryl Halides with Vinyl Bromides. *Angew. Chem. Int. Ed.* **2016**, *55* (50), 15544–15548. https://doi.org/10.1002/anie.201607959.

(49) Chen, H.; Ye, Y.; Tong, W.; Fang, J.; Gong, H. Formation of Allylated Quaternary Carbon Centers via C–O/C–O Bond Fragmentation of Oxalates and Allyl Carbonates. *Chem. Commun.* **2020**, *56* (3), 454–457. https://doi.org/10.1039/C9CC07072A.

(50) Ye, Y.; Chen, H.; Yao, K.; Gong, H. Iron-Catalyzed Reductive Vinylation of Tertiary Alkyl Oxalates with Activated Vinyl Halides. *Org. Lett.* **2020**, *22* (5), 2070–2075. https://doi.org/10.1021/acs.orglett.0c00561.

(51) Luo, Y.-R. *Handbook of Bond Dissociation Energies in Organic Compounds*; CRC Press: Boca Raton, 2002. https://doi.org/10.1201/9781420039863.

(52) Gui, Y.-Y.; Wang, Z.-X.; Zhou, W.-J.; Liao, L.-L.; Song, L.; Yin, Z.-B.; Li, J.; Yu, D.-G. Arylation of Aniline C(Sp3)−H Bonds with Phenols via an In Situ Activation Strategy. *Asian J. Org. Chem.* **2018**, *7* (3), 537–541. https://doi.org/10.1002/ajoc.201700450.

(53) Shaw, M. H.; Shurtleff, V. W.; Terrett, J. A.; Cuthbertson, J. D.; MacMillan, D. W. C. Native Functionality in Triple Catalytic Cross-Coupling: Sp3 C–H Bonds as Latent Nucleophiles. *Science* **2016**, *352* (6291), 1304–1308. https://doi.org/10.1126/science.aaf6635.

(54) Cong, F.; Lv, X.-Y.; Day, C. S.; Martin, R. Dual Catalytic Strategy for Forging Sp2–Sp3 and Sp3–Sp3 Architectures via β-Scission of Aliphatic Alcohol Derivatives. *J. Am. Chem. Soc.* **2020**, *142* (49), 20594–20599. https://doi.org/10.1021/jacs.0c11172.

(55) Heitz, D. R.; Tellis, J. C.; Molander, G. A. Photochemical Nickel-Catalyzed C–H Arylation: Synthetic Scope and Mechanistic Investigations. *J. Am. Chem. Soc.* **2016**, *138* (39), 12715–12718. https://doi.org/10.1021/jacs.6b04789.

(56) Ingold, K. U.; DiLabio, G. A. Bond Strengths: The Importance of Hyperconjugation. *Org. Lett.* **2006**, *8* (26), 5923–5925. https://doi.org/10.1021/ol062293s.

(57) Cai, Y.; Dang, H.-S.; Roberts, B. P. Regioselectivity in the Ring-Opening β-Scission of 2-Phenyl-1,3-Dioxan-2-Yl Radicals Derived from Bicyclic Benzylidene Acetals. *J. Chem. Soc. Perkin 1* **2002**, No. 22, 2449–2458. https://doi.org/10.1039/B208200B.

(58) Oderinde, M. Practical Syntheses of [2,2'-Bipyridine]Bis[3,5-Difluoro-2-[5-(Trifluoromethyl)-2-Pyridinyl]Phenyl]Iridium(III) Hexafluorophosphate, [Ir{dF(CF3)Ppy}2(Bpy)]PF6 and [4,4'-Bis(Tert-Butyl)-2,2'-Bipyridine]Bis[3,5-Difluoro-2-[5-(Trifluoromethyl)-2-Pyridinyl]Phenyl]Iridium(III) Hexafluorophosphate, [Ir{dF(CF3)Ppy}2(Dtbbpy)]PF6. *Org. Synth.* **2017**, *94*, 77–92. https://doi.org/10.15227/orgsyn.094.0077.

(59) Li, G.; Yang, L.; Liu, J.-J.; Zhang, W.; Cao, R.; Wang, C.; Zhang, Z.; Xiao, J.; Xue, D. Light-Promoted C–N Coupling of Aryl Halides with Nitroarenes. *Angew. Chem. Int. Ed.* **2021**, *60* (10), 5230–5234. https://doi.org/10.1002/anie.202012877.

(60) Meng, C.; Niu, H.; Ning, J.; Wu, W.; Yi, J. Nickel-Catalyzed Removal of Alkene Protecting Group of Phenols, Alcohols via Chain Walking Process. *Molecules* **2020**, *25* (3), 602. https://doi.org/10.3390/molecules25030602.

(61) Liu, W.; Leischner, T.; Li, W.; Junge, K.; Beller, M. A General Regioselective Synthesis of Alcohols by Cobalt-Catalyzed Hydrogenation of Epoxides. *Angew. Chem. Int. Ed.* **2020**, *59* (28), 11321–11324. https://doi.org/10.1002/anie.202002844.

(62) Shen, Y.; Gu, Y.; Martin, R. Sp3 C–H Arylation and Alkylation Enabled by the Synergy of Triplet Excited Ketones and Nickel Catalysts. *J. Am. Chem. Soc.* **2018**, *140* (38), 12200–12209. https://doi.org/10.1021/jacs.8b07405.

(63) Peng, H.; Cai, R.; Xu, C.; Chen, H.; Shi, X. Nucleophile Promoted Gold Redox Catalysis with Diazonium Salts: C–Br, C–S and C–P Bond Formation through Catalytic Sandmeyer Coupling. *Chem. Sci.* **2016**, *7* (9), 6190–6196. https://doi.org/10.1039/C6SC01742H.

(64) Li, W.; Tan, F.; Hao, X.; Wang, G.; Tang, Y.; Liu, X.; Lin, L.; Feng, X. Catalytic Asymmetric Intramolecular Homologation of Ketones with α-Diazoesters: Synthesis of Cyclic α-Aryl/Alkyl β-Ketoesters. *Angew. Chem. Int. Ed.* **2015**, *54* (5), 1608–1611. https://doi.org/10.1002/anie.201409572.

(65) Huang, K.; Zhang, X.; Emge, T. J.; Hou, G.; Cao, B.; Zhang, X. Design and Synthesis of a Novel Three-Hindered Quadrant Bisphosphine Ligand and Its Application in Asymmetric Hydrogenation. *Chem. Commun.* **2010**, *46* (45), 8555–8557. https://doi.org/10.1039/C0CC02620D.

(66) Bates, R. W.; Lu, Y.; Cai, M. P. Ring Opening of Cyclic N,O-Acetals with Allyltrimethylsilane under Lewis Acidic Conditions. *Tetrahedron* **2009**, *65* (37), 7852–7858. https://doi.org/10.1016/j.tet.2009.07.011.

Chapter 3.

sp^3 bis-organometallic reagents via catalytic 1,1-difunctionalisation of unactivated olefins

Research carried out in collaboration with

Shang-Zheng Sun, Philipp Spieß, and Craig Day

Published in: *Angew. Chem. Int. Ed.* **2021**, *60*, 11740-11744.

UNIVERSITAT ROVIRA I VIRGILI
FUNCTIONALISATION OF SP3 C-O BONDS AND OLEFINS ENABLED BY NICKEL CATALYSIS
Laura Talavera Codina

3.1. Nickel-catalysed alkene functionalisation

Transition metal catalysis has been broadly adopted due to its ability to activate and manipulate abundant and readily available feedstock chemicals. As discussed in Chapter 1 and 2, nickel offers unique advantages when compared to palladium. One notable feature of Ni is its ability to undergo facile oxidative addition into bonds that are traditionally unreactive under Pd catalysis (*e.g.*, ethers). Another distinguishing feature of Ni catalysts is their lower character to undergo β-hydride elimination, which allows to extend the scope of cross-coupling partners to alkyl reagents possessing β-hydrogens. This peculiarity has contributed to the fast development of nickel-catalysed processes aimed at avoiding β-hydride elimination. On the other hand, Ni-catalysed migratory functionalisations of alkenes, especially remote hydrofunctionalisation and difunctionalisation of unactivated alkenes via chain-walking, has progressed much more slowly compared to the corresponding Pd catalysis.

The aim of this chapter is to showcase the recent progresses made in nickel-catalysed remote hydrofunctionalisation and difunctionalisation strategies, especially targeting the manipulation at non-classical sites.

3.1.1. Nickel-catalysed remote hydrofunctionalisation of unactivated alkenes via chain-walking

The selective functionalisation of unbiased C(*sp*³)–H bonds presents significant challenges: *i*) high bond dissociation energy, *ii*) lack of adjacent π-bonds that readily interact with transition metals, and *iii*) difficulty in controlling site-selectivity, as multiple similar C(*sp*³)–H bonds are often present within a hydrocarbon framework.[1,2] In recent years, the field of Ni-catalysed chain-walking reactions of unactivated olefins has emerged as a powerful and practical alternative to commonly adopted C(*sp*³)–H functionalisation strategies.[3–6] This strategy enables innovative bond disconnections, providing opportunities to construct *sp*³-rich architectures from readily available and abundant starting materials.[7–12]

Although several mechanisms are known for specific systems, two main reaction pathways have been proposed for Ni-catalysed olefin isomerisation, namely 1,2- or 1,3-hydride shift mechanisms, and both pathways may compete with each other (Scheme 1).[7,9,13] In the 1,2-hydride shift mechanism, a Ni–H specie with a free coordination site binds to the olefin and undergoes migratory insertion, resulting in the formation of a well-defined alkyl-metal species (**II**). Subsequent β-hydride elimination furnishes the isomerised olefin π-complex (**III**) (Scheme 1, *top*). The β-hydride elimination step requires a vacant coordination site on the metal and a *syn*-coplanar rearrangement between the Ni-alkyl and the adjacent β-hydrogen bonds. The transfer of a hydride to the metal occurs in a concerted manner

through a four-centred transition state (**VII**), facilitated by the agnostic interaction between the d-orbitals of the metal and the C–H$_\beta$ σ-bond, promoting C–H bond cleavage (Scheme 1, *middle*). Alternatively, olefin isomerisation can proceed via a 1,3-hydride shift mechanism. In this case, the metal must possess two vacant orbitals, one for the olefin coordination and the other for allylic C–H activation. Initially, the Ni-insertion into the allylic C–H bond delivers a η^3-allyl Ni–H complex (**X**), which is followed by reductive elimination, to finally provide the isomerised olefin-metal complex (**XII**) (Scheme 1, *bottom*).

The repetition of this sequence of elementary steps (called "chain-walking") enables to the formal translocation of a double-bond across an alkyl chain, ultimately leading to the functionalisation at remote C(sp^3)–H sites. However, it is worth noting that all the steps are reversible.

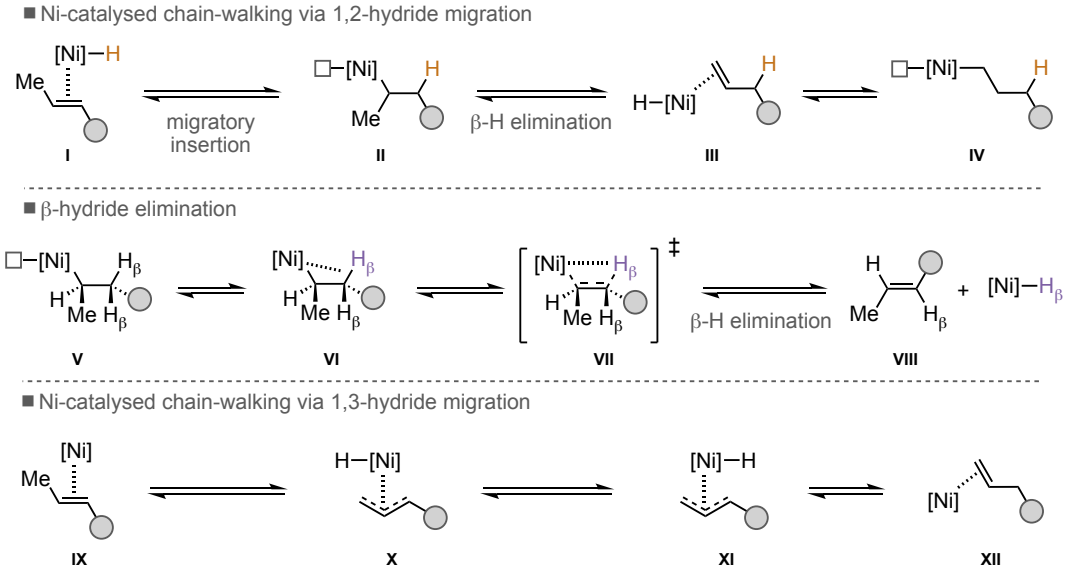

Scheme 1. Ni-catalysed chain-walking reactions and β-hydride elimination mechanism

The use of Ni-catalysts capable of olefin isomerisation has a long-standing history and has been widely recognised, particularly in multi-ton industrial processes. Two notable examples include the Shell higher olefin process (SHOP) for ethylene oligomerisation to produce α-olefins and DuPont's hydrocyanation of 1,3-butadiene for the production of adiponitrile.[14,15]

In addition to these industrial applications, significant progress has been made in the research area of nickel-catalysis over the last two decades. In 2013, Ong and co-workers developed a tandem olefin isomerisation/C–H bond functionalisation using nickel catalysts in combination with NHC ligands (Scheme 2, *top*).[16] This methodology enabled the coupling of a range of heteroarenes bearing acidic C–H bonds with activated α-olefins to form 1,1-diarylalkenes. Interestingly, regioselectivity control was achieved by modifying the ligand and

incorporating an Al co-catalyst, leading to the selective functionalisation to linear products. Although no detailed mechanistic studies were conducted, a proposed pathway involving of a 1,3-hydride shift was suggested. In 2014, Hartwig and co-workers reported a related transformation with trifluoromethyl-substituted arenes and unactivated terminal and internal alkenes (Scheme 2, *middle*). This reaction resulted in the functionalisation at the terminal, primary C(*sp*³)–H site.[17] The high selectivity observed was attributed to the steric hinderance imposed by the bulky NHC ligand (**L2**). The authors favoured a 1,2-hydride pathway, although other mechanistic scenarios could also be considered. Subsequently, in 2016, Fu and Liu successfully implemented a Ni-catalysed reductive hydroalkylation of alkenes using DEMS[18] – a catalytic version of the hydroalkylation of olefins previously developed by Hu[19] – (Scheme 2, *bottom*). This protocol enabled the synthesis of the desired products in an anti-Markovnikov fashion using a simple Ni/**L3** system, exhibiting high levels of chemo- and regio-selectivity. Although mechanistic experiments were carried and indicated a radical-type reaction mechanism, further investigations were needed to fully elucidate the details of this reaction mechanism.

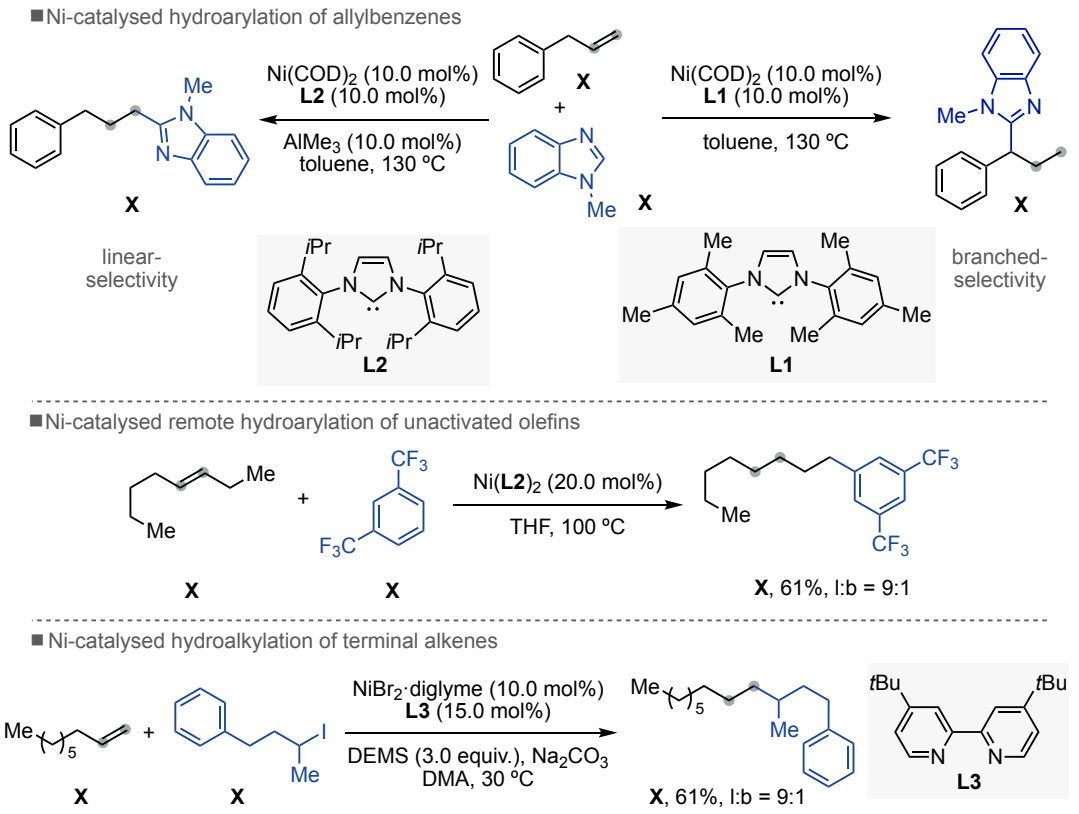

Scheme 2. Pioneering reports on nickel-catalysed hydrofunctionalisation reactions

Prompted by these findings, in 2017, Zhu and co-workers reported a reductive hydroarylation of olefins with (hetero)aryl iodides (Scheme 3, *top*).[20] This method allowed for the functionalisation of remote benzylic C(sp^3)–H sites using PMHS as the hydride source. In this case, high selectivity was attained using 2,2'-bipyridine ligands (**L4**) possessing substituents adjacent to the nitrogen motif. In an effort to expand the application of chain-walking strategies beyond the benzylic position, Zhu and Hu independently developed a hydroarylation of boron-containing olefins, which furnished various α-arylated alkyl boronates, that serve as versatile synthetic precursors (Scheme 3, *middle*).[21,22] These methods involved the generation of a boron-stabilised alkyl metal species, which served as a novel driving force for metal migration. Zhu employed a PyrOx type ligand (**L5**), while Hu utilised di-*ortho* substituted bipyridine ligands (**L4**). In both cases, $NiBr_2$·diglyme in combination with silane as hydride source (TES or DEMS) yielded the desired products. Subsequently, Zhu and co-workers disclosed a selective alkylation of alkyl iodides with internal alkenes occurring at the least sterically hindered terminal C(sp^3)–H site (Scheme 3, *bottom*).[23] Unlike the previously described olefin hydroarylation event,[20] the utilisation of a PyrOx type ligand (**L6**) resulted in the C–C bond formation at the unactivated primary site. This protocol demonstrated the potential for regioconvergent strategies using unrefined mixtures of olefins, leading to the formation of linear alkylated products with high site-selectivity. Although control and deuterium-labelling experiments suggested a chain-walking process, there remains some ambiguity regarding whether chain-walking occurs via Ni(I), as proposed by the authors, or through Ni(II) intermediates. Further investigations are still needed to fully elucidate the mechanism of chain-walking in this context.

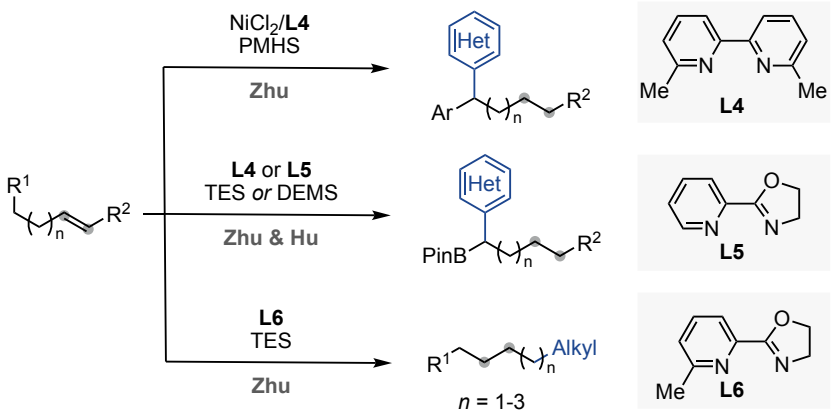

Scheme 3. Examples of Ni-catalysed remote C–H functionalisation at different reaction sites

In the methods described above, site-selectivity is predominantly dictated by carefully balancing electronic and steric effects, where bond formation typically occurs adjacent to a stabilising group on thermodynamic grounds or at a distal primary C(sp^3)–H bond due to

kinetic preferences. Recently, however, elegant disclosures have shown the feasibility for targeting other C(sp^3)–H sites within the alkyl side chain (Scheme 4). In this context, strongly chelating bidentate 8-aminoquinoline directing groups could be used to target β- and γ-selectivities. In 2020, Koh and co-workers reported the formation of β-alkylated products through remote hydroalkylation employing readily available primary and secondary haloalkanes as both the hydride and alkyl donor.[24] The method used a $Ni(PPh_3)_2Cl_2$ precatalyst in combination with manganese as reductant, without the need for additional ligands. The success of this method relied on the capability of the directing group to stabilise a five-membered nickelacycle intermediate. Similarly, in 2021 Hong and co-workers developed a γ-selective migratory hydroamination via stabilisation of a 6-membered nickelacycle by the 8-aminoquinoline directing group.[25] The method employed $NiCl_2$·glyme as the precatalyst, tris(4-methoxypehnly)phosphine (**L7**) as the ligand and DEMS as the hydride source. In another approach, Yu and co-workers achieved remote γ-methylene C–H bond amidation using a thioether-directed cyclometallation strategy.[26] In this case, the authors employed a di-*ortho* substituted phenanthroline ligand (**L8**), which delivered the product with high γ-selectivity. Later, Lu and Wang independently disclosed a switchable site-selective alkene hydroalkylation to generate a range of structurally diverse α- and β-branched protected amines via stabilisation of 5- and 6-membered nickelacycles respectively. Lu achieved such regiodivergent protocol by selection of reaction temperature using **L9**,[27] while Wang utilised a ligand-controlled strategy (**L10** *vs* **L11**).[28] Early this year, our group developed an interrupted deaminative Ni-catalysed chain-walking strategy that enables the formation of C(sp^3)–C(sp^3) architectures at remote methylene C(sp^3)–H sites using native amides as weakly coordinating directing groups.[29] This approach avoids the need for the strongly chelating quinoline or pyridine backbones used in previous methods. Interestingly, by careful selection of the ligand (**L12** to **L14**), different site-selectivity, including β-, γ- and δ-functionalisation, could be targeted.

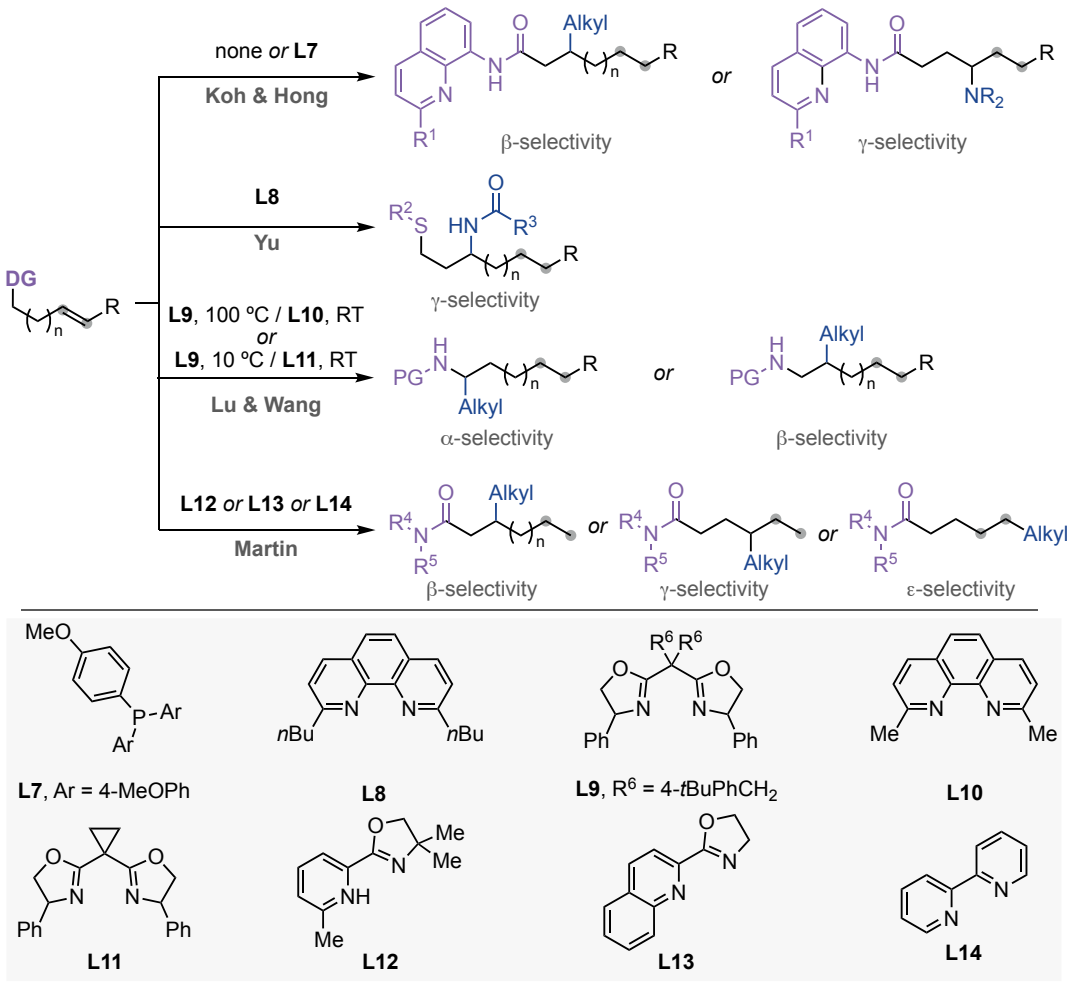

Scheme 4. Interrupted Ni-catalysed remote hydrofunctionalisation protocols

These advancements have significantly contributed to the manipulation at various remote C(sp^3)–H sites, providing novel opportunities for the construction of C–C and C–X bonds at previously unfunctionalised sites, even in the context of enantioselective transformations.[8,9,11,12]

3.1.2. Nickel-catalysed difunctionalisation of unactivated alkenes at non-classical sites

In recent years, the opportunity to perform the direct difunctionalisation of alkenes has garnered significant interest as a highly appealing strategy for enhancing molecular complexity.[30–32] These reactions enable the simultaneous incorporation of two distinct functional groups across a C–C double bond in a single synthetic step, offering notable advantages in terms of efficiency and atom economy. In contrast to the widely studied 1,2-

difunctionalisation of alkenes,[33–37] 1,*n*-difunctionalisations (where $n \neq 2$) involving metal migrations has received less attention.[38–41] These techniques provide a non-classical site-selectivity pattern in olefin functionalisation, thereby expanding the repertoire of bond disconnections available in modern organic synthesis.

The mechanism underlying these types of functionalisations is illustrated in Scheme 5.[39] Initially, a nucleophilic Ni–R complex is formed, which undergoes migratory insertion into an alkene double-bond to generate the key Ni-sec-alkyl complex (**XIII**). In the context of alkene 1,2-difunctionalisation, the primary goal is to intercept this intermediate **XIII** and inhibit the β-hydride elimination. However, if β-hydride elimination occurs more rapidly than the second bond formation, a 1,2-hydride shift takes place, resulting in the formation of a Ni–H species. This species can undergo migratory insertion into the newly formed olefin and trigger a chain-walking event, culminating in the generation of a stabilised metal intermediate (**XIV**). Subsequent bond formation ultimately delivers the desired 1,1-, 1,3-, or 1,*n*-difunctionalised products (where $n \geq 3$). Throughout this process, competitive pathways may favour the formation of monofunctionalised products, such as the premature dissociation of the Ni–H species from the olefinic intermediate.

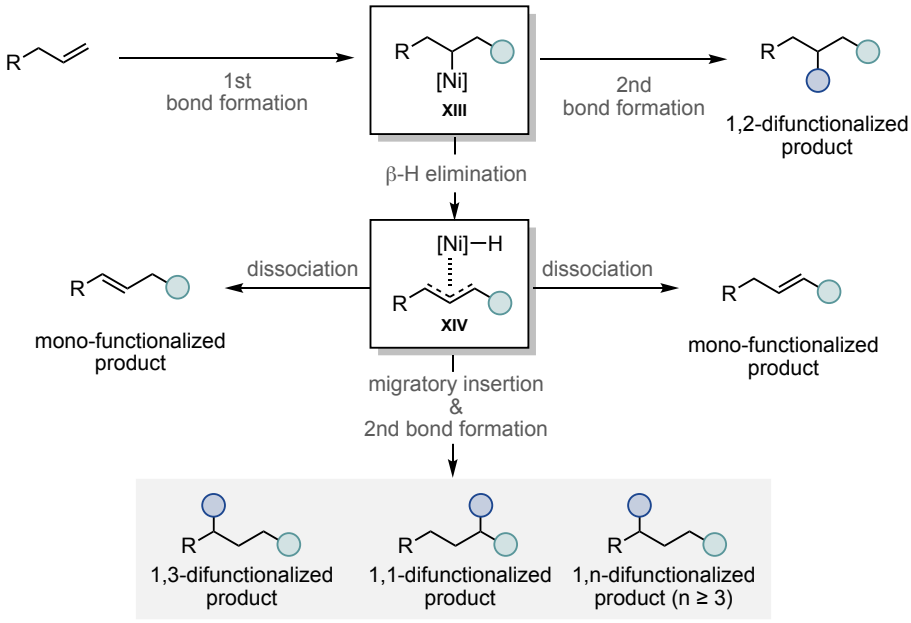

Scheme 5. Proposed mechanism for the difunctionalisation of alkenes

Unlike alkene migratory hydrofunctionalisation, where the reaction is initiated by alkene insertion into a metal hydride,[8,9] the olefin difunctionalisation poses the additional challenge of overcoming the steric effects exerted by the group present on the metal centre and to be installed on the hydrocarbon chain. Indeed, the initial olefin insertion into the Ni–R bond

(when R ≠ H), can significantly impact on the regioselectivity of the reaction. Therefore, subtle fine-tuning of the reaction conditions is necessary to promote the formation of the desired 1,*n*-difunctionalised products (where n ≠ 2).

3.1.2.1. 1,*n*-difunctionalisation

In 2018, Zhao and co-workers developed an unprecedented 1,3-difuncionalisation of alkenes bearing a coordinating group, using a Ni catalyst in combination with diphosphine ligands (Scheme 6).[42] Under these conditions, various aryl iodides, aryl and alkenyl boronic acids were successfully coupled with *N*-allylpyrimidin-2-amine. Unfortunately, the method is limited to terminal alkenes and could not be expanded to internal counterparts, even under more forcing reaction conditions. Mechanistic studies suggested that the formation of a five-membered metallacycle **XVI**, formed via β-hydride elimination and migratory insertion, played a crucial role in promoting the formation of the desired 1,3-dicarbofunctionalised products.

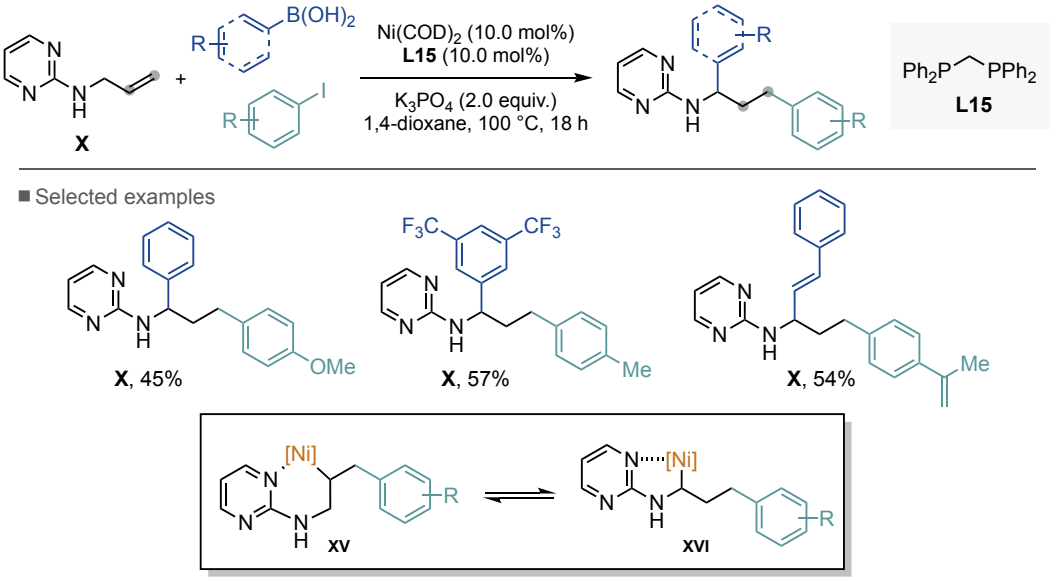

Scheme 6. Ni-catalysed 1,3-difunctionalisation of *N*-allylpyrimidin-2-amine

In the same year, Giri and co-workers disclosed an efficient and regioselective method for the 1,3-diarylation of unactivated olefins employing a ketimine-directed strategy (Scheme 7).[43] In this case, β,δ-diarylketones were obtained from alkenes, aryl halides and arylzinc reagents under a $NiBr_2$/**L16** regime. In analogy to the previously discussed 1,3-dicarbofunctinalisation, the authors proposed a pathway involving the formation of a five-membered nickelacycle prior to transmetallation/reductive elimination to furnish the desired products.

*sp*³ bis-organometallic reagents via catalytic 1,1-difunctionalisation of unactivated olefins

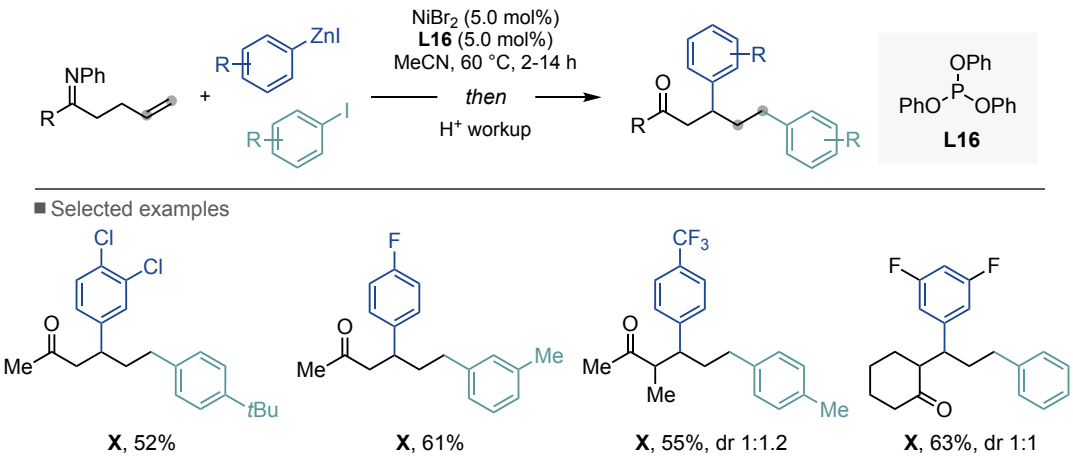

Scheme 7. Ni-catalysed β,δ,diarylation of unactivated olefins in ketimines

Inspired by a series of related Ni-catalysed hydrofunctionalisation techniques at remote benzylic C–H sites, in 2019, Yin and co-workers reported a Ni-catalysed 1,*n*-arylboration (*n* = 3 - 5) of terminal alkenes bearing a pendant aryl group by employing a $NiCl_2$·glyme/**L17** system (Scheme 8, *top*).[44] Unlike previous methodologies,[42,43] the utilisation of a PyrOx-type ligand (**L17**) resulted critical for the success of this three-component reaction. Interestingly, **L17** favoured the formation of a η^3-benzyl-nickel intermediate over the α-boryl Ni-alkyl species. More recently, the same group extended this methodology to the regio-, diastereo-, and enantioselective 1,3-alkylboration of heterocyclic alkenes with primary alkyl bromides and B_2Pin_2, providing access to the synthesis of 2,4-disubsituted heterocycles (Scheme 8, *bottom*).[45] In this case, bipyridine ligands substituted at the four position displayed exclusive 2,4-regioselectivity but suffered from low yields and poor diastereomeric ratios. On the other hand, diamine-based ligands exhibited superior performance (**L18**), delivering the desired product in good yield, excellent diastereoselectivity, and high enantioselectivity. Mechanistic investigations unveiled a radical-chain catalytic cycle for this transformation, in which an alkyl radical is generated from the alkyl bromide by SET from a Ni(I) species. Notably, the stereochemical outcome of the reaction suggested that the olefin intermediate does not dissociate from the nickel centre during chain-walking.

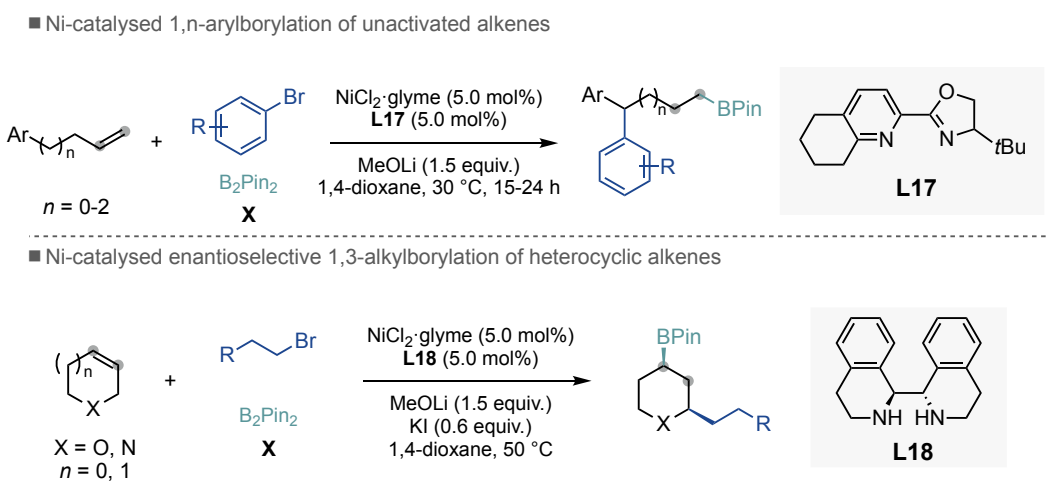

Scheme 8. Ni-catalysed 1,*n*-difunctionalisation of unactivated olefins

3.1.2.2. 1,1-difunctionalisation

Although palladium-catalysed 1,1-difunctionalisation reactions have been known since 1985 by the pioneering work from Yoshida and co-workers,[46] it was not until 2017 that Fu and co-workers demonstrated the first Ni-catalysed 1,1-difunctionalisation reaction of unactivated alkenes (Scheme 9).[47] In this case, a Ni/**L19** catalysed 1,1-diboration of terminal alkenes with B_2Pin_2 resulted in the formation of 1,1-diborylalkanes. This method constituted the first example demonstrating that migration towards a boron-containing moieties could serve as a driving force for olefin isomerisation. Bonding interaction between filled *d*-orbitals on the transition metal and the empty *p*-orbitals on the boron atom establishes the foundation for subsequent nickel-catalysed 1,1-carboboration protocols.

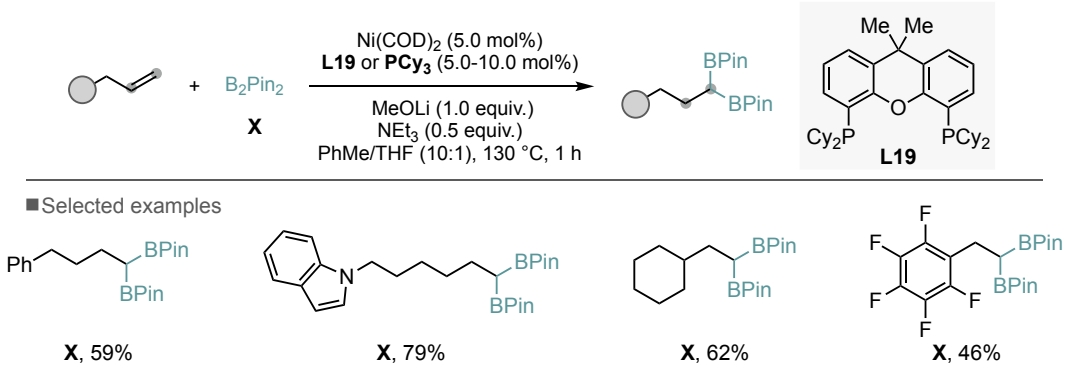

Scheme 9. Ni-catalysed 1,1-diborylation of terminal alkenes

In 2019, Yin and co-workers disclosed a 1,1-alkylboration of olefins using activated benzyl or allyl halides and B_2Pin_2 (Scheme 10).[48] The method used an unusual pyridyl carboxamide ligand with a methyl group adjacent to the nitrogen atom of the pyridine to furnish the

products with high regiocontrol. Interestingly, the authors demonstrated that high terminal regioselectivity was also achieved regardless the presence of potentially stabilising groups (such as phenyl, ester, amide, and cyano groups). Moreover, substrates containing multiple double bonds selectively reacted at the monosubsituted olefins.

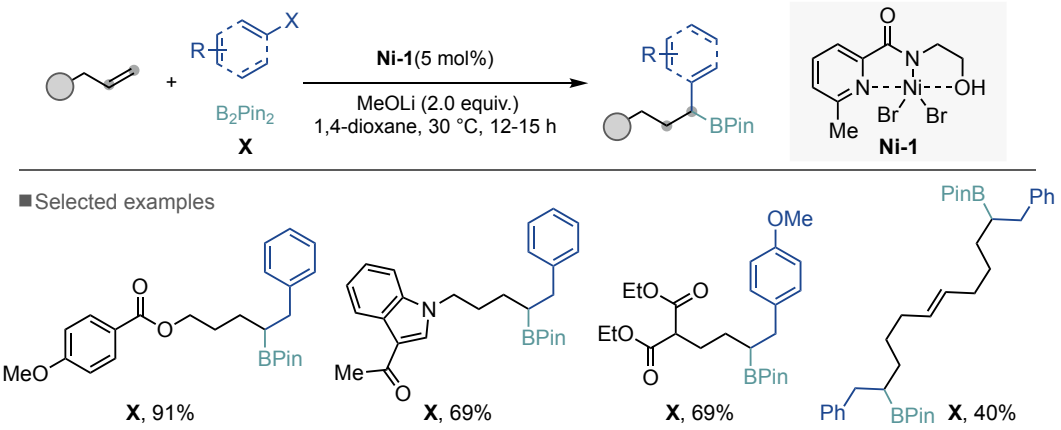

Scheme 10. Ni-catalysed 1,1-alkylboration of terminal alkenes

A year later, Yin and co-workers developed a chemodivergent 1,1-difunctionalisation strategy to access propargylic boronic esters and *gem*-dialkynylalkanes (Scheme 11).[49] The selectivity observed in these transformations was attributed to the specific ligand employed and the choice of solvent. Increasing steric hindrance on the pyridyl moiety while reducing it on the oxazoline fragment favoured the formation of dialkynylated products. Additionally, the use of polar aprotic solvents such as NMP facilitated the transmetallation step leading to propargylic boronic esters. Mechanistic investigations revealed that the 1,1-alkynylboration products served as intermediates in the dialkynylation reactions, and that the boron reagent acted as both stoichiometric reductant and transient assisting group.

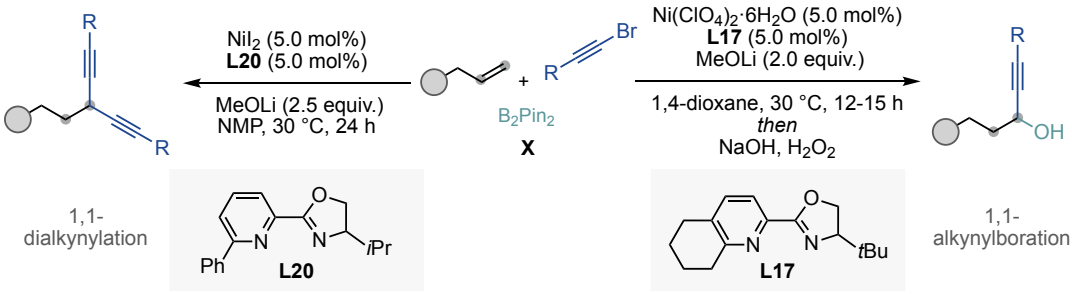

Scheme 11. Chemodivergent 1,1-difunctionalisation of unactived olefins

Recently, the same group extended the application of the 1,1-benzylboration strategy[48] to include methylenecyclohexane derivatives as viable starting materials (Scheme 12).[50] Through the introduction of a sterically demanding boron ester group adjacent to the

cyclohexane moiety, the authors successfully synthesised kinetically favoured disubstituted cyclohexane. These compounds often exhibit enhanced bioactivity compared to their thermodynamically favoured isomers, but their synthesis is typically challenging. The practical utility of this methodology was further demonstrated by the modification of complex bioactive molecules and their diversification through downstream transformations.

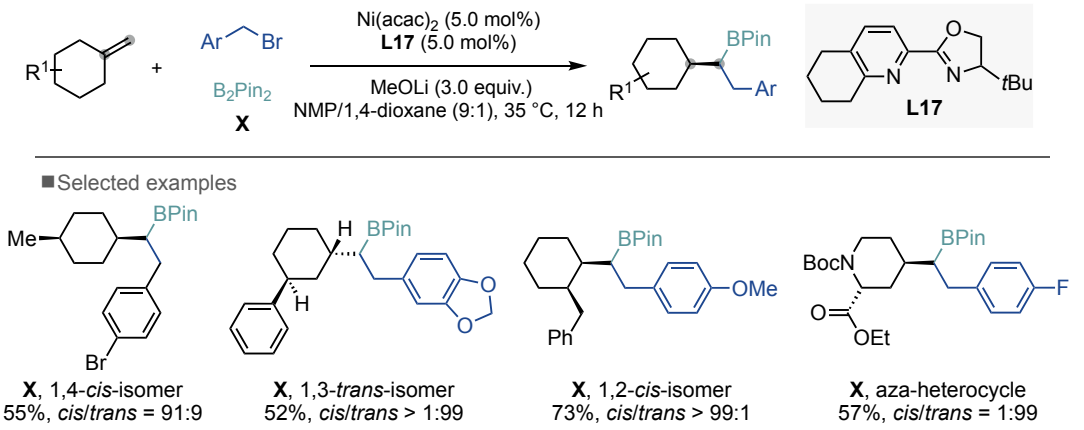

Scheme 12. Modular access to substituted cylohexanes with kinetic stereocontrol

Despite significant progress in catalytic 1,1-difunctionalisation of olefins, the development of enantioselective difunctionalisation reactions remains challenging. However, it is a highly desirable endeavour as it allows access to complex chiral molecules from simple racemic or achiral starting materials. In a notable breakthrough, Yin's group developed the asymmetric 1,1-difunctionalisation of unactivated olefins using B_2Pin_2 and aryl/vinyl halides (Scheme 13).[51,52] In both reports, high regio- and enantioselectivities were achieved by careful selection of the nickel/ligand catalytic system, with diamine ligands playing a crucial role (**Ni-2** and **L21**). Remarkably, the enantioselectivities remained relatively constant across various alkene substrates, whereas aryl halides with electron-rich substituents led to slightly lower enantiomeric excesses.[51] On the other hand, a broad scope of alkenyl halides was demonstrated, with 1,1,2- and 1,2,2-tri-subsituted alkenyl bromides affording moderate to good yields with high levels of enantioinduction. Regardless their configuration, di- and tri-substituted alkenyl electrophiles afforded the targeted enantioenriched products while retaining their initial geometry.[52] The versatility of the transformation was further demonstrated by converting the chiral alkyl boronate products into different chiral scaffolds through stereospecific transformations. Mechanistic investigations revealed that β-hydride elimination step is highly regioselective, while reductive elimination is the enantiodetermining step in the reaction.

*sp*³ bis-organometallic reagents via catalytic 1,1-difunctionalisation of unactivated olefins

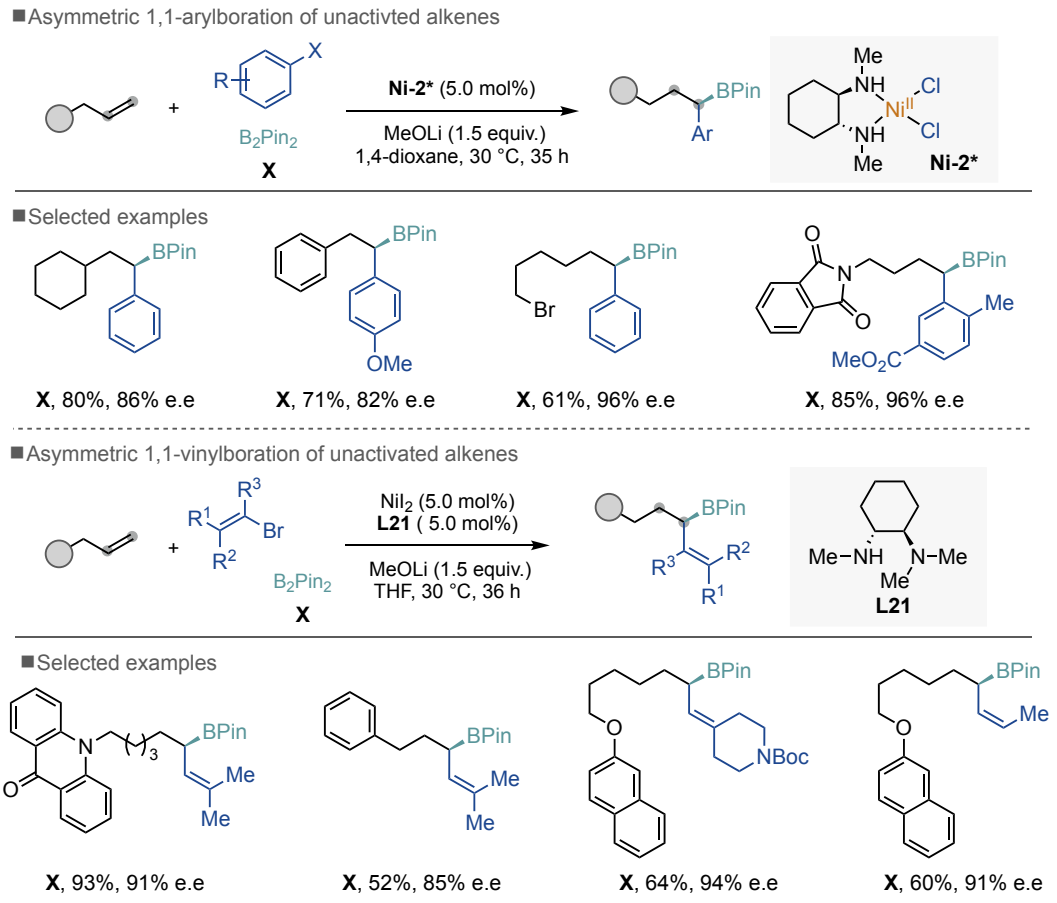

Scheme 13. Ni-catalysed asymmetric 1,1-carboboration of terminal alkenes

Despite the remarkable advancements in the field of olefin hydrofunctionalisation and difunctionalisation at remote, non-classical sites, a comprehensive understanding of the underlying mechanisms still remains elusive. The precise nature of the chain-walking mechanism, weather it involves Ni(I), Ni(II) or even Ni(III) intermediates, is still subject to ambiguity. Additionally, the role played by the ligand backbone in these transformations has yet to be fully elucidated. Thus, the lack of detailed mechanistic data currently forces the progress in this filed to be based on empirical discoveries.

3.2. General aim of the project

Metal-catalysed cross-coupling reactions of sp^3 mono-organometallic reagents have achieved remarkable advancements as vehicles to rapidly construct sp^3 architectures.[53–57] Although sp^3 poly-organometallics, *a priori*, might offer improved versatility and modularity for forging sp^3 linkages, a limited number of catalytic synthetic routes have been described for preparing these reagents from simple available precursors.[58,59] Currently, catalytic approaches for their synthesis involve olefin 1,2-bis-metallations[60–62] or 1,2-hydrometallation of vinyl metal species.[63–68]

At the outset of this Doctoral Thesis, the development of a catalytic technique for accessing sp^3 bis-organometallics via site-selective olefin 1,1-difunctionalisation remained a desirable scenario. We recognised that the successful implementation of such a technology would not only complement existing 1,1-difunctionalisation strategies that introduce boron fragments into olefins, but would also provide a new and valuable approach to efficiently access versatile homologated 1,2-bis-organometallic compounds.

3.3. *sp*³ bis-organometallic reagents via catalytic 1,1-difunctionalisation of unactivated olefins

3.3.1. Optimisation of the reaction conditions

Based on preliminary results obtained in the group by Dr Shang-Zheng Sun and inspired by Yin's and Brown's work on the catalytic borylation of olefins with B_2Pin_2,[48,69] the 1,1-difunctionalisation of olefin **1a** was evaluated using **2a** and B_2Pin_2 as coupling partners. The choice of **2a** was not arbitrary, as α-haloboronates are readily accessible on a large scale via Matteson homologation.[70] Specifically, it was found that the use of $NiBr_4{\cdot}TBA_2$ and a pyridine ligand possessing a tethered free alcohol (**LX**) in combination with *t*BuOLi in DME delivered the corresponding 1,1-difunctionalised product (**4a**) in 53% yield. During the screening of the reaction conditions, by-products originated by olefin isomerisation along the side-chain (**A**), vinyl boronate (**B**) and alkyl diboronates (**C**) were observed, accounting for the mass balance of the process. The formation of these compounds can be explained by competitive β-hydride elimination and homocoupling of α-bromoboronate.

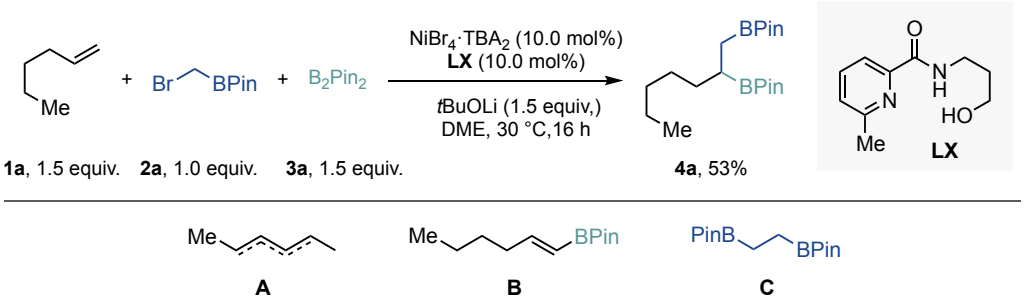

Reaction conditions: **1a** (0.30 mmol, 1.5 equiv.), **2a** (0.20 mmol, 1.0 equiv.), B_2Pin_2 (0.30 mmol, 1.5 equiv.), $NiBr_4{\cdot}TBA_2$ (10.0 mol%), **LX** (10.0 mol%), *t*BuOLi (0.30 mmol, 1.5 equiv.), DME (0.5 mL), 30 ºC for 16 h. GC yield using decane as internal standard.

Scheme 14. Initial reaction conditions

To enhance the efficiency of the reaction and address the issue of dimerisation of the α-bromoboranate by-product, we directed our attention towards evaluating the reaction stoichiometry (Table 1). Interestingly, improved results were found by utilising **1a** as the limiting reagent (entries 2-4). Further optimisation of the stoichiometric ratios revealed that employing 1.7 equiv. of **2a**, 1.7 equiv. of B_2Pin_2, and 2.0 equiv. of *t*BuOLi delivered the desired product in a 72% yield.

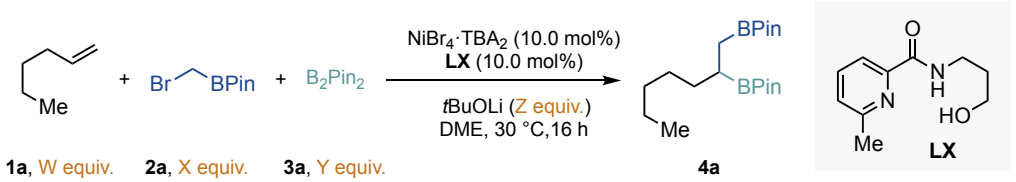

Entry	**1a** (W equiv.)	**2a** (X equiv.)	**3a** (Y equiv.)	*t*BuOLi (Z equiv.)	**4a** (%)
1	1.5	1.0	1.5	1.5	53
2	1	1.5	1.5	1.5	63
3	1	2.0	1.5	1.5	59
4	1	1.5	2.0	1.5	63
5	1	1.5	1.5	2.0	68
6	1	2.0	1.5	2.0	69
7	1	1.5	2.0	2.0	60
8	1	1.7	1.7	2.0	72

Reaction conditions: **1a** (W equiv.), **2a** (X equiv.), B_2Pin_2 (Y equiv.), $NiBr_4·TBA_2$ (10.0 mol%), **LX** (10.0 mol%), *t*BuOLi (Z equiv.), DME (0.5 mL), 30 ºC for 16 h. GC yield using decane as internal standard.

Table 1. Evaluation of the reaction stoichiometry

The optimisation of the reaction conditions was continued by studying the impact of different solvents and in the presence of additives (Table 2). While ethereal solvents, such as THF, dioxane or diglyme, gave the desired product in good yields (entries 1-3), amide-containing polar aprotic solvents, such as NMP, DMA and DMF, were not effective for this transformation (entries 4-6). Particularly interesting was the observation that a combination of DME with 4.0 equivalents of *t*BuOH provided the best results (entry 11).

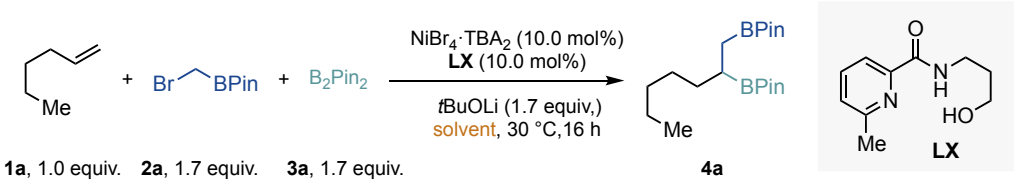

1a, 1.0 equiv. **2a**, 1.7 equiv. **3a**, 1.7 equiv. **4a**

Entry	Solvent	Additive	**4a** (%)
1	DME	none	72
2	1,4-dioxane	none	63
3	THF	none	55
4	NMP	none	trace
5	DMA	none	11
6	DMF	none	25
7	DMSO	none	0
8	DME	*t*BuOH (1.0 equiv.)	69
9	DME	*t*BuOH (2.0 equiv.)	78
10	DME	*t*BuOH (3.0 equiv.)	64
11	DME	*t*BuOH (4.0 equiv.)	78
12	DME	MeOH (4.0 equiv.)	10
13	DME	*i*PrOH (4.0 equiv.)	43

Reaction conditions: **1a** (0.20 mmol, 1.0 equiv.), **2a** (0.34 mmol, 1.7 equiv.), B_2Pin_2 (0.34 mmol, 1.7 equiv.), $NiBr_4 \cdot TBA_2$ (10.0 mol%), **LX** (10.0 mol%), *t*BuOLi (0.40 mmol, 2.0 equiv.), solvent (0.5 mL), 30 ºC for 16 h. GC yield using decane as internal standard.

Table 2. Screening of solvents and additives

With this set of conditions in hand, we proceeded to evaluate the effect of different nickel precatalysts (Table 3). Interestingly, comparable results were obtained when using other soluble Ni sources (entries 4-6). However, $NiBr_4 \cdot TBA_2$ was selected for further screenings due to its low hygroscopic nature, thus improving the practicality of the current methodology.

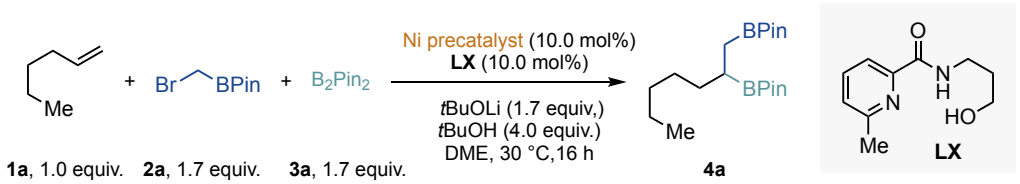

1a, 1.0 equiv. **2a**, 1.7 equiv. **3a**, 1.7 equiv. **4a**

Entry	Ni precatalyst	**4a** (%)
1	$NiBr_4 \cdot TBA_2$	78
2	$Ni(COD)_2$	64
3	$NiBr_2$	10
4	$NiBr_2 \cdot glyme$	76
5	$NiCl_2 \cdot glyme$	76
6	$NiBr_2 \cdot diglyme$	71
7	$NiCl_4 \cdot TBA_2$	54
8	$NiI_4 \cdot TBA_2$	45
9	$NiBr_4 \cdot TEA_2$	55
10	$NiBr_4 \cdot TBA_2$ (5 mol%)	63

Reaction conditions: **1a** (0.20 mmol, 1.0 equiv.), **2a** (0.34 mmol, 1.7 equiv.), B_2Pin_2 (0.34 mmol, 1.7 equiv.), nickel precatalyst (10.0 mol%), **LX** (10.0 mol%), *t*BuOLi (0.40 mmol, 2.0 equiv.), *t*BuOH (0.40 mmol, 2.0 equiv.), DME (0.5 mL), 30 ºC for 16 h. GC yield using decane as internal standard.

Table 3. Screening of nickel precatalysts

Although initial screenings identified **LX** as the optimal ligand, we decided to embark in a second evaluation to confirm its superiority under the optimised conditions (Scheme 15). In accordance to the results outlined by Yin and co-workers on their initial report,[48] ligands commonly employed in nickel catalysis – including bipyridine, phenanthroline, PyrBox, or terpyridine – proved unapplicable.[49,51,71–73]

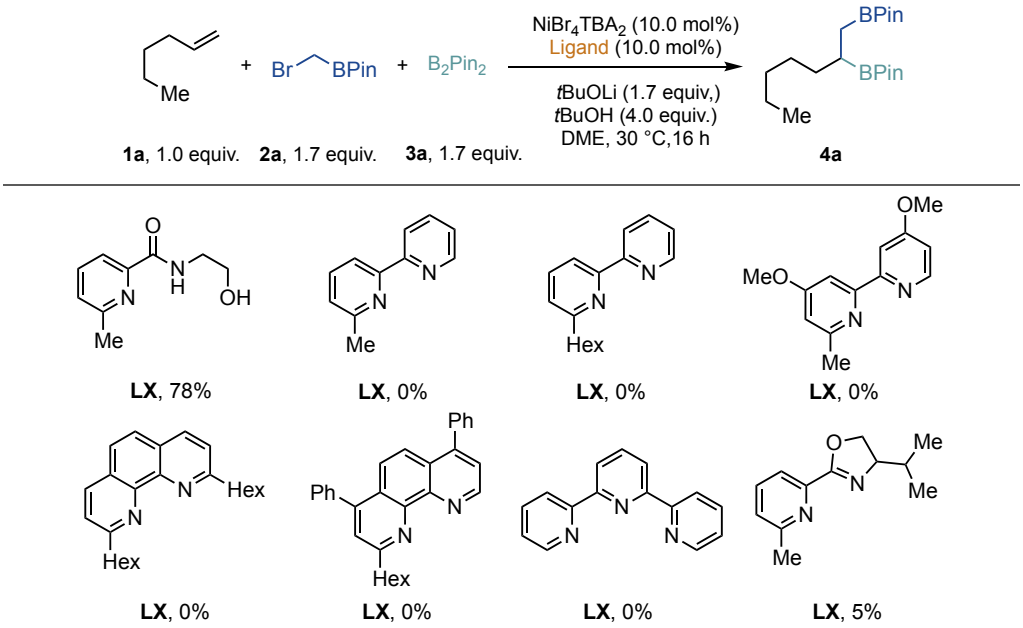

Reaction conditions: **1a** (0.20 mmol, 1.0 equiv.), **2a** (0.34 mmol, 1.7 equiv.), B_2Pin_2 (0.34 mmol, 1.7 equiv.), $NiBr_4 \cdot TBA_2$ (10.0 mol%), **ligand** (10.0 mol%), *t*BuOLi (0.40 mmol, 2.0 equiv.), *t*BuOH (0.40 mmol, 2.0 equiv.), DME (0.5 mL), 30 ºC for 16 h. GC yield using decane as internal standard.

Scheme 15. Screening of ligands (**I**)

Capitalising on these findings, we shifted our focus to investigating the ligand substitution using pyridyl carboxamide type structures (Scheme 16). The results showed that only pyridine-based ligands possessing a tethered free alcohol delivered the product, indicating that binding of the latter to the Ni centre play a non-negligible influence on reactivity.[48] This hypothesis was further supported by the catalytic competence of preformed Ni(**LX**)$_2$, and the lack of reactivity using the *O*-methylated (**LX**) or deoxygenated (**LX**) versions of the optimal ligand, highlighting the importance of the *N*,*N*,*O* binding mode. Remarkably, the substitution at the *ortho* position of the pyridyl carboxamide ligands significantly influenced the reaction outcome. In particular, the use of unsubstituted pyridyl carboxamide derivatives resulted in inefficient formation of the desired product. Although, substitution at the fourth position with electron-donating groups resulted in similar results, we continued the screening with **LX**, due to the ease of its synthesis.

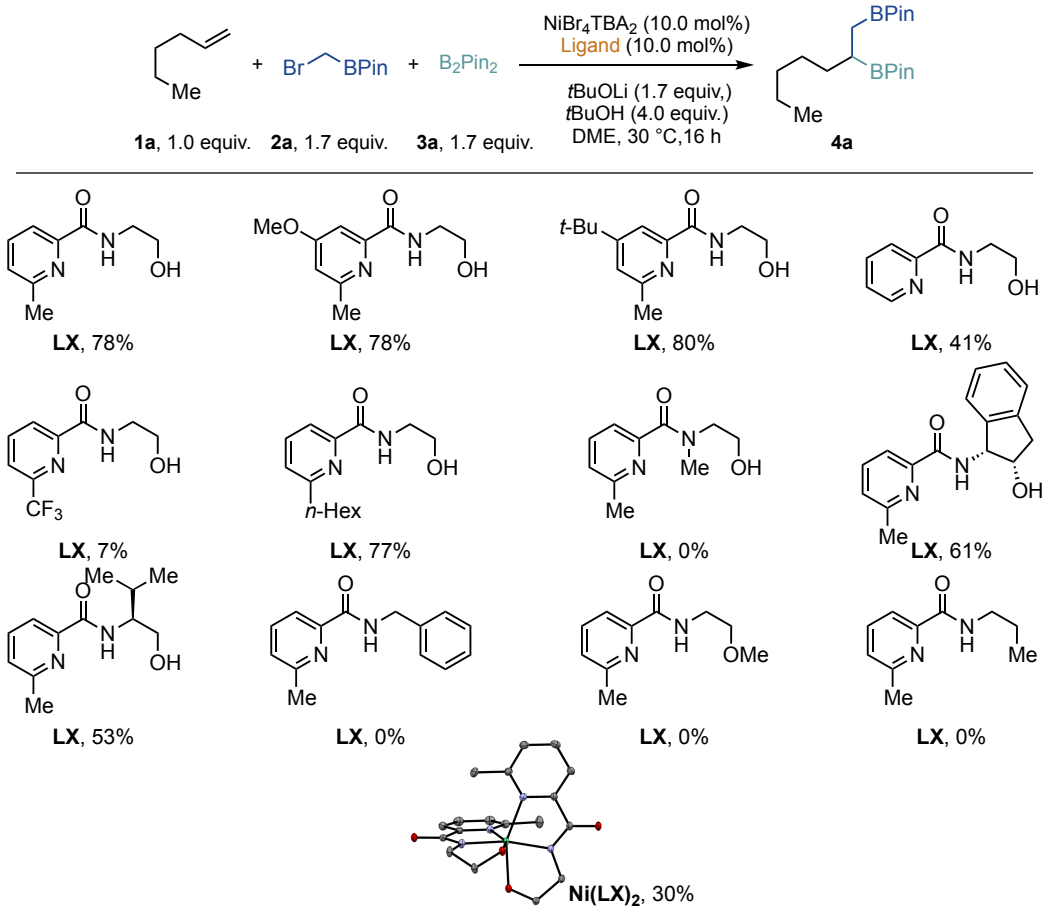

Reaction conditions: **1a** (0.20 mmol, 1.0 equiv.), **2a** (0.34 mmol, 1.7 equiv.), B_2Pin_2 (0.34 mmol, 1.7 equiv.), $NiBr_4{\cdot}TBA_2$ (10.0 mol%), **ligand** (10.0 mol%), *t*BuOLi (0.40 mmol, 2.0 equiv.), *t*BuOH (0.40 mmol, 2.0 equiv.), DME (0.5 mL), 30 ºC for 16 h. GC yield using decane as internal standard.

Scheme 16. Screening of ligands (**II**)

Finally, before moving to test the substrate scope, the temperature and reaction time were also tested (Table 4). Surprisingly, we found that the reaction reached completion within just 10 minutes. However, to ensure full consumption of the starting material and maximise the yield of the desired product, a reaction time of 30 minutes was chosen as the optimal condition. Additionally, control experiments revealed that all the reaction parameters were critical for success (entry 7).

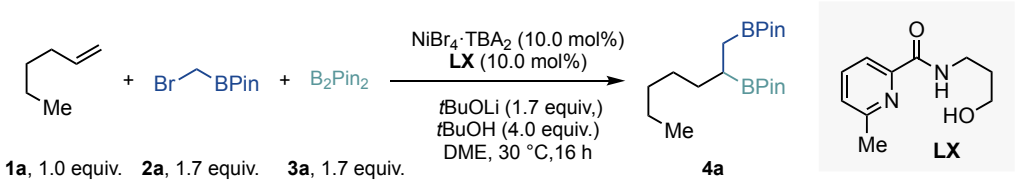

1a, 1.0 equiv. **2a**, 1.7 equiv. **3a**, 1.7 equiv. **4a**

Entry	Devation from standard conditions	**4a** (%)
1	none	78
2	5 minutes	65
3	10 minutes	77
4	30 minutes	80
5	20 ºC	78
6	45 ºC	71
7	*w/o* Ni, LX *or* *t*BuOLi	0

Reaction conditions: **1a** (0.20 mmol, 1.0 equiv.), **2a** (0.34 mmol, 1.7 equiv.), B_2Pin_2 (0.34 mmol, 1.7 equiv.), $NiBr_4 \cdot TBA_2$ (10.0 mol%), **LX** (10.0 mol%), *t*BuOLi (0.40 mmol, 2.0 equiv.), *t*BuOH (0.40 mmol, 2.0 equiv.), DME (0.5 mL), 30 ºC for 16 h. GC yield using decane as internal standard.

Table 4. Screening of temperature and reaction time

3.3.2. Scope of 1,1-difunctionalisation with α-bromoboronates

After having established the optimal reaction conditions, we proceeded to investigate the scope of the transformation by evaluating a wide variety of terminal olefins. As shown from the results complied in Scheme 17, a series of unactivated α-olefins could be employed as substrates, furnishing the desired 1,1-difunctionalisation products with excellent chemoselectivity and in good yields. The method readily accommodated a variety of functional groups, including nitriles (**4b**), ketones (**4c**), silyl ethers (**4d**), esters (**4j**, **4k**), and amides (**4l**). Likewise, the reaction proved compatible with heterocyclic cores (**4m**, **4n**, **4o**). Notably, alkyl halides (**4f**, **4g**) and aryl halides (**4k**) remained untouched, leaving an additional handle for further derivatisation via conventional cross-coupling reactions.[74] Remarkably, the reaction could be successfully conducted on a gram scale, affording **4a** in 75% yield.

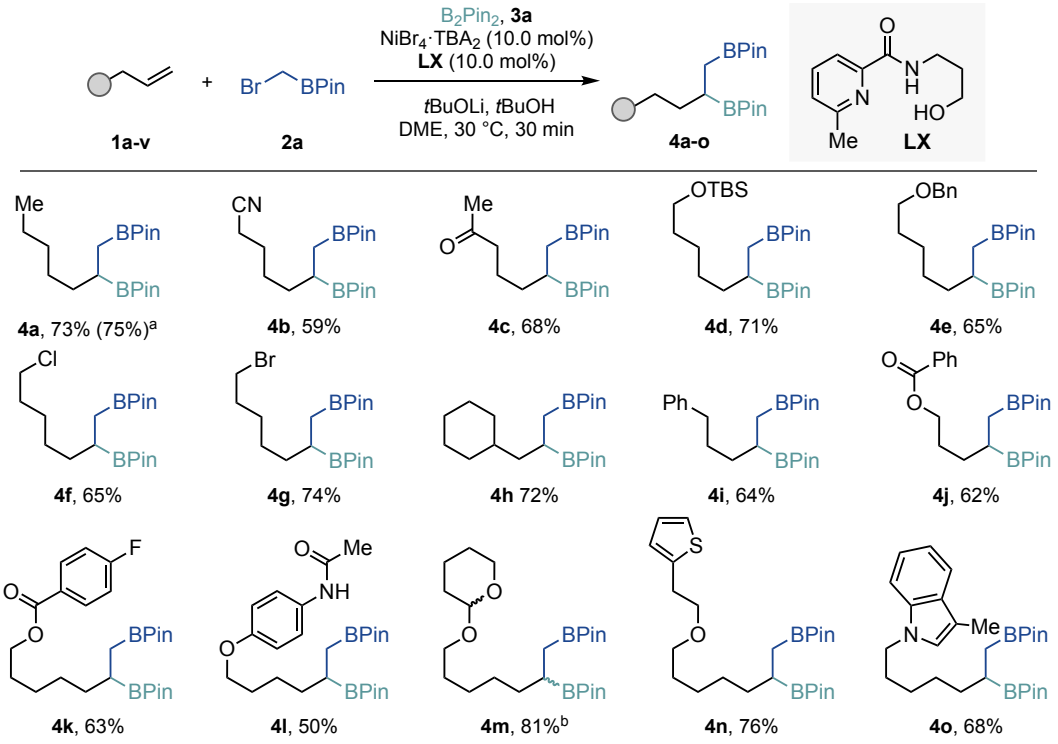

Reaction conditions: **1** (0.20 mmol, 1.0 equiv.), **2a** (0.34 mmol, 1.7 equiv.), B_2Pin_2 (0.34 mmol, 1.7 equiv.), $NiBr_4 \cdot TBA_2$ (10.0 mol%), **LX** (10.0 mol%), *t*BuOLi (0.40 mmol, 2.0 equiv.), *t*BuOH (0.80 mmol, 4.0 equiv.), DME (0.5 mL), 30 °C for 0.5 h. Isolated yields, average of two independent runs. [a] 5.0 mmol scale. [b] dr = 1:1.

Scheme 17. Scope of 1,1-difunctionalisation with α-bromoboronates (**I**)

Gratifyingly, 1,1-disubsituted olefins could be employed under the same reaction conditions, delivering the products with excellent selectivity (**4p**). The preparation of **4q** is particularly noteworthy as it enables the incorporation of both a chiral boron entity and two structurally different *sp*³ C–B bonds contemporarily. The successful preparation of **4r'** and **4s'** demonstrates that the reaction can also be extended to secondary α-halobonates, potentially opening up avenues for accessing diboryl fragments with two secondary *sp*³ alkyl sites. However, it is important to note that lower yields and diastereoselectivities were found in these cases.

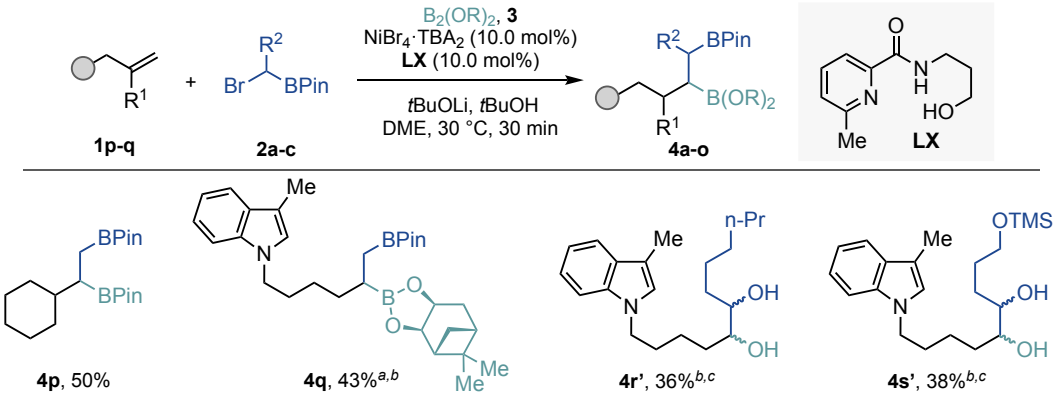

Reaction conditions: **1** (0.20 mmol, 1.0 equiv.), **2** (0.34 mmol, 1.7 equiv.), **$B_2(OR)_2$** (0.34 mmol, 1.7 equiv.), $NiBr_4 \cdot TBA_2$ (10.0 mol%), **LX** (10.0 mol%), *t*BuOLi (0.40 mmol, 2.0 equiv.), *t*BuOH (0.80 mmol, 4.0 equiv.), DME (0.5 mL), 30 ºC for 0.5 h. Isolated yields, average of two independent runs. [a] bis[(1R,2R,3S,5R)-pinanediolato]diboron used instead of B_2Pin_2 [b] dr = 1:1. [c] Isolated as diol upon quenching with $NaBO_3 \cdot H_2O$.

Scheme 18. Scope of 1,1-difunctionalisation with α-bromoboronates (**II**)

3.3.3. Scope of 1,1-difunctionalisation with α-bromosilanes

In light of the results shown in Scheme 17 and Scheme 18, we wondered whether our protocol could be extended to ambiphilic organometallic partners other than α-haloboronates.[75–77] Such an extension would be particularly fascinating as it would give access to 1,2-bisorganometallic reagents with intrinsically different C(sp^3)–X bonds, thus setting the stage for promoting site-selective sp^3 cross-coupling reactions at later stages. This turned out to be the case, and by employing readily accessible (bromomethyl)trimethylsilane, 1,2-silylboronates were successfully obtained in a 51% yield. By slight modification of the reaction conditions, such as using the more electron-rich **LX**, and LiCl as additive, the yield could be increased up to 80%.

As depicted in Scheme 19, these optimised conditions could be employed across a wide number of unactivated olefins bearing alkyl halides (**5b**), aryl halides (**5e**), heterocycles (**5f**, **5g**), and epoxides (**5h**).

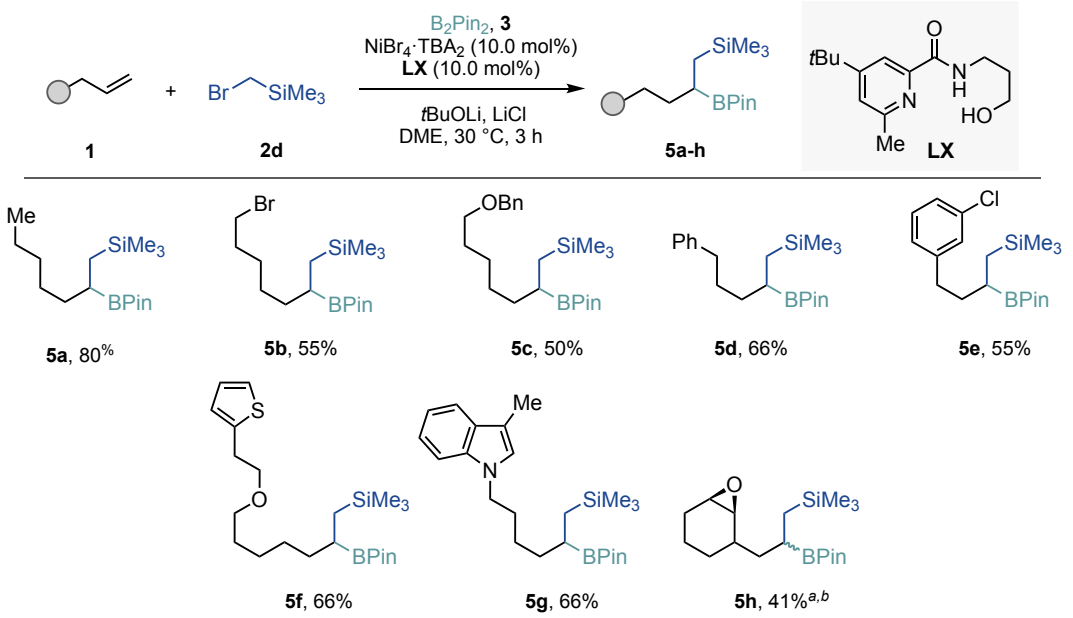

Reaction conditions: **1** (0.20 mmol, 1.0 equiv.), **2d** (0.50 mmol, 2.5 equiv.), B_2Pin_2 (0.34 mmol, 1.7 equiv.), $NiBr_4{\cdot}TBA_2$ (10.0 mol%), **LX** (10.0 mol%), *t*BuOLi (0.50 mmol, 2.5 equiv.), LiCl (0.40 mmol, 2.0 equiv.), DME (0.2 mL), 30 ºC for 3 h. Isolated yields, average of two independent runs. [a] starting alkene with dr = 1:1. [b] dr = 1.5:1.5:1:1.

Scheme 19. Scope of 1,1-difunctionalisation with α-bromosilanes

3.3.4. Application to advanced synthetic intermediates and ethylene revalorisation

With a reliable set of conditions in hand for forging both 1,2-diboronates and 1,2-silylboronates from unactivated olefins, we turned our attention their application to the modification of advanced synthetic intermediates.[78] As demonstrated in Scheme 20, a variety of products bearing either a diboronate (**6a**–**9a**) or silylboronate motif (**6b**–**9b**) could be readily accessed from common precursors. These results are particularly noteworthy as these intermediates hold the potential to serve as vehicles to access libraries of compounds of interest in drug discovery programs via site-selective C–B or C–Si bond-functionalisation. The synthetic value of our transformation is further illustrated by the ability to use ethylene – the largest-volume organic chemical produced in industry – as substrate, even at atmospheric pressure, delivering **10a** or **10b** in an unoptimised 40% and 28% yield, respectively.[79]

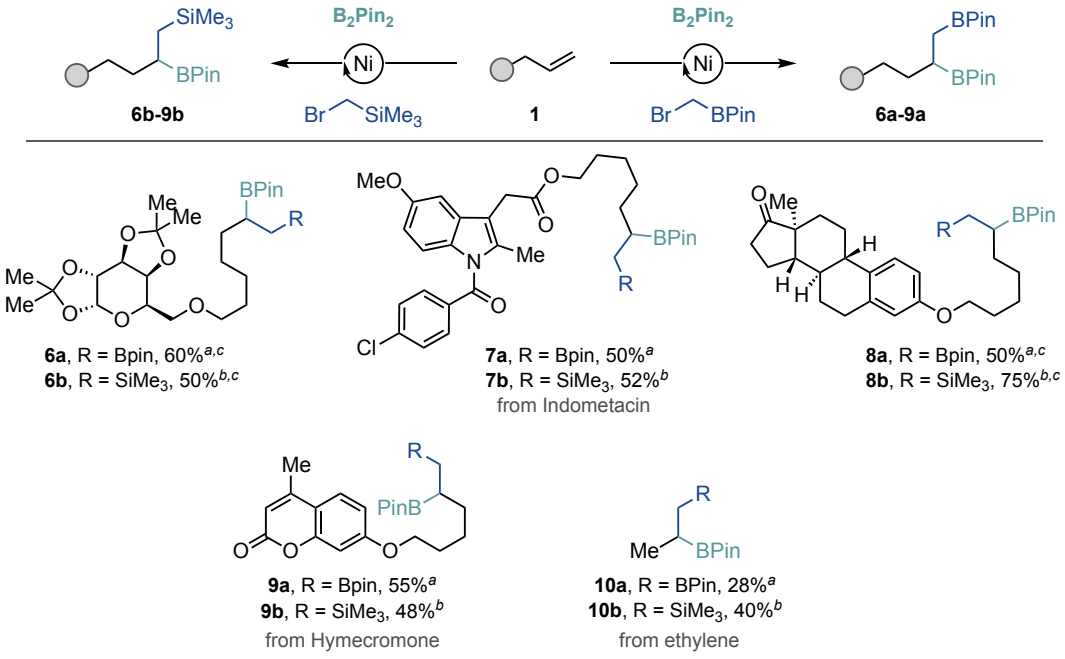

Reaction conditions: [a] as Scheme 17. [b] as Scheme 19. [c] dr = 1:1.

Scheme 20. Scope of 1,1-difunctionalisation in advanced synthetic intermediates and ethylene valorisation

3.3.5. Unsuccessful substrates

Unfortunately, our method displayed some limitations with a series of substrates, probably due to the presence of functional groups that interfere with the desired reactivity. For example, substrates possessing strong coordinating groups resulted in low yields or were completely unreactive (**X**, **X**, **X**). Moreover, activated olefins, such as styrene (**X**) resulted in the formation of 1,2-difunctionalised products in low efficiencies. Additionally, sterically more demanding substrates, such as internal alkenes, delivered only trace amounts of product (**X**, **X**, **X**).

In addition to some functionalised olefins, our methodology also failed with α-bromoalkyl boronic esters bearing quaternary carbon centres (**X**).

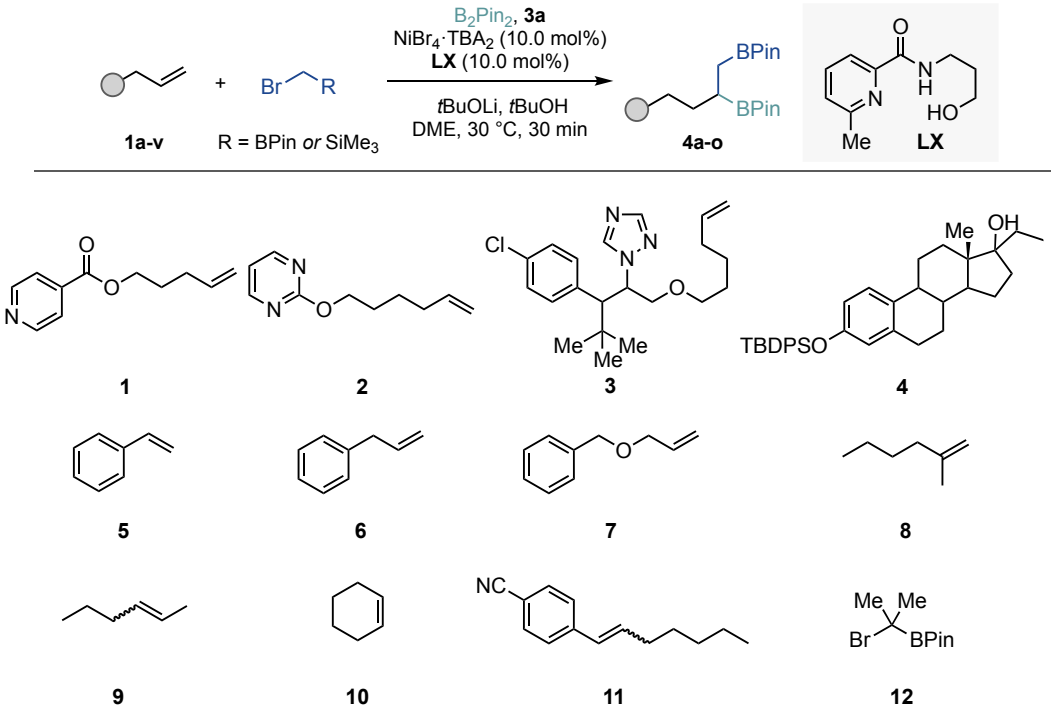

Scheme 21. Unsuccessful substrates

3.3.6. Synthetic applications

In order to further demonstrate the applicability of our protocol, we conducted a detailed investigation into the selective cleavage of the C–B or C–Si bond using the obtained 1,2-diboronates or 1,2-silylboronates products.

Interestingly, compounds **11**–**13** were easily prepared via site-selective sp^3 C–B bond-cleavage from **4a** under reported cross-coupling conditions.[80] Using bromobenzene as a model electrophile, homobenzylic boronic ester **11** was obtained. Similarly, replacing bromobenzene with vinyl chloride furnished the trisubstituted olefin **12** under identical conditions. Furthermore, by using dichloroethane under basic reaction conditions, terminal unsubstituted olefins could be obtained. Presumably, dichloroethane is converted to vinyl chloride – a highly toxic and gaseous electrophile that requires specialised equipment – under basic conditions and subsequently engages in the cross-coupling reaction. It is worth noting that, under the limits of detection, no cross-coupling product arising from the cleavage of the secondary sp^3 C–B bond was observed in the crude mixtures.

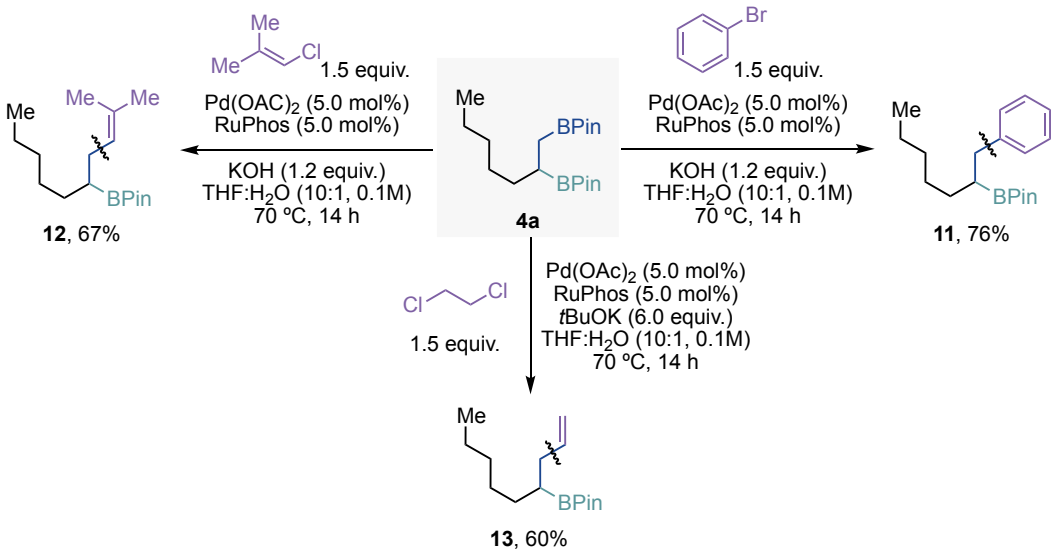

Scheme 22. Synthetic application of 1,2-diboronates

While cleavage of the primary sp^3 C–B bond was obtained using cross-coupling reactions, secondary sp^3 C–B bond cleavage using 1,2-silylboronates was performed utilising substituted Grignard reagents or organolithium compounds. By applying reported conditions from Aggarwal,[81] we successfully coupled the secondary boronic ester **5a** with the electron-rich furane to generate **14**. The reaction proceeds by the addition of the aryl lithium species (formed *in situ* from furane and *n*BuLi) to the boronic ester, producing the corresponding boronate intermediate. The latter reacts with NBS to generate a bromonium species, which triggers a subsequent 1,2-migration from boron, followed by elimination. Moreover, by

subjecting **5a** to modified Zweifel olefination conditions, we were able to isolate the terminal alkene **15** in 66% yield. This transformation involved the use of vinylmagnesium bromide, followed by the addition of iodine and sodium methoxide.[82] Likewise, 1,1-bromoalkylalkenes (**16**) could also be accessed employing vinyl bromide with LDA, followed by the addition of a methanolic solution of I_2 and subsequent warming to room-temperature, via the generation of a vinyl-boronate intermediate.[83]

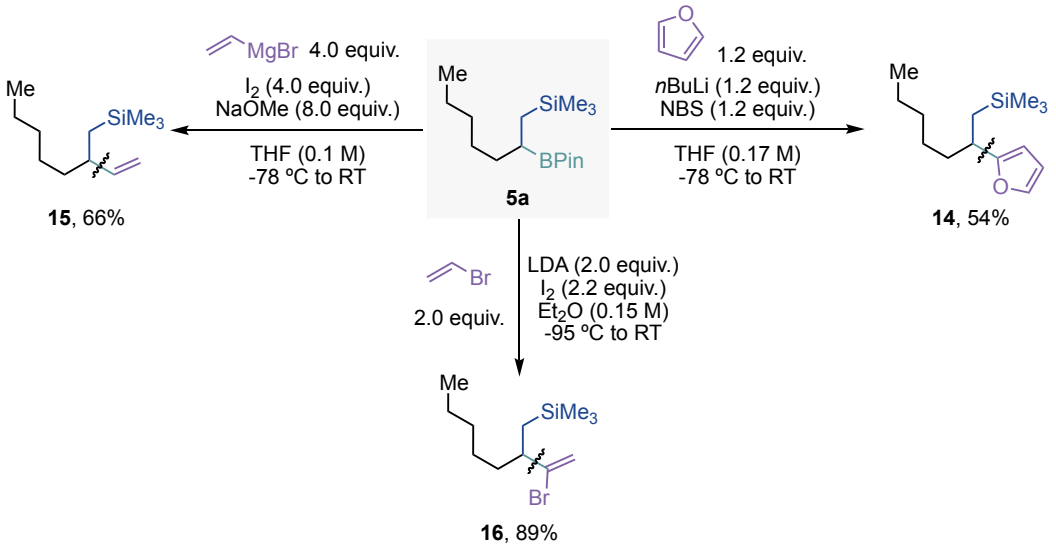

Scheme 23. Synthetic application of 1,2-silylboronates

3.3.7. Preliminary mechanistic studies

Once the generality and applicability of the current process was secured, we decided to gather indirect evidence regarding the underlying mechanism of our 1,1-difunctionalisation protocol. In principle, four different mechanisms are conceivable (Scheme 24): *i*) formation of a vinyl-BPin intermediate **I** prior to coupling with **2** (*path a*); *ii*) addition of two BPin fragments across the olefin in a 1,1-selective manner (**II**) followed by cross-coupling with **2** via C–B cleavage (*path b*);[47] *iii*) single electron transfer from Ni(0) to **2**, generating a boron-stabilised radical that adds across the olefin followed by recombination with Ni(I) (**III**), chain-walking and coupling with B_2Pin_2 (*path c*); *iv*) migratory insertion of *in situ* generated Ni–Bpin via **VI**, followed by 1,2-Ni migration via chain-walking[7–9,20,84] thus allowing to locate the metal centre adjacent to the boron atom prior to coupling with **2**[21,22,41] (*path d*).

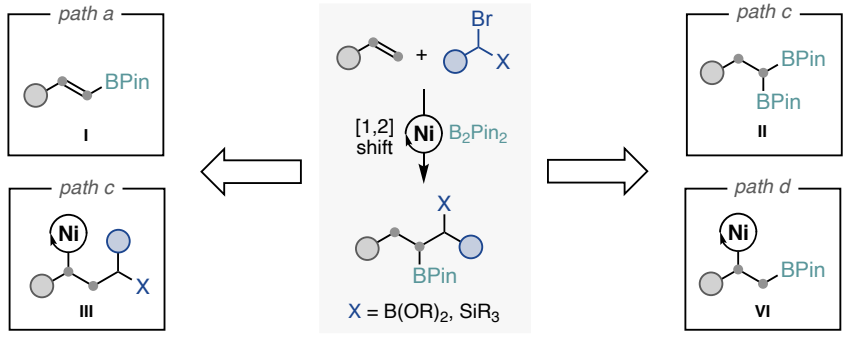

Scheme 24. Possible mechanistic scenarios

No reactivity was observed when exposing vinyl boronic ester **17** or 1,1-diborylated compound **18** to our optimised reaction conditions, thereby ruling out *path a* and *path b* (Scheme 25, *top*). To further explore the mechanistic details and differentiate between the remaining two pathways, we hypothesised that if a radical mechanism is involved, a 5-exo-trig cyclisation would occur with **19**. As depicted in Scheme 25, exclusive formation of **20a** was observed with no detectable traces of **20b** in the crude mixtures. This observation points against the involvement of a radical pathway (*path c*). Finally, the migratory insertion of Ni–BPin species followed by a 1,2-Ni migration was indirectly confirmed by subjecting **21** under the optimised conditions, resulting in significant deuterium incorporation at the C3 position (Scheme 25, *bottom*). Nonetheless, our available data did not allow us to distinguish between the participation of Ni(I)-alkyl or Ni(II)-alkyl entities.

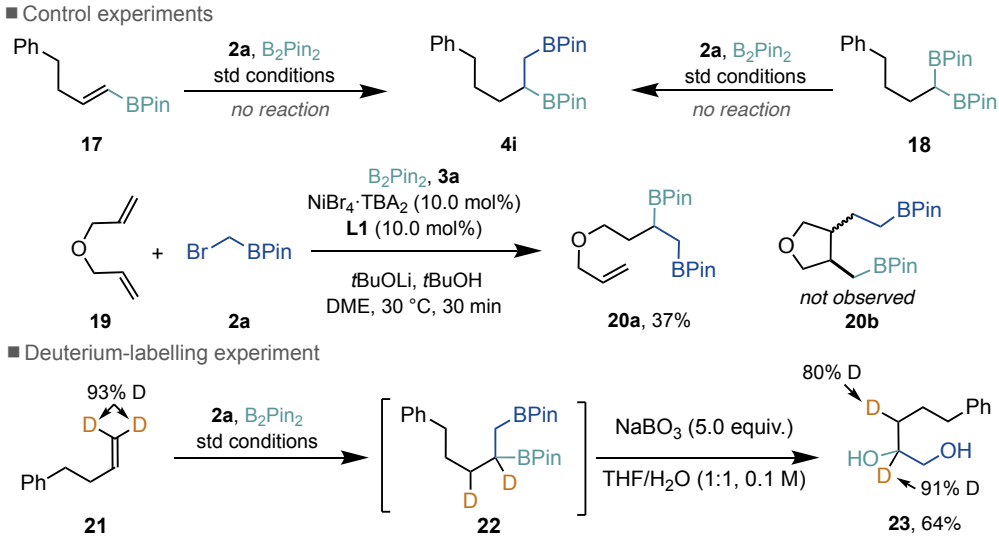

Scheme 25. Mechanistic experiments

3.4. Conclusions

This chapter summarises our efforts towards the development of a nickel-catalysed 1,1-difunctionalisation of unactivated olefins, leading to the generation of sp^3 bis-organometallic reagents bearing either B or Si motifs. The broad scope, mild conditions and exquisite chemo- and regio-selectivity makes this protocol an useful tool for the preparation of synthetically relevant building blocks from simple olefins as raw materials, while serving as an alternative strategy to existing catalytic approaches for the synthesis of sp^3 poly-organometallics. Furthermore, we have successfully implemented a site-selective C–B or C–Si bond-cleavage platform, allowing access to structurally different carbon linkages from simple olefin backbones. Preliminary mechanistic investigations suggest that difunctionalisation occurs via migratory insertion of an *in situ* generated Ni–BPin species, followed by a 1,2-Ni shift facilitated by the stabilisation of the boron atom. However, at this point, it is still unclear if the reaction occurs via Ni(I) or Ni(II) intermediates. Further mechanistic studies are required to gain a comprehensive picture of the reaction mechanism.

3.5. Experimental section

3.5.1. General information

Analytical methods

^{1}H and ^{13}C NMR spectra were recorded on Bruker 400 MHz and Bruker 500 MHz at 20 °C. All ^{1}H NMR spectra are reported in parts per million (ppm) downfield of TMS and were calibrated using the residual solvent peak of $CHCl_3$ (7.26 ppm), unless otherwise indicated. All ^{13}C NMR spectra are reported in ppm relative to TMS, were calibrated using the signal of residual $CHCl_3$ (77.16 ppm) and ^{19}F NMR were obtained with ^{1}H decoupling unless otherwise indicated. Coupling constants, *J*, are reported in Hertz. Gas chromatographic analyses were performed on Hewlett-Packard 6890 gas chromatography instrument with FID detector. Flash chromatography was performed with EM Science silica gel 60 (230-400 mesh). Thin layer chromatography was used to monitor reaction progress and analyse fractions from column chromatography. To this purpose TLC Silica gel 60 F_{254} aluminium sheets from Merck were used and visualisation was achieved using UV irradiation and/or staining with Cerium Molybdate solution. The yields reported in Tables XX and Schemes XX refer to isolated yields and represent an average of at least two independent runs. In the cases the High-Resolution Mass Spectra of the molecular ion could not be obtained using ESI and APCI ionisation modes the GC-MS of the compound was given. SFC analysis were carried out on a Waters Investigator SFC using a Waters Acquity UPC^2 equipped with PDA (Acquity) and an Agilent 1260 Infinity II SFC system.

Reagents

Commercially available materials were used as received without further purification. (Bromomethyl)boronic acid pinacol ester, Bis(pinacolato)diboron (B_2Pin_2) and bis[(1R,2R,3S,5R)-pinanediolato]diboron were purchased from Fluorochem. (bromomethyl)trimethylsilane was purchased from TCI. *t*BuOLi and Anhydrous *tert*-Butanol (99.5%) were purchased from Sigma-Aldrich. Anhydrous dimethoxyethane (DME, 99.5% purity), and anhydrous 1,4-dioxane (99.5% purity), were purchased from Acros

3.5.2. Optimisation of the reaction conditions

General procedure used for reaction optimisation (Tables XX – XX):

An oven-dried 8 mL screw-cap test tube containing a stirring bar was charged with $NiBr_4 \cdot TBA_2$ (10 mol%, 17.3 mg), the corresponding ligand (10 mol%), B_2Pin_2 (**3a,** 0.34 mmol, 86.3 mg). Subsequently, the tube was put into the glovebox under N_2 atmosphere, and *t*BuOLi (0.4 mmol, 32.0 mg) was added in the glovebox. Then the tube was sealed with a Teflon-lined screw cap and taken outside from the glovebox. Afterwards, 1-hexene (**1a**, 0.20

mmol, 25 μL, 1.0 equiv), (Bromomethyl)boronic acid pinacol ester (**2a**, 0.34 mmol, 61 μL, 1.7 equiv), *t*-BuOH (0.80 mmol, 76 μL, 4.0 equiv) and solvent (0.5 mL) were added via syringe, independently. Then, the tube was stirred at 30 ºC for 30 min. After the reaction was completed, the mixture was diluted with EtOAc or DCM, filtered through silica gel and concentrated under vacuum. The yields were determined by GC FID analysis using 1-decane (1.0 equiv.) as internal standard.

3.5.3. Ligands and starting materials synthesis

Commercially available compounds were used as received without further purification. *N*-benzyl-6-methylpicolinamide (**L1**),[48] 4-isopropyl-2-(6-methylpyridin-2-yl)-4,5-dihydrooxazole (**L11**)[85], *N*-benzyl-6-methylpicolinamide (**L13**)[86] *tert*-butyl(hex-5-en-1-yloxy)dimethylsilane (**1d**),[87] ((hex-5-en-1-yloxy)methyl)benzene (**1e)**,[87] but-3-en-1-yl benzoate (**1j**),[88] hex-5-en-1-yl 4-fluorobenzoate (**1k**),[89] *N*-(4-(pent-4-en-1-yloxy)phenyl)acetamide (**1l**),[90] (3a*R*,5*R*,5a*S*,8a*S*,8b*R*)-5-((hex-5-en-1-yloxy)methyl)-2,2,7,7-tetramethyltetrahydro-5*H*-bis([1,3]dioxolo)[4,5-*b*:4',5'-*d*]pyran (**1u**),[91] (8*R*,9*S*,13*S*,14*S*)-3-(hex-5-en-1-yloxy)-13-methyl-6,7,8,9,11,12,13,14,15,16-decahydro-17*H*-cyclopenta [*a*] phenanthren-17-one (**1w)**,[92] 4-methyl-7-(pent-4-en-1-yloxy)-2*H*-chromen-2-one (**1x**),[93] 2-(1-bromoheptyl)-4,4,5,5-tetramethyl-1,3,2-dioxaborolane (**2b**),[75] 4,4,5,5-tetramethyl-2-(4-phenylbut-1-en-1-yl)-1,3,2-dioxaborolane (**19**),[94] and 2,2'-(4-phenylbutane-1,1-diyl)bis(4,4,5,5-tetramethyl-1,3,2-dioxaborolane) (**20**),[95] were prepared by known procedures, the NMR data matched those reported previously in the literature.

Preparation of ligands

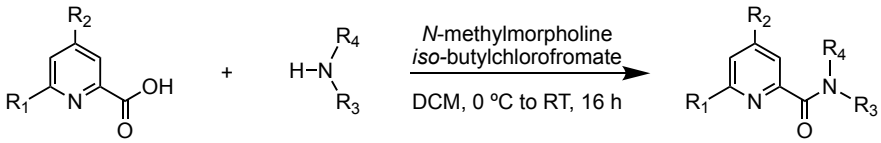

General procedure A: The ligands **L2-L10** were prepared according to a procedure reported in literature.[48] To a round-bottom flask containing a stirring bar was added the corresponding picolinic acid (10 mmol, 1.0 equiv.), then dry DCM (40 mL) was added via syringe under inert atmosphere. Subsequently, *N*-methylmorpholine (15 mmol, 1.5 equiv.) was added and the reaction mixture was cooled down to 0 °C. Subsequently, *iso*-butylchloroformate was added dropwise (12 mmol, 1.2 equiv.), and the mixture was stirred for further 20 min. Then the corresponding amine (12 mmol, 1.2 equiv.) dissolved in DCM (10 mL) and added via syringe. After the addition, the mixture was allowed to warm to room temperature and stirred for 16 h. Afterwards, the mixture was extracted with DCM (10 mL), washed with water (10 mL),

brine (10 mL), dried over $MgSO_4$ and concentrated in vacuum. The residue was purified by silica gel flash chromatography.

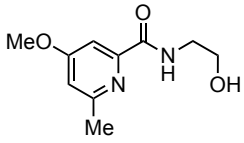

***N*-(2-hydroxyethyl)-4-methoxy-6-methylpicolinamide** (**L2**): Following the **general procedure A**, using 4-methoxy-6-methylpicolinonitrile (1.48 g, 10 mmol) and 2-aminoethan-1-ol (0.73 mL, 12 mmol). The product was purified by flash chromatography (*n*-hexane/EtOAc = 1:1) to afford the compound as a yellow oil, 1.68 g (80%). **^{1}H NMR** (400 MHz, $CDCl_3$): δ 8.57 (br s, 1H), 7.58 (d, *J* = 2.4 Hz, 1H), 6.78 (d, *J* = 2.9 Hz, 1H), 3.89 (s, 3H), 3.86 – 3.84 (m, 2H), 3.65 – 3.61 (m, 2H), 2.52 (s, 3H) ppm. No signal for OH-group has been observed. **^{13}C NMR** (101 MHz, $CDCl_3$): δ 167.7, 165.5, 158.7, 150.8, 112.4, 105.6, 62.8, 55.7, 43.0, 24.2 ppm. **IR** (neat, cm^{-1}): 3372, 2941, 2875, 1655, 1598, 1572, 1523, 1464, 1438, 1379, 1335, 1274, 1200, 1138, 1047. **HRMS**: m/z calcd. for ($C_{10}H_{15}N_2O_3$) $[M+H]^+$: 221.1077 found 211.1072.

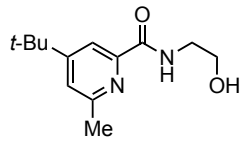

4-(*tert*-butyl)-*N*-(2-hydroxyethyl)-6-methylpicolinamide (**L3**): Following the **general procedure A**, using 4-(*tert*-butyl)-6-methylpicolinic acid (1.93 g, 10.0 mmol) and 2-aminoethan-1-ol (0.73 mL, 12.0 mmol). The product was purified by flash chromatography (*n*-hexane/EtOAc 2:1 to 1:1) to afford the compound as a brown oil, 1.65 g (70%). **^{1}H NMR** (400 MHz, $CDCl_3$): δ 8.50 (br s, 1H), 8.00 (d, *J* = 1.7 Hz, 1H), 7.23 (d, *J* = 1.7 Hz, 1H), 3.83 – 3.81 (m, 2H), 3.64 – 3.60 (m, 2H), 3.38 (br s, 1H), 2.52 (s, 3H), 1.30 (s, 9H) ppm. **^{13}C NMR** (101 MHz, $CDCl_3$): δ 166.4, 162.1, 157.2, 148.9, 123.0, 116.9, 62.7, 42.8, 35.0, 30.6, 24.4 ppm. **IR** (neat, cm^{-1}): 3370, 2961, 2874, 1698, 1656, 1603, 1523, 1469, 1248, 1147, 1069. **HRMS**: m/z calcd. for ($C_{13}H_{21}N_2O_2$) $[M+H]^+$: 237.1598 found 237.1598.

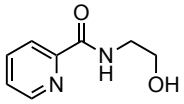

***N*-(2-hydroxyethyl)picolinamide** (**L7**): Following the **general procedure A**, using picolinic acid (1.2 g, 10.0 mmol) and 2-aminoethan-1-ol (0.73 mL, 12.0 mmol). The product was purified by flash chromatography (*n*-hexane/EtOAc 1:1 to 1:2), to afford the compound as a yellow oil, 495 mg (30%). **^{1}H NMR** (400 MHz, $CDCl_3$): δ 8.55 (ddd, *J* = 4.8, 1.7, 0.9 Hz, 1H),

8.44 (br s, 1H), 8.20 (dt, *J* = 7.8, 1.1 Hz, 1H), 7.86 (td, *J* = 7.7, 1.7 Hz, 1H), 7.44 (ddd, *J* = 7.6, 4.8, 1.3 Hz, 1H), 3.87 – 3.84 (m, 2H), 3.68 – 3.64 (m, 2H), 2.43 (br s, 1H) ppm. **^{13}C NMR** (101 MHz, $CDCl_3$): δ 165.6, 149.7, 148.2, 137.7, 126.5, 122.5, 62.7, 42.8 ppm. **IR** (neat, cm^{-1}): 3374, 3059, 2930, 2875, 1655, 1590, 1569, 1510, 1463, 1434, 1289, 1246, 1169, 1063, 1042, 997. **HRMS**: m/z calcd. for ($C_8H_{10}N_2NaO_2$) $[M+Na]^+$: 189.0634 found 189.0631.

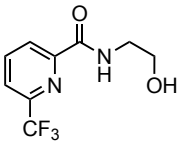

***N*-(2-hydroxyethyl)-6-(trifluoromethyl)picolinamide** (**L8**): Following the **general procedure A**, using 6-(trifluoromethyl)picolinic acid (1.9 g, 10.0 mmol) and 2-aminoethan-1-ol (0.73 mL, 12.0 mmol). The product was purified by flash chromatography (*n*-hexane/EtOAc 2:1), to afford the compound as a yellow oil, 491 mg (21%). **^{1}H NMR** (400 MHz, $CDCl_3$): δ 8.40 – 8.38 (m, 1H), 8.30 (br s, 1H), 8.08 – 8.04 (m, 1H), 7.82 (dd, *J* = 7.8, 1.1 Hz, 1H), 3.88 – 3.86 (m, 2H), 3.70 – 3.66 (m, 2H), 2.70 (br s, 1H) ppm. **^{13}C NMR** (101 MHz, $CDCl_3$): δ 164.2, 150.2, 147.1 (q, *J* = 35.4 Hz), 139.3, 125.2, 123.0 (q, *J* = 2.5 Hz), 121.2 (q, *J* = 274.4 Hz), 62.5, 42.8 ppm. **IR** (neat, cm^{-1}): 3460, 3314, 3109, 2957, 2957, 2957, 2924, 2882, 1650, 1598, 1532, 1461, 1430, 1362, 1341, 1311, 1275, 1249, 1213, 1131, 1110, 1083, 1066. **HRMS**: m/z calcd. for ($C_9H_9F_3N_2NaO_2$) $[M+Na]^+$: 257.0508 found 257.0511.

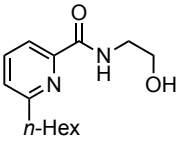

6-hexyl-*N*-(2-hydroxyethyl)picolinamide (**L9**): Following the **general procedure A**, using 6-hexanoylpicolinonitrile (2.0 g, 10.0 mmol) and 2-aminoethan-1-ol (0.73 mL, 12.0 mmol). The product was purified by flash chromatography (*n*-hexane/EtOAc 1:1), to afford the compound as a yellow oil, 950 mg (38%). **^{1}H NMR** (400 MHz, $CDCl_3$): δ 8.55 (br s, 1H), 8.08 (dd, *J* = 7.7, 1.1 Hz, 1H), 7.75 (t, *J* = 7.7 Hz, 1H), 7.29 (dd, *J* = 7.8, 1.1 Hz, 1H), 3.87 – 3.84 (m, 2H), 3.67 – 3.63 (m, 2H), 2.83 – 2.79 (m, 2H), 1.76 – 1.69 (m, 2H), 1.39 – 1.27 (m, 6H), 0.91 – 0.87 (m, 3H) ppm. No signal for OH-group has been observed. **^{13}C NMR** (101 MHz, $CDCl_3$): δ 165.9, 161.5, 148.8, 137.9, 125.8, 119.8, 62.9, 42.9, 38.0, 31.8, 29.7, 29.1, 22.7, 14.2 ppm. **IR** (neat, cm^{-1}): 3380, 2926, 2857, 1658, 1592, 1572, 1526, 1452, 1360, 1262, 1172, 1070. **HRMS**: m/z calcd. for ($C_{14}H_{23}N_2O_2$) $[M+H]^+$: 251.1754 found 251.1753.

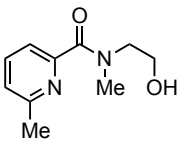

***N*-(2-hydroxyethyl)-*N*,6-dimethylpicolinamide** (**L10**): Following the **general procedure A**, using 6-methylpicolinic acid (1.37 g, 10.0 mmol) and 2-(methylamino)ethan-1-ol (1.07 mL, 12.0 mmol). The product was purified by flash chromatography (*n*-hexane/EtOAc 2:1), to afford the compound as a yellow oil, 854 mg (44%). **^{1}H NMR** (500 MHz, $CDCl_3$): δ 7.75 (t, *J* = 7.7 Hz, 1H), 7.63 (d, *J* = 7.7 Hz, 1H), 7.25 (d, *J* = 7.6 Hz, 1H), 3.89 – 3.78 (m, 2H), 3.56 – 3.54 (m, 2H), 3.16 (s, 3H), 2.58 (s, 3H) ppm. **^{13}C NMR** (126 MHz, $CDCl_3$): δ 168.8, 156.3, 152.7, 138.4, 124.9, 122.6, 58.8, 52.2, 33.2, 23.7 ppm. **IR** (neat, cm^{-1}): 3391, 2928, 2872, 1618, 1589, 1493, 1443, 1400, 1307, 1262, 1228, 1180, 1085, 1049, 1049, 1002. **HRMS**: m/z calcd. for ($C_{10}H_{14}N_2NaO_2$) $[M+Na]^+$: 217.0947 found 217.0944.

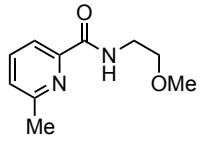

***N*-(2-methoxyethyl)-6-methylpicolinamide** (**L4**): Following **general procedure A**, using 6-methylpicolinic acid (1.37 g, 10.0 mmol) and 2-methoxyethan-1-amine (1.04 mL, 12.0 mmol). The product was purified by flash chromatography (*n*-hexane/EtOAc 2:1) to afford the compound as a yellow oil, 1.57 g (81%). **^{1}H NMR** (300 MHz, $CDCl_3$): δ 8.38 (br s, 1H), 8.00 (d, *J* = 7.7 Hz, 1H), 7.71 (t, *J* = 7.7 Hz, 1H), 7.28 – 7.25 (m, 1H), 3.70 – 3.65 (m, 2H), 3.61 – 3.57 (m, 2H), 3.41 (s, 3H), 2.57 (s, 3H) ppm. **^{13}C NMR** (101 MHz, CD_3Cl): δ 164.7, 157.3, 149.3, 137.6, 126.0, 119.5, 71.5, 59.0, 39.3, 24.3 ppm. **IR** (neat, cm^{-1}): 3396, 3342, 2977, 2927, 2881, 2831, 2817, 1670, 1593, 1574, 1519, 1452,1392, 1376, 1361, 1306, 1256, 1237, 1196, 1175, 1155, 1118, 1088, 1026, 993. **HRMS**: m/z calcd. for ($C_{10}H_{14}NaN_2O_2$) $[M+Na]^+$: 217.0937 found 217.0937.

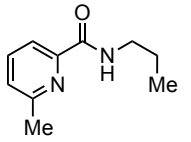

6-methyl-*N*-propylpicolinamide (**L5**): Following the **general procedure A**, using 6-methylpicolinic acid (1.37 g, 10.0 mmol) and propan-1-amine (1.0 mL, 12.0 mmol). The product was purified by flash chromatography (*n*-hexane/EtOAc 3:1 to 2:3), to afford the compound as a yellow oil, 1.13 g (63%). **^{1}H NMR** (400 MHz, $CDCl_3$): δ 8.14 (br s, 1H), 8.01 – 7.99 (m, 1H), 7.71 (t, *J* = 7.7 Hz, 1H), 7.27 – 7.25 (m, 1H), 3.46 – 3.41 (m, 2H), 2.57 (s, 3H), 1.71 – 1.62 (m, 2H), 0.99 (t, *J* = 7.4 Hz, 3H) ppm. **^{13}C NMR** (101 MHz, $CDCl_3$): δ 164.5, 157.2, 149.5, 137.6, 125.8, 119.4, 41.2, 24.4, 23.1, 11.7 ppm. **IR** (neat, cm^{-1}): 3388, 2963, 2874, 1665, 1593, 1573, 1522, 1453, 1377, 1305, 1256, 1172, 1084. **HRMS**: m/z calcd. for ($C_{10}H_{14}N_2NaO$) $[M+Na]^+$: 201.0998 found 201.0993.

Synthesis of unactivated olefins

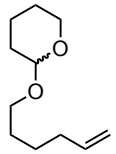

2-(hex-5-en-1-yloxy)tetrahydro-2*H*-pyran (**1m**): To a solution of hex-5-en-1-ol (3.51 mL, 2.91 g, 29.1 mmol, 1.0 equiv.) in DCM (50 mL) catalytic amounts of *p*-toluenesulfonic acid (100 mg) were added at 0 °C, following the dropwise addition of 3,4-dihydro-2*H*-pyran (5.32 mL, 4.88 g, 58.2 mmol, 2.0 equiv.). After complete addition, the reaction allowed to warm to RT and stirred for further 2 h. Then, the reaction was quenched with the addition of saturated aqueous $NaHCO_3$ solution. The organic phase was washed with water and brine, dried over $MgSO_4$ and concentrated under vacuum. The residue was purified by flash column chromatography (*n*-hexane/EtOAc 96:4) to provide **1m** (3.16 g, 17.2 mmol, 58%) as colourless oil. **^{1}H NMR** (400 MHz, $CDCl_3$): δ 5.86 – 5.76 (m, 1H), 5.03 – 4.92 (m, 2H), 4.58 – 4.56 (m, 1H), 3.89 – 3.83 (m, 1H), 3.74 (dt, *J* = 9.6, 6.7 Hz, 1H), 3.52 – 2.47 (m, 1H), 3.39 (dt, *J* = 9.6, 6.5 Hz, 1H), 2.11 – 2.05 (m, 2H), 1.89 – 1.78 (m, 1H), 1.74 – 1.67 (m, 1H), 1.65 – 1.43 (m, 8H) ppm. **^{13}C NMR** (101 MHz, $CDCl_3$): δ 138.9, 114.6, 99.0, 67.6, 62.4, 33.7, 30.9, 29.4, 25.73, 25.66, 19.8 ppm. **IR** (neat, cm^{-1}): 2938, 2866, 1640, 1440, 1352, 1323, 1261, 1200, 1119, 1076, 1032, 989. **HRMS**: m/z calcd. for ($C_{11}H_{20}NaO_2$) $[M+Na]^+$: 207.1356 found 207.1352.

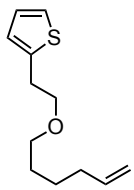

2-(2-(hex-5-en-1-yloxy)ethyl)thiophene (**1n**): Sodium hydride (132 mg, 5.50 mmol, 1.10 equiv.) was added to a solution of 2-(thiophen-2-yl)ethan-1-ol in dry THF (25 mL) at 0 °C. After stirring for 10 min, 5-hexenyl tosylate (1.34 g, 5.25 mmol, 1.05 equiv.) was added via syringe. Then, the reaction mixture was heated to 60 °C for 2 h. After cooling down to RT, saturated aqueous $NaHCO_3$ was added. The mixture was extracted with EtOAc (3 x 30 mL) and the combined organic phases were washed with brine (30 mL). The organic phase was dried over $MgSO_4$ and concentrated under vacuum. The crude was purified via flash column chromatography (*n*-hexane/EtOAc 98:2) to provide **1n** (713 mg, 3.39 mmol, 68 %) as a yellow oil. **^{1}H NMR** (400 MHz, $CDCl_3$): δ 7.14 (dd, *J* = 5.1, 1.2 Hz, 1H), 6.93 (dd, *J* = 5.1, 3.4 Hz, 1H), 6.86 – 6.84 (m, 1H), 5.87 – 5.77 (m, 1H), 5.04 – 4.94 (m, 2H), 3.65 (t, *J* = 6.9 Hz, 2H), 3.47 (t, *J* = 6.5 Hz, 2H), 3.10 (td, *J* = 6.8, 0.6 Hz, 2H), 2.11 – 2.05 (m, 2H), 1.65 – 1.58 (m, 2H), 1.51 – 1.43 (m, 2H) ppm. **^{13}C NMR** (101 MHz, $CDCl_3$): δ 141.6, 138.9, 126.7, 125.2,

123.7, 114.6, 71.5, 71.0, 33.7, 30.7, 29.3, 25.6 ppm. **IR** (neat, cm^{-1}): 3074, 2934, 2858, 2794, 1640, 1439, 1367, 1110, 1050. **HRMS**: m/z calcd. for ($C_{12}H_{19}OS$) $[M+H]^+$: 211.1157 found 211.1151.

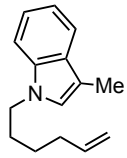

1-(hex-5-en-1-yl)-3-methyl-1*H*-indole (**1o**): 3-methyl-1H-indole (656 mg, 5.00 mmol, 1.00 equiv.) was dissolved in THF (25 mL). The solution was cooled down to 0 °C and sodium hydride (132 mg, 5.50 mmol, 1.10 equiv.) was added. After 10 min, 5-hexenyl tosylate (1.34 g, 5.25 mmol, 1.05 equiv.) was added and the reaction mixture was heated to 60 °C for 2 h. Saturated aqueous $NaHCO_3$ (20 mL) was added, and the mixture was extracted with EtOAc (3 × 30 mL). The organic phases were combined and washed with brine (30 mL), dried over $MgSO_4$ and concentrated under vacuum. The residue was purified by flash column chromatography (*n*-hexane/EtOAc, gradient 98:2 to 96:4) to provide **1o** (624 mg, 3.01 mmol, 60 %) as yellow oil. **^{1}H NMR** (400 MHz, $CDCl_3$): δ 7.60 – 7.57 (m, 1H), 7.32 – 7.29 (m, 1H), 7.24 – 7.19 (m, 1H), 7.14 – 7.09 (m, 1H), 6.88 (s, 1H), 5.84 – 5.73 (m, 1H), 5.05 – 4.95 (m, 2H), 4.09 – 4.05 (m, 2H), 2.35 (s, 3H), 2.13 – 2.06 (m, 2H), 1.88 – 1.80 (m, 2H), 1.48 – 1.39 (m, 2H) ppm. **^{13}C NMR** (126 MHz, $CDCl_3$): δ 138.4, 136.4, 128.8, 125.5, 121.4, 119.1, 118.5, 115.0, 110.2, 109.3, 46.1, 33.5, 29.9, 26.4, 9.7 ppm. **IR** (neat, cm^{-1}): 3074 ,3055, 3029, 2995, 2927, 2919, 2885, 2859, 1640, 1614, 1559, 1482, 1467, 1454, 1416, 1385, 1361, 1330, 1236, 1200, 1177, 1126, 1013, 993. **HRMS**: m/z calcd. for ($C_{15}H_{20}N$) $[M+H]^+$: 214.1596 found 214.1590.

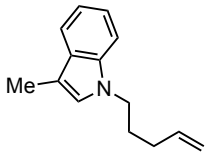

3-methyl-1-(pent-4-en-1-yl)-1*H*-indole (**1p**): To a solution of 3-methyl-1H-indole (1.31g, 10 mmol, 1.0 equiv.) in DMF (15 mL), was added 5-bromopent-1-ene (1.42 mL, 12 mmol, 1.2 equiv.) and KOH (673 mg, 12 mmol, 1.2 equiv.). The mixture was heated to 70 ºC and stirred for at least 3 h. The solution was allowed to cool to room temperature and water (40 mL) was added. Then, the solution was extracted with ethyl acetate (3 x 30 mL). The organic phases were combined, washed with water (6 x 30 mL), dried over Na_2SO_4 and concentrated under vacuum. The residue was purified by column chromatography (*n*-hexane/EtOAc 100:1 to 100:5) to provide **1p** (1.22g, 6.1mmol, 61%) as pale-yellow oil. **^{1}H NMR** (500 MHz, $CDCl_3$): δ 7.59 (dt, J = 7.8, 1.0 Hz, 1H), 7.32 – 7.30 (m, 1H), 7.23 – 7.20 (m, 1H), 7.13 – 7.10 (m,

1H), 6.88 (d, *J* = 1.1 Hz, 1H), 5.83 (ddt, *J* = 16.9, 10.2, 6.6 Hz, 1H), 5.09 – 5.03 (m, 2H), 4.08 (t, *J* = 7.0 Hz, 2H), 2.35 (d, *J* = 1.1 Hz, 3H), 2.12 – 2.07 (m, 2H), 1.96 – 1.90 (m, 2H) ppm. **^{13}C NMR** (126 MHz, $CDCl_3$): δ 137.6, 136.4, 128.9, 125.6, 121.4, 119.1, 118.6, 115.6, 110.3, 109.3, 45.4,31.1, 29.5, 9.7 ppm. **IR** (neat, cm^{-1}): 3075, 3029, 2996, 2929, 2918, 2875, 2862, 1640, 1614, 1558, 1467, 1450, 1361, 1330, 1243, 1202, 1179, 1126, 992, 911. **HRMS**: m/z calcd. for ($C_{14}H_{18}N$) $[M+H]^+$: 200.1434 found 200.1433.

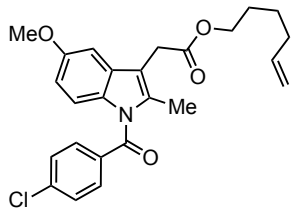

hex-5-en-1-yl 2-(1-(4-chlorobenzoyl)-5-methoxy-2-methyl-1H-indol-3-yl)acetate (**1u**): To a solution of 2-(1-(4-chlorobenzoyl)-5-methoxy-2-methyl-1H-indol-3-yl)acetic acid (4.0 mmol, 1.43g) and hex-5-en-1-ol (4.0 mmol, 475 μl) in DCM (40 mL), was added DMAP (0.2 mmol, 24 mg) and DCC (4.0 mmol, 824 mg). Then, the reaction mixture was stirring at room temperature for 2 h. After the reaction was completed, the mixture was extracted with EtOAc (3 x 30 mL) and the combined organic phases were washed with brine (30 mL). The organic phase was dried over $MgSO_4$ and concentrated under vacuum. The crude was purified via flash column chromatography (*n*-hexane/EtOAc 10:1) to provide **1u** 1.4 g (80% yield) as a yellow oil. **^{1}H NMR** (400 MHz, $CDCl_3$): δ 7.67 – 7.63 (m, 2H), 7.48 – 7.45 (m, 2H), 6.97 (d, *J* = 2.5 Hz, 1H), 6.87 (d, *J* = 9.0 Hz, 1H), 6.67 (dd, *J* = 9.0, 2.5 Hz, 1H), 5.74 (ddt, *J* = 16.9, 10.2, 6.7 Hz, 1H), 5.00 – 4.92 (m, 2H), 4.11 (t, *J* = 6.6 Hz, 2H), 3.83 (s, 3H), 3.66 (s, 2H), 2.39 (s, 3H), 2.07 – 2.00 (m, 2H), 1.67 – 1.60 (m, 2H), 1.44 – 1.36 (m, 2H) ppm. **^{13}C NMR** (101 MHz, $CDCl_3$): δ 171.0, 168.4, 156.2, 139.4, 138.3, 136.0, 134.1, 131.3, 130.9, 130.8, 129.2, 115.1, 115.0, 112.8, 111.8, 101.4, 65.1, 55.8, 33.3, 30.6, 28.2, 25.3, 13.5 ppm. **IR** (neat, cm^{-1}): 3075, 2933, 2859, 2834, 1731, 1591, 1476, 1456, 1399, 1368, 1355, 1300, 1258, 1164, 1087, 1066, 1035, 1014. **HRMS**: m/z calcd. for ($C_{25}H_{27}ClNO_4$) $[M+H]^+$: 440.1623 found 440.1620.

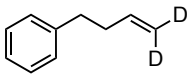

(but-3-en-1-yl-4,4-d2)benzene (**21**): To a solution of PPh_3CD_3I (10.0 mmol, 4.08 g) in THF (50 mL) at -78 °C, was added *n*-BuLi (10.0 mmol) dropwise over 5 min. The solution was stirred at -78 °C for 15 min, then warm to room temperature, stirred for another 30 min. After that, the solution was cooled back to -78 °C, 3-phenylpropanal (10 mmol, 1.3 mL) was added dropwise over 5 min via syringe, stirred at the same temperature for 20 min, then warmed to room temperature, and stirred for 24 h. After the reaction was completed, the mixture was

filtered with celite and concentrated under vacuum. The crude was purified via flash column chromatography (*n*-hexane) to provide **21**, 0.85 g (64%) as a colourless oil, with 93% D. **^{1}H NMR** (400 MHz, $CDCl_3$): δ 7.34 – 7.29 (m, 2H), 7.23 (m, 3H), 5.91 – 5.86 (m, 1H), 5.10 – 4.97 (m, 0.14H), 2.76 – 2.71 (m, 2H), 2.43 – 2.37 (m, 2H) ppm. **^{13}C NMR** (101 MHz, $CDCl_3$): δ 142.0, 138.0, 128.6, 128.4, 125.9, 35.5 (2C) ppm. **IR** (neat, cm^{-1}): 3063, 3027, 3000, 2924, 2855, 1602, 1496, 1454, 1075, 1031. **GC-MS** ($C_{10}H_{10}D_2$) [M]: found t = 3.839 min, m/z 134.1.

Preparation of α-bromo boronic esters

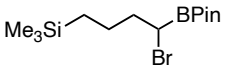

(4-bromo-4-(4,4,5,5-tetramethyl-1,3,2-dioxaborolan-2-yl)butyl)trimethylsilane (2c): The title compound was prepared according to a procedure reported in literature.[91] To an oven dried round flask equipped with a stirring bar was added CH_2Cl_2 (15 mmol, 0.96 mL) and THF (20 mL) by syringe, and the solution was cooled to −100°C using a methanol/dry ice bath. Then *n*-butyllithium (2.5 M solution in *n*-hexane, 11 mmol, 1.1 equiv.) was added dropwise under −100 ºC. After stirring for 45 min, a solution of trimethyl(3-(4,4,5,5-tetramethyl-1,3,2-dioxaborolan-2-yl)propyl)silane (10 mmol, 1.0 equiv.) in diethyl ether was directly added dropwise via syringe. Then the reaction mixture was allowed to slowly warm to room temperature overnight. After the reaction was completed, 50 mL of DCM was added to precipitate the lithium chloride (optional), the solution was directly filtered through a short pad of silica gel (*n*-hexane/EtOAc 10:1) and concentrated under reduced pressure. Subsequently, the compound was dissolved in 50 mL of acetone, and then added sodium bromide (5.0 equiv.). The reaction mixture was stirred under RT overnight. Then the mixture was extracted with EtOAc (3 x 40 mL), dried over $MgSO_4$, filtered, and concentrated under reduced pressure. The resulting crude product was purified by column chromatography (*n*-hexane/EtOAc 30:1 to 10:1) to provide **2c**, 1.73 g (51% yield) as a yellowish oil. **^{1}H NMR** (500 MHz, $CDCl_3$) δ 3.44 (t, *J* = 7.4 Hz, 1H), 1.84 (q, *J* = 7.5 Hz, 2H), 1.52 – 1.39 (m, 2H), 1.28 (s, 12H), 0.56 – 0.43 (m, 2H), -0.02 (s, 9H) ppm. **^{13}C NMR** (126 MHz, $CDCl_3$) δ 84.5, 37.9, 24.8, 24.7, 23.8, 16.3, -1.6 ppm. **IR** (neat, cm^{-1}): 2979, 2953, 2932, 2874, 1479, 1457, 1414, 1381, 1373, 1338, 1297, 1259, 1248, 1216, 1167, 1141, 1005. **HRMS**: m/z calcd. for ($C_{13}H_{28}BrNaO_2Si^{11}B$) $[M+Na]^+$: 357.1027 found 357.1026.

Synthesis of $(L1)_2Ni$

In the glovebox, $(pyridine)_2Ni(CH_2TMS)_2$ (41 mg, 0.10 mmol) was added to a 10 mL vial. A stirring bar was added and charged with 1 mL of cold THF (-36 ºC) and **L1** (40 mg, 0.22 mmol) where a white precipitate is immediately formed. The white suspension was then

filtered and washed with 0.5 mL x 3 cold pentane (-36 ºC) to afford (**L1**)$_2$Ni (19 mg, 43 % yield) as a white powder.

An alternative synthesis by deprotonating **L1** (2.0 equiv.) with NaH (2.0 equiv.) in THF and then adding $NiBr_2$(DME) (1.0 equiv.) also gives the desired product but the NaBr generated is challenging to separate from (**L1**)$_2$Ni.

^{1}H NMR (500 MHz, DMSO-d_6) δ 101.6 (broad s), 54.6 (broad s), 46.3 (broad s), 45.1 (broad s), 21.0 (broad s), 12.3 (broad s), -8.3 (broad s). **^{13}C NMR** omitted due to line broadening of paramagnetic (**L1**)$_2$Ni. Diamagnetic (δ 12-0 ppm) NMR of (**L1**)$_2$Ni has no signals corresponding to the free ligand **L1**.

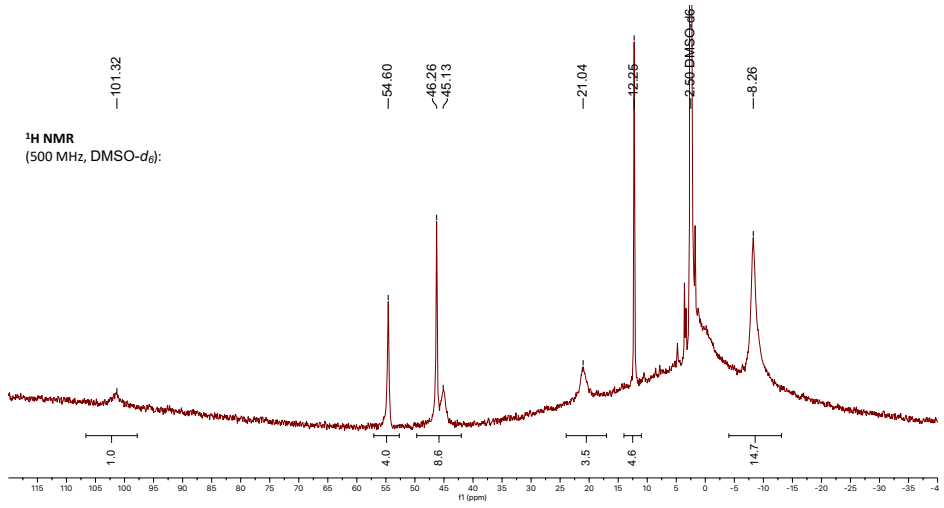

3.5.4. General procedure for Ni-catalysed 1,1-difunctionalisation with α-bromoboronates

General procedure B (Schemes XX -XX): An oven-dried 8 mL screw-cap test tube containing a stirring bar was charged with $NiBr_4 \cdot TBA_2$ (17.3 mg, 10 mol%), *N*-benzyl-6-methylpicolinamide (**L1**, 3.6 mg, 10 mol%), B_2Pin_2 (**3a,** 86.3 mg, 0.34 mmol). Subsequently, the tube was put into the glovebox under N_2 atmosphere, and *tBuOLi* (0.4 mmol, 32.0 mg) was added in the glovebox. Then the tube was sealed with a Teflon-lined screw cap and taken outside from the glovebox. Afterwards, the corresponding olefin (**1**, 0.20 mmol, 1.0 equiv.), α-Bromo boronic acid pinacol ester (**2**, 0.34 mmol, 1.7 equiv.), *t*-BuOH (0.80 mmol, 76 μL, 4.0 equiv.) and DME (0.5 mL) were added via syringe, independently. Then, the tube was stirred at 30 ℃ for 30 min. After the reaction was completed, the mixture was diluted with EtOAc, filtered through silica gel and concentrated under vacuum. The corresponding products **4a**–**4u** were purified by flash column chromatography on silica gel.

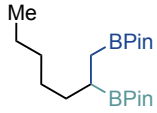

2,2'-(heptane-1,2-diyl)bis(4,4,5,5-tetramethyl-1,3,2-dioxaborolane) (**4a**): Following the **general procedure B**, using 1-hexene (**1a**, 25 μL, 0.20 mmol), the crude was purified by flash column chromatography (pentane/EtOAc 50:1 to 25:1), to afford **4a** (49 mg, 70% yield) as a colourless oil. In an independent experiment, 53 mg (76% yield) were obtained, giving an average of 73% yield. **^{1}H NMR** (500 MHz, $CDCl_3$): δ 1.46 – 1.39 (m, 1H), 1.35 – 1.25 (m, 7H), 1.22 (s, 12H), 1.22 (s, 12H), 1.13 – 1.07 (m, 1H), 0.88 – 0.76 (m, 5H) ppm. **^{13}C NMR** (126 MHz, $CDCl_3$): δ 82.93, 82.86, 33.9, 32.2, 28.7, 25.1, 25.0, 24.92, 24.89, 22.8, 14.2 ppm. **IR** (neat, cm^{-1}): 2977, 2925, 2856, 1467, 1369, 1310, 1267, 1215, 1140, 1007. **HRMS:** m/z calcd**.** for ($C_{19}H_{38}NaO_4{}^{11}B_2$) $[M+Na]^+$: 375.2853 found 375.2848.

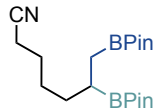

6,7-bis(4,4,5,5-tetramethyl-1,3,2-dioxaborolan-2-yl)heptanenitrile (**4b**): Following the **general procedure B**, using hex-5-enenitrile (**1b**, 19.0 mg, 0.20 mmol), the crude was purified by flash column chromatography (*n*-hexane/EtOAc 10:1 to 5:1), to afford **4b** (44 mg, 60% yield) as a colourless oil. In an independent experiment, 43 mg (59% yield) were obtained, giving an average of 59% yield. **^{1}H NMR** (400 MHz, $CDCl_3$): δ 2.31 (t, *J* = 7.2 Hz, 2H), 1.68 – 1.60 (m, 2H), 1.52 – 1.41 (m, 3H), 1.39 – 1.31 (m, 1H), 1.23 (s, 12H), 1.22 (s, 12H), 1.15 – 1.06 (m, 1H), 0.92 – 0.75 (m, 2H) ppm. **^{13}C NMR** (101 MHz, $CDCl_3$): δ 120.0,

83.1, 83.0, 32.8, 28.0, 25.7, 25.03, 24.99, 24.93, 24.88, 17.1 ppm. **IR** (neat, cm^{-1}): 2978, 2930, 2867, 1460, 1370, 1312, 1269, 1214, 1140, 967. **HRMS:** m/z calcd. for ($C_{19}H_{35}NNa^{11}O_4B_2$) $[M+Na]^+$: 386.2644 found 386.2637.

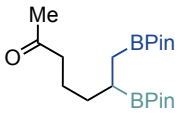

6,7-bis(4,4,5,5-tetramethyl-1,3,2-dioxaborolan-2-yl)heptan-2-one (**4c**): Following the **general procedure B**, using hex-5-en-2-one (**1c**, 19.6 mg, 0.20 mmol), the crude was purified by flash column chromatography (*n*-hexane/EtOAc 10:1 to 5:1), to afford **4c** (51 mg, 70% yield) as a colourless oil. In an independent experiment, 49 mg (67% yield) were obtained, giving an average of 68% yield. **^{1}H NMR** (500 MHz, $CDCl_3$): 2.40 – 2.37 (m, 2H), 2.09 (s, 3H), 1.59 – 1.53 (m, 2H), 1.25 – 1.22 (m, 6H), 1.20 (s, 24H), 0.81 (d, *J* = 6.8 Hz, 2H) ppm. **^{13}C NMR** (101 MHz, $CDCl_3$): δ 209.7, 83.0 (2C), 42.0, 32.7, 30.4, 29.8, 25.0, 24.9, 24.85, 24.7 ppm. **IR** (neat, cm^{-1}): 2978, 2928, 2856, 1715, 1451, 1368, 1313, 1272, 1214, 1141, 967. **HRMS:** m/z calcd. for ($C_{19}H_{36}NaO_5{}^{11}B_2$) $[M+Na]^+$: 389.2641 found 389.2645.

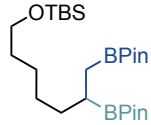

((6,7-bis(4,4,5,5-tetramethyl-1,3,2-dioxaborolan-2-yl)heptyl)oxy)(tert-butyl)dimethylsilane (**4d**): Following the **general procedure B**, using tert-butyl(hex-5-en-1-yloxy)dimethylsilane (**1d**, 43 mg, 0.20 mmol), the crude was purified by flash column chromatography (*n*-hexane/EtOAc 100:1 to 100:5), to afford **4d** (63 mg, 65% yield) as a colourless oil. In an independent experiment, 68 mg (70% yield) were obtained, giving an average of 68% yield. **^{1}H NMR** (400 MHz, CDCl3) δ 3.57 (t, *J* = 6.7 Hz, 2H), 1.52 – 1.25 (m, 10H), 1.22 (s, 12H), 1.22 (s, 12H), 1.13 –1.06 (m, 1H), 0.88 (s, 9H), 0.03 (s, 6H) ppm. **^{13}C NMR** (101 MHz, $CDCl_3$): δ 82.94, 82.88, 63.5, 34.0, 33.1, 28.9, 26.1, 25.05, 24.98, 24.96, 24.92, 24.89, 18.5, -5.1 ppm. **IR** (neat, cm^{-1}): 2977, 2953, 2928, 2856, 1470, 1463, 1406, 1370, 1311, 1255, 1214, 1142, 1099, 1038, 1006, 968. **HRMS:** m/z calcd. for ($C_{25}H_{52}NaO_5Si^{11}B_2$) $[M+Na]^+$:505.3662 found 505.3657.

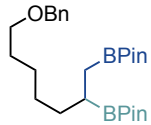

6,7-bis(4,4,5,5-tetramethyl-1,3,2-dioxaborolan-2-yl)heptan-2-one (**4e**): Following the **general procedure B**, using ((hex-5-en-1-yloxy)methyl)benzene (**1e**, 38.0 mg, 0.20 mmol), the crude was purified by flash column chromatography (*n*-hexane/EtOAc 30:1 to 15:1), to

afford **4e** (60 mg, 66% yield) as a colourless oil. In an independent experiment, 59 mg (64% yield) were obtained, giving an average of 65% yield. **^{1}H NMR** (400 MHz, $CDCl_3$): δ 7.33 – 7.32 (m, 4H), 7.28 – 7.23 (m, 1H), 4.48 (s, 2H), 3.44 (t, *J* = 6.7 Hz, 2H), 1.63 – 1.56 (m, 2H), 1.49 – 1.42 (m, 1H), 1.35 – 1.28 (m, 5H), 1.22 (s, 24H), 1.13 – 1.08 (m, 1H), 0.87 – 0.79 (m, 2H) ppm. **^{13}C NMR** (101 MHz, $CDCl_3$): δ 138.8, 128.4, 127.7, 127.5, 82.9, 82.8, 72.9, 70.7, 33.8, 29.9, 28.8, 26.5, 25.0, 24.95, 24.89, 24.8 ppm. **IR** (neat, cm^{-1}): 3401, 2978, 2931, 2860, 1720, 1706, 1449, 1370, 1315, 1271, 1142, 967. **HRMS:** m/z calcd. for ($C_{26}H_{44}NaO_5{}^{10}B^{11}B$) $[M+Na]^+$: 480.3303 found 480.3298.

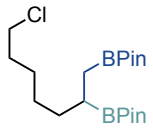

2,2'-(7-chloroheptane-1,2-diyl)bis(4,4,5,5-tetramethyl-1,3,2-dioxaborolane) (**4f**): Following the **general procedure B**, using 6-chloro-1-hexene (**1f**, 23.6 mg, 0.20 mmol), the crude was purified by flash column chromatography (*n*-hexane/EtOAc 30:1), to afford **4f** (50 mg, 65% yield) as a colourless oil. In an independent experiment, 50 mg (65% yield) were obtained, giving an average of 65% yield. **^{1}H NMR** (400 MHz, $CDCl_3$): δ 3.50 (t, *J* = 6.9 Hz, 2H), 1.78 – 1.71 (m, 2H), 1.49 – 1.27 (m, 6H), 1.22 (s, 12H), 1.21 (s, 12H), 1.13 – 1.06 (m, 1H), 0.89 – 0.74 (m, 2H) ppm. **^{13}C NMR** (101 MHz, $CDCl_3$): δ 83.0, 82.9, 45.2, 33.6, 32.7, 28.2, 27.2, 25.04, 24.98, 24.92, 24.89 ppm. **IR** (neat, cm^{-1}): 2977, 2929, 2857, 1369, 1310, 1272, 1214, 1140, 967. **HRMS:** m/z calcd. for ($C_{19}H_{37}NaO_4{}^{10}B^{11}BCl$) $[M+Na]^+$: 408.2495 found 408.2496.

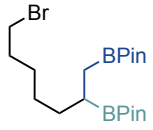

2,2'-(7-bromoheptane-1,2-diyl)bis(4,4,5,5-tetramethyl-1,3,2-dioxaborolane) (**4g**): Following the **general procedure B**, using 6-bromo-1-hexene (**1g**, 32.4 mg, 0.20 mmol), the crude was purified by flash column chromatography (*n*-hexane/EtOAc 30:1), to afford **4g** (64 mg, 75% yield) as a colourless oil. In an independent experiment, 63 mg (73% yield) were obtained, giving an average of 74% yield. **^{1}H NMR** (500 MHz, $CDCl_3$): δ 3.39 (t, *J* = 7.0 Hz, 2H), 1.87 – 1.81 (m, 2H), 1.48 – 1.38 (m, 3H), 1.35 – 1.28 (m, 3H), 1.23 (s, 12H), 1.23 (s, 12H), 1.14 – 1.08 (m, 1H), 0.89 – 0.76 (m, 2H) ppm. **^{13}C NMR** (101 MHz, $CDCl_3$): δ 83.00, 82.96, 34.2, 33.6, 32.9, 28.5, 28.1, 25.1, 25.0, 24.94, 24.90 ppm. **IR** (neat, cm^{-1}): 2977, 2927, 2856, 1461, 1369, 1311, 1270, 1246, 1214, 1140, 1109, 1067. **HRMS:** m/z calcd. for ($C_{19}H_{37}{}^{10}B^{11}BBrO_4$) $[M]^+$: 430.2061 found 430.2170.

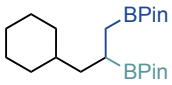

2,2'-(3-cyclohexylpropane-1,2-diyl)bis(4,4,5,5-tetramethyl-1,3,2-dioxaborolane) (**4h**): Following the **general procedure B**, using vinylcyclohexane (**1h,** 27 μL, 0.2 mmol), the crude was purified by flash column chromatography (*n*-hexane/EtOAc 99:1-95:5), to afford **4h** (55 mg, 73% yield) as a colourless oil. In an independent experiment, 54 mg (72% yield) were obtained, giving an average of 73% yield. **^{1}H NMR** (400 MHz, CDCl3) δ 1.73 – 1.58 (m, 6H), 1.38 – 1.31 (m, 4H), 1.22 (s, 12H), 1.22 (s, 12H), 1.17 – 1.06 (m, 4H), 0.84 – 0.75 (m, 2H) ppm. **^{13}C NMR** (101 MHz, $CDCl_3$): δ 82.9, 82.8, 41.6, 36.6, 33.7, 33.5, 26.9, 26.63, 26.61, 25.1, 24.93 (2C), 24.92 ppm. **IR** (neat, cm^{-1}): 2977, 2920, 2850, 1480, 1448, 1405, 1369, 1310, 1269, 1214, 1141, 1108, 1005, 967. **HRMS:** m/z calcd. for ($C_{21}H_{40}NaO_4{}^{11}B_2$) $[M+Na]^+$: 401.3005 found 401.3017.

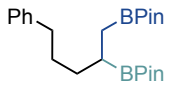

2,2'-(5-phenylpentane-1,2-diyl)bis(4,4,5,5-tetramethyl-1,3,2-dioxaborolane) (**4i**): Following the **general procedure B**, using 4-phenyl-1-butene (**1i**, 26.4 mg, 0.20 mmol), the crude was purified by flash column chromatography (*n*-hexane/EtOAc 50:1 to 25:1), to afford **4i** (50 mg, 63% yield) as a colourless oil. In an independent experiment, 52 mg (65% yield) were obtained, giving an average of 64% yield. **^{1}H NMR** (400 MHz, $CDCl_3$): δ 7.27 – 7.23 (m, 2H), 7.19 – 7.12 (m, 3H), 2.61 – 2.57 (m, 2H), 1.68 – 1.60 (m, 2H), 1.57 – 1.48 (m, 1H), 1.43 – 1.34 (m, 1H), 1.23 (s, 12H), 1.21 (s, 12H), 0.93 – 0.77 (m, 3H) ppm. **^{13}C NMR** (101 MHz, $CDCl_3$) δ 143.2, 128.5, 128.3, 125.5, 82.94, 82.92, 36.3, 33.6, 30.8, 25.01, 24.98, 24.89, 24.88 ppm. **IR** (neat, cm^{-1}): 3026, 2977, 2927, 2856, 1496, 1454, 1370, 1312, 1269, 1214, 1140, 1170, 1079, 1030, 1008, 968. **HRMS:** m/z calcd. for ($C_{23}H_{38}B_2O_4$) $[M]^+$: 400.2956 found 400.3065.

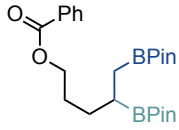

4,5-bis(4,4,5,5-tetramethyl-1,3,2-dioxaborolan-2-yl)pentyl benzoate (**4j**): Following the **general procedure B**, using but-3-en-1-yl benzoate (**1j**, 35.2 mg, 0.20 mmol), the crude purified by flash column chromatography (*n*-hexane/EtOAc 10:1 to 3:1), to afford **4j** (53 mg, 60% yield) as a colourless oil. In an independent experiment, 57 mg (64% yield) were obtained, giving an average of 62% yield. **^{1}H NMR** (400 MHz, $CDCl_3$): δ 8.13 – 7.95 (m, 2H), 7.54 (ddt, *J* = 8.0, 6.8, 1.4 Hz, 1H), 7.45 – 7.39 (m, 2H), 4.29 (t, *J* = 6.6 Hz, 2H), 1.81 – 1.74 (m, 2H), 1.69 – 1.56 (m, 2H), 1.54 – 1.44 (m, 1H) 1.23 (s, 12H), 1.22 (s, 12H), 0.95 – 0.80

(m, 2H) ppm. **^{13}C NMR** (101 MHz, $CDCl_3$): δ 166.8, 132.8, 130.8, 129.7, 128.4, 83.1, 83.0, 65.6, 30.2, 28.2, 25.03, 25.01, 24.93, 24.88 ppm. **IR** (neat, cm^{-1}): 2977, 2929, 1719, 1452, 1370, 1313, 1270, 1215, 1140, 1111, 1070, 1027, 1006, 968. **HRMS:** m/z calcd. for ($C_{24}H_{38}B_2O_6$) $[M]^+$: 444.2854 found 444.2964.

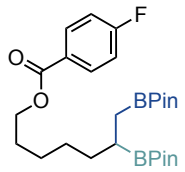

6,7-bis(4,4,5,5-tetramethyl-1,3,2-dioxaborolan-2-yl)heptyl 4-fluorobenzoate (**4k**): Following the **general procedure B**, using hex-5-en-1-yl 4-fluorobenzoate (**1k**, 45 mg, 0.20 mmol), the crude was purified by flash column chromatography (*n*-hexane/EtOAc 100:1 to 10:1), to afford **4k** (63 mg, 64% yield) as a colourless oil. In an independent experiment, 66 mg (67% yield) were obtained, giving an average of 66% yield. **^{1}H NMR** (400 MHz, $CDCl_3$): δ 8.07 – 8.02 (m, 2H), 7.12 – 7.06 (m, 2H), 4.28 (t, *J* = 6.7 Hz, 2H), 1.77 – 1.70 (m, 2H), 1.51 – 1.31 (m, 6H), 1.22 (s, 24H), 1.16 – 1.06 (m, 1H), 0.90 – 0.76 (m, 2H) ppm. **^{13}C NMR** (101 MHz, $CDCl_3$): 165.83, 165.81 (d, *J* = 253.2 Hz), 132.2 (d, *J* = 9.1 Hz), 127.0 (d, *J* = 3.3 Hz), 115.5 (d, *J* = 22.0 Hz), 83.0, 82.9, 65.4, 33.7, 28.8, 28.6, 26.4, 25.04, 24.98, 24.92, 24.88 ppm. **IR** (neat, cm^{-1}): 2997, 2927, 2856, 1720, 1604, 1508, 1465, 1410, 1370, 311, 1269, 1238, 1215, 1141, 1112, 1090, 1015, 968. **HRMS:** m/z calcd. for ($C_{26}H_{41}FNaO_6{}^{10}B^{11}B$) $[M+Na]^+$: 512.3002 found 512.3001.

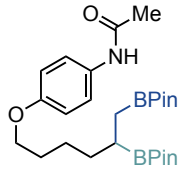

***N*-(4-((5,6-bis(4,4,5,5-tetramethyl-1,3,2-dioxaborolan-2-yl)hexyl)oxy)phenyl) acetamide** (**4l**): Following the **general procedure B**, using *N*-(4-(pent-4-en-1-yloxy)phenyl)acetamide (**1l**, 43.8 mg, 0.20 mmol), the crude was purified by flash column chromatography (*n*-hexane/EtOAc 1:1 to 1:2), to afford **4l** (49 mg, 50% yield) as a light yellow oil. In an independent experiment, 49 mg (50% yield) were obtained, giving an average of 50% yield. **^{1}H NMR** (400 MHz, $CDCl_3$): δ 7.64 (brs, 1H), 7.37 – 7.33 (m, 2H), 6.82 – 6.67 (m, 2H), 3.87 (t, *J* = 6.6 Hz, 2H), 2.10 (s, 3H), 1.75 – 1.68 (m, 2H), 1.53 – 1.33 (m, 4H), 1.21 (s, 12H), 1.20 (s, 12H), 1.15 – 1.09 (m, 1H), 0.90 – 0.77 (m, 2H) ppm. **^{13}C NMR** (101 MHz, $CDCl_3$): δ 168.3, 157.8, 156.2, 130.8, 121.9, 114.9, 83.00, 82.98, 68.4, 33.6, 29.6, 25.4, 25.04, 24.99, 24.92, 24.88, 24.5 ppm. **IR** (neat, cm^{-1}): 3299, 2977, 2931, 2868, 1663, 1604, 1543, 1510, 1472,

1457, 1411, 1370, 1312, 1269, 1240, 1166, 1141, 1111, 1037, 1008, 967. **HRMS:** m/z calcd. for ($C_{26}H_{43}B_2NO_6$) $[M]^+$: 487.3276 found 487.3386.

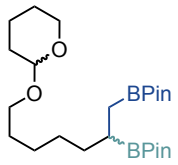

2,2'-(7-((tetrahydro-2H-pyran-2-yl)oxy)heptane-1,2-diyl)bis(4,4,5,5-tetramethyl-1,3,2-dioxaborolane) (**4m**): Following the **general procedure B**, using 2-(hex-5-en-1-yloxy)tetrahydro-2H-pyran (**1m**, 36.8 mg, 0.20 mmol), the crude was purified by flash column chromatography (*n*-hexane/EtOAc 50:1 to 25:1), to afford **4m** (73 mg, 81% yield) as a light yellow oil. In an independent experiment, 73mg (81% yield) were obtained, giving an average of 81% yield, as a 1:1 mixture of diastereoisomers, determined by ^{1}H NMR and ^{13}C NMR. **^{1}H NMR** (400 MHz, $CDCl_3$):δ 4.56 – 4.54 (m, 1H), 3.88 – 3.82 (m, 1H), 3.73 – 3.67 (m, 1H), 3.50 – 3.45 (m, 1H), 3.35 (dt, *J* = 9.5, 6.7 Hz, 1H), 1.85 – 1.77 (m, 1H), 1.73 – 1.66 (m, 1H), 1.60 – 1.47 (m, 6H), 1.37 – 1.27 (m, 6H), 1.22 (s, 12H), 1.21 (s, 12H), 1.12 – 1.06 (m, 1H), 0.89 – 0.75 (m, 2H) ppm. **^{13}C NMR** (126 MHz, $CDCl_3$): δ 98.88, 98.87, 82.91, 82.85, 67.79, 67.78, 62.3, 33.9, 30.9, 29.9, 28.9, 26.6, 25.6, 25.02, 24.96, 24.89, 24.86, 19.8 ppm. **IR** (neat, cm^{-1}): 2977, 2928, 2856, 1456, 1369, 1353, 1311, 1270, 1214, 1201, 1185, 1139, 1077, 1033, 1023, 968. **HRMS:** m/z calcd. for ($C_{24}H_{46}B_2NaO_6$) $[M+Na]^+$: 475.3378 found 475.3373.

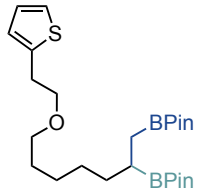

2,2'-(7-(2-(thiophen-2-yl)ethoxy)heptane-1,2-diyl)bis(4,4,5,5-tetramethyl-1,3,2-dioxaborolane) (**4n**): Following the **general procedure B**, using 2-(2-(hex-5-en-1-yloxy)ethyl)thiophene (**1n**, 42 mg, 0.20 mmol), the crude was purified by flash column chromatography (*n*-hexane/EtOAc 40:1 to 20:1), to afford **4n** (73 mg, 76% yield) as a light yellow oil. In an independent experiment, 74 mg (77% yield) were obtained, giving an average of 76% yield. **^{1}H NMR** (500 MHz, $CDCl_3$): δ 7.12 (dd, *J* = 5.1, 1.2 Hz, 1H), 6.92 (dd, *J* = 5.1, 3.4 Hz, 1H), 6.84 – 6.83 (m, 1H), 3.63 (t, *J* = 6.9 Hz, 2H), 3.43 (t, *J* = 6.8 Hz, 2H), 3.08 (td, *J* = 6.9, 0.6 Hz, 2H), 1.60 – 1.54 (m, 2H), 1.48 – 1.43 (m, 1H), 1.35 – 1.29 (m, 5H), 1.22 (s, 12H), 1.22 (s, 12H), 1.15 – 1.08 (m, 1H), 0.89 – 0.77 (m, 2H) ppm. **^{13}C NMR** (101 MHz, $CDCl_3$): δ 141.6, 126.7, 125.1, 123.7, 82.93, 82.88, 71.5, 71.3, 33.9, 30.6, 29.8, 28.8, 26.5, 25.04, 24.98, 24.91, 24.88 ppm. **IR** (neat, cm^{-1}): 2977, 2927, 2856, 1463, 1369, 1311, 1271, 1214, 1140, 968. **HRMS:** m/z calcd. for ($C_{25}H_{44}B_2NaO_5S$) $[M+Na]^+$: 501.2993 found 501.2988.

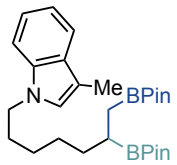

1-(6,7-bis(4,4,5,5-tetramethyl-1,3,2-dioxaborolan-2-yl)heptyl)-3-methyl-1H-indole (**4o**): Following the **general procedure B**, using 1-(hex-5-en-1-yl)-3-methyl-1H-indole (**1o**, 42.6 mg, 0.20 mmol), the crude was purified by flash column chromatography (*n*-hexane/EtOAc 20:1 to 10:1), to afford **4o** (65 mg, 67% yield) as a light yellow oil. In an independent experiment, 66 mg (69% yield) were obtained, giving an average of 68% yield. **^{1}H NMR** (400 MHz, $CDCl_3$): δ 7.57 (d, *J* = 7.9 Hz, 1H), 7.301 – 7.29 (m, 1H), 7.21 – 7.17 (m, 1H), 7.11 – 7.07 (m, 1H), 6.87 (br s, 1H), 4.04 (t, *J* = 7.2 Hz, 2H), 2.34 (d, *J* = 1.0 Hz, 3H), 1.84 – 1.76 (m, 2H), 1.50 – 1.43 (m, 1H), 1.37 – 1.31 (m, 5H), 1.24 (s, 24H), 1.15 – 1.09 (m, 1H), 0.90 – 0.80 (m, 2H) ppm. **^{13}C NMR** (101 MHz, $CDCl_3$): δ 136.4, 128.8, 125.6, 121.3, 119.0, 118.4, 110.0, 109.3, 82.95, 82.91, 46.1, 33.7, 30.4, 28.6, 27.3, 25.03, 24.98, 24.91, 24.88, 9.7 ppm. **IR** (neat, cm^{-1}): 2976, 2926, 2856, 1481, 1467, 1369, 1311, 1268, 1237, 1214, 1164, 1140, 1111, 968. **HRMS:** m/z calcd. for ($C_{28}H_{45}B_2NO_4$) $[M]^+$: 481.3535 found 481.3644.

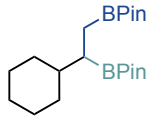

2,2'-(1-cyclohexylethane-1,2-diyl)bis(4,4,5,5-tetramethyl-1,3,2-dioxaborolane) (**4p**): Following the **general procedure B**, using methylenecyclohexane (**1p**, 25 μL, 0.2 mmol), the crude was purified by flash column chromatography (*n*-hexane/Et_2O 100:5), to afford **4p** (32 mg, 45% yield) as a colourless oil. In an independent experiment, 29 mg (40% yield) were obtained, giving an average of 43% yield. **^{1}H NMR** (400 MHz, $CDCl_3$): δ 1.68 – 1.65 (m, 4H), 1.42 – 1.30 (m, 2H), 1.23 (s, 12H) 1.21 (s, 12H), 1.10 – 0.73 (m, 8H) ppm. **^{13}C NMR** (101 MHz, $CDCl_3$): δ 82.90, 82.87, 41.6, 32.3, 32.1, 27.04, 27.00, 26.9, 25.11, 25.09, 25.01, 24.8 ppm. **IR** (neat, cm^{-1}): 2977, 2922, 2851, 1480, 1466, 1448, 1403, 1369, 1309, 127, 1238, 1214, 1141, 1105, 969. **HRMS:** m/z calcd. for ($C_{20}H_{38}NaO_4{}^{11}B_2$) $[M+Na]^+$: 387.2848 found 387.2846.

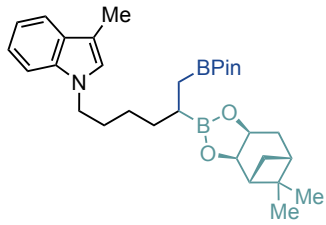

3-methyl-1-(6-(4,4,5,5-tetramethyl-1,3,2-dioxaborolan-2-yl)-5-((3a*S*,4*S*,6*S*,7a*R*)-3a,5,5-trimethylhexahydro-4,6-methanobenzo[*d*][1,3,2]dioxaborol-2-yl)hexyl)-1*H*-indole (**4q**): Following the **general procedure B**, using 3-methyl-1-(pent-4-en-1-yl)-1*H*-indole (**1q**, 40.0 mg, 0.20 mmol) and bis[(1R,2R,3S,5R)-pinanediolato]diboron (**3b**, 121.8 mg, 0.34 mmol), the mixture was purified by flash column chromatography (*n*-hexane/EtOAc 30:1), to afford **4q** (57.5 mg, 55% yield) as a colourless oil. In an independent experiment, 56.2 mg (54% yield) were obtained, giving an average of 54% yield, dr = 1:1, determined by SFC, IG-3 column (3µm, 3×10 mm), CO_2 / MeOH = 7.5% MeOH, 1.2 mL/min, λ = 230 nm, t_1 = 1.801 min, t_2 = 1.91 min. **^{1}H NMR** (400 MHz, $CDCl_3$): δ 7.55 (dt, *J* = 7.9, 1.0 Hz, 1H), 7.29 (m, 1H), 7.20 – 7.16 (m, 1H), 7.10 – 7.06 (m, 1H), 6.87 – 7.86 (m, 1H), 4.19 (td, *J* = 8.6, 2.1 Hz, 1H), 4.04 (t, *J* = 7.1 Hz, 2H), 2.32 (d, *J* = 1.1 Hz, 3H), 2.14 – 2.06 (m, 1H), 2.04 – 1.99 (m, 1H), 1.89 – 1.73 (m, 4H), 1.57 – 1.47 (m, 1H), 1.42 – 1.35 (m, 2H), 1.32 – 1.31 (m, 2H), 1.29 – 1.28 (m, 3H), 1.24 (s, 3H), 1.23 (s, 12H), 1.19 – 1.11 (m, 2H), 0.95 – 0.87 (m, 2H), 0.84 – 0.83 (m, 3H). **^{13}C NMR** (126 MHz, $CDCl_3$) δ. 136.4, 128.8, 125.6, 121.2, 119.0, 118.4, 109.9, 109.3, 85.4, 83.0, 77.62, 77.60, 51.4, 46.1, 39.63, 39.62, 38.3, 38.2, 35.7, 35.6, 33.8, 33.5, 30.7, 30.6, 28.76, 28.75, 27.2, 26.6, 26.50, 26.46, 26.43, 25.1, 25.0, 24.94, 24.88, 24.1, 9.73, 9.71. **IR** (neat, cm^{-1}):2976, 2918, 2869, 1468, 1453, 1364, 1340, 1315, 1278, 1237, 1209, 1164, 1143, 1123, 1078, 1055, 1030, 1014. **HRMS: m/z calcd.** for ($C_{31}H_{48}{}^{11}B^{10}BNO_4$) $[M+H]^+$: 519.3800 found 519.3809.

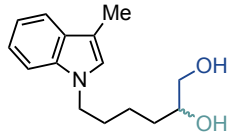

6-(3-methyl-1*H*-indol-1-yl)hexane-1,2-diol (**4q'**): 3-methyl-1-(6-(4,4,5,5-tetramethyl-1,3,2-dioxaborolan-2-yl)-5-((3a*S*,4*S*,6*S*,7a*R*)-3a,5,5-trimethylhexahydro-4,6-methanobenzo[*d*][1,3,2]dioxaborol-2-yl)hexyl)-1*H*-indole (**4q**, 57.1 mg, 0.11 mmol) was dissolved in THF and H_2O (1:1, 10 mL), and $NaBO_3{\cdot}H_2O$ (169 mg, 1.0 mmol, 10.0 equiv) was added. The reaction mixture was stirred at room temperature for 4 h. After the reaction was completed, water (20 mL) was added. The aqueous phase was extracted with EtOAc (3 x 20 mL), and the combined organic phases were dried over anhydrous Na_2SO_4 and concentrated. The corresponding product **4q'** was purified by column chromatography on silica gel (*n*-hexane/EtOAc 1:1 to 0:1), affording light pink oil 19.4 mg (70% yield), 0% ee,

determined by SFC, Chiralpak IG-3 column (3µm, 3×10 mm), CO_2 / MeOH = 5-40% MeOH, 1.2 mL/min, λ = 230 nm, t_1 = 3.063 min, t_2 = 3.214 min. **^{1}H NMR** (400 MHz, $CDCl_3$) δ 7.57 (d, *J* = 7.9 Hz, 1H), 7.29 (d, *J* = 8.2 Hz, 1H), 7.22 – 7.18 (m, 1H), 7.12 – 7.08 (m, 1H), 6.86 (d, *J* = 1.2 Hz, 1H), 4.07 (t, *J* = 7.0 Hz, 2H), 3.65 – 3.55 (m, 2H), 3.46 – 3.38 (m, 1H), 2.33 (d, *J* = 1.0 Hz, 3H), 1.88 – 1.80 (m, 2H), 1.50 – 1.35 (m, 4H) ppm. **^{13}C NMR** (126 MHz, $CDCl_3$) δ 136.4, 128.8, 125.6, 121.4, 119.2, 118.6, 110.3, 109.2, 72.1, 66.8, 46.0, 32.8, 30.5, 23.2, 9.7 ppm. **IR** (neat, cm^{-1}): 3376, 3050, 2928, 2862, 1736, 1614, 1481, 1467, 1453, 1385, 1360, 1331, 1284, 1239, 1198, 1166, 1125, 1045. **HRMS:** m/z calcd. for ($C_{15}H_{21}NO_2Na$) $[M+Na]^+$: 270.1465 found 270.1472.

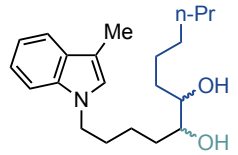

1-(3-methyl-1*H*-indol-1-yl)tridecane-6,7-diol (**4r**): Following the **general procedure B**, using 3-methyl-1-(pent-4-en-1-yl)-1*H*-indole (**1q**, 40.0 mg, 0.20 mmol) and 2-(1-bromoheptyl)-4,4,5,5-tetramethyl-1,3,2-dioxaborolane (**2b**, 183 mg, 0.6 mmol). After the reaction was completed, the mixture was filtered through a short silica plug (*n*-hexane/EtOAc 50:1) and concentrated under vacuum. Then the residue was dissolved in THF and H_2O (1:1, 4 mL), and $NaBO_3 \cdot H_2O$ (100 mg, 1.0 mmol, 5.0 equiv.) was added. The reaction mixture was stirred at room temperature for 4 h. After the reaction was completed, water (15 mL) was added. The aqueous phase was extracted with EtOAc (3 x 15 mL), and the combined organic phases were dried over $MgSO_4$ and concentrated. The corresponding product **4r** was purified by column chromatography on silica gel (Hexane/EtOAc 4:1 to 1:1), affording light yellow oil 26 mg (39% yield). In an independent experiment, 24 mg (36% yield) were obtained, giving an average of 37% yield, dr = 1:1, determined by SFC, Chiralpak IG (4.6mm x 150mm, 3µm) analytical chiral column using CO_2 / IPA = 73 : 27. **^{1}H NMR** (400 MHz, $CDCl_3$): δ 7.57 – 7-55 (m, 1H), 7.30 – 7.28 (m, 1H), 7.21 – 7.17 (m, 1H), 7.11 – 7.07 (m, 1H), 6.87 – 6.86 (m, 1H), 4.08 (t, *J* = 7.0 Hz, 2H), 3.63 – 3.50 (m, 1H), 3.37 – 3.33 (m, 1H), 2.33 (d, *J* = 1.0 Hz, 3H), 1.92 – 1.80 (m, 4H), 1.60 – 1.25 (m, 12H), 0.90 – 0.87 (m, 3H) ppm. **^{13}C NMR** (101 MHz, $CDCl_3$) δ 136.4, 128.9, 125.6, 121.4, 119.2, 118.6, 110.3, 109.3, 74.8, 74.6, 74.5, 74.3, 46.1, 33.8, 33.4, 31.9, 31.5, 30.8, 30.5, 29.4, 26.1, 25.7, 23.7, 23.4, 22.7, 14.2, 9.7 ppm. **IR** (neat, cm^{-1}): 3273, 3054, 2924, 2854, 1709, 1665, 1614, 1560, 1467, 1363, 1333, 1232, 1163, 1082, 968. **HRMS:** m/z calcd. for ($C_{21}H_{33}NNaO_2$) $[M+Na]^+$: 354.2404 found 354.2389.

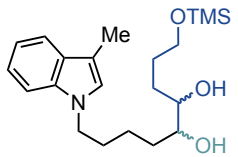

10-(3-methyl-1*H*-indol-1-yl)-1-(trimethylsilyl)decane-4,5-diol (**4s**): Following the **general procedure B**, using 3-methyl-1-(pent-4-en-1-yl)-1*H*-indole (**1q**, 40.0 mg, 0.20 mmol) and (4-bromo-4-(4,4,5,5-tetramethyl-1,3,2-dioxaborolan-2-yl)butyl) trimethylsilane (**2c**, 201 mg, 0.6 mmol). After the reaction was completed, the mixture was filtered through a short silica plug (Hexane/EtOAc 50:1) and concentrated under vacuum. Then the residue was dissolved in THF and H_2O (1:1, 4 mL), and $NaBO_3 \cdot H_2O$ (100 mg, 1.0 mmol, 5.0 equiv.) was added. The reaction mixture was stirred at room temperature for 4 h. After the reaction was completed, water (15 mL) was added. The aqueous phase was extracted with EtOAc (3 x 15 mL), and the combined organic phases were dried over $MgSO_4$ and concentrated. The corresponding product **4s** was purified by column chromatography on silica gel (*n*-hexane/EtOAc 4:1 to 1:1), affording light yellow oil 26 mg (39% yield). In an independent experiment, 27 mg (37% yield) were obtained, giving an average of 38% yield, as a 1:1 mixture of diastereoisomers, determined by SFC. **^{1}H NMR** (400 MHz, $CDCl_3$) δ 7.59 (d, *J* = 7.9 Hz, 1H), 7.32 – 7.29 (m, 1H), 7.24 – 7.18 (m, 1H), 7.15 – 7.09 (m, 1H), 6.89 – 6.87 (m, 1H), 4.12 – 4.06 (m, 2H), 3.85 – 3.74 (m, 1H), 3.61 – 3.50 and 3.39 – 3.32 (m, 1H), 3.36 (td, *J* = 7.6, 3.7 Hz, 0.5H), 2.35 (s, 3H), 1.91 – 1.82 (m, 2H), 1.60 – 1.30 (m, 10H), 0.98 – 0.87 (m, 1H), 0.61 – 0.44 (m, 1H), 0.02 (s, 9H) ppm. **^{13}C NMR** (101 MHz, $CDCl_3$) δ 136.3, 128.8, 125.5, 121.4, 119.1, 118.6, 110.2, 109.2, 74.6, 74.5, 74.4, 74.3, 46.1, 43.4, 37.6, 35.3, 33.3, 30.8, 30.5, 30.3, 29.9, 29.8, 23.7, 23.3, 20.6, 20.2, 16.8, 16.7, 9.7, -1.5 ppm. **IR** (neat, cm^{-1}): 3402, 3054, 2925, 2859, 1710, 1614, 1482, 1467, 1455, 1385, 1361, 1330, 1246, 1173, 1079, 921. **HRMS:** m/z calcd. for ($C_{21}H_{35}NNaO_2Si$) $[M+Na]^+$: 384.2329 found 384.2328.

Racemic dihydroxylation

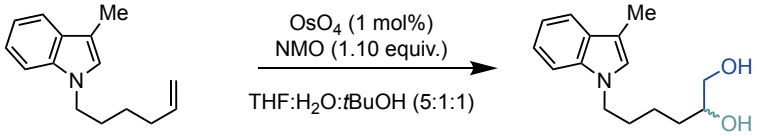

6-(3-methyl-1*H*-indol-1-yl)hexane-1,2-diol: The title compound was prepared according to a procedure reported in literature.[96] To a solution of 1-(hex-5-en-1-yl)-3-methyl-1H-indole (**1o**, 250 mg, 1.17 mmol) and 4-methylmorpholine *N*-oxide (151 mg, 1.29 mmol) in THF (8.5 mL), water (1.7 mL) and *tert*-butanol (1.7 mL) was added Osmiumtetraoxide (152 µL, 0.1 M in *tert*-butanol) at room temperature under stirring. After 24 hours, the reaction mixture was quenched with 10% aq Na_2SO_4 (20 mL) and extracted with 3 times with ethyl acetate (50 mL). The combined organic extracts were washed with Brine (50 mL), dried over anhydrous Na_2SO_4, and concentrated under reduced pressure to give a crude brown oil. The corresponding crude product was purified by column chromatography on silica gel (*n*-hexane/EtOAc 1:1 to 0:1), affording light pink oil, 116 mg (40% yield), 0% ee, determined by SFC, Chiralpak IG-3 column (3µm, 3×10 mm), CO_2 / MeOH = 5-40% MeOH, 1.2 mL/min, λ

= 230 nm, t_1 = 3.063 min, t_2 = 3.214 min. **^{1}H NMR** (400 MHz, $CDCl_3$) δ 7.57 – 7.55 (m, 1H), 7.30 – 7.27 (m, 1H), 7.21 – 7.17 (m, 1H), 7.11 – 7.07 (m, 1H), 6.86 (d, *J* = 1.2 Hz, 1H), 4.07 (t, *J* = 7.0 Hz, 2H), 3.72 – 3.59 (m, 2H), 3.42 – 3.37 (m, 1H), 2.32 (d, *J* = 1.1 Hz, 3H), 1.89 – 1.80 (m, 2H), 1.51 – 1.40 (m, 4H) ppm. **^{13}C NMR** (101 MHz, $CDCl_3$) δ 136.4, 128.9, 125.6, 121.4, 119.2, 118.6, 110.3, 109.2, 72.1, 66.9, 46.1, 32.9, 30.5, 23.2, 9.7 ppm. **IR** (neat, cm^{-1}): 3376, 3051, 2928, 2862, 1692, 1612, 1483, 1644, 1385, 1357, 1331, 1236, 1198, 1166, 1125, 1053, 1013.

Enantioselective dihydroxylation of Sharpless

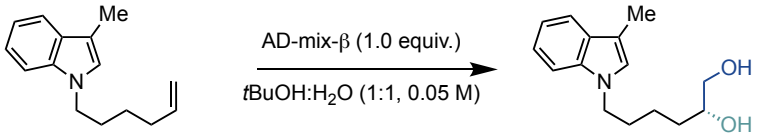

(*R*)-6-(3-methyl-1*H*-indol-1-yl)hexane-1,2-diol: The title compound was prepared according to a procedure reported in literature.[97] A stirred solution of AD-mix-β (1.65 g, 1.4 g/mmol of substrate) in a 1/1 mixture of *tert*-butanol (10 mL) and water (10 mL) was stirred for 10 min at 30 °C and then transferred to cooled bath at 4 ºC. After 15 min at 4 °C, 1-(hex-5-en-1-yl)-3-methyl-1H-indole (**1o**, 250 mg, 1.17 mmol) was added, and the reaction stirred overnight at 4 °C. After 16 hours, ethyl acetate (13 mL) was added and followed by careful addition of sodium metabisulfite (468 mg, 2.1 Eq, 2.46 mmol). The reaction was left for 1 hour at 4 °C and then treated with water (13 mL). The organic layer was separated and the aqueous extracted twice with ethyl acetate (5.0 mL). The combined organic phases were washed with water (5.0 mL) and brine (5.0 mL), dried over anhydrous Na_2SO_4, and concentrated under reduced pressure. The corresponding crude product was purified by column chromatography on silica gel (*n*-hexane/EtOAc 1:1 to 0:1), affording light pink oil, 167 mg (58% yield), 74% ee, determined by SFC, Chiralpak IG-3 column (3µm, 3×10 mm), CO_2 / MeOH = 5-40% MeOH, 1.2 mL/min, λ = 230 nm, t (minor) = 3.063 min, t (major) = 3.214 min. **^{1}H NMR** (400 MHz, $CDCl_3$) δ 7.59 – 7.56 (m, 1H), 7.30 – 7.28 (m, 1H), 7.22 – 7.18 (m, 1H), 7.12 – 7.08 (m, 1H), 6.86 – 6.85 (m, 1H), 4.06 (t, *J* = 7.0 Hz, 2H), 3.64 – 3.55 (m, 2H), 3.38 – 3.33 (m, 1H), 2.33 (d, *J* = 1.1 Hz, 3H), 1.87 – 1.78 (m, 2H), 1.51 – 1.30 (m, 4H) ppm. **^{13}C NMR** (101 MHz, $CDCl_3$) δ 136.4, 128.8, 125.5, 121.4, 119.2 118.6, 110.3, 109.2, 72.1, 66.8, 46.0, 32.8, 30.4, 23.2, 9.7 ppm. **IR** (neat, cm^{-1}): 3363, 3052, 2929, 2862, 1614, 1481, 1467, 1385, 1360, 1331, 1238, 1198, 1166, 1125, 1056, 1013.

3.5.5. General procedure for Ni-catalysed 1,1-difunctionalisation with a-bromosilanes

General procedure C (Scheme XX-XX): An oven-dried 8 mL screw-cap test tube containing a stirring bar was charged with $NiBr_4 \cdot TBA_2$ (17.3 mg, 10 mol%), 4-(*tert*-butyl)-*N*-(2-

hydroxyethyl)-6-methylpicolinamide (**L3**, 4.7 mg, 10 mol%), B_2Pin_2 (86.3 mg, 0.34 mmol), LiCl (16.8 mg, 0.40 mmol). Subsequently, the tube was put into the glovebox under N_2 atmosphere, and *tBuOLi* (0.5 mmol, 40.0 mg) was added in the glovebox. Then the tube was sealed with a Teflon-lined screw cap and taken outside from the glovebox. Afterwards, the corresponding olefin (**1**, 0.20 mmol, 1.0 equiv), (Bromomethyl)trimethylsilane (**2d**, 72 μL, 0.50 mmol, 2.5 equiv) and DME (0.2 mL) were added via syringe, independently. Then, the tube was stirred at 30 ℃ for 3 h. After the reaction was completed, the mixture was diluted with EtOAc, filtered through silica gel and concentrated under vacuum. The corresponding product **5a**–**5h** were purified by flash column chromatography on silica gel.

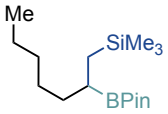

trimethyl(2-(4,4,5,5-tetramethyl-1,3,2-dioxaborolan-2-yl)heptyl)silane (**5a**): Following the **general procedure C**, using 1-hexene (**1a**, 25 μL, 0.20 mmol), the mixture was purified by flash column chromatography (*n*-hexane/EtOAc 150:1), to afford **5a** (48 mg, 80% yield) as a colourless oil. In an independent experiment, 48 mg (80% yield) were obtained, giving an average of 80% yield. **^{1}H NMR** (400 MHz, $CDCl_3$) δ 1.46 – 1.37 (m, 1H), 1.35 – 1.25 (m, 7H), 1.23 (s, 12H), 1.05 – 0.97 (m, 1H), 0.86 (t, *J* = 6.8 Hz, 3H), 0.70 (dd, *J* = 14.6, 8.6 Hz, 1H), 0.47 (dd, *J* = 14.6, 5.9 Hz, 1H), -0.02 (s, 9H) ppm. **^{13}C NMR** (101 MHz, $CDCl_3$) δ 82.9, 35.0, 32.3, 28.8, 25.1, 25.0, 22.8, 17.7, 14.2, -0.8 ppm. **IR** (neat, cm^{-1}): 2978, 2955, 2926, 2857, 1467, 1411, 1379, 1316, 1246, 1145. **HRMS:** m/z calcd. for ($C_{16}H_{35}NaO_2Si^{11}B$) $[M+Na]^+$: 321.2392 found 321.2387.

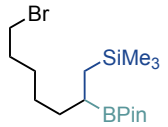

(6-bromo-2-(4,4,5,5-tetramethyl-1,3,2-dioxaborolan-2-yl)hexyl)trimethylsilane (**5b**): Following the **general procedure C**, using 5-bromo-1-pentene (**1g**, 24 μL, 0.20 mmol), the mixture was purified by flash column chromatography (*n*-hexane/EtOAc 120:1), to afford **5b** (42 mg, 58% yield) as a colourless oil. In an independent experiment, 38 mg (52% yield) were obtained, giving an average of 55% yield. **^{1}H NMR** (400 MHz, $CDCl_3$) δ 3.40 (t, *J* = 6.8 Hz, 2H), 1.90 – 1.78 (m, 2H), 1.50 – 1.37 (m, 4H), 1.24 (s, 12H), 1.06 – 0.99 (m, 1H), 0.73 (dd, *J* = 14.6, 8.7 Hz, 1H), 0.47 (dd, *J* = 14.7, 5.8 Hz, 1H), -0.01 (s, 9H) ppm. **^{13}C NMR** (101 MHz, $CDCl_3$) δ 83.1, 34.2, 34.1, 33.2, 27.7, 25.1, 25.0, 24.9, 17.7, -0.8 ppm. **IR** (neat, cm^{-1}): 2978, 2952, 2925, 2857, 1410, 1378, 1371, 1316, 1246, 1143, 969. **HRMS:** m/z calcd. for ($C_{15}H_{32}NaO_2Si^{10}B^{79}Br$) $[M+Na]^+$:384.1377 found 384.1371.

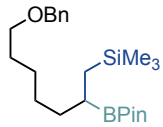

(7-(benzyloxy)-2-(4,4,5,5-tetramethyl-1,3,2-dioxaborolan-2-yl)heptyl) trimethylsilane (**5c**): Following the **general procedure C**, using ((hex-5-en-1-yloxy)methyl)benzene (**1e**, 38 mg, 0.20 mmol), the mixture was purified by flash column chromatography (*n*-hexane/EtOAc 50:1), to afford **5c** (40 mg, 50% yield) as a colourless oil. In an independent experiment, 41 mg (51% yield) were obtained, giving an average of 50% yield. **^{1}H NMR** (400 MHz, $CDCl_3$) δ 7.34 – 7.33 (m, 4H), 7.30 – 7.25 (m, 1H), 4.49 (s, 2H), 3.46 (t, *J* = 6.7 Hz, 2H), 1.65 – 1.58 (m, 2H), 1.48 – 1.30 (m, 6H), 1.23 (s, 12H), 1.07 – 0.97 (m, 1H), 0.71 (dd, *J* = 14.6, 8.7 Hz, 1H), 0.47 (dd, *J* = 14.7, 5.8 Hz, 1H), -0.02 (s, 9H) ppm. **^{13}C NMR** (101 MHz, $CDCl_3$) δ 138.9, 128.5, 127.8, 127.6, 82.9, 73.0, 70.7, 34.9, 29.9, 29.0, 26.6, 25.1, 25.0, 17.7, -0.8 ppm. **IR** (neat, cm^{-1}): 2977, 2928, 2855, 1455, 1410, 1378, 1371, 1315, 1246, 1143, 1103, 968, 857. **HRMS:** m/z calcd. for ($C_{23}H_{41}NaO_3Si^{11}B$) $[M+Na]^+$: 427.2810 found 427.2823.

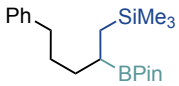

trimethyl(5-phenyl-2-(4,4,5,5-tetramethyl-1,3,2-dioxaborolan-2-yl)pentyl)silane (**5d**): Following the **general procedure C**, using 4-phenyl-1-butene (**1i**, 30 μL, 0.20 mmol), the mixture was purified by flash column chromatography (*n*-hexane/EtOAc 100:1), to afford **5d** (48 mg, 69% yield) as a colourless oil. In an independent experiment, 43 mg (63% yield) were obtained, giving an average of 66% yield. **^{1}H NMR** (400 MHz, $CDCl_3$) δ 7.29 – 7.24 (m, 2H), 7.20 – 7.14 (m, 3H), 2.60 (t, *J* = 7.7 Hz, 2H), 1.68 – 1.58 (m, 2H), 1.53 – 1.38 (m, 2H), 1.24 (s, 12H), 1.10 – 1.03 (m, 1H), 0.73 (dd, *J* = 14.6, 8.8 Hz, 1H), 0.49 (dd, *J* = 14.6, 5.8 Hz, 1H), -0.02 (s, 9H) ppm. **^{13}C NMR** (101 MHz, $CDCl_3$) δ 143.0, 128.5, 128.3, 125.6, 83.0, 36.3, 34.6, 31.0, 25.1, 25.0, 17.7, -0.8 ppm. **IR** (neat, cm^{-1}): 2978, 2927, 2857, 1638, 1454, 1378, 1371, 1315, 1246, 1143, 969. **HRMS:** m/z calcd. for ($C_{20}H_{35}NaO_2Si^{11}B$) $[M+Na]^+$: 369.2392 found 369.2391.

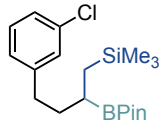

(4-(3-chlorophenyl)-2-(4,4,5,5-tetramethyl-1,3,2-dioxaborolan-2-yl)butyl) trimethylsilane (**5e**): Following the **general procedure C**, using 1-allyl-3-chlorobenzene (**1r**, 30.5 mg, 0.20 mmol), the mixture was purified by flash column chromatography (*n*-

hexane/EtOAc 120:1), to afford **5e** (40 mg, 55% yield) as a colourless oil. In an independent experiment, 41 mg (56% yield) were obtained, giving an average of 55% yield. **^{1}H NMR** (400 MHz, $CDCl_3$) δ 7.21 – 7.11 (m, 3H), 7.08 – 7.03 (m, 1H), 2.63 – 2.53 (m, 2H), 1.79 – 1.70 (m, 1H), 1.67 – 1.58 (m, 1H), 1.26 (s, 12H), 1.14 – 1.01 (m, 1H), 0.78 (dd, *J* = 14.6, 8.8 Hz, 1H), 0.53 (dd, *J* = 14.6, 5.7 Hz, 1H), -0.01 (s, 9H) ppm. **^{13}C NMR** (101 MHz, $CDCl_3$) δ 145.2, 134.1, 129.6, 128.7, 126.8, 125.9, 83.1, 36.7, 35.2, 25.1, 25.0, 17.6, -0.8 ppm. **IR** (neat, cm^{-1}): 2978, 2951, 2929, 2861, 1597, 1573, 1457, 1411, 1377, 1371, 1317, 1246, 1143, 1004, 967. **HRMS:** m/z calcd. for ($C_{19}H_{32}NaO_2Si^{11}BCl$) $[M+Na]^+$: 389.1845 found 389.1846.

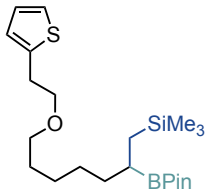

trimethyl(2-(4,4,5,5-tetramethyl-1,3,2-dioxaborolan-2-yl)-7-(2-(thiophen-2-yl)ethoxy)heptyl)silane (**5f**): Following the **general procedure C**, using 2-(2-(hex-5-en-1-yloxy)ethyl)thiophene (**1n**, 42 mg, 0.20 mmol), the mixture was purified by flash column chromatography (*n*-hexane/EtOAc 40:1), to afford **5f** (56 mg, 66% yield) as a colourless oil. In an independent experiment, 56 mg (66% yield) were obtained, giving an average of 66% yield. **^{1}H NMR** (400 MHz, $CDCl_3$) δ 7.13 (dd, *J* = 5.1, 1.2 Hz, 1H), 6.92 (dd, *J* = 5.1, 3.4 Hz, 1H), 6.88 – 6.83 (m, 1H), 3.64 (t, *J* = 6.9 Hz, 2H), 3.44 (t, *J* = 6.7 Hz, 2H), 3.09 (td, *J* = 6.8, 0.9 Hz, 2H), 1.63 – 1.54 (m, 2H), 1.46 – 1.30 (m, 6H), 1.24 (s, 12H), 1.07 – 0.97 (m, 1H), 0.71 (dd, *J* = 14.6, 8.7 Hz, 1H), 0.47 (dd, *J* = 14.6, 5.8 Hz, 1H), -0.02 (s, 9H) ppm. **^{13}C NMR** (101 MHz, $CDCl_3$) δ 141.6, 126.8, 125.1, 123.7, 82.9, 71.5, 71.3, 34.9, 30.7, 29.8, 29.0, 26.5, 25.1, 25.0, 17.7, -0.8 ppm. **IR** (neat, cm^{-1}): 2977, 2931, 2857, 1440, 1407, 1419, 1378, 1371, 1311, 1246, 1144, 1112, 968. **HRMS:** m/z calcd. for ($C_{22}H_{41}NaO_3SSi^{11}B$) $[M+Na]^+$: 447.2531 found 447.2533.

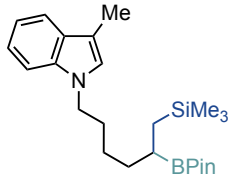

3-methyl-1-(5-(4,4,5,5-tetramethyl-1,3,2-dioxaborolan-2-yl)-6-(trimethylsilyl) hexyl)-1*H*-indole (**5g**): Following the **general procedure C**, using 3-methyl-1-(pent-4-en-1-yl)-1*H*-indole (**1q**, 39.6 mg, 0.20 mmol), the mixture was purified by flash column chromatography (*n*-hexane/EtOAc 100:1), to afford **5g** (51 mg, 62% yield) as a colourless oil. In an independent experiment, 55 mg (66% yield) were obtained, giving an average of 64% yield. **^{1}H NMR** (400 MHz, $CDCl_3$) δ 7.58 – 7.56 (m, 1H), 7.33 – 7.29 (m, 1H), 7.22 – 7.18 (m, 1H),

7.12 – 7.08 (m, 1H), 6.88 – 6.87 (m, 1H), 4.06 (t, *J* = 7.0 Hz, 2H), 2.34 (d, *J* = 1.1 Hz, 3H), 1.87 – 1.76 (m, 2H), 1.50 – 1.32 (m, 4H), 1.20 (s, 6H), 1.19 (s, 6H), 1.07 – 1.00 (m, 1H), 0.74 (dd, *J* = 14.6, 8.7 Hz, 1H), 0.47 (dd, *J* = 14.7, 5.8 Hz, 1H), 0.01 (s, 9H) ppm. **^{13}C NMR** (101 MHz, $CDCl_3$) δ 136.4, 128.8, 125.6, 121.3, 119.0, 118.4, 110.0, 109.3, 83.0, 46.1, 34.7, 30.7, 26.6, 25.0, 24.9, 17.8, 9.7, -0.8 ppm. **IR** (neat, cm^{-1}): 3053, 2977, 2950, 2929, 2860, 1615, 1468, 1412, 1378, 1370, 1316, 1245, 1164, 1149, 1046, 967. **HRMS:** m/z calcd. for ($C_{24}H_{40}NNaO_2Si^{11}B$) $[M+Na]^+$: 436.2814 found 436.2814.

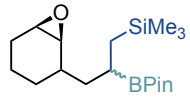

(3-(7-oxabicyclo[4.1.0]heptan-3-yl)-2-(4,4,5,5-tetramethyl-1,3,2-dioxaborolan-2-yl)propyl)trimethylsilane (**5h**): Following the **general procedure C**, using 3-vinyl-7-oxabicyclo[4.1.0]heptane (**1s**, 24.8 mg, 0.20 mmol), the mixture was purified by flash column chromatography (*n*-hexane/EtOAc 20:1), to afford **5h** (28 mg, 41% yield) as a colourless oil. In an independent experiment, 28 mg (41% yield) were obtained, giving an average of 41% yield, as a 3:3:2:2 mixture of diastereoisomers, determined by ^{13}C NMR and GC. **^{1}H NMR** (400 MHz, $CDCl_3$) δ 3.14 – 3.08 (m, 2H), 2.19 – 2.05 (m, 1H), 2.01 – 1.92 (m, 1H), 1.83 – 1.75 (m, 1H), 1.69 – 1.62 (m, 1H), 1.57 – 1.43 (m, 1H), 1.40 – 1.27 (m, 2H), 1.23 (s, 12H), 1.17 – 1.11 (m, 1H), 1.11 – 1.02 (m, 1H), 0.89 – 0.79 (m, 1H), 0.68 – 0.61 (m, 1H), 0.46 – 0.39 (m, 1H), -0.02 – -0.04 (m, 9H) ppm. **^{13}C NMR** (101 MHz, $CDCl_3$) δ 83.03, 83.01, 82.99, 82.97, 53.31, 53.25, 52.83, 52.80, 52.07, 52.05, 52.03, 52.09, 42.1, 41.7, 41.4, 41.2, 32.3, 32.1, 32.0, 31.1, 31.0, 28.8, 28.6, 27.4, 27.1, 25.5, 25.1, 25.05, 25.02, 24.99, 24.95, 24.4, 23.72, 23.69, 17.9, 17.8, 17.63, 17.58, -0.7, -0.77, -0.78 ppm. **IR** (neat, cm^{-1}): 2978, 2950, 2926, 2853, 1445, 1411, 1378, 1371, 1315, 1246, 1143, 973. **HRMS:** m/z calcd. for ($C_{18}H_{35}NaO_3Si^{11}B$) $[M+Na]^+$: 361.2341 found 361.2341.

3.5.6. Functionalisation of advanced synthetic intermediates and ethylene revalorisation

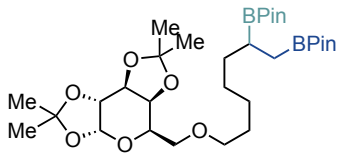

2,2'-(7-(((3a*R*,5*R*,5a*S*,8a*S*,8b*R*)-2,2,7,7-tetramethyltetrahydro-5*H*-bis([1,3]dioxolo)[4,5-*b*:4',5'-*d*]pyran-5-yl)methoxy)heptane-1,2-diyl)bis(4,4,5,5-tetramethyl-1,3,2-dioxaborolane) (**6a**): Following the **general procedure B**, using (3a*R*,5*R*,5a*S*,8a*S*,8b*R*)-5-((hex-5-en-1-yloxy)methyl)-2,2,7,7-tetramethyltetrahydro-5*H*-bis([1,3]dioxolo)[4,5-*b*:4',5'-*d*]pyran (**1t**, 68.4 mg, 0.20 mmol), the mixture was purified by flash column chromatography (*n*-hexane/EtOAc 10:1 to 5:1), to afford **6a** (73 mg, 60% yield) as a colourless oil. In an independent experiment, 61 mg (61% yield) were obtained, giving an average of 60% yield, as a 1:1 mixture of diastereoisomers, determined by chiral HPLC. **^{1}H NMR** (400 MHz, $CDCl_3$) δ 5.52 (d, *J* = 5.0 Hz, 1H), 4.58 (dd, *J* = 7.9, 2.4 Hz, 1H), 4.29 (dd, *J* = 5.0, 2.3 Hz, 1H), 4.25 (dd, *J* = 7.9, 1.9 Hz, 1H), 3.94 (td, *J* = 6.3, 1.9 Hz, 1H), 3.66 – 3.52 (m, 2H), 3.50 – 3.39 (m, 2H), 1.57 – 1.55 (m, 2H), 1.53 (s, 3H), 1.44 (s, 3H), 1.33 (s, 3H), 1.32 (s, 3H) 1.29 – 1.25 (m, 6H), 1.22 (s, 12H), 1.21 (s, 12H), 1.13 – 1.07 (m, 1H), 0.86 – 0.76 (m, 2H) ppm. **^{13}C NMR** (101 MHz, $CDCl_3$) δ 109.3, 108.6, 96.5, 82.93, 82.88, 71.8, 71.3, 70.82, 70.80, 69.4, 66.8, 33.9, 29.7, 28.9, 26.4, 26.2, 26.1, 25.1, 25.04, 24.98, 24.91, 24.88, 24.6 ppm. **IR** (neat, cm^{-1}): 2978, 2930, 2860, 1458, 1370, 1311, 1254, 1211, 1161, 1141, 1111, 1069, 1002, 968. **HRMS:** m/z calcd. for ($C_{31}H_{56}NaO_{10}{}^{11}B_2$) $[M+Na]^+$: 633.3952 found 633.3967.

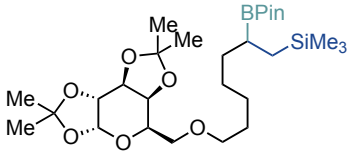

trimethyl(2-(4,4,5,5-tetramethyl-1,3,2-dioxaborolan-2-yl)-7-(((3a*R*,5*R*,5a*S*,8a*S*,8b*R*)-2,2,7,7-tetramethyltetrahydro-5*H*-bis([1,3]dioxolo)[4,5-*b*:4',5'-*d*]pyran-5-yl)methoxy)heptyl)silane (**6b**): Following the **general procedure C**, using (3a*R*,5*R*,5a*S*,8a*S*,8b*R*)-5-((hex-5-en-1-yloxy)methyl)-2,2,7,7-tetramethyl tetrahydro-5*H*-bis([1,3]dioxolo)[4,5-*b*:4',5'-*d*]pyran (**1t**, 68.4 mg, 0.20 mmol) and (bromomethyl)trimethylsilane (**2d**, 86 μL, 0.60 mmol), the reaction was stirred for 6 h and the mixture purified by flash column chromatography (*n*-hexane/EtOAc 30:1 to 15:1), to afford **6b** (55 mg, 49% yield) as a colourless oil. In an independent experiment, 57 mg (51% yield) were obtained, giving an average of 50% yield, as a 1:1 mixture of diastereoisomers, determined by chiral HPLC. **^{1}H NMR** (400 MHz, $CDCl_3$) δ 5.52 (d, *J* = 5.0 Hz, 1H), 4.58 (dd,

J = 7.9, 2.4 Hz, 1H), 4.28 (dd, *J* = 5.0, 2.4 Hz, 1H), 4.24 (dd, *J* = 7.9, 1.9 Hz, 1H), 3.94 (td, *J* = 6.3, 1.9 Hz, 1H), 3.63 – 3.52 (m, 2H), 3.50 – 3.39 (m, 2H), 1.59 – 1.54 (m, 2H), 1.52 (s, 3H), 1.43 (s, 3H), 1.33 (s, 3H), 1.31 (s, 3H), 1.30 – 1.24 (m, 6H), 1.22 (s, 12H), 1.01 – 0.94 (m, 1H), 0.69 (dd, *J* = 14.6, 8.7 Hz, 1H), 0.45 (dd, *J* = 14.6, 5.8 Hz, 1H), -0.04 (s, 9H) ppm. **^{13}C NMR** (101 MHz, $CDCl_3$) δ 109.3, 108.6, 96.5, 82.9, 71.8, 71.2, 70.8 (2C), 69.4, 66.9, 34.9, 29.8, 29.0, 26.4, 26.2, 26.1, 25.09, 25.07, 25.0, 24.6, 17.7, -0.8 ppm. **IR** (neat, cm^{-1}): 2979, 2932, 2859, 1457, 1378, 1372, 1315, 1247, 1211, 1144, 1113, 1069, 1001, 836. **HRMS:** m/z calcd. for ($C_{28}H_{53}NaO_8Si^{11}B$) $[M+Na]^+$: 579.3495 found 579.3499.

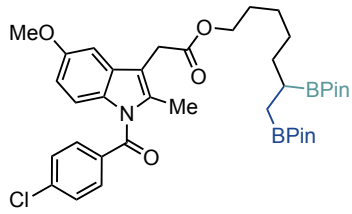

6,7-bis(4,4,5,5-tetramethyl-1,3,2-dioxaborolan-2-yl)heptyl 2-(1-(4-chlorobenzoyl)-5-methoxy-2-methyl-1*H*-indol-3-yl)acetate (**7a**): Following the **general procedure B**, using hex-5-en-1-yl 2-(1-(4-chlorobenzoyl)-5-methoxy-2-methyl-1*H*-indol-3-yl) acetate (**1u**, 87.8 mg, 0.20 mmol), the mixture was purified by flash column chromatography (*n*-hexane/EtOAc 10:1), to afford **7a** (71 mg, 50% yield) as a colourless oil. In an independent experiment, 71 mg (50% yield) were obtained, giving an average of 50% yield. **^{1}H NMR** (400 MHz, $CDCl_3$) δ 7.67 – 7.63 (m, 2H), 7.47 – 7.44 (m, 2H), 6.95 (d, *J* = 2.5 Hz, 1H), 6.86 (d, *J* = 9.0 Hz, 1H), 6.65 (dd, *J* = 9.0, 2.6 Hz, 1H), 4.07 (t, *J* = 6.8 Hz, 2H), 3.82 (s, 3H), 3.64 (s, 2H), 2.37 (s, 3H), 1.64 – 1.58 (m, 2H), 1.46 – 1.40 (m, 1H), 1.33 – 1.26 (m, 5H), 1.21 (s, 24H), 1.12 – 1.05 (m, 1H), 0.88 – 0.74 (m, 2H) ppm. **^{13}C NMR** (101 MHz, $CDCl_3$) δ 171.0, 168.4, 156.2, 139.3, 135.9, 134.1, 131.3, 130.9, 130.8, 129.2, 115.0, 112.9, 111.8, 101.4, 82.94, 82.90, 65.3, 55.8, 33.7, 30.5, 28.7, 28.5, 26.1, 25.01, 24.95, 24.89, 24.85, 13.5 ppm. **IR** (neat, cm^{-1}): 2976, 2929, 2856, 1734, 1684, 1593, 1478, 1457, 1369, 1355, 1310, 1217, 1139, 1067, 1014, 968. **HRMS:** m/z calcd. for ($C_{38}H_{52}NNaO_8{}^{11}B_2Cl$) $[M+Na]^+$: 730.3460 found 730.3464.

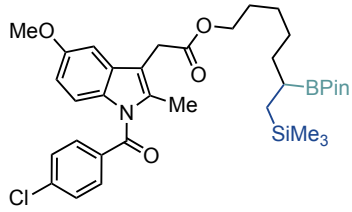

6-(4,4,5,5-tetramethyl-1,3,2-dioxaborolan-2-yl)-7-(trimethylsilyl)heptyl 2-(1-(4-chlorobenzoyl)-5-methoxy-2-methyl-1*H*-indol-3-yl)acetate (**7b**): Following the **general procedure C**, using hex-5-en-1-yl 2-(1-(4-chlorobenzoyl)-5-methoxy-2-methyl-1*H*-indol-3-

yl)acetate (**1u**, 87.8 mg, 0.20 mmol) and (Bromomethyl)trimethylsilane (**2d**, 86 μL, 0.60 mmol), the reaction was stirred for 6 h and the mixture purified by flash column chromatography (*n*-hexane/EtOAc 20:1 to 10:1), to afford **7b** (66 mg, 51% yield) as a light yellow oil. In an independent experiment, 69 mg (53% yield) were obtained, giving an average of 52% yield. **^{1}H NMR** (400 MHz, $CDCl_3$) δ 7.68 – 7.64 (m, 2H), 7.48 – 7.45 (m, 2H), 6.96 (d, *J* = 2.5 Hz, 1H), 6.87 (d, *J* = 9.0 Hz, 1H), 6.66 (dd, *J* = 9.0, 2.5 Hz, 1H), 4.08 (t, *J* = 6.8 Hz, 2H), 3.83 (s, 3H), 3.64 (s, 2H), 2.38 (s, 3H), 1.63 – 1.56 (m, 2H), 1.44 – 1.49 (m, 1H), 1.33 – 1.27 (m, 5H), 1.23 (s, 12H), 1.03 – 0.95 (m, 1H), 0.71 (dd, *J* = 14.6, 8.8 Hz, 1H), 0.45 (dd, *J* = 14.6, 5.6 Hz, 1H), -0.02 (s, 9H). **^{13}C NMR** (101 MHz, $CDCl_3$) δ 171.0, 168.4, 156.2, 139.3, 136.0, 134.1, 131.3, 131.0, 130.8, 129.2, 115.1, 112.9, 111.8, 101.5, 83.0, 65.3, 55.8, 34.8, 30.5, 28.73, 28.68, 26.2, 25.1, 25.0, 17.9, 13.5, -0.8 ppm. **IR** (neat, cm^{-1}): 2976, 2930, 2857, 1735, 1684, 1593, 1478, 1457, 1370, 1356, 1313, 1222, 1142, 1088, 1068, 835. **HRMS:** m/z calcd. for ($C_{35}H_{49}ClNNaO_6Si^{11}B$) $[M+Na]^+$: 676.3003 found 676.3001.

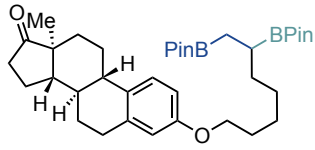

(8*R*,9*S*,13*S*,14*S*)-3-((6,7-bis(4,4,5,5-tetramethyl-1,3,2-dioxaborolan-2-yl)heptyl) oxy)-13-methyl-6,7,8,9,11,12,13,14,15,16-decahydro-17*H*-cyclopenta [*a*] phenanthrene-17-one (**8a**): Following the **general procedure B**, using (8*R*,9*S*,13*S*,14*S*)-3-(hex-5-en-1-yloxy)-13-methyl-6,7,8,9,11,12,13,14,15,16-decahydro-17*H*-cyclopenta[*a*]phenanthren-17-one (**1v**, 70.4 mg, 0.20 mmol), the mixture was purified by flash column chromatography (*n*-hexane/EtOAc 15:1), to afford **8a** (56 mg, 50% yield) as a colourless oil. In an independent experiment, 57 mg (50% yield) were obtained, giving an average of 50% yield, as a 1:1 mixture of diastereoisomers, determined by chiral HPLC. **^{1}H NMR** (500 MHz, $CDCl_3$): δ 7.17 (d, *J* = 8.5 Hz, 1H), 6.69 (dd, *J* = 8.6, 2.7 Hz, 1H), 6.63 (d, *J* = 2.6 Hz, 1H), 3.90 (t, *J* = 6.7 Hz, 2H), 2.90 – 2.87 (m, 2H), 2.52 – 2.47 (m, 1H), 2.41 – 2.37 (m, 1H), 2.26 – 2.22 (m, 1H), 2.16 – 1.93 (m, 4H), 1.77 – 1.72 (m, 2H), 1.66 – 1.31 (m, 12H), 1.23 (s, 24H), 1.15 – 1.10 (m, 1H), 0.91 (s, 3H), 0.88 – 0.79 (m, 2H) ppm. **^{13}C NMR** (126 MHz, $CDCl_3$): δ 157.4, 137.8, 131.9, 126.4, 114.7, 112.3, 83.0, 82.9, 68.1, 50.6, 48.2, 44.2, 38.6, 36.0, 33.8, 31.8, 29.8, 29.4, 28.8, 26.7, 26.4, 26.1, 25.1, 25.0, 24.94, 24.90, 21.8, 14.0 ppm. **IR** (neat, cm^{-1}): 2976, 2926, 2857, 1740, 1609, 1500, 1469, 1406, 1370, 1311, 1280, 1255, 1234, 1214, 1140, 1112, 1082, 1055, 1033, 1006. **HRMS:** m/z calcd. for ($C_{37}H_{58}NaO_6B_2$) $[M+Na]^+$: 643.4312 found 643.4317.

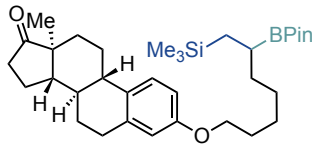

(8*R*,9*S*,13*S*,14*S*)-13-methyl-3-((6-(4,4,5,5-tetramethyl-1,3,2-dioxaborolan-2-yl)-7-(trimethylsilyl)heptyl)oxy)-6,7,8,9,11,12,13,14,15,16-decahydro-17*H*-cyclopenta[*a*]phenanthren-17-one (**8b**): Following the **general procedure C**, using (8*R*,9*S*,13*S*,14*S*)-3-(hex-5-en-1-yloxy)-13-methyl-6,7,8,9,11,12,13,14,15,16-decahydro-17*H*-cyclopenta[*a*]phenanthren-17-one (**1v**, 70.4 mg, 0.20 mmol), and (Bromomethyl)trimethylsilane (**2d**, 86 μL, 0.60 mmol), the reaction was stirred for 6 h and the mixture purified by flash column chromatography (*n*-hexane/EtOAc 10:1 to 5:1), to afford **8b** (94 mg, 76% yield) as a white solid. In an independent experiment, 92 mg (74% yield) were obtained, giving an average of 75% yield, as a 1:1 mixture of diastereoisomers, determined by chiral HPLC. **^{1}H NMR** (400 MHz, $CDCl_3$): δ 7.18 (d, *J* = 8.6 Hz, 1H), 6.70 (dd, *J* = 8.6, 2.8 Hz, 1H), 6.63 (d, *J* = 2.7 Hz, 1H), 3.91 (t, *J* = 6.6 Hz, 2H), 2.91 – 2.85 (m, 2H), 2.53 – 2.46 (m, 1H), 2.42 – 2.34 (m, 1H), 2.27 – 2.23 (m, 1H), 2.18 – 1.93 (m, 4H), 1.79 – 1.72 (m, 2H), 1.65 – 1.34 (m, 12H), 1.24 (s, 12H), 1.07 – 0.99 (m, 1H), 0.91 (s, 3H), 0.72 (dd, *J* = 14.6, 8.7 Hz, 1H), 0.48 (dd, *J* = 14.6, 5.8 Hz, 1H), -0.01 (s, 9H) ppm. **^{13}C NMR** (101 MHz, $CDCl_3$): δ 221.0, 157.3, 137.7, 131.9, 126.4, 114.7, 112.3, 82.9, 68.0, 50.6, 48.1, 44.1, 38.5, 36.0, 34.9, 31.7, 29.8, 29.4, 28.9, 26.7, 26.4, 26.1, 25.1, 25.0, 21.7, 17.7, 14.0, -0.8 ppm. **IR** (neat, cm^{-1}): 3388, 2975, 2930, 2862, 1738, 1609, 1499, 1473, 1454, 1372, 1315, 1246, 1144, 1007, 836. **HRMS:** m/z calcd. for ($C_{34}H_{55}NaO_4Si^{11}B$) $[M+Na]^+$: 589.3855 found 589.3845.

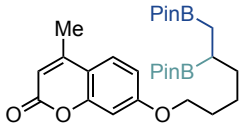

7-((5,6-bis(4,4,5,5-tetramethyl-1,3,2-dioxaborolan-2-yl)hexyl)oxy)-4-methyl-2*H*-chromen-2-one (**9a**): Following the **general procedure B**, using 4-methyl-7-(pent-4-en-1-yloxy)-2*H*-chromen-2-one (**1w**, 56 mg, 0.20 mmol), the mixture was purified by flash column chromatography (*n*-hexane/EtOAc 9:1 to 3:2), to afford **9a** (56 mg, 55% yield) as a white solid. In an independent experiment, 57 mg (55% yield) were obtained, giving an average of 55% yield. **^{1}H NMR** (500 MHz, $CDCl_3$) δ 7.48 – 7.46 (m, 1H), 6.85 – 6.80 (m, 1H), 6.79 – 6.78 (m, 1H), 6.11 – 6.11 (m, 1H), 3.99 (t, *J* = 6.5 Hz, 2H), 2.38 (d, *J* = 1.2 Hz, 3H), 1.82 – 1.76 (m, 2H), 1.57 – 1.35 (m, 4H), 1.23 (s, 12H), 1.22 (s, 12H), 1.17 – 1.12 (m, 1H), 0.93 – 0.78 (m, 2H). **^{13}C NMR** (126 MHz, $CDCl_3$) δ 162.5, 161.6, 155.4, 152.7, 125.1, 113.5, 112.8, 111.9, 101.5, 83.0 (2C), 68.7, 33.5, 29.3, 25.3, 25.03, 24.99, 24.92, 24.88, 18.8 ppm. **IR** (neat, cm^{-1}): 2979, 2922, 1723, 1609, 1557, 1510, 1472, 1423, 1387, 1368, 1331, 1262,

1138, 1068, 967. **HRMS:** m/z calcd. for ($C_{28}H_{42}NaO_7{}^{10}B^{11}B$) $[M+Na]^+$: 534.3045 found 534.3043.

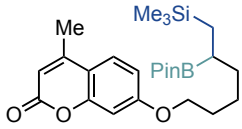

4-methyl-7-((5-(4,4,5,5-tetramethyl-1,3,2-dioxaborolan-2-yl)-6-(trimethylsilyl) hexyl)oxy)-2*H*-chromen-2-one (**9b**): Following the **general procedure C**, using 4-methyl-7-(pent-4-en-1-yloxy)-2*H*-chromen-2-one (**1w**, 48.8 mg, 0.20 mmol) and (Bromomethyl)trimethylsilane (**2d**, 86 μL, 0.60 mmol), the reaction was stirred for 6 h and the mixture purified by flash column chromatography (*n*-hexane/EtOAc 4:1 to 2:1), to afford **9b** (45 mg, 49% yield) as a white solid. In an independent experiment, 44 mg (48% yield) were obtained, giving an average of 48% yield. **^{1}H NMR** (400 MHz, $CDCl_3$): δ 7.24 – 7.18 (m, 1H), 6.95 – 6.93 (m, 1H), 6.89 – 6.82 (m, 2H), 2.65 – 2.55 (m, 2H), 1.80 – 1.59 (m, 3H), 1.34 – 1.19 (m, 18H), 1.12 – 1.02 (m, 1H), 0.78 (dd, *J* = 14.6, 8.7 Hz, 1H), 0.54 (dd, *J* = 14.6, 5.8 Hz, 1H), -0.01 (s, 9H) ppm. **^{13}C NMR** (101 MHz, $CDCl_3$): δ 164.3, 161.8, 145.84, 145.77, 129.74, 129.65, 124.20, 124.17, 115.4, 115.2, 112.6, 112.4, 83.1, 36.7, 35.3, 25.1, 25.0, 17.6, -0.8 ppm. **IR** (neat, cm^{-1}): 2982, 2949, 2915, 2863, 1721, 1607, 1387, 1372, 1282, 1262, 1202, 1138, 1070, 1019, 980. **HRMS:** m/z calcd. for ($C_{25}H_{40}O_5Si^{10}B$) $[M]^+$: 458.2769 found 458.2778.

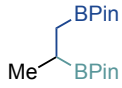

2,2'-(propane-1,2-diyl)bis(4,4,5,5-tetramethyl-1,3,2-dioxaborolane) (**10a**)**:** An oven-dried 8 mL screw-cap test tube containing a stirring bar was charged with $NiBr_4{\cdot}TBA_2$ (17.3 mg, 10 mol%), *N*-benzyl-6-methylpicolinamide (**L1**, 3.6 mg, 10 mol%), B_2Pin_2 (86.3 mg, 0.34 mmol). Subsequently, the tube was put into the glovebox under N_2 atmosphere, and *t*BuOLi (0.4 mmol, 32.0 mg) was added in the glovebox. Then the tube was sealed with a Teflon-lined screw cap and taken outside from the glovebox. Subsequently, the tube was sealed with a Teflon-lined screw cap, then evacuated and back-filled with ethylene (3 times). Afterwards, (Bromomethyl)boronic acid pinacol ester (**2a**, 36 μL, 0.20 mmol, 1.0 equiv.), *t*BuOH (0.80 mmol, 76 μL, 4.0 equiv.) and DME (0.5 mL) were added via syringe, independently. Then, the tube was stirred at 30 ºC for 3 hours. The reaction was performed under an ethylene atmosphere with an ethylene balloon. After the reaction was completed, the mixture was diluted with DCM, filtered through silica gel, and concentrated under vacuum. The corresponding product was purified by column chromatography on silica gel (*n*-hexane/Et_2O 95:5), to afford **10a** (24 mg, 40% yield) as colourless oil. In an independent experiment, 23 mg (39% yield) were obtained, giving an average of 40% yield. **^{1}H NMR** (400

MHz, $CDCl_3$) δ 1.22 (s, 24H), 0.99 (d, *J* = 7.4 Hz, 3H), 0.92 – 0.74 (m, 3H) ppm. **^{13}C NMR** (101 MHz, $CDCl_3$) δ 82.94, 82.92, 25.00, 24.96, 24.90, 24.85, 18.5 ppm. **IR** (neat, cm^{-1}): 2977, 2930, 2871, 1461, 1406, 1369, 1348, 1270, 1216, 1139, 1110, 1035, 968. **HRMS:** m/z calcd. for ($C_{15}H_{30}NaO_4{}^{11}B_2$) $[M+Na]^+$: 319.2216 found 319.2222.

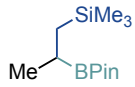

trimethyl(2-(4,4,5,5-tetramethyl-1,3,2-dioxaborolan-2-yl)propyl)silane (**10b**): An oven-dried 8 mL screw-cap test tube containing a stirring bar was charged with $NiBr_4{\cdot}TBA_2$ (17.3 mg, 10 mol%), 4-(*tert*-butyl)-*N*-(2-hydroxyethyl)-6-methylpicolinamide (**L3**, 4.7 mg, 10 mol%), B_2Pin_2 (86.3 mg, 0.34 mmol) and LiCl (16.8 mg, 0.40 mmol). Subsequently, the tube was put into the glovebox under N_2 atmosphere, and *t*BuOLi (0.5 mmol, 40.0 mg) was added in the glovebox. Then the tube was sealed with a Teflon-lined screw cap and taken outside from the glovebox. Subsequently, the tube was sealed with a Teflon-lined screw cap, then evacuated and back-filled with ethylene (3 times). Afterwards, (bromomethyl)trimethylsilane (**2d**, 28.8 μL, 0.20 mmol, 1.0 equiv.) and DME (0.5 mL) were added via syringe, independently. Then, the tube was stirred at 30 ºC for 3 h. The reaction was performed under an ethylene atmosphere with an ethylene balloon. After the reaction was completed, the mixture was diluted with EtOAc, filtered through silica gel, and concentrated under vacuum. The corresponding product was purified by column chromatography on silica gel (*n*-hexane/Et_2O 120:1), to afford **10b** (13 mg (27% yield) as colourless oil. In an independent experiment, 14 mg (29% yield) were obtained, giving an average of 28% yield. **^{1}H NMR** (500 MHz, $CDCl_3$) δ 1.23 (s, 12H), 1.11 – 1.05 (m, 1H), 1.00 (d, *J* = 7.2Hz, 3H), 0.78 (dd, *J* = 14.6, 7.5 Hz, 1H), 0.43 (dd, *J* = 14.7, 6.9 Hz, 1H), -0.02 (s, 9H) ppm. **^{13}C NMR** (126 MHz, $CDCl_3$) δ 82.9, 24.94, 24.92, 20.1, 19.5, -0.7 ppm. **IR** (neat, cm^{-1}): 2978, 2953, 2929, 2897, 2869, 1459, 1404, 1378, 1360, 1314, 1248, 1226, 1144, 1105, 1023, 698, 835. **HRMS:** m/z calcd. for ($C_{12}H_{27}NaO_2Si{}^{11}B$) $[M+Na]^+$: 256.1766 found 265.1765.

3.5.7. Synthetic application

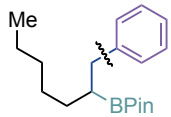

4,4,5,5-tetramethyl-2-(1-phenylheptan-2-yl)-1,3,2-dioxaborolane (**11**): An oven-dried 8 mL screw-cap test tube containing a stirring bar was charged with $Pd(OAc)_2$ (4.5 mg, 5 mol %), RuPhos (9.3 mg, 5 mol%) and KOH (67.2 mg, 1.2 mmol). Subsequently, the tube was sealed with a Teflon-lined screw cap, then evacuated and back-filled with Ar (3 times).

Afterwards, 2,2'-(heptane-1,2-diyl)bis(4,4,5,5-tetramethyl-1,3,2-dioxaborolane) (**4a**, 140.8 mg, 0.4 mmol, 1.0 equiv.), bromobenzene (PhBr, 94.2 mg, 0.6 mmol, 1.5 equiv.), THF and H_2O (10:1, 4.0 mL) were added via syringe. Then, the tube was stirred at 70 ºC for 14 h. After the reaction was completed, the mixture was quenched with H_2O, extracted with EtOAc, dried with Na_2SO_4 and concentrated under vacuum. The corresponding product **11** was purified by column chromatography on silica gel (*n*-hexane/EtOAc 70:1), to afford a colourless oil, 93 mg (76% yield). **^{1}H NMR** (400 MHz, $CDCl_3$): δ 7.29 – 7.11 (m, 5H), 2.74 – 2.64 (m, 2H), 1.46 – 1.37 (m, 2H), 1.30 – 1.22 (m, 7H), 1.16 (s, 6H), 1.13 (s, 6H), 0.87 (t, *J* = 6.8 Hz, 3H) ppm. **^{13}C NMR** (101 MHz, $CDCl_3$): δ 142.6, 129.0, 128.1, 125.7, 83.1, 37.6, 32.2, 31.3, 29.0, 24.9, 24.8, 22.7, 14.2 ppm. **IR** (neat, cm^{-1}): 2977, 2957, 2924, 2855, 1603, 1455, 1379, 1317, 1240, 1142, 967. **HRMS:** m/z calcd. for ($C_{19}H_{31}NaO_2{}^{10}B$) $[M+Na]^+$: 324.2346 found 324.2349.

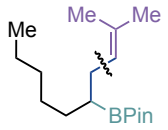

4,4,5,5-tetramethyl-2-(2-methyldec-2-en-5-yl)-1,3,2-dioxaborolane (**12**): An oven-dried 8 mL screw-cap test tube containing a stirring bar was charged with $Pd(OAc)_2$ (4.5 mg, 5 mol %), RuPhos (9.3 mg, 5 mol%) and KOH (67.2 mg, 1.2 mmol). Subsequently, the tube was sealed with a Teflon-lined screw cap, then evacuated and back-filled with Ar (3 times). Afterwards, 2,2'-(heptane-1,2-diyl)bis(4,4,5,5-tetramethyl-1,3,2-dioxaborolane) (**4a**, 140.8 mg, 0.4 mmol, 1.0 equiv.), 1-chloro-2-methyl-1-propen (54 mg, 0.6 mmol, 1.5 equiv.), THF and H_2O (10:1, 4.0 mL) were added via syringe. Then, the tube was stirred at 70 ºC for 14 h. After the reaction was completed, the mixture was quenched with H_2O, extracted with EtOAc, dried with Na_2SO_4, and concentrated under vacuum. The corresponding product **12** was purified by column chromatography on silica gel (*n*-hexane/EtOAc 70:1), to afford a light-yellow oil, 75 mg (67% yield). **^{1}H NMR** (400 MHz, $CDCl_3$): δ 5.13 – 5.08 (m, 1H), 2.11 – 2.01 (m, 2H), 1.65 (s, 3H), 1.59 (s, 3H), 1.33 – 1.24 (m, 8H), 1.22 (s, 6H), 1.21 (s, 6H), 1.06 – 0.96 (m, 1H), 0.86 (t, *J* = 6.8 Hz, 3H) ppm. **^{13}C NMR** (101 MHz, $CDCl_3$): δ 131.3, 124.8, 82.9, 32.3, 31.3, 30.0, 29.1, 25.9, 25.0, 24.8, 22.7, 18.0, 14.2 ppm. **IR** (neat, cm^{-1}): 2977, 2959, 2923, 2855, 1458, 1410, 1378, 1371, 1316, 1241, 1215, 1144, 967. **HRMS:** m/z calcd. for ($C_{17}H_{33}NaO_2{}^{10}B$) $[M+Na]^+$: 302.2502 found 302.2505.

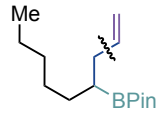

4,4,5,5-tetramethyl-2-(non-1-en-4-yl)-1,3,2-dioxaborolane (**13**): An oven-dried 8 mL screw-cap test tube containing a stirring bar was charged with $Pd(OAc)_2$ (4.5 mg, 5 mol %), RuPhos (9.3 mg, 5 mol%) and *t*BuOK (269 mg, 2.4 mmol). Subsequently, the tube was sealed with a Teflon-lined screw cap, then evacuated and back-filled with Ar (3 times).

Afterwards, 2,2'-(heptane-1,2-diyl)bis(4,4,5,5-tetramethyl-1,3,2-dioxaborolane) (**4a**, 140.8 mg, 0.4 mmol, 1.0 equiv.), 1,2-dichloroethane (96 μL, 1.2 mmol, 3.0 equiv.), THF and H_2O (10:1, 4.0 mL) were added via syringe. Then, the tube was stirred at 70 ºC for 14 h. After the reaction was completed, the mixture was quenched with H_2O, extracted with EtOAc, dried with Na_2SO_4, and concentrated under vacuum. The corresponding product **13** was purified by column chromatography on silica gel (*n*-hexane/EtOAc 70:1), to afford a brown oil, 61 mg (60% yield). **^{1}H NMR** (400 MHz, $CDCl_3$): δ 5.79 (ddt, *J* = 17.1, 10.1, 6.9 Hz, 1H), 5.02 – 4.96 (m, 1H), 4.91 (ddt, *J* = 10.1, 2.2, 1.1 Hz, 1H), 2.20 – 2.06 (m, 2H), 1.39 – 1.25 (m, 8H), 1.22 (s, 12H), 1.09 – 1.01 (m, 1H), 0.86 (t, *J* = 6.9 Hz, 3H) ppm. **^{13}C NMR** (101 MHz, $CDCl_3$): δ 138.9, 114.8, 83.0, 35.7, 32.2, 31.0, 28.9, 24.9 (2C), 22.7, 14.2 ppm. **IR** (neat, cm^{-1}): 2978, 2958, 2923, 2856, 1640, 1460, 1408, 1379, 1316, 1241, 1164, 1144, 967. **HRMS:** m/z calcd. for ($C_{15}H_{29}NaO_2{}^{10}B$) $[M+Na]^+$: 274.2189 found 274.2178.

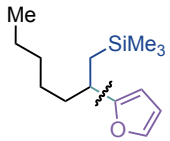

(2-(furan-2-yl)heptyl)trimethylsilane (**14**): To an oven-dried screw-cap tube containing a stirring bar, furan (1.2 equiv., 0.3 mmol, 22 μL) and THF (1 mL) were added via syringe, and the resulting solution was cooled to -78 ºC. Then *n*BuLi (1.2 equiv., 2.5 M, 0.3 mmol, 120 μL) was added dropwise under -78 ºC. The resultant mixture was allowed to warm to room temperature and stirred for 1h. Subsequently, the reaction mixture was cooled back to -78 ºC, and a solution of trimethyl(2-(4,4,5,5-tetramethyl-1,3,2-dioxaborolan-2-yl)heptyl)silane (**5a,** 74 mg, 0.25 mmol) in THF (0.5 ml) was added dropwise. The resulting mixture was stirred at the same temperature for 1h and a solution of NBS (1.2 equiv., 0.3 mmol, 54 mg) in THF (1 mL) was added dropwise. After 1h at -78 ºC, sat. aq. $Na_2S_2O_3$ (1 mL) was added, and the reaction mixture was allowed to warm to room temperature. The reaction mixture was diluted with EtOAc (10 mL) and water (5 mL). Then the mixture was extracted with EtOAc (3 x 10 mL), dried over $MgSO_4$, filtered, and concentrated under vacuum. The corresponding product **14** was purified by column chromatography on silica gel (*n*-hexane), to afford a colourless oil, 32 mg (54% yield). **^{1}H NMR** (400 MHz, $CDCl_3$) δ 7.28 – 7.26 (m, 1H), 6.25 (dd, *J* = 3.1, 1.9 Hz, 1H), 5.94 – 5.93 (m, 1H), 2.81 – 2.74 (m, 1H), 1.67 – 1.49 (m, 2H), 1.31 – 1.13 (m, 6H), 1.01 – 0.95 (m, 1H), 0.88 – 0.83 (m, 4H), -0.14 (s, 9H) ppm. **^{13}C NMR** (101 MHz, $CDCl_3$): δ 160.3, 140.3, 110.0, 104.5, 38.4, 35.2, 31.9, 27.2, 22.8, 22.6, 14.2, -1.3 ppm. **IR** (neat, cm-1): 2955, 2928, 2873, 2858, 1592, 1506, 1466, 1248, 1150, 1008. **HRMS:** m/z calcd. for ($C_{14}H_{27}OSi$) $[M+H]^+$: 239.1826 found 239.1825.

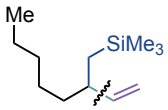

trimethyl(2-vinylheptyl)silane (15): To an oven-dried round bottom flask containing a stirring bar was added a solution of trimethyl(2-(4,4,5,5-tetramethyl-1,3,2-dioxaborolan-2-yl)heptyl)silane (**5a,** 0.4 mmol, 119.2 mg) in THF (4 mL) and subsequently vinylmagnesium bromide (4 equiv., 1M, 1.6 mmol, 1.6 mL) was added dropwise. The mixture was stirred as room temperature for 30 min. To the above solution at -78 ºC, a solution of I_2 (4 equiv., 1.6 mmol, 406 mg) in methanol (6.0 mL) was added dropwise. The reaction mixture was allowed to stir 30 min at the same temperature. Afterwards, to the mixture was added dropwise a solution of NaOMe (8 equiv., 3.2 mmol, 174 mg) in methanol (6 mL). After warming to room temperature, the mixture was stirred for another 1.5 h, diluted with pentane (40 mL), and washed with 10% aqueous solution of $Na_2S_2O_3$ (10 mL). Then, the mixture was extracted with EtOAc (3 x 10 mL), dried over $MgSO_4$, filtered, and concentrated under vacuum. The corresponding product **16** was purified by column chromatography on silica gel (*n*-hexane), to afford a colourless oil, 52 mg (66% yield). **^{1}H NMR** (400 MHz, $CDCl_3$) δ 5.56 (ddd, *J* = 17.1, 10.1, 8.8 Hz, 1H), 4.94 – 4.86 (m, 2H), 2.17 – 2.03 (m, 1H), 1.37 – 1.17 (m, 8H), 0.88 (t, *J* = 6.9 Hz, 3H), 0.67 – 0.54 (m, 2H), -0.01 (s, 9H) ppm. **^{13}C NMR** (101 MHz, $CDCl_3$): δ 145.7, 112.7, 40.5, 38.7, 32.1, 27.0, 23.5, 22.9, 14.3, -0.4 ppm. **IR** (neat, cm^{-1}): 2955, 2928, 2872, 2857, 1622, 1459, 1415, 1248, 1203. **HRMS:** m/z calcd. for $C_{12}H_{25}Si$ $[M-H]^+$: 197.1720 found 197.1724.

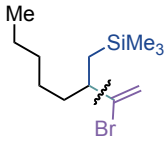

(2-(1-bromovinyl)heptyl)trimethylsilane (**16**): To an oven-dried round bottom flask containing a stirring bar, a solution of trimethyl(2-(4,4,5,5-tetramethyl-1,3,2-dioxaborolan-2-yl)heptyl)silane (**5a,** 0.3 mmol, 89.4 mg), vinyl bromide (0.6 mmol, 1M in THF, 0.6 mL) and diethyl ether (2 mL) were added sequentially. The above solution was stirred at -95 ºC, and then freshly prepared LDA (0.86 M, 0.7 mL) was added dropwise over 10 min. The reaction mixture was allowed to stir 1h at -95 ºC followed by dropwise addition of a solution of I_2 (0.66 mmol, 167.4 mg) in methanol (2 mL). After stirring for 5 min, the mixture was allowed warm to room temperature, after stirring for 1h a 20% aqueous solution of $Na_2S_2O_3$ (10 mL) was added. Then, the mixture was extracted with EtOAc (3 x 10 mL), dried over MgSO4, filtered, and concentrated under vacuum. The corresponding product **15** was purified by column chromatography on silica gel (*n*-hexane), to afford a colourless oil, 74 mg (89% yield). **^{1}H NMR** (400 MHz, $CDCl_3$) δ 5.59 (d, *J* = 1.4 Hz, 1H), 5.35 (d, *J* = 1.4, 1H), 2.31 – 2.22 (m, 1H), 1.50 – 1.41 (m, 1H), 1.34 – 1.21 (m, 6H), 1.19 – 1.11 (m, 1H), 0.88 (t, *J* = 6.9 Hz, 3H), 0.83

(dd, *J* = 14.8, 8.3 Hz, 1H), 0.64 (dd, *J* = 14.8, 5.8 Hz, 1H), 0.03 (s, 9H) ppm. **^{13}C NMR** (101 MHz, $CDCl_3$): δ 143.2, 115.9, 46.1, 36.8, 31.8, 26.9, 22.77, 22.77, 14.2, -0.7 ppm. **IR** (neat, cm-1): 3076, 2955, 2925, 2857, 1639, 1465, 1418, 1247, 995. **HRMS:** m/z calcd. for $C_{11}H_{22}BrSi$ $[M\text{-}CH_3]^+$: 261.0669 found 261.0662.

3.5.8. Mechanistic experiments

Reaction with potential intermediates 19 and 20

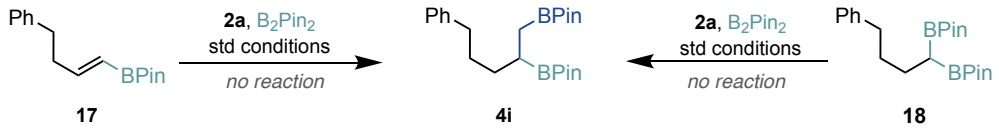

17 **4i** **18**

An oven-dried 8 mL screw-cap test tube containing a stirring bar was charged with $NiBr_4{\cdot}TBA_2$ (17.3 mg, 10 mol%), *N*-benzyl-6-methylpicolinamide (**L1**, 3.6 mg, 10 mol%), B_2Pin_2 (86.3 mg, 0.34 mmol). Subsequently, the tube was put into the glovebox under N_2 atmosphere, and *t*BuOLi (0.4 mmol, 32.0 mg) was added in the glovebox. Then the tube was sealed with a Teflon-lined screw cap and taken outside from the glovebox. Afterwards, 4,4,5,5-tetramethyl-2-(4-phenylbut-1-en-1-yl)-1,3,2-dioxaborolane (**17**, 51.6 mg, 0.20 mmol, 1.0 equiv.) or 2,2'-(4-phenylbutane-1,1-diyl)bis(4,4,5,5-tetramethyl-1,3,2-dioxaborolane) (**18**, 77.2 mg, 0.20 mmol, 1.0 equiv.), (bromomethyl)boronic acid pinacol ester (**2a**, 61 μL, 0.34 mmol, 1.0 equiv.), *t*BuOH (0.80 mmol, 76 μL, 4.0 equiv.) and DME (0.5 mL) were added via syringe, independently. Then, the tube was stirred at 30 ºC for 30 min. After the reaction was completed, the mixtures were diluted with EtOAc, filtered through silica gel. No desired product **4i** was detected by GC-MS determination.

Experiments with radical probe 17

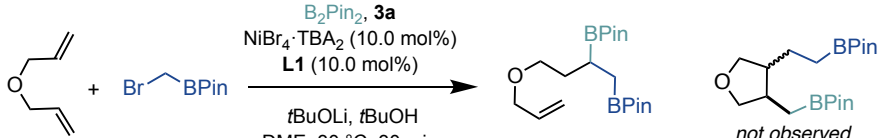

19 **2a** **20a**, 37% **20b**

An oven-dried 8 mL screw-cap test tube containing a stirring bar was charged with $NiBr_4{\cdot}TBA_2$ (17.3 mg, 10 mol%), N-benzyl-6-methylpicolinamide (**L1**, 3.6 mg, 10 mol%), B_2Pin_2 (86.3 mg, 0.34 mmol). Subsequently, the tube was put into the glovebox under N_2 atmosphere, and *t*BuOLi (0.4 mmol, 32.0 mg) was added in the glovebox. Then the tube was sealed with a Teflon-lined screw cap and taken outside from the glovebox. Afterwards, diallyl ether (**19**, 24 μL, 0.20 mmol, 1.0 equiv.), (bromomethyl)boronic acid pinacol ester (**2a**, 61 μL, 0.34 mmol, 1.0 equiv.), *t*BuOH (0.80 mmol, 76 μL, 4.0 equiv.) and DME (0.5 mL) were added

via syringe, independently. Then, the tube was stirred at 30 ºC for 30 min. After the reaction was completed, the mixture was diluted with EtOAc, filtered through silica gel, and concentrated under vacuum. The corresponding product **20a** was purified by column chromatography on silica gel (*n*-hexane/EtOAc 20:1), to afford a colourless oil, 27 mg (37% yield). The formation of the cyclisation product **20b**, was not observed either by GC-MS or column chromatography.

2,2'-(4-(allyloxy)butane-1,2-diyl)bis(4,4,5,5-tetramethyl-1,3,2-dioxaborolane) (20a): **^{1}H NMR** (400 MHz, $CDCl_3$) δ 5.90 (ddt, *J* = 17.2, 10.4, 5.6 Hz, 1H), 5.22 (ddd, *J* = 17.2, 3.5, 1.7 Hz, 1H), 5.07 (ddd, *J* = 10.4, 3.2, 1.3 Hz, 1H), 4.09 – 3.84 (m, 2H), 3.63 – 3.45 (m, 1H), 1.73 – 1.50 (m, 2H), 1.22 (s, 12H), 1.21 (s, 12H), 1.12 (dd, *J* = 15.2, 6.8 Hz, 1H), 1.00 (dd, *J* = 15.2, 7.1 Hz, 1H), 0.85 – 0.71 (m, 2H) ppm. **^{13}C NMR** (101 MHz, $CDCl_3$): δ 136.0, 116.1, 83.1, 83.0, 78.2, 69.7, 30.5, 25.0, 24.94 (2C), 24.9 ppm. **IR** (neat, cm^{-1}): 2978, 2931, 2868, 1458, 1370, 1317, 1272, 1214, 1143, 1078, 967. **HRMS:** m/z calcd. For $C_{19}H_{36}NaO_5{}^{10}B^{11}B$ $[M+Na]^+$: 388.2677 found 388.2666.

Isotopic-labelling experiment

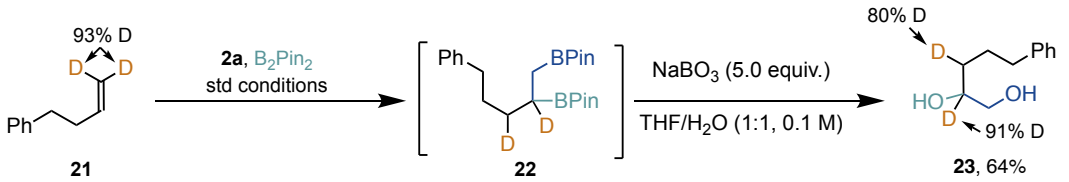

An oven-dried 8 mL screw-cap test tube containing a stirring bar was charged with $NiBr_4{\cdot}TBA_2$ (17.3 mg, 10 mol%), *N*-benzyl-6-methylpicolinamide (**L1**, 3.6 mg, 10 mol%), B_2Pin_2 (86.3 mg, 0.34 mmol). Subsequently, the tube was put into the glovebox under N_2 atmosphere, and *t*BuOLi (0.4 mmol, 32.0 mg) was added in the glovebox. Then the tube was sealed with a Teflon-lined screw cap and taken outside from the glovebox. Afterwards, (but-3-en-1-yl-4,4-D_2)benzene (**21**, 26.8 mg, 0.20 mmol, 1.0 equiv.), (bromomethyl)boronic acid pinacol ester (**2a**, 61 μL, 0.34 mmol, 1.0 equiv.), *t*BuOH (0.80 mmol, 76 μL, 4.0 equiv.) and DME (0.5 mL) were added via syringe, independently. Then, the tube was stirred at 30 ºC for 30 min. After the reaction was completed, the mixture was diluted with EtOAc, filtered through silica gel, and concentrated under vacuum. Then the residue was dissolved in THF and H_2O (1:1, 4 mL), and $NaBO_3{\cdot}H_2O$ (100 mg, 1.0 mmol, 5.0 equiv.) was added. The reaction mixture was stirred at room temperature for 4 h. After the reaction was completed, water (5 mL) was added. The aqueous phase was extracted with EtOAc (3 x 10 mL), and the combined organic phases were dried over $MgSO_4$ and concentrated. The corresponding product **23** was purified by column chromatography on silica gel (*n*-hexane/EtOAc 1:1), to afford a light-yellow oil, 23 mg (64% yield).

5-phenylpentane-1,2-diol (23): **^{1}H NMR** (400 MHz, $CDCl_3$) δ 7.31 – 7.23 (m, 2H), 7.21 – 7.16 (m, 3H), 3.71 – 3.65 (m, 0.15H), 3.60 (d, *J* = 11.2 Hz, 1H), 3.39 (d, *J* = 11.2 Hz, 1H), 2.96 (br s, 2H), 2.63 (t, *J* = 7.6 Hz, 2H), 1.83 – 1.73 (m, 1H), 1.70 – 1.61 (m, 1H), 1.48 – 1.37 (m, 1.2H) ppm. **^{13}C NMR** (101 MHz, $CDCl_3$): δ 142.2, 128.5, 128.4, 125.9, 71.8 (t, *J* = 19.7 Hz), 66.8, 35.9, 32.3 (t, *J* = 19.3 Hz), 27.3 ppm. **IR** (neat, cm^{-1}): 3355, 3105, 3085, 3062, 2927, 2860, 2152, 1603, 1496, 1453, 1382, 1147, 1122, 1030, 949. **HRMS:** m/z calcd. for ($C_{11}H_{16}NaO_2$) $[M+Na]^+$: 203.1043 found 204.1087 and **HRMS:** m/z calcd. for ($C_{11}H_{14}D_2NaO2$) $[M+Na]^+$: 205.1168 found 205.1168.

3.5.9. X-Ray crystallographic data

X-Ray Crystal structure for 9b (CCDC-2047528)

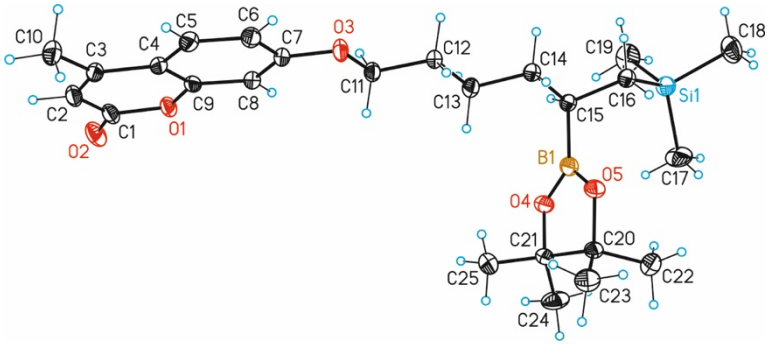

X-Ray Crystal structure for (L1)$_2$Ni (CCDC-2046367)

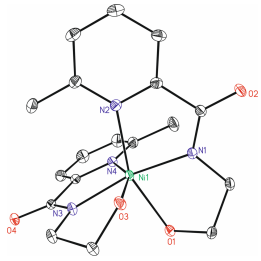

	9b	**$(L1)_2Ni$**
Formula	$C_{25}H_{39}BO_5Si$	$C_{22}H_{34}N_4NiO_6S_2$
Formula weight	458.48	573.36
T (K)	100(2)	100(2)
Wavelength (Å)	0.71073	0.71073
Crystal system	Triclinic	Triclinic
Space group	P-1	P-1
***a* (Å)**	6.83520(10)	10.1065(3)
***b* (Å)**	11.1658(2)	12.0082(4)
***c* (Å)**	17.3911(3)	12.2425(4)
***a* (deg)**	80.9320(10)	75.7108(8)
***b* (deg)**	84.6880(10)	76.3154(8)
***g* (deg)**	81.9640(10)	67.9818(7)
V ($Å^3$)	1294.46(4)	1317.51(7)
Z	6	2
Density (calc.) (Mg/m^3)	1.175	1.445
μ (mm^{-1})	0.122	0.938
F(000)	496	604
Crystal size (mm^3)	0.050 x 0.040 x 0.020	0.200 x 0.050 x 0.050
Theta range for data collection (deg)	2.352 to 31.937	1.739 to 33.160
Index ranges	-9<=h<=10, -16<=k<=13, -21<=l<=25	-15<=h<=15, -18<=k<=18, -14<=l<=17
Reflections collected	21731	27767
Independent reflections	8351[R(int) = 0.0262]	9665[R(int) = 0.0197]
Completeness to theta	93.3% 31.937°	95.9% 33.160°
Absorption correction	Multi-scan	Multi-scan
Max. and min. transmission	1.00 and 0.87	0.74 and 0.71
Refinement method	Full-matrix least-squares on F^2	Full-matrix least-squares on F^2
Data / restraints / parameters	8351/ 578/ 431	9665/ 0/ 330
Goodness-of-fit on F^2	1.027	1.042
Final R indices [I>2sigma(I)]	R1 = 0.0521, wR2 = 0.1305	R1 = 0.0266, wR2 = 0.0674
R indices (all data)	R1 = 0.0656, wR2 = 0.1363	R1 = 0.0326, wR2 = 0.0702
Largest diff. peak and hole	0.452 and -0.400 $e.Å^{-3}$	0.618 and -0.428 $e.Å^{-3}$

Table 5. Crystallographic data

3.5.10. NMR spectra

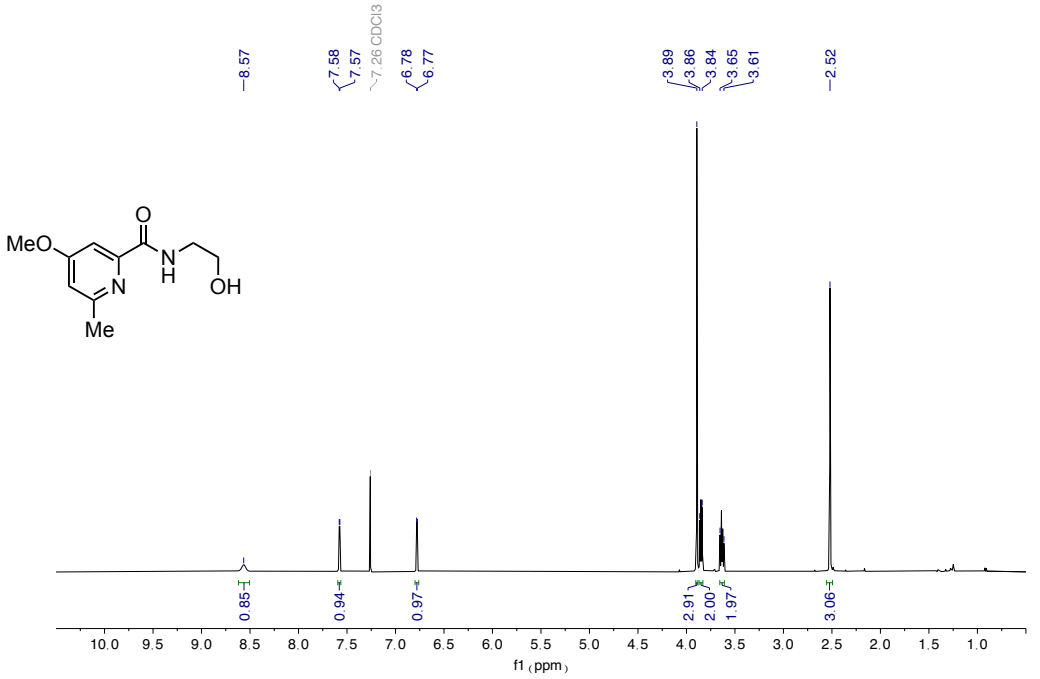

^{1}H NMR spectra (400 MHz) of **L2**

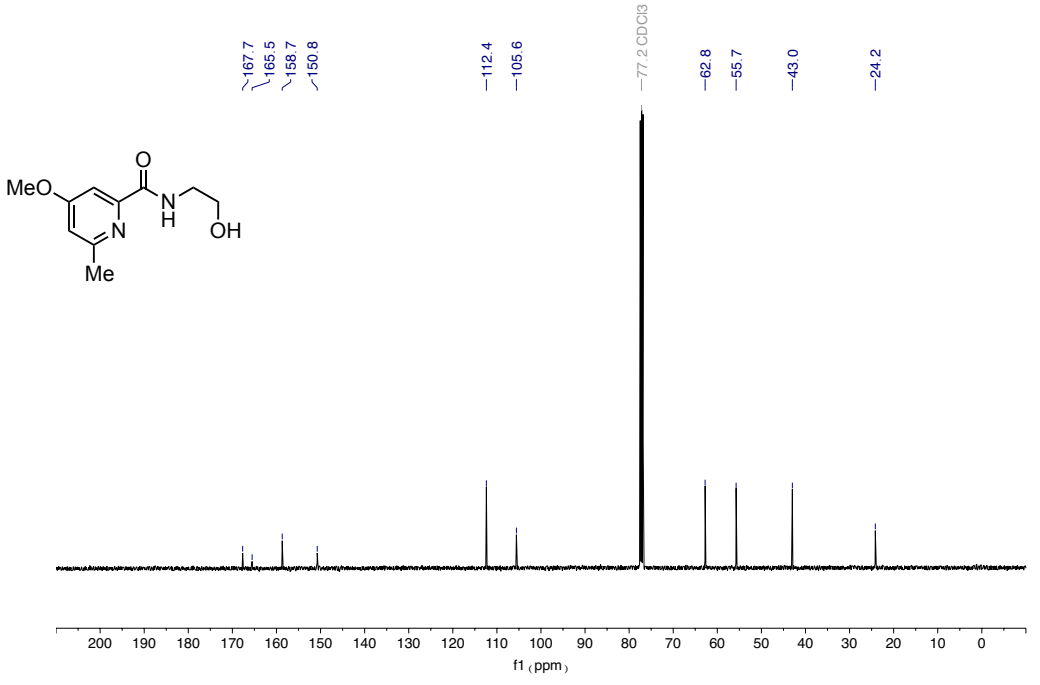

^{13}C NMR spectra (101 MHz) of **L2**

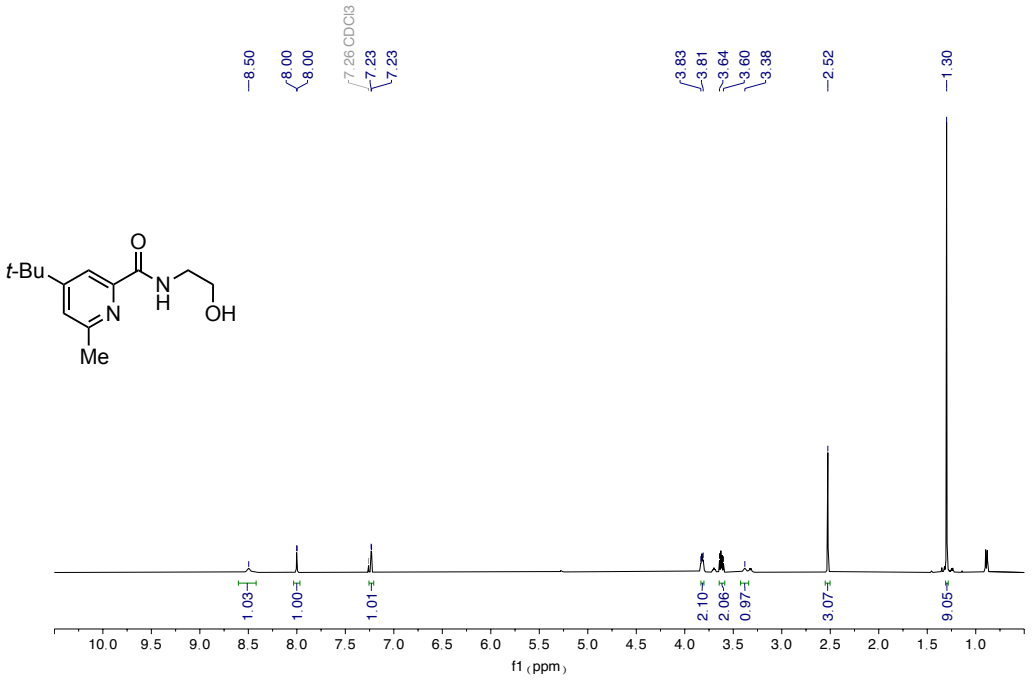

^{1}H NMR spectra (400 MHz) of **L3**

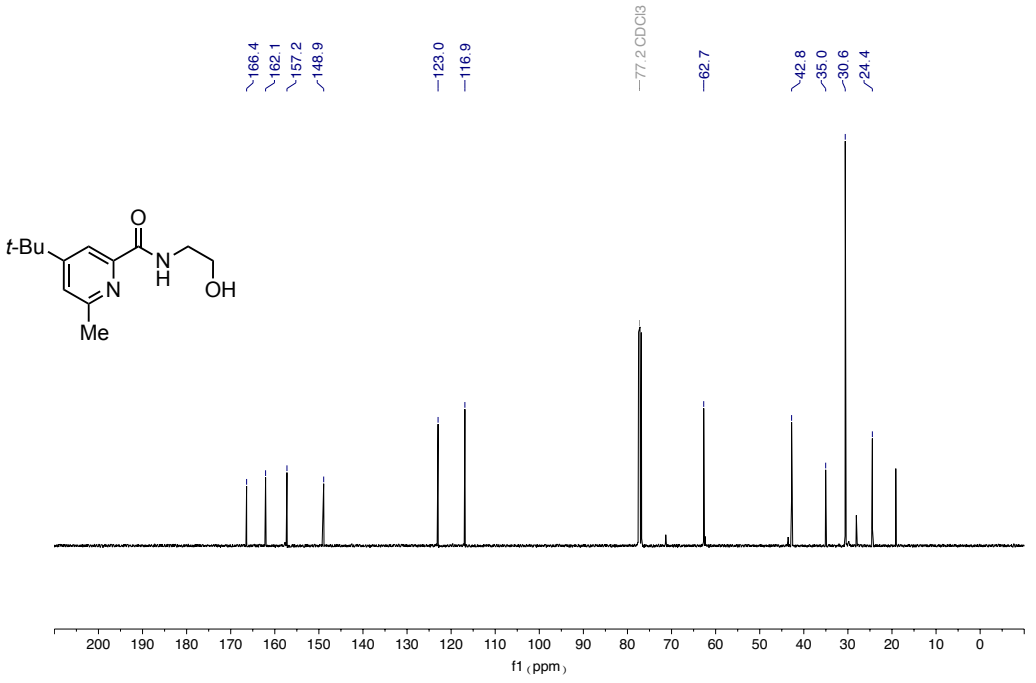

^{13}C NMR spectra (101 MHz) of **L3**

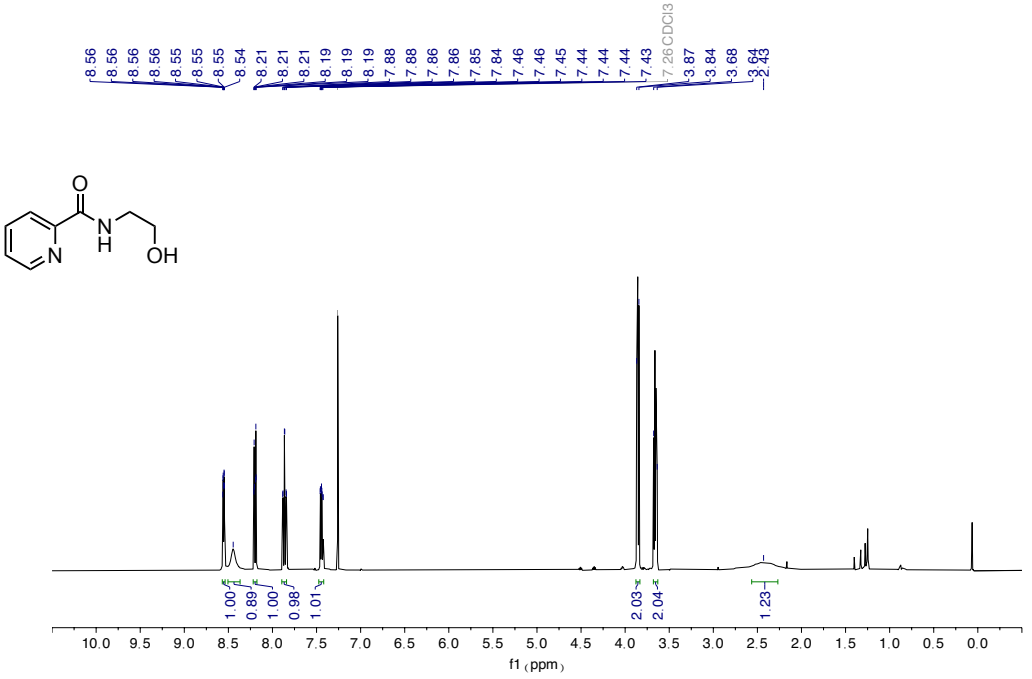

^{1}H NMR spectra (400 MHz) of **L7**

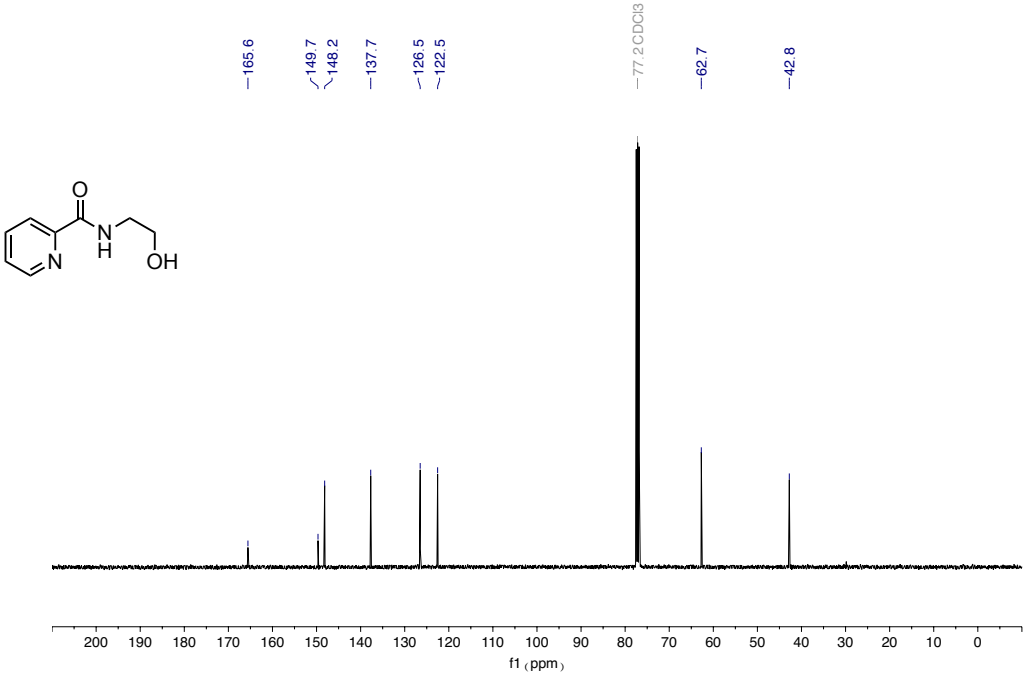

^{13}C NMR spectra (101 MHz) of **L7**

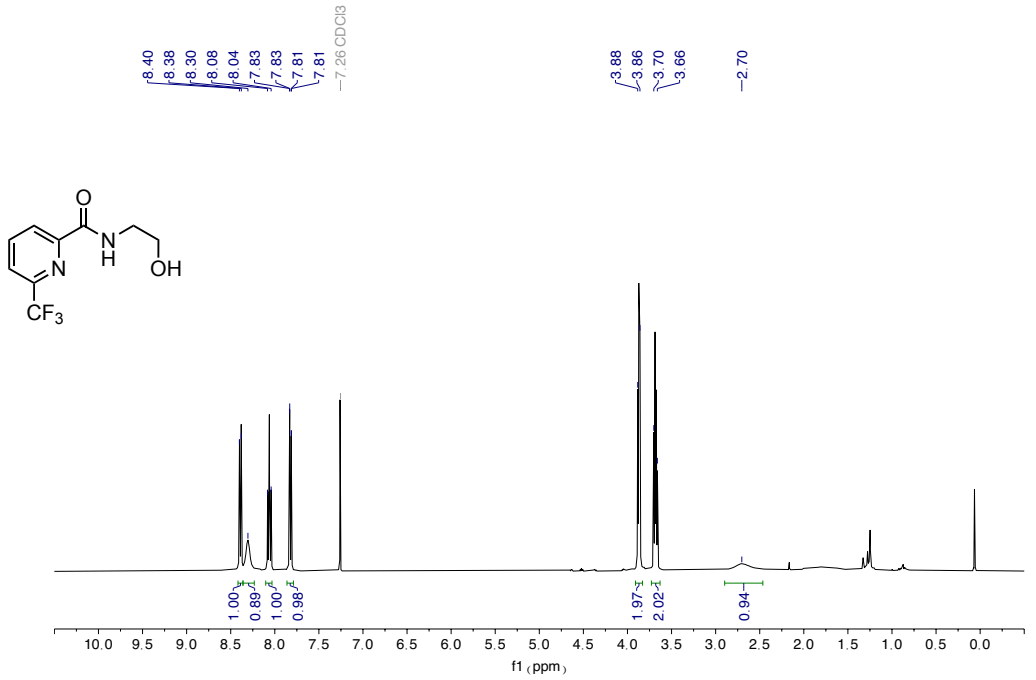

^{1}H NMR spectra (400 MHz) of **L8**

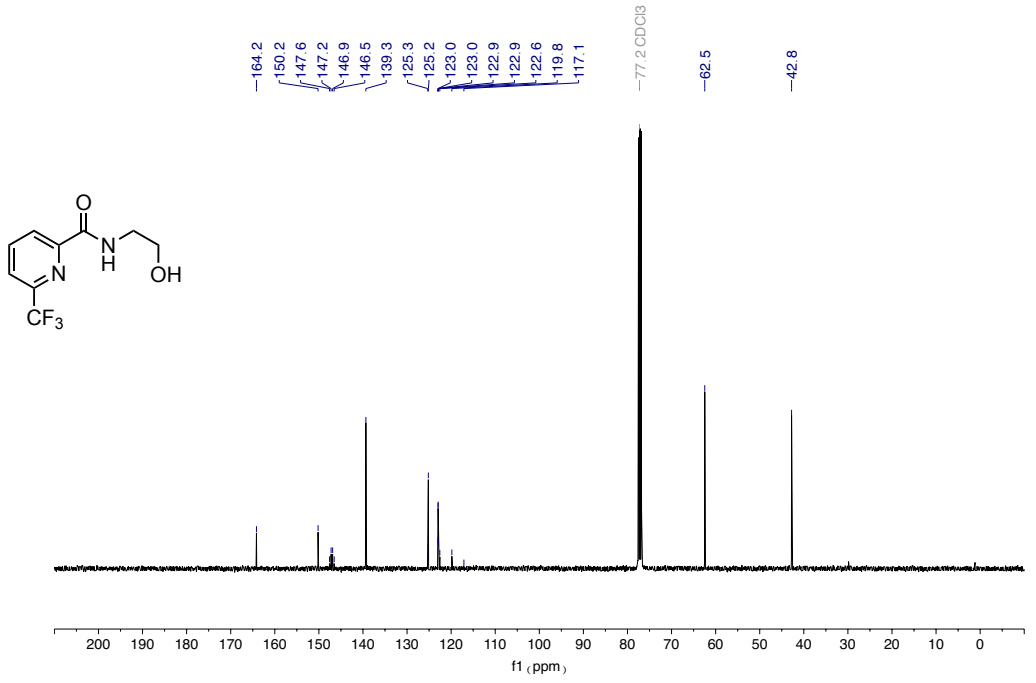

^{13}C NMR spectra (101 MHz) of **L8**

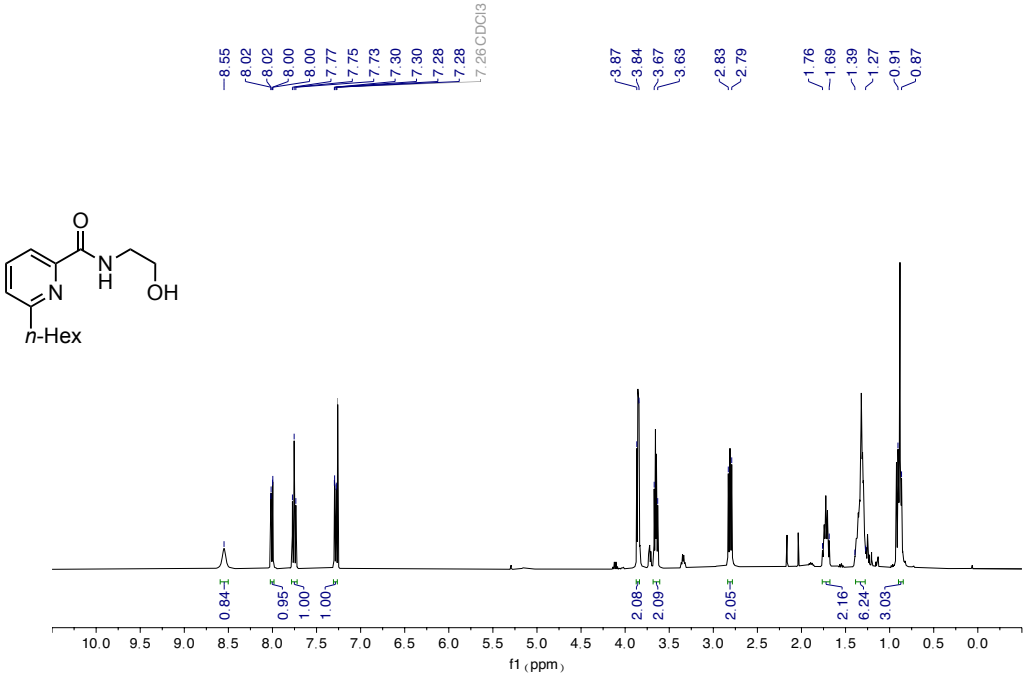

^{1}H NMR spectra (400 MHz) of **L9**

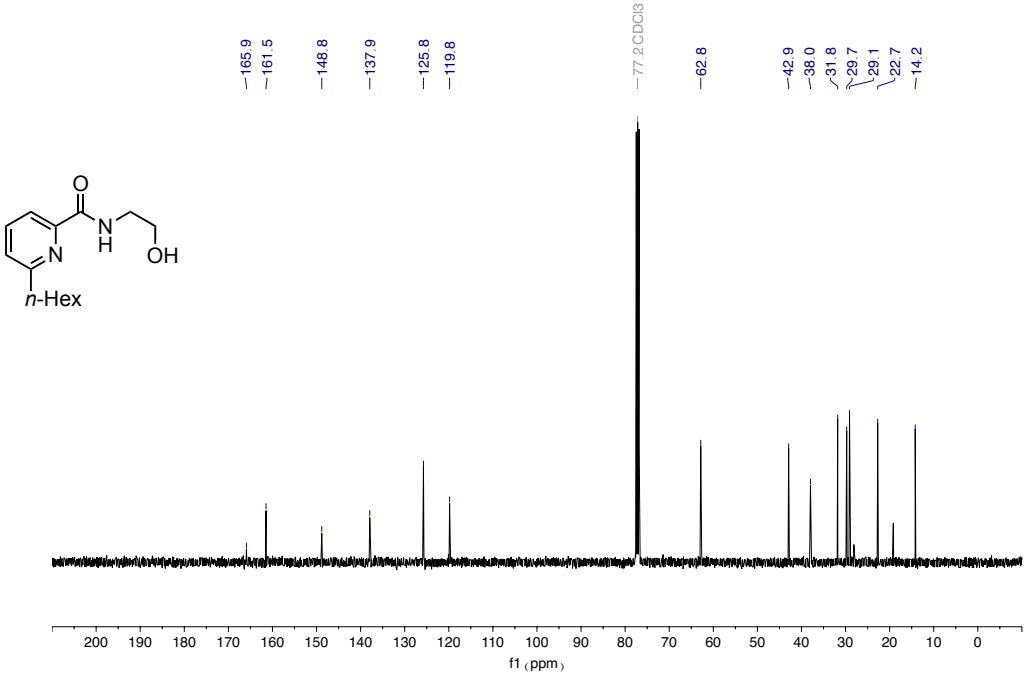

^{13}C NMR spectra (101 MHz) of **L9**

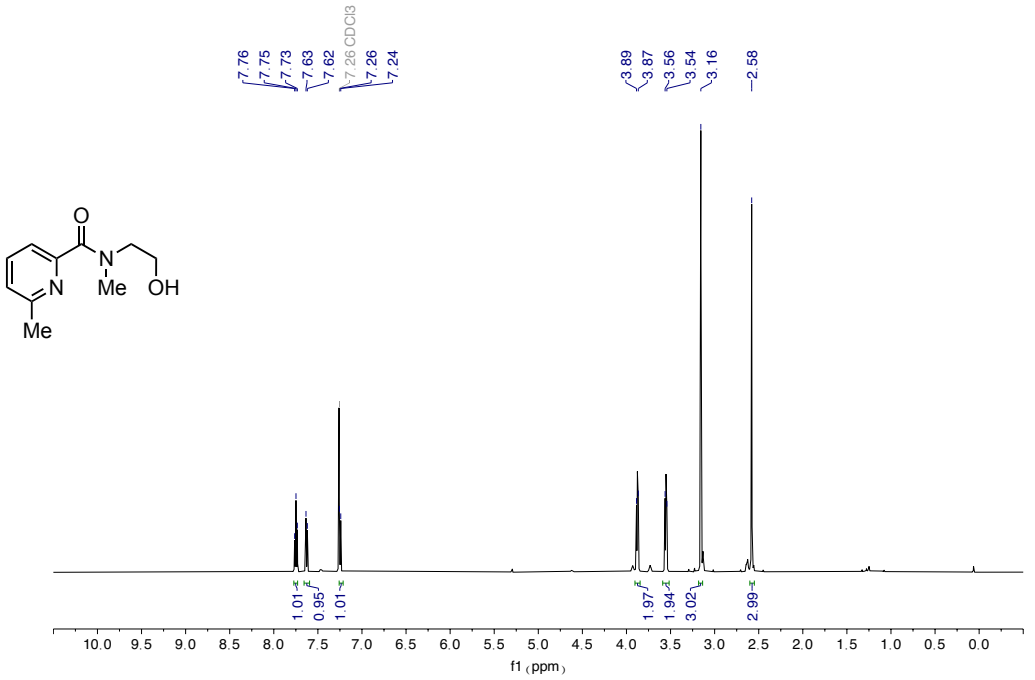

^{1}H NMR spectra (500 MHz) of **L10**

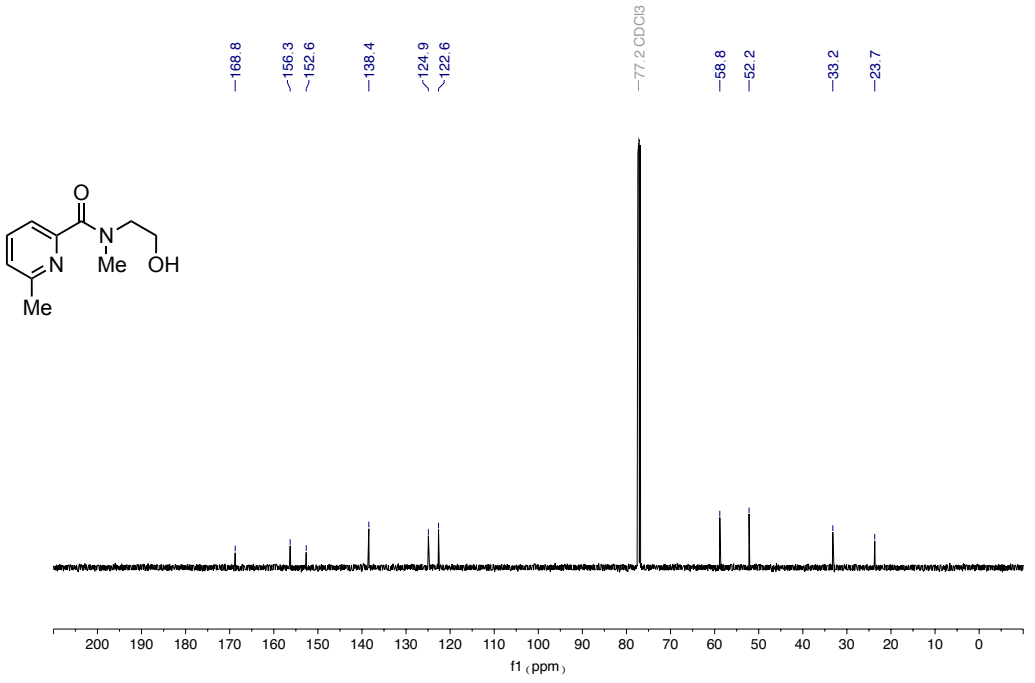

^{13}C NMR spectra (126 MHz) of **L10**

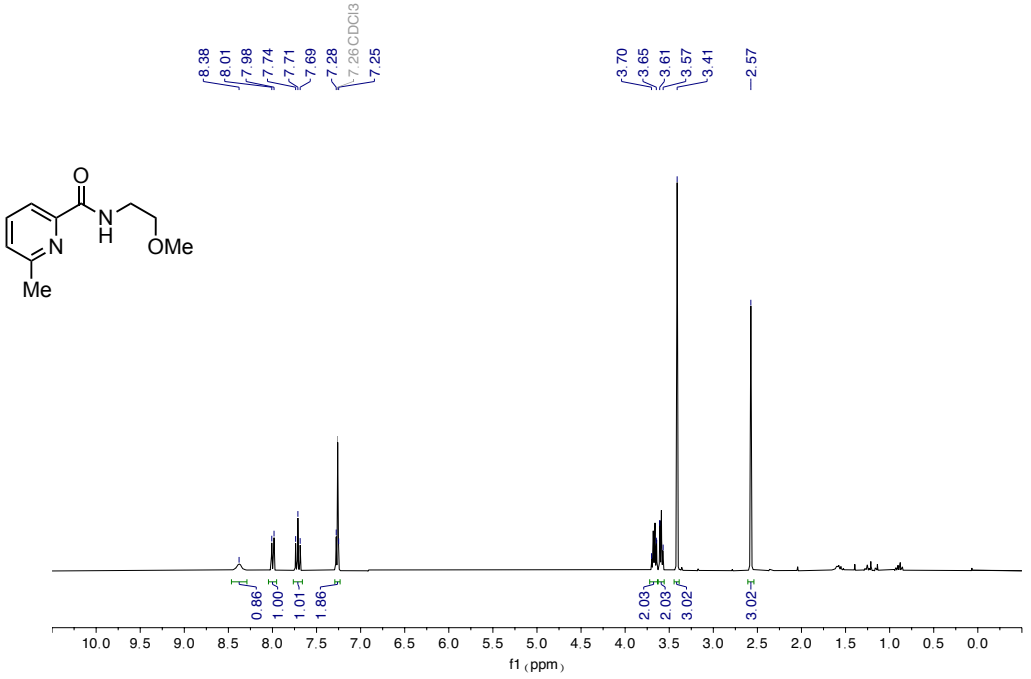

^{1}H NMR spectra (300 MHz) of **L4**

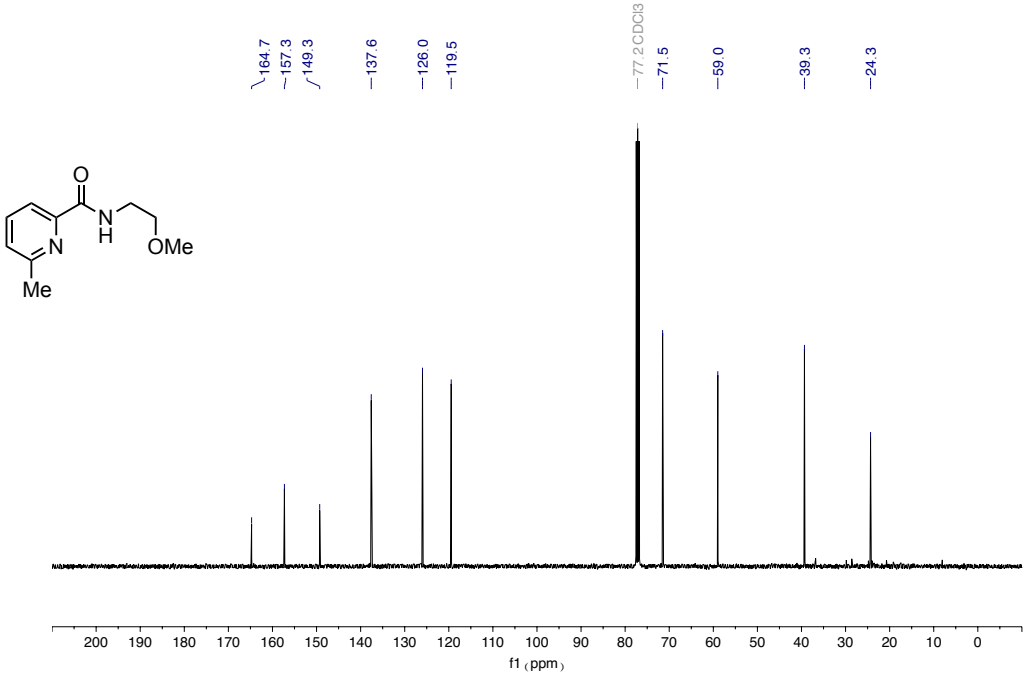

^{13}C NMR spectra (101 MHz) of **L3**

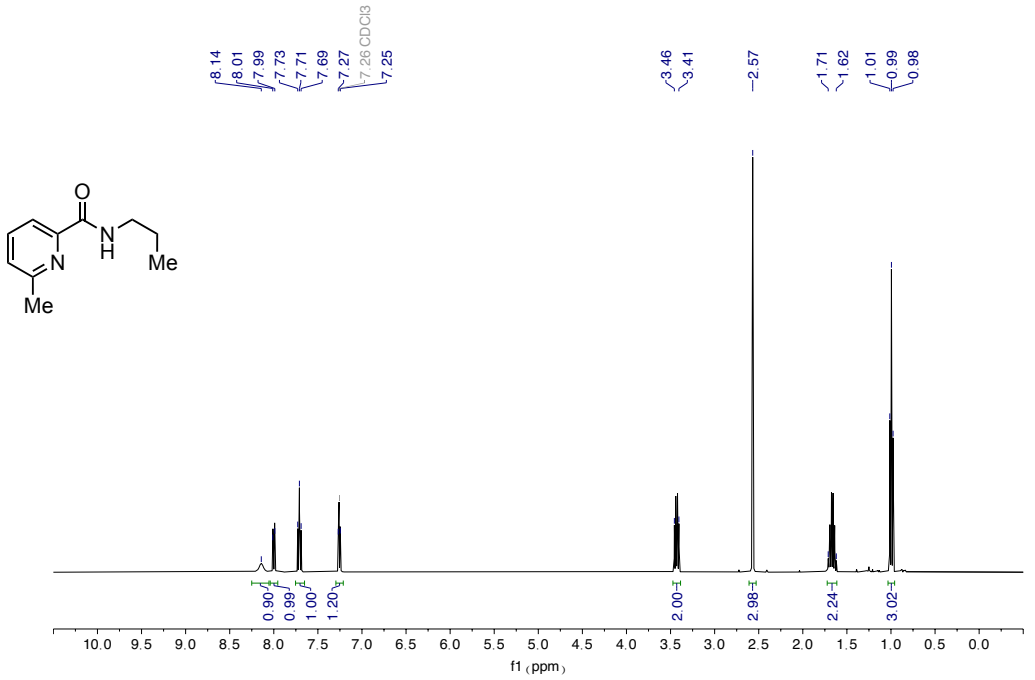

^{1}H NMR spectra (400 MHz) of **L5**

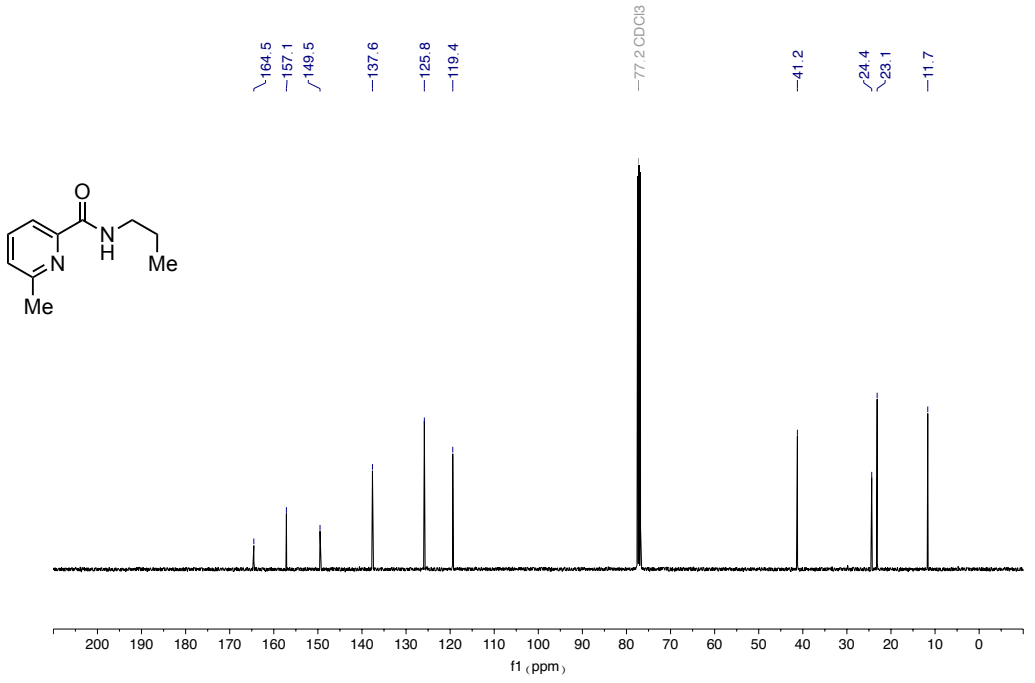

^{13}C NMR spectra (101 MHz) of **L5**

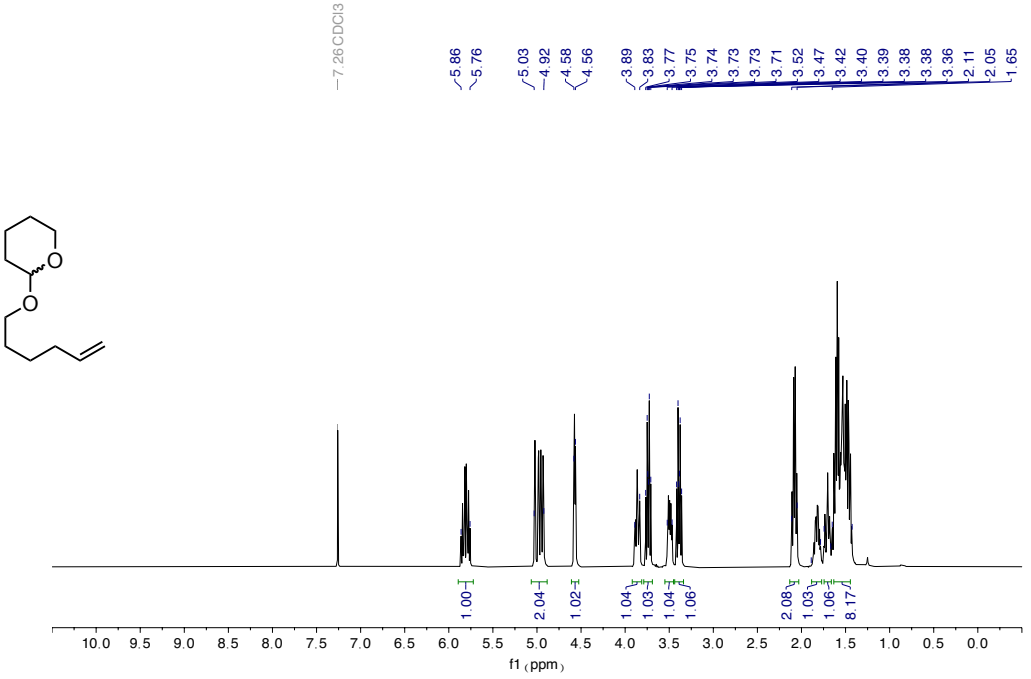

^{1}H NMR spectra (400 MHz) of **1m**

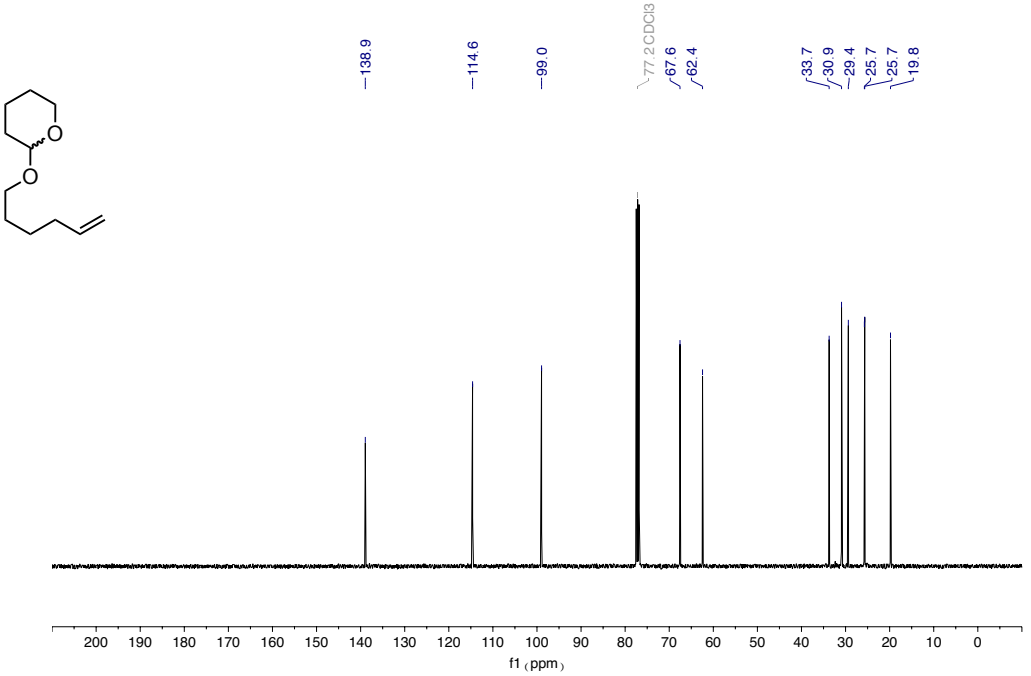

^{13}C NMR spectra (101 MHz) of **1m**

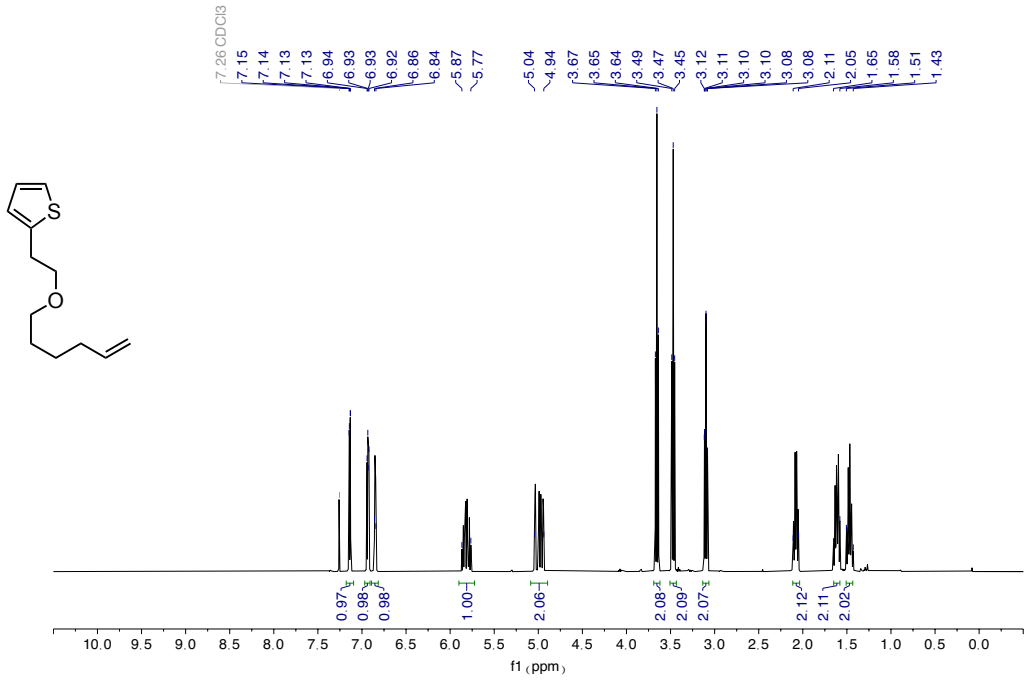

^{1}H NMR spectra (400 MHz) of **1n**

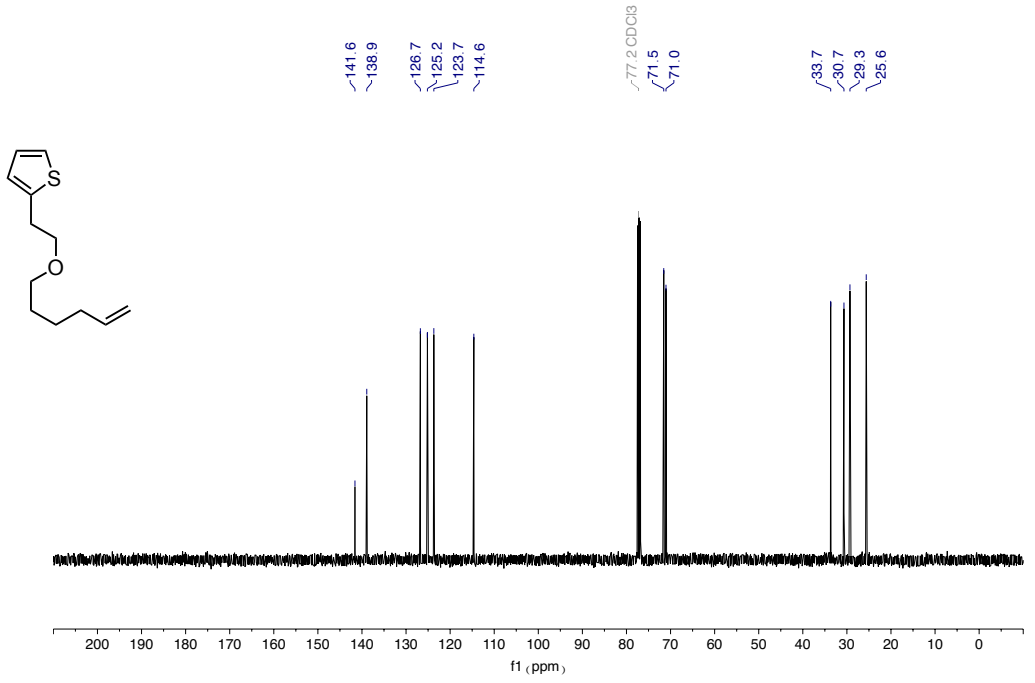

^{13}C NMR spectra (101 MHz) of **1n**

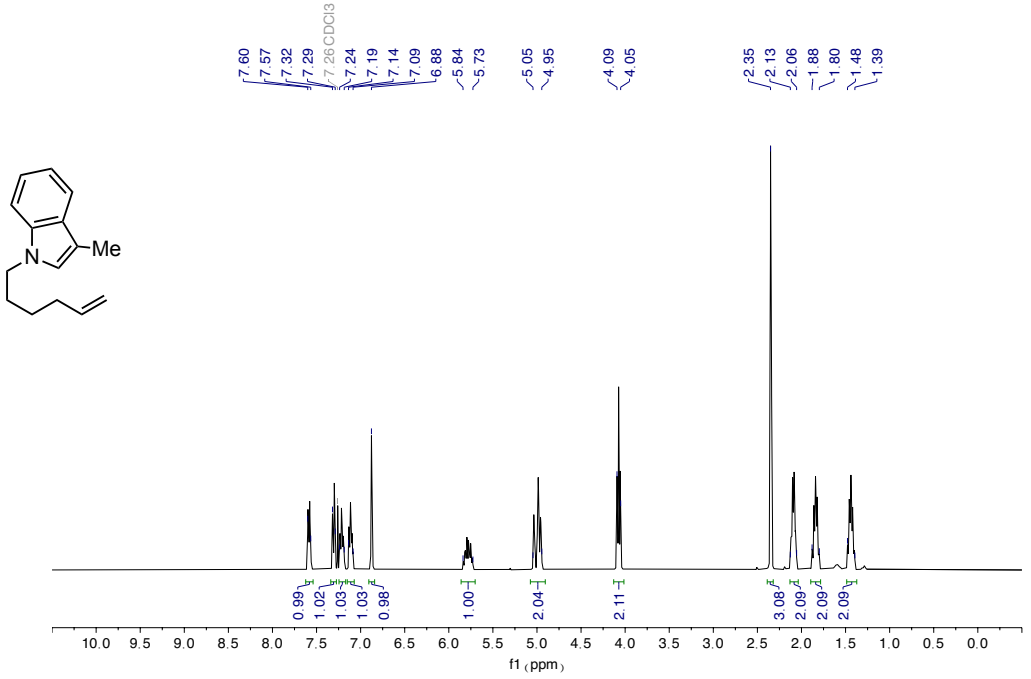

^{1}H NMR spectra (400 MHz) of **1o**

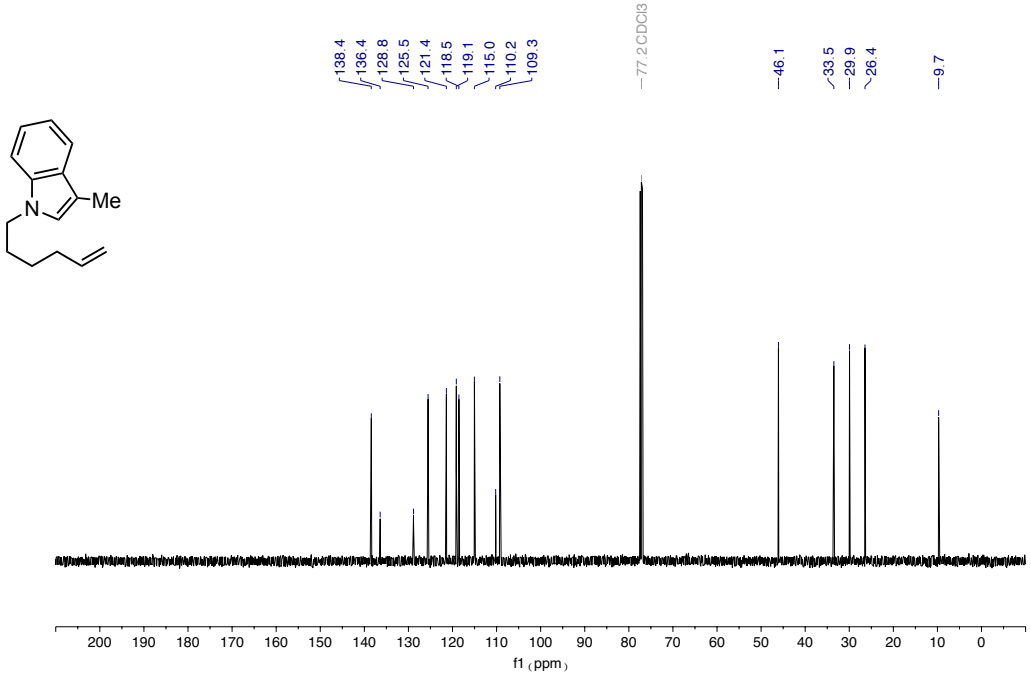

^{13}C NMR spectra (126 MHz) of **1o**

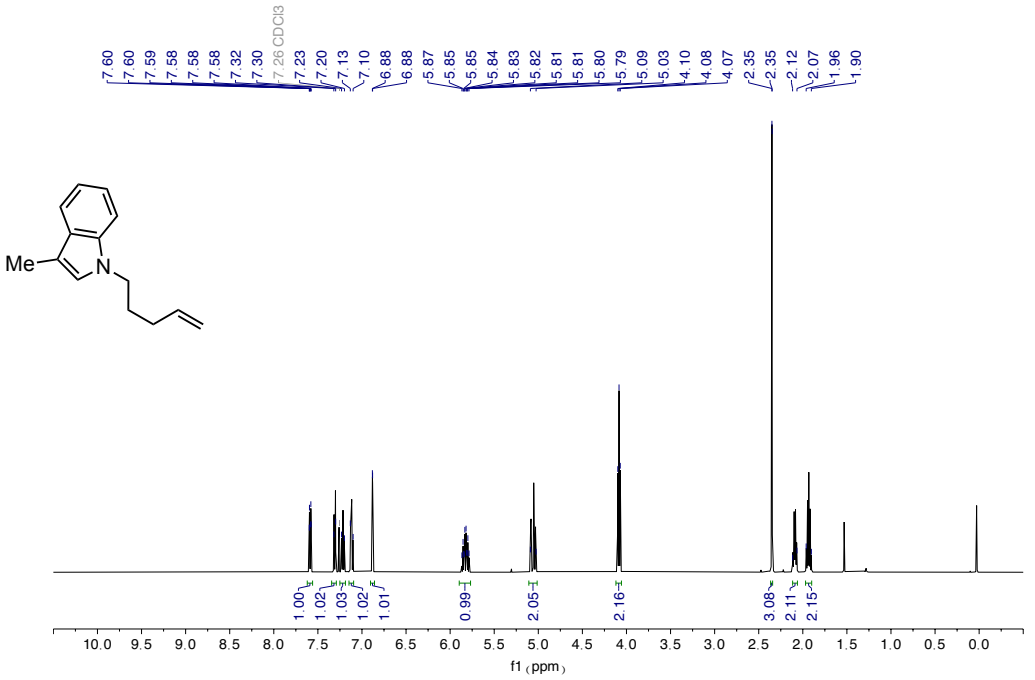

^{1}H NMR spectra (500 MHz) of **1q**

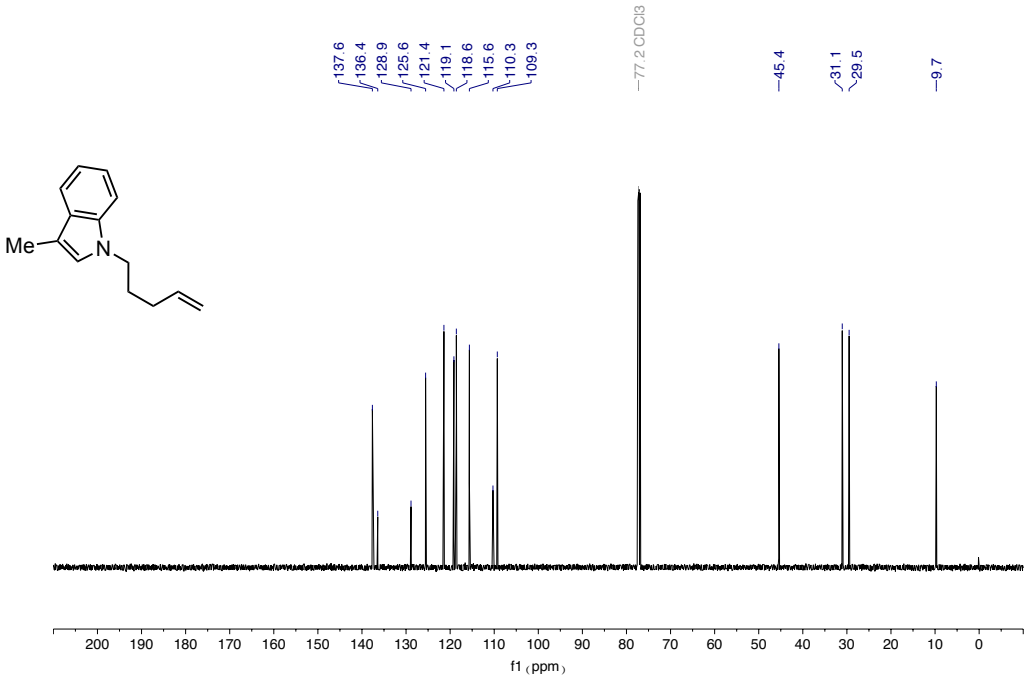

^{13}C NMR spectra (126 MHz) of **1q**

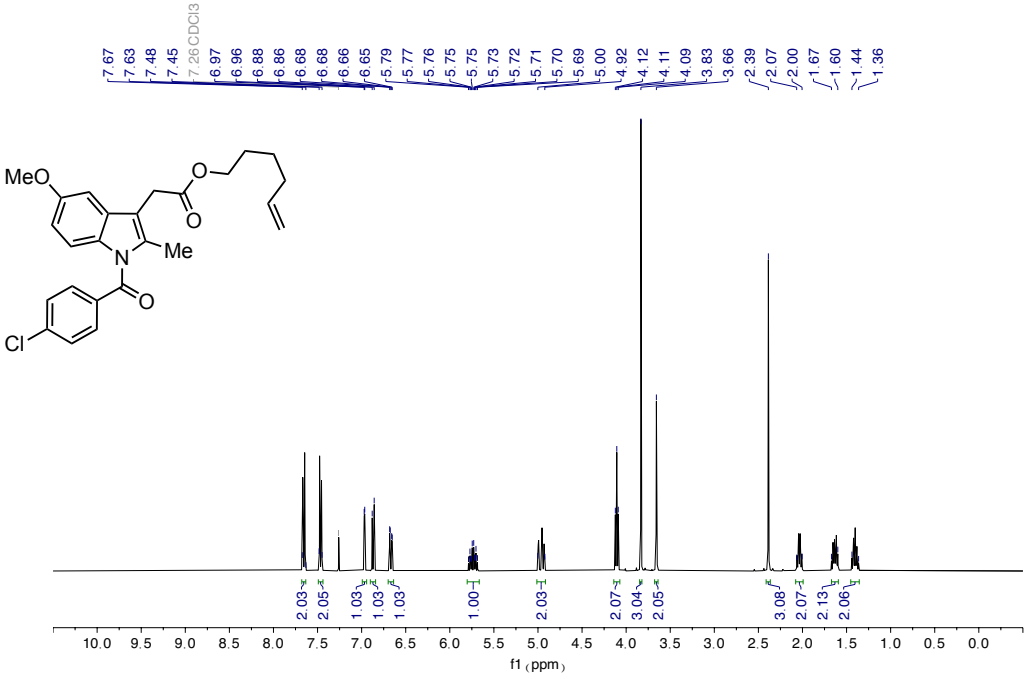

^{1}H NMR spectra (400 MHz) of **1u**

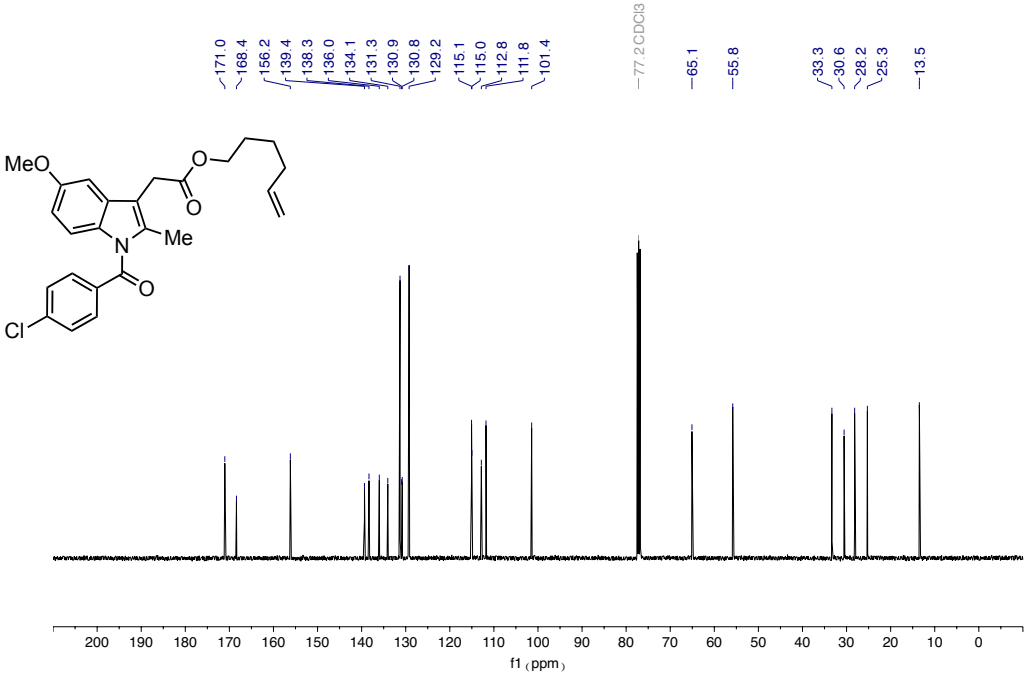

^{13}C NMR spectra (101 MHz) of **1u**

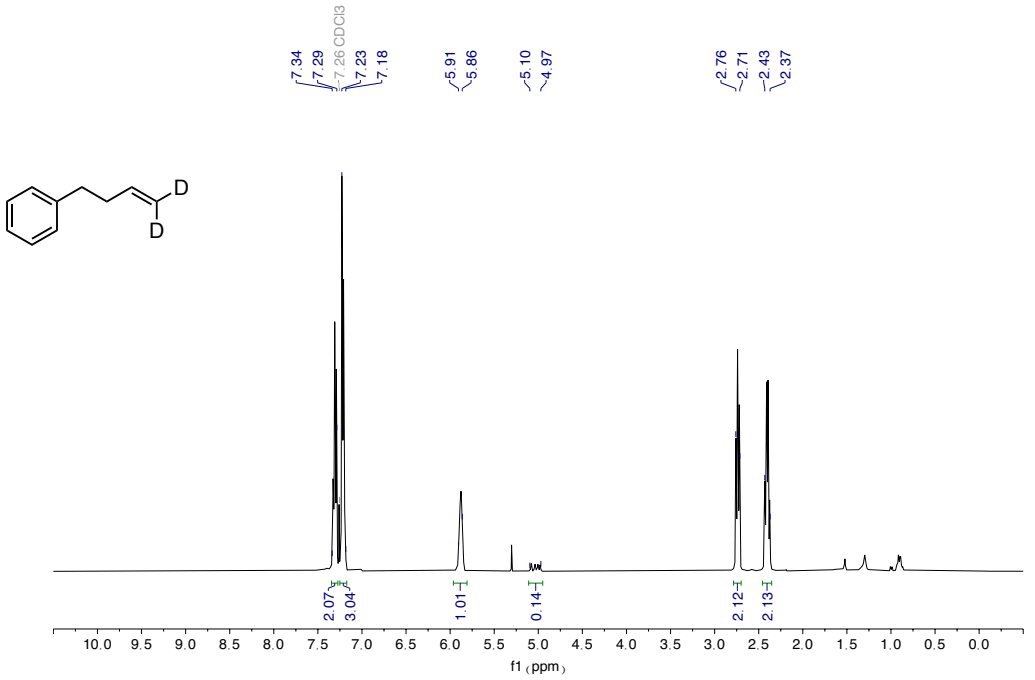

^{1}H NMR spectra (400 MHz) of **21**

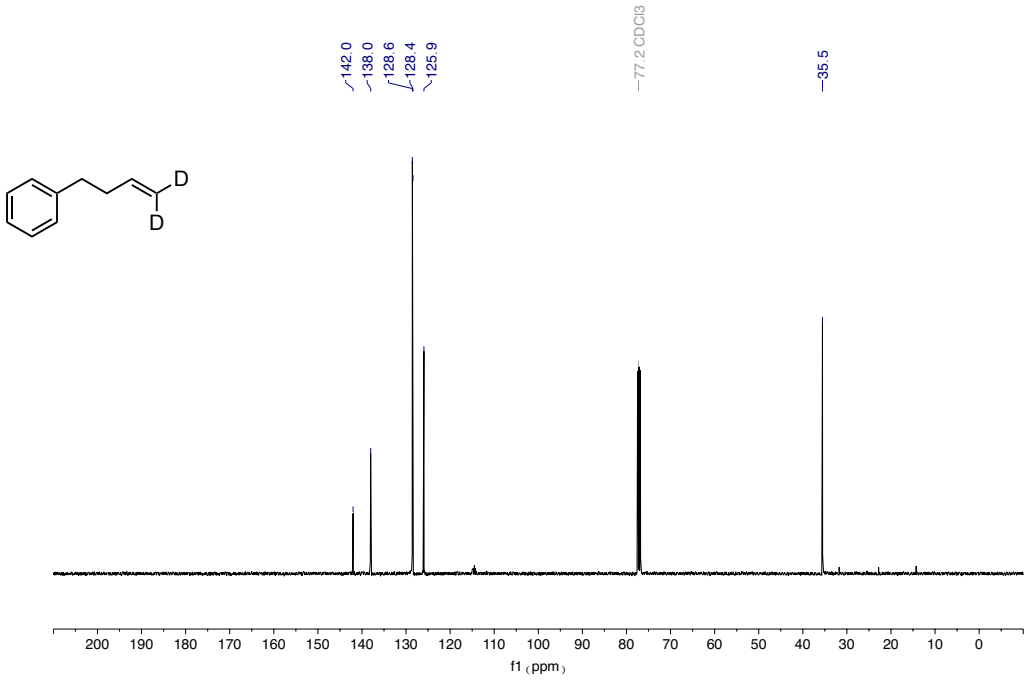

^{13}C NMR spectra (101 MHz) of **21**

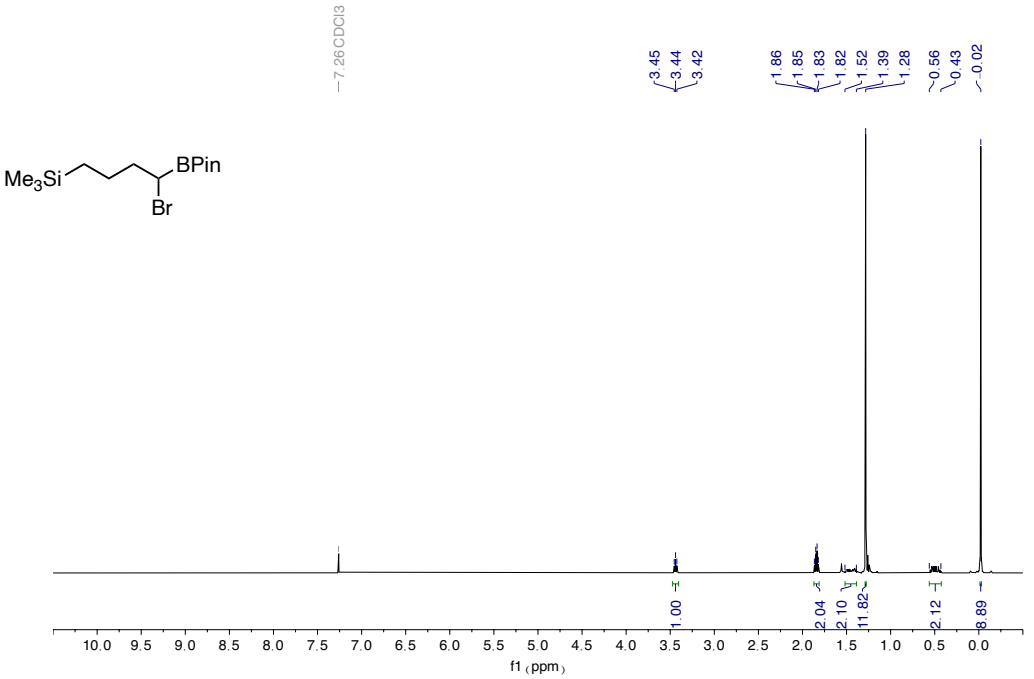

^{1}H NMR spectra (500 MHz) of **2c**

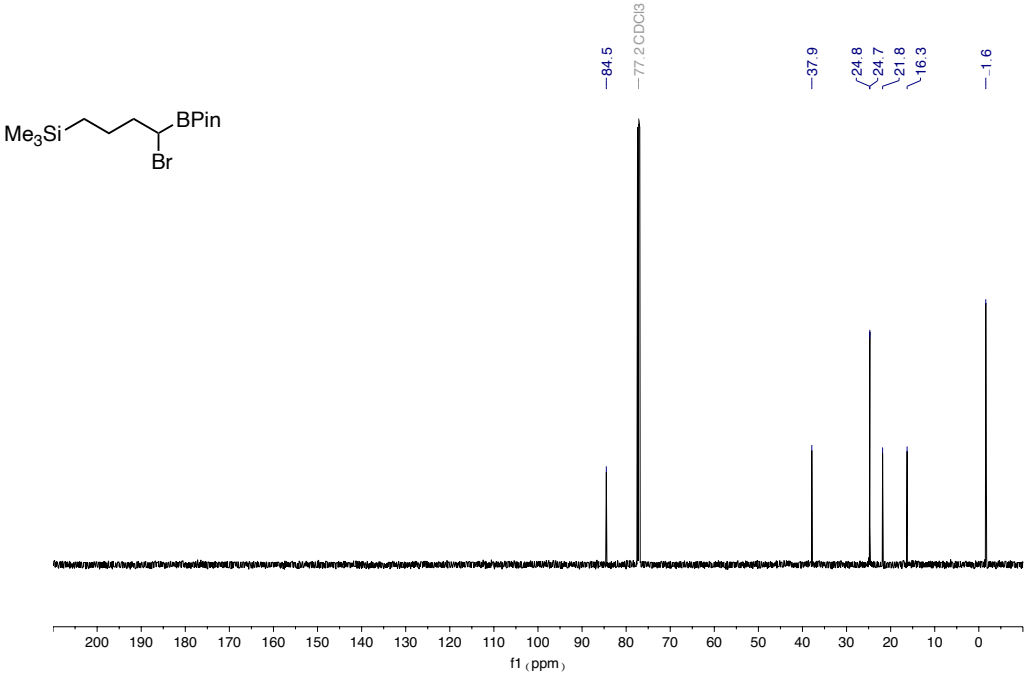

^{13}C NMR spectra (126 MHz) of **2c**

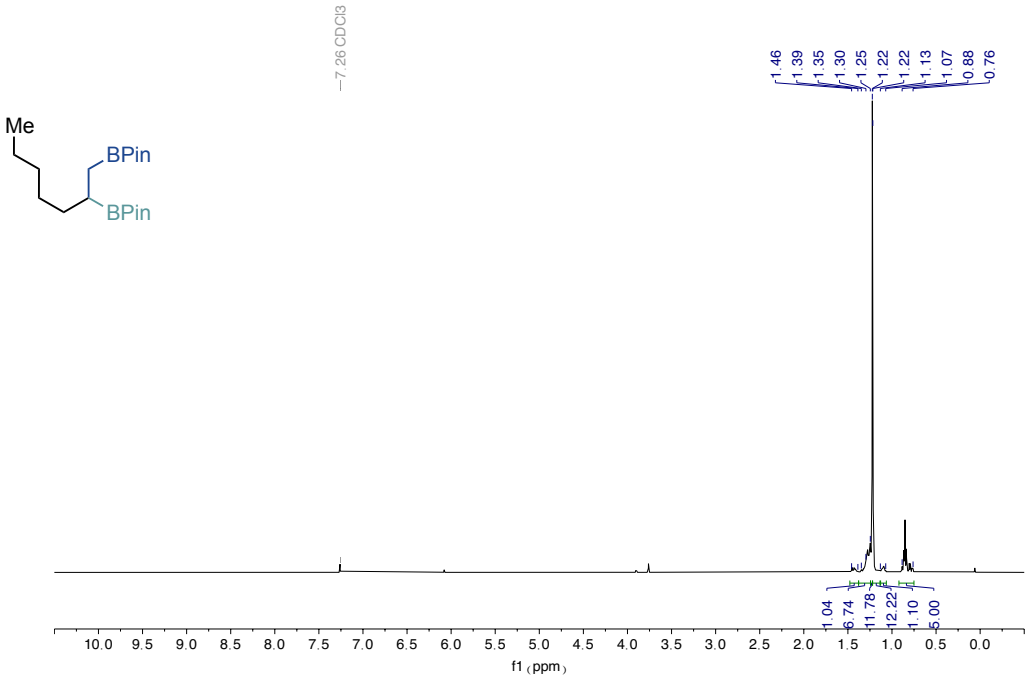

^{1}H NMR spectra (500 MHz) of **4a**

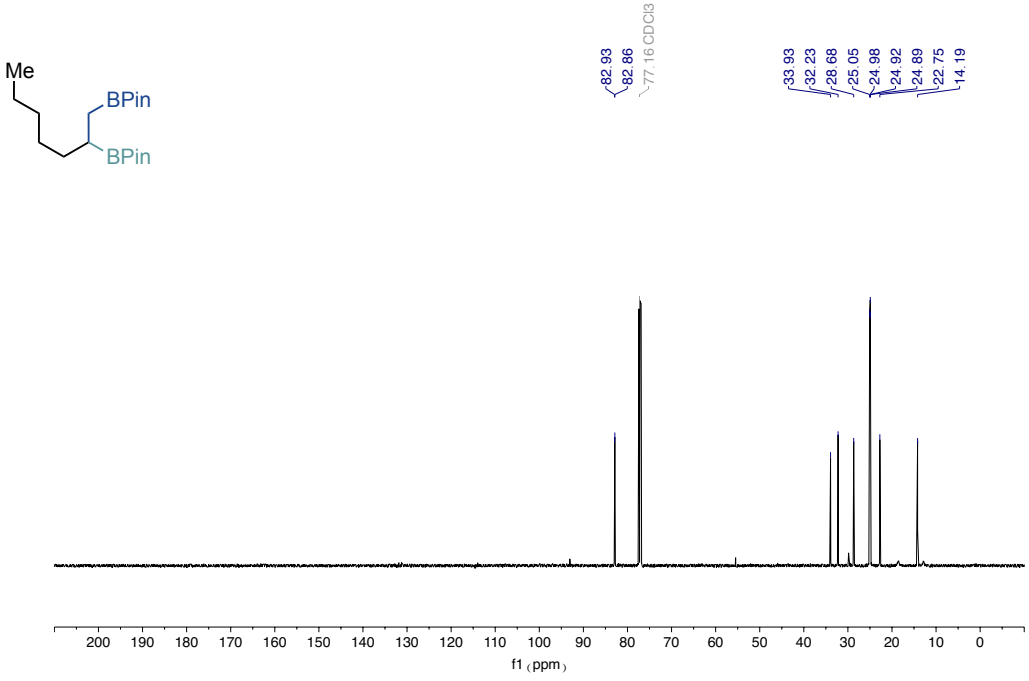

^{13}C NMR spectra (126 MHz) of **4a**

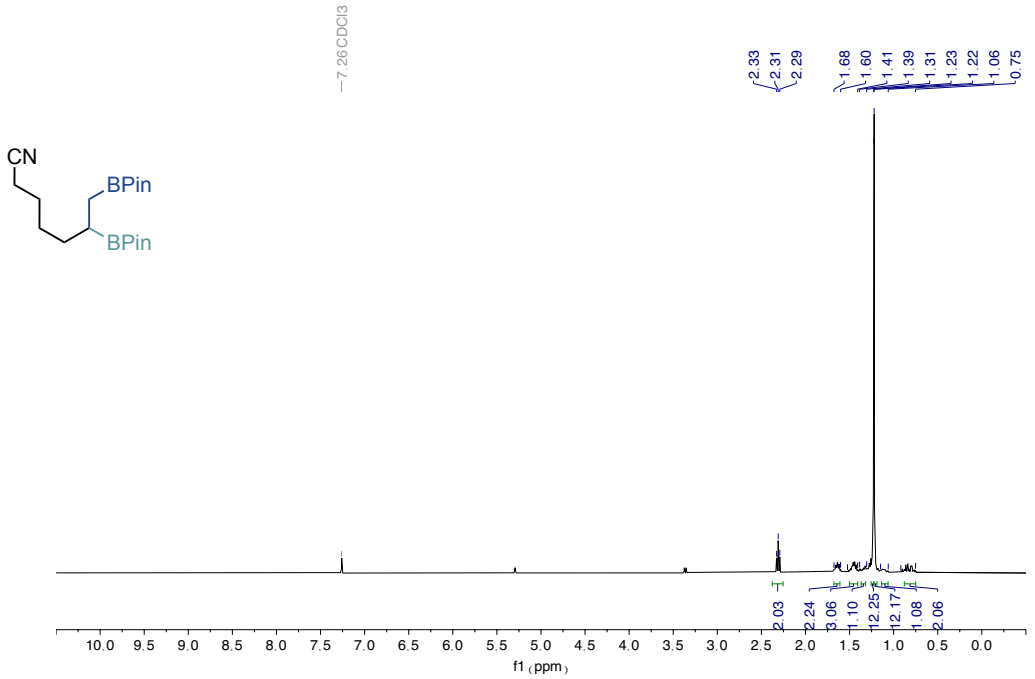

^{1}H NMR spectra (400 MHz) of **4b**

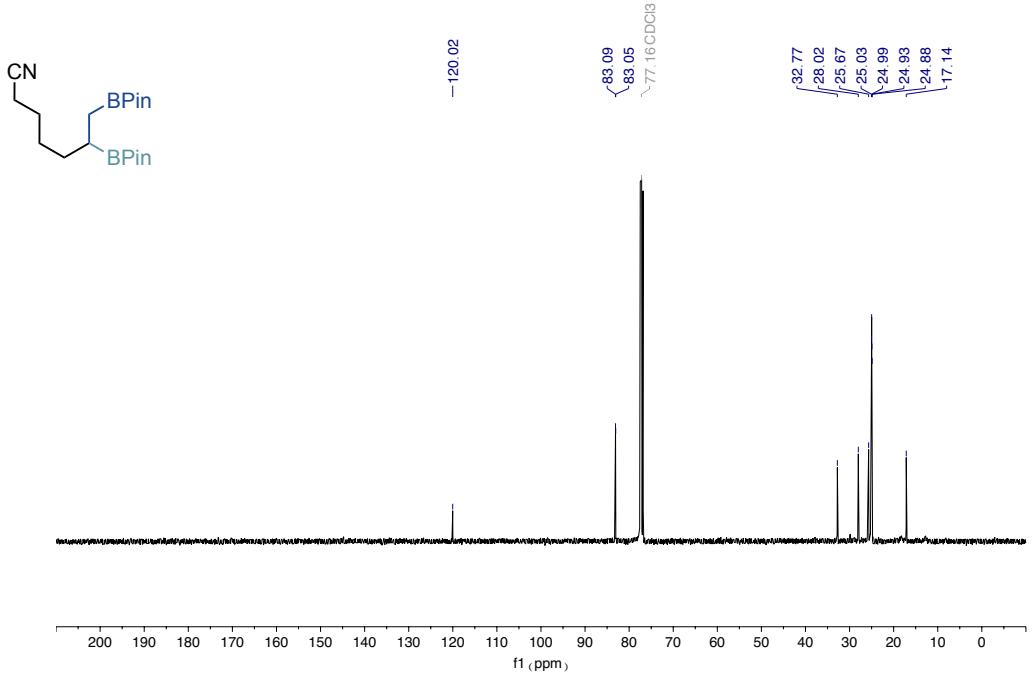

^{13}C NMR spectra (101 MHz) of **4b**

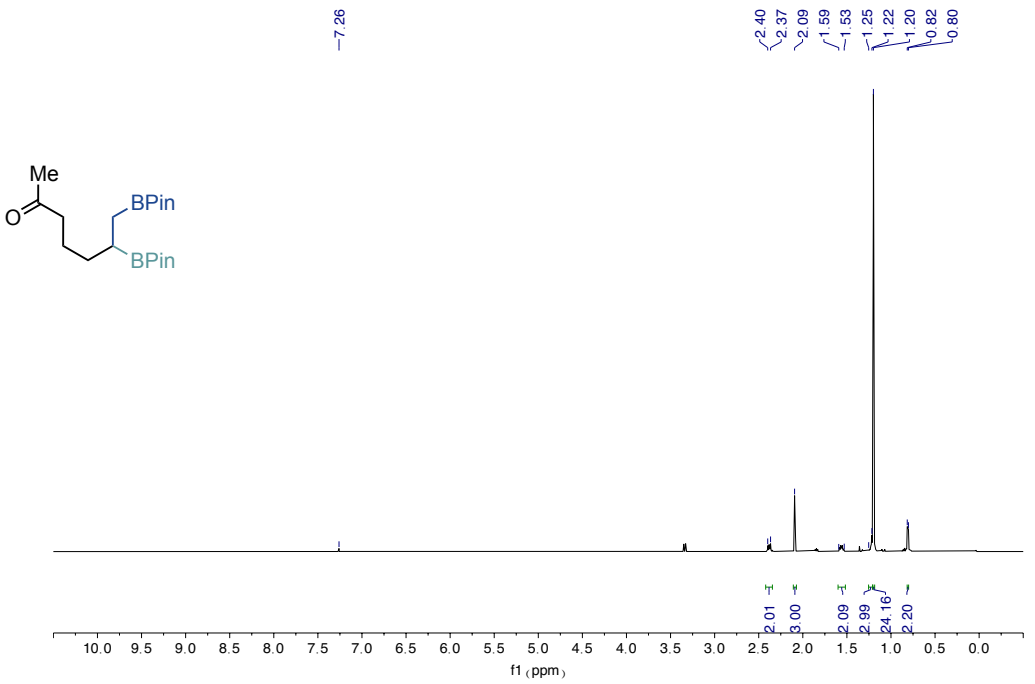

^{1}H NMR spectra (500 MHz) of **4c**

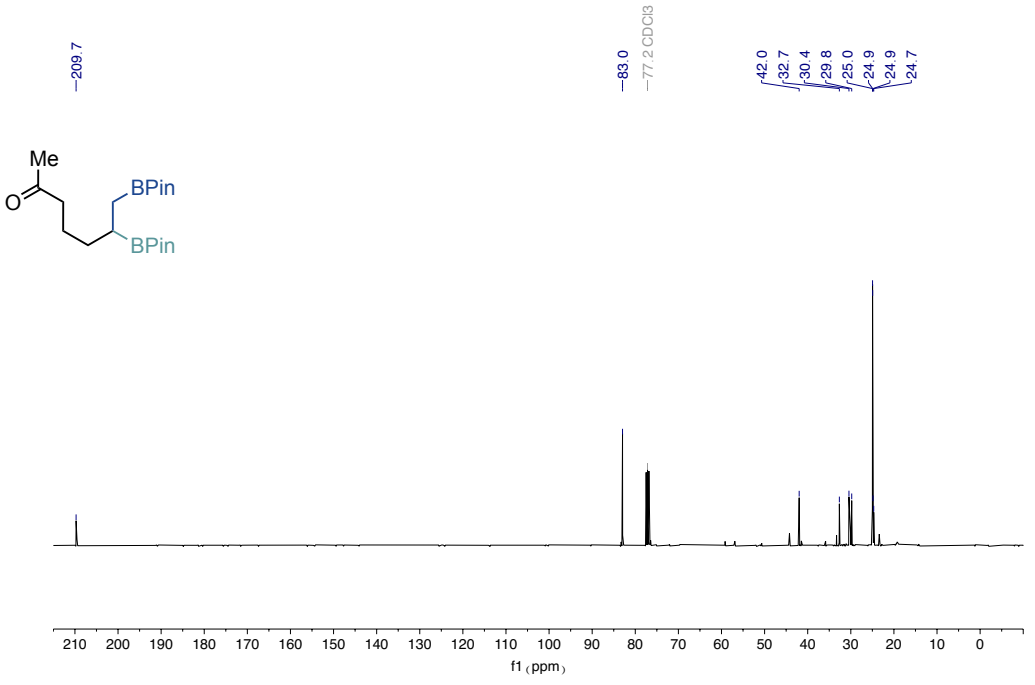

^{13}C NMR spectra (101 MHz) of **4c**

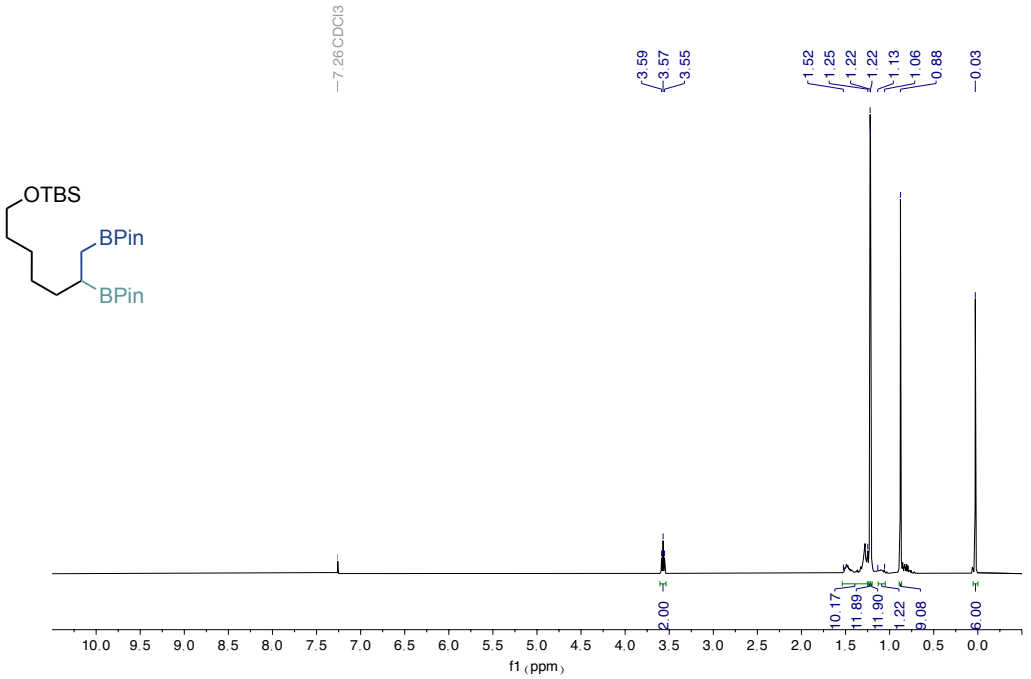

^{1}H NMR spectra (400 MHz) of **4d**

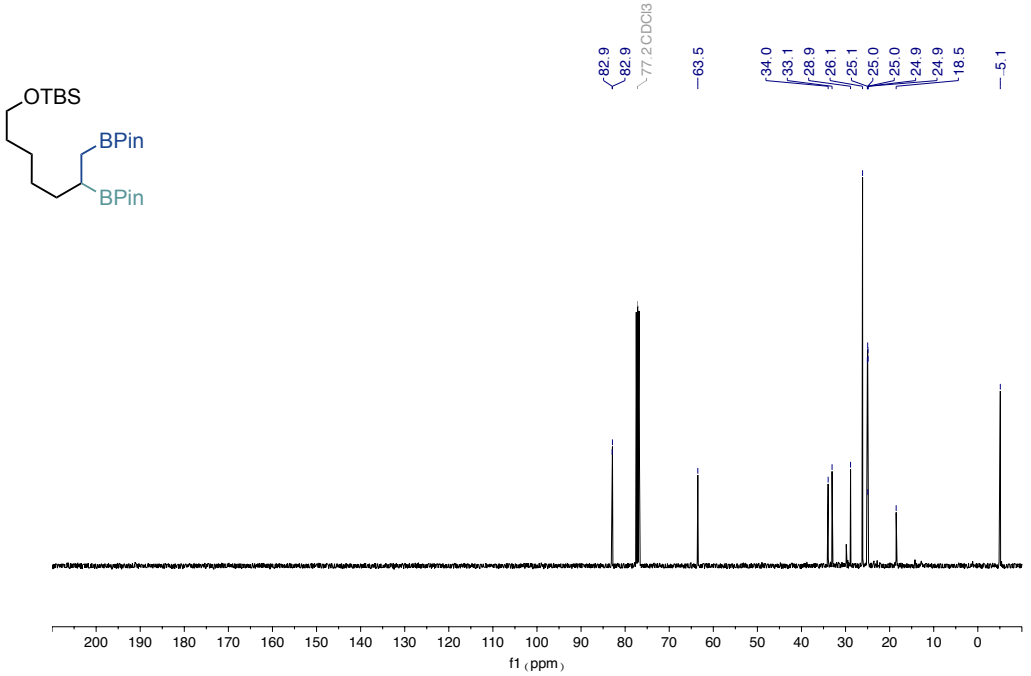

^{13}C NMR spectra (101 MHz) of **4d**

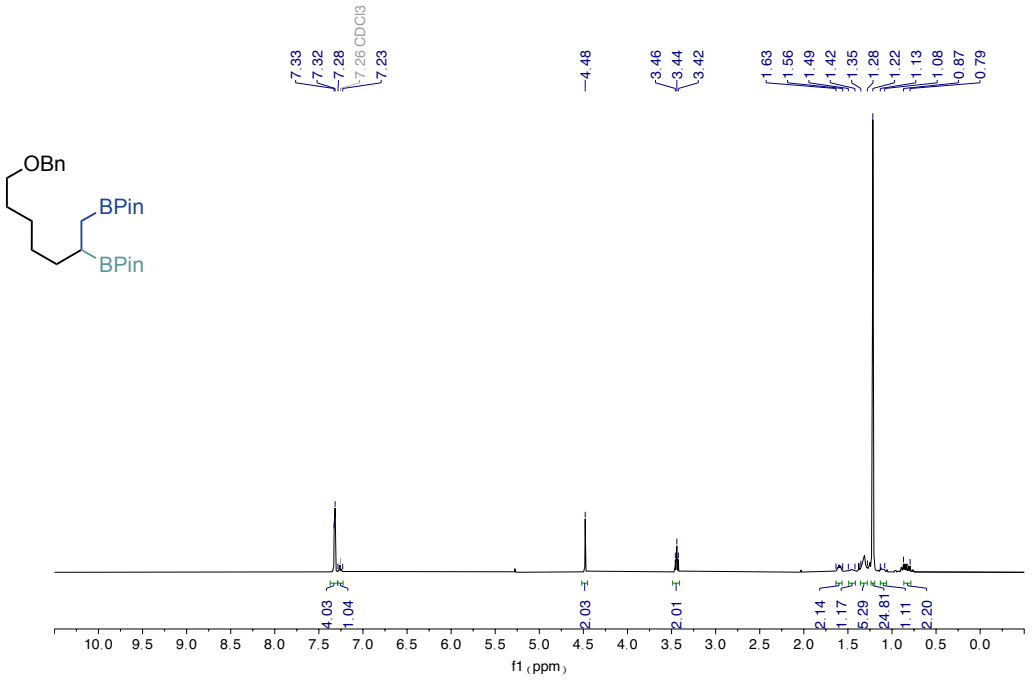

^{1}H NMR spectra (400 MHz) of **4e**

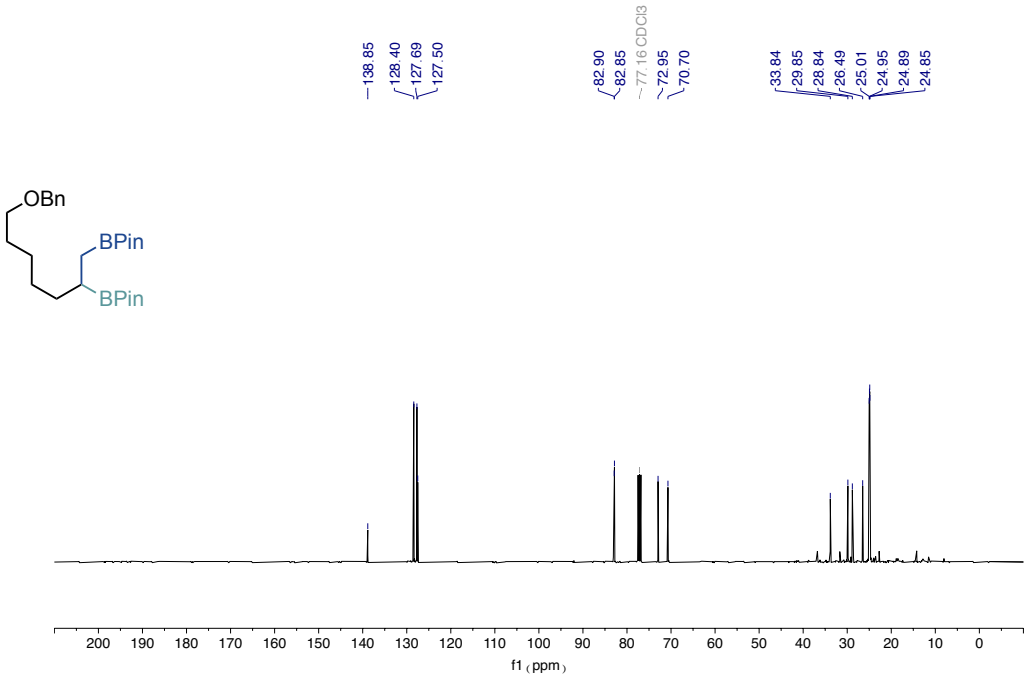

^{13}C NMR spectra (101 MHz) of **4e**

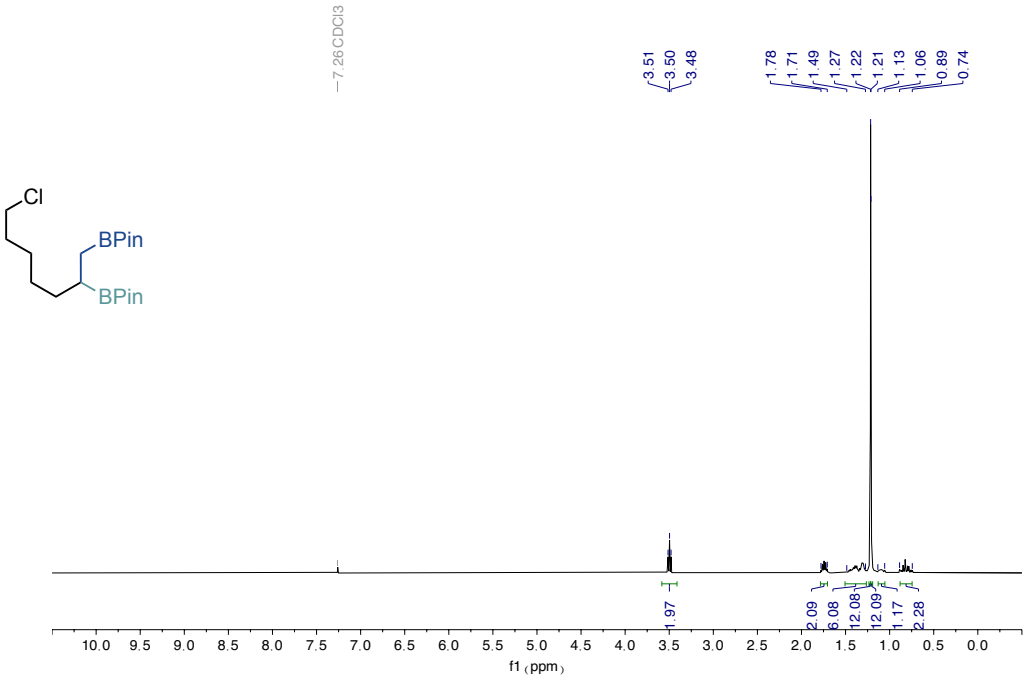

^{1}H NMR spectra (400 MHz) of **4f**

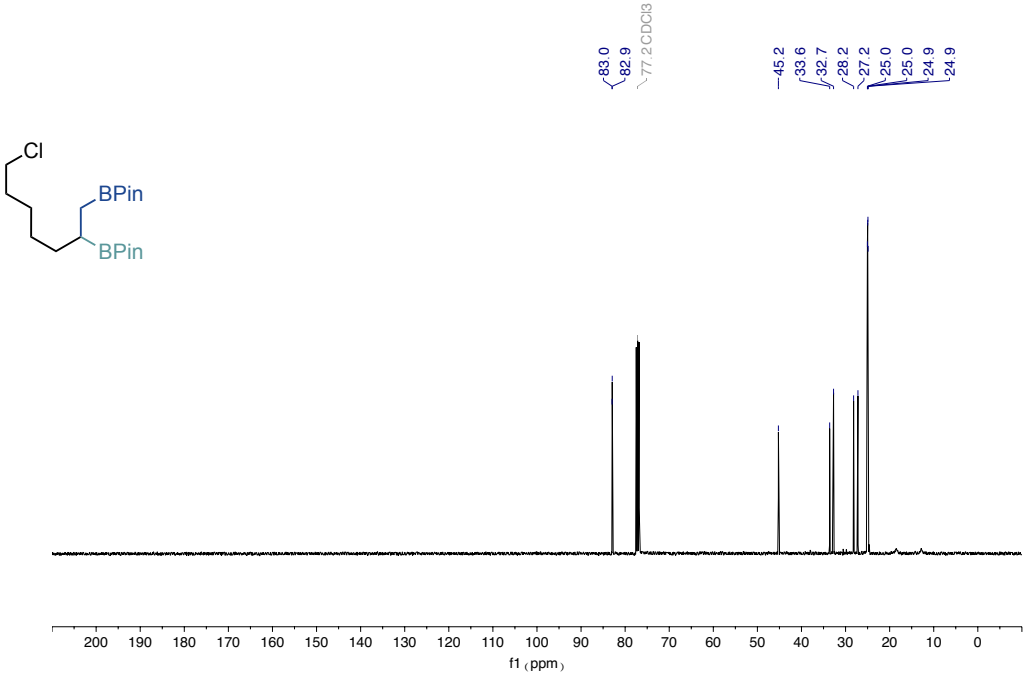

^{13}C NMR spectra (101 MHz) of **4f**

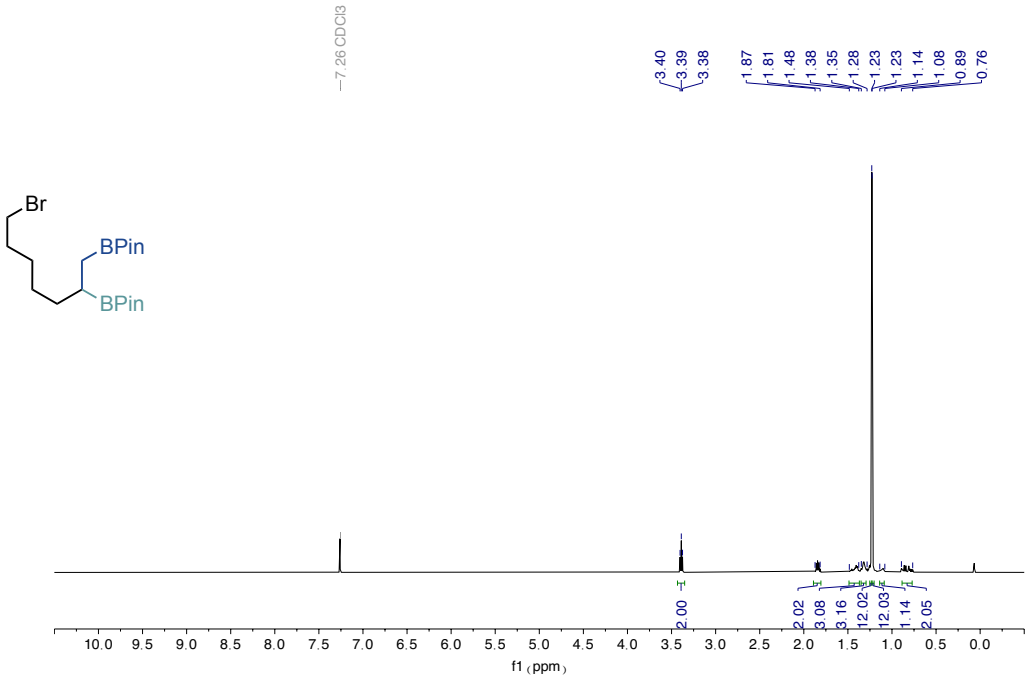

^{1}H NMR spectra (500 MHz) of **4g**

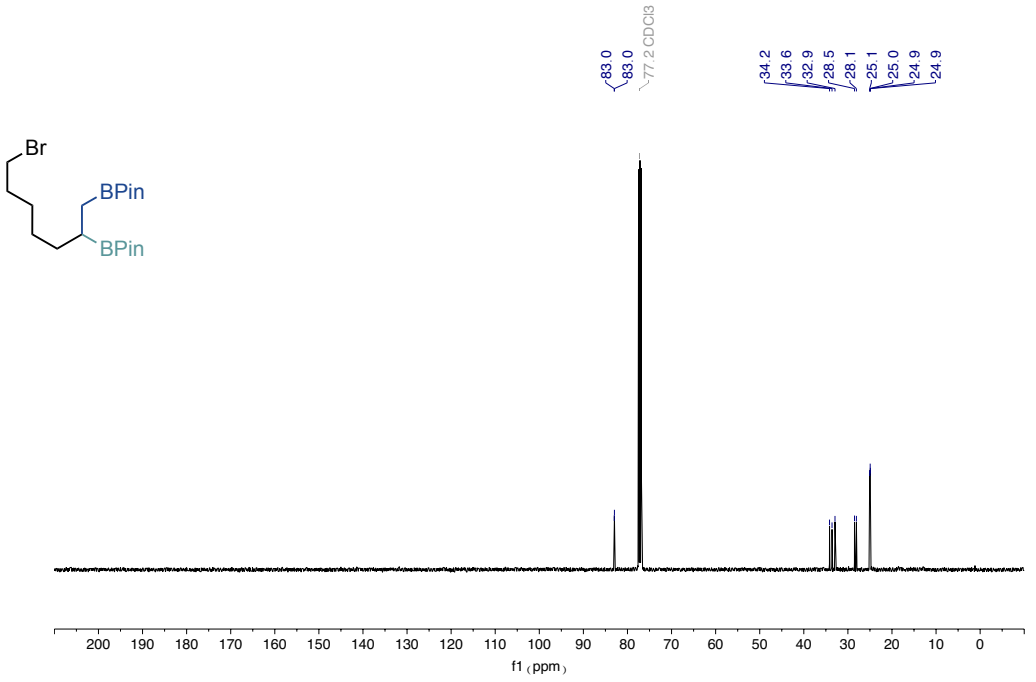

^{13}C NMR spectra (101 MHz) of **4g**

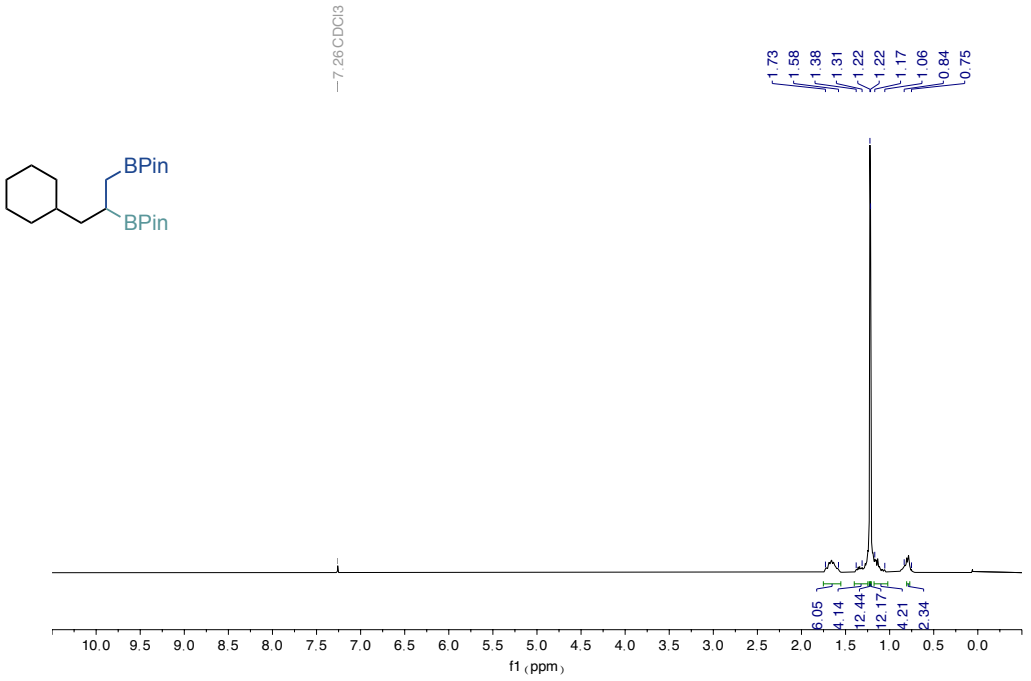

^{1}H NMR spectra (400 MHz) of **4h**

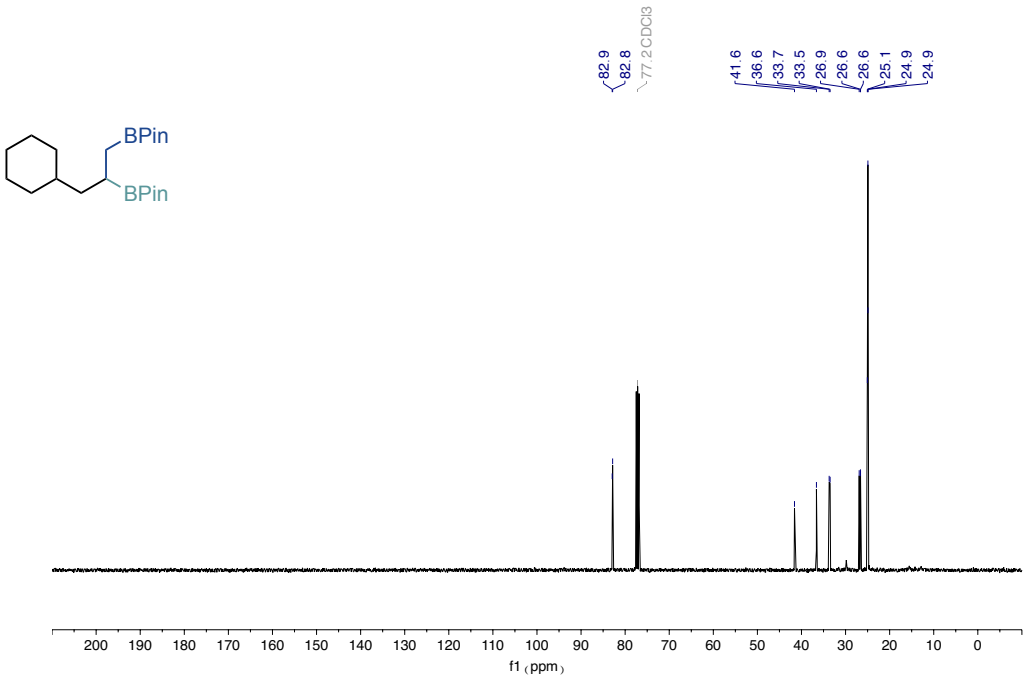

^{13}C NMR spectra (101 MHz) of **4h**

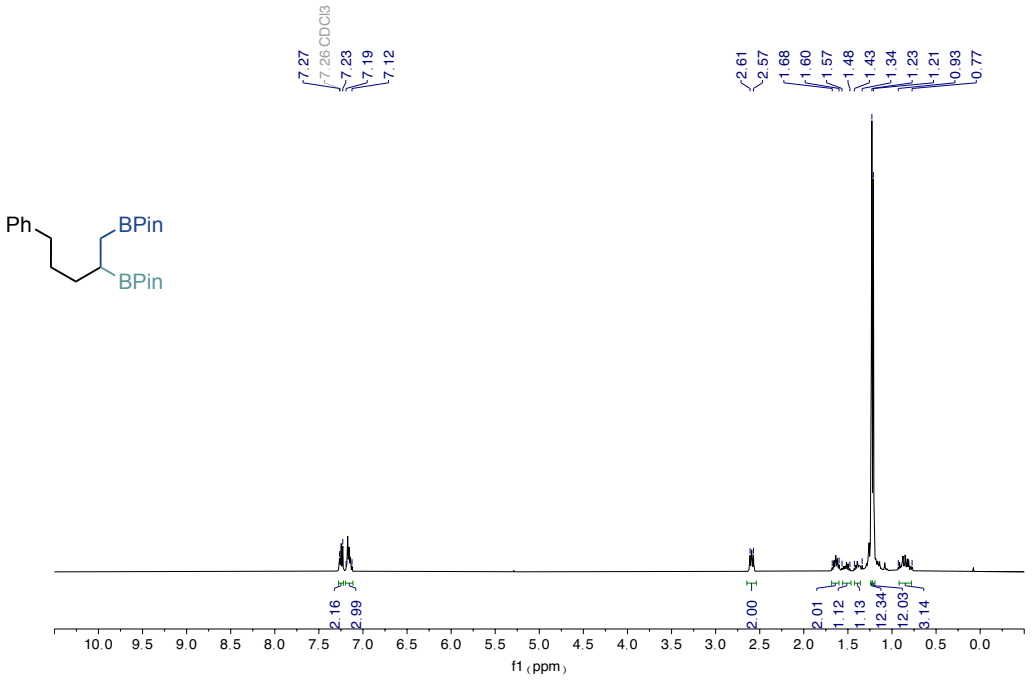

^{1}H NMR spectra (400 MHz) of **4i**

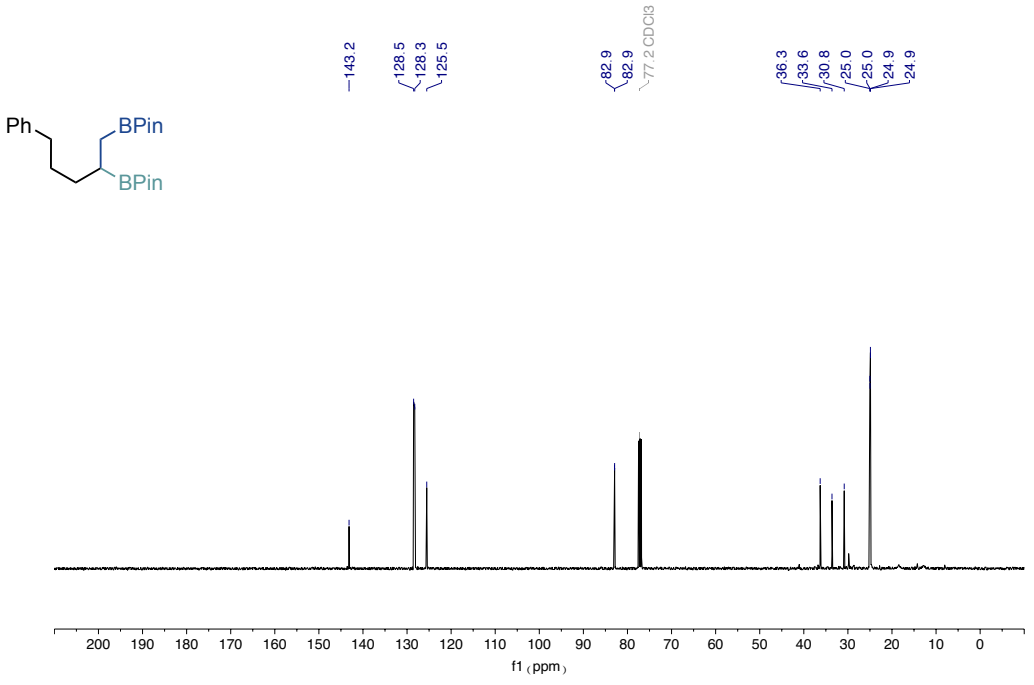

^{13}C NMR spectra (101 MHz) of **4i**

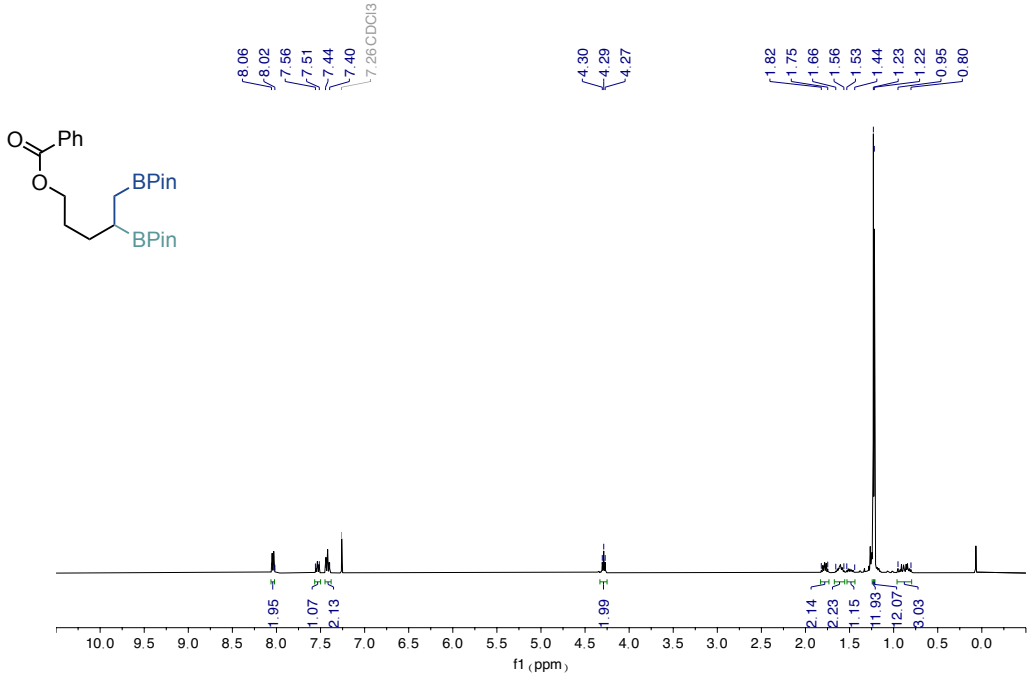

^{1}H NMR spectra (400 MHz) of **4j**

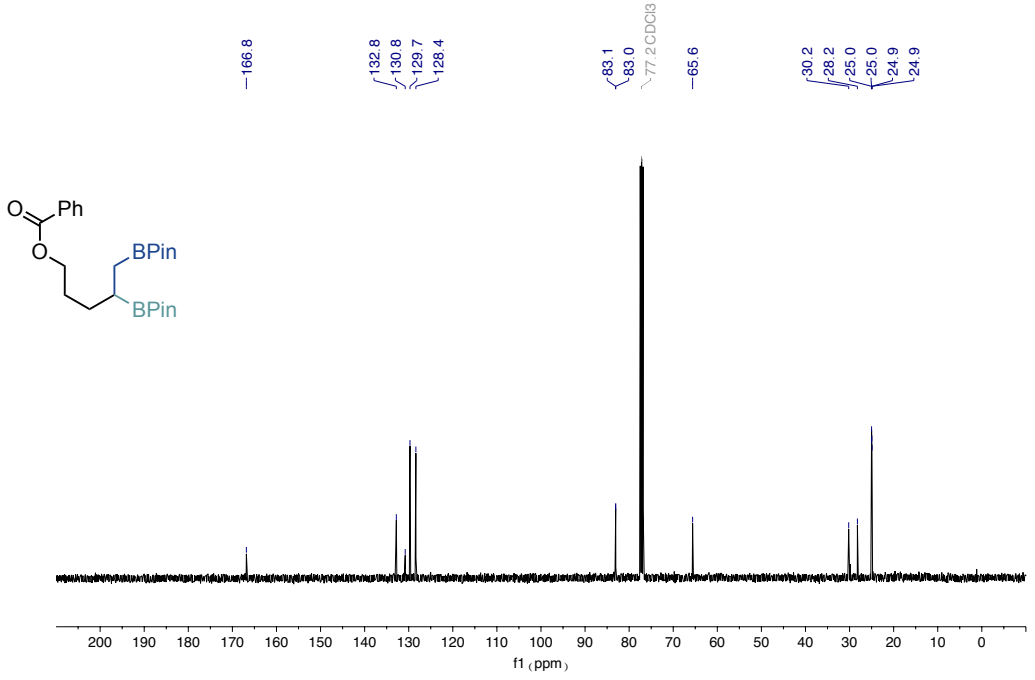

^{13}C NMR spectra (101 MHz) of **4j**

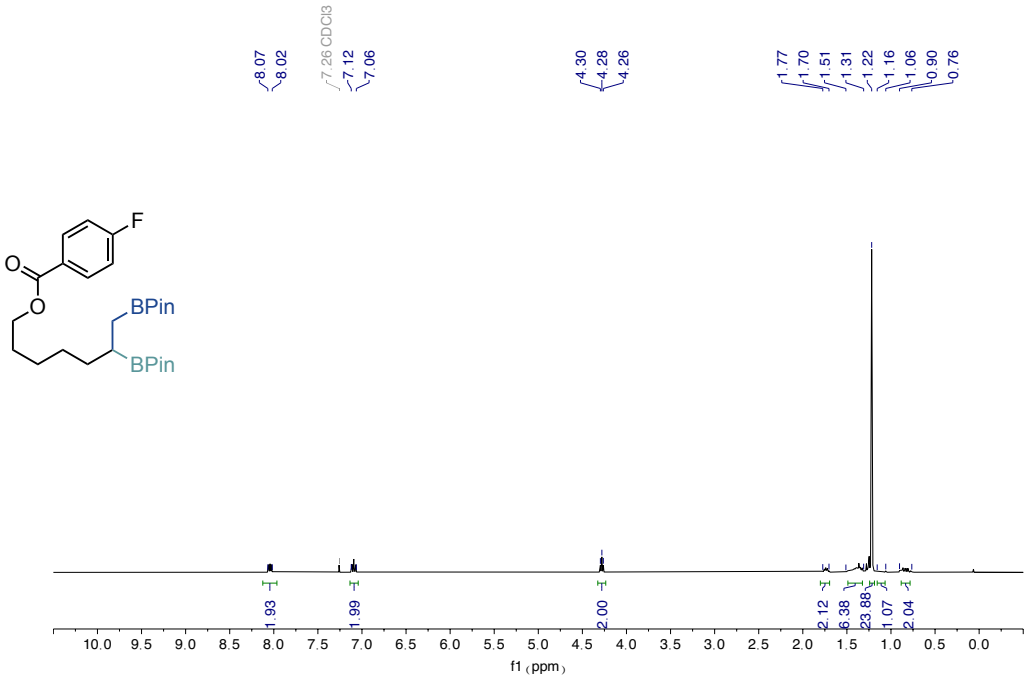

^{1}H NMR spectra (400 MHz) of **4k**

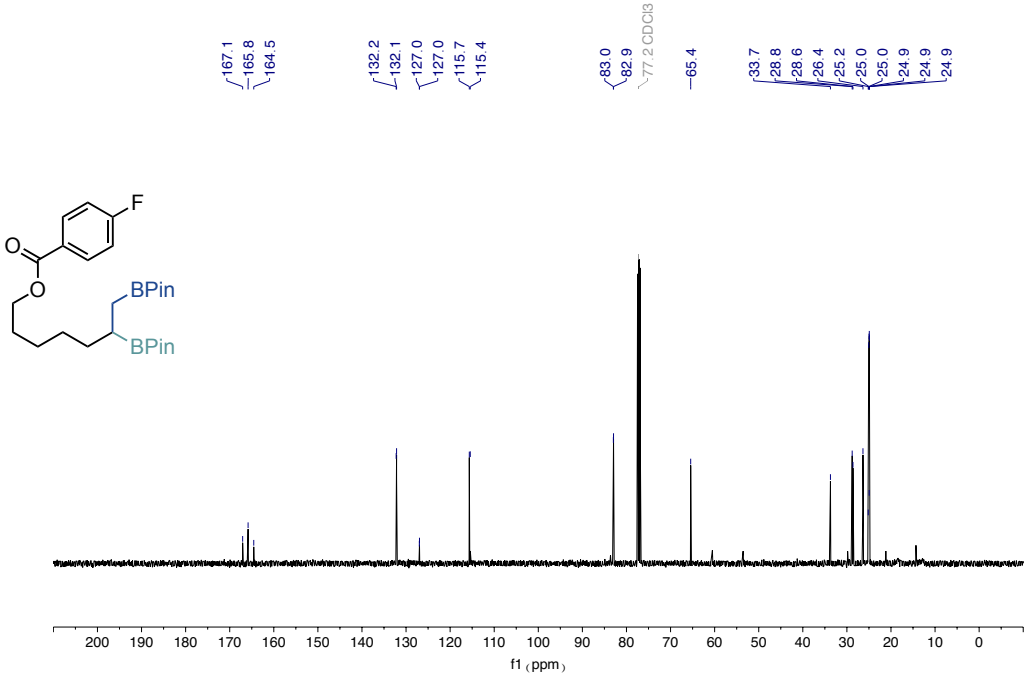

^{13}C NMR spectra (101 MHz) of **4k**

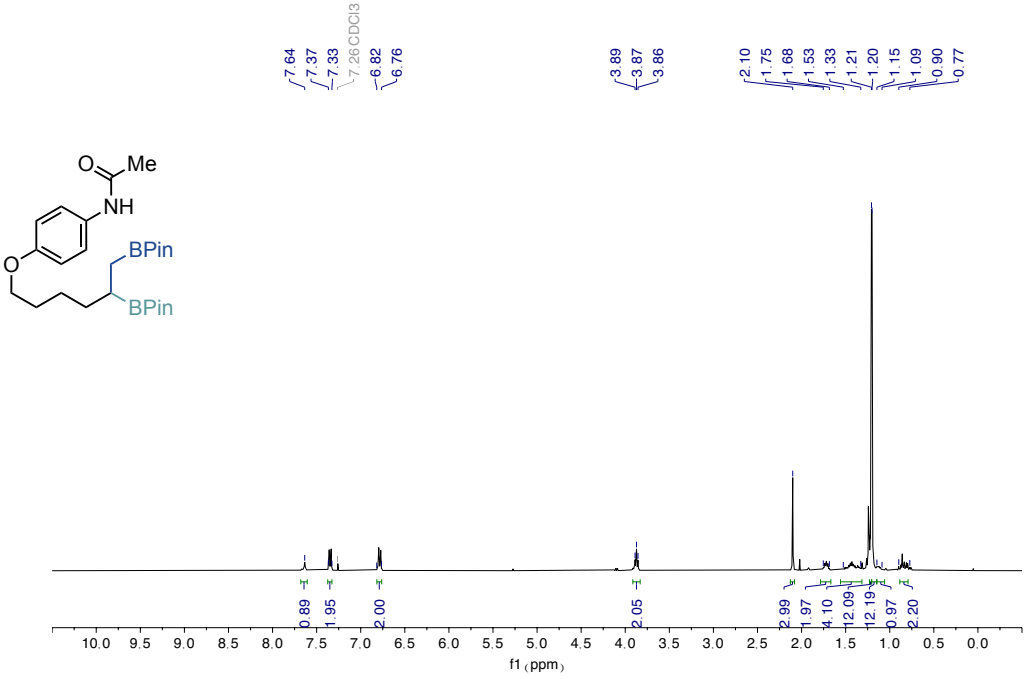

^{1}H NMR spectra (400 MHz) of **4l**

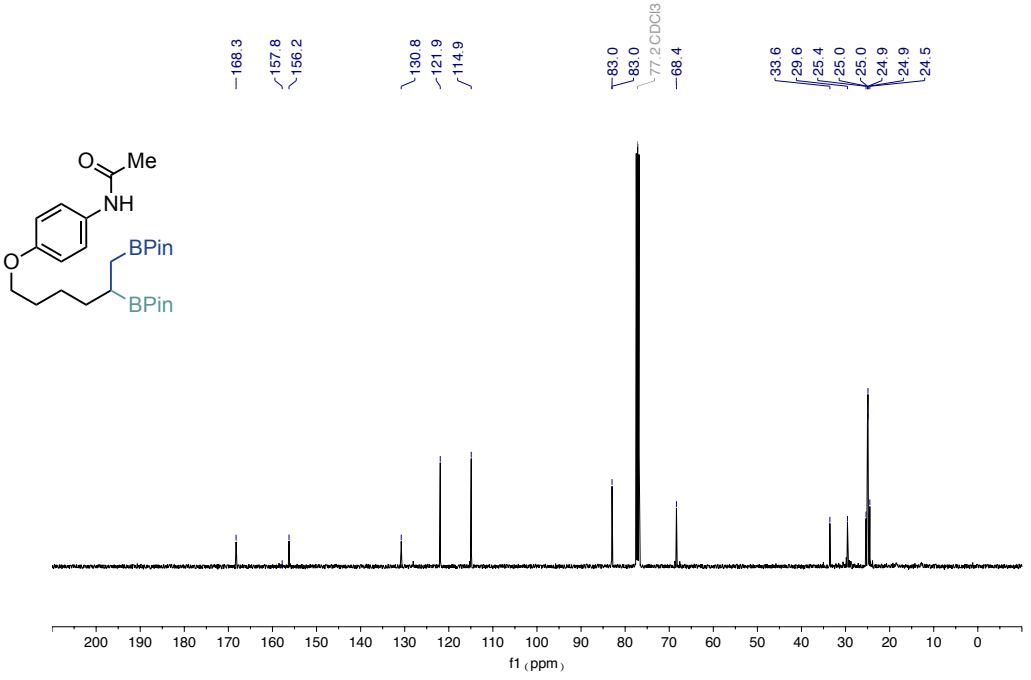

^{13}C NMR spectra (101 MHz) of **4l**

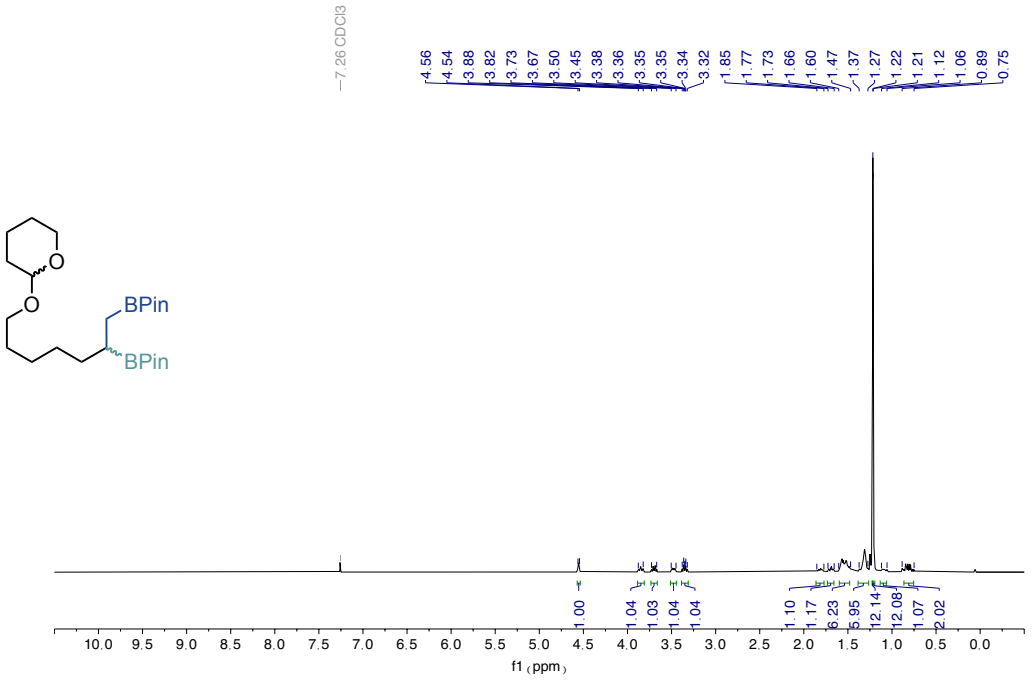

^{1}H NMR spectra (400 MHz) of **4m**

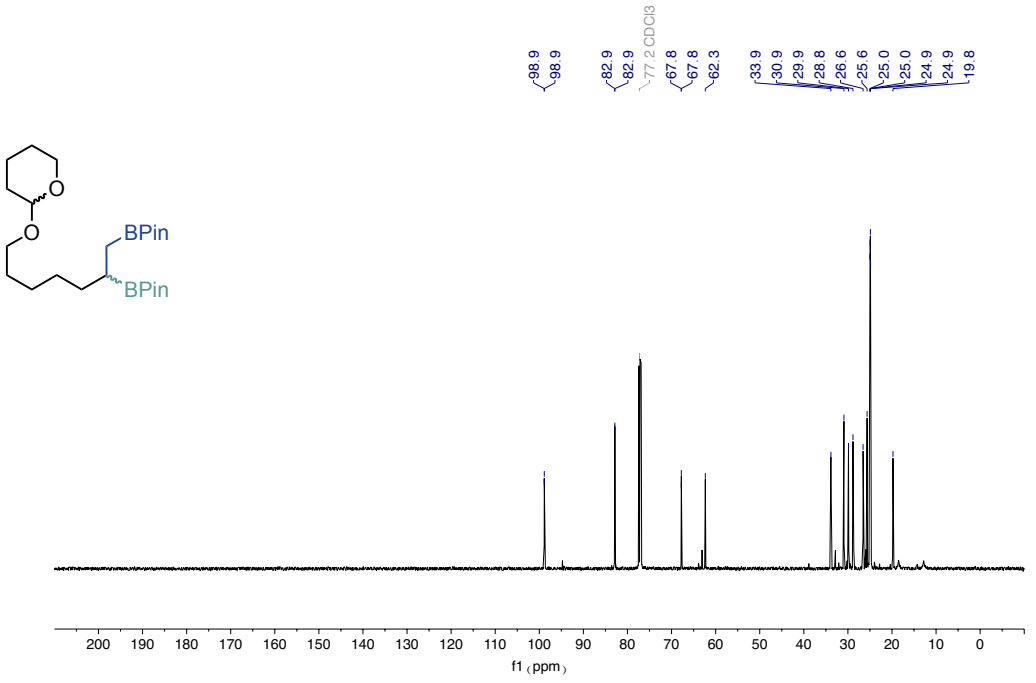

^{13}C NMR spectra (126 MHz) of **4m**

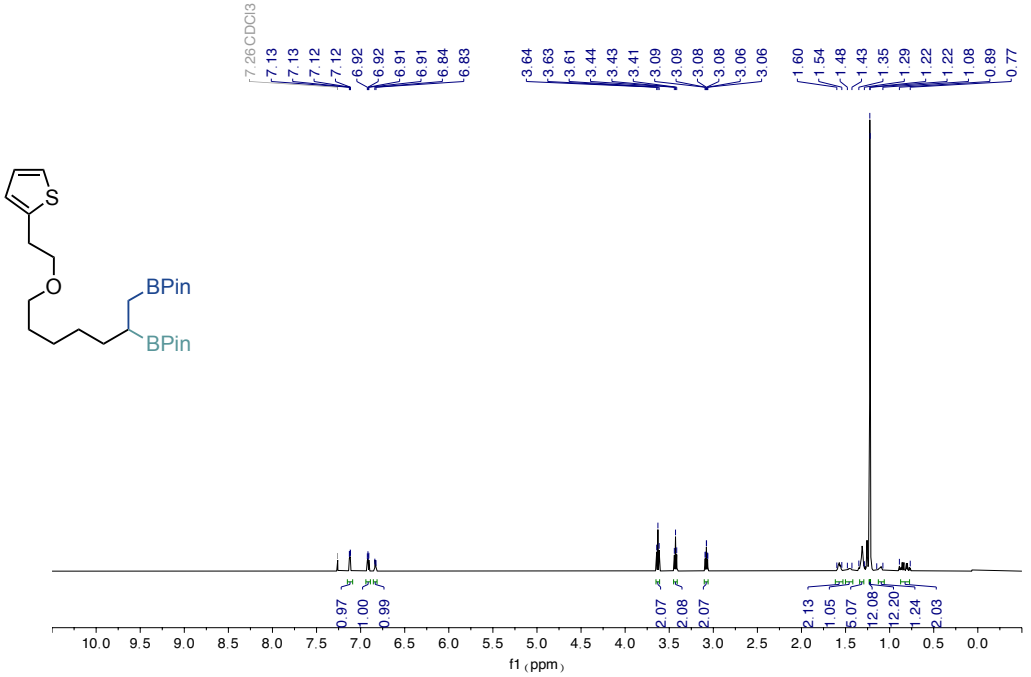

^{1}H NMR spectra (500 MHz) of **4n**

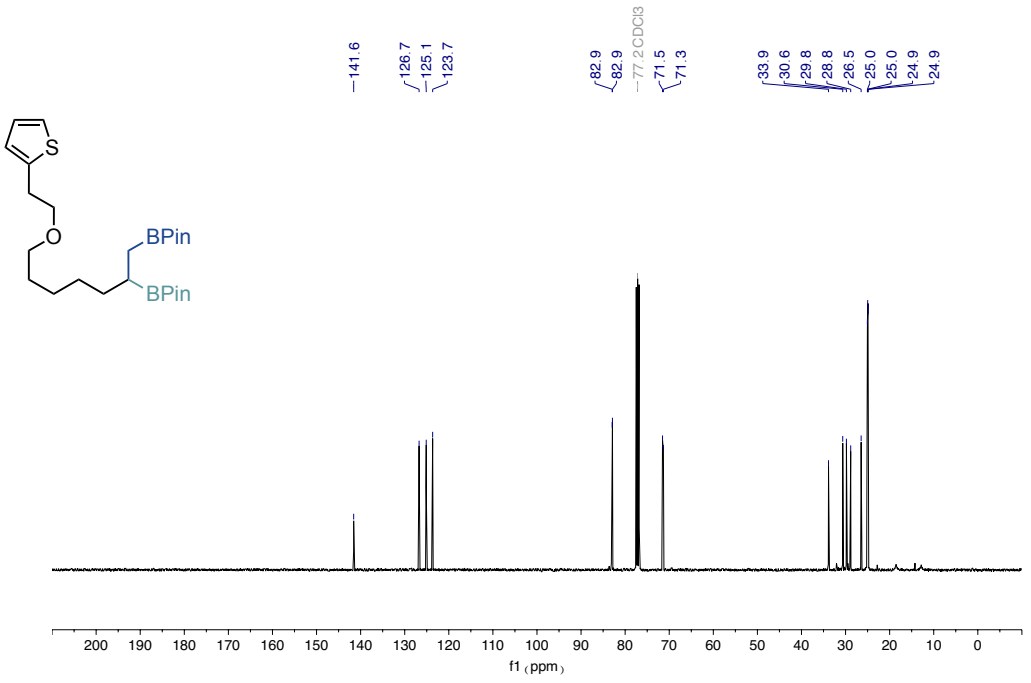

^{13}C NMR spectra (101 MHz) of **4n**

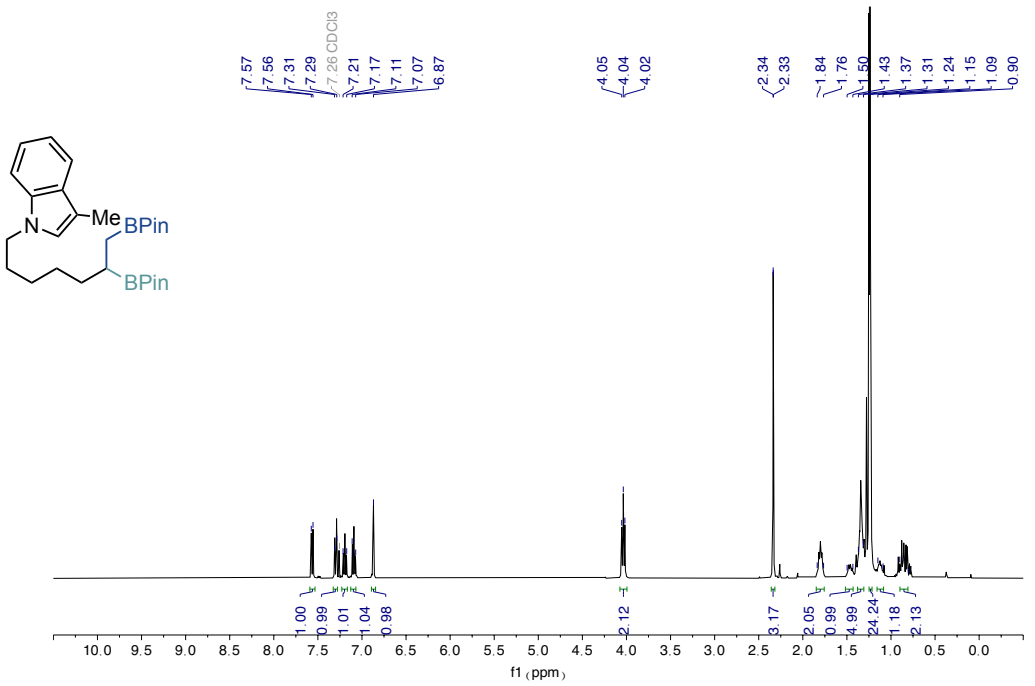

^{1}H NMR spectra (400 MHz) of **4o**

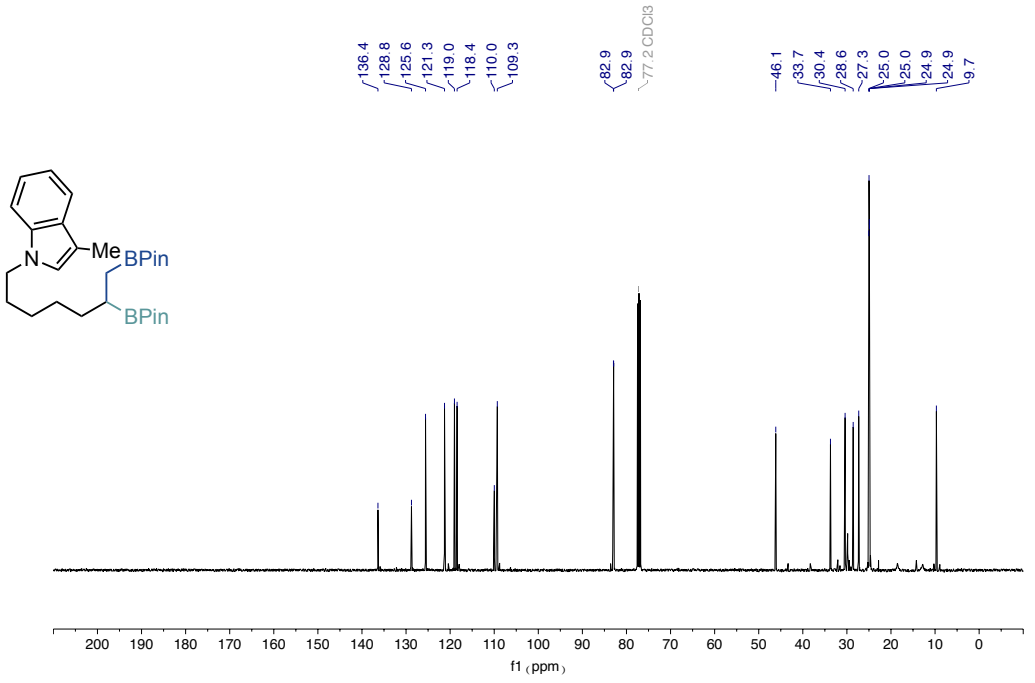

^{13}C NMR spectra (101 MHz) of **4o**

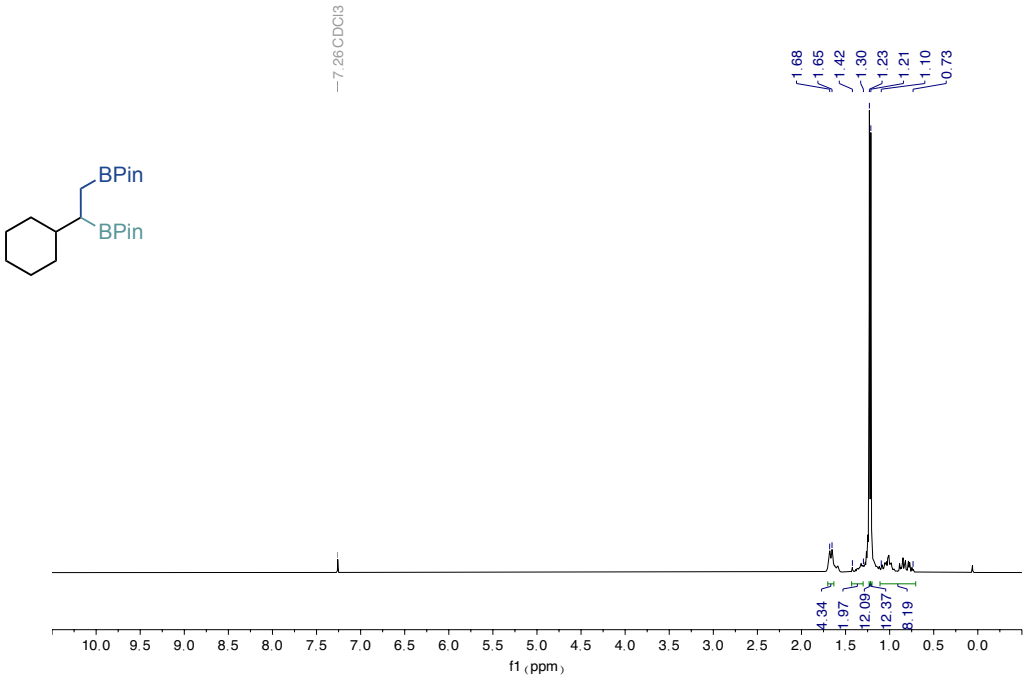

^{1}H NMR spectra (400 MHz) of **4p**

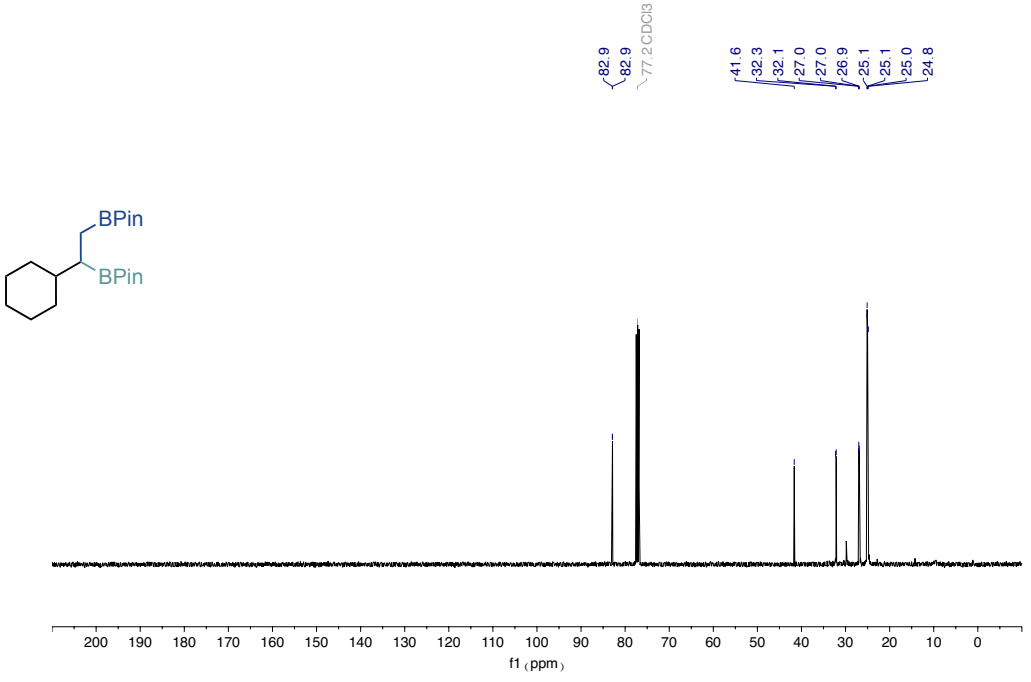

^{13}C NMR spectra (101 MHz) of **4p**

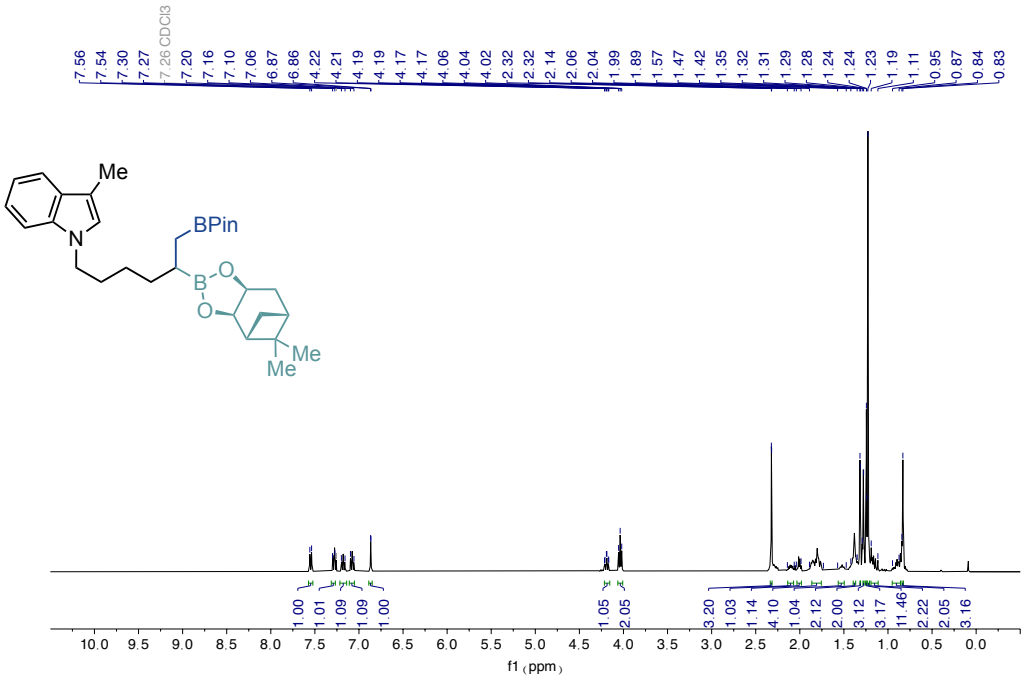

^{1}H NMR spectra (400 MHz) of **4q**

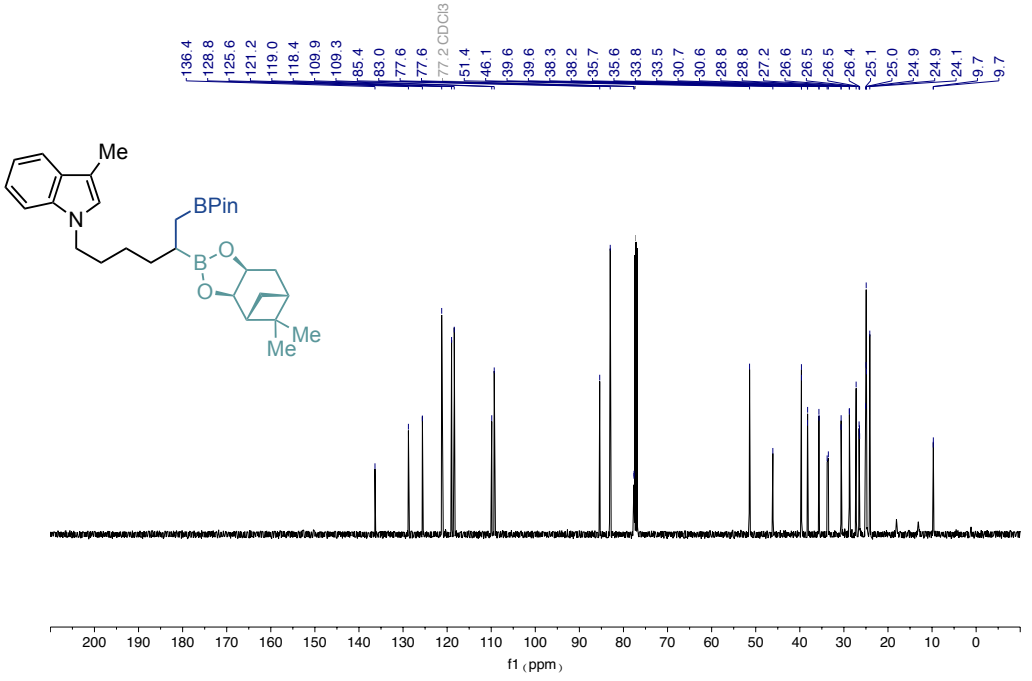

^{13}C NMR spectra (126 MHz) of **4q**

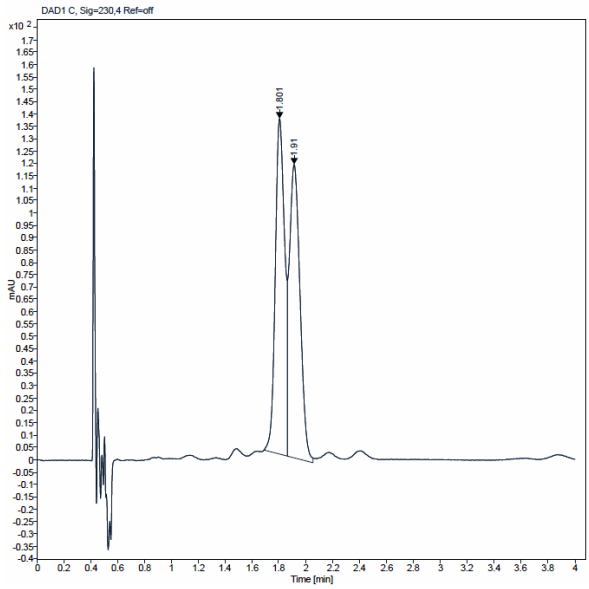

Peak	Ret. Time	Area	Area %
1	1.801 min	658.1146	50.2
2	1.910 min	652.9620	49.8

SFC chromatogram of **4q**

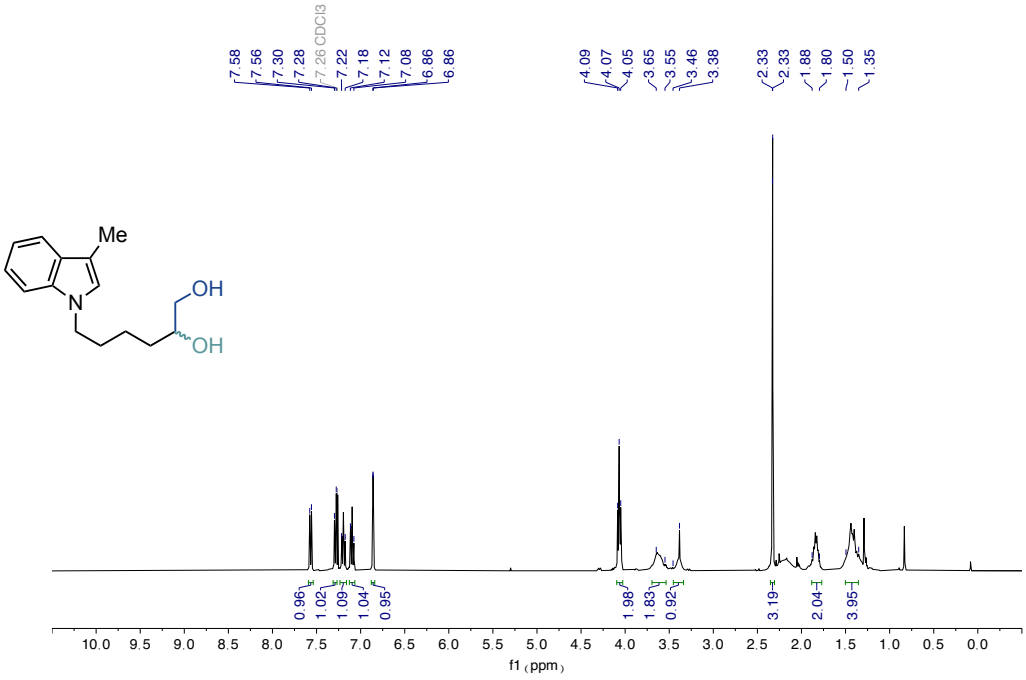

^{1}H NMR spectra (400 MHz) of **4q'**

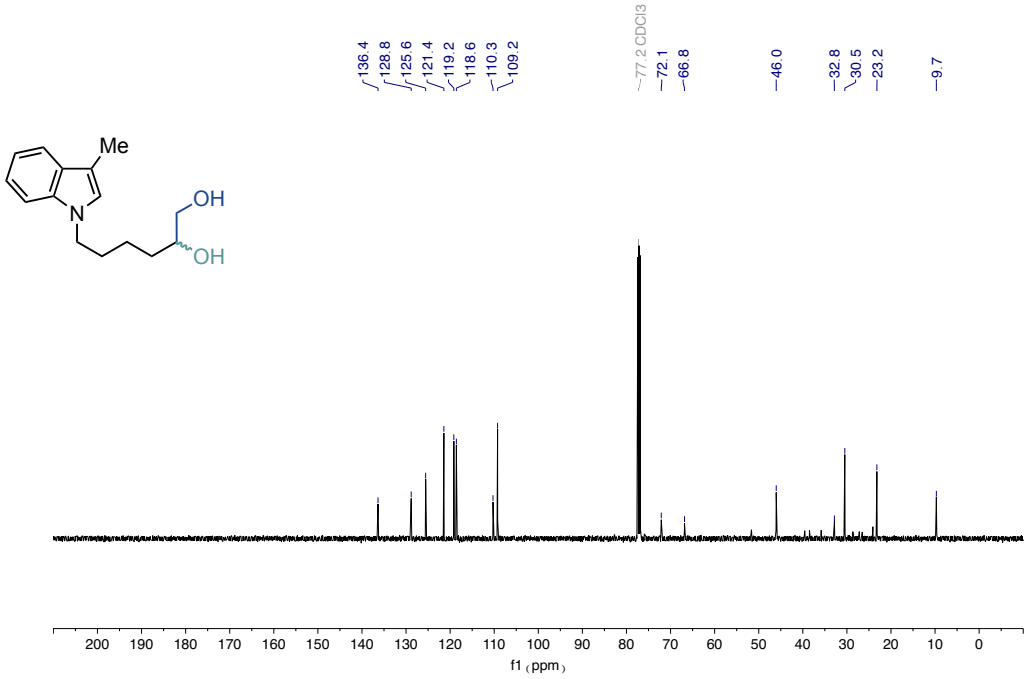

^{13}C NMR spectra (126 MHz) of **4q'**

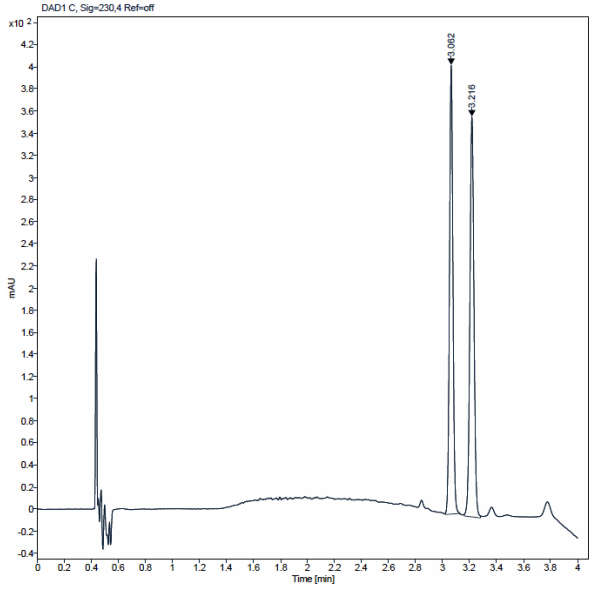

Peak	Ret. Time	Area	Area %
1	3.062 min	718.4263	48.7
2	3.216min	757.2715	51.3

SFC chromatogram of **4q'**

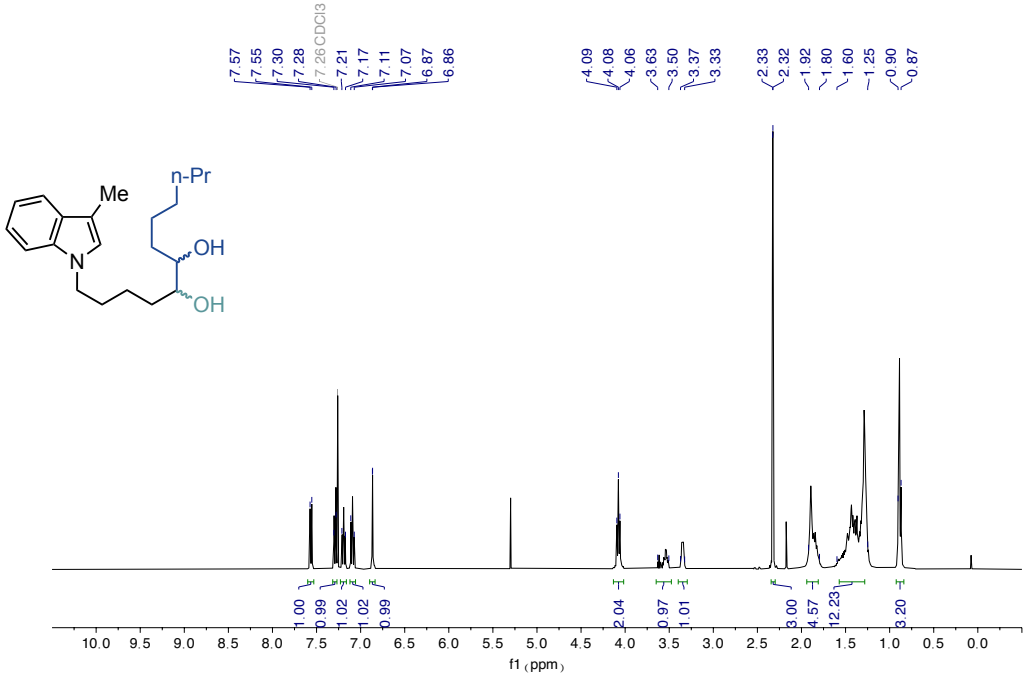

^{1}H NMR spectra (400 MHz) of **4r**

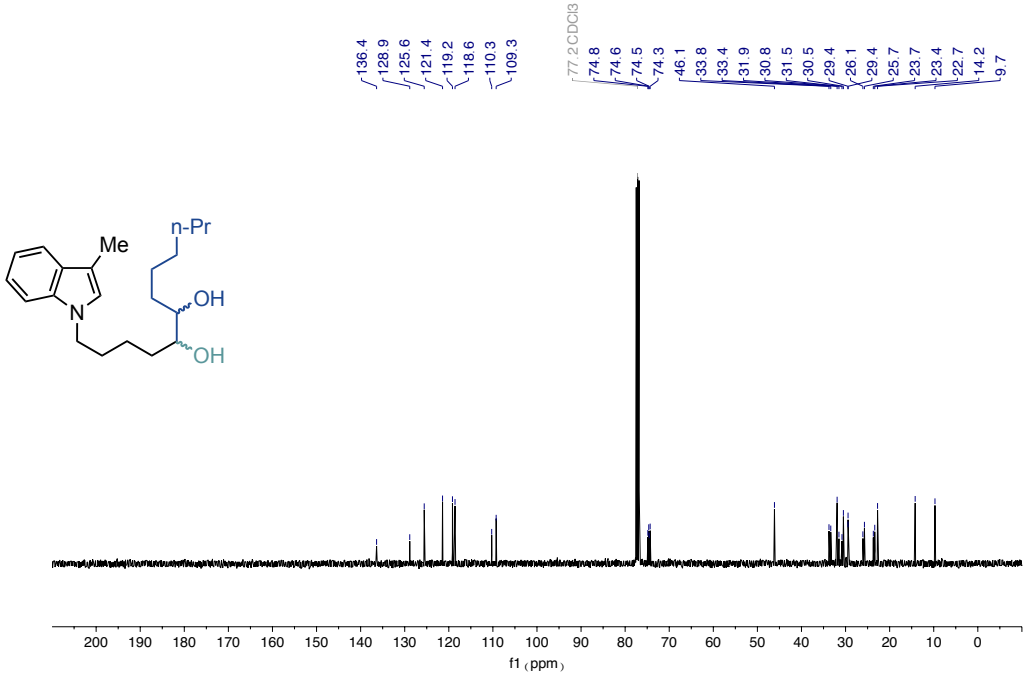

^{13}C NMR spectra (101 MHz) of **4r**

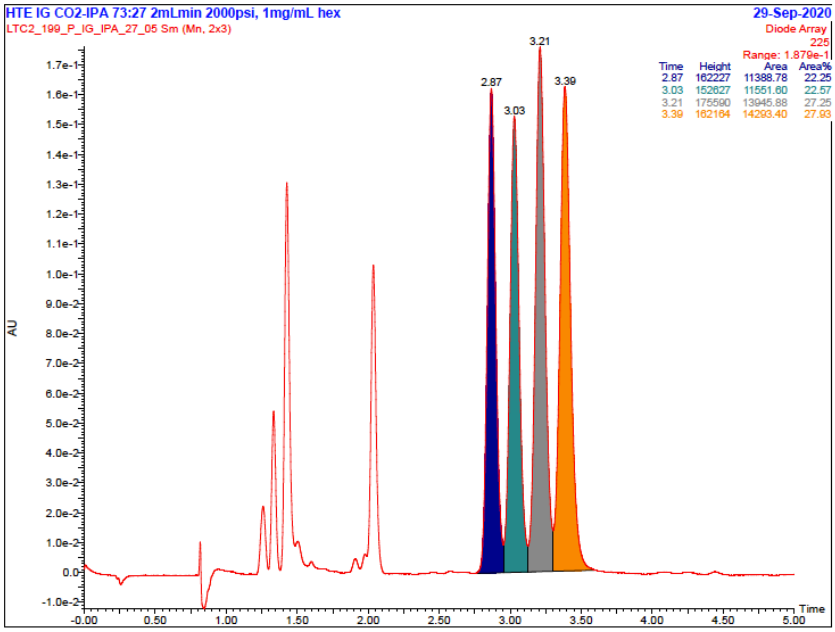

SFC chromatogram of **4r**

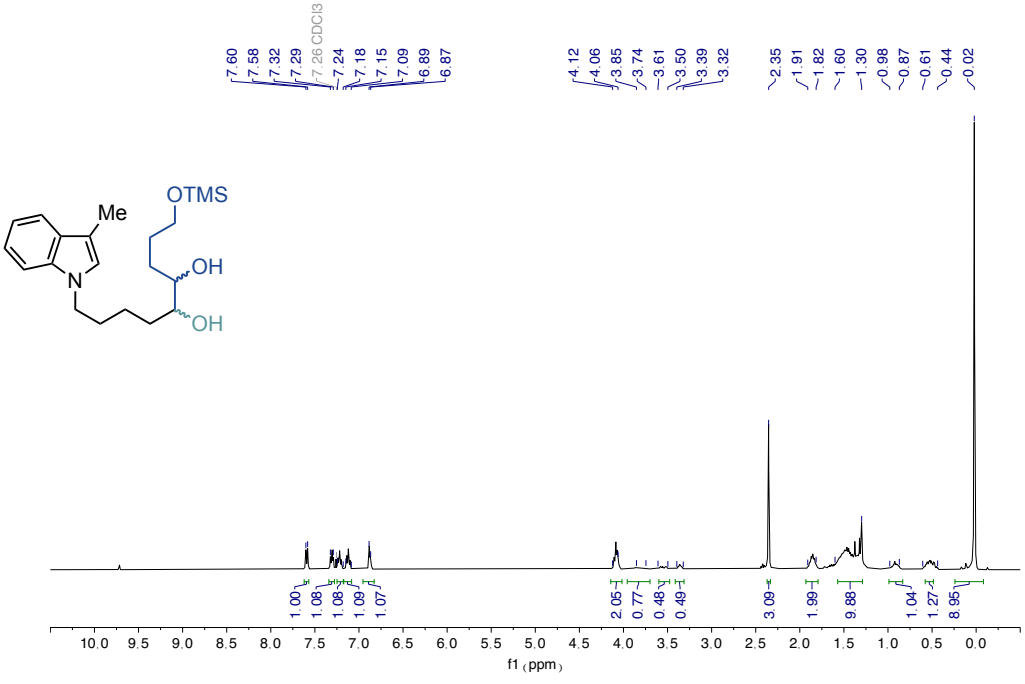

^{1}H NMR spectra (400 MHz) of **4s**

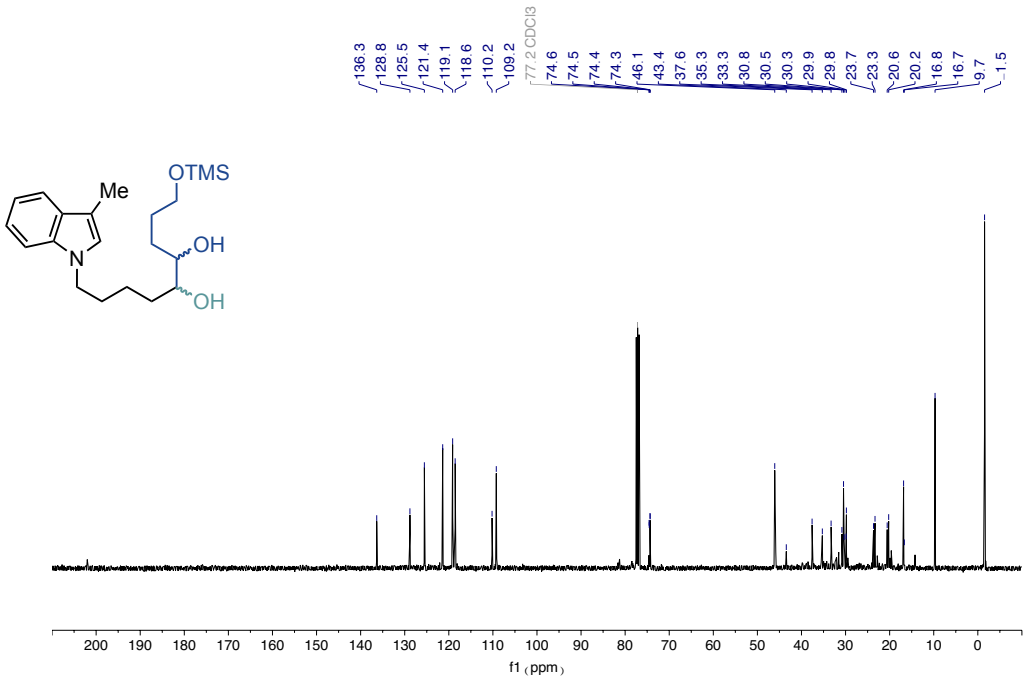

^{13}C NMR spectra (101 MHz) of **4s**

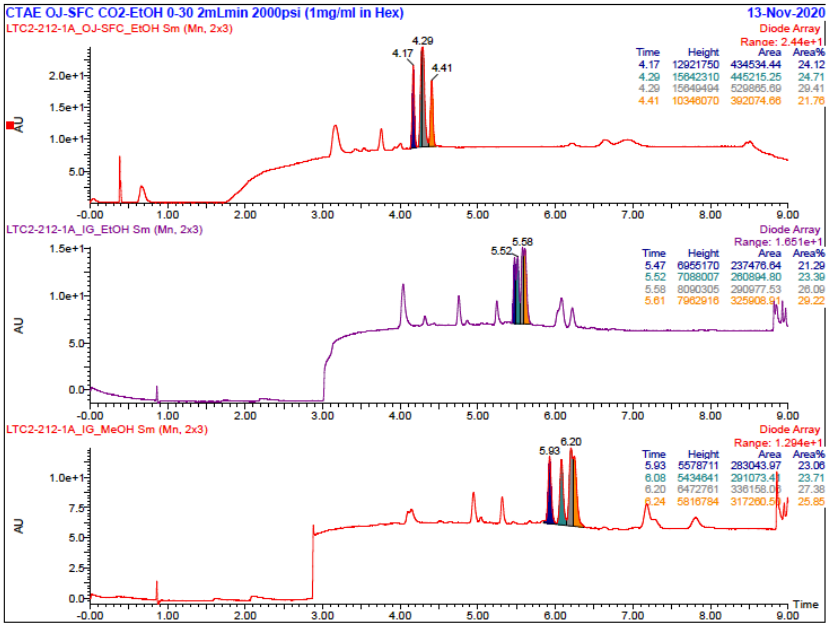

SFC chromatogram of **4s**

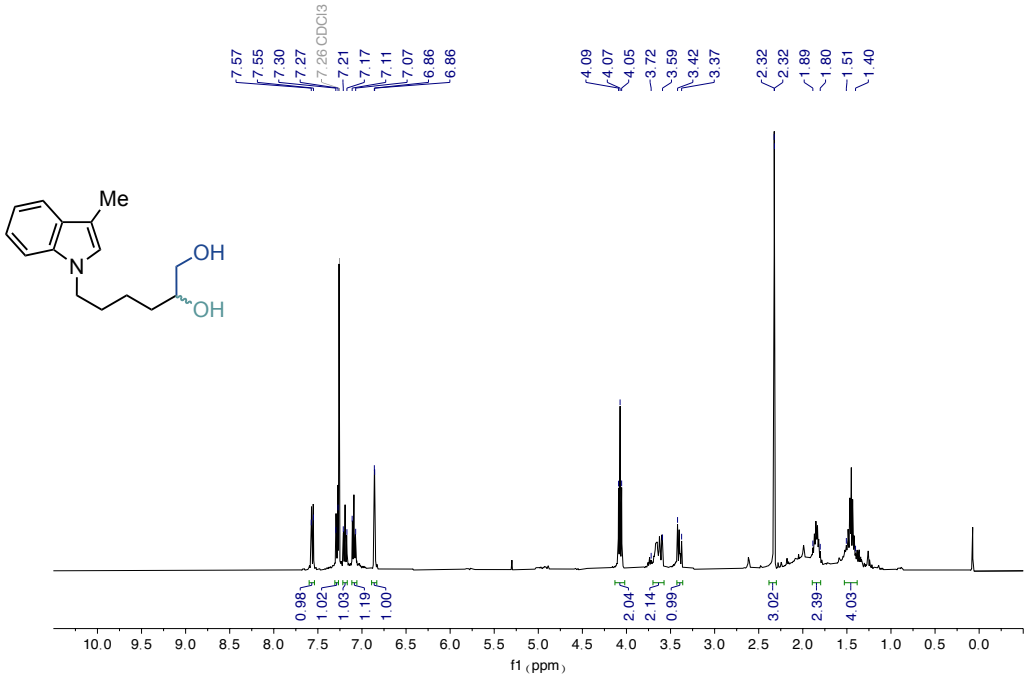

^{1}H NMR spectra (400 MHz) of ***rac*-6-(3-methyl-1*H*-indol-1-yl)hexane-1,2-diol**

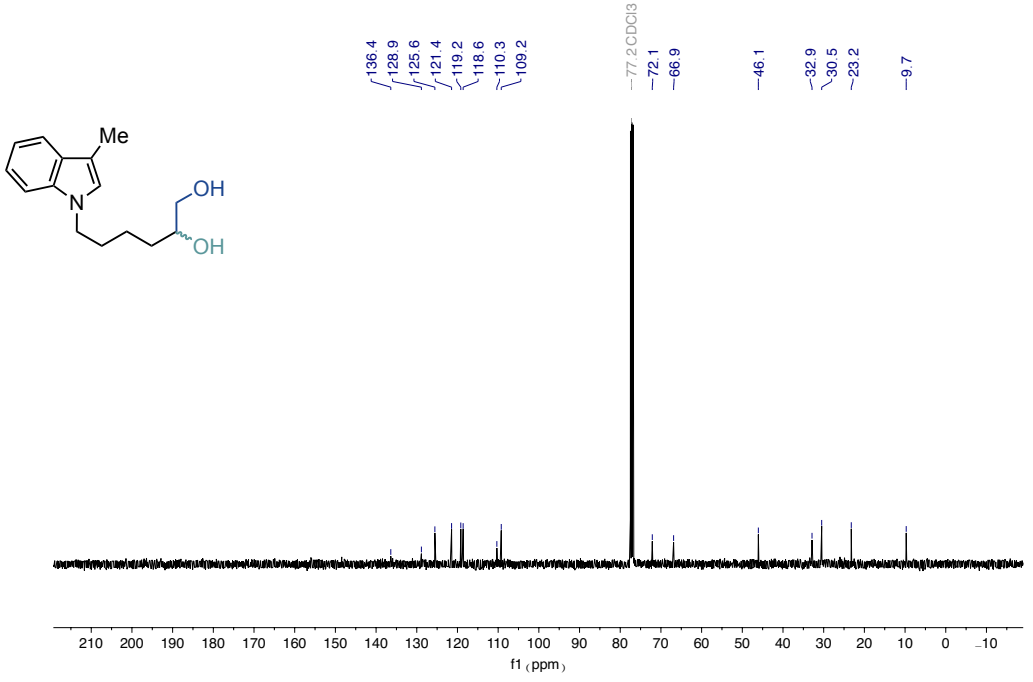

^{13}C NMR spectra (101 MHz) of ***rac*-6-(3-methyl-1*H*-indol-1-yl)hexane-1,2-diol**

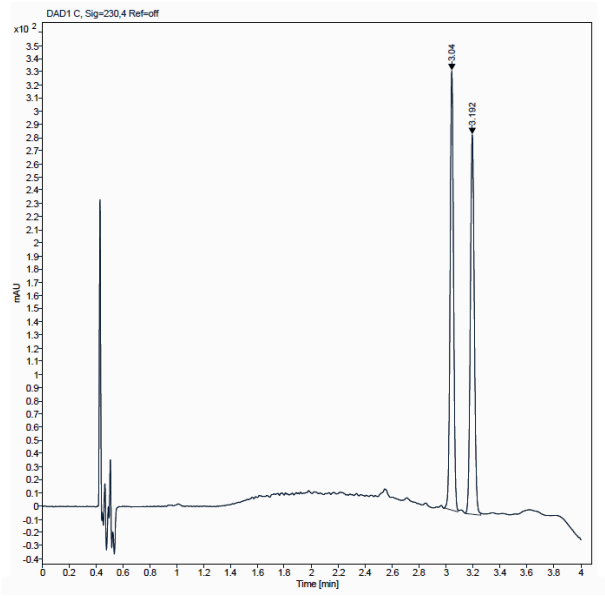

Peak	Ret. Time	Area	Area %
1	3.040 min	588.0927	50.0
2	3.192min	587.9526	50.0

SFC chromatogram of ***rac*-6-(3-methyl-1*H*-indol-1-yl)hexane-1,2-diol**

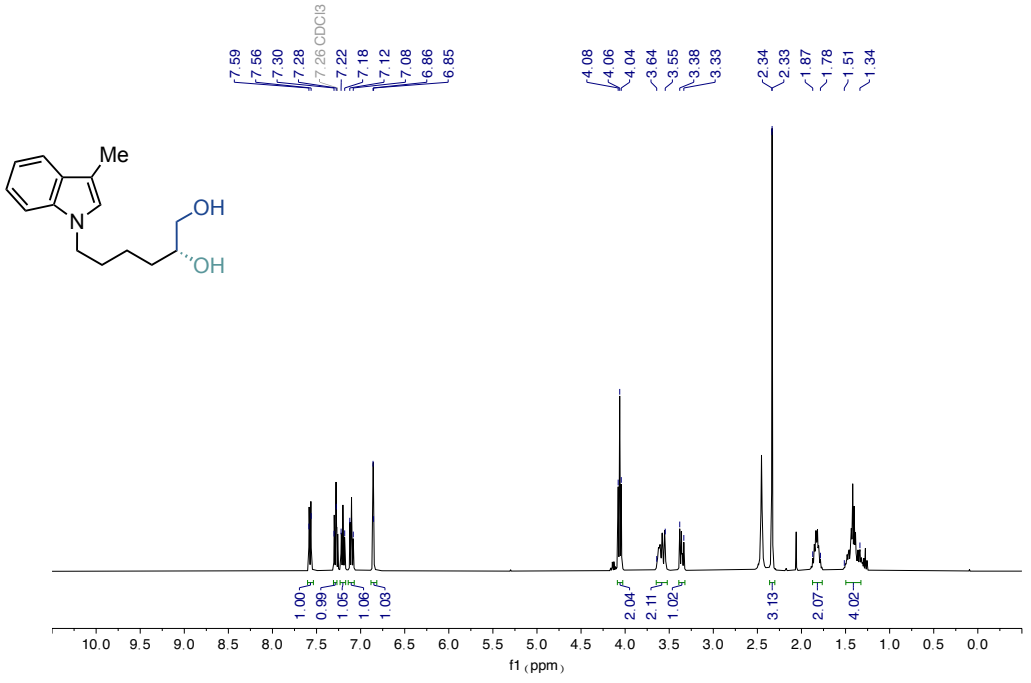

[1]H NMR spectra (400 MHz) of **(*R*)-6-(3-methyl-1*H*-indol-1-yl)hexane-1,2-diol**

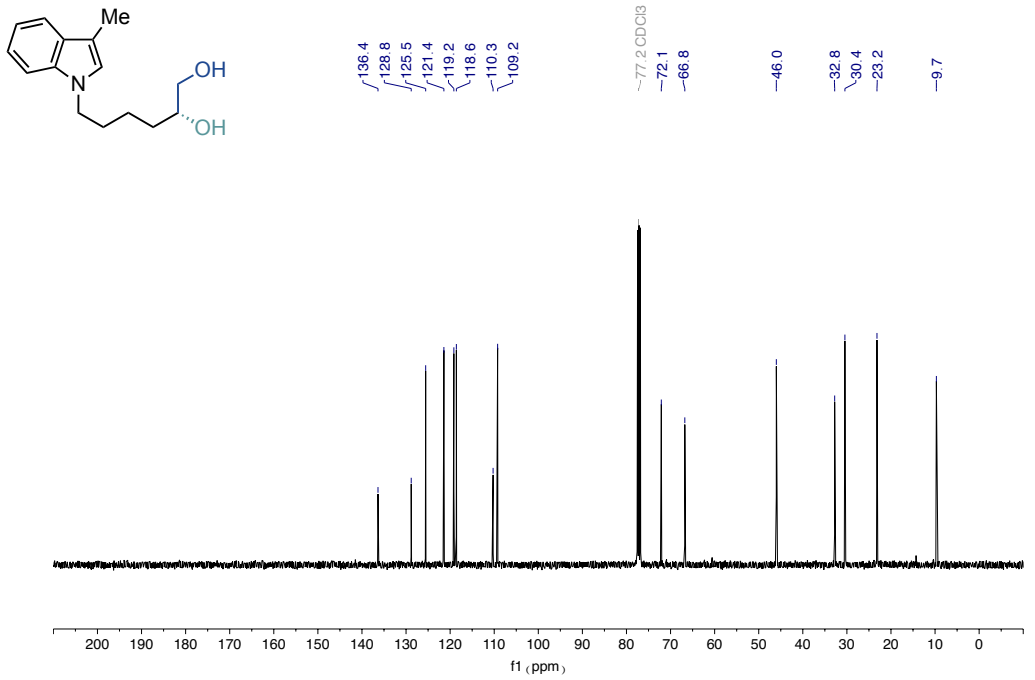

^{13}C NMR spectra (101 MHz) of **(*R*)-6-(3-methyl-1*H*-indol-1-yl)hexane-1,2-diol**

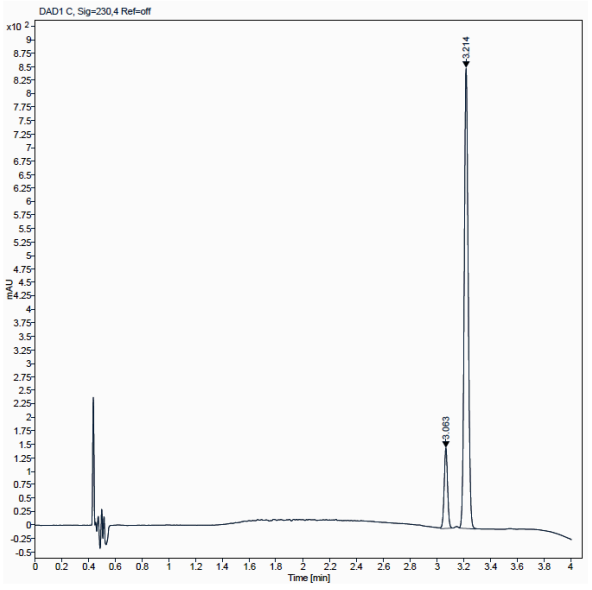

Peak	Ret. Time	Area	Area %
1	3.063 min	262.2455	13.0
2	3.214 min	1749.7922	87.0

SFC chromatogram of **(*R*)-6-(3-methyl-1*H*-indol-1-yl)hexane-1,2-diol**

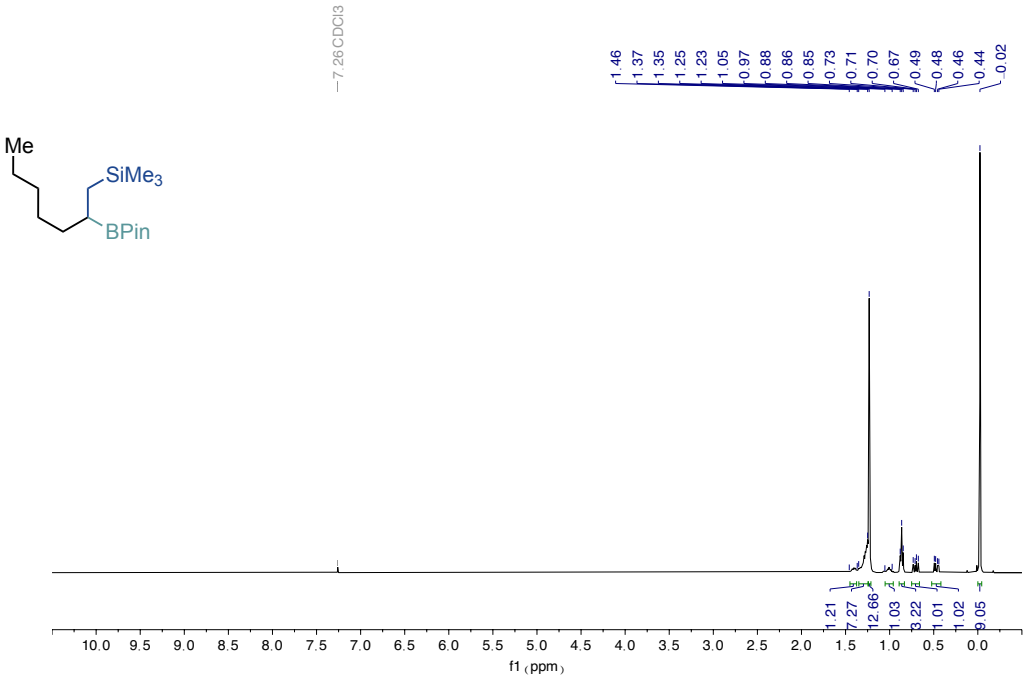

^{1}H NMR spectra (400 MHz) of **5a**

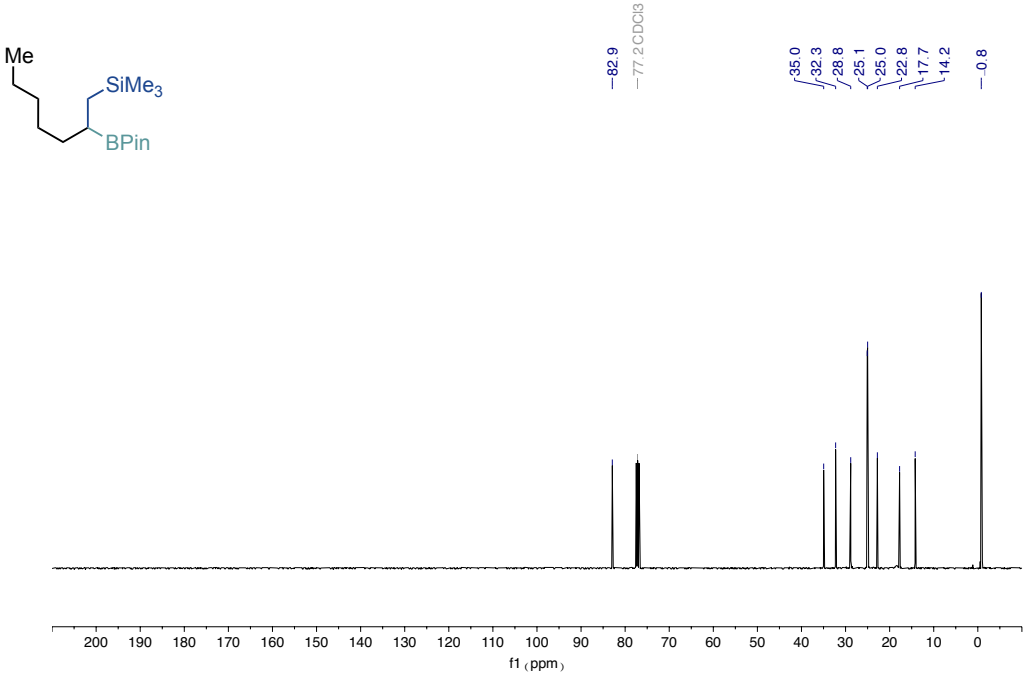

^{13}C NMR spectra (101 MHz) of **5a**

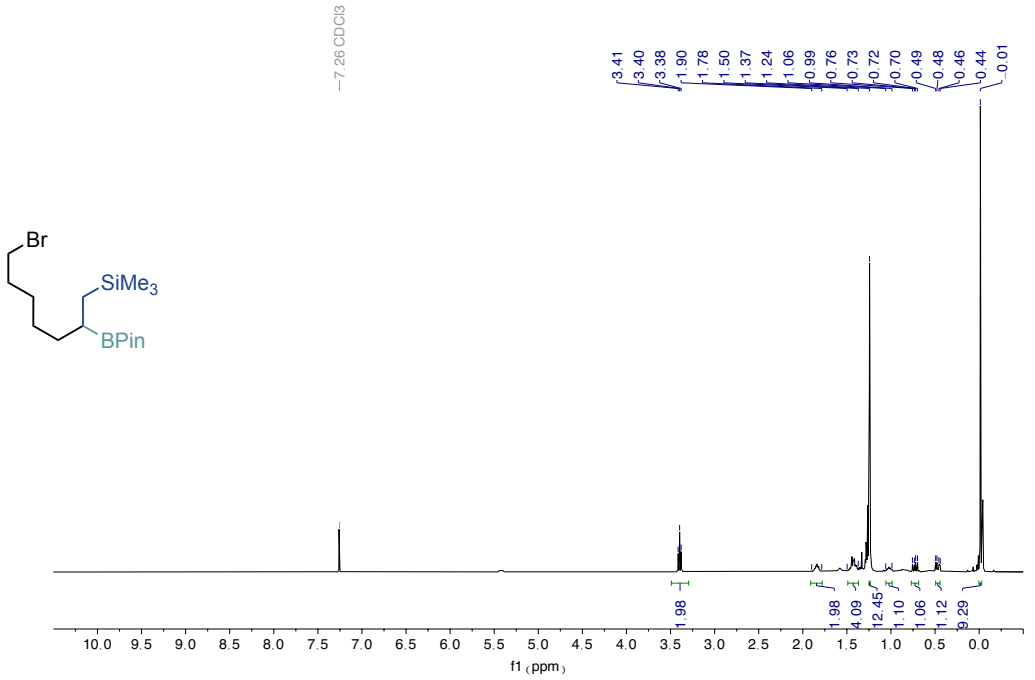

^{1}H NMR spectra (400 MHz) of **5b**

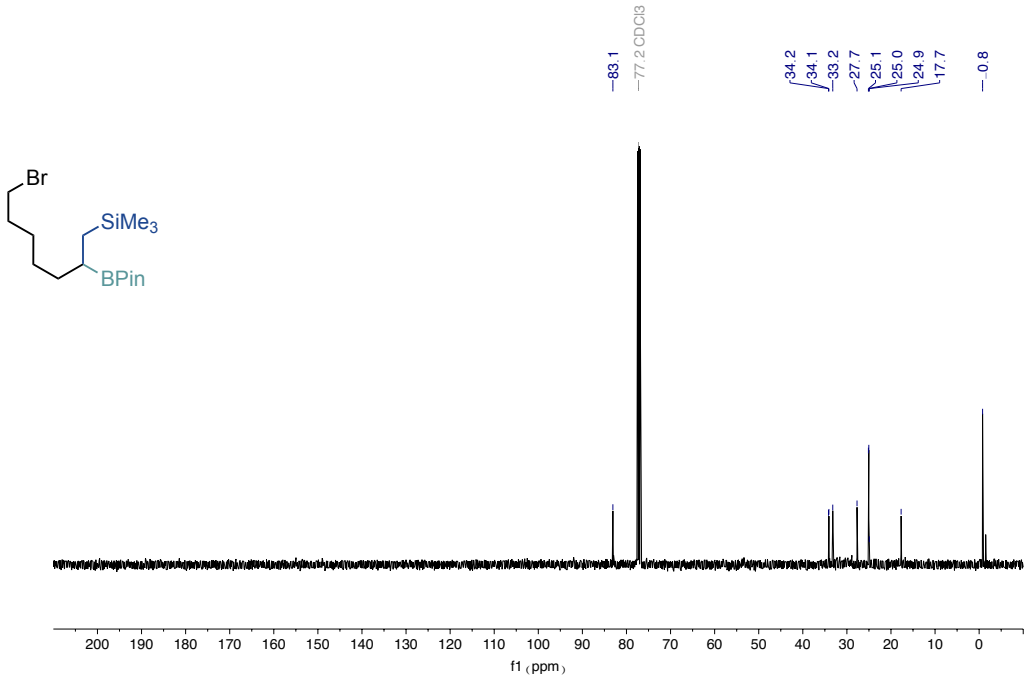

^{13}C NMR spectra (101 MHz) of **5b**

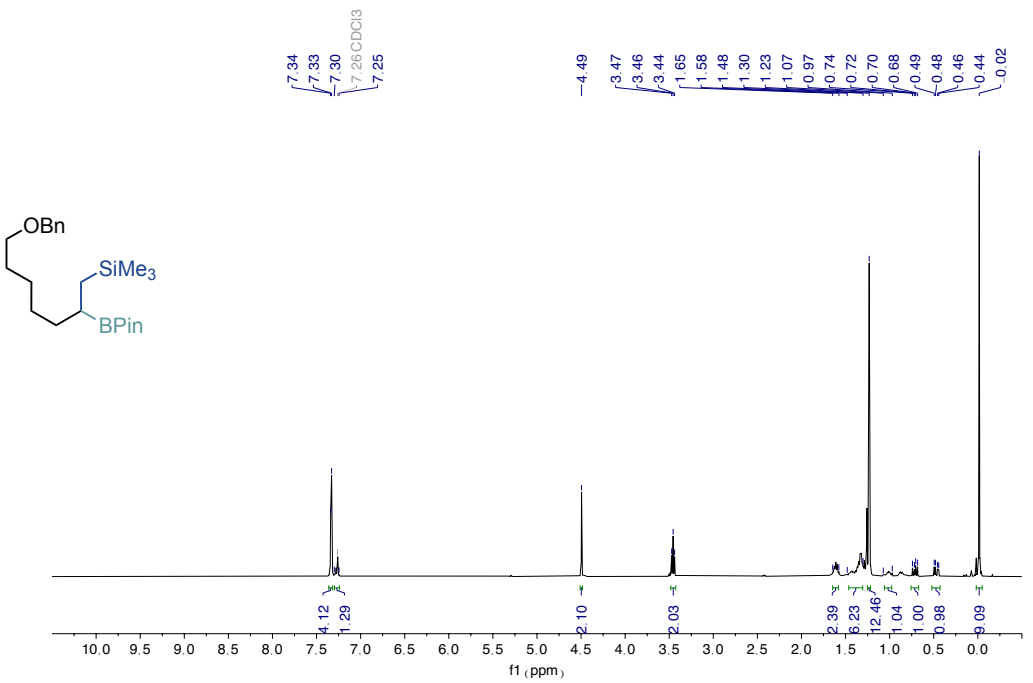

^{1}H NMR spectra (400 MHz) of **5c**

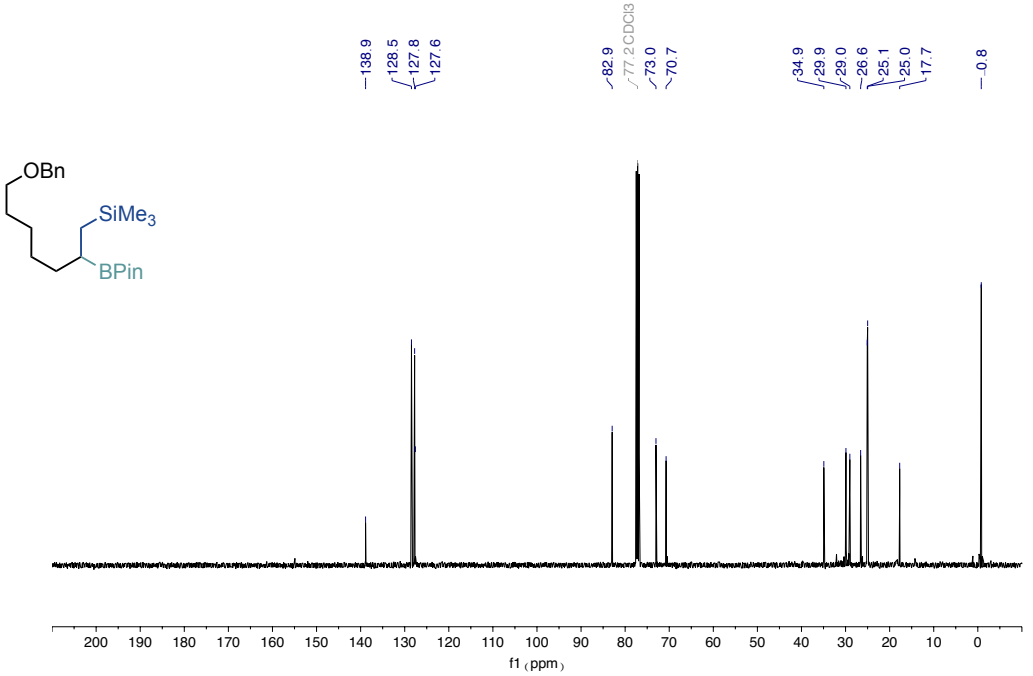

^{13}C NMR spectra (101 MHz) of **5c**

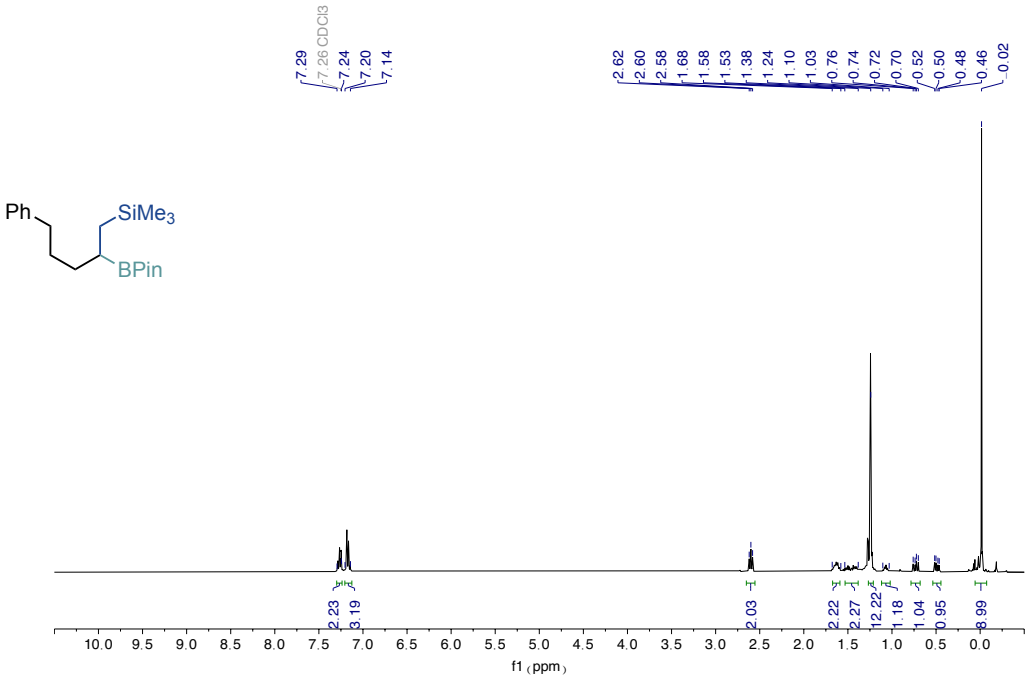

^{1}H NMR spectra (400 MHz) of **5d**

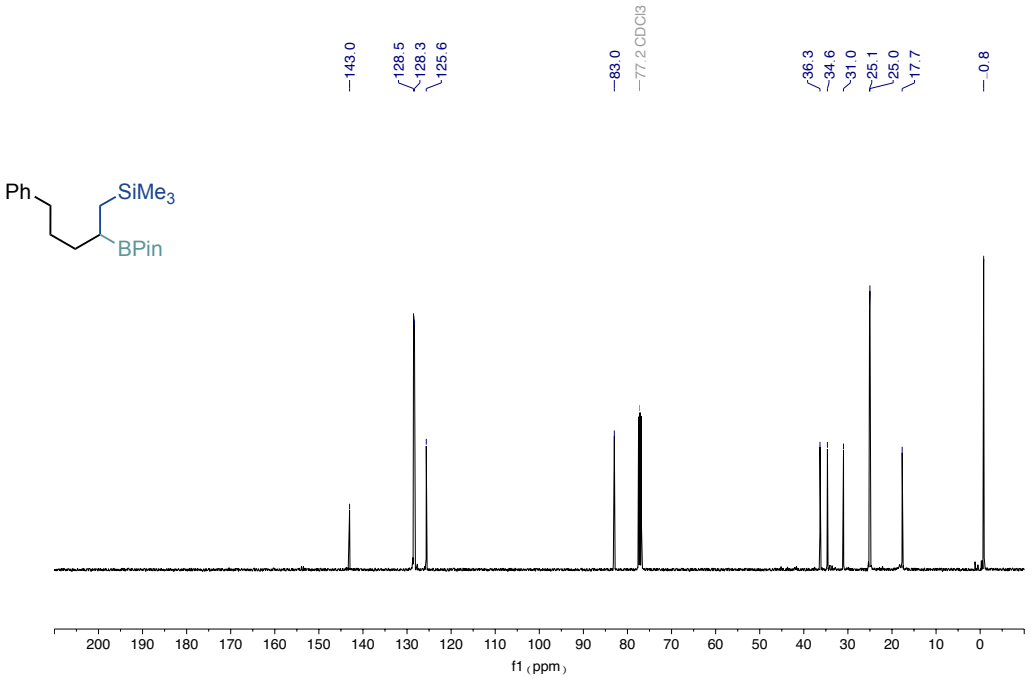

^{13}C NMR spectra (101 MHz) of **5d**

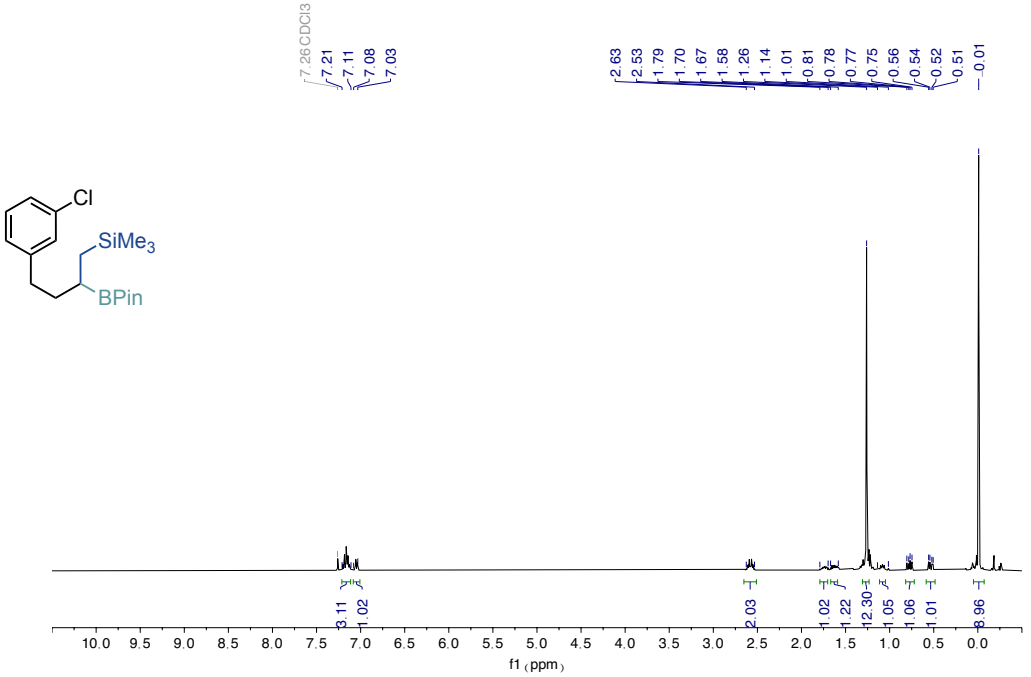

^{1}H NMR spectra (400 MHz) of **5e**

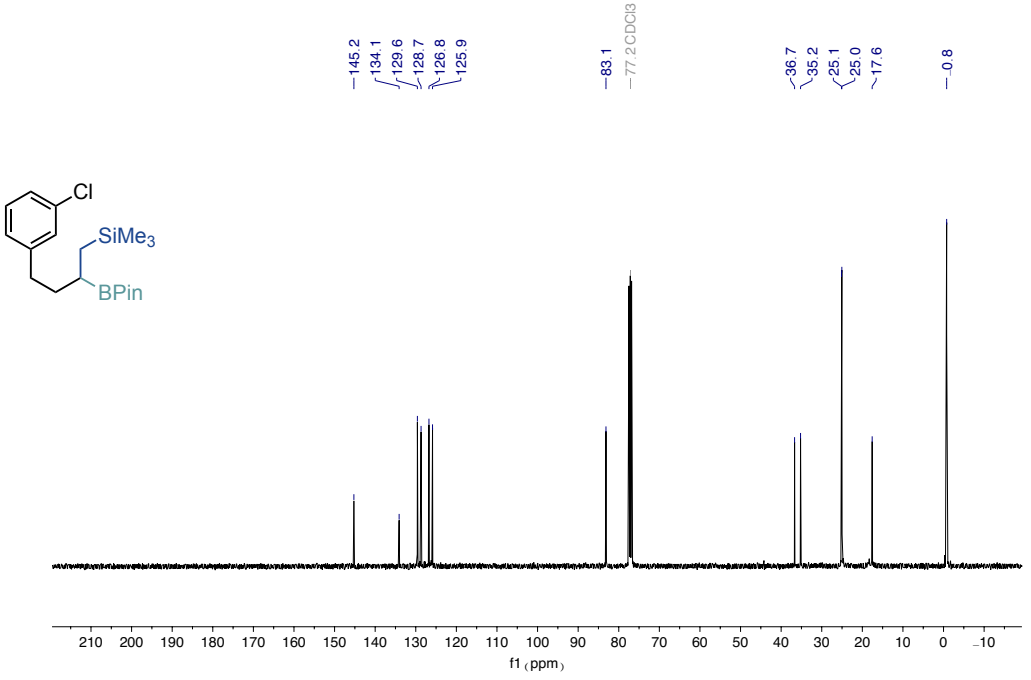

^{13}C NMR spectra (101 MHz) of **5e**

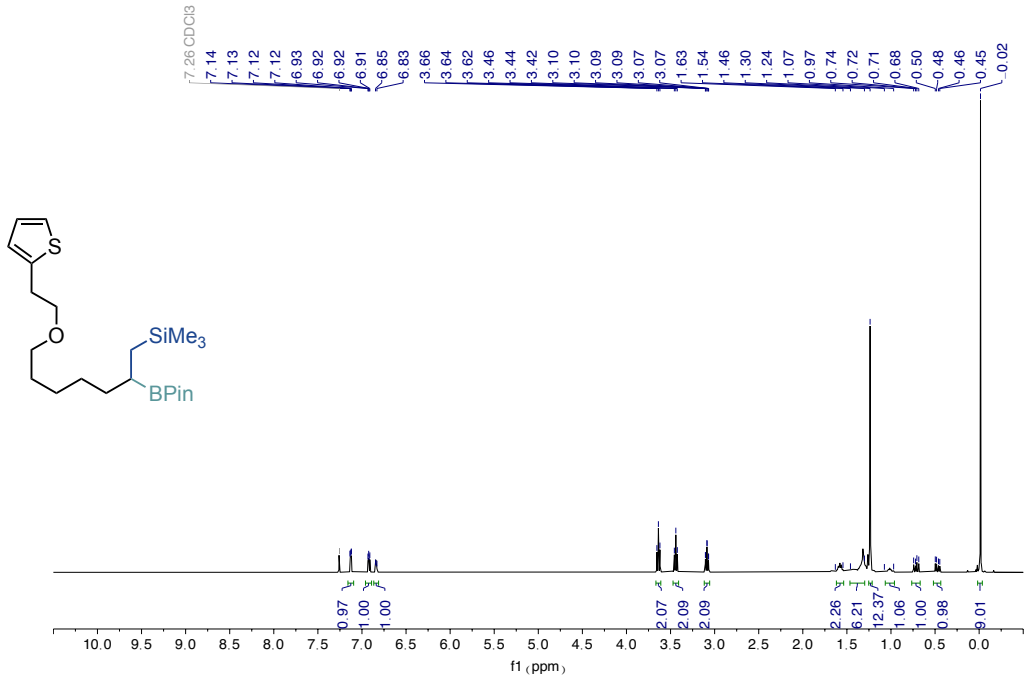

^{1}H NMR spectra (400 MHz) of **5f**

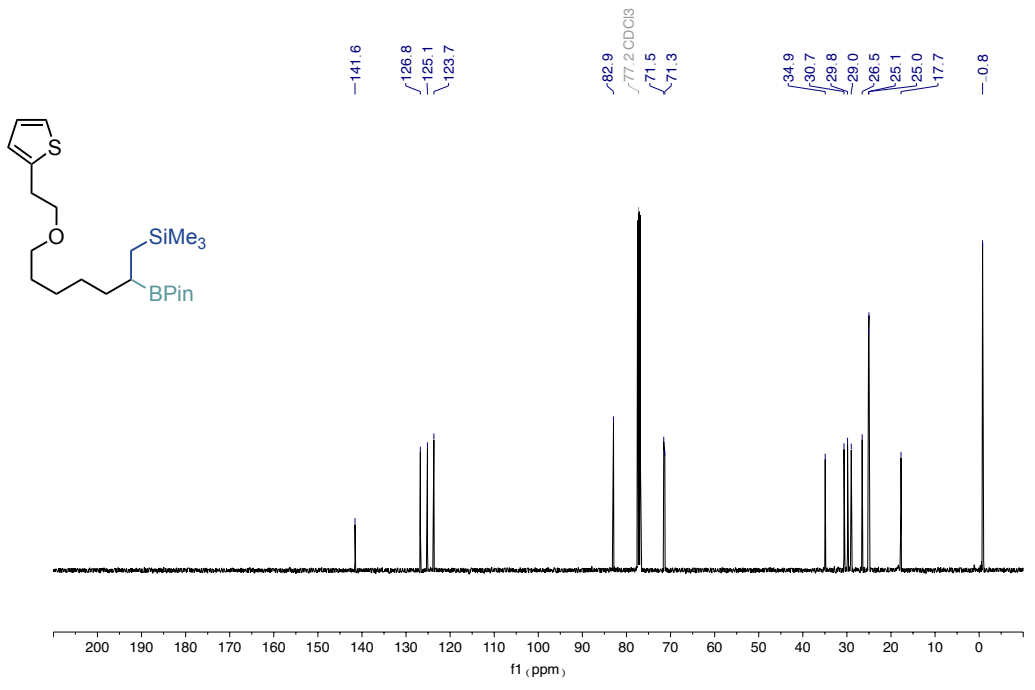

^{13}C NMR spectra (101 MHz) of **5f**

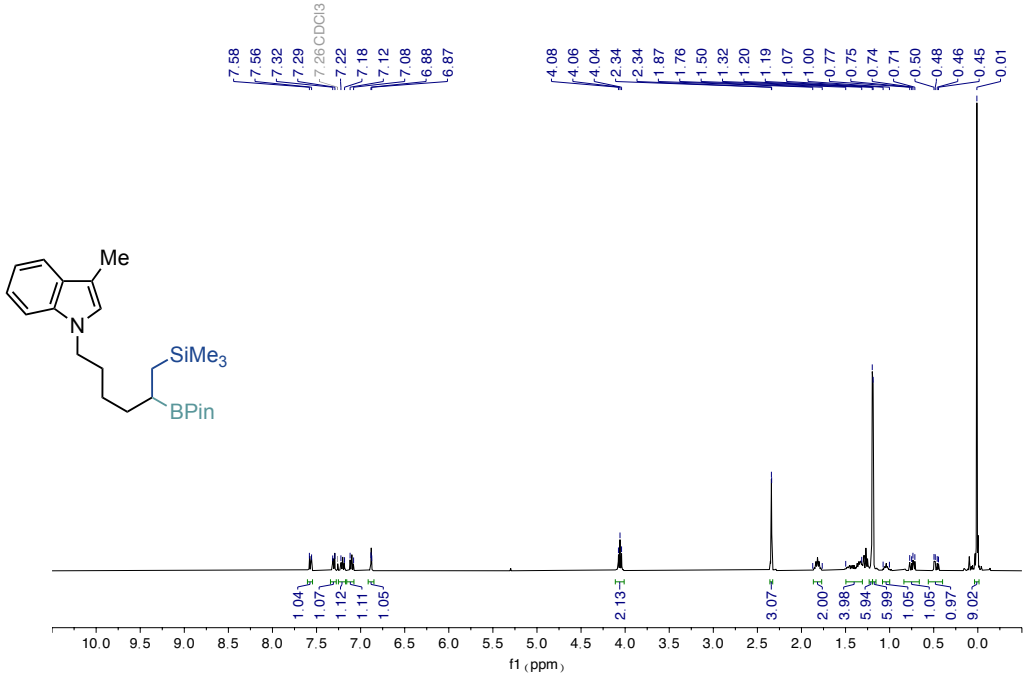

^{1}H NMR spectra (400 MHz) of **5g**

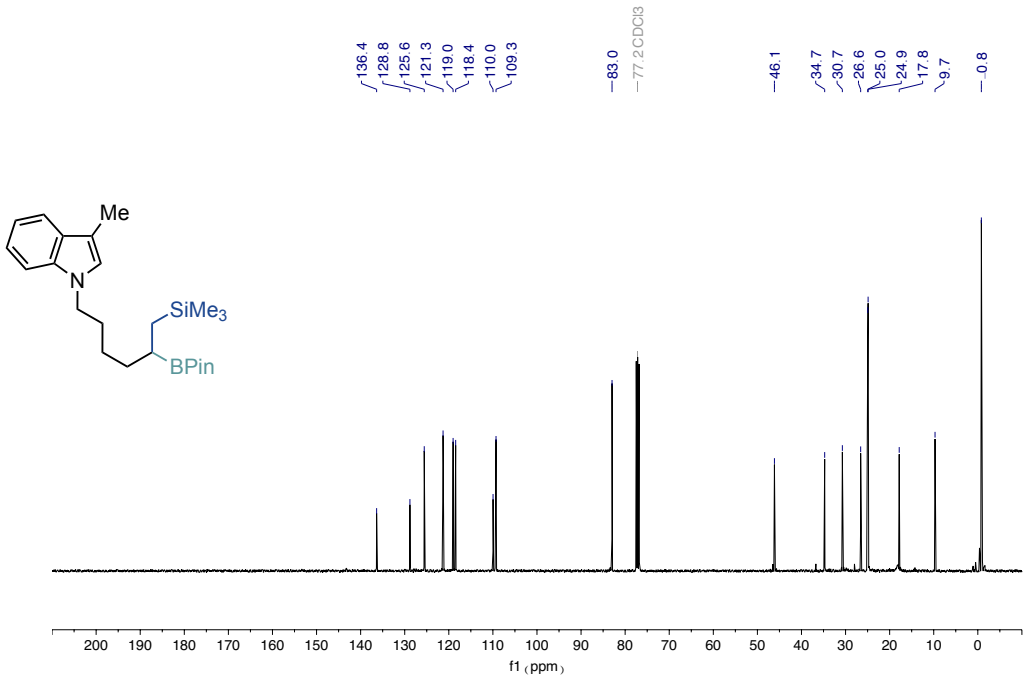

^{13}C NMR spectra (101 MHz) of **5g**

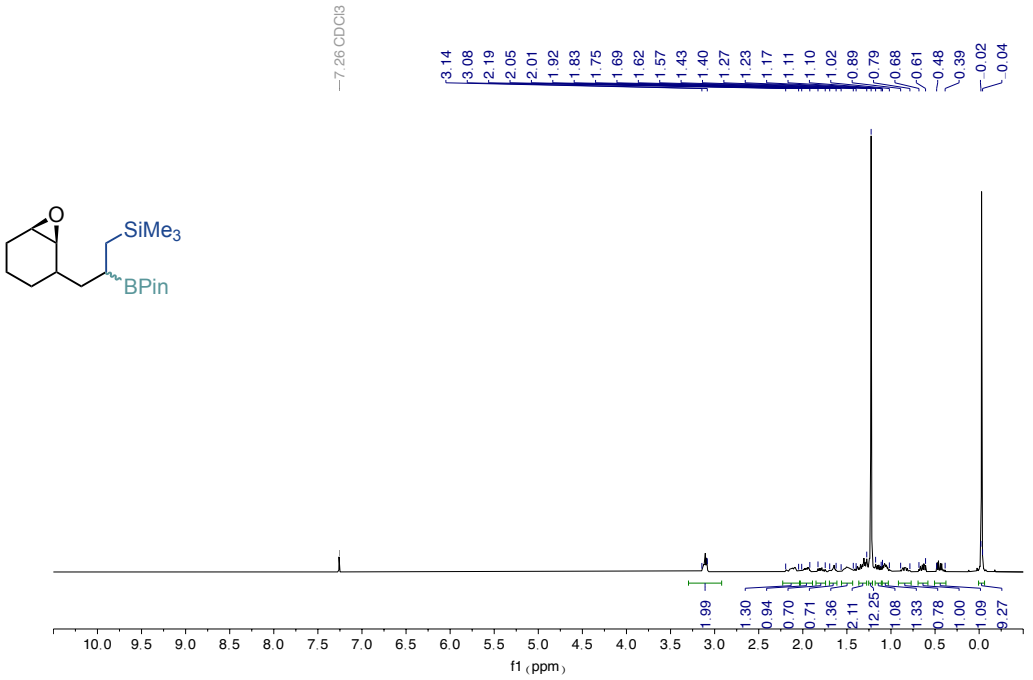

^{1}H NMR spectra (400 MHz) of **5h**

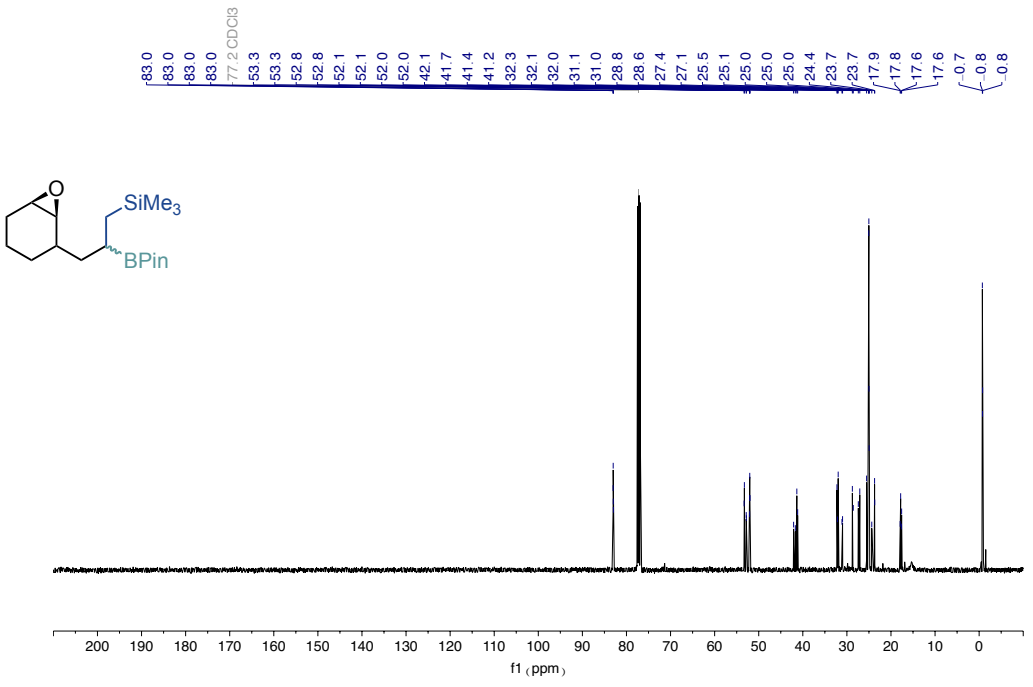

^{13}C NMR spectra (101 MHz) of **5h**

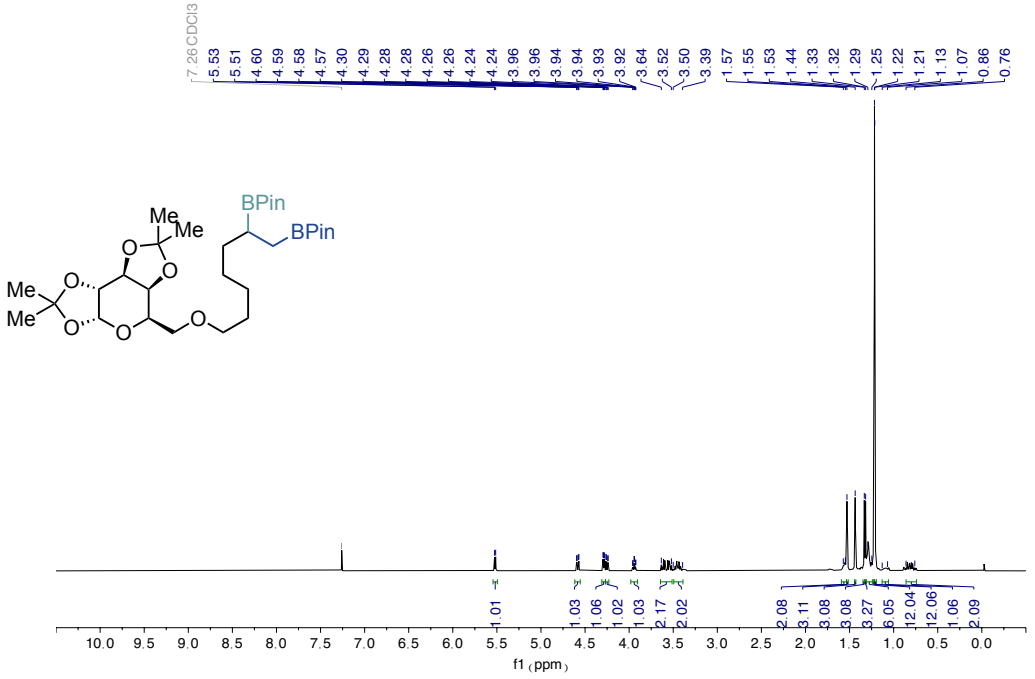

^{1}H NMR spectra (400 MHz) of **6a**

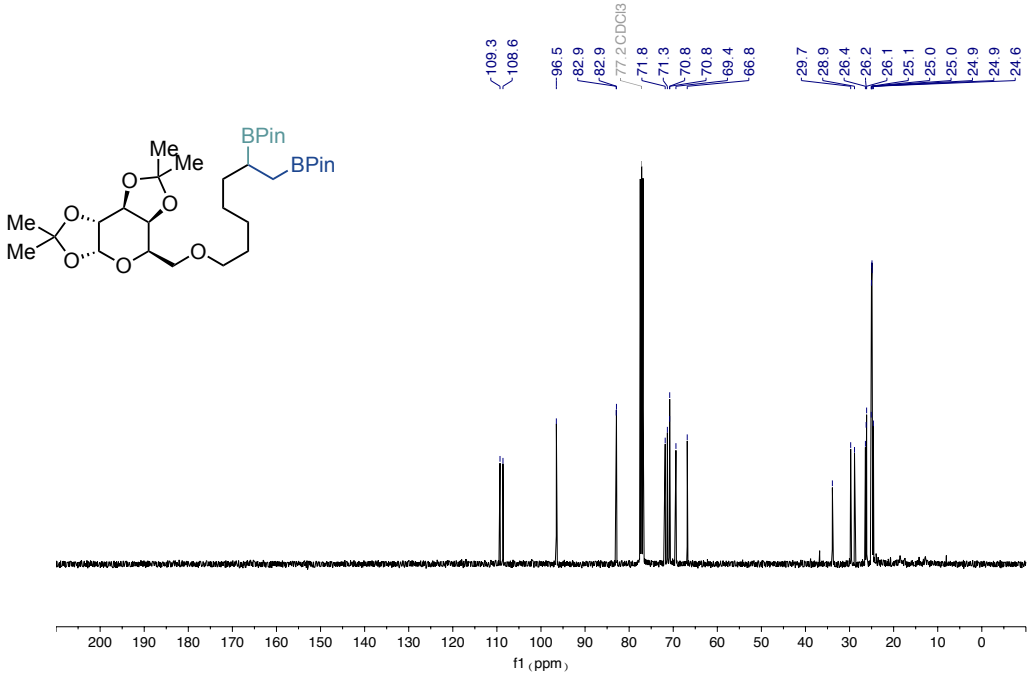

^{13}C NMR spectra (101 MHz) of **6a**

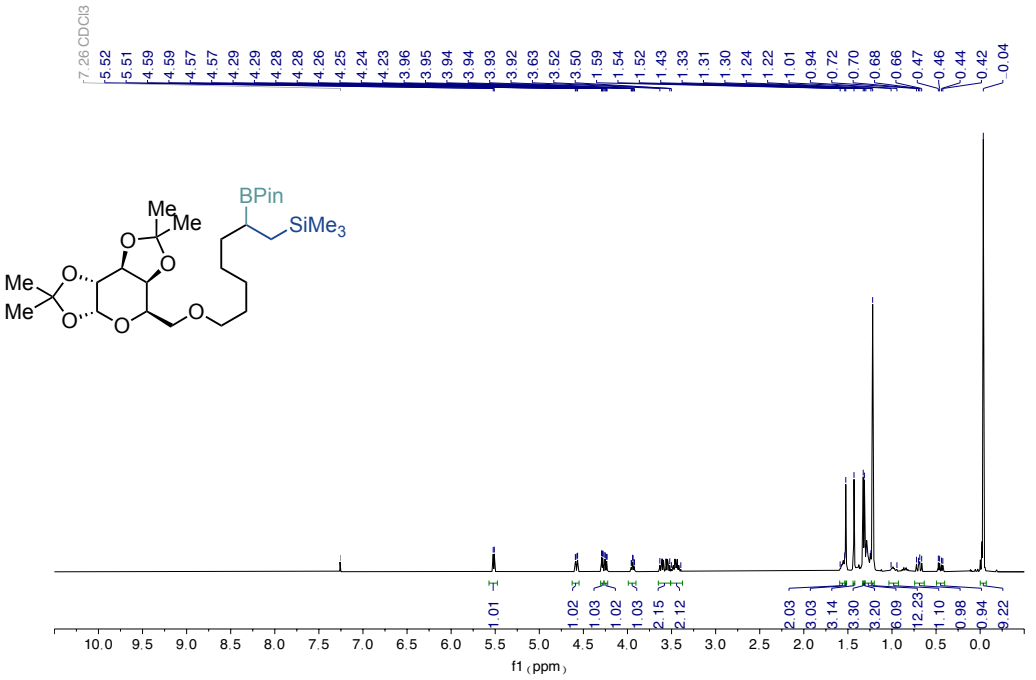

^{1}H NMR spectra (400 MHz) of **6b**

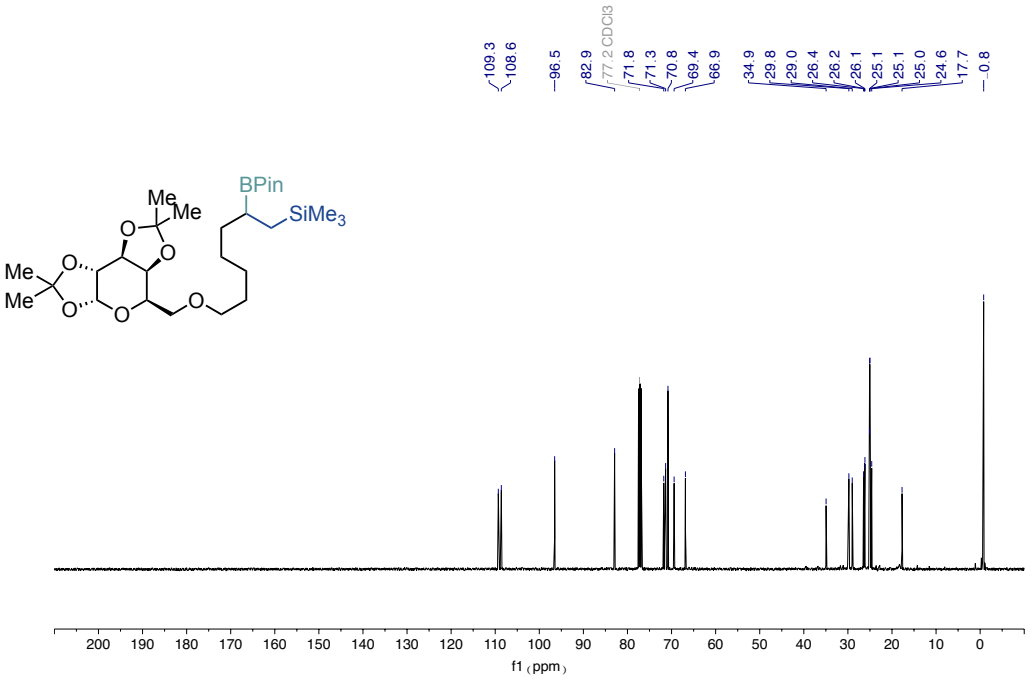

^{13}C NMR spectra (101 MHz) of **6b**

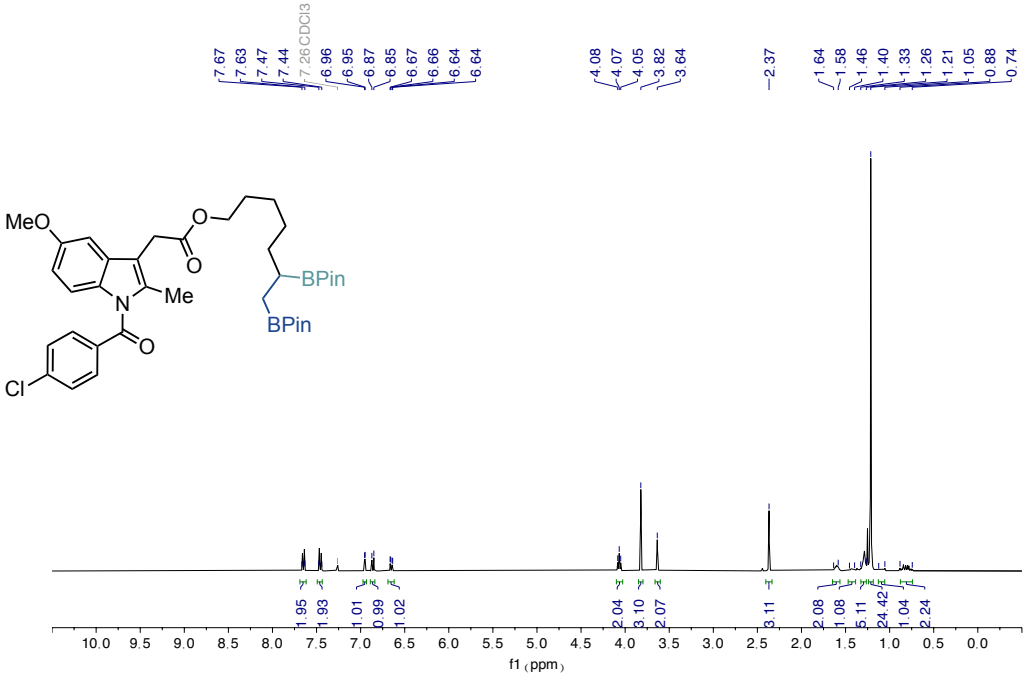

^{1}H NMR spectra (400 MHz) of **7a**

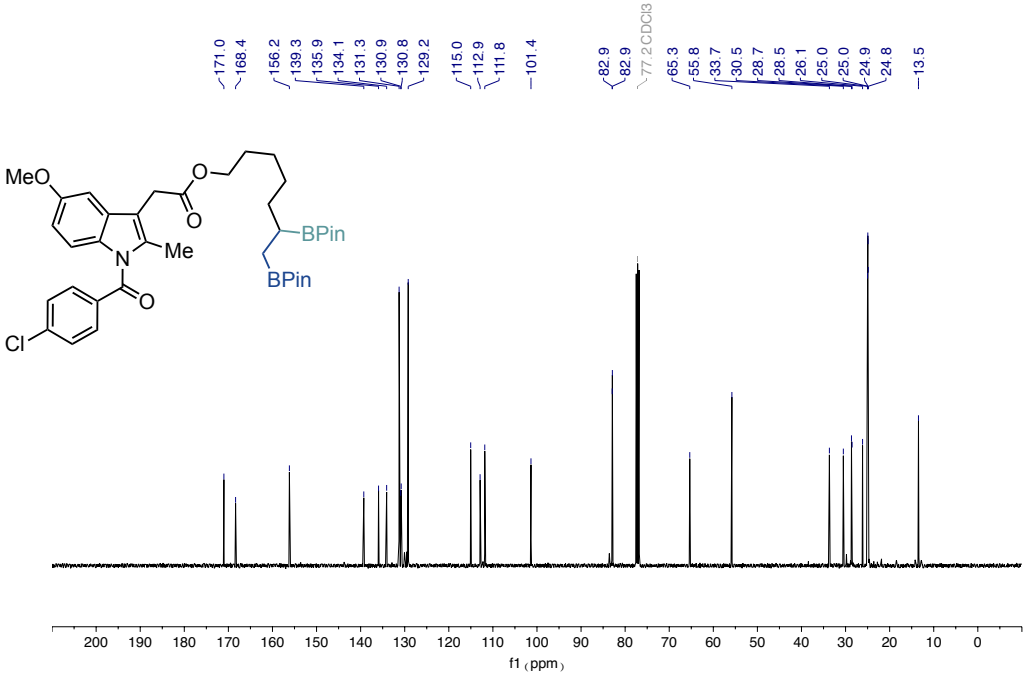

^{13}C NMR spectra (101 MHz) of **7a**

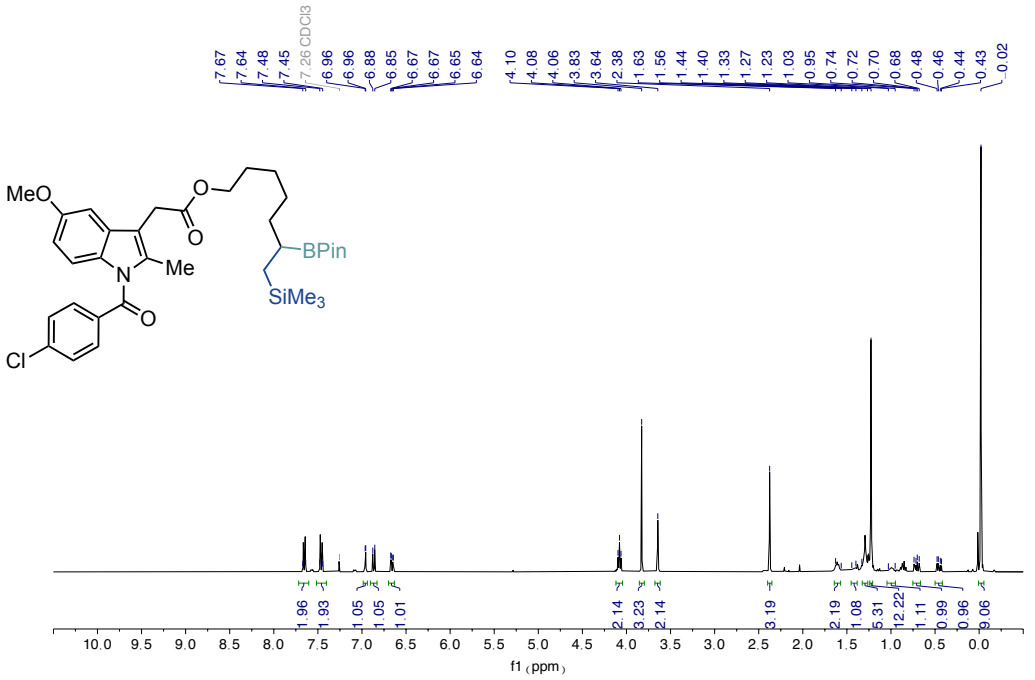

^{1}H NMR spectra (400 MHz) of **7b**

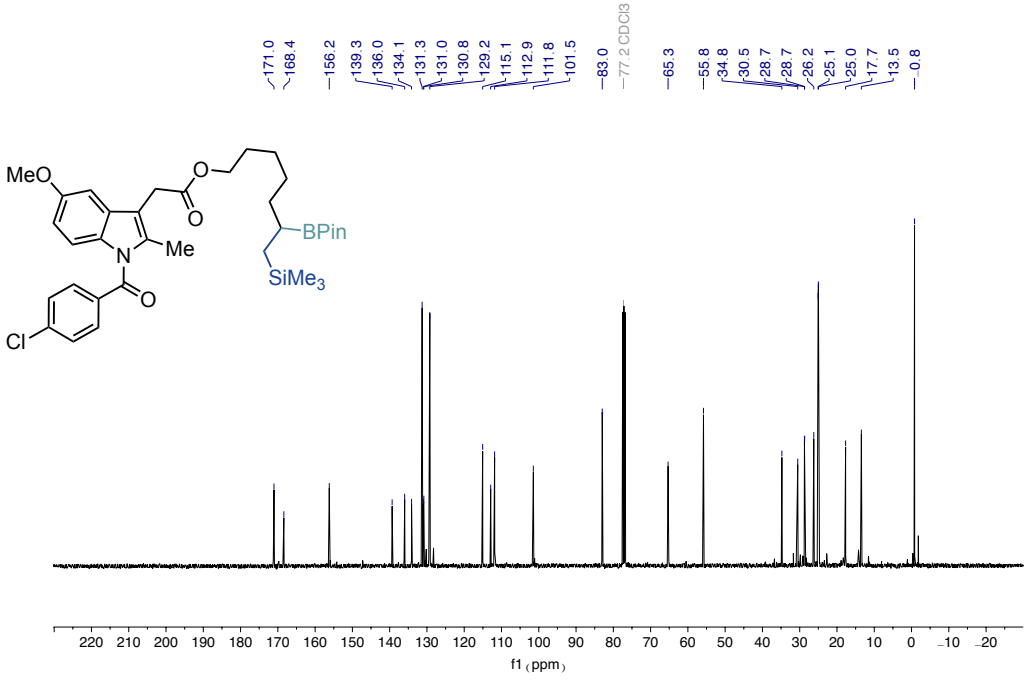

^{13}C NMR spectra (101 MHz) of **7b**

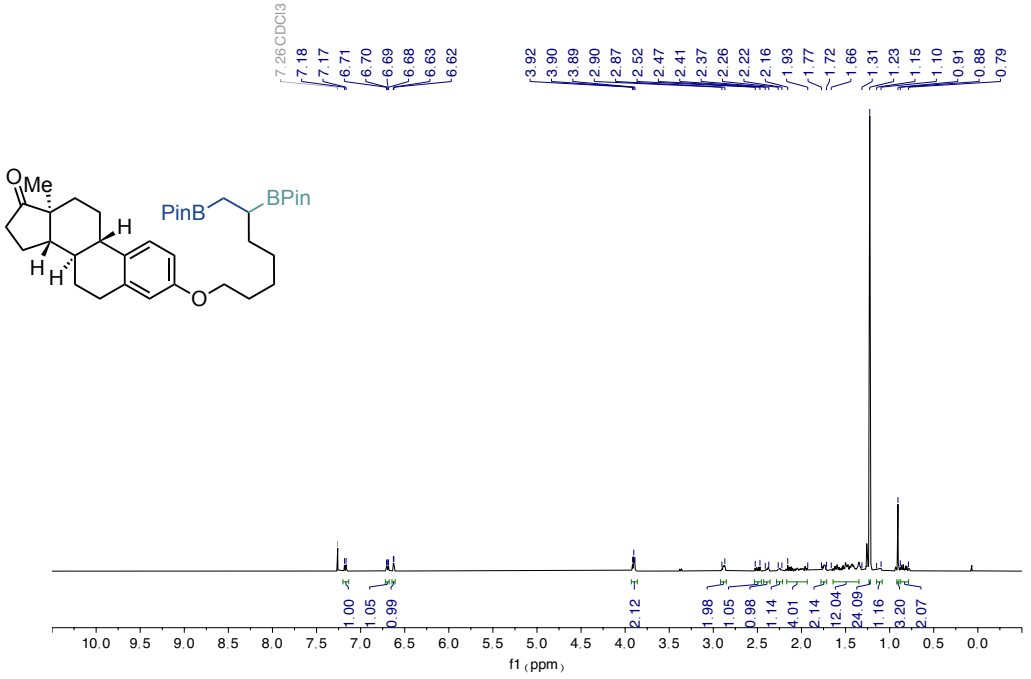

^{1}H NMR spectra (500 MHz) of **8a**

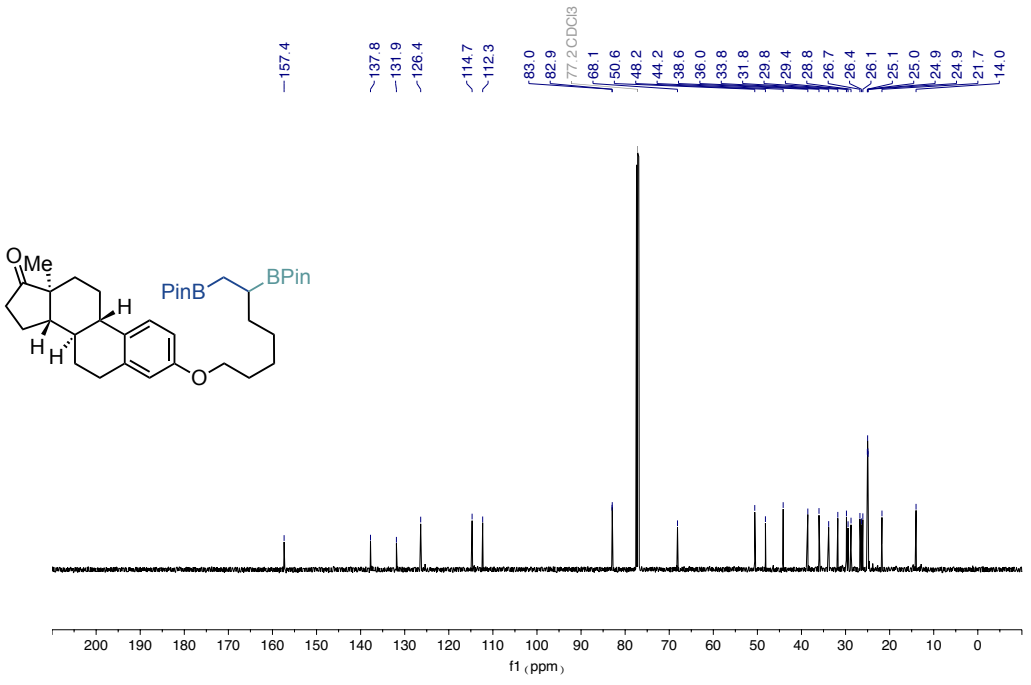

^{13}C NMR spectra (126 MHz) of **8a**

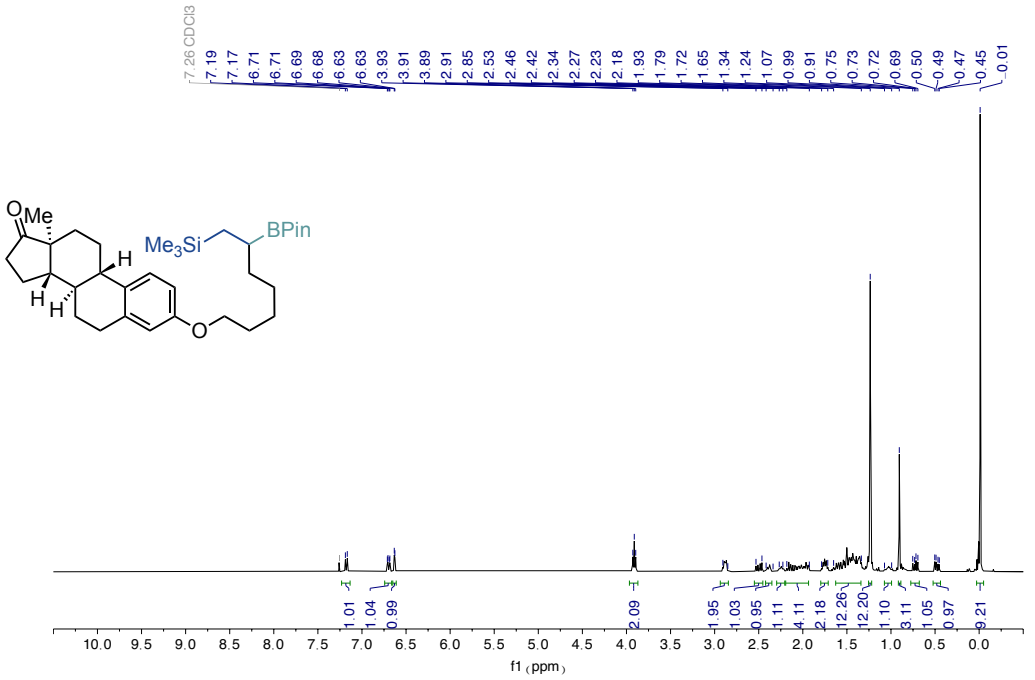

^{1}H NMR spectra (400 MHz) of **8b**

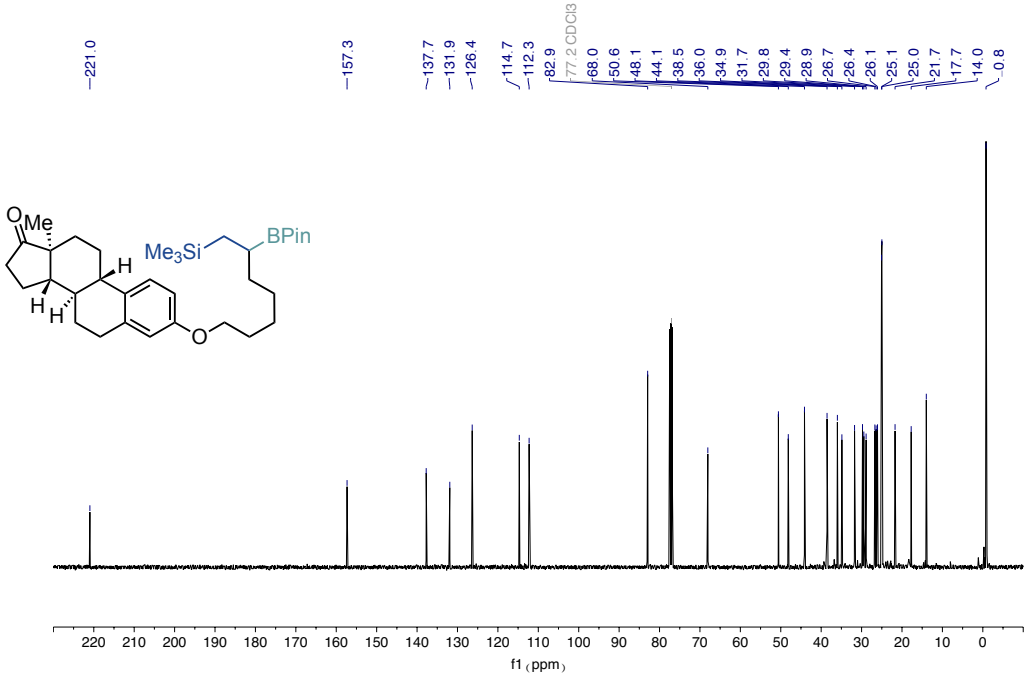

^{13}C NMR spectra (101 MHz) of **8b**

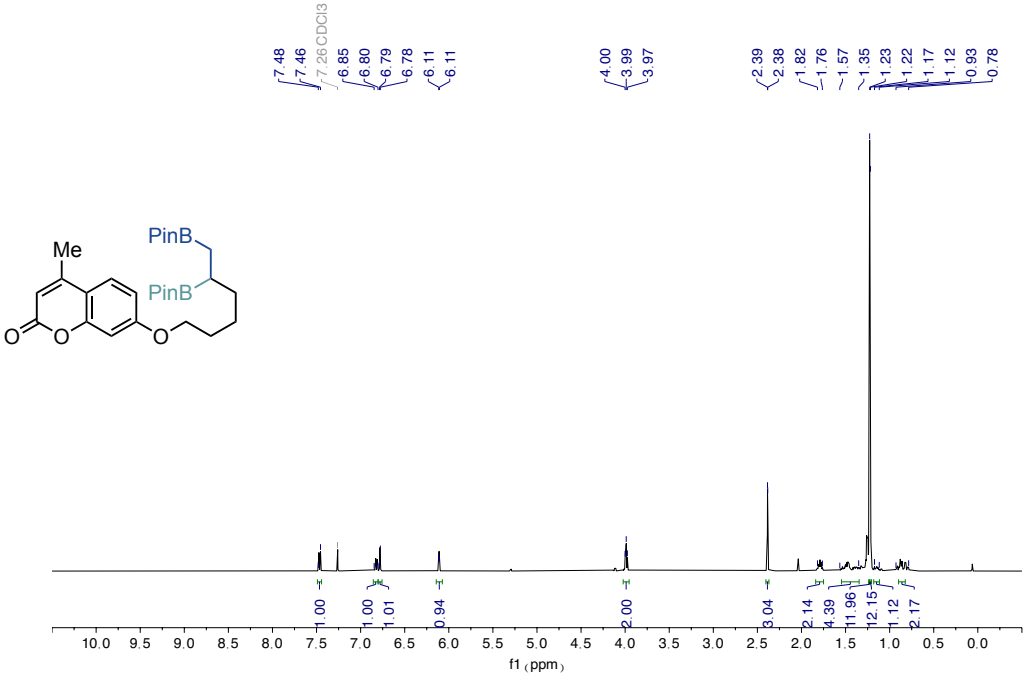

^{1}H NMR spectra (500 MHz) of **9a**

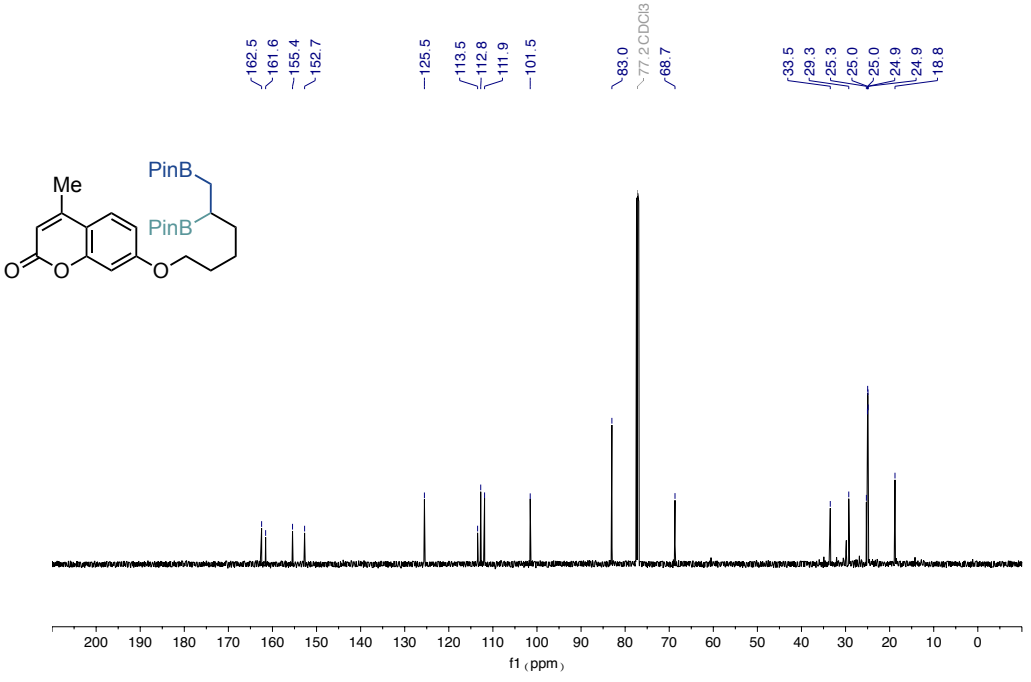

^{13}C NMR spectra (126 MHz) of **9a**

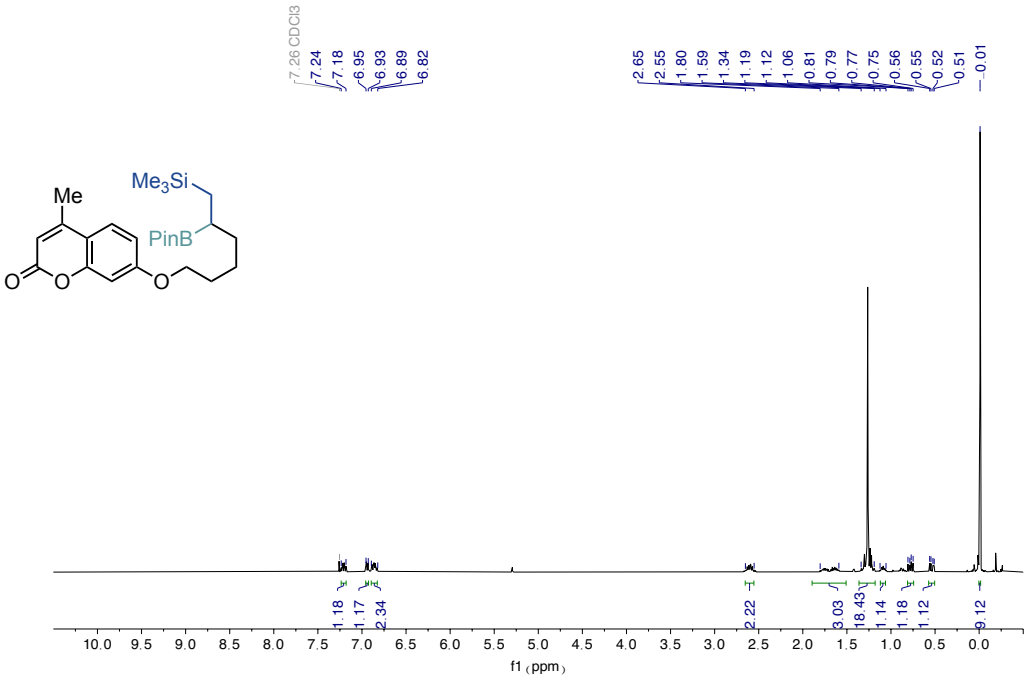

^{1}H NMR spectra (400 MHz) of **9b**

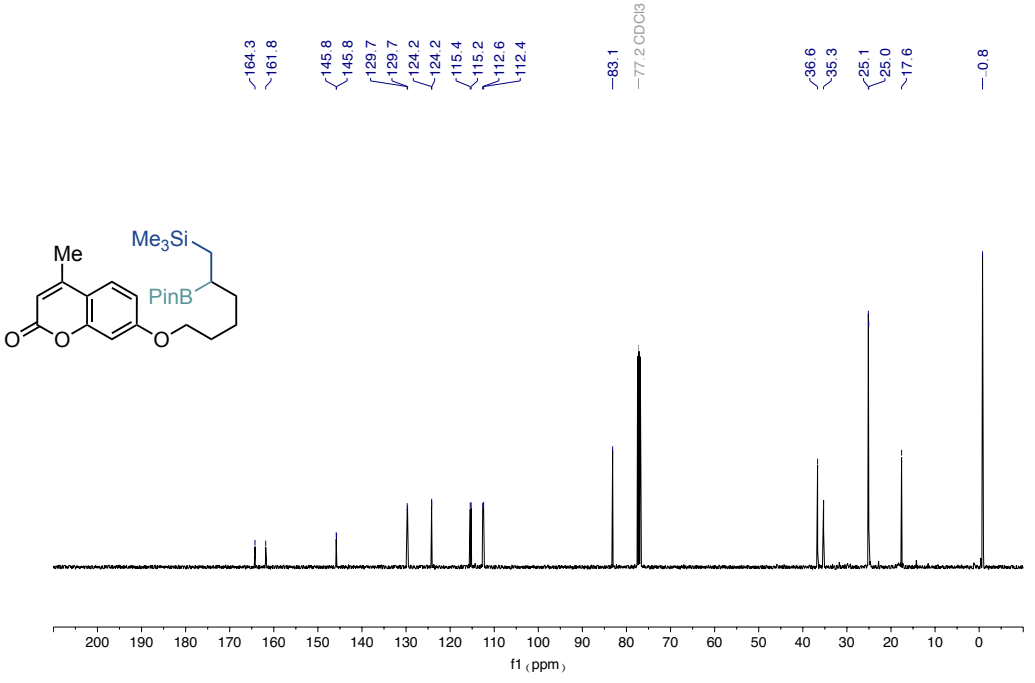

^{13}C NMR spectra (101 MHz) of **9b**

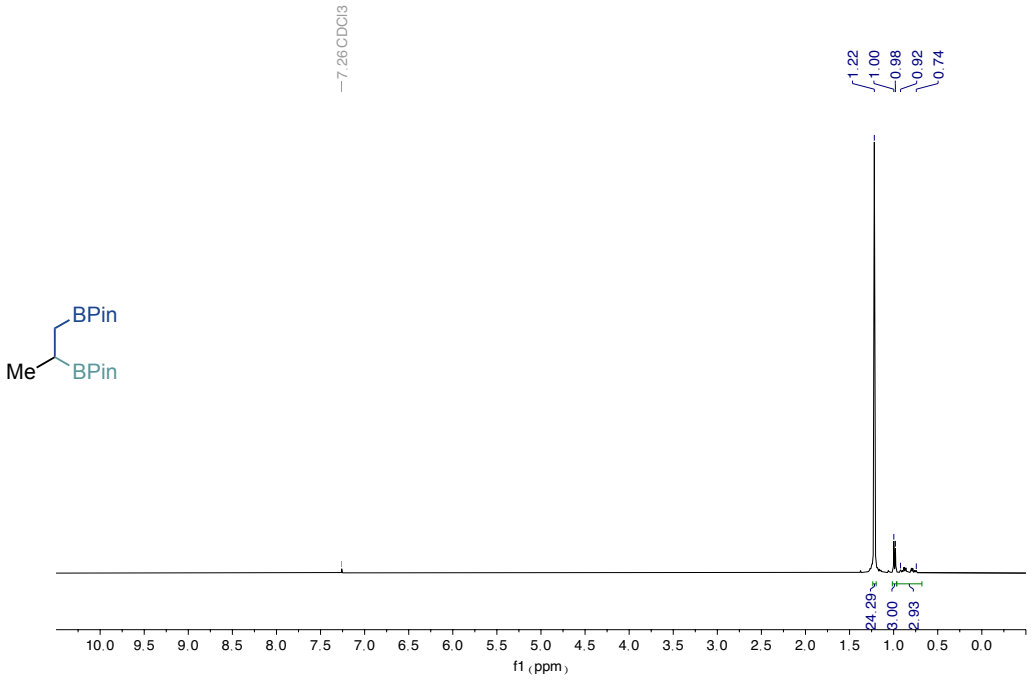

^{1}H NMR spectra (400 MHz) of **10a**

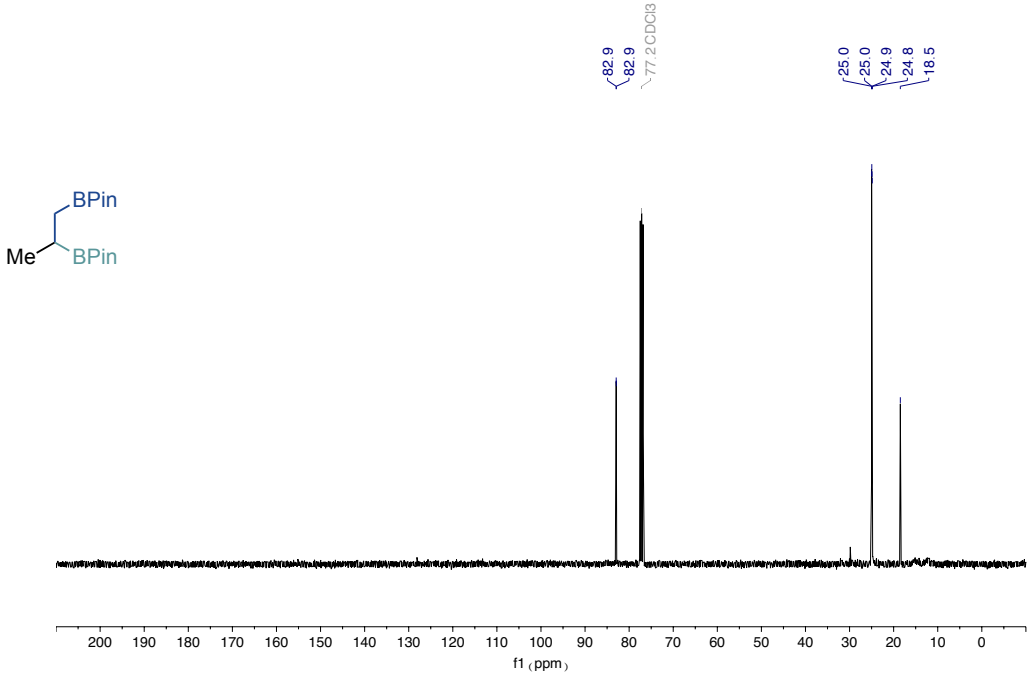

^{13}C NMR spectra (101 MHz) of **10a**

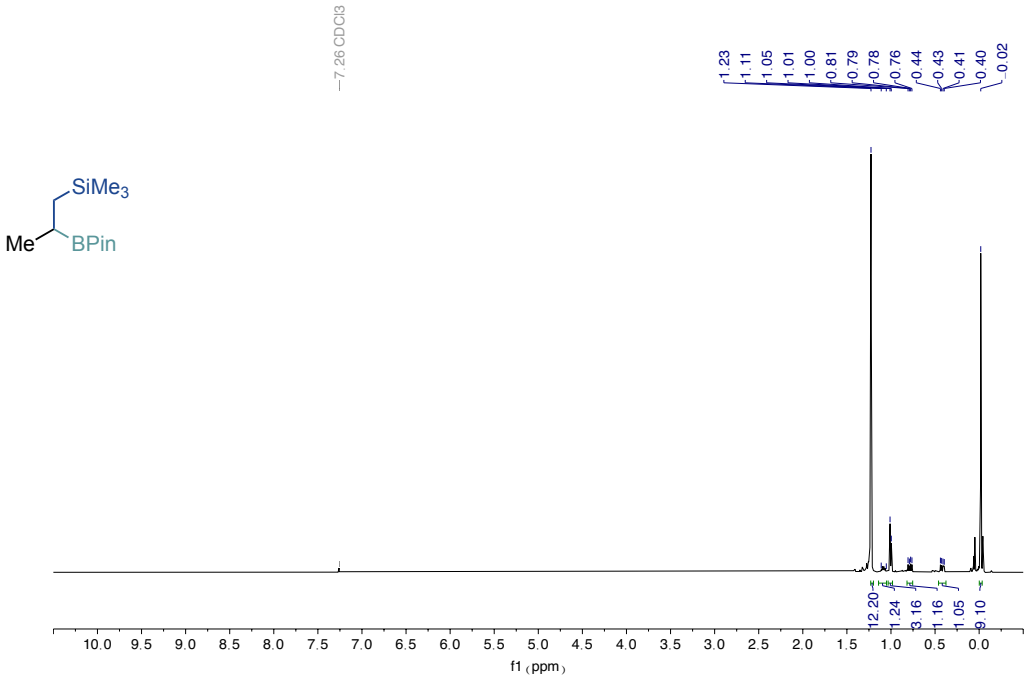

^{1}H NMR spectra (500 MHz) of **10b**

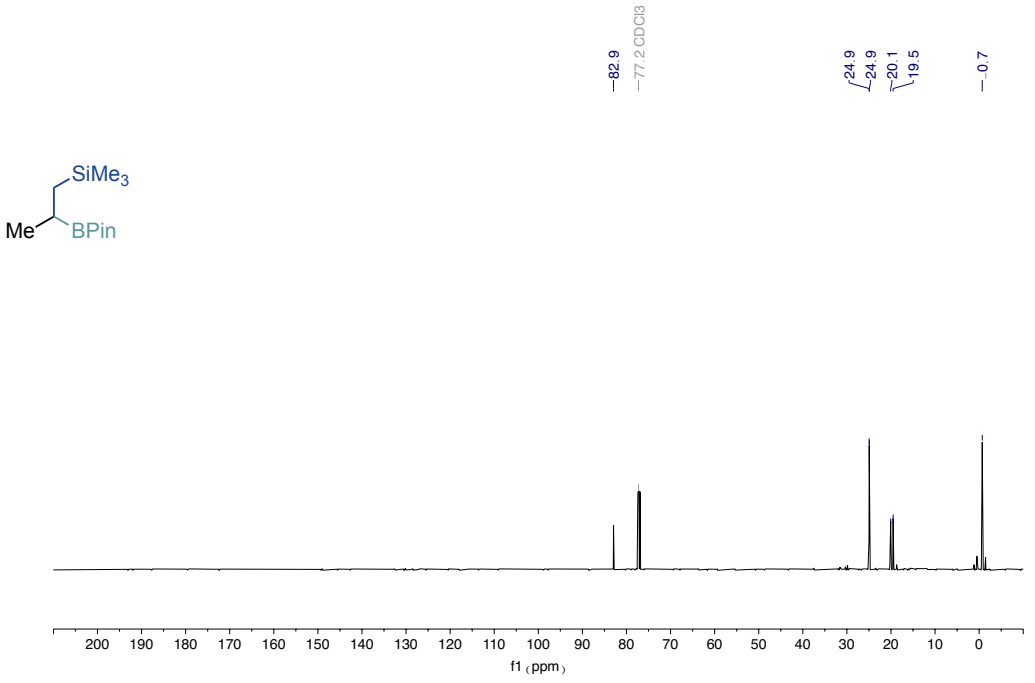

^{13}C NMR spectra (126 MHz) of **10b**

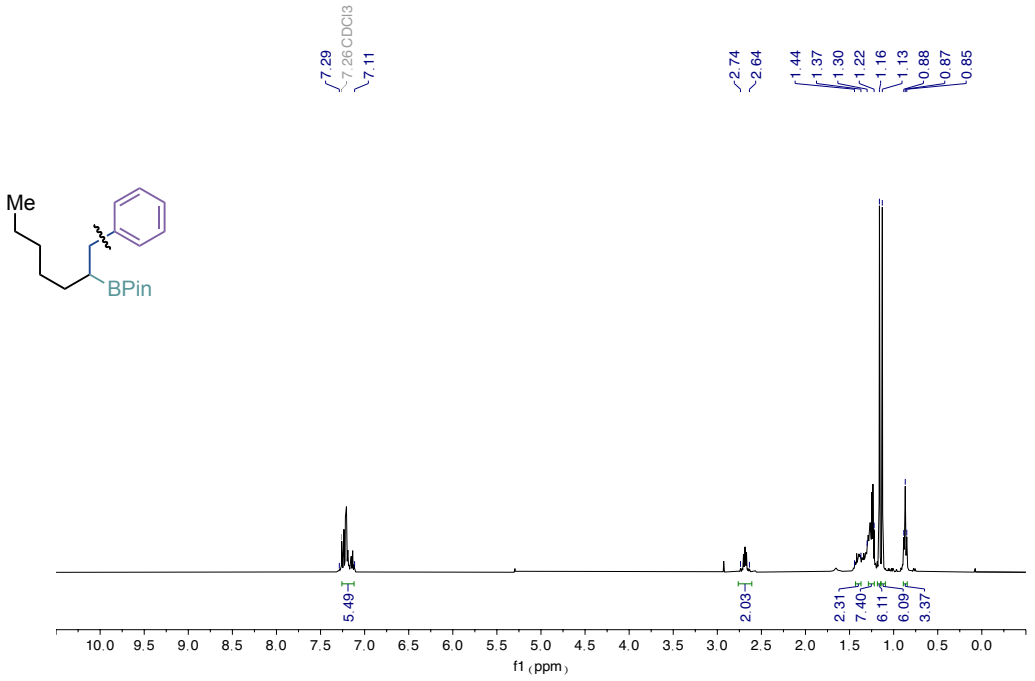

^{1}H NMR spectra (400 MHz) of **11**

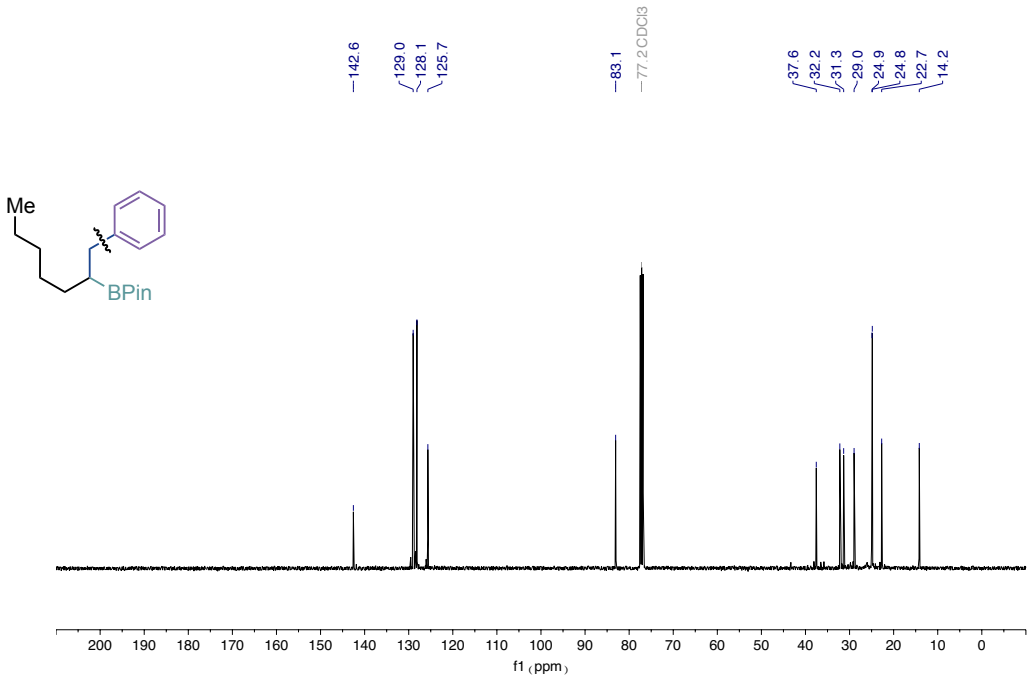

^{13}C NMR spectra (101 MHz) of **11**

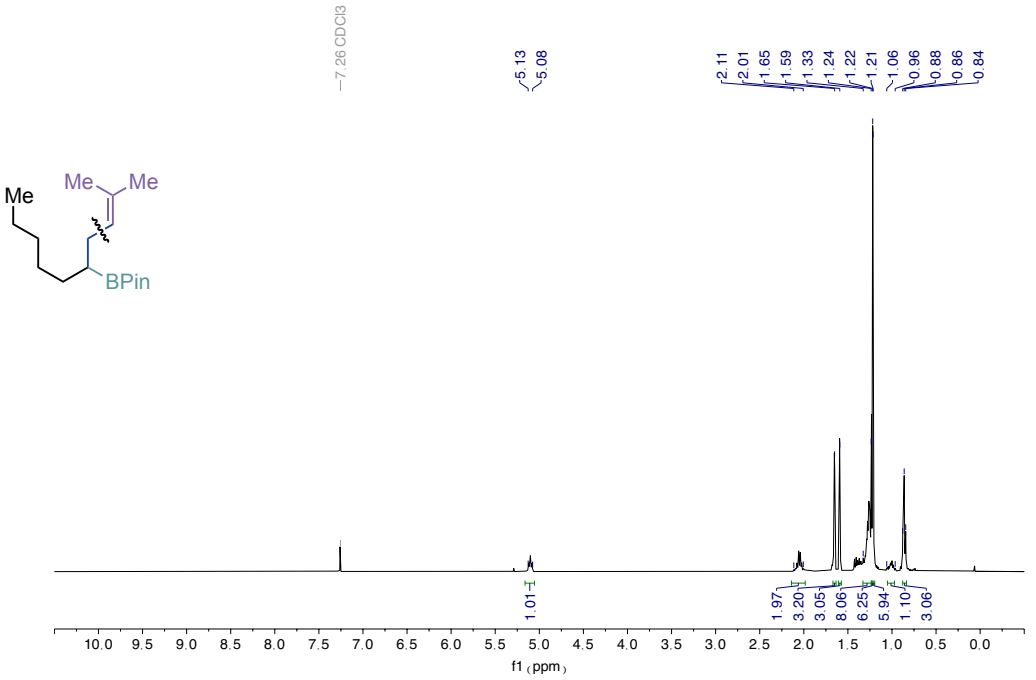

^{1}H NMR spectra (400 MHz) of **12**

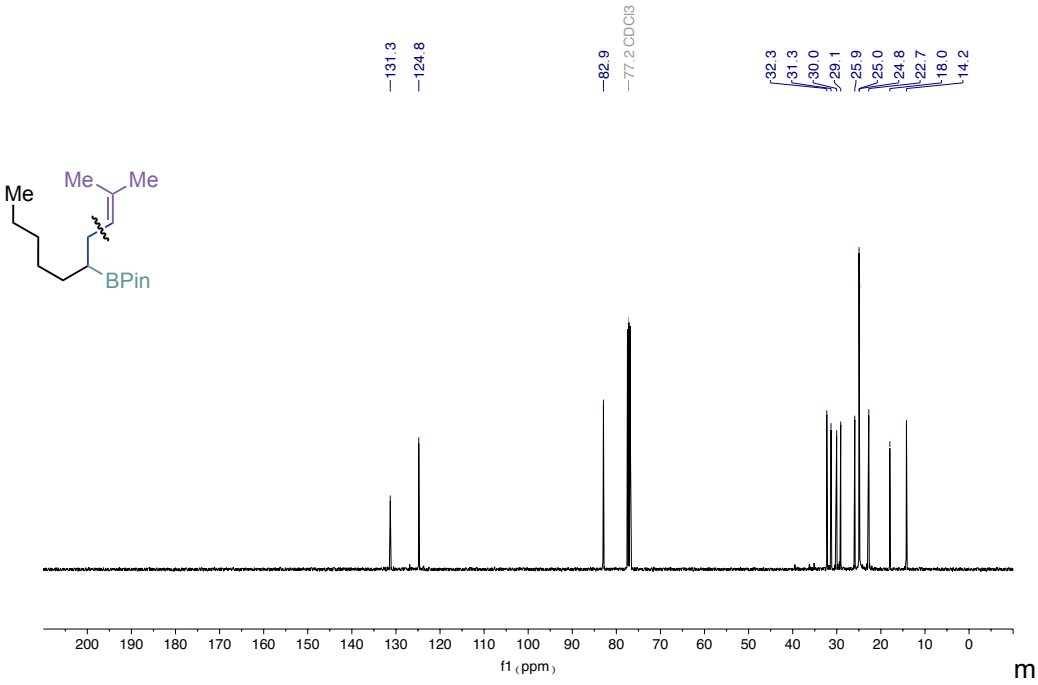

^{13}C NMR spectra (101 MHz) of **12**

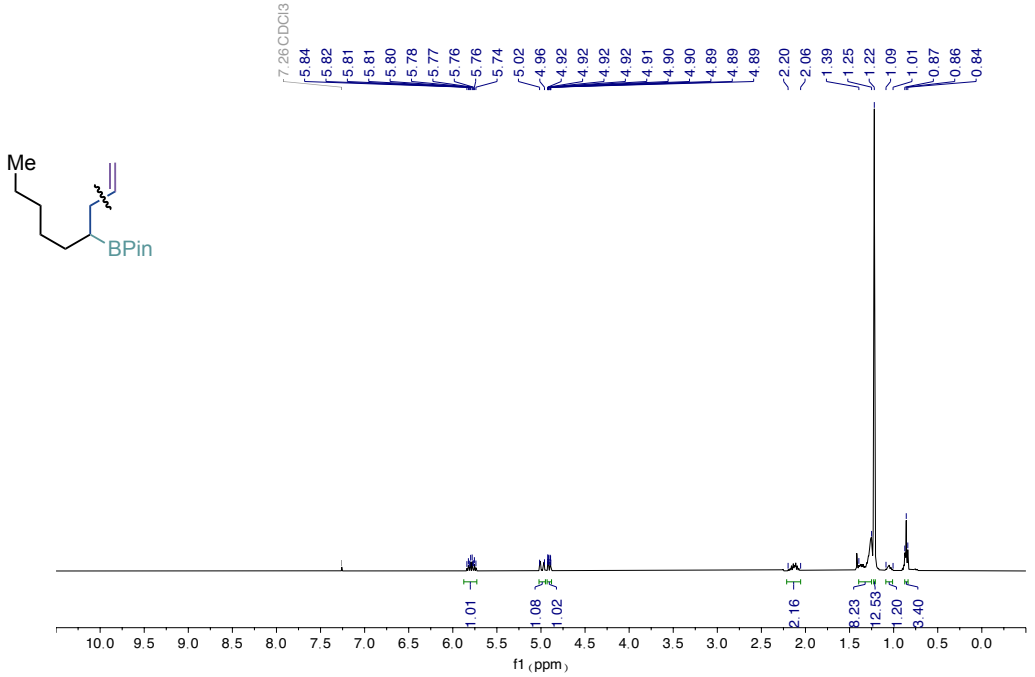

^{1}H NMR spectra (400 MHz) of **13**

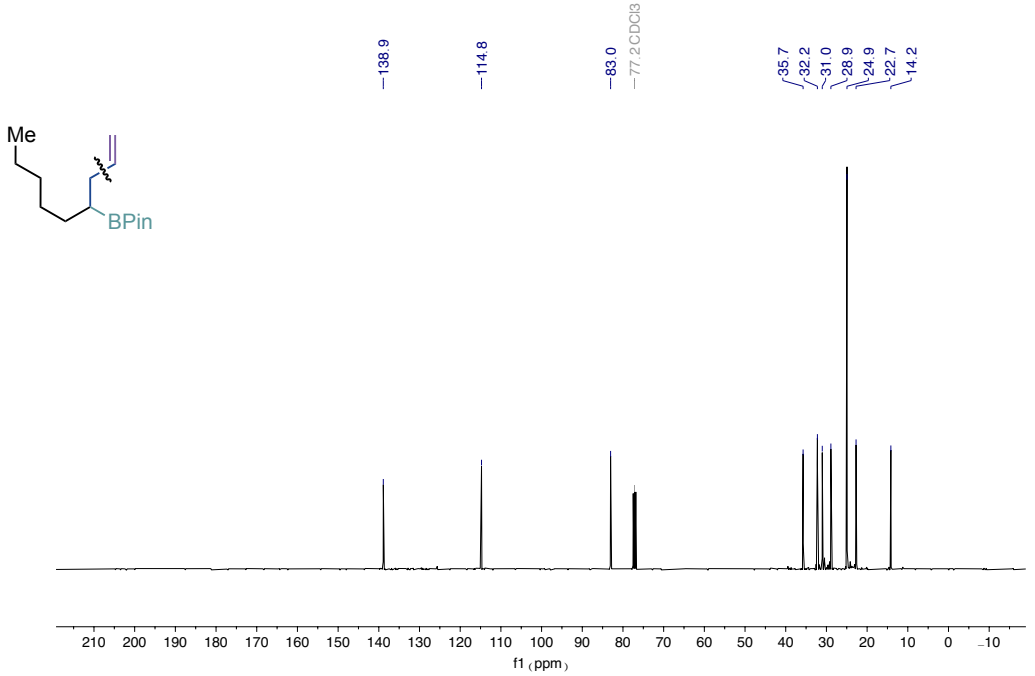

^{13}C NMR spectra (101 MHz) of **13**

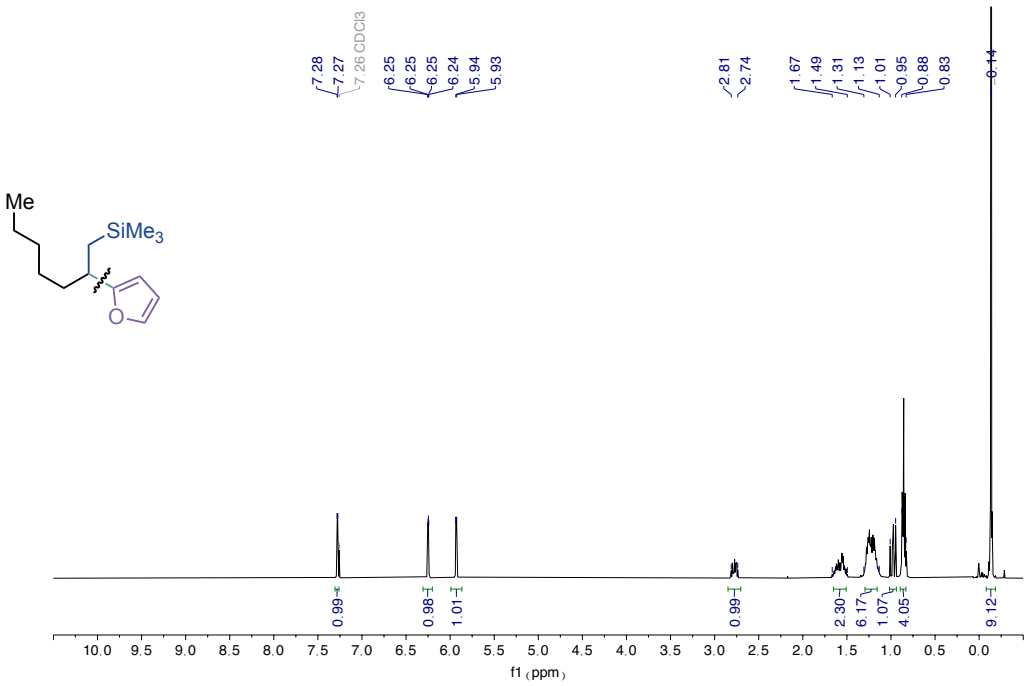

^{1}H NMR spectra (400 MHz) of **14**

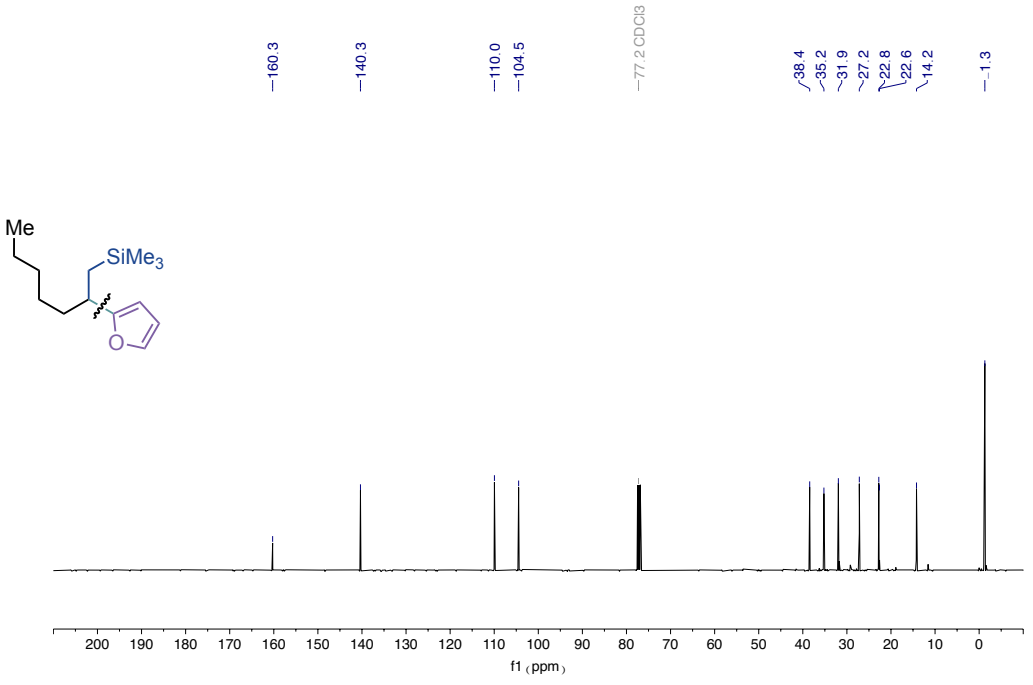

^{13}C NMR spectra (101 MHz) of **14**

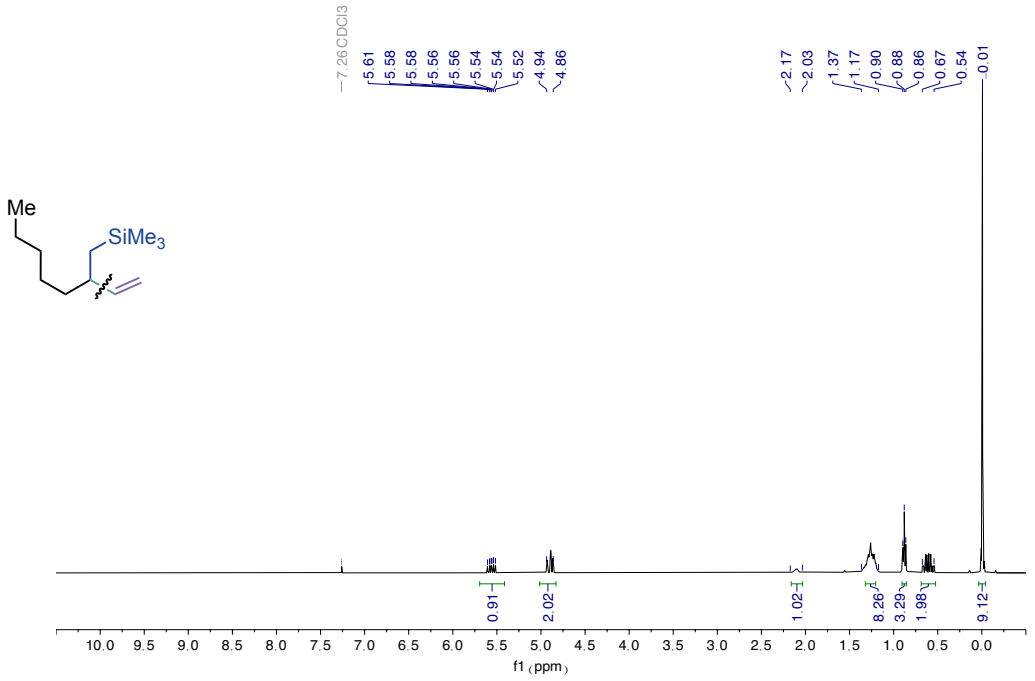

^{1}H NMR spectra (400 MHz) of **16**

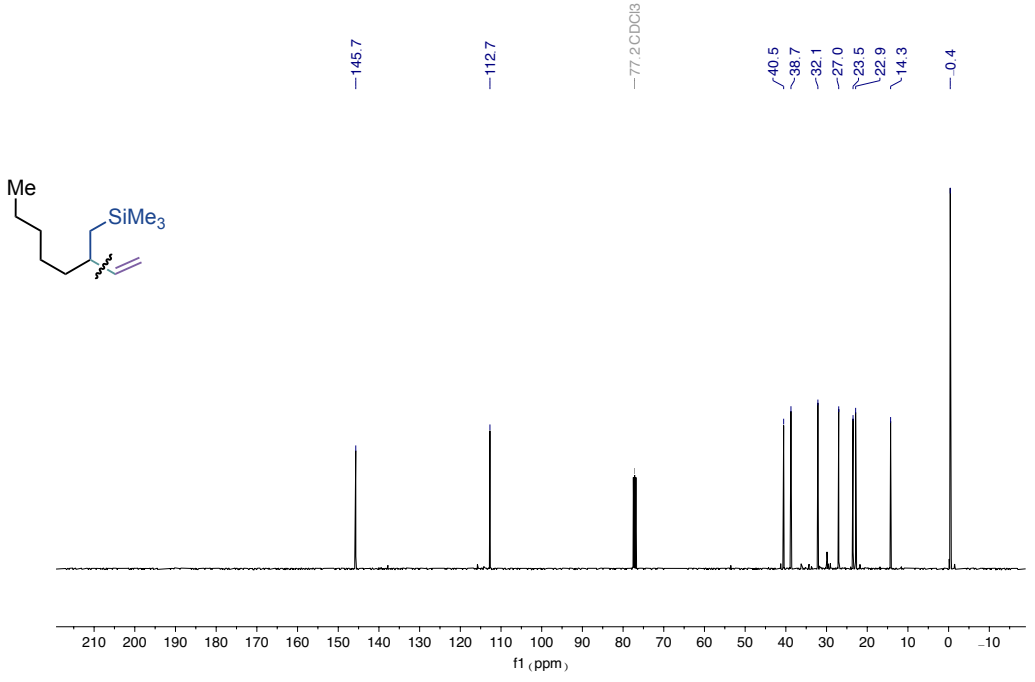

^{13}C NMR spectra (101 MHz) of **16**

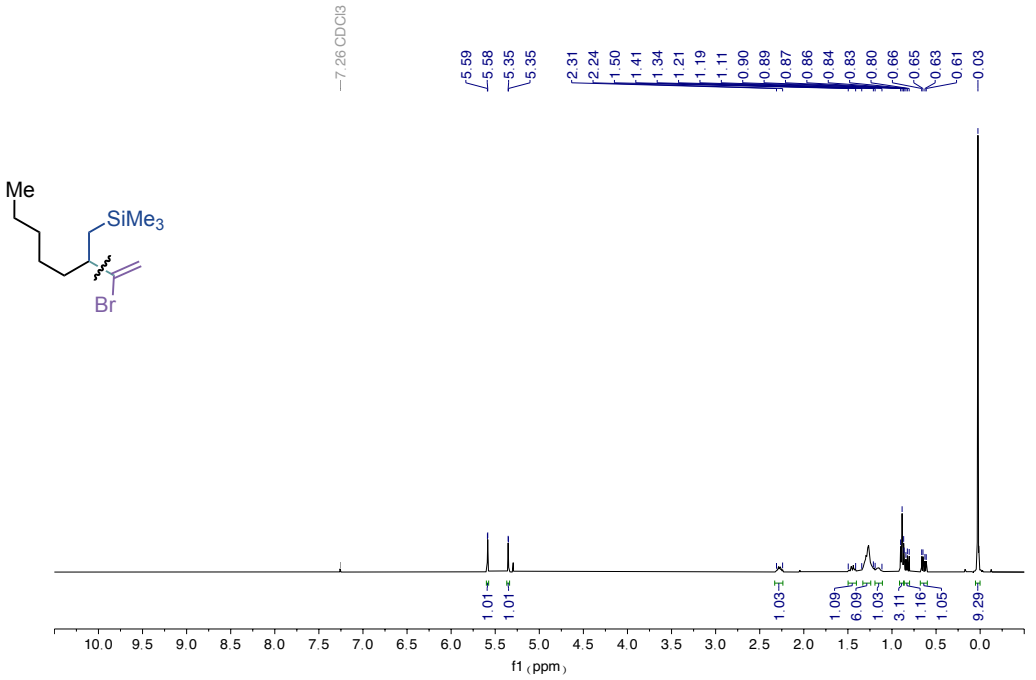

^{1}H NMR spectra (400 MHz) of **15**

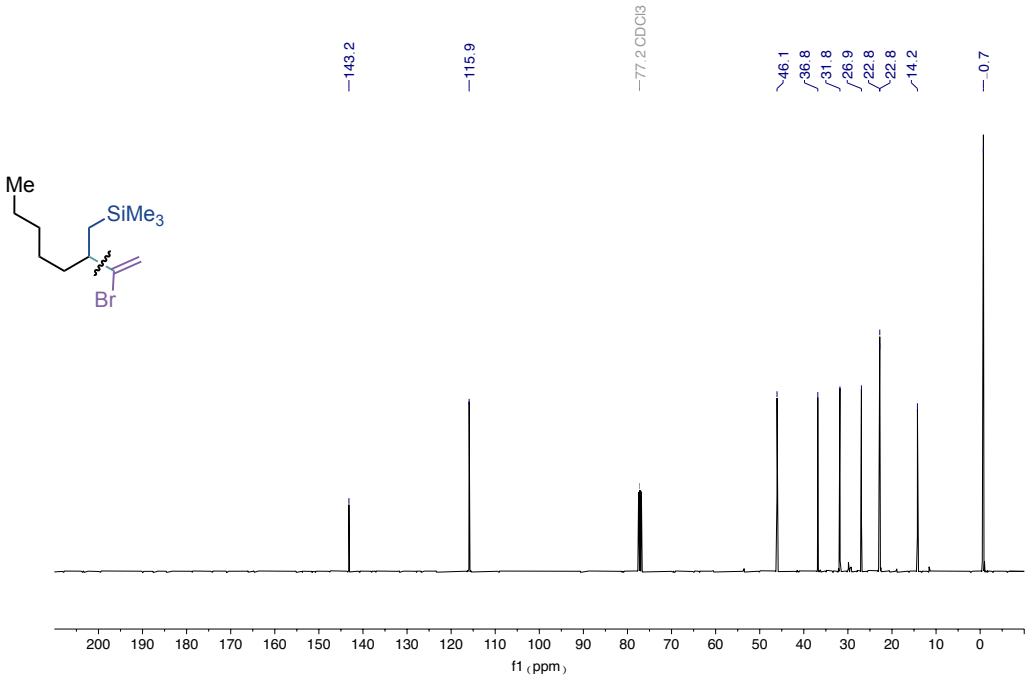

^{13}C NMR spectra (101 MHz) of **15**

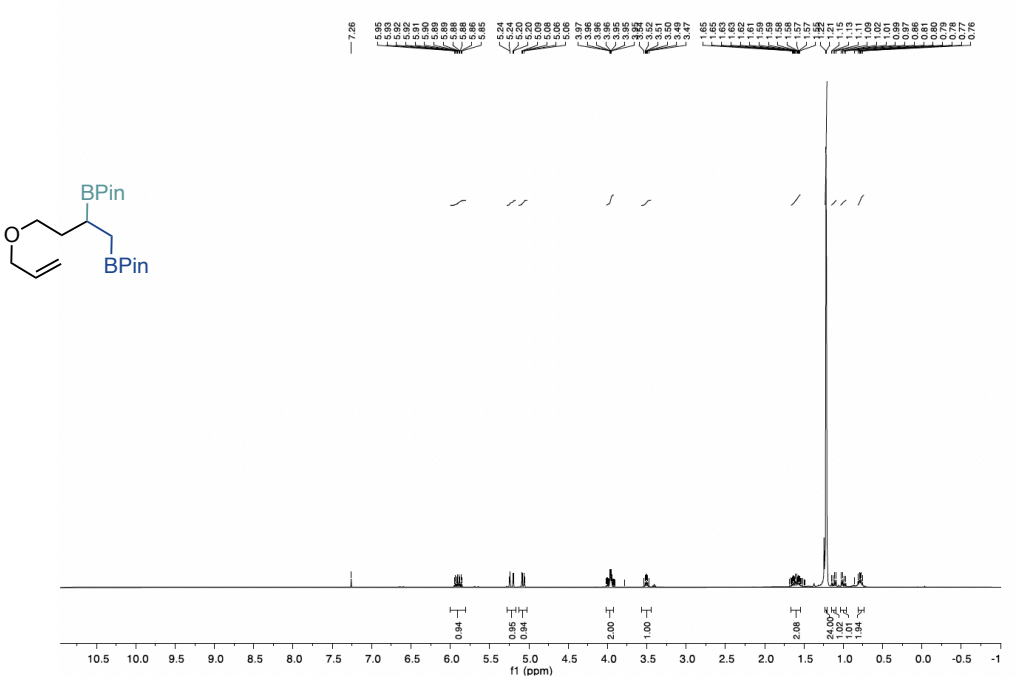

^{1}H NMR spectra (400 MHz) of **20a**

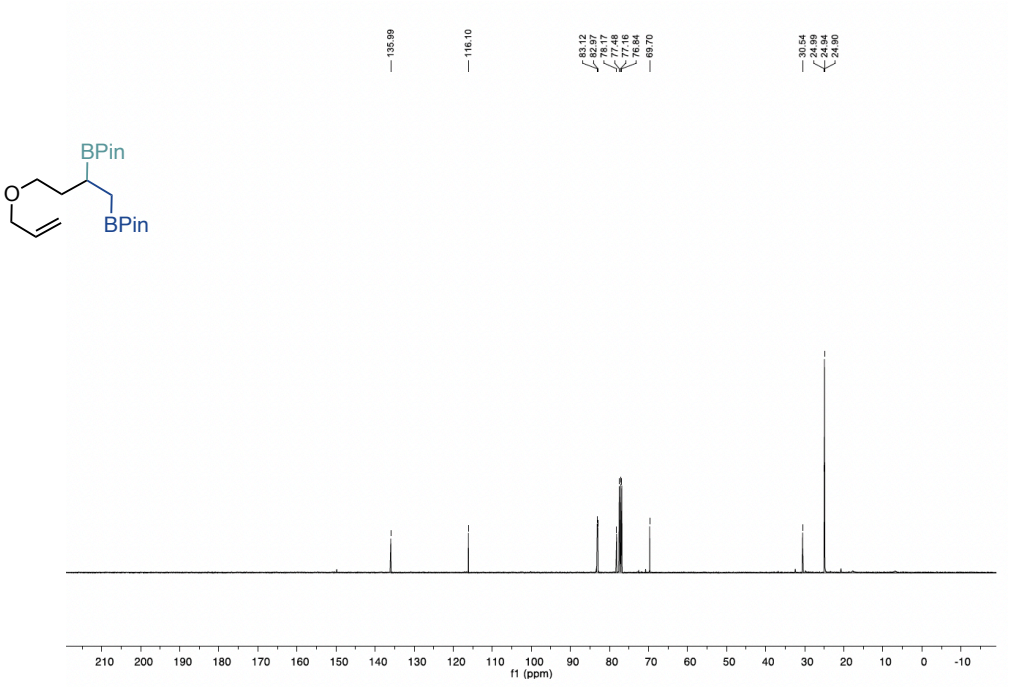

^{13}C NMR spectra (101 MHz) of **20a**

3.6. References

(1) Li, H.; Li, B.-J.; Shi, Z.-J. Challenge and Progress: Palladium-Catalyzed Sp3 C–H Activation. *Catal. Sci. Technol.* **2011**, *1* (2), 191–206. https://doi.org/10.1039/C0CY00076K.

(2) Xue, X.-S.; Ji, P.; Zhou, B.; Cheng, J.-P. The Essential Role of Bond Energetics in C–H Activation/Functionalization. *Chem. Rev.* **2017**, *117* (13), 8622–8648. https://doi.org/10.1021/acs.chemrev.6b00664.

(3) Recent Advances in C–H Functionalization. *J. Org. Chem.* **2016**, *81* (2), 343–350. https://doi.org/10.1021/acs.joc.5b02818.

(4) Gensch, T.; Hopkinson, M. N.; Glorius, F.; Wencel-Delord, J. Mild Metal-Catalyzed C–H Activation: Examples and Concepts. *Chem. Soc. Rev.* **2016**, *45* (10), 2900–2936. https://doi.org/10.1039/C6CS00075D.

(5) Rej, S.; Das, A.; Chatani, N. Strategic Evolution in Transition Metal-Catalyzed Directed C–H Bond Activation and Future Directions. *Coord. Chem. Rev.* **2021**, *431*, 213683. https://doi.org/10.1016/j.ccr.2020.213683.

(6) Holmberg-Douglas, N.; Nicewicz, D. A. Photoredox-Catalyzed C–H Functionalization Reactions. *Chem. Rev.* **2022**, *122* (2), 1925–2016. https://doi.org/10.1021/acs.chemrev.1c00311.

(7) Vasseur, A.; Bruffaerts, J.; Marek, I. Remote Functionalization through Alkene Isomerization. *Nat. Chem.* **2016**, *8* (3), 209–219. https://doi.org/10.1038/nchem.2445.

(8) Sommer, H.; Juliá-Hernández, F.; Martin, R.; Marek, I. Walking Metals for Remote Functionalization. *ACS Cent. Sci.* **2018**, *4* (2), 153–165. https://doi.org/10.1021/acscentsci.8b00005.

(9) Janssen-Müller, D.; Sahoo, B.; Sun, S.-Z.; Martin, R. Tackling Remote Sp3 C−H Functionalization via Ni-Catalyzed "Chain-Walking" Reactions. *Isr. J. Chem.* **2020**, *60* (3–4), 195–206. https://doi.org/10.1002/ijch.201900072.

(10) Ghosh, S.; Patel, S.; Chatterjee, I. Chain-Walking Reactions of Transition Metals for Remote C–H Bond Functionalization of Olefinic Substrates. *Chem. Commun.* **2021**, *57* (85), 11110–11130. https://doi.org/10.1039/D1CC04370F.

(11) Wang, Y.; He, Y.; Zhu, S. NiH-Catalyzed Functionalization of Remote and Proximal Olefins: New Reactions and Innovative Strategies. *Acc. Chem. Res.* **2022**, *55* (23), 3519–3536. https://doi.org/10.1021/acs.accounts.2c00628.

(12) Zhang, Z.; Bera, S.; Fan, C.; Hu, X. Streamlined Alkylation via Nickel-Hydride-Catalyzed Hydrocarbonation of Alkenes. *J. Am. Chem. Soc.* **2022**, *144* (16), 7015–7029. https://doi.org/10.1021/jacs.1c13482.

(13) Jardine, F. H. Hydrogenation & Isomerization of Alkenes. In *Encyclopedia of Inorganic and Bioinorganic Chemistry*; John Wiley & Sons, Ltd, 2011. https://doi.org/10.1002/9781119951438.eibc0087.

(14) Schneider, C.; Leischner, T.; Ryabchuk, P.; Jackstell, R.; Junge, K.; Beller, M. Development of Bulk Organic Chemical Processes—History, Status, and Opportunities for Academic Research. *CCS Chem.* **2021**, *3* (3), 512–530. https://doi.org/10.31635/ccschem.021.202000680.

(15) Clevenger, A. L.; Stolley, R. M.; Aderibigbe, J.; Louie, J. Trends in the Usage of Bidentate Phosphines as Ligands in Nickel Catalysis. *Chem. Rev.* **2020**, *120* (13), 6124–6196. https://doi.org/10.1021/acs.chemrev.9b00682.

(16) Lee, W.-C.; Wang, C.-H.; Lin, Y.-H.; Shih, W.-C.; Ong, T.-G. Tandem Isomerization and C–H Activation: Regioselective Hydroheteroarylation of Allylarenes. *Org. Lett.* **2013**, *15* (20), 5358–5361. https://doi.org/10.1021/ol402644y.

(17) Bair, J. S.; Schramm, Y.; Sergeev, A. G.; Clot, E.; Eisenstein, O.; Hartwig, J. F. Linear-Selective Hydroarylation of Unactivated Terminal and Internal Olefins with Trifluoromethyl-Substituted Arenes. *J. Am. Chem. Soc.* **2014**, *136* (38), 13098–13101. https://doi.org/10.1021/ja505579f.

(18) Lu, X.; Xiao, B.; Zhang, Z.; Gong, T.; Su, W.; Yi, J.; Fu, Y.; Liu, L. Practical Carbon–Carbon Bond Formation from Olefins through Nickel-Catalyzed Reductive Olefin Hydrocarbonation. *Nat. Commun.* **2016**, *7* (1), 11129. https://doi.org/10.1038/ncomms11129.

(19) Breitenfeld, J.; Scopelliti, R.; Hu, X. Synthesis, Reactivity, and Catalytic Application of a Nickel Pincer Hydride

Complex. *Organometallics* **2012**, *31* (6), 2128–2136. https://doi.org/10.1021/om201279j.

(20) He, Y.; Cai, Y.; Zhu, S. Mild and Regioselective Benzylic C–H Functionalization: Ni-Catalyzed Reductive Arylation of Remote and Proximal Olefins. *J. Am. Chem. Soc.* **2017**, *139* (3), 1061–1064. https://doi.org/10.1021/jacs.6b11962.

(21) Zhang, Y.; Han, B.; Zhu, S. Rapid Access to Highly Functionalized Alkyl Boronates by NiH-Catalyzed Remote Hydroarylation of Boron-Containing Alkenes. *Angew. Chem. Int. Ed.* **2019**, *58* (39), 13860–13864. https://doi.org/10.1002/anie.201907185.

(22) Bera, S.; Hu, X. Nickel-Catalyzed Regioselective Hydroalkylation and Hydroarylation of Alkenyl Boronic Esters. *Angew. Chem.* **2019**, *131* (39), 13992–13997. https://doi.org/10.1002/ange.201907045.

(23) Zhou, F.; Zhu, J.; Zhang, Y.; Zhu, S. NiH-Catalyzed Reductive Relay Hydroalkylation: A Strategy for the Remote C(Sp3)−H Alkylation of Alkenes. *Angew. Chem. Int. Ed.* **2018**, *57* (15), 4058–4062. https://doi.org/10.1002/anie.201712731.

(24) Chen, X.; Rao, W.; Yang, T.; Koh, M. J. Alkyl Halides as Both Hydride and Alkyl Sources in Catalytic Regioselective Reductive Olefin Hydroalkylation. *Nat. Commun.* **2020**, *11* (1), 5857. https://doi.org/10.1038/s41467-020-19717-6.

(25) Lee, C.; Seo, H.; Jeon, J.; Hong, S. γ-Selective C(Sp3)–H Amination via Controlled Migratory Hydroamination. *Nat. Commun.* **2021**, *12* (1), 5657. https://doi.org/10.1038/s41467-021-25696-z.

(26) Du, B.; Ouyang, Y.; Chen, Q.; Yu, W.-Y. Thioether-Directed NiH-Catalyzed Remote γ-C(Sp3)–H Hydroamidation of Alkenes by 1,4,2-Dioxazol-5-Ones. *J. Am. Chem. Soc.* **2021**, *143* (37), 14962–14968. https://doi.org/10.1021/jacs.1c05834.

(27) Wang, J.-W.; Liu, D.-G.; Chang, Z.; Li, Z.; Fu, Y.; Lu, X. Nickel-Catalyzed Switchable Site-Selective Alkene Hydroalkylation by Temperature Regulation**. *Angew. Chem. Int. Ed.* **2022**, *61* (31), e202205537. https://doi.org/10.1002/anie.202205537.

(28) Zhao, L.; Zhu, Y.; Liu, M.; Xie, L.; Liang, J.; Shi, H.; Meng, X.; Chen, Z.; Han, J.; Wang, C. Ligand-Controlled NiH-Catalyzed Regiodivergent Chain-Walking Hydroalkylation of Alkenes. *Angew. Chem. Int. Ed.* **2022**, *61* (30), e202204716. https://doi.org/10.1002/anie.202204716.

(29) Rodrigalvarez, J.; Wang, H.; Martin, R. Native Amides as Enabling Vehicles for Forging Sp3–Sp3 Architectures via Interrupted Deaminative Ni-Catalyzed Chain-Walking. *J. Am. Chem. Soc.* **2023**. https://doi.org/10.1021/jacs.2c12915.

(30) Dong, Z.; Ren, Z.; Thompson, S. J.; Xu, Y.; Dong, G. Transition-Metal-Catalyzed C–H Alkylation Using Alkenes. *Chem. Rev.* **2017**, *117* (13), 9333–9403. https://doi.org/10.1021/acs.chemrev.6b00574.

(31) Dhungana, R. K.; Kc, S.; Basnet, P.; Giri, R. Transition Metal-Catalyzed Dicarbofunctionalization of Unactivated Olefins. *Chem. Rec.* **2018**, *18* (9), 1314–1340. https://doi.org/10.1002/tcr.201700098.

(32) Patel, M.; Desai, B.; Sheth, A.; Dholakiya, B. Z.; Naveen, T. Recent Advances in Mono- and Difunctionalization of Unactivated Olefins. *Asian J. Org. Chem.* **2021**, *10* (12), 3201–3232. https://doi.org/10.1002/ajoc.202100666.

(33) Giri, R.; KC, S. Strategies toward Dicarbofunctionalization of Unactivated Olefins by Combined Heck Carbometalation and Cross-Coupling. *J. Org. Chem.* **2018**, *83* (6), 3013–3022. https://doi.org/10.1021/acs.joc.7b03128.

(34) Tu, H.-Y.; Zhu, S.; Qing, F.-L.; Chu, L. Recent Advances in Nickel-Catalyzed Three-Component Difunctionalization of Unactivated Alkenes. *Synthesis* **2020**, *52* (09), 1346–1356. https://doi.org/10.1055/s-0039-1690842.

(35) Badir, S. O.; Molander, G. A. Developments in Photoredox/Nickel Dual-Catalyzed 1,2-Difunctionalizations. *Chem* **2020**, *6* (6), 1327–1339. https://doi.org/10.1016/j.chempr.2020.05.013.

(36) Derosa, J.; Apolinar, O.; Kang, T.; Tran, V. T.; Engle, K. M. Recent Developments in Nickel-Catalyzed Intermolecular Dicarbofunctionalization of Alkenes. *Chem. Sci.* **2020**, *11* (17), 4287–4296. https://doi.org/10.1039/C9SC06006E.

(37) Qi, X.; Diao, T. Nickel-Catalyzed Dicarbofunctionalization of Alkenes. *ACS Catal.* **2020**, *10* (15), 8542–8556. https://doi.org/10.1021/acscatal.0c02115.

(38) Yang, S.; Chen, Y.; Ding, Z. Recent Progress of 1,1-Difunctionalization of Olefins. *Org. Biomol. Chem.* **2020**, *18* (36), 6983–7001. https://doi.org/10.1039/D0OB01323D.

(39) Li, Y.; Wu, D.; Cheng, H.; Yin, G. Difunctionalization of Alkenes Involving Metal Migration. *Angew. Chem. Int. Ed.* **2020**, *59* (21), 7990–8003. https://doi.org/10.1002/anie.201913382.

(40) Dhungana, R. K.; Sapkota, R. R.; Niroula, D.; Giri, R. Walking Metals: Catalytic Difunctionalization of Alkenes at Nonclassical Sites. *Chem. Sci.* **2020**, *11* (36), 9757–9774. https://doi.org/10.1039/D0SC03634J.

(41) Ye, Y.; Lin, Y.; Mao, N.-D.; Yang, H.; Ye, X.-Y.; Xie, T. Recent Progress in Nickel-Catalyzed Carboboration of Alkenes. *Org. Biomol. Chem.* **2022**, *20* (47), 9255–9271. https://doi.org/10.1039/D2OB01855A.

(42) Li, W.; Boon, J. K.; Zhao, Y. Nickel-Catalyzed Difunctionalization of Allyl Moieties Using Organoboronic Acids and Halides with Divergent Regioselectivities. *Chem. Sci.* **2018**, *9* (3), 600–607. https://doi.org/10.1039/C7SC03149A.

(43) Basnet, P.; Dhungana, R. K.; Thapa, S.; Shrestha, B.; Kc, S.; Sears, J. M.; Giri, R. Ni-Catalyzed Regioselective β,δ-Diarylation of Unactivated Olefins in Ketimines via Ligand-Enabled Contraction of Transient Nickellacycles: Rapid Access to Remotely Diarylated Ketones. *J. Am. Chem. Soc.* **2018**, *140* (25), 7782–7786. https://doi.org/10.1021/jacs.8b03163.

(44) Wang, W.; Ding, C.; Li, Y.; Li, Z.; Li, Y.; Peng, L.; Yin, G. Migratory Arylboration of Unactivated Alkenes Enabled by Nickel Catalysis. *Angew. Chem. Int. Ed.* **2019**, *58* (14), 4612–4616. https://doi.org/10.1002/anie.201814572.

(45) Ding, C.; Ren, Y.; Sun, C.; Long, J.; Yin, G. Regio- and Stereoselective Alkylboration of Endocyclic Olefins Enabled by Nickel Catalysis. *J. Am. Chem. Soc.* **2021**, *143* (48), 20027–20034. https://doi.org/10.1021/jacs.1c09214.

(46) Tamaru, Y.; Hojo, M.; Higashimura, H.; Yoshida, Z. PdII-Catalyzed Regioselective Arylchlorination and Oxyarylation of Unsaturated Alcohols. *Angew. Chem. Int. Ed. Engl.* **1986**, *25* (8), 735–737. https://doi.org/10.1002/anie.198607351.

(47) Li, L.; Gong, T.; Lu, X.; Xiao, B.; Fu, Y. Nickel-Catalyzed Synthesis of 1,1-Diborylalkanes from Terminal Alkenes. *Nat. Commun.* **2017**, *8* (1), 345. https://doi.org/10.1038/s41467-017-00363-4.

(48) Li, Y.; Pang, H.; Wu, D.; Li, Z.; Wang, W.; Wei, H.; Fu, Y.; Yin, G. Nickel-Catalyzed 1,1-Alkylboration of Electronically Unbiased Terminal Alkenes. *Angew. Chem. Int. Ed.* **2019**, *58* (26), 8872–8876. https://doi.org/10.1002/anie.201903890.

(49) Li, Y.; Wei, H.; Wu, D.; Li, Z.; Wang, W.; Yin, G. Nickel-Catalyzed Chemodivergent 1,1-Difunctionalization of Unactivated α-Olefins with Alkynyl Electrophiles and B2pin2. *ACS Catal.* **2020**, *10* (9), 4888–4894. https://doi.org/10.1021/acscatal.0c00898.

(50) Li, Y.; Li, Y.; Shi, H.; Wei, H.; Li, H.; Funes-Ardoiz, I.; Yin, G. Modular Access to Substituted Cyclohexanes with Kinetic Stereocontrol. *Science* **2022**, *376* (6594), 749–753. https://doi.org/10.1126/science.abn9124.

(51) Wang, W.; Ding, C.; Yin, G. Catalyst-Controlled Enantioselective 1,1-Arylboration of Unactivated Olefins. *Nat. Catal.* **2020**, *3* (11), 951–958. https://doi.org/10.1038/s41929-020-00523-8.

(52) Sun, C.; Li, Y.; Yin, G. Practical Synthesis of Chiral Allylboronates by Asymmetric 1,1-Difunctionalization of Terminal Alkenes. *Angew. Chem. Int. Ed.* **2022**, *61* (37), e202209076. https://doi.org/10.1002/anie.202209076.

(53) *Handbook of Functionalized Organometallics: Applications in Synthesis*, 1st ed.; Knochel, P., Ed.; Wiley, 2005. https://doi.org/10.1002/9783527619467.

(54) Jana, R.; Pathak, T. P.; Sigman, M. S. Advances in Transition Metal (Pd,Ni,Fe)-Catalyzed Cross-Coupling Reactions Using Alkyl-Organometallics as Reaction Partners. *Chem. Rev.* **2011**, *111* (3), 1417–1492. https://doi.org/10.1021/cr100327p.

(55) Choi, J.; Fu, G. C. Transition Metal–Catalyzed Alkyl-Alkyl Bond Formation: Another Dimension in Cross-Coupling Chemistry. *Science* **2017**, *356* (6334), eaaf7230. https://doi.org/10.1126/science.aaf7230.

(56) Campeau, L.-C.; Hazari, N. Cross-Coupling and Related Reactions: Connecting Past Success to the Development of New Reactions for the Future. *Organometallics* **2019**, *38* (1), 3–35. https://doi.org/10.1021/acs.organomet.8b00720.

(57) Ma, X.; Murray, B.; Biscoe, M. R. Stereoselectivity in Pd-Catalysed Cross-Coupling Reactions of Enantioenriched Nucleophiles. *Nat. Rev. Chem.* **2020**, *4* (11), 584–599. https://doi.org/10.1038/s41570-020-00222-9.

(58) Ohmura, T.; Suginome, M. Silylboranes as New Tools in Organic Synthesis. *Bull. Chem. Soc. Jpn.* **2009**, *82* (1), 29–49. https://doi.org/10.1246/bcsj.82.29.

(59) Cho, H. Y.; Morken, J. P. Catalytic Bismetallative Multicomponent Coupling Reactions: Scope, Applications, and Mechanisms. *Chem. Soc. Rev.* **2014**, *43* (13), 4368–4380. https://doi.org/10.1039/C3CS60482A.

(60) Burks, H. E.; Morken, J. P. Catalytic Enantioselective Diboration, Disilation and Silaboration: New Opportunities for Asymmetric Synthesis. *Chem. Commun.* **2007**, No. 45, 4717–4725. https://doi.org/10.1039/B707779C.

(61) Cuenca, A. B.; Shishido, R.; Ito, H.; Fernández, E. Transition-Metal-Free B–B and B–Interelement Reactions with Organic Molecules. *Chem. Soc. Rev.* **2017**, *46* (2), 415–430. https://doi.org/10.1039/C6CS00692B.

(62) *Diboron(4) Compounds: From Structural Curiosity to Synthetic Workhorse | Chemical Reviews*. https://pubs.acs.org/doi/10.1021/acs.chemrev.6b00193 (accessed 2023-06-06).

(63) Burgess, Kevin.; Ohlmeyer, M. J. Transition-Metal Promoted Hydroborations of Alkenes, Emerging Methodology for Organic Transformations. *Chem. Rev.* **1991**, *91* (6), 1179–1191. https://doi.org/10.1021/cr00006a003.

(64) Bonet, A.; Pubill-Ulldemolins, C.; Bo, C.; Gulyás, H.; Fernández, E. Transition-Metal-Free Diboration Reaction by Activation of Diboron Compounds with Simple Lewis Bases. *Angew. Chem. Int. Ed.* **2011**, *50* (31), 7158–7161. https://doi.org/10.1002/anie.201101941.

(65) Ito, H.; Horita, Y.; Yamamoto, E. Potassium Tert-Butoxide-Mediated Regioselective Silaboration of Aromatic Alkenes. *Chem. Commun.* **2012**, *48* (64), 8006–8008. https://doi.org/10.1039/C2CC32778C.

(66) Blaisdell, T. P.; Caya, T. C.; Zhang, L.; Sanz-Marco, A.; Morken, J. P. Hydroxyl-Directed Stereoselective Diboration of Alkenes. *J. Am. Chem. Soc.* **2014**, *136* (26), 9264–9267. https://doi.org/10.1021/ja504228p.

(67) Obligacion, J. V.; Chirik, P. J. Earth-Abundant Transition Metal Catalysts for Alkene Hydrosilylation and Hydroboration. *Nat. Rev. Chem.* **2018**, *2* (5), 15–34. https://doi.org/10.1038/s41570-018-0001-2.

(68) Chen, J.; Guo, J.; Lu, Z. Recent Advances in Hydrometallation of Alkenes and Alkynes via the First Row Transition Metal Catalysis. *Chin. J. Chem.* **2018**, *36* (11), 1075–1109. https://doi.org/10.1002/cjoc.201800314.

(69) Joung, S.; Bergmann, A. M.; Brown, M. K. Ni-Catalyzed 1,2-Benzylboration of 1,2-Disubstituted Unactivated Alkenes. *Chem. Sci.* **2019**, *10* (47), 10944–10947. https://doi.org/10.1039/C9SC04199K.

(70) Matteson, D. S.; Ray, R. Directed Chiral Synthesis with Pinanediol Boronic Esters. *J. Am. Chem. Soc.* **1980**, *102* (25), 7590–7591. https://doi.org/10.1021/ja00545a046.

(71) García-Domínguez, A.; Li, Z.; Nevado, C. Nickel-Catalyzed Reductive Dicarbofunctionalization of Alkenes. *J. Am. Chem. Soc.* **2017**, *139* (20), 6835–6838. https://doi.org/10.1021/jacs.7b03195.

(72) Zhao, X.; Tu, H.-Y.; Guo, L.; Zhu, S.; Qing, F.-L.; Chu, L. Intermolecular Selective Carboacylation of Alkenes via Nickel-Catalyzed Reductive Radical Relay. *Nat. Commun.* **2018**, *9* (1), 3488. https://doi.org/10.1038/s41467-018-05951-6.

(73) Shu, W.; García-Domínguez, A.; Quirós, M. T.; Mondal, R.; Cárdenas, D. J.; Nevado, C. Ni-Catalyzed Reductive Dicarbofunctionalization of Nonactivated Alkenes: Scope and Mechanistic Insights. *J. Am. Chem. Soc.* **2019**, *141* (35), 13812–13821. https://doi.org/10.1021/jacs.9b02973.

(74) *Metal-Catalyzed Cross-Coupling Reactions and More: DeMeijere/Metal-Catalyzed Cross-Coupling Reactions and More*; De Meijere, A., Bräse, S., Oestreich, M., Eds.; Wiley-VCH Verlag GmbH & Co. KGaA: Weinheim, Germany, 2014. https://doi.org/10.1002/9783527655588.

(75) Sun, S.-Z.; Martin, R. Nickel-Catalyzed Umpolung Arylation of Ambiphilic α-Bromoalkyl Boronic Esters.

Angew. Chem. Int. Ed. **2018**, *57* (14), 3622–3625. https://doi.org/10.1002/anie.201712428.

(76) Hofstra, J. L.; Cherney, A. H.; Ordner, C. M.; Reisman, S. E. Synthesis of Enantioenriched Allylic Silanes via Nickel-Catalyzed Reductive Cross-Coupling. *J. Am. Chem. Soc.* **2018**, *140* (1), 139–142. https://doi.org/10.1021/jacs.7b11707.

(77) Schmidt, J.; Choi, J.; Liu, A. T.; Slusarczyk, M.; Fu, G. C. A General, Modular Method for the Catalytic Asymmetric Synthesis of Alkylboronate Esters. *Science* **2016**, *354* (6317), 1265–1269. https://doi.org/10.1126/science.aai8611.

(78) Cernak, T.; Dykstra, K. D.; Tyagarajan, S.; Vachal, P.; Krska, S. W. The Medicinal Chemist's Toolbox for Late Stage Functionalization of Drug-like Molecules. *Chem. Soc. Rev.* **2016**, *45* (3), 546–576. https://doi.org/10.1039/C5CS00628G.

(79) Saini, V.; Sigman, M. S. Palladium-Catalyzed 1,1-Difunctionalization of Ethylene. *J. Am. Chem. Soc.* **2012**, *134* (28), 11372–11375. https://doi.org/10.1021/ja304344h.

(80) Mlynarski, S. N.; Schuster, C. H.; Morken, J. P. Asymmetric Synthesis from Terminal Alkenes by Cascades of Diboration and Cross-Coupling. *Nature* **2014**, *505* (7483), 386–390. https://doi.org/10.1038/nature12781.

(81) Bonet, A.; Odachowski, M.; Leonori, D.; Essafi, S.; Aggarwal, V. K. Enantiospecific Sp2–Sp3 Coupling of Secondary and Tertiary Boronic Esters. *Nat. Chem.* **2014**, *6* (7), 584–589. https://doi.org/10.1038/nchem.1971.

(82) Sonawane, R. P.; Jheengut, V.; Rabalakos, C.; Larouche-Gauthier, R.; Scott, H. K.; Aggarwal, V. K. Enantioselective Construction of Quaternary Stereogenic Centers from Tertiary Boronic Esters: Methodology and Applications. *Angew. Chem. Int. Ed.* **2011**, *50* (16), 3760–3763. https://doi.org/10.1002/anie.201008067.

(83) Wang, Y.; Noble, A.; Myers, E. L.; Aggarwal, V. K. Enantiospecific Alkynylation of Alkylboronic Esters. *Angew. Chem. Int. Ed.* **2016**, *55* (13), 4270–4274. https://doi.org/10.1002/anie.201600599.

(84) Juliá-Hernández, F.; Moragas, T.; Cornella, J.; Martin, R. Remote Carboxylation of Halogenated Aliphatic Hydrocarbons with Carbon Dioxide. *Nature* **2017**, *545* (7652), 84–88. https://doi.org/10.1038/nature22316.

(85) Sun, S.-Z.; Börjesson, M.; Martin-Montero, R.; Martin, R. Site-Selective Ni-Catalyzed Reductive Coupling of α-Haloboranes with Unactivated Olefins. *J. Am. Chem. Soc.* **2018**, *140* (40), 12765–12769. https://doi.org/10.1021/jacs.8b09425.

(86) Martínez, Á. M.; Rodríguez, N.; Arrayás, R. G.; Carretero, J. C. Synthesis of Alkylidene Pyrrolo[3,4-b]Pyridin-7-One Derivatives via RhIII-Catalyzed Cascade Oxidative Alkenylation/Annulation of Picolinamides. *Chem. Commun.* **2014**, *50* (46), 6105–6107. https://doi.org/10.1039/C4CC02322F.

(87) Ho, G.-M.; Judkele, L.; Bruffaerts, J.; Marek, I. Metal-Catalyzed Remote Functionalization of ω-Ene Unsaturated Ethers: Towards Functionalized Vinyl Species. *Angew. Chem. Int. Ed.* **2018**, *57* (27), 8012–8016. https://doi.org/10.1002/anie.201802434.

(88) Tokuyasu, T.; Kunikawa, S.; McCullough, K. J.; Masuyama, A.; Nojima, M. Synthesis of Cyclic Peroxides by Chemo- and Regioselective Peroxidation of Dienes with Co(II)/O2/Et3SiH. *J. Org. Chem.* **2005**, *70* (1), 251–260. https://doi.org/10.1021/jo048359j.

(89) Yang, T.; Lu, L.; Shen, Q. Iron-Mediated Markovnikov-Selective Hydro-Trifluoromethylthiolation of Unactivated Alkenes. *Chem. Commun.* **2015**, *51* (25), 5479–5481. https://doi.org/10.1039/C4CC08655D.

(90) Oh, H.; Park, A.; Jeong, K.-S.; Han, S. B.; Lee, H. Copper-Catalyzed 1,2-Bistrifluoromethylation of Terminal Alkenes. *Adv. Synth. Catal.* **2019**, *361* (9), 2136–2140. https://doi.org/10.1002/adsc.201801675.

(91) Sun, S.-Z.; Romano, C.; Martin, R. Site-Selective Catalytic Deaminative Alkylation of Unactivated Olefins. *J. Am. Chem. Soc.* **2019**, *141* (41), 16197–16201. https://doi.org/10.1021/jacs.9b07489.

(92) Wang, Y.; Wang, J.; Li, G.-X.; He, G.; Chen, G. Halogen-Bond-Promoted Photoactivation of Perfluoroalkyl Iodides: A Photochemical Protocol for Perfluoroalkylation Reactions. *Org. Lett.* **2017**, *19* (6), 1442–1445. https://doi.org/10.1021/acs.orglett.7b00375.

(93) Xu, J.; Fu, Y.; Luo, D.-F.; Jiang, Y.-Y.; Xiao, B.; Liu, Z.-J.; Gong, T.-J.; Liu, L. Copper-Catalyzed Trifluoromethylation of Terminal Alkenes through Allylic C–H Bond Activation. *J. Am. Chem. Soc.* **2011**, *133* (39), 15300–15303. https://doi.org/10.1021/ja206330m.

(94) Zhang, H.; Huang, W.; Wang, T.; Meng, F. Cobalt-Catalyzed Diastereo- and Enantioselective Hydroalkenylation of Cyclopropenes with Alkenylboronic Acids. *Angew. Chem. Int. Ed.* **2019**, *58* (32), 11049–11053. https://doi.org/10.1002/anie.201904994.

(95) Stephens, T. C.; Pattison, G. Transition-Metal-Free Homologative Cross-Coupling of Aldehydes and Ketones with Geminal Bis(Boron) Compounds. *Org. Lett.* **2017**, *19* (13), 3498–3501. https://doi.org/10.1021/acs.orglett.7b01474.

(96) Zhou, Z.; Liu, M.; Lv, L.; Li, C.-J. Silver(I)-Catalyzed Widely Applicable Aerobic 1,2-Diol Oxidative Cleavage. *Angew. Chem. Int. Ed.* **2018**, *57* (10), 2616–2620. https://doi.org/10.1002/anie.201711531.

(97) Biondi, S.; Bastia, E.; Ronsin, G. Nitric Oxide Releasing Naproxen. WO2011012400A2, February 3, 2011. https://patents.google.com/patent/WO2011012400A2/en (accessed 2023-04-18).

Chapter 3.

Chapter 4.

Nickel-catalysed 1,1-aminoborylation of unactivated terminal olefins

Research carried out in collaboration with

Robert R. A. Freund, Huihui Zhang, Matthew Wakeling and Mara Jensen

Published in: *ACS Catal.* **2023**, *13*, 5538-5543.

UNIVERSITAT ROVIRA I VIRGILI
FUNCTIONALISATION OF SP3 C-O BONDS AND OLEFINS ENABLED BY NICKEL CATALYSIS
Laura Talavera Codina

4.1. Introduction

4.1.1. α-aminoboronic acid derivatives

In recent years, α-aminoboronic acids have gained considerable attention in various fields. They have emerged as valuable molecular probes[1] and enzyme inhibitors in drug discovery, with notable examples including Bortezomib or Vaborbactam.[2–5] Furthermore, α-aminoboronic acids have also found extensive echo in organic synthesis as versatile intermediates,[6–8] and in material science as sensors.[9–11]

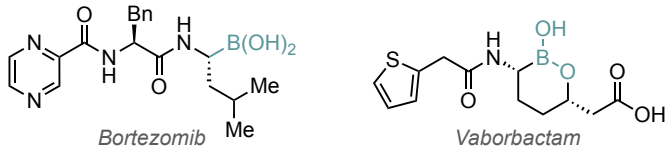

Scheme 1. Boron-containing drugs

The wide applicability of α-aminoboronic acids arises from the electronic properties of their trivalent boron atom, which acts as a Lewis acid due to its vacant p orbital. While the boron atom primarily displays electrophilic character, the C–B bond possesses nucleophilic properties. These unique properties provide access to additional synthetic opportunities.[12]

However, α-aminoboronic acids are inherently unstable when bearing unprotected or electron-rich amines possessing a high hurdle for conventional isolation procedures. The electron-deficient nature of the boron atom allows for the formation of a three-membered ring adduct with the nitrogen (1,2-azaboriridine, **I**), wherein subsequent protonation at the carbon leads to the cleavage of the C–B bond resulting in the formation of the corresponding amine (**2**) upon hydrolysis (Scheme 2, *top*). In the case of boronic esters bearing a tertiary amino group in the α-position, the rearrangement occurs via intramolecular nucleophilic attack of the amino group on boron, leading to intermediate **II**. The zwitterion (**II**) could then undergo ring-opening, in either a concerted or stepwise manner, terminated by 1,2-hydride migration to eventually generate **4** (Scheme 2, *bottom*). Subsequent oxidative work-up will finally give rise to primary alcohol **5**.[12] To overcome this intrinsic reactivity, α-aminoboronic acids are typically isolated as their protected derivatives.

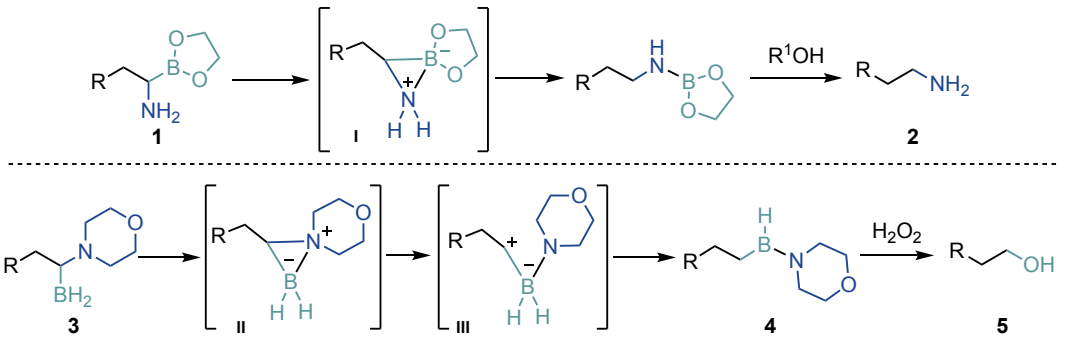

Scheme 2. Decomposition pathways of α-aminoboronic acids or esters

α-Aminoboronic acids derivatives were first synthesised by Matteson and co-workers in the 1960s through a stereoselective homologation reaction using chiral boronic esters.[13–15] In this process, the *in situ* generated (dichloromethyl)lithium species adds to the alkyl boronate from the convex side (**IV**), and zinc chloride binds to the less hindered oxygen atom (**V**), promoting the formation a chiral α-haloboronic ester via 1,2-migration of the benzyl fragment. Subsequent S_N2 substitution of the chlorine atom with a lithium hexamethyldisilazane derivative (LiHMDS), followed by N–Si bond cleavage and acetylation affords the chiral product (Scheme 3). Although practically useful, the stereoselectivity is controlled by the substrate and requires cryogenic conditions as well as stoichiometric amounts of $ZnCl_2$.

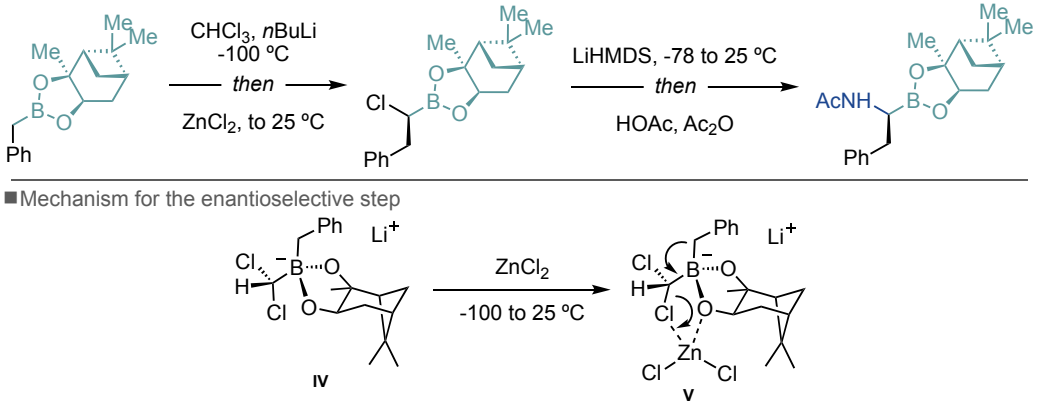

Scheme 3. Matteson seteroselective homologation reaction using chiral boronic esters

In recent years, various methods to synthesise α-aminoboronic acid derivatives had been developed. The aim of this chapter is to highlight the recent advances achieved using first-raw transition metal-catalysed reactions. Comprehensive summaries of existing methods were recently discussed by Cativiela, Časar and Marder.[16–18]

4.1.2. First-raw transition metal-catalysed synthesis of α-aminoboronic acid derivatives

4.1.2.1. Borylation of imines

A remarkable breakthrough in asymmetric synthesis of α-aminoboronic derivatives was the copper-catalysed hydroboration of *N-tert*-butyanesulfinyl amides achieved by the Ellman group in 2008 (Scheme 4, *left*).[19] The method utilised Sadighi's catalyst ([(**L1**)CuO*t*Bu]) to perform the direct addition of a boryl group to sulfinyl aldimines, which were synthesised from readily available aldehydes. However, the practicality of this method was limited by the use of a Cu(I) source, which is particularly air- and moisture-sensitive. Consequently, the groups of Sun and Ellman independently developed improved protocols to enhance the catalytic system's stability avoiding glovebox equipment. Sun utilised benzimidazole-based *N*-heterocyclic carbenes as ligands (Scheme 4, *middle*),[20] while Ellman employed a Cu(II) salt in combination with a phosphine ligand (PCy_3) (Scheme 4, *right*).[21]

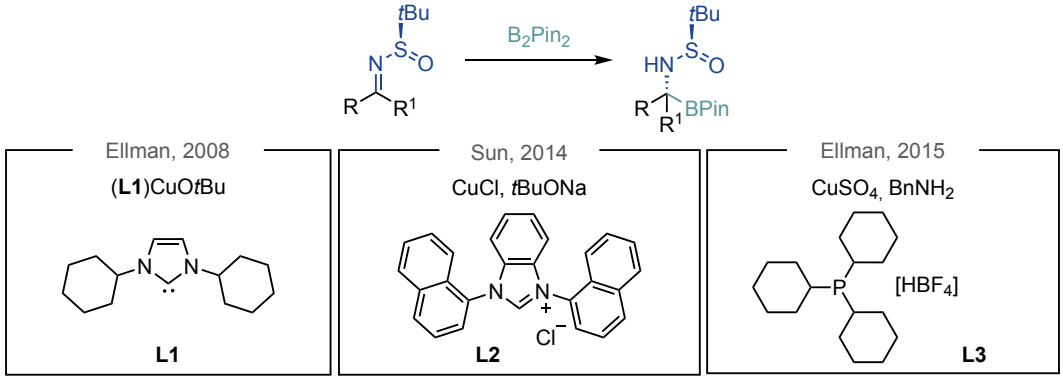

Scheme 4. Copper-catalysed hydroboration of sulfinyl aldimines and imines

In 2014, Tian, Lin and co-workers developed a method using Hoveyda's non-C_2-symmetric (*N*-alkyl, *N*-aryl)-hybrid chiral NHC/Cu(I) complex for the asymmetric hydroboration of *N*-benzoyl aldimines (Scheme 5, *a*).[22] While the method provided excellent yields, the enantioselectivities were only moderate. Additionally, the applicability of this method was limited to benzylamides, and moderate to low yields were obtained when employing the corresponding alkyl amines. To address these limitations, Cheong, Scheidt and co-workers expanded the scope of the reaction to include *N*-benzoyl alkyl-substituted aldimines, which were *in situ* generated via deprotonation of *N*-benzoyl protected α-tosylamines using an excess of Cs_2CO_3 (Scheme 5, *b*).[23] In this case, a planar-chiral NHC-copper complex controlled the stereoselectivity of the process via facial selectivity. Although diminished mass recovery was observed with BPin esters during conventional chromatographic purification, improved yields could be achieved by directly converting the unpurified α-amido-BPin esters into the corresponding BF_3K salts.

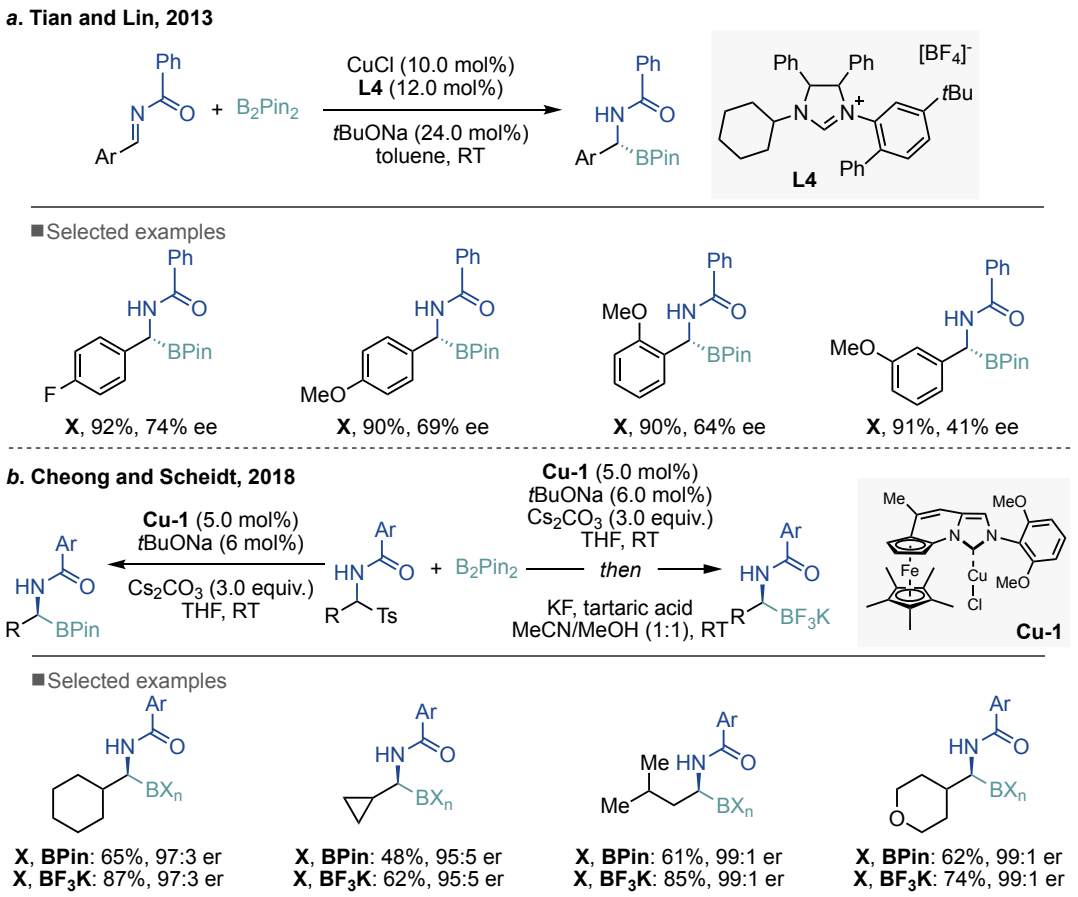

Scheme 5. Copper-catalysed hydroboration of *N*-benzoyl aldimines

In 2015, the Liao group, reported a novel approach using *N*-Boc-aldimines in enantioselective copper(I)-catalysed pinacolboryl additions.[24] In contrast to the *N*-acyl-α-amino boronic esters, *N*-Boc-imines are versatile and readily available starting materials which can be easily removed for further synthetic purposes. The authors observed that by employing a single chiral sulfoxide-(dialkyl)phosphine ligand, both enantiomers could be obtained with high enantioselectivities by simply changing the counter ion of the catalyst (Scheme 6). However, it should be noted that when the corresponding alkyl aldimines were used, low conversions and enantioselectivities were observed.

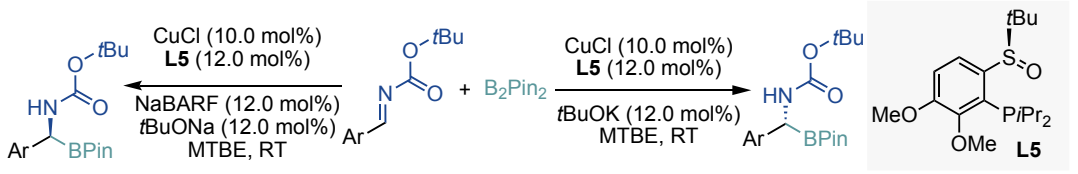

Scheme 6. Copper-catalysed hydroboration of *N*-Boc-imines

Multicomponent reactions have shown great potential for the synthesis of α-aminoboronates using Cu catalysis. Although no enantioselective transformations have been reported in this context, notable advances have been made in racemic synthesis. In 2018, Marder reported the first multicomponent Boron-Strecker reaction for the synthesis of racemic α-aminoboronates using readily available carbonyl compounds, amines and B_2Pin_2 (Scheme 7, *a*).[25] Importantly, the method demonstrated the inclusion of aryl-substituted (**XX**) and tertiary examples (**XX**), as well as the use of both coordinating and non-coordinating *N*-aryl groups (**XX**). In a separate study, Song and co-workers disclosed the borylacylation of aldimines with acyl chlorides and B_2Pin_2, using readily available aldehydes and amines. In this case, aldimines were generated *in situ* from the corresponding aldehyde and amine and could be used in the next step without purification (Scheme 7, *b*).[26]

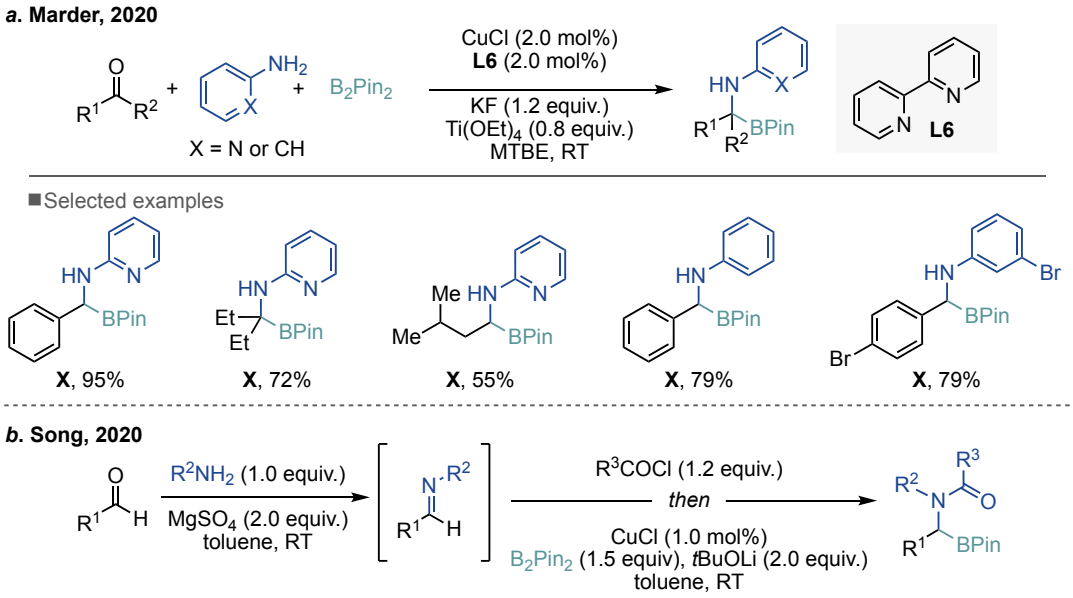

Scheme 7. Multicomponent reactions for the synthesis of α-aminoboronates

4.1.2.2. Decarboxylative borylation

The development of a catalytic platform to access α-aminoboronic acids from native peptides is particularly interesting as it provides a modular technique to react ubiquitous alkyl carboxylic acids with boronate esters to deliver boronic acid derivatives of high synthetic value. As part of their ongoing interest in harnessing alkyl carboxylic acids as alkyl halide surrogates through the intermediacy of redox-active esters, Baran and co-workers reported in 2017 a nickel-catalysed decarboxylative borylation of *N*-hydroxyphtalamide (NHP) redox-active esters to transform native peptides into α-aminoboronic acid derivatives (Scheme 8).[27] The applicability of this method was further illustrated by the late-stage functionalisation of

natural products and the synthesis of pharmaceutically relevant compounds (Bortezomib, **X**). Additionally, the method enabled the discovery of three highly potent human neutrophil elastase inhibitors.

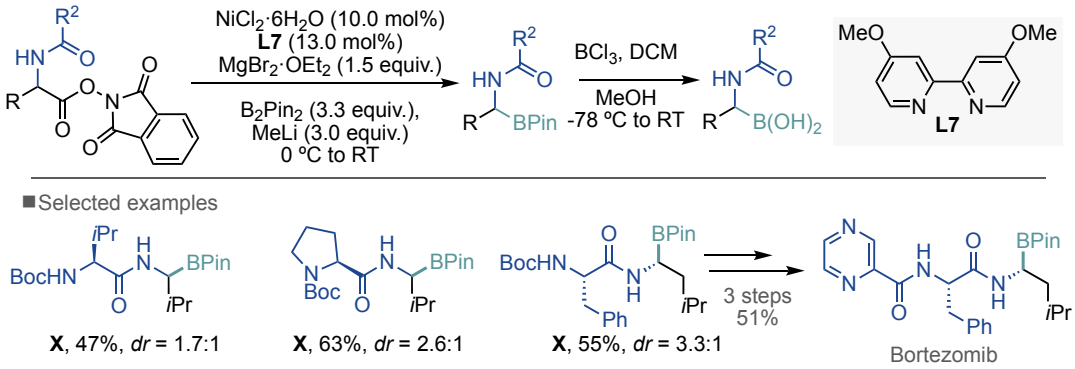

Scheme 8. Nickel-catalysed decarboxylative borylation using NHP redox-active esters

4.1.2.3. Hydroboration of enamides

Although methods for the regioselective and enantioselective hydroboration of alkenes for the synthesis of chiral α-amino boronic esters are known using noble transition metals such as rhodium,[28,29] when utilising first-raw transition metals the scope is limited to the use of α,β-unsaturated compounds. In 2017, two independent reports by the groups of Xu, and Parra and Tortosa, described a Cu-catalysed asymmetric hydroboration of β-amidoacrylonitriles and -acrylates, thus highlighting the necessity for an electron-withdrawing group in the side-chain of the precursor (Scheme 9).[30,31] The methods, however, used an inexpensive copper(I) catalyst bearing a chiral phosphine ligand, as (R)-SEGPHOS (**L10**), where the enantioselectivities could be controlled by the configuration of the substrate.

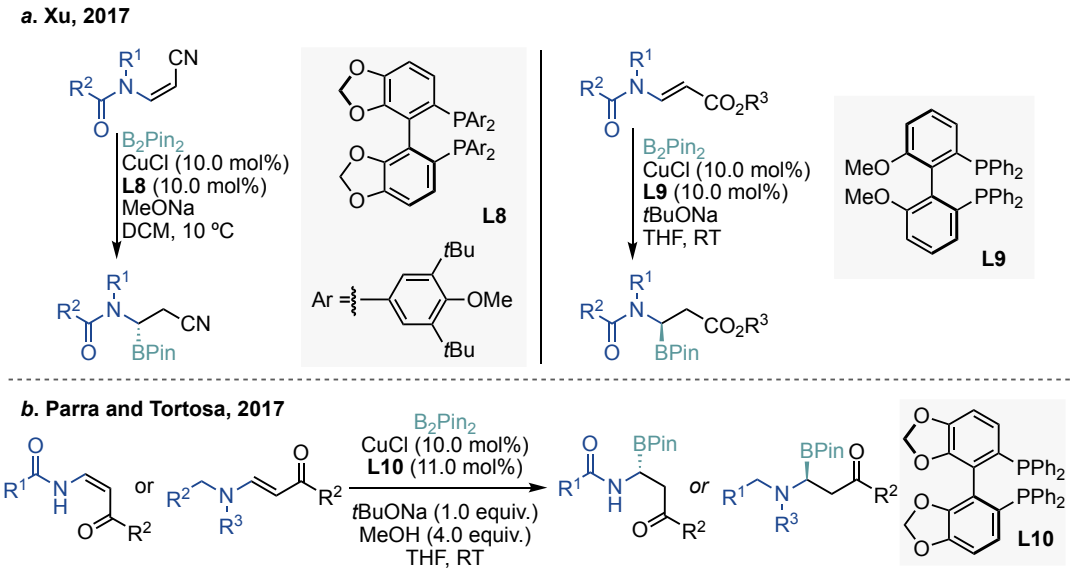

Scheme 9. Enantioselective Cu-catalysed hydroboration of α,β-unsaturated compounds

4.1.2.4. Hydroamination of alkenyl boron compounds

Hirano et al. introduced a Cu-catalysed regio- and enantioselective hydroamination of alkenyl Bdan with hydrosilanes and electrophilic *O*-benzoyl-*N,N*-dialkyl hydroxylamines to expand the substrate scope towards (Scheme 10).[32] Based on previous studies on Cu-catalysed hydroaminations independently developed by Miura's and Buchwald's groups,[33–39] the authors proposed that the enantioselectivity is determined during the alkene insertion step into the $L_nCu–H$ species, and the subsequent C–N bond formation occurs with retention of configuration. This method was particularly significant as it allowed for the synthesis of alkyl-substituted chiral α-aminoboronic acid derivatives, which were otherwise challenging to access using aliphatic aldimines.

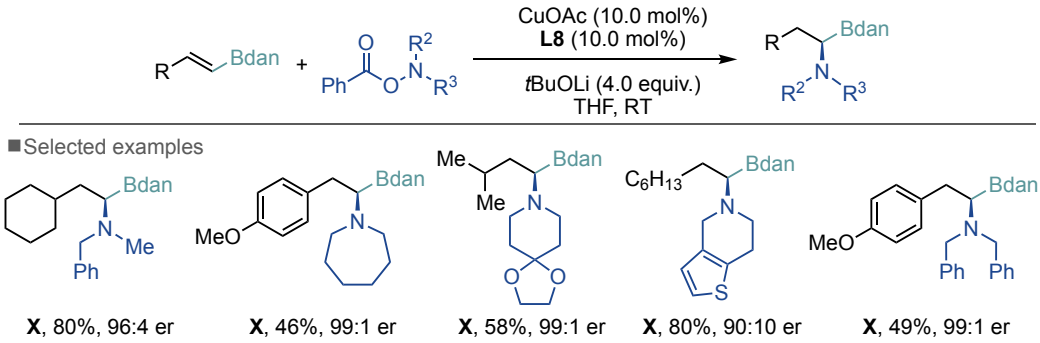

Scheme 10. Cu-catalysed hydroamination of alkenyl Bdans

Recently, Zhu and co-workers reported a Ni-catalysed asymmetric hydroamination of alkenyl boronates employing dioxazolones as suitable electrophilic amidating reagents (Scheme 11).[40] This strategy offered a complementary hydroamination approach that directly produced enantioenriched amides with an adjacent BPin unit, thereby simplifying the synthetic process to generate the targeted pharmacophores. Interestingly, the protocol utilised of a simple chiral amino alcohol ligand, (*S*)-3-amino-2-benzyl-1,4-diphenylbutan-2-ol (**L11**). The proposed mechanism involves a *syn*-hydronickelation reaction with the alkenyl-Bpin substrate, followed by an inner-sphere nitrenoid transfer to yield the corresponding C–N bond.

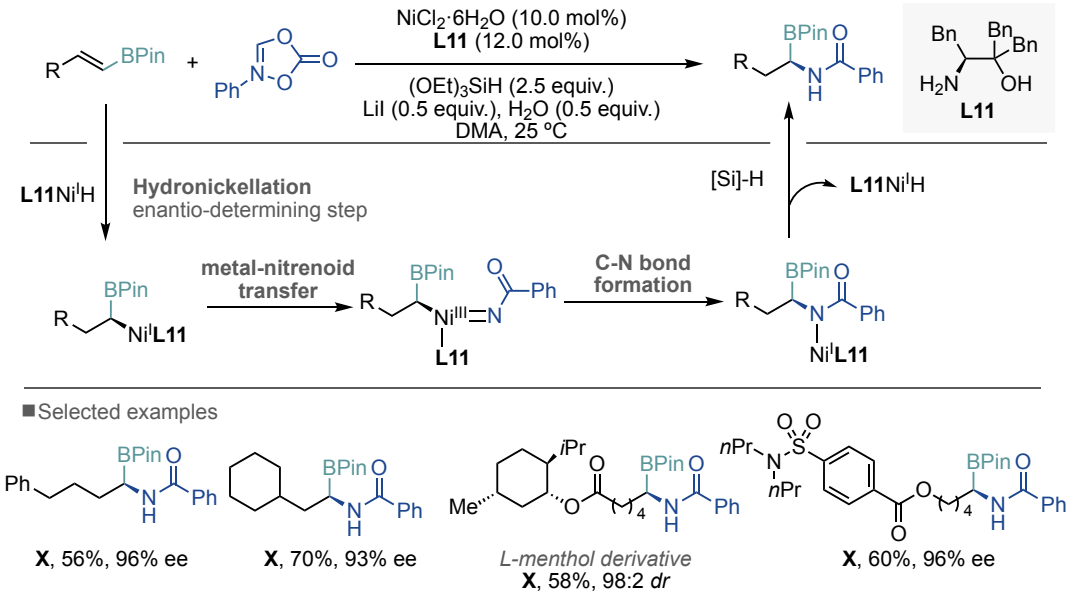

Scheme 11. Ni-catalysed hydroamination of alkenyl BPins

4.1.2.5. Hydroamination of *gem*-diborylalkanes

In 2019, Hirano, Miura and co-workers disclosed a related Cu-catalysed electrophilic amination of *gem*-diborylalkenes with *O*-benzoyl hydroxylamines (Scheme 12).[41] The successful development of this transformation was founded on the implementation of the silylated 1,2-bis(diphenylphosphino)benzene derivative (**L12**) as crucial ligand, in conjunction with the use of *gem*-diborylalkenes bearing the sterically less encumbered neopentylglycolborane derivative (Bneop). Remarkably, the use of the later allowed for the coupling of relatively sterically congested substrates, that otherwise exhibited lower reactivity. Unfortunately, benzyl-substituted and disubstituted *gem*-diborylalkanes did not yield any detectable amount of the desired products, even when Bneop was employed.

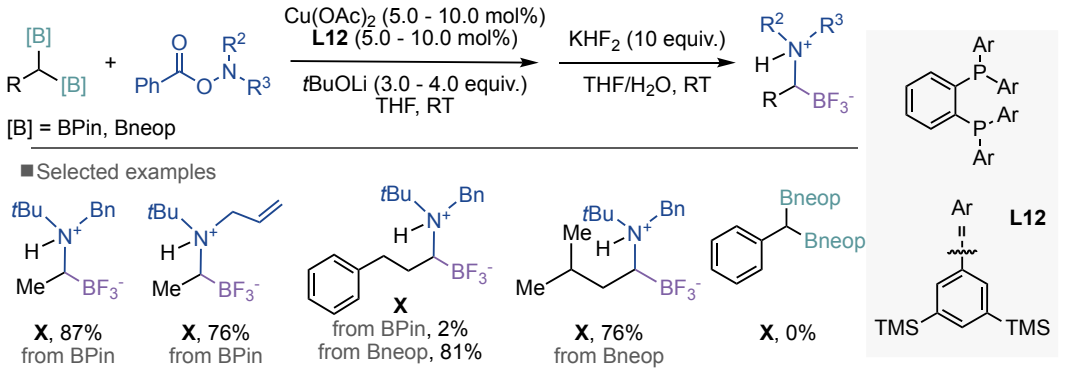

Scheme 12. Cu-catalysed amination of *gem*-diborylalkenes

4.1.2.6. Hydroboration/hydroamination of alkynes

Taking inspiration from seminal contributions by Hirano and Miura on the hydroamination of alkenes for the synthesis of α-aminoboronic ester derivatives,[32] Liu, Engle and co-workers developed a more efficient asymmetric Cu–H cascade hydroboration/hydroamination catalysis using terminal alkynes as starting materials (Scheme 13).[42] Interestingly, a single Cu–H catalyst was able to mediate sequential hydroboration and hydroamination. Mechanistic studies by subjecting each of the putative intermediates, alkenyl-Bdan and substituted enamine, showed that alkenyl-Bdan is a competent intermediate in this reaction, whereas enamine leads to unproductive decomposition pathways. Thus, initially hydroboration takes place to generate the intermediate alkenylBdan, followed by hydroamination. Interestingly, an intramolecular cascade reaction resulted in the enantioselective formation of azetidine-2-ylboronate (**X**), and pyrrolidine-2-ylboronate (**X**) derivatives, which represent an important class of heterocycles in pharmaceutical setups.[43]

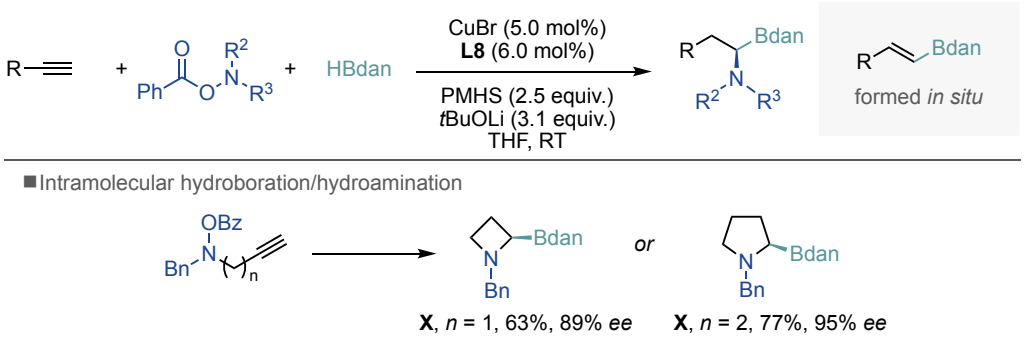

Scheme 13. Asymmetric Cu-H cascade hydroboration/hydroamination catalysis

4.1.2.7. Copper-catalysed asymmetric C–N bond formation of α-haloboroanes

Inspired by the pioneering work of Matteson and co-workers, the group of Fu has recently reported the enantioselective synthesis of α-aminoboronic derivatives via the coupling of racemic α-haloboronate esters with carbamates using a chiral copper catalyst (Scheme 14, *top*).[44] The enantioselective process employs a commercially available CuCl salt accompanied with a chiral 1,2-diamine (**L13**) and a secondary phosphine (**L14**). Mechanistic studies revealed that enantioselectivity is achieved through a kinetic resolution of the racemic electrophile, where only one of the two enantiomers of the electrophile reacts with the catalyst (Scheme 14, *bottom*).

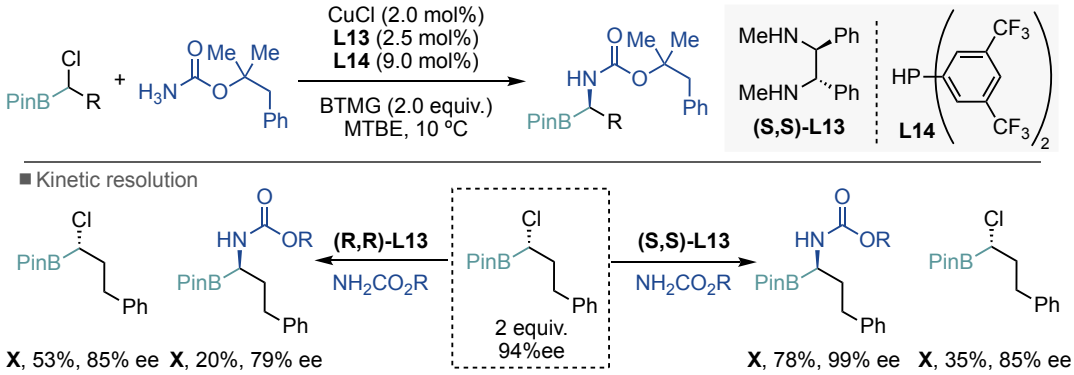

Scheme 14. Copper-catalysed asymmetric C–N bond of α-haloboroanes

4.2. General aim of the project

The utilisation of unactivated alkenes as versatile building blocks in catalytic 1,1-difunctionalisation reactions has opened up new possibilities to rapidly and reliably construct sp^3 fragments from readily available starting materials. These techniques provide innovative strategies in olefin functionalisation, enabling unconventional site-patterns. Despite the significant advances in C–C, and C-heteroatom bond-forming reactions, the incorporation of two different heteroatom motifs across the olefin backbone with 1,1-site selectivity remains underexplored.[45]

Motivated by the success of the transformation described in Chapter 3, we hypothesised that the development of a generic platform for synthesising α-aminoboronic acids through a 1,1-difunctionalisation of unactivated olefins would represent an attractive scenario. Unlike the remarkable achievements using alkynes[42] and well-defined vinyl boronates[32,40] as precursors, we recognised that the use of readily accessible alkenes and commercially available B_2Pin_2 as starting materials would enhance synthetic flexibility and provide cost-efficiency.

Building upon the knowledge gained in Chapter 3 and as part of our group interests in Ni-catalysed chain-walking reactions,[46–51] we envisioned a mechanism operating via migratory insertion of Ni–BPin via 1,2-addition (**I**), followed by a 1,2-Ni migration (**II**), facilitated by the stabilisation of the neighbouring boron atom, prior to C–N bond formation to afford the desired 1,1-aminoboron compounds (Scheme 15).

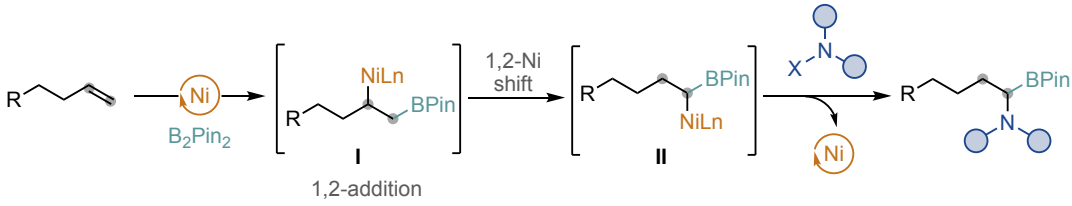

Scheme 15. Nickel-catalysed 1,1-aminborylation of olefins

4.3. Nickel-catalysed 1,1-aminoborylation of unactivated terminal olefins

4.3.1. Optimisation of the reaction conditions

The feasibility of the 1,1-aminoborylation of unactivated terminal alkenes was initially investigated using 4-phenyl-1-butene (**1a**) as the model substrate. Morpholine benzoate (**2**) was chosen as the electrophilic aminating reagent, and bis(pinacolato)diboron (B_2Pin_2) as the boron source. The choice of the model system was based on the knowledge acquired in Chapter 3, as well as on previous studies in the field, particularly in the areas of 1,1-difunctionalisation[45,52–54] and carboamination[55,56] of unactivated olefins. After initial screening of the reaction conditions, we were delighted to observe the desired 1,1-aminoborylation product in trace amounts (5% yield by GC-FID). The reaction conditions comprised of $NiBr_2$·glyme as precatalyst, CPhos (**L1**) as ligand, *t*BuOLi as base and 1,4-dioxane as solvent. In addition to the desired product, several side products were detected by GCMS analysis: (1) olefin isomerisation along the side chain (**A**, **B**) resulting from β-hydride elimination, (2) vinyl boron compound (**C**) formed through a Heck-type pathway, (3) monofunctionalised side products (**D** and **E**) generated via competitive dissociation, and (4) 1,*n*-difunctionalised products arising from 1,2-Ni migration at different positions (**F**, **G** and **H**) (Scheme 16). These findings highlighted the complexity of the reaction and the presence of various competing pathways leading to different products.

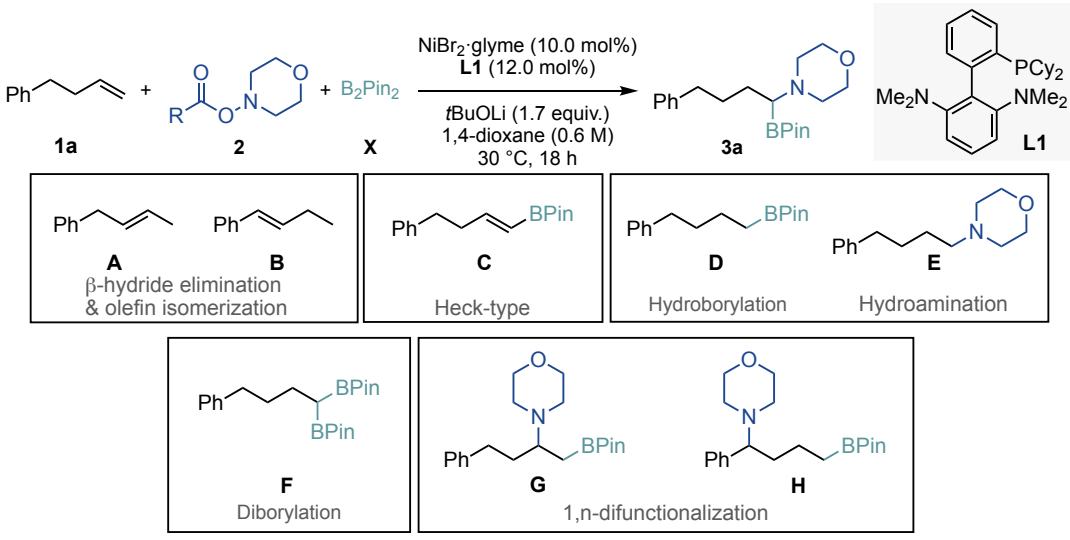

Reaction conditions: **1a** (0.20 mmol, 1.0 equiv.), **2a-l** (0.22 mmol, 1.1 equiv.), B_2Pin_2 (0.34 mmol, 1.7 equiv.), NBr_2·glyme (15.0 mol%), **L1** (12 mol%), *t*BuOLi (0.34 mmol, 1.7 equiv.), 1,4-dioxane (0.6 M), 30 ºC for 18 h.

Scheme 16. Preliminary evaluation of the 1,1-aminoborylation of unactivated terminal alkenes

Based on previous reports using electrophilic aminating reagents,[55,56] we hypothesised that the yield of the desired 1,1-aminoborylation could be enhanced by fine-tuning the steric and electronic properties of the *N*,*O*-electrophile (Scheme 17). Throughout our investigations, we observed a consistent trend wherein *N*,*O*-electrophiles bearing electron-rich benzoyl groups at the *para*-position of the aryl ring delivered higher yields of the desired product (**2a**-**2d**). To further explore this trend, we examined the impact of electron-donating groups at the *ortho*-position of the aryl ring. We found that the use of the sterically bulky mesityl group lead to the highest yields, while minimising side product formation at other positions (**F**, **G** and **H**). Unfortunately, the use of more electron-donating substituents (**2f**) did not further enhance the yield of the desired product.[57–59]

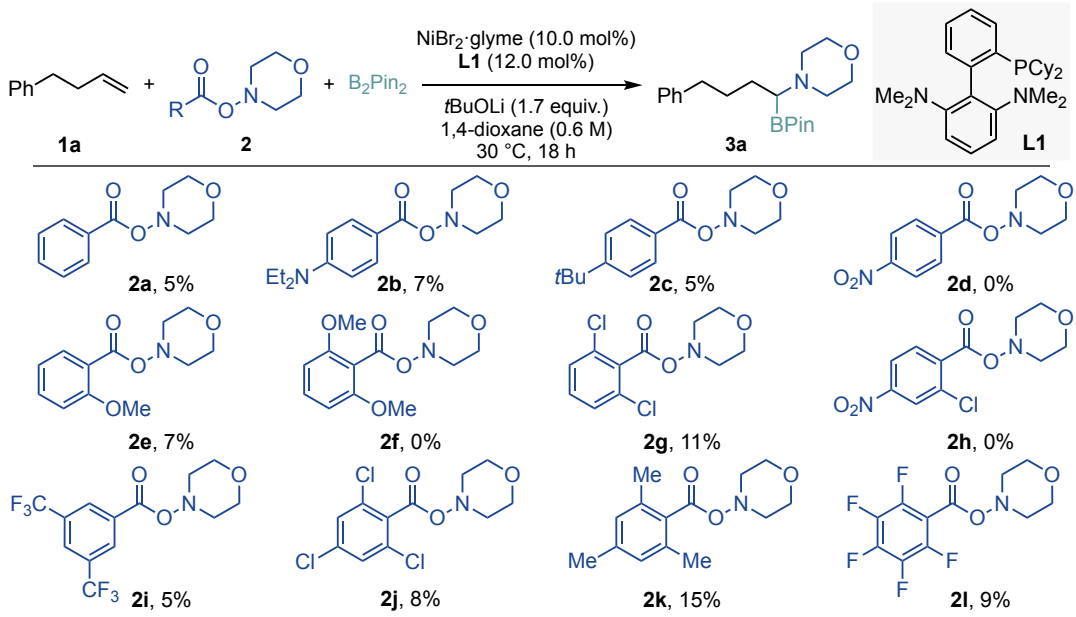

Reaction conditions: **1a** (0.20 mmol, 1.0 equiv.), **2a-l** (0.22 mmol, 1.1 equiv.), B_2Pin_2 (0.34 mmol, 1.7 equiv.), NBr_2·glyme (10.0 mol%), **L1** (12 mol%), *t*BuOLi (0.34 mmol, 1.7 equiv.), 1,4-dioxane (0.6 M), 30 ºC for 18 h. GC yields using decane (0.20 mmol, 1.0 equiv.) as internal standard.

Scheme 17. Screening of the steric and electronic properties of *N*,*O*-electrophiles

With this results in hand, our efforts shifted towards the identification of an optimal ligand. As shown in Scheme 18, similar results were obtained when using *P*,*N*-type ligands (**L1**-**L5**) Surprisingly, we observed that ligands previously reported to effectively enable 1,1-difunctionalisation of olefins did not yield significant amounts of the desired product (**L6**-**L10**).[49,60] Intriguingly, 19% yield was achieved when no ligand was added to the reaction mixture. This finding is reminiscent to the ligand-free 1,2-carboboration, where the absence of a ligand promotes the desired reaction.[61–64] Noteworthy, no side products arising from 1,2-aminoborylation functionalisation (**G**) could be detected by GC analysis under the limits of detection.

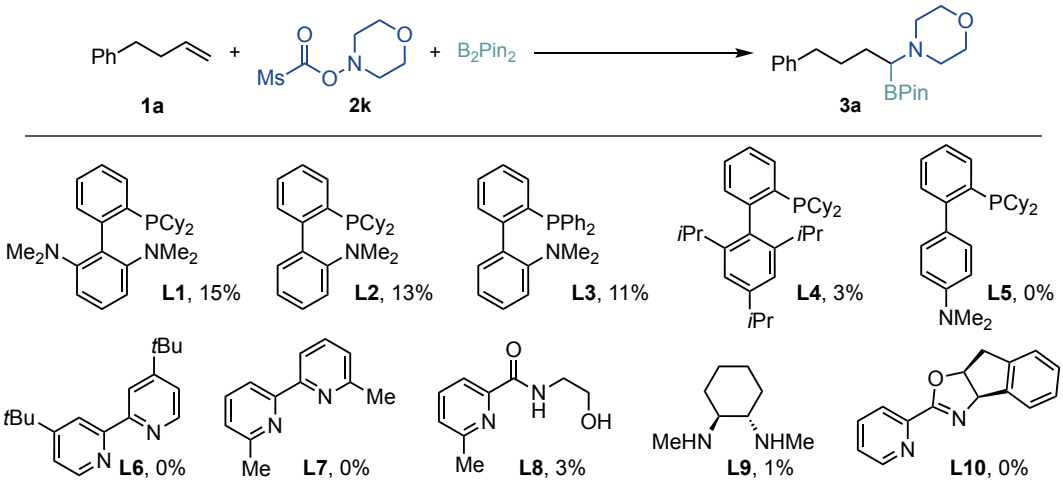

Reaction conditions: **1a** (0.20 mmol, 1.0 equiv.), **2k** (0.22 mmol, 1.1 equiv.), B_2Pin_2 (0.34 mmol, 1.7 equiv.), NBr_2·glyme (10.0 mol%), **Ligand** (12 mol%), *t*BuOLi (0.34 mmol, 1.7 equiv.), 1,4-dioxane (0.6 M), 30 ºC for 18 h. GC yields using decane (0.20 mmol, 1.0 equiv.) as internal standard.

Scheme 18. Screening of ligands

Next, we assessed the impact of the nickel precatalyst and the base (Table 1). As shown, significantly reduced yield was observed when employing $NiBr_2 \cdot TBA_4$ or $Ni(acac)_2$, whereas $NiCl_2 \cdot$glyme led to slightly improved yields. The use of $Ni(COD)_2$ resulted in only 3% yield of the desired product, however, employing a more stable 16 electron Ni(0) source with stilbene as the ancillary ligand significantly increased the yield to 13%.[65] The investigation of inorganic bases revealed *t*BuOLi as the optimal choice (entries 8-11).

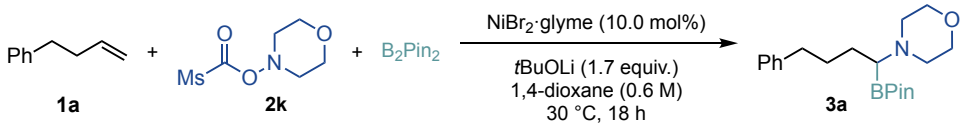

1a **2k** **3a**

Entry	Deviation from standard conditions	Conv **1a** (%)	**3a** (%)
1	$NiBr_2 \cdot$glyme	50	19
2	$NiBr_2 \cdot$diglyme	31	10
3	$NiCl_2 \cdot$glyme	67	28
4	$Ni(acac)_2$	100	4
5	$NiBr_2 \cdot TBA_4$	30	4
6	$Ni(COD)_2$	19	3
7	$Ni(^{CF3}stb)_3$	45	13
8	*t*BuONa	15	1
9	*t*BuOK	48	2
10	LiOMe	35	0
11	CsF	0	0

Reaction conditions: **1a** (0.20 mmol, 1.0 equiv.), **2k** (0.22 mmol, 1.1 equiv.), B_2Pin_2 (0.34 mmol, 1.7 equiv.), nickel precatalyst (10.0 mol%), *t*BuOLi (0.34 mmol, 1.7 equiv.), 1,4-dioxane (0.6 M), 30 ºC for 18 h. GC yields using decane (0.20 mmol, 1.0 equiv.) as internal standard. Mass balance accounts for isomerisation of **1a** and to a lower extend formation of the Heck-type product (**C**).

Table 1. Screening of nickel precatalyst and base

The intriguing increase in yield observed with $Ni(^{CF3}stb)_3$ prompted us to further investigate stilbenes and electron-deficient olefins as potential ligands, to enhance the reaction yield (Scheme 19).[66–69] Gratifyingly, when *trans*-stilbene (L11) or the 3,5-bis(trifluoromethylene) substituted analogue were employed, the yield was significantly increased to 47% and 43%, respectively. These findings tentatively suggest that the presence of electron-deficient olefins as ancillary ligands might facilitate the final sp^3 C–N bond reductive elimination step.[68] To determine if aminoborylation occurred at the *trans*-stilbene backbone, control experiments were conducted using *trans*-stilbene as the substrate. Interestingly, traces (if any) of the corresponding products were observed in the crude mixture.

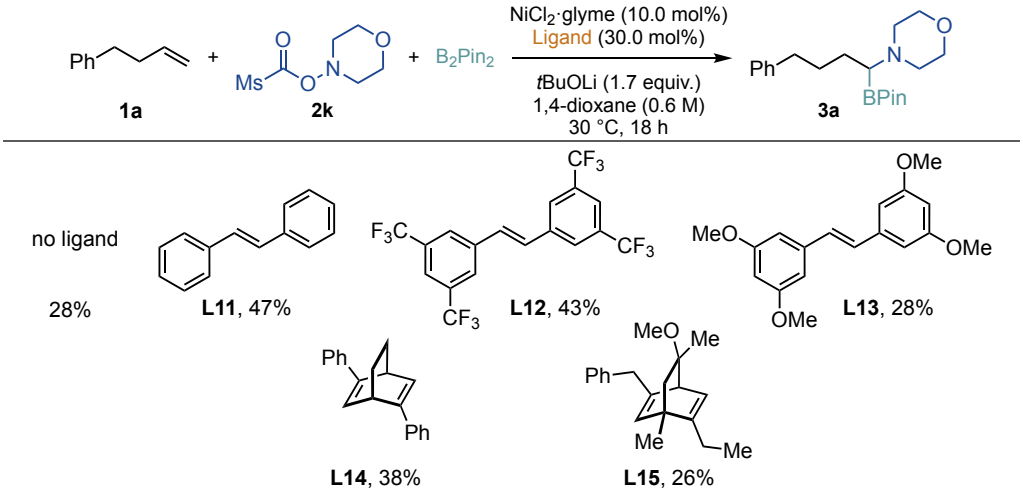

Reaction conditions: **1a** (0.20 mmol, 1.0 equiv.), **2k** (0.22 mmol, 1.1 equiv.), B_2Pin_2 (0.34 mmol, 1.7 equiv.), $NiCl_2$·glyme (10.0 mol%), **Ligand** (30.0 mol%), *t*BuOLi (0.34 mmol, 1.7 equiv.), 1,4-dioxane (0.6 M), 30 ºC for 18 h. GC yields using decane (0.20 mmol, 1.0 equiv.) as internal standard.

Scheme 19. Screening of electrodeficient ligands

As anticipated, the solvent had a strong influence on the reaction outcome (Table 2), revealing that ethereal solvents exhibit superior performance, with MTBE providing the best results. In contrast, amide containing solvents, such as DMF, DMA, or NMP, as well as strong solubilising solvents like DMSO, completely suppressed the reactivity.

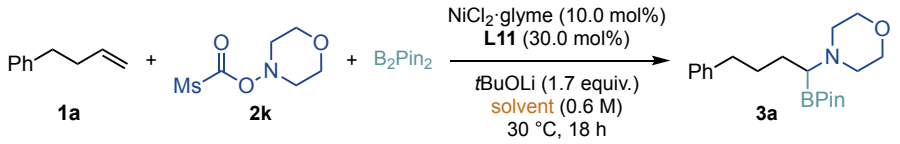

Entry	Solvent	Conv **1a** (%)	**3a** (%)
1	1,4-dioxane	85	47
2	THF	82	28
3	Et_2O	85	43
4	MTBE	84	51
5	toluene	85	40
6	CH_2Cl_2	41	7
7	DMF	0	0
8	DMA	13	3
9	NMP	0	0
10	DMSO	0	0
11	*t*BuOH	64	26

Reaction conditions: **1a** (0.20 mmol, 1.0 equiv.), **2k** (0.22 mmol, 1.1 equiv.), B_2Pin_2 (0.34 mmol, 1.7 equiv.), $NiCl_2$·glyme (10.0 mol%), **L11** (30.0 mol%), *t*BuOLi (0.34 mmol, 1.7 equiv.), **solvent** (0.6 M), 30 ºC for 18 h. GC yields using decane (0.20 mmol, 1.0 equiv.) as internal standard. Mass balance accounts for isomerisation of **1a** and to a lower extend formation of the Heck-type product (**C**).

Table 2. Screening of solvents

Subsequently, we evaluated the effect of the temperature (Table 3) and optimal results were obtained within the temperature range of 20 to 40 ºC. Improved mass balance was observed at 20 ºC, whereas lower temperatures slowed down the reaction progress (11% of **3a**, 18% conversion) and higher temperatures led to diminished product formation.

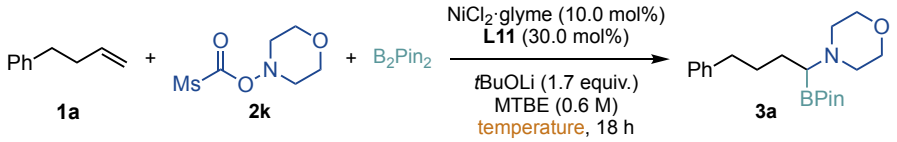

Entry	Temperature	Conv **1a** (%)	**3a** (%)
1	0 ºC	18	11
2	10 ºC	52	33
3	20 ºC	80	52
4	30 ºC	84	51
5	40 ºC	85	49
6	60 ºC	53	33

Reaction conditions: **1a** (0.20 mmol, 1.0 equiv.), **2k** (0.22 mmol, 1.1 equiv.), B_2Pin_2 (0.34 mmol, 1.7 equiv.), $NiCl_2$·glyme (10.0 mol%), **L11** (30.0 mol%), *t*BuOLi (0.34 mmol, 1.7 equiv.), MTBE (0.6 M), **temperature**, for 18 h. GC yields using decane (0.20 mmol, 1.0 equiv.) as internal standard. Mass balance accounts for isomerisation of **1a** and to a lower extend formation of the Heck--type product (**C**).

Table 3. Screening of reaction temperature

Next, we focused our attention on the impact of reaction stoichiometry (Table 4). Varying the equivalents of the **2k** had a noticeable effect on the reactivity, as an increase in equivalents resulted in decreased product formation (entries 1-4). On the other hand, altering the equivalents of the base did not significantly influence the reaction efficiency (entries 1, 5-7). However, a negative influence was observed when the base was in an excess compared to B_2Pin_2, as shown in entry 8. Consequently, despite similar yields being obtained with 1.7 or 1.5 equivalents, it was decided to reduce the equivalents of the base relative to the B_2Pin_2 to suppress unproductive pathways (entry 9).

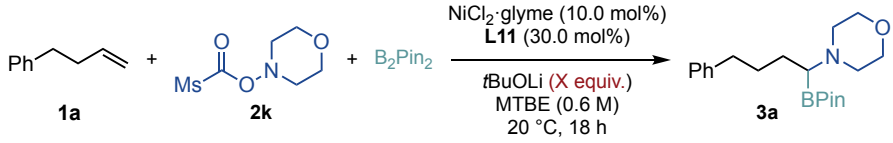

Entry	**2k** (X equiv.)	B_2Pin_2 (Y equiv.)	*t*BuOLi (Z equiv.)	Conv **1a** (%)	**3a** (%)
1	1.1	1.7	1.7	80	52
2	1.5	1.7	1.7	69	55
3	2.0	1.7	1.7	53	30
4	2.5	1.7	1.7	47	20
5	1.1	1.1	1.1	51	46
6	1.1	1.5	1.5	70	49
7	1.1	2.0	2.0	50	46
8	1.1	1.7	1.9	30	16
9	1.5	1.7	1.5	71	52

Reaction conditions: **1a** (0.20 mmol, 1.0 equiv.), **2k** (X equiv.), B_2Pin_2 (Y equiv.), $NiCl_2$·glyme (10.0 mol%), **L11** (30.0 mol%), *t*BuOLi (Z equiv.), MTBE (0.6 M), 20 ºC, for 18 h. GC yields using *decane* (0.20 mmol, 1.0 equiv.) as internal standard. Mass balance accounts for isomerisation of **1a** and to a lower extend formation of the Heck-type product (**C**).

Table 4. Screening of reaction stoichiometry

In light with these findings, we wondered if subtle modification of the reaction conditions could enhance the selectivity and yield, while minimising the formation of side-reactions (Table 5). Fortunately, employing a two-batch sequence involving an additional charge of *N*,*O*-electrophile, B_2Pin_2, and base proved to increase the efficiency of the reaction, resulting in a 76% yield. Intriguingly, a decrease in yield was observed when an additional 1.5 equivalents of **2k** were added (entry 4), whereas no improvement was observed upon the addition of B_2Pin_2 and base (entry 3). These results suggest a synergistic effect among the three components in the reaction.

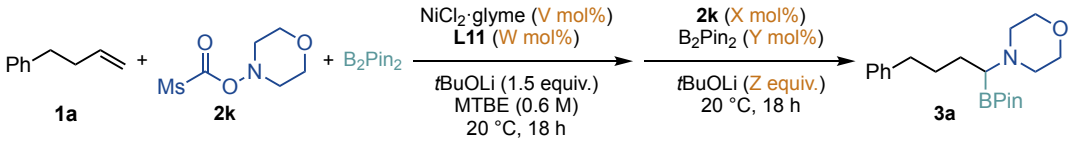

Entry	$NiCl_2$·glyme (V mol%.)	**L11** (W mol%.)	**2k** (X equiv.)	B_2Pin_2 (Y equiv.)	*t*BuOLi (Z equiv.)	Conv **1a** (%)	**3a** (%)
1	10.0	30.0	-	-	-	71	52
2	15.0	45.0	-	-	-	71	67
3	15.0	45.0	0	1.7	1.5	100	55
4	15.0	45.0	1.5	0	0	76	25
5	15.0	45.0	1.5	1.7	1.5	99	76
6	10.0	30.0	1.5	1.7	1.5	96	62
7	15.0	45.0	1.0	1.2	1.0	99	76
8	15.0	45.0	0.5	0.7	0.5	91	69

Reaction conditions: **1a** (0.20 mmol, 1.0 equiv.), **2k** (0.30 mmol, 1.5 equiv.), B_2Pin_2 (0.34 mmol, 1.7 equiv.), $NiCl_2$·glyme (V mol%), **L11** (W mol%), *t*BuOLi (0.30 mmol, 1.5 equiv.), MTBE (0.6 M), 20 ºC, for 18 h, *then* **2k** (X equiv.), B_2Pin_2 (Y equiv.) and *t*BuOLi (Z equiv.), at 20 ºC for 18 hours. GC yields using decane (0.20 mmol, 1.0 equiv.) as internal standard. Mass balance accounts for isomerisation of **1a** and to a lower extend formation of the Heck-type product (**C**).

Table 5. Screening of a two-batch sequence

Despite extensive screening of additional parameters, including additives, solvent concentration as well as additional ligands, we were unable to achieve a significant improvement in the yield of the reaction. Additionally, we conducted several reactions using chiral dienes as ligands (**L14** and **L15**), as we anticipated that a certain degree of enantiocontrol could be induced; however, in all cases racemic products were observed. Finally, we tackled the challenges for isolation of **3a**, following our efforts towards the derivatisation of **3a** into a product that could be isolated under standard purification techniques (crystallisation and/or column chromatography). The inherent instability of α-aminobornic acids (**3a**) under various conditions (column chromatography, basic aqueous conditions, or high temperature) hampered its isolation in pure form.

4.3.2. Isolation of the product

α-aminoboronic acids are inherently unstable, however, they can be stabilised through various methods. One approach is to convert them into their hydrochloride salts or amide derivatives.[15] Another strategy involves the transformation of the pinacol borane ester into the corresponding ammonium trifluoroborate inner salt, or the generation of a Lewis acid-base adduct, wherein the Lewis base amine and the Lewis acid borane (BH_3) are attached on the same molecule.[70,71]

Further experimentation revealed two reliable processes to generate the corresponding ammonium trifluoroborate inner salt (**4a**) or the Lewis acid-base adduct with BH_3 (**5a**) from the crude α-aminoboronic ester derivative (**3a**). Although similar yields were obtained with both methods, the protocol based on KHF_2/AcOH was chosen for study the generality of our reaction due to their increased crystallinity and potential ease of purification on larger scale by crystallisation techniques.

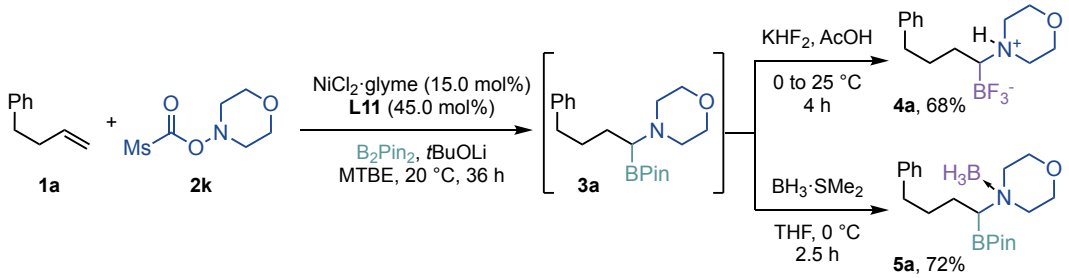

Scheme 20. Isolation of α-aminoboronic acid derivatives

It is worth noting that recent methods have also introduced the use of Bdan derivatives as a more stable boron source. However, all our attempts to use the unsymmetrical boron source, PinB-Bdan or to perform the *in situ* conversion of the BPin to the corresponding Bdan derivatives were unsuccessful.[32,42,72]

4.3.3. Substrate scope

Having established a reliable procedure for isolating and purifying the targeted α-aminoboronic acid derivatives, we proceeded to explore the generality of our nickel-catalysed 1,1-aminborylation of unactivated terminal olefins. Initially, we evaluated a wide range of *N*,*O*-electrophiles. As illustrated in Scheme 21, six-membered azaheterocycles, such as morpholine (**4a**), piperidine (**4d, 4g**), *N*-Boc-protected piperazine (**4b**), *N*-(2-pyridinyl) substituted piperazine (**4e**), and thiomorpholine (**4c**), did not interfere with productive 1,1-aminoboration. Notably, the reaction could be extended to seven-membered cyclic amine electrophiles, albeit with reduced yield (**4h, 4i**). Acyclic amines were also investigated;

however, moderate to low yields were obtained (**4j-4l**). Importantly, the formation of the desired products was confirmed by X-ray diffraction analysis of **4a** and **4i**.

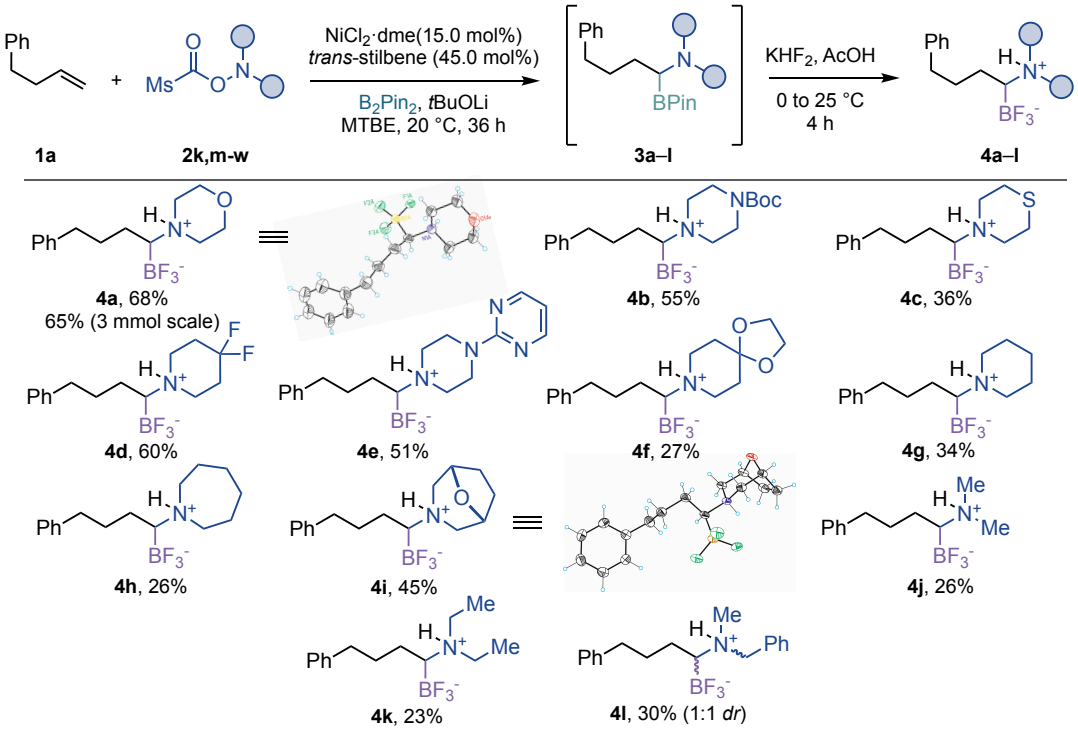

Reaction conditions: **1a** (0.20 mmol, 1.0 equiv.), **2k**,**m-w** (0.30 mmol, 1.5 equiv.), B_2Pin_2 (0.34 mmol, 1.7 equiv.), $NiCl_2$·glyme (15.0 mol%), *trans*-stilbene (45.0 mol%), *t*BuOLi (0.30 mmol, 1.5 equiv.), MTBE (0.6 M), 20 ºC for 18 h, *then* **2k** (0.20 mmol, 1.0 equiv.), B_2Pin_2 (0.24 mmol, 1.2 equiv.) and *t*BuOLi (0.2 mmol, 1.0 equiv.), at 20 ºC for 18 hours, then add KHF2 (20 equiv.) in AcOH for 4. Isolated yields, average of two independent runs.

Scheme 21. Screening of *N*,*O*-electrophiles

Next, we investigated the preparative scope of the unactivated olefin counterparts. We focused on determining whether the presence of arenes or strongly coordinating groups in the vicinity might compromise the 1,1-site selectivity via translocation of the nickel catalyst throughout the side chain. Gratifyingly, no sp^3 C–N bond formation was observed adjacent to an arene or amide groups via chain-walking at remote sp^3 C–H sites. Interestingly, our protocol displayed highly chemoselectivity, as amides (**4w, 4x**), esters (**4p-4r**), acetals (**4ac-4ae**) or phthalimide protected amines (4y) could participate in equal efficiencies. Notably, our method tolerated the presence of nitrogen-containing heterocycles, as exemplified by the incorporation of pyrrole (**4y**), indole (**4ab**), or pyrimidine derivatives (**4aa**).

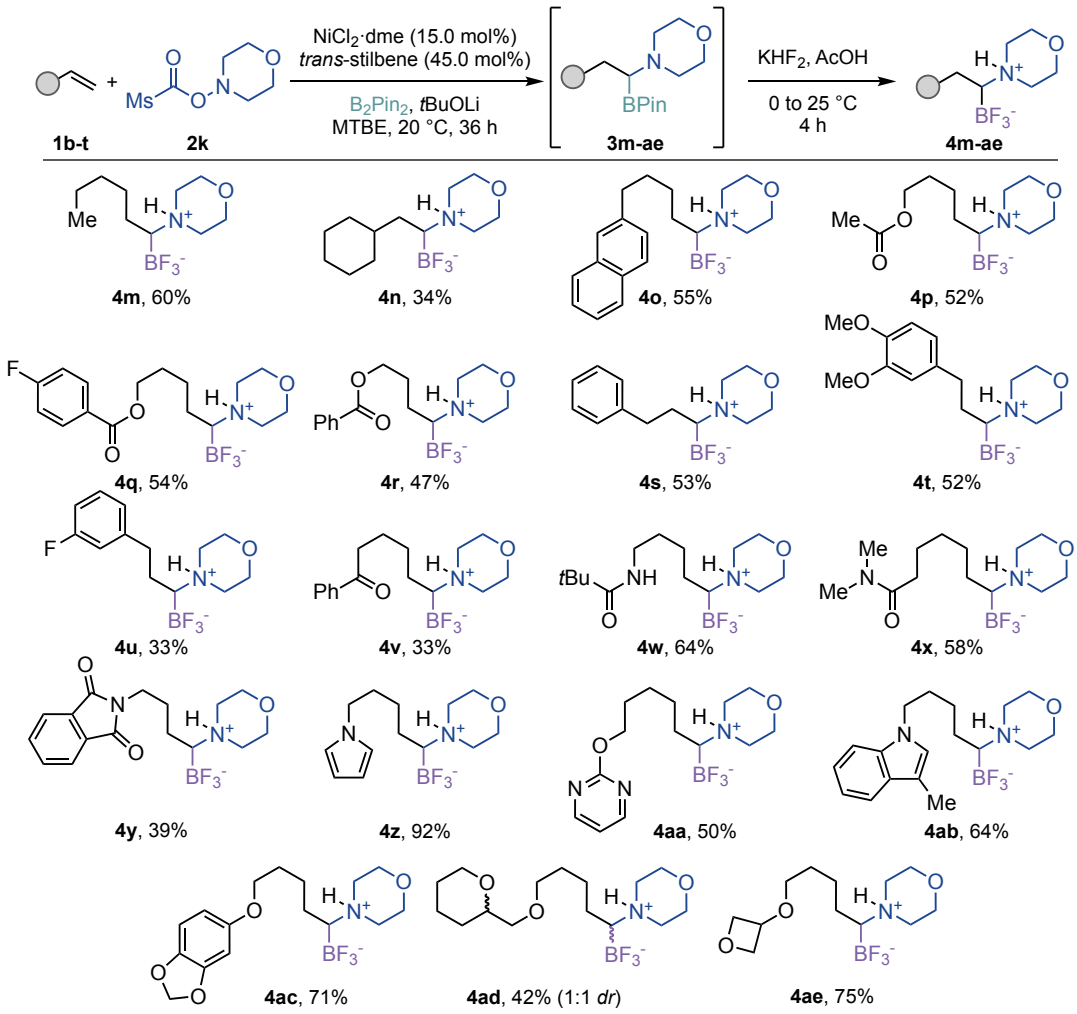

Reaction conditions: **1b-t** (0.20 mmol, 1.0 equiv.), **2k** (0.30 mmol, 1.5 equiv.), B_2Pin_2 (0.34 mmol, 1.7 equiv.), $NiCl_2$·glyme (15.0 mol%), *trans*-stilbene (45.0 mol%), *t*BuOLi (0.30 mmol, 1.5 equiv.), MTBE (0.6 M), 20 ºC for 18 h, *then* **2k** (0.20 mmol, 1.0 equiv.), B_2Pin_2 (0.24 mmol, 1.2 equiv.) and *t*BuOLi (0.2 mmol, 1.0 equiv.), at 20 ºC for 18 hours, then add KHF2 (20 equiv.) in AcOH for 4. Isolated yields, average of two independent runs.

Scheme 22. Screening of unactivated terminal olefins

Additionally, the functionalisation of advanced synthetic intermediates further demonstrated the synthetic feasibility of our method. Carbohydrate (**4af**) and drug derivatives, such as Hymecromone (**4ah**) and Indometacine (**4ai**), were successfully functionalised in synthetically useful yields (55%-74%), providing opportunities for further diversification.

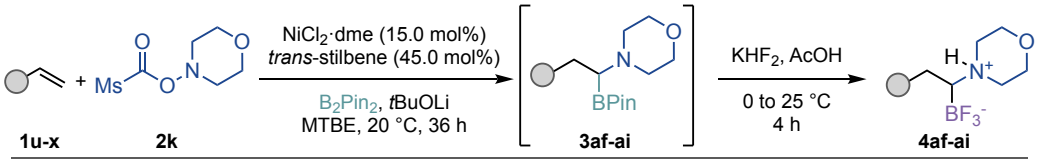

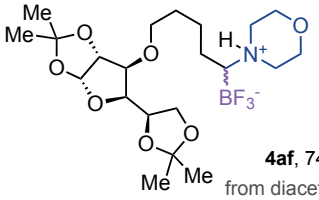

4af, 74% (1:1 *dr*)
from diacetone-D-glucose

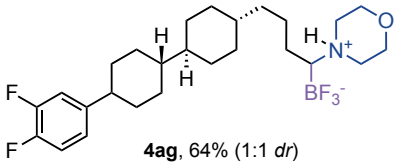

4ag, 64% (1:1 *dr*)
from Liquid Crystal Bulding Block

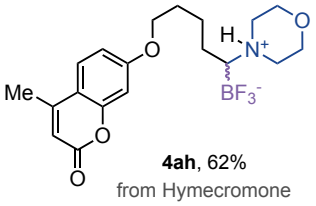

4ah, 62%
from Hymecromone

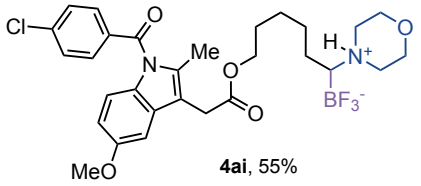

4ai, 55%
from Indometacin

Reaction conditions: **1u-x** (0.20 mmol, 1.0 equiv.), **2k** (0.30 mmol, 1.5 equiv.), B_2Pin_2 (0.34 mmol, 1.7 equiv.), $NiCl_2$·glyme (15.0 mol%), *trans*-stilbene (45.0 mol%), *t*BuOLi (0.30 mmol, 1.5 equiv.), MTBE (0.6 M), 20 ºC for 18 h, *then* **2k** (0.20 mmol, 1.0 equiv.), B_2Pin_2 (0.24 mmol, 1.2 equiv.) and *t*BuOLi (0.2 mmol, 1.0 equiv.), at 20 ºC for 18 hours, then add KHF2 (20 equiv.) in AcOH for 4. Isolated yields, average of two independent runs.

Scheme 23. Screening of synthetic advanced intermediates

Although our 1,1-aminoborylation method has shown a wide substrate scope and successful functionalisation of terminal unactivated olefins, it is important to note that there were certain limitations, and some substrates failed to provide the target product, or functionalisation occurred at other positions within the alkyl chain. Specifically, pyrrolidine derivatives (**2x**) or cyclic and acyclic benzyl amine *N*,*O*-electrophiles (**2y, 2z**) resulted in negligible reactivity, possibly arising from undesired β-hydride elimination upon nickel insertion into the *N*,*O*-bond. Moreover, substrates possessing alkyl bromides, alkyl alcohols, amides, aryl boronic esters or pyridine type functionalities led to the formation of complex mixtures (**1y**-**ac**). Unfortunately, no reaction occurred with 1,1-disubstituted or internal olefins, which only resulted in recovered starting materials, highlighting that functionalisation of sterically encumbered olefins is highly challenging (**1ad**-**ae**). The utilisation of styrene or coordinating group with shorter alkyl chains resulted in the formation of the 1,2-

difunctionalised product in low yields, which can be attributed to the strong chelation exerted by these groups to the metal centre (**1af-ag**).

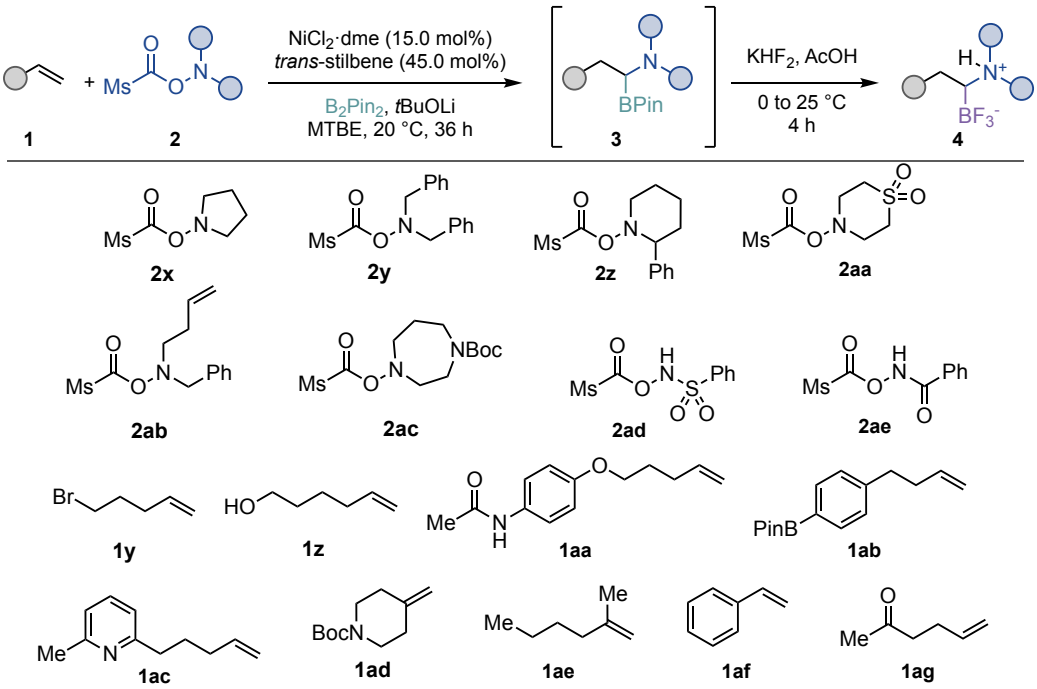

Scheme 24. Unsuccessful substrates

4.3.4. Synthetic applications

To investigate the synthetic applicability of our methodology, we examined the conversion of the trifluoroborate moiety (**4a**) into the boronic acid **6a** (Scheme 25). To this end, we synthesised the corresponding analogue **6a** in quantitative yield by simple exposure to hexamethyldisiloxane (HMDSO) in the presence of aqueous HCl in methanol.[73]

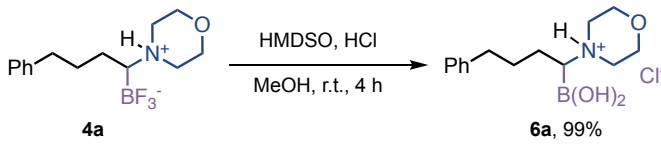

Scheme 25. Preparation of α-aminoboronic acids

Subsequently, we focused our attention to the widely employed Matteson homologation as a means to access β-aminoboronic esters from the corresponding α-substituted derivatives (Scheme 26). Initially, direct conversion of compound **3a** into the desired β-amino analogue proved unsuccessful. However, by fine-tuning of the reaction conditions, we found that treating the crude reaction mixture with CH_2ILi – generated *in situ* from CH_2I_2 and *n*BuLi,

at -78 ºC –, followed by the addition of $ZnCl_2$, led to the formation of the desired β-amino-alkylboronate. Due to the challenges associated with isolating the resulting product via column chromatography, we performed an *in situ* oxidation to convert the boronic acid to the corresponding alcohol, followed by protection with the benzyl group. This four-step synthetic sequence afforded compound **7a** in 27% yield. Although the yield of this transformation is modest, it represents an important proof-of-concept for the synthesis of β-amino-alcohols using our methodology.[74]

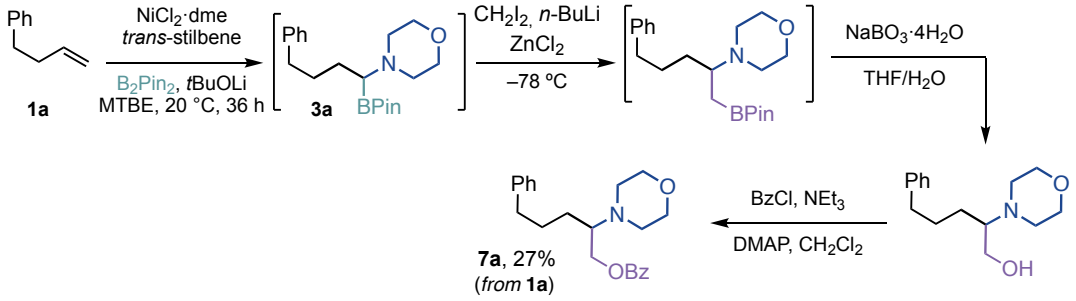

Scheme 26. *In situ* homologation of α-aminoboronc acids *en route* to β-amino-alcohols

Although α-aminotrifuoroboronates have been shown to undergo cross-coupling reactions under palladium or photoredox catalysis, all our attempts to subject these more substituted substrates to cross-coupling conditions were meet with no success. The lack of success could be tentatively attributed to the increased steric demands and basicity of the substrates or potential oxidative degradation pathways.[75–83]

4.3.5. Preliminary mechanistic studies

In a similar manner as explained in the Chapter 3 (*vide supra*), control experiments and isotope labelling experiments were conducted to gain further insights into the reaction mechanism. Firstly, the potential intermediate 1,1-diborylakane (**8**) was prepared and subjected to the optimised reaction conditions. However, no desired product was observed, likely indicating that 1,1-diboryl compounds are not productive reaction intermediates.

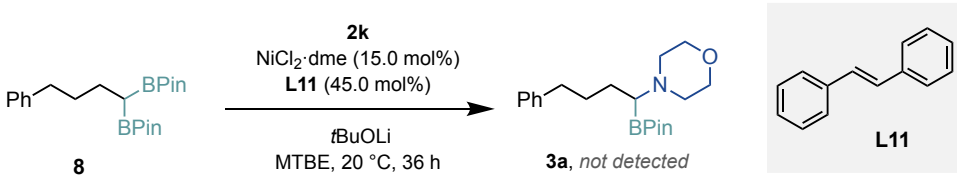

Scheme 27. Control experiments using 1,1-diborylalkane **8**

Additionally, a terminal deuterium-labelled olefin (**9**) was used as the starting material in the reaction. Consistent with the findings in the previous Chapter, migration of the deuterium atom to the adjacent carbon was observed, suggesting that a 1,2-nickel shift is involved in the reaction.

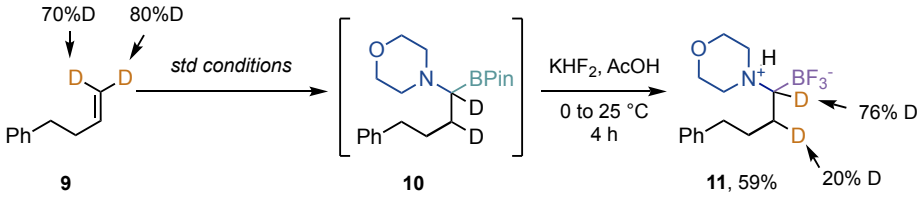

Scheme 28. Deuterium-labelling experiments

4.3.5.1. Plausible mechanism

Based on the available data gathered in Chapter 3, together with control and deuterium-labelling experiments, and previous literature reports,[60,84,85] we proposed a plausible mechanism for the 1,1-aminoborylation reaction. It is expected that a Ln[Ni]^{I} species is generated from the Ln[Ni]^{II} precatalyst via comproportionation. The generated Ln[Ni]^{I} undergoes transmetallation with B_2Pin_2 in the presence of the base (*t*BuOLi), resulting in the formation of a Ln[Ni]^{I}-BPin complex. Subsequently, olefin insertion takes place to afford **I**. A 1,2-nickel migration then occurs, translocating the metal centre adjacent to the boron atom to generate **II**. Finally, *N*-O insertion followed by reductive elimination yields the desired product. However, at this stage, it is not possible to exclude the possibility of a mechanisms involving Ln[Ni]^{II}-alkyl species. Further studies and additional evidence are required to fully elucidate the detailed mechanism of the reaction.

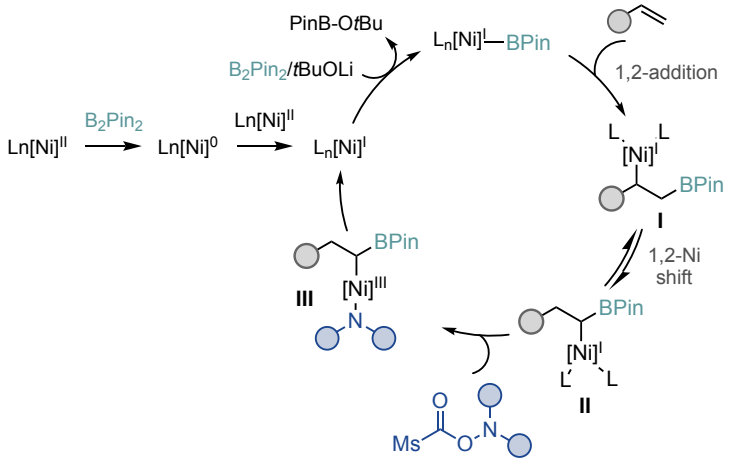

Scheme 29. Proposed mechanism

4.4. Conclusions

In summary, we have developed a nickel-catalysed 1,1-aminoborylation of terminal olefins to generate α-aminotrifluoroboronic salts. This protocol offers the possibility to utilise simple olefin feedstocks to generate bioisosters of amino acids, thus complementing existing techniques for their preparation. While it may be argued that in our catalytic 1,1-aminoborylation generally moderate yields are achieved, it is important to consider the challenges addressed in this transformation. A close look into the literature (*vide supra*) reveals that the majority of modern synthetic routes aiming to prepare 1,1-aminoboranes require the inclusion of non-particularly basic amide backbones. In contrast, the synthesis of 1,1-aminoboranes possessing amine functions remains a challenging endeavour. Therefore, our method may serve as an entry point for accessing elusive amino acid isosteres, which could find applications in medicinal chemistry.

Presently, this methodology is restricted to the formation of racemic α-aminoboronic acid derivatives, therefore additional optimisation of the reaction conditions would be required to achieve an enantioselective transformation. Preliminary mechanistic experiments were carried out, indicating that 1,2-Ni shift is operative. However, further experimental evidence is required in order to confirm the origin of such Ni-alkyl intermediate and to elucidate the subtitles of the chain-walking process.

4.5. Experimental section

4.5.1. General information

Analytical methods

^{1}H and ^{13}C NMR spectra were recorded on Bruker 400 MHz and Bruker 500 MHz at 20 °C. All ^{1}H NMR spectra are reported in parts per million (ppm) downfield of TMS and were calibrated using the residual solvent peak of $CHCl_3$ (7.26 ppm), unless otherwise indicated. All ^{13}C NMR spectra are reported in ppm relative to TMS, were calibrated using the signal of residual $CHCl_3$ (77.16 ppm) and ^{19}F NMR were obtained with ^{1}H decoupling unless otherwise indicated. Coupling constants, *J*, are reported in Hertz. Gas chromatographic analyses were performed on Hewlett-Packard 6890 gas chromatography instrument with FID detector. Flash chromatography was performed with Sigma-Aldrich silica gel, pore size 60 Å (230-400 mesh). Thin layer chromatography was used to monitor reaction progress and analyse fractions from column chromatography. To this purpose TLC Silica gel 60 F_{254} aluminium sheets from Sigma-Aldrich were used and visualisation was achieved using UV irradiation and/or staining with Potassium Permanganate solution.

Reagents

Commercially available materials were used as received without further purification. Nickel (II) chloride ethylene glycol dimethyl ether complex ($NiCl_2$·glyme) and lithium *tert*-butoxide (*t*BuOLi) were purchased from Sigma-Aldrich and stored in a nitrogen-filled glovebox. Potassium hydrogen fluoride was purchased from Sigma-Aldrich, dried at room temperature under vacuum for three days using P_2O_5, and stored in a nitrogen-filled glovebox. Anhydrous methyl *tert*-butyl ether (MTBE, 99% purity) was purchased from Sigma-Aldrich and stored using molecular sieves. *trans*-stilbene was purchased from TCI. Bis(pinacolato)diboron (B_2Pin_2) was purchased from Fluorochem and recrystallised from pentane.

4.5.2. Optimisation of the reaction conditions

General procedure used for reaction optimisation (Schemes 16-18, Tables 1 – 5):

Under air, a Schlenk tube equipped with a stirring bar was loaded with recrystallised, free-flowing B_2Pin_2 (1.70 equiv.), ligand **L** (12 mol%), and N–O electrophile **2** (1.10 equiv.). The tube was transferred into a N_2-filled glovebox, followed by addition of the nickel source (10.0 mol%) and base (1.7 equiv.), assisted by an anti-static device to ensure complete aggregation at the bottom. The tube was closed, brought out of the glovebox, and connected to a N_2-filled Schlenk line. Stirring was started, alkene **1a** (0.20 mmol, 1.00 equiv.) and anhydrous solvent (0.30 mL) were added sequentially via syringe, independently. The tube was closed, and the suspension was stirred at a specified temperature (external thermostat)

and 800 rpm for a specified time, during which several colour changes occurred from yellow to deep violet and finally to a slightly green solution. Then, the reaction was terminated by addition of CH_2Cl_2 (6.00 mL) and *decane* (0.39 μL, 0.20 mmol, 1.00 equiv.) as an internal standard (IS), followed by GC FID (and GC MS) analysis.

4.5.3. Starting materials synthesis

Commercially available compounds were used as received without further purification. Non-commercially available terminal olefins: 2-(pent-4-en-1-yl)naphthalene (**1d**),[86] pent-4-en-1-yl acetate (**1e**),[87] pent-4-en-1-yl 4-fluorobenzoate (**1f**),[88] but-3-en-1-yl benzoate (**1g**),[89] 1-phenylhex-5-en-1-one (**1k**),[90] *N*,*N*-dimethylhept-6-enamide (**1m**),[91] 2-(pent-4-en-1-yl)isoindoline-1,3-dione (**1n**),[92] 1-(pent-4-en-1-yl)-1*H*-pyrrole (**1o**),[93] 3-methyl-1-(pent-4-en-1-yl)-1*H*-indole (**1q**),[49] 5-(pent-4-en-1-yloxy)benzo[*d*][1,3]dioxole (**1r**),[94] 2-(hex-5-en-1-yloxy)tetrahydro-2*H*-pyran (**1s**),[49] 3-(pent-4-en-1-yloxy)oxetane (**1t**),[95] 5-(2,2-dimethyl-1,3-dioxolan-4-yl)-2,2-dimethyl-6-(pent-4-en-1-yloxy)tetrahydrofuro[2,3-*d*][1,3]dioxole (**1u**),[96] 4-methyl-7-(pent-4-en-1-yloxy)-2*H*-chromen-2-one (**1w**),[97] and hex-5-en-1-yl 2-(1-(4-chlorobenzoyl)-5-methoxy-2-methyl-1*H*-indol-3-yl)acetate (**1x**),[49] and ligands: (*E*)-1,2-bis(3,5-bis(trifluoromethyl)phenyl)ethene (**L12**),[98] and (*E*)-1,2-bis(3,5-dimethoxyphenyl)ethene (**L13**),[99] were prepared according to given literature procedures. The NMR data for all these compounds is in agreement with those reported previously.

Preparation of N–O electrophiles

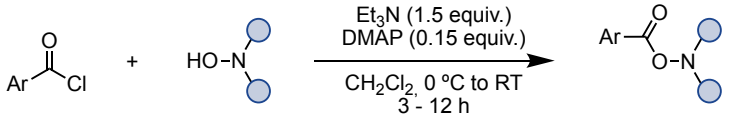

General procedure A: Hydroxyl amine (1.00 equiv.) and DMAP (0.15 equiv.) were dissolved in anhydrous CH_2Cl_2 (0.4 M) with stirring. Anhydrous Et_3N (1.50 equiv.) was added, and the solution was cooled to 0 °C, followed by the dropwise addition of acyl chloride (1.05 equiv.) over 5 min. The solution was allowed to slowly warm to RT (3 h) and stirred at this temperature or kept at 5 °C until completion (TLC control). Next, sat. aq. $NaHCO_3$ solution (same volume as CH_2Cl_2) was added, and the mixture was vigorously stirred for 10 min. The organic layer was separated, and the aqueous layer extracted with CH_2Cl_2 (same volume as sat. aq. $NaHCO_3$). The combined organic extracts were washed with brine (half the volume of the organics), dried over Na_2SO_4, filtered, and the volatiles removed in vacuo at 40 °C. The residue was purified by flash column chromatography on silica gel (see details below) to afford the title compound.

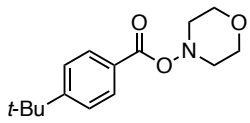

Morpholino 4-(*tert*-butyl)benzoate (**2c**): Following the **general procedure A**, using 4-(*tert*-butyl)benzoyl chloride (1.16 g, 5.5 mmol) and morpholin-4-ol (516 mg, 5.00 mmol, 1.0 equiv.), flash column chromatographic purification (*n*-hexane/EtOAc 9:1 to 7:3) afforded **2c** (700 mg, 53% yield) as an amorphous colourless solid. **^{1}H NMR** (500 MHz, $CDCl_3$): *δ* 7.95 – 7.92 (m, 2H), 7.46 – 7.43 (m, 2H), 3.97 – 3.82 (m, 4H), 3.44 – 3.41 (m, 2H), 3.05 – 3.00 (m, 2H), 1.32 (s, 9H) ppm. **^{13}C NMR** (126 MHz, $CDCl_3$): *δ* 164.7, 157.0, 129.4, 126.4, 125.5, 65.9, 57.1, 35.2, 31.2 ppm. **IR** (neat, cm^{-1}): 2963, 2927, 2859, 2843, 1735, 1605, 1457, 1268, 1254, 1099, 1071, 1047, 853. **HRMS**: m/z calcd. for ($C_{15}H_{21}NNaO_3$) $[M+Na]^+$: 286.1414 found 286.1406. **MP**: 67 – 68 ºC.

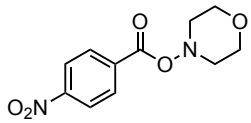

Morpholino 4-nitrobenzoate (**2d**): Following the **general procedure A**, using 4-nitrobenzoyl chloride (500 mg, 1.51 mmol, 1.0 equiv.) and morpholin-4-ol (262 mg, 2.26 mmol, 1.5 equiv.), flash column chromatographic purification (*n*-hexane/EtOAc 3:2) afforded **2d** (146 mg, 39% yield) as an amorphous colourless solid. **^{1}H NMR** (400 MHz, $CDCl_3$): *δ* 8.32 – 8.28 (m, 2H), 8.20 – 8.17 (m, 2H), 4.01 – 3.84 (m, 4H), 3.49 – 3.46 (m, 2H), 3.11 – 3.06 (m, 2H) ppm. **^{13}C NMR** (101 MHz, $CDCl_3$): *δ* 162.9, 150.8, 134.7, 130.8, 123.8, 66.0, 57.3 ppm. **IR** (neat, cm^{-1}): 3115, 2964, 2929, 2909, 2863, 1724, 1604, 1513, 1472, 1455, 1391, 1347, 1321, 1258, 1162, 1102, 1091, 1050, 1007, 873, 855, 843, 713, 635. **HRMS**: m/z calcd. for ($C_{11}H_{12}N_2NaO_5$) $[M+Na]^+$: 275.0638 found 275.0637. **MP**: 130 – 131 ºC.

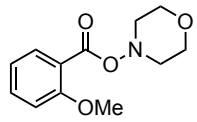

Morpholino 2-methoxybenzoate (**2e**): Following the **general procedure A**, using 2-methoxybenzoyl chloride (273 mg, 1.60 mmol) and morpholin-4-ol (150 mg, 1.45 mmol, 1.0 equiv.), flash column chromatographic purification (*n*-hexane/EtOAc 1:1) afforded **2e** (295 mg, 86% yield) as an amorphous pale-yellow solid. **^{1}H NMR** (400 MHz, $CDCl_3$): δ 7.67 – 7.65 (m, 1H), 7.48 – 7.43 (m, 1H), 6.99 – 6.94 (m, 2H), 3.97 – 3.90 (m, 2H), 3.87 (s, 3H), 3.84 – 3.80 (m, 2H), 3.46 – 3.44 (m, 2H), 3.04 – 2.99 (m, 2H) ppm. **^{13}C NMR** (101 MHz, $CDCl_3$): δ 165.0, 158.8, 133.5, 131.1, 120.3, 119.6, 112.2, 65.8, 57.0, 56.1 ppm. **IR** (neat, cm^{-1}): 2970, 2931, 2911, 2870, 2846, 1743, 1599, 1463, 1291, 1255, 1231, 1068, 1038, 1008, 851. **HRMS**: m/z calcd. for ($C_{12}H_{15}NNaO_4$) $[M+Na]^+$: 260.0893 found 260.0894. **MP**: 62 – 64 ºC.

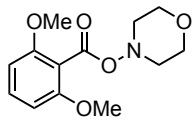

Morpholino 2,6-dimethoxybenzoate (**2f**): Following the **general procedure A**, using 2,6-dimethoxybenzoyl chloride (600 mg, 3.00 mmol, 1.0 equiv.) and morpholin-4-ol (325 mg, 3.15 mmol, 1.05 equiv.), flash column chromatographic purification (*n*-hexane/EtOAc 8:1 to 2:3) afforded **2f** (665 mg, 89% yield) as an amorphous colourless solid. **^{1}H NMR** (400 MHz, $CDCl_3$): δ 7.29 (t, *J* = 8.4 Hz, 1H), 6.54 (d, *J* = 8.4 Hz, 2H), 3.93 – 3.86 (m, 4H), 3.81 (s, 6H), 3.47 – 3.43 (m, 2H), 3.02 – 2.97 (m, 2H) ppm. **^{13}C NMR** (101 MHz, $CDCl_3$): δ 164.8, 157.8, 131.7, 111.6, 104.1, 66.0, 57.0, 56.1 ppm. **IR** (neat, cm^{-1}): 3008, 2967, 2942, 2906, 2859, 1728, 1587, 1476, 1436, 1296, 1258, 1242, 102, 1043, 1010, 855, 787, 762, 646, 585. **HRMS**: m/z calcd. for ($C_{13}H_{17}NNaO_5$) $[M+Na]^+$: 290.0999 found 290.0992. **MP**: 88 – 89 ºC.

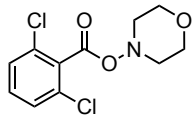

Morpholino 2,6-dichlorobenzoate (**2g**): Following the **general procedure A**, using 2,6-dichlorobenzoyl chloride (328 mg, 1.42 mmol) and morpholin-4-ol (154 mg, 1.49 mmol, 1.0 equiv.), flash column chromatographic purification (*n*-hexane/EtOAc 3:1) afforded **2g** (313 mg, 76% yield) as an amorphous colourless solid. **^{1}H NMR** (300 MHz, $CDCl_3$): *δ* 7.34 – 7.31 (m, 3H), 3.99 – 3.95 (m, 2H), 3.88 – 3.81 (m, 2H), 3.52-3.49 (m, 2H), 3.09 – 3.01 (m, 2H) ppm. **^{13}C NMR** (75 MHz, $CDCl_3$): *δ* 163.0, 132.4, 132.1, 131.5, 128.0, 65.9, 57.2 ppm. **IR** (neat, cm^{-1}): 2973, 2926, 2902, 2863, 1746, 1577, 1561, 1431, 1254, 1097, 1039, 786. **HRMS**: m/z calcd. for ($C_{11}H_{11}Cl_2NNaO_3$) $[M+Na]^+$: 298.0008 found 298.0008. **MP**: 83 – 86 ºC.

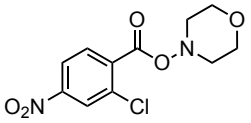

Morpholino 2-chloro-4-nitrobenzoate (**2h**): Following the **general procedure A**, using 2-chloro-4-nitrobenzoyl chloride (1.21 g, 6.00 mmol, 1.2 equiv.) and morpholin-4-ol (973 mg, 6.00 mmol, 1.0 equiv.), flash column chromatographic purification (*n*-hexane/EtOAc 3:1 to 1:1) afforded **2h** (505 mg, 35% yield) as an amorphous colourless solid. **^{1}H NMR** (400 MHz, $CDCl_3$): *δ* 8.33 (d, *J* = 2.2 Hz, 1H), 8.18 (dd, *J* = 8.5, 2.2 Hz, 1H), 7.86 (d, *J* = 8.5 Hz, 1H), 4.01 – 3.98 (m, 2H), 3.88 – 3.82 (m, 2H), 3.52 – 3.49 (m, 2H), 3.11 – 3.07 (m, 2H) ppm. **^{13}C NMR** (101 MHz, $CDCl_3$): *δ* 163.0, 149.7, 135.6, 134.5, 131.7, 126.0, 121.8, 66.0, 57.3 ppm. **IR** (neat, cm^{-1}): 3090, 3029, 2961, 2907, 2864, 1741, 1522, 1461, 1391, 1349, 1272, 1237,

1094, 1035, 1005, 840, 741, 626. **HRMS**: m/z calcd. for ($C_{11}H_{11}ClN_2NaO_5$) $[M+Na]^+$: 309.0249 found 309.0243. **MP**: 131 – 133 ºC.

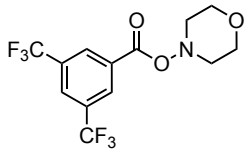

Morpholino 3,5-bis(trifluoromethyl)benzoate (**2i**): Following the **general procedure A**, using 3,5-bis(trifluoromethyl)benzoyl chloride (422 mg, 1.53 mmol) and morpholin-4-ol (150 mg, 1.45 mmol, 1.0 equiv.), flash column chromatographic purification (*n*-hexane/EtOAc 3:1) afforded **2i** (338 mg, 68% yield) as an amorphous colourless solid. **^{1}H NMR** (400 MHz, $CDCl_3$): δ 8.44 – 8.43 (m, 2H), 8.08 – 8.07 (m, 1H), 4.02 – 3.98 (m, 2H), 3.90 – 3.84 (m, 2H), 3.49 – 3.46 (m, 2H), 3.13 – 3.07 (m, 2H) ppm. **^{13}C NMR** (101 MHz, $CDCl_3$): δ 162.1, 132.5 (q, *J* = 34.0 Hz), 131.5, 129.7 (q, *J* = 4.0 Hz), 127.0 – 126.7 (m), 124.3, 122.9 (q, *J* = 271.0 Hz), 66.0, 57.4 ppm. **^{19}F NMR** (376 MHz, $CDCl_3$): δ –63.1 ppm. **IR** (neat, cm^{-1}): 3034, 2994, 2971, 2909, 2871, 1749, 1681, 1462, 1275, 1232, 1160, 1124, 1093, 919, 858, 761. **HRMS**: m/z calcd. for ($C_{13}H_{11}F_6NNaO_3$) $[M+Na]^+$: 366.0535 found 366.0553. **MP**: 92 – 93 ºC.

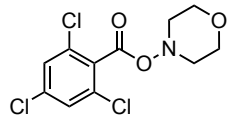

Morpholino 2,4,6-trichlorobenzoate (**2j**): Following the **general procedure A**, using 2,4,6-trichlorobenzoyl chloride (447 mg, 1.83 mmol) and morpholin-4-ol (180 mg, 1.75 mmol, 1.0 equiv.), flash column chromatographic purification (*n*-hexane/EtOAc 4:1) afforded **2j** (427 mg, 83% yield) as an amorphous colourless solid. **^{1}H NMR** (300 MHz, $CDCl_3$): δ 7.36 (s, 2H), 3.98 – 3.79 (m, 4H), 3.50 – 3.47 (m, 2H), 3.08 – 3.01 (m, 2H) ppm. **^{13}C NMR** (75 MHz, $CDCl_3$): δ 162.3, 136.8, 133.1, 130.7, 128.2, 65.9, 57.2 ppm. **IR** (neat, cm^{-1}): 3087, 2968, 2932, 2865, 2846, 1759, 1575, 1550, 1461, 1373, 1269, 12243, 1094, 1036, 1004, 850. **HRMS**: m/z calcd. for ($C_{11}H_{10}Cl_3NNaO_3$) $[M+Na]^+$: 331.9618 found 331.9619. **MP**: 100 – 103 ºC.

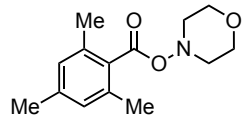

Morpholino 2,4,6-trimethylbenzoate (**2k**): Following the **general procedure A**, using 2,4,6-trimethylbenzoyl chloride (6.51 g, 35.6 mmol) and morpholin-4-ol (3.50 g, 33.9 mmol, 1.0 equiv.), flash column chromatographic purification (*n*-hexane/EtOAc 3:1) afforded **2k** (6.40 g, 76% yield) as an amorphous colourless solid. **^{1}H NMR** (400 MHz, $CDCl_3$): δ 6.86 (s, 2H), 3.97 – 3.94 (m, 2H), 3.89 – 3.85 (m, 2H), 3.46 (d, *J* = 10.5 Hz, 2H), 3.03 – 2.99 (m, 2H),

2.31 (s, 6H), 2.28 (s, 3H) ppm. **^{13}C NMR** (126 MHz, $CDCl_3$): δ 168.2, 140.0, 135.3, 129.3, 128.5, 66.0, 57.1, 21.3, 19.6 ppm. **IR** (neat, cm^{-1}): 2963, 2924, 2894, 2854, 1741, 1610, 1444, 1240, 1164, 1101, 1039, 1007, 854. **HRMS**: m/z calcd. for ($C_{14}H_{19}NNaO_3$) $[M+Na]^+$: 272.1257 found 272.1261. **MP**: 150 – 153 ºC.

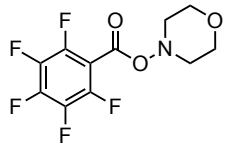

Morpholino 2,3,4,5,6-pentafluorobenzoate (**2l**): Following the **general procedure A**, using 2,3,4,5,6-pentafluorobenzoyl chloride (267 mg, 1.16 mmol) and morpholin-4-ol (120 mg, 1.16 mmol, 1.0 equiv.), flash column chromatographic purification (*n*-hexane/EtOAc 4:1) afforded **2l** (300 mg, 87% yield) as an amorphous colourless solid. **^{1}H NMR** (400 MHz, $CDCl_3$): δ 3.99 – 3.96 (m, 2H), 3.85 – 3.79 (m, 2H), 3.48 – 3.45 (m, 2H), 3.08 – 3.03 (m, 2H) ppm. **^{13}C NMR** (101 MHz, $CDCl_3$): δ 157.4, 145.3 (d, *J* = 263.1 Hz), 143.5 (dm, *J* = 260.2 Hz), 137.8 (dm, *J* = 257.2 Hz), 107.3, 65.9, 57.3 ppm. **^{19}F NMR** (376 MHz, $CDCl_3$) δ –137.9 (dp, *J* = 16.9, 5.7 Hz, 2F), –148.0 (td, *J* = 20.7, 4.0 Hz, 1F), –(159.9–160.0) (m, 2F) ppm. **IR** (neat, cm^{-1}): 2984, 2965, 2932, 2901, 2862, 1754, 1652, 1524, 1494, 1418, 1323, 1267, 1197, 1098, 989, 940, 858, 829, 735. **HRMS**: m/z calcd. for ($C_{11}H_8F_5NNaO_3$) $[M+Na]^+$: 320.0317 found 320.0323. **MP**: 40 – 41 ºC.

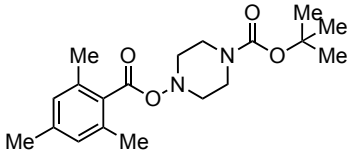

***tert*-Butyl 4-((2,4,6-trimethylbenzoyl)oxy)piperazine-1-carboxylate** (**2m**): Following the **general procedure A**, using 2,4,6-trimethylbenzoyl chloride (575 mg, 3.15 mmol) and *tert*-butyl 4-hydroxypiperazine-1-carboxylate (607 mg, 3.00 mmol, 1.0 equiv.), flash column chromatographic purification (*n*-hexane/EtOAc 3:1) afforded **2m** (625 mg, 60% yield) as an amorphous colourless solid. **^{1}H NMR** (400 MHz, $CDCl_3$): δ 6.85 (s, 2H), 4.03 (br, 2H), 3.45 – 3.28 (m, 4H), 2.84 (br, 2H), 2.29 (s, 6H), 2.27 (s, 3H), 1.46 (s, 9H) ppm. **^{13}C NMR** (101 MHz, $CDCl_3$) δ 168.2, 154.5, 140.0, 135.3, 129.3, 128.5, 80.4, 56.0, 28.5, 21.3, 19.6 ppm. **IR** (neat, cm^{-1}): 2971, 1928, 2899, 2856, 1739, 1685, 1422, 1363, 1248, 1141, 1018, 859. **HRMS**: m/z calcd. for ($C_{19}H_{28}N_2NaO_4$) $[M+Na]^+$: 371.1941 found 371.1930. **MP**: 102 – 105 ºC.

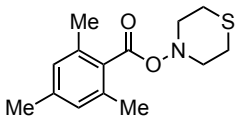

Thiomorpholino 2,4,6-trimethylbenzoate (**2n**): Following the **general procedure A**, using 2,4,6-trimethylbenzoyl chloride (575 mg, 3.15 mmol) and thiomorpholine-4-ol (358 mg, 3.00 mmol, 1.0 equiv.), flash column chromatographic purification (*n*-hexane/EtOAc 7:1 to 5:1) afforded **2n** (605 mg, 76% yield) as an amorphous pale-yellow solid. **^{1}H NMR** (300 MHz, $CDCl_3$): δ 6.86 (s, 2H), 3.72 – 2.78 (m, 8H), 2.30 (s, 6H), 2.28 (s, 3H) ppm. **^{13}C NMR** (75 MHz, $CDCl_3$): δ 168.1, 140.0, 135.2, 129.3, 128.5, 58.0, 27.1, 21.3, 19.6 ppm. **IR** (neat, cm^{-1}): 2949, 2922, 2845, 1747, 1610, 1458, 1238, 1160, 1061, 975, 848. **HRMS**: m/z calcd. for ($C_{14}H_{19}NNaO_2S$) $[M+Na]^+$: 288.1029; found 288.1041. **MP**: 57 – 59ºC.

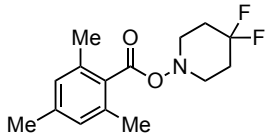

4,4-Difluoropiperidin-1-yl 2,4,6-trimethylbenzoate (**2o**): Following the **general procedure A**, using 2,4,6-trimethylbenzoyl chloride (622 mg, 3.41 mmol) and 4,4-difluoropiperidin-1-ol (445 mg, 3.25 mmol, 1.0 equiv.), flash column chromatographic purification (*n*-hexane/EtOAc 7:1) afforded **2o** (721 mg, 78% yield) as an amorphous colourless solid (slow solidification). **^{1}H NMR** (400 MHz, $CDCl_3$): δ 6.87 – 6.86 (m, 2H), 3.47 – 3.25 (m, 4H), 2.30 (s, 6H), 2.29 (s, 3H), 2.26 – 2.16 (m, 4H) ppm. **^{13}C NMR** (101 MHz, $CDCl_3$): δ 168.2, 140.1, 135.3, 129.2, 128.5, 120.6 (t, J = 242.3 Hz), 52.7 (t, J = 4.6 Hz), 31.8 (t, J = 24.2 Hz), 21.3, 19.7 ppm. **^{19}F NMR** (376 MHz, $CDCl_3$): δ -96.2 – (-99.0) (m), -100.0 (d, J = 232.9 Hz) ppm. **IR** (neat, cm^{-1}): 2970, 2946, 2921, 2851, 1747, 1365, 1239, 1129, 1052, 953. **HRMS**: m/z calcd. for ($C_{15}H_{19}F_2NNaO_2$) $[M+Na]^+$: 306.1276; found 306.1263. **MP**: 122 – 123 ºC.

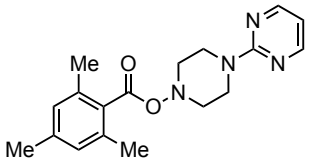

4-(pyrimidin-2-yl)piperazin-1-yl 2,4,6-trimethylbenzoate (**2p**): Following the **general procedure A**, using 2,4,6-trimethylbenzoyl chloride (253 mg, 1.39 mmol) and 4-(pyrimidin-2-yl)piperazin-1-ol (250 mg, 1.39 mmol, 1.0 equiv.), flash column chromatographic purification (*n*-hexane/EtOAc 3:1) afforded **2p** (337 mg, 74% yield) as an amorphous colourless solid. **^{1}H NMR** (400 MHz, $CDCl_3$): δ 8.32 (d, J = 4.8 Hz, 2H), 6.87 – 6.85 (m, 2H), 6.53 (t, J = 4.7 Hz, 1H), 4.73 – 4.67 (m, 2H), 3.64 – 3.40 (m, 4H), 3.00 – 2.92 (m, 2H), 2.32 (s, 6H), 2.28 (s, 3H) ppm. **^{13}C NMR** (101 MHz, $CDCl_3$): δ 168.4, 161.5, 157.9, 140.0, 135.3,

129.4, 128.5, 110.6, 56.1, 42.4, 21.3, 19.7 ppm. **IR** (neat, cm^{-1}): 3018, 2971, 2919, 2905, 2865, 2855, 1736, 1610, 1584, 1549, 1513, 1492, 1452, 1372, 1352, 1268, 1237, 1161, 1129, 1062, 1024, 982, 954, 848, 808, 725. **HRMS**: m/z calcd. for ($C_{18}H_{22}N_4NaO_2$) $[M+Na]^+$: 349.1635; found 349.1634. **MP**: 158 – 161 ºC.

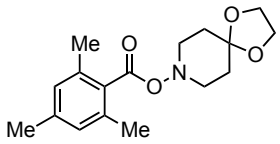

1,4-dioxa-8-azaspiro[4.5]decan-8-yl 2,4,6-trimethylbenzoate (**2q**): Following the **general procedure A**, using 2,4,6-trimethylbenzoyl chloride (1.51 g, 8.3 mmol, 1.1 equiv.) and 1,4-dioxa-8-azaspiro[4.5]decan-8-ol (1.20 g, 7.5 mmol, 1.0 equiv.), flash column chromatographic purification (*n*-hexane/EtOAc 3:1) afforded **2q** (2.00 g, 87% yield) as an amorphous colourless solid. **^{1}H NMR** (400 MHz, $CDCl_3$): δ 6.85 (s, 2H), 3.96 (s, 4H), 3.48 – 3.47 (m, 2H), 3.19 – 3.12 (m, 2H), 2.30 (s, 6H), 2.27 (s, 3H), 2.06 – 1.84 (m, 4H) ppm. **^{13}C NMR** (101 MHz, $CDCl_3$): δ 168.5, 139.8, 135.3, 129.6, 128.5, 106.0, 64.7, 64.5, 54.2, 33.0, 21.3, 19.6 ppm. **IR** (neat, cm^{-1}): 2966, 2932, 2884, 2841, 1742, 1608, 1477, 1423, 1365, 1280, 1255, 1242, 1151, 1116, 1060, 1038, 965, 928, 895, 850. **HRMS**: m/z calcd. for ($C_{17}H_{23}NNaO_4$) $[M+Na]^+$: 328.1519; found 328.1517. **MP**: 61 – 64 ºC.

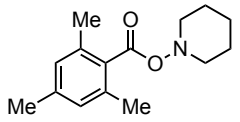

Piperidin-1-yl 2,4,6-trimethylbenzoate (**2r**): Following the **general procedure A**, using 2,4,6-trimethylbenzoyl chloride (590 mg, 3.23 mmol) and piperidin-1-ol (311 mg, 3.07 mmol, 1.0 equiv.), flash column chromatographic purification (*n*-hexane/EtOAc 7:1) afforded **2r** (663 mg, 87% yield) as a colourless oil. **^{1}H NMR** (400 MHz, $CDCl_3$): 6.84 (s, 2H), 3.56 – 3.54 (m, 2H), 2.74 – 2.69 (m, 2H), 2.30 (s, 6H), 2.27 (s, 3H), 1.87 – 1.80 (m, 4H), 1.69 – 1.64 (m, 1H), 1.33 – 1.19 (m, 1H) ppm. **^{13}C NMR** (101 MHz, $CDCl_3$): δ 168.4, 139.6, 135.2, 129.9, 128.4, 57.7, 25.2, 23.4, 21.3, 19.6 ppm. **IR** (neat, cm^{-1}): 2941, 1857, 2832, 1743, 1612, 1443, 1241, 1163, 1063, 1012, 850. **HRMS**: m/z calcd. for ($C_{15}H_{21}NNaO_2$) $[M+Na]^+$: 270.1464 found 270.1472.

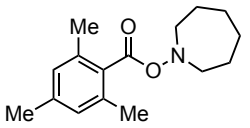

Azepan-1-yl 2,4,6-trimethylbenzoate (**2s**): Following the **general procedure A**, using 2,4,6-trimethylbenzoyl chloride (767 mg, 4.20 mmol) and azepan-1-ol (461 mg, 4.00 mmol, 1.0 equiv.), flash column chromatographic purification (*n*-hexane/EtOAc 7:1) afforded **2s**

(961 mg, 92% yield) as a colourless oil. **^{1}H NMR** (400 MHz, $CDCl_3$): δ 6.84 (s, 2H), 3.32 – 3.29 (m, 4H), 2.30 (s, 6H), 2.27 (s, 3H), 1.83 – 1.77 (m, 4H), 1.68 – 1.62 (m, 4H) ppm. **^{13}C NMR** (101 MHz, $CDCl_3$): δ 168.5, 139.6, 135.2, 130.0, 128.4, 59.8, 26.4, 24.1, 21.3, 19.6 ppm. **IR** (neat, cm^{-1}): 2925, 2856, 1741, 1612, 1449, 1234, 1161, 1056, 850. **HRMS**: m/z calcd. for ($C_{16}H_{23}NNaO_2$) $[M+Na]^+$: 284.1621; found 284.1631. **MP**: 90 – 91 ºC.

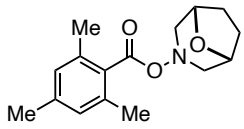

(1R,5S)-8-oxa-3-ayabicyclo[3.2.1]ocatan-3-yl 2,4,6-trimethylbenzoate (**2t**): Following the **general procedure A**, using 2,4,6-trimethylbenzoyl chloride (1.21 g, 6.4 mmol, 1.1 equiv.) and (1R,5S)-8-oxa-3-ayabicyclo[3.2.1]ocatan-3-ol (780 mg, 6.0 mmol, 1.0 equiv.), flash column chromatographic purification (*n*-hexane/EtOAc 4:1) afforded **2t** (1.39 g, 84% yield) as an amorphous colourless solid. **^{1}H NMR** (400 MHz, $CDCl_3$): δ 6.85 (s, 2H), 4.47 – 4.43 (m, 2H), 3.42 – 3.39 (m, 2H), 3.04 – 3.01 (m, 2H), 2.29 (s, 6H), 2.28 (s, 3H), 2.23 – 2.18 (m, 2H), 1.95 – 1.90 (m, 2H) ppm. **^{13}C NMR** (101 MHz, $CDCl_3$): δ 168.1, 139.8, 135.3, 129.7, 128.5, 75.2, 61.9, 28.4, 21.3, 19.7 ppm. **IR** (neat, cm^{-1}): 2982, 29445, 2924, 2851, 1737, 1609, 1575, 1463, 1427, 1381, 1253, 1239, 1193, 1163, 1067, 1037, 991, 980, 879, 846, 760. **HRMS**: m/z calcd. for ($C_{16}H_{21}NNaO_3$) $[M+Na]^+$: 298.1414; found 298.1402. **MP**: 92 – 96 ºC.

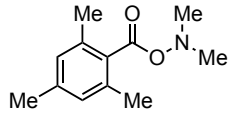

N,N-dimethyl-O-(2,4,6-trimethylbenzoyl)hydroxylamine (**2u**): Following the **general procedure A**, using 2,4,6-trimethylbenzoyl chloride (2.06 g, 11.3 mmol, 1.1 equiv.), N,N-dimethylhydroxylamine hydrochloride (1.0 g, 10.3 mmol, 1.0 equiv.), and triethylamine (4.3 mL, 30.8 mmol, 3 equiv.), flash column chromatographic purification (*n*-hexane/EtOAc 9:1 to 7:3) afforded **2u** (1.80 g, 85% yield) as a colourless oil. **^{1}H NMR** (500 MHz, $CDCl_3$): δ 6.85 (s, 2H), 2.88 (s, 6H), 2.30 (s, 6H), 2.27 (s, 3H) ppm. **^{13}C NMR** (126 MHz, $CDCl_3$): δ 168.6, 139.7, 135.2, 129.6, 128.4, 48.6, 21.3, 19.5 ppm. **IR** (neat, cm^{-1}): 2996, 2963, 2922, 2864, 1743, 1612, 1442, 1430, 1254, 1153, 1050, 851. **HRMS**: m/z calcd. for ($C_{12}H_{17}NNaO_2$) $[M+Na]^+$: 230.1151; found 230.1149.

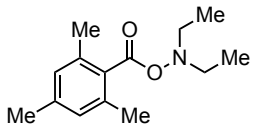

N,N-diethyl-O-(2,4,6-trimethylbenzoyl)hydroxylamine (**2v**): Following the **general procedure A**, using 2,4,6-trimethylbenzoyl chloride (575 mg, 3.15 mmol, 1.05 equiv.) and N,N-diethylhydroxylamine (267 mg, 3.0 mmol, 1.0 equiv.), flash column chromatographic purification (*n*-hexane/EtOAc 6:1) afforded **2v** (540 mg, 77% yield) as a colourless oil. **^{1}H NMR** (500 MHz, $CDCl_3$): δ 6.85 (s, 2H), 3.07 (q, *J* = 7.1 Hz, 4H), 2.33 (s, 6H), 2.28 (s, 3H), 1.23 (t, *J* = 7.1 Hz, 6H) ppm. **^{13}C NMR** (126 MHz, $CDCl_3$): δ 169.4, 139.6, 135.2, 130.0, 128.5, 52.6, 21.3, 19.9, 11.9 ppm. **IR** (neat, cm^{-1}): 2979, 2939, 1744, 1612, 1448, 1378, 1239, 1166, 1049, 865. **HRMS**: m/z calcd. for ($C_{14}H_{21}NNaO_2$) $[M+Na]^+$: 258.1464; found 258.1474.

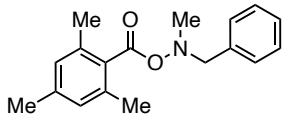

***N*-benzyl-*N*-methyl-*O*-(2,4,5-trimethylbenzoyl)hydroxylamine** (**2w**): Following the **general procedure A**, using 2,4,6-trimethylbenzoyl chloride (1.33 g, 7.29 mmol) and *N*-benzyl-*N*-methylhydroxylamine (1.00 g, 7.29 mmol, 1.0 equiv.), flash column chromatographic purification (*n*-hexane/EtOAc 9:1) afforded **2w** (1.64 g, 79% yield) as an amorphous colourless solid. **^{1}H NMR** (400 MHz, $CDCl_3$): δ 7.45 – 7.43 (m, 2H), 7.34 – 7.27 (m, 3H), 6.77 – 6.76 (m, 2H) 4.09 (s, 2H), 2.97 (s, 3H), 2.24 (s, 3H), 2.01 (s, 6H) ppm. **^{13}C NMR** (101 MHz, $CDCl_3$): δ 168.6, 139.5, 136.2, 135.1, 129.8, 129.5, 128.5, 128.3, 127.9, 65.3, 46.7, 21.3, 19.1 ppm. **IR** (neat, cm^{-1}): 3029, 2999, 2971, 2918, 2855, 2794, 1736, 1612, 1581, 1495, 1454, 1441, 1360, 1255, 1199, 1162, 1067, 1047, 961, 851, 751, 723, 698. **HRMS**: m/z calcd. for ($C_{18}H_{21}NNaO_2$) $[M+Na]^+$: 306.1464; found 306.1467. **MP**: 41 – 43 ºC.

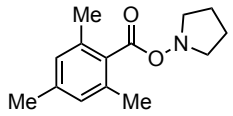

Pyrrolidin-1-yl 2,4,6-trimethylbenzoate (**2x**): Following the **general procedure A**, using 2,4,6-trimethylbenzoyl chloride (726 mg, 3.97 mmol) and pyrrolidin-1-ol (330 mg, 3.79 mmol, 1.0 equiv.), flash column chromatographic purification (*n*-hexane/EtOAc 5:2) afforded **2x** (597 mg, 68% yield) as a colourless oil. **^{1}H NMR** (400 MHz, $CDCl_3$): 6.87 – 6.82 (m, 2H), 3.35 – 3.25 (m, 4H), 2.29 (s, 6H), 2.27 (s, 3H), 2.01 – 1.71 (m, 4H) ppm. **^{13}C NMR** (101 MHz, $CDCl_3$): δ 168.9, 139.7, 135.3, 129.9, 128.4, 57.8, 22.3, 21.3, 19.6 ppm. **IR** (neat, cm^{-1}): 2953, 2919, 2858, 1740, 1707, 1611, 1541, 1435, 1377, 1255, 1062, 850. **HRMS**: m/z calcd. for ($C_{14}H_{20}NO_2$) $[M+H]^+$: 234.1489 found 234.1492.

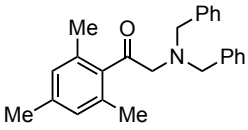

***N*,*N*-dibenzyl-*O*-(2,4,6-trimethylbenzoyl)hydroxylamine** (**2y**): Following the **general procedure A**, using 2,4,6-trimethylbenzoyl chloride (480 mg, 2.63 mmol) and *N*,*N*-dibenzylhydroxylamine (533mg, 2.50 mmol, 1.0 equiv.), flash column chromatographic purification (*n*-hexane/EtOAc 9:1) afforded **2y** (732 mg, 82% yield) as a colourless oil. **^{1}H NMR** (400 MHz, $CDCl_3$): 7.54 – 7.51 (m, 4H), 7.37 – 7.32 (m, 4H), 7.30 – 7.26 (m, 2H), 6.73 (s, 2H), 4.19 (s, 4H), 2,23 (s, 3H), 1.84 (s, 6H) ppm. **^{13}C NMR** (101 MHz, $CDCl_3$): δ 168.4, 139.3, 136.5, 135.2, 129.9, 129.4, 128.5, 128.2, 127.8, 62.6, 21.2, 19.0 ppm. **IR** (neat, cm^{-1}):3061, 3034, 2870, 2841, 1746, 1453, 1243, 1059, 982, 695. **HRMS**: m/z calcd. for ($C_{24}H_{25}NNaO_2$) $[M+Na]^+$: 382.1777 found 382.1779.

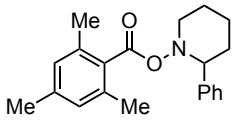

2-Phenylpiperidin-1-yl 2,4,6-trimethylbenzoate (**2z**): Following the **general procedure A**, using 2,4,6-trimethylbenzoyl chloride (575 mg, 3.15 mmol) and 2-phenylpiperidin-1-ol (548 mg, 3.00 mmol, 1.0 equiv.), flash column chromatographic purification (*n*-hexane/EtOAc 9:1 to 6:1) afforded **2z** (881 mg, 91% yield) as an amorphous colourless solid.**^{1}H NMR** (400 MHz, $CDCl_3$): δ 7.48 – 7.39 (m, 2H), 7.33 – 7.17 (m, 3H), 6.71 – 6.65 (m, 2H), 3.86 – 3.76 (m, 1H), 3.72 (dd, *J* = 10.7, 3.6 Hz, 1H), 2.87 (ddd, *J* = 12.5, 9.4, 3.0 Hz, 1H), 2.19 (s, 3H), 2.14 – 1.83 (m, 4H), 1.85 – 1.74 (m, 7H), 1.52 – 1.33 (m, 1H) ppm. **^{13}C NMR** (101 MHz, $CDCl_3$): δ 168.3, 142.8, 139.2, 135.0, 123.0, 128.5, 128.1, 127.5, 127.5, 72.1, 58.4, 36.3, 25.7, 24.2, 21.2, 18.7 ppm. **IR** (neat, cm^{-1}): 2944, 2849, 2829, 1751, 1441, 1235, 1045, 763. **HRMS**: m/z calcd. for ($C_{21}H_{25}NO_2$) $[M+H]^+$: 324.1958; found 324.1973.

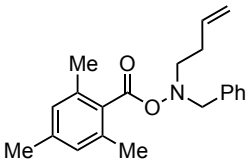

***N*-benzyl-*N*-(but-3-en-1-yl)-*O*-(2,4,6-trimethylbenzoyl)hydroxylamine** (**2aa**): Following the **general procedure A**, using 2,4,6-trimethylbenzoyl chloride (605 mg, 3.31 mmol) and 2*N*-benzyl-*N*-(but-3-en-1-yl)hydroxylamine (587 mg, 3.31 mmol, 1.0 equiv.), flash column chromatographic purification (*n*-hexane/EtOAc 98:2) afforded **2aa** (896mg, 84% yield) as an amorphous colourless oil.**^{1}H NMR** (400 MHz, $CDCl_3$): δ 7.47 – 7.44 (m, 2H), 7.34 – 7.27 (m, 3H), 5.86 (ddt, *J* = 17.0, 10.2, 6.7 Hz, 1H), 5.12 – 5.07 (m, 1H), 5.06 – 5.02 (m, 1H), 4.51 (s, 2H), 3.13 – 3.09 (m, 2H), 2.50 – 2.44 (m, 2H), 2.25 (s, 3H), 2.07 (s, 6H) ppm. **^{13}C NMR** (101

MHz, $CDCl_3$): δ 168.7, 139.5, 136.3, 135.5, 135.3, 129.9, 129.5, 128.5, 128.4, 127.9, 116.5, 63.1, 58.1, 31.3, 21.2, 19.5 ppm. **IR** (neat, cm^{-1}): 3030, 3004, 2921, 2853, 1747, 1611, 1437, 1235, 1161, 1055, 1031, 739. **HRMS**: m/z calcd. for ($C_{21}H_{25}NNaO_2$) $[M+Na]^+$: 346.1777; found 346.1776.

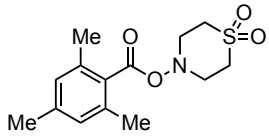

1,1-dioxidothiomorpholino 2,4,6-trimethylbenzoate (**2ab**): Following the **general procedure A**, using 2,4,6-trimethylbenzoyl chloride (804 mg, 4.40 mmol) and 4-hydroxythiomorpholine 1,1-dioxide (605 mg, 4.00 mmol, 1.0 equiv.), flash column chromatographic purification (*n*-hexane/EtOAc 2:1 to 1:2) afforded **2ab** (870mg, 73% yield) as an amorphous colourless oil.**^{1}H NMR** (400 MHz, $CDCl_3$): δ 6.89 (s, 2H), 3.81, (t, *J* = 5.4 Hz, 4H), 3.25 (br s, 4H), 2.30 (s, 3H), 2.29 (s, 6H) ppm. **^{13}C NMR** (101 MHz, $CDCl_3$): δ 167.6, 135.3, 128.7, 128.4, 53.7, 48.1, 21.3, 19.8 ppm. **IR** (neat, cm^{-1}): 2991, 2940, 2921, 1750, 1611, 1426, 1296, 1236, 1131, 1034, 846. **HRMS**: m/z calcd. for ($C_{14}H_{19}NNaO_4S$) $[M+Na]^+$: 320.0927; found 320.0934.

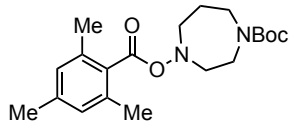

***tert*-butyl 4-((2,4,6-trimethylbenzoyl)oxy)-1,4-diazepane-1-carboxylate** (**2ac**): Following the **general procedure A**, using 2,4,6-trimethylbenzoyl chloride (1.2 g, 6.57 mmol, 1.0 equiv.) and *tert*-butyl 4-hydroxy-1,4-diazepane-1-carboxylate (1.42 g, 6.57 mmol, 1.0 equiv.), flash column chromatographic purification (*n*-hexane/EtOAc 10:1 to 7:3) afforded **2ac** (1.21 g, 51% yield) as an amorphous colourless oil, in a 1:1 mixture of diastereomers .**^{1}H NMR** (500 MHz, $CDCl_3$): δ 6.85 (s, 2H), 3.64 – 3.57 (m, 2H), 3.54 – 3.46 (m, 2H), 3.31 (br, 4H), 2.29 (s, 6H), 2.28 (s, 3H), 2.06 – 2.01 (m, 2H), 1.46 (s, 9H) ppm. **^{13}C NMR** (126 MHz, $CDCl_3$): δ 168.3, 139.9, 135.2, 129.5, 128.5, 80.0, 60.0, 59.7, 58.2, 57.8, 45.6, 44.4, 42.6, 41.8, 28.6, 23.9, 23.8, 21.3, 19.6 ppm. **IR** (neat, cm^{-1}): 2972, 2926, 2856, 1744, 1688, 1457, 1407, 1329, 1160, 1147, 1051, 851. **HRMS**: m/z calcd. for ($C_{20}H_{30}N_2NaO_4$) $[M+Na]^+$: 385.2098; found 385.2105.

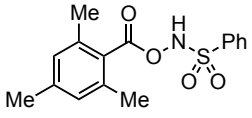

***N*-((2,4,6-Trimethylbenzoyl)oxy)benzenesulfonamide** (**2ad**): Following the **general procedure A**, using 2,4,6-trimethylbenzoyl chloride (1.11 g, 6.06 mmol) and *N*-hydroxy-

benzenesulfonamide (1.00 g, 5.77 mmol, 1.0 equiv.), flash column chromatographic purification (*n*-hexane/EtOAc/MeOH 4:2:1) afforded **2ad** (981 mg, 53% yield) as an amorphous colourless solid. **^{1}H NMR** (400 MHz, $CDCl_3$): δ 9.32 (s, 1H), 7.99 – 7.96 (m, 2H), 7.69 – 7.65 (m, 1H), 7.58 – 7.53 (m, 2H), 6.86 (s, 2H), 2.27 (s, 3H), 2.09 (s, 6H) ppm. **^{13}C NMR** (101 MHz, $CDCl_3$): δ 168.2, 141.5, 137.0, 136.0, 134.6, 129.5, 129.1, 128.9, 125.5, 21.3, 19.9 ppm. **IR** (neat, cm^{-1}): 3156, 1738, 1609, 1447, 1387, 1239, 1179, 1160, 1047, 857, 742, 679. **HRMS**: m/z calcd. for ($C_{16}H_{17}NNaO_4S$) $[M+Na]^+$: 342.0770 found 342.0785.

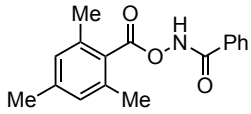

***N*-((2,4,6-Trimethylbenzoyl)oxy)benzamide** (**2ae**): Following the **general procedure A**, using 2,4,6-trimethylbenzoyl chloride (419 mg, 2.29 mmol) and *N*-hydroxybenzamide (300 mg, 2.19 mmol, 1.0 equiv.), flash column chromatographic purification (*n*-hexane/EtOAc 4:1 to 2:1) afforded **2ae** (460 mg, 74% yield) as an amorphous colourless solid. **^{1}H NMR** (400 MHz, $CDCl_3$): δ 9.61 (s, 1H), 7.91 – 7.88 (m, 2H), 7.61 – 7.57 (m, 1H), 7.52 – 7.46 (m, 2H), 6.91 (s, 2H), 2.43 (s, 6H), 2.31 (s, 3H) ppm. **^{13}CNMR** (101 MHz, $CDCl_3$): δ 168.6, 166.8, 141.1, 137.1, 133.0, 131.0, 129.0, 128.9, 127.7, 126.6, 21.4, 20.2 ppm. **IR** (neat, cm^{-1}): 3202, 2970, 2923, 1771, 1658, 1602, 1503, 1482, 1252, 1233, 1157, 1020, 986, 851. **HRMS**: m/z calcd. for ($C_{17}H_{17}NNaO_3$) $[M+Na]^+$: 306.1101 found 306.1103.

Synthesis of unactivated olefins

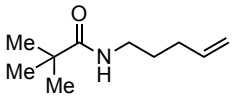

N-(pent-4-en-1-yl)pivalamide (**1l**): In an oven dried round bottom flask with magnetic stirring, 4-penten-1-amine hydrochloride (190 mg, 1.56 mmol, 1.0 equiv.) was dissolved in dry dichloromethane (5 mL). Then triethylamine (480 μL, 3.44 mmol, 2.2 equiv.), followed trimethylacetylchloride (226 mg, 1.9 mmol, 1.2 equiv.) were added dropwise. The reaction mixture was stirred overnight at room temperature. The reaction mixture was quenched with an aqueous saturated solution of NH_4Cl. The layers were separated, and the organic phase was washed with water (2x 10 mL). The combined organic phases were dried over Na_2SO_4, filtered, and concentrated in vacuo. The residue was purified by flash column chromatographic (*n*-hexane/EtOAc 9:1 to 4:1) to afford **1l** (210 mg, 79% yield) as a colourless oil. **^{1}H NMR** (400 MHz, $CDCl_3$): δ 5.81 (ddt, *J* = 16.9, 10.2, 7.7, 1H), 5.65 (br, 1H), 5.04 (dq, *J* = 17.1, 1.7, 1H), 4.98 (ddt, *J* = 10.2, 2.0, 1.2, 1H), 3.28 – 3.23 (m, 2H), 2.12 – 2.06 (m, 2H), 1.64 – 1.57 (m, 2H), 1.19 (s, 9H) ppm. **^{13}C NMR** (101 MHz, $CDCl_3$): δ 178.5, 138.1, 115.3, 39.3, 38.8, 31.4, 28.9, 27.8 ppm. **IR** (neat, cm^{-1}): 3343, 3078, 2960, 2932, 2870, 1636, 1531,

1480, 1437, 1366, 1299, 1211, 992, 908, 646. **HRMS**: m/z calcd. for ($C_{10}H_{19}NNaO$) $[M+Na]^+$: 192.1359; found 192.1353.

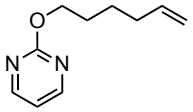

2-(hex-5-en-1-yloxy)pyrimidine (**1p**): To a suspension of sodium hydride (396 mg, 16.5 mmol, 1.1 equiv.) in THF (50 mL) was added 2-chloro-pyrimidine (1.72 g, 15.0 mmol, 1.0 equiv.) followed by careful, dropwise addition of hex-5-en-1-ol (1.65 g, 16.5 mmol, 1.1 equiv.) at room temperature. After 2 hours, water (25 mL) was added, and the mixture extracted with EtOAc (25 mL). The layers were separated, and the organic layer was washed with water (25 mL) and brine (25 mL). The combined organic phases were dried over Na_2SO_4, filtered, and concentrated in vacuo. The residue was purified by flash column chromatography on silica gel (*n*-hexane/EtOAc 9:1 to 7:3) to give **1p** (2.01 g, 75% yield) as a colourless oil. **^{1}H NMR** (500 MHz, $CDCl_3$): δ 8.50 (d, *J* = 4.8 Hz, 2H), 6.91 (t, *J* = 4.8 Hz, 1H), 5.81 (ddt, *J* = 16.9, 10.2, 6.7 Hz, 1H), 5.02 (dq, *J* = 17.1, 1.7 Hz, 1H), 4.95 (ddt, *J* = 10.2, 2.2, 1.2 Hz, 1H), 4.35 (t, *J* = 6.6 Hz, 2H), 2.15 – 2.10 (m, 2H), 1.86 – 1.80 (m, 2H), 1.61 – 1.55 (m, 2H) ppm. **^{13}C NMR** (126 MHz, $CDCl_3$): δ 165.5, 159.4, 138.6, 114.9, 114.8, 67.6, 33.5, 28.4, 25.4 ppm. **IR** (neat, cm^{-1}): 2939, 2860, 1739, 1578, 1561, 1424, 1378, 1320, 1024, 996, 808. **HRMS**: m/z calcd. for ($C_{10}H_{14}N_2NaO$) $[M+Na]^+$: 201.0998; found 201.1006.

4.5.4. General procedure for nickel-catalysed 1,1-aminoborylation of unactivated alkenes

Product isolation as ammonium trifluoroborate inner salt

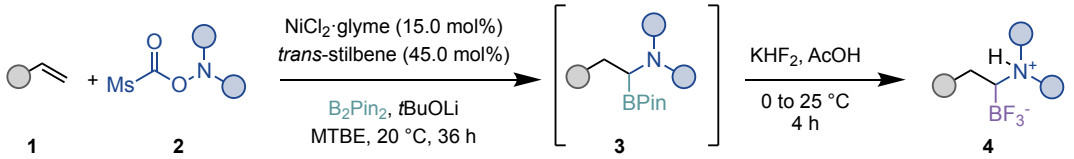

General procedure B (Schemes 20-22): Under air, a Schlenk tube equipped with a stirring bar was loaded with recrystallised, free-flowing B_2Pin_2 (86.3 mg, 0.34 mmol, 1.70 equiv.), *trans*-stilbene (16.2 mg, 0.09 mmol, 0.45 equiv.), and N–O electrophile (*if solid*, 0.30 mmol, 1.50 equiv.). The tube was transferred into a N_2-filled glovebox, followed by addition of $NiCl_2$·glyme (6.60 mg, 0.03 mmol, 0.15 equiv.) and *t*BuOLi (24.0 mg, 0.30 mmol, 1.50 equiv.), assisted by an anti-static device to ensure complete aggregation at the bottom. The tube was closed, brought out of the glovebox and connected to a N_2-filled Schlenk line. Stirring was started and the alkene (0.20 mmol, 1.00 equiv.), and anhydrous MTBE (0.3 mL) were added sequentially via syringe, followed by addition of the N–O electrophile by syringe (*if liquid*, by

weight, 0.30 mmol, 1.50 equiv.). The tube was closed, and the suspension was stirred at 20 °C (external thermostat) and 800 rpm for 18 h, during which several colour changes occurred from yellow to deep violet and finally to a slightly green solution.

Under air, a second Schlenk tube equipped with a stirring bar was loaded with another portion of B_2Pin_2 (60.9 mg, 0.24 mmol, 1.20 equiv.), and N–O electrophile (*if solid*, 0.20 mmol, 1.00 equiv.), transferred into a N_2-filled glovebox, followed by addition of *t*BuOLi (16.0 mg, 0.20 mmol, 1.00 equiv.), assisted by an anti-static device to ensure complete aggregation at the bottom. The tube was closed, brought out of the glovebox and connected to a N_2-filled Schlenk line. Then, the primary reaction solution was transferred into the newly prepared Schlenk tube by a syringe, followed by addition of N–O electrophile by syringe (*if liquid*, by weight, 0.20 mmol, 1.00 equiv.). The primary tube was rinsed with anh. MTBE (0.1 mL), which was transferred to the second tube using the previous syringe. Stirring was continued at 20 °C (external thermostat) and 800 rpm for another 18 h (GC FID control).

Then, the reaction solution was cooled to 0 °C with stirring, and a solution of anhydrous KHF_2 (312 mg, 4.00 mmol, 20.0 equiv.) in anh. AcOH (2.00 mL) was added dropwise within 2 min. After 5 min, the cooling bath was removed, and the mixture was stirred at RT for additional 4 h (GC FID control). The suspension was transferred into a 50 mL flask using 20 mL of acetone. Celite (1.00 g) was added, and the volatiles were briefly removed in vacuo at 40 °C. Toluene (30 mL) was added, and the volatiles were again removed in vacuo at 40 °C. The latter treatment was repeated, and the resulting solid was dried at 15 mbar and 40 °C for 15 min, before being purified by flash column chromatography on silica gel to isolate the ammonium BF_3 salt **4**.

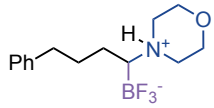

4-[1-(Difluoroboraneyl)-4-phenylbutyl]morpholin-4-ium fluoride (**4a**): Following the **general procedure B**, using 4-phenyl-1-butene (**1a**, 30.0 µL, 0.20 mmol) and N–O electrophile **2k** (solid, 1. batch: 74.8 mg, 0.30 mmol, 1.50 equiv., 2. batch: 49.9 mg, 0.20 mmol, 1.00 equiv.), flash column chromatographic purification (*n*-hexane/MTBE/acetone 2:1:1 + 1v% AcOH) afforded **4a** (38 mg, 67% yield) as an amorphous colourless solid. In an independent experiment, 40 mg (69% yield) were obtained, giving an average yield of 68%. **^{1}H NMR** (400 MHz, $CDCl_3$): δ 7.30 – 7.24 (m, 2H), 7.20 – 7.15 (m, 3H), 6.80 (br, 1H), 4.03 – 3.94 (m, 3H), 3.82 – 3.76 (m, 1H), 3.38 (d, *J* = 12.8 Hz, 1H), 3.23 – 3.12 (m, 2H), 2.97 – 2.88 (m, 1H), 2.67 (t, *J* = 7.4 Hz, 2H), 2.36 – 2.33 (m, 1H), 2.00 – 1.89 (m, 1H), 1.78 – 1.69 (m, 1H), 1.67 – 1.49 (m, 2H) ppm. **^{13}C NMR** (101 MHz, $CDCl_3$): δ 141.9, 128.6, 128.5, 126.0, 64.64, 64.659, 51.8, 48.5, 36.0, 28.2, 23.3 ppm. The carbon (CH) adjacent to boron was not observed, due to quadrupolar coupling with ^{11}B (*I* = 3/2) and ^{10}B (*I* = 3). **^{11}B NMR** (128 MHz,

$CDCl_3$): δ 2.60 ppm. **^{19}F NMR** (376 MHz, $CDCl_3$): δ -142.8 ppm. **IR** (neat, cm^{-1}): 3172, 2957, 2935, 2871, 1739, 1438, 1415, 1245, 1131, 1085, 1027, 956, 935, 902, 703. **HRMS**: m/z calcd. for ($C_{14}H_{21}F_3NNaO^{11}B$) $[M+Na]^+$: 310.1561; found 310.1568. **MP**: 165 – 167ºC.

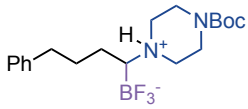

4-(*tert*-Butoxycarbonyl)-1-[1-(difluoroboraneyl)-4-phenylbutyl]piperazin-1-ium fluoride (**4b**): Following the **general procedure B**, using 4-phenyl-1-butene (**1a**, 30.0 µL, 0.20 mmol) and N-O electrophile **2m** (solid, 1. batch: 105 mg, 0.30 mmol, 1.50 equiv., 2. batch: 69.7 mg, 0.20 mmol, 1.00 equiv.), flash column chromatographic purification (*n*-hexane/MTBE/acetone 4:2:2 + 1v% AcOH to 4:2:3 + 1v% AcOH) afforded **4a** (42 mg, 54% yield) as an amorphous colourless solid. In an independent experiment, 43 mg (56% yield) were obtained, giving an average yield of 55%. **^{1}H NMR** (500 MHz, $CDCl_3$): δ 7.28 – 7.25 (m, 2H), 7.19 – 7.16 (m, 3H), 6.65 (brs, 1H), 3.46 – 3.38 (m, 2H), 3.18 – 2.99 (m, 3H), 2.77 – 2.72 (m, 1H), 2.67 – 2.64 (m, 2H), 2.39 – 2.37 (m, 1H), 1.95 – 1.91 (m, 1H), 1.70 (qd, J = 11.1, 4.1 Hz, 1H), 1.64 – 1.47 (m, 4H), 1.45 (s, 9H) ppm. **^{13}C NMR** (101 MHz, $CDCl_3$): δ 153.9, 141.9, 128.6, 128.5, 126.0, 81.4, 51.8 (2C), 48.3 (2C), 36.0, 28.4, 28.2, 23.3 ppm. The carbon (CH) adjacent to boron was not observed, due to quadrupolar coupling with ^{11}B (I = 3/2) and ^{10}B (I = 3). **^{11}B NMR** (128 MHz, $CDCl_3$): δ 2.34 ppm. **^{19}F NMR** (376 MHz, $CDCl_3$): δ -142.6 ppm. **IR** (neat, cm^{-1}): 3169, 3021, 2983, 2926, 2900, 2864, 1686, 1477, 1455, 1415, 1396, 1372, 1327, 1298, 1283, 1267, 1244, 1180, 1133, 1079, 1049, 1030, 990, 956, 936, 901, 746, 697. **HRMS**: m/z calcd. for ($C_{19}H_{30}F_3N_2NaO_2{}^{11}B$) $[M+Na]^+$: 409.2245; found 409.2256. **MP:** 198 – 200 ºC.

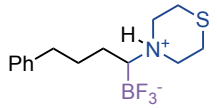

4-[1-(Difluoroboraneyl)-4-phenylbutyl]thiomorpholin-4-ium fluoride (**4c**): Following the **general procedure B**, using 4-phenyl-1-butene (**1a**, 30.0 µL, 0.20 mmol) and N-O electrophile **2n** (solid, 1. batch: 79.6 mg, 0.30 mmol, 1.50 equiv., 2. batch: 53.1 mg, 0.20 mmol, 1.00 equiv.), flash column chromatographic purification (*n*-hexane/MTBE/acetone 3:1:1 + 1v% AcOH to 2:1:1 + 1v% AcOH) afforded **4c** (23.1 mg, 38% yield) as an amorphous colourless solid. In an independent experiment, 20.0 mg (33% yield) were obtained, giving an average yield of 36%. **^{1}H NMR** (400 MHz, $CDCl_3$): δ 7.29 – 7.25 (m, 2H), 7.20 – 7.15 (m, 3H), 6.47 (brs, 1H), 3.80 (d, J = 12.8 Hz, 1H), 3.47 – 3.39 (m, 2H), 3.30 – 3.21 (m, 1H), 3.13 – 3.05 (m, 1H), 3.00 – 2.91 (m, 1H), 2.69 – 2.63 (m, 4H), 2.37 – 2.34 (m, 1H), 2.00 – 1.91 (m, 1H), 1.78 – 1.69 (m, 1H), 1.65 – 1.51 (m, 2H) ppm. **^{13}C NMR** (101 MHz, $CDCl_3$): δ 141.9, 128.6, 128.5, 126.0, 54.7, 51.0, 36.0, 28.2, 26.3, 25.9, 23.2 ppm. The carbon (CH) adjacent

to boron was not observed, due to quadrupolar coupling with ^{11}B (I = 3/2) and ^{10}B (I = 3). **^{11}BNMR** (128 MHz, $CDCl_3$): δ 2.49 ppm. **^{19}F NMR** (376 MHz, $CDCl_3$): δ -142.3 ppm. **IR** (neat, cm^{-1}): 3174, 3019, 2970, 2920, 2862, 1739, 1450, 1366, 1216, 1101, 1016, 921, 896. **HRMS**: m/z calcd. for ($C_{14}H_{21}F_3NNaS^{11}B$ $[M+Na]^+$: 326.1332; found 326.1348. **MP**: 126 – 128 ºC.

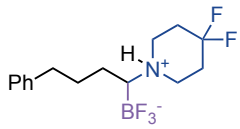

1-(1-(Difluoroboraneyl)-4-phenylbutyl)-4,4-difluoropiperidin-1-ium fluoride (**4d**): Following the **general procedure B**, using 4-phenyl-1-butene (**1a**, 30.0 µL, 0.20 mmol) and N-O electrophile **2o** (oil, 1. batch: 85.0 mg, 0.30 mmol, 1.50 equiv., 2. batch: 56.7 mg, 0.20 mmol, 1.00 equiv.), flash column chromatographic purification (*n*-hexane/MTBE/acetone 3:1:1 + 1v% AcOH to 2:1:1 + 1v% AcOH) afforded **4d** (39 mg, 60% yield) as an amorphous colourless solid. In an independent experiment, 39 mg (60% yield) were obtained, giving an average yield of 60%. **^{1}H NMR** (400 MHz, $CDCl_3$): δ 7.30 – 7.25 (m, 2H), 7.21 – 7.16 (m, 3H), 6.74 (brs, 1H), 3.61 – 3.55 (m, 1H), 3.31 – 3.22 (m, 2H), 3.00 – 2.90 (m, 1H), 2.69 – 2.51 (m, 3H), 2.44 – 2.41 (m, 1H), 2.34 – 2.18 (m, 3H), 2.01 – 1.88 (m, 1H), 1.78 – 1.68 (m, 1H), 1.65 – 1.50 (m, 2H) ppm. **^{13}C NMR** (101 MHz, $CDCl_3$): δ 141.8, 128.6, 128.5, 126.1, 118.5 (dd, J = 248.3, 239.2 Hz), 50.1 (d, J = 10.6 Hz), 45.7 (d, J = 9.9 Hz), 35.6, 31.9 (dt, J = 25.3, 22.0 Hz), 28.2, 23.2 ppm. The carbon (CH) adjacent to boron was not observed, due to quadrupolar coupling with ^{11}B (I = 3/2) and ^{10}B (I = 3). **^{11}B NMR** (128 MHz, $CDCl_3$): δ 2.72 ppm. **^{19}F NMR** (376 MHz, $CDCl_3$): δ -97.0 (d, J = 243.8 Hz), – -103.7 (d, J = 243.8 Hz), – -143.1 ppm. **IR** (neat, cm^{-1}): 3156, 2954, 2923, 2876, 1739, 1419, 1388, 1131, 1024, 1001, 930, 750. **HRMS**: m/z calcd. for ($C_{15}H_{21}F_5NNa^{11}B$) $[M+Na]^+$: 344.1579; found 344.1584. **MP**: 131 – 132 ºC.

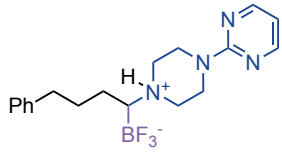

1-(1-(difluoroboraneyl)-4-phenylbutyl)-4-(pyrimidin-2-yl)piperazin-1-ium fluoride (**4e**): Following the **general procedure B**, using 4-phenyl-1-butene (**1a**, 30.0 µL, 0.20 mmol) and N-O electrophile **2p** (solid, 1. batch: 98.2 mg, 0.30 mmol, 1.50 equiv., 2. batch: 65.5 mg, 0.20 mmol, 1.00 equiv.), flash column chromatographic purification (*n*-hexane/MTBE/acetone 4:2:2 + 1v% AcOH to 4:2:3 + 1v% AcOH) afforded **4e** (39 mg, 53% yield) as an amorphous colourless solid. In an independent experiment, 37 mg (49% yield) were obtained, giving an average yield of 51%. **^{1}H NMR** (400 MHz, DMSO-d_6): δ 8.42 (d, J = 4.8 Hz, 2H), 8.30 (brs, 1H), 7.29 – 7.14 (m, 5H), 6.73 (t, J = 4.8 Hz, 1H), 4.67 – 4.62 (m, 2H), 3.28 – 3.18 (m, 4H),

3.09 – 3.01 (m, 2H), 2.60 – 2.52 (m, 2H), 2.14 (brs, 1H), 1.75 – 1.47 (m, 4H) ppm. **^{13}C NMR** (101 MHz, DMSO-d_6): δ 160.7, 158.1, 142.2, 128.24, 128.19, 125.6, 111.1, 49.3, 49.2, 40.8, 40.6, 35.6, 28.8, 25.7 ppm. The carbon (CH) adjacent to boron was not observed, due to quadrupolar coupling with ^{11}B (I = 3/2) and ^{10}B (I = 3). **^{11}B NMR** (128 MHz, $CDCl_3$): δ 2.68 ppm. **^{19}F NMR** (376 MHz, $CDCl_3$): δ -142.7 ppm. **IR** (neat, cm^{-1}): 3170, 3020, 2943, 2898, 2865, 1587, 1552, 1500, 1446, 1366, 1247, 1132, 1093, 1027, 952, 902. **HRMS**: m/z calcd. for ($C_{18}H_{24}F_3N_4Na^{11}B$) $[M+Na]^+$:387.1938; found 387.1947. **MP**: 145 - 147 ºC.

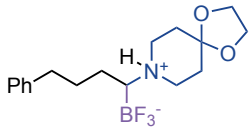

8-(1-(Difluoroboraneyl)-4-phenylbutyl)-1,4-dioxa-8-azaspiro[4.5]decan-8-ium fluoride (**4f**): Following the **general procedure B**, using 4-phenyl-1-butene (**1a**, 30.0 µL, 0.20 mmol) and N-O electrophile **2q** (solid, 1. batch: 91.6 mg, 0.30 mmol, 1.50 equiv., 2. batch: 61.1 mg, 0.20 mmol, 1.00 equiv.), flash column chromatographic purification (*n*-hexane/MTBE/acetone 3:1:1 + 1v% AcOH to 2:1:1 + 1v% AcOH) afforded **4f** (16 mg, 23% yield) as an amorphous colourless solid. In an independent experiment, 21 mg (31% yield) were obtained, giving an average yield of 27%. **^{1}H NMR** (400 MHz, $CDCl_3$): δ 7.28 – 7.24 (m, 2H), 7.20 – 7.14 (m, 3H), 6.46 (brs, 1H), 4.00 – 3.91 (m, 4H), 3.54 – 3.50 (m, 1H), 3.34 – 3.23 (m, 2H), 3.03 – 2.93 (m, 1H), 2.66 (t, J = 7.5 Hz, 2H), 2.41 – 2.29 (m, 2H), 2.08 – 1.99 (m, 1H), 1.97 – 1.88 (m, 1H), 1.81 (d, J = 14.0 Hz, 2H), 1.76 – 1.69 (m, 1H), 1.66 – 1.52 (m, 2H) ppm. **^{13}C NMR** (101 MHz, $CDCl_3$): δ 142.1, 128.6, 128.4, 125.8, 104.2, 65.0, 64.7, 51.3, 46.9, 36.1, 33.3, 33.1, 28.3, 23.3 ppm. The carbon (CH) adjacent to boron was not observed, due to quadrupolar coupling with ^{11}B (I = 3/2) and ^{10}B (I = 3). **^{11}B NMR** (128 MHz, $CDCl_3$): δ 2.79 ppm. **^{19}F NMR** (376 MHz, $CDCl_3$): δ -144.4 ppm. **IR** (neat, cm^{-1}): 3623, 3534, 3167, 3085, 3062, 3030, 2989, 2950, 2922, 2892, 1649, 1597, 1496, 1470, 1414, 1379, 1347, 1299, 1249, 1162, 1100, 1074, 1034, 993, 970, 949, 929, 850, 813, 759, 722, 698. **HRMS**: m/z calcd. for ($C_{17}H_{25}F_3NNaO_2^{11}B$) $[M+Na]^+$: 366.1823; found 366.1824. **MP**: 170 – 174 ºC.

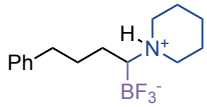

1-[1-(Difluoroboraneyl)-4-phenylbutyl]piperidin-1-ium fluoride (**4g**): Following the **general procedure B**, using 4-phenyl-1-butene (**1a**, 30.0 µL, 0.20 mmol) and N-O electrophile **2r** (solid, 1. batch: 74.2 mg, 0.30 mmol, 1.50 equiv., 2. batch: 49.5 mg, 0.20 mmol, 1.00 equiv.), flash column chromatographic purification (*n*-hexane/MTBE/acetone 3:1:1 + 1v% AcOH to 2:1:1 + 1v% AcOH) afforded **4g** (20 mg, 33% yield) as an amorphous colourless solid. In an independent experiment, 21 mg (35% yield) were obtained, giving an

average yield of 34%. **^{1}H NMR** (400 MHz, $CDCl_3$): δ 7.30 – 7.26 (m, 2H), 7.22 – 7.16 (m, 3H), 6.23 (brs, 1H), 3.57 (d, *J* = 12.4 Hz, 1H), 3.25 (d, *J* = 12.0 Hz, 1H), 3.01 – 2.91 (m, 1H), 2.74 – 2.59 (m, 3H), 2.37 – 2.33 (m, 1H), 2.12 – 1.93 (m, 2H), 1.89 – 1.79 (m, 3H), 1.77 – 1.70 (m, 1H), 1.69 – 1.58 (m, 1H), 1.54 – 1.44 (m, 1H), 1.39 – 1.26 (m, 2H) ppm. **^{13}C NMR** (101 MHz, $CDCl_3$): δ 142.2, 128.6, 128.4, 125.9, 53.6, 49.7, 36.1, 28.3, 24.2, 23.9, 23.4, 22.2 ppm. The carbon (CH) adjacent to boron was not observed, due to quadrupolar coupling with ^{11}B (*I* = 3/2) and ^{10}B (*I* = 3). **^{11}B NMR** (128 MHz, $CDCl_3$): *δ* 2.66 ppm. **^{19}F NMR** (376 MHz, $CDCl_3$): *δ* -142.3 ppm. **IR** (neat, cm^{-1}): 3186, 3015, 2969, 2931, 2869, 1739, 1453, 1376, 1217, 1094, 1060, 943, 923, 751, 700. **HRMS**: m/z calcd. for ($C_{15}H_{23}F_3NNa^{11}B$) $[M+Na]^+$: 308.1768; found 308.1772. **MP**: 145 – 146 ºC.

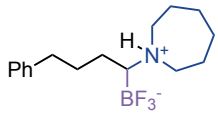

1-[1-(Difluoroboraneyl)-4-phenylbutyl]azepan-1-ium fluoride (**4h**): Following the **general procedure B**, using 4-phenyl-1-butene (**1a**, 30.0 µL, 0.20 mmol) and N-O electrophile **2s** (oil, 1. batch: 78.4 mg, 0.30 mmol, 1.50 equiv., 2. batch: 52.3 mg, 0.20 mmol, 1.00 equiv.), flash column chromatographic purification (*n*-hexane/MTBE/acetone 3:1:1 + 1v% AcOH to 2:1:1 + 1v% AcOH) afforded **4h** (15.5 mg, 26% yield) as an amorphous colourless solid. In an independent experiment, 15.5 mg (26% yield) were obtained, giving an average yield of 26%. **^{1}H NMR** (400 MHz, $CDCl_3$): *δ* 7.30 – 7.26 (m, 2H), 7.22 – 7.15 (m, 3H), 6.33 (brs, 1H), 3.57 (dd, *J* = 13.4, 6.7 Hz, 1H), 3.38 – 3.33 (m, 1H), 3.17 – 3.09 (m, 1H), 2.89 – 2.81 (m, 1H), 2.68 (t, *J* = 7.6 Hz, 2H), 2.45 (d, *J* = 12.6 Hz, 1H), 2.08 – 1.74 (m, 7H), 1.68 – 1.54 (m, 4H), 1.35 – 1.28 (m, 1H) ppm. **^{13}C NMR** (101 MHz, $CDCl_3$): *δ* 142.2, 128.6, 128.4, 125.9, 56.4, 51.1, 36.1, 28.2, 26.5, 25.9, 25.6, 25.2, 23.4 ppm. The carbon (CH) adjacent to boron was not observed, due to quadrupolar coupling with ^{11}B (*I* = 3/2) and ^{10}B (*I* = 3). **^{11}B NMR** (128 MHz, $CDCl_3$): *δ* 2.55 ppm. **^{19}F NMR** (376 MHz, $CDCl_3$): *δ* -144.3 ppm. **IR** (neat, cm^{-1}): 3207, 2925, 2861, 1739, 1454, 1422, 1366, 1090, 1058, 1018, 996. **HRMS**: m/z calcd. for ($C_{16}H_{25}F_3NNa^{11}B$) $[M+Na]^+$: 322.1924; found 322.1925. **MP**: 135 – 138 ºC.

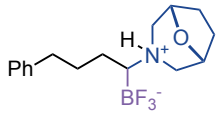

(1R*,5S*)-3-(1-(Difluoroboraneyl)-4-phenylbutyl)-8-oxa-3-azabicyclo[3.2.1]octan-3-ium fluoride (**4i**): Following the **general procedure B**, using 4-phenyl-1-butene (**1a**, 30.0 µL, 0.20 mmol) and N-O electrophile **2t** (solid, 1. batch: 82.6 mg, 0.30 mmol, 1.50 equiv., 2. batch: 55.1 mg, 0.20 mmol, 1.00 equiv.), flash column chromatographic purification (*n*-hexane/MTBE/acetone 3:1:1 + 1v% AcOH to 2:1:1 + 1v% AcOH) afforded **4i** (29 mg, 46% yield) as a colourless oil. In an independent experiment, 28 mg (44% yield) were obtained,

giving an average yield of 45%. **^{1}H NMR** (400 MHz, $CDCl_3$): δ 7.28 – 7.23 (m, 2H), 7.21 – 7.14 (m, 3H), 6.60 (brs, 1H), 4.43 (dd, *J* = 12.4, 7.1 Hz, 2H), 3.28 – 3.14 (m, 3H), 3.07 (ddd, *J* = 12.9, 11.0, 2.5 Hz, 1H), 2.65 (t, *J* = 7.4 Hz, 2H), 2.45 – 2.39 (m, 2H), 2.23 – 2.04 (m, 2H), 1.98 – 1.87 (m, 2H), 1.76 – 1.55 (m, 2H), 1.46 – 1.42 (m, 1H) ppm. **^{13}C NMR** (101 MHz, $CDCl_3$): δ 141.9, 128.6, 128.4, 125.9, 73.0, 72.3, 54.8, 52.9, 35.9, 28.2, 26.5, 26.4, 22.8 ppm. The carbon (CH) adjacent to boron was not observed, due to quadrupolar coupling with ^{11}B (*I* = 3/2) and ^{10}B (*I* = 3). **^{11}B NMR** (128 MHz, $CDCl_3$): *δ* 2.64 ppm. **^{19}F NMR** (376 MHz, $CDCl_3$): *δ* -143.6 ppm. **IR** (neat, cm^{-1}): 3186, 3085, 3060, 3026, 2957, 2938, 2866, 1707, 1654, 1603, 1496, 1479, 1454, 1350, 1299, 1251, 1142, 1063, 1025, 988, 967, 913, 878, 729, 700. **HRMS**: m/z calcd. for ($C_{16}H_{23}F_3NNaO^{11}B$) $[M+Na]^+$: 336.1717; found 336.1728.

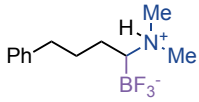

1-(Difluoroboraneyl)-N,N-dimethyl-4-phenylbutan-1-aminium fluoride (**4j**): Following the **general procedure B**, using 4-phenyl-1-butene (**1a**, 30.0 µL, 0.20 mmol) and N-O electrophile **2u** (oil, 1. batch: 62.2 mg, 0.30 mmol, 1.50 equiv., 2. batch: 41.5 mg, 0.20 mmol, 1.00 equiv.), flash column chromatographic purification (*n*-hexane/MTBE/acetone 3:1:1 + 1v% AcOH to 2:1:1 + 1v% AcOH) afforded **4j** (12 mg, 25% yield) as an amorphous colourless solid. In an independent experiment, 13 mg (27% yield) were obtained, giving an average yield of 26%. **^{1}H NMR** (400 MHz, $CDCl_3$): δ 7.29 – 7.24 (m, 2H), 7.19 – 7.15 (m, 3H), 6.90 (brs, 1H), 2.77 (d, *J* = 5.3 Hz, 3H), 2.73 – 2.60 (m, 5H), 2.36 – 2.23 (m, 1H), 2.02 – 1.89 (m, 1H), 1.77 – 1.58 (m, 2H), 1.51 – 1.43 (m, 1H) ppm. **^{13}C NMR** (101 MHz, $CDCl_3$): δ 142.0, 128.6, 128.5, 126.0, 44.1, 39.6, 36.0, 28.1, 22.6 ppm. The carbon (CH) adjacent to boron was not observed, due to quadrupolar coupling with ^{11}B (*I* = 3/2) and ^{10}B (*I* = 3). **^{11}B NMR** (128 MHz, $CDCl_3$): *δ* 2.63 ppm. **^{19}F NMR** (376 MHz, $CDCl_3$): *δ* -146.6 ppm. **IR** (neat, cm^{-1}): 3209, 3025, 2955, 2925, 2867, 1739, 1474, 1372, 1088, 1033, 979, 955, 700. **HRMS**: m/z calcd. for ($C_{12}H_{19}F_3NNa^{11}B$) $[M+Na]^+$: 268.1455; found 268.1458. **MP**: 135 – 138 ºC.

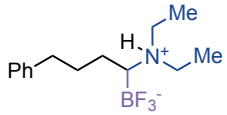

1-(Difluoroboraneyl)-N,N-diethyl-4-phenylbutan-1-aminium fluoride (**4k**): Following the **general procedure B**, using 4-phenyl-1-butene (**1a**, 30.0 µL, 0.20 mmol) and amination agent **2v** (oil, 1. batch: 70.6 mg, 0.30 mmol, 1.50 equiv., 2. batch: 47.1 mg, 0.20 mmol, 1.00 equiv.), flash column chromatographic purification (*n*-hexane/MTBE/acetone 3:1:1 + 1v% AcOH to 2:1:1 + 1v% AcOH) afforded **4k** (13 mg, 23% yield) as an amorphous colourless solid. In an independent experiment, 12 mg (22% yield) were obtained, giving an average yield of 23%. **^{1}H NMR** (400 MHz, $CDCl_3$): δ 7.28 – 7.24 (m, 2H), 7.20 – 7.14 (m, 3H), 5.79

(br s, 1H), 3.60 – 3.51 (m, 1H), 3.24 – 3.14 (m, 1H), 2.97 – 2.86 (m, 1H), 2.74 – 2.61 (m, 3H), 2.53 – 2.51 (m, 1H), 2.02 – 1.92 (m, 1H), 1.76 – 1.58 (m, 2H), 1.48 – 1.37 (m, 1H), 1.35 – 1.30 (m, 6H) ppm. **^{13}C NMR** (101 MHz, $CDCl_3$): δ 142.0, 128.6, 128.4, 125.9, 47.5, 46.8, 36.1, 28.1, 23.0, 11.5, 11.0 ppm. The carbon (CH) adjacent to boron was not observed, due to quadrupolar coupling with ^{11}B (*I* = 3/2) and ^{10}B (*I* = 3). **^{11}B NMR** (128 MHz, $CDCl_3$): δ 2.55 ppm. **^{19}F NMR** (376 MHz, $CDCl_3$): δ -144.3 ppm. **IR** (neat, cm^{-1}): 3189, 3022, 2944, 2926, 2867, 1739, 1464, 1028, 990, 971. **HRMS**: m/z calcd. for ($C_{14}H_{23}F_3NNa^{10}B$) $[M+Na]^+$: 295.1804; found 295.1818. **MP**: 140 – 143 ºC.

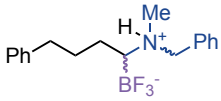

***N*-benzyl-1-(difluoroboraneyl)-N-methyl-4-phenylbutan-1-aminium fluoride** (**4l**): Following the **general procedure B**, using 4-phenyl-1-butene (**1a**, 30.0 µL, 0.20 mmol) and N-O electrophile **2w** (solid, 1. batch: 85.0 mg, 0.30 mmol, 1.50 equiv., 2. batch: 56.7 mg, 0.20 mmol, 1.00 equiv.), flash column chromatographic purification (*n*-hexane/MTBE/acetone 4:2:2 + 1v% AcOH to 4:2:3 + 1v% AcOH) afforded **4l** (21 mg, 33% yield) as an amorphous colourless solid. In an independent experiment, 17 mg (27% yield) were obtained, giving an average yield of 30%. **^{1}H NMR** (500 MHz, $CDCl_3$): *δ* 7.44 – 7.26 (m, 7H), 7.23 – 7.16 (m, 3H), 6.54 (brs, 1H), 4.71 and 3.48 (d, *J* = 13.0 Hz and *J* = 13.1, 1H), 4.19 – 3.96 (m, 1H), 2.72 and 2.65 (d, *J* = 5.4 Hz and *J* = 5.4 Hz, 3H), 2.72 – 2.59 and 2.45 – 2.43 (m, 1H), 2.07 – 1.96 (m, 1H), 1.90 – 1.83 and 1.81 – 1.75 (m, 1H), 1.74 – 1.67 (m, 1H), 1.63 – 1.54 (m, 3H) ppm. **^{13}C NMR** (126 MHz, $CDCl_3$): *δ* 142.1, 142.0, 130.9, 130.5, 130.2, 130.1, 129.9, 129.69, 129.67, 128.7, 128.6, 128.5, 126.01, 125.95, 59.6, 56.9, 39.3, 37.6, 36.0, 35.9, 28.0, 22.9, 22.5 ppm. The carbon (CH) adjacent to boron was not observed, due to quadrupolar coupling with ^{11}B (*I* = 3/2) and ^{10}B (*I* = 3). **^{11}B NMR** (128 MHz, $CDCl_3$): *δ* 2.70 ppm. **^{19}F NMR** (376 MHz, $CDCl_3$): *δ* -144.0, -145.2 ppm. **IR** (neat, cm^{-1}): 3175, 2925, 2853, 1495, 1471, 1454, 1435, 1411, 1279, 1214, 1154, 1134, 1095, 1076, 1051, 1039, 1016, 983, 945, 928, 914, 862, 801, 759, 700. **HRMS**: m/z calcd. for ($C_{18}H_{23}F_3NNa^{11}B$) $[M+Na]^+$:344.1768; found 344.1768. **MP**: 163 – 167 ºC.

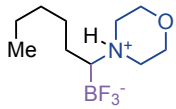

4-(1-(Difluoroboraneyl)hexyl)morpholin-4-ium fluoride (**4m**): Following the **general procedure B**, using 1-hexene (**1b**, 25.0 µL, 0.20 mmol) and N-O electrophile **2k** (solid, 1. batch: 74.8 mg, 0.30 mmol, 1.50 equiv., 2. batch: 49.9 mg, 0.20 mmol, 1.00 equiv.), flash column chromatographic purification (*n*-hexane/MTBE/acetone 2:1:1 + 1v% AcOH to 1:1:1 *n*-hexane/MTBE/acetone) afforded **4m** (27.6 mg, 58% yield) as an amorphous colourless

solid. In an independent experiment, 29.5 mg (62% yield) were obtained, giving an average yield of 60%. **^{1}H NMR** (500 MHz, $CDCl_3$): δ 6.86 (brs, 1H), 4.07 – 3.98 (m, 3H), 3.85 – 3.80 (m, 1H), 3.43 – 3.40 (m, 1H), 3.29 (ddt, *J* = 15.1, 10.9, 5.7 Hz, 1H), 3.20 – 3.18 (m, 1H), 3.02 – 2.94 (m, 1H), 2.35 – 2.31 (m, 1H), 1.74 – 1.67 (m, 1H), 1.60 – 1.54 (m, 1H), 1.50 – 1.46 (m, 1H), 1.35 – 1.27 (m, 5H), 0.90 – 0.87 (m, 3H) ppm. **^{13}C NMR** (126 MHz, $CDCl_3$): δ 64.64, 64.59, 51.8, 48.5, 32.4, 26.6, 24.0, 22.6, 14.2 ppm. The carbon (CH) adjacent to boron was not observed, due to quadrupolar coupling with ^{11}B (*I* = 3/2) and ^{10}B (*I* = 3). **^{11}B NMR** (160 MHz, $CDCl_3$): δ 2.59 ppm. **^{19}F NMR** (471 MHz, $CDCl_3$): δ -142.8 ppm. **IR** (neat, cm^{-1}): 3168, 2931, 2863, 1460, 1372, 1252, 1127, 1023, 947, 901. **HRMS**: m/z calcd. for ($C_{10}H_{21}F_3NNaO^{11}B$) $[M+Na]^+$: 262.1561; found 262.1570. **MP:** 134 – 137 °C.

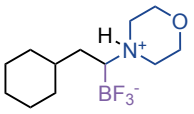

4-(2-Cyclohexyl-1-(difluoroboraneyl)ethyl)morpholin-4-ium fluoride (**4n**): Following the **general procedure B**, using vinylcyclohexane (**1c**, 22.0 mg, 0.20 mmol) and N-O electrophile **2k** (solid, 1. batch: 74.8 mg, 0.30 mmol, 1.50 equiv., 2. batch: 49.9 mg, 0.20 mmol, 1.00 equiv.), flash column chromatographic purification (*n*-hexane/MTBE/acetone 3:2:2 + 1v% AcOH) afforded **4n** (20 mg, 38% yield) as an amorphous colourless solid. In an independent experiment, 16 mg (30% yield) were obtained, giving an average yield of 34%. **^{1}H NMR** (400 MHz, $CDCl_3$): δ 6.84 (brs, 1H), 4.06 – 3.97 (m, 3H), 3.85 – 3.78 (m, 1H), 3.45 – 3.41 (m, 1H), 3.26 (brs, 1H), 3.18 – 3.15 (m, 1H), 3.01 – 2.95 (m, 1H), 2.50 – 2.45 (m, 1H), 1.84 (d, *J* = 12.7 Hz, 1H), 1.76 – 1.63 (m, 4H), 1.54 – 1.44 (m, 1H), 1.32 – 1.12 (m, 5H), 1.01 – 0.91 (m, 1H), 0.83 – 0.74 (m, 1H) ppm. **^{13}C NMR** (101 MHz, $CDCl_3$): δ 64.7, 64.6, 51.6, 48.4, 34.9, 34.8, 32.7, 31.4, 26.7, 26.4, 26.2 ppm. The carbon (CH) adjacent to boron was not observed, due to quadrupolar coupling with ^{11}B (*I* = 3/2) and ^{10}B (*I* = 3). **^{11}B NMR** (128 MHz, $CDCl_3$): δ 2.76 ppm. **^{19}F NMR** (376 MHz, $CDCl_3$): δ -143.4 ppm. **IR** (neat, cm^{-1}): 3154, 2924, 2850, 1459, 1448, 1370, 1346, 1283, 1252, 1181, 1129, 1100, 1074, 1048, 1014, 973, 962, 930, 903, 869, 581. **HRMS**: m/z calcd. for ($C_{12}H_{23}F_3NNaO^{11}B$) $[M+Na]^+$: 288.1717; found 288.1721. **MP**: 186 – 189 ºC.

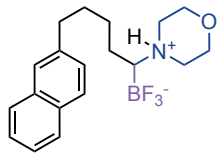

4-(1-(Difluoroboraneyl)-5-(naphthalen-2-yl)pentyl)morpholin-4-ium fluoride (**4o**): Following the **general procedure B**, using 2-(pent-4-en-1-yl)naphthalene (**1d**, 39.3 mg, 0.20 mmol) and N-O electrophile **2k** (solid, 1. batch: 74.8 mg, 0.30 mmol, 1.50 equiv., 2. batch: 49.9 mg, 0.20 mmol, 1.00 equiv.), flash column chromatographic purification (*n*-

hexane/MTBE/acetone 3:2:2 + 1v% AcOH) afforded **4o** (41 mg, 58% yield) as an amorphous colourless solid. In an independent experiment, 36 mg (51% yield) were obtained, giving an average yield of 55%. **^{1}H NMR** (400 MHz, $CDCl_3$) δ 7.81 – 7.75 (m, 3H), 7.61 (brs, 1H), 7.47 – 7.39 (m, 2H), 7.32 (dd, *J* = 8.4, 1.8 Hz, 1H), 6.81 (brs, 1H), 4.02 – 3.89 (m, 3H), 3.83 – 3.76 (m, 1H), 3.39 (d, *J* = 12.7 Hz, 1H), 3.22 – 3.07 (m, 2H), 2.97 – 2.72 (m, 3H), 2.29 (br, 1H), 1.82 – 1.62 (m, 4H), 1.57 – 1.44 (m, 1H), 1.42 – 1.32 (m, 1H) ppm. **^{13}C NMR** (101 MHz, $CDCl_3$) δ 140.1, 133.8, 132.1, 128.0, 127.7, 127.54, 127.49, 126.5, 126.0, 125.2, 64.6, 64.5, 51.8, 48.5, 36.1, 31.8, 26.6, 24.0 ppm. The carbon (CH) adjacent to boron was not observed, due to quadrupolar coupling with ^{11}B (*I* = 3/2) and ^{10}B (*I* = 3). **^{11}B NMR** (128 MHz, $CDCl_3$) δ 2.68 ppm. **^{19}F NMR** (376 MHz, $CDCl_3$) δ -142.9 ppm. **IR** (neat, cm^{-1}): 3196, 3166, 3051, 3016, 2972, 2946, 2925, 2896, 2876, 2862, 2823, 1454, 1423, 1285, 1254, 1161, 1122, 1087, 1056, 1041, 980, 959, 931, 917, 850, 782, 726. **HRMS**: m/z calcd. for ($C_{19}H_{25}F_3NNaO^{11}B$) $[M+Na]^+$: 374.1874; found 374.1878. **MP**: 155 – 159 ºC.

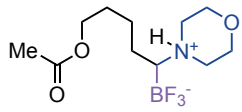

4-(5-Acetoxy-1-(difluoroboraneyl)pentyl)morpholin-4-ium fluoride (**4p**): Following the **general procedure B**, using pent-4-en-1-yl acetate (**1e**, 25.6 mg, 0.20 mmol) and N-O electrophile **2k** (solid, 1. batch: 74.8 mg, 0.30 mmol, 1.50 equiv., 2. batch: 49.9 mg, 0.20 mmol, 1.00 equiv.), flash column chromatographic purification (*n*-hexane/MTBE/acetone 3:2:2 + 1v% AcOH) afforded **4p** (27 mg, 48% yield) as an amorphous colourless solid. In an independent experiment, 32 mg (56% yield) were obtained, giving an average yield of 52%. **^{1}H NMR** (400 MHz, $CDCl_3$) δ 6.84 (brs, 1H), 4.12 – 3.98 (m, 5H), 3.85 – 3.78 (m, 1H), 3.41 (d, *J* = 12.7 Hz, 1H), 3.34 – 3.25 (m, 1H), 3.18 (d, *J* = 12.1 Hz, 1H), 3.03 – 2.93 (m, 1H), 2.33 -2.31 (m, 1H), 2.04 (s, 3H), 1.78 – 1.60 (m, 4H), 1.58 – 1.47 (m, 1H), 1.41 – 1.29 (m, 1H) ppm. **^{13}C NMR** (101 MHz, $CDCl_3$) δ 171.4, 64.6, 64.5, 64.2, 51.8, 48.6, 29.0, 23.6, 23.2, 21.1 ppm. The carbon (CH) adjacent to boron was not observed, due to quadrupolar coupling with ^{11}B (*I* = 3/2) and ^{10}B (*I* = 3). **^{11}B NMR** (128 MHz, $CDCl_3$) δ 2.51 ppm. **^{19}F NMR** (376 MHz, $CDCl_3$) δ -142.9 ppm. **IR** (neat, cm^{-1}): 3170, 2969, 2945, 2867, 1736, 1469, 1453, 1439, 1383, 1368, 1332, 1244, 1125, 1100, 1039, 995, 952, 931, 899, 821. **HRMS**: m/z calcd. for ($C_{11}H_{21}F_3NNaO_3{}^{11}B$) $[M+Na]^+$: 306.1459; found 306.1467. **MP**: 112 – 114 ºC.

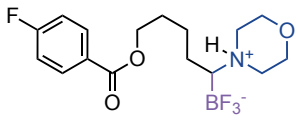

4-(1-(Difluoroboraneyl)-6-((4-fluorobenzoyl)oxy)hexyl)morpholin-4-ium fluoride (**4q**): Following the **general procedure B**, using hex-5-en-1-yl 4-fluorobenzoate (**1f**, 44.5 mg, 0.20 mmol) and N-O electrophile **2k** (solid, 1. batch: 74.8 mg, 0.30 mmol, 1.50 equiv., 2. batch:

49.9 mg, 0.20 mmol, 1.00 equiv.), flash column chromatographic purification (*n*-hexane/MTBE/acetone 3:2:2 + 1v% AcOH) afforded **4q** (40 mg, 53% yield) as an amorphous colourless solid. In an independent experiment, 41 mg (55% yield) were obtained, giving an average yield of 54%. **^{1}H NMR** (400 MHz, $CDCl_3$): δ 8.07 – 8.02 (m, 2H), 7.13 – 7.07 (m, 2H), 6.84 (brs, 1H), 4.30 (t, *J* = 6.6 Hz, 2H), 4.06 – 3.98 (m, 3H), 3.86 – 3.79 (m, 1H), 3.42 (d, *J* = 12.5 Hz, 1H), 3.34 – 3.26 (m, 1H), 3.18 (d, *J* = 12.4 Hz, 1H), 3.03 – 2.93 (m, 1H), 2.35 – 2.32 (m, 1H), 1.84 – 1.61 (m, 4H), 1.55 – 1.45 (m, 3H), 1.40 – 1.29 (m, 1H) ppm. **^{13}C NMR** (101 MHz, $CDCl_3$): δ 165.84 (d, *J* = 253.8 Hz), 165.83, 132.2 (d, *J* = 9.2 Hz), 126.8 (d, *J* = 2.9 Hz), 115.6 (d, *J* = 22.0 Hz), 65.2, 64.64, 64.57, 51.8, 48.5, 28.7, 26.7, 26.6, 24.0 ppm. The carbon (CH) adjacent to boron was not observed, due to quadrupolar coupling with ^{11}B (*I* = 3/2) and ^{10}B (*I* = 3). **^{11}B NMR** (128 MHz, $CDCl_3$): δ 2.72 ppm. **^{19}F NMR** (376 MHz, $CDCl_3$): δ -106.0, -142.9 ppm. **IR** (neat, cm^{-1}): 3170, 2955, 2930, 2891, 2871, 1720, 1604, 1509, 1473, 1455, 1413, 1384, 1299, 1274, 1256, 1230, 1126, 1075, 1055, 1011, 957, 947, 858, 766, 687, 609. **HRMS**: m/z calcd. for ($C_{17}H_{24}F_4NNaO_3{}^{11}B$) $[M+Na]^+$: 400.1678; found 400.1671. **MP**: 121 – 124 ºC.

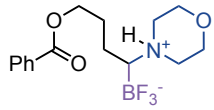

4-(4-(Benzoyloxy)-1-(difluoroboraneyl)butyl)morpholin-4-ium fluoride (**4r**): Following the **general procedure B**, using but-3-en-1-yl benzoate (**1g**, 35.2 mg, 0.20 mmol) and N-O electrophile **2k** (solid, 1. batch: 74.8 mg, 0.30 mmol, 1.50 equiv., 2. batch: 49.9 mg, 0.20 mmol, 1.00 equiv.), flash column chromatographic purification (*n*-hexane/MTBE/acetone 3:2:2 + 1v% AcOH) afforded **4r** (33 mg, 49% yield) as an amorphous colourless solid. In an independent experiment, 30 mg (45% yield) were obtained, giving an average yield of 47%. **^{1}H NMR** (400 MHz, $CDCl_3$): δ 8.06 – 8.03 (m, 2H), 7.58 – 7.54 (m, 1H), 7.47 – 7.42 (m, 2H), 6.88 (brs, 1H), 4.44 – 4.32 (m, 2H), 4.07 – 3.98 (m, 3H), 3.87 – 3.80 (m, 1H), 3.44 (d, *J* = 12.6 Hz, 1H), 3.34 – 3.19 (m, 2H), 3.06 – 2.97 (m, 1H), 2.44 – 2.42 (m, 1H), 2.14 – 2.02 (m, 1H), 1.89 – 1.76 (m, 2H), 1.74 – 1.68 (m, 1H) ppm. **^{13}C NMR** (101 MHz, $CDCl_3$): δ 166.8, 133.1, 130.4, 129.7, 128.6, 64.7, 64.62, 64.55, 51.8, 48.7, 26.1, 20.5 ppm. The carbon (CH) adjacent to boron was not observed, due to quadrupolar coupling with ^{11}B (*I* = 3/2) and ^{10}B (*I* = 3). **^{11}B NMR** (128 MHz, $CDCl_3$): δ 2.61 ppm. **^{19}F NMR** (376 MHz, $CDCl_3$): δ -142.7 ppm. **IR** (neat, cm^{-1}): 3180, 2962, 2923, 2883, 1709, 1600, 1454, 1395, 1314, 1282, 1255, 1123, 1097, 1052, 1023, 976, 932, 904, 876, 714, 678. **HRMS**: m/z calcd. for ($C_{15}H_{21}F_3NNaO_3{}^{11}B$) $[M+Na]^+$: 354.1459; found 354.1450. **MP**: 144 – 147 ºC.

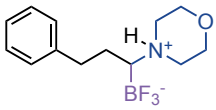

4-(1-(Difluoroboraneyl)-3-phenylpropyl)morpholin-4-ium fluoride (**4s**): Following the **general procedure B**, using allylbenzene (**1h**, 23.6 mg, 0.20 mmol) and N-O electrophile **2k** (solid, 1. batch: 74.8 mg, 0.30 mmol, 1.50 equiv., 2. batch: 49.9 mg, 0.20 mmol, 1.00 equiv.), flash column chromatographic purification (*n*-hexane/MTBE/acetone 3:2:2 + 1v% AcOH) afforded **4s** (30 mg, 55% yield) as an amorphous colourless solid. In an independent experiment, 28 mg (51% yield) were obtained, giving an average yield of 53%. **^{1}H NMR** (400 MHz, $CDCl_3$): δ 7.32 – 7.16 (m, 5H), 6.80 (brs, 1H), 4.03 – 3.96 (m, 3H), 3.83 – 3.77 (m, 1H), 3.43 (d, *J* = 12.7 Hz, 1H), 3.28 – 3.18 (m, 1H), 3.10 (d, *J* = 12.2 Hz, 1H), 3.01 – 2.91 (m, 2H), 2.60 – 2.52 (m, 1H), 2.41 – 2.38 (m, 1H), 2.15 – 2.02 (m, 1H), 1.81 – 1.78 (m, 1H) ppm. **^{13}C NMR** (101 MHz, $CDCl_3$): δ 141.9, 128.7, 128.6, 126.3, 64.64, 64.56, 51.6, 48.8, 32.9, 26.3 ppm. The carbon (CH) adjacent to boron was not observed, due to quadrupolar coupling with ^{11}B (*I* = 3/2) and ^{10}B (*I* = 3). **^{11}B NMR** (128 MHz, $CDCl_3$): δ 2.78 ppm. **^{19}F NMR** (376 MHz, $CDCl_3$): δ -142.2 ppm. **IR** (neat, cm^{-1}): 3192, 3085, 3061, 3030, 2961, 2922, 2853, 1602, 1497, 1456, 1412, 1278, 1217, 1146, 1124, 1087, 1051, 1018, 963, 941, 906, 865, 820, 786, 734, 701, 582. **HRMS**: m/z calcd. for ($C_{13}H_{19}F_3NNaO^{11}B$) $[M+Na]^+$: 296.1404; found 296.1404. **MP**: 190 – 195 ºC.

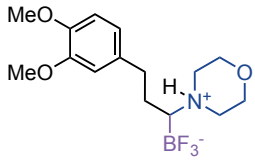

4-(1-(Difluoroboraneyl)-3-(3-fluorophenyl)propyl)morpholin-4-ium fluoride (**4t**): Following the **general procedure B**, using 4-allyl-1,2-dimethoxybenzene (**1i**, 35.6 mg, 0.20 mmol) and N-O electrophile **2k** (solid, 1. batch: 74.8 mg, 0.30 mmol, 1.50 equiv., 2. batch: 49.9 mg, 0.20 mmol, 1.00 equiv.), flash column chromatographic purification (*n*-hexane/MTBE/acetone 3:2:2 + 1v% AcOH) afforded **4t** (36 mg, 54% yield) as an amorphous colourless solid. In an independent experiment, 33 mg (50% yield) were obtained, giving an average yield of 52%. **^{1}H NMR** (400 MHz, $CDCl_3$): *δ* 6.86 – 6.76 (m, 4H), 4.03 – 3.97 (m, 3H), 3.87 (s, 3H), 3.85 (s, 3H), 3.83 – 3.76 (m, 1H), 3.43 (d, *J* = 12.7 Hz, 1H), 3.30 – 3.20 (m, 1H), 3.13 – 3.10 (m, 1H), 3.03 – 2.85 (m, 2H), 2.54 – 2.47 (m, 1H), 2.41 – 2.39 (m, 1H), 2.09 – 1.99 (m, 1H), 1.79 – 1.77 (m, 1H) ppm. **^{13}C NMR** (126 MHz, $CDCl_3$): *δ* 149.1, 147.6, 134.6, 120.3, 112.1, 111.5, 64.6, 64.5, 56.1, 56.0, 51.7, 48.8, 32.5, 26.6. The carbon (CH) adjacent to boron was not observed, due to quadrupolar coupling with ^{11}B (*I* = 3/2) and ^{10}B (*I* = 3). **^{11}B NMR** (128 MHz, $CDCl_3$): *δ* 2.92 ppm. **^{19}F NMR** (376 MHz, $CDCl_3$): *δ* -142.5 ppm. **IR** (neat, cm^{-1}): 3167, 3018, 2973, 2954, 2923, 2878, 2834, 1591, 1517, 1464, 1444, 1416,

1372, 1261, 1225, 1155, 1135, 1121, 1081, 1046, 1026, 979, 954, 926, 901. **HRMS**: m/z calcd. for ($C_{15}H_{23}F_3NNaO_3{}^{11}B$) $[M+Na]^+$: 356.1615; found 356.1617. **MP**: 168 – 171 ºC.

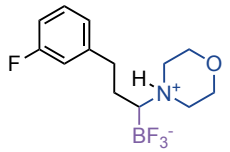

4-(1-(Difluoroboraneyl)-3-(3-fluorophenyl)propyl)morpholin-4-ium fluoride (**4u**): Following the **general procedure B**, using 1-allyl-3-fluorobenzene (**1j**, 27.2 mg, 0.20 mmol) and N-O electrophile **2k** (solid, 1. batch: 74.8 mg, 0.30 mmol, 1.50 equiv., 2. batch: 49.9 mg, 0.20 mmol, 1.00 equiv.), flash column chromatographic purification (*n*-hexane/MTBE/acetone 3:2:2 + 1v% AcOH) afforded **4u** (22 mg, 37% yield) as an amorphous colourless solid. In an independent experiment, 17 mg (29% yield) were obtained, giving an average yield of 33%. **^{1}H NMR** (400 MHz, DMSO-d_6): δ 8.36 (brs, 1H), 7.34 – 7.29 (m, 1H), 7.06 – 6.97 (m, 3H), 3.88 (d, J = 12.1 Hz, 2H), 3.76 – 3.64 (m, 2H), 3.21 – 3.10 (m, 4H), 2.77 – 2.70 (m, 1H), 2.63 – 2.55 (m, 1H), 2.08 (brs, 1H), 1.92 – 1.80 (m, 2H) ppm. **^{13}C NMR** (101 MHz, DMSO-d_6): δ 162.3 (d, J = 242.9 Hz), 145.3 (d, J = 7.3 Hz), 124.4 (d, J = 2.6 Hz), 114.8 (d, J = 20.7 Hz), 112.5 (d, J = 20.9 Hz), 63.7, 63.6, 49.82, 49.79, 32.3, 27.5 ppm. The carbon (CH) adjacent to boron was not observed, due to quadrupolar coupling with ^{11}B (I = 3/2) and ^{10}B (I = 3). **^{11}B NMR** (128 MHz, DMSO-d_6): δ 2.44 ppm. **^{19}F NMR** (376 MHz, DMSO-d_6): δ -114.0, -138.6 ppm. **IR** (neat, cm^{-1}): 3193, 2952, 2921, 1874, 2854, 1614, 1585, 1488, 1456, 1411, 1383, 1290, 1278, 1254, 1175, 1145, 1124, 1088, 1079, 1052, 1019, 964, 929, 905, 868, 790, 744, 684. **HRMS**: m/z calcd. for ($C_{13}H_{18}F_4NO^{11}B$) $[M+Na]^+$: 314.1310; found 314.1310. **MP**: 175 – 181 ºC.

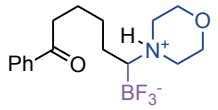

4-(1-(Difluoroboraneyl)-6-oxo-6-phenylhexyl)morpholin-4-ium fluoride (**4v**): Following the **general procedure B**, using 1-phenylhex-5-en-1-one (**1k**, 34.8 mg, 0.20 mmol) and N-O electrophile **2k** (solid, 1. batch: 74.8 mg, 0.30 mmol, 1.50 equiv., 2. batch: 49.9 mg, 0.20 mmol, 1.00 equiv.), flash column chromatographic purification (*n*-hexane/MTBE/acetone 3:2:2 + 1v% AcOH) afforded **4v** (21 mg, 32% yield) as an amorphous colourless solid. In an independent experiment, 22 mg (34% yield) were obtained, giving an average yield of 33%. **^{1}H NMR** (400 MHz, $CDCl_3$): δ 7.96 – 7.93 (m, 2H), 7.58 – 7.53 (m, 1H), 7.48 – 7.43 (m, 2H), 6.91 (brs, 1H), 4.03 – 3.99 (m, 3H), 3.92 – 3.85 (m, 1H), 3.42 – 3.29 (m, 2H), 3.21 – 3.09 (m, 2H), 3.02 (t, J = 7.1 Hz, 2H), 2.41 – 2.38 (m, 1H), 1.84 – 1.73 (m, 3H), 1.63 – 1.56 (m, 2H), 1.47 – 1.39 (m, 1H) ppm. **^{13}C NMR** (101 MHz, $CDCl_3$): δ 200.8, 137.0, 133.3, 128.8, 128.2, 64.7, 64.6, 51.5, 49.1, 38.4, 26.4, 24.1 (2C) ppm. The carbon (CH) adjacent to boron was

not observed, due to quadrupolar coupling with ^{11}B (I = 3/2) and ^{10}B (I = 3). **^{11}B NMR** (128 MHz, $CDCl_3$): δ 2.75 ppm. **^{19}F NMR** (376 MHz, $CDCl_3$): δ -142.7 ppm. **IR** (neat, cm^{-1}): 3179, 3140, 2928, 2887, 2868, 1686, 1662, 1594, 1578. 1450, 1405, 1363, 1301, 1281, 1259, 1231, 1199, 1126, 1090, 1064, 1045, 1026, 1001, 969, 930, 908, 731, 692. **HRMS**: m/z calcd. for ($C_{16}H_{23}F_3NNaO_2{}^{11}B$) $[M+Na]^+$: 352.1666; found 352.1660. **MP**: 149 – 152 ºC.

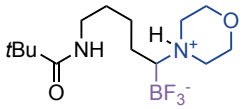

4-(1-(Difluoroboraneyl)-5-pivalamidopentyl)morpholin-4-ium fluoride (**4w**): Following the **general procedure B**, using N-(pent-4-en-1-yl)pivalamide (**1l**, 33.9 mg, 0.20 mmol) and N-O electrophile **2k** (solid, 1. batch: 74.8 mg, 0.30 mmol, 1.50 equiv., 2. batch: 49.9 mg, 0.20 mmol, 1.00 equiv.), flash column chromatographic purification (*n*-hexane/MTBE/acetone 3:2:2 + 1v% AcOH) afforded **4w** (43 mg, 67% yield) as an amorphous colourless solid. In an independent experiment, 39 mg (60% yield) were obtained, giving an average yield of 64%. **^1H NMR** (400 MHz, $CDCl_3$) δ 7.19 (brs, 1H), 6.04 (t, J = 5.9 Hz, 1H), 4.00 – 3.95 (m, 3H), 3.92 – 3.86 (m, 1H), 3.42 – 3.31 (m, 2H), 3.30 – 3.22 (m, 3H), 3.17 – 3.09 (m, 1H), 2.26 (brs, 1H), 1.78 – 1.69 (m, 1H), 1.57 – 1.48 (m, 4H), 1.33 – 1.27 (m, 1H), 1.17 (s, 9H) ppm. **^{13}C NMR** (101 MHz, $CDCl_3$) δ 179.6, 64.50, 64.46, 51.0, 50.4, 38.8, 38.6, 29.7, 27.7, 24.2, 23.8 ppm. The carbon (CH) adjacent to boron was not observed, due to quadrupolar coupling with ^{11}B (I = 3/2) and ^{10}B (I = 3). **^{11}B NMR** (128 MHz, $CDCl_3$) δ 2.70 ppm. **^{19}F NMR** (376 MHz, $CDCl_3$) δ -141.8 ppm. **IR** (neat, cm^{-1}): 3415, 2969, 2869, 1739, 1625, 1535, 1457, 1366, 1215, 1127, 995. **HRMS**: m/z calcd. for ($C_{14}H_{28}F_3N_2NaO_2{}^{11}B$) $[M+Na]^+$: 347.2088; found 347.2080. **MP:** 111 – 113 ºC.

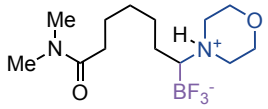

4-(1-(Difluoroboraneyl)-7-(dimethylamino)-7-oxoheptyl)morpholin-4-ium fluoride (**4x**): Following the **general procedure B**, using N,N-dimethylhept-6-enamide (**1m**, 31.0 mg, 0.20 mmol) and N-O electrophile **2k** (solid, 1. batch: 74.8 mg, 0.30 mmol, 1.50 equiv., 2. batch: 49.9 mg, 0.20 mmol, 1.00 equiv.), flash column chromatographic purification (*n*-hexane/MTBE/acetone 3:2:2 + 1v% AcOH) afforded **4x** (36 mg, 58% yield) as an amorphous colourless solid. In an independent experiment, 36 mg (58% yield) were obtained, giving an average yield of 58%. **^1H NMR** (400 MHz, $CDCl_3$): δ 7.09 (brs, 1H), 3.99 – 3.95 (m, 3H), 3.89 – 3.83 (m, 1H), 3.37 – 3.27 (m, 2H), 3.20 – 3.07 (m, 2H), 2.99 (s, 3H), 2.91 (s, 3H), 2.33 – 2.29 (m, 3H), 1.78 – 1.68 (m, 1H), 1.66 – 1.59 (m, 2H), 1.58 – 1.47 (m, 2H), 1.41 – 1.28 (m, 3H) ppm. **^{13}C NMR** (101 MHz, $CDCl_3$): δ 173.5, 64.52, 64.46, 51.1, 49.4, 37.5, 35.6, 33.0, 29.2, 26.2, 24.6, 24.3 ppm. The carbon (CH) adjacent to boron was not observed, due to

quadrupolar coupling with ^{11}B (I = 3/2) and ^{10}B (I = 3). **^{11}B NMR** (128 MHz, $CDCl_3$): δ 2.43 ppm. **^{19}F NMR** (376 MHz, $CDCl_3$): δ -142.6 ppm. **IR** (neat, cm^{-1}): 2931, 2866, 1738, 1614, 1457, 1402, 1368, 1125, 1036. **HRMS**: m/z calcd. for ($C_{13}H_{26}F_3N_2NaO_2{}^{11}B$) $[M+Na]^+$: 333.1932; found 333.1938. **MP:** 142 – 147 ºC.

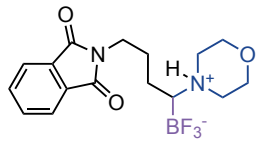

4-(1-(Difluoroboraneyl)-5-(1,3-dioxoisoindolin-2-yl)pentyl)morpholin-4-ium fluoride (**4y**): Following the **general procedure B**, using 2-(pent-4-en-1-yl)isoindoline-1,3-dione (**1n**, 43.1 mg, 0.20 mmol) and N-O electrophile **2k** (solid, 1. batch: 74.8 mg, 0.30 mmol, 1.50 equiv., 2. batch: 49.9 mg, 0.20 mmol, 1.00 equiv.), flash column chromatographic purification (*n*-hexane/MTBE/acetone 2:1:1 + 1v% AcOH to 1:1:1 *n*-hexane/MTBE/acetone) afforded **4y** (29 mg, 39% yield) as an amorphous colourless solid. In an independent experiment, 29 mg (39% yield) were obtained, giving an average yield of 39%. **^1H NMR** (400 MHz, DMSO-d_6): δ 8.25 (brs, 1H), 7.87 – 7.81 (m, 4H), 3.90 – 3.82 (m, 2H), 3.74 – 3.61 (m, 2H), 3.55(t, J = 3.6 Hz, 2H), 3.23 – 3.02 (m, 4H), 2.06 – 1.96 (m, 1H), 1.64 – 1.24 (m, 6H) ppm. **^{13}C NMR** (101 MHz, DMSO-d_6): δ 168.0, 134.4, 131.6, 123.0, 63.7, 63.6, 49.9, 49.8, 37.4, 28.3, 25.4, 24.1 ppm. The carbon (CH) adjacent to boron was not observed, due to quadrupolar coupling with ^{11}B (I = 3/2) and ^{10}B (I = 3). **^{11}B NMR** (128 MHz, DMSO-d_6): δ 2.36 ppm. **^{19}F NMR** (471 MHz, $CDCl_3$): δ -142.8 ppm. **IR** (neat, cm^{-1}): 3187, 2928, 2872, 1766, 1710, 1398, 1368, 1125, 1037, 917, 719. **HRMS**: m/z calcd. for ($C_{17}H_{22}F_3N_2NaO_3{}^{11}B$) $[M+Na]^+$: 393.1568 found 393.1576. **MP:** 144 – 145 ºC.

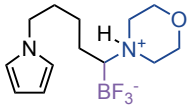

4-(1-(Difluoroboraneyl)-5-(1*H*-pyrrol-1-yl)pentyl)morpholin-4-ium fluoride (**4z**): Following the **general procedure B**, using 1-(pent-4-en-1-yl)-1*H*-pyrrole (**1o**, 27.0 mg, 0.20 mmol) and N-O electrophile **2k** (solid, 1. batch: 74.8 mg, 0.30 mmol, 1.50 equiv., 2. batch: 49.9 mg, 0.20 mmol, 1.00 equiv.), flash column chromatographic purification (*n*-hexane/MTBE/acetone 2:1:1 + 1v% AcOH to 1:1:1 *n*-hexane/MTBE/acetone) afforded **4z** (56.3 mg, 97% yield) as a colourless oil. In an independent experiment, 50.5 mg (87% yield) were obtained, giving an average yield of 92%. **^1H NMR** (500 MHz, $CDCl_3$): δ 6.80 (brs, 1H), 6.66 (t, J = 2.1 Hz, 2H), 6.13 (t, J = 2.1 Hz, 2H), 4.01 – 3.78 (m, 6H), 3.39 – 3.36 (m, 1H), 3.26 – 3.18 (m, 1H), 3.14 – 3.10 (m, 1H), 2.97. – 2.89 (m, 1H), 2.29 – 2.26 (m, 1H), 1.85 – 1.79 (m, 2H), 1.73 – 1.66 (m, 1H), 1.64 – 1.56 (m, 1H), 1.45 – 1.37 (m, 1H), 1.34 – 1.28 (m, 1H) ppm. **^{13}C NMR** (126 MHz, $CDCl_3$): δ 120.6, 108.1, 64.6, 64.5, 51.8, 49.6, 48.5, 31.9,

24.3, 23.6 ppm. The carbon (CH) adjacent to boron was not observed, due to quadrupolar coupling with ^{11}B (I = 3/2) and ^{10}B (I = 3). **^{11}B NMR** (160 MHz, $CDCl_3$): δ 2.49 ppm. **^{19}F NMR** (282 MHz, $CDCl_3$): δ -142.6 ppm. **IR** (neat, cm^{-1}): 3191, 2921, 2854, 1500, 1455, 1281, 1126, 1092, 1051, 993, 935, 904. **HRMS**: m/z calcd. for ($C_{13}H_{22}F_3N_2NaO^{11}B$) $[M+Na]^+$: 313.1669 found 313.1678.

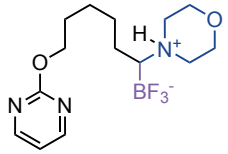

4-(1-(Difluoroboraneyl)-6-(pyrimidin-2-yloxy)hexyl)morpholin-4-ium fluoride (**4aa**): Following the **general procedure B**, using 2-(hex-5-en-1-yloxy)pyrimidine (**1p**, 35.6 mg, 0.20 mmol) and N-O electrophile **2k** (solid, 1. batch: 74.8 mg, 0.30 mmol, 1.50 equiv., 2. batch: 49.9 mg, 0.20 mmol, 1.00 equiv.), flash column chromatographic purification (*n*-hexane/MTBE/acetone 2:1:1 + 1v% AcOH to 1:1:1 to 1:1:2 *n*-hexane/MTBE/acetone) afforded **4aa** (33.3 mg, 50% yield) as a colourless oil. In an independent experiment, 33.0 mg (50% yield) were obtained, giving an average yield of 50%. **^1H NMR** (400 MHz, $CDCl_3$): δ 8.49 (d, J = 4.8 Hz, 2H), 7.00 – 6.90 (m, 2H), 4.34 (t, J = 6.6, 2H), 4.06 – 3.97 (m, 3H), 3.86 – 3.79 (m, 1H), 3.43 – 3.40 (m, 1H), 3.34 – 3.25 (m, 1H), 3.20 – 3.17 (m, 1H), 3.04 – 2.94 (m, 1H), 2.33 – 2.31 (m, 1H), 1.89 – 1.70 (m, 3H), 1.69 – 1.46 (m, 4H), 1.40 – 1.31 (m, 1H) ppm. **^{13}C NMR** (126 MHz, $CDCl_3$): δ 165.3, 159.4, 114.9, 67.5, 64.6, 64.5, 51.7, 48.6, 28.7, 26.6, 26.5, 24.1 ppm. The carbon (CH) adjacent to boron was not observed, due to quadrupolar coupling with ^{11}B (I = 3/2) and ^{10}B (I = 3). **^{11}B NMR** (160 MHz, $CDCl_3$): δ 2.71 ppm. **^{19}F NMR** (282 MHz, $CDCl_3$): δ -142.8 ppm. **IR** (neat, cm^{-1}): 3171, 2926, 2862, 1578, 1427, 1379, 1323, 1022, 936. **HRMS**: m/z calcd. for ($C_{14}H_{23}F_3N_3NaO_2{}^{11}B$) $[M+Na]^+$: 356.1728; found 356.1739.

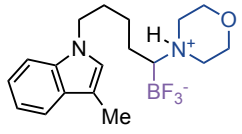

4-(1-(Difluoroboraneyl)-6-(3-methyl-1H-indol-1-yl)hexyl)morpholin-4-ium fluoride (**4ab**): Following the **general procedure B**, using 1-(hex-5-en-1-yl)-3-methyl-1H-indole (**1q**, 42.7 mg, 0.20 mmol) and N-O electrophile **2k** (solid, 1. batch: 74.8 mg, 0.30 mmol, 1.50 equiv., 2. batch: 49.9 mg, 0.20 mmol, 1.00 equiv.), flash column chromatographic purification (*n*-hexane/MTBE/acetone 3:2:2 + 1v% AcOH) afforded **4ab** (49 mg, 67% yield) as an amorphous colourless solid. In an independent experiment, 44 mg (60% yield) were obtained, giving an average yield of 64%. **^1H NMR** (400 MHz, $CDCl_3$) δ 7.58 (dt, J = 7.9, 1.0 Hz, 1H), 7.32 – 7.29 (m, 1H), 7.22 – 7.18 (m, 1H), 7.12 – 7.08 (m, 1H), 6.89 – 6.77 (m, 2H),

4.07 (t, *J* = 6.9 Hz, 2H), 4.00 – 3.93 (m, 3H), 3.83 – 3.76 (m, 1H), 3.36 (d, *J* = 12.6 Hz, 1H), 3.19 – 3.04 (m, 2H), 2.93 – 2.83 (m, 1H), 2.34 (d, *J* = 1.1 Hz, 3H), 2.28 – 2.23 (m, 1H), 1.88 – 1.80 (m, 2H), 1.70 – 1.55 (m, 2H), 1.44 – 1.24 (m, 4H) ppm. **^{13}C NMR** (101 MHz, $CDCl_3$) δ 136.4, 128.8, 125.6, 121.3, 119.1, 118.5, 110.1, 109.3, 64.5, 64.4, 51.6, 48.4, 45.9, 30.1, 27.4, 26.4, 23.8, 9.7. ppm. The carbon (CH) adjacent to boron was not observed, due to quadrupolar coupling with ^{11}B (*I* = 3/2) and ^{10}B (*I* = 3). **^{11}B NMR** (128 MHz, $CDCl_3$) δ 2.93 ppm. **^{19}F NMR** (376 MHz, $CDCl_3$) δ -142.7 ppm. **IR** (neat, cm^{-1}): 3167, 3079, 3054, 2947, 2934, 2863, 1709, 1613, 1469, 1455, 1356, 1332, 1279, 1257, 1209, 1165, 1156, 1125, 1081, 1043, 1003, 961, 943, 908, 888, 757. **HRMS**: m/z calcd. for ($C_{19}H_{28}F_3N_2NaO^{11}B$) $[M+Na]^+$: 391.2139; found 391.2144. **MP:** 139 – 145 ºC.

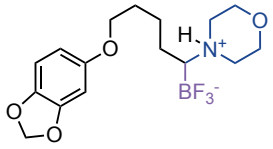

4-(5-(Benzo[*d*][1,3]dioxol-5-yloxy)-1-(difluoroboraneyl)pentyl)morpholin-4-ium fluoride (**4ac**): Following the **general procedure B**, using 5-(pent-4-en-1-yloxy)benzo[*d*][1,3]dioxole (**1r**, 41.2 mg, 0.20 mmol) and N-O electrophile **2k** (solid, 1. batch: 74.8 mg, 0.30 mmol, 1.50 equiv., 2. batch: 49.9 mg, 0.20 mmol, 1.00 equiv.), flash column chromatographic purification (*n*-hexane/MTBE/acetone 2:1:1 + 1v% AcOH to 1:1:1 *n*-hexane/MTBE/acetone) afforded **4ac** (52.8 mg, 73% yield) as an amorphous colourless solid. In an independent experiment, 49.5 mg (69% yield) were obtained, giving an average yield of 71%. **^{1}H NMR** (500 MHz, $CDCl_3$): δ 6.82 (brs, 1H), 6.69 (d, *J* = 8.5 Hz, 1H), 6.47 (d, *J* = 2.5 Hz, 1H), 6.30 (dd, *J* = 8.5, 2.5 Hz, 1H), 5.90 (s, 2H), 4.06 – 3.99 (m, 3H), 3.93 – 3.80 (m, 3H), 3.44 (d, *J* = 12.6 Hz, 1H), 3.33 – 3.26 (m, 1H), 3.20 (d, *J* = 12.2 Hz, 1H), 3.03 – 2.95 (m, 1H), 2.37 (brs, 1H), 1.83 – 1.66 (m, 3H), 1.57 (brs, 2H), 1.52 – 1.43 (m, 1H) ppm. **^{13}C NMR** (126 MHz, $CDCl_3$): δ 154.7, 148.4, 141.7, 108.1, 105.8, 101.2, 98.2, 68.8, 64.7, 64.6, 51.9, 48.6, 29.7, 23.9, 23.6 ppm. The carbon (CH) adjacent to boron was not observed, due to quadrupolar coupling with ^{11}B (*I* = 3/2) and ^{10}B (*I* = 3). **^{11}B NMR** (161 MHz, $CDCl_3$): δ 2.47 ppm. **^{19}F NMR** (471 MHz, $CDCl_3$): δ -142.8 ppm. **IR** (neat, cm^{-1}): 3191, 2933, 2869, 1630, 1503, 1488, 1469, 1261, 1242, 1182, 1101, 1032, 935, 903. **HRMS**: m/z calcd. for ($C_{16}H_{23}F_3NNaO_4{}^{11}B$) $[M+Na]^+$: 384.1564; found 384.1571. **MP:** 140 – 142 °C.

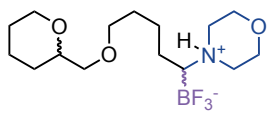

4-(1-(Difluoroboraneyl)-6-((tetrahydro-2H-pyran-2-yl)oxy)hexyl)morpholin-4-ium fluoride (**4ad**): Following the **general procedure B**, using 2-(hex-5-en-1-yloxy)tetrahydro-2H-pyran (**1s**, 36.9 mg, 0.20 mmol) and N-O electrophile **2k** (solid, 1. batch: 74.8 mg, 0.30

mmol, 1.50 equiv., 2. batch: 49.9 mg, 0.20 mmol, 1.00 equiv.), flash column chromatographic purification (*n*-hexane/MTBE/acetone 3:2:2 + 1v% AcOH) afforded **4ad** (32 mg, 47% yield) as an amorphous colourless solid in a 1:1 mixture of diastereomers. In an independent experiment, 26 mg (38% yield) were obtained, giving an average yield of 42%. **^{1}H NMR** (400 MHz, $CDCl_3$, mixture of diastereomers): δ 6.88 (brs, 1H), 4.59 – 4.52 (m, 1H), 4.06 – 3.94 (m, 3H), 3.88 – 3.79 (m, 2H), 3.72 (dtd, *J* = 9.6, 6.8, 0.9 Hz, 1H), 3.51 – 3.46 (m, 1H), 3.45 – 3.34 (m, 2H), 3.33 – 3.24 (m, 1H), 3.22 – 3.13 (m, 1H), 3.06 – 2.88 (m, 1H), 2.37 – 2.22 (m, 1H), 1.85 – 1.27 (m, 14H) ppm. **^{13}C NMR** (101 MHz, $CDCl_3$): δ 99.1, 99.0, 67.6, 64.61, 64.55, 62.8, 62.58, 62.55, 51.8, 48.6, 48.5, 32.5, 30.9, 29.7, 26.9, 26.8, 26.1, 25.6, 24.0, 24.0, 19.87, 19.85 ppm. The carbon (CH) adjacent to boron was not observed, due to quadrupolar coupling with ^{11}B (*I* = 3/2) and ^{10}B (*I* = 3). **^{11}B NMR** (128 MHz, $CDCl_3$): δ 2.43 ppm. **^{19}F NMR** (376 MHz, $CDCl_3$): δ -142.8 ppm. **IR** (neat, cm^{-1}): 3168, 2939, 2864, 1459, 1442, 1408, 1370, 1323, 1254, 1184, 1126, 1066, 1020, 952, 931, 903, 865, 812. **HRMS**: m/z calcd. for ($C_{15}H_{29}F_3NNaO_3{}^{11}B$) $[M+Na]^+$: 362.2085; found 362.2082.

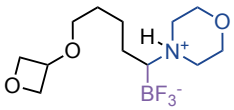

4-(1-(Difluoroboraneyl)-5-(oxetan-3-yloxy)pentyl)morpholin-4-ium fluoride (**4ae**): Following the **general procedure B**, using 3-(pent-4-en-1-yloxy)oxetane (**1t**, 28.4 mg, 0.20 mmol) and N-O electrophile **2k** (solid, 1. batch: 74.8 mg, 0.30 mmol, 1.50 equiv., 2. batch: 49.9 mg, 0.20 mmol, 1.00 equiv.), flash column chromatographic purification (*n*-hexane/MTBE/acetone 2:1:1 + 1v% AcOH to 1:1:1 to 1:1:2 *n*-hexane/MTBE/acetone) afforded **4ae** (44.4 mg, 75% yield) as a pale yellow oil. In an independent experiment, 43.7 mg (74% yield) were obtained, giving an average yield of 75%. **^{1}H NMR** (400 MHz, $CDCl_3$): δ 6.86 (brs, 1H), 4.73 (t, *J* = 6.7 Hz, 2H), 4.57 – 4.54 (m, 2H), 4.51 – 4.46 (m, 1H), 4.02 – 3.94 (m, 3H), 3.83 – 3.76 (m, 1H), 3.44 – 3.22 (m, 4H), 3.18 – 3.14 (m, 1H), 3.02 – 2.92 (m, 1H), 2.31 – 2.28 (m, 1H), 1.75 – 1.66 (m, 1H), 1.64 – 1.42 (m, 4H), 1.40 – 1.32 (m, 1H) ppm. **^{13}C NMR** (126 MHz, $CDCl_3$): δ 78.9, 72.3, 68.7, 64.5, 64.4, 51.7, 48.5, 30.1, 23.9, 23.6 ppm. The carbon (CH) adjacent to boron was not observed, due to quadrupolar coupling with ^{11}B (*I* = 3/2) and ^{10}B (*I* = 3). **^{11}B NMR** (161 MHz, $CDCl_3$) δ 2.64 ppm. **^{19}F NMR** (471 MHz, $CDCl_3$): δ –142.7 ppm. **IR** (neat, cm^{-1}): 3566, 3166, 2947, 2872, 1622, 1457, 1367, 1256, 1127, 1028, 967. **HRMS**: m/z calcd. for ($C_{12}H_{23}F_3NNaO_3{}^{11}B$) $[M+Na]^+$: 320.1615; found 320.1623.

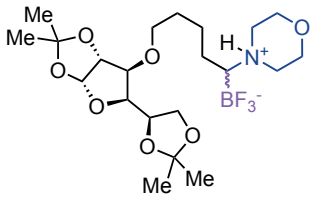

4(5-(((3aR,5R,6S,6aR)-5-((R)-2,2-Dimethyl-1,3-dioxolan-4-yl)-2,2-dimethyltetrahydro-furo[2,3-d][1,3]dioxol-6-yl)oxy)-1-(morpholino-4-ium)pentyl)trifluoroborate (**4af**): Following the **general procedure B**, using (3aR,5R,6S,6aR)-5-((R)-2,2-dimethyl-1,3-dioxolan-4-yl)-2,2-dimethyl-6-(pent-4-en-1-yloxy)tetrahydrofuro[2,3-d][1,3]dioxole (**1u**, 65.7 mg, 0.20 mmol) and N-O electrophile **2k** (solid, 1. batch: 74.8 mg, 0.30 mmol, 1.50 equiv., 2. batch: 49.9 mg, 0.20 mmol, 1.00 equiv.), flash column chromatographic purification (*n*-hexane/MTBE/acetone 3:2:2 + 1v% AcOH) afforded **4af** (70 mg, 72% yield) as an amorphous colourless solid. In an independent experiment, 72 mg (75% yield) were obtained, giving an average yield of 74%. **^{1}H NMR** (400 MHz, $CDCl_3$): δ 6.89 (brs, 1H), 5.84 – 5.83 (m, 1H), 4.51 – 4.50 (m, 1H), 4.29 – 4.25 (m, 1H), 4.09 (dd, *J* = 7.4, 3.0 Hz, 1H), 4.06 – 3.93 (m, 5H), 3.83 – 3.77 (m, 2H), 3.61 – 3.48 (m, 2H), 3.38 (d, *J* = 12.5 Hz, 1H), 3.31 – 3.21 (m, 1H), 3.13 (d, *J* = 11.9 Hz, 1H), 2.99 – 2.91 (m, 1H), 2.29 – 2.26 (m, 1H), 1.75 – 1.51 (m, 6H), 1.46 (s, 3H), 1.39 (s, 3H), 1.32 (s, 3H), 1.28 (s, 3H) ppm. **^{13}C NMR** (101 MHz, $CDCl_3$): δ 111.8, 108.9, 105.3, 82.6, 82.5, 82.24, 82.21, 81.1, 72.6, 70.5, 70.3, 67.2, 64.5, 64.4, 51.7, 48.5, 30.2, 30.1, 26.89, 26.86, 26.3, 25.48, 25.46, 23.8, 23.5, 23.4 ppm. The carbon (CH) adjacent to boron was not observed, due to quadrupolar coupling with ^{11}B (*I* = 3/2) and ^{10}B (*I* = 3). **^{11}B NMR** (128 MHz, $CDCl_3$): δ 2.77 ppm. **^{19}F NMR** (376 MHz, $CDCl_3$): δ -142.7 ppm. **IR** (neat, cm^{-1}): 3164, 2986, 2937, 2872, 1738, 1714, 1456, 1372, 1216, 1127, 1069, 1012, 846. **HRMS**: m/z calcd. for ($C_{21}H_{37}F_3NNaO_7{}^{11}B$) $[M+Na]^+$: 506.2507; found 506.2512. **MP:** 160 – 165 ºC.

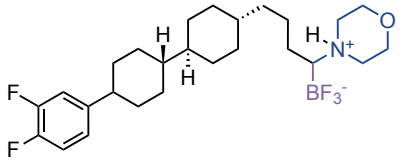

4-(1-(Difluoroboraneyl)-4-((1*s*,1'*r*,4*R*,4'*R*)-4'-(3,4-difluorophenyl)-[1,1'-bi(cyclohexan)]-4-yl)butyl)morpholin-4-ium fluoride (**4ag**): Following the **general procedure B**, using *trans*,*trans*-4'-(3-Butenyl)-4-(3,4-difluorophenyl)bicyclohexyl (**1v**, 66.5 mg, 0.20 mmol) and N-O electrophile **2k** (solid, 1. batch: 74.8 mg, 0.30 mmol, 1.50 equiv., 2. batch: 49.9 mg, 0.20 mmol, 1.00 equiv.), flash column chromatographic purification (*n*-hexane/MTBE/acetone 2:1:1 + 1v% AcOH to 1:1:1 *n*-hexane/MTBE/acetone) afforded **4ag** (61.5 mg, 63% yield) as an amorphous colourless solid in a 1:1 mixture of diastereomers. In an independent experiment, 62.2 mg (65% yield) were obtained, giving an average yield of 64%. **^{1}H NMR**

(500 MHz, DMSO-d_6): δ 8.22 (brs, 1H), 7.32 – 7.24 (m, 2H), 7.05 (brs, 1H), 3.88 – 3.85 (m, 2H), 3.75 – 3.64 (m, 2H), 3.16 – 3.07 (m, 4H), 2.48 – 2.43 (m, 1H), 2.02 (brs, 1H), 1.82 – 1.69 (m, 8H), 1.58 – 1.52 (m, 1H), 1.44 – 1.34 (m, 4H), 1.29 – 1.23 (m, 1H), 1.16 – 1.07 (m, 6H), 1.05 – 0.94 (m, 3H), 0.87 – 0.80 (m, 2H) ppm. **^{13}C NMR** (126 MHz, DMSO-d_6): δ 149.3 (dd, J = 256.9, 12.6 Hz), 147.7 (dd, J = 243.0, 12.6 Hz), 145.2, 123.2, 117.0 (d, J = 16.5 Hz), 115.5 (d, J = 16.5 Hz), 63.6, 63.5, 49.8, 49.7, 43.0, 42.8, 42.1, 37.4, 37.3, 33.9, 33.2, 33.1, 29.7, 29.5, 26.1, 24.1 ppm. The carbon (CH) adjacent to boron was not observed, due to quadrupolar coupling with ^{11}B (I = 3/2) and ^{10}B (I = 3). **^{11}B NMR** (160 MHz, DMSO-d_6): δ 2.42 ppm. **^{19}F NMR** (471 MHz, DMSO-d_6): δ -138.6, -139.2 (d, J = 22.7 Hz), -143.0 (d, J = 22.7 Hz) ppm. **IR** (neat, cm^{-1}): 3129, 2912, 2846, 1514, 1432, 1276, 1134, 1036, 1018, 939. **HRMS**: m/z calcd. for ($C_{26}H_{39}F_5NNaO^{11}B$) [M+Na]$^+$: 510.2937; found 510.2942. **MP:** 226 – 230 °C.

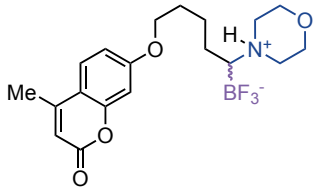

4-(1-(Difluoroboraneyl)-5-(4-methyl-2-oxo-2H-chromen-8-yl)pentyl)morpholin-4-ium fluoride (**4ah**): Following the **general procedure B**, using 4-methyl-8-(pent-4-en-1-yloxy)-2H-chromen-2-one (**1w**, 48.9 mg, 0.20 mmol) and N-O electrophile **2k** (solid, 1. batch: 74.8 mg, 0.30 mmol, 1.50 equiv., 2. batch: 49.9 mg, 0.20 mmol, 1.00 equiv.), flash column chromatographic purification (*n*-hexane/MTBE/acetone 3:2:2 + 1v% AcOH) afforded **4ah** (52 mg, 65% yield) as an amorphous colourless solid. In an independent experiment, 46 mg (58% yield) were obtained, giving an average yield of 62%. **^{1}H NMR** (400 MHz, DMSO-d_6): δ 8.33 (brs, 1H), 7.67 (d, J = 9.3 Hz, 1H), 6.96 – 6.94 (m, 2H), 6.19 (brs, 1H), 4.07 (t, J = 6.5 Hz, 2H), 3.89 – 3.86 (m, 2H), 3.73 – 3.68 (m, 2H), 3.16 (brs, 4H), 2.39 (s, 3H), 2.05 (brs, 1H), 1.76 – 1.38 (m, 6H) ppm. **^{13}C NMR** (101 MHz, DMSO-d_6): 161.8, 160.2, 154.8, 153.4, 126.4, 113.0, 112.4, 111.0, 101.1, 68.3, 63.6, 63.5, 49.8, 30.7, 28.9, 25.5, 23.3, 18.1 ppm. The carbon (CH) adjacent to boron was not observed, due to quadrupolar coupling with ^{11}B (I = 3/2) and ^{10}B (I = 3). **^{11}B NMR** (128 MHz, DMSO-d_6): δ 2.42 ppm. **^{19}F NMR** (376 MHz, DMSO-d_6): δ -138.8 ppm. **IR** (neat, cm^{-1}): 3170, 3069, 2922, 2870, 1720, 1610, 1512, 1460, 1427, 1389, 1372, 1264, 1203, 1138, 1127, 1099, 1070, 1006, 935, 900, 857, 811, 706. **HRMS**: m/z calcd. for ($C_{19}H_{25}F_3NNaO_4{}^{11}B$) [M+Na]$^+$: 422.1721; found 422.1726. **MP**: 233 – 235 ºC.

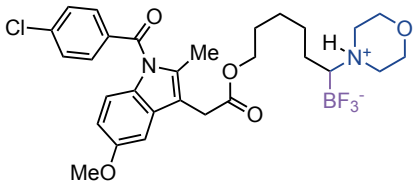

4-(6-(2-(1-(4-Chlorobenzoyl)-5-methoxy-2-methyl-1H-indol-3-yl)acetoxy)-1-(difluoro-boraneyl)hexyl)morpholin-4-ium fluoride (**4ai**): Following the **general procedure B**, using hex-5-en-1-yl 2-(1-(4-chlorobenzoyl)-5-methoxy-2-methyl-1H-indol-3-yl)acetate (**1x**, 88.0 mg, 0.20 mmol) and N-O electrophile **2k** (solid, 1. batch: 74.8 mg, 0.30 mmol, 1.50 equiv., 2. batch: 49.9 mg, 0.20 mmol, 1.00 equiv.), flash column chromatographic purification (*n*-hexane/MTBE/acetone 3:2:2 + 1v% AcOH) afforded **4ai** (71 mg, 60% yield) as an amorphous colourless solid. In an independent experiment, 60 mg (50% yield) were obtained, giving an average yield of 55%. **^{1}H NMR** (400 MHz, $CDCl_3$) δ 7.67 – 7.64 (m, 2H), 7.49 – 7.45 (m, 2H), 6.97 (d, *J* = 2.5 Hz, 1H), 6.90 (d, *J* = 9.0 Hz, 1H), 6.77 (brs, 1H), 6.67 (dd, *J* = 9.0, 2.5 Hz, 1H), 4.10 (t, *J* = 6.5 Hz, 2H), 4.01 – 3.97 (m, 3H), 3.84 (s, 3H), 3.79 (d, *J* = 11.7 Hz, 1H), 3.65 (s, 2H), 3.38 (d, *J* = 12.6 Hz, 1H), 3.30 – 3.20 (m, 1H), 3.11 (d, *J* = 12.0 Hz, 1H), 3.00 – 2.91 (m, 1H), 2.37 (s, 3H), 2.26 – 2.24 (m, 1H), 1.68 – 1. 59 (m, 3H), 1.57 – 1.49 (m, 1H), 1.41 – 1.20 (m, 4H) ppm. **^{13}C NMR** (101 MHz, $CDCl_3$) δ 171.1, 168.5, 156.2, 139.4, 136.0, 134.0, 131.3, 131.0, 130.8, 129.3, 115.1, 112.9, 111.8, 101.5, 65.0, 64.65, 64.56, 55.9, 51.7, 48.5, 30.6, 28.6, 26.4, 23.9, 13.5 ppm. The carbon (CH) adjacent to boron was not observed, due to quadrupolar coupling with ^{11}B (*I* = 3/2) and ^{10}B (*I* = 3). **^{11}B NMR** (128 MHz, $CDCl_3$) δ 2.84 ppm. **^{19}F NMR** (376 MHz, $CDCl_3$) δ -143.0 ppm. **IR** (neat, cm^{-1}): 3163, 2932, 2864, 1728, 1679, 1591, 1477, 1456, 1399, 1357, 1318, 1258, 1222, 1169, 1144, 1128, 1087, 1067, 1034, 1014, 926, 833, 754. **HRMS**: m/z calcd. for ($C_{29}H_{35}F_3N_2NaO_5{}^{11}B^{35}Cl$) $[M+Na]^+$: 617.2172; found 617.2178. **MP:** 210 – 213 ºC.

Product isolation as *N*-BH3 Lewis acid-base adduct

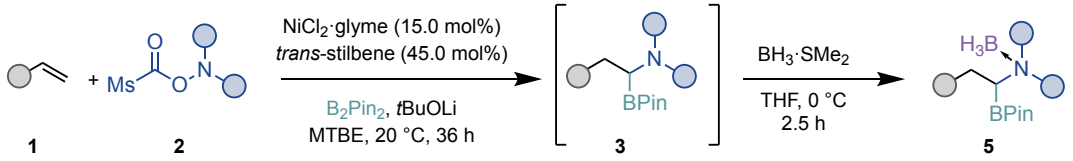

General procedure C (Scheme 19): Under air, a Schlenk tube equipped with a stirring bar was loaded with recrystallised, free-flowing B_2Pin_2 (86.3 mg, 0.34 mmol, 1.70 equiv.), *trans*-stilbene (16.2 mg, 0.09 mmol, 0.45 equiv.), and N–O electrophile **2k** (0.30 mmol, 1.5 equiv.). The tube was transferred into a N_2-filled glovebox, followed by addition of $NiCl_2$·glyme (6.60 mg, 0.03 mmol, 0.15 equiv.) and *t*BuOLi (24.0 mg, 0.30 mmol, 1.50 equiv.), assisted by an anti-static device to ensure complete aggregation at the bottom. The tube was closed,

brought out of the glovebox, and connected to a N_2-filled Schlenk line. Stirring was started and the alkene **1a** (0.20 mmol, 1.00 equiv.) was added as a solution in anhydrous MTBE (0.30 mL). The tube was closed, and the suspension was stirred at 20 °C (external thermostat) and 800 rpm for 18 h, during which several colour changes occurred from yellow to deep violet and finally to a slightly green solution.

Under air, a second Schlenk tube equipped with a stirring bar was loaded with another portion of B_2Pin_2 (60.9 mg, 0.24 mmol, 1.20 equiv.), and N–O electrophile (**2k**, 0.20 mmol, 1.00 equiv.), transferred into a N_2-filled glovebox, followed by addition of *t*BuOLi (16.0 mg, 0.20 mmol, 1.00 equiv.), assisted by an anti-static device to ensure complete aggregation at the bottom. The tube was closed, brought out of the glovebox, and connected to a N_2-filled Schlenk line. Then, the primary reaction solution was transferred into the newly prepared Schlenk tube by a syringe. The primary tube was rinsed with anhydrous MTBE (0.1 mL), which was transferred to the second tube using the previous syringe. Stirring was continued at 20 °C (external thermostat) and 800 rpm for another 18 h (GC FID control).

Then, the reaction solution was diluted with anhydrous, degassed THF (1.0 mL) and cooled to 0 °C with stirring. $BH_3 \bullet SMe_2$ (0.28 µL, 3.00 mmol, 15.0 equiv.) was added dropwise within 2 min, resulting in a black suspension. The reaction mixture was stirred at 0 °C for 2.5 h, followed by removal of all volatiles in vacuo at 0 °C, down to 0.1 mbar (liquid N_2 trap). The residue was suspended in EtOAc, assisted by sonification, and then filtered through a pad of silica gel (3 × 3 cm, EtOAc). Celite (1.00 g) was added to the filtrate and the volatiles were briefly removed in vacuo at 20 °C, before being purified by flash column chromatography on silica gel to isolate the borane adduct (details see compound data below).

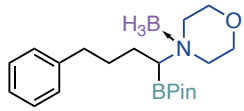

4-(4-Phenyl-1-(4,4,5,5-tetramethyl-1,3,2-dioxaborolan-2-yl)butyl)morpholine *N*-BH_3 adduct (5a) : Following the **general procedure C**, using but-3-en-1-ylbenzene (**1a**, 26.4 mg, 0.20 mmol) and N–O electrophile **2k** (solid, 1. batch: 74.8 mg, 0.30 mmol, 1.50 equiv., 2. batch: 49.9 mg, 0.20 mmol, 1.00 equiv.), flash column chromatographic purification (*n*-hexane/ethyl acetate 4:1) afforded ***N*-BH_3 adduct** (51.7 mg, 72% yield) as an amorphous colourless solid. In an independent experiment, 53.2 mg (74% yield) were obtained, giving an average yield of 73%. **^{1}H NMR** (400 MHz, $CDCl_3$): δ 7.30 – 7.26 (m, 2H), 7.21 – 7.14 (m, 3H), 4.36 – 4.26 (m, 2H), 3.68 – 3.61 (m, 2H), 3.16 – 3.05 (m, 2H), 2.84 (td, *J* = 11.8, 3.9 Hz, 1H), 2.74 – 2.57 (m, 4H), 1.90 – 1.47 (m, 7H), 1.28 –1.27 (m, 12H) ppm. **^{13}C NMR** (101 MHz, $CDCl_3$): δ 141.7, 128.52, 128.45, 126.1, 84.1, 62.4, 62.3, 56.1, 53.8, 35.9, 29.1, 25.02, 25.00, 23.5 ppm. The carbon (CH) adjacent to boron was not observed, due to quadrupolar coupling with ^{11}B (*I* = 3/2) and ^{10}B (*I* = 3). **^{11}B NMR** (128 MHz, $CDCl_3$): δ 30.23, -13.76 ppm. **IR** (neat,

cm^{-1}): 3017, 2978, 2933, 2858, 2420, 2371, 2280, 1739, 1453, 1372, 1328, 1264, 1184, 1140, 1116, 991, 855, 697. **HRMS**: m/z calcd. for ($C_{20}H_{35}NNaO_3{}^{10}B^{11}B$) [M+Na]$^+$: 381.2732; found 381.2717. **MP**:76 – 78 ºC.

4.5.5. Transformations of the α-aminoboronic acid derivatives

α-aminoboronic acid formation

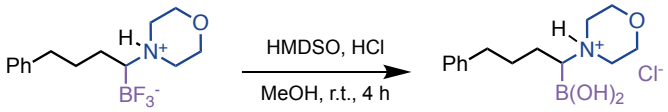

4a **6a**

(1-morpholino-4-phenylbutyl)boronic acid hydrochloride (**6a**) was prepared in analogy to a literature procedure.[22] In a round bottom flask, the corresponding α-aminotrifluoroborate (**4a**, 11 mg, 38 μmol, 1.00 equiv.) was dissolved in CH_3OH (0.05 M). To this solution, HCl (2M aq, 4 equiv.) and hexamethyldisiloxane (3.0 equiv.) were added and the solution was left at room temperature for 4 hours. Then, the volatiles were removed under reduced pressure, keeping the bath temperature at 30 ºC. The residue was further dried under high vacuum overnight, to afford **6a** (11 mg, 99% yield) as a white solid. **Note**: the compound begins to decompose and signs indicative of protodeboration are observed in NMR when stored in solution. **^{1}H NMR** (400 MHz, CD_3OD): δ 7.29 – 7.12 (m, 5H), 4.02 – 3.94 (m, 2H), 3.78 – 3.69 (m, 2H), 3.50 – 3.35 (m, 2H), 3.28 – 3.13 (m, 2H), 3.07 – 3.02 (m, 1H), 2.74 – 2.62 (m, 2H), 1.86 – 1.65 (m, 4H) ppm. Suppressed signals for NH and OH occurred in MeOD.**^{13}C NMR** (101 MHz, CD_3OD): δ 142.5, 129.4, 127.0, 65.0, 64.9, 53.2, 52.1, 36.4, 29.1, 26.5 ppm. The carbon (CH) adjacent to boron was not observed, due to quadrupolar coupling with ^{11}B (I = 3/2) and ^{10}B (I = 3). **IR** (neat, cm^{-1}): 2936, 2865, 1453, 1415, 1379, 1262, 1125, 1045, 749. **HRMS**: m/z calcd. for ($C_{14}H_{23}NO_3{}^{10}B$) [M+H]$^+$: 263.1802; found 263.1792. **MP:** 58 – 59ºC.

In situ Matteson homologation and further transformations

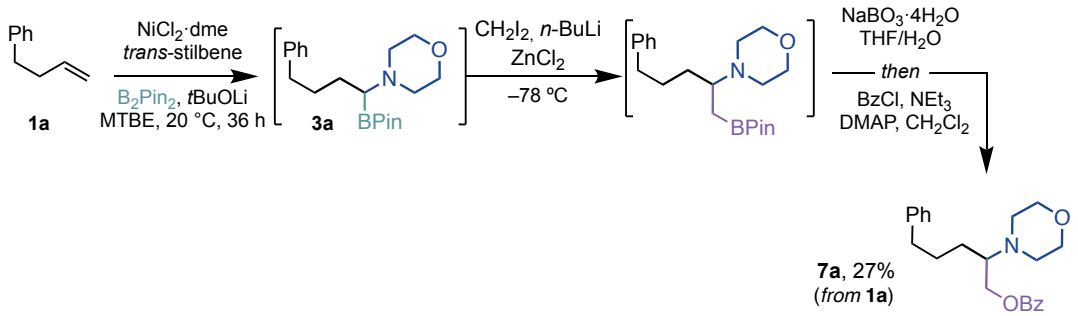

2-morpholino-5-phenylpentyl benzoate (**7a**): Under air, a Schlenk tube equipped with a stirring bar was loaded with recrystallised, free-flowing B_2Pin_2 (130 mg, 0.51 mmol, 1.70 equiv.), *trans*-stilbene (24.3 mg, 0.14 mmol, 0.45 equiv.), and N–O electrophile **2k** (0.45 mmol, 1.50 equiv.). The tube was transferred into a N_2-filled glovebox, followed by addition of $NiCl_2$·glyme (9.9 mg, 0.05 mmol, 0.15 equiv.) and *t*BuOLi (36.0 mg, 0.45 mmol, 1.50 equiv.), assisted by an anti-static device to ensure complete aggregation at the bottom. The tube was closed, brought out of the glovebox and connected to a N_2-filled Schlenk line. Stirring was started and the alkene **1a** (0.30 mmol, 1.00 equiv.) was added as a solution in anhydrous MTBE (0.50 mL). The tube was closed, and the suspension was stirred at 20 °C (external thermostat) and 800 rpm for 18 h, during which several colour changes occurred from yellow to deep violet and finally to a slightly green solution.

Under air, a second Schlenk tube equipped with a stirring bar was loaded with another portion of B_2Pin_2 (74.8 mg, 0.30 mmol, 1.20 equiv.), and N-O electrophile **2k** (0.30 mmol, 1.00 equiv.), transferred into a N_2-filled glovebox, followed by addition of *t*BuOLi (24.0 mg, 0.30 mmol, 1.00 equiv.), assisted by an anti-static device to ensure complete aggregation at the bottom. The tube was closed, brought out of the glovebox and connected to a N_2-filled Schlenk line. Then, the primary reaction solution was transferred into the newly prepared Schlenk tube by a syringe. The primary tube was rinsed with anhydrous MTBE (0.15 mL), which was transferred to the second tube using the previous syringe. Stirring was continued at 20 °C (external thermostat) and 800 rpm for another 18 h.

Then, the reaction solution was concentrated to dryness under inert atmosphere. The crude **3a**, was dissolved in THF (3.0 mL), and CH_2I_2 (6.0 mmol, 20.0 equiv.) was added. The reaction mixture was cooled to -78 ºC, and *n*BuLi (5.4 mmol, 18 equiv.) was added dropwise under N_2 atmosphere within 5 minutes. The reaction was stirred at -78 ºC for 30 minutes and then $ZnCl_2$ (900 μL, 3.0 equiv., 1.0 M in Et_2O) was added. The mixture was allowed to warm to room temperature and stirred for 1 hour. Water (10 mL) was added, and the solution was extracted with CH_2Cl_2 (2 x 10 mL). The combined organic layers were dried over Na_2SO_4, filtered, and concentrated under vacuum. The homologated crude product was dissolved in a 1:1 mixture of THF:H_2O (4 mL) in a vial containing a stir bar. $NaBO_3$·$4H_2O$ (277 mg, 1.8 mmol, 6.0 equiv.) was added to the solution. The suspension was stirred at room temperature for 4 hours. Water (4 mL) was added, and the solution extracted with CH_2Cl_2 (4 x 15 mL). The combined organic layers were dried over Na_2SO_4, filtered, and concentrated under vacuum. The crude amino alcohol was dissolved in dry CH_2Cl_2 (3 mL) in an oven-dried Schlenk flask with stir bar. DMAP (4 mg, 10.0 mol%), Et_3N (63 μL, 1.5 equiv.), and BzCl (42 μL, 1.2 equiv.) were added sequentially. The mixture was stirred at room temperature for 6 hours. The reaction mixture was diluted with CH_2Cl_2 (75 mL) and washed with HCl (20 mL, 5%), $NaHCO_3$ (20 mL, saturated), and H_2O (20 mL). The organic layer was dried with Na_2SO_4, filtered, and concentrated under vacuum. The crude benzoate ester was purified by

column chromatography on silica gel (*n*-hexane/EtOAc 85:15) to afforded **7a** (29 mg, 27% yield) as a colourless oil.

^{1}H NMR (400 MHz, $CDCl_3$): δ 8.05 – 8.00 (m, 2H), 7.60 – 7.55 (m, 1H), 7.48 – 7.43 (m, 2H), 7.29 – 7.25 (m, 2H), 7.20 – 7.16 (m, 3H), 4.44 (dd, *J* = 11.6, 6.7 Hz, 1H), 4.30 (dd, *J* = 11.5, 4.6 Hz, 1H), 3.71 – 3.61 (m, 4H), 2.87 – 2.58 (m, 7H), 1.88 – 1.46 (m, 4H) ppm. **^{13}C NMR** (101 MHz, $CDCl_3$): δ 166.6, 142.3, 133.1, 130.3, 129.7, 128.6, 128.5, 128.4, 125.9, 67.8, 64.3, 62.7, 49.7, 35.9, 28.4, 28.0 ppm. **IR** (neat, cm^{-1}): 2950, 2854, 2816, 1717, 1452, 1271, 1115, 1069, 711. **HRMS**: m/z calcd. for ($C_{22}H_{28}NO_3$) $[M+H]^+$: 354.2064; found 354.2069.

4.5.6. Mechanistic experiments

Control experiments with 8

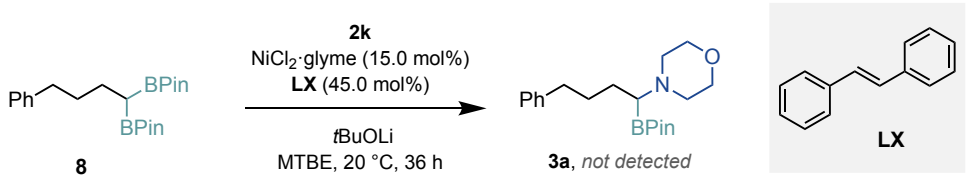

Under air, a Schlenk tube equipped with a stirring bar was loaded with *trans*-stilbene (16.2 mg, 0.09 mmol, 0.45 equiv.), and **2k** (0.30 mmol, 1.50 equiv.). The tube was transferred into a N_2-filled glovebox, followed by addition of $NiCl_2$·glyme (6.60 mg, 0.03 mmol, 0.15 equiv.) and *t*BuOLi (24.0 mg, 0.30 mmol, 1.50 equiv.). The tube was closed, brought out of the glovebox and connected to a N_2-filled Schlenk line. Stirring was started and 2,2'-(4-phenylbutane-1,1-diyl)bis(4,4,5,5-tetramethyl-1,3,2-dioxaborolane) (**8**, 0.20 mmol, 1.00 equiv.) and anhydrous MTBE (0.30 mL) were sequentially added via syringe. The tube was closed, and the suspension was stirred at 20 ºC (external thermostat) and 800 rpm for 18 h. After this time, under air, a second Schlenk tube equipped with a stirring bar was loaded with **2k** (0.20 mmol, 1.00 equiv.), transferred into a N_2-filled glovebox, followed by addition of *t*BuOLi (16.0 mg, 0.20 mmol, 1.00 equiv.). The tube was closed, brought out of the glovebox and connected to a N_2-filled Schlenk line. Then, the primary reaction solution was transferred into the newly prepared Schlenk tube by a syringe. The primary tube was rinsed with anh. MTBE (0.1 mL), which was transferred to the second tube using the previous syringe. Stirring was continued at 20 ºC (external thermostat) and 800 rpm for another 18 h. After the reaction was completed, the mixture was diluted with DCM, filtered through syringe filter. No desired product **3a** was detected by GC-MS analysis.

Isotopic-labelling experiment

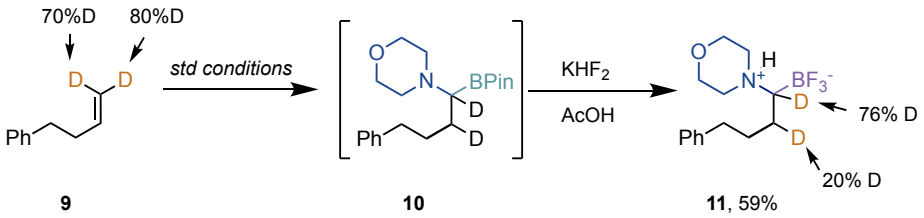

9 **10** **11**, 59%

Under air, a Schlenk tube equipped with a stirring bar was loaded with B_2Pin_2 (86.3 mg, 0.34 mmol, 1.70 equiv.), *trans*-stilbene (16.2 mg, 0.09 mmol, 0.45 equiv.), and **2k** (0.30 mmol, 1.50 equiv.). The tube was transferred into a N_2-filled glovebox, followed by addition of $NiCl_2$·glyme (6.60 mg, 0.03 mmol, 0.15 equiv.) and *t*BuOLi (24.0 mg, 0.30 mmol, 1.50 equiv.). The tube was closed, brought out of the glovebox and connected to a N_2-filled Schlenk line. Stirring was started and the alkene **9** (0.20 mmol, 1.00 equiv.) was added followed by anhydrous MTBE (0.30 mL). The tube was closed, and the suspension was stirred at 20 ºC (external thermostat) and 800 rpm for 18 h. After this time, under air, a second Schlenk tube equipped with a stirring bar was loaded with B_2Pin_2 (60.9 mg, 0.24 mmol, 1.20 equiv.), and **2k** (0.20 mmol, 1.00 equiv.), transferred into a N_2-filled glovebox, followed by addition of *t*BuOLi (16.0 mg, 0.20 mmol, 1.00 equiv.). The tube was closed, brought out of the glovebox and connected to a N_2-filled Schlenk line. Then, the primary reaction solution was transferred into the newly prepared Schlenk tube by a syringe. The primary tube was rinsed with anh. MTBE (0.1 mL), which was transferred to the second tube using the previous syringe. Stirring was continued at 20 ºC (external thermostat) and 800 rpm for another 18 h. Then, the reaction solution was cooled to 0 °C with stirring, and a solution of anhydrous KHF_2 (312 mg, 4.00 mmol, 20.0 equiv.) in anh. AcOH (2.00 mL) was added dropwise within 2 min. After 5 min, the cooling bath was removed, and the mixture was stirred at RT for additional 4 h. The suspension was transferred into a 50 mL flask using 20 mL of acetone. Celite (1.00 g) was added, and the volatiles were briefly removed in vacuo at 40 °C. Toluene (30 mL) was added, and the volatiles were again removed in vacuo at 40 °C. The latter treatment was repeated, and the resulting solid was dried at 15 mbar and 40 ºC for 15 min. The corresponding ammonium BF_3 salt **11** was purified by flash column chromatography on silica gel (*n*-hexane/MTBE/acetone 2:1:1 + 1v% AcOH), to afford a colourless oil, 34 mg (59 % yield).

4-(1-(difluoroboraneyl)-4-phenylbutyl-1,2-*d*$_2$)morpholin-4-ium fluoride (**11**): **^{1}H NMR** (500 MHz, $CDCl_3$): *δ* 7.28 – 7.25 (m, 2H), 7.19 – 7.16 (m, 3H), 6.80 (br, 1H), 4.02 – 3.94 (m, 3H), 3.82 – 3.76 (m, 1H), 3.37 (d, *J* = 12.8 Hz, 1H), 3.21 – 3.12 (m, 2H), 2.95 – 2.88 (m, 1H), 2.67 (t, *J* = 7.4 Hz, 2H), 2.37 – 2.31 (m, 0.24H), 1.96 – 1.90 (m, 1H), 1.75 – 1.69 (m, 0.8H), 1.66 – 1.58 (m, 1H), 1.53 – 1.50 (m, 0.8H) ppm. **^{13}C NMR** (126 MHz, $CDCl_3$): *δ* 141.9, 128.6, 128.5, 126.0, 64.6, 64.5, 51.7, 48.5, 36.01 – 35.98 (m), 28.2 – 28.1 (m), 23.3 – 23.2 (m) ppm. The carbon (CH) adjacent to boron was not observed, due to quadrupolar coupling with ^{11}B

(I = 3/2) and ^{10}B (I = 3). **^{11}B NMR** (128 MHz, $CDCl_3$): δ 2.64 ppm. **^{19}F NMR** (376 MHz, $CDCl_3$): δ -142.7 ppm. **IR** (neat, cm^{-1}): 3170, 2956, 2925, 2870, 1603, 1460, 1414, 1260, 1149, 1058, 1028, 953, 941, 747, 700. **HRMS**: m/z calcd. for ($C_{14}H_{21}F_3NNaO^{10}B$) $[M+Na]^+$: 309.1597; found 309.1584, ($C_{14}H_{20}DF_3NNaO^{11}B$) $[M+Na]^+$: 311.1623; found 311.1648 and ($C_{14}H_{19}D_2F_3NNaO^{11}B$) $[M+Na]^+$: 312.1686; found 312.1691. **MP**: 165 – 167ºC.

4.5.7. X-Ray crystallographic data

	4a	**4i**
Formula	$C_{14}H_{21}BF_3NO$	$C_{64}H_{92}B_4F_{12}N_4O_4$
Formula weight	287.17	1252.65
T (K)	298(2)	100(2)K
Wavelength (Å)	0.71073	0.71073
Crystal system	Orthorhombic	monoclinic
Space group	P b c a	P 21/
***a* (Å)**	9.0038(8)	21.3843(4)
***b* (Å)**	30.495(5)	14.1566(3)
***c* (Å)**	11.1854(13)	21.6516(5)
α (deg)	90	90
β (deg)	90	90.151
γ (deg)	90	90
V (Å^3)	3071.2(7)	6554.5(2)
Z	8	4
Density (calc.) (Mg·m^{-3})	1.242	1.269
μ (mm^{-1})	0.101	0.100
F(000)	1216	2656
Crystal size (mm^3)	0.200 x 0.200 x 0.100	0.400 x 0.100 x 0.100
Theta range for data collection (deg)	2.980 to 28.683	3.333 to 29.754
Index ranges	-11<=h<=10,-29<=k<=41,-12<=l<=14	27<=h<=28,-18<=k<=17,-23<=l<=30
Reflections collected	16903	59001
Independent reflections	3502[R(int) = 0.0528]	16439[R(int) = 0.0636]
Completeness to theta	88.3%	87.9%
Absorption correction	Multi-scan	Multi-scan
Max. and min. transmission	1.00 and 0.46	1.00 and 0.84
Refinement method	Full-matrix least-squares on F^2	Full-matrix least-squares on F^2
Data / restraints / parameters	3502/ 399/ 361	16439/ 290/ 849
Goodness-of-fit on F^2	1.071	1.071
Final R indices [I>2sigma(I)]	R1 = 0.1297, wR2 = 0.3749	R1 = 0.0490, wR2 = 0.1316
R indices (all data)	R1 = 0.1883, wR2 = 0.4110	R1 = 0.0653, wR2 = 0.1396
Largest diff. peak and hole	0.617 and -0.344 e.Å^{-3}	0.562 and -0.235 e.Å^{-3}

Table 6. Crystallographic data

X-Ray Crystal structure for 4a (CCDC-2243931)

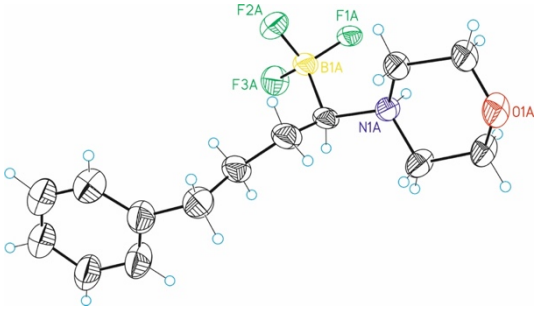

X-Ray Crystal structure for 4i (CCDC-2243932)

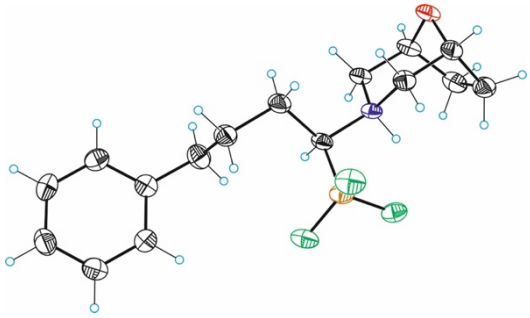

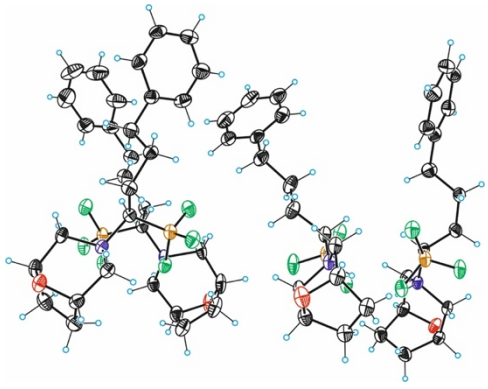

4.5.8.NMR spectra

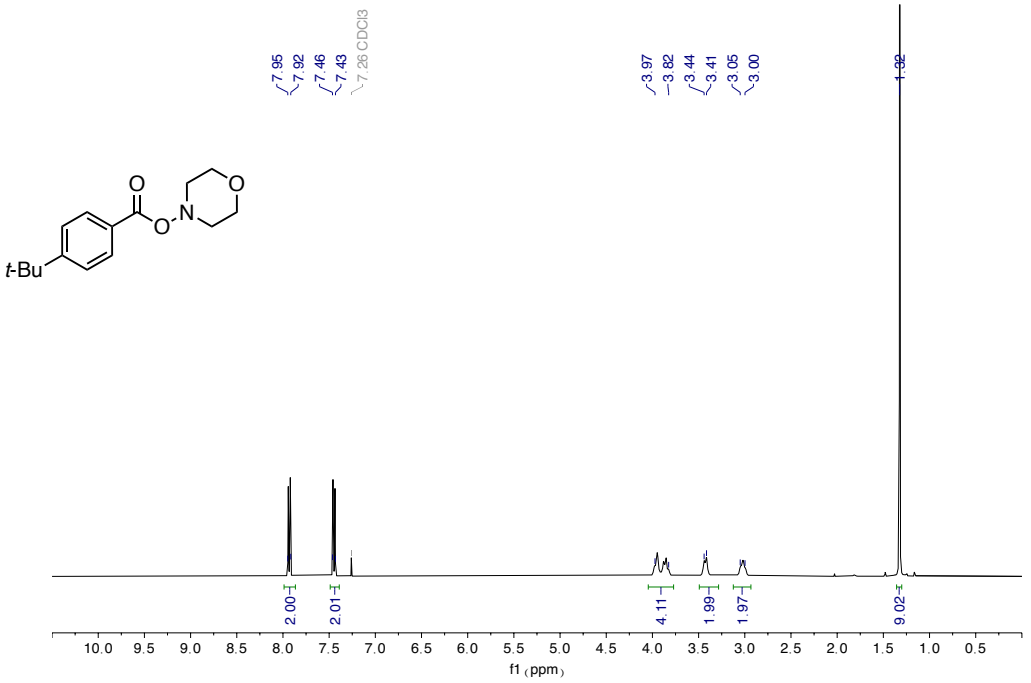

*[1]H NMR spectra (500 MHz) of **2c***

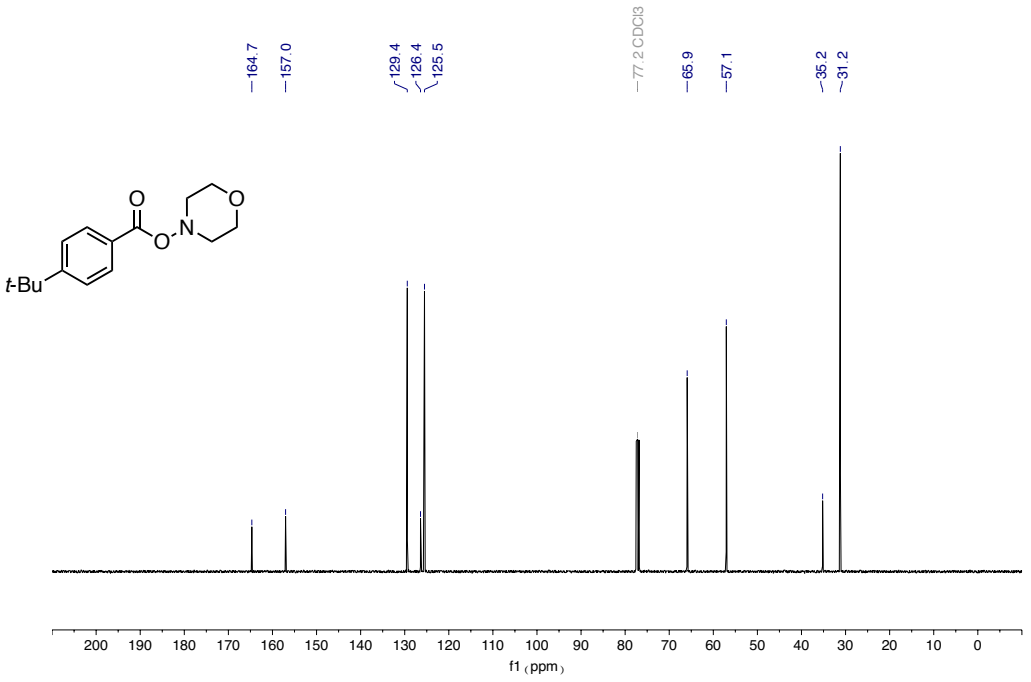

*[13]C NMR spectra (126 MHz) of **2c***

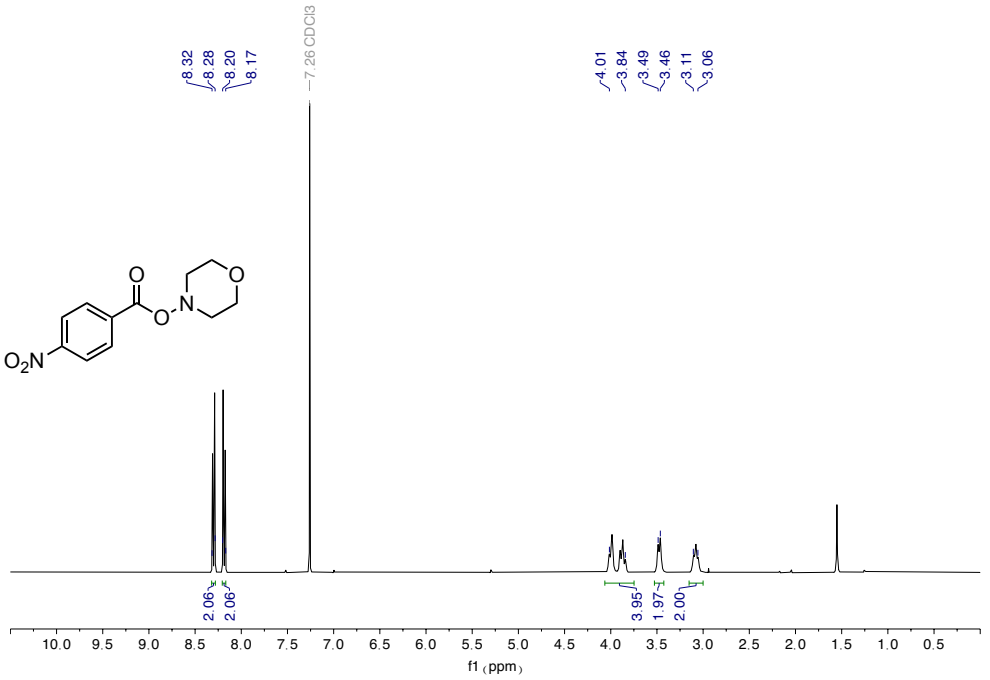

*^{1}H NMR spectra (400 MHz) of **2d***

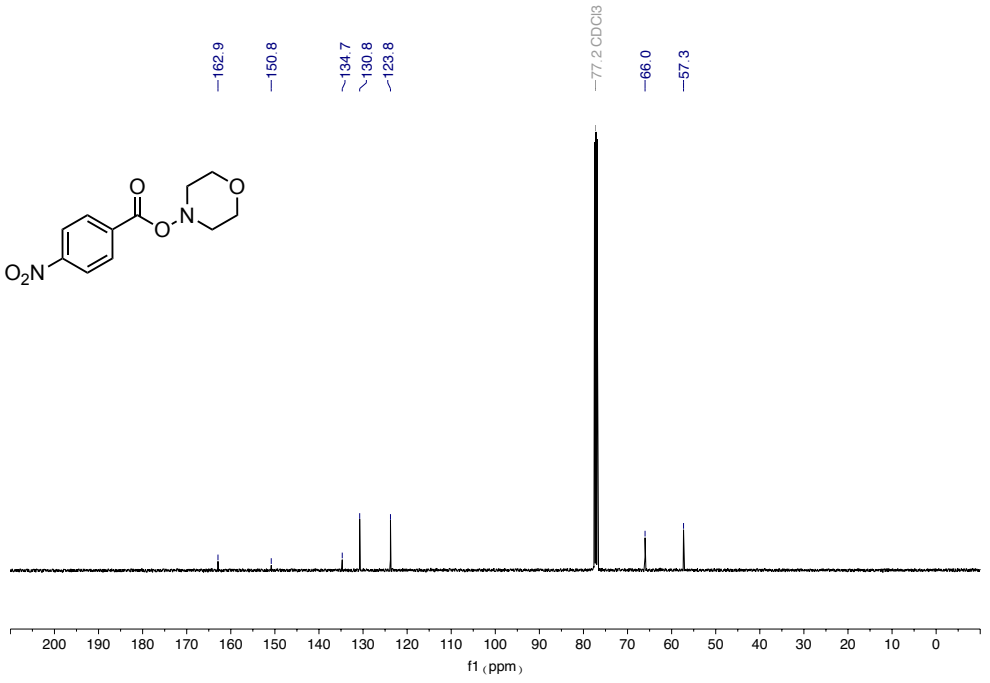

*^{13}C NMR spectra (101 MHz) of **2d***

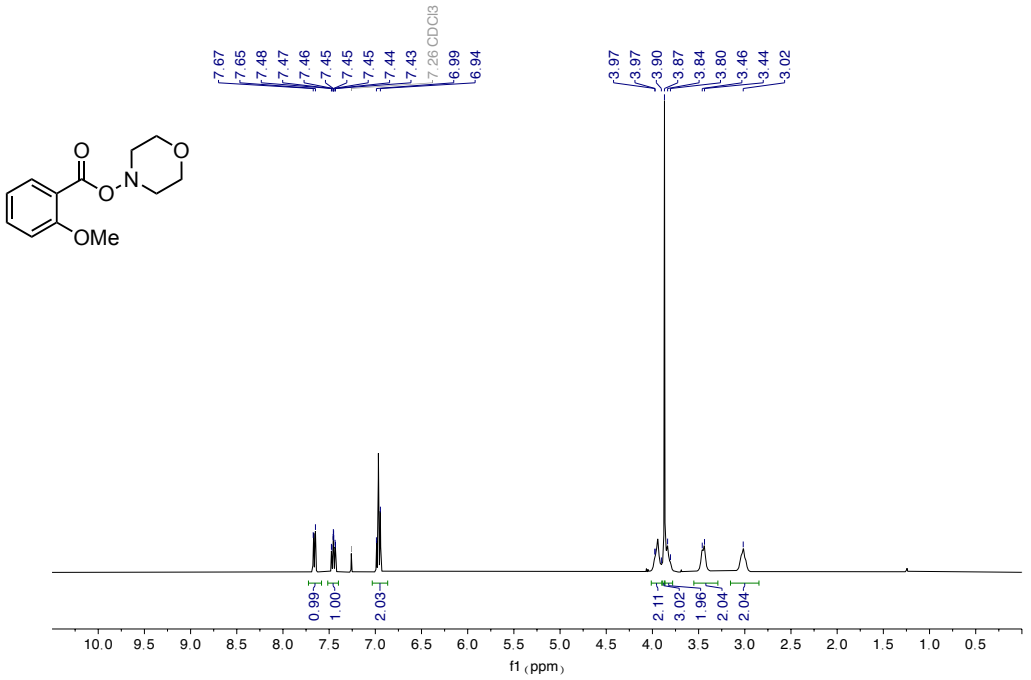

*^{1}H NMR spectra (400 MHz) of **2e***

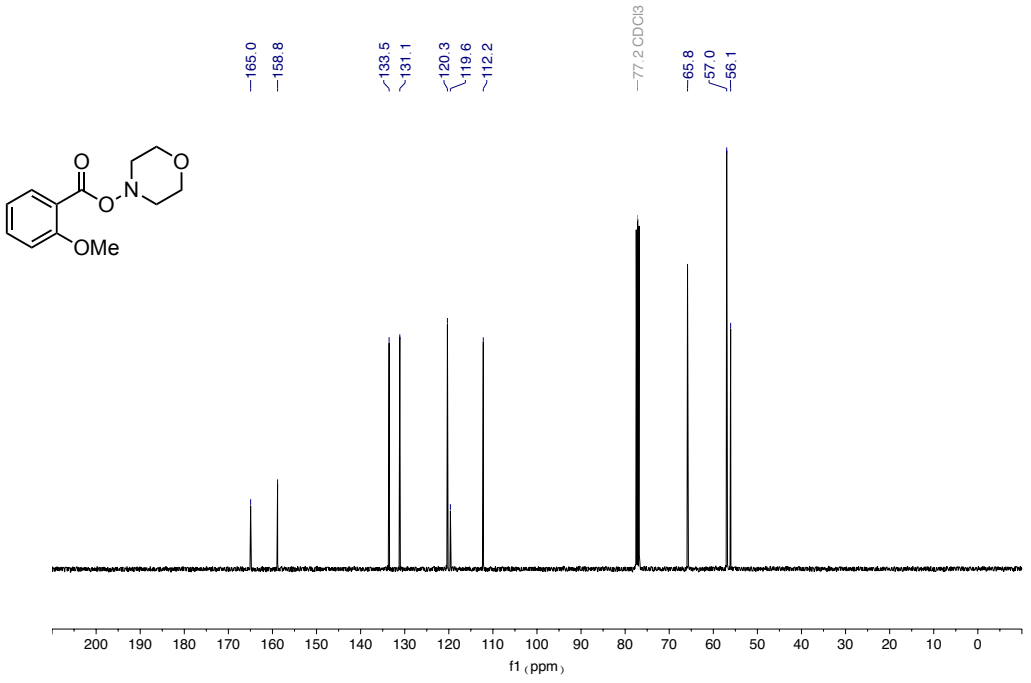

*^{13}C NMR spectra (101 MHz) of **2e***

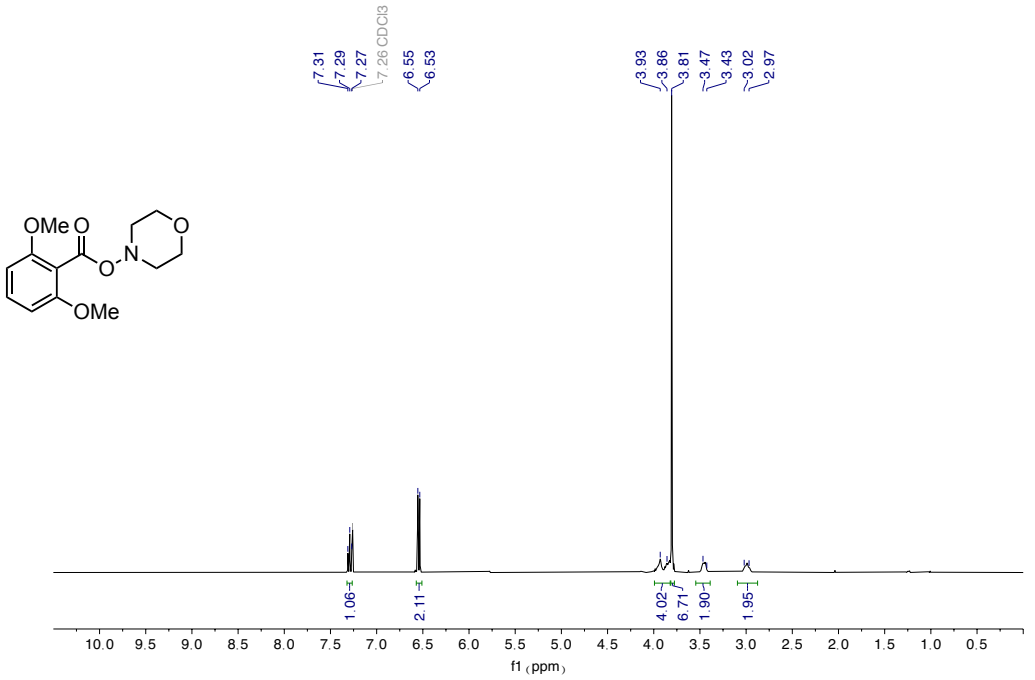

*[1]H NMR spectra (400 MHz) of **2f***

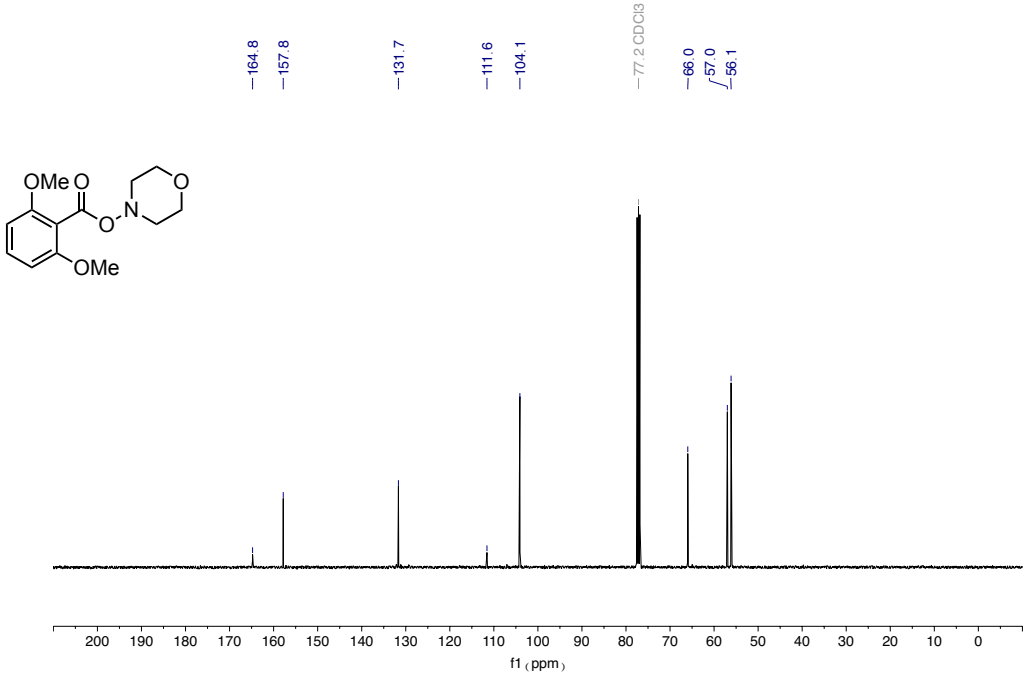

*[13]C NMR spectra (101 MHz) of **2f***

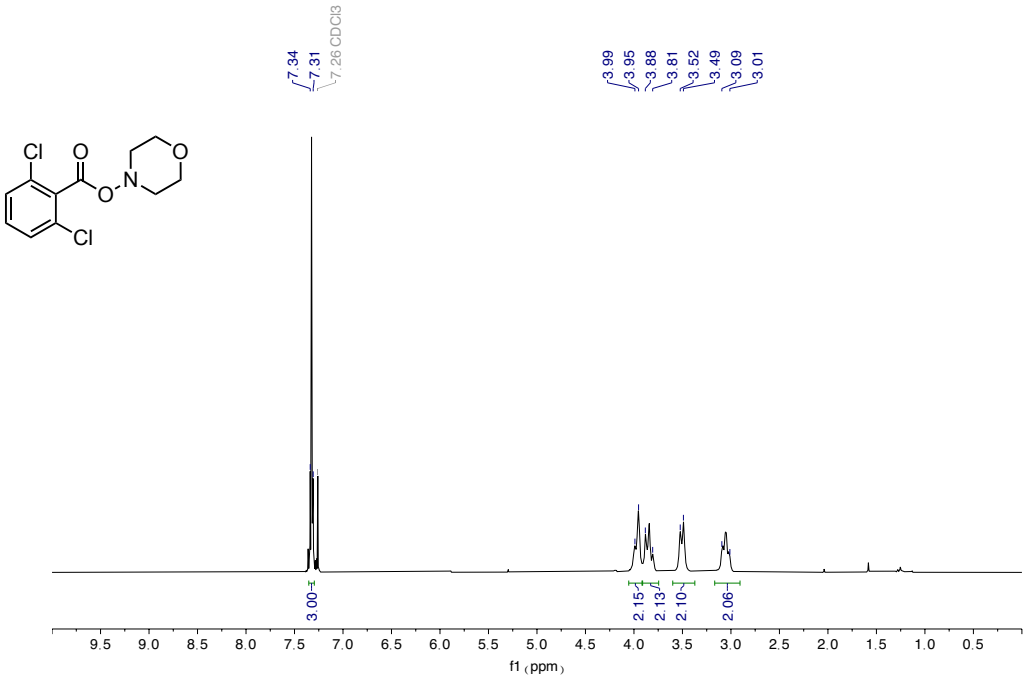

*^{1}H NMR spectra (300 MHz) of **2g***

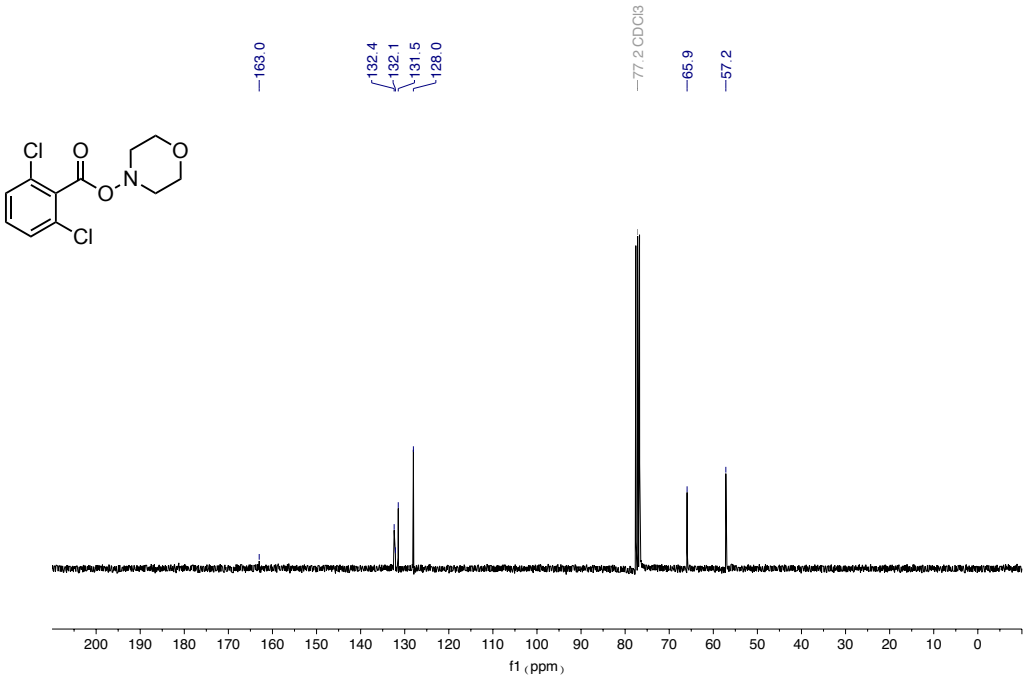

*^{13}C NMR spectra (75 MHz) of **2g***

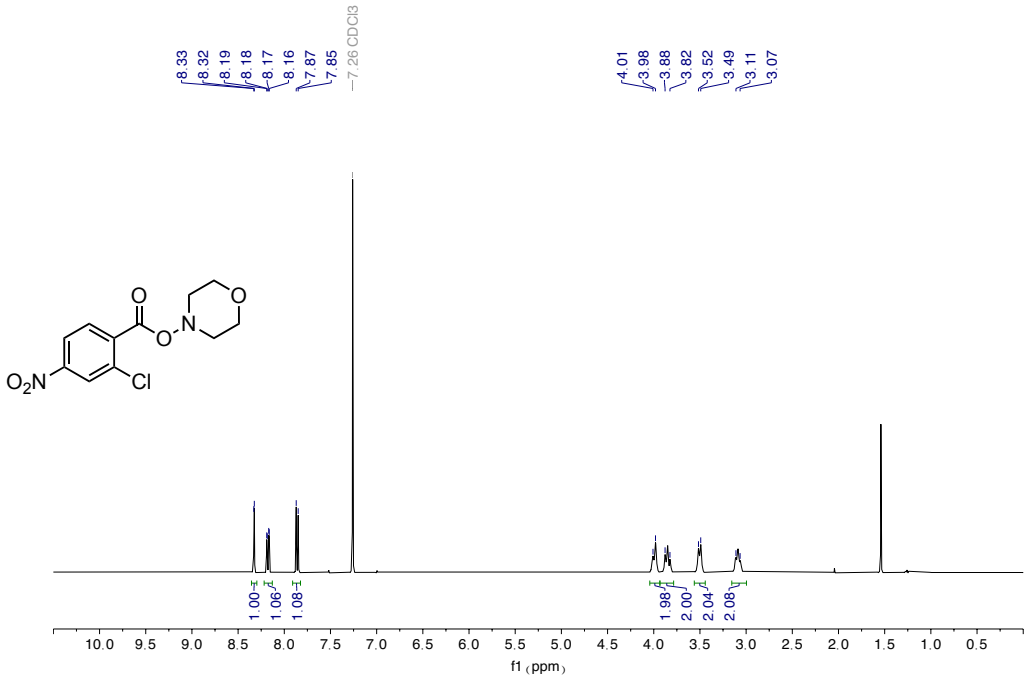

*^{1}H NMR spectra (400 MHz) of **2h***

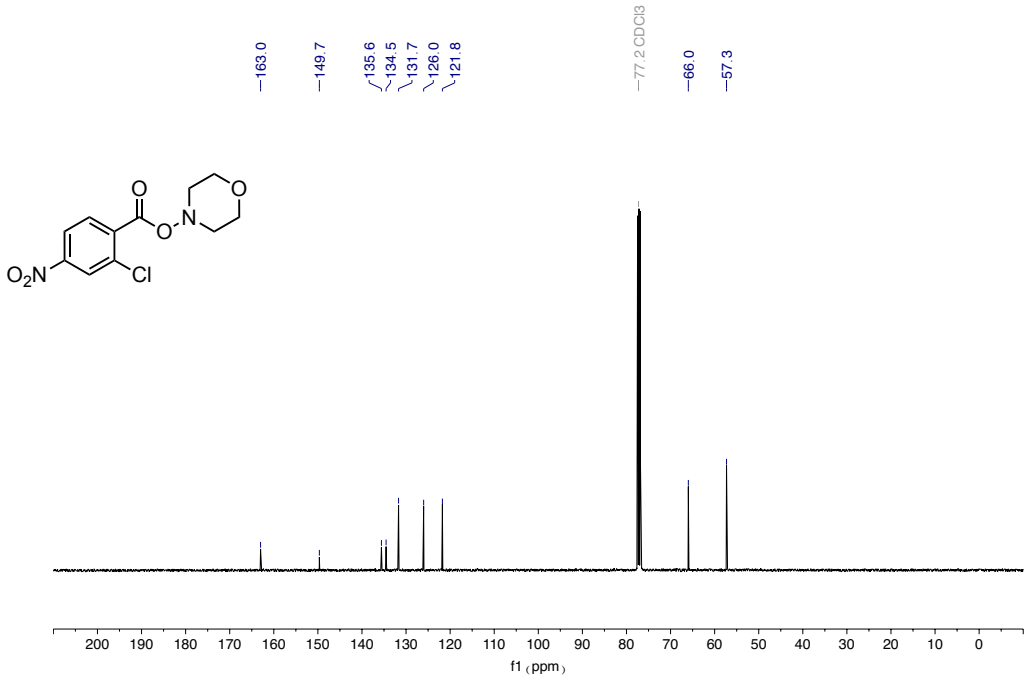

*^{13}C NMR spectra (101 MHz) of **2h***

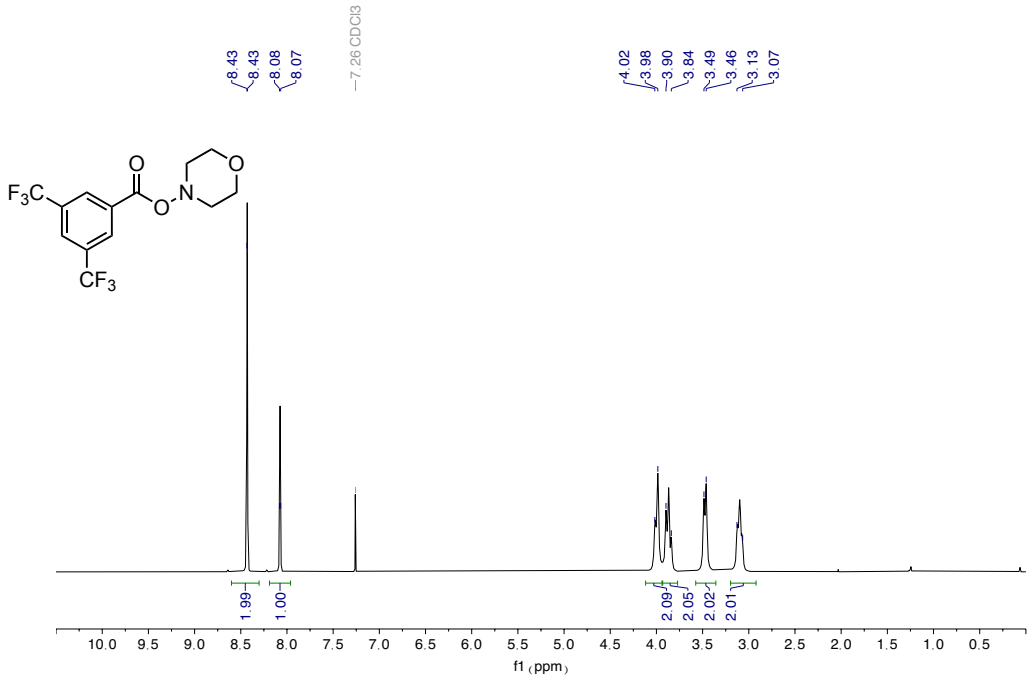

*^{1}H NMR spectra (400 MHz) of **2i***

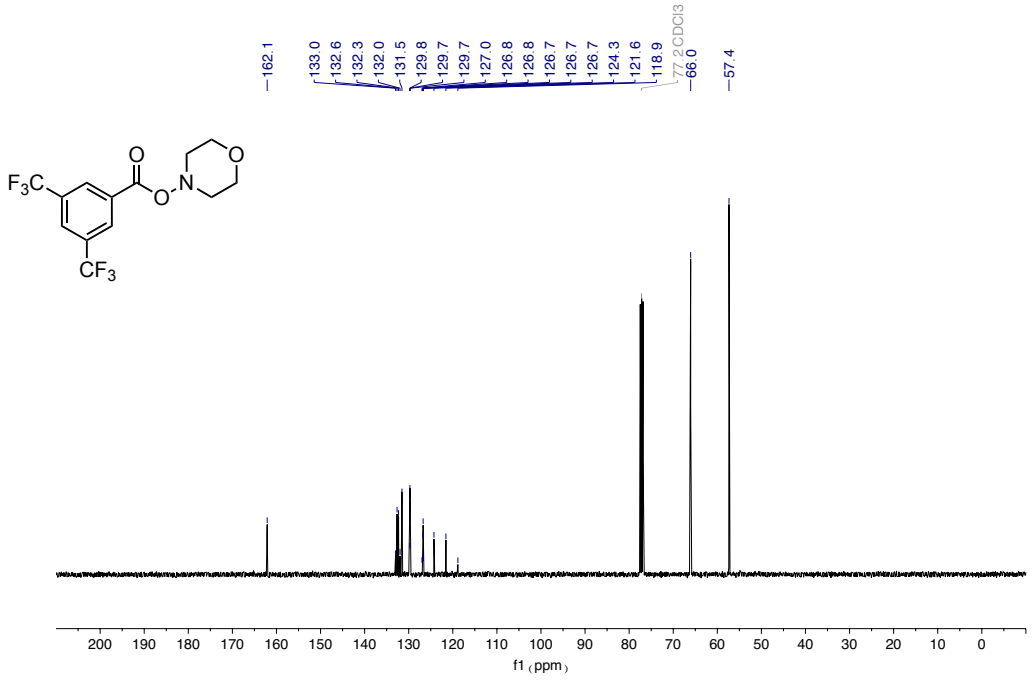

*^{13}C NMR spectra (101 MHz) of **2i***

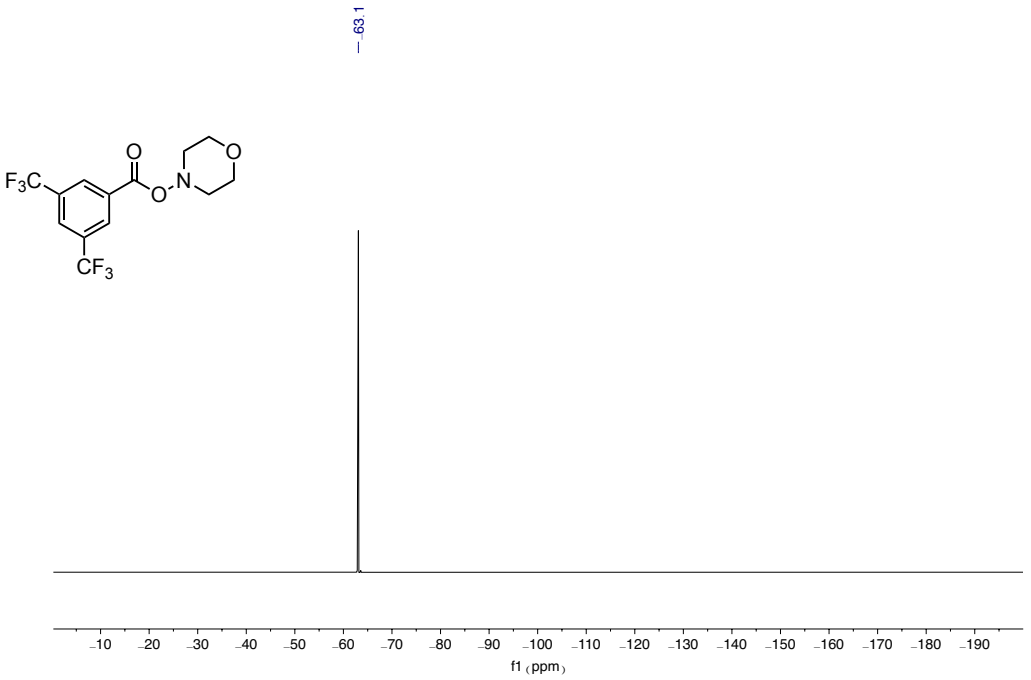

*^{19}F NMR spectra (376 MHz) of **2i***

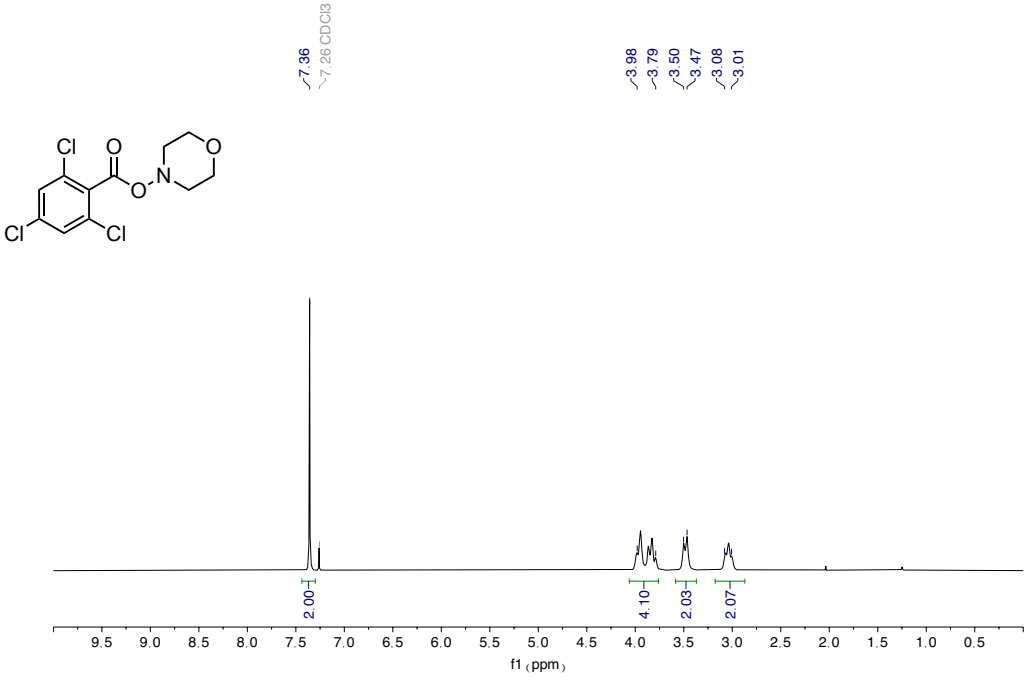

*^{1}H NMR spectra (300 MHz) of **2j***

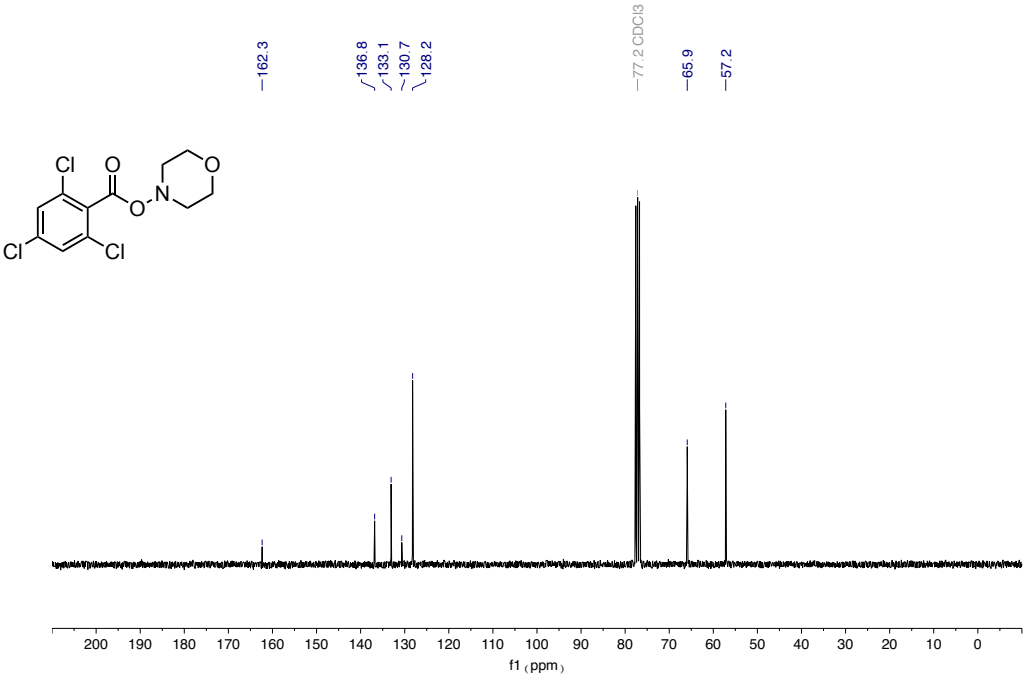

*^{13}C NMR spectra (76 MHz) of **2j***

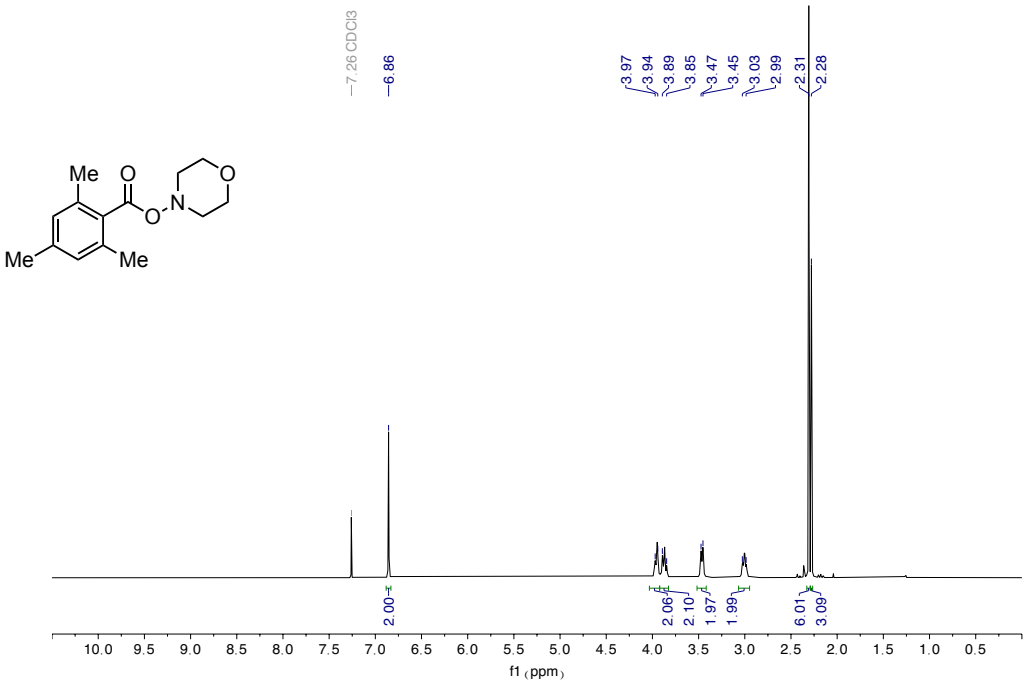

*^{1}H NMR spectra (400 MHz) of **2k***

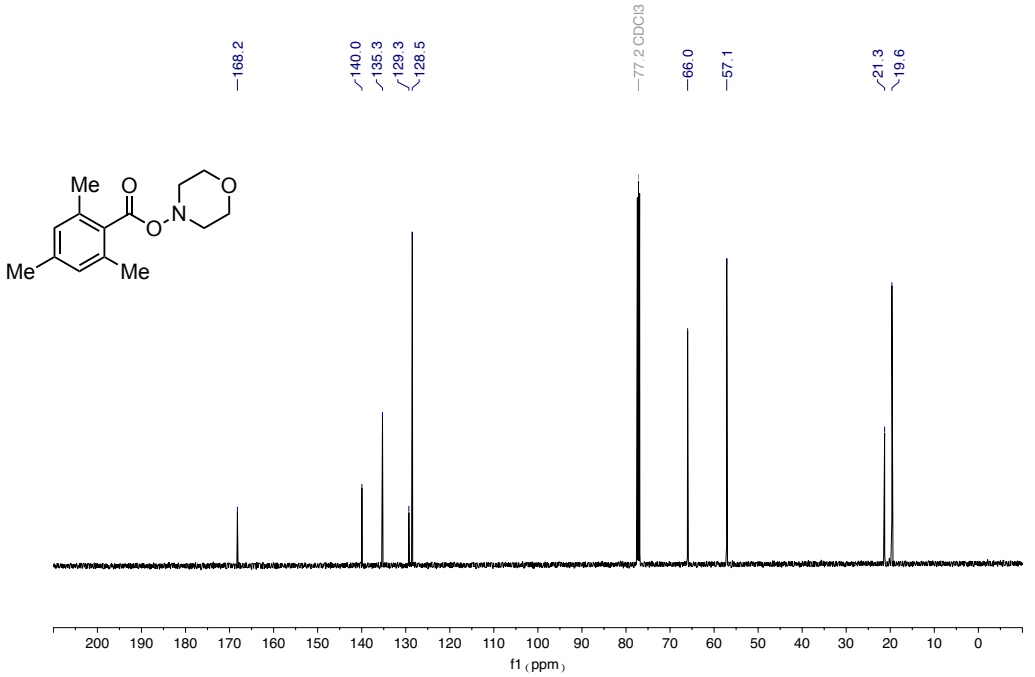

*^{13}C NMR spectra (126 MHz) of **2k***

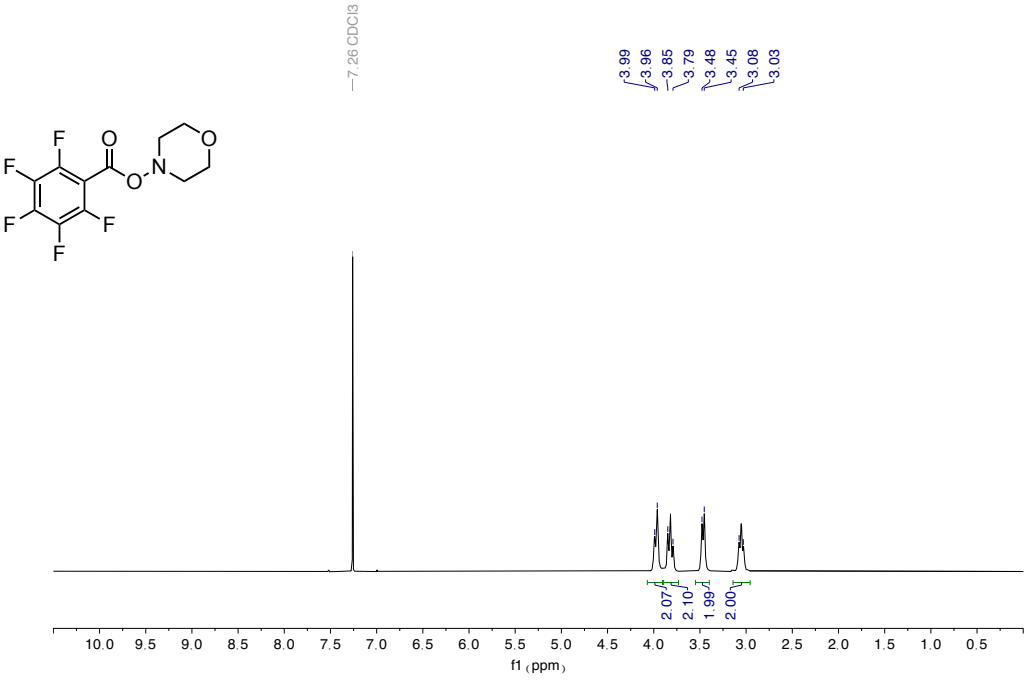

*^{1}H NMR spectra (400 MHz) of **2l***

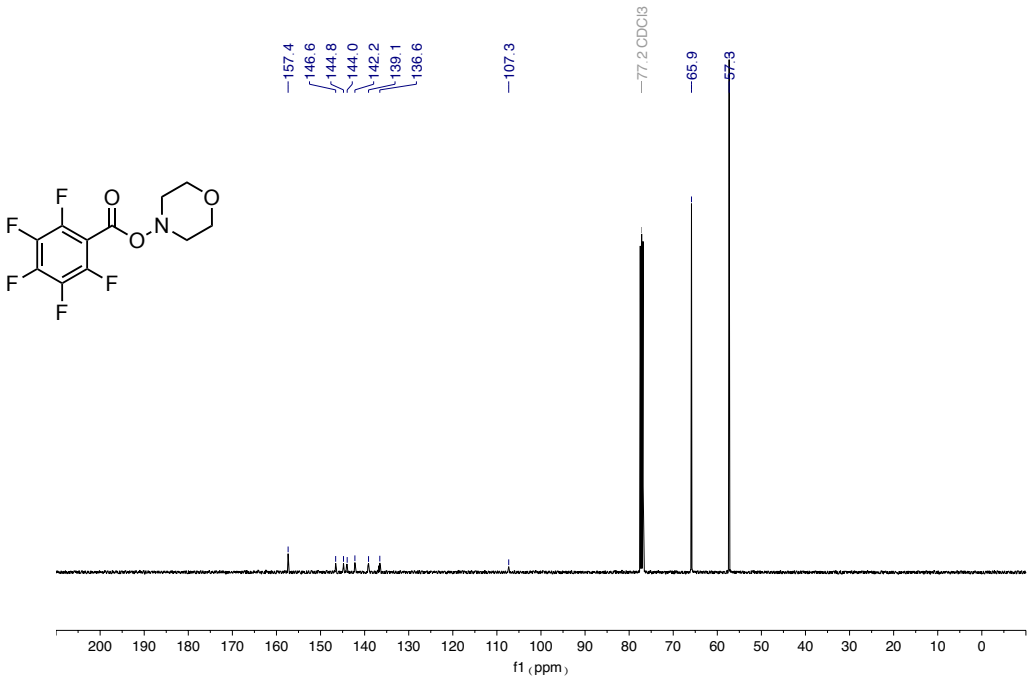

*^{13}C NMR spectra (101 MHz) of **2l***

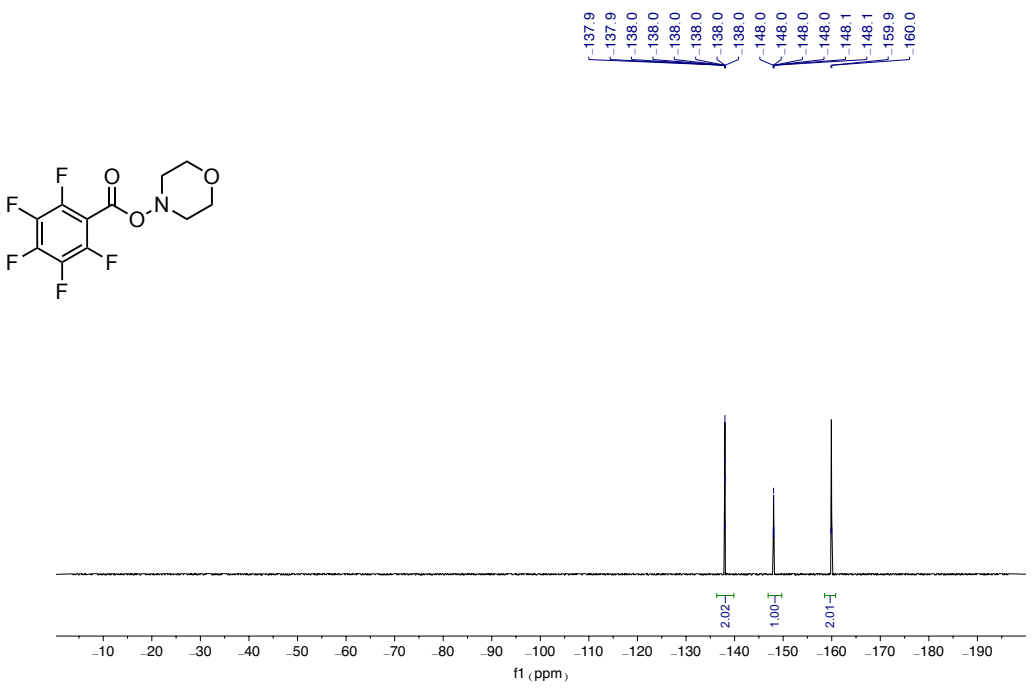

*^{19}F NMR spectra (376 MHz) of **2l***

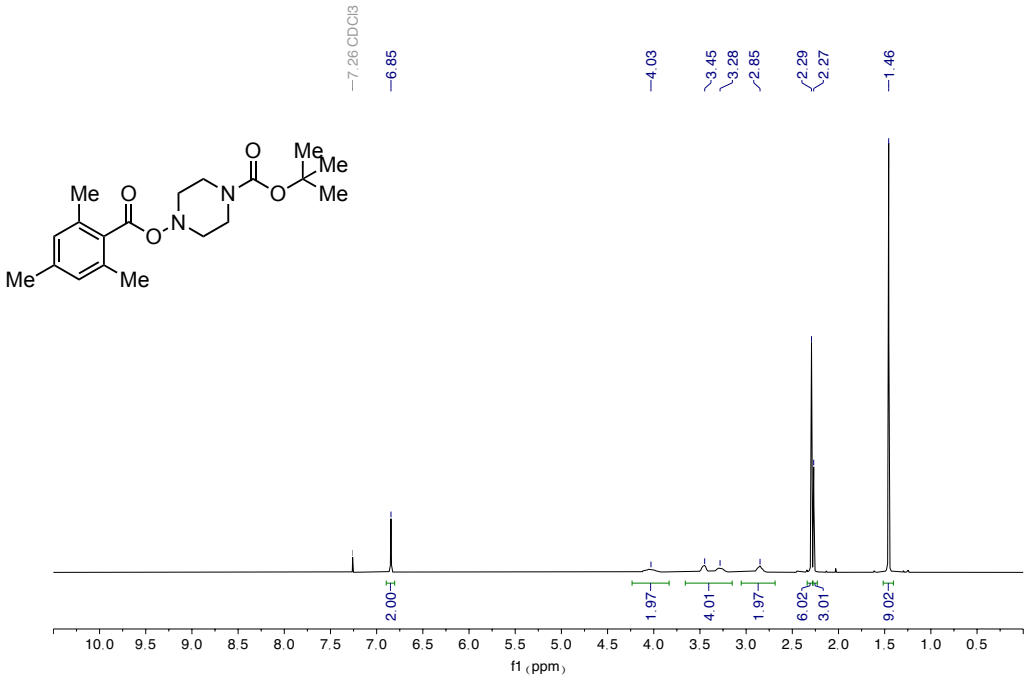

*^{1}H NMR spectra (400 MHz) of **2m***

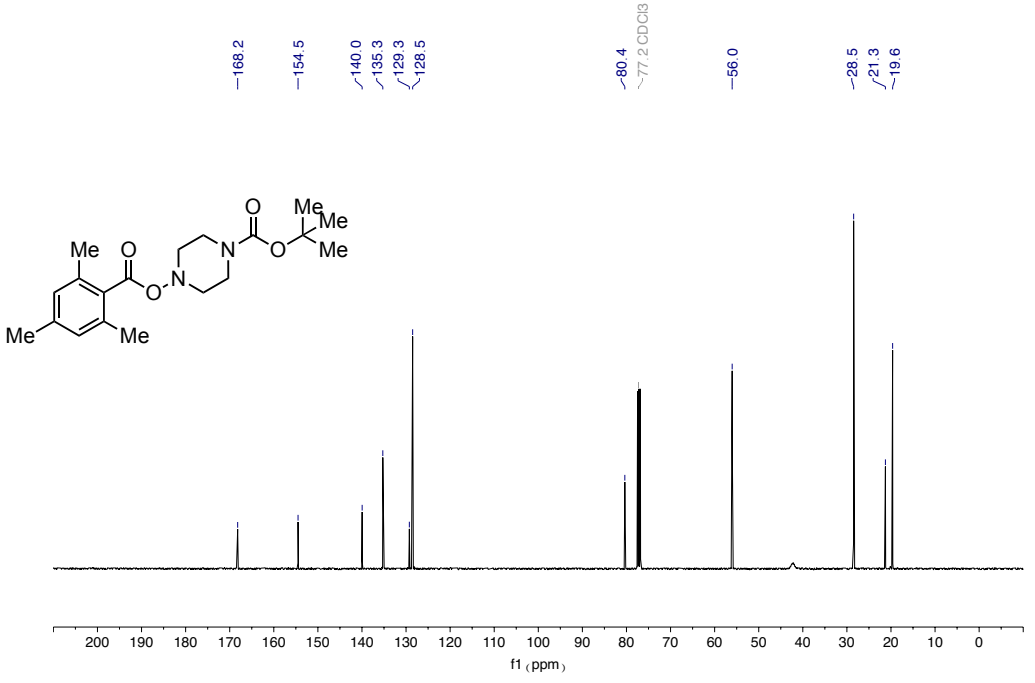

*^{13}C NMR spectra (101 MHz) of **2m***

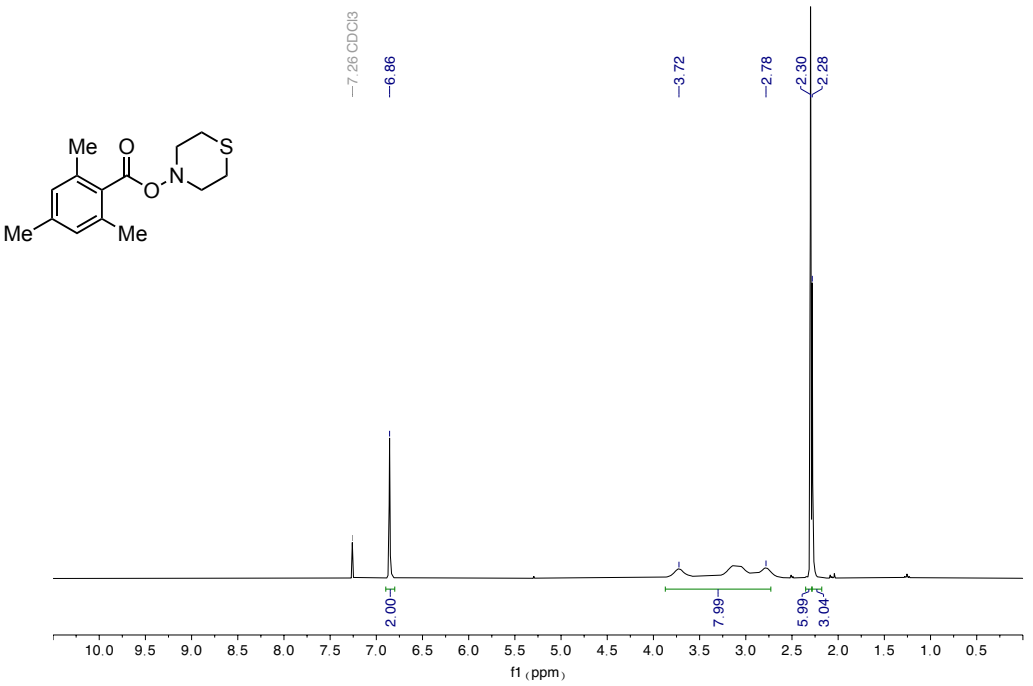

*^{1}H NMR spectra (300 MHz) of **2n***

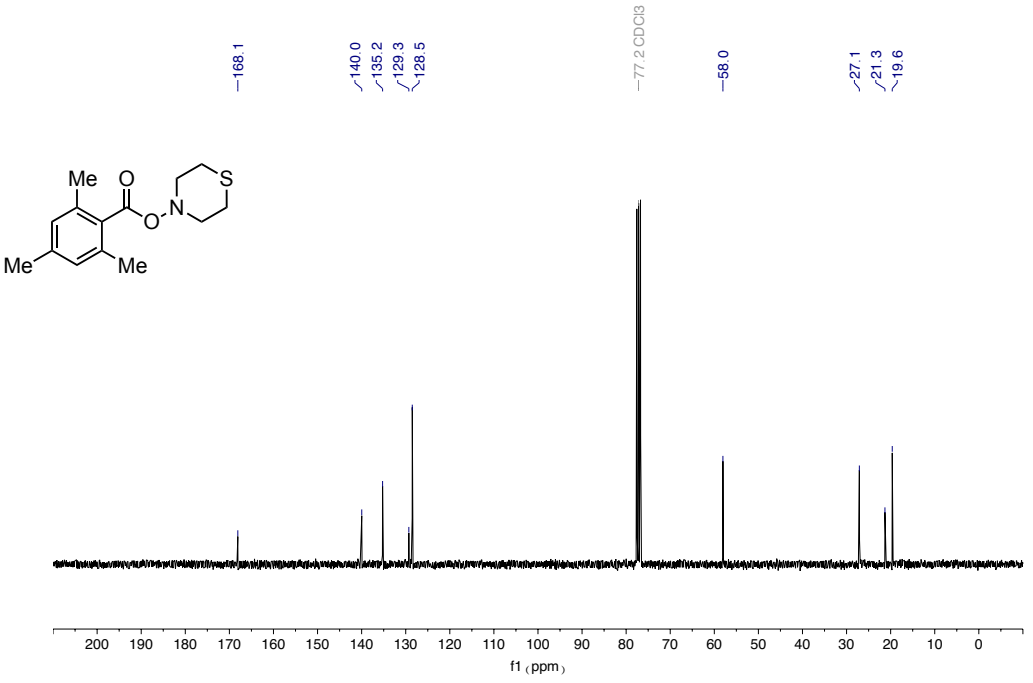

*^{13}C NMR spectra (75 MHz) of **2n***

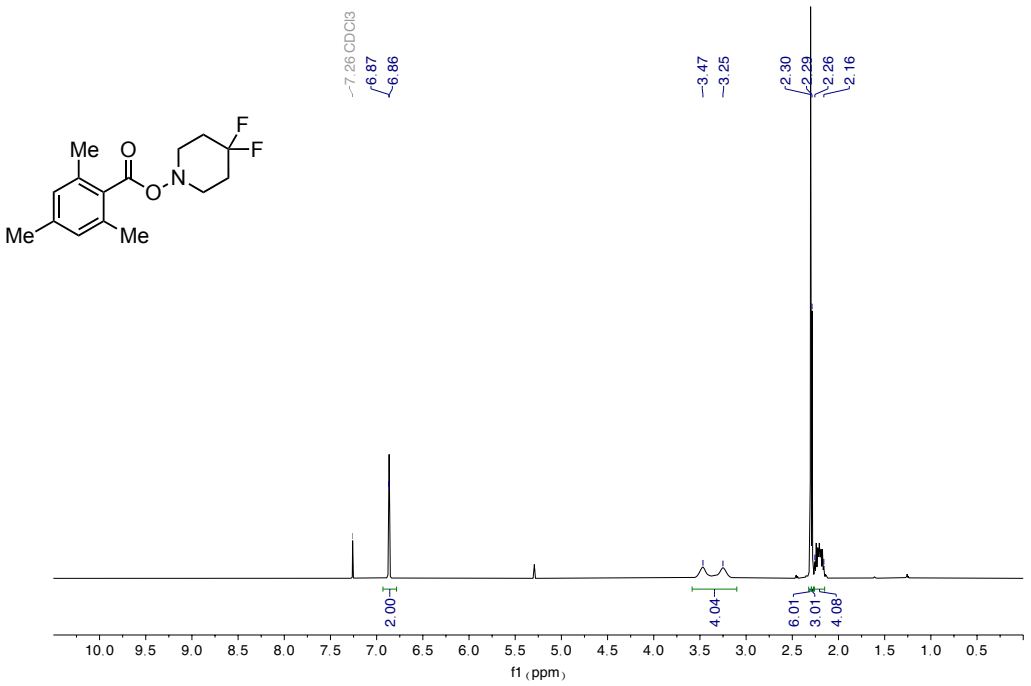

*^{1}H NMR spectra (400 MHz) of **2o***

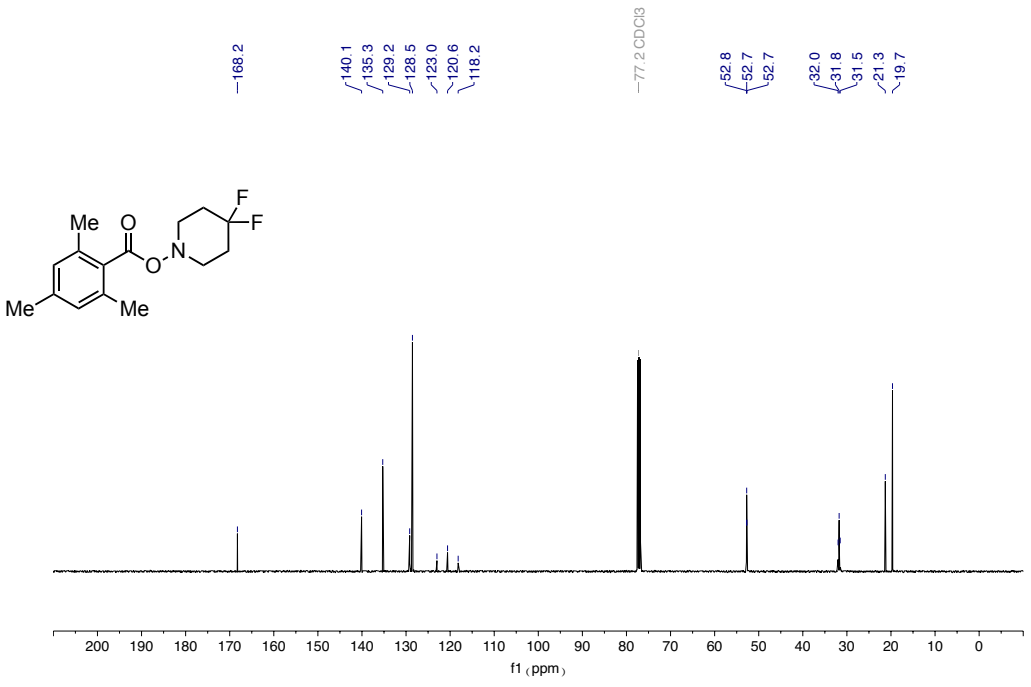

*^{13}C NMR spectra (101 MHz) of **2o***

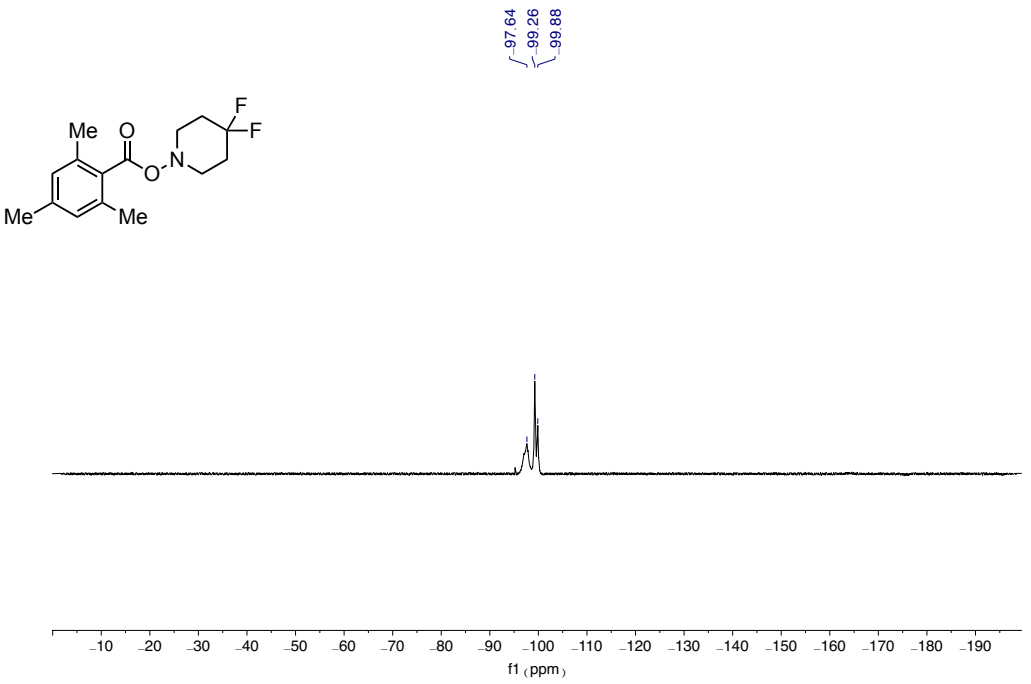

*^{19}F NMR spectra (376 MHz) of **2o***

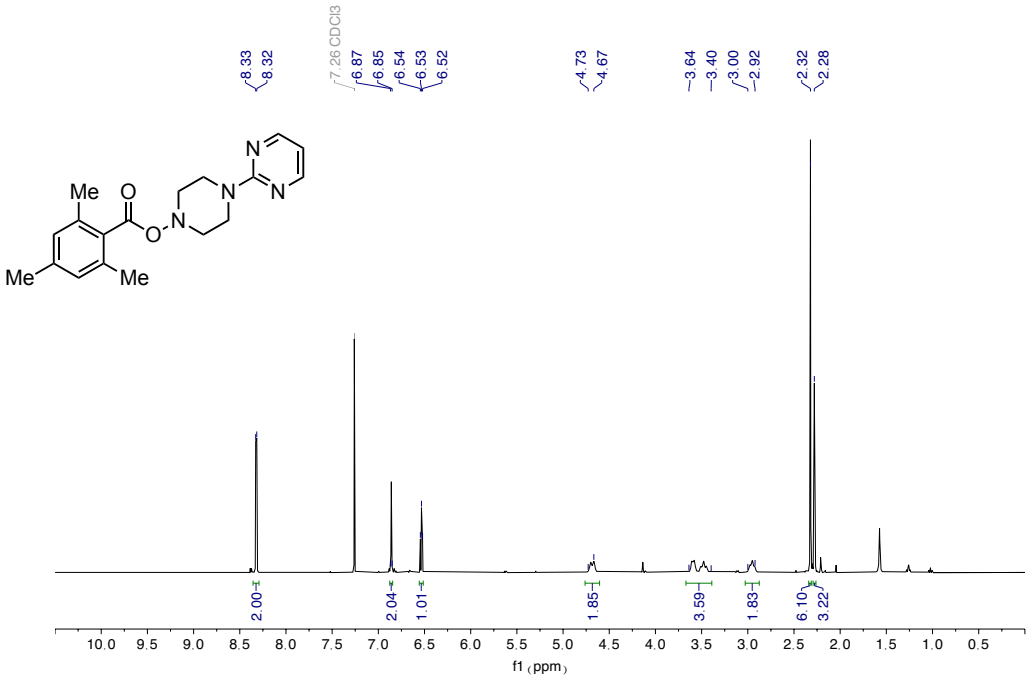

*^{1}H NMR spectra (400 MHz) of **2p***

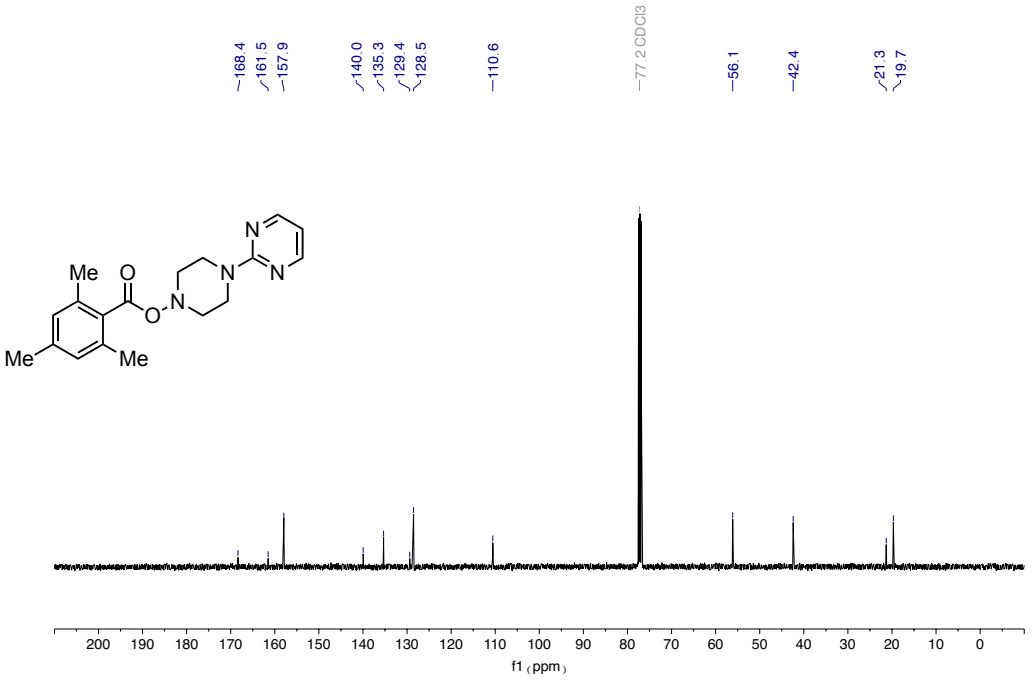

*^{13}C NMR spectra (101 MHz) of **2p***

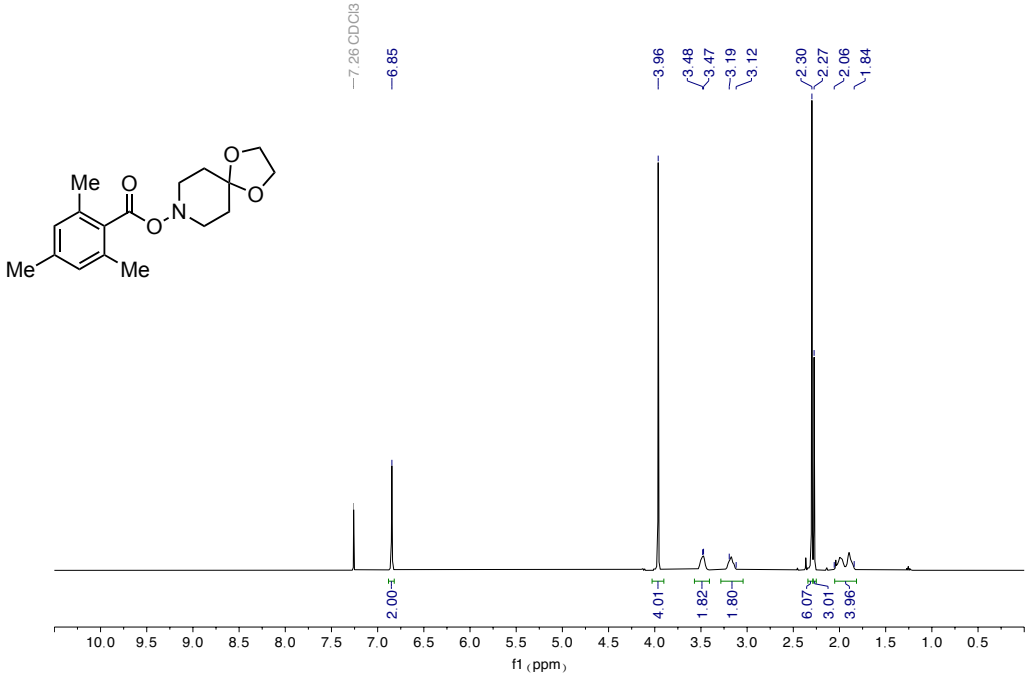

*^{1}H NMR spectra (400 MHz) of **2q***

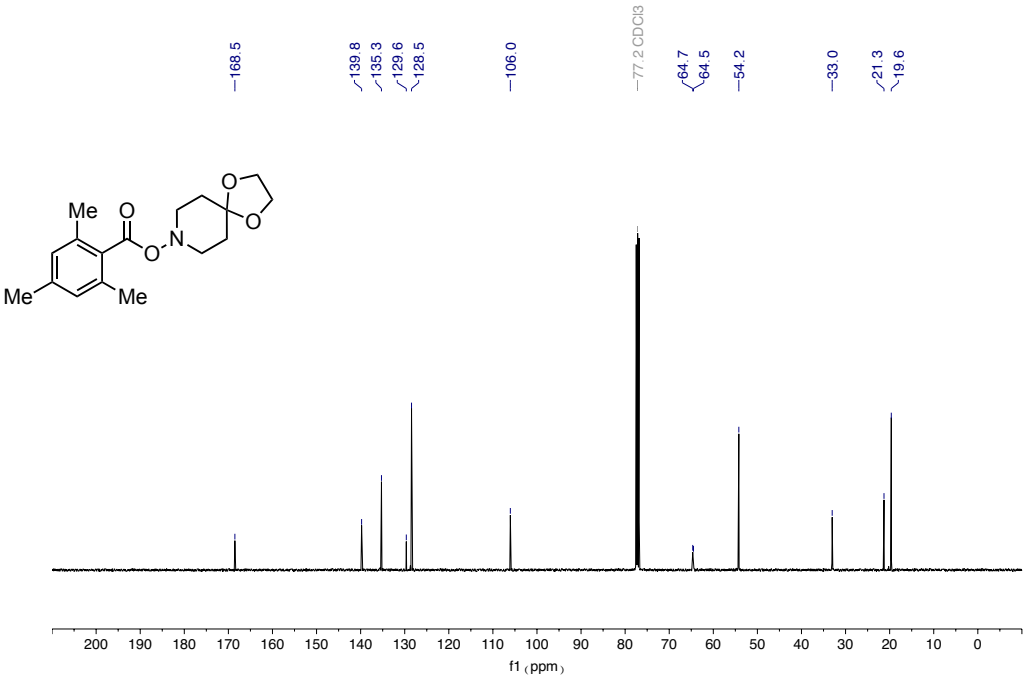

*^{13}C NMR spectra (101 MHz) of **2q***

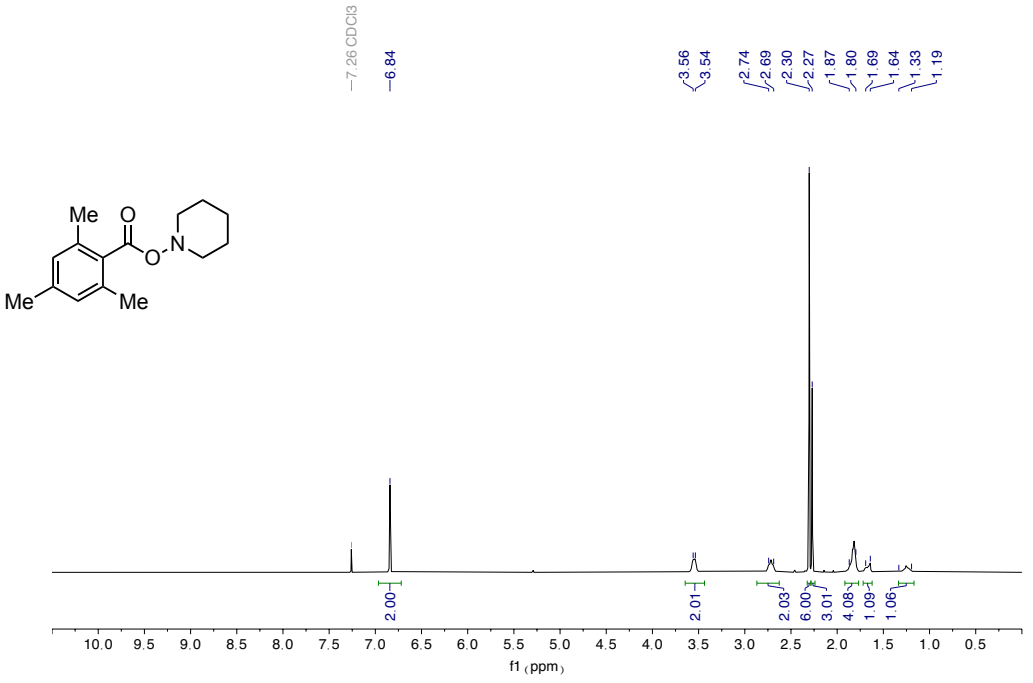

*^{1}H NMR spectra (400 MHz) of **2r***

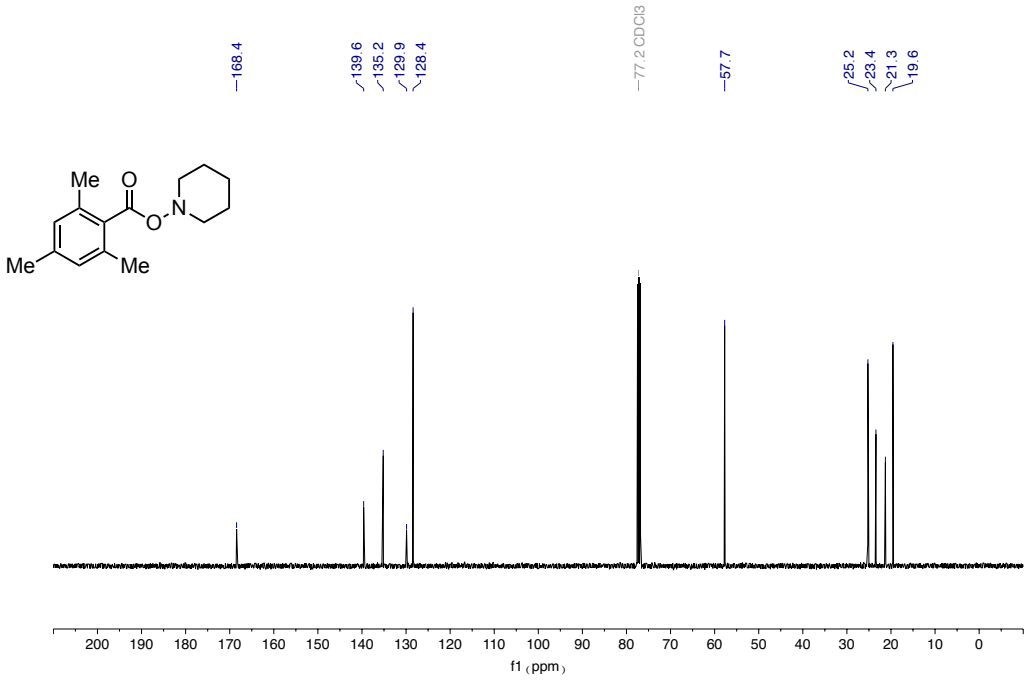

*^{13}C NMR spectra (101 MHz) of **2r***

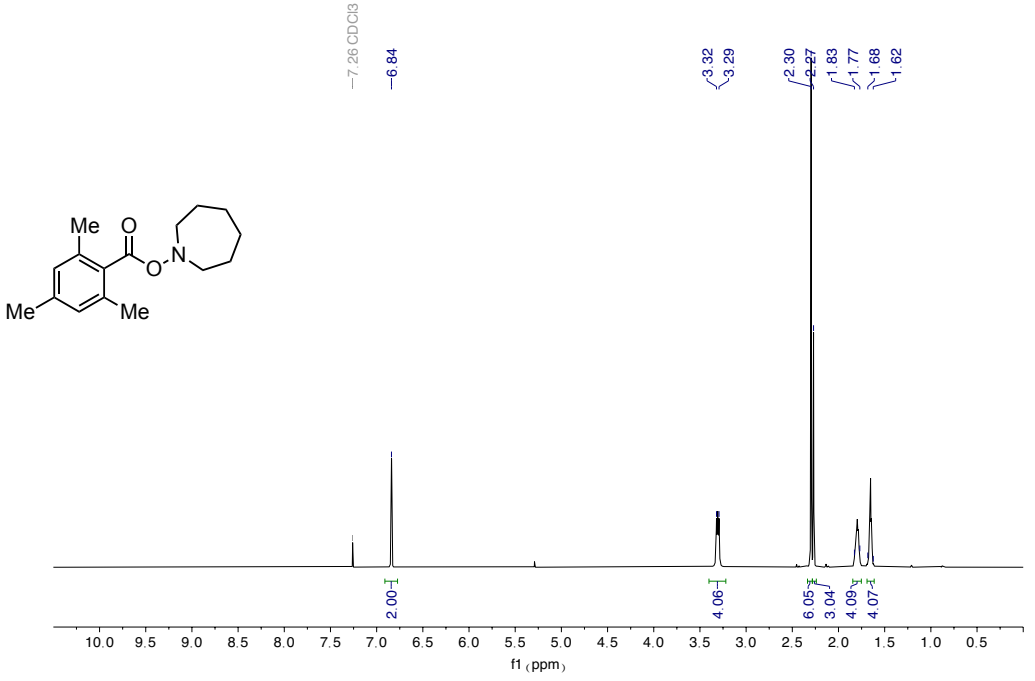

*^{1}H NMR spectra (400 MHz) of **2s***

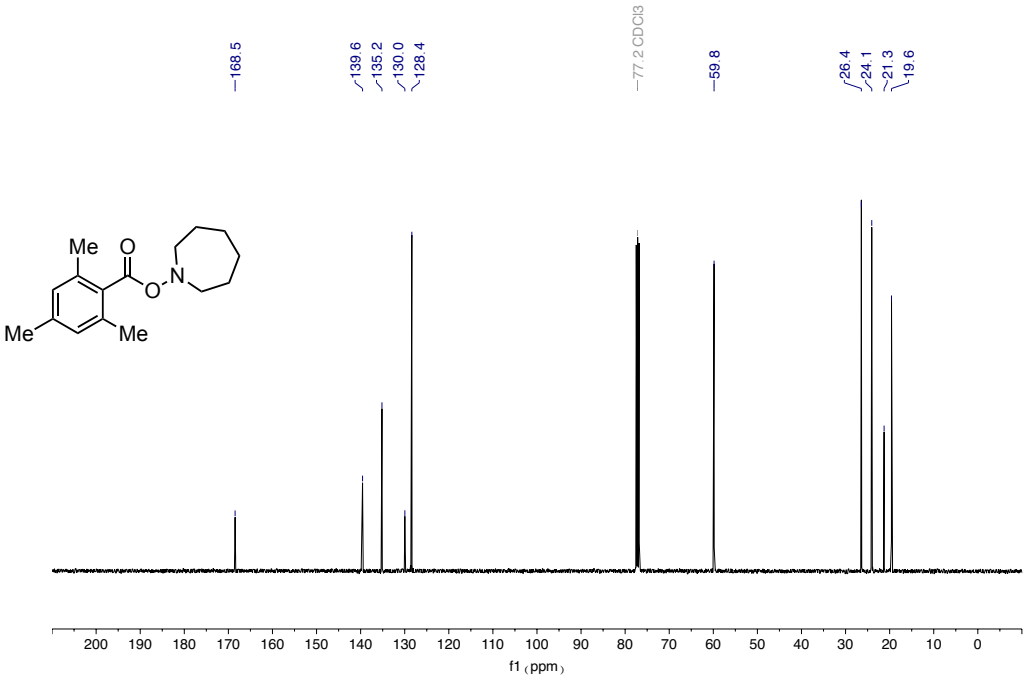

*^{13}C NMR spectra (101 MHz) of **2s***

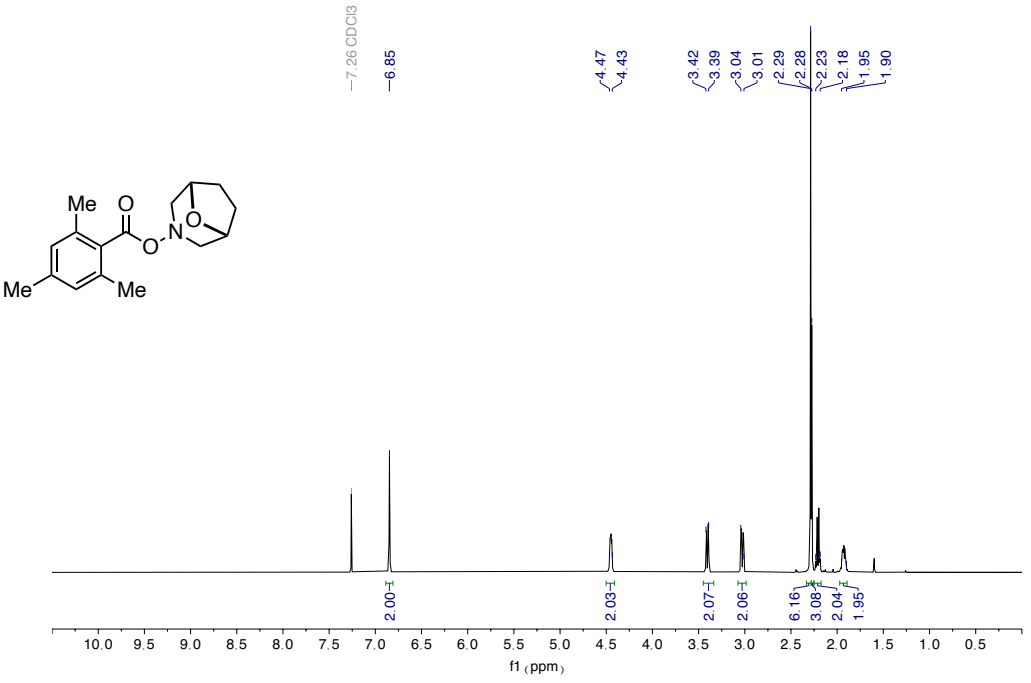

*^{1}H NMR spectra (400 MHz) of **2t***

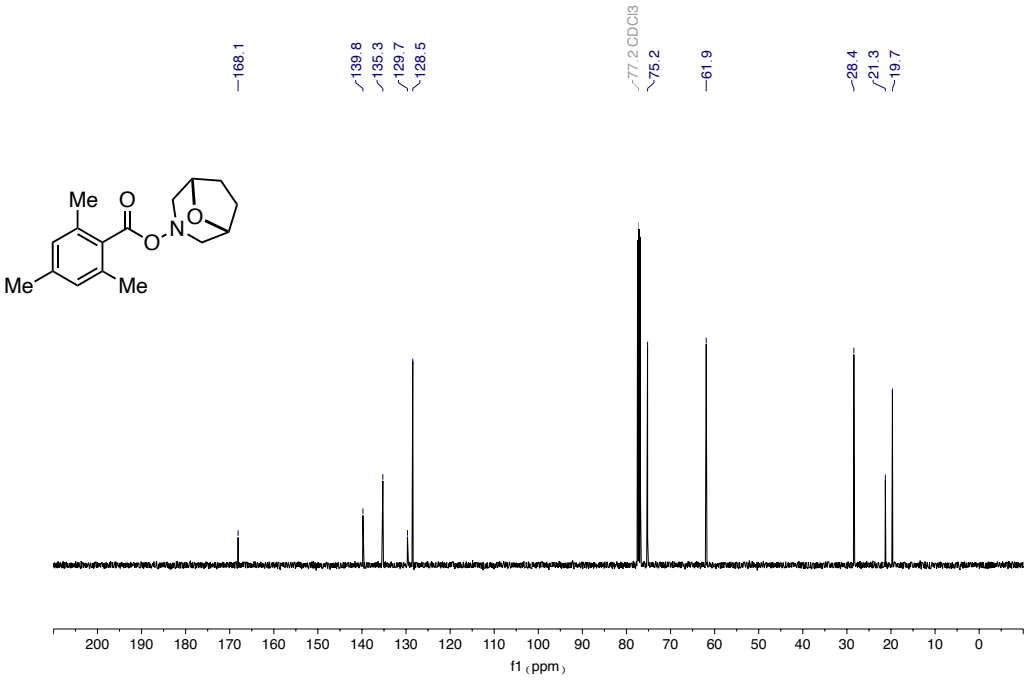

*^{13}C NMR spectra (101 MHz) of **2t***

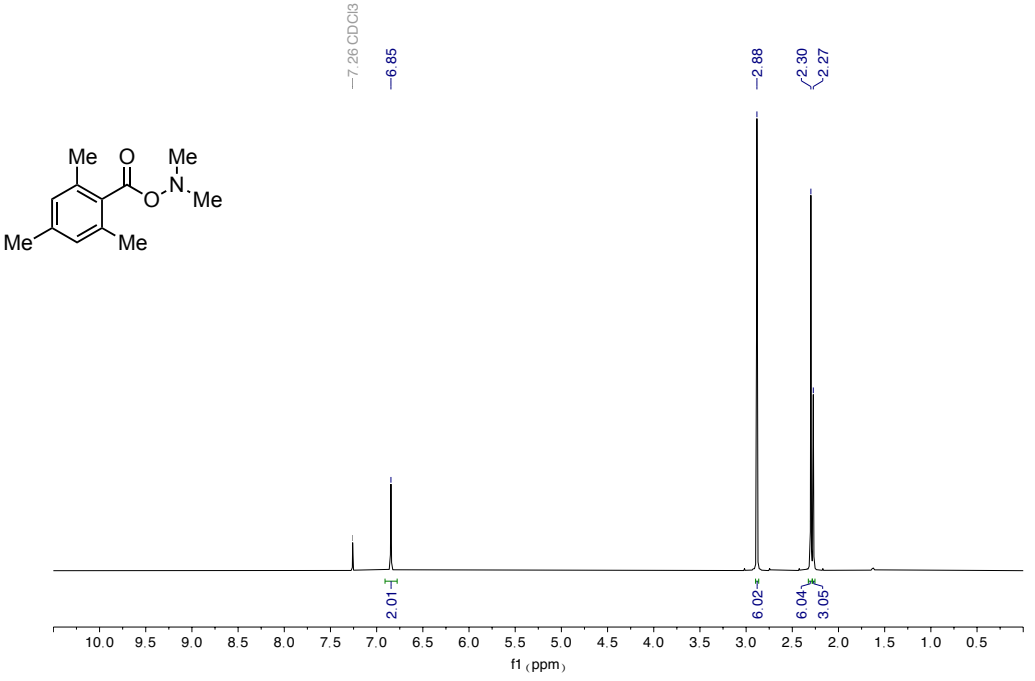

*^{1}H NMR spectra (500 MHz) of **2u***

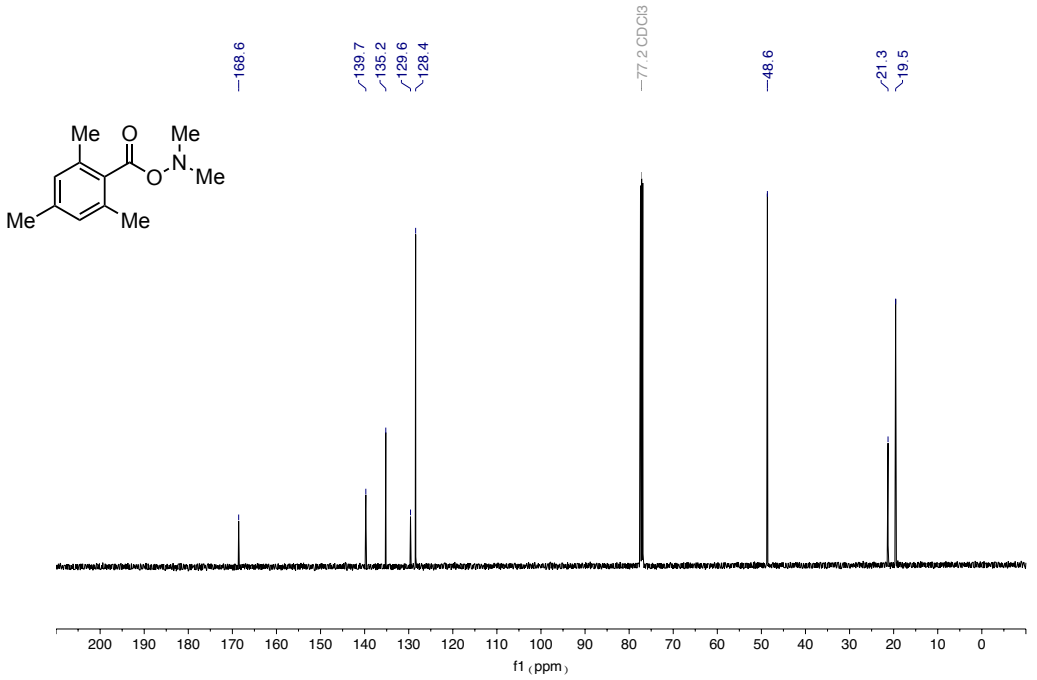

*^{13}C NMR spectra (126 MHz) of **2u***

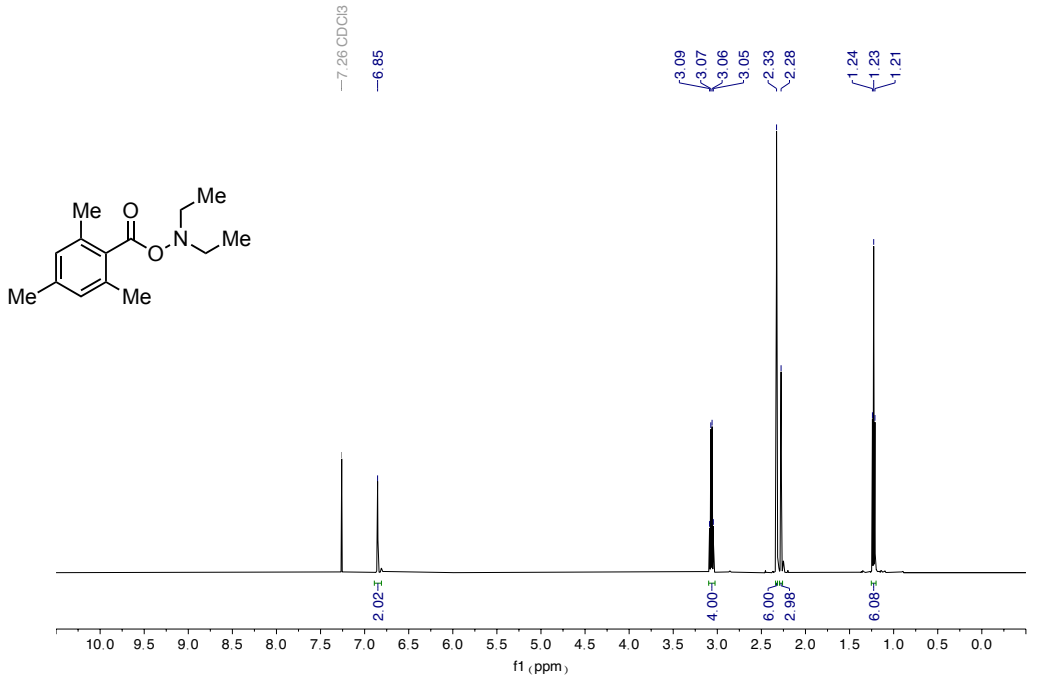

*^{1}H NMR spectra (400 MHz) of **2v***

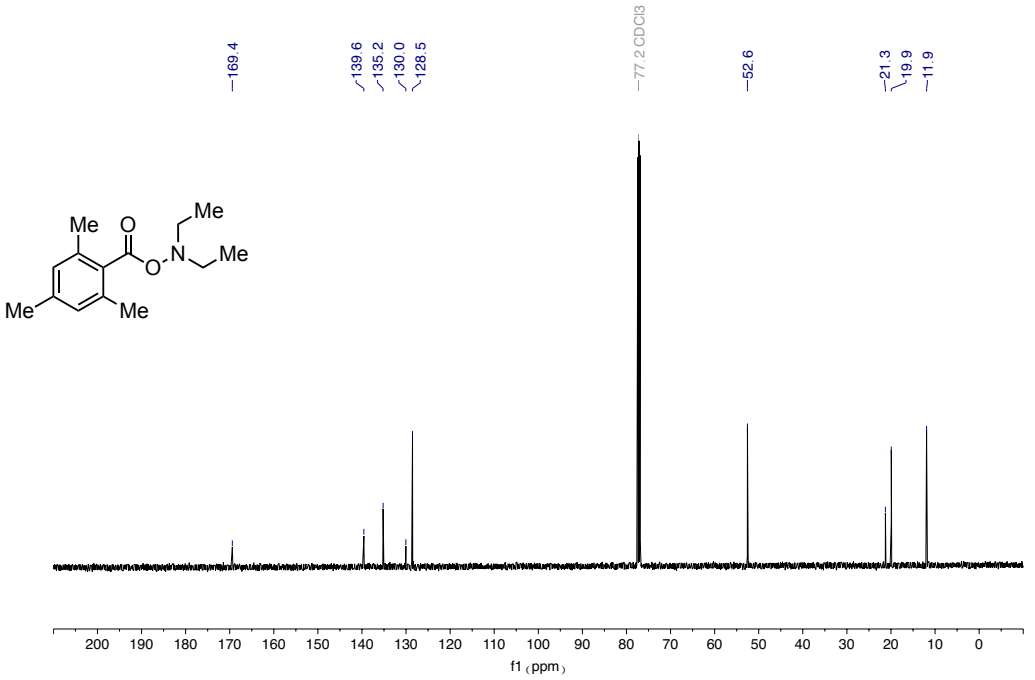

*^{13}C NMR spectra (101 MHz) of **2v***

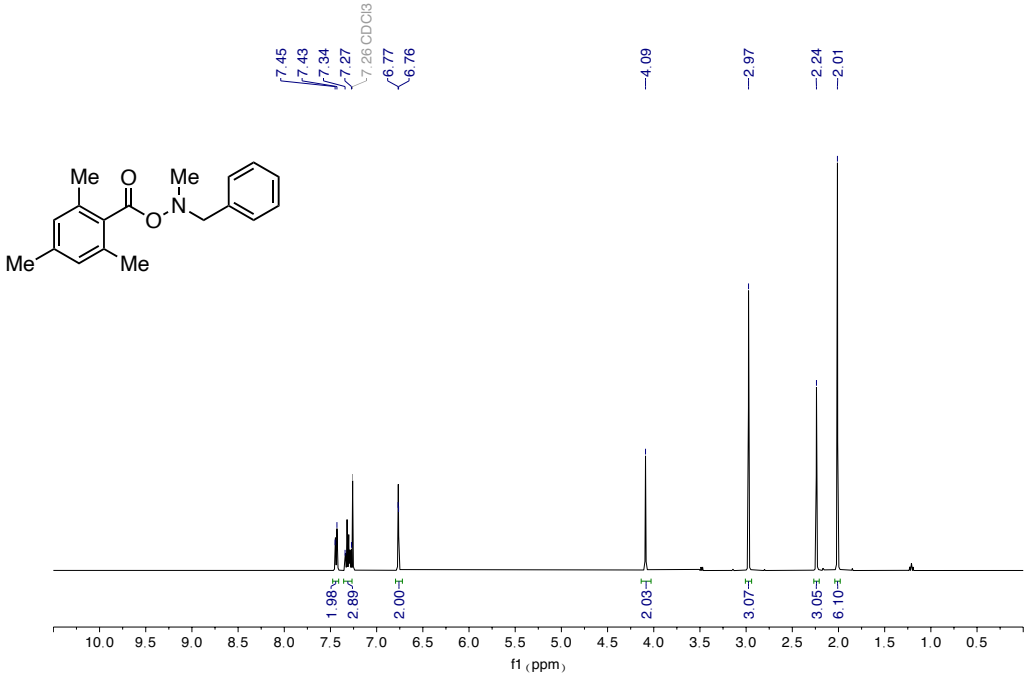

*^{1}H NMR spectra (400 MHz) of **2w***

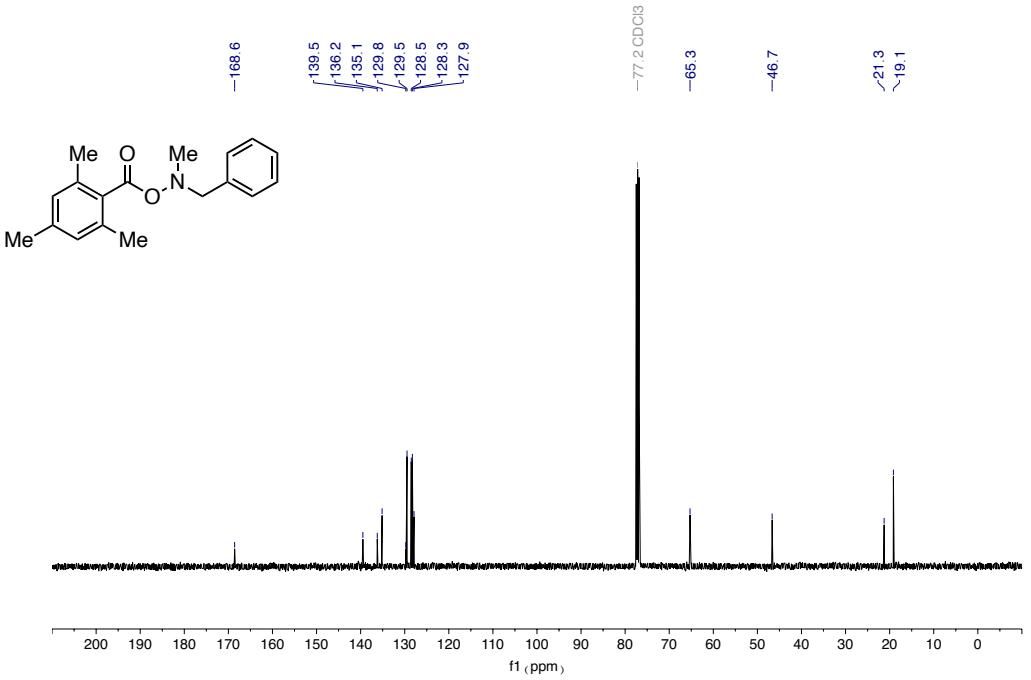

*^{13}C NMR spectra (101 MHz) of **2w***

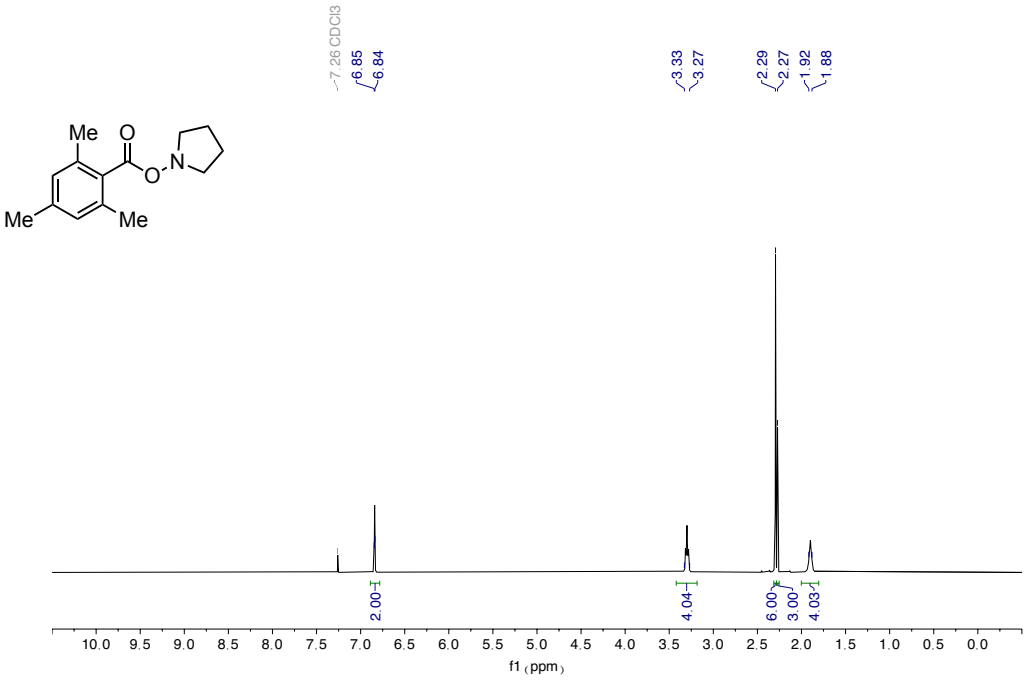

*^{1}H NMR spectra (400 MHz) of **2x***

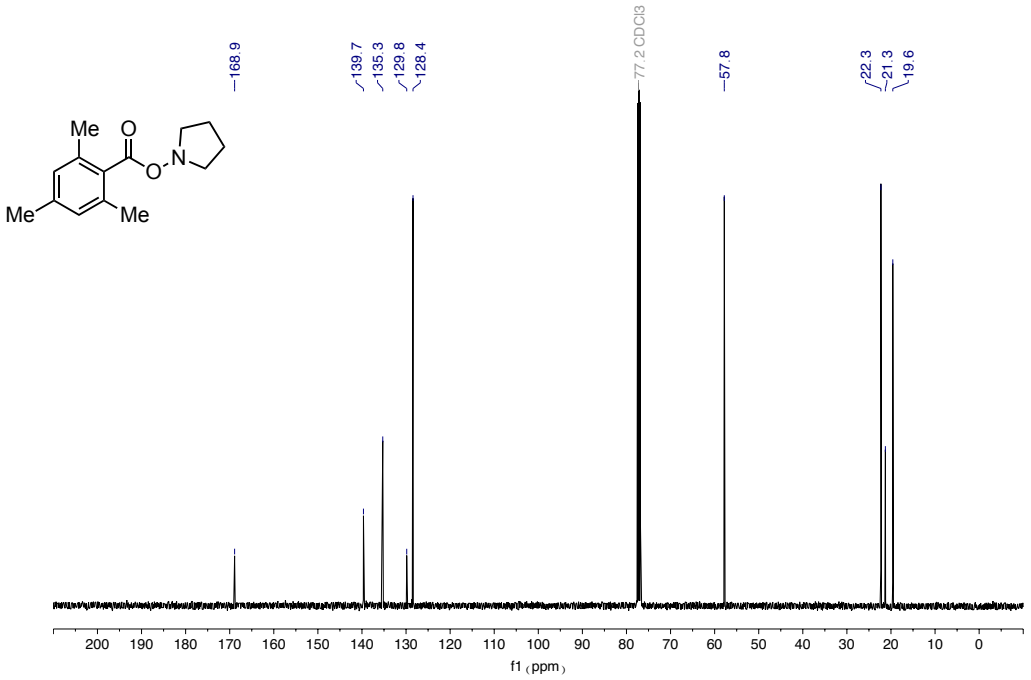

*^{13}C NMR spectra (101 MHz) of **2x***

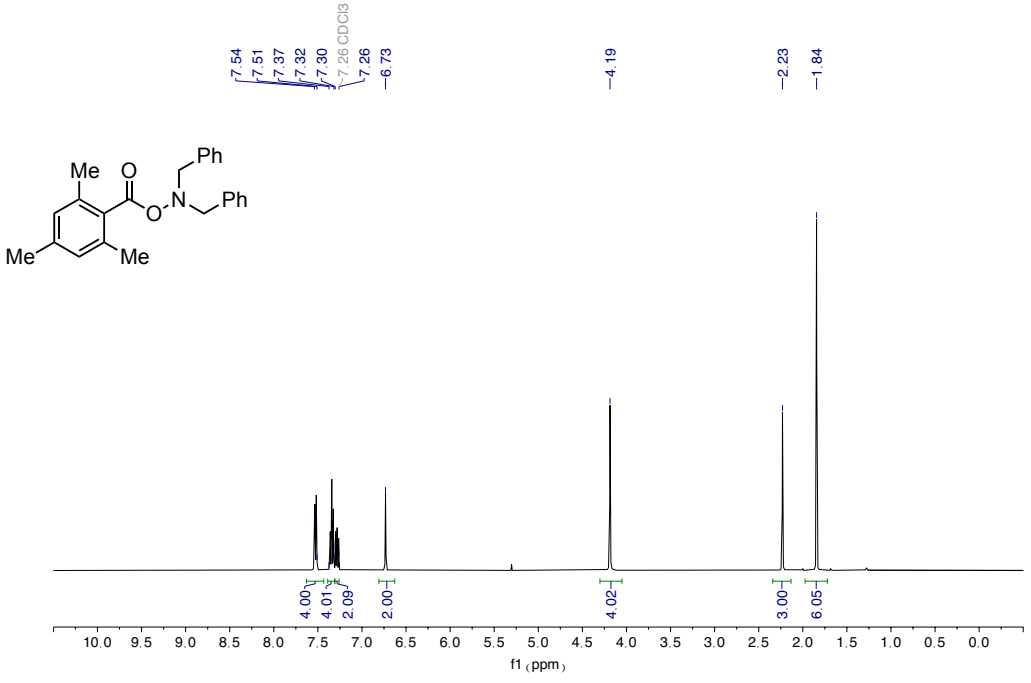

*^{1}H NMR spectra (400 MHz) of **2y***

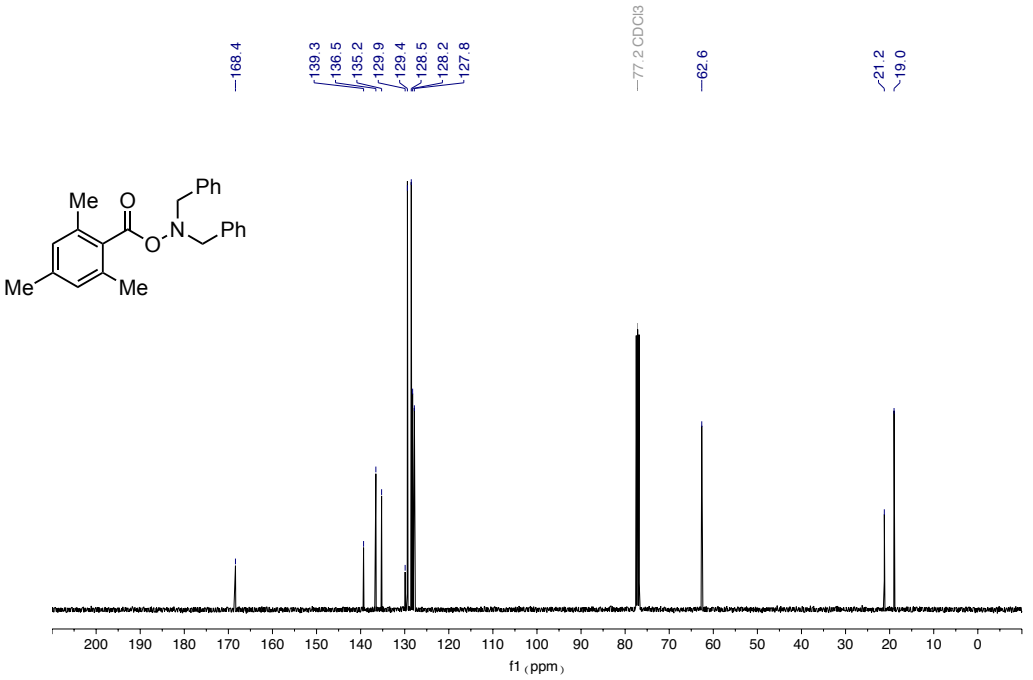

*^{13}C NMR spectra (101 MHz) of **2y***

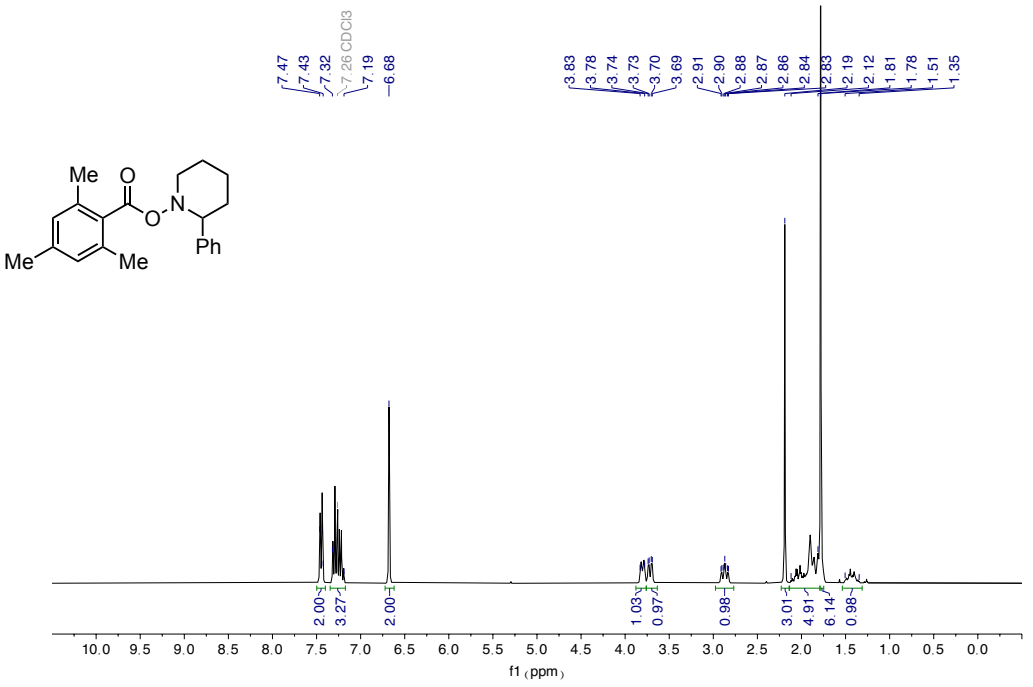

*^{1}H NMR spectra (400 MHz) of **2z***

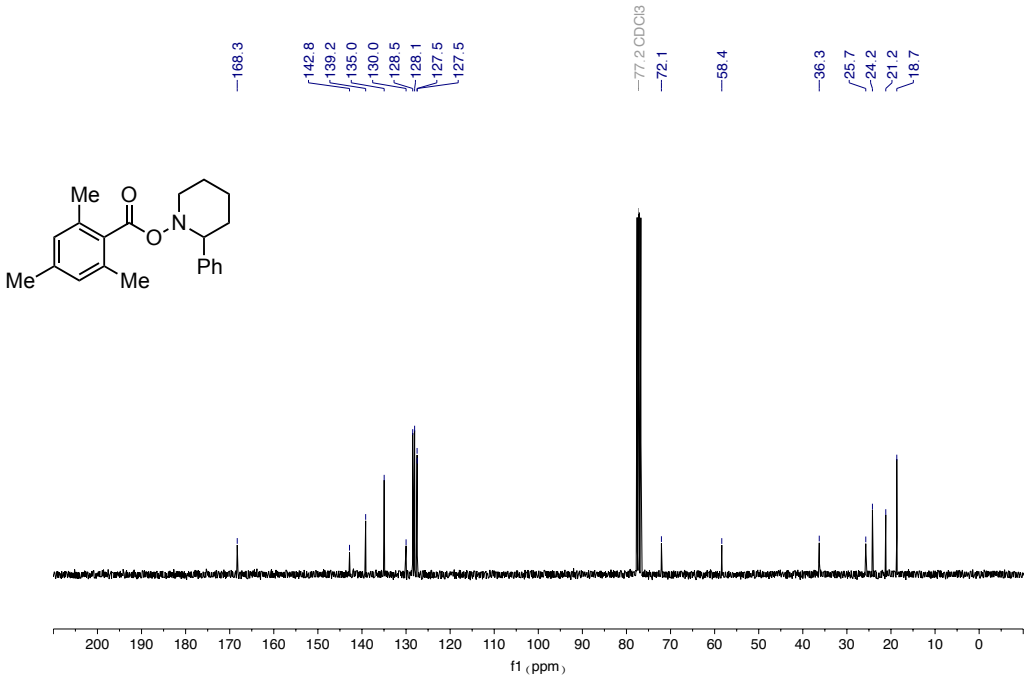

*^{13}C NMR spectra (101 MHz) of **2z***

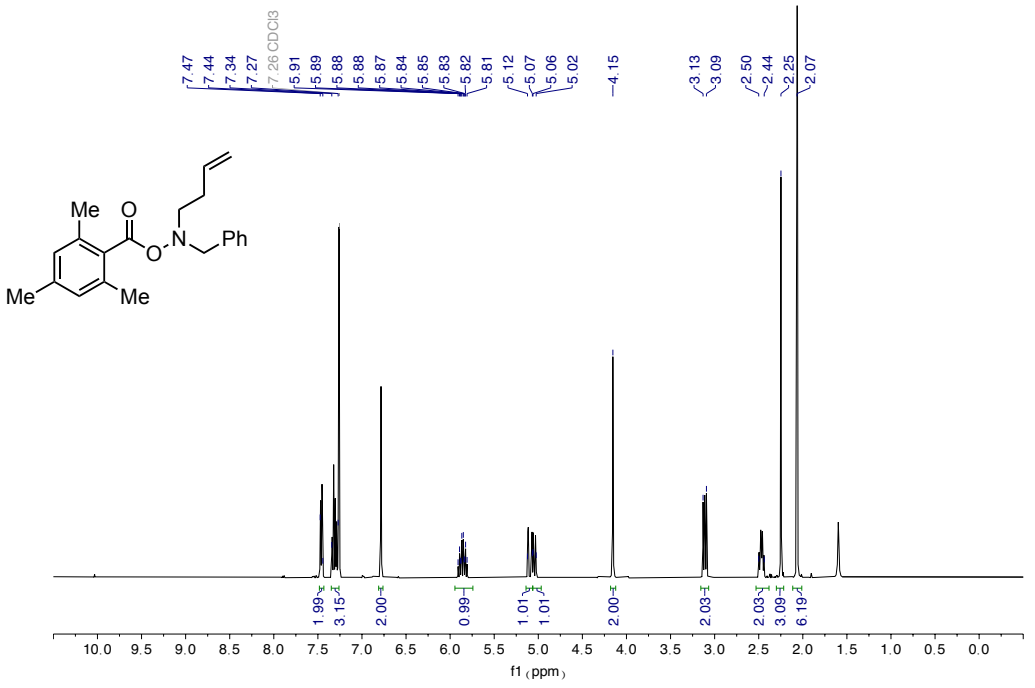

*^{1}H NMR spectra (400 MHz) of **2aa***

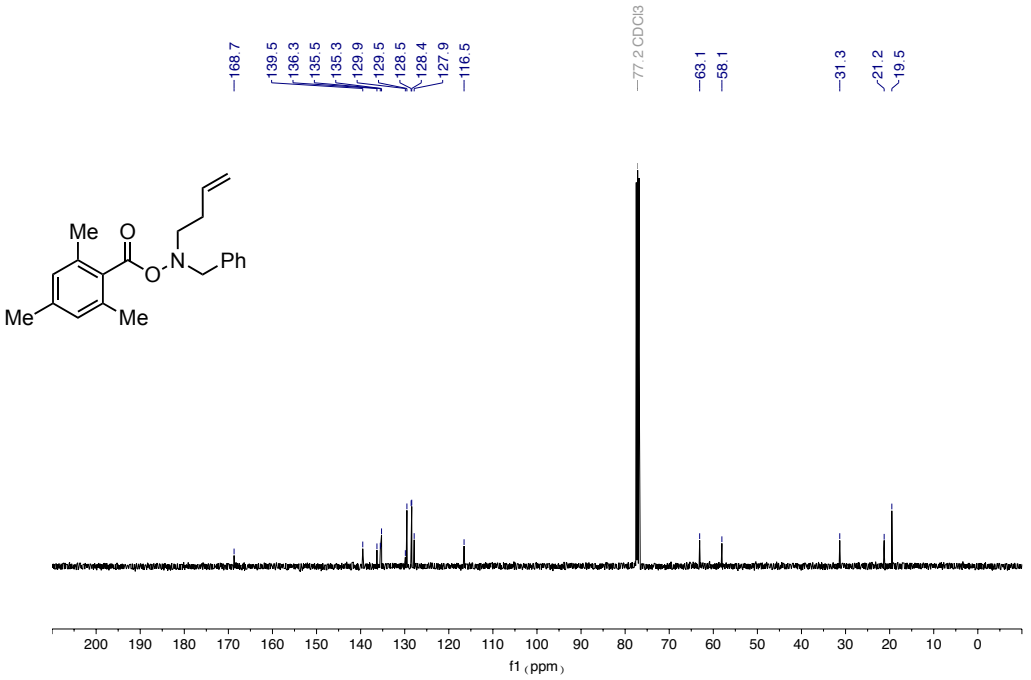

*^{13}C NMR spectra (101 MHz) of **2aa***

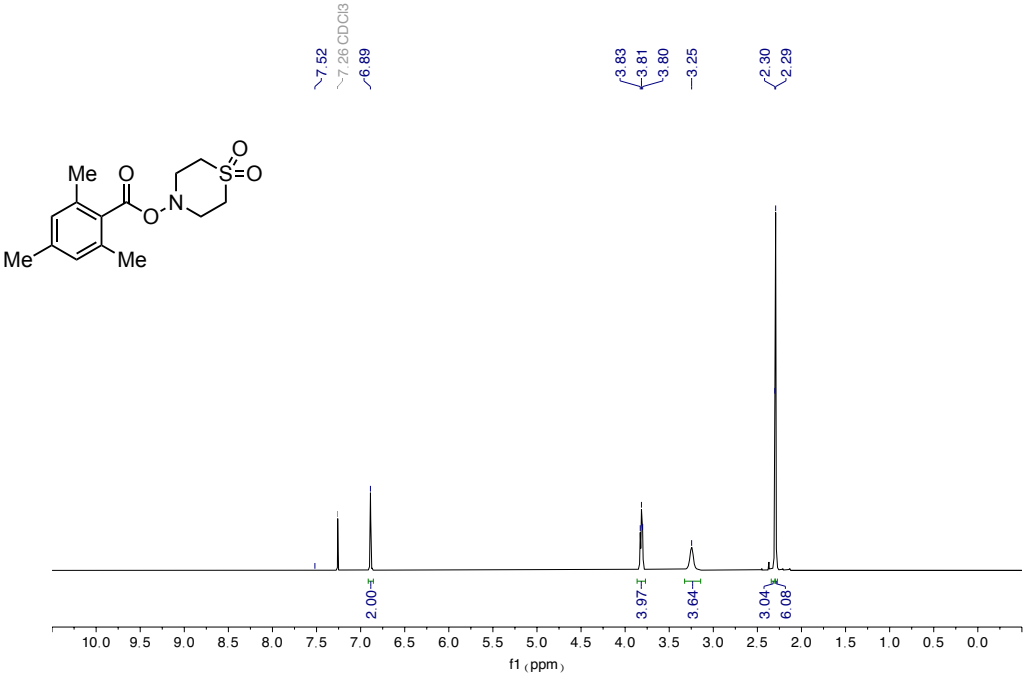

*^{1}H NMR spectra (400 MHz) of **2ab***

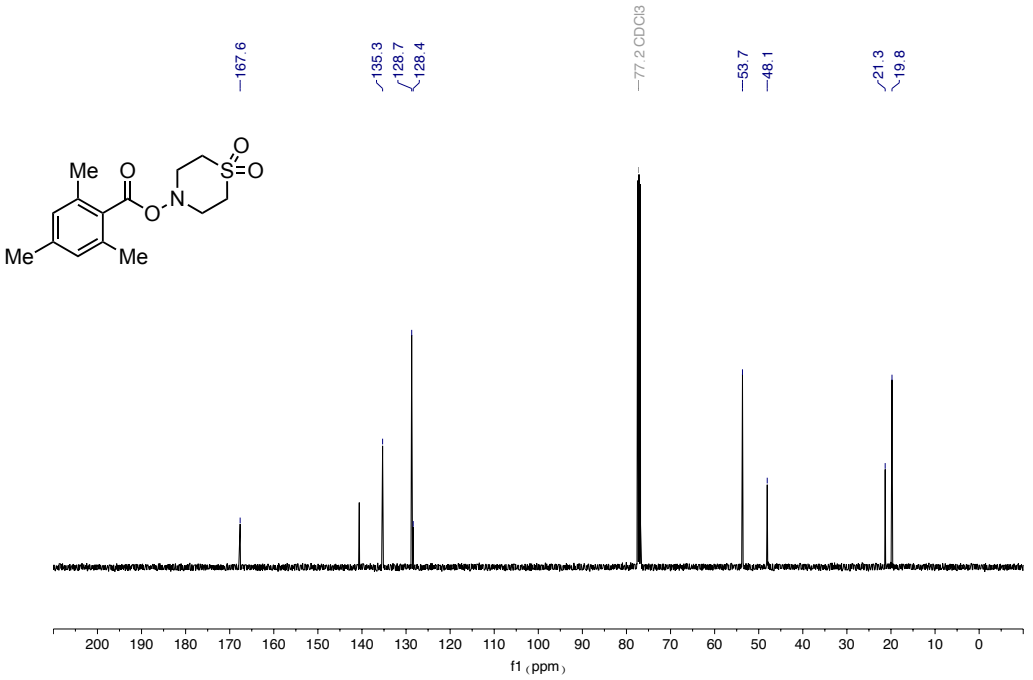

*^{13}C NMR spectra (101 MHz) of **2ab***

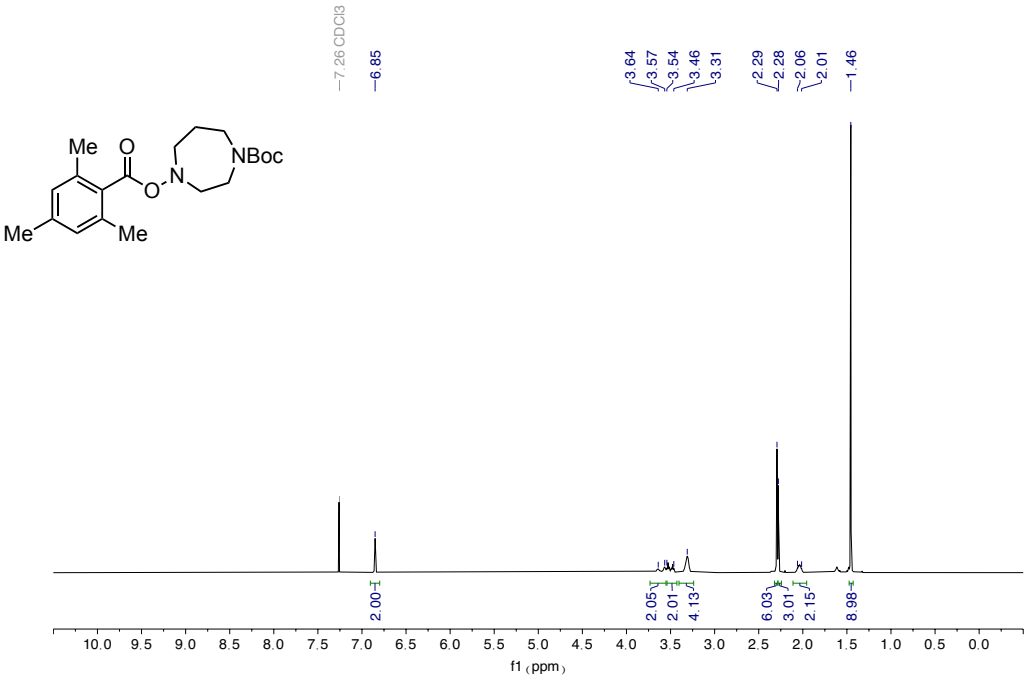

*^{1}H NMR spectra (400 MHz) of **2ac***

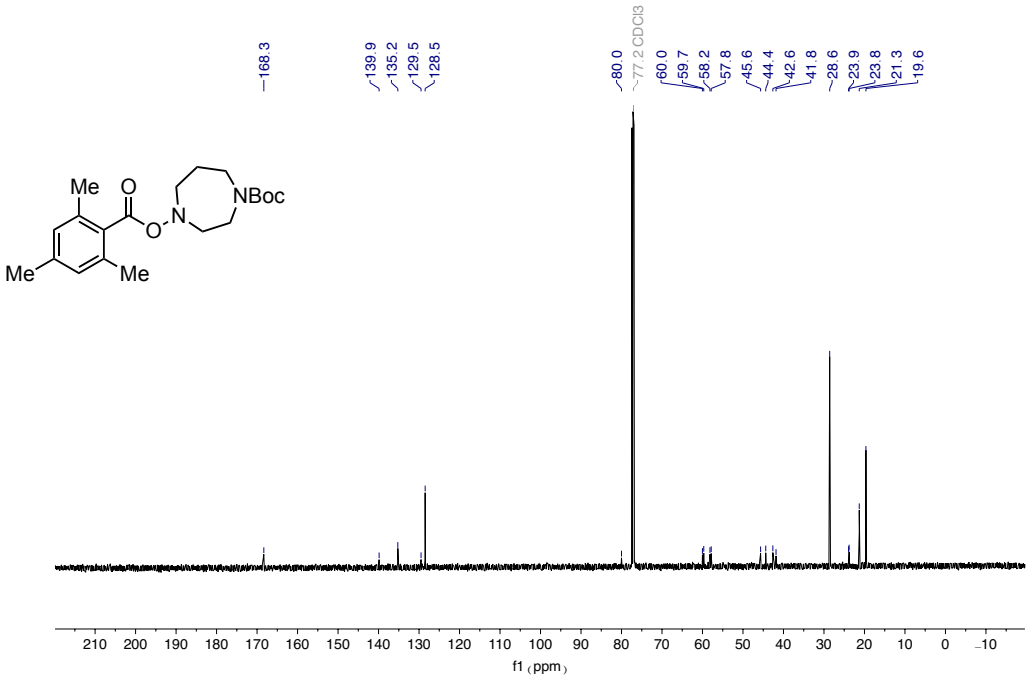

*^{13}C NMR spectra (101 MHz) of **2ac***

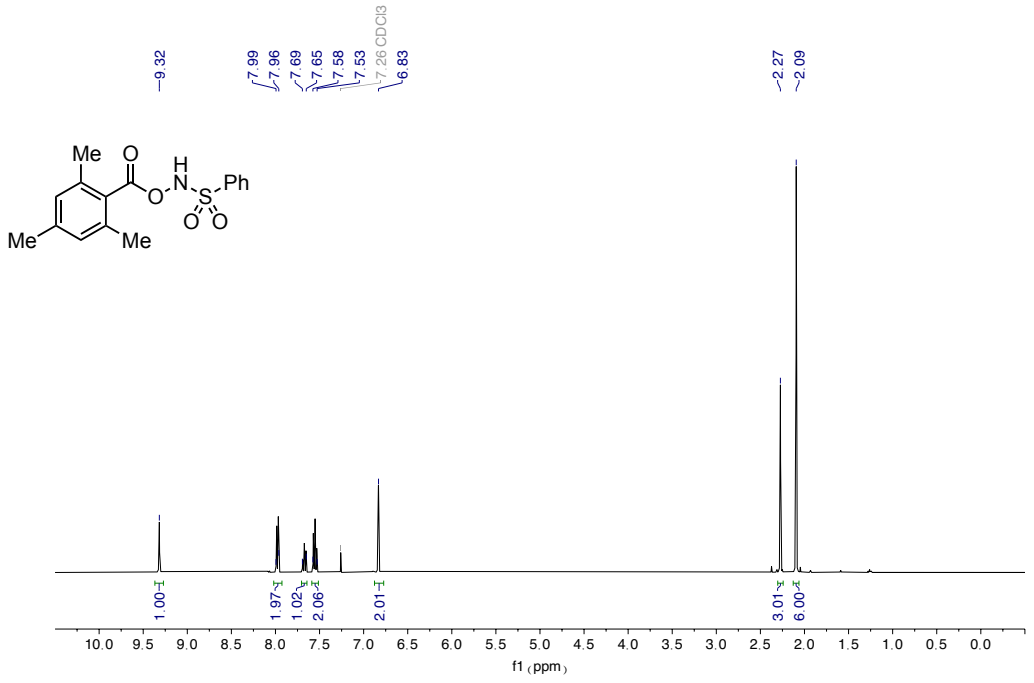

*^{1}H NMR spectra (400 MHz) of **2ad***

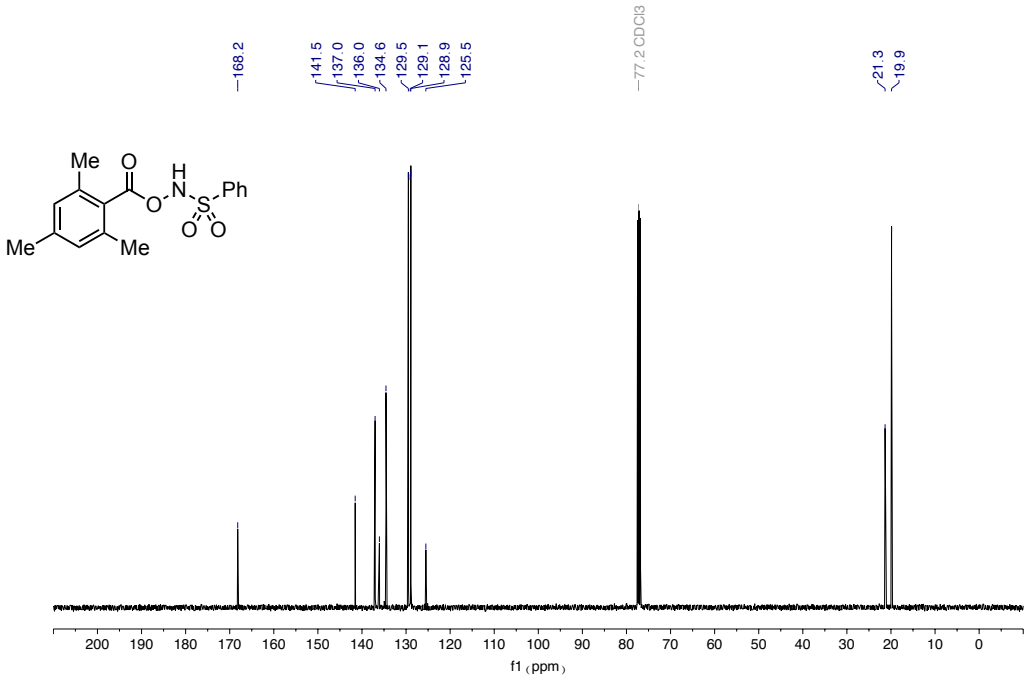

*^{13}C NMR spectra (101 MHz) of **2ad***

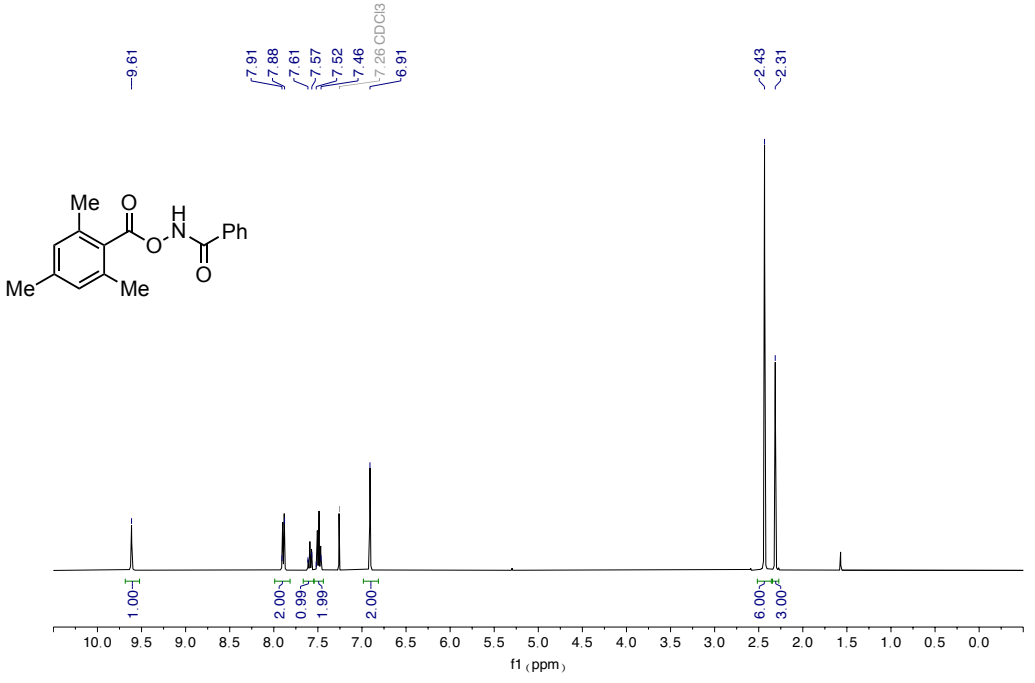

*^{1}H NMR spectra (400 MHz) of **2ae***

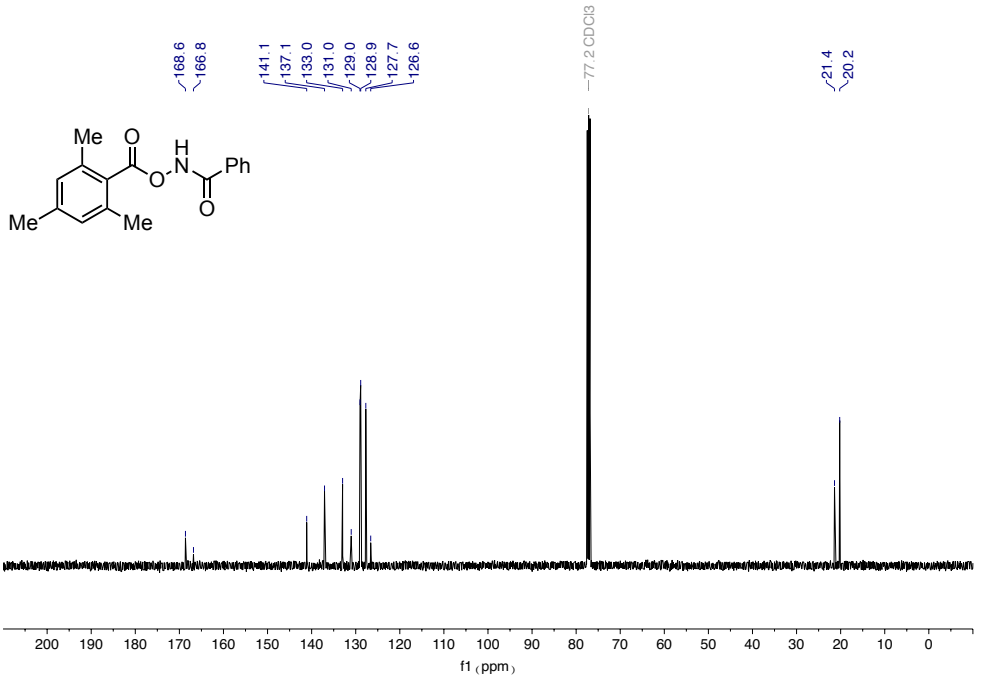

*^{13}C NMR spectra (101 MHz) of **2ae***

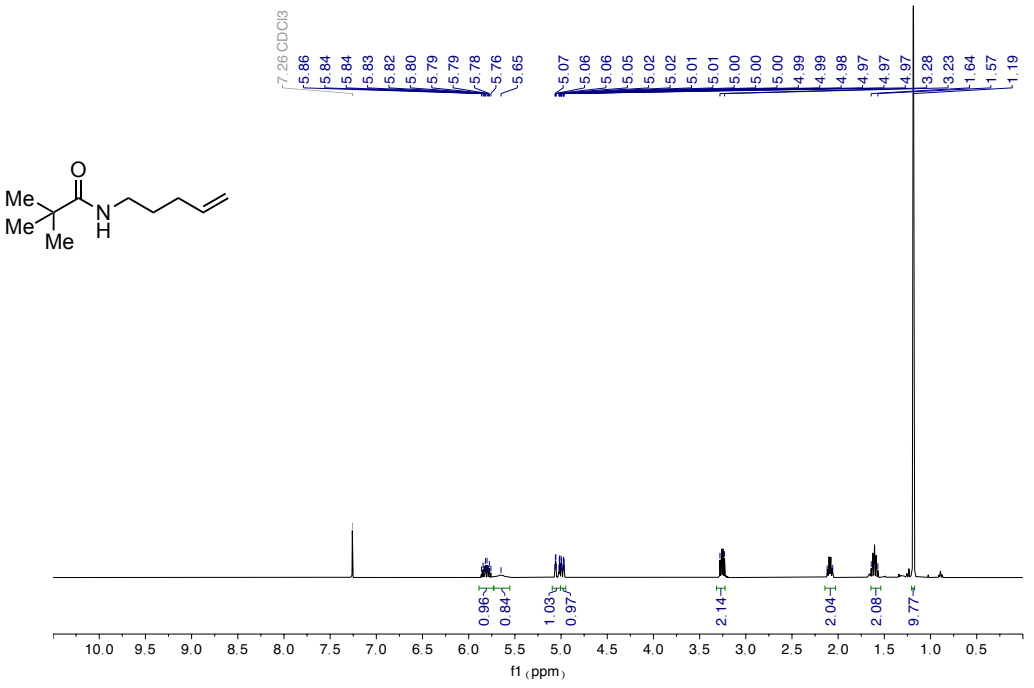

*^{1}H NMR spectra (400 MHz) of **1l***

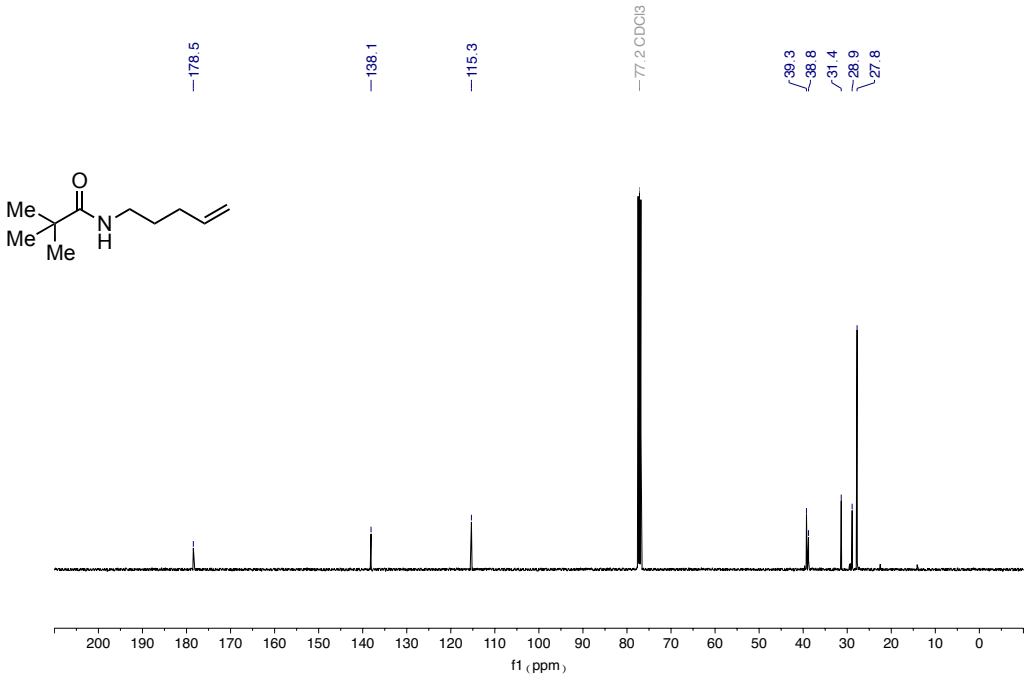

*^{13}C NMR spectra (101 MHz) of **1l***

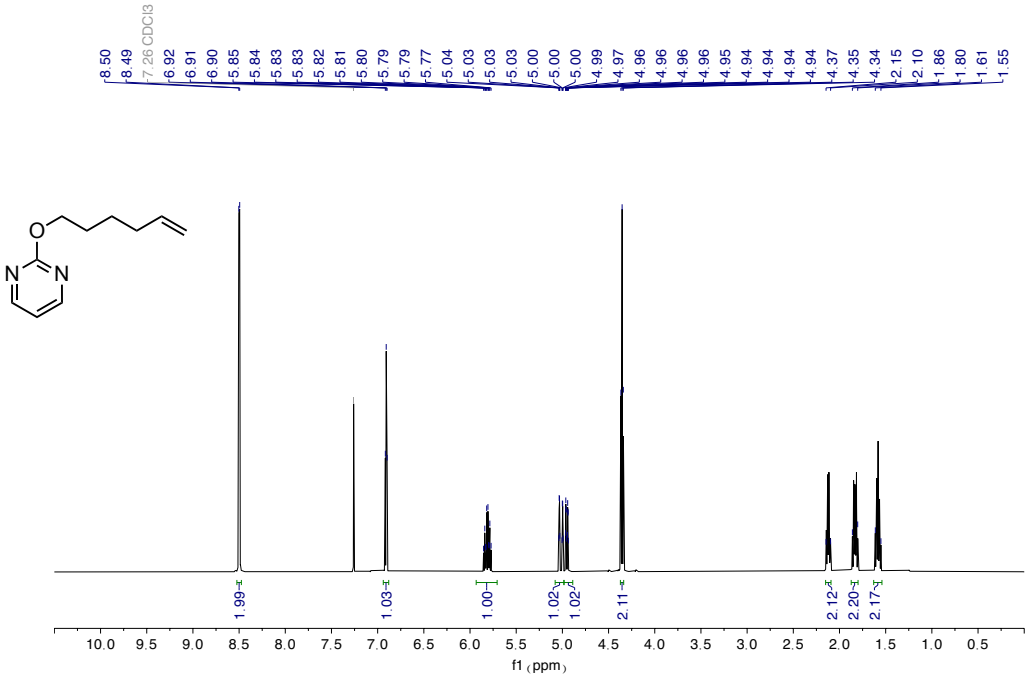

*^{1}H NMR spectra (400 MHz) of **1p***

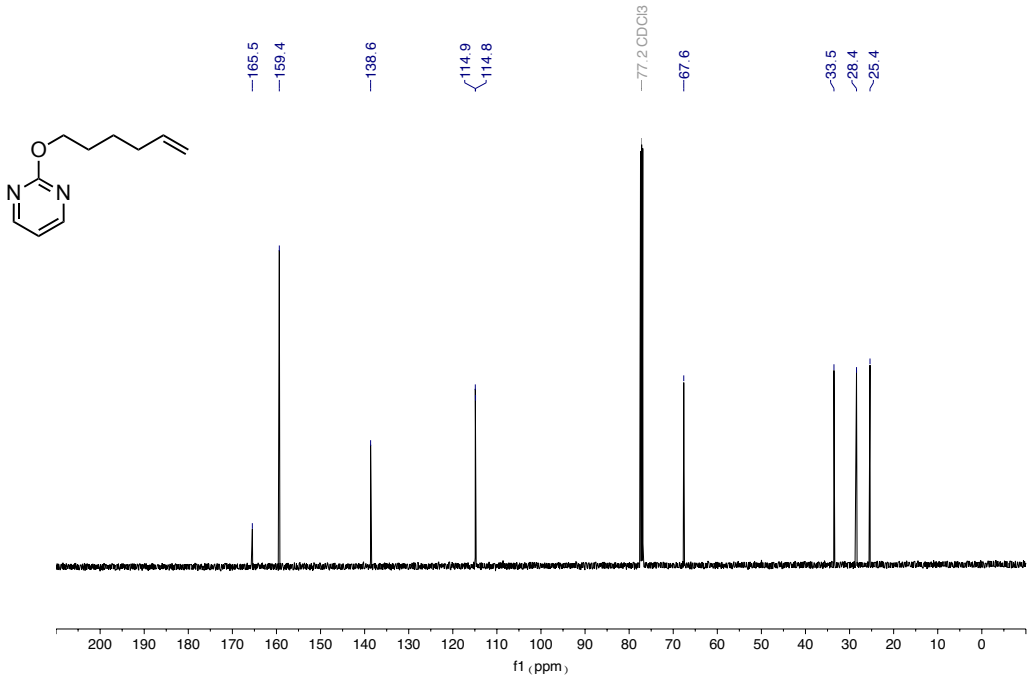

*^{13}C NMR spectra (101 MHz) of **1p***

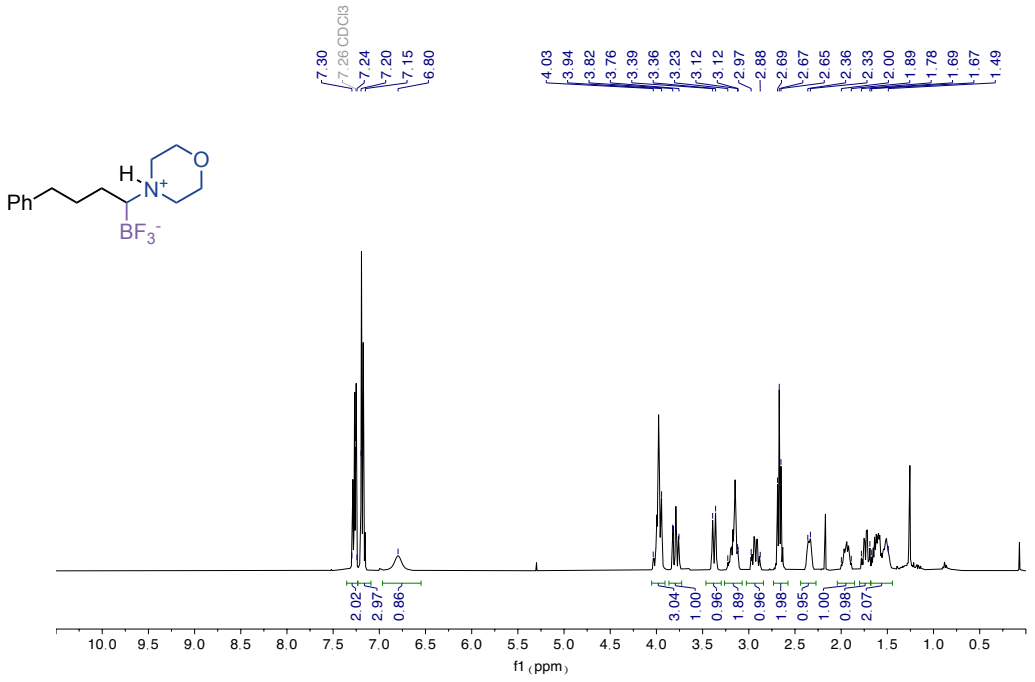

*^{1}H NMR spectra (400 MHz) of **4a***

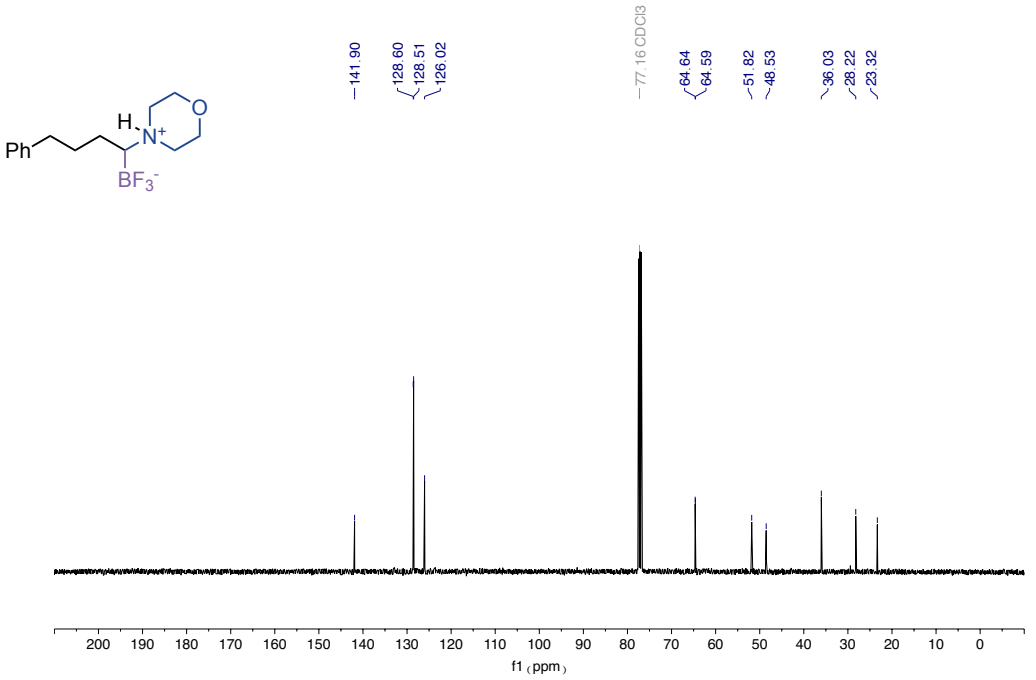

*^{13}C NMR spectra (101 MHz) of **4a***

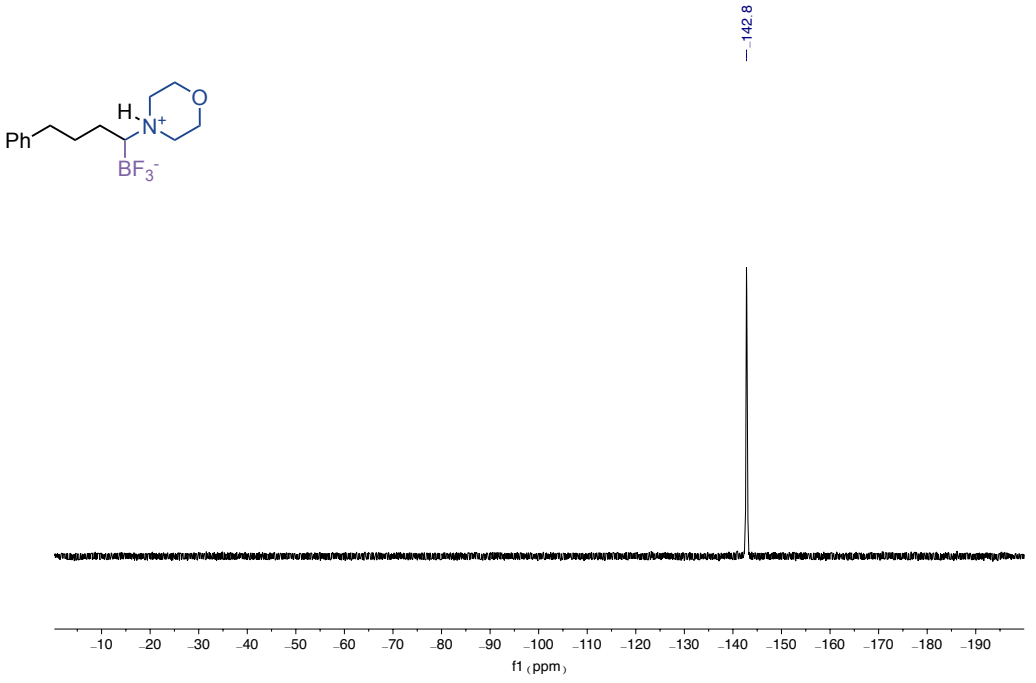

*^{19}F NMR spectra (376 MHz) of **4a***

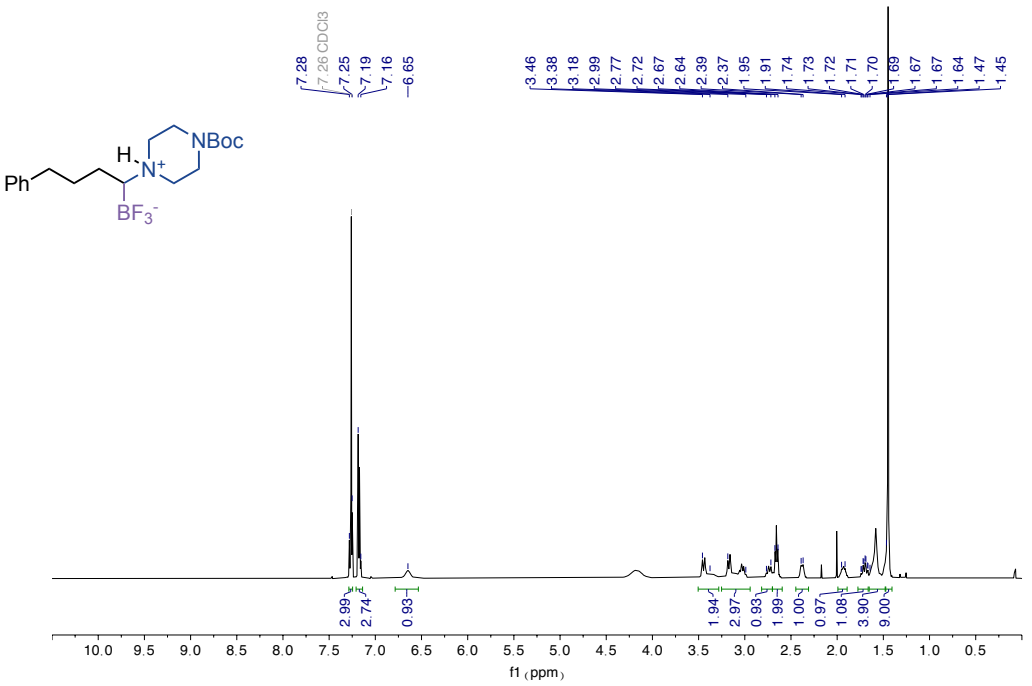

*[1]H NMR spectra (400 MHz) of **4b***

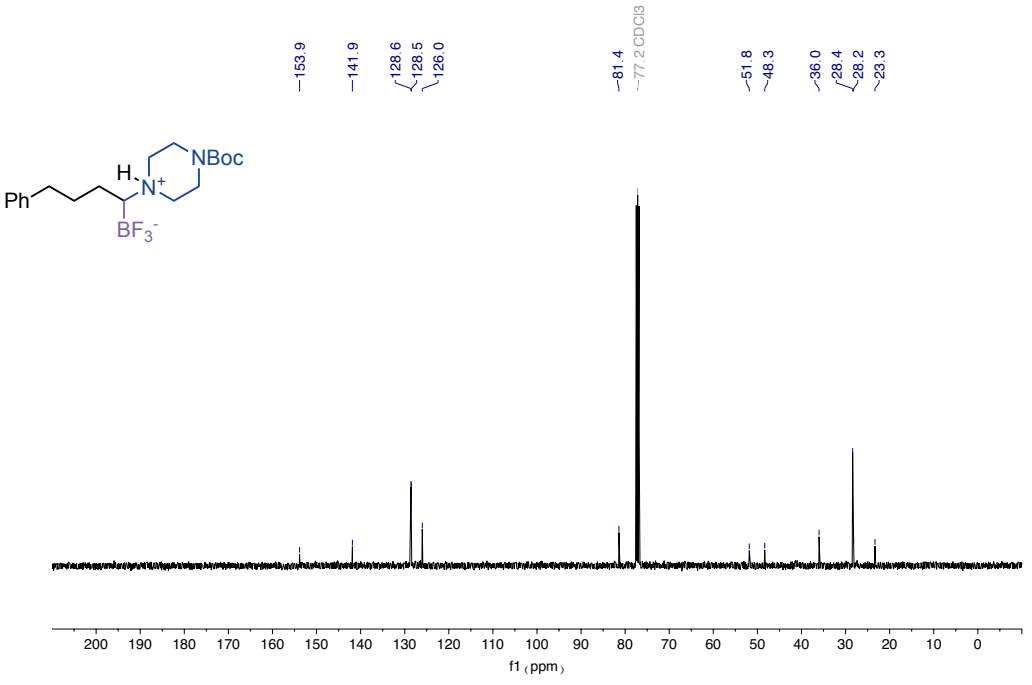

*[13]C NMR spectra (101 MHz) of **4b***

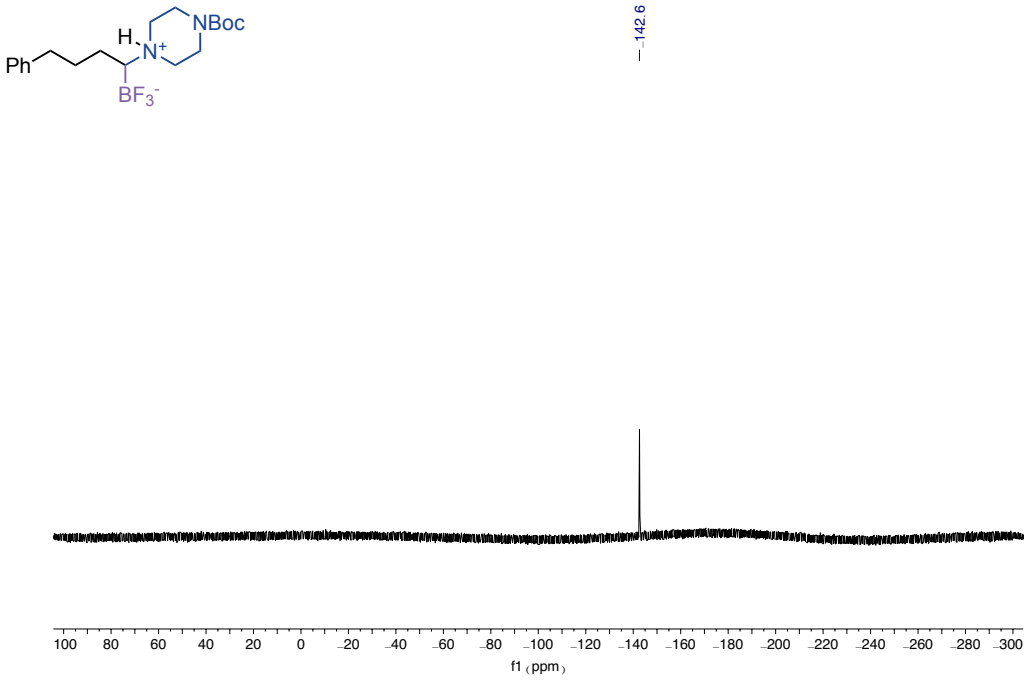

*^{19}F NMR spectra (376 MHz) of **4b***

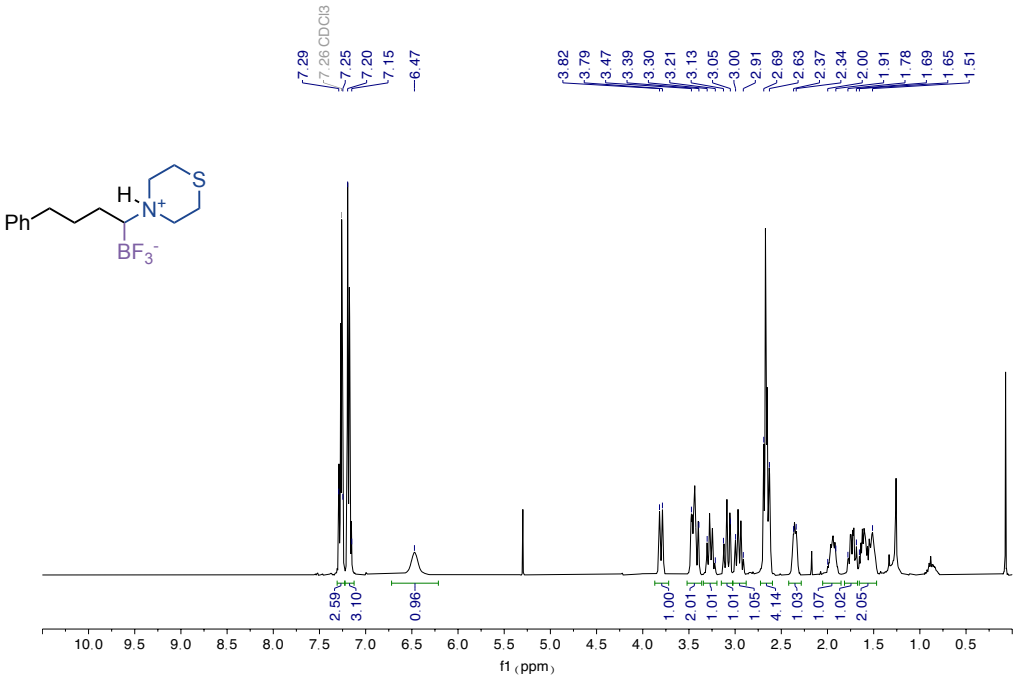

*^{1}H NMR spectra (400 MHz) of **4c***

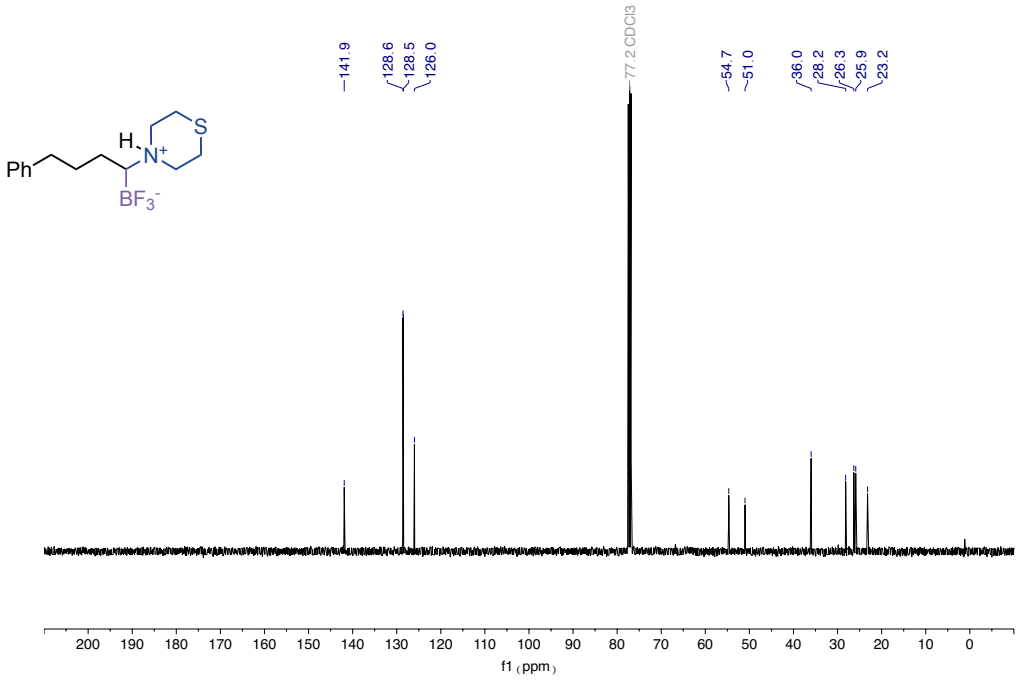

*^{13}C NMR spectra (101 MHz) of **4c***

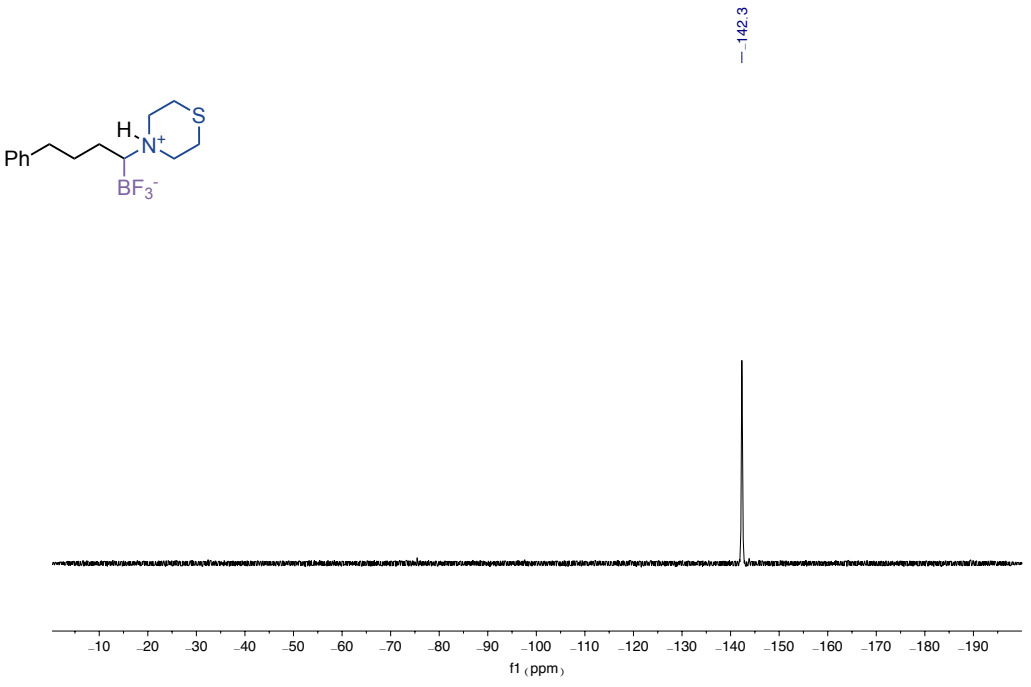

*^{19}F NMR spectra (376 MHz) of **4c***

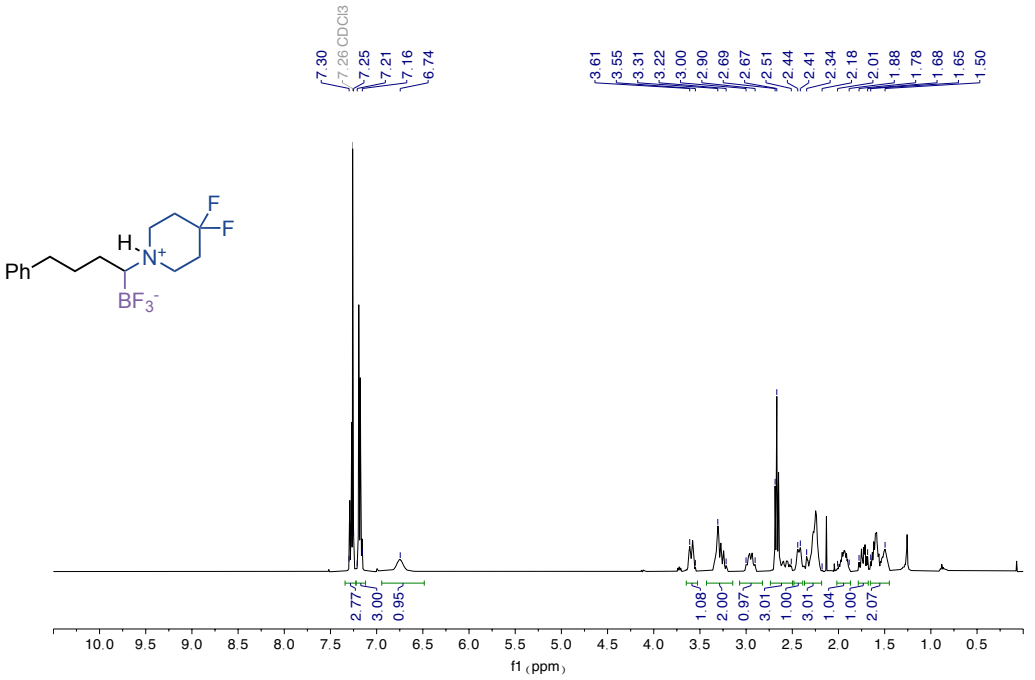

*^{1}H NMR spectra (400 MHz) of **4d***

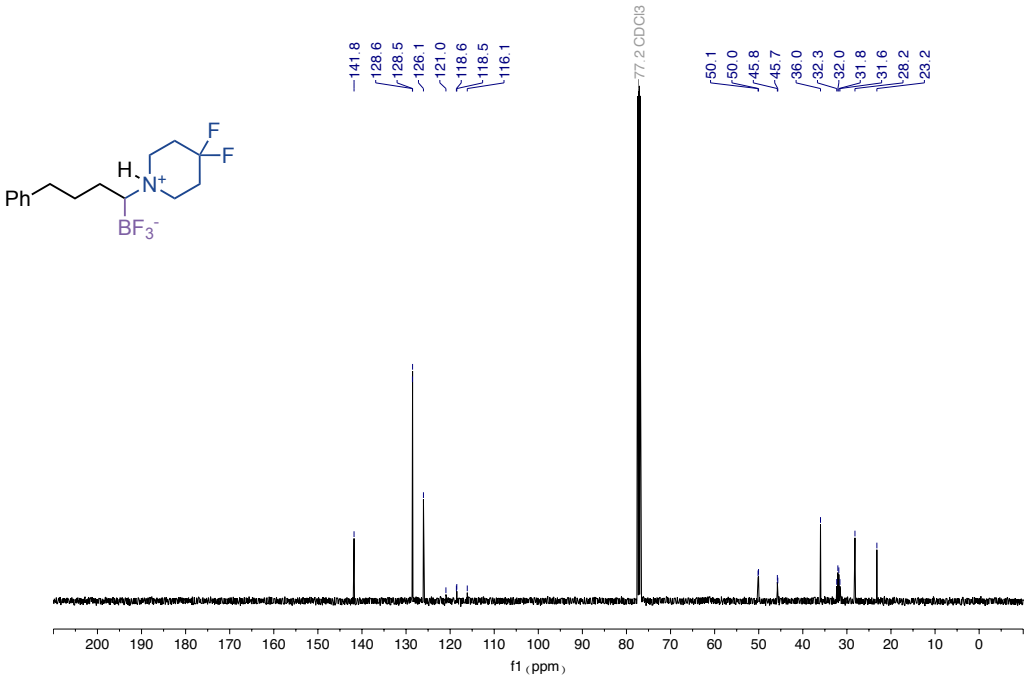

*^{13}C NMR spectra (101 MHz) of **4d***

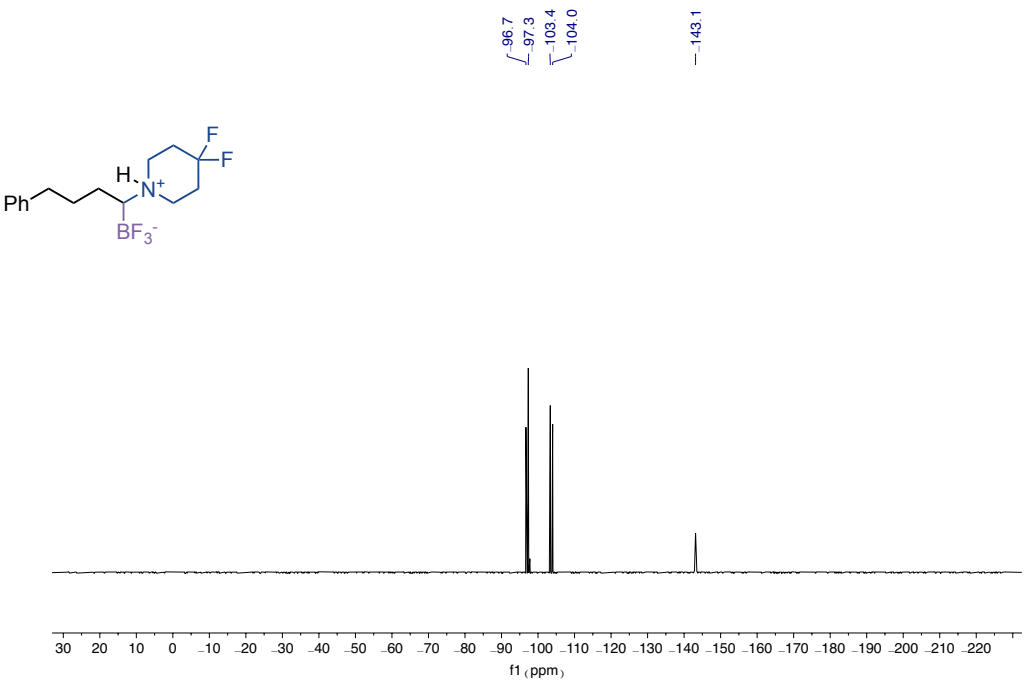

*^{19}F NMR spectra (376 MHz) of **4d***

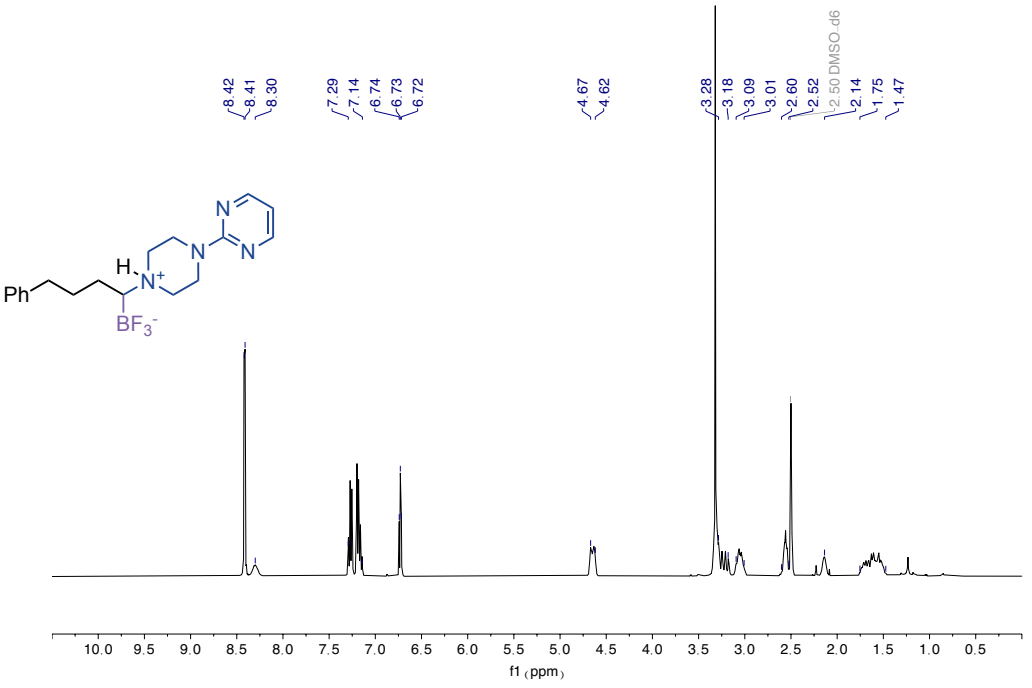

*^{1}H NMR spectra (400 MHz) of **4e***

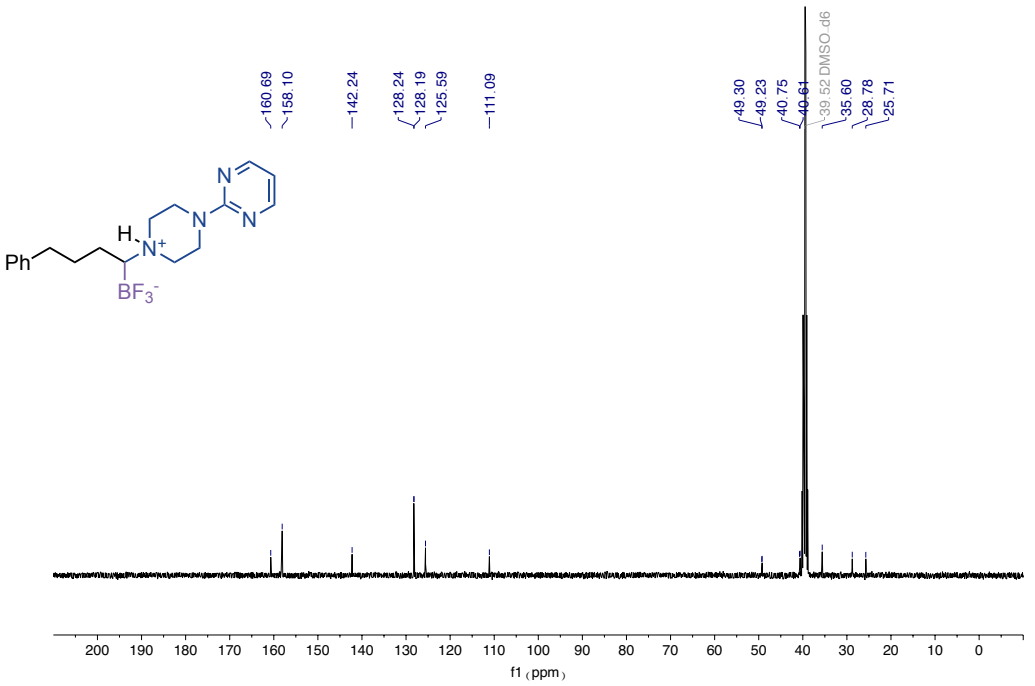

*^{13}C NMR spectra (101 MHz) of **4e***

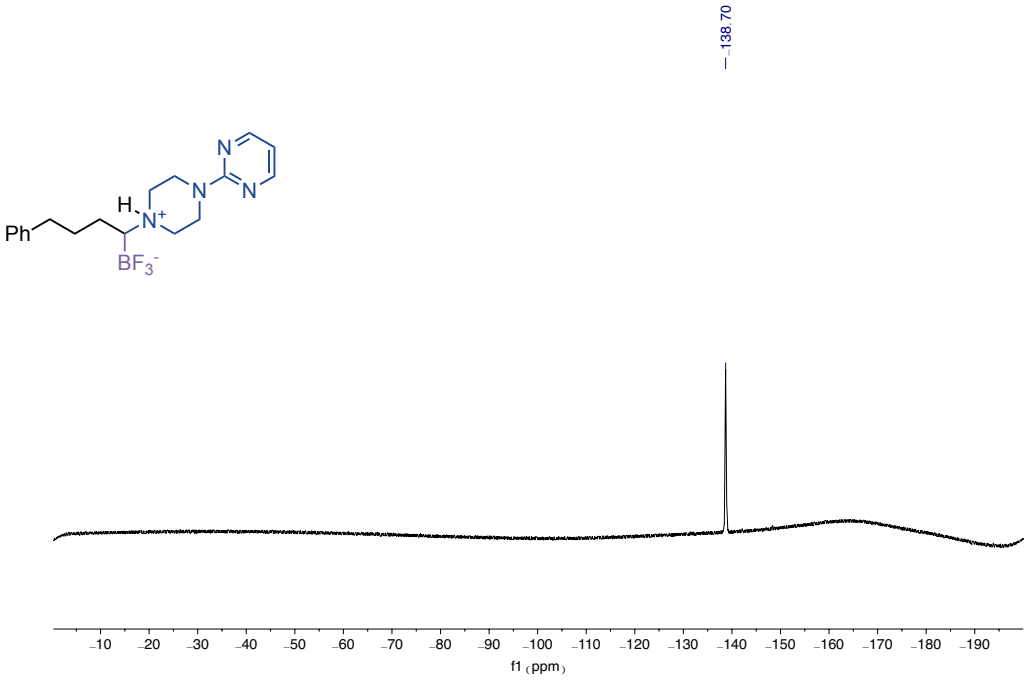

*^{19}F NMR spectra (376 MHz) of **4e***

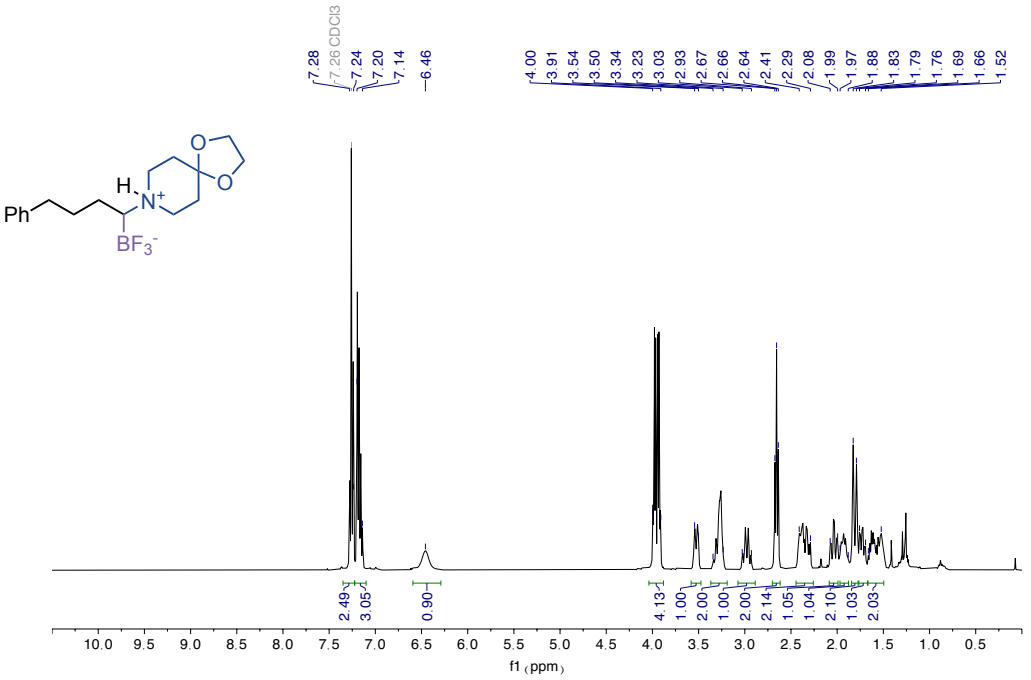

*^{1}H NMR spectra (400 MHz) of **4f***

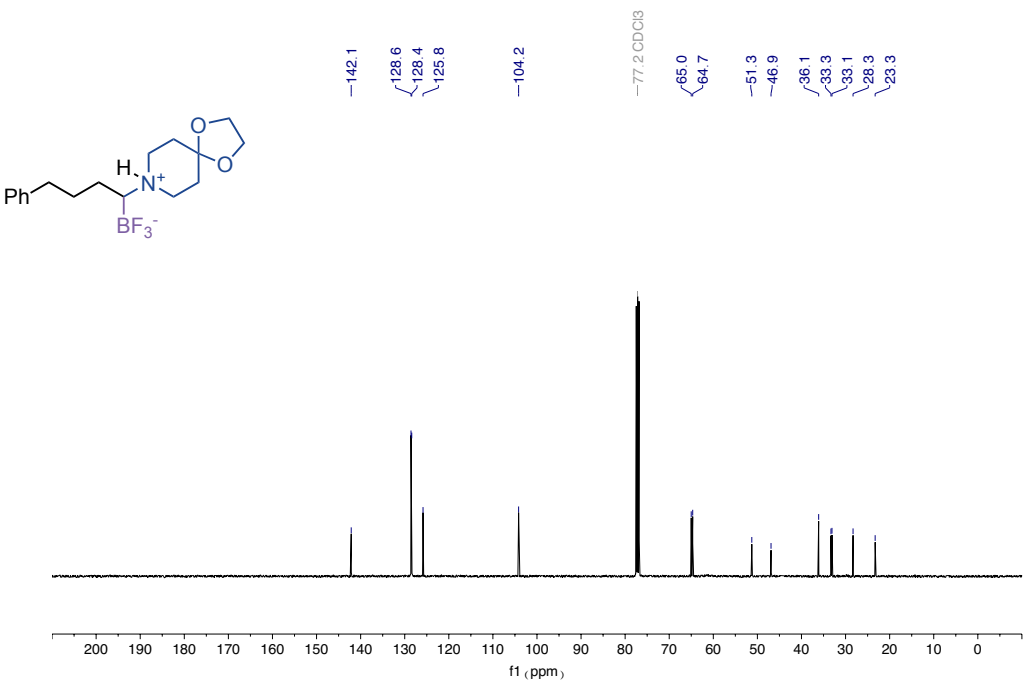

*^{13}C NMR spectra (101 MHz) of **4f***

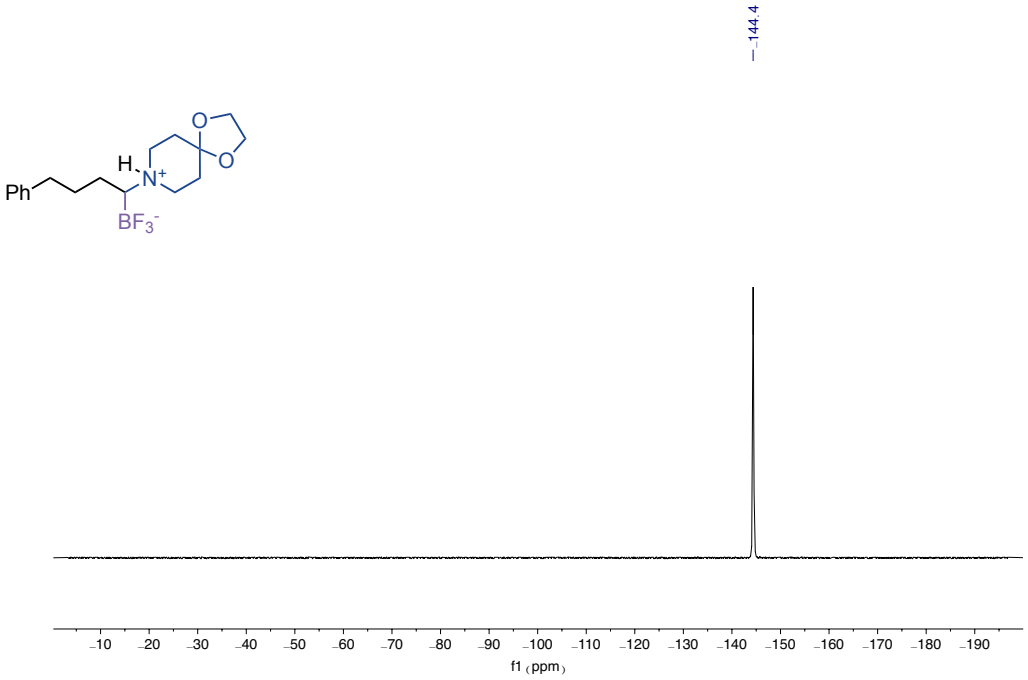

*[19]F NMR spectra (376 MHz) of **4f***

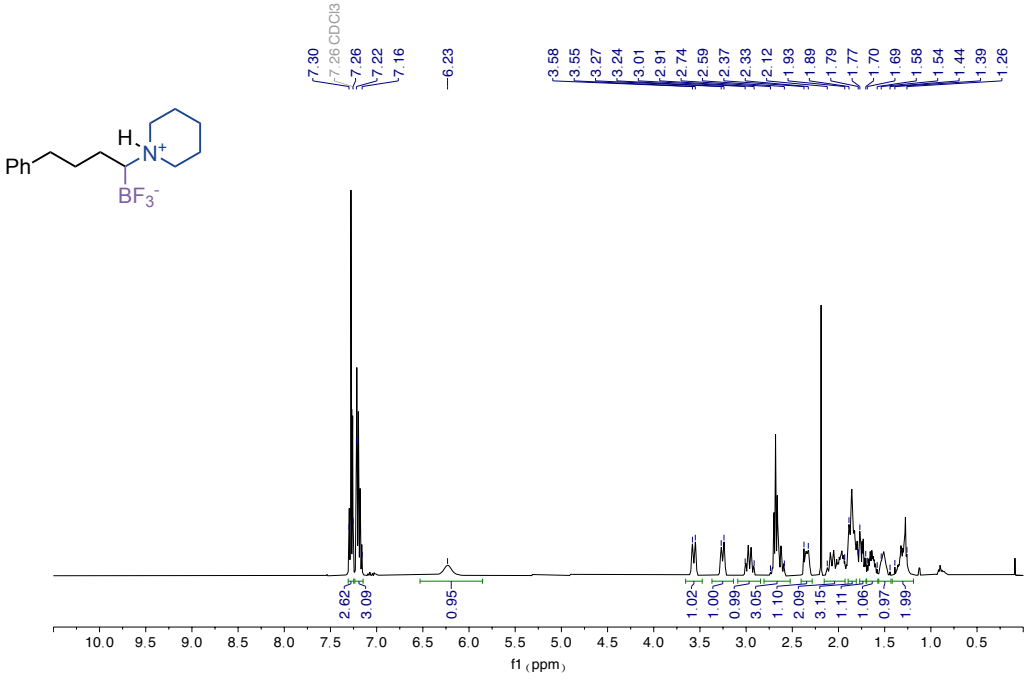

*[1]H NMR spectra (400 MHz) of **4g***

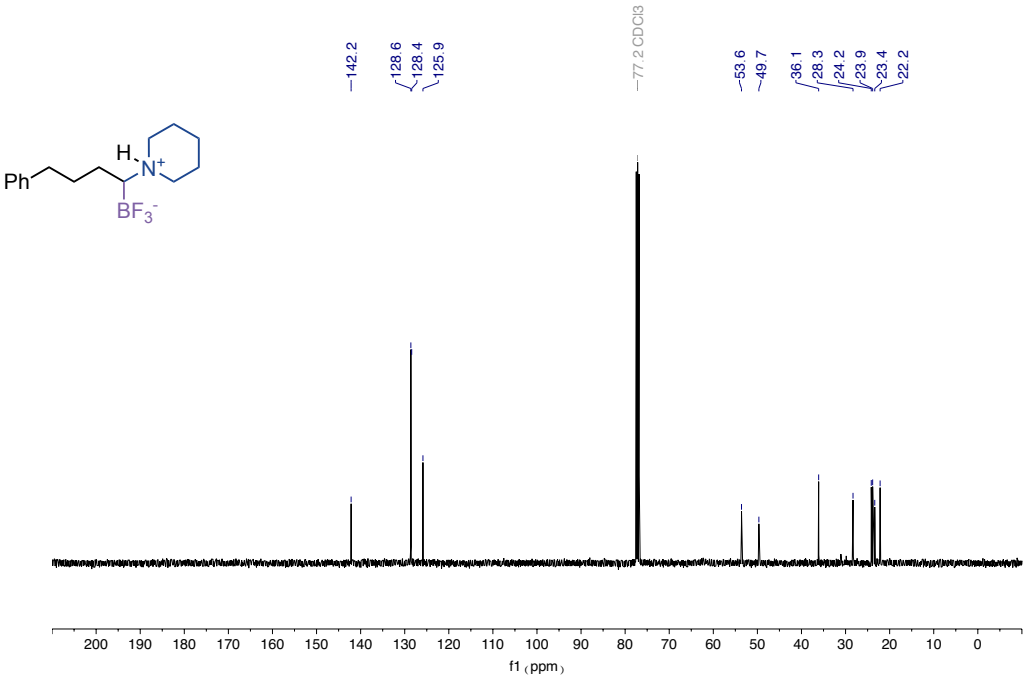

*^{13}C NMR spectra (101 MHz) of **4g***

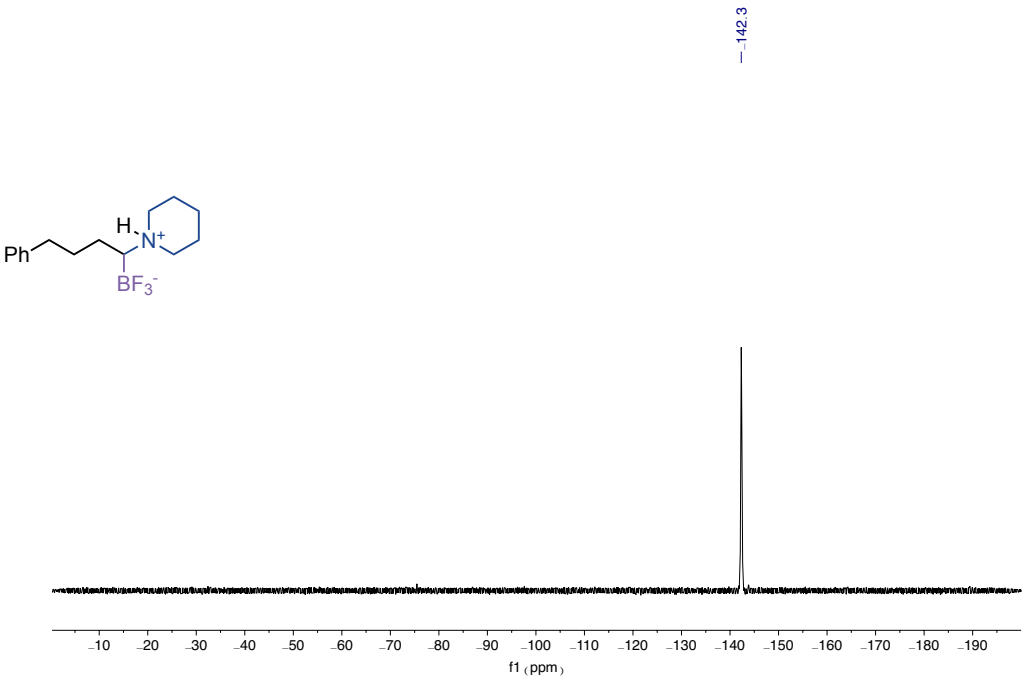

*^{19}F NMR spectra (376 MHz) of **4g***

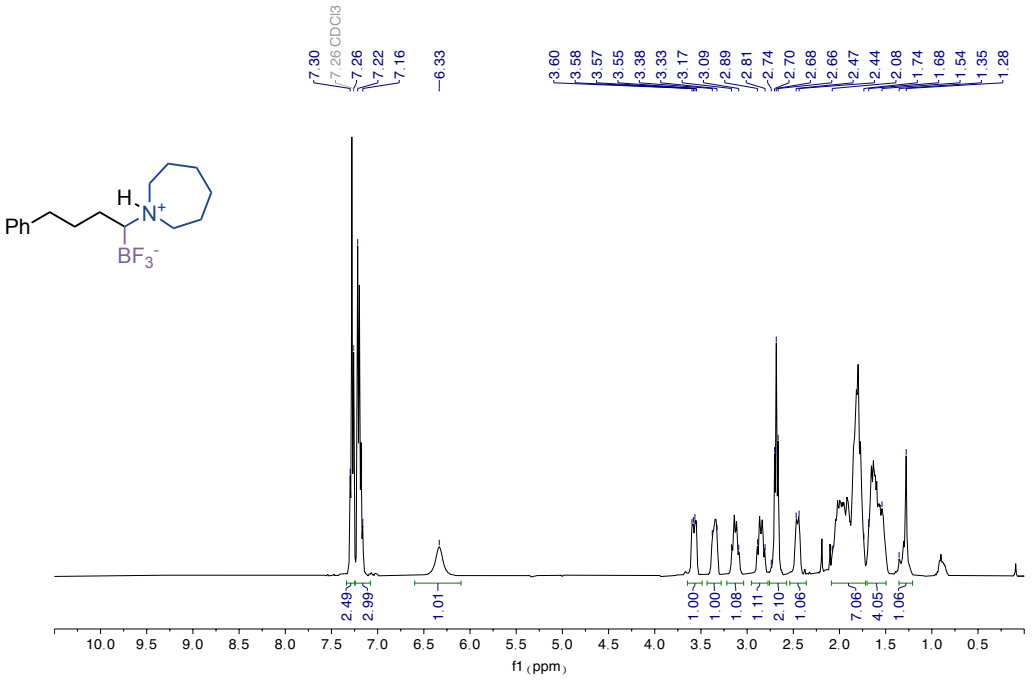

*^{1}H NMR spectra (400 MHz) of **4h***

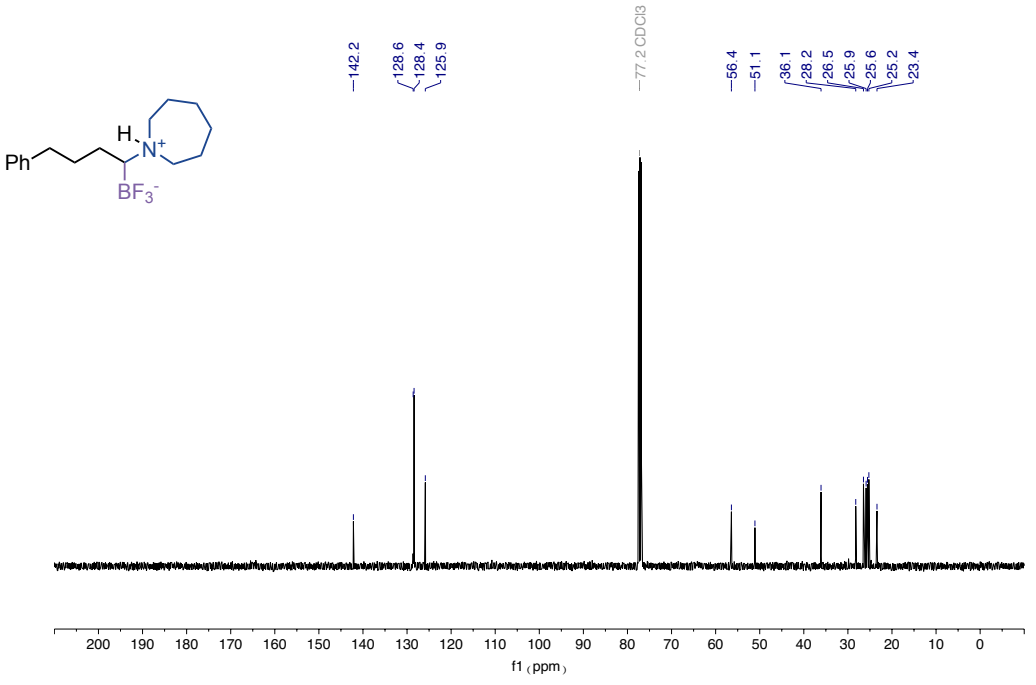

*^{13}C NMR spectra (101 MHz) of **4h***

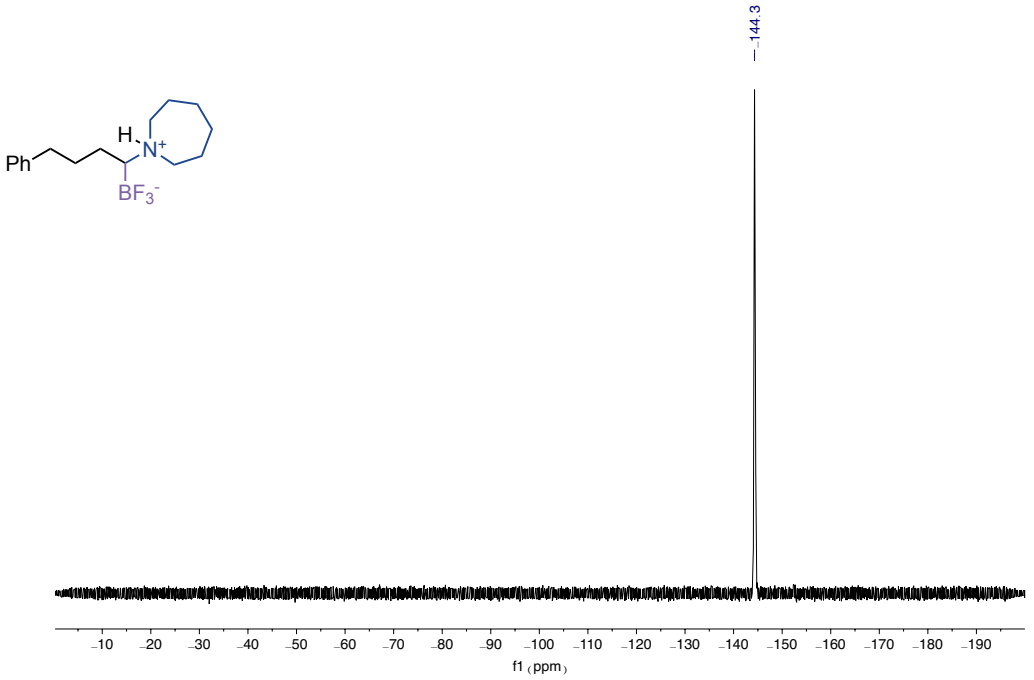

*^{19}F NMR spectra (376 MHz) of **4h***

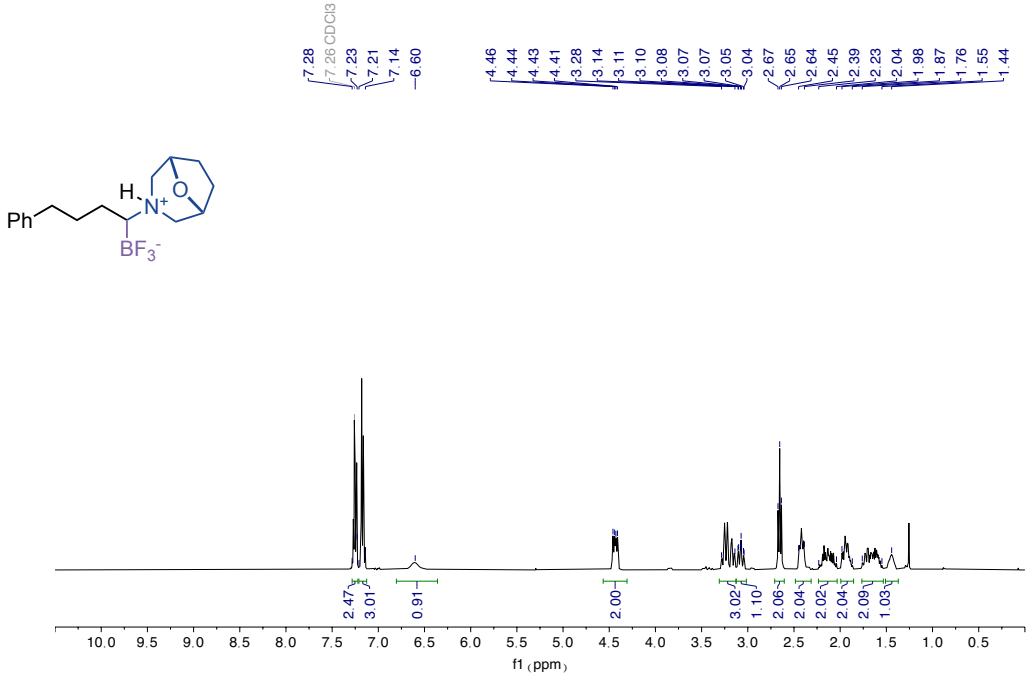

*^{1}H NMR spectra (400 MHz) of **4i***

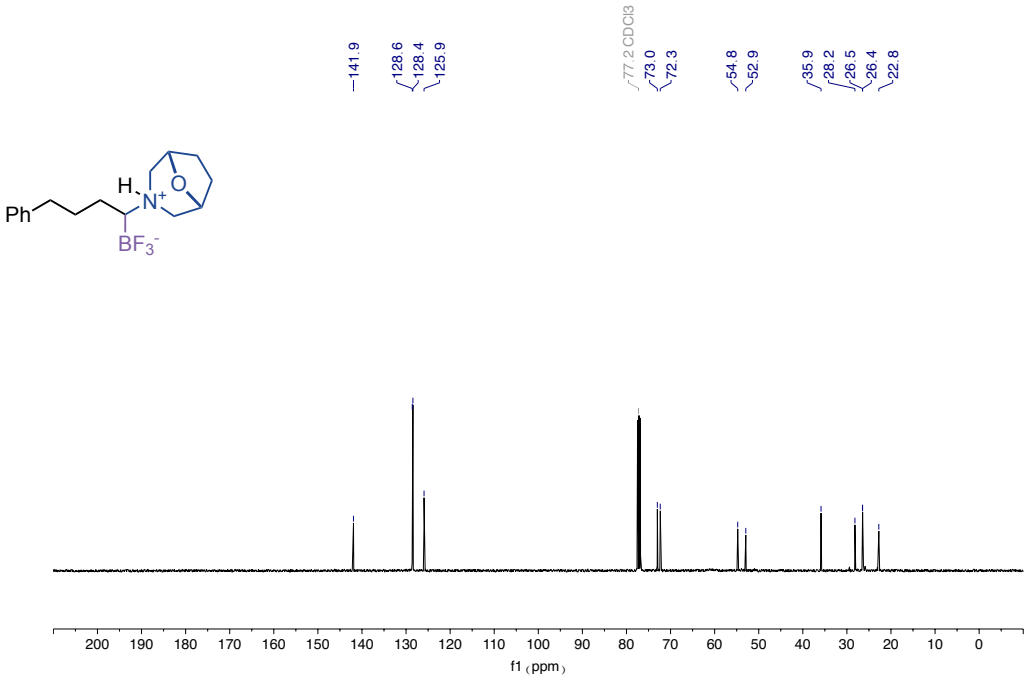

*^{13}C NMR spectra (101 MHz) of **4i***

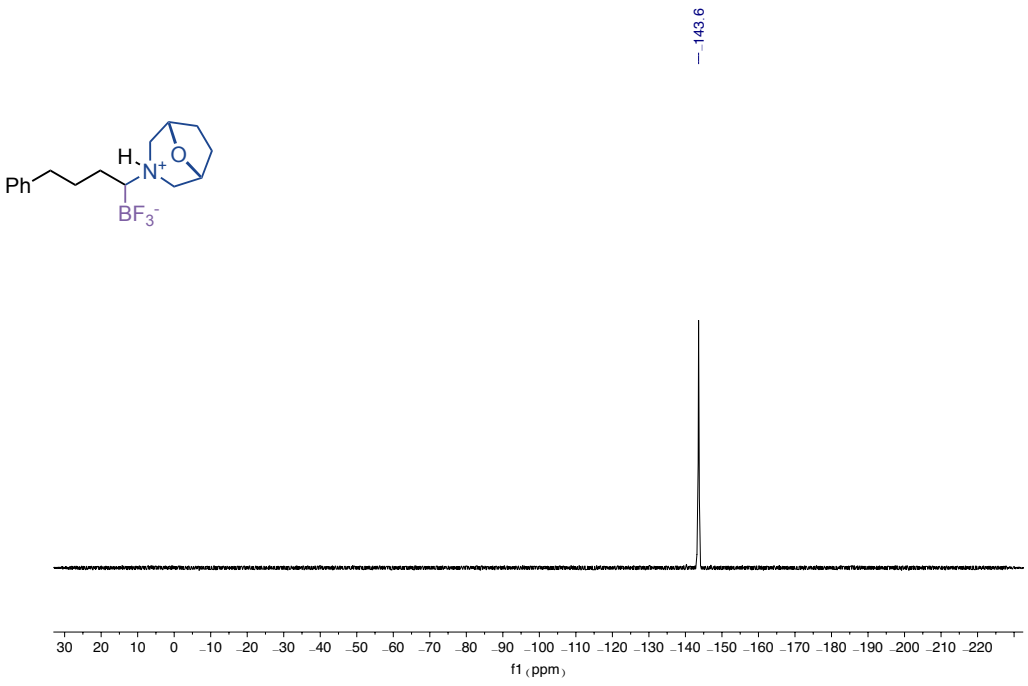

*^{19}F NMR spectra (376 MHz) of **4i***

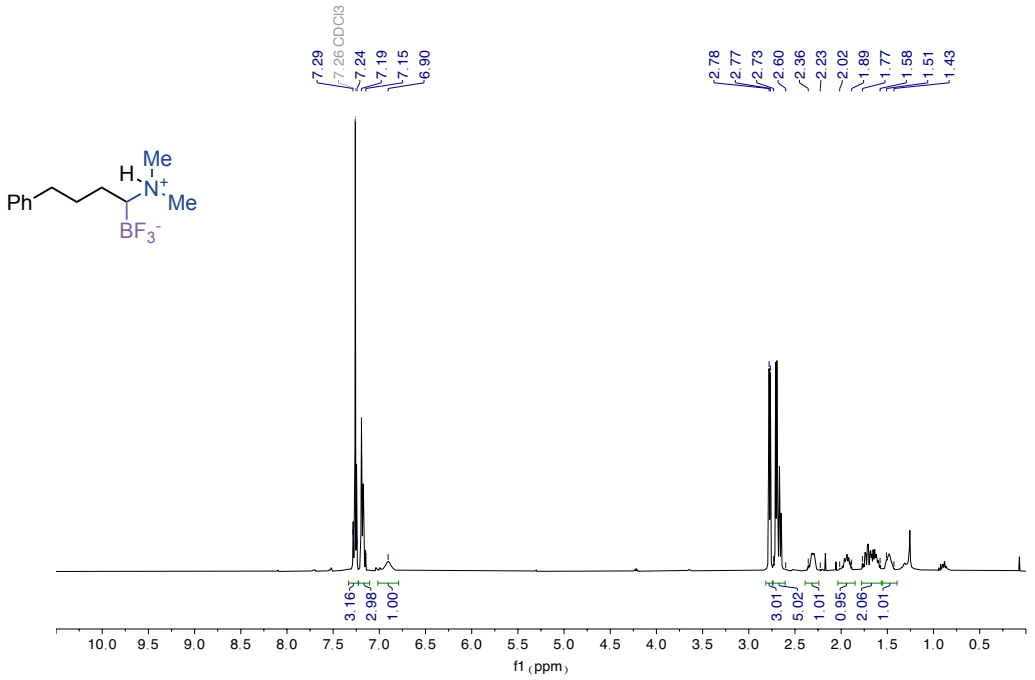

*^{1}H NMR spectra (400 MHz) of **4j***

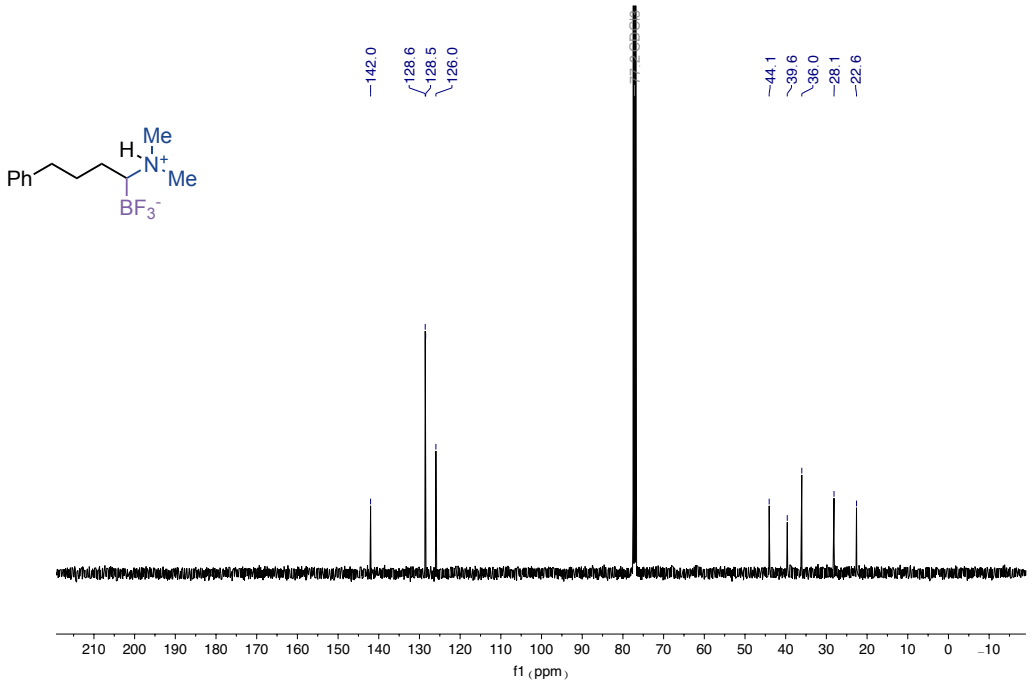

*^{13}C NMR spectra (101 MHz) of **4j***

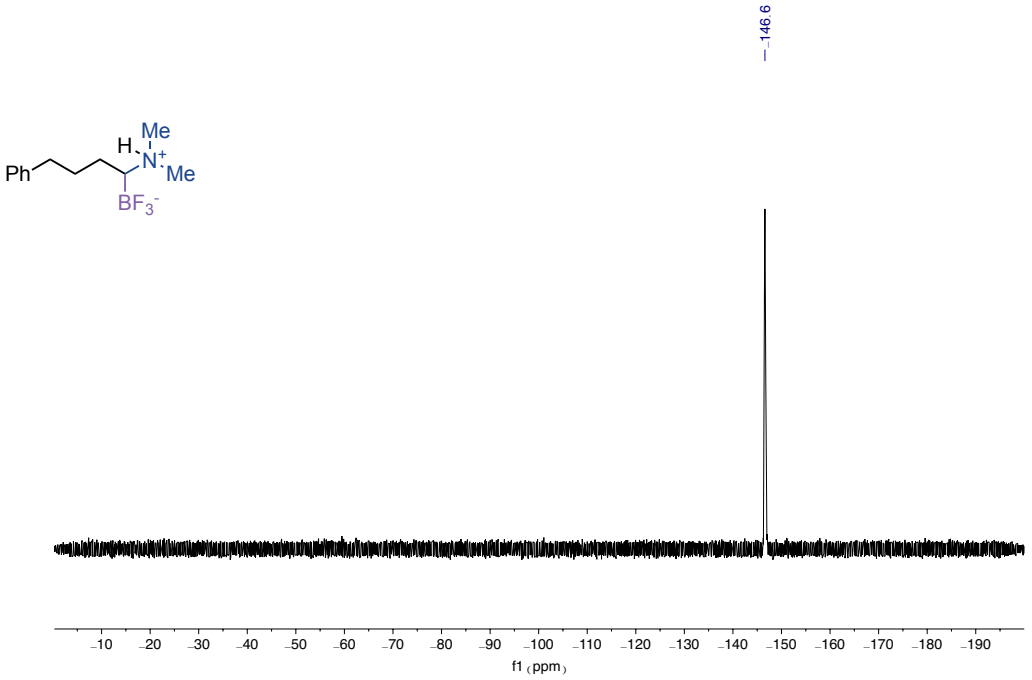

*^{19}F NMR spectra (376 MHz) of **4j***

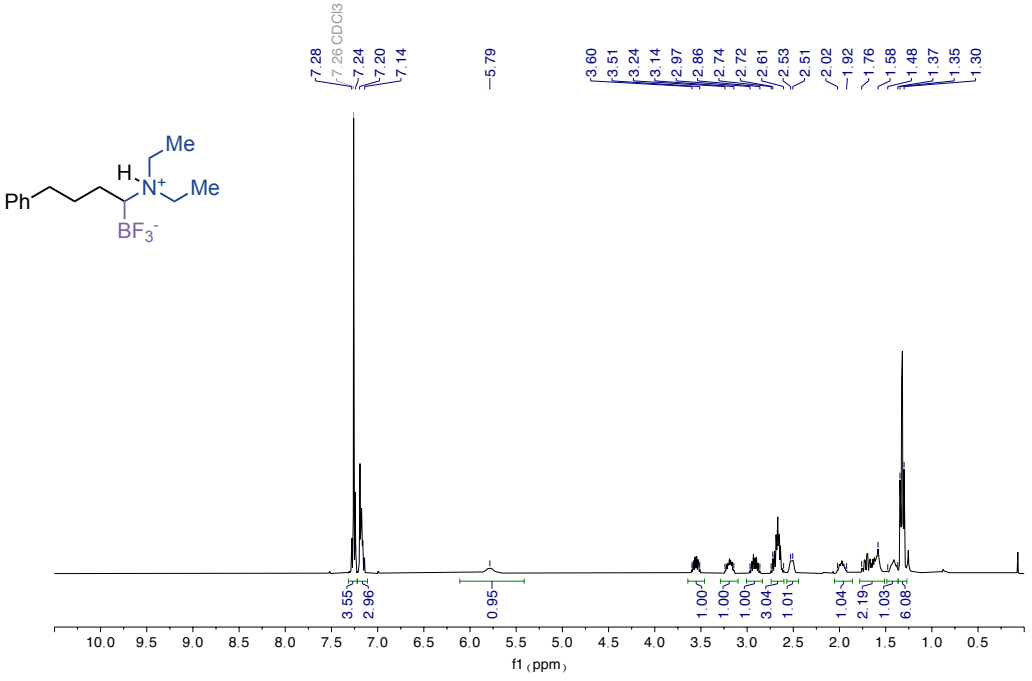

*^{1}H NMR spectra (400 MHz) of **4k***

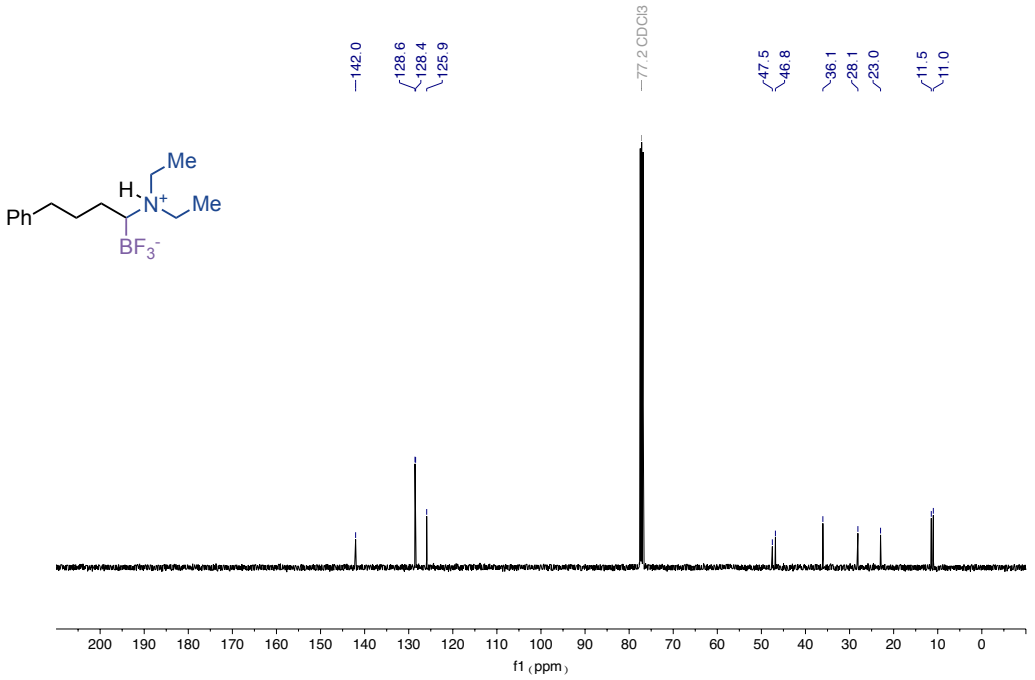

*^{13}C NMR spectra (101 MHz) of **4k***

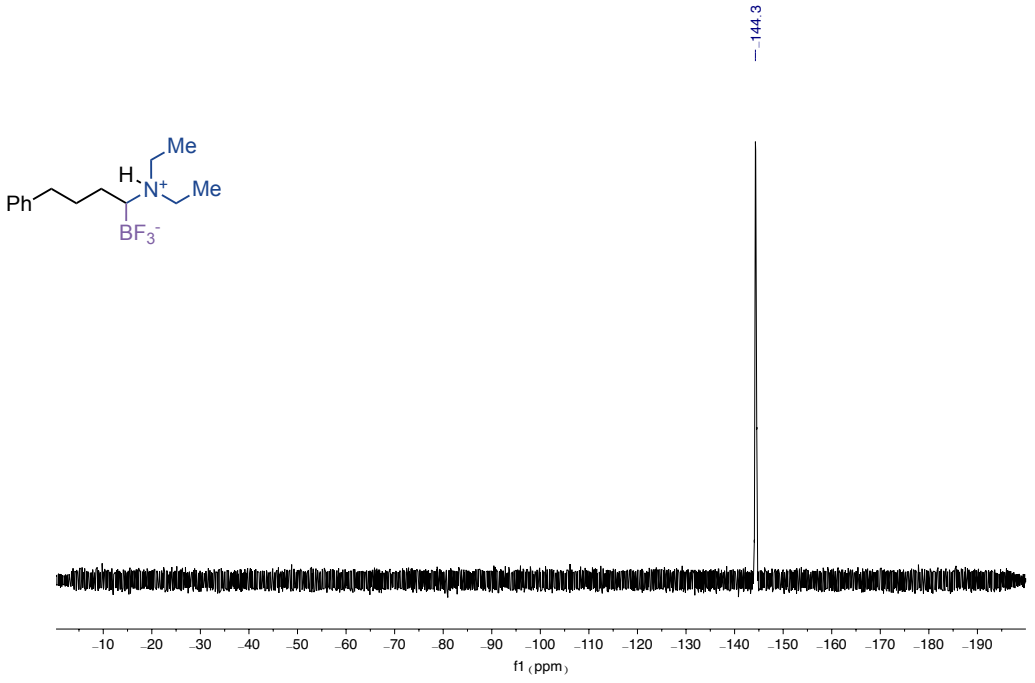

*^{19}F NMR spectra (376 MHz) of **4k***

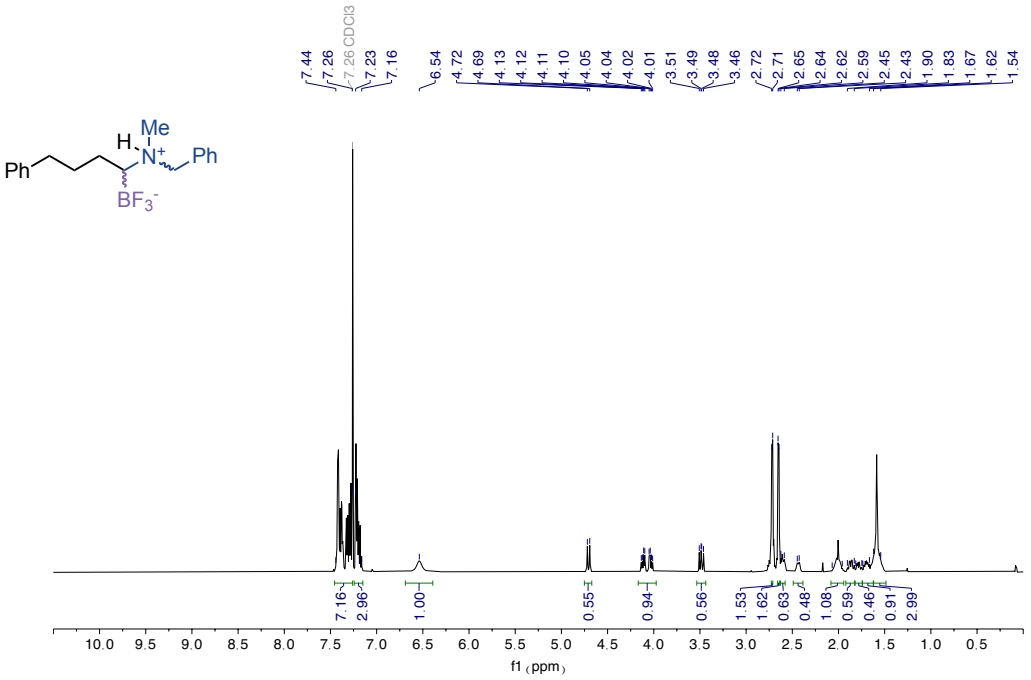

*^{1}H NMR spectra (400 MHz) of **4l***

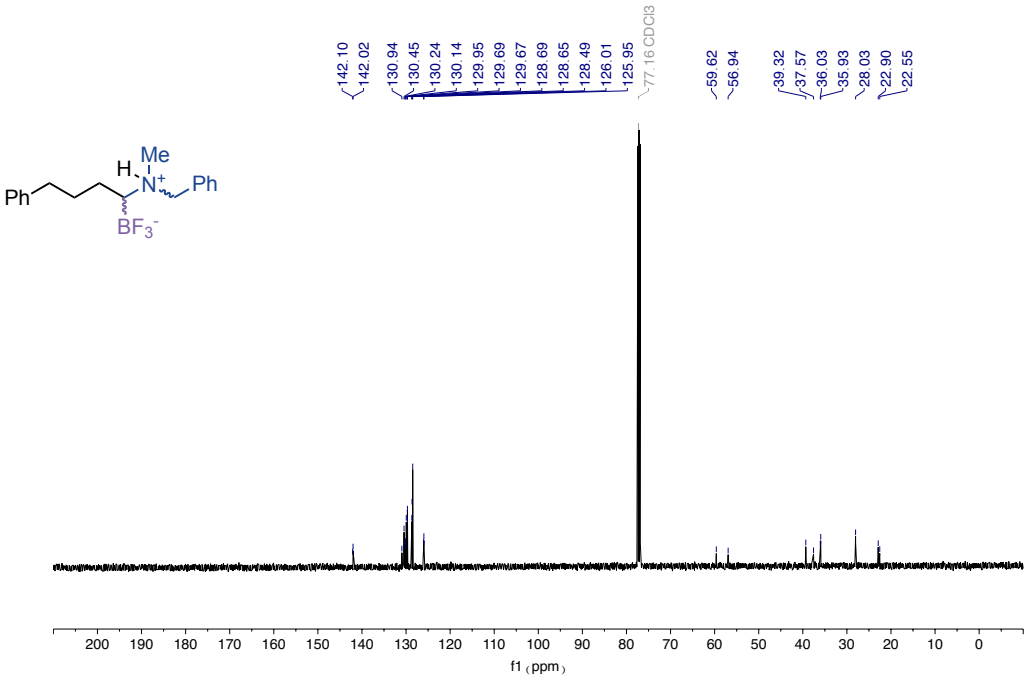

*^{13}C NMR spectra (101 MHz) of **4l***

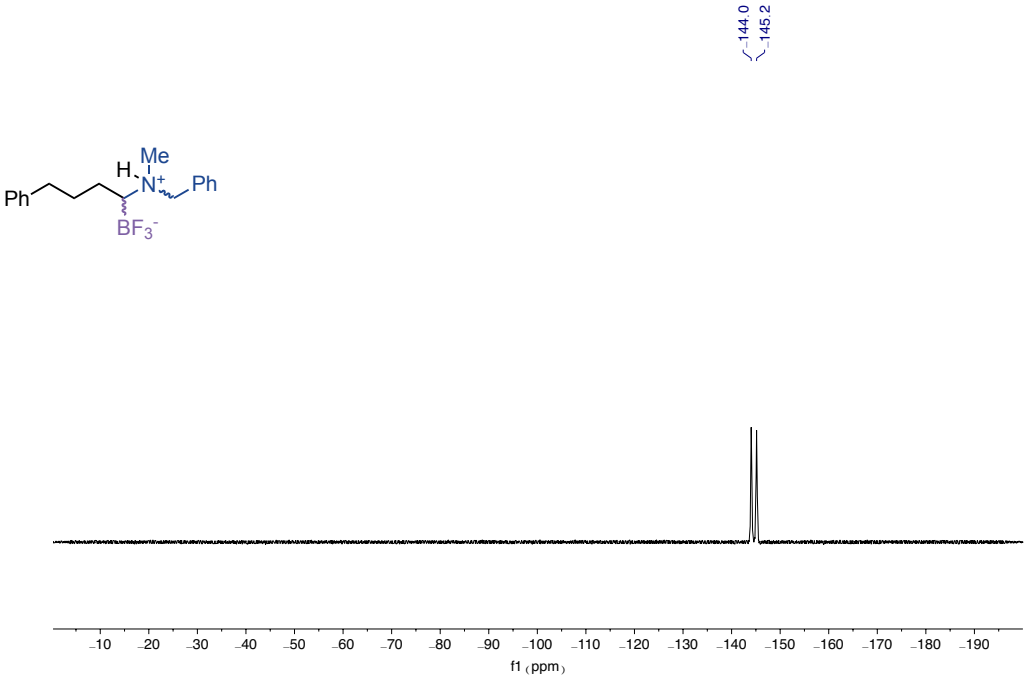

*^{19}F NMR spectra (376 MHz) of **4l***

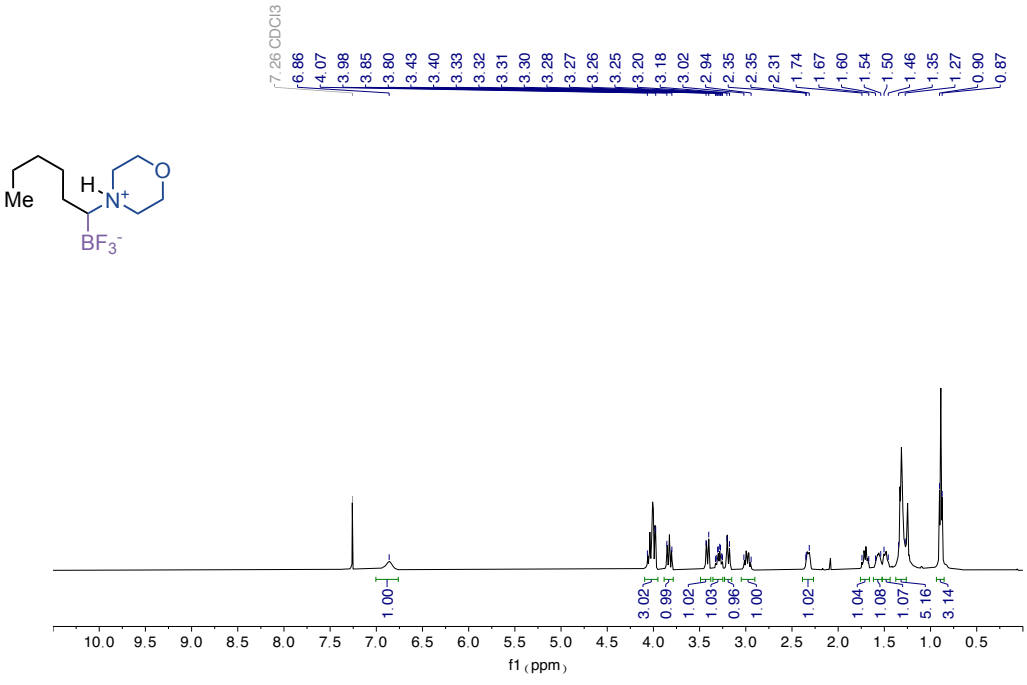

*^{1}H NMR spectra (400 MHz) of **4m***

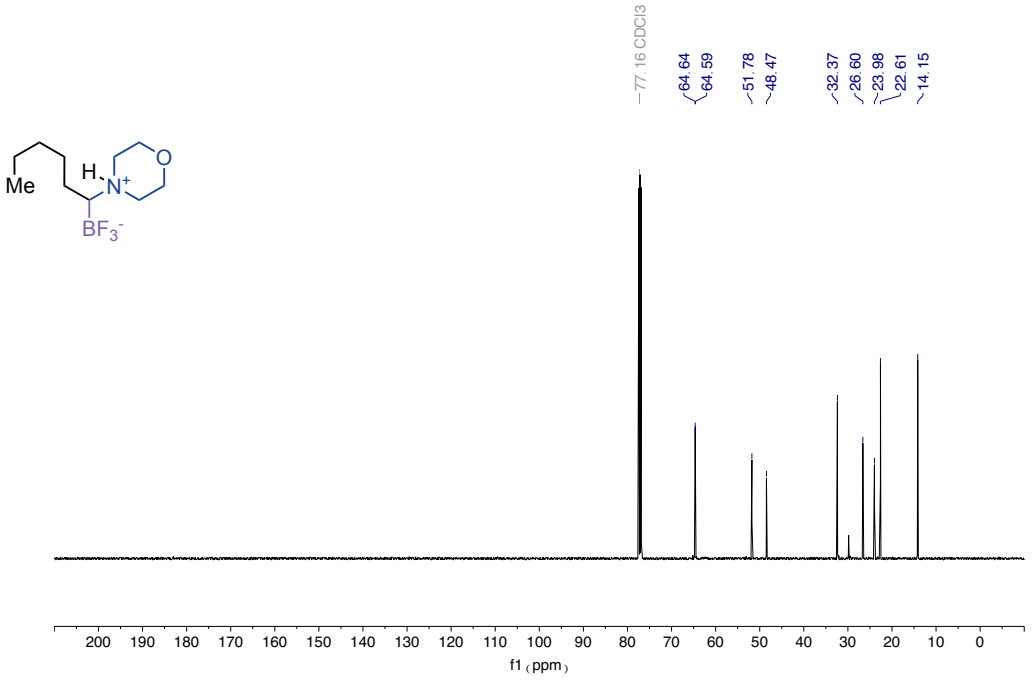

*^{13}C NMR spectra (101 MHz) of **4m***

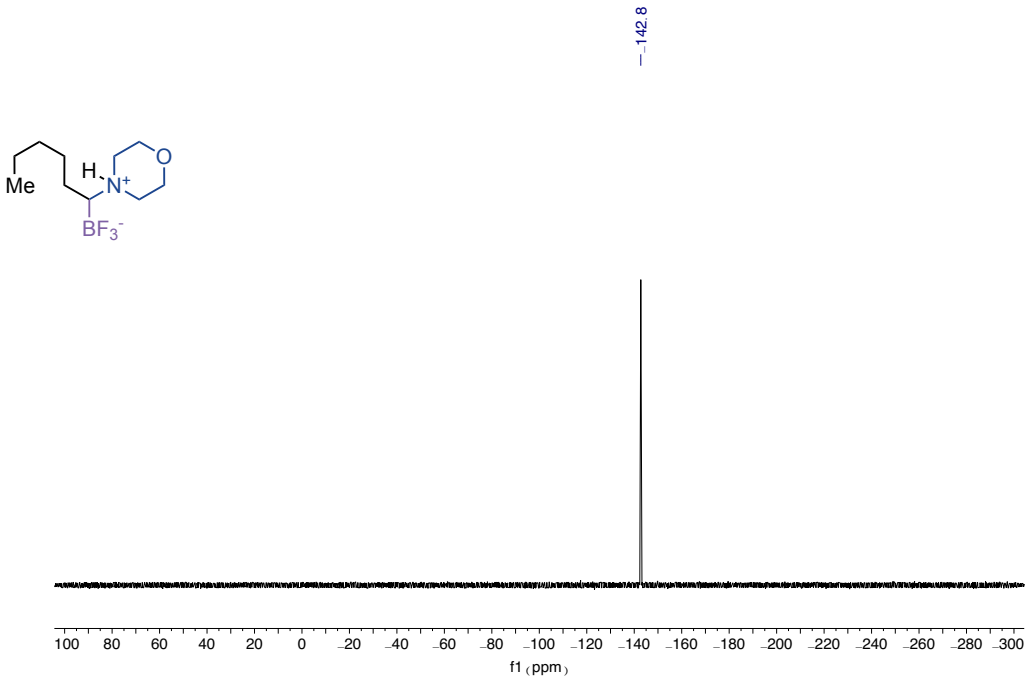

*^{19}F NMR spectra (376 MHz) of **4m***

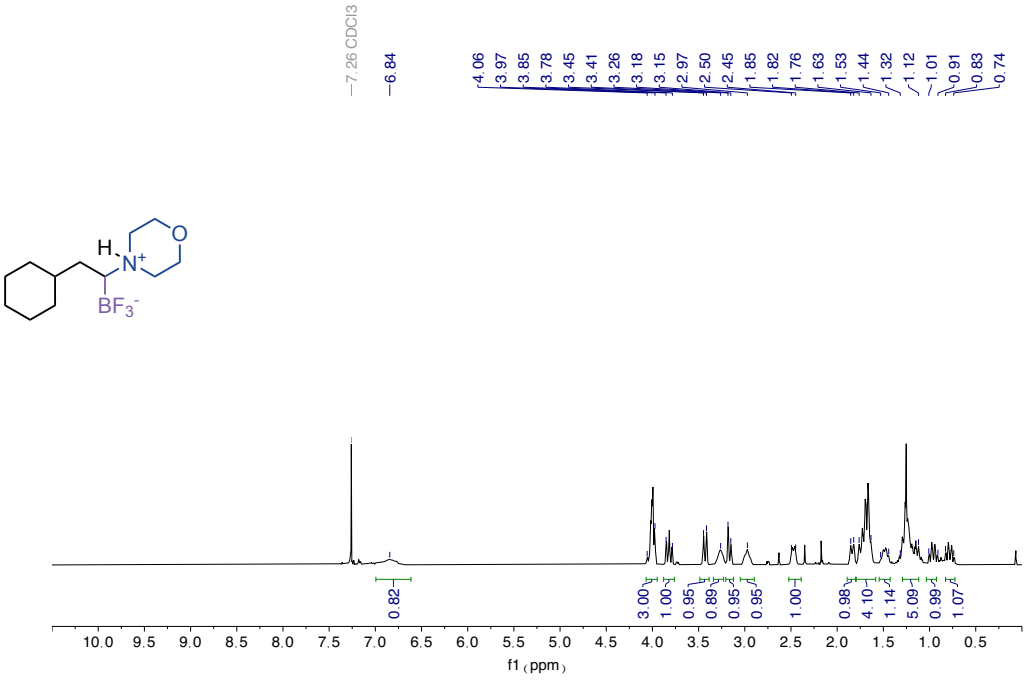

*[1]H NMR spectra (400 MHz) of **4n***

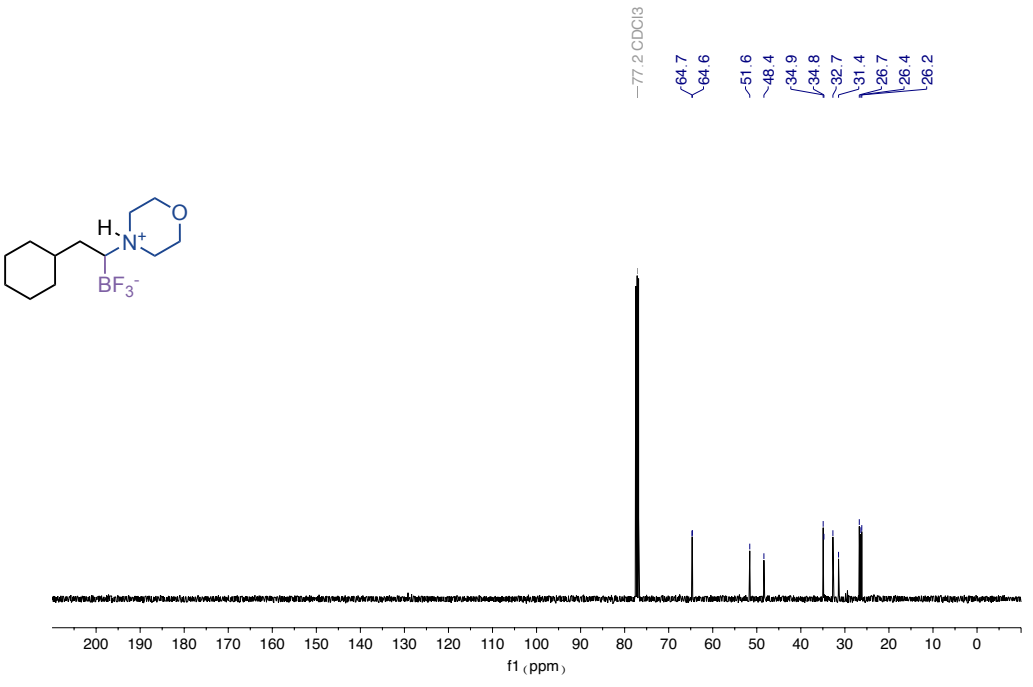

*[13]C NMR spectra (101 MHz) of **4n***

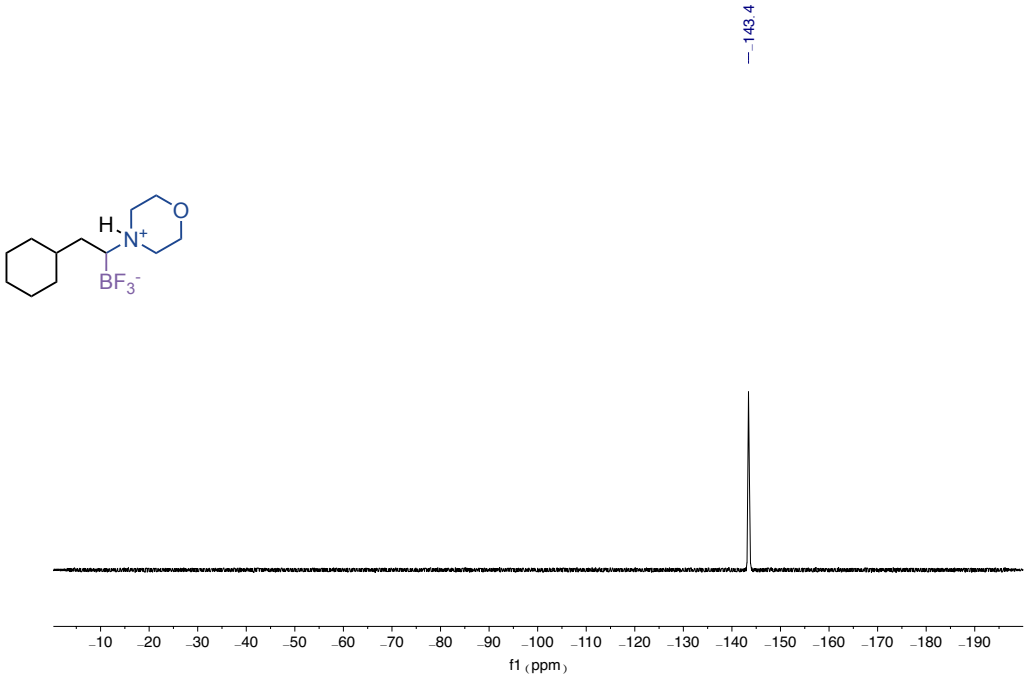

*^{19}F NMR spectra (376 MHz) of **4n***

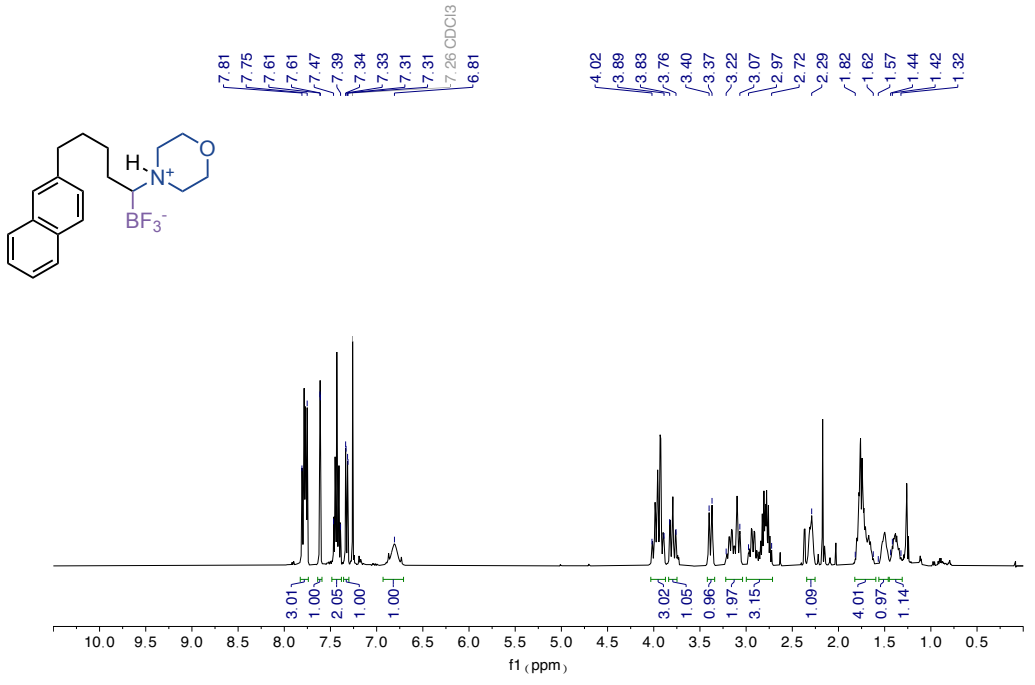

*^{1}H NMR spectra (400 MHz) of **4o***

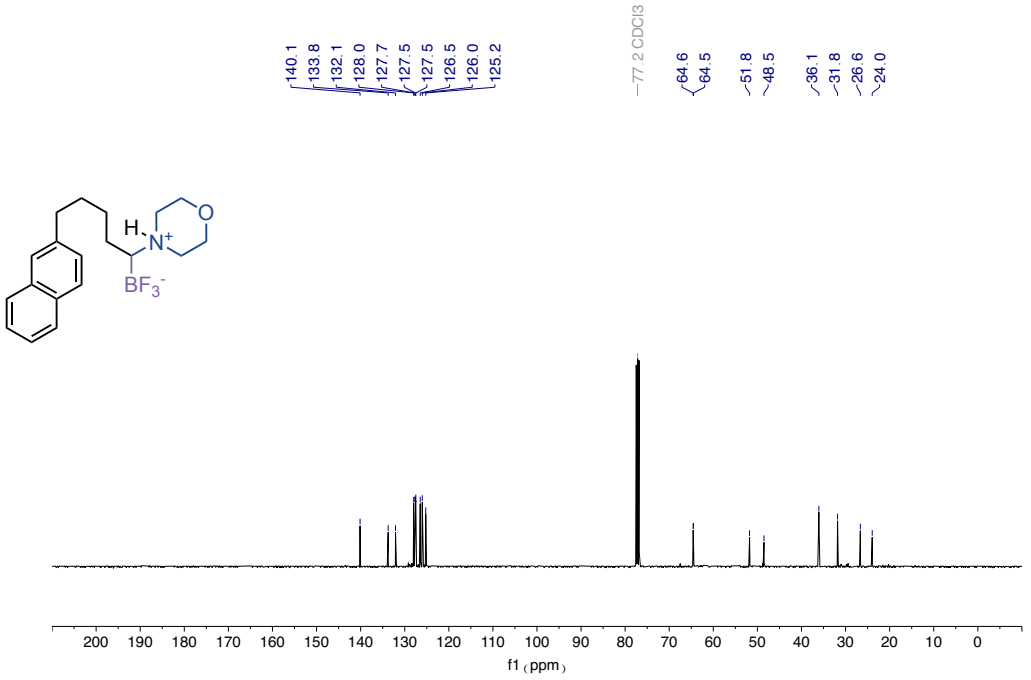

*^{13}C NMR spectra (101 MHz) of **4o***

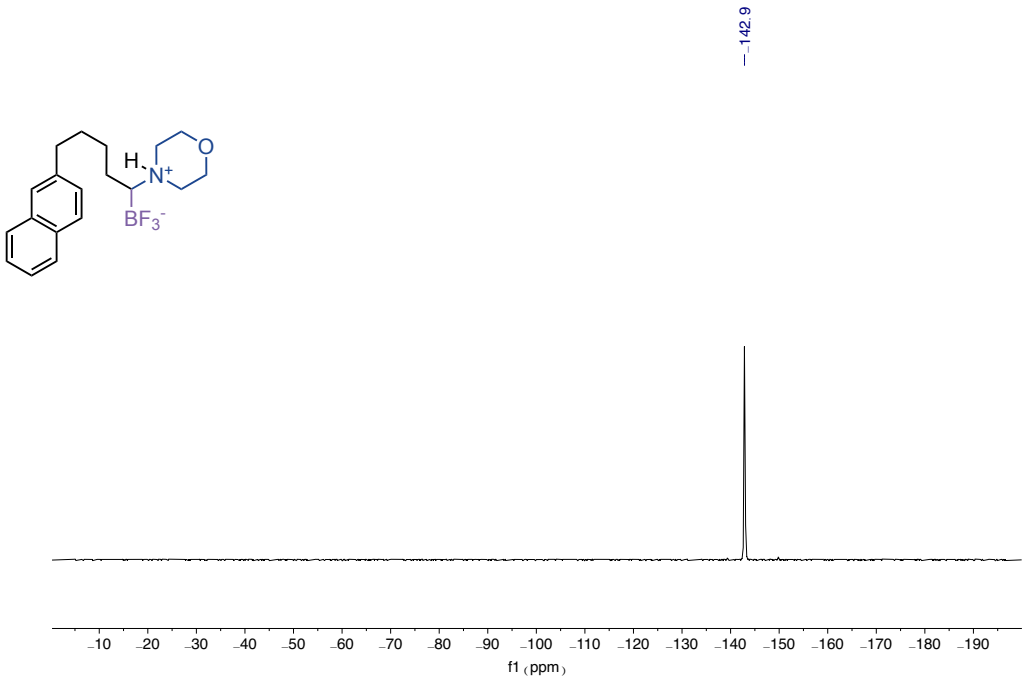

*^{19}F NMR spectra (376 MHz) of **4o***

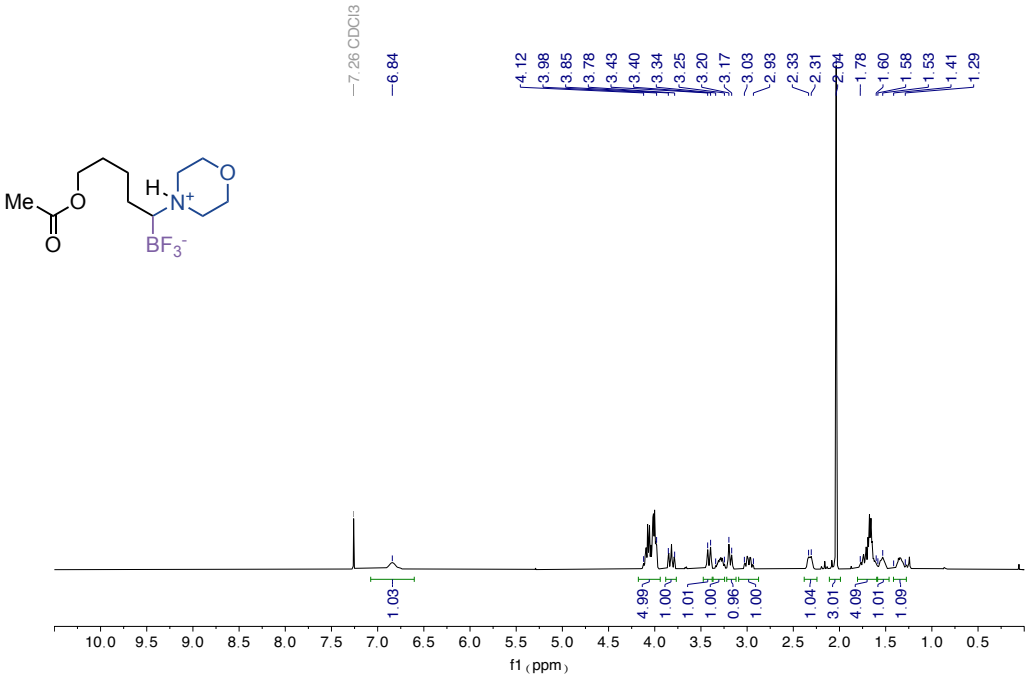

*^{1}H NMR spectra (400 MHz) of **4p***

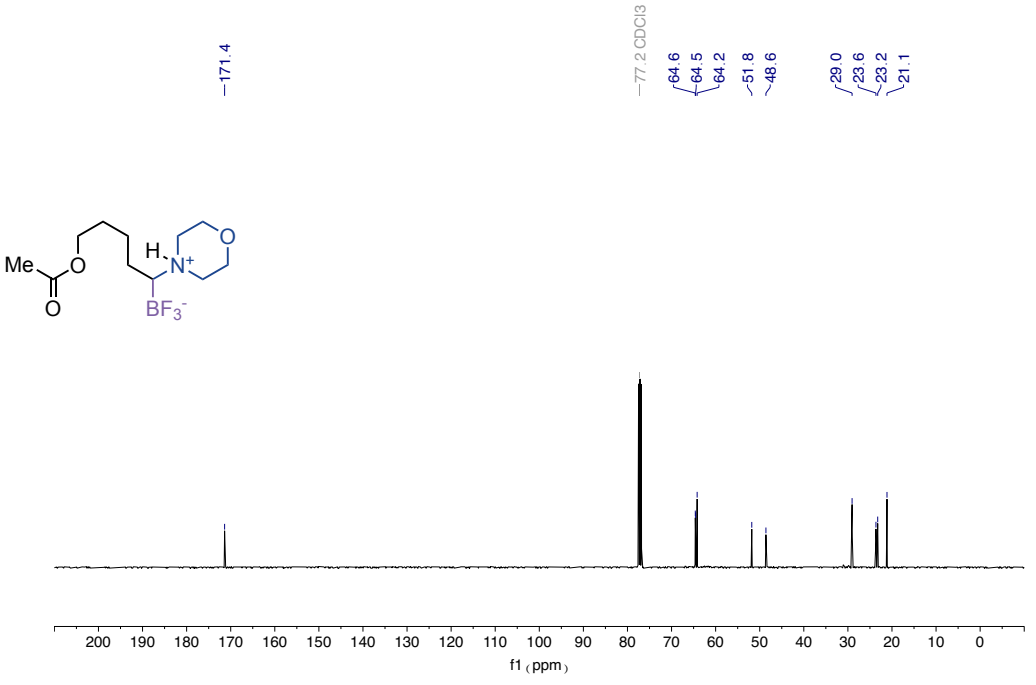

*^{13}C NMR spectra (101 MHz) of **4p***

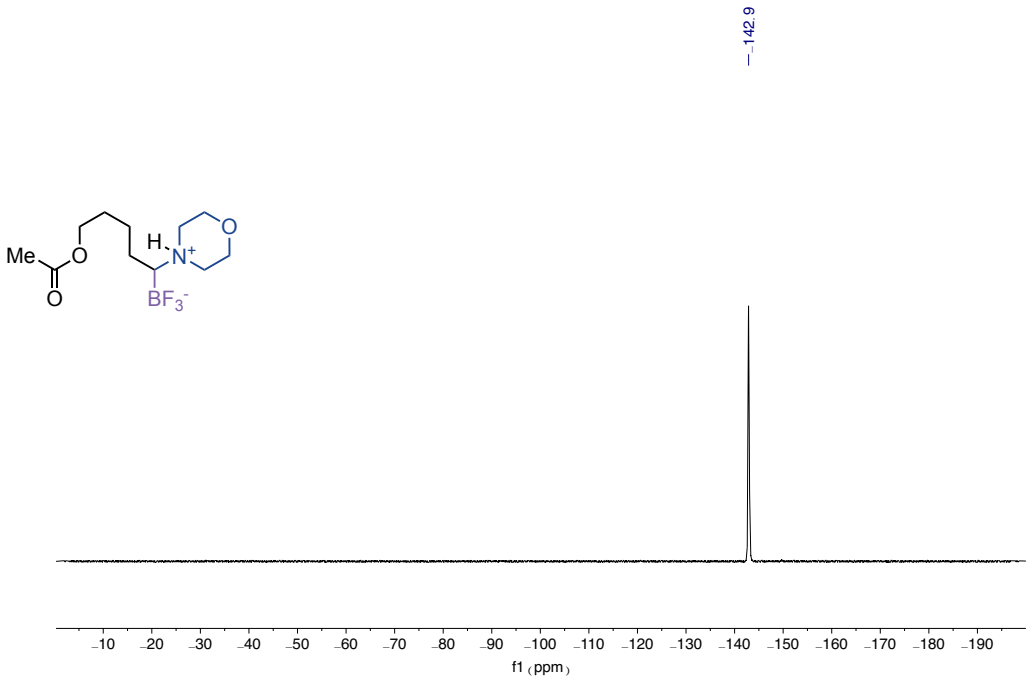

*^{19}F NMR spectra (376 MHz) of **4p***

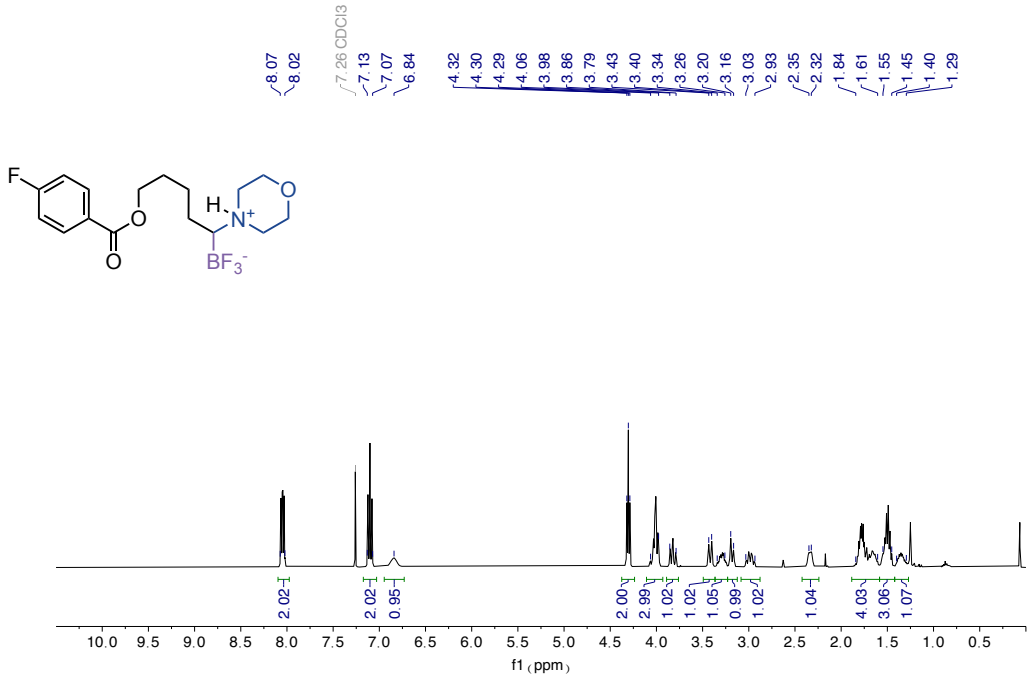

*^{1}H NMR spectra (400 MHz) of **4q***

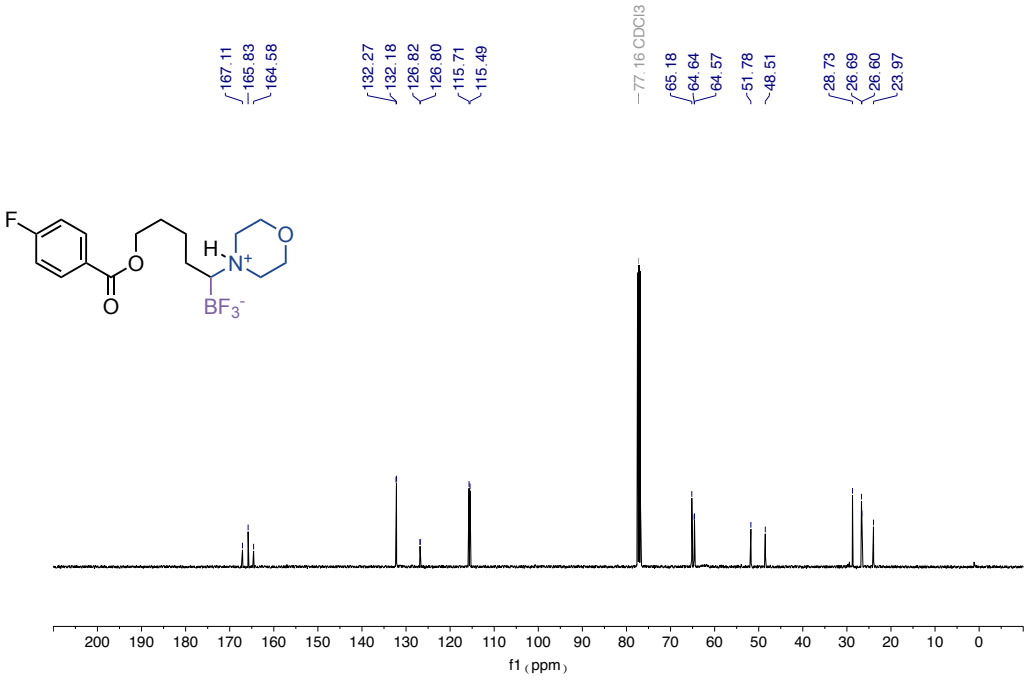

*^{13}C NMR spectra (101 MHz) of **4q***

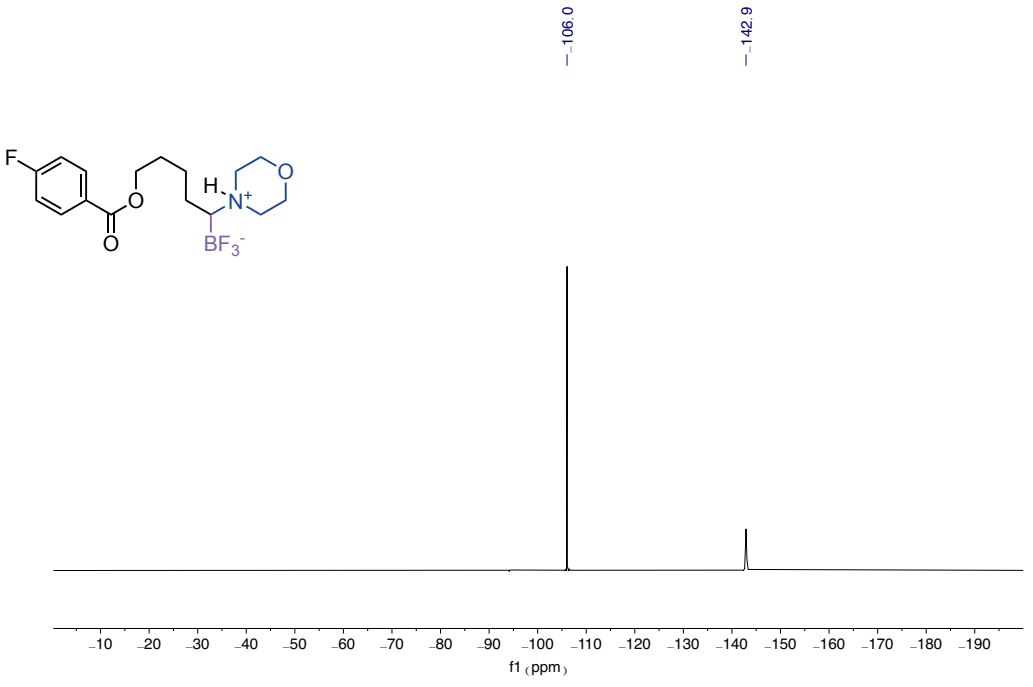

*^{19}F NMR spectra (376 MHz) of **4q***

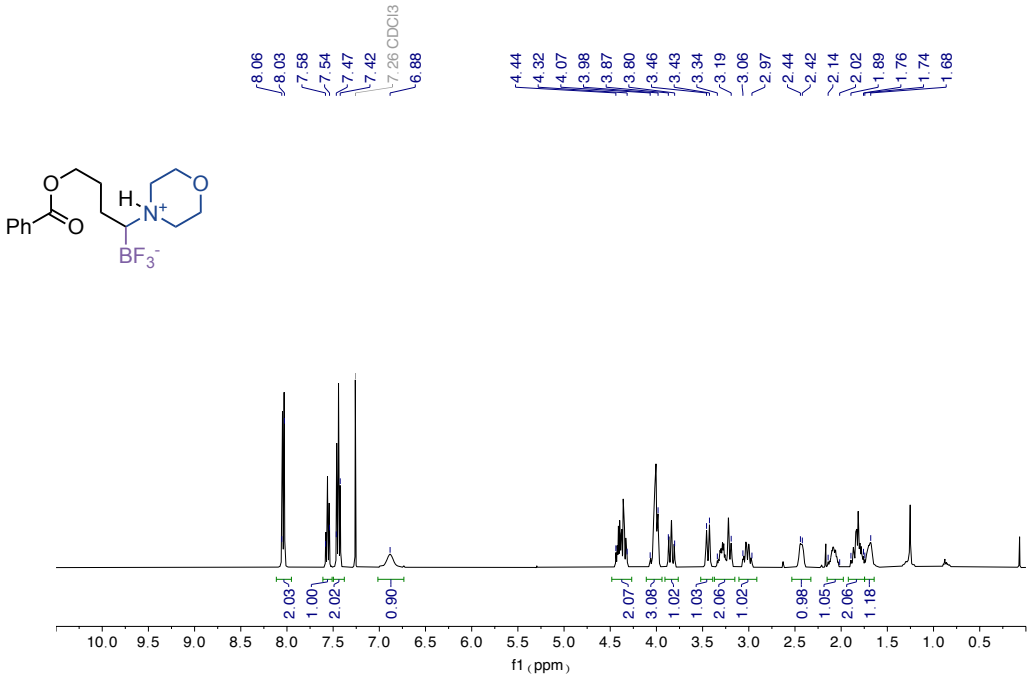

*^{1}H NMR spectra (400 MHz) of **4r***

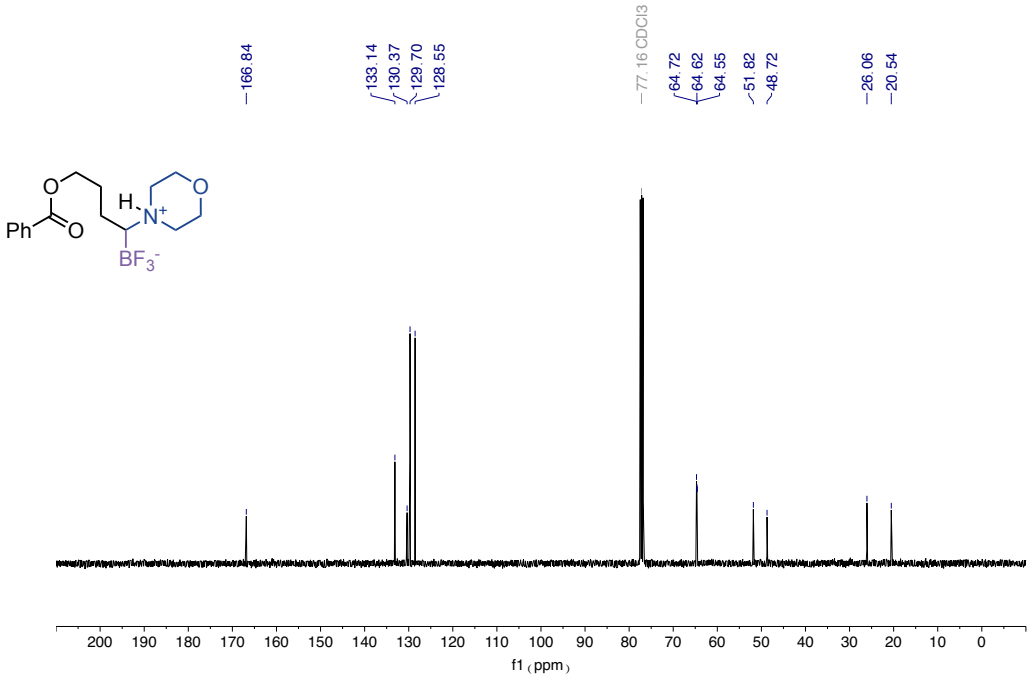

*^{13}C NMR spectra (101 MHz) of **4r***

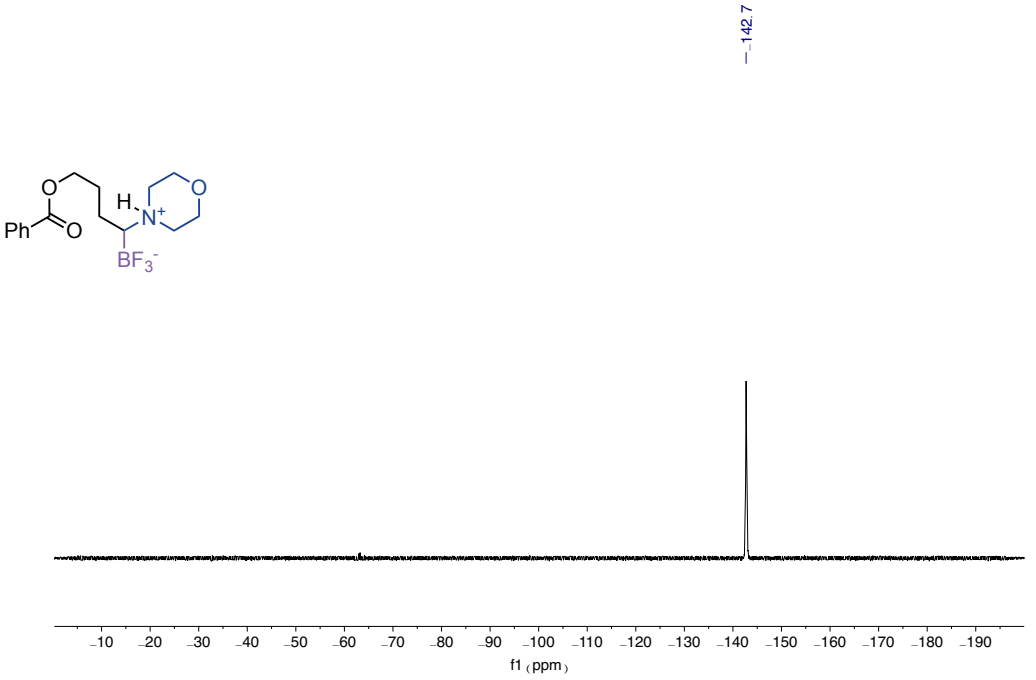

*^{19}F NMR spectra (376 MHz) of **4r***

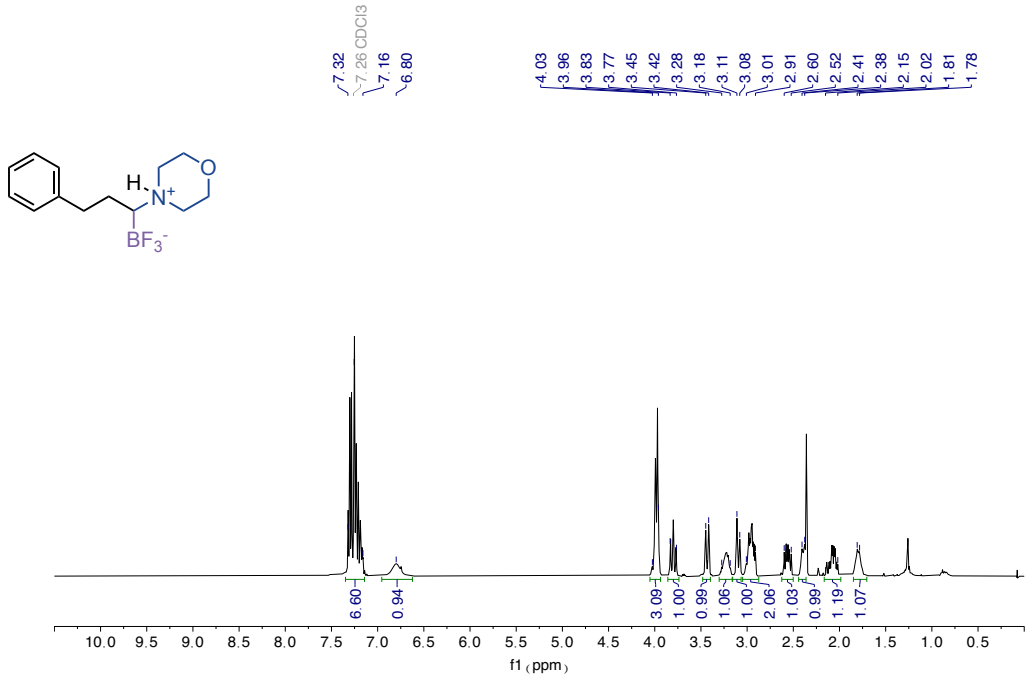

*^{1}H NMR spectra (400 MHz) of **4s***

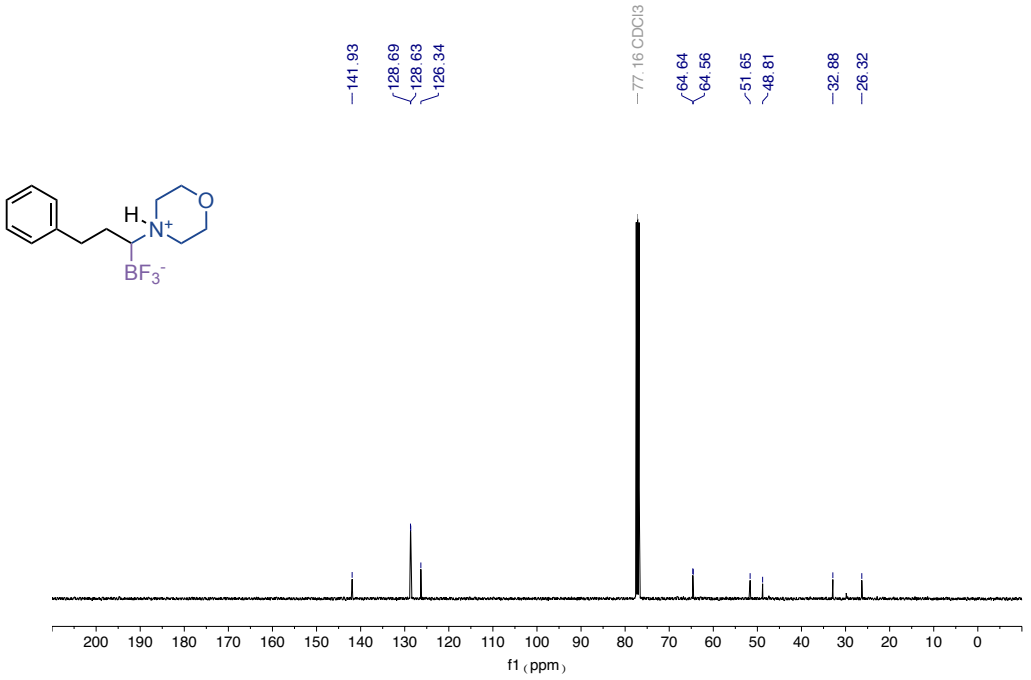

*^{13}C NMR spectra (101 MHz) of **4s***

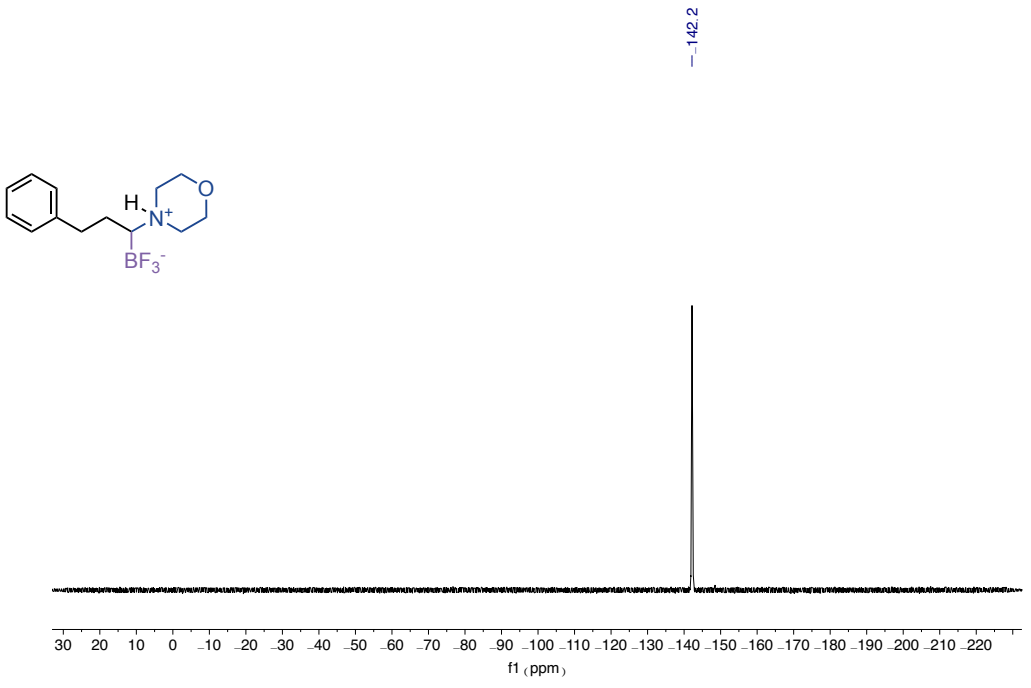

*^{19}F NMR spectra (376 MHz) of **4s***

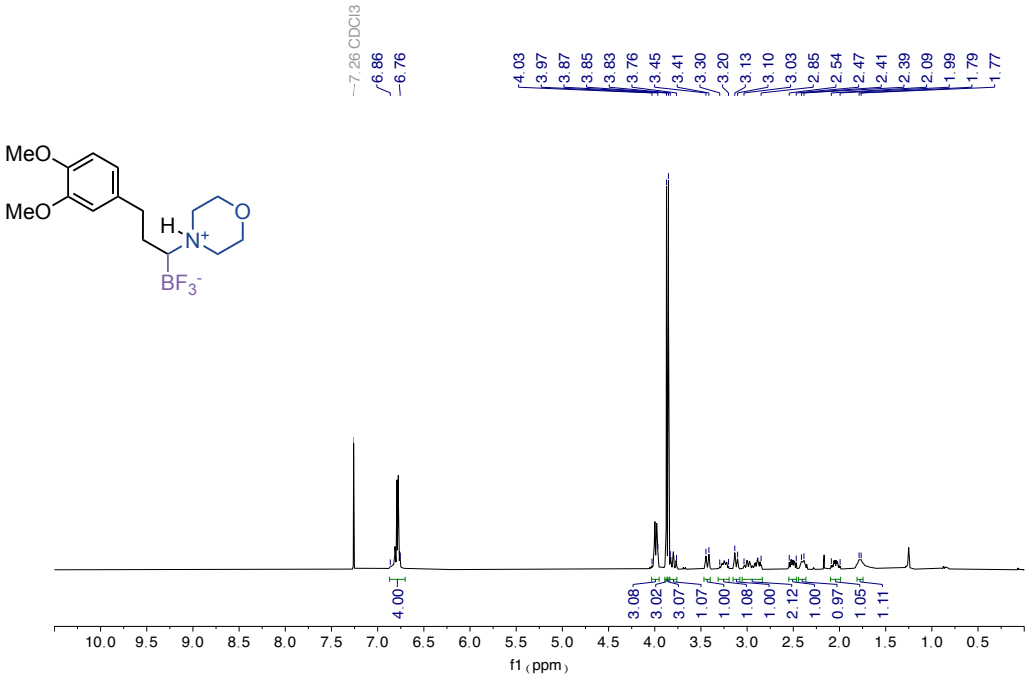

*^{1}H NMR spectra (400 MHz) of **4t***

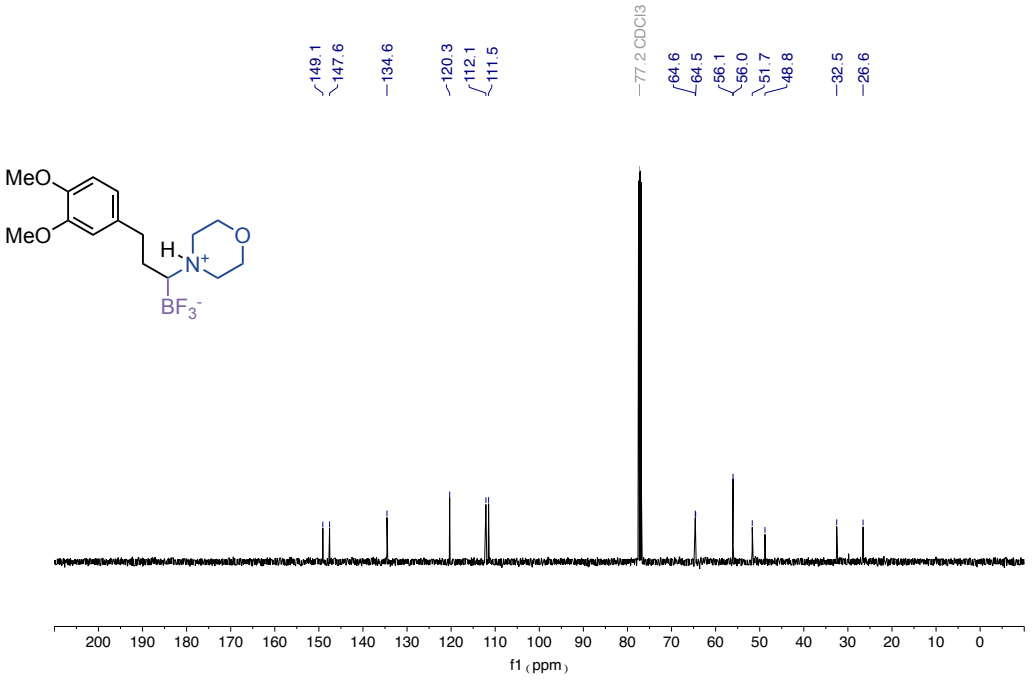

*^{13}C NMR spectra (101 MHz) of **4t***

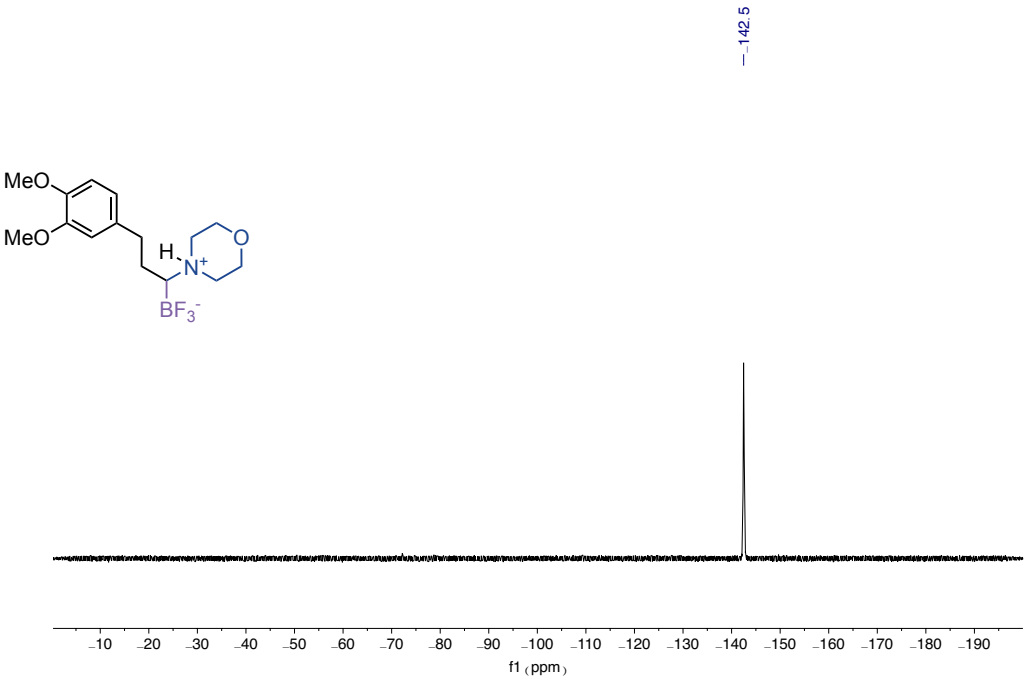

*^{19}F NMR spectra (376 MHz) of **4t***

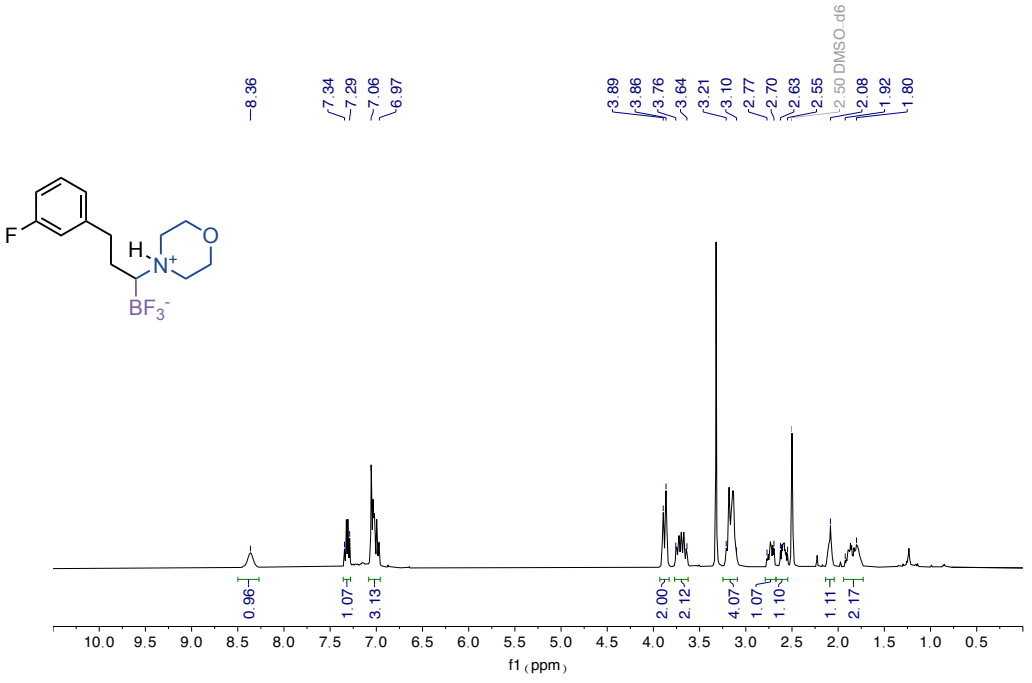

*^{1}H NMR spectra (400 MHz) of **4u***

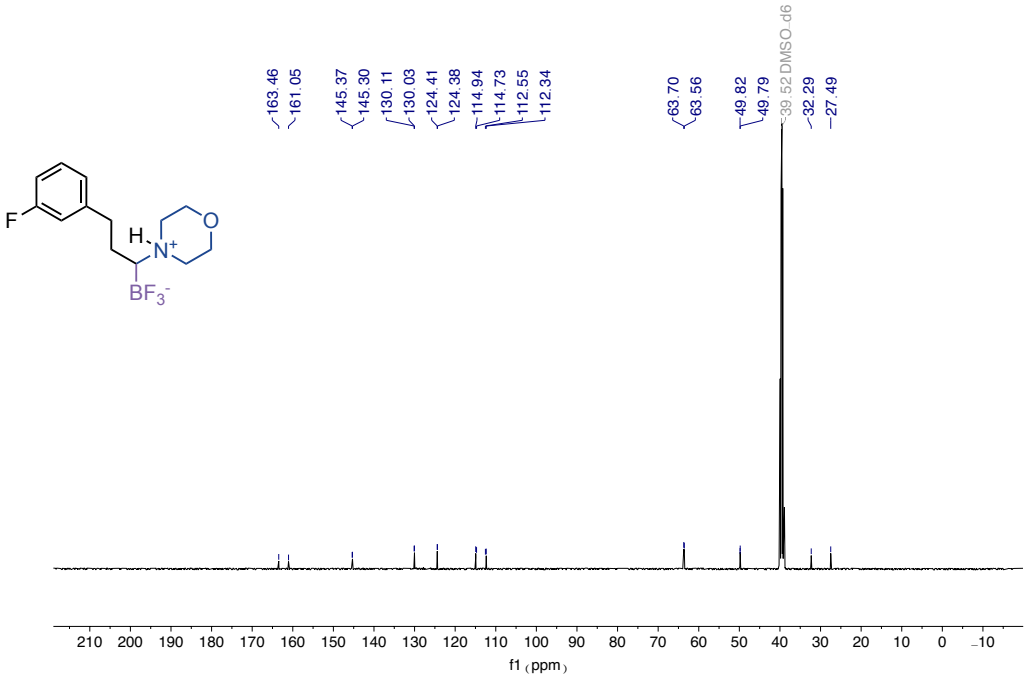

*^{13}C NMR spectra (101 MHz) of **4u***

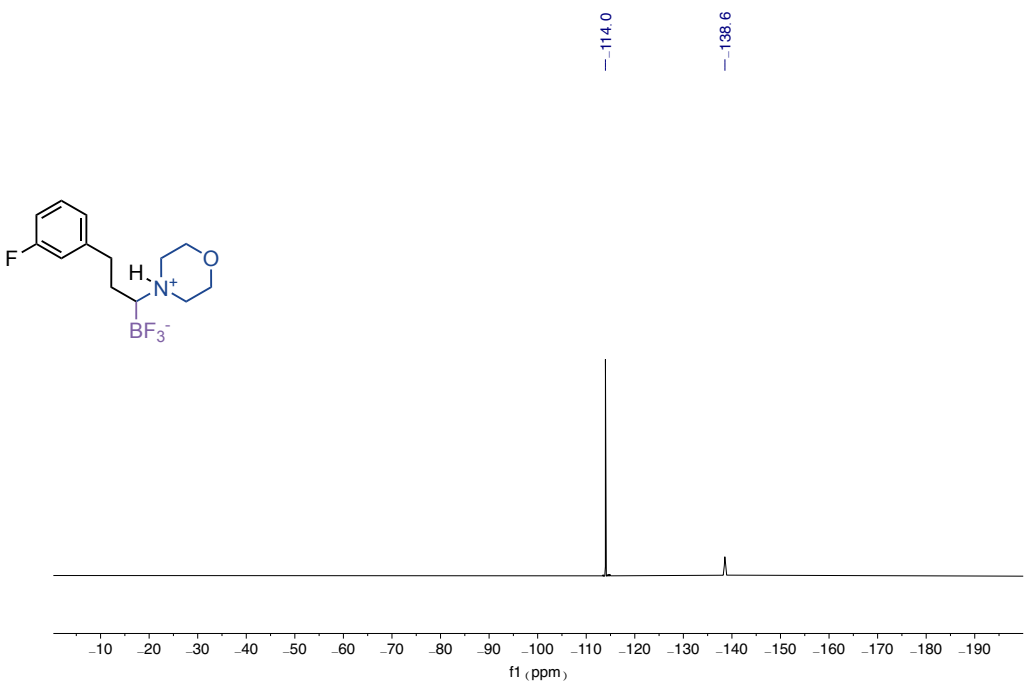

*^{19}F NMR spectra (376 MHz) of **4u***

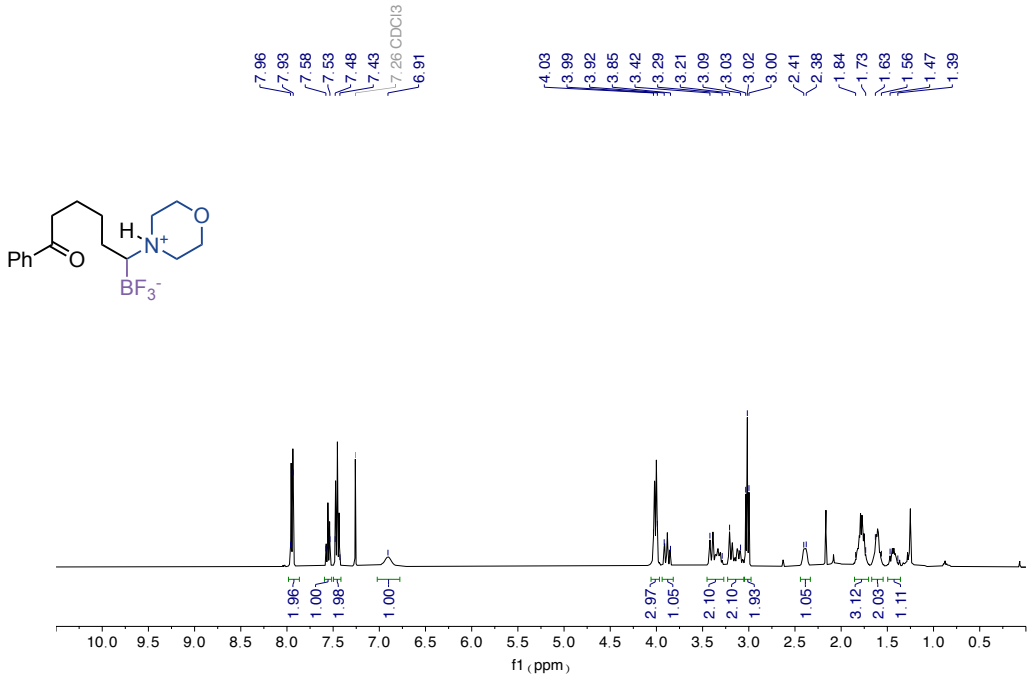

*^{1}H NMR spectra (400 MHz) of **4v***

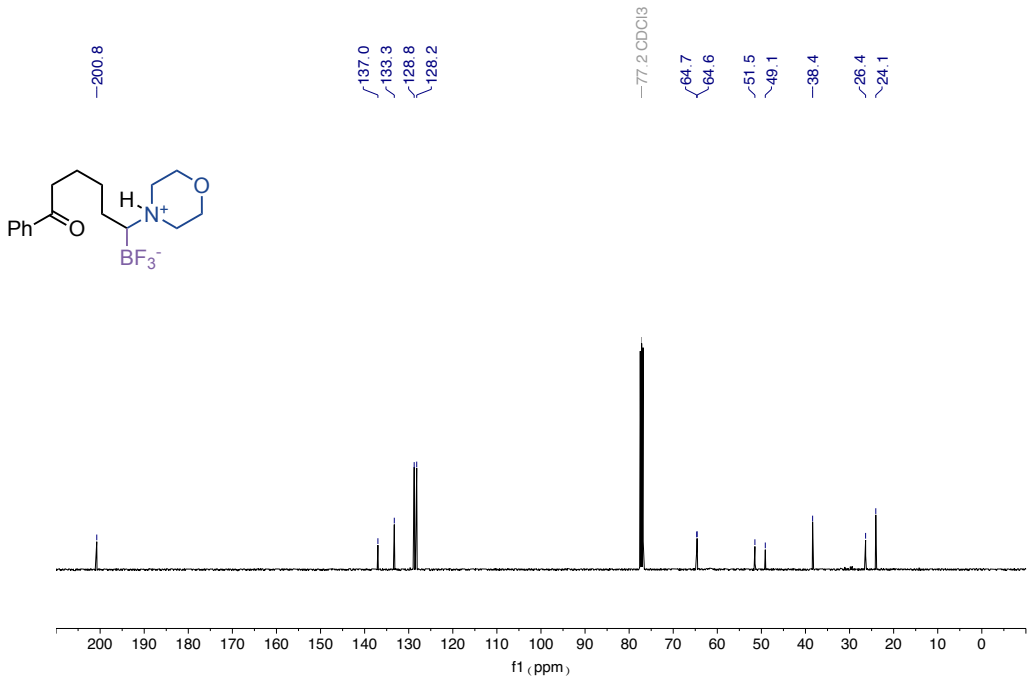

*^{13}C NMR spectra (101 MHz) of **4v***

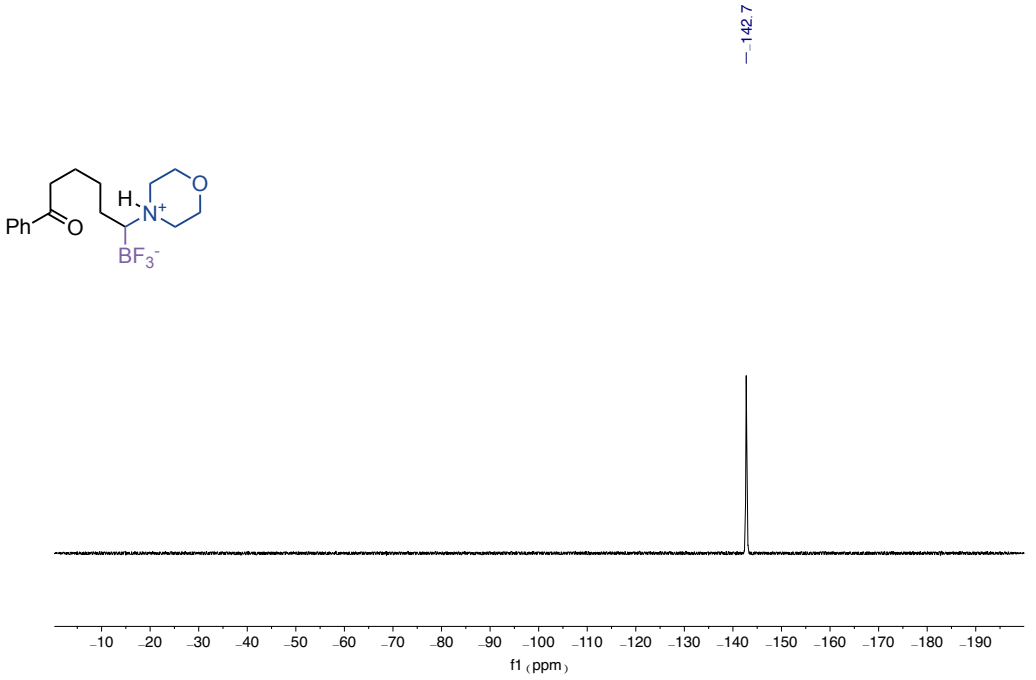

*^{19}F NMR spectra (376 MHz) of **4v***

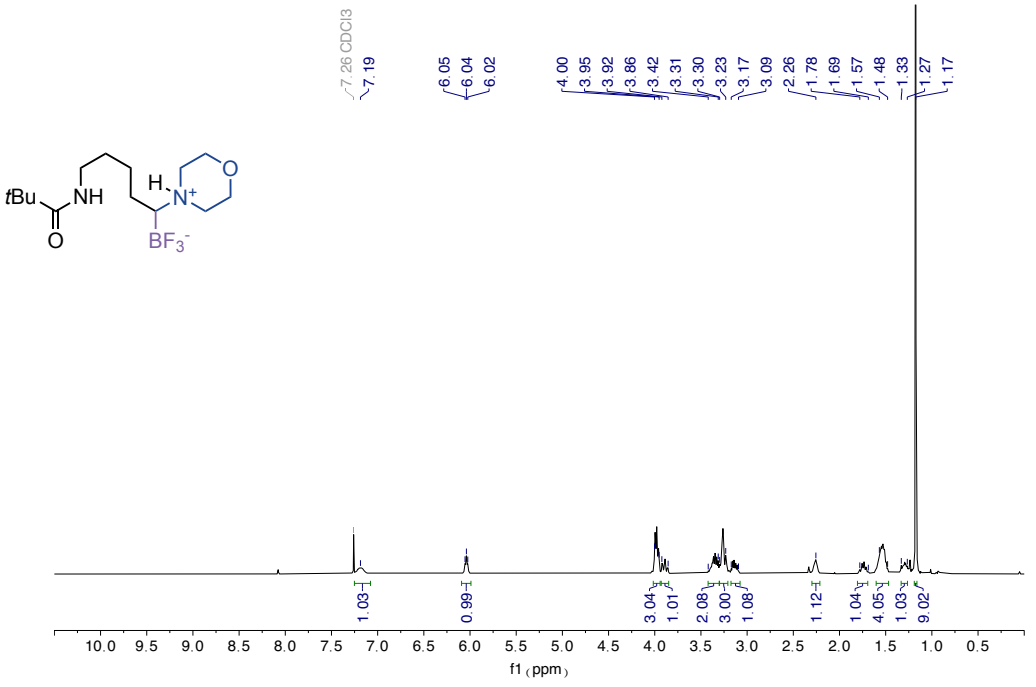

*^{1}H NMR spectra (400 MHz) of **4w***

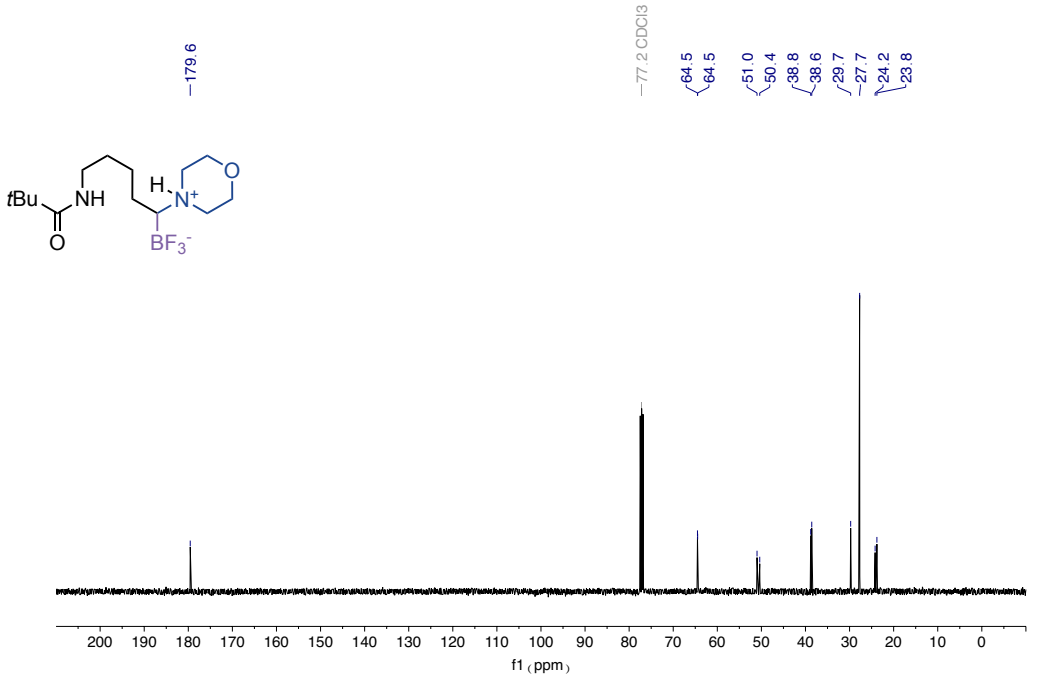

*^{13}C NMR spectra (101 MHz) of **4w***

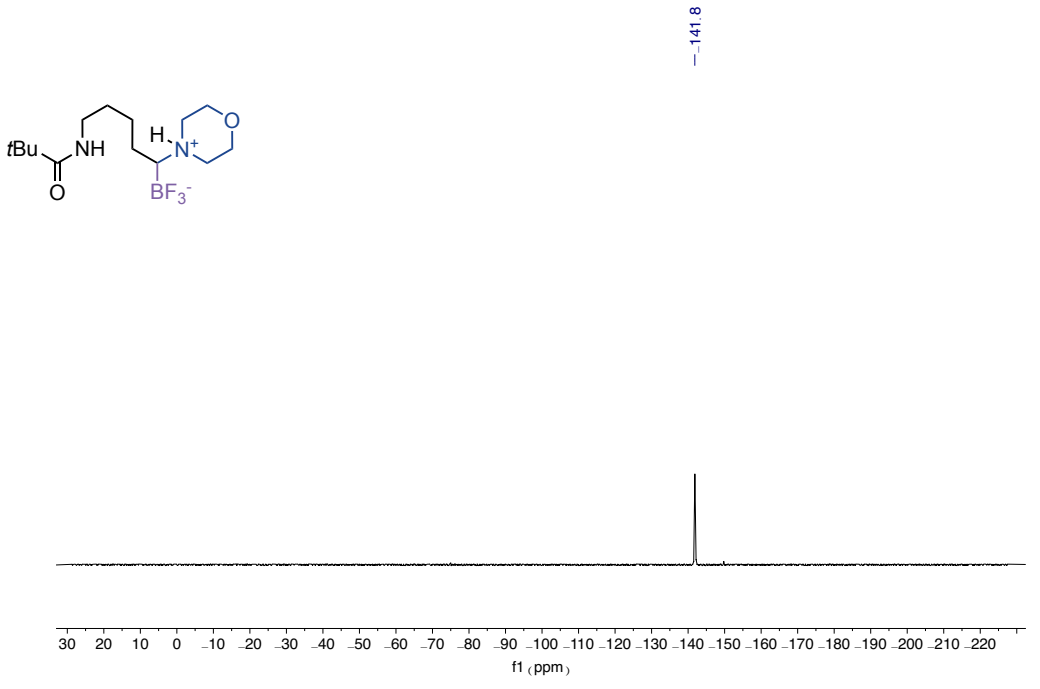

*^{19}F NMR spectra (376 MHz) of **4w***

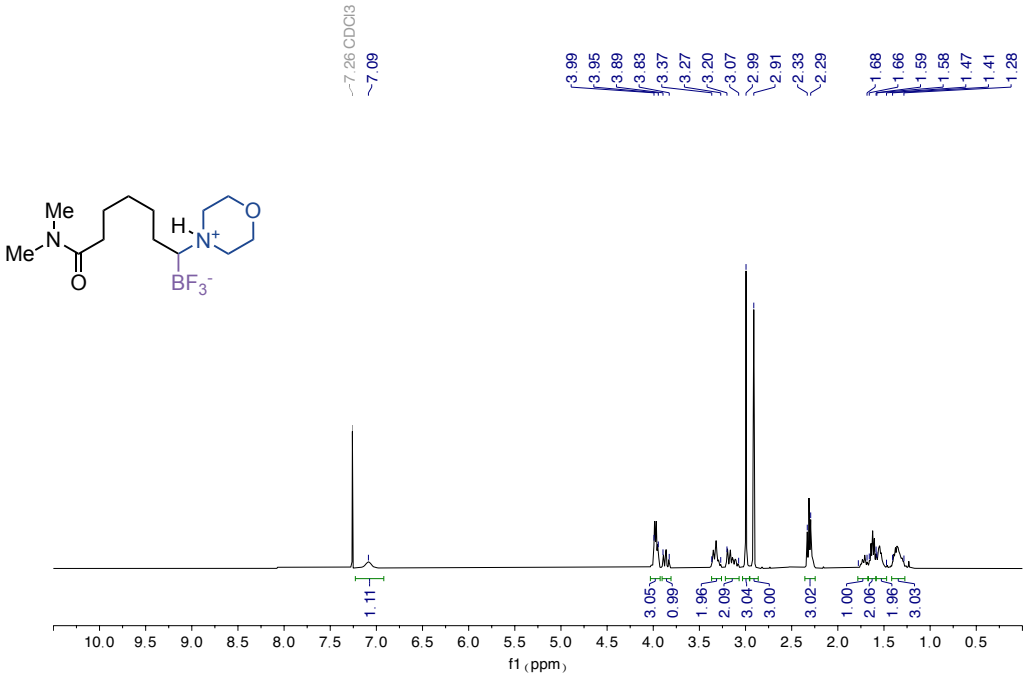

*^{1}H NMR spectra (400 MHz) of **4x***

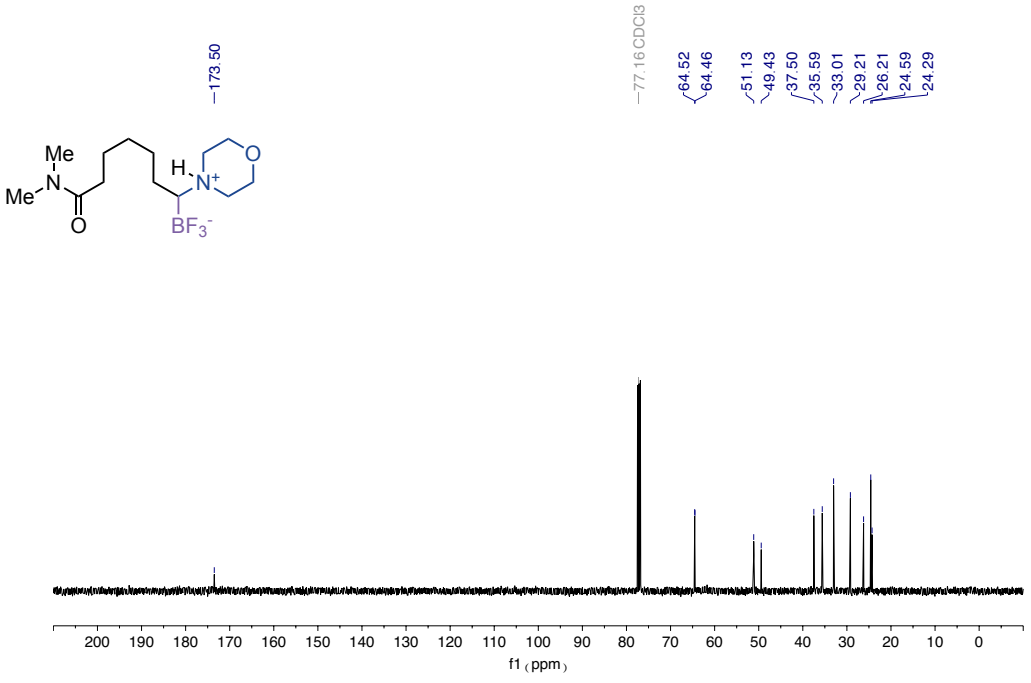

*^{13}C NMR spectra (101 MHz) of **4x***

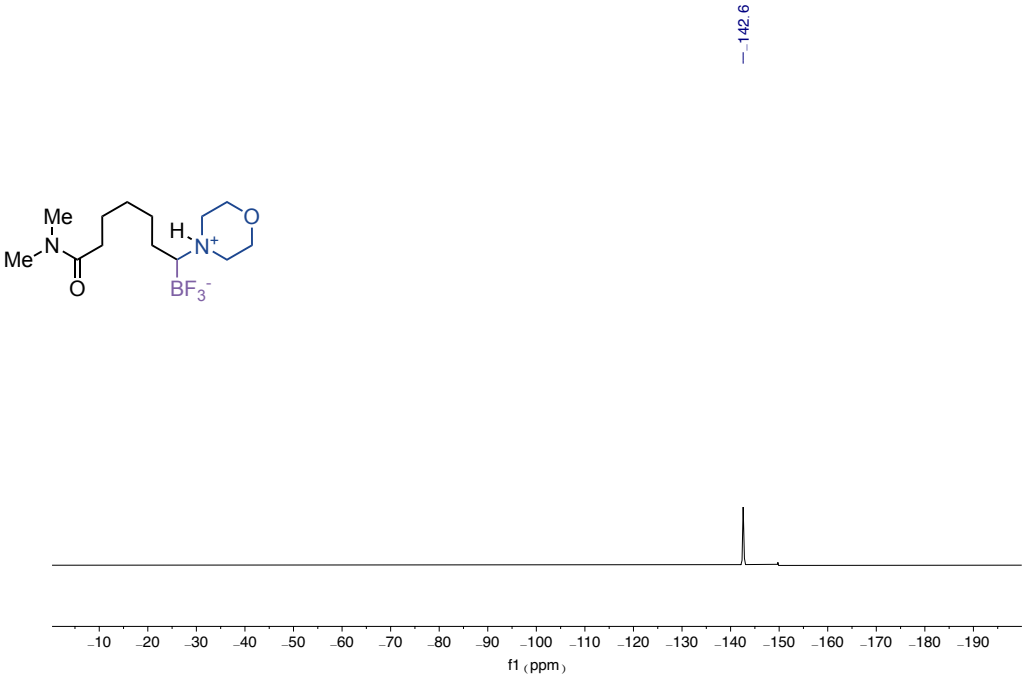

*^{19}F NMR spectra (376 MHz) of **4x***

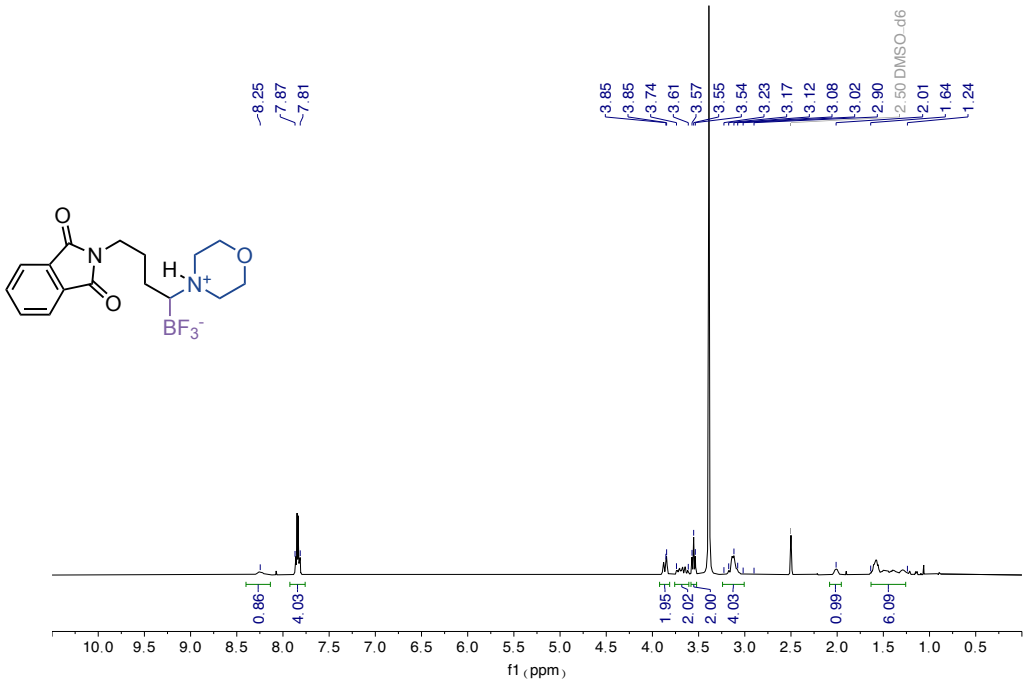

*^{1}H NMR spectra (400 MHz) of **4y***

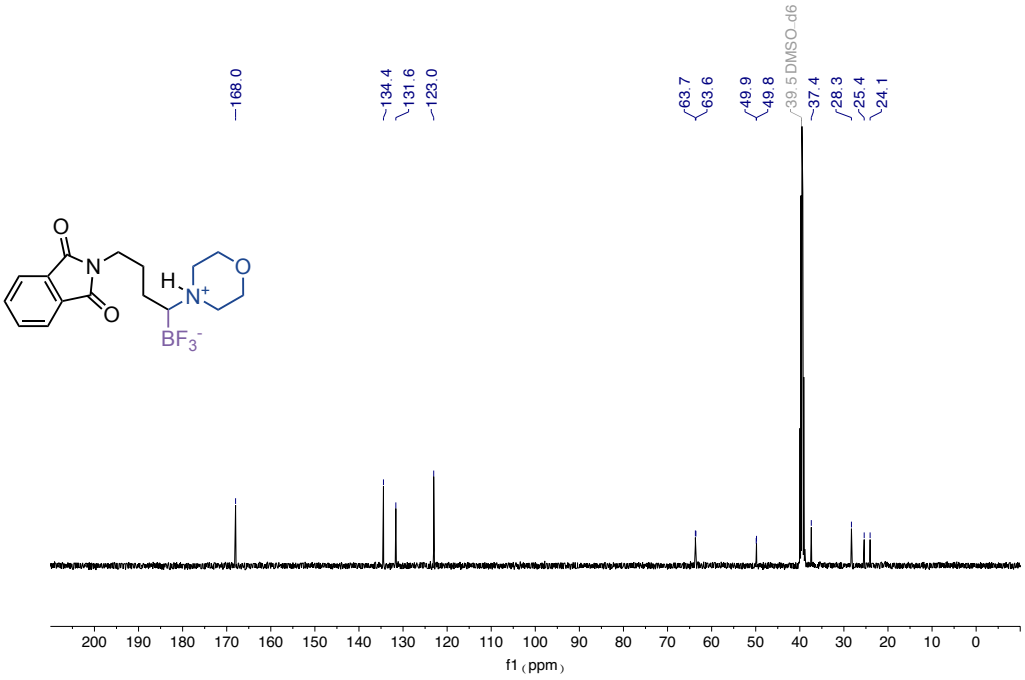

*^{13}C NMR spectra (101 MHz) of **4y***

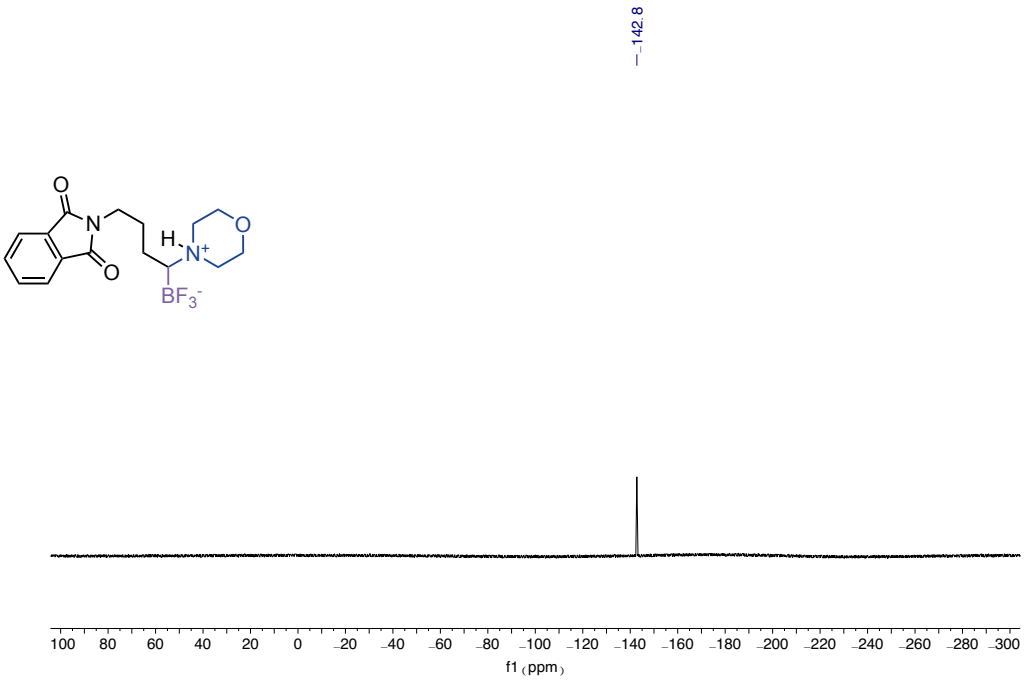

*^{19}F NMR spectra (376 MHz) of **4y***

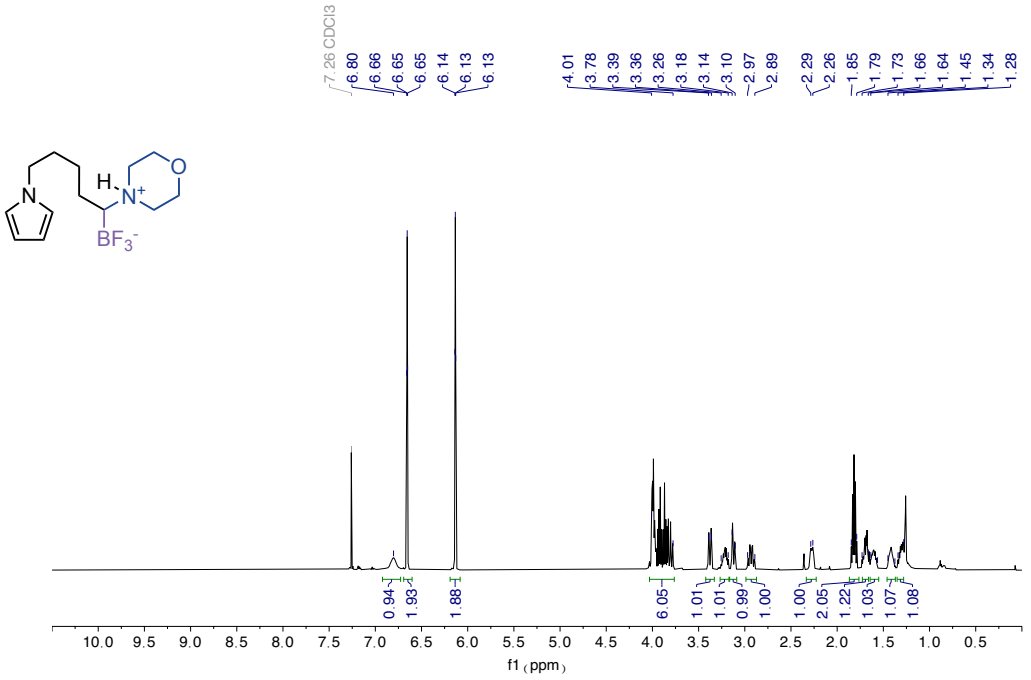

*[1]H NMR spectra (400 MHz) of **4z***

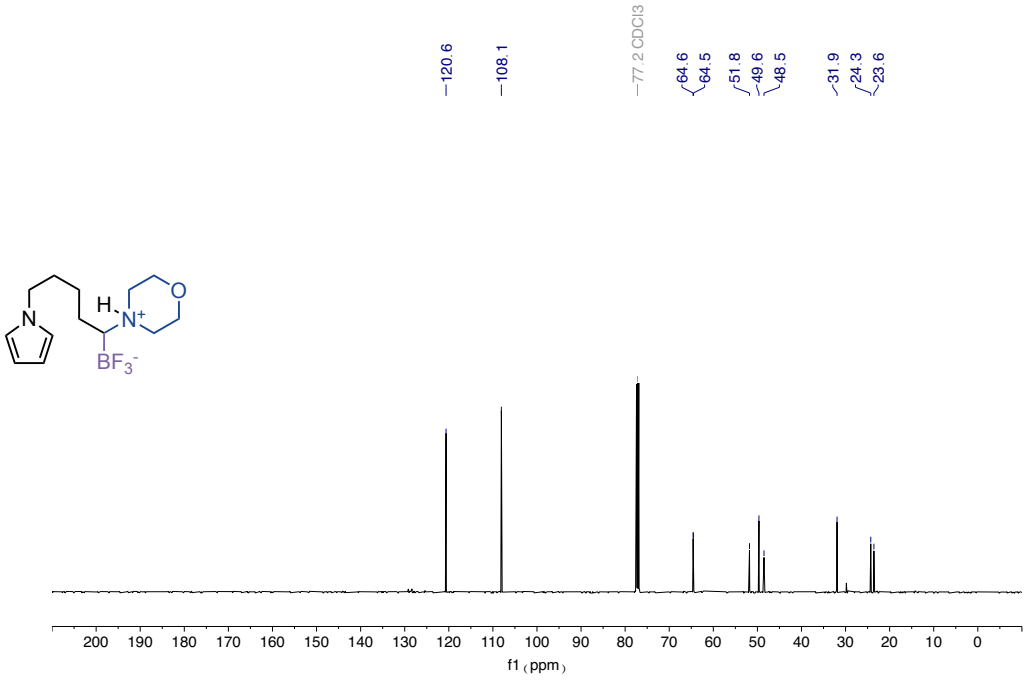

*[13]C NMR spectra (101 MHz) of **4z***

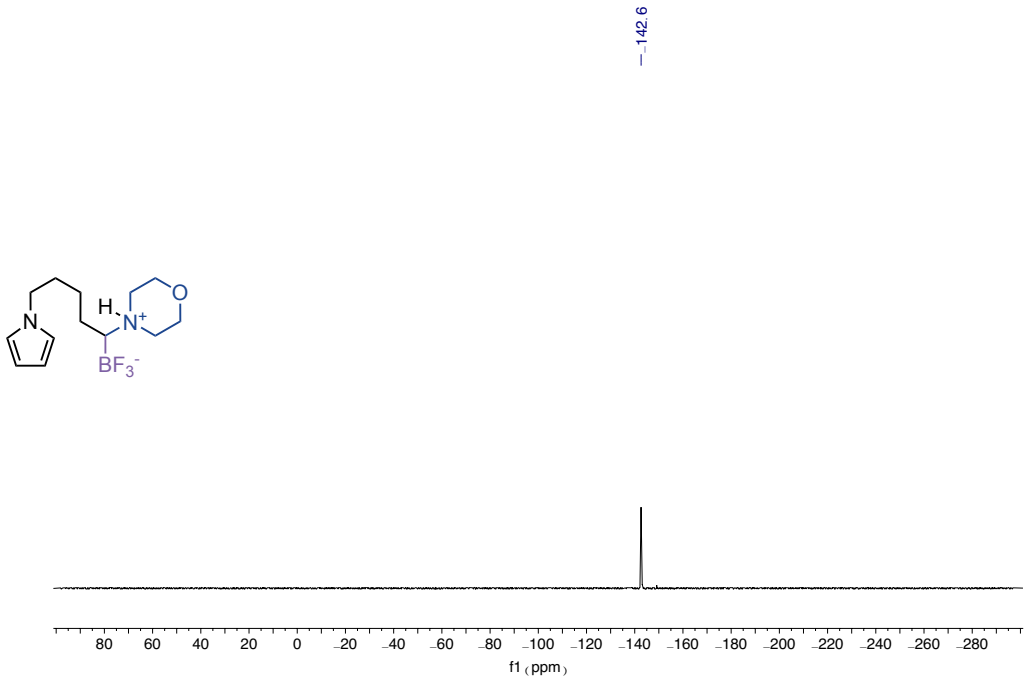

*^{19}F NMR spectra (376 MHz) of **4z***

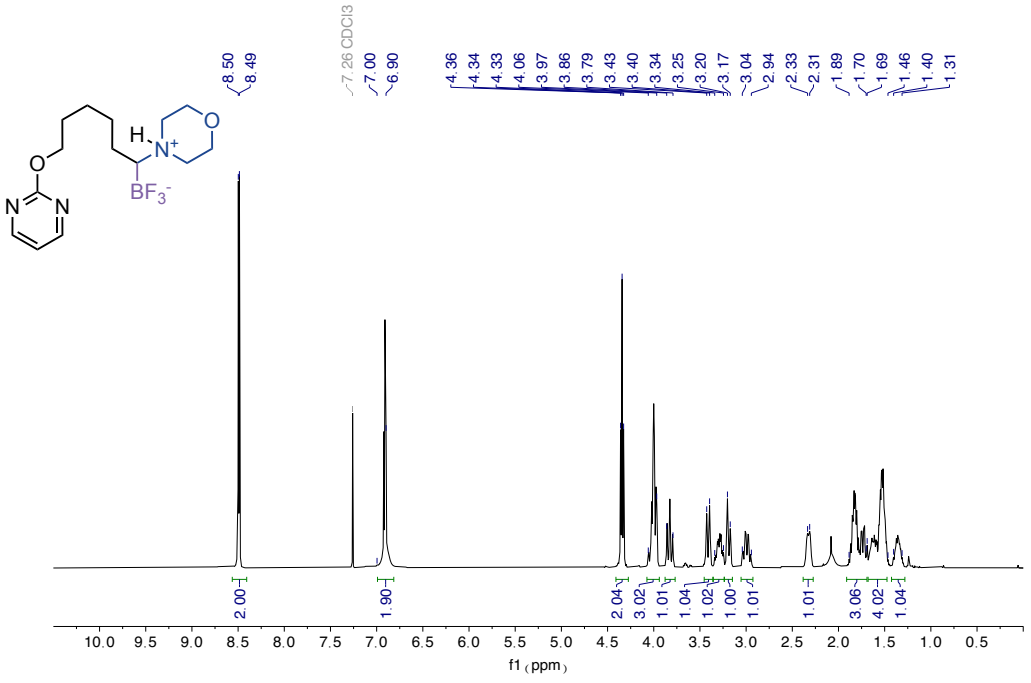

*^{1}H NMR spectra (400 MHz) of **4aa***

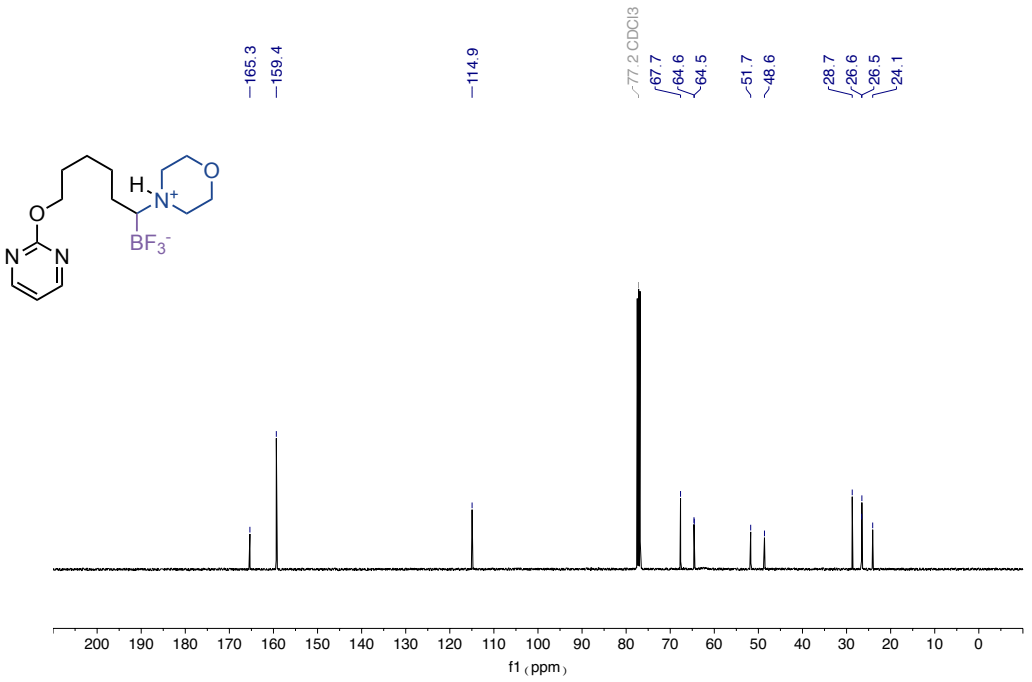

*^{13}C NMR spectra (101 MHz) of **4aa***

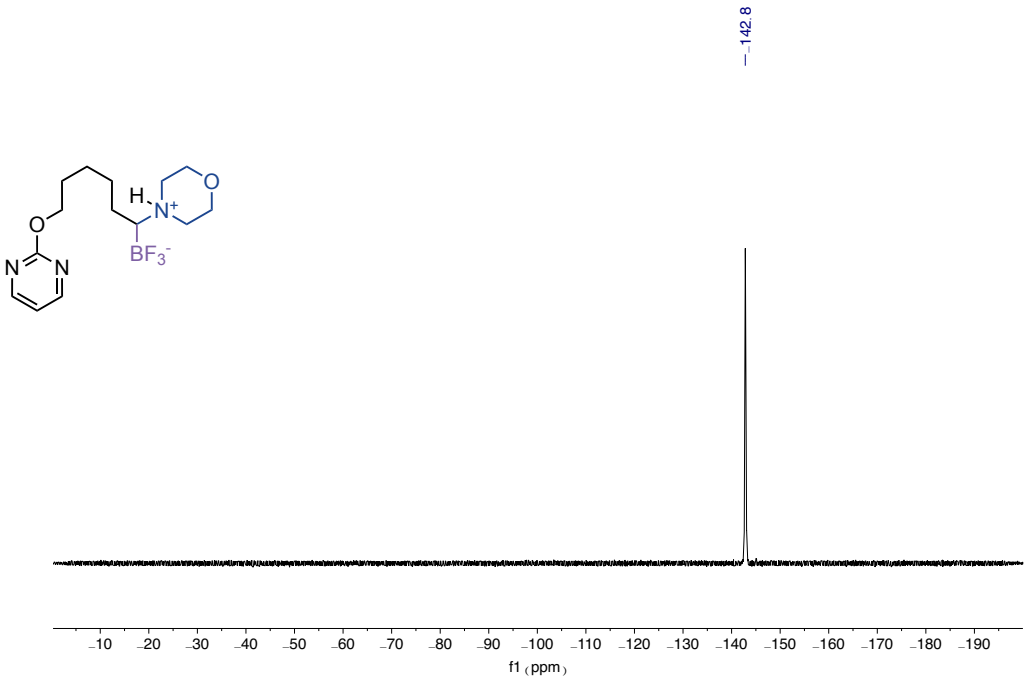

*^{19}F NMR spectra (376 MHz) of **4aa***

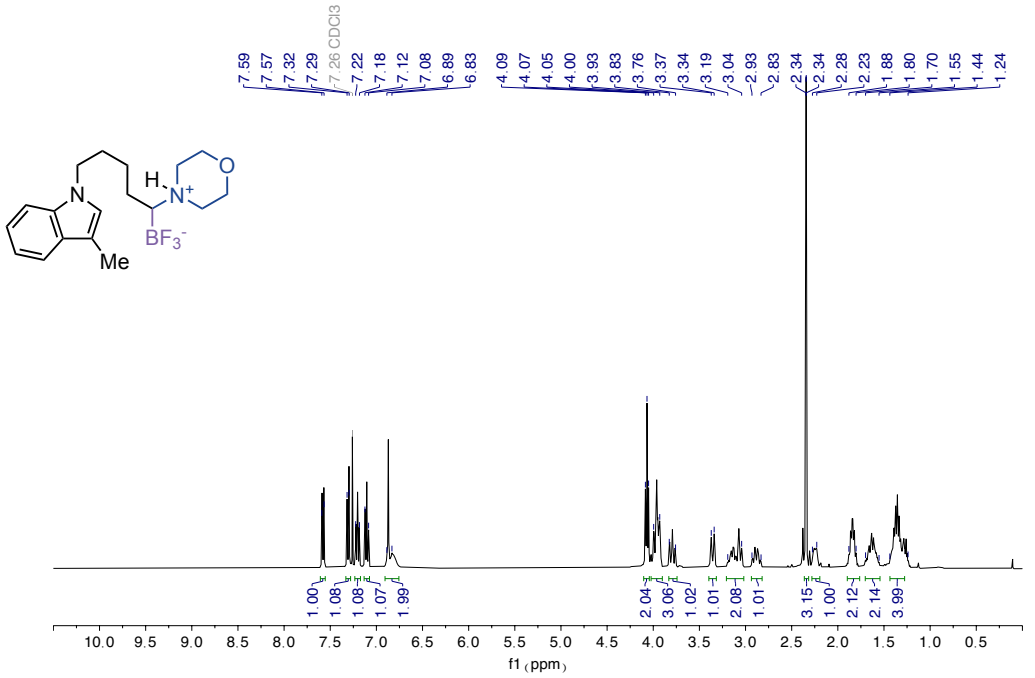

*[1]H NMR spectra (400 MHz) of **4ab***

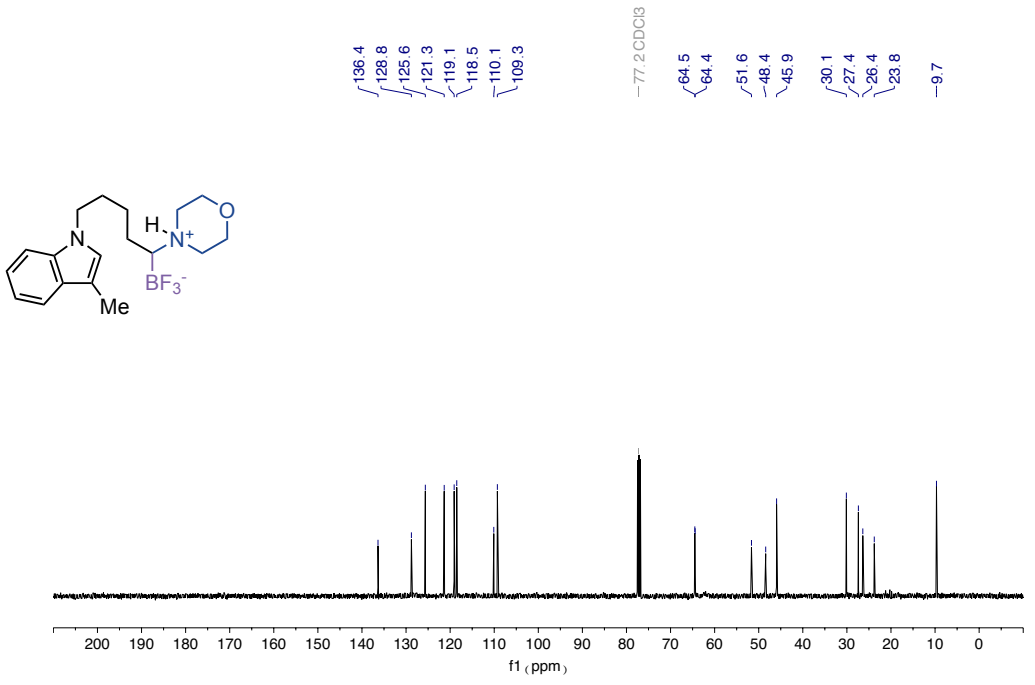

*[13]C NMR spectra (101 MHz) of **4ab***

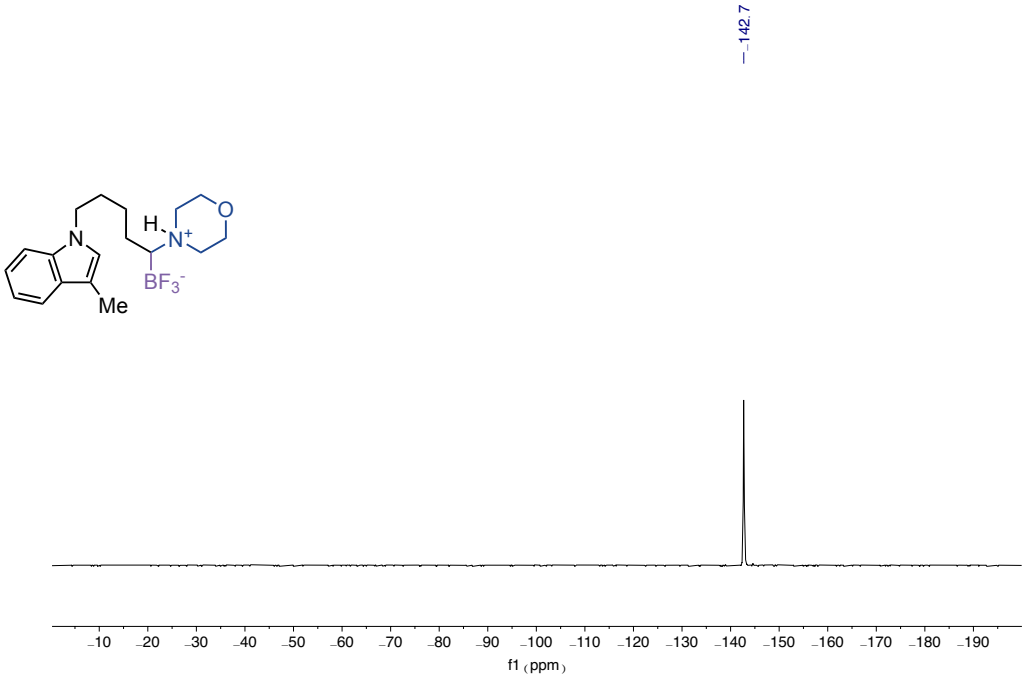

*^{19}F NMR spectra (376 MHz) of **4ab***

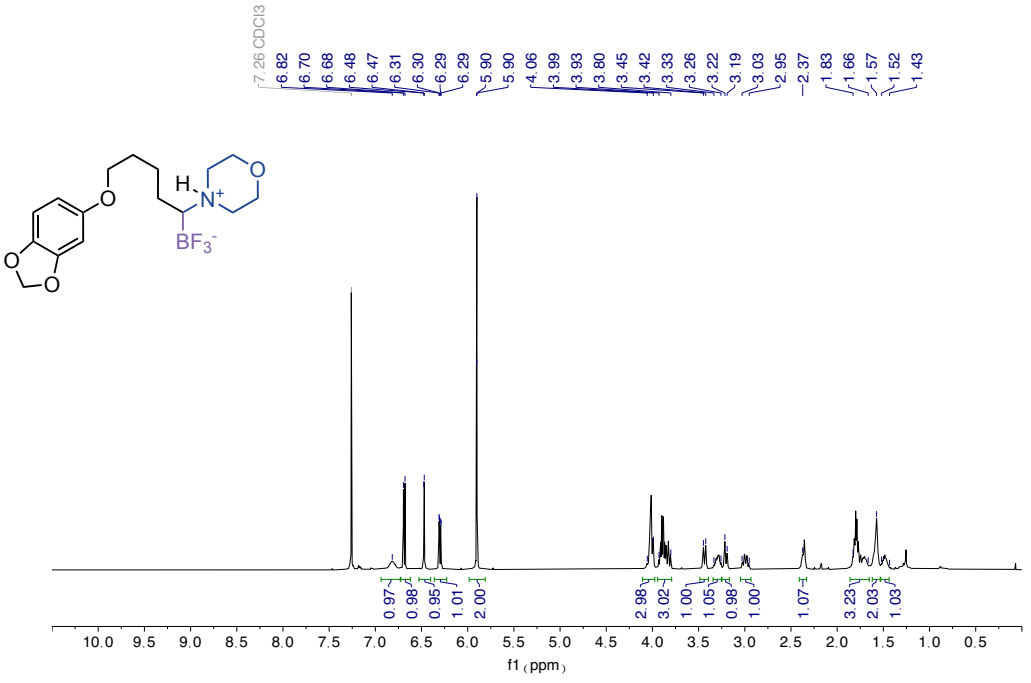

*^{1}H NMR spectra (400 MHz) of **4ac***

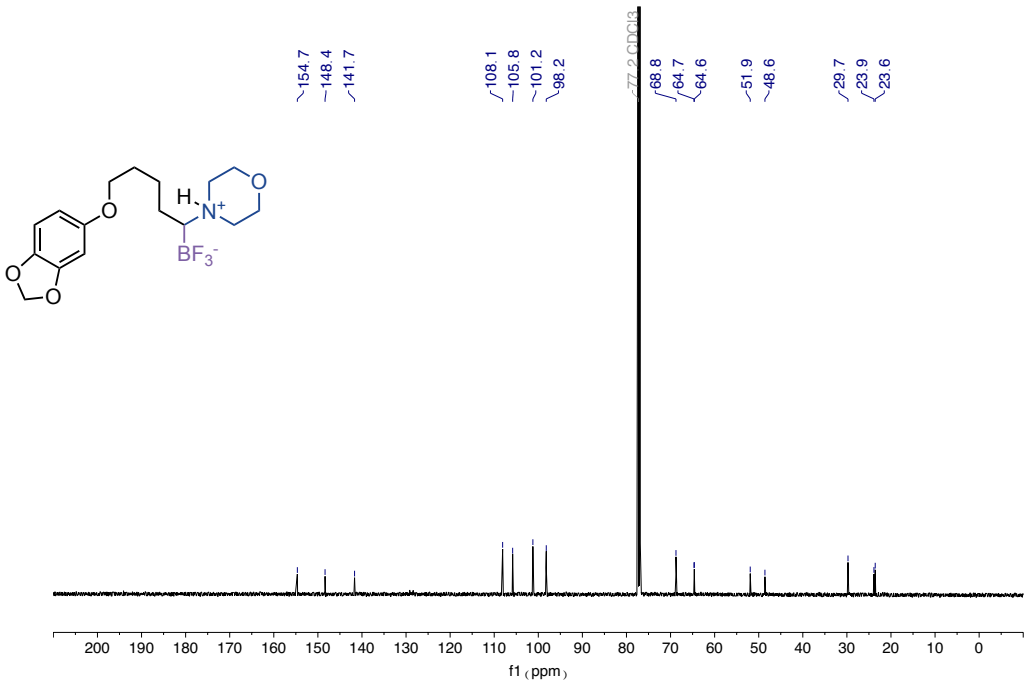

*^{13}C NMR spectra (101 MHz) of **4ac***

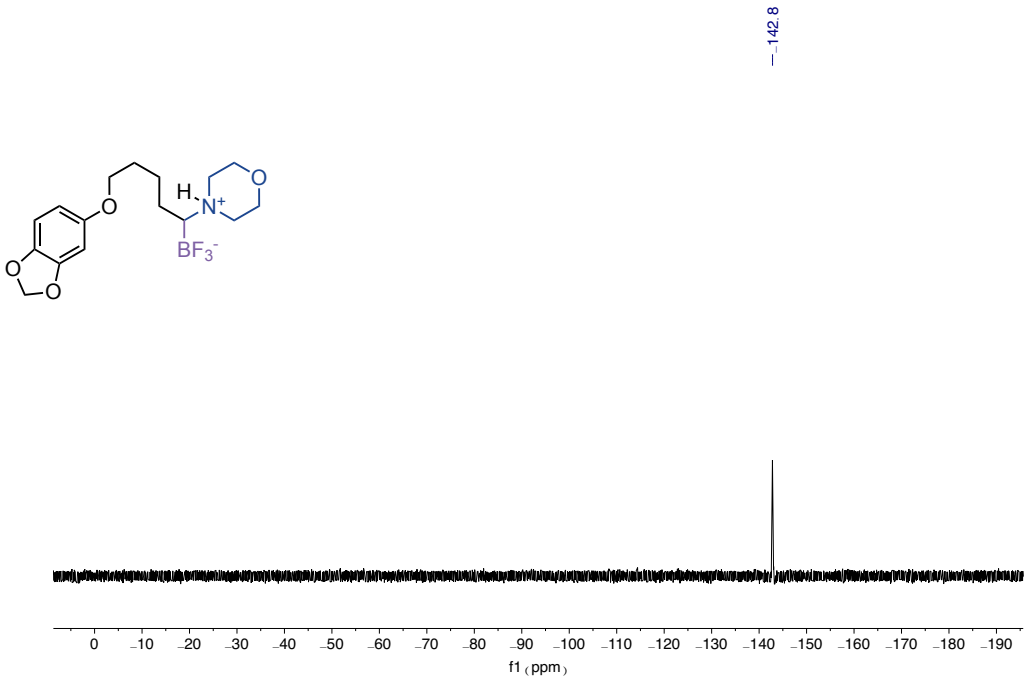

*^{19}F NMR spectra (376 MHz) of **4ac***

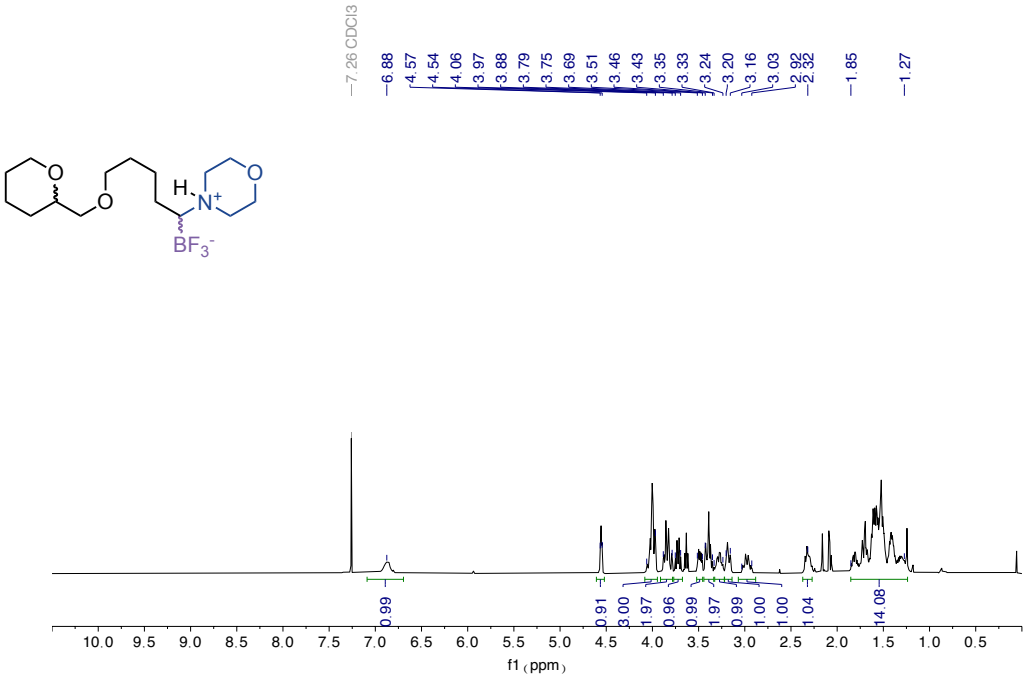

*^{1}H NMR spectra (400 MHz) of **4ad***

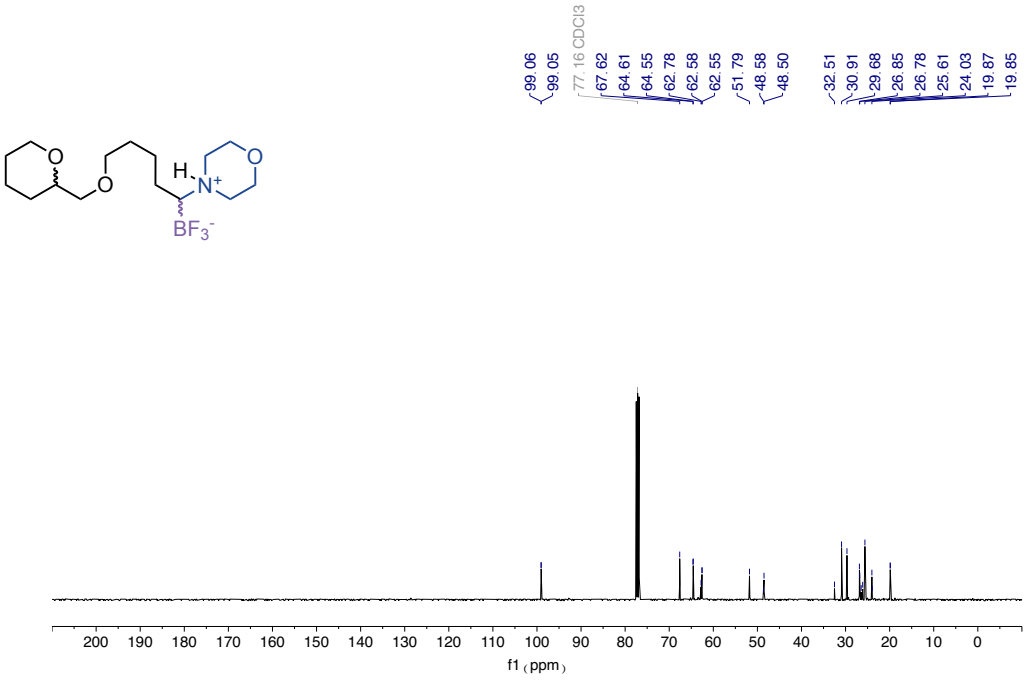

*^{13}C NMR spectra (101 MHz) of **4ad***

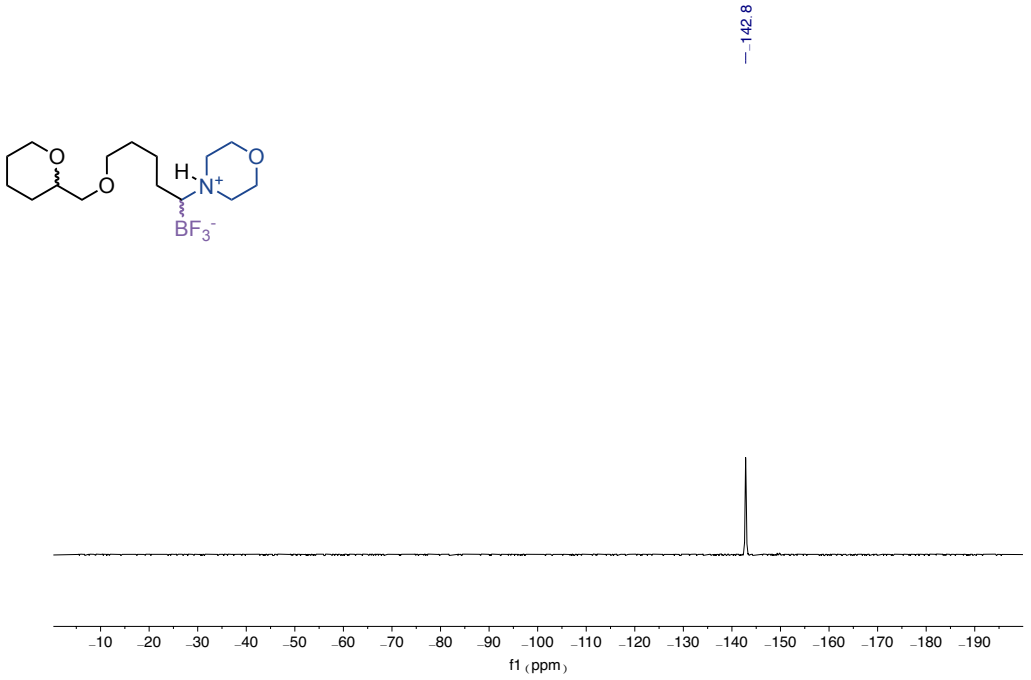

*^{19}F NMR spectra (376 MHz) of **4ad***

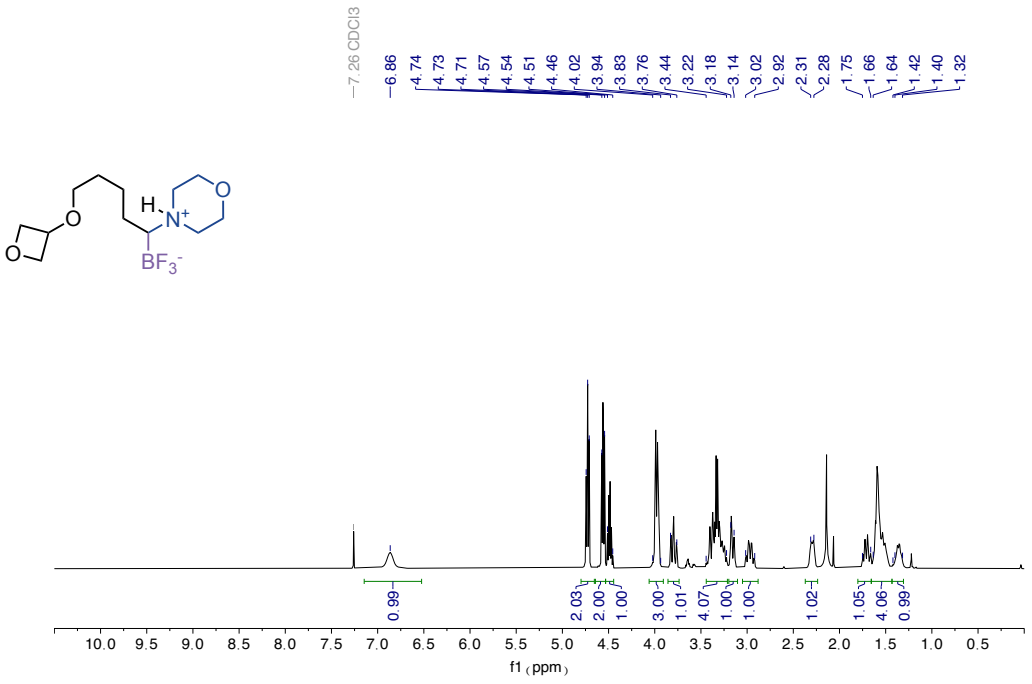

*^{1}H NMR spectra (400 MHz) of **4ae***

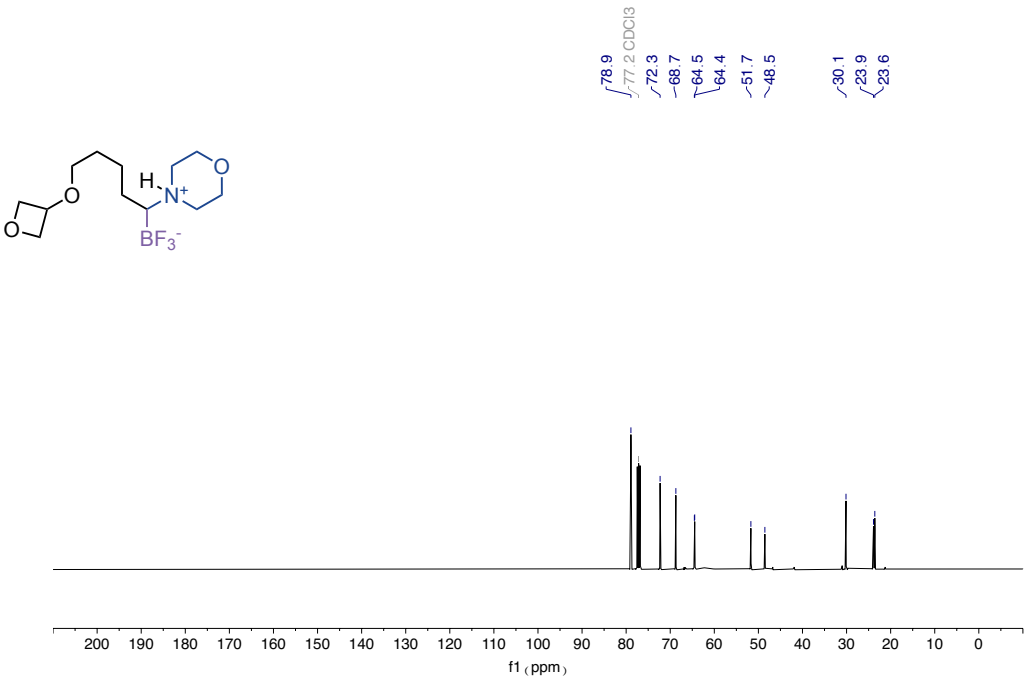

*^{13}C NMR spectra (101 MHz) of **4ae***

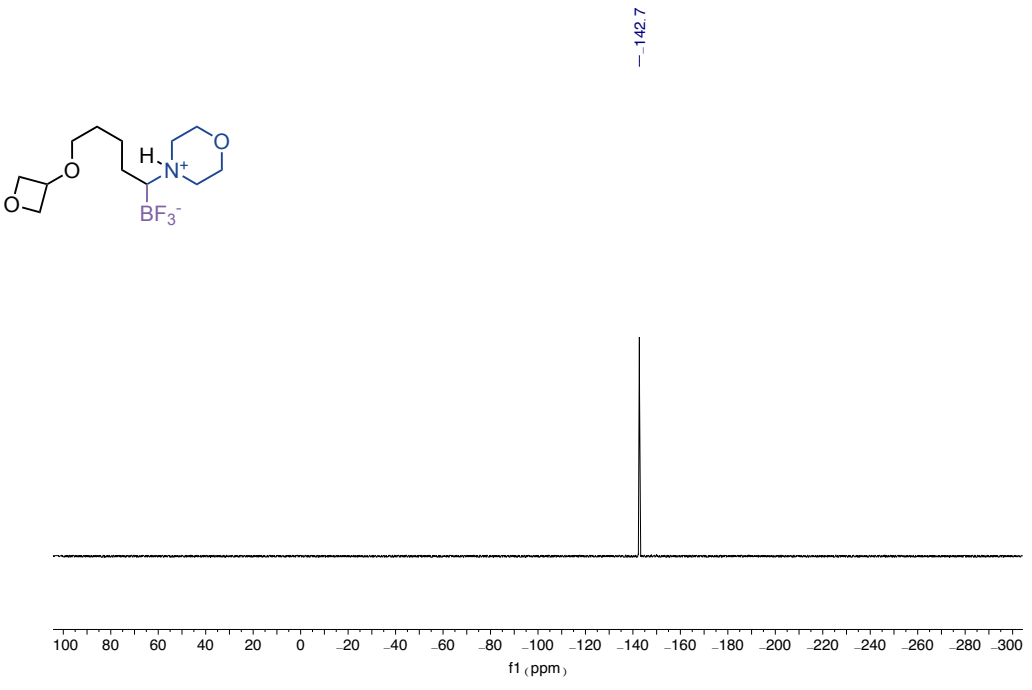

*^{19}F NMR spectra (376 MHz) of **4ae***

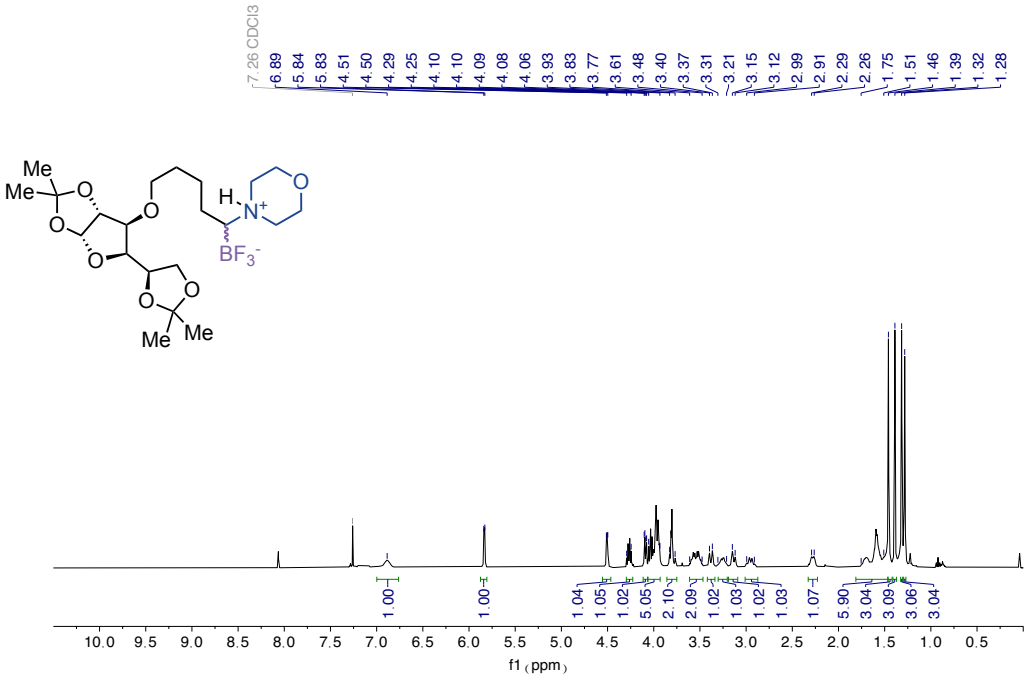

*[1]H NMR spectra (400 MHz) of **4af***

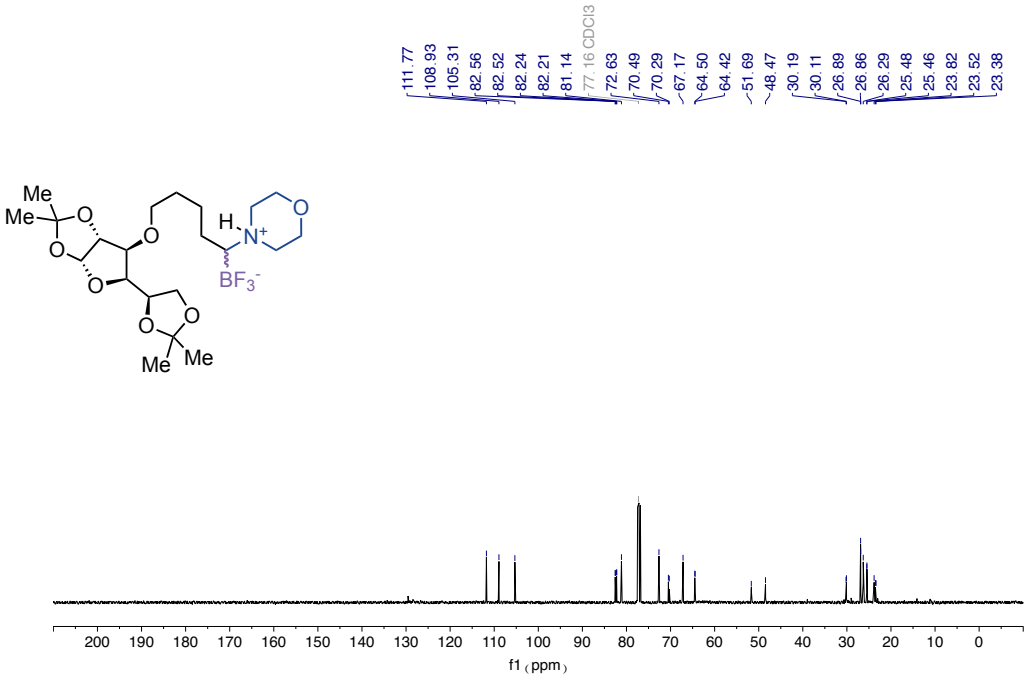

*[13]C NMR spectra (101 MHz) of **4af***

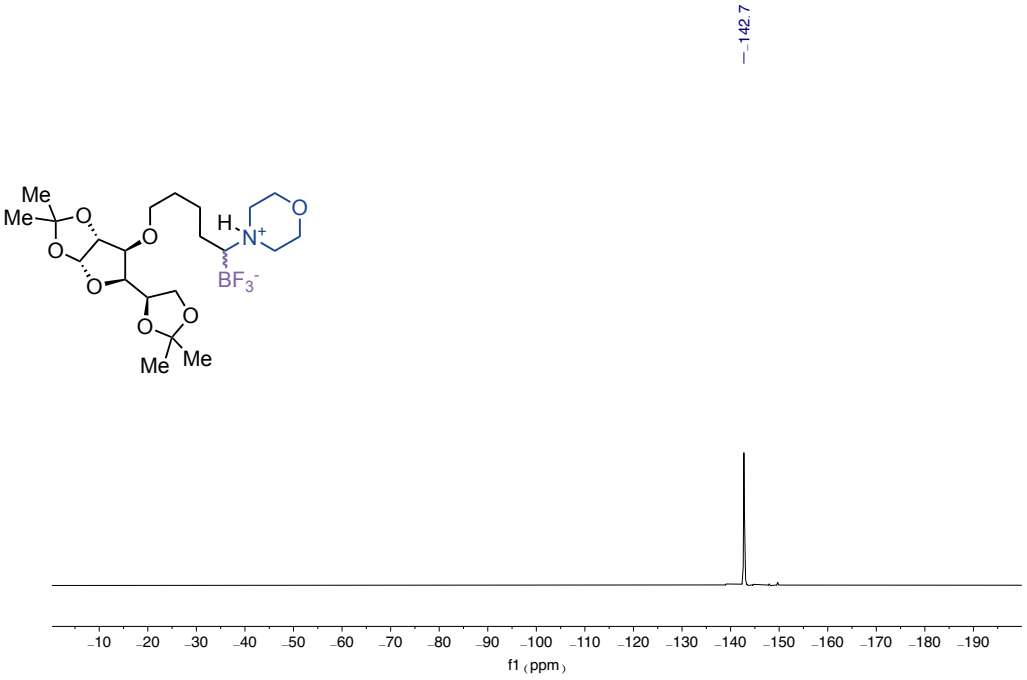

*^{19}F NMR spectra (376 MHz) of **4af***

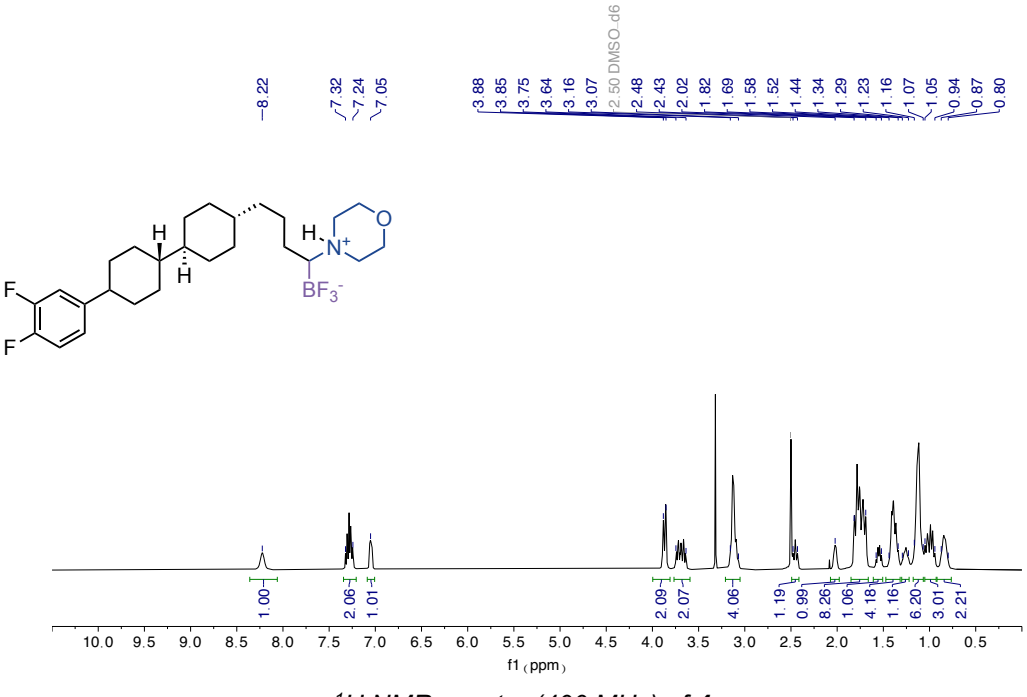

*^{1}H NMR spectra (400 MHz) of **4ag***

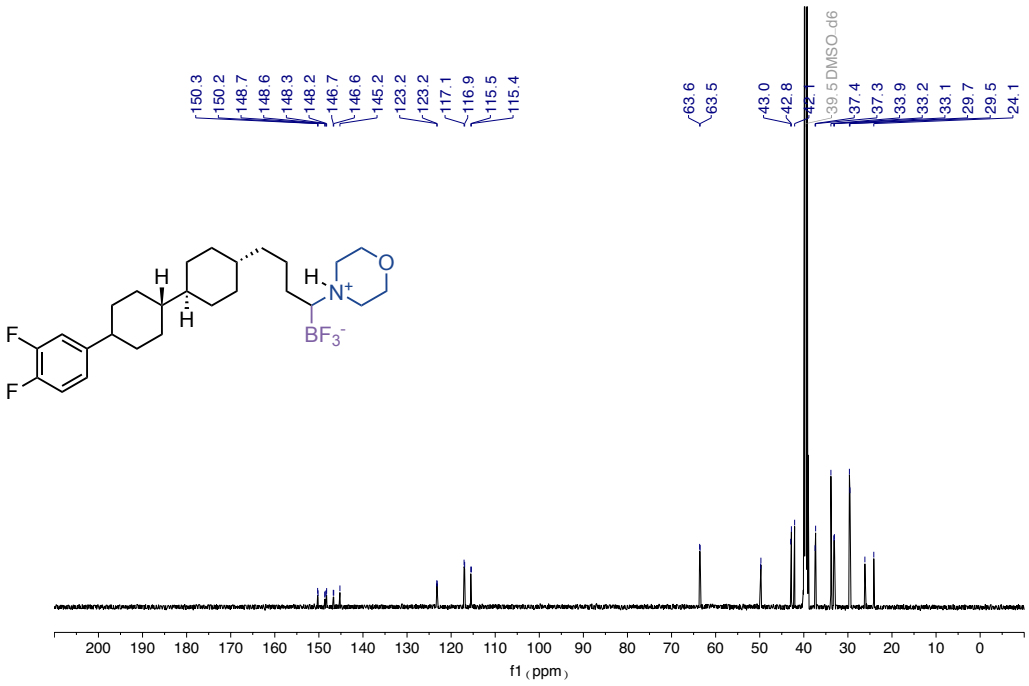

*^{13}C NMR spectra (101 MHz) of **4ag***

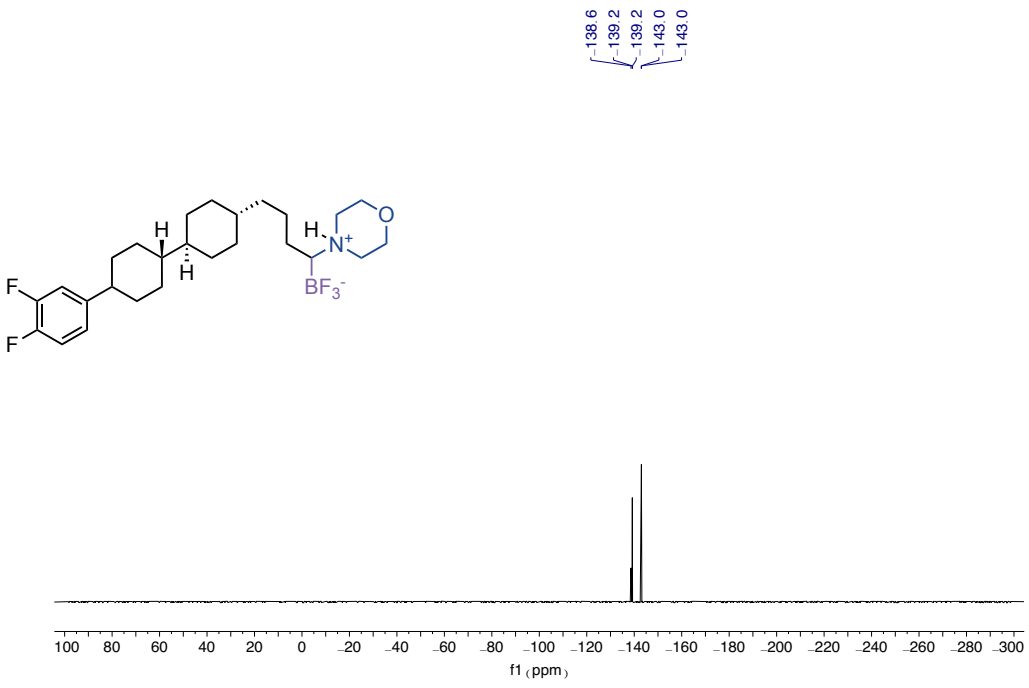

*^{19}F NMR spectra (376 MHz) of **4ag***

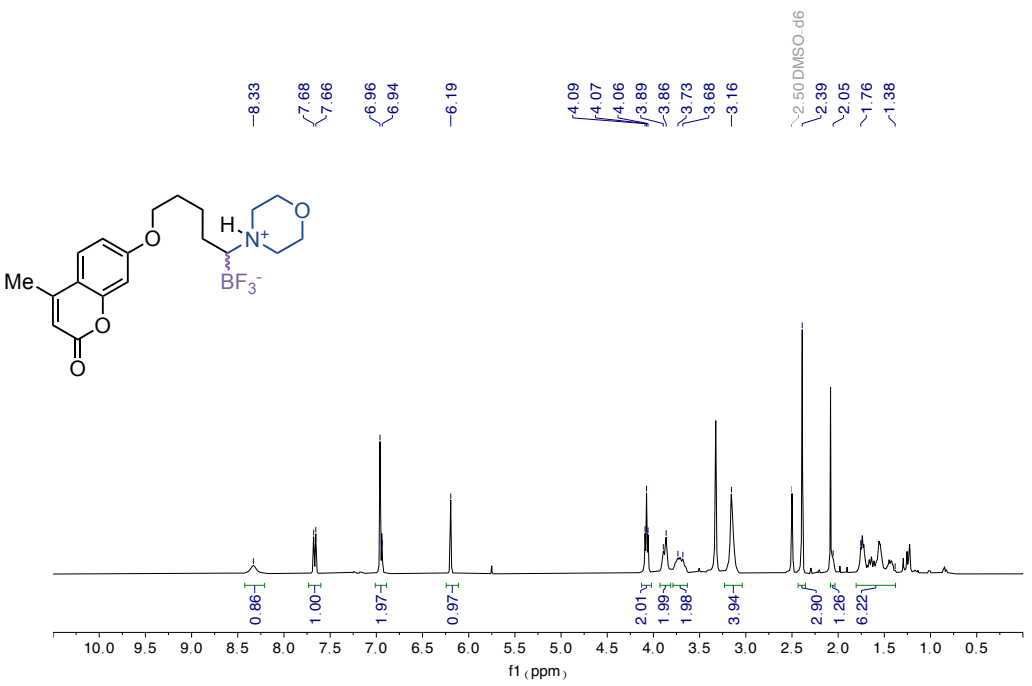

*[1]H NMR spectra (400 MHz) of **4ah***

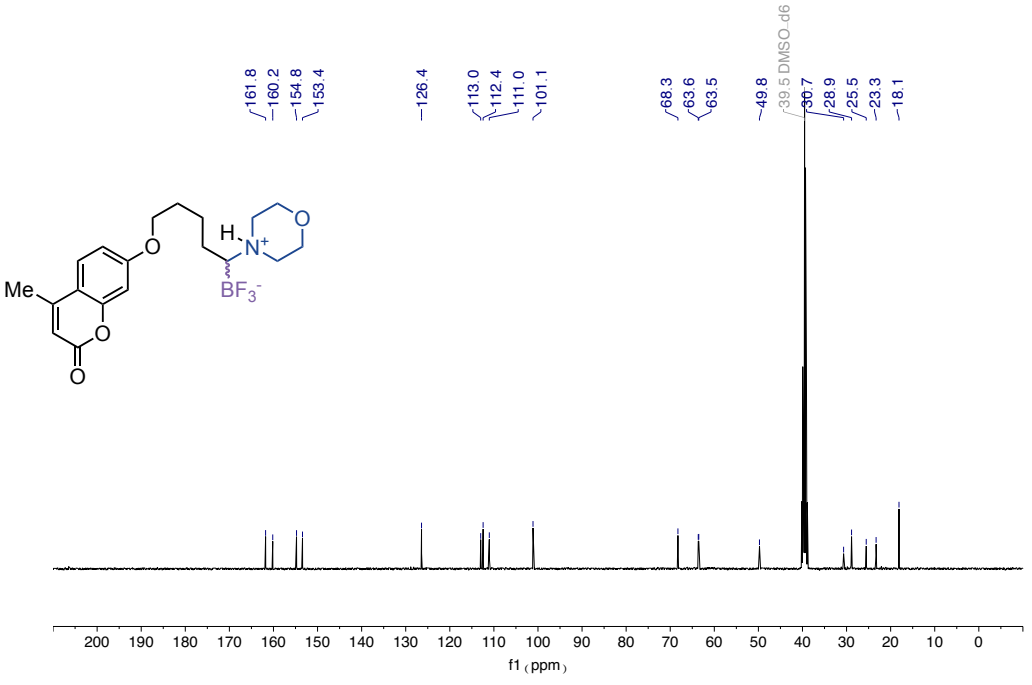

*[13]C NMR spectra (101 MHz) of **4ah***

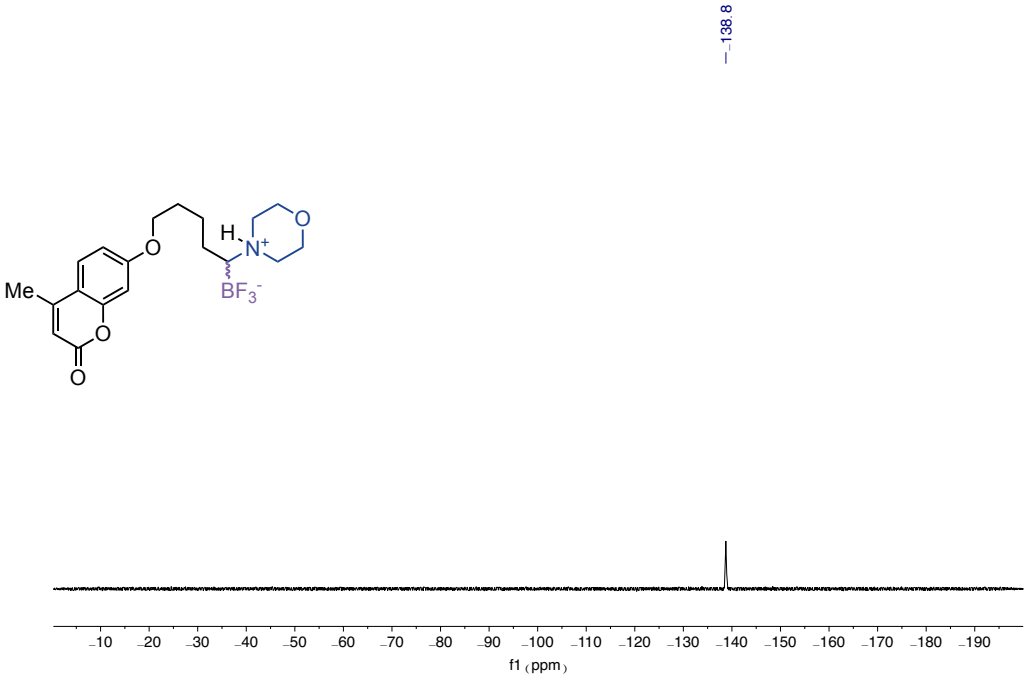

*^{19}F NMR spectra (376 MHz) of **4ah***

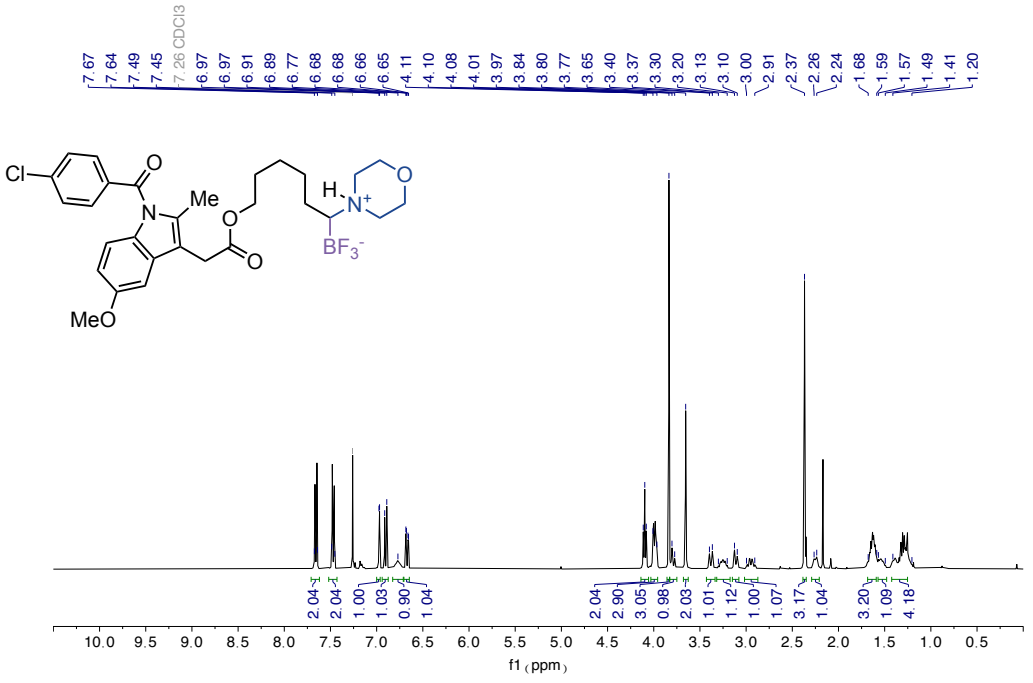

*^{1}H NMR spectra (400 MHz) of **4ai***

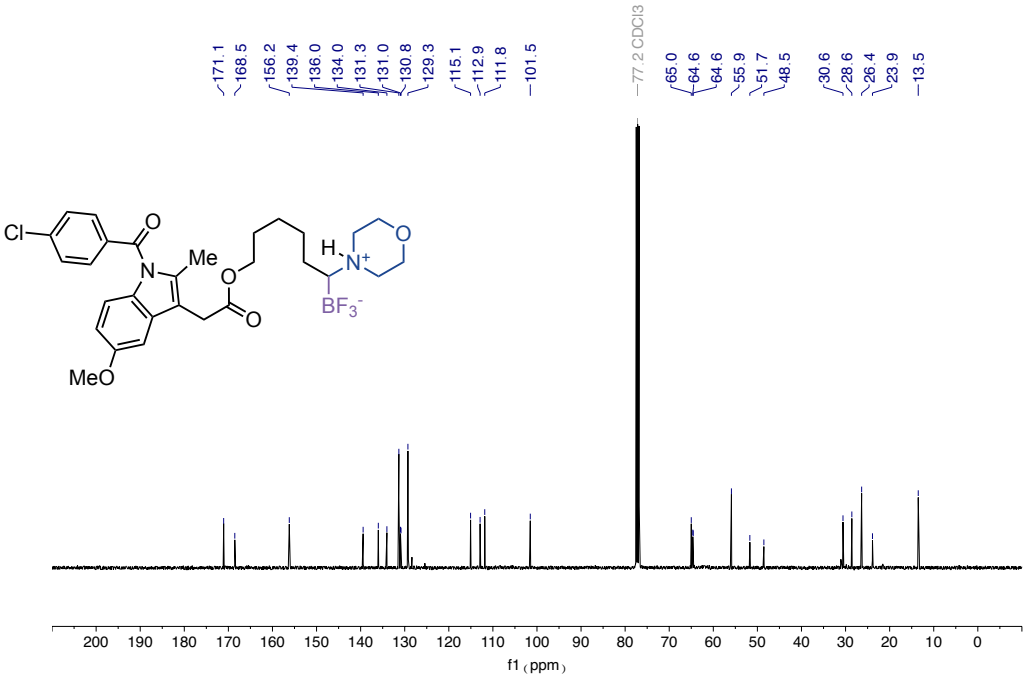

*^{13}C NMR spectra (101 MHz) of **4ai***

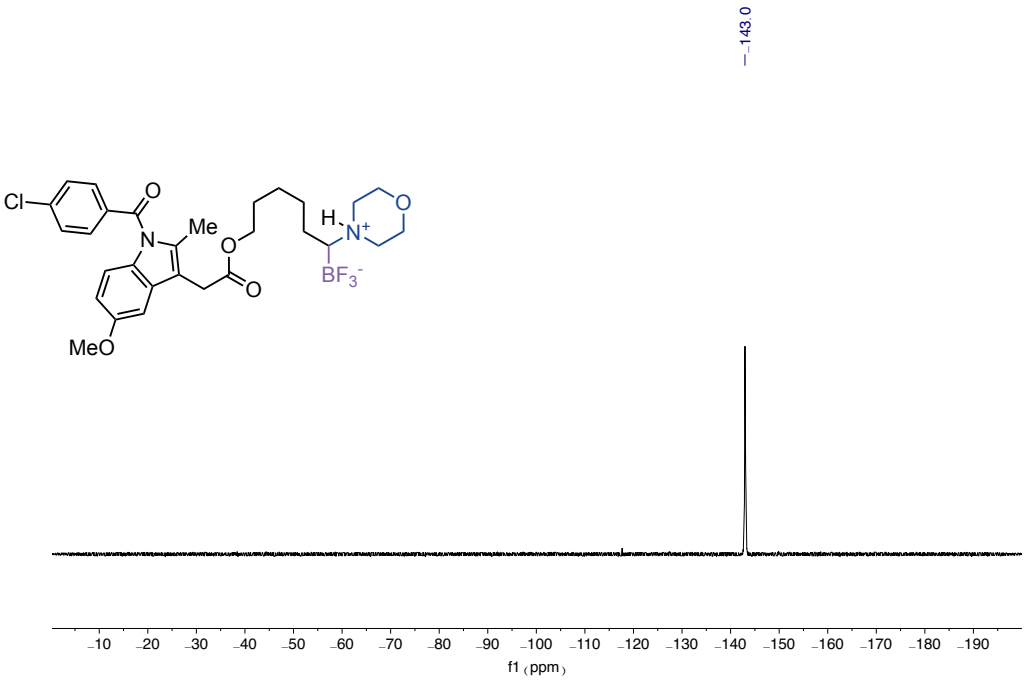

*^{19}F NMR spectra (376 MHz) of **4ai***

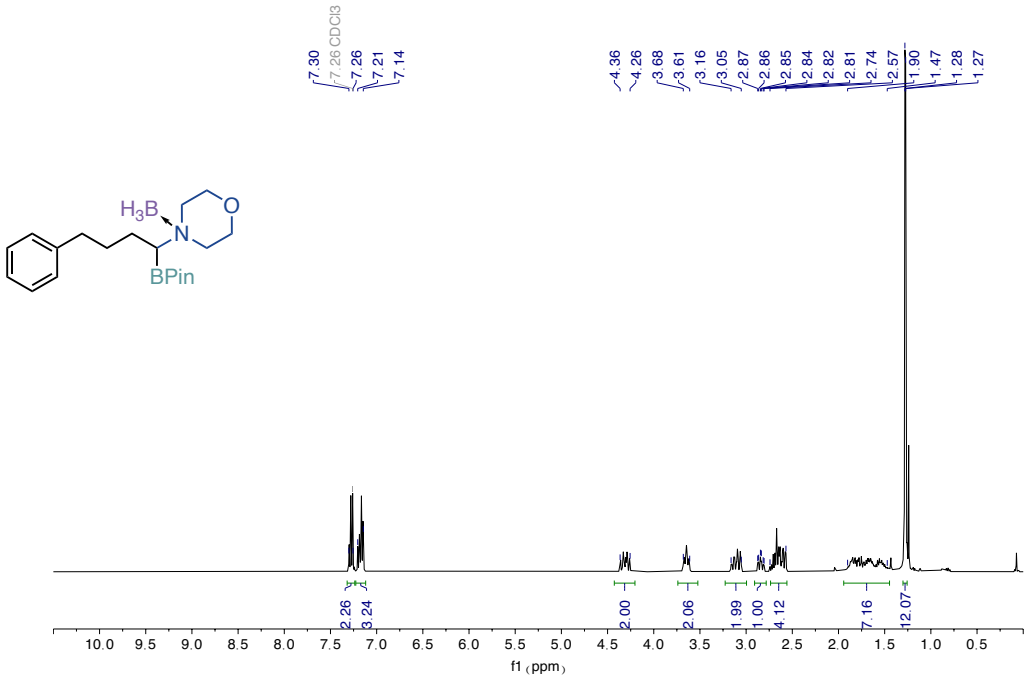

*^{1}H NMR spectra (400 MHz) of **5a***

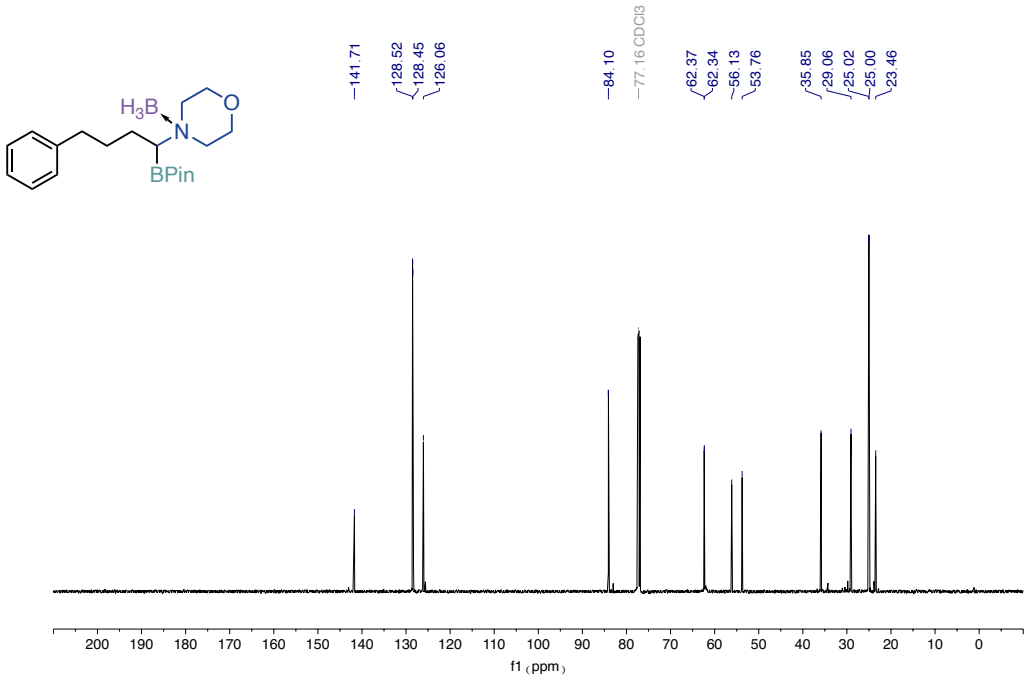

*^{13}C NMR spectra (101 MHz) of **5a***

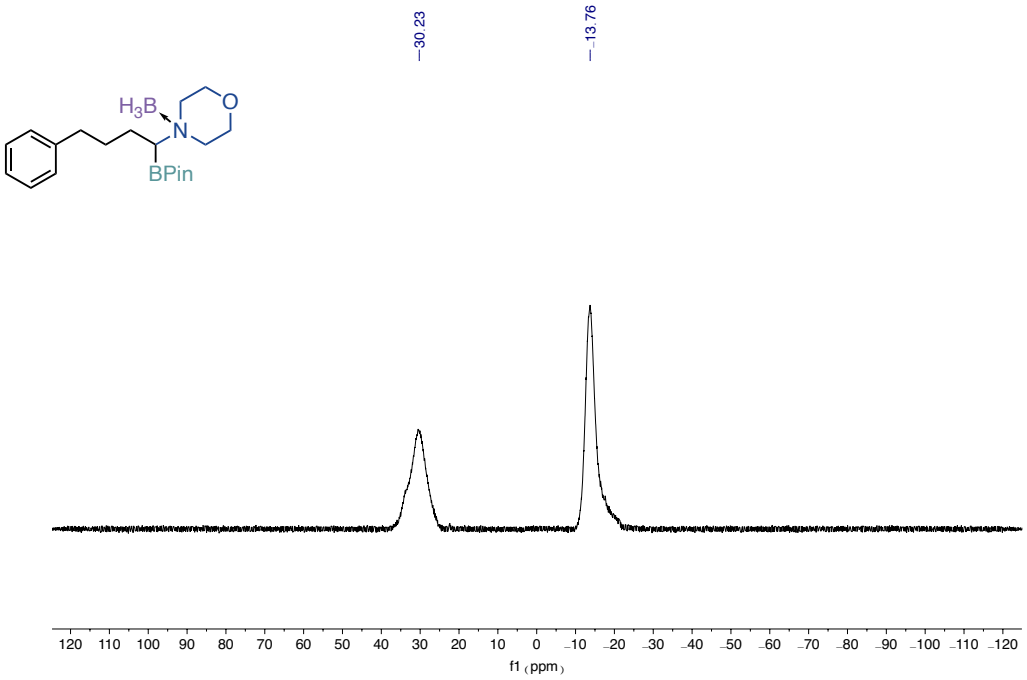

*^{11}B NMR spectra (xx MHz) of **5a***

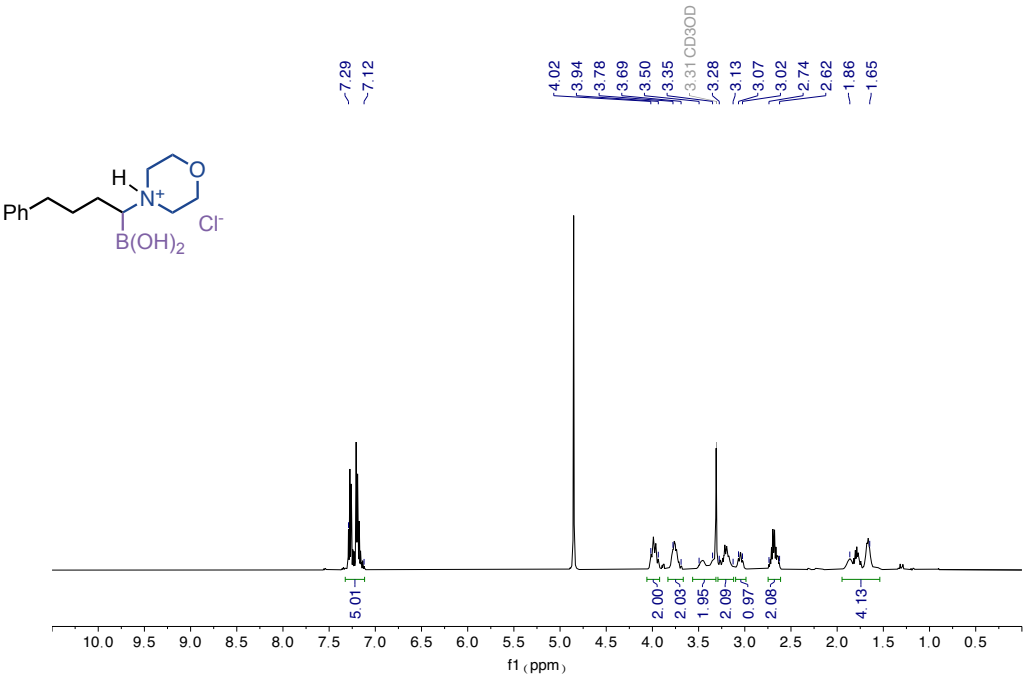

*^{1}H NMR spectra (400 MHz) of **6a***

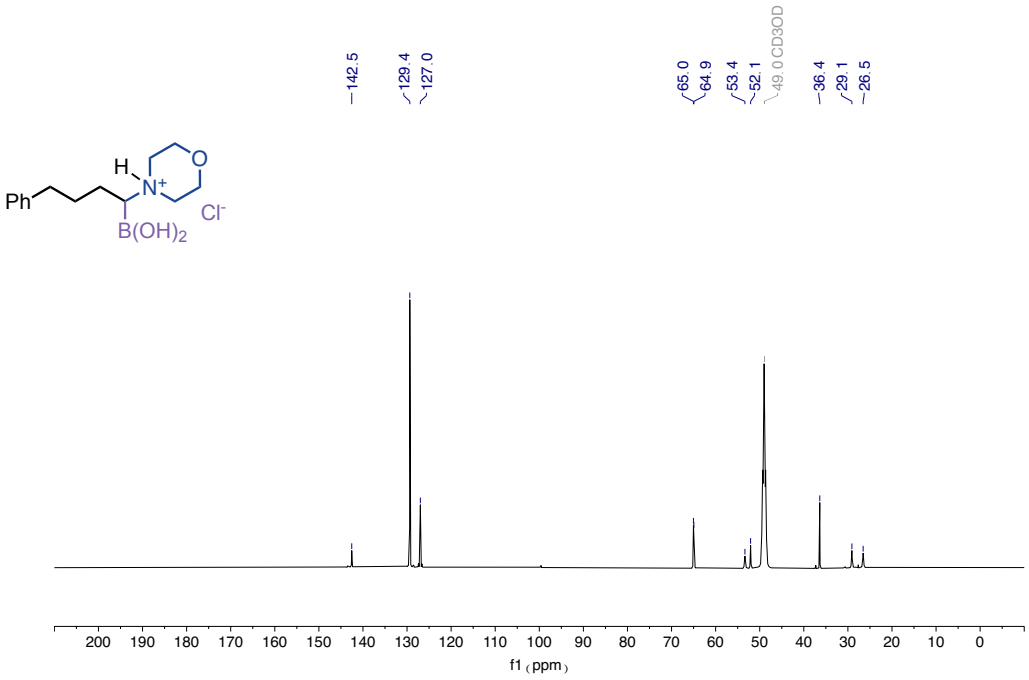

*^{13}C NMR spectra (101 MHz) of **6a***

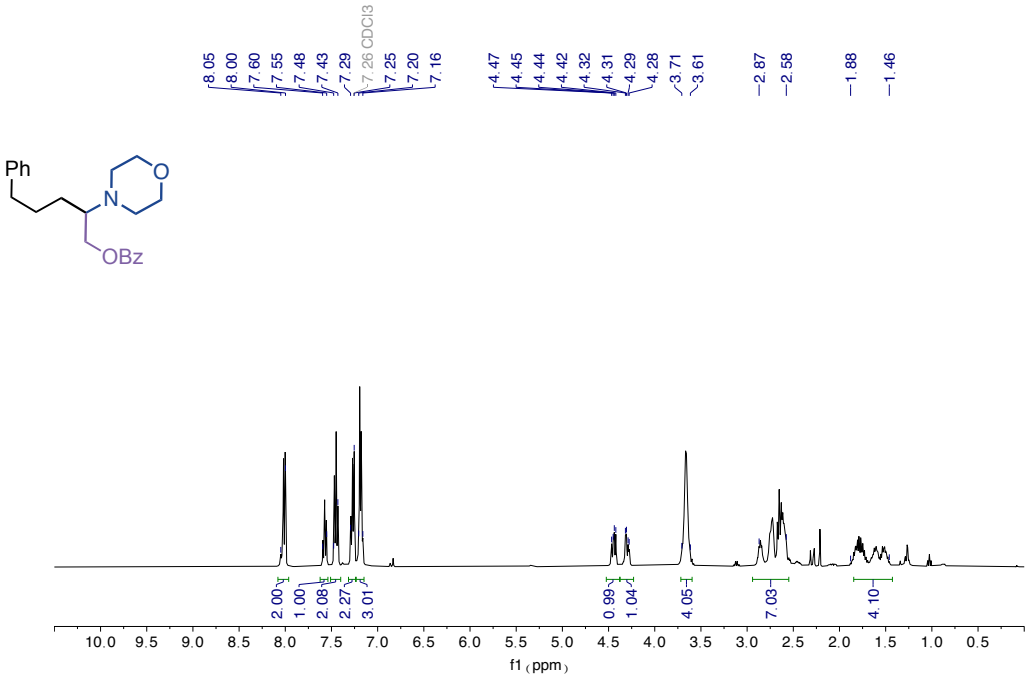

*^{1}H NMR spectra (400 MHz) of **7a***

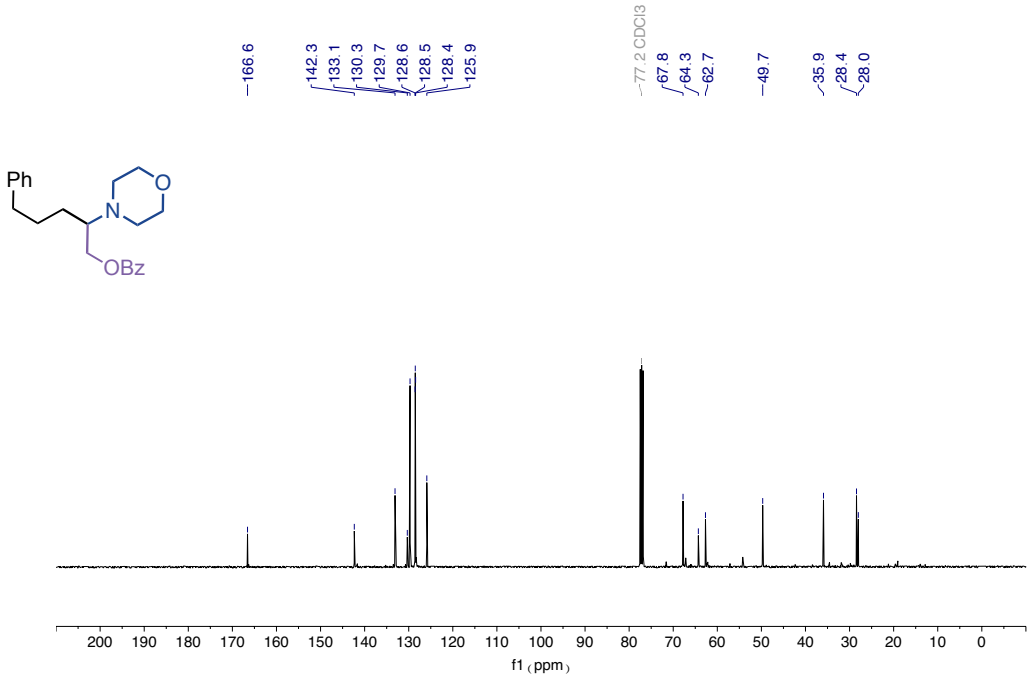

*^{13}C NMR spectra (101 MHz) of **7a***

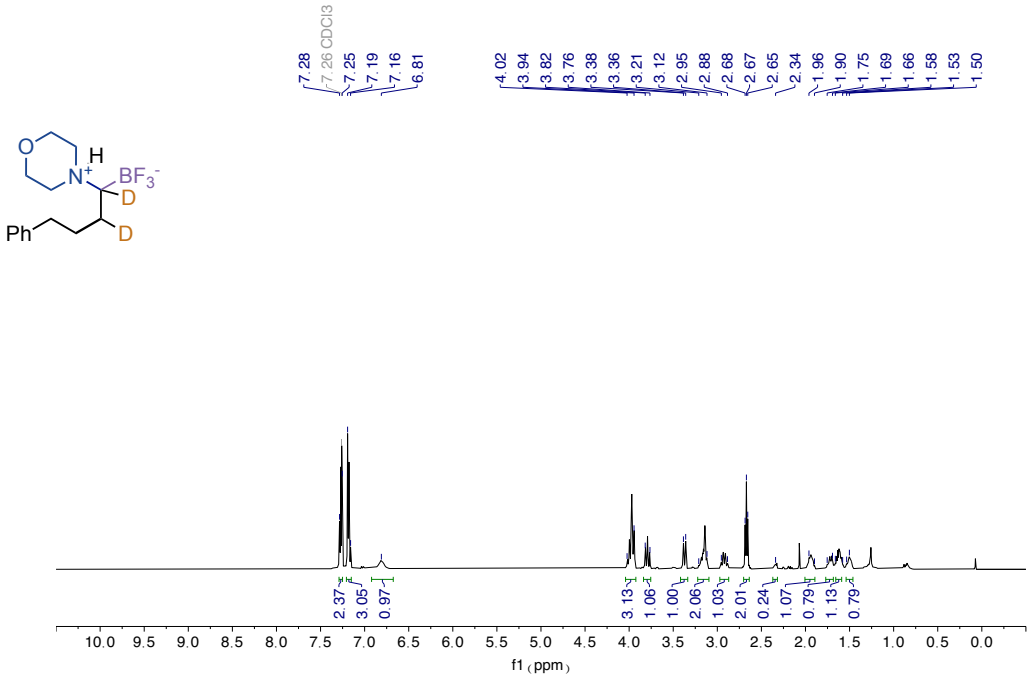

*^{1}H NMR spectra (500 MHz) of **11***

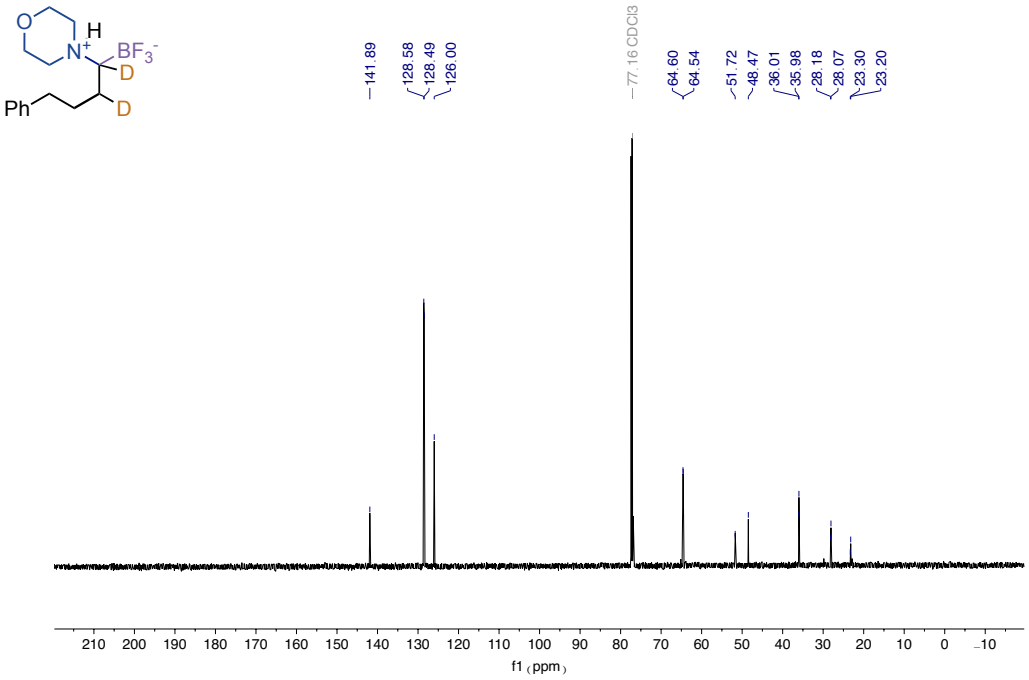

*^{13}C NMR spectra (126 MHz) of **11***

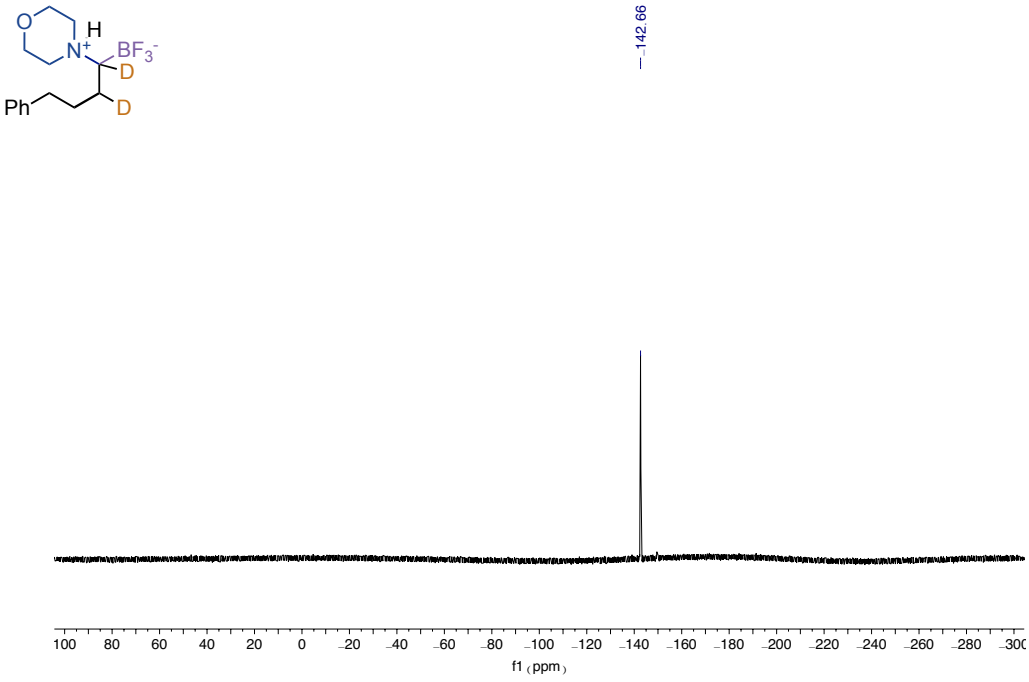

*^{19}F NMR spectra (376 MHz) of **11***

4.6. References

(1) Hosmane, N. S.; Eagling, R. *Handbook of Boron Science: With Applications in Organometallics, Catalysis, Materials and MedicineVolume 4: Boron in Medicine*; WORLD SCIENTIFIC (EUROPE), 2018; Vol. 4. https://doi.org/10.1142/q0130-vol4.

(2) Adams, J.; Kauffman, M. Development of the Proteasome Inhibitor Velcade™ (Bortezomib). *Cancer Invest.* **2004**, *22* (2), 304–311. https://doi.org/10.1081/CNV-120030218.

(3) Hecker, S. J.; Reddy, K. R.; Totrov, M.; Hirst, G. C.; Lomovskaya, O.; Griffith, D. C.; King, P.; Tsivkovski, R.; Sun, D.; Sabet, M.; Tarazi, Z.; Clifton, M. C.; Atkins, K.; Raymond, A.; Potts, K. T.; Abendroth, J.; Boyer, S. H.; Loutit, J. S.; Morgan, E. E.; Durso, S.; Dudley, M. N. Discovery of a Cyclic Boronic Acid β-Lactamase Inhibitor (RPX7009) with Utility vs Class A Serine Carbapenemases. *J. Med. Chem.* **2015**, *58* (9), 3682–3692. https://doi.org/10.1021/acs.jmedchem.5b00127.

(4) Miller, Z.; Ao, L.; Kim, K. B.; Lee, W. Inhibitors of the Immunoproteasome: Current Status and Future Directions. *Curr. Pharm. Des.* **2013**, *19* (22), 4140–4151.

(5) Zhang, W.; Bai, H.; Han, L.; Zhang, H.; Xu, B.; Cui, J.; Wang, X.; Ge, Z.; Li, R. Synthesis and Biological Evaluation of Curcumin Derivatives Modified with α-Amino Boronic Acid as Proteasome Inhibitors. *Bioorg. Med. Chem. Lett.* **2018**, *28* (14), 2459–2464. https://doi.org/10.1016/j.bmcl.2018.06.004.

(6) Chatterjee, S.; Tripathi, N. M.; Bandyopadhyay, A. The Modern Role of Boron as a 'Magic Element' in Biomedical Science: Chemistry Perspective. *Chem. Commun.* **2021**, *57* (100), 13629–13640. https://doi.org/10.1039/D1CC05481C.

(7) Das, B. C.; Nandwana, N. K.; Das, S.; Nandwana, V.; Shareef, M. A.; Das, Y.; Saito, M.; Weiss, L. M.; Almaguel, F.; Hosmane, N. S.; Evans, T. Boron Chemicals in Drug Discovery and Development: Synthesis and Medicinal Perspective. *Molecules* **2022**, *27* (9), 2615. https://doi.org/10.3390/molecules27092615.

(8) Messner, K.; Vuong, B.; Tranmer, G. K. The Boron Advantage: The Evolution and Diversification of Boron's Applications in Medicinal Chemistry. *Pharmaceuticals* **2022**, *15* (3), 264. https://doi.org/10.3390/ph15030264.

(9) Ingram, A.; Moore, B. D.; Graham, D. Simultaneous Detection of Alkaline Phosphatase and β-Galactosidase Activity Using SERRS. *Bioorg. Med. Chem. Lett.* **2009**, *19* (6), 1569–1571. https://doi.org/10.1016/j.bmcl.2009.02.030.

(10) Jin, S.; Zhu, C.; Cheng, Y.; Li, M.; Wang, B. Synthesis and Carbohydrate Binding Studies of Fluorescent α-Amidoboronic Acids and the Corresponding Bisboronic Acids. *Bioorg. Med. Chem.* **2010**, *18* (4), 1449–1455. https://doi.org/10.1016/j.bmc.2010.01.017.

(11) Inglis, S. R.; Strieker, M.; Rydzik, A. M.; Dessen, A.; Schofield, C. J. A Boronic-Acid-Based Probe for Fluorescence Polarization Assays with Penicillin Binding Proteins and β-Lactamases. *Anal. Biochem.* **2012**, *420* (1), 41–47. https://doi.org/10.1016/j.ab.2011.08.036.

(12) Dembitsky, V. M.; Srebnik, M. Chemistry of A-Aminoboronic Acids and Their Derivatives. In *Amino Acids, Peptides and Proteins in Organic Chemistry*; Hughes, A. B., Ed.; Wiley, 2009; pp 145–187. https://doi.org/10.1002/9783527631780.ch4.

(13) Matteson, D. S.; Cheng, T.-C. Displacement Reactions of Dibutyl Iodomethaneboronate and the Synthesis of Boron-Substituted Pyrimidines. *J. Org. Chem.* **1968**, *33* (8), 3055–3060. https://doi.org/10.1021/jo01272a008.

(14) Matteson, D. S. ..Alpha.-Halo Boronic Esters: Intermediates for Stereodirected Synthesis. *Chem. Rev.* **1989**, *89* (7), 1535–1551. https://doi.org/10.1021/cr00097a009.

(15) Matteson, D. S. Boronic Esters in Asymmetric Synthesis. *J. Org. Chem.* **2013**, *78* (20), 10009–10023. https://doi.org/10.1021/jo4013942.

(16) Andrés, P.; Ballano, G.; Calaza, M. I.; Cativiela, C. Synthesis of α-Aminoboronic Acids. *Chem. Soc. Rev.* **2016**, *45* (8), 2291–2307. https://doi.org/10.1039/C5CS00886G.

(17) Šterman, A.; Sosič, I.; Gobec, S.; Časar, Z. Synthesis of Aminoboronic Acid Derivatives: An Update on Recent Advances. *Org. Chem. Front.* **2019**, *6* (16), 2991–2998. https://doi.org/10.1039/C9QO00626E.

(18) Ming, W.; Soor, H. S.; Liu, X.; Trofimova, A.; Yudin, A. K.; Marder, T. B. α-Aminoboronates: Recent Advances

in Their Preparation and Synthetic Applications. *Chem. Soc. Rev.* **2021**, *50* (21), 12151–12188. https://doi.org/10.1039/D1CS00423A.

(19) Beenen, M. A.; An, C.; Ellman, J. A. Asymmetric Copper-Catalyzed Synthesis of α-Amino Boronate Esters from N-Tert-Butanesulfinyl Aldimines. *J. Am. Chem. Soc.* **2008**, *130* (22), 6910–6911. https://doi.org/10.1021/ja800829y.

(20) Wen, K.; Wang, H.; Chen, J.; Zhang, H.; Cui, X.; Wei, C.; Fan, E.; Sun, Z. Improving Carbene–Copper-Catalyzed Asymmetric Synthesis of α-Aminoboronic Esters Using Benzimidazole-Based Precursors. *J. Org. Chem.* **2013**, *78* (7), 3405–3409. https://doi.org/10.1021/jo4000477.

(21) Buesking, A. W.; Bacauanu, V.; Cai, I.; Ellman, J. A. Asymmetric Synthesis of Protected α-Amino Boronic Acid Derivatives with an Air- and Moisture-Stable Cu(II) Catalyst. *J. Org. Chem.* **2014**, *79* (8), 3671–3677. https://doi.org/10.1021/jo500300t.

(22) Zhang, S.-S.; Zhao, Y.-S.; Tian, P.; Lin, G.-Q. Chiral NHC/Cu(I)-Catalyzed Asymmetric Hydroboration of Aldimines: Enantioselective Synthesis of α-Amido Boronic Esters. *Synlett* **2013**, *24* (4), 437–442. https://doi.org/10.1055/s-0032-1318145.

(23) Schwamb, C. B.; Fitzpatrick, K. P.; Brueckner, A. C.; Richardson, H. C.; Cheong, P. H.-Y.; Scheidt, K. A. Enantioselective Synthesis of α-Amidoboronates Catalyzed by Planar-Chiral NHC-Cu(I) Complexes. *J. Am. Chem. Soc.* **2018**, *140* (34), 10644–10648. https://doi.org/10.1021/jacs.8b05045.

(24) Wang, D.; Cao, P.; Wang, B.; Jia, T.; Lou, Y.; Wang, M.; Liao, J. Copper(I)-Catalyzed Asymmetric Pinacolboryl Addition of N-Boc-Imines Using a Chiral Sulfoxide–Phosphine Ligand. *Org. Lett.* **2015**, *17* (10), 2420–2423. https://doi.org/10.1021/acs.orglett.5b00934.

(25) Ming, W.; Liu, X.; Friedrich, A.; Krebs, J.; Marder, T. B. The Borono–Strecker Reaction: Synthesis of α-Aminoboronates via a Multicomponent Reaction of Carbonyl Compounds, Amines, and B2pin2. *Org. Lett.* **2020**, *22* (2), 365–370. https://doi.org/10.1021/acs.orglett.9b03773.

(26) Xia, Q.; Chang, H.-R.; Li, J.; Wang, J.-Y.; Peng, Y.-Q.; Song, G.-H. Tunable Synthesis of α-Amino Boronic Esters from Available Aldehydes and Amines through Sequential One-Pot Dehydration and Copper-Catalyzed Borylacylation. *J. Org. Chem.* **2020**, *85* (4), 2716–2724. https://doi.org/10.1021/acs.joc.9b02887.

(27) Li, C.; Wang, J.; Barton, L. M.; Yu, S.; Tian, M.; Peters, D. S.; Kumar, M.; Yu, A. W.; Johnson, K. A.; Chatterjee, A. K.; Yan, M.; Baran, P. S. Decarboxylative Borylation. *Science* **2017**, *356* (6342), eaam7355. https://doi.org/10.1126/science.aam7355.

(28) Hu, N.; Zhao, G.; Zhang, Y.; Liu, X.; Li, G.; Tang, W. Synthesis of Chiral α-Amino Tertiary Boronic Esters by Enantioselective Hydroboration of α-Arylenamides. *J. Am. Chem. Soc.* **2015**, *137* (21), 6746–6749. https://doi.org/10.1021/jacs.5b03760.

(29) Bai, X.-Y.; Zhao, W.; Sun, X.; Li, B.-J. Rhodium-Catalyzed Regiodivergent and Enantioselective Hydroboration of Enamides. *J. Am. Chem. Soc.* **2019**, *141* (50), 19870–19878. https://doi.org/10.1021/jacs.9b10578.

(30) Chen, L.; Zou, X.; Zhao, H.; Xu, S. Copper-Catalyzed Asymmetric Protoboration of β-Amidoacrylonitriles and β-Amidoacrylate Esters: An Efficient Approach to Functionalized Chiral α-Amino Boronate Esters. *Org. Lett.* **2017**, *19* (13), 3676–3679. https://doi.org/10.1021/acs.orglett.7b01740.

(31) López, A.; Clark, T. B.; Parra, A.; Tortosa, M. Copper-Catalyzed Enantioselective Synthesis of β-Boron β-Amino Esters. *Org. Lett.* **2017**, *19* (23), 6272–6275. https://doi.org/10.1021/acs.orglett.7b02784.

(32) Nishikawa, D.; Hirano, K.; Miura, M. Asymmetric Synthesis of α-Aminoboronic Acid Derivatives by Copper-Catalyzed Enantioselective Hydroamination. *J. Am. Chem. Soc.* **2015**, *137* (50), 15620–15623. https://doi.org/10.1021/jacs.5b09773.

(33) Miki, Y.; Hirano, K.; Satoh, T.; Miura, M. Copper-Catalyzed Intermolecular Regioselective Hydroamination of Styrenes with Polymethylhydrosiloxane and Hydroxylamines. *Angew. Chem. Int. Ed.* **2013**, *52* (41), 10830–10834. https://doi.org/10.1002/anie.201304365.

(34) Zhu, S.; Niljianskul, N.; Buchwald, S. L. Enantio- and Regioselective CuH-Catalyzed Hydroamination of Alkenes. *J. Am. Chem. Soc.* **2013**, *135* (42), 15746–15749. https://doi.org/10.1021/ja4092819.

(35) Zhu, S.; Buchwald, S. L. Enantioselective CuH-Catalyzed Anti-Markovnikov Hydroamination of 1,1-Disubstituted Alkenes. *J. Am. Chem. Soc.* **2014**, *136* (45), 15913–15916. https://doi.org/10.1021/ja509786v.

(36) Miki, Y.; Hirano, K.; Satoh, T.; Miura, M. Copper-Catalyzed Enantioselective Formal Hydroamination of Oxa- and Azabicyclic Alkenes with Hydrosilanes and Hydroxylamines. *Org. Lett.* **2014**, *16* (5), 1498–1501. https://doi.org/10.1021/ol5003219.

(37) Shi, S.-L.; Buchwald, S. L. Copper-Catalysed Selective Hydroamination Reactions of Alkynes. *Nat. Chem.* **2015**, *7* (1), 38–44. https://doi.org/10.1038/nchem.2131.

(38) Niljianskul, N.; Zhu, S.; Buchwald, S. L. Enantioselective Synthesis of α-Aminosilanes by Copper-Catalyzed Hydroamination of Vinylsilanes. *Angew. Chem. Int. Ed.* **2015**, *54* (5), 1638–1641. https://doi.org/10.1002/anie.201410326.

(39) Yang, Y.; Shi, S.-L.; Niu, D.; Liu, P.; Buchwald, S. L. Catalytic Asymmetric Hydroamination of Unactivated Internal Olefins to Aliphatic Amines. *Science* **2015**, *349* (6243), 62–66. https://doi.org/10.1126/science.aab3753.

(40) Zhang, Y.; Qiao, D.; Duan, M.; Wang, Y.; Zhu, S. Enantioselective Synthesis of α-Aminoboronates by NiH-Catalysed Asymmetric Hydroamidation of Alkenyl Boronates. *Nat. Commun.* **2022**, *13* (1), 5630. https://doi.org/10.1038/s41467-022-33411-9.

(41) Nishino, S.; Hirano, K.; Miura, M. Copper-Catalyzed Electrophilic Amination of Gem-Diborylalkanes with Hydroxylamines Providing α-Aminoboronic Acid Derivatives. *Org. Lett.* **2019**, *21* (12), 4759–4762. https://doi.org/10.1021/acs.orglett.9b01640.

(42) Gao, D.-W.; Gao, Y.; Shao, H.; Qiao, T.-Z.; Wang, X.; Sanchez, B. B.; Chen, J. S.; Liu, P.; Engle, K. M. Cascade CuH-Catalysed Conversion of Alkynes into Enantioenriched 1,1-Disubstituted Products. *Nat. Catal.* **2020**, *3* (1), 23–29. https://doi.org/10.1038/s41929-019-0384-6.

(43) *NCATS Inxight Drugs — PINANEDIOL PYRROLIDIN-2-YLBORONATE, (+)-*. https://drugs.ncats.io/substance/UX8XOB7FWD (accessed 2023-06-13).

(44) Zuccarello, G.; Batiste, S. M.; Cho, H.; Fu, G. C. Enantioselective Synthesis of α-Aminoboronic Acid Derivatives via Copper-Catalyzed N-Alkylation. *J. Am. Chem. Soc.* **2023**, *145* (6), 3330–3334. https://doi.org/10.1021/jacs.3c00038.

(45) Ye, Y.; Lin, Y.; Mao, N.-D.; Yang, H.; Ye, X.-Y.; Xie, T. Recent Progress in Nickel-Catalyzed Carboboration of Alkenes. *Org. Biomol. Chem.* **2022**, *20* (47), 9255–9271. https://doi.org/10.1039/D2OB01855A.

(46) Juliá-Hernández, F.; Moragas, T.; Cornella, J.; Martin, R. Remote Carboxylation of Halogenated Aliphatic Hydrocarbons with Carbon Dioxide. *Nature* **2017**, *545* (7652), 84–88. https://doi.org/10.1038/nature22316.

(47) Sun, S.-Z.; Börjesson, M.; Martin-Montero, R.; Martin, R. Site-Selective Ni-Catalyzed Reductive Coupling of α-Haloboranes with Unactivated Olefins. *J. Am. Chem. Soc.* **2018**, *140* (40), 12765–12769. https://doi.org/10.1021/jacs.8b09425.

(48) Sun, S.-Z.; Romano, C.; Martin, R. Site-Selective Catalytic Deaminative Alkylation of Unactivated Olefins. *J. Am. Chem. Soc.* **2019**, *141* (41), 16197–16201. https://doi.org/10.1021/jacs.9b07489.

(49) Sun, S.-Z.; Talavera, L.; Spieß, P.; Day, C. S.; Martin, R. Sp3 Bis-Organometallic Reagents via Catalytic 1,1-Difunctionalization of Unactivated Olefins. *Angew. Chem. Int. Ed.* **2021**, *60* (21), 11740–11744. https://doi.org/10.1002/anie.202100810.

(50) Rodrigalvarez, J.; Wang, H.; Martin, R. Native Amides as Enabling Vehicles for Forging Sp3–Sp3 Architectures via Interrupted Deaminative Ni-Catalyzed Chain-Walking. *J. Am. Chem. Soc.* **2023**. https://doi.org/10.1021/jacs.2c12915.

(51) Jankins, T. C.; Martin-Montero, R.; Cooper, P.; Martin, R.; Engle, K. M. Low-Valent Tungsten Catalysis Enables Site-Selective Isomerization–Hydroboration of Unactivated Alkenes. *J. Am. Chem. Soc.* **2021**, *143* (37), 14981–14986. https://doi.org/10.1021/jacs.1c07162.

(52) Yang, S.; Chen, Y.; Ding, Z. Recent Progress of 1,1-Difunctionalization of Olefins. *Org. Biomol. Chem.* **2020**, *18* (36), 6983–7001. https://doi.org/10.1039/D0OB01323D.

(53) Dhungana, R. K.; Sapkota, R. R.; Niroula, D.; Giri, R. Walking Metals: Catalytic Difunctionalization of Alkenes

at Nonclassical Sites. *Chem. Sci.* **2020**, *11* (36), 9757–9774. https://doi.org/10.1039/D0SC03634J.

(54) Li, Y.; Wu, D.; Cheng, H.; Yin, G. Difunctionalization of Alkenes Involving Metal Migration. *Angew. Chem. Int. Ed.* **2020**, *59* (21), 7990–8003. https://doi.org/10.1002/anie.201913382.

(55) Barker, T. J.; Jarvo, E. R. Developments in Transition-Metal-Catalyzed Reactions Using Electrophilic Nitrogen Sources. *Synthesis* **2011**, 3954–3964. https://doi.org/10.1055/s-0031-1289581.

(56) Hirano, K.; Miura, M. Hydroamination, Aminoboration, and Carboamination with Electrophilic Amination Reagents: Umpolung-Enabled Regio- and Stereoselective Synthesis of N-Containing Molecules from Alkenes and Alkynes. *J. Am. Chem. Soc.* **2022**, *144* (2), 648–661. https://doi.org/10.1021/jacs.1c12663.

(57) Niu, D.; Buchwald, S. L. Design of Modified Amine Transfer Reagents Allows the Synthesis of α-Chiral Secondary Amines via CuH-Catalyzed Hydroamination. *J. Am. Chem. Soc.* **2015**, *137* (30), 9716–9721. https://doi.org/10.1021/jacs.5b05446.

(58) Kang, T.; Kim, N.; Cheng, P. T.; Zhang, H.; Foo, K.; Engle, K. M. Nickel-Catalyzed 1,2-Carboamination of Alkenyl Alcohols. *J. Am. Chem. Soc.* **2021**, *143* (34), 13962–13970. https://doi.org/10.1021/jacs.1c07112.

(59) Nishino, S.; Nishii, Y.; Hirano, K. Anti-Selective Synthesis of β-Boryl-α-Amino Acid Derivatives by Cu-Catalysed Borylamination of α,β-Unsaturated Esters. *Chem. Sci.* **2022**, *13* (48), 14387–14394. https://doi.org/10.1039/D2SC06003E.

(60) Li, Y.; Pang, H.; Wu, D.; Li, Z.; Wang, W.; Wei, H.; Fu, Y.; Yin, G. Nickel-Catalyzed 1,1-Alkylboration of Electronically Unbiased Terminal Alkenes. *Angew. Chem. Int. Ed.* **2019**, *58* (26), 8872–8876. https://doi.org/10.1002/anie.201903890.

(61) Logan, K. M.; Sardini, S. R.; White, S. D.; Brown, M. K. Nickel-Catalyzed Stereoselective Arylboration of Unactivated Alkenes. *J. Am. Chem. Soc.* **2018**, *140* (1), 159–162. https://doi.org/10.1021/jacs.7b12160.

(62) Sardini, S. R.; Lambright, A. L.; Trammel, G. L.; Omer, H. M.; Liu, P.; Brown, M. K. Ni-Catalyzed Arylboration of Unactivated Alkenes: Scope and Mechanistic Studies. *J. Am. Chem. Soc.* **2019**, *141* (23), 9391–9400. https://doi.org/10.1021/jacs.9b03991.

(63) Simlandy, A. K.; Lyu, M.-Y.; Brown, M. K. Catalytic Arylboration of Spirocyclic Cyclobutenes: Rapid Access to Highly Substituted Spiro[3.n]Alkanes. *ACS Catal.* **2021**, *11* (20), 12815–12820. https://doi.org/10.1021/acscatal.1c03491.

(64) Simlandy, A. K.; Sardini, S. R.; Brown, M. K. Construction of Congested Csp3–Csp3 Bonds by a Formal Ni-Catalyzed Alkylboration. *Chem. Sci.* **2021**, *12* (15), 5517–5521. https://doi.org/10.1039/D1SC00900A.

(65) Nattmann, L.; Saeb, R.; Nöthling, N.; Cornella, J. An Air-Stable Binary Ni(0)–Olefin Catalyst. *Nat. Catal.* **2020**, *3* (1), 6–13. https://doi.org/10.1038/s41929-019-0392-6.

(66) Nattmann, L.; Cornella, J. Ni(4-TBustb)3: A Robust 16-Electron Ni(0) Olefin Complex for Catalysis. *Organometallics* **2020**, *39* (18), 3295–3300. https://doi.org/10.1021/acs.organomet.0c00485.

(67) Xu, J.; Bercher, O. P.; Watson, M. P. Overcoming the Naphthyl Requirement in Stereospecific Cross-Couplings to Form Quaternary Stereocenters. *J. Am. Chem. Soc.* **2021**, *143* (23), 8608–8613. https://doi.org/10.1021/jacs.1c03898.

(68) Estrada, J. G.; Williams, W. L.; Ting, S. I.; Doyle, A. G. Role of Electron-Deficient Olefin Ligands in a Ni-Catalyzed Aziridine Cross-Coupling To Generate Quaternary Carbons. *J. Am. Chem. Soc.* **2020**, *142* (19), 8928–8937. https://doi.org/10.1021/jacs.0c02237.

(69) Aryal, V.; Chesley, L. J.; Niroula, D.; Sapkota, R. R.; Dhungana, R. K.; Giri, R. Ni-Catalyzed Regio- and Stereoselective Alkylarylation of Unactivated Alkenes in γ,δ-Alkenylketimines. *ACS Catal.* **2022**, *12* (12), 7262–7268. https://doi.org/10.1021/acscatal.2c01697.

(70) Shibli, A.; Srebnik, M. Synthesis of Novel α-Aminoboronate Complexes of Aminoboranes and Aminocyanoboranes. *Eur. J. Inorg. Chem.* **2006**, *2006* (8), 1686–1689. https://doi.org/10.1002/ejic.200501085.

(71) Shiro, T.; Schuhmacher, A.; Jackl, M. K.; Bode, J. W. Facile Synthesis of α-Aminoboronic Acids from Amines and Potassium Acyltrifluoroborates (KATs) via Trifluoroborate-Iminiums (TIMs). *Chem. Sci.* **2018**, *9* (23), 5191–5196. https://doi.org/10.1039/C8SC01486H.

(72) Nishikawa, D.; Hirano, K.; Miura, M. Copper-Catalyzed Regio- and Stereoselective Aminoboration of Alkenylboronates. *Org. Lett.* **2016**, *18* (19), 4856–4859. https://doi.org/10.1021/acs.orglett.6b02338.

(73) Šterman, A.; Sosič, I.; Časar, Z. Primary Trifluoroborate-Iminiums Enable Facile Access to Chiral α-Aminoboronic Acids via Ru-Catalyzed Asymmetric Hydrogenation and Simple Hydrolysis of the Trifluoroborate Moiety. *Chem. Sci.* **2022**, *13* (10), 2946–2953. https://doi.org/10.1039/D1SC07065G.

(74) Xie, Q.; Dong, G. Aza-Matteson Reactions via Controlled Mono- and Double-Methylene Insertions into Nitrogen–Boron Bonds. *J. Am. Chem. Soc.* **2021**, *143* (36), 14422–14427. https://doi.org/10.1021/jacs.1c06186.

(75) Ohmura, T.; Awano, T.; Suginome, M. Stereospecific Suzuki−Miyaura Coupling of Chiral α-(Acylamino)Benzylboronic Esters with Inversion of Configuration. *J. Am. Chem. Soc.* **2010**, *132* (38), 13191–13193. https://doi.org/10.1021/ja106632j.

(76) Raushel, J.; Sandrock, D. L.; Josyula, K. V.; Pakyz, D.; Molander, G. A. Reinvestigation of Aminomethyltrifluoroborates and Their Application in Suzuki−Miyaura Cross-Coupling Reactions. *J. Org. Chem.* **2011**, *76* (8), 2762–2769. https://doi.org/10.1021/jo2001066.

(77) Molander, G. A.; Wisniewski, S. R. Stereospecific Cross-Coupling of Secondary Organotrifluoroborates: Potassium 1-(Benzyloxy)Alkyltrifluoroborates. *J. Am. Chem. Soc.* **2012**, *134* (40), 16856–16868. https://doi.org/10.1021/ja307861n.

(78) Fleury-Brégeot, N.; Raushel, J.; Sandrock, D. L.; Dreher, S. D.; Molander, G. A. Rapid and Efficient Access to Secondary Arylmethylamines. *Chem. – Eur. J.* **2012**, *18* (31), 9564–9570. https://doi.org/10.1002/chem.201200831.

(79) El Khatib, M.; Serafim, R. A. M.; Molander, G. A. α-Arylation/Heteroarylation of Chiral α-Aminomethyltrifluoroborates by Synergistic Iridium Photoredox/Nickel Cross-Coupling Catalysis. *Angew. Chem. Int. Ed.* **2016**, *55* (1), 254–258. https://doi.org/10.1002/anie.201506147.

(80) Alam, R.; Molander, G. A. Direct Synthesis of Secondary Benzylic Alcohols Enabled by Photoredox/Ni Dual-Catalyzed Cross-Coupling. *J. Org. Chem.* **2017**, *82* (24), 13728–13734. https://doi.org/10.1021/acs.joc.7b02589.

(81) Yuan, M.; Song, Z.; Badir, S. O.; Molander, G. A.; Gutierrez, O. On the Nature of C(Sp3)–C(Sp2) Bond Formation in Nickel-Catalyzed Tertiary Radical Cross-Couplings: A Case Study of Ni/Photoredox Catalytic Cross-Coupling of Alkyl Radicals and Aryl Halides. *J. Am. Chem. Soc.* **2020**, *142* (15), 7225–7234. https://doi.org/10.1021/jacs.0c02355.

(82) Greenwood, J. W.; Boyle, B. T.; McNally, A. Pyridylphosphonium Salts as Alternatives to Cyanopyridines in Radical–Radical Coupling Reactions. *Chem. Sci.* **2021**, *12* (31), 10538–10543. https://doi.org/10.1039/D1SC02324A.

(83) Cauley, A. N.; Sezen-Edmonds, M.; Simmons, E. M.; Cavallaro, C. L. Increasing Saturation: Development of Broadly Applicable Photocatalytic Csp2–Csp3 Cross-Couplings of Alkyl Trifluoroborates and (Hetero)Aryl Bromides for Array Synthesis. *React. Chem. Eng.* **2021**, *6* (9), 1666–1676. https://doi.org/10.1039/D1RE00192B.

(84) Chen, L.-A.; Lear, A. R.; Gao, P.; Brown, M. K. Nickel-Catalyzed Arylboration of Alkenylarenes: Synthesis of Boron-Substituted Quaternary Carbons and Regiodivergent Reactions. *Angew. Chem. Int. Ed.* **2019**, *58* (32), 10956–10960. https://doi.org/10.1002/anie.201904861.

(85) Wang, W.; Ding, C.; Yin, G. Catalyst-Controlled Enantioselective 1,1-Arylboration of Unactivated Olefins. *Nat. Catal.* **2020**, *3* (11), 951–958. https://doi.org/10.1038/s41929-020-00523-8.

(86) Zhu, D.; Shi, L. Ni-Catalyzed Cross-Coupling of Aryl Thioethers with Alkyl Grignard Reagents via C–S Bond Cleavage. *Chem. Commun.* **2018**, *54* (67), 9313–9316. https://doi.org/10.1039/C8CC03665A.

(87) García-Vázquez, V.; Hoteite, L.; Lakeland, C. P.; Watson, D. W.; Harrity, J. P. A. A Pd-Catalyzed [4 + 2] Annulation Approach to Fluorinated N-Heterocycles. *Org. Lett.* **2021**, *23* (7), 2811–2815. https://doi.org/10.1021/acs.orglett.1c00752.

(88) Yang, T.; Lu, L.; Shen, Q. Iron-Mediated Markovnikov-Selective Hydro-Trifluoromethylthiolation of

Unactivated Alkenes. *Chem. Commun.* **2015**, *51* (25), 5479–5481. https://doi.org/10.1039/C4CC08655D.

(89) Tokuyasu, T.; Kunikawa, S.; McCullough, K. J.; Masuyama, A.; Nojima, M. Synthesis of Cyclic Peroxides by Chemo- and Regioselective Peroxidation of Dienes with Co(II)/O2/Et3SiH. *J. Org. Chem.* **2005**, *70* (1), 251–260. https://doi.org/10.1021/jo048359j.

(90) Reid, J. P.; McAdam, C. A.; Johnston, A. J. S.; Grayson, M. N.; Goodman, J. M.; Cook, M. J. Base-Mediated Cascade Rearrangements of Aryl-Substituted Diallyl Ethers. *J. Org. Chem.* **2015**, *80* (3), 1472–1498. https://doi.org/10.1021/jo502403n.

(91) Buswell, M.; Fleming, I.; Ghosh, U.; Mack, S.; Russell, M.; Clark, B. P. The Extraordinary Reactions of Phenyldimethylsilyllithium with N,N-Disubstituted Amides. *Org. Biomol. Chem.* **2004**, *2* (20), 3006–3017. https://doi.org/10.1039/B412768D.

(92) Zhao, H.; McMillan, A. J.; Constantin, T.; Mykura, R. C.; Juliá, F.; Leonori, D. Merging Halogen-Atom Transfer (XAT) and Cobalt Catalysis to Override E2-Selectivity in the Elimination of Alkyl Halides: A Mild Route toward Contra-Thermodynamic Olefins. *J. Am. Chem. Soc.* **2021**, *143* (36), 14806–14813. https://doi.org/10.1021/jacs.1c06768.

(93) Olivier, W. J.; Gardiner, M. G.; Bissember, A. C.; Smith, J. A. Brønsted Acid-Mediated Annulations of Pyrroles Featuring N-Tethered α,β-Unsaturated Ketones and Esters: Total Syntheses of (±)-Tashiromine and (±)-Indolizidine 209I. *Tetrahedron* **2018**, *74* (38), 5436–5441. https://doi.org/10.1016/j.tet.2018.04.067.

(94) Hoffmann, N.; Pete, J.-P. Intramolecular Photochemical Reactions of Bichromophoric 3-(Alkenyloxy)Phenols and 1-(Alkenyloxy)-3-(Alkyloxy)Benzene Derivatives. Acid-Catalyzed Transformations of the Primary Cycloadducts. *J. Org. Chem.* **1997**, *62* (20), 6952–6960. https://doi.org/10.1021/jo970554t.

(95) Legnani, L.; Prina-Cerai, G.; Delcaillau, T.; Willems, S.; Morandi, B. Efficient Access to Unprotected Primary Amines by Iron-Catalyzed Aminochlorination of Alkenes. *Science* **2018**, *362* (6413), 434–439. https://doi.org/10.1126/science.aat3863.

(96) Wang, M.; Zhang, H.; Liu, J.; Wu, X.; Zhu, C. Radical Monofluoroalkylative Alkynylation of Olefins by a Docking–Migration Strategy. *Angew. Chem. Int. Ed.* **2019**, *58* (49), 17646–17650. https://doi.org/10.1002/anie.201910514.

(97) Xu, J.; Fu, Y.; Luo, D.-F.; Jiang, Y.-Y.; Xiao, B.; Liu, Z.-J.; Gong, T.-J.; Liu, L. Copper-Catalyzed Trifluoromethylation of Terminal Alkenes through Allylic C–H Bond Activation. *J. Am. Chem. Soc.* **2011**, *133* (39), 15300–15303. https://doi.org/10.1021/ja206330m.

(98) Donnoli, M. I.; Scafato, P.; Superchi, S.; Rosini, C. Synthesis and Stereochemical Characterization of Optically Active 1,2-Diarylethane-1,2-Diols: Useful Chiral Controllers in the Ti-Mediated Enantioselective Sulfoxidation. *Chirality* **2001**, *13* (5), 258–265. https://doi.org/10.1002/chir.1028.

(99) Diéguez, H. R.; López, A.; Domingo, V.; Arteaga, J. F.; Dobado, J. A.; Herrador, M. M.; Quílez del Moral, J. F.; Barrero, A. F. Weakening C−O Bonds: Ti(III), a New Reagent for Alcohol Deoxygenation and Carbonyl Coupling Olefination. *J. Am. Chem. Soc.* **2010**, *132* (1), 254–259. https://doi.org/10.1021/ja906083c.

Chapter 5.

General conclusions

UNIVERSITAT ROVIRA I VIRGILI
FUNCTIONALISATION OF SP3 C-O BONDS AND OLEFINS ENABLED BY NICKEL CATALYSIS
Laura Talavera Codina

5.1. General conclusions

To conclude this Doctoral thesis, the main points from each of the experimental chapters will be highlighted. The developed methods highlight the versatility and distinct reactivity modes of nickel catalysis, providing valuable tools for the functionalisation of unactivated C–O bonds via metallaphotoredox strategies and the synthesis of diverse sp^3 functionalised linkages using olefins as readily available starting materials.

Chapter 2

- The functionalisation of *unbiased* C(sp^3)–O bonds in cyclic acetals has been successfully achieved.
- The C–O cleavage occurs through selective HAT at the benzylidene C–H bond, followed by a subsequent β-fragmentation.
- The β-fragmentation occurs only with an appropriate σ*-p orbital overlap, emphasising the importance of conformational flexibility.
- The reaction scope has been extended to the formation of C(sp^3)–C(sp^3) bonds, broadening the synthetic possibilities.

Chapter 3

- A protocol for the synthesis of *bis*-organometallics via nickel-catalysed 1,1-difunctionalisation of unactivated olefins has been developed.
- The incorporation of a boron sources serves as a driving force for metal migration, enabling precise 1,1-site selectivity.
- The applicability of this methodology has been demonstrated through the functionalisation of advanced synthetic intermediates and the use of ethylene as starting materials.
- The introduction of both B and a Si motif and selective cleavage of the primary boron or secondary boron over silicon allows for downstream reactions and further derivatisation.

Chapter 4

- A method for the incorporation of two different heteroatom motifs across the olefin backbone with a 1,1-selectivity has been successfully realized.
- This reaction enables the synthesis of valuable α-aminoboronic acid derivatives.
- This methodology offers enhanced synthetic versatility and flexibility by utilising readily available alkenes and commercially available starting materials.
- β-aminoboronic esters can be readily accessed via *in situ* Matteson homologation of the reaction crude.

Chapter 5.

UNIVERSITAT ROVIRA I VIRGILI
FUNCTIONALISATION OF SP3 C-O BONDS AND OLEFINS ENABLED BY NICKEL CATALYSIS
Laura Talavera Codina

UNIVERSITAT
ROVIRA i VIRGILI